



# Handbook on the Physics and Chemistry of Rare Earths volume 6

Elsevier, 1984

*Edited by: Karl A. Gschneidner, Jr. and LeRoy Eyring*  
ISBN: 978-0-444-86592-2

## PREFACE

Karl A. GSCHNEIDNER, Jr., and LeRoy EYRING

---

*These elements perplex us in our rearches [sic], baffle us in our speculations, and haunt us in our very dreams. They stretch like an unknown sea before us – mocking, mystifying, and murmuring strange revelations and possibilities.*

Sir William Crookes (February 16, 1887)

---

This lament of Sir William Crookes, which introduced the preface to the previous volumes of this series, still beckons hauntingly for satisfaction. Although many of the greatest mysteries he contemplated have been satisfactorily solved, there still remains the need for voyages of discovery on the “unknown sea”.

The first five volumes of the *Handbook of the Physics and Chemistry of Rare Earths* served primarily as navigational guides for the “elemental sea” and the “sea of binary materials”. Although some information in volumes three, four and five dealt with ternary and higher order materials, this vast “sea” is still virtually unknown. Volume six is the beginning of an intensive exploration of the “sea of ternary and higher order materials”. But even with this volume only a small portion will be duly recorded in our log (Handbook), and future volumes will be needed to help map out the unknown and bring it into the realm of our knowledge. Even though our knowledge of the “elemental sea” and “sea of binary materials” is vast, it is, nevertheless, incomplete, and portions of the future volumes will help fill in these unexplored bays and inlets.

The four chapters in volume six deal with ternary (and higher order) systems, compounds, etc. which contain at least one rare earth metal and at least one nonmetallic element (H, B, C or Si). The first chapter deals with hydrogen absorption by intermetallic compounds. The next two chapters are quite complementary, dealing with the crystal chemistry of ternary borides and silicides, and phase equilibria in ternary and higher order systems involving boron. A companion chapter on phase equilibria in ternary and higher order systems involving silicon is scheduled for volume seven. The last chapter of volume six is a little more specialized and is concerned with divalent samarium and ytterbium in organic chemistry. Future volumes are scheduled to contain more reviews on the organic chemistry of rare earths—a rapidly growing and dynamic “bay” in the “sea of ternary and higher order materials”.

It is our intent that the handbook will continue to serve as a chronicle, charts, and navigational aids to those who would explore the mysteries of this unknown sea, the rare earths.

## CONTENTS

Preface v

Contents vii

Contents of volumes 1–5 ix

47. K.H.J. Buschow

*Hydrogen absorption in intermetallic compounds* 1

48. E. Parthé and B. Chabot

*Crystal structures and crystal chemistry of ternary rare earth–transition metal borides, silicides and homologues* 113

49. P. Rogl

*Phase equilibria in ternary and higher order systems with rare earth elements and boron* 335

50. H.B. Kagan and J.L. Namy

*Preparation of divalent ytterbium and samarium derivatives and their use in organic chemistry* 525

*Subject index* 567

## CONTENTS OF VOLUMES 1-5

### VOLUME 1: METALS

1. Z.B. Goldschmidt, *Atomic properties (free atom)* 1
2. B.J. Beaudry and K.A. Gschneidner, Jr., *Preparation and basic properties of the rare earth metals* 173
3. S.H. Liu, *Electronic structure of rare earth metals* 233
4. D.C. Koskenmaki and K.A. Gschneidner, Jr., *Cerium* 337
5. L.J. Sundström, *Low temperature heat capacity of the rare earth metals* 379
6. K.A. McEwen, *Magnetic and transport properties of the rare earths* 411
7. S.K. Sinha, *Magnetic structures and inelastic neutron scattering: metals, alloys and compounds* 489
8. T.E. Scott, *Elastic and mechanical properties* 591
9. A. Jayaraman, *High pressure studies: metals, alloys and compounds* 707
10. C. Probst and J. Wittig, *Superconductivity: metals, alloys and compounds* 749
11. M.B. Maple, L.E. DeLong and B.C. Sales, *Kondo effect: alloys and compounds* 797
12. M.P. Dariel, *Diffusion in rare earth metals* 847
- Subject index* 877

### VOLUME 2: ALLOYS AND INTERMETALLICS

13. A. Iandelli and A. Palenzona, *Crystal chemistry of intermetallic compounds* 1
14. H.R. Kirchmayr and C.A. Poldy, *Magnetic properties of intermetallic compounds of rare earth metals* 55
15. A.E. Clark, *Magnetostrictive RFe<sub>2</sub> intermetallic compounds* 231
16. J.J. Rhyne, *Amorphous magnetic rare earth alloys* 259
17. P. Fulde, *Crystal fields* 295
18. R.G. Barnes, *NMR, EPR and Mössbauer effect: metals, alloys and compounds* 387
19. P. Wachter, *Europium chalcogenides: EuO, EuS, EuSe and EuTe* 507
20. A. Jayaraman, *Valence changes in compounds* 575
- Subject index* 613

### VOLUME 3: NON-METALLIC COMPOUNDS - I

21. L.A. Haskin and T.P. Paster, *Geochemistry and mineralogy of the rare earths* 1
22. J.E. Powell, *Separation chemistry* 81
23. C.K. Jørgensen, *Theoretical chemistry of rare earths* 111
24. W.T. Carnall, *The absorption and fluorescence spectra of rare earth ions in solution* 171
25. L.C. Thompson, *Complexes* 209
26. G.G. Libowitz and A.J. Maeland, *Hydrides* 299
27. L. Eyring, *The binary rare earth oxides* 337
28. D.J.M. Bevan and E. Summerville, *Mixed rare earth oxides* 401
29. C.P. Khattak and F.F.Y. Wang, *Perovskites and garnets* 525
30. L.H. Brixner, J.R. Barkley and W. Jeitschko, *Rare earth molybdates (VI)* 609
- Subject index* 655

**VOLUME 4: NON-METALLIC COMPOUNDS - II**

31. J. Flahaut, *Sulfides, selenides and tellurides* 1
32. J.M. Haschke, *Halides* 89
33. F. Hulliger, *Rare earth pnictides* 153
34. G. Blasse, *Chemistry and physics of R-activated phosphors* 237
35. M.J. Weber, *Rare earth lasers* 275
36. F.K. Fong, *Nonradiative processes of rare-earth ions in crystals* 317
- 37A. J.W. O'Laughlin, *Chemical spectrophotometric and polarographic methods* 341
- 37B. S.R. Taylor, *Trace element analysis of rare earth elements by spark source mass spectrometry* 359
- 37C. R.J. Conzemius, *Analysis of rare earth matrices by spark source mass spectrometry* 377
- 37D. E.L. DeKalb and V.A. Fassel, *Optical atomic emission and absorption methods* 405
- 37E. A.P. D'Silva and V.A. Fassel, *X-ray excited optical luminescence of the rare earths* 441
- 37F. W.V. Boynton, *Neutron activation analysis* 457
- 37G. S. Schuhmann and J.A. Philpotts, *Mass-spectrometric stable-isotope dilution analysis for lanthanides in geochemical materials* 471
38. J. Reuben and G.A. Elgavish, *Shift reagents and NMR of paramagnetic lanthanide complexes* 483
39. J. Reuben, *Bioinorganic chemistry: lanthanides as probes in systems of biological interest* 515
40. T.J. Haley, *Toxicity* 553  
*Subject index* 587

**VOLUME 5**

41. M. Gasgnier, *Rare earth alloys and compounds as thin films* 1
42. E. Gratz and M.J. Zuckermann, *Transport properties (electrical resistivity, thermoelectric power and thermal conductivity) of rare earth intermetallic compounds* 117
43. F.P. Netzer and E. Bertel, *Adsorption and catalysis on rare earth surfaces* 217
44. C. Boulesteix, *Defects and phase transformation near room temperature in rare earth sesquioxides* 321
45. O. Greis and J.M. Haschke, *Rare earth fluorides* 387
46. C.A. Morrison and R.P. Leavitt, *Spectroscopic properties of triply ionized lanthanides in transparent host crystals* 461  
*Subject index* 693

## Chapter 47

# HYDROGEN ABSORPTION IN INTERMETALLIC COMPOUNDS

K.H.J. BUSCHOW

*Philips Research Laboratories, Eindhoven, The Netherlands*

---

Contents		4.4. Metastable character of ternary hydrides	44
1. Introduction	1	5. Physical properties	47
2. Intermetallic compounds	4	5.1. Crystal structures	48
2.1. Preparation, phase diagrams, composition, structure and relative stability	4	5.2. Magnetic properties	53
2.2. Magnetic properties	10	5.3. Miscellaneous properties	78
3. Hydrogen sorption in intermetallic compounds	17	6. Technical applications	80
3.1. Pressure-composition isotherms	17	6.1. Hydrogen storage	80
3.2. Activation	18	6.2. Hydrogen purification and hydrogen getters	82
3.3. Hydriding kinetics	20	6.3. Heat pumps	82
3.4. Surface effects and poisoning	24	6.4. Energy storage	84
3.5. Sorption hysteresis	26	6.5. Electrochemical cells	85
3.6. Diffusion of hydrogen atoms	28	6.6. Thermal compressors and heat engines	86
4. Thermodynamic aspects	32	6.7. H and D isotope separation	87
4.1. Pressure-composition isotherms	32	6.8. Neutron moderators and neutron generators	88
4.2. Experimental values of $\Delta H$ and $\Delta S$	35	7. Concluding remarks	88
4.3. Empirical relations for estimating $\Delta H$ of the hydrides of intermetallic compounds	37	Appendix	90
		References	104

---

### 1. Introduction

It cannot be said that research on metal hydrides has had a history of continuous growth. Prior to 1950 the relatively small amount of interest was confined to binary hydrides, at that time usually referred to as solid solutions of hydrogen in metals. Activity in the field of metal hydride research intensified in the 1950s, mainly stimulated by the possibility of using stable hydrides for neutron moderators. After another period of relatively little activity, research on metal hydrides started to grow again in the 1970s and has since then been experiencing a period of proliferation. This second time, too, the renewed interest in metal hydride research was triggered

by a potential application of these materials, namely as an energy carrier. The energy crisis in the early 1970s led to a search for alternative energy sources and to a search for methods which would enable more effective use to be made of the energy available. The use of metal hydrides comprises heat pumping and energy storage in conjunction with the generation of hydrogen by electrolysis and thermolysis of water. Apart from the energy-related applications of hydrides there are applications involving hydrogen purification, neutron and tritium generation, hydrogen isotope separation, interaction of the hydrogen plasma with container walls in nuclear fusion reactors, hydrogen getters, hydrogen pressure regulators, thermal compressors and cold accumulators. The investigations concerned with applications have gone hand in hand with an even larger number of investigations in areas of fundamental scientific research. These investigations comprise not only thermodynamics, kinetics, crystal structure, phase relations and surface effects but also magnetic and superconducting properties, electronic properties and band structures. The range of tools used to study all these quantities is impressive. The experimental methods involve nearly all of the techniques nowadays available to solid state scientists. Among these are nuclear magnetic resonance, paramagnetic resonance, the Mössbauer effect performed on a variety of nuclei, muon spin resonance, de Haas-van Alphen effect, X-ray photo-emission and Auger spectroscopy, neutron- and X-ray diffraction, calorimetry, volumetric measurements, magnetic measurements and standard metallography.

The proliferation of studies in this area of research has of course meant that metal hydrides have become a separate topic of solid state physics. Research is now being carried out by more than 4000 researchers and encompasses hundreds of laboratories all over the world.

Basic to all metal hydrides is their ability to sorb hydrogen gas reversibly. Examples of the metals involved are Pd, Nb, V and Ta. The hydrogen-to-metal atomic ratio in these binary hydrides is only moderate, however. Substantially larger quantities of  $H_2$  gas can be absorbed by the metals Ti, Zr, Hf, Sc, by the alkaline earths and by the rare earths (comprising the lanthanides plus yttrium). The hydrides of these metals are, in general, highly stable. This, in fact, implies a rather low equilibrium  $H_2$  pressure so that, at room temperature, the  $H_2$  absorption in these metals can be considered as being virtually irreversible. This rules out most technological applications and makes these materials less amenable to investigations of their sorption properties. More promising in this respect are intermetallic compounds in which the strongly hydrogen-attracting metals mentioned are combined with one or more metals that have no or only a small hydrogen-attracting power. Numerous investigations of such compounds have shown that such a combination can shift the equilibrium pressure to a more convenient range without much reduction of the hydrogen-to-metal atomic ratio. In contradistinction to the hydrides of pure metals, called "binary hydrides", we will refer to the hydrides of intermetallics as "ternary hydrides". The ternary hydrides reviewed in this chapter are mainly those in which one of the parent metals is a rare-earth element. Since there is an intimate relation between the properties of ternary hydrides based on rare-earth elements and ternary hydrides based on metals of groups 2 and 4a of the periodic

system, it seems desirable to include incidentally some of the properties of the latter materials in this review. For a more detailed treatment of these ternary hydrides we refer to reviews published by Oesterreicher (1981) and Buschow et al. (1982a). Useful information is also contained in "Hydrides for Energy Storage", edited by Andresen and Maeland (1978). Properties of binary hydrides have been reviewed by Libowitz (1972), by Libowitz and Maeland (1978) and by Bos and Gayer (1966).

The present review is organized as follows. The section that follows (section 2) gives a brief survey of the composition, crystal structure and physical properties of the uncharged rare-earth intermetallics. Reference is made to previous volumes of this Handbook and to related reviews, and the more recent developments are described herein. A brief account is given of how the different types of intermetallics can be prepared in single phase condition. The La-Ni phase diagram is presented and used as an example in the discussion of such features as homogeneity range, congruently and incongruently melting compounds etc. The number and composition of intermetallics occurring in other rare-earth 3d binary systems are briefly considered on the basis of three schematic representations. Anticipating the changes brought about by the absorption of hydrogen, this section also gives an indication of some of the physical properties of the uncharged intermetallic compounds.

In section 3 the phenomenon of hydrogen sorption in intermetallic compounds is described. Topics dealt with in this section are: activation treatment, pressure-composition isotherms, miscibility gap, sorption hysteresis, lattice expansion, diffusion, sorption kinetics, surface effects, poisoning, impurity effects and decomposition of ternary hydrides. The sorption characteristics of all ternary rare-earth hydrides investigated are listed in several tables given in the appendix. For comparison the sorption characteristics of some selected ternary hydrides based on non-rare-earth metals are given in a separate table.

Section 4 treats the thermodynamic aspects of the hydrogen sorption. The treatment includes: the van 't Hoff relationship between plateau pressure and heat and entropy of formation, the validity of the van 't Hoff relationship close to the critical point, the maximum hydrogen capacity, and the extension of the Lacher and Rees description to multiplateau isotherms. Also discussed are various models that relate the hydrogen sorption to other physical properties of the intermetallics such as formation enthalpy, elastic properties and interstitial hole sizes.

Section 5 considers changes in physical properties upon charging. These changes take place in magnetic, superconducting, electronic and transport properties and also effect the crystal structure. The emphasis is placed on magnetic properties, electronic properties and crystal structures and on their relation to the bonding of hydrogen in these materials. Attention is given to the large amount of experimental results obtained by means of various resonance techniques (NMR, EPR, Mössbauer effect), neutron diffraction and magnetic measurements. The magnetic properties of charged and uncharged materials are compared in several tables given in the appendix.

Some technical applications of metal hydride systems are described in section 6. They are: heat pumping, energy storage in conjunction with the generation of hydrogen by electrolysis and thermolysis of water, hydrogen purification, hydrogen



TABLE 1  
Conversion factors for various pressure units

Units	Pa	bar	atm	cm Hg
1 Pa	1	$10^{-5}$	$9.869 \times 10^{-6}$	$7.501 \times 10^{-4}$
1 bar	$10^5$	1	0.987	75.006
1 atm	$1.013 \times 10^5$	1.013	1	76.000
1 cm Hg (0°C)	$1.333 \times 10^3$	$1.333 \times 10^{-2}$	$1.316 \times 10^{-2}$	1
1 lbf/in <sup>2</sup>	$6.895 \times 10^{-1}$	$6.895 \times 10^{-6}$	$6.804 \times 10^{-6}$	$5.171 \times 10^{-4}$
1 kg/cm <sup>2</sup>	$9.807 \times 10^4$	0.981	0.968	73.556
1 psi	$6.895 \times 10^3$	$6.895 \times 10^{-2}$	$6.804 \times 10^{-2}$	5.171
1 Torr (mm Hg at 0°C)	$1.333 \times 10^2$	$1.333 \times 10^{-3}$	$1.316 \times 10^{-3}$	$10^{-1}$

Table 1 (cont.)

Units	lbf/in <sup>2</sup>	kg/cm <sup>2</sup>	psi	Torr
1 Pa	1.450	$1.020 \times 10^{-5}$	$1.450 \times 10^{-4}$	$7.501 \times 10^{-3}$
1 bar	$1.450 \times 10^5$	1.020	14.504	$7.501 \times 10^2$
1 atm	$1.470 \times 10^5$	1.033	14.696	$7.601 \times 10^2$
1 cm Hg (0°C)	$1.934 \times 10^3$	$1.359 \times 10^{-2}$	0.193	10
1 lbf/in <sup>2</sup>	1	$7.031 \times 10^{-6}$	$10^{-4}$	$5.171 \times 10^{-3}$
1 kg/cm <sup>2</sup>	$1.422 \times 10^5$	1	14.223	$7.356 \times 10^2$
1 psi	$10^4$	$7.031 \times 10^{-2}$	1	51.715
1 Torr (mm Hg at 0°C)	$1.933 \times 10^2$	$1.359 \times 10^{-3}$	$1.934 \times 10^{-2}$	1

getters, thermal compressor, hydrogen isotope separation, neutron generation and neutron moderators.

The main conclusions drawn in sections 4, 5 and 6 are presented in general in the last section (section 7), which also looks at the future and indicates areas of interest still open to experimental investigations.

We include with this introductory section a table of conversion factors for the most common pressure units employed by different investigators (table 1). Since most of these units have been converted into atm in this chapter, the table will enable readers who may prefer their own units to compare the data presented here with their own data.

## 2. Intermetallic compounds

### 2.1. Preparation, phase diagrams, composition, structure and relative stability

One of the most common methods of preparation is melting the parent metals together in an oxide crucible ( $\text{Al}_2\text{O}_3$ ,  $\text{ThO}_2$  or  $\text{MgO}$ ) using either a resistance furnace or an inductance furnace. If a relatively high purity is required levitation melting or arc melting are to be preferred since these methods avoid the possibility of a contamination due to the reaction with the crucible material.

The procedures described above cannot be used if the vapour pressure of one or both of the parent metals is high at elevated temperatures (for instance Mg, Zn or Cd and incidentally also Eu, Yb and Sm). In these cases the intermetallics can be prepared by sealing the starting materials into tantalum or molybdenum capsules in a protective atmosphere and heating at temperatures sufficiently high for the reaction to take place. Quite often annealing is required after melting the samples. In these cases knowledge of the corresponding binary phase diagram is of value. The La–Ni phase diagram is shown in fig. 1. The compounds  $\text{La}_7\text{Ni}_3$ ,  $\text{LaNi}$  and  $\text{LaNi}_5$  melt congruently and can be obtained directly from the melt. The other compounds melt incongruently and as a rule will require annealing. For instance, solidification of a melt of the formal composition  $\text{La}_2\text{Ni}_7$  first leads to the formation of primary crystals of the phase  $\text{LaNi}_5$ , leaving a melt richer in La than corresponding to  $\text{La}_2\text{Ni}_7$ . At the peritectic temperature ( $995^\circ\text{C}$ ) this La-rich melt will react with the primary  $\text{LaNi}_5$  crystals to form  $\text{La}_2\text{Ni}_7$ . At current cooling rates this reaction will be incomplete. The corresponding sample is not single phase and contains, apart from  $\text{La}_2\text{Ni}_7$ , a certain amount of the phases  $\text{LaNi}_5$ ,  $\text{LaNi}_3$  and possibly some  $\text{LaNi}_2$  as well. The formation of  $\text{La}_2\text{Ni}_7$  can be completed by vacuum annealing below  $995^\circ\text{C}$ . Since the reaction rates are diffusion controlled, high temperatures (as close as possible to the peritectic temperature) are preferred if relatively short annealing times are required. The application of high annealing temperatures can give rise to difficulties, however, due to the presence of  $\text{LaNi}_2$  in the sample. As seen in the diagram, this phase will melt above  $795^\circ\text{C}$  and heavy con-

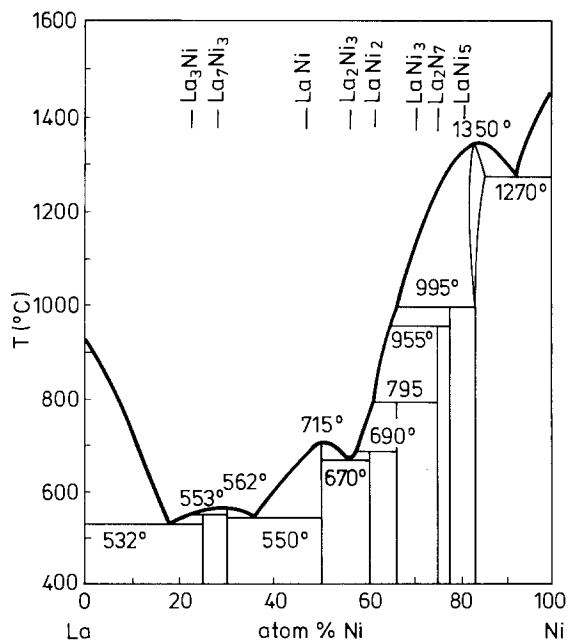


Fig. 1. La–Ni phase diagram, constructed from results compiled by Gschneidner (1961), from results published by Buschow and van Mal (1972), from results of DSC (differential scanning calorimetry) and microscopic investigations (Buschow, 1982c).

tamination of the sample may occur due to reaction of the molten phase (during the long annealing period) with the crucible material. This problem can be solved by gradually increasing the annealing temperature from below 795°C to below 995°C.

Binary phase diagrams involving rare earths as one of the components have been collected by Gschneidner (1961) and by Savitsky and Terekhova (1975). Specific series of binary phase diagrams such as R-Co and R-Al can be found in Buschow (1971) and Buschow and van Vucht (1967).

Details regarding the crystal structure of intermetallic compounds based on rare earth elements can be found in Volume 2 of the Handbook on the Physics and Chemistry of Rare Earths (Iandelli and Palenzona, 1979). Lattice constants and structure type of these intermetallics have furthermore been compiled in the two reviews published by Buschow (1977a, 1979). As will be shown in the following sections, many investigations of hydrogen sorption in intermetallics pertain to compounds formed between rare earth elements and 3d transition elements.

Given the fact that there are 15 rare earth elements, there are 60 combinations comprising one of these rare earth elements and one of the 3d metals Ni, Fe, Co, or Mn. As shown in fig. 1, each of these combinations can give rise to more than one compound. It will be clear, therefore, that the group of R-3d intermetallics is quite a substantial one. A survey of the R-Ni compounds reported in the literature up to now is given schematically in fig. 2. The lack of information on Pm-Ni is

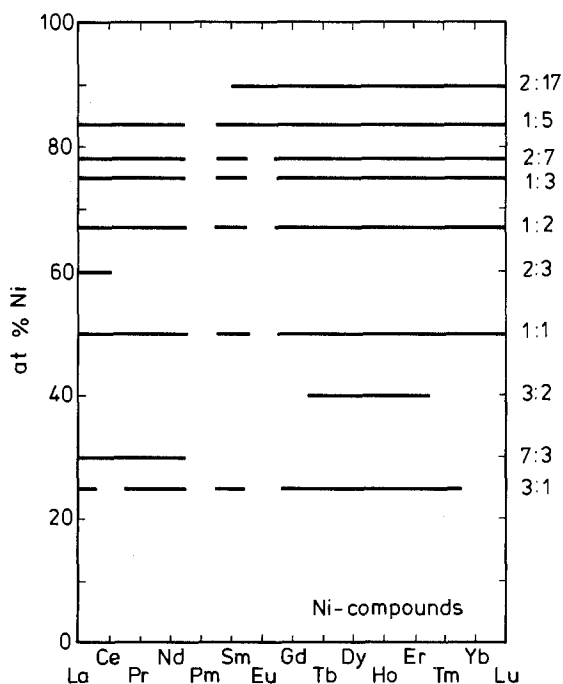


Fig. 2. Schematic representation of intermetallic compounds occurring in various R-Ni systems. This diagram was constructed using the compilation of compounds given in Buschow's review (1977a), the results published by Parthé and Moreau (1977) and those given by van Vucht and Buschow (1976).

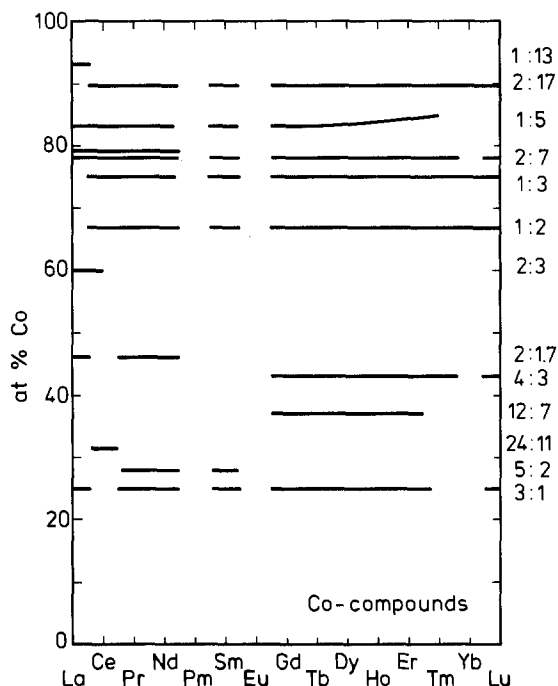


Fig. 3. Schematic representation of intermetallic compounds occurring in R-Co systems. This diagram was constructed from the data listed in Buschow's review (1977a) and the data published by Parthé and Moreau (1977) and van Vucht and Buschow (1976).

evident since Pm is radioactive. The voids in the various series of compounds occurring with the elements Eu, Yb and, to a lesser extent, also Ce, is due to the abnormal valency of these elements. The number of R-Co compounds is comparable in magnitude to the number of R-Ni intermetallics. A survey of the occurrence of R-Co compounds is given in fig. 3. Differences with R-Ni compounds are primarily restricted to the range of intermediate rare-earth concentration. For instance, there are no equiatomic R-Co compounds. At the 3d-rich end (top part of figs. 1 and 3) it can be seen that the  $R_2Co_{17}$  phase extends from Ce to Lu, compared to  $R_2Ni_{17}$  occurring only for elements heavier than Pm.

A peculiar behaviour is shown by the  $CaCu_5$  type R-Co compounds. As one proceeds through the rare earth series from La to Lu the stoichiometry changes from 1:5 to approximately 1:6. All these  $CaCu_5$  type compounds decompose at low temperatures into  $R_2Co_{17}$  and  $R_2Co_7$  (Buschow, 1974; den Broeder and Buschow, 1980).

The occurrence of R-Fe and R-Mn compounds is presented schematically in fig. 4. Compared to the Ni and Co systems there are few Fe compounds and even fewer Mn compounds; furthermore the compounds in the R-Fe and R-Mn systems are seen to be restricted exclusively to 3d-rich concentrations.

Melting together of a rare earth metal and a second metal does not always give

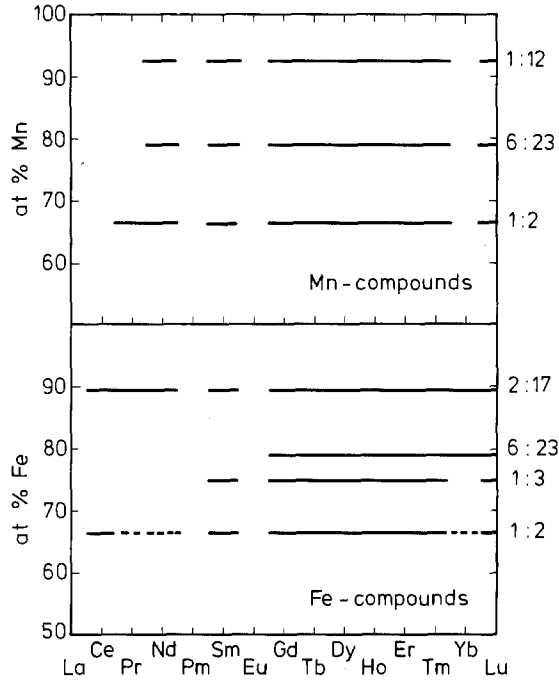


Fig. 4. Schematic representation of intermetallic compounds occurring in R-Fe and R-Mn systems. The diagrams were constructed from the data compiled in Buschow's review (1977a). The broken parts in the R-Fe diagram indicate the existence of metastable  $RFe_2$  compounds (Meyer et al., 1981).

rise to the formation of intermetallic compounds. No compounds are formed, for instance, when rare earth elements are melted together with Cr, V, Nb, Mo, Ta or W. In general, the combination of two metals will lead to the formation of intermetallic compounds only when the heat of formation (with respect to the pure parent metals as standard states) is negative. Miedema et al. (1980) proposed a simple model by means of which heats of formation can be estimated in terms of interactions between the neighbouring individual atoms.

We will discuss this model in somewhat more detail because a simple extension of this model can also be used to describe the heat of formation of ternary hydrides.

In Miedema's model the heat of formation  $\Delta H$  of an intermetallic compound  $R_{1-x}M_x$  comprises two contributions:

$$\Delta H = F(x)[-P(\Delta\phi^*)^2 + Q(\Delta n_{ws}^{1/3})^2]. \quad (1)$$

Here  $F(x)$  is a function of concentration, while  $P$  and  $Q$  are constants for a given group of metal combinations.

The first contribution is proportional to the electronegativity difference  $\Delta\phi^* = \phi_M - \phi_R$  between the two metals R and M. This term contributes negatively to  $\Delta H$ . It takes account of the fact that the electrons have a preference for one of the two metals, which leads to a displacement of electrons to locations of a more negative potential and hence to a lowering of the energy of the alloy.

The second contribution originates from the discontinuity in electron density at the interface between dissimilar atoms when R and M atoms are combined. This difference in electron density at the Wigner-Seitz atomic cell boundaries  $\Delta n_{ws} = n_{ws}^M - n_{ws}^R$  makes a positive contribution to the heat of compound formation or heat of alloying. The electronegativities  $\phi^*$  are related to the work functions  $\phi$  of the metals. For simple metals and for a few transition metals self-consistent band structure calculations exist, so that the values of  $n_{ws}$  can be derived theoretically by summation of atomic electron charge densities. These theoretical values show quite an accurate linear correlation with an experimentally observable quantity, namely with the value of  $(B/V_m)^{1/2}$ , where  $B$  is the bulk modulus and  $V_m$  the molar volume. Semi-empirical values of  $\phi^*$  and  $n_{ws}$  are listed for all common metals, so that  $\Delta H$  can be calculated for almost all metal combinations (Miedema et al., 1980). Values of  $\Delta H$  calculated on the basis of Miedema's model for a representative number of compounds are reproduced in table 2.

Miedema's model is able to give quite a reliable answer to the question of whether

TABLE 2

Formation enthalpies of intermetallic compounds of the rare earth metals La, Y and Sc with 3d, 4d and 5d elements (in kJ/mol). The values listed represent model calculations according to the results published by Miedema et al. (1980). Light rare earth elements interpolate between La and Y, heavy rare earth between Y and Sc.

M	ScM <sub>5</sub>	ScM <sub>3</sub>	ScM <sub>2</sub>	ScM	YM <sub>5</sub>	YM <sub>3</sub>	YM <sub>2</sub>	YM	LaM <sub>5</sub>	LaM <sub>3</sub>	LaM <sub>2</sub>	LaM
Sc	+0	+0	+0	+0	+4	+4	+4	+3	+9	+9	+9	+6
Ti	+24	+24	+22	+17	+56	+54	+49	+35	+77	+74	+67	+45
V	+32	+31	+29	+21	+82	+79	+71	+45	+114	+108	+96	+63
Cr	+3	+3	+3	+2	+56	+54	+48	+32	+90	+54	+74	+47
Mn	-36	-37	-35	-25	-7	-7	-6	-4	+13	+13	+11	+7
Fe	-52	-51	-47	-34	-6	-5	-5	-3	+24	+22	+20	+13
Co	-135	-132	-122	-86	-104	-103	-92	-61	-89	-84	-74	-47
Ni	-175	-171	-158	-113	-155	-149	-133	-88	-141	-133	-177	-75
Y	+3	+3	+3	+3	+0	+0	+0	+0	+1	+1	+1	+1
Zr	+12	+12	+12	+9	+34	+33	+31	+23	+50	+49	+45	+33
Nb	+66	+66	+43	+48	+123	+120	+111	+80	+159	+154	+140	+98
Mo	+44	+43	+41	+31	+110	+107	+98	+70	+151	+145	+132	+90
Tc	-157	-156	-149	-115	-126	-125	-116	-84	-108	-105	-96	-66
Ru	-179	-178	-170	-130	-152	-149	-138	-99	-133	-129	-118	-81
Rh	-249	-247	-236	-181	-244	-239	-222	-259	-238	-230	-211	-145
Pd	-342	-340	-327	-257	-366	-360	-338	-247	-377	-367	-340	-239
La	+7	+7	+7	+6	+1	+1	+1	+1	+0	+0	+0	+0
Hf	+17	+16	+16	+13	+43	+42	+39	+29	+61	+60	+55	+40
Te	+65	+65	+62	+47	+122	+120	+111	+80	+159	+154	+140	+98
W	+38	+37	+36	+28	+107	+104	+97	+70	+149	+145	+133	+92
Re	-145	-145	-139	-109	-108	-107	-100	-73	-84	-82	-76	-53
Os	-157	-156	-149	-116	-123	-121	-113	-81	-101	-98	-90	-63
Ir	-248	-246	-237	-185	-234	-230	-216	-157	-223	-218	-201	-141
Pt	-344	-343	-332	-266	-355	-350	-332	-247	-358	-351	-328	-235

or not compound formation in a given binary system will occur. It also gives a rough indication of whether the number of intermetallics formed in a given binary system will be large or small. The model does not entail the prediction of the precise composition or of the crystal structure of the compounds formed. Predictions of such quantities are in general extremely difficult to make, since they depend on often subtle differences in free energy between the compounds possible in a small concentration range. Long-range interactions between atoms may be of importance, too, in the determination of the crystal structure. These interactions comprise energy effects associated with a favourable match of the various interatomic distances in a given compound with the consecutive minima of the pair potential function. Such long-range energy effects are not included explicitly in Miedema's model. Here it is assumed that the long-range energy effects contributing to  $\Delta H$  are of the same order of magnitude as those operative in the pure starting metals.

Since  $\Delta H$  refers to these parent metals in their standard state the overall effect will more or less cancel or be of minor importance compared with the absolute value of  $\Delta H$ . We wish to mention that Miedema's model is able to give a description of several other physical quantities and phenomena, such as the monovacancy enthalpies in pure metals and intermetallic compounds, interfacial energies including the surface energy at metal-vacuum interfaces, and surface segregation in alloys. The model also comprises a description of compound formation in relation to the valency changes in binary systems where the rare earth component is Ce, Eu, or Yb (Miedema, 1976; de Boer et al., 1979). Of particular interest in the present context is the calculation of monovacancy energies in alloys or compounds since they play an important role in the diffusion behaviour. The heat of formation of a vacancy at an M site in the compound  $RM_n$  can be represented as (Miedema, 1979):

$$\Delta H_{iv}^M(\text{in } RM_n) = f_M^M(\Delta H_{iv}^M) + f_R^M(\Delta H_{iv}^R)(V_M/V_R)^{5/6}. \quad (2)$$

Here  $\Delta H_{iv}^R$ ,  $\Delta H_{iv}^M$  represent the monovacancy energies of R and M atoms in the pure metals R and M, and  $V_R$  and  $V_M$  are the atomic volumes of these metals. The quantities  $f_M^M$  and  $f_R^M$  are the atomic fractions of M and R atoms surrounding a given M site in  $RM_n$ . All these quantities are listed by Miedema for practically all metals, so that  $\Delta H_{iv}$  can be calculated for given metal combinations  $RM_n$  as a function of concentration  $n$ . In fig. 5 the vacancy energies at Ni sites in various  $LaNi_n$  intermetallics have been calculated and plotted as a function of Ni concentration. Note that  $\Delta H_{iv}^{Ni}$  in La-rich compounds is considerably less than in pure Ni metal. The initial concentration independence of  $\Delta H_{iv}^{Ni}$  results from the fact that in intermetallic compounds the Ni atoms try to surround themselves with an optimal number of the larger La atoms. The broken line represents the results for a solid solution, realized more or less in amorphous La-Ni alloys.

## 2.2. Magnetic properties

The majority of intermetallics on which the  $H_2$  absorption studies were performed comprise combinations of 3d transition elements and rare earth elements. Depending on the type of combination of these elements in a given intermetallic compound and

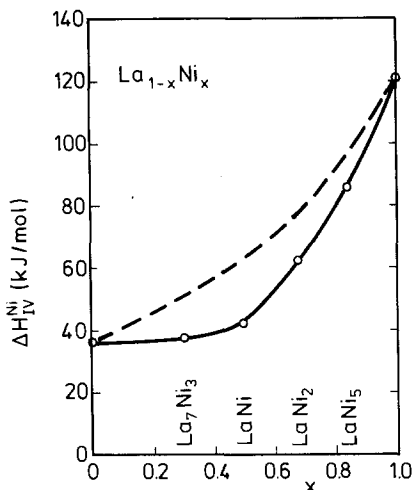


Fig. 5. Monovacancy energies of Ni atoms in La-Ni intermetallic compounds (full line) and La-Ni amorphous alloys (broken line).

its ternary hydride, one or more of the following magnetic interactions will be involved:

- (i) magnetic interaction between 4f moments,
- (ii) magnetic interaction between 3d moments,
- (iii) magnetic interaction between 3d and 4f moments.

These interactions are quite different in nature. This is a result of the fact that the 4f wave functions are highly localized and have no or only small overlap with those of neighbour atoms. The 3d wave functions are more extended in space, and there is considerable overlap with wave functions of neighbour atoms.

Anticipating the changes in magnetic properties brought about by the absorption of H<sub>2</sub> we will in this section briefly summarize some general results obtained in numerous investigations of the uncharged rare earth-3d transition metal compounds (see for instance Buschow, 1977a, 1979; Kirchmayr and Poldy, 1979).

### 2.2.1. Interaction of 4f moments

The magnitude of the 4f moments is in general equal to  $gJ\mu_B$ , where  $g$  is the Landé factor and  $J$  the total angular momentum. For the light rare earth elements  $J = L - S$ , while for the heavy rare earth elements  $J = L + S$ . With the exception of Gd ( $J = S$ ,  $L = 0$ ) the magnitude of the 4f moments can be less than  $gJ\mu_B$  due to crystal field effects. The magnitude of the rare earth moments is otherwise independent of factors such as electron concentration and charge transfer effects.

The most widely accepted form of magnetic interaction between the 4f moments is the RKKY interaction. Since there is virtually no overlap between the 4f wavefunctions on different 4f atoms, magnetic coupling proceeds indirectly via polarization of the conduction electrons. Due to the sharp discontinuity of filled and empty conduction electron states at the Fermi energy  $E_F$ , this conduction electron



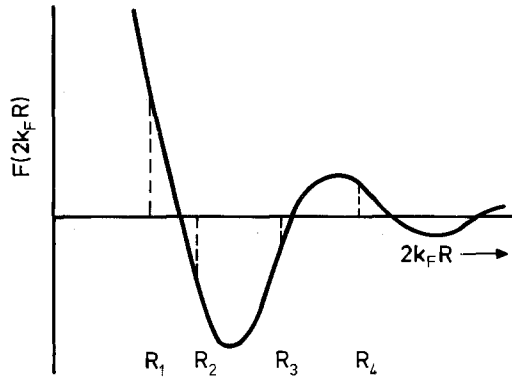


Fig. 6. Schematic representation of the spatial extent of the conduction electron polarization produced by a 4f moment located at the origin ( $R = 0$ ). The broken lines at  $R_n$  can be considered as representing the conduction electron polarization at  $R = 0$  due to the polarizing influence of a 4f moment at  $R_n$ . For a more complete definition of  $F(2k_F R)$ , see text.

spin polarization is spatially non-uniform. In its simplest form the oscillatory spin polarization produced by a 4f spin at  $R = 0$  can be described by the function  $F(x) = (x \cos x - \sin x)/x^4$ , where  $x = 2k_F R$ . The quantity  $k_F$  is the Fermi wave vector which, in the free electron approximation, is a measure of the number of conduction electrons  $Z$  per unit volume  $V$ , since  $k_F^3 = 3\pi^2 Z/V$ . This non-uniform conduction electron polarization is shown schematically in fig. 6. In a given compound  $k_F$  is a fixed quantity. The total exchange interaction experienced by a given 4f moment due to the polarizing influence of the neighbouring 4f moments can then be obtained by summing the contributions of the various neighbours. As seen in fig. 6, these may be contributions of either sign (broken lines). These contributions have to be weighted by the number of neighbour atoms present at the distance  $R_n$ . The sign and magnitude of the sum of these contributions  $\sum_n F(2k_F R_n)$  determine the sign and magnitude of the paramagnetic Curie temperature  $\theta_p$ . Apart from this sum  $\theta_p$  depends on the magnitude of the 4f spin moment  $S$  and on the s-f exchange integral  $\Gamma_{sf}$ , leading to the expression

$$\theta_p \propto -S(S+1)\Gamma_{sf}^2 \sum_n F(2k_F R_n). \quad (3)$$

Due to the presence of the function  $\sum F(2k_F R)$  in eq. (3) the value of  $\theta_p$  depends on the crystal structure. Furthermore, through  $k_F$  appearing in eq. (3) the value of  $\theta_p$  is also dependent on the number of conduction electrons. The effect of changes of  $k_F$  can rather conveniently be illustrated by means of fig. 6. For larger or smaller  $k_F$  values the distances  $R$ , where the function  $F(2k_F R)$  passes through zero, are reduced or increased, respectively. The oscillations are, as it were, compressed or expanded in the  $R$  direction. For a given crystal structure, i.e. for fixed neighbour atom distances, this gives rise to an altered contribution for each of the neighbour shells, which may seriously affect the value of  $\theta_p$ .

In practice the magnetic behaviour of 4f-base intermetallics is often more complicated than would follow from the RKKY model outlined above. For more details the reader is referred to the reviews by Kirchmayr and Poldy (1979) and Buschow (1980a).

### 2.2.2. 3d-electron magnetism

Due to the fact that the 3d atom wave functions of neighbouring 3d atoms show a strong overlap, the 3d electrons are accommodated in 3d bands rather than in localized 3d levels. The relatively strong effective Coulomb repulsion between the 3d electrons can lead to a situation where the number of spin-up and spin-down electrons is no longer equal, i.e. to the formation of a magnetic moment. This inequality between the number of spin-up and spin-down electrons is realized by means of an exchange splitting between the two corresponding spin subbands. Such a situation is schematically represented in fig. 7. In its most simple form the collective electron model predicts the occurrence of such an exchange splitting if the Stoner criterion is satisfied, i.e. if

$$IN(E_F) > 1,$$

where  $I$  is the effective Coulomb interaction between the 3d electrons. For a given density of states the extent of the 3d band splitting is proportional to the interaction parameter and to the magnetic moment resulting from this splitting.

When 3d metals are alloyed with other metals the magnetic moment per 3d atom may change for at least two reasons. In the first place the alloying (or compounding) may be associated with transfer of charge from or to the 3d band. Since  $N(E_F)\uparrow \neq N(E_F)\downarrow$ , this charge transfer then leads to a change in magnetic moment. In the second place hybridization of the valence electrons of the non-3d component with the 3d electrons of the 3d transition metal component can lead to a substantial broadening of the 3d band and reduce the effective Coulomb repulsion. This leads to a reduction in band splitting, which can cause a reduction in 3d moment. In a discussion where the possibility of electron transfer to or from d bands has to be considered, it is important to realize that the position of the 3d band with respect to the s-p band and  $E_F$  is also influenced by the d-d Coulomb interaction mentioned above, because the energy of each 3d electron includes a Coulomb term that increases with increasing number of 3d electrons.

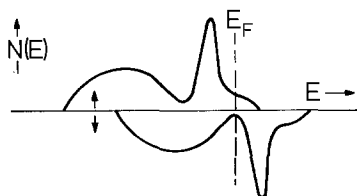


Fig. 7. Schematic representation of the density of 3d band states  $N(E)$  as a function of energy. The Fermi level at  $E_F$  is represented by the broken line.

The band model and the above features of the Coulomb interaction have three important implications which will enter the discussion of the magnetic properties of 3d intermetallics and their changes upon hydrogen absorption. These are briefly summarized below.

(i) Relatively large changes in the number of 3d electrons will be counteracted by the Coulomb interaction since the 3d band is raised or lowered with respect to the s-p band if the number of 3d electrons is increased or decreased, respectively (feed-back mechanism).

(ii) Any 3d moment changes will be enhanced by the exchange interaction since the band splitting is proportional to the moment.

(iii) The effect of a changing number of 3d electrons on the magnetic moment can be inferred from the fact that the occupancy of the two subbands changes in proportion to their density of states at the Fermi level. A consequence of the last observation is that in a strong ferromagnet, where the majority subband is full, only, the minority subband will change its occupancy, leading to a reduction of magnetic moment with increasing number of 3d electrons.

Alloying of the 3d elements with rare earth elements, or with elements of a comparably low electronegativity like Ti, Zr, Hf or Th, leads to a reduction in 3d magnetic moment. This reduction is most pronounced in the Ni compounds and least pronounced in Fe compounds. It has been suggested that this moment reduction is a consequence of electron transfer from R to 3d (2.5 electrons per R atom), leading to a partial or total filling of the 3d band (Wallace 1979, 1982). Band structure calculations on  $\text{RCo}_5$  made by Malik et al. (1977a), with the simplifying assumption that all Co sites are equal in  $\text{RCo}_5$ , show the presence of a partial transfer of charge. This appears to be too small, however, to explain the moment reduction in terms of charge transfer effects alone. It is therefore proposed that the major portion of the moment reduction is more likely due to a strong broadening of the 3d band caused by hybridization of the 3d electrons with the valence electrons of the rare earth component. (This assumption fully agrees with the band structure calculations.) As a result, the intra-atomic Coulomb repulsion decreases, which in turn gives rise to a reduced exchange splitting between the majority and minority in spin subbands. This view is in accordance with the numerous experimental results available, comprising (a) bulk magnetic measurement, (b) Mössbauer spectroscopy and (c) photoemission spectroscopy.

(a) In the series  $\text{Y}_2\text{Co}_{17}$ ,  $\text{YCo}_5$ ,  $\text{Y}_2\text{Co}_7$ ,  $\text{YCo}_3$  and  $\text{YCo}_2$  the moment per Co atom gradually decreases and vanishes in  $\text{YCo}_2$  (Pauli paramagnetic). Comparison with the magnetic properties of the corresponding Gd compounds makes it clear, however, that the moment reduction is mainly due to a decreased exchange splitting in the Y-Co compounds and that charge transfer is not the main reason for this reduction. Here one has to keep in mind that the metals Gd and Y are expected to behave similarly with regard to charge transfer, but that the strongly polarizing influence of the Gd spin can at least partially restore the reduced exchange splitting between the majority and the minority band. Indeed, the Co moment in  $\text{GdCo}_5$  is only slightly smaller ( $1.7 \mu_B$ ) than in Co metal. In  $\text{GdCo}_2$  the Co moment equals  $1.1 \mu_B$ , so that even at this rare earth concentration the number of holes present in the Co 3d band is still appreciable. A similar situation, also refuting the existence of large charge

transfer effects, is present in  $\text{GdFe}_{2-2x}\text{Al}_{2x}$  (Besnus et al., 1979; van der Kraan et al., 1982). Here the Fe moment remains constant throughout the whole concentration range.

(b) Measurements of the isomer shift derived by means of Mössbauer spectroscopy on the nuclei of the rare earth as well as on the 3d component indicate that the charge transfer is not only moderate but that it is composed of both d and s electrons (de Graaf et al., 1982a; Buschow et al., 1978).

(c) A comparable situation arises when 3d elements are combined with elements like Zr also having a relatively low electronegativity. Studies of the core level shifts obtained by means of photoemission experiments show that even when the Zr concentration is high, as it is in  $\text{Zr}_3\text{Fe}$ , the increase in d band occupation amounts to only 0.5 electron per Fe atom (Kübler et al., 1981). Also the photoemission results of Azoulay and Ley (1979) on Gd-Fe intermetallics refute explanations of 3d moment changes based on charge transfer.

Charge transfer is expected to have a larger effect, however, on the magnetic properties of compounds of rare earth elements with Ni. This is not so much due to the fact that the difference in electronegativity between R and Ni is slightly larger than between R and Co. It originates rather from a larger vulnerability of the magnetization in alloys of Ni with a low electronegativity element, owing to the comparatively small number of holes in the Ni 3d band. A slight decrease of this number will usually result in a collapse of the magnetic moment. In R-Ni compounds a magnetic Ni moment is still present in  $\text{R}_2\text{Ni}_{17}$ , while the  $\text{RNi}_5$  compounds are Pauli paramagnetic when R represents La, Y or Lu. An increase of the rare earth concentration brings the magnetism back (Gignoux et al., 1980). In  $\text{Y}_2\text{Ni}_7$  and  $\text{YNi}_3$  this resurgence of magnetism arises as a result of an increase of the density of states  $N(E_F)$  at the Fermi level due to hybridization between the 3d electrons of Ni with the 4d electrons of Y. In this rather exceptional case the increase in  $N(E_F)$  due to hybridization offsets the decrease of  $N(E_F)$  due to filling of the 3d band. The 3d band moment has disappeared again in  $\text{RNi}_2$  and in compounds of higher R concentration.

### 2.2.3. *Magnetic coupling between 4f and 3d moments*

The coupling involving the 4f moments is again an indirect one. It proceeds mainly via polarization of the 5d electrons of the rare earth component. It can be shown that the interaction mediated by 5d electrons leads to an antiferromagnetic coupling between the 4f electron spin moment and the 3d moment when the latter pertains to a 3d element having its 3d shell more than half filled. With respect to the 4f moment of the light rare earth ( $J = L - S$ ) and heavy rare earth ( $J = L + S$ ) the following important relation therefore exists: when R is a light rare earth element (Ce-Sm) the coupling between the 4f and 3d moments is ferromagnetic; when R is a heavy rare earth element (Gd-Yb) this coupling is antiferromagnetic. Experimentally no exceptions are known to these rules [see for instance the compilation of experimental data given in the reviews by Buschow (1977a) and Kirchmayr and Poldy (1979)].

The strength of the various interactions discussed above decreases in the sense

$$3d-3d > 3d-4f > 4f-4f.$$

In general this implies that upon cooling from elevated temperatures, ordering of the 3d moments will occur first. Particularly in compounds of not too high rare earth concentrations, ordering of the 4f moments will occur at significantly lower temperatures. In compounds that are composed of heavy rare earth elements this has the interesting consequence that the total magnetization (3d sublattice magnetization minus 4f sublattice magnetization) starts to decrease somewhat below the Curie temperature owing to the increasing ordering of the rare earth moments. At a given temperature (compensation temperature,  $T_{\text{comp}}$ ) the magnetizations of the 3d and 4f sublattices have become of equal magnitude so that the total magnetization vanishes. At temperatures below  $T_{\text{comp}}$  the magnetization of the rare earth sublattice prevails. Some examples of magnetization versus temperature curves, illustrating this type of magnetic ordering, are shown in fig. 8. It is seen that the compensation temperature decreases as the relative strength of the 3d sublattice magnetization increases (increasing 3d concentration). If the mutual compensation of the 4f and 3d sublattice magnetizations occurs at temperatures not too much below the Curie temperature ( $T_c$ ) the molecular field model leads to the following expression for  $T_{\text{comp}}$  (Buschow and van Stapele, 1970):

$$T_{\text{comp}} = Kg(g - 1)J(J + 1) + \theta, \quad (4)$$

where  $g$  is the Landé  $g$ -factor. The constants  $K$  and  $\theta$  are a measure of the 3d-4f and 4f-4f coupling strengths.

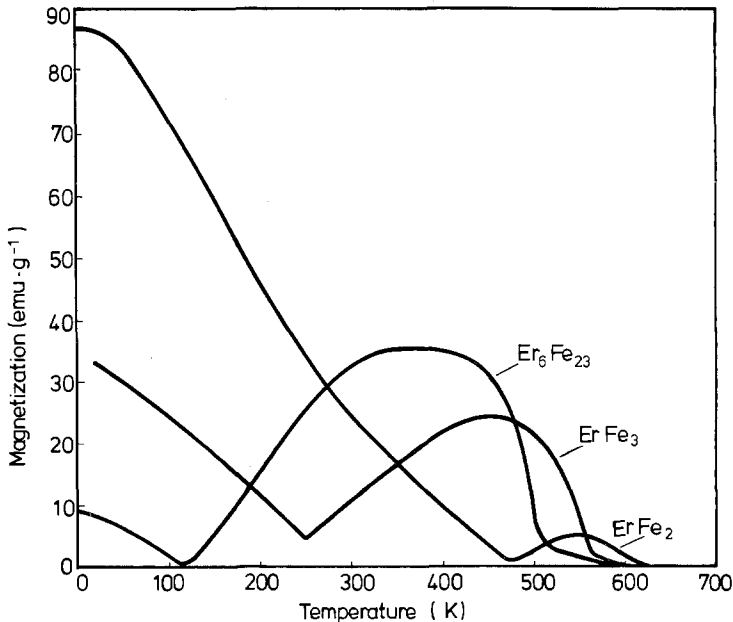


Fig. 8. Examples of temperature dependences of the magnetization in rare earth-iron compounds. The minima in the curves ( $T_{\text{comp}}$ ) reflect mutual cancellation of the magnetization contributions of the rare earth and 3d sublattices.

It was mentioned already in section 2.2.2 that the size of the 3d moment depends to a certain degree on the polarizing influence of the rare earth spin moment. It will be clear therefore that the Curie temperature in such compounds will also depend on this 3d-4f interaction. The following expression for  $T_c$  has been proposed (Bloch et al., 1975; Cyrot et al., 1979; Wohlfarth, 1979):

$$T_c = \Gamma_{fd}^2 \frac{(g-1)^2 J(J+1)}{12\mu_B^2 k} \chi_{3d}(T_c), \quad (5)$$

where  $\Gamma_{fd}$  represents the 4f-3d exchange constant and  $\chi_{3d}$  the 3d electron susceptibility. The effect of this 4f-3d interaction leads to Curie temperatures that are substantially higher than the Curie temperature ( $T'_c$ ) observed in the absence of a 4f moment (compounds of Y, La or Lu). Particularly for compounds where  $T'_c$  is low, one may use the relation  $\chi_{3d} \propto (T'_c)^2$  to estimate  $\chi_{3d}$  (Wohlfarth, 1979). It follows then from eq. (5) that, owing to the factor  $(g-1)^2 J(J+1)$ , the Curie temperature can vary by more than an order of magnitude in going through the rare earth series. This dependence of  $T_c$  on the rare earth component becomes less effective as the 3d concentration increases, and the 3d moment is large already without the polarizing influence of the 4f spin.

### 3. Hydrogen sorption in intermetallic compounds

#### 3.1. Pressure-composition isotherms

The sorption of hydrogen in metal systems can most conveniently be studied by isothermal measurements of the hydrogen pressure  $p_{H_2}$  as a function of the hydrogen concentration  $x$ . Typical examples of such isotherms are schematically represented in fig. 9. The following features may be discerned: The absorption of the first quantity of hydrogen gas in an intermetallic compound  $AB_n$  gives rise to a relatively strong increase of the hydrogen pressure. This equilibrium pressure refers to the original compound, which is able to absorb a small fraction of hydrogen gas without changing its crystal structure. In the following this will be called the  $\alpha$  phase. The next stage in the isotherm involves a region where the hydrogen pressure is concentration independent and where the  $\alpha$  phase is in equilibrium with the first ternary hydride ( $\beta_1$  phase). The pressure corresponding to the reaction  $\alpha + H_2 \rightleftharpoons \beta_1$  is usually referred to as the plateau pressure ( $p_p$ ). A further increase of  $x$ , after the  $\alpha$  phase has completely been transformed into the  $\beta_1$  phase, is again accompanied by a strong rise in  $p$ . Very often a second hydride ( $\beta_2$ ) with a higher H content than  $\beta_1$  exists. In these cases one observes a second "plateau" pressure due to the reaction  $\beta_1 + H_2 \rightleftharpoons \beta_2$ . These  $\beta$  phases can be looked upon as ternary intermetallic compounds in which one of the components consists of hydrogen.

The concentration region determined by the horizontal part of the isotherm between points 1 and 3 (or between 4 and 5) can be regarded as a miscibility gap. Samples of such H concentrations consist of two phases ( $\alpha$  and  $\beta_1$ , or  $\beta_1$  and  $\beta_2$ ). The presence of this miscibility gap arises from the fact that the heat of solution in the intermetallic compound decreases (becomes increasingly negative) with increasing H

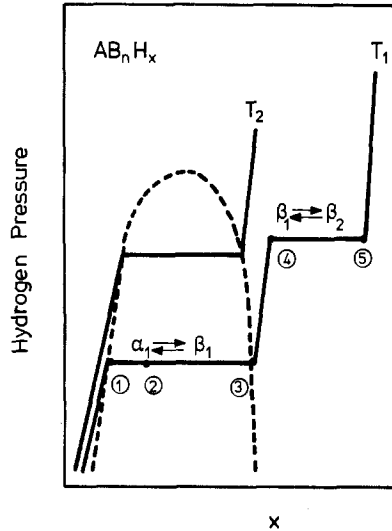


Fig. 9. Schematic representation of two pressure-composition isotherms of a hydride of the composition  $AB_nH_x$ . At the temperature  $T_1$  the two-phase regions (miscibility gaps) are confined to within the concentrations denoted by 1 and 3 and by 4 and 5, respectively. The miscibility gap corresponding to the formation of the first hydride  $\beta_1$  is indicated by means of a broken line.

concentration. This means that the process of solution becomes more exothermic so that it is energetically more favourable for the H atoms to be concentrated locally than to be distributed in a uniform manner throughout the metal. At higher temperature the influence of entropy will counteract this tendency to form two separate phases. The extent of the miscibility gap can then be expected to decrease until finally the gap disappears. For the first hydrogenation reaction this is schematically represented by means of the broken line in fig. 9; the maximum of the cigar-shaped region defines a critical pressure ( $p_c$ ), occurring at a critical temperature ( $T_c$ ), above which the isotherms have no horizontal part. The absence of a flat region in the isotherm does not therefore always mean that the sample is inhomogeneous or contains a high density of stacking faults such as impurities. A consequence of the presence of the miscibility gap is that at low temperatures ( $T_1$  in fig. 9) it is not possible to prepare a hydride with the composition  $AB_nH_{x_2}$ , where  $x_2$  corresponds to point 2 in the figure. Charging  $AB_n$  up to  $AB_nH_{x_2}$  results in the presence of two phases in equilibrium with each other. One of these is the  $\alpha$  phase with the composition  $x_1$ . The second phase is the hydride  $\beta_1$  with the composition  $x_3$ . The relative amount of these phases is given by the lever rule.

### 3.2. Activation

Spontaneous absorption of hydrogen gas by a sample of an intermetallic compound after it has been brought into an atmosphere of hydrogen gas is observed relatively seldom. In general, hydrogen absorption takes place only if the sample has been subjected to a so-called activation treatment. The activation process can be considered as consisting of two steps (Sandrock, 1978). In the first step the thin

surface oxide film is destroyed, making direct contact possible between the  $H_2$  and the metallic surface. For instance, the first step in the activation of the compound TiFe consists of heating it in a hydrogen atmosphere to a few hundred degrees C. With many compounds based on rare earth metals, which are much more brittle, such a heat treatment is not necessary. Activation can be performed by applying  $H_2$  pressures considerably in excess of the corresponding plateau pressure. The second step of the activation consists of the conversion of the entire sample for the first time into the hydride. Sandrock (1978) showed by means of a detailed microscopic examination of the hydrogenation process in TiFe that the hydride initially grows as an envelope around the partially activated particles of the compound, with the hydride phase penetrating as an assembly of fine platelets. The volume increase associated with the formation of the ternary hydride leads to stresses exerted by the hydride envelope on the unhydrided core material. This stress causes cracks which provide new surfaces (Wang, 1976). In brittle intermetallic compounds the first hydrogenation process already breaks the sample down into an assembly of tiny particles. For instance in  $LaNi_5$ , the particle diameter is a broad distribution peaked at about  $50 \mu m$  (Belkbir et al., 1980; Schlapbach, 1980). Further charging–discharging cycles shift the mean particle diameter to even lower values (see fig. 10). The diameter is seen to decrease rapidly within the first ten cycles. No substantial

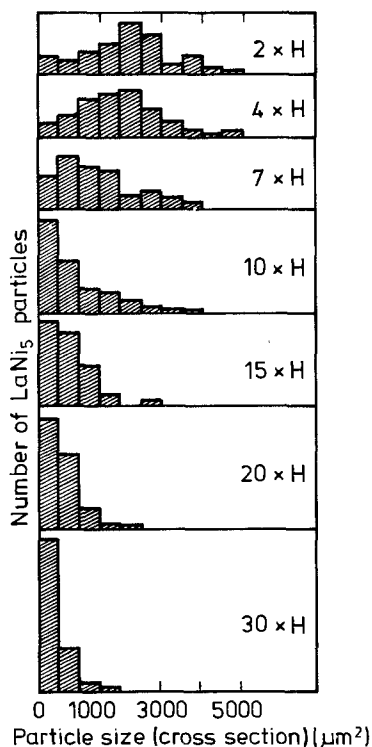


Fig. 10. Particle size of  $LaNi_5$ , as a function of the number of charging–discharging cycles (after Schlapbach, 1980).



changes are generally observed upon continued cycling, the ultimate particle diameter being approximately  $10\ \mu\text{m}$ .

Second-phase particles, dispersed in the matrix of the intermetallic compounds, are able to promote as well as to retard activation (Sandrock, 1978). Second-phase particles richer in the hydrogen-attracting element than the main phase will usually promote activation since they form sites favourable to hydride nucleation. They may also serve as canals by means of which the hydrogen enters the bulk of the main phase. Furthermore, if the presence of the second-phase particles leads to an increase in the brittleness of the alloy, the major activation cracks will form more easily and activation can proceed much more rapidly.

### 3.3. Hydriding kinetics

The reaction kinetics associated with the absorption and desorption of hydrogen in metal systems is an important factor in the technical application of these materials. Several investigations of binary and pseudobinary intermetallics based on rare earths and 3d transition metals had shown that the desorption rate of the corresponding hydrides is extremely fast and second order in the hydrogen concentration (van Vucht et al., 1970; Raichlen and Doremus, 1971; Boser, 1976; Goudy et al., 1978). Later on Goodell et al. (1980a, b) extended the kinetic studies on rechargeable intermetallics by concentrating primarily on the dynamic continuous reaction test procedure, keeping in mind that most technical devices based on rechargeable metal hydrides operate on a continuous reaction basis. Some of their results for  $\text{LaNi}_5\text{H}_x$  are shown in fig. 11. The quantities plotted are the time to half completion of the reaction  $t_{1/2}$  and the corresponding rate  $R_{1/2}$ . For comparative purposes data of  $t_{1/2}$

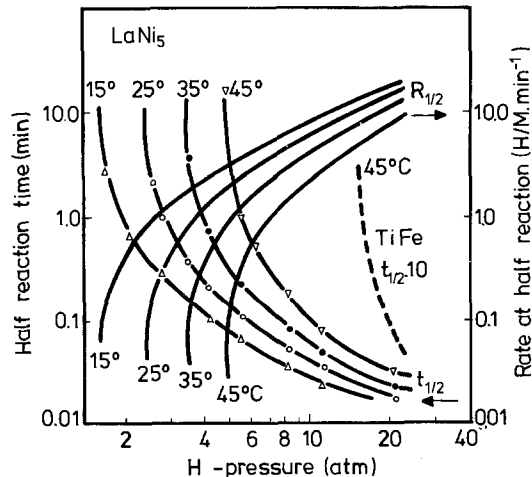


Fig. 11. Isobaric absorption kinetic test data for  $\text{LaNi}_5$  and  $\text{TiFe}$  showing the time ( $t_{1/2}$ , left-hand scale) and the rate ( $R_{1/2}$ , right-hand scale) when the reaction is half completed ( $\text{H}/\text{M} = 0.5$ ). The data shown in this figure are those published by Goodell et al. (1980a).

for  $\text{TiFeH}_x$  are included (broken lines). The response of  $\text{LaNi}_3\text{H}_x$  is clearly much more rapid. It is seen that, under the given test conditions, the response of  $\text{LaNi}_3\text{H}_x$  is nearly an order of magnitude faster than that of  $\text{FeTiH}_x$ . Goodell et al. (1980a) also show that the  $\text{LaNi}_5$  reaction, even when performed in a sample holder of high thermal conductivity, is completely governed by heat transfer. For this reason the data obtained do not reflect the intrinsic reaction kinetics of the alloy. The authors furthermore note that in dynamic tests the plateau pressures and reaction enthalpies are slightly different from those obtained under static conditions. However, these differences prove to be quite reproducible so that it is possible to take them into consideration in the selection of operating pressures and temperatures for hydride device design.

Larsen and Livesay (1980) chose  $\text{SmCo}_5$  as a representative compound on which to study the intrinsic hydriding kinetics of compounds of the  $\text{RCO}_5$  family. The compound  $\text{LaNi}_5$  and several pseudobinaries were studied by Belkbir et al. (1980, 1981). All these authors analysed their data in terms of the Johnson–Mehl equation (Johnson and Mehl, 1939; Avrami, 1940)

$$F(t) = 1 - \exp[-(t/\tau)^n], \quad (6)$$

where  $F(t)$  is the fraction of the reaction completed at time  $t$  and  $\tau$  is the reaction time rate constant. The latter quantity obeys the empirical expression

$$\tau = \tau_0[\exp(-K/T)] \times (p - p_p),$$

$K$  being an energy (Larsen and Livesay, 1980). The value of  $n$  is determined by the geometry associated with the rate-controlling process. Belkbir et al. (1980) as well as Larsen and Livesay (1980) found that formation reaction of the hydride phase in the various  $\text{CaCu}_5$ -type intermetallics is second order in time ( $n = 2$ ). The Johnson–Mehl equation is usually considered as describing a metallurgical phase transformation that proceeds by means of a nucleation and growth mechanism. It is still difficult to tell which of these latter two quantities is the rate-determining step (Christian 1965). The formation of the  $\beta$  phase was described by Belkbir et al. as a precipitation of a new phase in the bulk. These authors were not able to observe, by means of microscopic investigation, nucleation or growth of a new phase but only saw the formation of parallel ridges up to a stage marking the onset of fragmentation.

In general, the pressure–composition isotherms will not contain plateau pressures as sharp as shown in fig. 9. For instance, the part between points 1 and 3 in fig. 9 will not be completely horizontal but will show a slight increase with  $x$ . Also the edges (points 1 and 3) will tend to be slightly rounded. This phenomenon can be interpreted as arising through different portions of the same sample showing slightly different plateau pressures. This behaviour is often observed in binary compounds that are not true line compounds (i.e. exhibit a homogeneity region), and in pseudobinary compounds. Concentration fluctuations on a fine scale may be present in all these materials. The phenomenon is rather pronounced in amorphous materials (Spit et al., 1980; Suzuki, 1983). Larsen and Livesay showed that one has to take account of this effect even in the kinetic investigation of a vacuum-annealed sample. For a

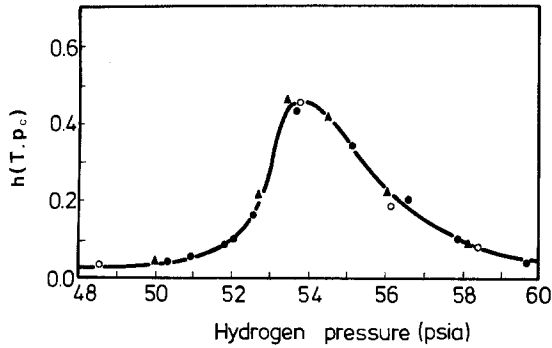


Fig. 12. Derivative  $h(T, p_c) = dx/dp$  associated with the composition ( $x$ ) versus pressure ( $p$ ) isotherms for various temperatures: ● 25°C, ○ 40°C, ▲ 80°C (Larsen and Livesay, 1980).

theoretical  $p(x)$  isotherm, like that shown in fig. 9, the function

$$h(T, p) = dx(T, p)/dp \quad (7)$$

has a singularity at  $p = p(\alpha \rightarrow \beta)$ . In a practical case investigated by Larsen and Livesay, the function  $h(T, p)$  looks like that shown in fig. 12. By using this result in conjunction with the empirical exponential dependence of  $\tau$  on  $K/T$  Larsen and Livesay were able to analyse their data quite satisfactorily.

The reaction kinetics of hydride formation as a function of charging–discharging cycles was investigated by Belkbir et al. (1980). They found that in the first few cycles considerable differences in reaction rate exist between  $\text{LaNi}_5$  and related pseudobinaries. The reaction rates increase with the number of cycles and after 20 cycles have levelled off to a constant value, this value being the same for  $\text{LaNi}_5$  and the pseudobinaries investigated ( $\text{LaNi}_{4.9}\text{X}_{0.1}$  with  $\text{X} = \text{Cu}, \text{Ti}$  and  $\text{Al}$ ). Belkbir et al. also studied the desorption of hydrogen in these materials as a function of different parameters. In the first few charging–discharging cycles the desorption can be described by a rate equation of the type  $1 - (1 - F)^{1/3} = (K_i/a_i)t$ , where  $K_i$  is the rate constant and  $a_i$  the grain size (corresponding to a given cycle  $i$ ). This was taken by the authors as an indication that the desorption proceeds by means of a reaction in which many nuclei appear on the surface and form a continuous layer. (The dependence of the grain size on the number of cycles is different in the materials studied but is basically similar to that shown in fig. 10.) The number of cycles affects the ratio  $K_i/a_i$  in the compounds investigated in quite a different way. However, in  $\text{LaNi}_{4.9}\text{Cu}_{0.1}$  the rate constant is independent of the number of cycles. It reaches a constant value after 20 cycles in  $\text{LaNi}_5$  and  $\text{LaNi}_{4.9}\text{Ti}_{0.1}$  and after 90 cycles in  $\text{LaNi}_{4.9}\text{Al}_{0.1}$ . After the desorption reaction rate has reached this maximum value the desorption process is described by the equation  $\ln(1 - F) = -Kt$ , indicating the formation of nuclei with constant probability and no further growth.

Apart from the number of cycles the frequency of the cycles also plays a role. Results of Belkbir et al. for  $\text{LaNi}_{4.9}\text{Ti}_{0.1}\text{H}_x$  are reproduced in fig. 13. In this compound and also in  $\text{LaNi}_5$  a short period ( $\Delta t$ ) of the charging–discharging cycle favours a high desorption rate. The hydride of  $\text{LaNi}_{4.9}\text{Al}_{0.1}$  has a lower desorption rate and does not show this dependence on  $\Delta t$ . Belkbir et al. suggest that the differences in sorption

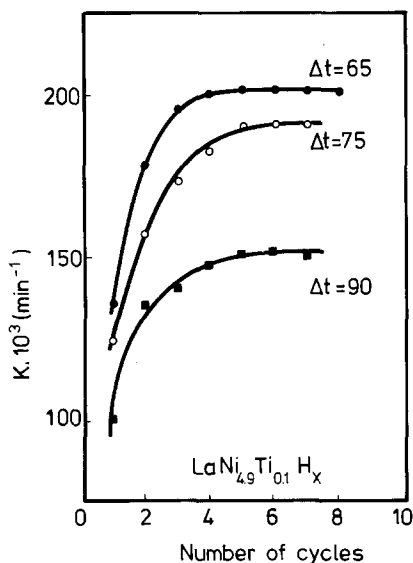


Fig. 13. Evolution of the rate constant  $K$  as a function of the number of cycles for various cycling times ( $\Delta t$ ) in  $\text{LaNi}_{4.9}\text{Ti}_{0.1}\text{H}_x$ . The hydrogen pressure and the temperature are equal to 1 atm and 298 K, respectively (after Belkbir et al., 1980).

behaviour observed may originate from differences in the mechanical properties of these compounds.

It cannot be derived unambiguously from the kinetic studies mentioned above which the rate-determining step is in the reaction of hydrogen with intermetallic compounds. Possible rate determinants are mass transport of  $\text{H}_2$  gas, dissociative chemisorption, surface migration of the protons after this chemisorption, transition from the adsorbed state to the absorbed state and diffusion of the (screened) protons in the bulk. The various steps were discussed by Flanagan (1978a), who presented arguments to show that in intermetallic compounds mass transport of  $\text{H}_2$  gas along channels between small particles may become the rate-determining step (see also Tanaka et al., 1977). A different view is taken by Wallace et al. (1979a) who propose that the dissociation of  $\text{H}_2$  and the recombination of monatomic hydrogen are the rate-controlling steps in the absorption and desorption reaction, respectively. Lü Man-qi et al. (1979) and Park and Lee (1982) showed that the rate-controlling step can change during the absorption process. The rate controlling step may be due to chemical adsorption of  $\text{H}_2$  molecules on the Ni surface at an early stage of the hydriding process, while later on diffusion of hydrogen through the hydride phase may become rate controlling. At the end of the absorption process the chemical reaction becomes again rate controlling (Park and Lee, 1982). Miyamoto et al. (1983) assumed that the rate controlling step in the plateau range is due to the chemical reaction at the interface between the unreacted core and the hydride phase. Goodell and Rudman (1983) showed that the bulk process tends to become rate controlling at low temperatures and high pressures while a surface process controls the rate during dehydriding. It will be clear that the nature of the metal surface plays an important role in the sorption behaviour. This will be discussed in more detail below.

### 3.4. *Surface effects and poisoning*

There are several mechanisms that cause the composition of the surface of intermetallics to be different from that of the bulk. The fact that the surface energy of the rare earth elements is smaller than that of the 3d elements can lead to a surface (equilibrium) concentration of rare earths atoms that exceeds that of the bulk. Surface segregation is quite a general phenomenon, and is expected to occur whenever the constituent elements have sufficiently different properties (Miedema, 1978). Often small amounts of oxygen or water are present as an impurity in the hydrogen gas. These give rise to the formation of rare earth oxides or hydroxides. The combination of surface segregation and oxidation may eventually result in a surface relatively rich in 3d transition metal. Siegmann et al. (1978) investigated  $\text{LaNi}_5$  by means of X-ray photoemission (XPS) and magnetic measurements. They showed that La diffuses to the surface in the presence of  $\text{O}_2$  or  $\text{H}_2\text{O}$ , where  $\text{La}_2\text{O}_3$ ,  $\text{La}(\text{OH})_3$  and metallic Ni are formed up to a certain concentration. However, in the presence of  $\text{H}_2$  gas the process can continue. This was ascribed by Siegmann et al. to the heat of hydrogenation, the widening of the  $\text{LaNi}_5$  lattice or the formation of cracks during hydrogen uptake. They note that as a result of the segregation of La atoms to the surface one can speak here of a self-cleaning mechanism, the occurrence of a fresh precipitation of metallic Ni explaining the favourable surface properties of  $\text{LaNi}_5$ , and also explaining why  $\text{LaNi}_5$  is relatively easily activated and not very sensitive to impurities contained in the hydrogen gas. Similar surface segregation effects of the strongly hydrogen-attracting component of intermetallic compounds were reported to occur in  $\text{Mg}_2\text{Ni}$  and  $\text{FeTi}$  (Schlapbach et al., 1980a; Shenoy et al., 1980; Bläsius and Gonser, 1980; Shaltiel et al., 1981). The presence of elemental 3d metals at the surface and the observation that the sorption reactions are second order in the hydrogen concentration led Wallace et al. (1979a) to propose that the sorption reaction rates in various intermetallics based on rare earth and 3d metals are controlled by dissociation into (or recombination from) monatomic hydrogen at the top of the interfacial region between rare earth oxide and elemental 3d metal. In this model the transition metal segregation is of crucial importance. Belkbir et al. (1981) report that they did not observe this second-order reaction rate during absorption, and they point to the possibility that the rate-determining steps proposed by Wallace et al. (1979a) and Schlapbach et al. (1980a) are less generally valid.

Current photoemission studies on surfaces of intermetallics provide experimental information on whether the constituent metal atoms on the surface are present in the form of non-metals. While the evidence clearly shows the rare earth atoms to be present in non-metallic form and the 3d atoms in metallic form, there is no compelling evidence that it is the segregated 3d metal that plays an important role in the hydrogen sorption. In this respect the photoemission studies performed on  $\text{ErFe}_2$  by Landolt et al. (1979) are quite revealing. These authors used spin-polarized photoelectrons and showed that freshly cut surfaces, when exposed to hydrogen or oxygen, did not result in large changes of the Er and Fe surface concentrations. Moreover, from the sign of the spin polarization they concluded that the Fe atoms are not present in clusters of elemental Fe, but still form part of the intermetallic

compound (the Fe moments remain coupled antiparallel to the Er moments). They argue that the freshly broken surface first becomes contaminated, but that exposure to hydrogen gas involves a reduction reaction which leads again to the presence of pure  $\text{ErFe}_2$ . In other words, the chemisorption of the hydrogen gas induces a self-cleaning mechanism of the  $\text{ErFe}_2$  surface for hydrogen absorption. These photoemission results refute explanations of hydrogen sorption in which the presence of clusters of elemental 3d metals is required. Again we note that the incidental observation of clusters of 3d atoms on the surface by means of  $^{57}\text{Fe}$  conversion electron Mössbauer spectroscopy, or the derivation of their presence from the results of magnetic measurements, does not imply that their presence is essential for the hydrogen sorption. The formation of such 3d metal clusters may be expected in all cases where the hydriding conditions are such that the pressure ratio  $p_{\text{H}_2}/p_{\text{H}_2\text{O}}$  is smaller than a critical value, determined mainly by the difference in formation energy of water and rare earth oxide. Furthermore, 3d metal clusters may also arise as a result of the metastable nature of the ternary hydride. This often leads to a decomposition of the ternary hydride into the binary rare earth hydride and 3d metal. This aspect will be discussed in more detail in section 4.

Surface poisoning is a phenomenon that is observed when impure hydrogen gas is used. It leads to a reduction of the hydrogen sorption properties and is currently ascribed to the formation of some type of surface structure that hampers the hydrogen sorption (Gualtieri et al., 1976a; Semenenko et al., 1978; Sandrock and Goodell, 1980; Block and Bahs, 1983). It is evident that surface poisoning is an unwanted complication in all technical applications of the hydrides. Solid state physicists alone have sometimes profited from the phenomenon and used the hampered hydrogen sorption to prevent hydrogen desorption during measurement of physical properties. Common impurities in hydrogen gas are  $\text{O}_2$ ,  $\text{H}_2\text{O}$  and  $\text{CO}$ . Their effects on materials like  $\text{LaNi}_5$  and  $\text{TiFe}$  have been studied in detail by Sandrock and Goodell (1980). The contamination of  $\text{H}_2$  gas by  $\text{O}_2$  and  $\text{H}_2\text{O}$  leads to comparable effects, resulting in the formation of a thick oxide film. Although there is some preferential oxidation of La (or Ti), the complex oxides formed initially also comprise at least part of the 3d atoms. After some time these complex oxides disproportionate into a composite film consisting of 3d atom clusters imbedded in a stable oxide or hydroxide ( $\text{La}_2\text{O}_3$ ,  $\text{TiO}_x$ ,  $\text{La}(\text{OH})_3$ ). When the charging-decharging cycling is carried out, and with  $\text{H}_2$  gas containing  $\text{O}_2$  or  $\text{H}_2\text{O}$  as an impurity (300 ppm), there is an initial loss of the sorption capacity in  $\text{LaNi}_5$  as well as in  $\text{TiFe}$  and related pseudobinaries. As can be seen from the results of Sandrock and Goodell, reproduced in fig. 14, there is quite a difference in response between these materials upon continued cycling. In  $\text{TiFe}$  poisoning continues, whereas in  $\text{LaNi}_5$  recovery sets in and leads eventually to a situation where the material is more or less immune to poisoning. This is an interesting result since in both materials the cyclic poisoning has led to a similar surface structure, containing clusters of 3d metal. Sandrock and Goodell note that the lack of self-restoration of the activity in  $\text{TiFe}$  suggests that metallic iron is not a catalyst for the hydrogen dissociation under the experimental conditions, unless the  $\text{TiO}_x$  film, unlike  $\text{La}_2\text{O}_3$ , is impermeable to hydrogen penetration. It can also be inferred from the results shown in fig. 14 that the poisoning

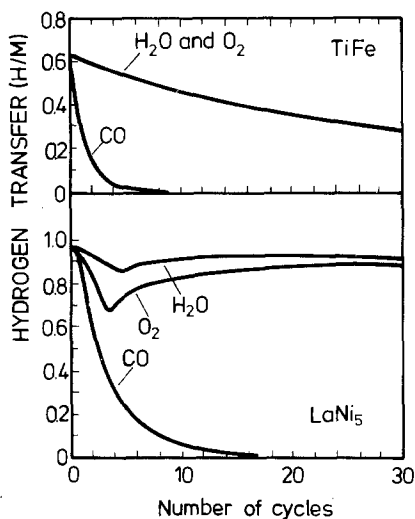


Fig. 14. Response of TiFe and LaNi<sub>5</sub> to cycling with H<sub>2</sub> containing 300 ppm of H<sub>2</sub>O, O<sub>2</sub> or CO (after Sandrock and Goodell, 1980).

effect of a CO impurity is large in the case of LaNi<sub>5</sub> as well as in the case of TiFe. Somewhat better results are obtained with materials like TiMn<sub>1-x</sub>Fe<sub>x</sub>.

### 3.5. Sorption hysteresis

The thermodynamic efficiency of rechargeable metal hydrides is reduced not only by the phenomenon of surface poisoning mentioned above but also, though to a smaller extent, by the occurrence of a sorption hysteresis.

The sorption process mentioned in connection with the isotherms shown in fig. 9 is not strictly reversible. The occurrence of a sorption hysteresis has been observed by many authors (van Mal, 1976; Kuijpers, 1973; Lundin and Lynch, 1978; Bowerman et al., 1980). Results obtained by Kuijpers and van Mal (1971) on the hydride SmCo<sub>5</sub>H<sub>x</sub> are schematically represented in fig. 15. The sorption hysteresis ( $\Delta p$ ) increases with temperature, but then the ratio  $\Delta p/p$  seems to remain nearly constant. Kuijpers and van Mal relate the occurrence of a hysteresis to the volume expansion and postulate that the extent of the hysteresis is proportional to the hydrogen-to-metal (H/M) ratio of the corresponding hydride. The nature of the sorption hysteresis was investigated by Lundin and Lynch (1978). They argue that in the absorption isotherms the  $\alpha$  phase and the  $\beta$  phase are compressively strained, whereas, in the desorption isotherms both phases are more or less strain-free. Owing to the microplastic deformation of the  $\alpha$  and  $\beta$  phases in the absorption process the hysteresis is irreversible (see the minor hysteresis loops in fig. 15). This would mean that the high-pressure absorption isotherm cannot be regarded as representing a metastable condition. In order to account thermodynamically for the two separate paths in the sorption process, Lundin and Lynch modified the phase rule by

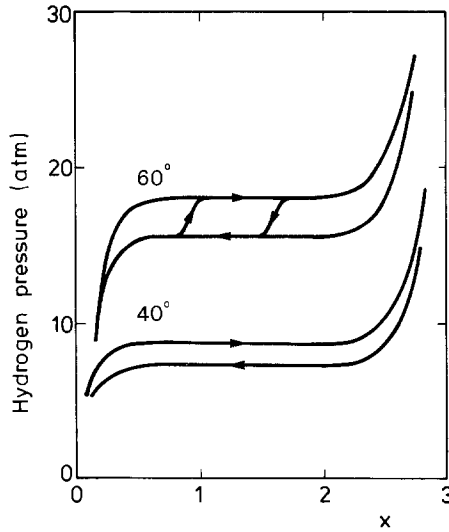


Fig. 15. Schematic representation of the sorption hysteresis observed in  $\text{SmCo}_5\text{H}_x$  at  $60^\circ\text{C}$  (upper) and  $40^\circ\text{C}$  (lower). In the set of curves pertaining to  $60^\circ\text{C}$  a minor hysteresis loop is included (after Kuijpers and van Mal, 1971).

incorporating a strain term:

$$F = C - P + 2 + \pi(\text{strain}).$$

In some respects this analysis is analogous to that used by Scholtus and Hall (1963) to explain the hysteresis in the Pd-H system. The Lundin and Lynch approach provides more directly a rationale pertaining to the pressure differential, in particular to that of the plateau region. According to these authors the plateau pressure increase is a consequence of the decrease in size of the interstitial holes in the uncharged material. The interstitial sites in either the  $\alpha$  or the  $\beta$  phase, which phases are compressively strained during the absorption, are relatively smaller than the sites in either of the unstrained  $\alpha$  and  $\beta$  phases during desorption. Accordingly, the pressure observed in the absorption isotherms is higher than in the desorption isotherms. Although the explanation in terms of compressive strain seems to be generally valid, one has to be careful in relating the pressure difference between the two isotherms to strain-induced changes in interstitial hole sizes, since Busch et al. (1978a) showed that the linear relationship between the plateau pressures of various  $\text{RCo}_5\text{H}_x$  and  $\text{RNi}_5\text{H}_x$  systems ( $R = \text{rare earth}$ ) is difficult to explain in terms of elastic deformation of the interstitial volume.

Interesting results with regard to the hysteresis phenomenon were also found by Flanagan and Biehl (1981), who showed that there is a marked increase in the plateau absorption pressure of  $\text{LaNi}_5\text{H}_x$  if this material is annealed (1025 K) after desorption. From this the authors conclude that at least two effects may be of importance: the occurrence of some mechanical disruption required in the more perfect sample (annealed sample), and the greater ease with which dislocations are formed in the less perfect sample (activated sample).



Hysteresis effects are extremely pronounced in hydrides based on intermetallic compounds containing Ce (van Vucht et al., 1970; Huang et al., 1978; Dayan et al., 1980). Here one has to take account of the fact that the valence state of the Ce ions in the hydride can be different from that in the starting material. A reduction in hysteresis was found upon substitution of elements of group 3 or 4 of the periodic table for Ni in  $\text{LaNi}_5$  (Mendelsohn et al., 1979).

Finally we mention that the occurrence of hysteresis in the sorption isotherms was used by Bowerman et al. (1980) to determine the relative partial molar enthalpies of  $\text{H}_2$  solution in the two coexisting phases in  $\text{LaNi}_5\text{H}_x$ . Their calorimetric measurements comprised absorption hysteresis scans starting from the desorption plateau pressure and ending near the absorption plateau pressure. The single-phase value obtained for the relative partial molar enthalpy of the hydrogen-saturated  $\text{LaNi}_5$  is slightly less negative ( $-13.5$  kJ/mol H) than the  $\alpha \rightarrow \beta$  reaction enthalpy ( $-14.8$  kJ/mol H), whereas the single-phase value for the hydride phase is slightly more negative ( $-16.8$  kJ/mol H). From these results it was concluded that small discontinuities in the thermodynamic parameters must exist at the phase boundaries.

### 3.6. Diffusion of hydrogen atoms

The diffusion of hydrogen atoms in ternary hydrides can be most conveniently studied by means of proton nuclear magnetic resonance (see for instance Barnes et al., 1976). By applying different pulse sequences, experimental information can be obtained about the spin-lattice relaxation time  $T_1$  and the spin-spin relaxation time  $T_{2m}$ . By means of the relation  $T_{2d}^{-1} = T_{2m}^{-1} - T_1^{-1}$  it is possible to derive the dipolar relaxation time  $T_{2d}$ , which is related to the mean time between H atom jumps  $\tau_c$ :

$$T_{2d}^{-1} = \gamma_H^2 M_{2d} \tau_c. \quad (8)$$

In this expression  $\gamma_H$  is the proton gyromagnetic moment and  $M_{2d}$  the dipolar second moment. This latter quantity is determined by the arrangement of the protons in the crystal structure and can be calculated if structural data are available for a given ternary hydride. It is also possible to derive the dipolar second moment from the NMR line shape. For a random walk diffusion process the mean jump time  $\tau_c$  is related to the diffusion constant  $D$  via the expression (Cotts, 1972)

$$D = d^2/n\tau_c, \quad (9)$$

where  $d$  is the mean jump distance and  $n$  the number of possible jump paths in the crystal structure. The diffusion constant  $D$  is usually written in a typical Arrhenius expression:

$$D = D_0 \exp(-E_A/kT), \quad (10)$$

where  $E_A$  is an activation energy and  $k$  is Boltzmann's constant. Combining relations (8)–(10) one has

$$T_{2d} = D_0(n/d^2)\gamma_H^{-2}M_{2d}^{-1} \exp(-E_A/kT). \quad (11)$$

Plots of  $T_{2d}$  versus  $1/T$  are expected to be linear. From their slope the corresponding

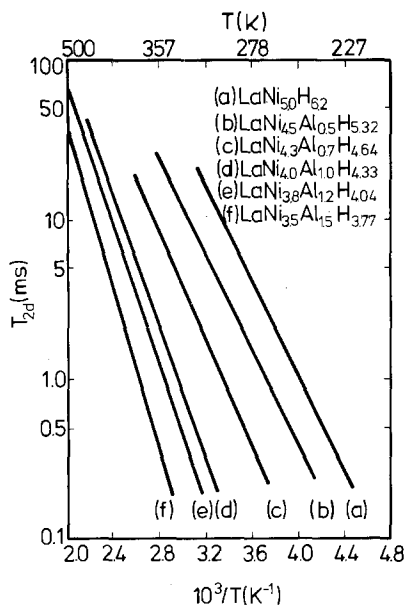


Fig. 16. Arrhenius plot of the dipolar proton relaxation time  $T_{2d}$  in various  $\text{LaNi}_{5-y}\text{Al}_x\text{H}_x$  alloys (after Bowman et al., 1980).

values of the activation energy  $E_A$  can be derived, while from the intercepts on the vertical axis values of  $D_0$  can be obtained (provided values for the other quantities in eq. (11) are known). A typical set of such plots is shown for various  $\text{LaNi}_5$  base materials in fig. 16 (Bowman et al., 1979). The activation energies are of the order of 0.3 eV. The room temperature diffusion constants derived from the NMR data are plotted versus Al content in fig. 17. Bowman et al. were able to show in this way that the room temperature diffusion constant decreases by more than two orders of magnitude upon substitution of Al for about 25% of the Ni in  $\text{LaNi}_5$ .

Apart from the spin-spin relaxation time one can also use the spin-lattice relaxation time to obtain information on the proton jump frequencies. For completeness it is mentioned that in current NMR investigations the spin lattice relaxation time is studied either in the laboratory reference frame ( $T_1$ ) or in the rotating reference frame ( $T_{1\rho}$ ). A method of measuring  $D$  directly has been described by Karlicek and Lowe (1980), using an alternating pulsed field gradient technique (APFG). The results obtained on a number of ternary hydrides by means of various methods are compared in table 3. Also given in the table are data obtained by means of the quasi-elastic neutron scattering technique (QNS). In this technique the quasi-elastic line width  $\Gamma$  is determined as a function of momentum transfer  $Q$ . The diffusion constant  $D$  can be derived from the initial slope of a plot of  $\Gamma$  versus  $Q^2$ . Comparison of the data collected for  $\text{LaNi}_5\text{H}_x$  in the table shows that there is satisfactory agreement between most of them. Furthermore, the diffusion of H atoms at room temperature is seen to be considerably faster in the  $\text{LaNi}_5$  hydride than in the Ti-base materials.

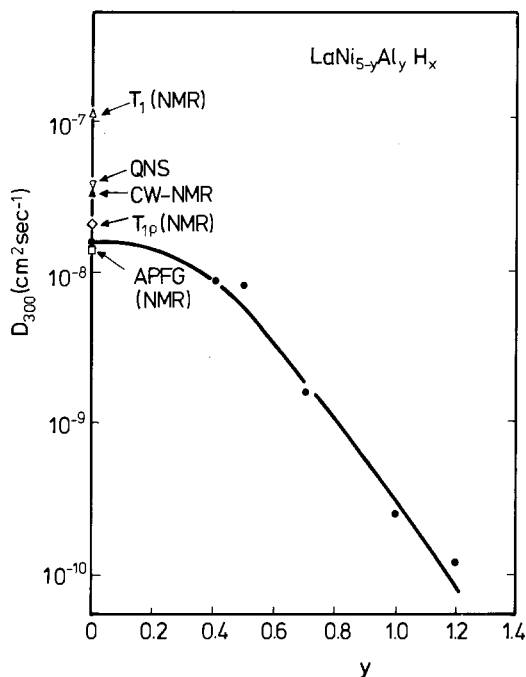


Fig. 17. Influence of the Al concentration ( $y$ ) on the room temperature hydrogen diffusion coefficients in  $\text{LaNi}_{5-y}\text{Al}_y\text{H}_x$ . For the various measuring techniques indicated in the figure, see text (after Bowman et al., 1979).

Apart from the  $\text{La}(\text{Ni}, \text{Al})_5$  ternaries, diffusion of H atoms was also studied in several  $\text{La}(\text{Ni}, \text{Cu})_5$  ternaries and in  $\text{LaCu}_5$ . Shinar et al. (1980) found that increasing Cu concentration leads to an increase in the activation energy  $E_A$ , the value in  $\text{LaCu}_5\text{H}_{1.5}$  being almost twice as high as in  $\text{LaNi}_5\text{H}_6$ .

In more detailed investigations Karlicek and Lowe (1980), Achard et al. (1982) and Noréus et al. (1983) found that the assumption of a single thermally activated diffusion process in the  $\text{LaNi}_5$  hydride is an oversimplification. According to their results the hydrogen motion in the  $\text{LaNi}_5$  hydride is rather complicated and involves at least two different diffusion processes (with activation energies differing by more than a factor of two). They ascribe this to the possibility that the movement of hydrogen involves the crossing of several potential energy wells of different depths. In this connection they point to the crystal structure of the  $\text{LaNi}_5$  deuteride (see section 5) where the deuterium atoms occupy more than one inequivalent lattice position. These lattice positions are interconnected by a multitude of different jump paths.

Shinar et al. (1981) found experimental evidence indicating that an analysis of the diffusion-related experimental data in terms of a simple Arrhenius type of activation law is an over-simplification for other reasons as well. For a number of hydrides based on binary and pseudobinary compounds they show that the activation energy  $E_A$  cannot be taken to be temperature independent, as is usually done.

TABLE 3  
 Diffusion coefficients for hydrogen in some ternary hydrides. The various quantities listed are related through the expression  $D = D_0 \exp(-E_A/kT)$ . The value of  $D_0$  for  $\text{LaNi}_5\text{H}_{6.6}$  was calculated by Lebsanft et al. (1979) from the data of Khodosov et al. (1978a, b).

Hydride	Temperature range (K)	$D_0$ ( $\text{cm}^2/\text{s}$ )	$E_A$ (eV)	$D(300\text{ K})$ ( $\text{cm}^2/\text{s}$ )	Method	Reference
$\text{LaNi}_5\text{H}_6$	280-400	$2.1 \times 10^{-3}$	0.27	$5 \times 10^{-8}$	QNS	Richter et al. (1982)
$\text{LaNi}_{5.00}\text{H}_{6.2}$	230-311	$1.6 \times 10^{-3}$	0.30	$1.5 \times 10^{-8}$	NMR( $T_{2d}$ )	Bowman et al. (1979)
$\text{LaNi}_{5.03}\text{H}_{4.95}$	215-301	$5.0 \times 10^{-6}$	0.17	$0.7 \times 10^{-8}$	NMR( $T_{2d}$ )	Bowman et al. (1979)
$\text{LaNi}_{5.3}\text{H}_6$	140-300	$1.5 \times 10^{-4}$	0.22	$2.1 \times 10^{-8}$	NMR(CW)	Halstead (1974)
$\text{LaNi}_{5.0}\text{H}_6$	150-300	$3.2 \times 10^{-4}$	0.25	$1.7 \times 10^{-8}$	NMR( $T_1$ )	Halstead et al. (1976)
$\text{LaNi}_5\text{H}_{6.6}$	230-280	$8 \times 10^{-4\text{b}}$	0.23	$11 \times 10^{-8}$	NMR( $T_1$ )	Khodosov et al. (1977)
$\text{LaNi}_{5.0}\text{H}_{6.5}$	331-375	0.14	0.42	$1.4 \times 10^{-8}$	NMR(APFG)	Karlicek and Lowe (1980)
$\text{LaNi}_5\text{H}_6$	248-318	$1.5 \times 10^{-5}$	0.15	$3.4 \times 10^{-8}$	QNS	Lebsanft et al. (1979)
$\text{TiFeH}_{1.03}$	350-413	$4.2 \times 10^{-7}$	0.33	$1.2 \times 10^{-12}$	NMR( $T_{2d}$ )	Bowman and Tadlock (1979)
$\text{TiFeH}_{1.03}$	633-759	$7.2 \times 10^{-4}$	0.50	$2.9 \times 10^{-12}$	QNS	Lebsanft et al. (1979)
$\text{TiCuH}_{0.94}$	420-560	-	0.79	$9.9 \times 10^{-16}$	NMR( $T_{2d}$ )	Bowman et al. (1978)

## 4. Thermodynamic aspects

### 4.1. Pressure–composition isotherms

The plateau pressures corresponding to the equilibrium  $\alpha + \frac{1}{2}x\text{H}_2 \rightleftharpoons \beta$  are found to depend strongly on the temperature. The results obtained for the pseudobinary compound  $\text{LaNi}_{4.7}\text{Al}_{0.3}$  by Huston and Sandrock (1980), shown in fig. 18, may serve to illustrate this point. It is seen that, starting from room temperature, an increase in temperature of about 100 degrees pushes the pressure from about 0.4 atm to above 5 atm.

The plateau pressure of the ternary hydride  $\text{AB}_n\text{H}_{2m}$ , formed by means of the reaction



can be taken as a measure of its stability. According to the van 't Hoff equation the corresponding plateau pressure can be approximated in a limited temperature range ( $T \ll T_c$ ) by means of the Arrhenius relation

$$\ln p_{\text{H}_2} = \Delta H/RT - \Delta S/R, \quad (13)$$

where  $R$  represents the gas constant, while  $\Delta H$  and  $\Delta S$  are the standard enthalpy and entropy of formation of the hydride, respectively (relative to  $\text{AB}_n$  and  $\text{H}_2$  gas). It follows from eq. (13) that  $\ln p_{\text{H}_2}$  is expected to vary linearly with  $1/T$ . From the slope of a plot of  $\ln p_{\text{H}_2}$  versus  $1/T$  it is therefore possible to derive the value of  $\Delta H$ , and

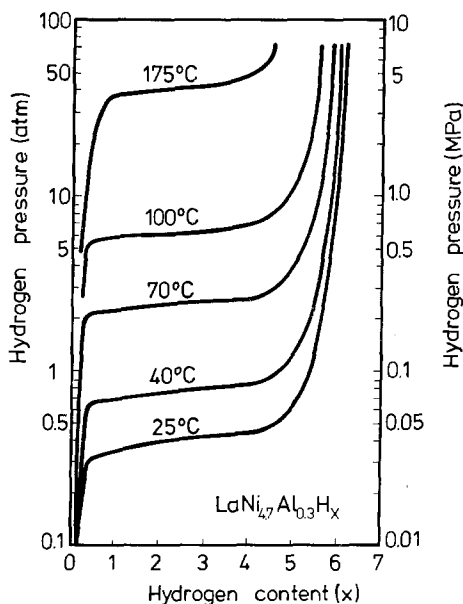


Fig. 18. Hydrogen absorption isotherms for the pseudobinary compound  $\text{LaNi}_{4.7}\text{Al}_{0.3}$  (after Huston and Sandrock, 1980).

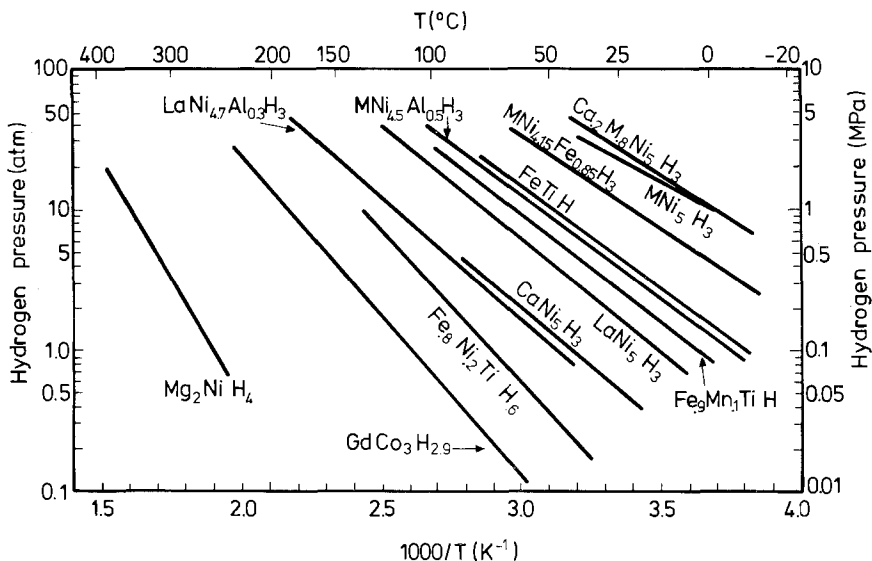


Fig. 19. Van 't Hoff type plots, describing the temperature dependence of the hydrogen desorption pressures in various materials. (Data are from Huston and Sandrock, 1980; Goudy et al., 1978; Kierstead, 1981a).

from the intercept with the vertical axis one can obtain the corresponding value of  $\Delta S$ . Using the data of fig. 18 such a plot is shown for  $\text{LaNi}_{4.7}\text{Al}_{0.3}\text{H}_3$  in the middle part of fig. 19. (The fact that the isotherms are not strictly horizontal in the plateau region was already discussed in section 3.3. The plot given in fig. 19 corresponds to the middle part of the plateau region.) The  $\Delta H$  and  $\Delta S$  values that can be derived for  $\text{LaNi}_{4.7}\text{Al}_{0.3}\text{H}_3$  from this plot are 33.9 kJ/mole and 120.1 J/K mole  $\text{H}_2$ . In some cases it is not justified to identify the  $\Delta H$  and  $\Delta S$  values obtained by means of the Arrhenius plot as the formation enthalpy and formation entropy of the ternary hydride  $\text{AB}_n\text{H}_{2m}$ . In most systems there is not only a substantial solubility of hydrogen in the intermetallic compound, but also an appreciable deviation of the hydride phase from the stoichiometric composition. It is therefore more appropriate to look upon  $\Delta H$  and  $\Delta S$  as the enthalpy and entropy changes associated with the reaction  $\alpha + x\text{H}_2 \rightleftharpoons \beta$  ( $x < m$ ). There is yet another complication. It can be seen from fig. 9 (and to some extent also from fig. 18) that close to the critical temperature in particular, the composition both of the  $\alpha$  phase and of the  $\beta$  phase varies considerably with temperature. This means that plateau pressures measured at different temperatures do not necessarily correspond to the same reactants and reaction products. Flanagan (1978b) has presented arguments showing that, in spite of this latter feature, conditions may be such that the linear relationship between  $\ln p_{\text{H}_2}$  and  $1/T$  can still be expected to hold. Values of  $\Delta H$  and  $\Delta S$  obtained by means of a linear  $\ln p_{\text{H}_2}$  versus  $1/T$  plot at temperatures where the compositional changes of the  $\alpha$  and  $\beta$  phases are quite severe therefore have to be interpreted with some caution. This is particularly true if the compositional dependence of the curve that

defines the two-phase region in fig. 9 is less symmetric about the critical composition (Flanagan 1978b).

Kierstead (1980a–d, 1981a, b) has had considerable success in fitting multiplateau hydrogen absorption isotherms in terms of the Lacher (1973) and Rees (1954) models. The phase separation corresponding to a given plateau pressure is taken to be governed by an attractive interaction between the hydrogen atoms. In order to describe more than one plateau one has to postulate the presence of various groups of sites ( $i$ ) having different heats ( $\Delta H_i$ ) and entropies ( $\Delta S_i$ ) of absorption. If there is a number  $n_i$  of sites of type  $i$  the corresponding hydrogen plateau pressure is determined by the four parameters  $n_i$ ,  $\Delta H_i$ ,  $\Delta S_i$  and  $T_i$ , where  $T_i$  represents the critical temperature (or heat of interaction  $H'_i = RT_i$ ) corresponding to these sites. In the modified Lacher model the various groups of hydrogen absorption sites are occupied independently and their presence persists after multiple phase changes and lattice expansion. In the modified Rees model there is a specific type of interdependence between the sites, since hydrogen absorption on a site of the type  $i$  produces new sites dissimilar from  $i$  owing to the presence of a H atom on the neighbouring type  $i$  site. An example of the data analysis based on the Rees model is shown in fig. 20 for  $\text{DyCo}_3\text{H}_x$ . Four different types of sites were assumed. Isotherms were calculated for five different temperatures (full lines in fig. 20). The total number of parameters used in this fitting procedure equals 16 ( $i = 4$ ). Later Kierstead (1981c) was able to obtain even better fits by introducing entropies of interaction ( $T_i = H'_i - TS'_i$ ) as well as temperature dependent enthalpies  $\Delta H_i(T)$  and entropies  $\Delta S_i(T)$  associated with the change in constant-pressure heat capacity ( $\Delta C_i$ ). The number of parameters required for fitting the isotherm then equals  $6m$  ( $n_i$ ,  $\Delta H_i^0$ ,  $\Delta S_i^0$ ,  $\Delta C_i^0$ ,  $H'_i$  and  $S'_i$ ;  $i = 1, \dots, m$ ). Here we wish to stress that the model used by Kierstead is useful for analysing measured data but it is not able to make any *a priori* predictions of the hydrogen absorption tendency in the various intermetallic compounds.

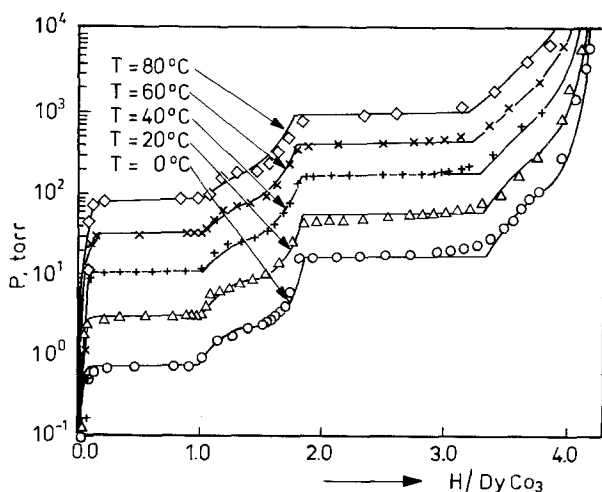


Fig. 20. Isotherms of  $\text{DyCo}_3\text{H}_x$  fitted by means of the Rees model (after Kierstead, 1981c).

To end this section it should be mentioned that the study of pressure–composition isotherms is not the only method that can be used to determine the values of  $\Delta H$  and  $\Delta S$  associated with the hydrogen sorption process. These values can also be derived from direct calorimetric measurements (see for instance Ohlendorf and Flotow, 1980a; Murray et al., 1981a, b; Wemple and Northrup, 1975; Mikheeva et al., 1978) and from magnetic measurements (Yamaguchi et al. 1982).

#### 4.2. Experimental values of $\Delta H$ and $\Delta S$

In tables A1 to A5 in the appendix some experimental hydrogen sorption characteristics for a number of intermetallic compounds are listed. Inspection of the  $\Delta H$  and  $\Delta S$  values given in the tables shows that the former values vary considerably, whereas there are only relatively small differences between the latter. This feature is also apparent from the results shown in fig. 19. There is a considerable difference in the slope of the lines, whereas extrapolation of the lines leads to about the same intercept on the left-hand vertical axis. The corresponding values of  $\Delta S$  and the various values of  $\Delta S$  given in the tables are not far off from the entropy of hydrogen gas ( $\Delta S^{\text{gas}}$ ) (about 130 J/K mole  $\text{H}_2$  at 1 atm and room temperature). The near constancy of the  $\Delta S$  values reflects the fact that in all the hydrogenation reactions the entropy of the hydrogen as a gas is lost upon entering the metal. Compared to this large entropy term other entropy effects, arising in the solid, can be shown to be relatively unimportant in most cases. If one neglects the solubility of hydrogen in the starting material the excess entropy  $\Delta S^{\text{ex}}$  in the ternary hydride can be expressed as

$$\Delta S^{\text{ex}} = \Delta S_{\text{H}}^{\text{vib}} + \Delta S_{\text{host}}^{\text{vib}} + \Delta S^{\text{el}} + \Delta S^{\text{conf}}. \quad (14)$$

The contribution  $\Delta S_{\text{H}}^{\text{vib}}$  represents the vibrational entropy of the hydrogen atoms in the ternary hydride,  $\Delta S_{\text{host}}^{\text{vib}}$  represents the entropy associated with the modifications of the the vibrational spectrum of the host compound. The contribution  $\Delta S^{\text{el}}$  is the entropy effect due to the changes in the electronic heat capacity upon charging, while  $\Delta S^{\text{conf}}$  represents the configurational entropy, originating from the statistical distribution of the hydrogen atoms over the more abundant interstitial sites in the hydride. By means of the same arguments presented elsewhere (Buschow et al., 1982a) it can be shown that the first three terms of eq. (14) are relatively small: The vibrational spectrum of the H atoms in a metallic hydride can be treated approximately as an assembly of Einstein oscillators. Experimental results obtained on binary and ternary hydrides so far suggest that the characteristic Einstein temperature ( $\theta_{\text{E}}$ ) is relatively high. This follows for instance from neutron scattering results obtained by Rush et al. (1980) in the hydride of TiCu (fig. 21) using the relation  $k\theta_{\text{E}} = hW_{\text{H}}$ . It also follows from the specific heat data obtained by Wenzl and Pietz (1980) in various hydrides based on TiFe. A high value of  $\theta_{\text{E}}$  is consistent with the fact that the mass of the hydrogen atoms is relatively low. With values of  $\theta_{\text{E}}$  in the range 1000–1500 K one expects the vibrational heat capacity to rise steeply at temperatures between 300 K and 500 K, approaching the value  $3R$  per mole of H atoms. Consequently, the heat capacity of  $\text{H}_2$  gas and that of hydrogen in the hydrides will cross at a temperature



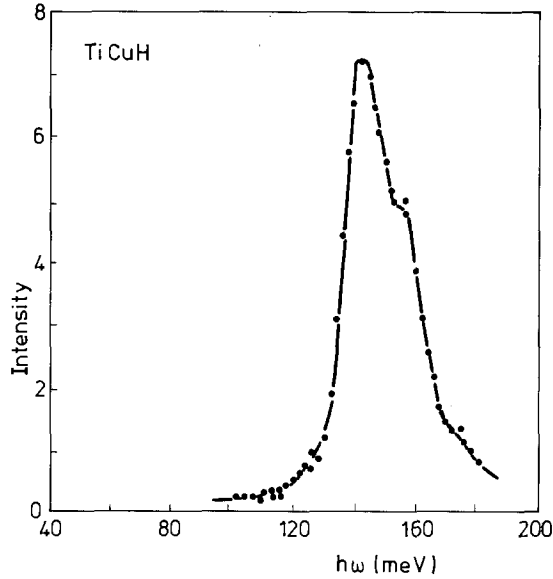


Fig. 21. Neutron scattering spectra measured at 78 K for  $\text{TiCuH}_{1-x}$ . Data are from Rush et al. (1980).

not much exceeding room temperature ( $T/\theta_E \approx 0.4$ ), after which the change of  $\Delta S^{\text{gas}}$  with temperature will be smaller than that of  $\Delta S_{\text{H}}^{\text{vib}}$ . In any case the term  $\Delta S_{\text{H}}^{\text{vib}}$  will be relatively small compared to  $\Delta S^{\text{gas}}$  at room temperature. Even in the case of Pd hydride, where  $\theta_E = 800$  K, the contribution is only of the order of 10 J/K mole  $\text{H}_2$  at 300 K (Boureau et al., 1979). In  $\text{LaNi}_5\text{H}_{6.4}$  a value equal to 2 J/K mole  $\text{H}_2$  was estimated (Ohlendorf and Flotow, 1980b). The two terms  $\Delta S_{\text{host}}^{\text{vib}}$  and  $\Delta S^{\text{el}}$  are even smaller. In Pd hydride Boureau et al. obtained the values +2 J/K mole  $\text{H}_2$  and -5 J/K mole  $\text{H}_2$ . The corresponding values estimated by Ohlendorf and Flotow (1980b) in  $\text{LaNi}_5\text{H}_{6.4}$  are 9.2 J/K mole  $\text{H}_2$  and -0.3 J/K mole  $\text{H}_2$ , respectively.

The configurational entropy can be derived by means of the relation  $\Delta S^{\text{conf}} = k \ln W$ , where  $W$  is the number of complexions associated with the distribution of the number of hydrogen atoms over the available crystallographic sites. Application of Stirling's approximation leads to

$$\Delta S^{\text{conf}} = -kN \sum_i G_i [\theta_i \ln \theta_i + (1 - \theta_i) \ln(1 - \theta_i)], \quad (15)$$

where  $\theta_i$  is the fractional occupancy of site  $i$  and  $G_i$  is the site multiplicity. If neutron diffraction data of the ternary deuteride of a given intermetallic compound are available the experimental values of  $\theta_i$  and  $G_i$  can be used to calculate  $\Delta S^{\text{conf}}$  by means of eq. (15). In  $\text{LaNi}_5\text{H}_6$  values of  $\Delta S^{\text{conf}}$  equal to 20 J/(K g at) have been estimated. However, we will return to this point later on, after having discussed experimental data on the crystal structure of ternary hydrides in more detail. In any case, even though  $\Delta S^{\text{conf}}$  is the largest contribution in eq. (14), the corresponding values are small compared with the value of  $\Delta S^{\text{gas}}$ .

#### 4.3. Empirical relations for estimating $\Delta H$ of the hydrides of intermetallic compounds

Given the fact that hydrogen absorption leads to rather similar values of the associated entropy change in the various intermetallics, it follows from the van 't Hoff relationship (eq. 13) that the equilibrium pressure would be predictable if  $\Delta H$  were known. It is clear that such formation enthalpies can be derived from ab initio band structure calculations. For CsCl-type compounds like  $\text{TiFeH}_2$  and  $\text{TiPdH}_2$  such calculations were made by Gelatt (1978), who obtained calculated  $\Delta H$  values of the right order of magnitude. Such calculations are, however, rather cumbersome and lengthy in cases where the crystallographic unit cell is composed of many different inequivalent metal atom positions. For this reason the prediction of  $\Delta H$  values and equilibrium pressures based on band structure calculations cannot be regarded as a universal method applicable to a large variety of intermetallics.

Methods in which the enthalpies were correlated with other physical quantities have proved to be more suitable for predicting the hydrogen absorption behaviour of intermetallics. In the empirical model described by van Mal et al. (1974) and Miedema et al. (1977) the enthalpy of formation of the ternary hydride  $\text{RMH}_{2m}$  is expressed in terms of the formation enthalpy of the binary hydrides of the metals R and M and the formation enthalpy of the uncharged intermetallic compound  $\text{RM}_n$ . This model is an extension of Miedema's models to describe formation enthalpies of intermetallic compounds and alloys (Miedema et al., 1980). A brief description of this model was given in section 2. Hydrides of transition metals are treated as alloys composed of hydrogen metal atoms. The component R in  $\text{RM}_n$  that forms a relatively stable binary hydride is taken to be a minority element ( $n > 1$ ). In the same way as in the heat of formation of the pure compound  $\text{RM}_n$  (see section 2.1) it is assumed that the main energy contributions to the heat of formation of the ternary hydride  $\text{RM}_n\text{H}_{x+y}$  are due to energy effects at the atomic cell boundaries. In the ternary hydride the hydrogen atoms will completely surround the minority atoms. The expression for  $\Delta H$  is composed of three terms:

$$\Delta H(\text{RM}_n\text{H}_{x+y}) = \Delta H(\text{RH}_x) + \Delta H(\text{M}_n\text{H}_y) - (1 - F)\Delta H(\text{RM}_n). \quad (16)$$

The first two terms on the right hand side of eq. (16) account for the energy effects associated with the R-H and M-H atomic cell boundaries. The third term accounts for the contacts between R and M being broken upon formation of the hydride. The factor  $(1 - F)$  in front of the last term of eq. (16) accounts for the fact that the separation of R atoms from M atoms by means of the H atoms becomes less effective as  $n$  decreases. For more details we refer to the papers by Miedema et al. (1977), and Buschow et al. (1982a), where values for the different quantities appearing in eq. (16) are also listed. Some of the computational results are reproduced in table 4. The  $\Delta H$  values of the corresponding Gd compounds are virtually the same as those listed for Y. In the case of the (trivalent) heavy lanthanides or light lanthanides one may extrapolate between the values of Y and Sc and between the values of La and Y, respectively. With a value of  $-130 \text{ J/K mol H}_2$  for the hydrogenation entropy a plateau pressure of 1 atm at room temperature corresponds to  $\Delta H = -39 \text{ kJ/mol H}_2$  (eq. 13). By means of the results given in table 4 a quick indication can be obtained of the possible existence of a stable hydride ( $p_p \leq 1 \text{ atm}$ ) for a given compound.

TABLE 4

Calculated values of the formation enthalpies of ternary hydrides of several intermetallic compounds of La, Y and Sc with 3d, 4d and 5d transition metals. The formation enthalpies are expressed in kJ/mol  $H_2$ . The hydride compositions were taken to be equal to  $RM_5H_6$ ,  $RM_3H_5$ ,  $RM_2H_4$ , and  $RMH_{2.5}$  for R=La or Y and  $RM_3H_5$ ,  $RM_3H_4$ ,  $RM_2H_{3.5}$  and  $RMH_2$  for R=Sc.

M	ScM <sub>5</sub>	ScM <sub>3</sub>	ScM <sub>2</sub>	ScM	YM <sub>5</sub>	YM <sub>3</sub>	YM <sub>2</sub>	YM	LaM <sub>5</sub>	LaM <sub>3</sub>	LaM <sub>2</sub>	LaM
V	-130	-142	-147	-185	-136	-144	-152	-181	-139	-146	-149	-173
Cr	-34	-101	-113	-162	-93	-106	-122	-163	-97	-108	-120	-156
Mn	-66	-33	-98	-151	-72	-55	-104	-151	-72	-83	-100	-143
Fe	-47	-65	-54	-141	-55	-73	-96	-147	-61	-74	-93	-140
Co	-25	-40	-64	-123	-36	-49	-75	-131	-35	-47	-70	-123
Ni	-14	-26	-53	-114	-24	-36	-64	-123	-22	-33	-59	-115
Mo	-93	-113	-122	-172	-105	-119	-134	-174	-110	-123	-134	-169
Tc	+4	-12	-34	-103	-2	-24	-54	-116	-8	-23	-50	-110
Ru	+15	+0	-30	-95	+2	-13	-45	-110	+3	-12	-41	-114
Rh	+30	+18	-15	-80	+18	+6	-27	-95	+24	+12	-20	-87
Pd	+31	+29	-6	-63	+24	+15	-12	-77	+34	+29	-2	-68
W	-76	-99	-111	-165	-91	-107	-126	-170	-97	-112	-126	-165
Re	+10	-9	-36	-101	-5	-22	-53	-117	-6	-22	-50	-111
Os	+11	-6	-34	-100	-3	-19	-51	-115	-3	-19	-47	-109
Ir	+40	+27	-7	-74	+26	+13	-22	-92	+30	+17	-16	-85
Pt	+65	+58	+19	-45	+53	+43	+7	-66	+51	+51	+16	+58

Owing to the simple formulation used in eq. (16) the model is sometimes misinterpreted. As already mentioned, the ternary hydrides are regarded as ternary intermetallic compounds, one of the components being hydrogen. Nishimiya et al. (1982) assume incorrectly that the model encompasses the formation of  $RH_2$  ( $ZrH_2$ ) clusters after a complete rupture of the alloys. (Such clusters may arise incidentally after decomposition of the ternary hydride, which is a different matter, not under discussion here.)

It should be realized that the crude approximations made set a limit to the applicability of the model. We have only considered energy effects associated with the nearest neighbour interaction and the distribution of H atoms between the R-H and M-H contact surfaces ( $x$  and  $y$  in eq. 16) is arbitrary. Calculations made by means of eq. (16) therefore can give only a first-order estimate of the enthalpy of the ternary hydrides. For the purpose of comparison relative energies are required, however, and due to the cancellation of errors the accuracy of eq. (16) is much better. The applicability of eq. (16) is quite useful, therefore, in predicting trends. These comprise:

(i) In a series of compounds  $RM_n$  with fixed composition  $n$  and the same non-rare earth component M the equilibrium pressures increase in the direction from La to Lu.

(ii) In a series of compounds  $RM_n$  with fixed composition  $n$  and rare earth component R the equilibrium pressure is lower as the heat of compounding of R with the component M into  $RM_n$  is less negative (rule of reversed stability).

(iii) If R and M are fixed the equilibrium pressure increases with increasing  $n$ .

For some series of intermetallic hydrides listed in tables A1 to A4 in the appendix the  $p_{eq}$  data are fairly complete. For these series we have plotted the plateau pressures

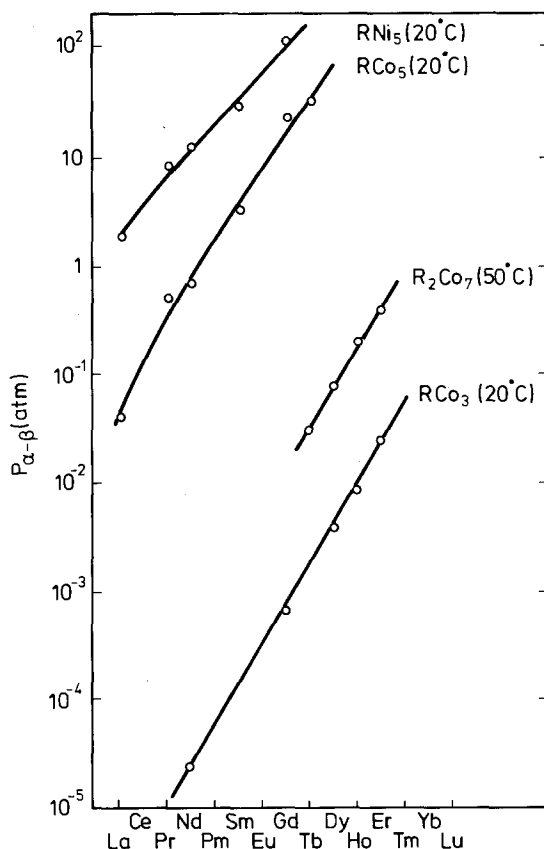


Fig. 22. Hydrogen plateau pressures in various series of rare earth compounds.

as a function of the rare earth component in fig. 22. These data reflect the trends (i) to (iii) mentioned above.

There are only a few exceptions where the model predictions were found to lead to the wrong answer. The most serious one is  $\text{LaPt}_5$ , which compound, according to the positive  $\Delta H$  value in table A4, should not give rise to a stable ternary hydride. Takeshita et al. (1981) reported the formation of a hydride phase  $\text{LaPt}_5\text{H}_4$  from  $\text{LaPt}_5$  at 1000 atm  $\text{H}_2$  and room temperature. This discrepancy is as yet unexplained.

The wrong trend in the hydrogen sorption properties is predicted in the series  $\text{TiM}$ , where the ternary hydride stability should decrease in the sense  $M = \text{Fe}, \text{Co}, \text{Ni}$ . Experimentally, however, an increase is observed (Yamanaka et al., 1975; Lundin et al., 1977). It should be noted that the three ternary hydrides observed differ considerably in hydrogen concentration, the composition at the end of the first plateau being approximately  $\text{TiFeH}_2$ ,  $\text{TiCoH}_{1.2}$  and  $\text{TiNiH}_{1.2}$ . The model calculations are based on the same hydrogen content ( $\text{TiMH}_2$ ) and thus underestimate the (absolute)  $\Delta H$  values of the ternary hydrides  $\text{TiCoH}_{1.2}$  and  $\text{TiNiH}_{1.2}$  when expressed per mole absorbed  $\text{H}_2$  gas. Further complications which make the series  $\text{TiFe}$ ,  $\text{TiCo}$ ,  $\text{TiNi}$  less suitable for a comparison between model and experiment have been discussed in detail elsewhere (Buschow and Miedema, 1978).

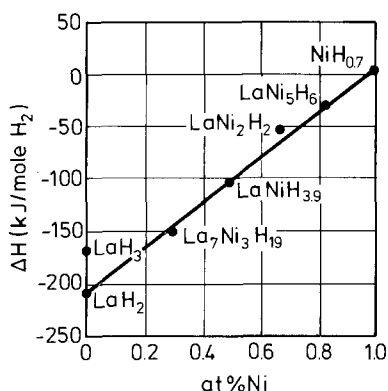


Fig. 23. Formation enthalpy of La-Ni hydrides plotted as a function of Ni concentration. The full line connects the experimental  $\Delta H$  values of  $\text{NiH}_{0.7}$  and  $\text{LaH}_2$  (after Busch et al., 1978a).

If one neglects the last term in eq. (16) the enthalpy of hydride formation takes the form of a sum of the weighted heat of formation of the binary hydrides of the two parent metals. Such an approach to estimating  $\Delta H$  values has been advocated by Clinton et al. (1975) and by Busch et al. (1978b, c). Results of the latter authors are reproduced in fig. 23. Here the full line connects the  $\Delta H$  data of  $\text{NiH}_{0.7}$  and  $\text{LaH}_2$ . It is clear that this phenomenological relationship between the heat of formation of the ternary and binary hydrides is quite useful for estimating  $\Delta H$  values of ternary hydrides based on rare earth metals where the first term in eq. (16) is the dominant one. It is obvious that the procedure of weighted averages is adequate for dealing with trend (iii) mentioned above. Trend (i) is also predicted correctly. This can be seen by taking account of the fact that in a series  $\text{RM}_n$  with M and  $n$  fixed the value of the binary hydride  $\text{RH}_2$ , which determines the intercept of the straight line with the left-hand vertical axis in fig. 23, moves in an upward direction as one proceeds from La to Lu. Difficulties are met if one considers very stable  $\text{RM}_n$  compounds with fixed R and  $n$  and a variable M component, such as  $\text{RRu}_n$ ,  $\text{RRh}_n$ ,  $\text{RPt}_n$  (trend ii). Since the heat of formation of the binary metal hydrides  $\text{MH}_{0.5}$  becomes more positive in the direction Pt, Rh, Ru (Bouten and Miedema, 1980), this means that the straight line corresponding to the weighted  $\Delta H$  averages (such as in fig. 23) lies lowest for  $\text{RPt}_n$  and highest for  $\text{RRu}_n$ . Consequently, the stability of the ternary hydrides  $\text{RM}_n\text{H}_x$  is expected to become more negative in the sense  $\text{RRu}_n\text{H}_x$ ,  $\text{RRh}_n\text{H}_x$ ,  $\text{RPt}_n\text{H}_x$ . This trend is opposite to that usually observed. For instance, the  $\Delta H$  values of the ternary hydrides of  $\text{GdRu}_2$ ,  $\text{GdRh}_2$  and  $\text{GdPt}_2$  are reported (Jacob and Shaltiel, 1979) to become less negative in going from  $\text{GdRu}_2$  to  $\text{GdPt}_2$  ( $\Delta H = -60.3$ ,  $49.4$  and  $> -39$  kJ/mole  $\text{H}_2$ , respectively). Difficulties will furthermore be met, even in reproducing trend (iii), in cases where the formation enthalpy of the binary hydrides of the parent metals is relatively low while the enthalpy of compound formation is relatively high (for instance in ternary hydrides of Pd-Nb compounds).

Jacob et al. (1977, 1980a) have proposed a model in which an important role is attributed to the local environment of the absorbed hydrogen atoms. These authors

suggest that the energy effects associated with the occupancy of a hydrogen atom of a given interstitial hole position ( $j$ ) be determined by the weighted average of the heat of formation of the binary hydrides that surround this position ( $\Delta H_j^f$ ). These latter quantities were estimated by means of the model of Miedema et al. (1980). The model given by Jacob et al. is suited, in particular, to predicting relative hole site occupancies  $N_j$ . According to Jacob et al. the  $N_j$  values can be obtained by using Boltzmann statistics, leading to the expression

$$N_j = N \frac{\exp(-\Delta H_j^f/k_B T)}{\sum_i \exp(-\Delta H_i^f/k_B T)} \quad (17)$$

Note that this model leads to a quantitative description of the temperature dependence of the relative hole site occupancies. For predicting ternary hydride stabilities the model would seem less suited since, in principle, it would require a knowledge of crystallographic details of the ternary hydride. Fortunately most of the ternary hydrides do not give rise to crystal structures where the metal atoms are arranged in a completely different way from the arrangement in the crystal structure of the uncharged intermetallics. Model calculations can then be made based on structural details of these latter compounds (see for instance Shinar et al., 1978a, b).

Lundin et al. (1977) and Magee et al. (1981) have analysed the hydrogen absorption behaviour of intermetallic compounds in terms of hole sizes present in these compounds. In the Haucke compounds, in particular, a rather close correlation was found between the stability of the  $RM_5H_x$  hydrides and the tetrahedral hole sizes in  $RM_5$ . It is not quite clear in how far these correlations have a physical basis. In the first place the differences in  $\ln p$  or  $\Delta H$  are explained in terms of tetrahedral hole radii differences of only several thousandths of Å, whereas it is known that hydrogen uptake gives rise to lattice expansions about two orders of magnitude larger. Secondly, if the hole size in the uncharged Haucke compounds  $RCO_5$  or  $RNi_5$  were really important, one would expect the correlation to hold for compounds in which the R component has a valence different from 3. This seems not to be the case. It is also not clear why compounds in which the R elements have opposite valence deviations, as in  $CeCo_5$  ( $Ce^{4+}$ ) and  $CaNi_5$  ( $Ca^{2+}$ ), often show deviations from the mentioned correlation in the same directions while  $CeCo_5$  and  $ThCo_5$  (Ce and Th both tetravalent) deviate in opposite directions. The correlation is further less well established if Ni in  $LaNi_5$  is wholly or partly replaced by Pt. Further arguments against the importance of hole sizes are the fact that the linear relationship between  $\ln p$  and the hole size cannot be explained by elastic deformation of these interstitial holes. Also the volume expansion per hydrogen in a given series of compounds is not related to the associated plateau pressures (Busch et al., 1978a). It is conceivable that the variation in hole size across a series of compounds reflects the variation of other parameters determining the hydride stability. For instance, the lattice parameters (and hence also the corresponding hole sizes) tend to be smaller as the uncharged compounds have higher stabilities or as the R components are less electropositive (Buschow et al., 1982). Nevertheless, the established correlation between tetrahedral hole size and ternary hydride stability can be used in tailoring the absorption properties to satisfy the conditions required in a given application of

the ternary hydrides. This is the more so since, instead of the hole size itself, one can use the corresponding unit cell volume, which is more easily accessible and, in addition, is an experimental quantity (Mendelsohn et al., 1977; Gruen et al., 1977; Buschow and Miedema, 1978).

Takeshita et al. (1980a, b, 1981) and Chung et al. (1980) have postulated the existence of a correlation between hydrogen absorption behaviour and the compressibility ( $\kappa$ ) of the uncharged materials. This correlation was taken by these authors to be a result of the fact that the work required for the metal lattice expansion upon charging is less the softer the metal. The  $\kappa$  values used in their analysis were derived from the Debye temperatures obtained for several Haucke compounds by means of specific heat measurements. For several compounds of the series  $\text{La}(\text{Ni}_{1-x}\text{Co}_x)_5$  experimental results are available relating to the hydrogen absorption behaviour (van Mal et al., 1979) as well as to compressibilities obtained by means of high-pressure equipment (Brouha and Buschow, 1975). These data have been used in fig. 24 to plot the plateau pressure versus the corresponding  $\kappa$  values. Although the  $\kappa$  values used in this plot are not directly comparable with the values used by Takeshita et al. (1981), the trend of  $\ln p$  is the same in both cases, thus confirming the correlation mentioned above. Also included in fig. 24 are data pertaining to the compounds  $\text{YCo}_5$  and  $\text{YCo}_2$  (Brouha et al., 1974). The correlation seems therefore to be less satisfactory when compounds varying widely in electronic and crystallographic properties are included.

Although the presence of an open d band does not represent a condition sine qua non for the hydrogen absorption, it may have some influence on details of the hydrogen sorption characteristics. Gschneidner et al. (1982) investigated a number of Haucke phases  $\text{R}(\text{Ni}_{1-x}\text{Cu}_x)_5$  and  $\text{R}(\text{Ni}_{1-x}\text{Al}_x)_5$  and found a correlation to exist between the variation in the normalized electronic specific heat  $\gamma(x)/\gamma(0)$  and the

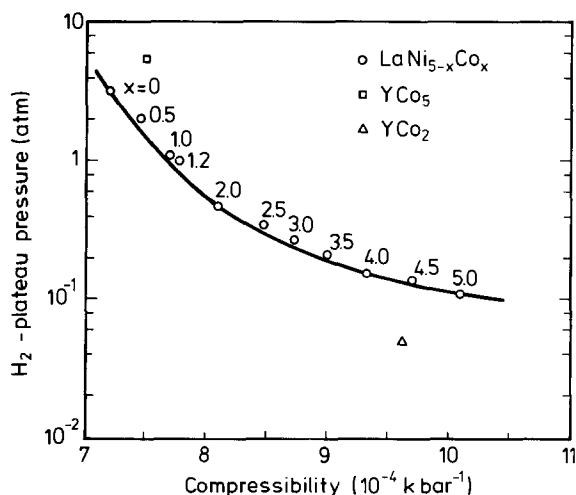


Fig. 24.  $\text{H}_2$  absorption plateau pressure versus compressibility of various  $\text{LaNi}_{5-x}\text{Co}_x$  compounds,  $\text{YCo}_5$  and  $\text{YCo}_2$ .

variation in the number of H atoms ( $N_H$ ) absorbed per formula unit when Ni is replaced by Cu or Al. The existence of this correlation was interpreted in terms of the rigid band model, increasing  $x$  leading to more electrons ( $\eta$ ) added to the 3d band and hence to a more complete filling of the Ni 3d band. In the case of Al substitution the authors assume that three electrons are added to the Ni 3d band for each Al atom. This latter assumption raises several questions. In the first place it is difficult to understand on the basis of electronegativity considerations why a relatively large charge transfer should take place between Al and Ni while the charge transfer between Gd and Ni is taken to be negligible. (Note that Gd has an even lower electronegativity than Al.) In the second place the large charge transfer from Al to Ni in  $R(Ni_{1-x}Al_x)_5$  is not in keeping with results of investigations made on a pseudobinary series, of the C15 type: magnetic and Mössbauer effect investigations of  $Gd(Fe_{1-x}Al_x)_2$  compounds showed that the 3d band filling remains more or less the same up to Al concentrations higher than  $x = 0.9$  (Besnus et al., 1979; van der Kraan et al., 1982). Although the above-mentioned correlation between  $\gamma(x)/\gamma(0)$  and  $N_H$  is quite convincing, the rigid band and charge transfer models seem to be too crude a picture. Hybridization effects will also lead to serious changes of the 3d band structure. The hybridization effects will be larger for Al substitution than for Cu substitution so that one may look upon the band filling parameter  $\eta$  also as reflecting to some extent an increasing 3d band hybridization.

For completeness we will conclude this section by mentioning that it is highly unlikely that the tendency towards hydrogen absorption is determined by the presence of a partially empty d band in the uncharged compounds. Formerly the presence of a partially depleted d band in metals like Pd, Nb and V has often been taken to be intimately connected with the capability of these elements to absorb hydrogen, the hydrogen donating its electron to the d band of the metal.

Starting from the experimental point of view, one could mention that the hydrogen absorption in  $Mg_2Cu$  (Reilly, 1978a),  $Ti_3Sn$  (Rudman et al., 1978)  $Th_2Al$  (Bergsma et al., 1963),  $HfAl$  (van Essen and Buschow, 1979) or  $La_2Mg_{17}$  (Yajima and Kayano, 1977) does not point to the presence of an open d band as being the driving force of the  $H_2$  absorption. The compound  $LaNi_5$  and its hydride resemble closely the Pd-H system in that there is a relatively high d electron density of states, corresponding to the presence of an almost filled d band.

Arguments were presented (Buschow and van Mal, 1982) showing that the presence of the partially depleted 3d band in, for instance,  $LaNi_5$  is not a prerequisite for the  $H_2$  absorption: In elementary Ni the number of unoccupied 3d band states is about 0.6 electron per Ni atom. This number will even be smaller in  $LaNi_5$ , so that one may consider it as an upper limit. If the donation of electrons to the 3d band were really important, the maximum hydrogen absorption capacity would be near  $LaNi_5H_3$ . The large number of experimental results (see for instance table A1) show that  $LaNi_5$  is able to absorb more than twice this amount. Also Gschneidner et al. (1982) concluded that relatively large amounts of hydrogen (0.5 H atom per metal atom) can be absorbed in  $RM_5$  compounds without the necessity of having holes in the 3d band.

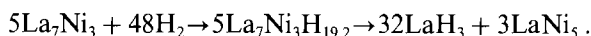
Further evidence against the necessity of d band filling upon hydrogen absorption



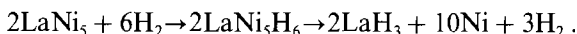
can be derived from results of specific heat measurements reported for several Haucke phases by Takeshita et al. (1980b, 1981). These authors conclude that the density of states at the Fermi surface is less likely to be an important factor in governing the hydrogen absorption behaviour.

#### 4.4. *Metastable character of ternary hydrides*

A comparison of the free energy of formation of a given ternary hydride (with H<sub>2</sub> gas and the corresponding intermetallic compound as standard states) with the free energy of formation of the binary hydrides of the corresponding constituent metals shows that formation of the ternary hydride is often not the energetically most favourable reaction (Buschow, 1977b). By means of experimental values of  $\Delta H$  and  $\Delta S$  or by means of values calculated on the basis of Miedema's model (see sections 2.1 and 4.3) one may derive quite generally that under not too high pressures and at room temperature most of the ternary hydrides (RM<sub>n</sub>H<sub>x</sub>) are metastable and decompose into the corresponding hydrides RH<sub>2</sub> (or RH<sub>3</sub>) and an M-richer compound RM<sub>p</sub> ( $p > n$ ). In the case of hydrogenation of La<sub>7</sub>Ni<sub>3</sub> Busch et al. (1978b) found the reaction



If an M-richer compound does not occur in the R–M phase diagram, pure M metal will be formed instead (Cohen et al., 1980a, b; Rummel et al., 1982):



Ternary hydrides are, nevertheless, formed upon hydrogenation owing to the fact that the charging with H<sub>2</sub> gas is usually performed at temperatures low enough to make diffusion of metal atoms impossible. This diffusion of the metal atoms is a necessary step to bring about separation of the phases RH<sub>3</sub> and RM<sub>p</sub> associated with the decomposition of the ternary hydride. In cases where the reaction between H<sub>2</sub> and RM<sub>n</sub> is allowed to proceed rapidly enough to make the transfer of the heat of hydrogenation to the surroundings in thermal contact with the sample insufficient, it can happen that the temperature of the sample becomes high enough for diffusion to take place. In many cases the thermal contact of the sample with its environment is such that a relatively high temperature is reached only during a short period. The phase separation mentioned above will then not reach completion. As a result, considerable atomic disorder may be present after charging. One may visualize the ternary hydride as an alloy supersaturated with respect to the phases H<sub>2</sub> and RM<sub>p</sub>. Precipitation of these phases may, for instance, proceed by means of a nucleation and growth mechanism and hence be strongly temperature dependent. Insufficient growth can give rise to precipitate particles too small to be observed by standard X-ray diffraction. This would explain the absence of diffraction lines after charging, as reported on several occasions in the literature (Clinton et al., 1975; Malik and Wallace, 1977). In some cases one of the reaction products after decomposition is ferromagnetic, whereas the original ternary hydride is not. It is then possible to follow rather closely by means of magnetic measurements the stage of the decom-

position process after repeated charging and desorption cycles (Buschow, 1978; Irvine and Harris, 1978; Siegman et al., 1978; Hempelmann et al., 1978). Such magnetic measurements have the advantage that the presence of the ferromagnetic phase will show up even though the decomposition has not yet reached a stage where this precipitated ferromagnetic phase can be detected by means of standard X-ray diffraction.

Since the transformation of the metastable ternary hydride into the decomposition products is diffusion controlled, one may use eq. (10) to show that the decomposition rate depends exponentially on the temperature [ $\propto \exp(E_A/kT)$ ]. It also depends exponentially on the activation energy  $E_A$  pertaining to the atomic motion of metal atoms. This activation energy is generally considered to comprise two terms, viz. the energy needed to create a vacancy ( $\Delta H_{iv}$ ) and the energy needed for a given atom to jump into the vacancy (saddle point energy). In pure metals both energies are found to be almost equal or to differ at least not much in magnitude (see for instance Christian, 1975). For the present purpose it is reasonable therefore to assume that  $E_A$  is proportional to  $\Delta H_{iv}$ . Studies of precipitations like those in the eutectoid decomposition of rare earth cobalt Haucke phases have indicated that the first precipitation is due to the movement of the smaller type of atoms. This would mean that  $E_A$  can be taken to be determined by  $\Delta H_{iv}^M$ , where M is the smaller (non-rare earth) component in the  $RM_n$  compounds. For the special case of La-Ni alloys we can use the results depicted in fig. 5. These results suggest that the decomposition of the ternary hydride of, for instance,  $La_7Ni_3$  involves an activation energy more than twice as low as in  $LaNi_5$ , for instance. It will be clear that due to the presence of the hydrogen atoms, the values of  $\Delta H_{iv}^{Ni}$  in the ternary hydrides will be substantially lower than those in the parent compounds. Nevertheless it seems plausible that the trend of  $\Delta H_{iv}^{Ni}$  in both types of materials will be the same. Considerations like those given above can then be used to show that the decomposition of ternary R-3d hydrides is expected to proceed more rapidly as the R concentration increases. Furthermore the  $\Delta H_{iv}^M$  value corresponding to the point on the left-hand vertical axis in fig. 5 can be shown to increase by more than 50% if one moves from R = La to Lu. This means that for a given 3d concentration of R-3d compounds the decomposition will proceed less easily in the same sense. The two trends of the decomposition of ternary hydrides as a function of 3d concentration and as a function of the nature of the R element are in keeping with experimental observations. In the case of compounds between light rare earth elements and 3d metals well-defined ternary hydrides (observable by X-ray diffraction) are generally obtained only for 3d-rich intermetallics (Busch et al., 1978b; Clinton et al., 1975). For a fixed 3d composition like  $RFe_2$  there is a tendency towards diminished decomposition as the atomic number of the rare earth component increases. This follows for instance from the increasing sharpness of the lines seen by means of  $^{57}Fe$  Mössbauer spectroscopy (Vicarò et al., 1979c, Buschow et al., 1980). Although the decomposition of the ternary hydride is of minor importance in compounds like  $LaNi_5$ , it may give rise to difficulites in those applications in which use is made of many repeated absorption-desorption cycles (McHenry, 1977; Holleck et al., 1980; Schlapbach, 1980).

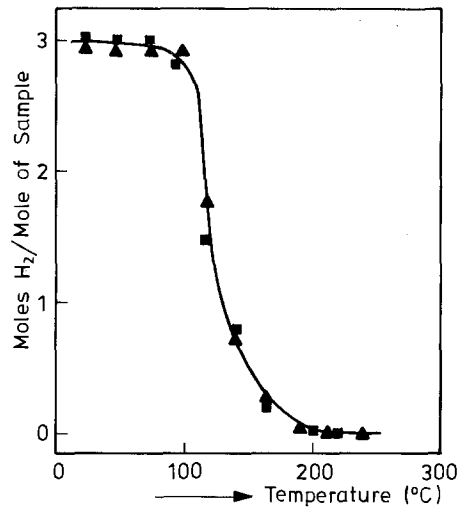


Fig. 25. Effect of temperature variation on the amount of absorbed hydrogen gas at 14.4 atm of the compound  $\text{La}_{0.9}\text{Eu}_{0.1}\text{Ni}_{4.6}\text{Mn}_{0.4}$  (after Cohen et al., 1980b). Heating is indicated by triangles, cooling by squares.

A detailed study of the degradation of ternary hydrides by repeated cycling was performed by Cohen et al. (1978, 1980a, b). The degradation in  $\text{LaNi}_3$  and pseudobinaries was studied by performing many temperature-induced absorption-desorption cycles. The response of  $\text{La}_{0.9}\text{Eu}_{0.1}\text{Ni}_{4.6}\text{Mn}_{0.4}$  in 14.4 atm  $\text{H}_2$  to temperature variation is shown in fig. 25. Cohen et al. found that through more than 1500 cycles the amount of reversibly absorbed hydrogen decreases markedly. By means of  $^{151}\text{Eu}$

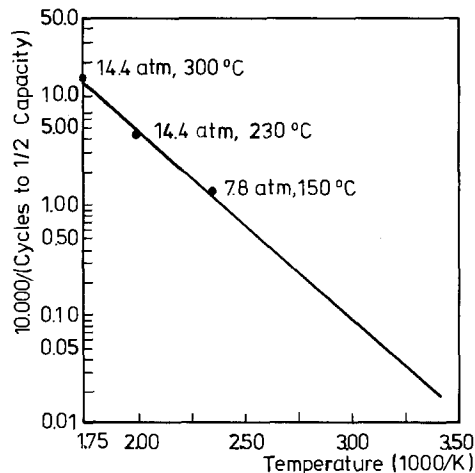


Fig. 26. Dependence of the degradation rate on the upper temperature limit used in temperature-induced cycling of  $\text{La}_{0.3}\text{Eu}_{0.1}\text{Ni}_{4.6}\text{Mn}_{0.4}$ . The vertical axis represents  $10^4$  divided by the number of cycles needed to achieve a loss of 50% of the absorption capacity (after Cohen et al., 1980a).

Mössbauer spectroscopy they established that the decrease mentioned is the result of the formation of a stable binary rare earth hydride. A straight line was obtained when the degradation rates were plotted versus  $1/T$  (see fig. 26). From the slope of the line they obtained a value of the activation energy equal to 32 kJ/mol. (Note that this value is indeed substantially lower than the activation energy for Ni in uncharged  $\text{LaNi}_5$ , mentioned above.) Cohen et al. suggest that pressure-cycled material gives rise to even faster degradation than temperature-cycled material.

The possibility to prepare amorphous alloys via charging with hydrogen gas was discussed by Buschow and Beekmans (1979). These authors argued that the disappearance of sharp reflection lines after charging is due to the formation of microcrystalline decomposition products rather than to the formation of amorphous alloys. Diffusion of metal atoms is a step necessary to bring about phase separation after, or better, during charging. The possibility of metal atom diffusion would, however, lead to spontaneous crystallization if the alloys were amorphous.

## 5. Physical properties

This section is concerned mainly with crystallographic and magnetic properties. In contrast to the vast amount of experimental work done on these properties, relatively little has been published on other properties such as transport properties. The few examples of specific heat measurements are not included in this section as they have already been discussed at more relevant places elsewhere in this review (see section 4.3). Since the NMR investigations performed on the ternary hydride dealt mainly with the motion of the H atoms, these properties were discussed in the section on diffusion (section 3.6).

The proliferation of research work on the magnetic properties of intermetallics and their ternary hydrides is primarily due to the interest in the fundamental physics aspects. Magnetism in metallic systems is not yet completely understood. Various theories exist, with often conflicting models. The possibility of changing the local conduction electron concentrations by the incorporation of hydrogen atoms is of relevance to many of these theories.

There is also interest from the technological side, since upon absorption of hydrogen a compound may change from ferromagnetic to paramagnetic or vice versa. This would imply an additional contribution to the sorption entropy. It follows from the discussion in section 4.2 that the entropy effect in a hydrogen sorption reaction is mainly determined by the hydrogenated material. In several applications involving a combination of two different metal-hydrogen systems (see section 6) it can be of advantage if not only reaction enthalpies but also reaction entropies can be freely chosen. The possibility to vary  $\Delta S$  by using magnetic effects would therefore provide a welcome degree of freedom. More trivially, one could mention that a knowledge of the changes in magnetic properties upon charging would make it possible to obtain information on the hydride degradation by means of magnetic monitoring. It was mentioned earlier (section 4.4) that ternary hydrides are metastable. Compounds  $\text{RM}_n\text{H}_{2m}$  tend to decompose into a hydride  $\text{RH}_m$ , M metal and

hydrogen gas. This magnetic monitoring could rather easily be performed, in particular, if the uncharged and charged compounds were non-magnetic or only weakly magnetic and the free M metal were ferromagnetic.

To deal with the fairly complex aspect of magnetic property changes, the section on magnetism is organized as follows.

In order to distinguish between changes in 3d electron magnetism and changes brought about by a modified coupling involving the localized 4f moments, we will first discuss results obtained upon H<sub>2</sub> absorption in intermetallics consisting of 3d elements and mainly those rare earth elements that are non-magnetic. These include the elements La, Y, Lu or Sc. In passing we will also discuss results obtained on compounds of 3d metals with Ti, Zr, Hf or Th. In a separate section we will discuss the changes observed in compounds where the rare earth element also carries a magnetic moment. Finally we will give an evaluation of the experimental results and discuss the conclusions that can be derived from them regarding the bonding of the H atoms in the ternary hydrides.

### 5.1. *Crystal structures*

As far as the lattice of metal atoms is concerned one can say that the structural changes accompanying the hydrogen sorption are of minor importance. In most cases the symmetry of the crystal lattice is preserved and the effect of the hydrogen is merely to produce a lattice expansion. Incidentally the H<sub>2</sub> absorption is accompanied by a small distortion which lowers the symmetry (Kuijpers, 1973; Viccaro et al., 1979b; Cho et al., 1982; Andreev et al., 1982). The X-ray diagrams of some of the compounds investigated did not contain diffraction peaks after H<sub>2</sub> absorption. This shows that long-range lattice periodicity has been lost. The loss in long-range atomic ordering is closely connected with the fact that the ternary hydrides are metastable under certain conditions of H<sub>2</sub> pressure and temperature and tend to decompose, a point already discussed in section 4. Further evidence in support of this decomposition follows from magnetic measurements (see section 5.2).

Owing to the small atomic scattering power of the H atoms no conclusive information on the crystallographic position of these atoms in the hydrides can be derived from results of X-ray and neutron diffraction. For a structure determination involving both the metal atoms and the H atoms one therefore has to rely on neutron diffraction studies made on the deuterium equivalents of the ternary hydrides. Until now only relatively few such studies have been undertaken. Kuijpers (1973) and Kuijpers and Loopstra (1974) investigated several hydrides of the RCo<sub>5</sub> family and found that hydrogen absorption leads to a small orthorhombic distortion. The crystal structure of LaNi<sub>5</sub>D<sub>6</sub> has been studied by several investigators (Bowman et al., 1973; Fischer et al., 1977; Andresen, 1978; Furrer et al., 1978; Burnasheva et al., 1978, Percheron-Guégan et al., 1980; Noréus et al., 1983). With respect to the original LaNi<sub>5</sub> unit cell, hydriding has led to a volume increase of about 25%. In several investigations the symmetry was reported to have decreased from P6/mm to P31m (see table 5).

TABLE 5

Comparison of the refinement results of the  $\text{LaNi}_5$  deuteride structure in the two-site model and the five-site model (after Achard et al., 1981). The values of  $[(\sin \theta)/\lambda]_{\max}$  correspond to the last reflection used in the refinement.

Deuteride	Occupancy $N$					Number of reflections	$[(\sin \theta)/\lambda]_{\max}$ ( $\text{\AA}^{-1}$ )	Reliability $R$ -factor (%)	Ref.
	3c sites		6d sites						
$\text{LaNi}_5\text{D}_{6.8}$	3		3.8			19	0.44	qualitative	1
$\text{LaNi}_5\text{D}_6$	2.86		3.14			21	0.39	5.4	2
$\text{LaNi}_5\text{D}_{6.4}$	3		3.4			—	—	5.4	2
$\text{LaNi}_5\text{D}_{5.8}$	3		2.8			—	0.52	6.4	3
$\text{LaNi}_5\text{D}_{5.6}$	3		2.6			not known	not known	4	4
$\text{LaNi}_5\text{D}_6$	3		3			23	0.44	12	5
$\text{LaNi}_5\text{D}_{6.5}$	3		3.5			—	0.72	16	6
$\text{LaNi}_5\text{D}_{5.5}$	3		2.5			92	—	8.3	7
	3f	4h	6m	12n	12o				
$\text{LaNi}_5\text{D}_{6.5}$	0.64	0.52	1.91	2.14	1.29	43	0.55	7.3	6

1. Bowman et al. (1973). 3. Furrer et al. (1978). 5. Burnasheva et al. (1978). 7. Noréus et al. (1983).  
 2. Fischer et al. (1977). 4. Andresen (1978). 6. Percheron-Guégan (1980).

The results of the refinements of the  $\text{LaNi}_5\text{D}_6$  structure obtained in the various investigations are summarized in table 5. It is seen that the number of reflections considered in the investigation by Percheron-Guégan et al. and Noréus et al. (1983) is relatively large and adds weight to the low value of the reliability factor  $R$  found in these studies. It can also be seen from the table that the number of hole sites is five in the structure proposed by Percheron-Guégan et al., while it is only two in the other structures. This latter fact has led Wallace et al. (1981) to cast doubt on the validity of this structure determination, arguing that the configurational entropy  $S$  corresponding to this structure would be incompatible with the results of thermodynamic measurements. The value of  $S_c$  calculated for the five-site structure by Wallace et al. on the basis of eq. (15) given in section 4.2 equals  $21.2 \text{ J K}^{-1} (\text{g atom})^{-1}$ . This value is much higher than  $S_c = 4.3 \text{ J K}^{-1} (\text{g atom})^{-1}$  derived by Ohlendorf and Flotow (1980b) from an analysis of their specific heat data based on eq. (15). It was shown subsequently by Archard et al. (1981) that the value  $S_c = 21.2 \text{ J K}^{-1} (\text{g atom})^{-1}$  calculated by Wallace et al. is far from realistic. Considerably lower values are obtained if account is taken of the fact that at a given time the occupation of one deuterium site prevents the occupation of sites closer than the minimum H-H separation (see also below).

The structure of  $\text{LaNi}_{4.5}\text{Al}_{0.5}\text{D}_{4.5}$  was investigated by Crowder et al. (1982). The distribution of Co atoms in  $\text{LaNi}_4\text{Co}$  and the structure of the corresponding deuteride was investigated by Gurewitz et al. (1983).

Closely related to the  $\text{CaCu}_5$ -type structure of  $\text{LaNi}_5$  are the crystal structures of  $\text{LaNi}_3$  ( $\text{CeNi}_3$ -type) and  $\text{HoNi}_3$  ( $\text{PuNi}_3$ ), the deuterides of which were investigated by

TABLE 6  
 Interstitial hole sites in  $R_6Mn_{23}$  compounds. In the  $Th_6Mn_{23}$  structure type there are four different Mn sites, indicated by Mn(*i*); *i* = 1, 2, 3, 4 corresponds to the sites 4b, 24d, 32f<sub>1</sub> and 32f<sub>2</sub>.

Wyckoff symbol	Polyhedron type	Corner atoms
4a	octahedron	6 R
32f <sub>3</sub>	tetrahedron	3 R + 1 Mn(4)
96k	tetrahedron	2 R + 1 Mn(4) + 1 Mn(2)
48i	octahedron	2 R + 1 Mn(1) + 1 Mn(2) + 2 Mn(3)

means of neutron diffraction by Andresen et al. (1978) and Solov'ev et al. (1981), respectively. The results of the structure determination of  $HoNi_3D_{1.8}$  obtained by Solov'ev et al. are reproduced in fig. 27. The deuterium atoms are accommodated in two types of interstitial holes (indicated close to the basal plane of the unit cell). The major part of the D atoms occupies the (deformed) tetrahedral hole sites of the type 18h (11.47 D atoms per unit cell  $Ho_9Ni_{27}$ ). These hole sites are surrounded by two Ho atoms and two Ni atoms. The remaining D atoms (4.72 D atoms per

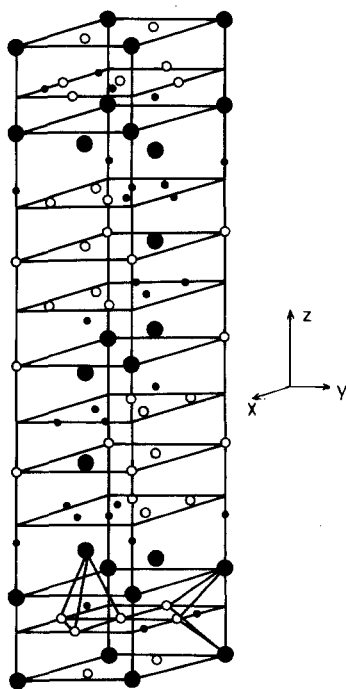


Fig. 27. Schematic illustration of the crystal structure of  $HoNi_3D_{1.8}$  as proposed by Solov'ev et al. (1981). The large filled circles represent the Ho positions, the medium-sized open circles the Ni positions, and the smaller filled circles the deuterium positions. The two types of tetrahedral holes corresponding to the deuterium positions are indicated in the lower part of the figure.

$\text{Ho}_9\text{Ni}_{27}$ ) are located at tetrahedral hole sites of the type 6c, surrounded by one Ho atom and three Ni atoms.

Neutron diffraction studies on  $\text{R}_6\text{Mn}_{23}\text{D}_x$  were made by Commandré et al. (1979) for  $\text{R} = \text{Y}$  and by Hardman et al. (1980) for  $\text{R} = \text{Th}$ . The energetically interstitial sites in the cubic  $\text{Th}_6\text{Mn}_{23}$  structure are summarized in table 6 (Jacob, 1981). Included in this table are the number and kinds of metal atoms occurring at the corners of the polyhedrons. It can be derived from the results of Commandré et al. (1979) on  $\text{Y}_6\text{Mn}_{23}\text{D}_{8.3}$  that the hole sites 4a and 32f<sub>3</sub> are preferentially occupied (0.6 and 7.7 D atoms, respectively). Results obtained on  $\text{Th}_6\text{Mn}_{23}\text{D}_{16}$  (Hardman et al., 1980) show that further deuteration had resulted in a preferential occupation of the 48i site. Only at concentrations as high as  $\text{Y}_6\text{Mn}_{23}\text{D}_{23}$  is there a (partial) occupation of the 96k site.

Jacob (1981) analysed the interstitial hole occupancies in the above materials by means of the semi-empirical model proposed by Jacob et al. (1980a) and mentioned in section 4.3. From top to bottom the hole sites in table 6 correspond to lower absolute values of the hole site enthalpies. The preferential occupancy of the 48i site, occurring before accommodation of D atoms in the 96k site takes place, is rather unexpected. Jacob et al. explained this discrepancy by noting that there is only a rather short separation ( $\approx 1.6 \text{ \AA}$ ) between the already filled 32f<sub>3</sub> site and the empty 96k site. The strong electrostatic repulsion between the H atoms raises the 96k hole site enthalpy and makes this site less attractive to occupation by D atoms. Jacob et al. also suggested that the electrostatic repulsion between the H atoms is sensitive to small changes in the relative H-H interatomic distance between 96k and 32f<sub>3</sub>. This would mean that in the light rare earth compounds, which have relatively large lattice constants (see fig. 28), the repulsion is less than in the case of compounds of the heavy rare earths. Consequently, the former are expected to have a somewhat higher absorption capacity than the latter. This would be in agreement with the fact that the change in lattice constant upon charging decreases in going from left to right in fig. 28.

Apart from the results mentioned above, structural information regarding the H positions in ternary rare earth base hydrides is still lacking. Nevertheless it is interesting to mention some results obtained on other ternary hydrides. Neutron diffraction experiments on intermetallics charged with deuterium comprise TiFe (Fruchart et al., 1980a; Thompson et al., 1979; Fischer et al., 1978b), ZrV<sub>2</sub> (Didisheim et al., 1979a, 1981; Fruchart et al., 1980b), ZrMn<sub>2</sub> (Didisheim et al., 1979b) and HfV<sub>2</sub> (Irodova et al., 1981). These experiments, too, support the notion that once a hydrogen atom is absorbed, other similar positions are not allowed to become occupied when they are present at too short a distance. Didisheim et al. (1981) investigated ZrNi<sub>2</sub>H<sub>3.6</sub> and showed that the hydrogen atoms are distributed in a disordered way at high temperatures, although there is a minimum distance associated with the H-H interseparation. From the diffuse background peak in the neutron scattering patterns it was derived that this minimum distance is equal to about 2.2 Å. In the hydride of TiFe there are many more sites than H atoms and the results derived from neutron diffraction measurements are still under discussion. Leaving this hydride out of consideration, one could say that the experimentally determined site occupancies agree quite well with the concept that the driving force



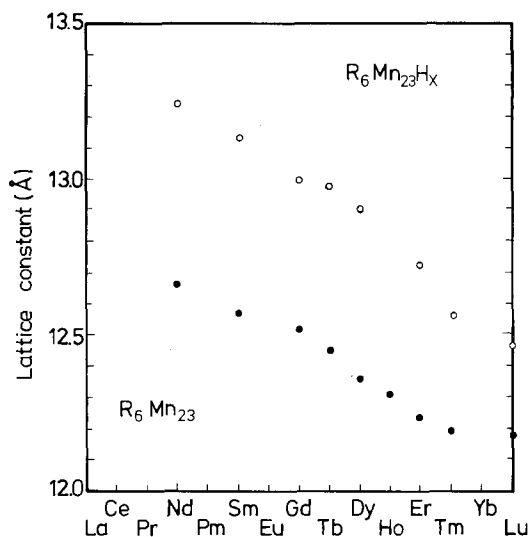


Fig. 28. Lattice constants as a function of the R component in various  $R_6Mn_{23}$  compounds (lower part) and the corresponding hydrides (upper part).

underlying ternary hydride formation is the creation of an optimal area of contact between the H atoms and the atoms of the strongly hydrogen-attracting component (van Mal et al., 1974; Jacob et al., 1980a).

We conclude this section on crystal structures by mentioning that there are also cases where the absorption of hydrogen has resulted in well-defined structural changes of the lattice of metal atoms as well. Some results have been collected in table 7. It can be seen that the structure changes can lead to a lowering as well as to an increase of the metal atom lattice symmetry.

TABLE 7  
Changes in crystal structure observed in some intermetallic compounds.

Compound	Structure	Hydride	Structure	Ref.
ZrCo	CsCl(c)	ZrCoH <sub>2.6</sub>	CrB(o.r.)	1, 2
HfCo	CsCl(c)	HfCoH <sub>3.2</sub>	CrB(o.r.)	2
EuPd	CrB(o.r.)	EuPdH <sub>3</sub>	CsCl(c)	3
YbNi	FeB(o.r.)	YbNiH <sub>x</sub>	CsCl(c)	4
Mg <sub>2</sub> Ni	MgNi <sub>2</sub> (h)	Mg <sub>2</sub> NiD <sub>4</sub>	fcc	5, 6
GdCu <sub>2</sub>	CeCu <sub>2</sub> (o.r.)	GdCu <sub>2</sub> H <sub>x</sub>	MoSi <sub>2</sub> (tetr.)	7

- Irvine and Harris (1978).
- Van Essen and Buschow (1979).
- Buschow et al. (1977).
- Buschow (unpublished results).
- Gavra et al. (1979).
- Schefer et al. (1980).
- De Graaf et al. (1982b).

## 5.2. Magnetic properties

### 5.2.1. Ni compounds

As mentioned in section 4.4, the ternary hydrides are actually metastable with respect to the binary rare earth hydrides and the pure 3d metals (or a more 3d-rich intermetallic compound). Partial or complete decomposition of the ternary hydrides during the sorption reaction can therefore lead to reaction products that are no longer single phase. This would seriously hamper the investigation of the magnetic properties of the ternary hydrides. Difficulties of this kind have been encountered, for instance, in charging the Pauli paramagnetic compound  $\text{La}_7\text{Ni}_3$ , which was found to decompose into  $\text{LaH}_3$  and  $\text{LaNi}_5$  (Busch et al., 1978b). Magnetically more revealing information was obtained from charging experiments with the Pauli paramagnetic compound  $\text{Th}_7\text{Ni}_3$ , isotypic with  $\text{La}_7\text{Ni}_3$ . Malik et al. (1980) found a decrease of the susceptibility upon charging. They interpreted their results as indicating that charging is accompanied by a decrease of the density of states. Evidently decomposition of the ternary hydride was avoided here or was of minor importance. This would be the case if the reaction products of the decomposition were of the same type as in  $\text{La}_7\text{Ni}_3$  (i.e. the binary hydride of Th and  $\text{ThNi}_5$ ). Tiny amounts of the decomposition products are likely to remain unnoticed in the magnetic measurements, since  $\text{ThNi}_5$  is Pauli paramagnetic and has a magnetic susceptibility equal to  $1.9 \times 10^{-3}$  emu/mole (Elemans et al., 1975), which is of the same order of magnitude as that of  $\text{Th}_7\text{Ni}_3$  and its hydride.

Charging of the paramagnetic compound  $\text{LaNi}_5$  usually leads to the presence of increasing amounts of Ni as a ferromagnetic impurity phase after repeated cycling (Siegmann et al., 1978). Busch and Schlapbach (1978) were able to show, however, that the magnetic susceptibility had decreased after each charging operation, indicating a smaller susceptibility in  $\text{LaNi}_5\text{H}_6$ . This was explained in terms of a decreasing density of states (Schlapbach, 1980). A decrease of the susceptibility was also reported by Palleau and Chouteau (1980). Experimental results of these authors are reproduced in fig. 29. Palleau and Chouteau furthermore studied the effect of Ni

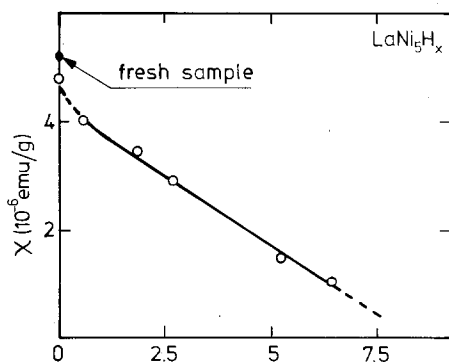


Fig. 29. Dependence of the magnetic susceptibility on  $x$  in  $\text{LaNi}_5\text{H}_x$  after continued charging of  $\text{LaNi}_5$  (after Palleau and Chouteau, 1980).

precipitation after cycling and question whether this precipitation arises as a consequence of the absorption reaction. According to their experimental results the Ni precipitation would occur during the dehydriding rather than during hydriding. Finally a decreasing intrinsic magnetic susceptibility in  $\text{LaNi}_5$  was also proposed by Walsh et al. (1976) on the basis of EPR measurements on Gd-doped  $\text{LaNi}_5\text{H}_6$ .

More obvious changes in magnetic properties upon charging with hydrogen gas occur in  $\text{YNi}_3$ . As already mentioned in section 2, Gignoux et al. reported  $\text{YNi}_3$  to be a weak itinerant ferromagnet. Similar results were also obtained by Buschow and van Essen (1979). These latter authors furthermore showed that the ferromagnetism disappears upon absorption of hydrogen gas. This was interpreted as being the result of a decrease in the density of states or a weakening of the intra-atomic Coulomb repulsion. A different type of change in magnetic properties was found in  $\text{CeNi}_3$ . Owing to the tetravalent character of Ce in this compound, the Ce atoms do not have a magnetic moment and also the 3d electron magnetism resurgence is not present here. Hydrogen uptake in  $\text{CeNi}_3$  leads to a change in valence of Ce from  $4+$  to  $3+$ . This follows from the observation of a Curie-Weiss-type temperature dependence of the reciprocal susceptibility in the hydride with an effective moment appropriate to  $\text{Ce}^{3+}$  (Buschow, 1980b). Further results reflecting the changes in magnetic properties of Ni-base intermetallics after charging with hydrogen are given in table A6.

### 5.2.2. Co compounds

The compound  $\text{YCo}_2$  is a strongly exchange-enhanced Pauli paramagnet. The absorption of  $\text{H}_2$  has been reported to lead to an increase of the magnetic susceptibility (Buschow, 1977b), which was ascribed to atomic disordering. The occurrence of atomic disordering upon charging has already been discussed in section 4.4. It arises as a consequence of the metastable nature of the ternary hydrides. Support for this interpretation was obtained from  $^{57}\text{Fe}$  Mössbauer spectroscopy performed on  $\text{YCo}_2$  doped with a small amount of enriched Fe (Buschow and van der Kraan, 1983). Hydrogen uptake was found to lead to small clusters of Co atoms too small to be observable by standard X-ray diffraction. As can be seen from the results shown in fig. 30, a large hyperfine field is present on the Fe atoms owing to magnetic ordering within the Co clusters. The mutual magnetic coupling of the Co clusters is weak, so that their presence does not contribute much to the bulk magnetization. The formation of small clusters of free Co resulting from a partial decomposition of the ternary hydride after charging was also studied in detail in  $\text{PrCo}_2\text{H}_x$  (de Jongh et al., 1981). The temperature dependence of the zero field a.c. susceptibility gives rise to a maximum, reminiscent of a spin glass or of a magnetic glass. The shift of this maximum to higher temperatures when the a.c. frequency is increased (see fig. 31) was interpreted in terms of the Néel model for superparamagnetic particles with randomly oriented local anisotropy axes. The amount of Co present as clusters was estimated to be as high as 70%, although it remains almost unnoticed in the temperature dependence of the magnetization (see also fig. 43 in section 5.2.5).

In this connection it is interesting to mention the results of Malik et al. (1980), who studied the effect of hydrogen absorption on the magnetic properties of  $\text{Th}_7\text{Co}_3$ . This

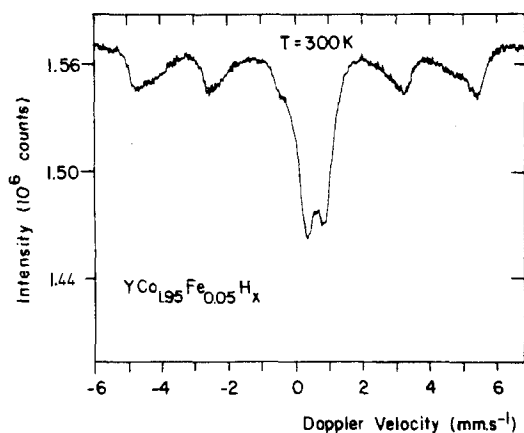


Fig. 30.  $^{57}\text{Fe}$  Mössbauer effect spectra of  $\text{YCo}_2$  (doped with enriched Fe) after charging with hydrogen gas (after Buschow and van der Kraan, 1983).

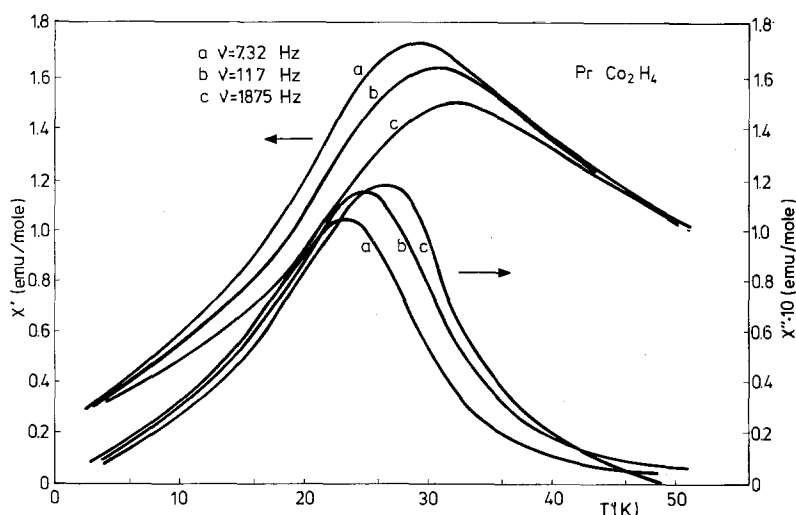


Fig. 31. Real ( $\chi'$ ) and imaginary ( $\chi''$ ) parts of the complex a.c. susceptibility  $\chi = \chi' - i\chi''$  as measured with various frequencies in  $\text{PrCo}_2\text{H}_4$  as a function of temperature (after de Jong et al., 1981).

compound is isotypic with  $\text{Th}_7\text{Ni}_3$  and  $\text{La}_7\text{Ni}_3$  mentioned in the preceding section. Their results indicate an increase in susceptibility upon  $\text{H}_2$  absorption. This was ascribed to a decreasing number of 3d electrons owing to charge transfer from Co to H. In this case, too, one cannot exclude the possibility that this increase of the susceptibility is not an intrinsic effect but results from traces of decomposition products not detectable by standard X-ray diffraction. From the results mentioned in the preceding section and from the results of Schlapbach et al. (1982) obtained on  $\text{Th}_7\text{Fe}_3$  it follows that some decomposition is likely to occur, so that an increase

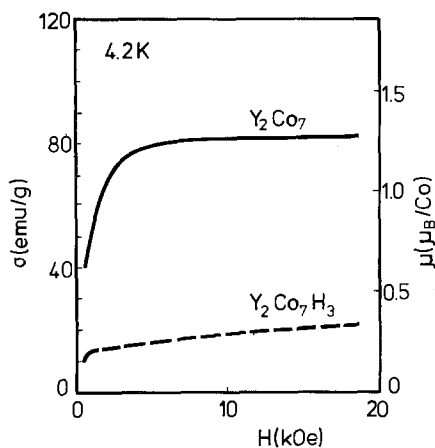


Fig. 32. Field dependence of the magnetization at 4.2 K in  $\text{Y}_2\text{Co}_7$  and  $\text{Y}_2\text{Co}_7\text{H}_3$  (after Buschow, 1982b).

of the susceptibility has to be treated with some reserve (Busch, 1978b; Siegmann et al., 1978; Stucki and Schlapbach, 1980). Here it should be kept in mind that the situation in  $\text{Th}_7\text{Co}_3$  is rather unfavourable compared to that in  $\text{Th}_7\text{Ni}_3$  since decomposition products like  $\text{ThCo}_5$ ,  $\text{Th}_2\text{Co}_{17}$  or  $\text{Co}$  are all strongly ferromagnetic. Even slight traces of these phases are able to mask any changes of the intrinsic bulk susceptibility of  $\text{Th}_7\text{Co}_3$  upon  $\text{H}_2$  absorption.

The above-mentioned uncertainty in the interpretation of changes in magnetic properties is considerably reduced when the original uncharged compounds are ferromagnetic. As an example we show in fig. 32 the effect of  $\text{H}_2$  absorption on

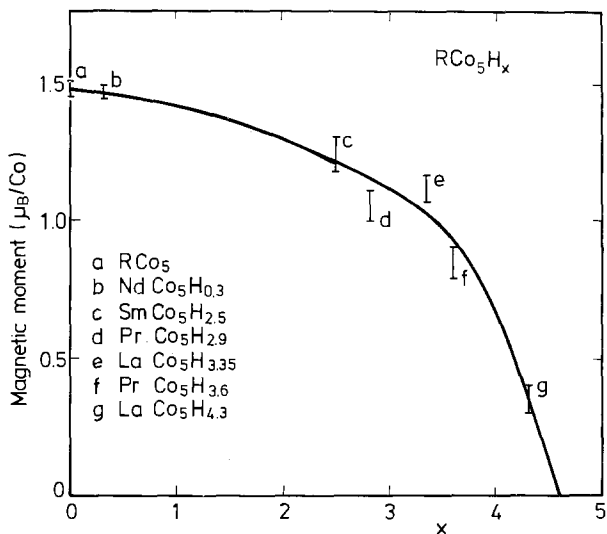


Fig. 33. Dependence of the Co moment on hydrogen concentration, as determined by means of neutron diffraction in various hydrides of the type  $\text{RCo}_5\text{H}_x$ . The data were taken from results published by Kuijpers (1973) and Kuijpers and Loopstra (1974).

TABLE 8  
Co moments in various intermetallics before and after charging with hydrogen.

Compound	$\mu_{\text{Co}}$ ( $\mu_{\text{B}}$ )	Hydride	$\mu_{\text{Co}}$ ( $\mu_{\text{B}}$ )	References
LaCo <sub>5</sub>	1.5	LaCo <sub>5</sub> H <sub>3.3</sub>	1.1	Kuijpers (1973)
		LaCo <sub>5</sub> H <sub>4.3</sub>	0.3	Kuijpers (1973)
La <sub>2</sub> Co <sub>7</sub>	1.0	La <sub>2</sub> Co <sub>7</sub> H <sub>5</sub>	0.6	Buschow et al. (1980)
YCo <sub>5</sub>	1.5	YCo <sub>5</sub> H <sub>2.8</sub>	1.2	Yamaguchi et al. (1983)
Y <sub>2</sub> Co <sub>7</sub>	1.3	Y <sub>2</sub> Co <sub>7</sub> H <sub>3</sub>	0.3	Buschow (1982a)
YCo <sub>3</sub>	0.8	YCo <sub>3</sub> H	0.3	Buschow and de Châtel (1979)
		YCo <sub>3</sub> H <sub>3</sub>	0.0	Buschow and de Châtel (1979)

Y<sub>2</sub>Co<sub>7</sub>. Here the ternary hydride is seen to have a considerably lower magnetization than the uncharged compound. The fact that the magnetization is more field dependent in the hydride may indicate that the charging has resulted in a certain degree of lattice disorder—giving rise to local deviations from a collinear spin arrangement. Even more reliable data with respect to the moment changes have been obtained by means of neutron diffraction measurements in RCo<sub>5</sub> compounds and their hydrides. Results obtained by Kuijpers (1973) and Kuijpers and Loopstra (1974) are collected in fig. 33. A reduction in Co moment upon hydrogen absorption was also observed in several other Co compounds. Results of the magnetic measurements are summarized in table 8. All these results show quite convincingly that in ferromagnetic Co compounds, where effects due to a possible decomposition of part of the hydride phase are relatively unimportant, H<sub>2</sub> absorption has the effect of lowering the Co moment. Further results of magnetic measurements on Co compounds and their hydrides are given in table A7.

### 5.2.3. Fe compounds

The changes in magnetic properties in the Fe compounds occur in the opposite direction from those in the Ni and Co compounds. The results shown in fig. 34 may serve to illustrate this point. As seen from the full line in fig. 34, the Fe moment increases with  $x$  in ScFe<sub>2</sub>H <sub>$x$</sub> , which contrasts with the behaviour of the RCo<sub>5</sub>H <sub>$x$</sub> .

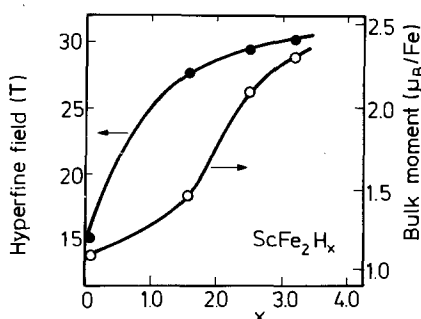


Fig. 34. <sup>57</sup>Fe Mössbauer effect hyperfine field (filled circles) and bulk magnetic moment (open circles) as a function of H concentration in ScFe<sub>2</sub>H <sub>$x$</sub>  (after Niarchos et al., 1980a).

TABLE 9  
Fe moments in various intermetallics before and after charging with hydrogen.

Compound	$\mu_{\text{Fe}} (\mu_{\text{B}})$	Hydride	$\mu_{\text{Fe}} (\mu_{\text{B}})$	References
ScFe <sub>2</sub>	1.4	ScFe <sub>2</sub> H <sub>2</sub>	2.2	Smit and Buschow (1980)
CeFe <sub>2</sub>	1.3	CeFe <sub>2</sub> H <sub>4</sub>	2.1	van Diepen and Buschow (1977)
YFe <sub>2</sub>	1.4	YFe <sub>2</sub> H <sub>4</sub>	1.8	Buschow (1976)
LuFe <sub>2</sub>	1.3	LuFe <sub>2</sub> H <sub>4,2</sub>	1.7	Buschow et al. (1980)
Y <sub>6</sub> Fe <sub>23</sub>	1.7	Y <sub>6</sub> Fe <sub>23</sub> H <sub>21</sub>	1.9	Buschow (1976)
Lu <sub>6</sub> Fe <sub>23</sub>	1.5	Lu <sub>6</sub> Fe <sub>23</sub> H <sub>8</sub>	1.6	Gubbens et al. (1981)
Hf <sub>2</sub> Fe	0	Hf <sub>2</sub> FeH <sub>3</sub>	0.9	Buschow and van Diepen (1979)

systems, where the 3d moment decreases with  $x$ . Results of magnetic measurements obtained on several other rare earth-iron compounds and their ternary hydrides are listed in table 9. As can be seen, hydrogen absorption in all compounds studied is accompanied by a substantial increase in Fe moment. The most drastic increase in Fe moment occurs in ScFe<sub>2</sub> and CeFe<sub>2</sub>, where  $\mu_{\text{Fe}}$  changes from about 1  $\mu_{\text{B}}/\text{Fe}$  to more than 2  $\mu_{\text{B}}/\text{Fe}$ . (Ce is not far from tetravalent and has no magnetic moment.) An increasing Fe moment is also associated with the transitions from paramagnetism to ferromagnetism after hydrogen absorption, reported to occur in Th<sub>7</sub>Fe<sub>3</sub> (Malik et al., 1978a) and in Hf<sub>2</sub>Fe (Buschow and van Diepen, 1979). The changes in magnetic properties after charging of Th<sub>7</sub>Fe<sub>3</sub> were reinvestigated by Schlapbach et al. (1982), who showed that the ternary hydride of this compound remains paramagnetic when the charging is performed sufficiently slowly to avoid decomposition of the material. A similar situation might also exist in CeFe<sub>2</sub> and to a lesser extent also in YFe<sub>2</sub>. In these cases X-ray diffraction of the hydrided material did not give rise to a sharp pattern. In fact, in CeFe<sub>2</sub> all diffraction lines had disappeared after charging (van Diepen and Buschow, 1977). Furthermore the <sup>57</sup>Fe Mössbauer spectra obtained on the charged materials were rather broadened. The results listed in table 9 for the CeFe<sub>2</sub> compound therefore have to be treated with some reserve since here, too, the increase in Fe moment may be an apparent one, brought about by decomposition and the formation of small Fe clusters.

The changes in magnetic ordering temperatures ( $T_c$ ) accompanying the hydrogen take-up can be in either direction (see the results listed in table A8). It was mentioned on several occasions that H<sub>2</sub> absorption leads to a large expansion of the crystal lattice. If the changes in interatomic distances were responsible for the changes in  $T_c$ , the published data on the pressure dependence of  $T_c$  in the uncharged intermetallics could give an indication as to whether  $T_c$  is expected to increase or decrease upon charging. Such a correlation between magnetovolume effects and the changes in magnetic ordering temperatures upon charging was proposed by Buschow (1978). A similar correlation was also observed by Coey et al. (1982) on amorphous Y-Fe alloys and by Hilscher et al. (1980) in TiFe<sub>1-x</sub>Co<sub>x</sub> and their hydrides. It should be realized that it is only the magnetic coupling between the moments that can be correlated with the magnetovolume effects and not the change in size of the moments.

<sup>57</sup>Fe Mössbauer spectroscopy investigations were made on several of the ternary

hydrides, such as  $\text{YFe}_2$ ,  $\text{CeFe}_2$  and  $\text{ThFe}_3$  (van Diepen and Buschow, 1977; Buschow and van Diepen, 1976; Okamoto et al., 1982; Fujii et al., 1983). The appearance of hyperfine splitting upon a decrease in temperature was found to agree with the onset of magnetic ordering derived from the magnetization measurements. Although the hyperfine splitting in the hydride of  $\text{YFe}_2$  was found to be larger than in uncharged  $\text{YFe}_2$ , a quantitative analysis of the hyperfine spectra of the hydrides below  $T_c$  is made difficult by an extremely strong line broadening. As mentioned above, this broadening reflects the presence of some atomic disorder brought about by the tendency toward phase separation (Buschow and Miedema, 1978; Buschow, 1977b). In some cases it has been possible to prepare ternary hydrides of  $\text{RFe}_2$  compounds which do not give rise to broadened Mössbauer spectra. These comprise the hydrides of  $\text{DyFe}_2$  and  $\text{ErFe}_2$  (Viccaro et al., 1979a),  $\text{LuFe}_2$  (Buschow et al., 1980) and  $\text{ScFe}_2$  (Smit and Buschow, 1980; Smit et al., 1982; Niarchos et al., 1980a). Evidently in these hydrides the atoms occupy highly ordered positions, i.e., the onset of phase separation had not yet taken place. The fact that no observable decomposition of the ternary hydrides of  $\text{RFe}_2$  occurs when R is a rare earth at the end of the lanthanide series is in keeping with results discussed in section 2, where it was shown that the diffusion of metal atoms proceeds less easily in these cases than in cases where the R element occurs more to the beginning of the series. (In the context of section 2.2 the element Sc can be regarded as being located at the end of the lanthanide series and the element Y in the middle of it.) In  $\text{ScFe}_2\text{H}_3$  the hyperfine splitting at 4.2 K was found to have increased by a factor of two relative to  $\text{ScFe}_2$  (see the upper line in fig. 34). This compares favourably with the results of the magnetic measurements (lower line in fig. 34) and seems to suggest that there is no drastic change in the relative magnitude of the various hyperfine field contributions such as core polarization and transferred hyperfine field. Sharp Mössbauer spectra (fig. 35) were also obtained upon charging of  $\text{Lu}_6\text{Fe}_{23}$  (Gubbens et al., 1981). The amount of hydrogen absorbed by this compound corresponds to the formula composition  $\text{Lu}_6\text{Fe}_{23}\text{H}_9$ . From an analysis of the Mössbauer spectra it was derived that the hydrogen atoms occupy primarily the tetrahedral hole consisting of three Lu atoms and one Fe atom. A preferential occupancy of this hole site is in keeping with model considerations put forward by Jacob (1981). Gubbens et al. furthermore indicate the possibility of a correlation existing between the change in Curie temperature  $T_c$  upon charging and the change in transferred hyperfine field.

In most of the compounds investigated by means of  $^{57}\text{Fe}$  Mössbauer spectroscopy the  $\text{H}_2$  uptake was found to be accompanied by a marked change of the isomer shift (IS). In all cases the IS in the hydrides takes more positive values than in uncharged compounds. These changes of the IS in the positive direction were found in quite a number of compounds. The IS data collected in table 10 may serve to illustrate this behaviour. To permit a quick comparison between the various data we have transformed the IS values reported into values relative to  $\alpha\text{-Fe}$ .

It can be seen in table 10 that in all cases the IS values are shifted to more positive values. It was assumed on several occasions that the change of the isomer shift upon charging is a result of the volume expansion associated with the  $\text{H}_2$  uptake. In order to separate out this volume effect we will first briefly discuss the effect of  $\Delta V/V$  on



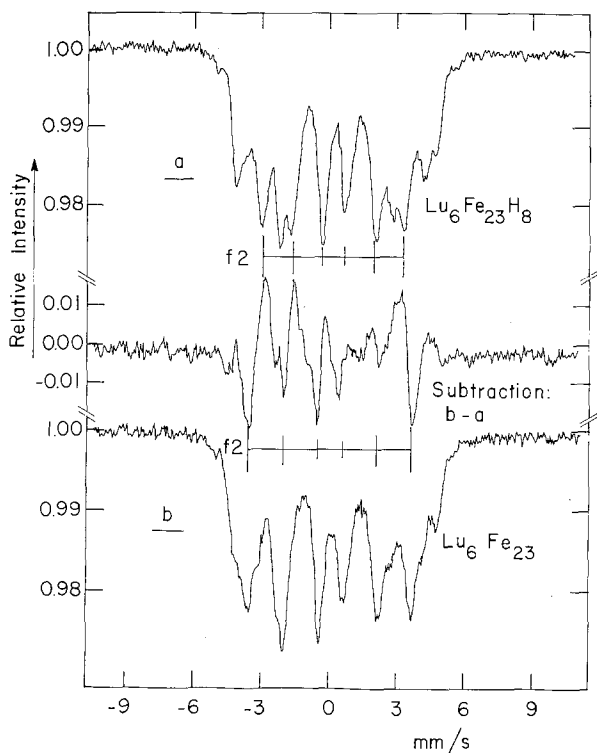


Fig. 35.  $^{57}\text{Fe}$  Mössbauer effect measured at 80 K by Gubbens et al. (1981) on  $\text{Lu}_6\text{Fe}_{23}$  and its hydride  $\text{Lu}_6\text{Fe}_{23}\text{H}_8$ . The subspectra of the  $f_2$  type Fe sites are obtained by subtraction of the two subspectra (middle part). This indicates that hydrogen absorption leads mainly to the filling of the  $32f_3$  tetrahedral hole, formed by three Lu atoms and one Fe atom.

TABLE 10

The  $^{57}\text{Fe}$  isomer shift observed in several intermetallic compounds (in  $\text{mm s}^{-1}$  relative to  $\alpha\text{-Fe}$ ) before and after charging with  $\text{H}_2$  gas.

Hydride	$x$	$\Delta V/V$	IS( $x \neq 0$ )	IS( $x = 0$ )	References
$\text{Hf}_2\text{FeH}_x$	3	0.2	+0.28	-0.12	Buschow and van Diepen (1979)
$\text{TiFeH}_x$	1.7	0.2	+0.27	-0.14	Swartzendruber et al. (1976)
$\text{ScFe}_2\text{H}_x$	2	0.2	+0.19	-0.18	Smit and Buschow (1980)
$\text{YFe}_2\text{H}_x$	4	0.2	+0.32	-0.12	Buschow and van Diepen (1979)
$\text{LuFe}_2\text{H}_x$	4	0.2	+0.25	-0.11	Buschow et al. (1980)
$\text{ErFe}_2\text{H}_x$	3.65	0.25	+0.31	-0.14	Viccaro et al. (1979a)
$\text{Th}_7\text{Fe}_3\text{H}_x$	14.2	0.3	+0.08	-0.22	Viccaro et al. (1979c)
$\text{ThFe}_3\text{H}_x$	2	-	+0.37	-0.16	van Diepen and Buschow (1977)

the isomer shift. Using the data in the review published by Kalvius et al. (1974), an estimate of this effect can be obtained, showing that an increase in volume of 10% leads to a change of IS of  $0.15 \text{ mm s}^{-1}$  in the positive direction. Taking account of the  $\Delta V/V$  values listed in table 10, the volume correction of IS would nearly be equal to  $+0.4 \text{ mm s}^{-1}$ . There are some doubts, however, as to whether one is justified in applying such a volume correction. The increase in volume accompanying the hydrogen absorption is mainly a result of the additional space required by the H atoms when they are accommodated in the lattice. The hydride can, in fact, be regarded as a ternary intermetallic compound, hydrogen being one of the three components. If more space became available to the Fe atoms after  $\text{H}_2$  uptake, it would at best be only a small fraction of  $\Delta V/V$ . The volume effect can therefore better be left out of consideration.

The data listed by Walker et al. (1961) can be used for a further interpretation of the changes in isomer shift. At the top in fig. 36 are indicated the changes in IS expected to follow the removal of one 3d electron and one 4s electron. The small positive change of IS observed is indicated in the middle part of the figure. It would correspond to an *increase* in d character of about 0.4 electron. However, in order to explain the changes of the Fe moment,  $\Delta\mu_{\text{Fe}}$ , in  $\text{ScFe}_2$  and  $\text{Hf}_2\text{Fe}$  a *decrease* in 3d electron character is required which is of the order of 1 electron per Fe atom. As indicated in the bottom part of fig. 36, this large decrease in 3d character would only be compatible with the change observed for IS if simultaneously there were a reduction in s character of at least the same order of magnitude. The total amount of charge transferred from the Fe atoms, in for instance  $\text{ScFe}_2\text{H}_2$ , would then be more

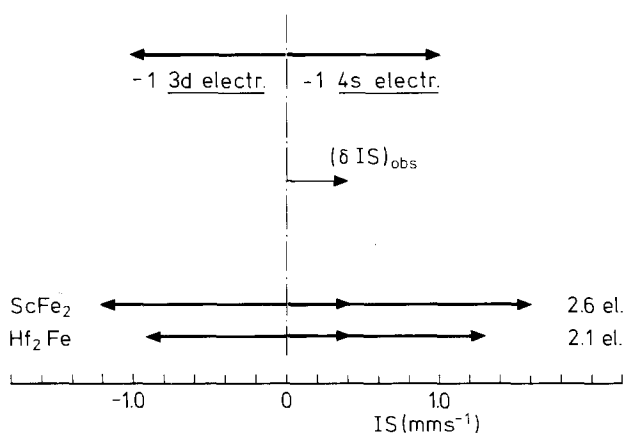


Fig. 36. Schematic representation of the effect on the  $^{57}\text{Fe}$  isomer shift upon removal of one 3d electron or one 4s electron per Fe atom (top part). The experimentally observed IS change is indicated in the middle part. The bottom part (left-hand side) shows the IS change expected on the basis of 3d electron removal as estimated from the 3d moment increase upon charging of  $\text{ScFe}_2$  and  $\text{Hf}_2\text{Fe}$ . (This is a lower minimum since the 3d band depletion will probably involve majority as well as minority spin subbands.) The bottom right-hand side indicates the simultaneous removal of 4s electrons in order to make the combined effect of 3d and 4s electrons equal to the experimental value. The corresponding total number of 3d + 4s electrons that would have to be removed by charge transfer effects is indicated on the extreme right-hand side. For more details see text.

than two electrons per Fe (or H) atom. It is clear that this is an unrealistically high number. Similar arguments refuting the existence of large charge transfer effects between Fe and H atoms can be presented by using the results of an analysis of the isomer shifts in compounds and alloys of Fe given by van der Kraan and Buschow (1982). These authors used an extension of the model of Miedema and van der Woude (1980) to show that in a wide class of different Fe-base materials  $A_{1-x}Fe_x$  the various contributions to IS can be given by means of the expression

$$\delta(\text{IS})_{\text{max}} = 1.0 \Delta\phi^* - 2.2 \Delta n_{\text{ws}}/n_{\text{ws}} + R, \quad (18)$$

where  $\delta(\text{IS})_{\text{max}}$  represents the isomer shift in  $\text{mm s}^{-1}$  relative to  $\alpha\text{-Fe}$  when the Fe atoms have exclusively A atoms as nearest neighbours. The quantities  $\Delta\phi^* = \phi_A^* - \phi_B^*$  and  $\Delta n_{\text{ws}} = n_{\text{ws}}^A - n_{\text{ws}}^{\text{Fe}}$  are the electronegativity difference and difference in electron density at the Wigner-Seitz atomic cell boundary, respectively (see section 2.1 for more details). The first term on the right-hand side of eq. (18) is the charge transfer term. The second term describes the intra-atomic s-d conversion. The third term accounts for effects of hybridization of the Fe 3d band states with the s,p band states of polyvalent non-transition metals. For simple metals and transition metals the  $R$  term is absent as it is in the present class of materials. A difference in electronegativity  $\phi_A^* - \phi_B^* = -1\text{V}$  corresponds to the transfer of 0.5 electron to Fe and an associated change in isomer shift of  $-2\text{ mm s}^{-1}$ .

In view of the smallness of the electronegativity difference between H and Fe ( $\Delta\phi^* = 5.0\text{--}4.93\text{ V}$ ) one expects almost no charge transfer between Fe and H and hence no significant charge transfer contribution to the isomer shift. A small positive contribution is expected on the basis of the  $\Delta n_{\text{ws}}$  term in eq. (18). In a more detailed approach one has to take into consideration that upon formation of the ternary hydride of, for instance,  $\text{Th}_7\text{Fe}_3$  part of the contact area between Fe and Th will be lost in favour of the Fe-H contact area. This means that one has to subtract part of the Fe-Th contributions from the isomer shift and add the Fe-H contribution. The results are summarized in table 11. According to these calculations one expects a change in isomer shift from  $-0.26\text{ mm s}^{-1}$  in uncharged  $\text{Th}_7\text{Fe}_3$  to  $+0.09\text{ mm s}^{-1}$  in  $\text{Th}_7\text{Fe}_3\text{H}_{14}$ . These results compare favourably with the data obtained by Viccaro et al. (see table 11). There is some ambiguity in these calculations regarding the

TABLE 11

Analysis of the isomer shift in  $\text{Th}_7\text{Fe}_3$  and its hydride in terms of eq. (18) (van der Kraan and Buschow, 1982). The values for  $\Delta\phi^*$  and  $\Delta n_{\text{ws}}$  are derived from the tables of Miedema (1973) and Miedema et al. (1980).

Contact area	$\Delta\phi^*$	$\Delta n_{\text{ws}}$	$1.0 \Delta\phi^*$	$-2.2 \Delta n_{\text{ws}}/n_{\text{ws}}^{\text{Fe}}$	$\delta(\text{IS})_{\text{max}}^{\text{calc}}$
100% Fe-Th	-1.63	-3.45	-1.63	+1.37	-0.26
100% Fe-H	+0.07	-0.95	+0.07	+0.38	+0.44
50% Fe-Th } 50% Fe-H }	—	—	—	—	+0.09

relative distribution of the contact area between Fe and Th and Fe and H in  $\text{Th}_7\text{Fe}_3\text{H}_{14}$ . Since this hydride is not yet fully charged (Schlapbach, 1982) it was assumed that some part of the Fe-Th contact area has still remained intact. We choose 50% more or less deliberately. The choice of a different partitioning will not, however, change the essence of the analysis, showing that the isomer shift changes from negative to positive upon charging.

#### 5.2.4. Mn compounds

In the Mn compounds, too, the changes in magnetic properties occurring when hydrogen is absorbed by rare earth manganese compounds are quite spectacular (Buschow, 1977a, b; Buschow and Sherwood, 1977a, b). As seen in figs. 37 and 38, these entail changes from paramagnetism to ferromagnetism as well as changes in the opposite direction. Like  $\text{ScMn}_2$  the compounds  $\text{LuMn}_2$ ,  $\text{YMn}_2$ ,  $\text{ZrMn}_2$  and  $\text{TiMn}_{1.2}$  are paramagnetic. In these cases, too, ferromagnetism is observed after hydrogen uptake (Buschow and Sherwood, 1977a, b; Jacob et al., 1980b; Hempelman and Hilscher, 1980; van Essen and Buschow, 1980a).

In several of these compounds it was found that the temperature dependence of the magnetization gives rise to a broad maximum below the magnetic ordering temperature ( $T_c$ ) when the samples, before the magnetization measurements, were cooled to 4.2 K without the presence of a magnetic field. A more or less normal ferromagnetic type of  $\sigma$  versus  $T$  behaviour was obtained, when the samples, prior to the measurements, were cooled to 4.2 K in the presence of a magnetic field. The presence of such features in the temperature dependence of the magnetization are quite well known in systems in which the atoms that carry the magnetic moment have a partial crystallographic disorder (Kouvel, 1961; Beck, 1972).

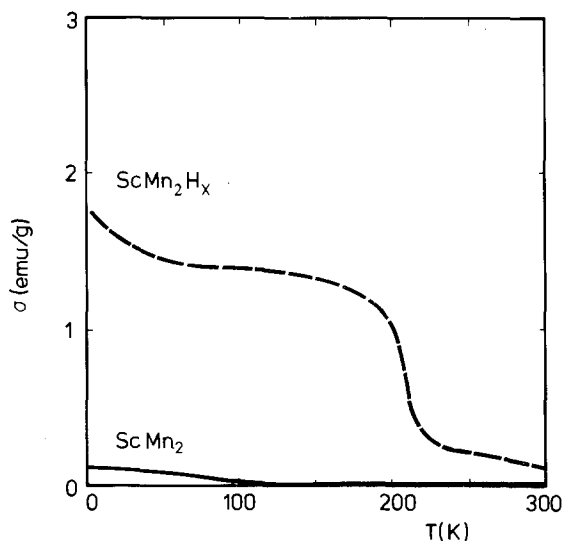


Fig. 37. Temperature dependence of the magnetization in  $\text{ScMn}_2$  (full line) and its hydride (broken line) measured in a field of 3 kOe (after Buschow, 1982a).

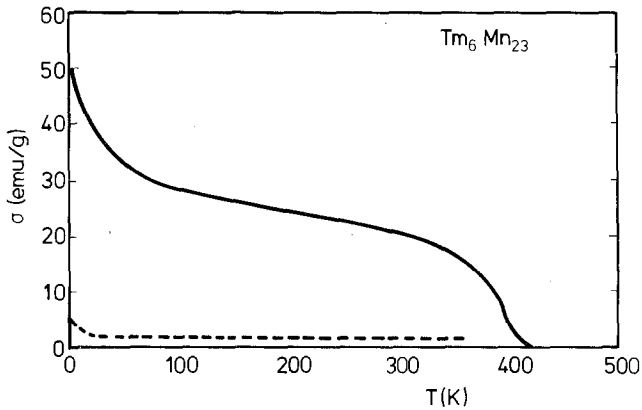


Fig. 38. Temperature dependence of the magnetization in  $Tm_6Mn_{23}$  (full line) and  $Tm_6Mn_{23}H_x$  (broken line) measured in a field of 3 kOe (after Gubbens et al., 1982).

We note that it was found by means of X-ray diffraction that long-range order remains intact after hydrogen uptake. Indications of the presence of local atomic disorder were obtained from some broadening of the reflection lines observed in the X-ray diagrams of the hydrides of  $Y Mn_2$  and  $Lu Mn_2$ . In regions where the atomic disordering is relatively high, ferromagnetic ordering can be lost. The difference in magnetic coupling of the Mn moments located in these regions with those located in the ferromagnetic regions may be responsible for the peculiar  $\sigma$  versus  $T$  behaviour observed. More details regarding this point can be found in the paper by Buschow and Sherwood (1977b).

Pronounced changes in magnetic behaviour, such as the ferromagnetic-paramagnetic transitions and vice versa mentioned above, are not observed in all the R-Mn compounds. For instance the compound  $Th Mn_2$  remains paramagnetic. In these compounds the changes in magnetic properties are only gradual ones (Buschow and Sherwood, 1977b).

Inspection of all of the magnetic data found in the literature on R-Mn compounds and the corresponding ternary hydrides shows that the presence or absence of a magnetic moment on the Mn atoms seems not to be correlated with the presence or absence of hydrogen. It was proposed that a correlation might exist between the presence of a Mn moment and a critical distance between the nearest neighbour Mn atoms (Buschow, 1978). Neutron diffraction studies made on  $Y_6 Mn_{23}$  (Delapalme et al. 1979) and its hydride (Commandré et al., 1979) do not seem to support this view. These studies showed that the magnetic structure entails many different Mn-Mn interactions and the definition of a critical Mn-Mn distance is at best an oversimplification. Nevertheless there are many experimental results (see table A9) showing that hydrogen absorption in paramagnetic Mn compounds leads to the creation of ferromagnetic behaviour. Continued hydrogen absorption further enhances the ferromagnetic properties, while at still higher hydrogen concentrations the ferromagnetism is lost again. Such features were observed for instance in  $Y Mn_2 H_x$  (Buschow and Sherwood, 1977b) and in  $Zr Mn_2 H_x$  (Jacob et al., 1980b). It should

be noted that in terms of a local moment description, and assuming the persistence of magnetic moments, the disappearance of the magnetization in hydrides with a relatively large separation between the Mn atoms could equally well be ascribed to the creation of antiferromagnetic order or to a breaking down of the magnetic coupling between the Mn moments as a consequence of a too large interatomic separation between the Mn atoms.

The hydrogen-induced loss of ferromagnetism in some  $R_6Mn_3$  compounds and the creation of ferromagnetism in others was explained by Wallace (1979) in quite a different way. Wallace assumed that the exchange interaction between the magnetic moment depends strongly on the electron concentration and based his explanation on results of a molecular field analysis of  $Er_6(Mn_{1-x}Fe_x)_{23}$  pseudo-binaries by Hilscher and Rais (1978). This explanation does not seem to be wholly satisfactory if one includes all the available experimental data on  $R_6Mn_{23}$  and  $R_6Fe_{23}$  compounds and their hydrides (Buschow et al., 1982). The assumption that the Mn atoms become non-magnetic after  $H_2$  absorption in  $Y_6Mn_{23}$  was made by several authors (Buschow, 1977; Malik et al., 1977b; Oesterreicher and Bittner, 1977). There are indications that this assumption is not wholly justified. Experimental results obtained by Commandré et al. (1979) are shown in fig. 39. It can be seen that hydrogen absorption leads ultimately to a strong reduction in magnetization, which indeed suggests the disappearance of the Mn magnetic moments. Closer inspection of the data shows, however, that there is a step-like change in the magnetization near 160 K. A similar discontinuity can also be found in the data of Malik et al. (1977b). Stewart et al. (1981a) reinvestigated the magnetic properties of the hydride of  $Y_6Mn_{23}$  and supplemented their results by performing Mössbauer spectroscopy on samples of

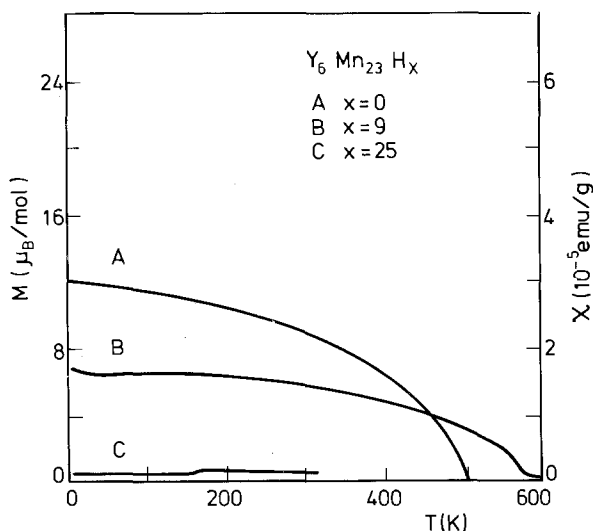


Fig. 39. Temperature dependence of the magnetization in  $Y_6Mn_{23}$  (A) and its hydride  $Y_6Mn_{23}H_9$  (B) (left-hand scale). The susceptibility of  $Y_6Mn_{23}H_{25}$  (C) is given on the right-hand scale (after Commandré et al., 1979).

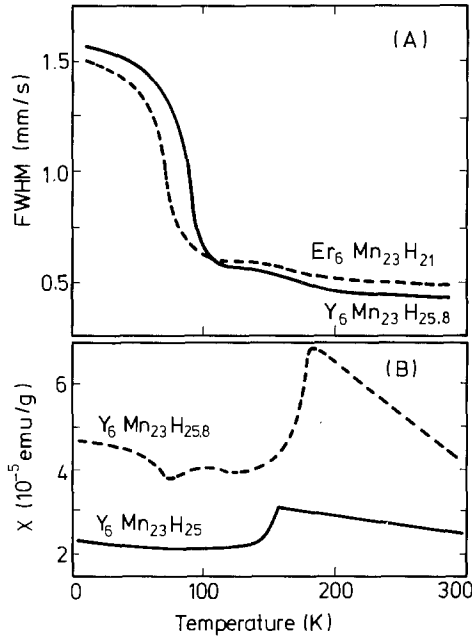


Fig. 40. Top part: Temperature dependence of the line width observed by means of  $^{57}\text{Fe}$  Mössbauer spectroscopy in  $Y_6\text{Mn}_{23}\text{H}_{25.8}$  (full line) and  $Er_6\text{Mn}_{23}\text{H}_{21}$  (broken line). Both results were obtained on samples doped with Fe (0.5%). Bottom part: Temperature dependence of the magnetization in  $Y_6\text{Mn}_{23}\text{H}_{25.8}$  mentioned above (broken line) and temperature dependence of the magnetization in  $Y_6\text{Mn}_{23}\text{H}_{25}$  (full line). The results reproduced in this figure were taken from data published by Stewart et al. (1981a).

$Y_6\text{Mn}_{23}$  and its hydride doped with traces of  $^{57}\text{Fe}$ (0.5%). The results of these authors' magnetic measurements and those of Malik et al. are reproduced in the lower part of fig. 40. Results of Mössbauer spectroscopy on Fe-doped  $Y_6\text{Mn}_{23}\text{H}_{25.8}$  are shown in the top part of the figure. The results show that below about 110 K a small magnetic splitting develops on the Fe nuclei. These results were interpreted by Stewart et al. as indicating the antiferromagnetic ordering to be present in the hydrides at low temperatures. It was mentioned by Buschow (1981) that the intensity of the cusp-like peak that marks the antiferromagnetic ordering in the hydride might depend on the amount of hydrogen absorbed (as measured by the relative volume expansion  $\Delta V/V$  after charging).

In this connection it is worth recalling that the comparison of the lattice constants of the various  $R_6\text{Mn}_{23}$  compounds and their ternary hydrides has indicated that the relative amount of  $\text{H}_2$  absorbed and/or the relative volume change associated with it, decreases in going from the light to the heavy lanthanides (see section 5.1). Here, too, no ordering of the Mn sublattice shows up in the  $\sigma(T)$  curve when  $\Delta V/V$  is comparatively small (as in  $\text{Tm}_6\text{Mn}_{23}\text{H}_x$ , see fig. 38). On the other hand, when  $\Delta V/V$  is comparatively large (as in  $\text{Nd}_6\text{Mn}_{23}\text{H}_x$  and  $\text{Sm}_6\text{Mn}_{23}\text{H}_x$ ) magnetic ordering of the Mn sublattice shows up in the  $\sigma(T)$  curve as a strong increase of the magnetization (fig. 41).

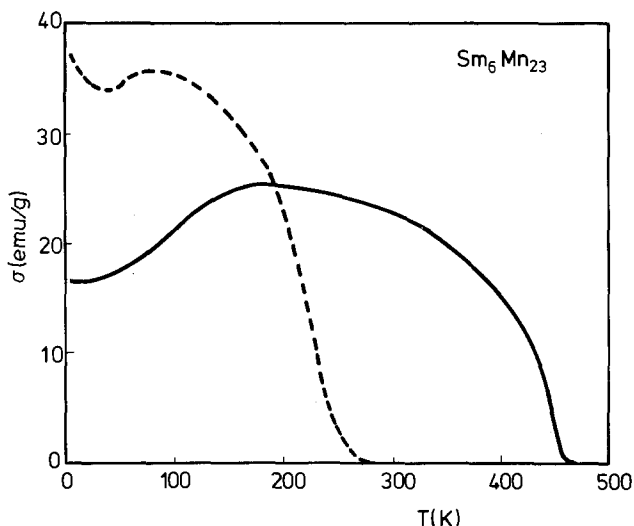


Fig. 41. Temperature dependence of the magnetization in  $\text{Sm}_6\text{Mn}_{23}$  (full line) and its hydride (broken line).

#### 5.2.5. Compounds with a magnetic rare earth component

The results arrived at from bulk magnetization measurements on hydrides of rare earth 3d intermetallics in which both the 4f atoms and the 3d atoms are magnetic are in general less conclusive (Kuijpers, 1973; Zijlstra and Westendorp, 1969; Maartense, 1973; Buschow and Sherwood, 1977b; Buschow, 1977d; Malik et al., 1978b; Pourarian et al., 1982b).

The compounds in which the rare earth component consists of Gd (having no orbital momentum) are the most favourable to study, since, in the interpretation of the magnetic data, one is not hampered by uncertainties associated with the moment reduction due to changes in the crystalline electric fields upon charging. Changes in magnetic properties due to hydrogen absorption have been studied in relatively few Gd compounds in which the M component in  $\text{RM}_n$  has no magnetic moment. It can be seen from the data collected in table A10 that the hydrogen absorption can result in a decrease of the paramagnetic Curie temperature as well as in an increase. In all cases a reduction of the saturation moment is observed. Changes of the gadolinium 4f moment itself upon charging can safely be excluded. The rather low values of the saturation moments observed may therefore point to deviations from collinear ferromagnetic ordering. The hydrogenation reaction can lead to some disorder among the metal atoms, so that there will be Gd sites where the coupling is no longer ferromagnetic. Even if the atomic order of the metal atoms is preserved after charging, there will be a distribution of the H atoms over the various sites available. This leads to concentration fluctuations of H atoms over a few atomic distances. On an atomic scale the electron concentration may therefore differ from one Gd site to the other, so that one may expect changes in the magnitude and sign of the local magnetic coupling strength.



The atomic disorder mentioned above will affect the sharpness of the magnetic transition at  $T_c$ . When atomic disorder is present the magnetic order-disorder transition will be smeared out appreciably. Even in the absence of atomic disorder, the introduction of hydrogen leads to substantial changes in the electronic properties of the compound which will affect sign and magnitude of the magnetic coupling. If this coupling proceeds by means of an indirect exchange interaction via polarization of the s conduction electrons (RKKY-type coupling, see section 2.2) the increase of the lattice parameters ( $\Delta a$ ) and the changes in s conduction electron concentration ( $\Delta k_F$ ) can bring about a decrease or an increase of the asymptotic Curie temperature  $\theta_p$ . An example of a decrease of  $\theta_p$  after charging was found in  $\text{GdRh}_2$  (Jacob et al., 1980c). The opposite effect was found in  $\text{GdCu}_2$  (de Graaf et al., 1982b). It is also possible that the coupling not only changes its magnitude but reverses its sign. Experimental evidence for a change from antiferromagnetism to ferromagnetism was observed in  $\text{GdAg}$  (Buschow, 1982c). In uncharged condition  $\text{GdAg}$  is an antiferromagnet ( $T_N = 143 \text{ K}$ ) with a strongly negative asymptotic Curie temperature ( $\theta_p = -57 \text{ K}$ ). The magnetic properties observed after charging have been reproduced in fig. 42. It is seen that the antiferromagnetic properties have disappeared. The (average) magnetic coupling is of the ferromagnetic type ( $\theta_p = +50 \text{ K}$ ). The change in  $\theta_p$  is extremely large and extends over more than 100 K.

There is one more effect which has to be taken into consideration. The RKKY-type interaction is of fairly long range. Even if atomic order of the metal atoms were preserved, the non-uniform spatial distribution of H atoms would lead to an enhanced scattering of the conduction electrons and hence to a decrease of the mean free path. It can be shown (de Gennes, 1962b) that this leads to a damping of the RKKY oscillations shown in fig. 6. This damping implies an effective decrease of the range of the interaction and tends to decrease the overall coupling strengths. This

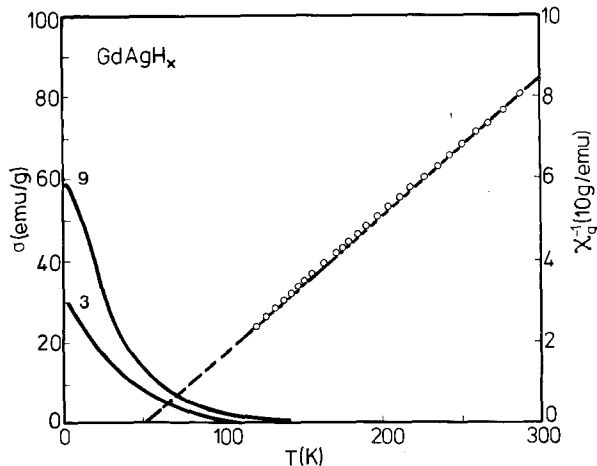


Fig. 42. Temperature dependence of the magnetization ( $\sigma$ , left-hand scale,  $H = 3$  and  $9 \text{ kOe}$ ) and temperature dependence of the reciprocal susceptibility ( $\chi^{-1}$ , right-hand scale) observed in  $\text{GdAgH}_x$  (Buschow, 1982c).

effect may counteract, or even overcompensate, a possible increase of  $\theta_p$  due to the effect of  $\Delta a$  and/or  $\Delta k_F$ .

The reduction in mean free path of the conduction electrons is probably also the reason for the weakening of the coupling strengths between the 4f and 3d moments in compounds where both the 3d and 4f atoms carry a magnetic moment. As an example one might consider the changes observed in the compound  $\text{GdCo}_2$  (listed in table A7). In this compound and its hydride the 4f–4f exchange interactions will not differ much from those in  $\text{GdNi}_2$  and its hydride. The large Curie temperature in  $\text{GdCo}_2$  is mainly due to the Gd–Co interaction, which leads to the formation of a magnetic moment on the Co atoms. (Note that  $\text{YCo}_2$  is paramagnetic.) After  $\text{H}_2$  uptake the Gd–Co interaction is reduced, which results in a large decrease of the ordering temperature (Buschow, 1977b). Similar changes take place in other members of the  $\text{RCO}_2$  series. The results obtained by means of magnetic measurements on  $\text{PrCo}_2$  are shown in fig. 43. Owing to the reduced Pr–Co exchange interaction the ferromagnetic properties, giving rise to a Curie temperature near 50 K, are seen to be lost after charging (de Jongh et al., 1981). Here we recall that it is often difficult to determine the intrinsic magnetic properties of the ternary hydrides owing to the decomposition of the ternary hydride and Co cluster formation. A reduction of the R–Co coupling strength was also observed in  $\text{GdCo}_3\text{H}_x$  and other members of the  $\text{RCO}_3\text{H}_x$  family (Malik et al., 1978b). In the  $\text{RCO}_3$  compounds the Co atoms have a magnetic moment even in the absence of the R–Co exchange interaction ( $\text{YCo}_3$ , unlike  $\text{YCo}_2$ , is ferromagnetic). In the  $\text{RCO}_3$  compounds, therefore, a large effect already results from the disappearance of the Co moments upon charging with hydrogen. This is illustrated by means of the results of Malik et al. (1978b) shown in fig. 44. Here one has to consider that the Co moments are coupled antiparallel

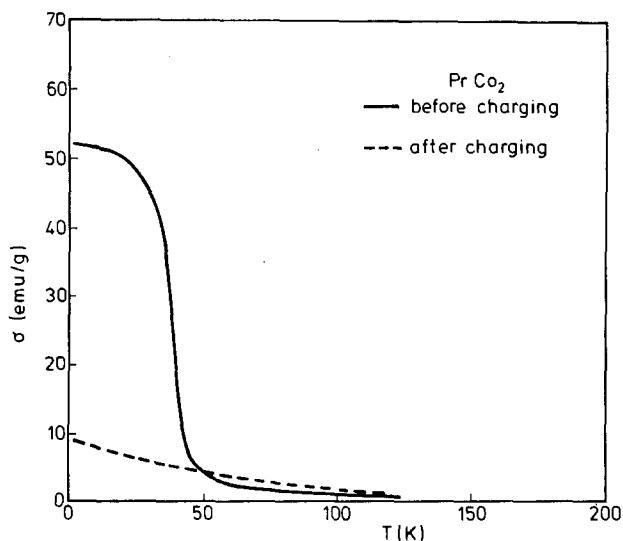


Fig. 43. Temperature dependence of the magnetization in  $\text{PrCo}_2$  before charging (full line) and after charging (broken line). Results are reproduced from the data published by de Jongh et al. (1981).

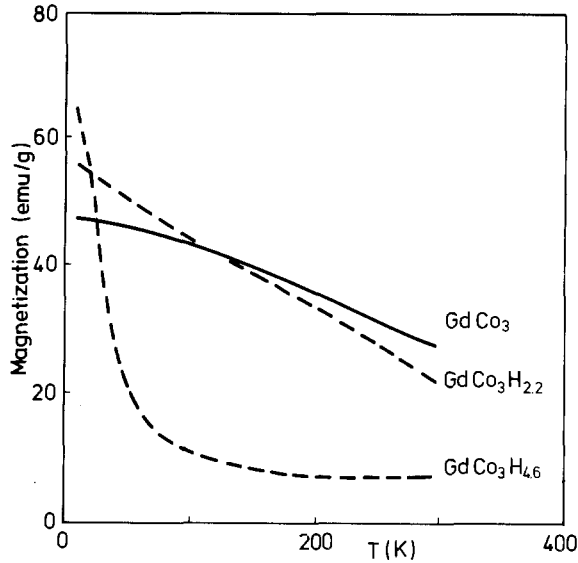


Fig. 44. Temperature dependence of the magnetization (21 kOe) in  $\text{GdCo}_3$  and its hydrides (after Malik et al., 1978b).

to the Gd moments. More conclusive evidence of a decreasing 4f–3d interaction was obtained by Niarchos et al. (1980b) in an investigation where magnetic measurements were combined with  $^{161}\text{Dy}$  and  $^{57}\text{Fe}$  Mössbauer spectroscopy. Three different hydride phases of  $\text{DyFe}_3\text{H}_x$  were studied. The temperature dependences of the magnetization of these phases and of uncharged  $\text{DyFe}_3$  are shown in fig. 45. In all these materials the  $\sigma(T)$  curves give rise to compensation temperatures (see also section 2.2). In uncharged  $\text{DyFe}_3$   $T_{\text{comp}}$  is above room temperature. It can be seen from the figure that the values of  $T_{\text{comp}}$  decrease with increasing  $x$ . Niarchos et al. showed that the Dy moment corresponds to the  $|\pm 15/2\rangle$  doublet state and does not change much with  $x$ . Qualitatively the decrease of  $T_{\text{comp}}$  with  $x$  in  $\text{DyFe}_3\text{H}_x$  can then be understood in terms of a molecular field approach (mentioned in section 2.2.3) where  $T_{\text{comp}}$  is given by expression (4). The value of  $\theta$  in expression (4), which measures the Dy–Dy coupling strength, can be derived from the magnetic properties of  $\text{DyNi}_3$  in which compound the Dy–Dy coupling is predominant. In  $\text{DyNi}_3$  the value of  $\theta$  is small (69 K), and therefore it may be concluded that a possible reduction of  $\theta$  with  $x$  is not able to account for the observed decrease of  $T_{\text{comp}}$ . Since  $J$  and  $g$  do not change either, this means that the decrease of  $T_{\text{comp}}$  originates from a corresponding decrease of the 3d–4f exchange interaction. It can be seen in fig. 46 that there is a linear relationship between  $T_{\text{comp}}$  and  $\Delta V$ . This led Niarchos et al. to suggest that the reduction of the 3d–4f exchange coupling is primarily a result of the lattice expansion.

Further experimental evidence for a gross decoupling of the rare earth and 3d sublattice magnetizations was obtained from  $^{166}\text{Er}$  and  $^{57}\text{Fe}$  Mössbauer effect spectroscopy in  $\text{ErFe}_2\text{H}_x$  (Viccaro et al., 1979a, b; Dunlap et al., 1979) and from  $^{166}\text{Er}$  and  $^{161}\text{Dy}$  Mössbauer spectroscopy in  $\text{ErMn}_2$  (Viccaro et al., 1980) and  $\text{DyMn}_2$

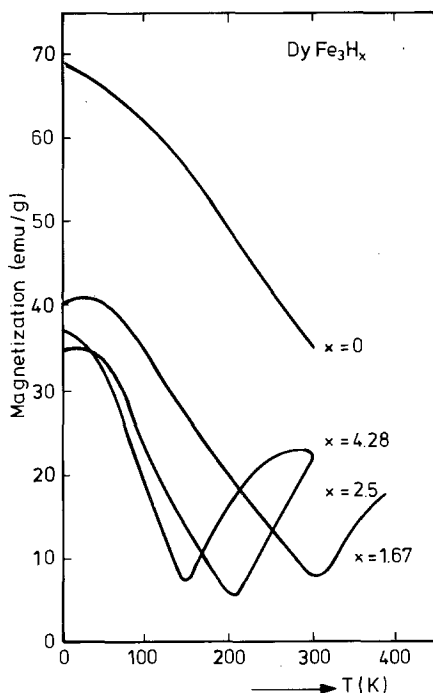


Fig. 45. Temperature dependence of the magnetization in  $\text{DyFe}_3$  and its hydrides (after Niarchos et al., 1980b).

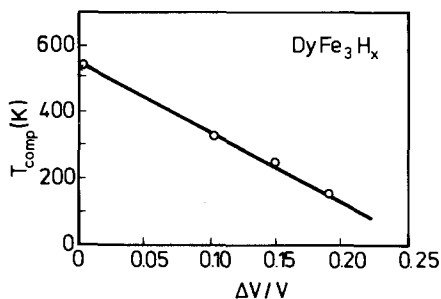


Fig. 46. Dependence of the compensation temperatures observed in  $\text{DyFe}_3\text{H}_x$  on the corresponding volume expansions  $\Delta V/V$  (after Niarchos et al., 1980b).

(Gubbens et al., 1983). Similar information was obtained from neutron scattering experiments (Fish et al., 1979). Results of these latter experiments are shown in fig. 47. It seems as if the Er sublattice becomes magnetically ordered more or less independently from the Fe sublattice.

Of all the ternary hydrides in which the 4f as well as the 3d atoms carry a magnetic moment, those of the type  $\text{R}_6\text{Mn}_{23}\text{H}_x$  seem to be of unusually complex behaviour. Pourarian et al. (1980a, b) performed magnetization measurements on various

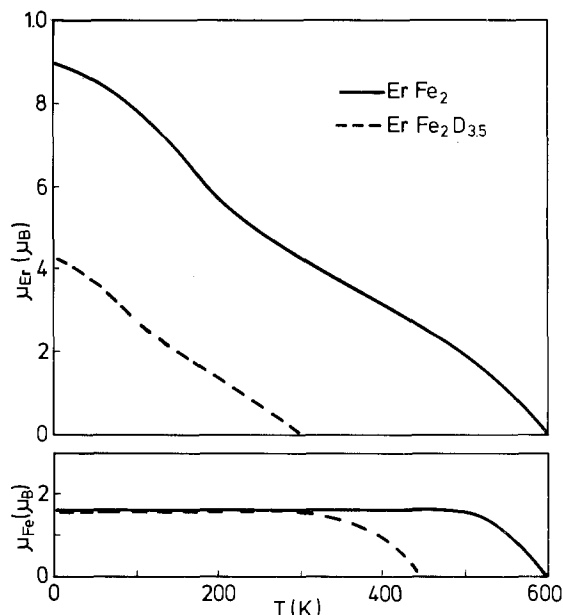


Fig. 47. Temperature dependence of the Er and Fe sublattice moments in  $\text{ErFe}_2$  and  $\text{ErFe}_2\text{D}_{3.5}$  as derived from neutron diffraction measurements by Fish et al. (1979).

$\text{R}_6\text{Mn}_{23}$  compounds and their hydrides. They conclude that hydrogenation leads to a non-magnetic Mn sublattice. Definite magnetic transitions were reported to occur only for  $\text{R} = \text{Tb}$  and  $\text{Gd}$  and were ascribed to the R-R coupling. The hydrides of  $\text{R}_6\text{Mn}_{23}$  with  $\text{R} = \text{Dy}$ ,  $\text{Ho}$  and  $\text{Er}$  appear to remain paramagnetic down to 4.2 K. The R-R interaction was assumed by Pourarian et al. to be of the RKKY type, where the Curie temperatures vary as  $T_c \propto J_s^2(g-1)^2J(J+1)$ ; the absence of magnetic ordering in  $\text{R}_6\text{Mn}_{23}$  for R having a higher atomic number than Tb could then be understood as being a logical consequence of the strong decrease of the de Gennes factor for R elements beyond Tb. As a second alternative Pourarian et al. propose antiferromagnetic ordering in the hydrides involving Dy, Ho and Er. This seems incompatible, however, with the first assumption (i.e. the presence of an RKKY-type interaction), since the RKKY interaction does not involve a sign reversal within a series of isotopic compounds. Mössbauer spectroscopy performed by other authors on various  $\text{R}_6\text{Mn}_{23}$  compounds and their hydrides showed that the situation is more complex than bulk magnetic measurements would suggest.  $^{57}\text{Fe}$  Mössbauer spectroscopy performed on  $\text{Er}_6\text{Mn}_{23}\text{H}_{21}$  doped with traces of  $^{57}\text{Fe}$  provided additional support for the conclusions reached already on the basis of Mössbauer spectroscopy on doped  $\text{Y}_6\text{Mn}_{23}\text{H}_{25}$ , namely that the Mn sublattice gives rise to magnetic ordering in the range below about 100 K. This refutes the assumption of a nonmagnetic Mn sublattice. The results obtained on  $\text{Er}_6\text{Mn}_{23}\text{H}_{21}$  have been included in fig. 40. From results of Mössbauer spectroscopy involving the isotopes  $^{161}\text{Dy}$ ,  $^{166}\text{Er}$  and  $^{169}\text{Tm}$  in the corresponding  $\text{R}_6\text{Mn}_{23}$  compounds and their hydrides one might conclude that in all cases a magnetically ordered R sublattice is present at 4.2 K (Stewart et al.,

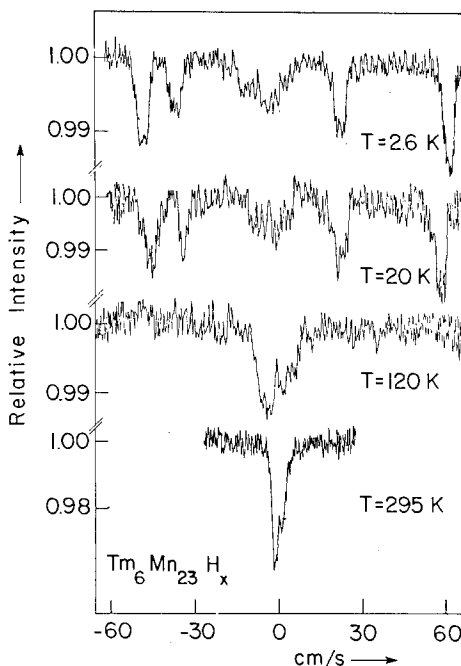


Fig. 48.  $^{169}\text{Tm}$  Mössbauer spectra of  $\text{Tm}_6\text{Mn}_{23}\text{H}_x$  measured at various temperatures (after Gubbens et al., 1983a).

1981b; Buschow et al., 1982b; Gubbens et al., 1983a). The R moments are not quenched but have values which are not far from those of the free  $\text{R}^{3+}$  ions. Detailed studies of the temperature dependences of the  $^{169}\text{Tm}$  hyperfine splitting and the quadrupolar splitting in  $\text{Tm}_6\text{Mn}_{23}\text{H}_x$  showed that an exchange field is exerted on the Tm moment up to temperatures at least as high as 50 K. Examples of a few  $^{169}\text{Tm}$  Mössbauer spectra are shown in fig. 48. It is not clear whether these splittings are a result of the R–R or the R–Mn interaction. In conjunction with the rather low bulk magnetization (see for instance the results shown in fig. 38) it follows that the magnetic structure of the R sublattice is not ferromagnetic with all the R spins pointing in the same direction. Several possibilities can be mentioned comprising antiferromagnetism, a spin-glass like arrangement, or ferromagnetic clusters that are coupled more or less antiparallel. It would appear from the experimental data available at present that the magnetic properties of the hydrides  $\text{R}_6\text{Mn}_{23}\text{H}_x$  are even more complex in nature than those of the parent compounds. Here we recall that it was shown in section 5.1 that the differences in lattice expansion through the  $\text{R}_6\text{Mn}_{23}$  series suggest differences in H concentration. This forms an additional complication.

The Mössbauer effect investigations have not only proved helpful in investigations of changes in the coupling strength; they have also provided conclusive information on the changes in Fe moment upon hydrogenation. Results of the  $^{57}\text{Fe}$  Mössbauer spectroscopy in  $\text{ErFe}_2\text{H}_x$  obtained by Dunlap et al. (1980) are schematically

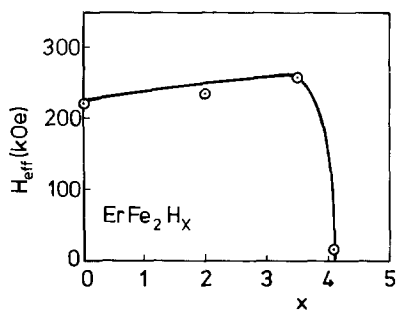


Fig. 49. Concentration dependence of the  $^{57}\text{Fe}$  Mössbauer hyperfine splitting in various hydrides of the types  $\text{ErFe}_2\text{H}_x$  as derived from the data published by Dunlap et al. (1979).

represented in fig. 49. It follows from these data that continued  $\text{H}_2$  absorption in  $\text{ErFe}_2$  eventually leads to a disappearance of the hyperfine splitting at the Fe nuclei. Assuming that the hyperfine splitting approximately scale to the Fe moments, these results indicate that the Fe moments in  $\text{ErFe}_2\text{H}_x$  first increase with  $x$  but then decrease in such a way that the Fe moments in  $\text{ErFe}_2\text{H}_{4.1}$  have virtually vanished ( $> 0.2 \mu_B$  per Fe compared to  $1.6 \mu_B$  in  $\text{ErFe}_2$ ). Measurements made in the presence of an externally applied magnetic field support this view. In the hydrides  $\text{ErFe}_3\text{H}_x$  a more or less similar situation is found. Niarchos et al. (1979) showed that the Fe moment increases initially but then decreases. In  $\text{ErFe}_3\text{H}_x$  the decrease at the highest  $x$  values is less severe than in the case of  $\text{ErFe}_2\text{H}_x$ .

Niarchos et al. (1980a) investigated the absorption of hydrogen in the pseudo-binary compound  $\text{LaNi}_4\text{Fe}$  and found that the absorption capacity is lower than that of  $\text{LaNi}_5$  ( $\text{LaNi}_4\text{FeH}_{5.2}$ ). At 4.2 K the  $^{57}\text{Fe}$  Mössbauer spectrum of the hydride shows the presence of exchange splitting, from which they infer the presence of an Fe moment equal to  $1.2 \mu_B$ . This is slightly less than in uncharged  $\text{LaNi}_4\text{Fe}$  ( $1.4 \mu_B/\text{Fe}$ ) and might also indicate a change of the Ni moment present in uncharged  $\text{LaNi}_4\text{Fe}$  (Elemans et al., 1975).

Apart from probing the local hyperfine field at the rare earth site, Mössbauer spectroscopy involving isotopes such as  $^{151}\text{Eu}$ ,  $^{155}\text{Gd}$  and  $^{161}\text{Dy}$  can also be employed to study changes in local charge density by means of the isomer shift. Results obtained by Cohen et al. (1980c) in several Laves phase compounds give evidence of a strong decrease of the Dy isomer shift upon charging. This was also observed in  $\text{DyFe}_3\text{H}_x$  by Niarchos et al. (1980b) and in  $\text{Dy}_6\text{Mn}_{23}\text{H}_x$  by Gubbens et al. (1983b). This points to a severe decrease of the s electron charge density at the Dy nucleus. Supplementary experimental evidence of a reduction in s electron density at the rare earth sites comes from  $^{155}\text{Gd}$  and  $^{151}\text{Eu}$  Mössbauer spectroscopy in several  $\text{RX}_2$  compounds and their hydrides (Jacob et al., 1980c; de Graaf et al., 1982b),  $\text{Gd}_{0.1}\text{La}_{0.9}\text{Ni}_5$  and  $\text{Gd}_{0.1}\text{La}_{0.9}\text{Co}_5$  (Bauminger et al., 1977),  $\text{EuPd}$  and  $\text{EuRh}_2$  (Buschow et al., 1977),  $\text{EuNi}_5$  and  $\text{EuMg}_2$  (Oliver et al., 1978) and  $\text{La}_{0.9}\text{Eu}_{0.1}\text{Ni}_{4.6}\text{Mn}_{0.4}$  (Cohen et al., 1980a, b). The results obtained on the  $\text{RX}_2$  compounds and their hydrides are shown in fig. 50, where the isomer shift is plotted versus the corresponding hyperfine field. The total hyperfine field  $H_{\text{hf}}$  is composed of two parts:  $H_{\text{hf}} = H_{\text{cp}} + H_{\text{cep}}$ . The

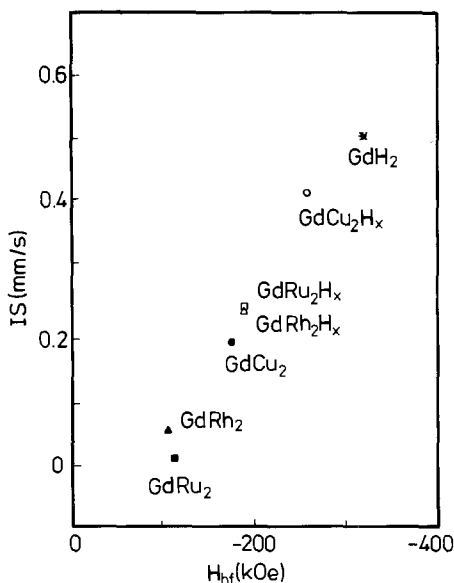


Fig. 50.  $^{155}\text{Gd}$  isomer shift in various  $\text{RX}_2$  compounds and their hydrides plotted versus the corresponding hyperfine fields (after de Graaf et al., 1982b).

core polarization  $H_{cp}$  is negative and equals  $-340$  kOe. The conduction electron polarization  $H_{cep}$  is usually positive. In  $^{155}\text{Gd}$  Mössbauer spectroscopy an increase in isomer shift corresponds to decreasing charge density at the Gd site. The results shown in fig. 50 then show that the decreasing charge density at the Gd site is accompanied by a decrease of the conduction electron polarization  $H_{cep}$ , leaving in  $\text{GdH}_2$  (which is a semimetal) only the contribution due to the core polarization.

#### 5.2.6. Hydrogen bonding, charge transfer and valency changes

This last section on magnetic properties will examine in how far the changes in magnetic properties allow conclusions to be drawn regarding the charge transfer and the bonding of the hydrogen atoms in the ternary hydrides. The many results discussed above make it clear that the most spectacular changes involve the 3d electrons. The 3d band magnetism in metals is still the subject of current experimental and theoretical studies and an analysis of the data presented above in terms of the 3d band model is not free of ambiguity. The same argument as already presented elsewhere will be used (Buschow and de Châtel, 1979) in order to show that some general conclusions can nevertheless be reached.

Malik et al. (1978b) and Wallace (1982) explained the reduction in Co moment after  $\text{H}_2$  uptake as being due to a further depletion of the 3d band. In view of the discussion on 3d band magnetism given in section 2.2.2 this is a very unlikely explanation. The rather large value of  $\mu_{Co}$ , especially in  $\text{LaCo}_5$ , suggests a filled majority (say, spin-up) subband, in which case the depletion of the d band should lead to an increasing moment. One would have to assume a considerable number of



d holes per Co atom to meet the condition  $N(E_F)\uparrow > N(E_F)\downarrow$ , which, according to implication (iii) of the discussion in section 2.2.2. is necessary for the mechanism proposed by Malik et al. to give the desired reduction of  $\mu_{Co}$ . As pointed out in section 2.2.2, the number of d holes is not expected to deviate much in R-Co compounds from its value in pure Co. The low electronegativities of Y and La make an *increased* number of holes especially unlikely in the compounds listed in table 8. If one sticks to explaining the moment changes in terms of charge transfer, one is left with conclusions like the one given by Kuijpers (1973) that the d band must become gradually filled upon  $H_2$  uptake. Here we recall that, as a result of the feedback mechanism mentioned in section 2.2.2, the change in the number of d electrons may actually be somewhat smaller than the change in  $\mu_{Co}/\mu_B$ .

We have seen that hydrogen absorption in Fe compounds, in contradistinction to Co compounds, leads to an increase in 3d moment (see table 9). As the 3d moments quoted in table 9 are generally  $1 \mu_B$  higher than the ones given for  $\mu_{Co}$  in table 8, the same arguments can be used for the Fe compounds as for the Co compounds to show that  $N(E_F)\uparrow < N(E_F)\downarrow$  is more likely to hold than the opposite inequality. Therefore, implication (iii) in section 2.2.2. entails a depletion of the 3d band upon hydrogen absorption. Similar conclusions have been reached before (Wallace, 1982; Malik, 1978a; Buschow and van Diepen, 1976). However, it should be pointed out again that our explanation does not necessitate a charge transfer of d electrons of the order of  $\Delta\mu_{Fe}/\mu_B$ , because of the feedback effect referred to earlier (section 2.2.2). It has already been noted in connection with the analysis of IS in section 5.2.3. that the small positive change in IS implies that the transfer of charge has to be composed of about equal amounts of s and d electrons. If the number of transferred d electrons were significantly below  $\Delta\mu_{Fe}/\mu_B$ , the total number of electrons transferred could reach a magnitude that would be in keeping with the redistribution of charge based on the electronegativity differences between the composing elements (Miedema, 1973). In other words, because of the feedback effect the discrepancy between the large change in  $\mu_{Fe}$ , and the comparatively small change of the corresponding IS is less strong than it seemed initially. Nevertheless it is doubtful whether this reasoning is still applicable in cases where  $\Delta\mu_{Fe}$  becomes of the order of a whole Bohr magneton or more, such as in  $ScFe_2H_x$ .

A further difficulty with explanations based on charge transfer arises if one compares the results obtained in Fe compounds with those in Co compounds. If one wishes to ascribe a decisive role to d-band occupancy changes in the decrease of  $\mu_{Co}$  and in the increase of  $\mu_{Fe}$  upon hydrogen absorption, one has to assume that H donates electrons to the Co 3d band but accepts electrons from the Fe 3d band. Attempts have been made to explain this apparently contradictory situation in terms of electronegativities (Buschow, 1978), the value for metallic H being lower than that of Co and higher than that of Fe (Miedema, 1973). Although the decrease of the Ni moment observed in the meantime in  $YNi_3H_x$  is in keeping with the sequence of electronegativities, the decrease in magnetic susceptibility observed in  $TiFeH_x$  (Stucki and Schlapbach, 1980) does not support the assumption that the H accepts electrons from the Fe 3d band.

It follows from the foregoing discussion that there is more evidence against major

$H \leftrightarrow 3d$  charge transfer effects than there is in favour of it. In terms of the 3d band model there is still the possibility of explaining the changes in magnetic properties in terms of changes of the d-d interaction parameter. In fact, equally convincing arguments can be found for an increase of the interaction parameter upon hydrogen absorption. If Fe is combined with R metals the 3d electrons of the former will mix or hybridize with the d and s, p electrons of the latter and in this way cause a reduction in the d-d interaction parameter and hence a reduction in band splitting. In the hydrides the R-Fe distances are increased and a large part of the R-Fe contacts are lost due to the absorbed H atoms. This will reduce the hybridization and partially restore the exchange splitting. Note that the influence of an increasing lattice constant is also beneficial in so far as it leads to much narrower 3d bands. The results obtained on  $ScFe_2$  are very illustrative in this respect. Compared to  $\alpha$ -Fe the Fe moments in these compounds are strongly reduced. However, in the hydrides the spin imbalance has become almost as large again as that in  $\alpha$ -Fe. This means that the presence of the H atoms has neutralized the unfavourable effect of the Sc atoms almost completely. This notion is in keeping with the fact that the H atoms (at not too high H concentrations) are located close to the R atoms and, as it were, "screen" the R atoms from the 3d atoms (see section 4.1). Increasing hydrogen concentration is found to lead to a larger occupancy of those interstitial holes where the situation is less favourable, i.e., where the area of contact of the H atomic cells with the 3d atomic cells has become larger and that with the R atomic cells has become smaller. One may expect therefore that an increase in hybridization between the 3d electrons and the 1s electrons of H will take place. In addition more dissimilar interstitial holes will become occupied so that disorder of the lattice is increased. Both occurrences will eventually lead to a reduction of exchange splitting. This agrees with the results obtained for  $ErFe_3H_x$  and the disappearance of an Fe moment in  $ErFe_2H_x$  when  $x > 4.1$  (see fig. 49). In off-stoichiometric  $ScFe_2$  an effective shielding of the Fe sublattice from the Sc sublattice by means of a symmetric filling of interstitial hole sites with H atoms is not possible. In this case the moment increase upon charging is considerably less than the moment increase in stoichiometric  $ScFe_2$  (Smit et al., 1982).

A reasoning similar to that given above can also be applied to Co (and Ni) compounds. Here we have to take into account that the 3d moment formation in Co and its compounds is much more vulnerable. Arguments have been presented elsewhere (Buschow et al., 1980) that the 3d moments in Co intermetallics are less localized than those in Fe intermetallics. The detrimental effect on the 3d moment formation of increasing 3d-H contacts at the expense of 3d-3d contacts upon charging is much stronger and overcompensates the beneficial influence of the reduced hybridization of the 3d electrons with the d and s, p electrons of the R component.

From the results discussed above the following conclusions can be drawn:

(i) If one wishes to explain the controversial changes in 3d moment in Fe and Co compounds by means of a unified model one has to accept that charge transfer is not the main reason for the hydrogen-induced change of moment.

(ii) A relatively large transfer of charge takes place between the H atoms and the

R atoms. This follows from the isomer shift results obtained by means of  $^{151}\text{Eu}$ ,  $^{161}\text{Dy}$  and  $^{161}\text{Gd}$  Mössbauer effect spectroscopy, which indicate that the R atoms donate electrons to the H atoms. These findings are in agreement with the fact that there is virtually no difference in electronegativity between H and the 3d metals but a considerable electronegativity difference between R and H.

In terms of Miedema's cellular model, the changes in 3d magnetism can be explained as follows (Buschow et al., 1982a): In the ternary hydride the contact area of a given 3d atom comprises 3d-3d contacts as well as a substantial portion of 3d-H contacts. In many respects the situation is similar to the one that would be present in the binary 3d transition metal hydrides, so that an analogous magnetic behaviour can be anticipated.

In the case of Ni and Co the introduction of hydrogen leads to a decrease of  $T_c$  and to a lower spontaneous magnetization (Wagner and Wortmann, 1978). Hence one expects similar effects upon ternary hydride formation of Co and Ni compounds, which agrees with experiments. It should be noted that the reduction of the ferromagnetic properties in the 3d metal hydrides is a result of the magnetic exchange parameters, charge transfer between Ni or Co and hydrogen being very small.

In the case of Mn and Fe the situation is less clear than in the case of Ni and Co. There are experimental indications that the presence of hydrogen is not an unfavourable factor with respect to magnetic moment formation. Antonov et al. (1978) found high Curie temperatures and an appreciable spontaneous magnetization in hybridized  $\text{Fe}_{65}(\text{NiMn})_{35}$  alloys containing up to 17 at% manganese. These alloys are non-magnetic without hydrogen. Local moment formation is a delicate matter, however, so that accurate predictions of the change in magnetic properties of Fe and Mn compounds upon hydrogen absorption are hardly possible.

Finally we note that the cellular model also provides a hint as to the direction of possible valence changes in the intermetallics  $\text{RM}_n$  upon hydrogenation, when R is one of the elements Ce, Eu or Yb. Hydrogen absorption results in the formation of an appreciable area of contact between R atoms and H atoms at the expense of R-M contacts. The R atoms therefore will tend to adopt the same valences they have in the binary hydrides, i.e., Ce tends to be trivalent, Eu and Yb tend to be divalent. This agrees with experimentally observed valence changes (Buschow et al., 1977; Buschow, 1980b).

Apart from the volume change due to the  $\text{H}_2$  uptake, one has an additional volume effect owing to the valence change. It should be emphasized that the valence change is driven by the energy effects associated with the creation of R-H interfaces and the loss of R-M interfaces. This has as a consequence the occurrence of an additional volume effect. Alternatively one could say that the additional volume effect is driven by the valence change and *not vice versa*, as is sometimes assumed.

### 5.3. Miscellaneous properties

A serious drawback in the study of the changes in physical properties due to hydrogen absorption is the fact that the material pulverizes during charging. Using standard methods it therefore seems impossible to determine electrical transport

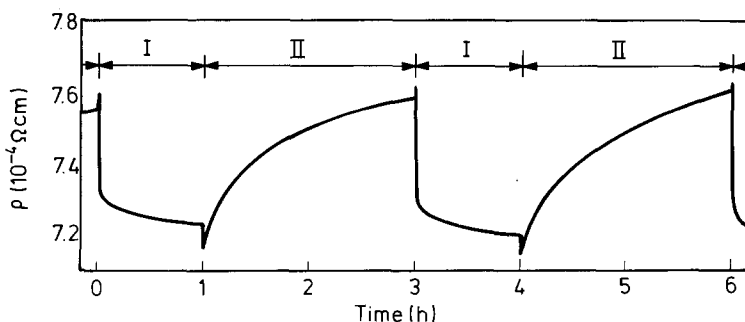


Fig. 51. Effect of hydrogen sorption (at 50°C) on the electrical resistivity of a 3000 Å thick  $\text{LaNi}_5$  film: I, absorption; II, desorption. The results represent data published by Adachi et al. (1981).

properties of ternary hydrides. Adachi et al. (1981) were able to avoid sample pulverization by using for their resistivity measurements a sample of  $\text{LaNi}_5$  prepared in the form of a thin film (3000 Å thick) by means of flash evaporation. Their results are reproduced in fig. 51, where the change in resistivity during cycling is shown after initial activation and after allowing the changes to become reproducible during the first 20 cycles. It can be seen from the figure that charging results in an initial small increase followed by a strong decrease. The initial increase was interpreted by the authors as being due to chemisorption, dissociation of  $\text{H}_2$  and dissolution in the film as  $\text{H}^-$  ions. The strong decrease of  $\rho$  was ascribed to the formation of a highly conductive ternary hydride. The authors verified that the properties of a La or Ni film prepared in this way were quite different. They also checked the composition of the films and concluded from X-ray data that they were amorphous (Adachi et al., 1982). The results of Adachi et al. show that the resistivity of  $\text{LaNi}_5$  remains the same within 10% after charging. This result is rather surprising in view of the large changes in structure and bonding resulting from the introduction of H atoms. The experimental results of Adachi et al., showing the presence of highly conductive material after charging, are at odds with the findings of Walsh et al. (1976), who concluded from ESR experiments that  $\text{LaNi}_5$  after charging has quite a low carrier concentration, reminiscent of semiconducting or barely metallic materials.

Although somewhat less interesting from the point of view of solid state physics, the thermal conductivity is of paramount importance in all cases where intermetallic compounds and their hydrides are employed as hydrogen storage materials. In hydrides with a good thermal conductivity the heat released upon charging can easily be dissipated and decomposition can be avoided. Good thermal conductivity is essential if these materials are to be used in heat pump devices. Unfortunately, no investigations of this kind have been performed on rare earth intermetallics and their hydrides.

Because of their relevance to these materials we would like to mention here briefly the results of Suda et al. (1980), who studied the thermal conductivity of  $\text{TiMn}_{1.5}$  and its hydride. These authors found different thermal conductivity values during

absorption and desorption, which reflect the presence of hysteresis in the temperature composition relationship. Suda et al. derived an empirical expression for the thermal conductivity, comprising a contribution proportional to the H/M ratio and pressure-dependent contributions of the type  $(\ln p)^n$ , where  $n$  ranges from 1 to 3.

The effect of hydrogen absorption on superconductive properties was studied on relatively few compounds. These comprise  $\text{Th}_7\text{Fe}_3$  (Malik et al., 1978a),  $\text{CeCo}_2$  (Buschow and Sherwood, 1978), several La–Ni compounds (Oesterreicher et al., 1976) and several Th–R alloys (Oesterreicher et al., 1977). In all cases it was found that the absorption of hydrogen gas leads to disappearance or lowering of the superconducting state.

## 6. Technical applications

Research on hydrogen absorption in metals has been stimulated for some considerable time now by the possibility of using hydrogen–metal systems as chemical and nuclear energy carriers. We recall here some of the prominent features of hydrogen metal systems:

(i) Extremely high mobility of hydrogen when dissolved in the metallic host, leading to high rates of absorption and desorption.

(ii) The hydrogen density in the metallic host phase surpasses the density of pure liquid or solid hydrogen.

(iii) Large heats of reaction occur during the hydrogen sorption processes.

(iv) A large choice of different materials is available owing to the high reactivity of hydrogen with a large number of metals or intermetallics.

A brief description of some applications of hydrogen metal systems is given below.

### 6.1. *Hydrogen storage*

Hydrogen gas to be used as fuel can be stored as compressed gas in steel cylinders, as liquid hydrogen at about 20 K and in the form of a metal hydride. The great advantage of the metal hydride storage system is obvious: owing to the equilibrium existing between the hydrogen and the host metal, cooling of the latter leads to reabsorption, in contrast to the first two storage systems where the once liberated hydrogen remains in this state.

Intermetallics such as  $\text{LaNi}_5$ ,  $\text{TiFe}$ ,  $\text{TiMn}_{1.5}$ ,  $\text{ZrMn}_2$  and related ternary compounds have proved to be the most promising candidates in hydrogen storage applications. Hydrogen storage systems based on these intermetallics have been discussed in several publications (Reilly, 1978b; Gruen et al., 1978; Guinet et al., 1980; McCue, 1980; Ron et al., 1980; Sheft et al., 1980; Swisher, 1980; Töpler et al., 1980a, b; van Mal, 1976; Wenzl and Lebsaft, 1980; Wenzl, 1982).

For storage purposes the intermetallic compound is usually contained as a coarse powder in a stainless steel vessel having specific provisions for improved heat exchange. After activation and several hydriding–dehydriding cycles the particle size

of the powder becomes reduced by brittle fracture due to elastic stresses (see section 3.1). This leads to a considerable increase of the surface area and the corresponding catalytic activity, so that after the attainment of a critical grain diameter chemical reaction kinetics ceases to control the flow rate. This stage is reached after only one or two cycles in  $\text{LaNi}_5$  and  $\text{TiMn}_{1.5}$ ; in TiFe-base intermetallics some more cycles are required. Since the equilibrium plateau pressure of the ternary hydride strongly depends on the temperature, the pressure level desired can be adjusted by heating the ternary hydride via an internal or external heating system attached to the steel container.

As an example fig. 52 shows results of the storage source described by McCue (1980). The device is relatively compact, portable and rechargeable and is based on encapsulated  $\text{LaNi}_5$ , able to store more than 200 litres of hydrogen. An internal heating system allows the pressure and flow rate to be increased. Refilling can, for instance, take place "overnight" by means of an electrolytic hydrogen generator since low pressures and low flow rates can be applied during recharging. All storage devices based on ternary hydrides have in common that the supply pressure remains virtually constant during almost the total delivery period. Other advantages over conventional pressurized gas vessels are the substantial reduction in volume and some reduction in weight, and the fact that the safety risk is considerably reduced. A sudden rupture of the container vessel will only lead to a rather gradual decharging, the large recoil momentum associated with the rupture of a high pressure vessel being absent. A disadvantage is the deterioration of the ternary hydride power as a result of poisoning (section 3.4) or as a result of phase separation (section 4.4). In most cases, however, restoration of the hydrogen sorption properties can be achieved by gently

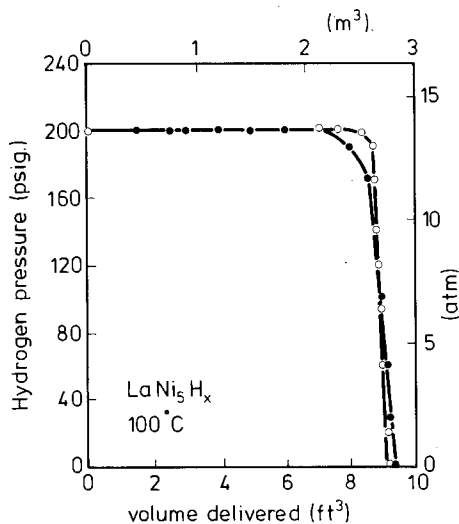


Fig. 52. Hydrogen pressure versus volume delivered (at STP) for a compact portable hydrogen storage device described by McCue (1980). The temperature of the internal heating system equals  $100^{\circ}\text{C}$ ; pressure switch control  $200\text{ lbf/in}^2$ ; open circles represent performance with a flow rate of  $17\text{ l/h}$  (total delivery period  $13.5\text{ h}$ ) full circles represent performance with a flow rate of  $170\text{ l/h}$  (total delivery period  $1.5\text{ h}$ ).

heating in vacuum. Further points to note in the conduction and operation of such storage systems are the large volume expansion of the metallic host upon charging ( $\Delta V/V = 0.25$  in the case of  $\text{LaNi}_5$ ) and the exponential pressure increase during accidental heating.

### 6.2. *Hydrogen purification and hydrogen getters*

Heated membranes of palladium–silver alloys have been commonly used (Fromm and Hörz, 1980) to obtain hydrogen gas of very high purity. Only the hydrogen gas is capable of diffusing through these membranes. The fact that palladium–silver sheets are less susceptible to embrittlement than most metals reacting with hydrogen makes them suitable for use in membranes. Such diffusion cells are fairly expensive and the process is rather slow. Moreover, constant supervision of the palladium–silver membranes is required to prevent malfunctioning arising from leaks.

As an alternative one may consider hydrogen purification by means of absorption–desorption cycles based on metal hydrides, operating at room temperature. Wenzl and Klatt (1978) showed that by selective absorption of hydrogen in  $\text{FeTi}$ , hydrogen gas of technical purity (99.9%) can be converted into hydrogen of ultra-high purity (99.9999%). At the same time a hydrogen gas source with a certain storage capacity is created. The pressure of the very pure hydrogen gas can be varied by changing the temperature.

A somewhat different application was reported by Reilly and Wiswall (1972), who noted that  $\text{RM}_3$  compounds are still able to form ternary hydrides when brought into contact with gas mixtures having a composition like that resulting from the steamreforming of hydrocarbons followed by CO shifts and methanation steps. They found that  $\text{CO}_2$ , even when present in large concentrations, does not interfere with the  $\text{H}_2$  uptake. On the other hand, small amounts of CO have an inhibiting effect (see also section 3.4). The inhibition can be reduced somewhat by raising the temperature or substituting Cu partly for Ni in  $\text{LaNi}_5$ . It will be clear that these poisoning effects set a limit to large scale applications of this method of hydrogen purification when operations on a continuous reaction basis are required.

Materials that can rapidly bind gases liberated from the interior of an evacuated vessel after it has been sealed off are called getters. Such materials are widely used in the field of vacuum tube fabrication. Examples are Th–Ce–Al (van Vucht, 1963) and  $\text{Zr}(\text{V}_{1-x}\text{Fe}_x)_2$  (Mendelsohn and Gruen, 1980).

### 6.3. *Heat pumps*

The coupling of the absorption–desorption cycles of two different hydrides (I and II) can be used to transfer heat from a low-temperature reservoir ( $T = T_c$ ) to a high temperature reservoir ( $T = T_h$ ). The principle of this heat pump is illustrated by fig. 53. In the first stage (a) the two metal hydrides I and II are in open communication with each other. As can be seen from the top part of fig. 53, hydride II is less stable than the hydride I. It reaches a given equilibrium pressure  $p_2$  at a substantially lower

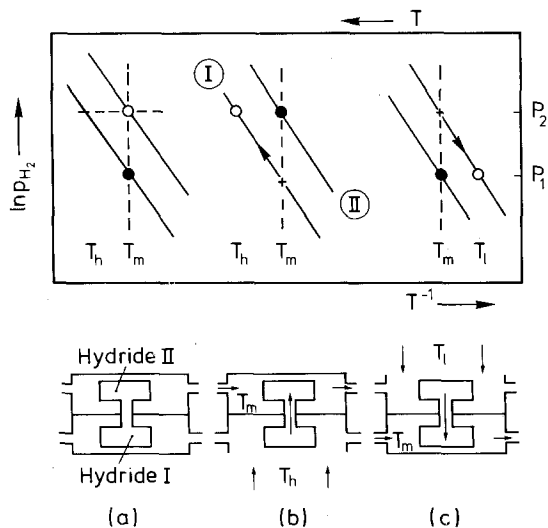


Fig. 53. Principle of a heat pump based on two hydrides. Hydride I is more stable than hydride II. The lower part of the figure shows the flow of hydrogen gas (see the arrows inside the closed hydride systems) when hydride I is exposed to a high temperature source (situation b) or when hydride II is brought into contact with a low temperature source (situation c). In both situations the heat of absorption is dissipated to the environment at  $T = T_m$  ( $T_l < T_m < T_h$ ). This can be done by cooling with water or air, indicated by the smaller arrows in the  $T_m$  system. A description of these processes in terms of  $\ln p$  versus  $1/T$  characteristics is schematically given in the upper part of the figure. Open circles represent hydrides in discharged condition, full circles represent hydrides in recharged condition. The situations in the upper part of the figure correspond to those in the lower part after completion of the hydrogen transfer shown by the arrows within the closed hydride systems in the lower part.

temperature ( $T_m$ ) than hydride I ( $T_h$ ). When hydride I, being saturated with hydrogen, is heated to  $T_h$  the hydrogen pressure rises to  $p_2$  and the hydrogen desorbs. The hydrogen is absorbed again by the hydride II, which therefore increases in temperature until it reaches  $T_m$  corresponding to  $p_2$ . This situation is represented in fig. 53b. The heat of absorption  $\Delta H_{II}$  is dissipated at  $T_m$ . When nearly all the hydrogen from hydride I has been desorbed, thermal contact between system I and the heat source at  $T_h$  is broken. The hydride I is brought now into contact with the environment having a temperature  $T_m$ . The temperature in system I now decreases and hydrogen is re-absorbed (fig. 53c). The hydrogen pressure drops to  $p_1$  and the desorption from system II causes its temperature to drop to  $T_l$ . During the desorption process system II takes up heat from the reservoir at  $T_l$  while the heat of reaction  $\Delta H_I$  corresponding to the absorption by system I is dissipated to the environment at  $T_m$ . When all the hydrogen has been re-absorbed by I, system I is coupled again to the heat source at  $T_h$  and the cycle is repeated.

The total heat dissipated to the environment at  $T_m$  is equal to  $\Delta H_I + \Delta H_{II}$ . The heat input at  $T_h$  is  $\Delta H_I$ . The efficiency is therefore

$$\eta = 1 + \Delta H_{II}/\Delta H_I.$$

It can be shown that this expression can be re-written as  $\eta = (1 - T_l/T_h)(1 - T_l/T_m)$ ,



Carnot efficiency being attained when  $T_h = T_m^2/T_c$  (van Mal, 1976). Temperature gradients needed for the heat exchange at the various levels were taken to be infinitely small in the above discussion. More sophisticated heat pumps based on more than two different hydrides have been discussed by van Mal (1976) and Buschow and van Mal (1982).

In the above discussion it was tacitly assumed that the heat of reaction  $\Delta H$  is temperature independent. It follows from the results described in section 4.1 that this is often not the case. A further complication is the presence of a sorption hysteresis in the isotherms and the absence of really flat portions in the sorption isotherm. Important factors affecting the efficiency are undoubtedly the thermal conductivity and the heat transfer of the hydride powder particles (Lynch, 1980; Töpler et al., 1980a,b). Since the thermal conductivity of the hydride particles is rather low and therefore the heat transfer is rather limited, large temperature gradients have to be employed. Considerable improvement can be achieved by using hydrides that have been compacted to form porous solids supported by a thin metal matrix. The technical feasibility of this was shown by Ron et al. (1980) on  $\text{LaNi}_5$ -15% Al compacts. These authors reported high thermal conductivities and rapid sorption kinetics. Further studies in this field were made by Suda et al. (1983a, b).

A chemical heat pump based on two hydrides designed for the storage and recovery of thermal energy for heating, cooling and energy conversion (HYCSOS) was developed at the Argonne National Laboratory (Sheft et al., 1980; Gruen et al., 1978). The two hydrides used are those of the compounds  $\text{LaNi}_5$  and  $\text{CaNi}_5$  or pseudobinary compounds based on them. The system has been tested for several years and is reported to compare favourably with a unit combining solar cooling with direct solar heating.

#### 6.4. Energy storage

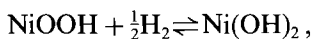
Energy storage systems based on metal hydrides were described by several authors (Wakao et al., 1983; Yonezu et al., 1983; Kawamura et al., 1983a, b).

An interesting application of metal hydrides as energy storage systems is utility load levelling or peak shaving: electrical energy produced during off-peak hours is stored for use during peak demand hours. An engineering model of such a peak shaving system was described by Reilly (1978b). The hydrogen generated electrolytically in off-peak hours is slightly compressed and stored in a hydrogen-absorbing intermetallic compound. During peak hours the hydrogen is released and fed into a fuel cell to generate electricity.

Metal hydride systems can also be used as storage media for heat and fuel in automotive applications (Töpler et al., 1980). The use of hydrogen in vehicles with internal combustion engines has the advantages of giving the engine a large thermal efficiency and producing exhaust gases virtually free from pollutants. A disadvantage is the weight penalty of the hydride tank, which is 10–20 times heavier than a filled petrol tank. This still compares favourably, however, with a lead-acid accumulator for electrically propelled vehicles. The feasibility of using hydrides in motor vehicles has been studied by Daimler-Benz in Berlin and Stuttgart on hydrogen-driven passenger cars and small buses (Töpler et al., 1980a, b; Buchner, 1978a).

### 6.5. Electrochemical cells

Ternary hydrides can also be used for the chemical storage of hydrogen (Justi et al., 1970; Gutjahr et al., 1973; Ewe et al., 1973; Earl and Dunlop, 1974; Buchner, 1976; Bronoel et al., 1976; Markin et al., 1978; van Rijswick, 1978; Videm, 1978; Holleck et al., 1980). A schematic representation of a Ni-H<sub>2</sub> cell is given in fig. 54. Here the ternary hydride is seen to be completely isolated from the electrolyte in a separate hydride compartment (E). The access of H<sub>2</sub> gas is made possible via holes in the compartment which are covered by a microporous membrane such as teflon. Oxygen can be prevented from reaching the ternary hydride by passing the H<sub>2</sub> gas over a large catalytic surface (platinum black) to recombine O<sub>2</sub> and H<sub>2</sub> to H<sub>2</sub>O. The reaction in the electrochemical cell can be represented by



where the upper and lower arrows pertain to discharging and charging, respectively. During the charging period the hydrogen pressure would normally increase from 3 to 33 atm, but because the hydrogen is stored in a suitable ternary hydride the operating pressure does not exceed a few atmospheres. The hydrogen desorbs from the ternary hydride during electrical discharge and the nickel hydroxide is regenerated. The electromotive force (emf) between the two electrodes is larger the less firmly the hydrogen is bonded in the ternary hydride. For a hydride having an absorption equilibrium pressure near 1 atm at room temperature the emf with a Ni(OH)<sub>2</sub> counter electrode is about 1.35 V. Each factor of 10 in the equilibrium

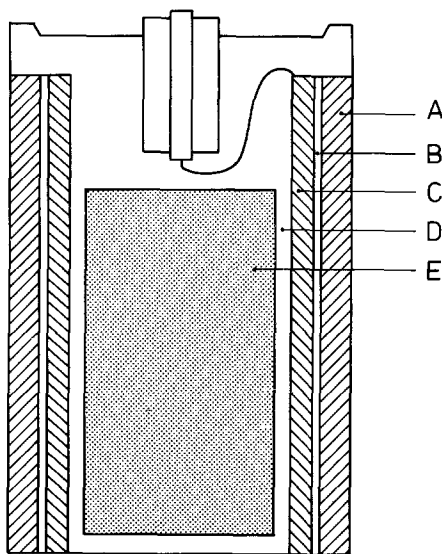


Fig. 54. Schematic representation of a Ni-H<sub>2</sub> cell. A: Ni oxide electrode, B: separating intermediate layer, C: H<sub>2</sub> electrode, D: gas space, E: ternary hydride (after Holleck et al., 1980).

pressure of the metal–gas sorption reaction corresponds to a change of 30 mV in the emf of the cell.

Selection criteria for ternary hydrides are: (i) they must be capable of operating over a convenient pressure range (0.5–5 atm), and (ii) they must be sufficiently corrosion-resistant to make the application of the KOH electrolyte possible. In addition the presence of small amounts of oxygen generated if overcharging occurs must not lead to deterioration. The hydride  $\text{LaNi}_5\text{H}_x$  seems to meet these requirements reasonably well. An advantage of the described cell based on  $\text{LaNi}_5\text{H}_x$  is its relatively high electrochemical capacity (0.37 A h/g). Somewhat smaller values are found for the hydrides  $\text{TiNiH}_x$  and  $\text{Ti}_2\text{NiH}_x$  (0.25 A h/g). A disadvantage of the  $\text{Ni-H}_2$  cells is the continuous decrease in their storage capacity (Holleck et al., 1980).

#### 6.6. *Thermal compressors and heat engines*

A number of favourable properties of  $\text{LaNi}_5\text{H}_x$ , comprising the fast rate of the sorption reactions, the constancy of the  $\text{H}_2$  pressure during charging and discharging at a given temperature, the large absorption capacity, and the favourable pressure range of  $\text{LaNi}_5$  hydride have been exploited by van Mal (1976) and Nomura (1983) to build a thermal absorption compressor for hydrogen gas.

The working principle of the compressor can be sketched as follows: Hydrogen gas is absorbed at a low temperature level ( $20^\circ\text{C}$ ) where the pressure is relatively low (1.5 atm). The hydride is then heated to  $140^\circ\text{C}$ , leading to a pressure of about 50 atm. After desorption the pressure drops and recharging at the lower temperature is necessary. Despite the dead volume (at least 60% for a container with  $\text{LaNi}_5$  hydride in powdered form) a relatively high pressure ratio can still be reached owing to the large absorption capacity of  $\text{LaNi}_5$ .

In a prototype three containers were used and mounted in a vacuum enclosure (van Mal, 1976). Each of these containers was equipped with its own electric heating and water cooling. This multiple system, operated with the appropriate differences in phase between the charging and discharging modes, was used to obtain a nearly steady flow of 10 mg/s of hydrogen at 45 atm and  $160^\circ\text{C}$  with a heat input of about 1 kW. Since thermal energy is used for the work of compression, the compressor may be driven by waste heat or solar energy. A hydride compressor in conjunction with highly efficient power conserving systems was also suggested by Powel et al. (1975).

Closely related to the working principle of the hydrogen compressor is the working principle of a heat engine based on metal hydrides. A water pump operating as a heat engine was devised by Northrup and Heckes (1980). This device is schematically shown in fig. 55. The system operates between two heat reservoirs  $R_h$  and  $R_c$ . A ternary hydride in a storage container C is discharged by the heat supplied by  $R_h$ . The generated hydrogen gas expands a flexible bulk B. Its expansion presses the water out of the container and lifts it to the height desired. This water can be used as a low-temperature heat reservoir to cool the hydride in C. Hydrogen is reabsorbed and the container around B becomes filled with water again, one-way valves V preventing the backflow of water.

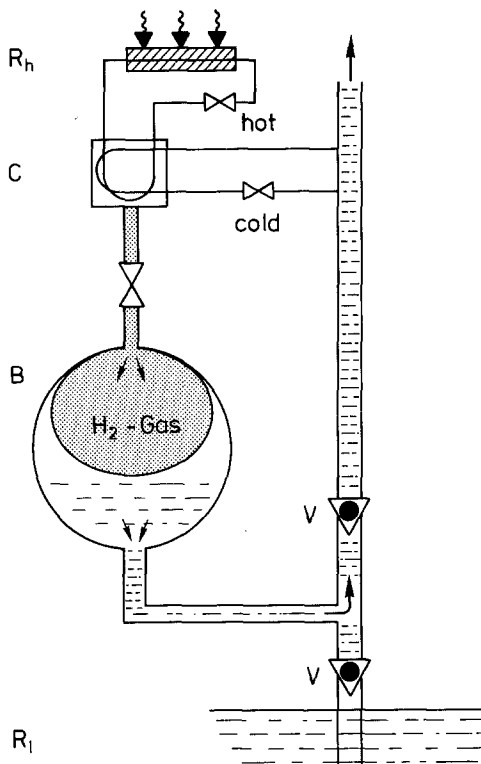


Fig. 55. Schematic representation of a hydrogen-actuated water pump, lifting the water from an underground reservoir  $R_1$  to a higher level. The ternary hydride in C is discharged by the heat provided by the heat source  $R_h$  and becomes charged again after cooling via the relatively cold water originating from  $R_1$ . The pumping operation proceeds by means of the  $H_2$  gas inside the flexible bulb B and one-way valves (V). This schematic representation is similar to that given by Wenzl (1982).

In practical cases one can use the heat provided by a solar collector ( $R_h$ ) able to heat the hydride to about  $80^\circ\text{C}$ , which is sufficiently above the temperature of underground water (about  $20^\circ\text{C}$ ) to bring about the large  $H_2$  pressure difference needed for the pumping (0.4 to 3 atm when  $\text{CaNi}_5\text{H}_x$  is used). For more details the reader is referred to the papers by Northrup and Heckes (1980) and Wenzl (1982).

### 6.7. H and D isotope separation

Owing to the large difference in mass between hydrogen and deuterium atoms pronounced isotope effects may occur with hydrogen in metals. The difference in free energy upon absorption of  $H_2$  and  $D_2$  can be regarded as an algebraic sum of a number of contributions pertaining to the differences in enthalpy and entropy of the two gases and those of the hydride (deuteride) phase. Isotopic separation experiments using ternary hydrides based on Ti and Mg were reported by Wiswall et al. (1977), Tanaka et al. (1978a, b) and Buchner (1978a, b). In TiNi the deuteride is significantly

less stable than the hydride, leading to a difference of a factor of 10 in the plateau pressure. This difference can be used to obtain a gas phase enriched in deuterium. In  $\text{LaNi}_5$ , too, the deuteride is less stable than the hydride. Here the plateau pressure difference is comparatively small (van Mal, 1976; Biris et al., 1976).

#### 6.8. Neutron moderators and neutron generators

The extremely large hydrogen density in combination with the high thermal stability of several hydrides makes these materials suitable for applications as moderators in nuclear fission reactors (Keinert, 1971; Mueller et al., 1968). A small-scale application of metal hydrides is found in neutron generators. Here a thin layer of the metal hydride saturated with deuterium or tritium is used as a target for accelerated D and T ions, where the DT reaction leads to a high neutron flux (Reifenschweiler, 1972).

### 7. Concluding remarks

The future technological applications of metal hydrides are to a large extent based on the general notion of achieving a more economical use of the energy available. A few points will be mentioned that are worth keeping in mind. Firstly, some of the applications that are technically feasible at the moment are not the cheapest solutions. However, since the cost of hydrocarbon fuels will tend to rise, it may be expected that these applications will eventually become more attractive. Secondly, hydrogen is a widely used industrial commodity, albeit hydrogen is only an energy carrier and not an energy source. It seems unlikely therefore that there will be any slackening of interest in metal-hydrogen systems in the foreseeable future.

A central problem in several of the possible technological applications is the heat transfer. A low heat transfer is intimately connected with the fine partial character of the ternary hydrides and with the circumstance that continued cycling leads to a repeated swelling and shrinking of the particles. The poor heat transfer not only affects the thermodynamic efficiency but reduces the lifetime of the ternary hydrides owing to the increased decomposition into binary hydrides and 3d metal.

A somewhat related situation exists in electrochemical applications of the ternary hydrides. In these cases the electrode composed of the hydride is immersed in an aqueous solution and the charging does not involve a violent reaction. Decomposition of the sample due to heating cannot therefore be a major problem. The swelling and shrinking, however, are also present here. Fine particles may lose contact with the main body of the electrode and the formation of new microcracks accelerates deterioration. Much effort in research and development will be required to solve these problems. Here one may think not only of finding an engineering solution (for instance by imbedding the powder particles into a suitable matrix material). One may also tackle the problem from the metallurgical side by looking for composite systems or for ternary hydrides that are less brittle. Investigations of

the sorption properties of amorphous materials also deserve more attention than they receive at the moment.

If one looks at the research effort that has been spent on the physical properties of rare earth-base intermetallics one will discover that most of the effort has gone into investigations of the magnetic properties. The results described in this chapter make it clear that the situation is not much different in the case of their ternary hydrides. It has been mentioned that the formation of microcracks during charging and discharging has hampered the investigation of transport properties on these materials. The presence of microcracks is less disturbing as far as the study of superconducting properties is concerned, and it is surprising that from this quarter such relatively little interest has been shown in ternary hydrides. A possible reason is that the few examples studied invariably showed no superconductivity in the ternary hydrides. It should be borne in mind, however, that these examples refer to compounds of a composition susceptible to easy decomposition upon charging. The presence of 3d atom metal clusters may then either suppress superconductivity altogether or mask it from observation. Similar studies are to be recommended on compounds that absorb the hydrogen gas less violently, or studies starting with materials where the hydrogenation is performed under carefully controlled conditions. The advantages of studying superconductivity in ternary hydrides are obvious, since it makes it possible to vary the Debye temperature, the density of states and the electron-phonon coupling constant over wide ranges. Of special interest are cases where the  $\beta$  phase is not a line compound but comprises a range of hydrogen concentrations, making it possible to achieve a gradual variation of the various parameters. Finally, in materials in which rare earths are combined with non-magnetic metals one has the possibility to reduce the interaction between the 4f moments by hydrogen absorption. In compounds of low magnetic ordering temperatures, hydrogen absorption could be used to obtain a reduction of the pair-breaking parameter.

Proton NMR experiments have received a relatively large amount of attention. The study of hydrogen diffusion in the hydrides is of interest both from the technological point of view and from that of fundamental physics. Systematic studies seem to be desirable in order to establish a relationship between the experimentally observed activation energies and the occupancy of particular interstitial sites. The choice should fall on hydrides for which a firm basis regarding the site occupancies has already been laid by neutron diffraction studies on the corresponding deuterides.

Of particular interest is furthermore the mutual interaction of the H atoms in the ternary hydrides. Estimates of a minimum H-H interatomic distance have been made on the basis of theoretical considerations (Switendick, 1978a, b), as well as on the basis of thermodynamic arguments (Bouten and Miedema, 1980; Buschow et al., 1982). Both estimates are in satisfactory agreement and point to a minimum H-H interatomic distance of about 2.2 Å. This minimum distance implies a blocking of nearest neighbour interstitial sites and the presence of a maximum hydrogen concentration. A few structural studies dealing with this blocking phenomenon have been published. Extensions of such studies to other series of compounds would be highly welcome.

## Appendix

## Tables A1-4

Hydrogen sorption characteristics of some rare earth-base compounds. The composition of the uncharged compounds  $RM_n$  has been listed in the first column. The maximal value of  $x$  in  $RM_nH_x$  has been listed under  $x(\max)$ , where the  $H_2$  pressure applied (atm) has been given in brackets. The composition of the first hydride  $\beta_1$  has been listed under  $x(\beta_1)$  and the corresponding plateau pressure under  $p(\alpha-\beta_1)$ . In both cases the temperature ( $^{\circ}C$ ) at which these data were obtained has been indicated in brackets. From the values reported in the literature we choose those that were as close to room temperature as possible. Experimental values of the formation enthalpy and entropy have been given in columns 5 and 6. The type of the corresponding reaction (whenever such information was specified in the literature) has been indicated in column 7. The compounds and hydrides given in the various tables have been listed in order of increasing rare earth concentration.

TABLE A1  
Compounds of rare earths and nickel.

Comp.	$x(\max)$	$x(\beta_1)$	$p(\alpha-\beta_1)$ (atm)	$\Delta H$ (kJ/mol $H_2$ )	$\Delta S$ (J/deg mol $H_2$ )	Reaction type	Refs.
LaNi <sub>5.5</sub>	5.5 (12)	5 (40°)	9.2 (40°)	—	—	$\alpha-\beta_1$	1
LaNi <sub>5</sub>	6.7 (50)	5.5 (40°)	1.9 (25°)	-30.2	-109.1	$\alpha-\beta_1$	1-17
LaNi <sub>4.9</sub>	6.2 (12)	6 (40°)	2.9 (40°)	—	—	—	1
CeNi <sub>5</sub>	6 (50)	6 (23°)	48 (25°)	-14.2	-80.0	$\alpha-\beta_1$	15
PrNi <sub>5</sub>	6 (9)	—	8.3 (23°)	-30.5	-120.2	$\alpha-\beta_1$	3
NdNi <sub>5</sub>	5.5	4	12.7 (20°)	-27.8	-116.0	$\alpha-\beta_1$	3, 16
SmNi <sub>5</sub>	3-4	—	30 (23°)	—	—	—	3
GdNi <sub>5</sub>	2-3	—	120 (23°)	—	—	—	3
YbNi <sub>5</sub>	2-3	—	120 (25°)	—	—	—	3
YNi <sub>5</sub>	3.5 (1550)	1 (22°)	300 (22°)	—	—	—	18
La <sub>2</sub> Ni <sub>7</sub>	11.4 (50)	4 (20°)	<1 (20°)	—	—	—	19-21
Ce <sub>2</sub> Ni <sub>7</sub>	4.2 (10)	4 (50°)	0.2 (50°)	—	—	—	22
Pr <sub>2</sub> Ni <sub>7</sub>	9.5 (50)	5.7 (25°)	9 (25°)	—	—	—	23
Y <sub>2</sub> Ni <sub>7</sub>	3 (50)	1.1 (50)	2.5 (50°)	—	—	—	22
LaNi <sub>3</sub>	5 (50)	—	—	—	—	—	19, 24
CeNi <sub>3</sub>	4.2 (10)	2.2 (50°)	0.09 (50°)	-43.9	—	—	22, 32
ErNi <sub>3</sub>	3.5 (50)	<2 (50°)	—	—	—	—	23
YNi <sub>3</sub>	4 (50)	1.5 (50°)	0.25 (50°)	—	—	—	22
LaNi <sub>2</sub>	4.6 (50)	2	—	54.5	—	—	20, 24, 25, 27
CeNi <sub>2</sub>	4 (40)	—	<10 <sup>-5</sup>	—	—	—	22
GdNi <sub>2</sub>	4.1	—	—	-89.7	-136.6	$\alpha-\beta_1$	28, 29
DyNi <sub>2</sub>	>4 (150)	—	—	—	—	—	30
YbNi <sub>2</sub>	3.1 (10)	—	—	-51.9	—	—	32
YNi <sub>2</sub>	3.6	—	—	—	—	—	22, 26
LaNi	3.6 (50)	—	—	—	—	—	19, 20, 26, 27
CeNi	2.7	—	—	—	—	—	26
YNi	3.0	—	—	—	—	—	26

TABLE A1 (cont.)

Comp.	$x(\max)$	$x(\beta_1)$	$p(\alpha-\beta_1)$ (atm)	$\Delta H$ (kJ/mol H <sub>2</sub> )	$\Delta S$ (J/deg mol H <sub>2</sub> )	Reaction type	Refs.
La <sub>2</sub> Ni <sub>3</sub>	4.4 (1)	-	-	-	-	-	26
La <sub>7</sub> Ni <sub>3</sub>	21 (50)	-	-	-	-	-	20
La <sub>3</sub> Ni	8.8 (1)	-	-	-	-	-	19, 26, 27
Ce <sub>3</sub> Ni	8.4	-	-	-	-	-	26
Y <sub>3</sub> Ni	8.0	-	-	-	-	-	26

- |                                     |                                   |
|-------------------------------------|-----------------------------------|
| 1. Buschow and van Mal (1972)       | 17. Takeshita et al. (1980)       |
| 2. van Vucht et al. (1970)          | 18. Takeshita et al. (1981)       |
| 3. Anderson et al. (1973)           | 19. Mikheeva et al. (1978)        |
| 4. van Mal et al. (1979)            | 20. Oesterreicher et al. (1976)   |
| 5. Biris et al. (1976)              | 21. Andresen (1978)               |
| 6. Kost and Mikheeva (1976)         | 22. van Essen and Buschow (1980b) |
| 7. van Mal (1976)                   | 23. Goudy et al. (1978)           |
| 8. Tanaka et al. (1978b)            | 24. Maeland et al. (1976)         |
| 9. Andreef et al. (1978)            | 25. Kost and Shilov (1979)        |
| 10. Bowerman et al. (1979)          | 26. van Mal et al. (1976)         |
| 11. Ohlendorf and Flotow (1980a, b) | 27. Carstens (1978)               |
| 12. Murray et al. (1980a, b)        | 28. Jacob and Shaltiel (1979)     |
| 13. Chung et al. (1980)             | 29. Malik and Wallace (1977)      |
| 14. van Mal et al. (1974)           | 30. Cohen et al. (1980c)          |
| 15. Lundin et al. (1977)            | 31. Jacob et al. (1981)           |
| 16. Gruen et al. (1977)             | 32. Oesterreicher et al. (1982)   |



TABLE A2  
Compounds of rare earths and cobalt.

Comp.	x(max)	x( $\beta_1$ )	p( $\alpha$ - $\beta_1$ ) (atm)	$\Delta H$ (kJ/mol H <sub>2</sub> )	$\Delta S$ (J/deg mol H <sub>2</sub> )	Reaction type	Refs.
LaCo <sub>13</sub>	2.8 (10)	-	-	-	-	-	1
LaCo <sub>5</sub>	9 (1500)	3.4 (20°)	0.04	-45.2	-127.8	$\alpha$ - $\beta_1$	2-6
CeCo <sub>5</sub>	2.9 (10)	2.5 (20°)	1.5	-39.0	-136.6	$\alpha$ - $\beta_1$	3
PrCo <sub>5</sub>	3.4	2.9 (20°)	0.5	-(38.5-34.3)	-126.1	$\alpha$ - $\beta_2$	3, 7
NdCo <sub>5</sub>	3.2	2.7 (20°)	0.7	-	-	-	3
SmCo <sub>5</sub>	2.5	2.5 (20°)	3.3	-32.7	-121.5	$\alpha$ - $\beta_1$	3
GdCo <sub>5</sub>	2.3	-	24	-	-	-	3
TbCo <sub>5.1</sub>	-	-	34	-	-	-	3
YCo <sub>5</sub>	2.5-4	-	5.5-21	-32.3	-133.5	-	8-11
La <sub>2</sub> Co <sub>7</sub>	5 (10)	-	-	-	-	-	12
Ce <sub>2</sub> Co <sub>7</sub>	9 (100)	6.1 (50°)	0.1-0.5	-43.6	-	$\alpha$ - $\beta_1$	13, 14
Pr <sub>2</sub> Co <sub>7</sub>	9 (100)	2.5 (150°)	0.1	-64.9	-	$\alpha$ - $\beta_1$	7, 14
Nd <sub>2</sub> Co <sub>7</sub>	9 (100)	2.7 (125°)	0.03	-72.1	-	$\alpha$ - $\beta_1$	14
Gd <sub>2</sub> Co <sub>7</sub>	9 (100)	2.6 (75°)	0.03	-57.8	-	$\alpha$ - $\beta_1$	14
Tb <sub>2</sub> Co <sub>7</sub>	9 (100)	2.7 (50°)	0.03	-48.2	-	$\alpha$ - $\beta_1$	14
Dy <sub>2</sub> Co <sub>7</sub>	9 (100)	2.6 (50°)	0.08	-46.1	-	$\alpha$ - $\beta_1$	14
Ho <sub>2</sub> Co <sub>7</sub>	9 (100)	-	0.2	-41.9	-	$\alpha$ - $\beta_1$	14
Er <sub>2</sub> Co <sub>7</sub>	9 (100)	-	0.4	-39.4	-	$\alpha$ - $\beta_1$	14
Y <sub>2</sub> Co <sub>7</sub>	8 (40)	1.5	0.01	-	-	-	13
CeCo <sub>3</sub>	4.2 (10)	4 (50°)	0.2	-	-	-	13, 1
PrCo <sub>3</sub>	4	-	0.02	-54.5	-	-	7
NdCo <sub>3</sub>	>4.2 (1)	2 (80°)	2.5 × 10 <sup>-3</sup> (20°)	-64.23	-130.8	$\alpha$ - $\beta_1$	15
GdCo <sub>3</sub>	5 (200)	2 (20°)	6.8 × 10 <sup>-4</sup> (20°)	-54.76	-121.3	$\beta_1$ - $\beta_2$	15
TbCo <sub>3</sub>	4.5 (68)	1.5	2.3 × 10 <sup>-3</sup> (20°)	-52.2	-117.6	$\alpha$ - $\beta_1$	15, 16
DyCo <sub>3</sub>	5 (40)	1.0 (20°)	3.9 × 10 <sup>-3</sup> (20°)	43.9	-114.7	$\beta_1$ - $\beta_2$	15
				-(44.4-49.4)	-117.9	$\alpha$ - $\beta_1$	16, 30
				-45.1	-123.5	$\beta_1$ - $\beta_2$	30
				-47.89	-117.3	$\alpha$ - $\beta_1$	16, 17, 19
				-40.85	-117.3	$\beta_1$ - $\beta_2$	19

HoCo <sub>3</sub>	5	(40)	1	(20°)	$8.5 \times 10^{-3}$	(20°)	-47.26	-121.5	$\alpha$ - $\beta_1$	16, 17, 29
ErCo <sub>3</sub>	5	(40)	1.1	(20°)	$2.5 \times 10^{-2}$	(20°)	-38.80	-117.1	$\beta_1$ - $\beta_2$	29
TmCo <sub>3</sub>	3.3				<1	(20°)	-44.2	-120.0	$\alpha$ - $\beta_1$	16, 17, 18
YCo <sub>3</sub>	4	(20)	1	(20°)	$2.5 \times 10^{-4}$	(20°)	-36.7	-116.8	$\beta_1$ - $\beta_2$	18
	3.8	(20°)	3.8	(20°)	0.03	(20°)	-	-	-	20
CeCo <sub>2</sub>	4	(10)			< $10^{-5}$	(50°)	56.2	-122.5	$\alpha$ - $\beta_1$	13, 30
PrCo <sub>2</sub>	4				< $10^{-3}$	(100°)	-43.9	-120.6	$\beta_1$ - $\beta_2$	30
GdCo <sub>2</sub>	4.5	(61)					-	-	-	13, 31
TbCo <sub>2</sub>							-	-	-	7
DyCo <sub>2</sub>	>4	(150)					-	-	-	24, 26
HoCo <sub>2</sub>							-	-	-	27
ErCo <sub>2</sub>	3.6	(<1)					-	-	-	28
YCo <sub>2</sub>	3.7				0.05	(25°)	-	-	-	13, 21, 22
Y <sub>4</sub> Co <sub>3</sub>	11.6						-	-	-	21
Y <sub>3</sub> Co	8						-	-	-	21

1. Guidotti et al. (1977)	17. Takeshita et al. (1974b)
2. Lakner et al. (1980)	18. Kierstead (1981b)
3. Kuijpers (1973)	19. Kierstead (1980b)
4. Kuijpers and Loopstra (1974)	20. Malik et al. (1981)
5. van Mal et al. (1979)	21. van Mal et al. (1976)
6. van Mal et al. (1974)	22. Shaltiel et al. (1977)
7. Clinton et al. (1975)	23. van Diepen and Buschow (1977)
8. Anderson et al. (1973)	24. Buschow (1977c)
9. Takeshita et al. (1974a)	25. Beck (1967)
10. Sarynin et al. (1977)	26. Jacob and Shaltiel (1979)
11. Gruen et al. (1977)	27. Cohen et al. (1980c)
12. Buschow et al. (1980)	28. Gualtieri and Wallace (1977)
13. van Essen and Buschow (1980b)	29. Kierstead (1981d)
14. Goudy et al. (1978)	30. Kierstead (1981e)
15. Kierstead (1981a)	31. Jacob et al. (1981)
16. Bechman et al. (1976)	

TABLE A3  
Compounds of rare earths and iron or manganese.

Comp.	$x(\text{max})$	$x(\beta_1)$	$p(\alpha-\beta)$ (atm)	$\Delta H$ (kJ/mol H <sub>2</sub> )	$\Delta S$ (J/deg mol H <sub>2</sub> )	Reaction type	Refs.
Ho <sub>6</sub> Fe <sub>23</sub>	16 (40)	-	-	-	-	-	1
Er <sub>6</sub> Fe <sub>23</sub>	14 (40)	-	-	-	-	-	1
Lu <sub>6</sub> Fe <sub>23</sub>	-	-	-	-	-	-	2
Y <sub>6</sub> Fe <sub>23</sub>	22.5	-	$< 10^{-5}$	(50°)	-	-	3
GdFe <sub>3</sub>	3.2	-	0.18	(150°)	-50.7	-	$\alpha-\beta_2$ 4
TbFe <sub>3</sub>	4.2	-	0.13	(125°)	-48.2	-	$\alpha-\beta_2$ 4
DyFe <sub>3</sub>	3.9 (13)	2 (0°)	$1.05 \times 10^{-3}$	(20°)	-45.7	-99.5	$\alpha-\beta_1$ 5, 6
HoFe <sub>3</sub>	3.6	-	0.28	(125°)	-44.8	-	$\alpha-\beta_2$ 4
ErFe <sub>3</sub>	4 (13)	-	0.53	(125°)	-43.5	-	$\alpha-\beta_2$ 4
YFe <sub>3</sub>	4.2	-	$< 10^{-5}$	(50°)	-	-	3
CeFe <sub>2</sub>	~4	-	-	-	-	-	7
SmFe <sub>2</sub>	~4	-	-	-	-	-	8
GdFe <sub>2</sub>	4.1 (20)	-	-	-29.3	-58.7	-	9
TbFe <sub>2</sub>	4	-	-	-	-	-	8
DyFe <sub>2</sub>	8 (1400)	2.0 (20°)	$5 \times 10^{-6}$	(20°)	-58.2	-96.4	- 12, 14
HoFe <sub>2</sub>	4.5	-	-	-	-	-	10
ErFe <sub>2</sub>	4.2 (13)	2	$5 \times 10^{-5}$	(20°)	-57.8	-109.8	$\alpha-\beta_1$ 11, 14
					-46.1	-110.2	$\beta_1-\beta_2$ 14
TmFe <sub>2</sub>	3.5-4.3	-	-	-	-	-	10
LuFe <sub>2</sub>	4	-	-	-	-	-	1.15
YFe <sub>2</sub>	4.2	2	$< 10^{-5}$	(50°)	-	-	3
ScFe <sub>2</sub>	3.2 (67)	2 (20°)	0.06	(20°)	-	-	22, 23
Nd <sub>6</sub> Mn <sub>23</sub>	~23	-	-	-	-	-	24
Sm <sub>6</sub> Mn <sub>23</sub>	~23	-	-	-	-	-	24
Gd <sub>6</sub> Mn <sub>23</sub>	~26	-	$< 1$	(20°)	-	-	33
Tb <sub>6</sub> Mn <sub>23</sub>	23 (60)	-	-	-	-	-	19
Dy <sub>6</sub> Mn <sub>23</sub>	23 (60)	-	-	-	-	-	19
Tm <sub>6</sub> Mn <sub>23</sub>	23	-	-	-	-	-	25
Lu <sub>6</sub> Mn <sub>23</sub>	~20 (1)	-	$< 1$	(20°)	-	-	17
Y <sub>6</sub> Mn <sub>23</sub>	23 (60)	-	$< 1$	(20°)	-	-	18, 20
GdMn <sub>2</sub>	3 (20)	-	-	-87.6	-134.0	-	3
DyMn <sub>2</sub>	>4 (150)	-	-	-	-	-	16
ErMn <sub>2</sub>	4.9 (13)	4 (22°)	$< 1.3 \times 10^{-3}$	(22°)	-	-	21
LuMn <sub>2</sub>	>4	-	-	-	-	-	17
YMn <sub>2</sub>	3.4 (2)	-	-	-	-	-	18

- |                                  |   |
|----------------------------------|---|
| 1. Boltich et al. (1981)         | 14. Kierstead (1980a)                             |
| 2. Gubbens et al. (1981)         | 15. Buschow and Donkersloot (unpublished results) |
| 3. van Essen and Buschow (1980b) | 16. Cohen et al. (1980c)                          |
| 4. Bechman et al. (1976)         | 17. Buschow and Sherwood (1977b)                  |
| 5. Kierstead (1980c)             | 18. van Mal et al. (1976)                         |
| 6. Niarchos et al. (1980b)       | 19. Pourarian et al. (1980b)                      |
| 7. van Diepen and Buschow (1977) | 20. Commandré and Sauvage (1979)                  |
| 8. Buschow (1977d)               | 21. Viccaro et al. (1980)                         |
| 9. Jacob and Shaltiel (1979)     | 22. Smit et al. (1982)                            |
| 10. Gualtieri et al. (1976b)     | 23. Niarchos et al. (1980a)                       |
| 11. Kierstead et al. (1979)      | 24. Buschow (1982b)                               |
| 12. Pourarian (1980c)            | 25. Gubbens et al. (1982)                         |
| 13. Buschow et al. (1980)        |   |

TABLE A4  
Miscellaneous compounds.

Comp.	$x(\max)$	$x(\beta_1)$	$p(\alpha-\beta)$ (atm)	$\Delta H$ (kJ/mol H <sub>2</sub> )	$\Delta S$ (J/deg mol H <sub>2</sub> )	Reaction type	Refs.
LaMg <sub>12</sub>	20 (30)	—	—	—	—	—	1
CeMg <sub>12</sub>	20 (30)	2 (325°)	3 (325°)	—	—	—	1, 3
La <sub>2</sub> Mg <sub>17</sub>	33 (30)	—	—	—	—	—	1, 3, 4
Ce <sub>2</sub> Mg <sub>17</sub>	31	—	—	—	—	—	4
Ce <sub>5</sub> Mg <sub>41</sub>	86 (30)	—	—	—	—	—	3
LaMg <sub>2</sub>	4 (65)	—	—	—	—	—	5
CeMg <sub>2</sub>	4.5 (12)	—	—	—	—	—	5
NdMg <sub>2</sub>	4 (28)	—	—	—	—	—	5
SmMg <sub>2</sub>	3 (2)	—	—	—	—	—	5
EuMg <sub>2</sub>	—	—	—	—	—	—	6
LaCu <sub>5</sub>	2.2	0.3 (20°)	—	—	—	—	8
PrCu <sub>5</sub>	2.6	—	—	—	—	—	4
NdCu <sub>5</sub>	3.0	—	—	—	—	—	4
LaRu <sub>2</sub>	4.5 (3.4)	—	—	—	—	—	5, 7, 9
CeRu <sub>2</sub>	5.2 (10)	—	—	—	—	—	5, 14
GdRu <sub>2</sub>	3.7 (70)	2.7 (164°)	0.05 (164°)	-60.34	-125.7	—	7, 9
DyRu <sub>2</sub>	3.1 (10)	—	—	-56.6	—	—	16
YRu <sub>2</sub>	3.3 (62)	—	—	—	—	—	5
LaRh <sub>2</sub>	4.9 (70)	1.4 (115°)	0.05 (195°)	-44.40	-85.06	$\alpha-\beta_1$	7, 9
EuRh <sub>2</sub>	5 (1)	—	—	—	—	—	10, 11
GdRh <sub>2</sub>	3.3 (10)	2.8 (101°)	0.9 (83°)	-49.4	-134.0	—	7, 9
EuPd	2.9 (1)	—	<1 (20°)	—	—	—	10
YbPd	2.2	—	—	—	—	—	13
YPd	3.1 (2)	—	—	—	—	—	12
LaPt <sub>5</sub>	4 (1350)	1.2 (21°)	200 (20°)	—	—	—	8
LaPt	2.8	—	—	—	—	—	15

- |                              |                                 |
|------------------------------|---------------------------------|
| 1. Darriet et al. (1979)     | 9. Shaltiel et al. (1977)       |
| 2. Yajima and Kayano (1977)  | 10. Buschow et al. (1977)       |
| 3. Pezat et al. (1980)       | 11. Cohen et al. (1978)         |
| 4. Reilly and Wiswall (1972) | 12. van Mal et al. (1976)       |
| 5. Shaltiel (1978)           | 13. Newkirk (1972)              |
| 6. Oliver et al. (1978)      | 14. Tessema et al. (1979)       |
| 7. Jacob and Shaltiel (1979) | 15. Anderson et al. (1973)      |
| 8. Takeshita et al. (1981)   | 16. Oesterreicher et al. (1982) |

Table A5

Selected examples of several hydrogen absorbing non-rare earth intermetallics and the corresponding hydrogen sorption parameters. The compounds are arranged in order of increasing concentration of the strongly hydrogen attracting component in  $AB_nH_x$ . The second column gives the values of maximum hydrogen content with the  $H_2$  pressures applied in parentheses. The plateau pressures (first plateau) given in the third column are those closest to room temperature available in the literature. Values of the sorption enthalpies and entropies are listed in the 4th and 5th columns.

TABLE A5

Compound	$x(\max)$	$p(\alpha-\beta)$ (atm)	$\Delta H$ (kJ/mole $H_2$ )	$\Delta S$ (J/K mole $H_2$ )	Refs.
CaNi <sub>5</sub>	4.2 (25)	0.5 (25°)	-34.2	-	1
ZrV <sub>2</sub>	5.3 (1)	$10^{-8}$ (20°)	-199.7	-	2
ZrCr <sub>2</sub>	3.8 (1)	0.01 (20°)	-46.1	-98	2
ZrMn <sub>2</sub>	3.6 (8)	0.01 (20°)	-53.2	-121.5	2
TiCr <sub>2</sub>	1.2 (50)	-	-23	-	3
TiCu	1 (1)	-	-75	-113	4
ZrCo	2.5 (1)	-	-84.2	-133.7	5
HfNi	3.2 (20)	0.02 (50°)	-	-	6
LiPt	0.7	-	-134	-149	7
Mg <sub>2</sub> Ni	4 (14)	1.2 (298°)	-64.5	-122.3	8

- |                           |                                 |
|---------------------------|---------------------------------|
| 1. Murray et al. (1980)   | 5. Irvine and Harris (1978)     |
| 2. Shaltiel et al. (1977) | 6. van Essen and Buschow (1979) |
| 3. Machida et al. (1978)  | 7. Nacken and Bronger (1978)    |
| 4. Macland et al. (1978)  | 8. Reilly (1978a)               |

## Tables A6–A10

Magnetic properties of compounds of rare earth elements and 3d transition metals ( $RM_n$ ) before and after charging with hydrogen gas. The composition of the ternary hydride has been listed as  $RM_nH_x$  if no details were given regarding the hydrogen concentration. The abbreviation n.l.o. in the second column indicates no long-range order as deduced from the absence of reflection lines in the X-ray diagram of the hydrides. The magnetic ordering temperatures have been listed under  $T_c$ . The values of  $T_{\text{comp}}$  refer to the minimum in the temperature dependence of the magnetization, corresponding to a cancellation of the R and M sublattice contributions. The saturation moments  $\mu_s$  are expressed in  $\mu_B$  per formula unit. Values expressed per 3d moment are given in column 6 only when R is non-magnetic or when more detailed information is available from neutron diffraction. The various compounds and hydrides have been listed in the order of increasing rare earth concentration. For a given concentration  $n$  the sequence is R = Y, La through Lu.

TABLE A6  
Magnetic properties of rare earth–nickel compounds and their hydrides.

Compound	Structure	Magnetic properties	Refs.
LaNi <sub>5</sub>	CaCu <sub>5</sub>	$\chi_g = 5 \times 10^{-6}$ emu/g	1, 2
LaNi <sub>5</sub> H <sub>6,9</sub>	CaCu <sub>5</sub>	$\chi_g = 1 \times 10^{-6}$ emu/g	1, 2
Y <sub>2</sub> Ni <sub>7</sub>	Gd <sub>2</sub> Co <sub>7</sub>	$T_c = 57$ K, $\mu_s = 0.08 \mu_B/\text{Ni}$	3
Y <sub>2</sub> Ni <sub>7</sub> H <sub>x</sub>	Gd <sub>2</sub> Co <sub>7</sub>	$T_c = 98$ K, $\mu_s = 0.05 \mu_B/\text{Ni}$	3
La <sub>2</sub> Ni <sub>7</sub>	Ce <sub>2</sub> Ni <sub>7</sub>	$T_N = 54$ K	3
La <sub>2</sub> Ni <sub>7</sub> H <sub>x</sub>	–	$\chi_g = 1 \times 10^{-5}$ emu/g	3
YNi <sub>3</sub>	PuNi <sub>3</sub>	$T_c = 35$ K, $\mu_s = 0.06 \mu_B/\text{Ni}$	4
YNi <sub>3</sub> H <sub>4</sub>	PuNi <sub>3</sub>	$\chi_g = 7 \times 10^{-6}$ emu/g	4
CeNi <sub>3</sub>	CeNi <sub>3</sub>	$\chi_g = 2 \times 10^{-6}$ emu/g	5
CeNi <sub>3</sub> H <sub>x</sub>	CeNi <sub>3</sub>	$\theta_p < 0$ , $\mu_{\text{eff}} = 2.5 \mu_B/\text{Ce}$	5
GdNi <sub>2</sub>	MgCu <sub>2</sub>	$T_c = 8$ K, $\mu_s = 6.9 \mu_B$	6
GdNi <sub>2</sub> H <sub>3,5</sub>	n.l.o.	$T_c = 8$ K, $\mu_s = 4.2 \mu_B$	6

1. Palleau and Chouteau (1980)
2. Stucki and Schlapbach (1980)
3. Buschow (1982c)
4. Buschow and van Essen (1979)
5. Buschow (1980a)
6. Malik and Wallace (1977)

TABLE A7  
Magnetic properties of rare earth-cobalt compounds and their hydrides.

Compound	Structure	$T_c$ (K)	$T_{\text{comp}}$ (K)	$\mu_s$ ( $\mu_B/\text{FU}$ )	$\mu_{\text{Co}}$ ( $\mu_B/\text{Co}$ )	Refs.
LaCo <sub>5</sub>	CaCu <sub>5</sub>	840	—	7.3	1.5	1
LaCo <sub>5</sub> H <sub>0.17</sub>	CaCu <sub>5</sub>	> 300	—	—	—	2
LaCo <sub>5</sub> H <sub>3.35</sub>	orthor.	> 300	—	5.60	1.14	2
LaCo <sub>5</sub> H <sub>4.3</sub>	orthor.	—	—	1.64	0.33	2
CeCo <sub>5</sub>	CaCu <sub>5</sub>	737	—	6.5	—	1
CeCo <sub>5</sub> H <sub>2.55</sub>	orthor.	—	—	4.4	0.98	2, 3
PrCo <sub>5</sub>	CaCu <sub>5</sub>	912	—	9.95	—	1
PrCo <sub>5</sub> H <sub>2.8</sub>	orthor.	—	—	—	1.05	2
PrCo <sub>5</sub> H <sub>3.6</sub>	orthor.	> 300	—	3.70	0.83	2, 3
NdCo <sub>5</sub>	CaCu <sub>5</sub>	910	—	10.6	—	1
NdCo <sub>5</sub> H <sub>0.3</sub>	CaCu <sub>5</sub>	> 300	—	—	1.45	2
NdCo <sub>5</sub> H <sub>2.8</sub>	orthor.	> 300	—	5.06	—	2, 4
SmCo <sub>5</sub>	CaCu <sub>5</sub>	1020	—	7.3	—	1
SmCo <sub>5</sub> H <sub>2.5</sub>	orthor.	> 300	—	—	0.2	2
Y <sub>2</sub> Co <sub>7</sub>	Gd <sub>2</sub> Co <sub>7</sub>	639	—	8.75	1.3	1, 5
Y <sub>2</sub> Co <sub>7</sub> H <sub>3</sub>	Gd <sub>2</sub> Co <sub>7</sub>	—	—	1.5	0.3	5, 6
La <sub>2</sub> Co <sub>7</sub>	Gd <sub>2</sub> Co <sub>7</sub>	490	—	7.0	1.0	7
La <sub>2</sub> Co <sub>7</sub> H <sub>5</sub>	Gd <sub>2</sub> Co <sub>7</sub>	> 300	—	4.2	0.6	7, 8
Ce <sub>2</sub> Co <sub>7</sub>	Ce <sub>2</sub> Ni <sub>7</sub>	50	—	0.9	—	10
Ce <sub>2</sub> Co <sub>7</sub> H <sub>7</sub>	Ce <sub>2</sub> Ni <sub>7</sub>	233	—	3.8	—	9, 10
YCo <sub>3</sub>	PuNi <sub>3</sub>	305	—	2.4	0.8	1, 8
YCo <sub>3</sub> H	PuNi <sub>3</sub>	—	—	1.0	0.3	8, 9
YCo <sub>3</sub> H <sub>3</sub>	PuNi <sub>3</sub>	—	—	~0	~0	8, 9
CeCo <sub>3</sub>	PuNi <sub>3</sub>	< 10	—	< 0.1	—	10
CeCo <sub>3</sub> H <sub>4</sub>	PuNi <sub>3</sub>	80	—	0.8	—	10
GdCo <sub>3</sub>	PuNi <sub>3</sub>	611	—	2.29	—	1
GdCo <sub>3</sub> H <sub>2.2</sub>	PuNi <sub>3</sub>	> 300	—	3.37	1.2	11
GdCo <sub>3</sub> H <sub>4.6</sub>	PuNi <sub>3</sub>	28	—	3.92	1.03	11
DyCo <sub>3</sub>	PuNi <sub>3</sub>	452	—	4.4	—	1
DyCo <sub>3</sub> H <sub>4.3</sub>	PuNi <sub>3</sub>	18	—	3.82	—	11
HoCo <sub>3</sub>	PuNi <sub>3</sub>	418	—	5.45	—	1
HoCo <sub>3</sub> H <sub>4.2</sub>	PuNi <sub>3</sub>	15	—	3.16	—	11
ErCo <sub>3</sub>	PuNi <sub>3</sub>	395	226	4.2	—	1, 14
ErCo <sub>3</sub> H <sub>4.2</sub>	PuNi <sub>3</sub>	—	170	1.04	—	14
TmCo <sub>3</sub>	PuNi <sub>3</sub>	401	122	3.0	—	1, 14
TmCo <sub>3</sub> H <sub>3.3</sub>	PuNi <sub>3</sub>	—	164	2.04	—	14
YCo <sub>2</sub>	MgCu <sub>2</sub>			Pauli paramagnetic		1
YCo <sub>2</sub> H <sub>4</sub>	n.l.o.			complex behavior		12, 15
PrCo <sub>2</sub>	MgCu <sub>2</sub>	49	—	2.83		1
PrCo <sub>2</sub> H <sub>4</sub>	n.l.o.			complex behavior		13

TABLE A7(cont.)

Compound	Structure	$T_c$ (K)	$T_{\text{comp}}$ (K)	$\mu_s$ ( $\mu_B/\text{FU}$ )	$\mu_{\text{Co}}$ ( $\mu_B/\text{Co}$ )	Refs.
GdCo <sub>2</sub>	MgCu <sub>2</sub>	398	–	4.8		12
GdCo <sub>2</sub> H <sub>4</sub>	MgCu <sub>2</sub>	~90	–	4.7		12
TbCo <sub>2</sub>	MgCu <sub>2</sub>	230	–	6.65		16
TbCo <sub>2</sub> H <sub>3.2</sub>	MgCu <sub>2</sub>	50	–	4.15		16
DyCo <sub>2</sub>	MgCu <sub>2</sub>	140	–	6.75		16
DyCo <sub>2</sub> H <sub>3.3</sub>	MgCu <sub>2</sub>	40	–	4.1		16
HoCo <sub>2</sub>	MgCu <sub>2</sub>	76	–	7.4		17
HoCo <sub>2</sub> H <sub>3.5</sub>	MgCu <sub>2</sub>	40	–	4.7		17
ErCo <sub>2</sub>	MgCu <sub>2</sub>	35	–	7		17
ErCo <sub>2</sub> H <sub>3.4</sub>	MgCu <sub>2</sub>	25	–	4.35		17

1. Buschow (1977a)

2. Kuijpers (1973)

3. Kuijpers and Loopstra (1974)

4. Kuijpers (1972b)

5. Buschow (1982c)

6. Buschow and van Essen (1980b)

7. Buschow et al. (1980)

8. Buschow and de Châtel (1979)

9. van Essen and Buschow (1980b)

10. Buschow (1980b)

11. Malik et al. (1978b)

12. Buschow (1977b)

13. De Jongh et al. (1981)

14. Malik et al. (1981)

15. Buschow and

van der Kraan (1983)

16. Pourarian et al. (1982a)

17. Pourarian et al. (1982b)



TABLE A8  
Magnetic properties of rare earth-iron compounds and their hydrides.

Compound	Structure	$T_c$ (K)	$T_{comp}$ (K)	$\mu_s$ ( $\mu_B/FU$ )	$\mu_{Fe}$ ( $\mu_B/Fe$ )	Refs.
$Y_6Fe_{23}$	$Th_6Mn_{23}$	481	–	43.1	1.65	1
$Y_6Fe_{23}H_{20}$	$Th_6Mn_{23}$	630	–	39.6	1.72	2
$Y_6Fe_{23}H_{22}$	$Th_6Mn_{23}$	743	–	45.1	1.96	3
$Ho_6Fe_{23}$	$Th_6Mn_{23}$	530	205	14.6	–	1
$Ho_6Fe_{23}H_{16}$	$Th_6Mn_{23}$	> 300	75	7.8	–	4
$Er_6Fe_{23}$	$Th_6Mn_{23}$	494	112	6.4	–	1
$Er_6Fe_{23}H_{14}$	tetr.	> 300	19.5	8.0	–	4
$Tm_6Fe_{23}$	$Th_6Mn_{23}$	480	–	15.2	–	5
$Tm_6Fe_{23}H_x$	$Th_6Mn_{23}$	550	–	23.6	–	5
$Lu_6Fe_{23}$	$Th_6Mn_{23}$	–	–	35.4	1.54	6
$Lu_6Fe_{23}H_8$	$Th_6Mn_{23}$	–	–	37.7	1.64	6
$YFe_3$	$PuNi_3$	549	–	5.01	1.67	2
$YFe_3H_5$	$PuNi_3$	545	–	5.70	1.90	2
$GdFe_3$	$PuNi_3$	729	618	1.79	–	1
$GdFe_3H_{3,1}$	$PuNi_3$	–	170	1.39	–	7
$DyFe_3$	$PuNi_3$	606	465	3.97	–	1
$DyFe_3H_{1,67}$	$PuNi_3$	–	310	–	–	8
$DyFe_3H_{2,5}$	$PuNi_3$	–	210	–	–	8
$DyFe_3H_3$	$PuNi_3$	–	175	2.2	–	7, 9
$DyFe_3H_{4,28}$	$PuNi_3$	–	145	–	–	8
$HoFe_3$	$PuNi_3$	571	393	4.53	–	1
$HoFe_3H_3$	$PuNi_3$	–	112	2.53	–	7
$ErFe_3$	$PuNi_3$	552	236	3.45	–	1
$ErFe_3H_x$	$PuNi_3$	–	–	–	–	10
$YFe_2$	$MgCu_2$	545	–	2.90	1.45	11
$YFe_2H_x$	$MgCu_2$	308	–	3.4	1.7	11
$CeFe_2$	$MgCu_2$	230	–	2.59	1.24	11
$CeFe_2H_x$	–	358	–	4.8	–	11
$SmFe_2$	$MgCu_2$	676	–	2.75	–	11
$SmFe_2H_x$	$MgCu_2$	333	–	3.2	–	11
$GdFe_2$	$MgCu_2$	785	–	2.80	–	11
$GdFe_2H_x$	$MgCu_2$	388	–	4.0	–	11
$GdFe_2H_{4,1}$	$MgCu_2$	338	180	5.39	–	12
$TbFe_2$	$MgCu_2$	711	–	4.72	–	11
$TbFe_2H_x$	$MgCu_2$	303	–	4.6	–	11
$TbFe_2H_3$	$MgCu_2$	> 300	–	7.8	–	13
$DyFe_2$	$MgCu_2$	635	–	5.50	–	11
$DyFe_2H_{1,9}$	$MgCu_2$	> 500	–	3.5	1.7	14
$DyFe_2H_x$	$MgCu_2$	385	–	4.9	–	11
$DyFe_2H_{3,5}$	–	> 300	–	7.5	–	13, 15

TABLE A8 (cont.)

Compound	Structure	$T_c$ (K)	$T_{comp}$ (K)	$\mu_s$ ( $\mu_B$ /FU)	$\mu_{Fe}$ ( $\mu_B$ /Fe)	Refs.
HoFe <sub>2</sub>	MgCu <sub>2</sub>	612	—	5.50	1.5	11, 16
HoFe <sub>2</sub> D <sub>3.5</sub>	MgCu <sub>2</sub>	—	—	—	1.9	16
HoFe <sub>2</sub> H <sub>x</sub>	MgCu <sub>2</sub>	298	—	5.5	—	11
HoFe <sub>2</sub> H <sub>4.5</sub>	MgCu <sub>2</sub>	287	60	2.35	—	17
ErFe <sub>2</sub>	MgCu <sub>2</sub>	587	486	4.85	1.6	1, 16
ErFe <sub>2</sub> H <sub>0.5</sub>	MgCu <sub>2</sub>	—	395	—	—	12
ErFe <sub>2</sub> H <sub>2</sub>	MgCu <sub>2</sub>	—	251	—	—	12
ErFe <sub>2</sub> H <sub>3.4</sub>	MgCu <sub>2</sub>	—	152	—	—	12
ErFe <sub>2</sub> D <sub>3.5</sub>	MgCu <sub>2</sub>	440	—	—	1.6	16
ErFe <sub>2</sub> H <sub>3.6</sub>	MgCu <sub>2</sub>	270	—	—	—	18
ErFe <sub>2</sub> H <sub>3.9</sub>	MgCu <sub>2</sub>	280	42	5.60	—	17
ErFe <sub>2</sub> H <sub>4</sub>	MgCu <sub>2</sub>	< 4	—	—	—	12
ErFe <sub>2</sub> H <sub>4.1</sub>	—	< 4.2	—	—	~0.2	18, 19
TmFe <sub>2</sub>	MgCu <sub>2</sub>	599	236	2.61	—	1
TmFe <sub>2</sub> H <sub>4.3</sub>	MgCu <sub>2</sub>	270	18	6.45	—	17
LuFe <sub>2</sub>	MgCu <sub>2</sub>	596	—	2.70	1.35	1, 20
LuFe <sub>2</sub> H <sub>4</sub>	MgCu <sub>2</sub>	—	—	3.34	1.67	20
ScFe <sub>2</sub>	MgZn <sub>2</sub>	542	—	2.30	1.15	21, 22
ScFe <sub>2</sub> H <sub>1.7</sub>	MgZn <sub>2</sub>	—	—	2.9	1.45	21
ScFe <sub>2</sub> H <sub>2</sub>	MgZn <sub>2</sub>	< 542	—	4.46	2.23	22
ScFe <sub>2</sub> H <sub>2.5</sub>	MgZn <sub>2</sub>	—	—	4.2	2.1	21
ScFe <sub>2</sub> H <sub>3.2</sub>	MgZn <sub>2</sub>	—	—	4.6	2.3	21

- |                                     |                                       |
|-------------------------------------|---------------------------------------|
| 1. Buschow (1977a)                  | 12. Oesterreicher and Bittner (1980b) |
| 2. Oesterreicher and Bittner (1977) | 13. Pourarian et al. (1982a)          |
| 3. Buschow (1976)                   | 14. Viccaro et al. (1979b)            |
| 4. Boltich et al. (1981)            | 15. Pourarian et al. (1980c)          |
| 5. Gubbens et al. (1983b)           | 16. Fish et al. (1979)                |
| 6. Gubbens et al. (1981)            | 17. Gualtieri et al. (1976b)          |
| 7. Malik et al. (1976)              | 18. Viccaro et al. (1979a)            |
| 8. Niarchos et al. (1980b)          | 19. Dunlap et al. (1979)              |
| 9. Wallace (1979)                   | 20. Buschow et al. (1980)             |
| 10. Niarchos et al. (1979)          | 21. Niarchos et al. (1980a)           |
| 11. Buschow (1977d)                 | 22. Smit and Buschow (1980)           |

TABLE A9  
Magnetic properties of rare earth-manganese compounds and their hydrides.

Compound	Structure	$T_c$ (K)	$T_{comp}$ (K)	$\mu_s$ ( $\mu_B$ /FU)	$\mu_{Mn}$ ( $\mu_B$ /Mn)	Refs.
$Y_6Mn_{23}$	$Th_6Mn_{23}$	486	—	13.2	1.8–2.8	1
$Y_6Mn_{23}H_9$	$Th_6Mn_{23}$	563	—	5	—	2
$Y_6Mn_{23}H_{22}$	$Th_6Mn_{23}$	—	—	$\sim 0$	—	4–7
$Nd_6Mn_{23}$	$Th_6Mn_{23}$	445	—	10.1	—	8
$Nd_6Mn_{23}H_x$	$Th_6Mn_{23}$	220	—	20.8	—	9
$Sm_6Mn_{23}$	$Th_6Mn_{23}$	442	—	10.3	—	8
$Sm_6Mn_{23}H_x$	$Th_6Mn_{23}$	230	—	15.3	—	9
$Gd_6Mn_{23}$	$Th_6Mn_{23}$	461	—	49	—	4
$Gd_6Mn_{23}H_x$	$Th_6Mn_{23}$	145	—	14.2	—	4, 7
$Tb_6Mn_{23}$	$Th_6Mn_{23}$	455	—	44.4	—	10
$Tb_6Mn_{23}H_x$	$Th_6Mn_{23}$	220	—	17.7	—	7
$Dy_6Mn_{23}$	$Th_6Mn_{23}$	435	—	49.8	—	10, 11
$Dy_6Mn_{23}H_x$	$Th_6Mn_{23}$	$> 10$	—	—	—	7, 11
$Ho_6Mn_{23}$	$Th_6Mn_{23}$	434	—	49.2	—	10
$Ho_6Mn_{23}H_x$	$Th_6Mn_{23}$	—	—	—	—	7
$Er_6Mn_{23}$	$Th_6Mn_{23}$	420	—	45.6	—	10, 3
$Er_6Mn_{23}H_x$	$Th_6Mn_{23}$	85	—	—	—	12
$Tm_6Mn_{23}$	$Th_6Mn_{23}$	404	—	29.5	—	15
$Tm_6Mn_{23}H_x$	$Th_6Mn_{23}$	—	—	6.5	—	15
$Lu_6Mn_{23}$	$Th_6Mn_{23}$	378	—	8.9	—	3, 6
$Lu_6Mn_{23}H_x$	$Th_6Mn_{23}$	266	—	3.4	—	3, 6
$YMn_2$	$MgCu_2$	—	—	0	—	10
$YMn_2H_x$	$MgCu_2$	284	—	0–0.5	—	3, 4, 6
$GdMn_2$	$MgCu_2$	(10)	—	4.8	—	4
$GdMn_2H_x$	$MgCu_2$	260	—	3.2	—	4
$DyMn_2$	$MgCu_2$	41	—	6.7	—	11
$DyMn_2H_x$	n.l.o.	$< 4.2$	—	—	—	11
$ErMn_2$	$MgZn_2$	25	—	7.9	—	10
$ErMn_2H_4$	$MgZn_2$	$> 4.2$	—	—	—	13
$ErMn_2H_{4.6}$	$MgZn_2$	$< 1.5$	—	—	—	13
$LuMn_2$	$MgZn_2$	—	—	—	—	4, 6
$LuMn_2H_x$	$MgZn_2$	201	—	0.16	—	4, 6
$ScMn_2$	$MgZn_2$	—	—	$\sim 0$	—	14
$ScMn_2H_x$	$MgZn_2$	217	—	0.1	—	14

1. Delapalme et al. (1979)

2. Commandré et al. (1979, 1980)

3. Buschow (1977b)

4. Buschow and Sherwood (1977b)

5. Malik et al. (1977b)

6. Buschow and Sherwood (1977a)

7. Pourarian et al. (1980a, b)

8. Parker and Oesterreicher (1982)

9. Buschow (1981)

10. Buschow (1977a)

11. Gubbens et al. (1983)

12. Stewart et al. (1981b)

13. Viccaro et al. (1980)

14. Buschow (1982a)

15. Gubbens et al. (1983a)

TABLE A10

Magnetic properties of intermetallic compounds and ternary hydrides consisting of rare earth elements and non-magnetic metals.

Compound	Structure	$T_c, T_N$ (K)	$\theta_p$ (K)	$\mu_s$ ( $\mu_B/R$ )	$\mu_{\text{eff}}$ ( $\mu_B/R$ )	Refs.
GdCu <sub>2</sub>	CeCu <sub>2</sub>	$T_N = 37$	+7	—	8.70	1
GdCu <sub>2</sub>	MoSi <sub>2</sub>	$T_c = 45$	+57	1.62	8.63	1
GdRu <sub>2</sub>	MgZn <sub>2</sub>	$T_c = 83$	100	7.9	7.9	2
GdRu <sub>2</sub> H <sub>3</sub>	—	$T_c = 65$	—	—	—	3
GdRh <sub>2</sub>	MgCu <sub>2</sub>	$T_c = 73$	77	6.9	7.9	2
GdRh <sub>2</sub> H <sub>3</sub>	orthorh.	$T_c = 35$	—	6.2	—	3
EuRh <sub>2</sub>	MgCu <sub>2</sub>		no Curie-Weiss behaviour			
EuRh <sub>2</sub> H <sub>5</sub>	MgCu <sub>2</sub>	15.5	9	5	7.85	4
GdCu	CsCl	$T_N = 150$	-86	—	8.45	5
GdCuH <sub>x</sub>		$T_c = 30$	15	3.6	8.40	6
GdAg	CsCl	$T_N = 123$	-57	—	8.81	6
GdAgH <sub>x</sub>		$T_c = 25$	50	4.38	7.81	6
GdAu	CsCl	—	25	—	8.52	6
GdAuH <sub>x</sub>		—	27	2.85	8.16	6
GdPd	CrB	$T_c = 32$	29	—	—	6
GdPdH <sub>x</sub>		$T_c = 40$	16	3.36	8.27	6
Gd <sub>3</sub> Pd <sub>4</sub>	Pu <sub>3</sub> Pd <sub>4</sub>	$T_N = 18$	-18	—	8.80	6
Gd <sub>3</sub> Pd <sub>4</sub> H <sub>x</sub>		$T_c \approx 20$	-10	3.83	8.70	6
Gd <sub>3</sub> Pd <sub>2</sub>		$T_N = 30$	-30	—	9.85	6
Gd <sub>3</sub> Pd <sub>2</sub> H <sub>x</sub>		—	~0	2.04	8.17	6
Gd <sub>7</sub> Pd <sub>3</sub>	Th <sub>7</sub> Fe <sub>3</sub>	$T_c = 311$	276	8.24	8.22	6
Gd <sub>7</sub> Pd <sub>3</sub> H <sub>x</sub>		—	-15	—	8.11	6
EuPd	CrB	48	~0	—	8.2	9
EuPdH <sub>2.9</sub>	CsCl	21	5	1.5	7.5	4
Eu <sub>2</sub> Ru	—	—	—	—	—	
Eu <sub>2</sub> RuH <sub>6</sub>	Sr <sub>2</sub> RuH <sub>6</sub>	$T_c = 29$	+29	—	7.5	7, 8

1. de Graaf et al. (1982b)
2. Buschow (1979)
3. Jacob et al. (1980c)
4. Buschow et al. (1977)
5. van Dongen et al. (1983)
6. Buschow (1982c)
7. Thompson et al. (1975)
8. Lindsay and Moyer (1981)
9. Buschow (1979)

## References

- Adachi, G.Y., K.I. Niki and J. Shiokawa, 1981, *J. Less-Common Met.* **81**, 345-348.
- Adachi, G., K. Niki, H. Nagai and J. Shiokawa, 1982, *J. Less-Common Met.* **88**, 213-216.
- Anderson, J.L., T.C. Wallace, A.L. Bowman, C.L. Radosevich and M.L. Courtney, 1973, Los Alamos Sci. Lab. Rept. LA-5320-MS.
- Andreef, B.M., Ya.D. Zelvenskii, A.I. Shaviev and V.V. Shitikov, 1978, *Russ. J. Phys.* **52**, 879-880.
- Andreev, A.V., A.V. Deryagin, V.N. Moskalev and N.V. Mushnikov, 1982, *Phys. Stat. Sol. (a)* **73**, K69-71.
- Andresen, A.F., 1978, in: *Hydrides for Energy Storage*, eds. A.F. Andresen and A.J. Maeland (Pergamon, Oxford) pp. 61-66.
- Andresen A.F. and A.J. Maeland, eds., 1978, *Hydrides for Energy Storage* (Pergamon, Oxford).
- Antonov, V.E., I.T. Belash, B.K. Ponomarev, E.G. Ponyatovskii and V.G. Tissen, 1978, *Sov. Phys. Solid State* **20**, 242.
- Archard, J.C., C. Lartigue, A. Percheron-Guégan, J.C. Mathieu, A. Pasturel and F. Tasset, 1981, *J. Less-Common Met.* **79**, 161-164.
- Archard, J.C., C. Lartigue and A. Percheron-Guégan, 1982, *J. Less-Common Met.* **88**, 89-96.
- Avrami, M., 1940, *J. Chem. Phys.* **8**, 212.
- Azoulay, J. and L. Ley, 1979, *Solid State Commun.* **31**, 31-34.
- Barnes, R.G., W.C. Harper, S.C. Nelson, D.K. Thome and D.R. Torgeson, 1976, *J. Less-Common Met.* **49**, 483-491.
- Bauminger, E.R., D. Davidov, I. Felner, I. Nowick, S. Ofer and D. Shaltiel, 1977, *Physica* **86-88B**, 201.
- Bechman, C.A., A. Goudy, T. Takeshita, W.E. Wallace and R.S. Craig, 1976, *Inorg. Chem.* **15**, 2184.
- Beck, P.A., 1972, *J. Less-Common Met.* **28**, 193.
- Belkbir, L., E. Joly, N. Gerard, J.C. Archard and A. Percheron-Guégan, 1980, *J. Less-Common Met.* **73**, 69-77.
- Belkbir, L., E. Joly and N. Gerard, 1981, *J. Less-Common Met.* **81**, 199-206.
- Bergsma, J., J.A. Goedkoop and J.H.N. van Vucht, 1963, *Acta Crystallogr.* **14**, 223-228.
- Besnus, M.J., A. Herr and G. Fischer, 1979, *J. Phys. F: Metal Phys.* **9**, 745-751.
- Biris, A., R.V. Bucur, P. Ghete, E. Indrea and D. Lupu, 1976, *J. Less-Common Met.* **49**, 477-482.
- Bläsius, A. and U. Gonsler, 1980, *J. Appl. Phys.* **22**, 331-332.
- Bloch, D., D.M. Edwards, M. Shimizu and J. Voiron, 1975, *J. Phys. F: Metal Phys.* **5**, 1217.
- Block, F.R. and H.J. Bahs, 1983, *J. Less-Common Met.* **89**, 77-84.
- Boltich, E., W.E. Wallace, F. Pourarian and S.K. Malik, 1982, *J. Magn. Magn. Mater.* **25**, 295-298.
- Boltich, H.B., F. Pourarian, W.E. Wallace, H.K. Smith and S.K. Malik, 1981, *Solid State Commun.* **40**, 117-120.
- Boom, R., F.R. de Boer and A.R. Miedema, 1976, *J. Less-Common Met.* **45**, 237; **46**, 271.
- Bos, W.G. and K.H. Gayer, 1966, *J. Nucl. Mater.* **18**, 1-30.
- Boser, O., 1976, *J. Less-Common Met.* **46**, 91-99.
- Boureau, G., O.J. Kleppa and Pd. Antonioni, 1979, *J. Solid State Chem.* **28**, 223.
- Bouten, P.C.P. and A.R. Miedema, 1980, *J. Less-Common Met.* **71**, 147-160.
- Bowerman, B.S., C.A. Wulff and T.B. Flanagan, 1979, *Z. Phys. Chem.* **116**, 179-181.
- Bowerman, B.S., C.A. Wulff, G.E. Biehl and T.B. Flanagan, 1980, *J. Less-Common Met.* **73**, 1-15.
- Bowman, A.L., J.L. Anderson and N.G. Nere-son, 1973, *Proc. 10th Rare Earth Research Conf., Carefree, AZ (1973)*, eds. C.J. Kevane and T. Moeller, pp. 485-491.
- Bowman, R.C. and W.E. Tadlock, 1979, *Solid State Commun.* **32**, 313-318.
- Bowman, R.C., A. Attalla and A.J. Maeland, 1978, *Solid State Commun.* **72**, 501-505.
- Bowman, R.C., D.M. Gruen and M.H. Mendelsohn, 1979, *Solid State Commun.* **32**, 501-506.
- Bowman, Jr., R.C., B.D. Craft and A. Attalla, 1980, *J. Less-Common Met.* **73**, 227-232.
- Bronoel, G., J. Saradin, M. Bonnemey, A. Percheron, J.C. Achard and J.L. Schlapbach, 1976, *Int. J. Hydr. Energy* **1**, 251.
- Brouha, M. and K.H.J. Buschow, 1975, *J. Phys. F: Metal Phys.* **5**, 543-554.
- Brouha, M., K.H.J. Buschow and A.R. Miedema, 1974, *IEEE Trans. Magn. MAG-10*, 182-185.
- Buchner, H., 1976, U.S. Patent 3,940,912; *J. Phys. F: Metal Phys.* **9**, L141-142.
- Buchner, H., 1978a, in: *Hydrides for Energy Storage*, eds. A.F. Andresen and A. J. Maeland (Pergamon, Oxford) pp. 569-573.
- Buchner, H., 1978b, *Int. J. Hydr. Energy* **3**, 85.
- Buchner, H., 1981, *Chemie-Techn.* **10**, 289-292.
- Buchner, H., M.A. Gutjahr, K.D. Beccu and H. Säufferer, 1972, *Z. Metallkde* **63**, 497.
- Bührer, W., A. Furrer, W. Hälgl and L. Schlapbach, 1979, *J. Phys. F: Metal Phys.* **9**, L141-142.
- Burnasheva, V.V., A.V. Ivanov and K.N. Semenenko, 1978, *Izv. Akad. Nauk SSSR, Neorg. Mater.* **14**, 1302-1307.
- Busch, G. and L. Schlapbach, 1978, *Helv. Phys. Acta* **51**, 5.
- Busch, G., L. Schlapbach, W. Thoeni, Th. von Waldkirch, P. Fischer, A. Furrer and W. Haelg, 1977, *Proc. 2nd Intern. Cong. Hydrogen in Metals (Paris)*, paper 1D7.
- Busch, G., L. Schlapbach and A. Seiler, 1978a, in: *Hydrides for Energy Storage*, eds. A.F. Andresen and A.J. Maeland (Pergamon, Oxford) pp. 293-300.
- Busch, G., L. Schlapbach and Th. von Waldkirch, 1978b, *J. Less-Common Met.* **60**, 83.
- Busch, G., L. Schlapbach and Th. von Waldkirch, 1978c, in: *Hydrogen for Energy Storage*,

- eds. A.F. Andresen and A.J. Maeland (Pergamon, Oxford) pp. 287-292.
- Buschow, K.H.J., 1971, *Philips Res. Repts.* **26**, 49-64.
- Buschow, K.H.J., 1974, *J. Less-Common Met.* **37**, 91-101.
- Buschow, K.H.J., 1976, *Solid State Commun.* **19**, 421-423.
- Buschow, K.H.J., 1977a, *Repts. Prog. Phys.* **40**, 1179.
- Buschow, K.H.J., 1977b, *J. Less-Common Met.* **51**, 173-175.
- Buschow, K.H.J., 1977c, *Solid State Commun.* **21**, 1031-1033.
- Buschow, K.H.J., 1977d, *Physica* **86-88B**, 79-80.
- Buschow, K.H.J., 1978, in: *Hydrides for Energy Storage*, eds. A.F. Andresen and A.J. Maeland (Pergamon, Oxford) pp. 273-285.
- Buschow, K.H.J., 1979, *Repts. Prog. Phys.* **42**, 1373-1477.
- Buschow, K.H.J., 1980a, in: *Ferromagnetic Materials*, Vol. 1, ed. E.P. Wohlfarth (North-Holland, Amsterdam) pp. 297-414.
- Buschow, K.H.J., 1980b, *J. Less-Common Met.* **72**, 257-263.
- Buschow, K.H.J., 1981, *Solid State Commun.* **40**, 207-210.
- Buschow, K.H.J., 1982a, *J. Magn. Magn. Mater.* **29**, 91-99.
- Buschow, K.H.J., 1982b, *Solid State Commun.*
- Buschow, K.H.J., 1982c, unpublished results.
- Buschow, K.H.J. and N.H. Beekmans, 1979, *Phys. Stat. Sol. (a)* **60**, 193-200.
- Buschow, K.H.J. and P.F. de Châtel, 1979, *Pure Appl. Chem.* **52**, 135-140.
- Buschow, K.H.J. and A.R. Miedema, 1978, in: *Hydrides for Energy Storage*, eds. A.F. Andresen and A.J. Maeland (Pergamon, Oxford), pp. 253-259.
- Buschow, K.H.J. and R.C. Sherwood, 1977a, *IEEE Trans. Magn. MAG-13*, 1571-1573.
- Buschow, K.H.J. and R.C. Sherwood, 1977b, *J. Appl. Phys.* **48**, 4643-4648.
- Buschow, K.H.J. and R.C. Sherwood, 1978, *J. Appl. Phys.* **49**, 1480-1485.
- Buschow, K.H.J. and A.M. van der Kraan, 1983, *J. Less-Common Met.* **91**.
- Buschow, K.H.J. and A.S. van der Goot, 1969, *Phys. Stat. Sol.* **35**, 515-522.
- Buschow, K.H.J. and A.M. van Diepen, 1976, *Solid State Commun.* **19**, 79-81.
- Buschow, K.H.J. and A.M. van Diepen, 1979, *Solid State Commun.* **31**, 469-471.
- Buschow, K.H.J. and R.M. van Essen, 1979, *Solid State Commun.* **32**, 1241-1242.
- Buschow, K.H.J. and H.H. van Mal, 1972, *J. Less-Common Met.* **29**, 203.
- Buschow, K.H.J. and H.H. van Mal, 1982, in: *Intercalation Chemistry*, eds. M.S. Whittingham and A.J. Jacobson (Academic Press, New York) Ch. 13, pp. 405-444.
- Buschow, K.H.J. and R.P. van Stapele, 1970, *J. Appl. Phys.* **41**, 4066-4069.
- Buschow, K.H.J. and J.H.N. van Vucht, 1967, *Philips Res. Repts.* **22**, 233-245.
- Buschow, K.H.J., R.L. Cohen and K.W. West, 1977, *J. Appl. Phys.* **48**, 5289-5295.
- Buschow, K.H.J., A.M. van Diepen, N.M. Beekmans and J.W.M. Biesterbos, 1978, *Solid State Commun.* **28**, 181-185.
- Buschow, K.H.J., P.H. Smit and R.M. van Essen, 1980, *J. Magn. Magn. Mater.* **15-18**, 1261-1263.
- Buschow, K.H.J., P.C.P. Bouten and A.R. Miedema, 1982a, *Repts. Prog. Phys.* **45**, 937-1038.
- Buschow, K.H.J., P.C.M. Gubbens, W. Ras and A.M. van der Kraan, 1982b, *J. Appl. Phys.* **53**, 8329-8331.
- Carstens, D.H.W., 1978, *J. Less-Common Met.* **61**, 253-259.
- Carter, F.L., 1980, *J. Less-Common Met.* **74**, 245.
- Cho, Y.K., R. Yamamoto, M. Doyama, S. Ono, K. Imanari and T. Tabata, 1982, *J. Less-Common Met.* **88**, 125-131.
- Christian, J.W., 1965, in: *Physical Metallurgy*, ed. R.W. Cahn, (North-Holland, Amsterdam) pp. 443-540.
- Christian, J.W., 1975, *The Theory of Transformations in Metals and Alloys*, Part I (Pergamon, Oxford).
- Chung, Y., T. Takeshita, O.D. McMasters and K.A. Gschneidner, 1980, *J. Less-Common Met.* **74**, 217-223.
- Clinton, J., H. Bittner and H. Oesterreicher, 1975, *J. Less-Common Met.* **41**, 187-189.
- Coey, J.D.M., D.H. Ryan, D. Gignoux and A. Lienard, 1982, *J. Appl. Phys.* **53**, 7804-7805.
- Cohen, R.L. and J.H. Wernick, 1982, *Science*.
- Cohen, R.L., K.W. West and K.H.J. Buschow, 1978, *Solid State Commun.* **25**, 293-295.
- Cohen, R.L., K.W. West and J.H. Wernick, 1980a, *J. Less-Common Met.* **73**, 273-279.
- Cohen, R.L., K.W. West and J.H. Wernick, 1980b, *J. Less-Common Met.* **70**, 229-241.
- Cohen, R.L., K.W. West, F. Oliver and K.H.J. Buschow, 1980c, *Phys. Rev.* **21**, 941-944.
- Commandré, M., D. Fruchart, A. Rouault, D. Sauvage, C.B. Shoemaker and D.P. Shoemaker, 1979, *J. Physique* **40**, L639-642.
- Commandré, M., D. Sauvage, D. Fruchart, A. Rouault, C.B. Shoemaker and D.P. Shoemaker, 1980, *J. Less-Common Met.* **74**, 14.
- Cotts, R.M., 1972, *Ber. Bunsenges. Phys. Chem.* **76**, 760.
- Crowder, C., W.J. James and W. Yelon, 1982, *J. Appl. Phys.* **53**, 2637-2639.
- Cyrot, M., D. Gignoux, F. Givord and M. Lavagna, 1979, *J. Physique* **40**, C5-171-176.
- Darriet, B., M. Pezat, A. Hbika and P. Hagenmuller, 1979, *Mat. Res. Bull.* **14**, 377-385.
- Dayan, D., M.H. Mintz and M.P. Dariel, 1980, *J. Less-Common Met.* **73**, 15-24.
- De Boer, F.R., W.H. Dijkman, W.C.M. Mattens and A.R. Miedema, 1979, *J. Less-Common Met.* **64**, 241.
- De Gennes, P.G., 1962a, *J. Phys. Radium* **23**, 510-520.
- De Gennes, P.G., 1962b, *J. Phys. Radium* **23**, 630-641.
- De Graaf, H., R.C. Thiel and K.H.J. Buschow, 1982a, *J. Phys. F: Metal Phys.* **12**, 1239-1245.
- De Graaf, H., R.C. Thiel and K.H.J. Buschow, 1982b, *J. Phys. F: Metal Phys.* **12**, 2079-2090.

- De Jongh, L.J., J. Bartholomé, F.J.A.M. Greidanus, H.J.M. de Groot, H.L. Stipdonk and K.H.J. Buschow, 1981, *J. Magn. Magn. Mater.* **25**, 207-214.
- Delapalme, A., J. Déportes, R. Lemaire, K. Hardman and W.J. James, 1979, *J. Appl. Phys.* **50**, 1987-1989.
- Den Broeder, F.J.A. and K.H.J. Buschow, 1980, *J. Less-Common Met.* **70**, 289-292.
- Didisheim, J.J., K. Yvon, D. Shaltiel, P. Fischer, P. Bujard and E. Walker, 1979a, *Solid State Commun.* **32**, 1087-1090.
- Didisheim, J.J., K. Yvon, D. Shaltiel and P. Fischer, 1979b, *Solid State Commun.* **31**, 47-50.
- Didisheim, J.J., K. Yvon, P. Fischer and D. Shaltiel, 1980, *J. Less-Common Met.* **73**, 355-362.
- Didisheim, J.J., K. Yvon, P. Fischer and P. Tissot, 1981, *Solid State Commun.* **38**, 637-641.
- Dunlap, B.D., G.K. Shenoy, J.M. Friedt, P.J. Viccaro, D. Niarchos, H. Kierstead, A.T. Aldred and D.G. Westlake, 1979, *J. Appl. Phys.* **50**, 7682-7686.
- Dunlap, B.D., P.J. Viccaro and G.K. Shenoy, 1980, *J. Less-Common Met.* **74**, 75-79.
- Earl, M.W. and J.D. Dunlop, 1974, *Proc. 26th Power Sources Symposium*, Atlanta City, NJ (June 1974), (PSC Publications Committee, Red Bank, NJ) p. 24.
- Elemans, J.B.A.A., K.H.J. Buschow, H.W. Zandbergen and J.P. de Jong, 1975, *Phys. Stat. Sol. (a)* **29**, 595-600.
- Evans, J., I.R. Harris and P.F. Martin, 1980, *J. Less-Common Met.* **75**, 49-53.
- Ewe, H., E.W. Justi and K. Stephen, 1973, *Energy Conversion* **13**, 109.
- Fischer, P., A. Furrer, G. Busch and L. Schlapbach, 1977, *Helv. Phys. Acta* **50**, 421.
- Fischer, P., W. Hälgl, L. Schlapbach and K. Yvon, 1978a, *J. Less-Common Met.* **60**, 1-9.
- Fischer P., W. Hälgl, L. Schlapbach, F. Stucki and A.F. Andresen, 1978b, *Mat. Res. Bull.* **13**, 931.
- Fish, G.E., J.J. Rhyne, S.G. Sankar and W.E. Wallace, 1979, *J. Appl. Phys.* **50**, 2003-2006.
- Flanagan, T.B., 1978a, in: *Hydrides for Energy Storage*, eds. A.F. Andresen and A.J. Maeland (Pergamon, Oxford) pp. 43-60.
- Flanagan, T.B., 1978b, in: *Hydrides for Energy Storage*, eds. A.F. Andresen and A.J. Maeland (Pergamon, Oxford) pp. 135-150.
- Flanagan, T.B. and G.E. Biehl, 1981, *J. Less-Common Met.* **82**, 385-389.
- Fromm, E. and G. Hörz, 1980, *Int. Metals Rev.* **5/6**, 269-283.
- Fruchart, D., M. Commandré, D. Sauvage, A. Raoult and R. Tellgren, 1980a, *J. Less-Common Met.* **74**, 55-63.
- Fruchart, D., A. Raoult, C.B. Shoemaker and D.P. Shoemaker, 1980b, *J. Less-Common Met.* **73**, 362; *Phys. Stat. Sol. (a)* **57**, K119-122.
- Fujii, H., F. Fujimoto, S. Takeda, T. Hihara and T. Okamoto, 1983, *J. Magn. Magn. Mater.* **31-34**, 223-224.
- Furrer, A., P. Fischer, W. Hälgl and L. Schlapbach, 1978, in: *Hydrides for Energy Storage*, eds. A.F. Andresen and A.J. Maeland (Pergamon, Oxford) pp. 73-79.
- Gavra, Z., H.H. Mintz, G. Kimmel and Z. Hadari, 1979, *Inorg. Chem.* **18**, 3595.
- Gelatt, C.D., 1978, in: *Hydrides for Energy Storage*, eds. A.F. Andresen and A.J. Maeland (Pergamon, Oxford) pp. 193-204.
- Gelatt, C.D., 1980, in: *Theory of Alloy Phase Formation*, ed. L.D. Bennett (The Metallurgical Soc. AIME) p. 451.
- Gignoux, D., R. Lemaire, P. Molho and F. Tasset, 1980, *J. Magn. Magn. Mater.* **21**, 307-315.
- Goodell, P.D., G.D. Sandrock and E.L. Huston, 1980a, *J. Less-Common Met.* **73**, 135-142.
- Goodell, P.D., G.D. Sandrock and E.L. Huston, 1980b, *Sandia Nat. Lab. Rept. SAND79-7095*, UC-94d.
- Goodell, P.D. and P.S. Rudman, 1983, *J. Less-Common Met.* **83**, 117-125.
- Goudy, A., W.E. Wallace, R.S. Craig and T. Takeshita, 1978, *Adv. Chem.* **157**, 212-226.
- Gruen, D.M., M.H. Mendelsohn and I. Sheft, 1977, *The Electrochem. Soc. Proc.* **77-6**, 482-488.
- Gruen, D.M., F. Schreiner, I. Sheft, 1978, *Int. J. Hydro. Energy* **3**, 303-310.
- Gschneidner, K.A., 1961, *Rare Earth Alloys*, (Van Nostrand, Princeton, NJ).
- Gschneidner, K.A., T. Takeshita, Y. Chung and O.D. McMasters, 1982, *J. Phys. F: Metal. Phys.* **12**, L1-6.
- Gualtieri, D.M. and W.E. Wallace, 1977, *J. Less-Common Met.* **55**, 53-59.
- Gualtieri, D.M. and W.E. Wallace, 1978, *J. Less-Common Met.* **61**, 261-267.
- Gualtieri, D.M., K.S.V.L. Narasimhan and T. Takeshita, 1976a, *J. Appl. Phys.* **47**, 3432-3435.
- Gualtieri, D.M., K.S.V.L. Narasimhan and W.E. Wallace, 1976b, *AIP Conf. Proc.* **34**, 219-221.
- Gubbens, P.C.M., A.M. van der Kraan and K.H.J. Buschow, 1981, *Solid State Commun.* **37**, 635-639.
- Gubbens, P.C.M., A.M. van der Kraan and K.H.J. Buschow, 1983a, *J. Magn. Magn. Mater.* **30**, 383-388.
- Gubbens, P.C.M., A.M. van der Kraan and K.H.J. Buschow, 1983b, *J. Phys. F: Metal. Phys.* (in press).
- Guidotti, R.A., G.B. Atkinson and M.M. Wong, 1977, *J. Less-Common Met.* **52**, 13-28.
- Guinet, Ph., P. Perroud and J. Rabière, 1980, *Int. J. Hydr. Energy* **5**, 609-618.
- Gurewitz, E., Pinto, M.P. Dariel and H. Shaked, 1983, *J. Phys. F: Metal Phys.* **13**, 545-554.
- Gutjahr, M.A., H. Buchner, K.D. Beccu and H. Säufferer, 1973, *Power Sources* **4**, 79.
- Halstead, T.K., 1974, *Solid State Commun.* **11**, 114-117.
- Halstead, T.K., N.A. Abood and K.H.J. Buschow, 1976, *Solid State Commun.* **19**, 425-428.
- Hardman, K., J.J. Rhyne, K. Smith and W.E. Wallace, 1980, *J. Less-Common Met.* **74**, 97.
- Hempelmann, H. and G. Hilscher, 1980, *J. Less-Common Met.* **74**, 103-109.
- Hempelmann, R., D. Ohlendorf and E. Wicke, 1978, in: *Hydrides for Every Storage*, eds. A.F. Andresen and A.J. Maeland (Pergamon, Oxford) pp. 407-415.

- Hilscher, G. and H. Rais, 1978, *J. Phys. F: Metal Phys.* **8**, 511-520.
- Hilscher, G., G. Wiesinger and E. Lebsanft, 1980, *J. Magn. Magn. Mater.* **15-18**, 1273-1274.
- Holleck, G.L., J.R. Driscoll and B.E. Paul, 1980, *J. Less-Common Met.* **74**, 379-384.
- Huang, Y.C., M. Tada, T. Watanabe and K. Fusita, 1978, *Proc. 2nd World Hydrogen Energy Conf.*, Vol. 3, eds. T.N. Veziroglu and W. Seifritz (Pergamon, Oxford) p. 1613.
- Huston, E.L. and G.D. Sandrock, 1980, *J. Less-Common Met.* **74**, 435-443.
- Iandelli, A. and A. Palenzona, 1979, in: *Handbook on the Physics and Chemistry of Rare Earths*, Vol. 2, eds. K.A. Gschneidner and L. Eyring (North-Holland, Amsterdam) pp. 1-54.
- Irodova, A.V., V.P. Gluzkov, V.A. Somenkov and S.Sh. Shilstein, 1981, *J. Less-Common Met.* **77**, 89-98.
- Irvine, S.J.C. and I.R. Harris, 1978, in: *Hydrogen for Energy Storage*, eds. A.F. Andresen and A.J. Maeland (Pergamon, Oxford) pp. 431-446.
- Irvine, S.J.C. and I.R. Harris, 1980, *J. Less-Common Met.* **74**, 33-43.
- Jacob, I., 1981, *Solid State Commun.* **40**, 1015-1018.
- Jacob, I. and D. Shaltiel, 1979, *J. Less-Common Met.* **65**, 117-128.
- Jacob, I., D. Shaltiel, D. Davidov and I. Miloslavski, 1977, *Solid State Commun.* **23**, 669-672.
- Jacob, I., J.M. Bloch, D. Shaltiel and D. Davidov, 1980a, *Solid State Commun.* **35**, 155-158.
- Jacob, I., D. Davidov and D. Shaltiel, 1980b, *J. Magn. Magn. Mater.* **20**, 226-230.
- Jacob, I., E.R. Bauminger, D. Davidov, I. Felner, S. Ofer and D. Shaltiel, 1980c, *J. Magn. Magn. Mater.* **15-18**, 1269-1270.
- Jacob, I., V. Shargorodski, D. Davidov and D. Shaltiel, 1981, *J. Less-Common Met.* **82**, 391-393.
- Johnson, W.A. and R.F. Mehl, 1939, *Trans. Am. Inst. Mineral Metall. Petrol. Eng.* **135**, 416.
- Justi, E.W., H.H. Ewe, A.W. Kalberlah, N.M. Saridakis and H.H. Schaefer, 1970, *Energy Conversion* **10**, 183.
- Kadel, R. and A. Weiss, 1979, *J. Less-Common Met.* **65**, 89-101.
- Kalvius, G.M., U.F. Klein and G. Wortmann, 1974, *J. Physique* **35**, C6-139.
- Karlicek, R.F. and I.J. Lowe, 1979, *Solid State Commun.* **31**, 163-165.
- Karlicek, R.F. and I.J. Lowe, 1980, *J. Less-Common Met.* **73**, 219-225.
- Kawamura, M., S. Ono, S. Higano and K. Kamino, 1983a, *J. Less-Common Met.* **89**, 359-363.
- Kawamura, M., S. Ono and Y. Mizuno, 1983b, *J. Less-Common Met.* **89**, 365-372.
- Keinert, J., 1971, *Atomkernenergie (ATKE)* **18**, 261.
- Khodosov, Ye.F., A.I. Linnik, G.F. Kobzenko and V.G. Ivanchenko, 1978a, *Fiz. Metal. Metallogr.* **44**(2), 178-180.
- Khodosov, E.F., M.I. Eremina, G.F. Kobzenko and V.G. Ivanchenko, 1978b, *Izv. Akad. Nauk SSSR, Neorg. Mater.* **14**, 1632-1634.
- Kierstead, H.A., 1980a, *J. Less-Common Met.* **70**, 199-207.
- Kierstead, H.A., 1980b, *J. Less-Common Met.* **73**, 61-68.
- Kierstead, H.A., 1980c, *J. Less-Common Met.* **71**, 311-315.
- Kierstead, H.A., 1980d, *J. Less-Common Met.* **71**, 303-309.
- Kierstead, H.A., 1981a, *J. Less-Common Met.* **78**, 29-34.
- Kierstead, H.A., 1981b, *J. Less-Common Met.* **78**, 61-68.
- Kierstead, H.A., 1981c, *J. Less-Common Met.* **77**, 281-285.
- Kierstead, H.A., 1981d, *J. Less-Common Met.* **80**, 115-120.
- Kierstead, H.A., 1981e, *J. Less-Common Met.* **81**, 221-227.
- Kierstead, H.A., P.J. Viccaro, G.K. Shenoy and B.D. Dunlap, 1979, *J. Less-Common Met.* **66**, 219-222.
- Kirchmayr, H.R. and C. Poldy, 1979, in: *Handbook on the Physics and Chemistry of Rare Earths*, Vol. 2, eds. K.A. Gschneidner and L. Eyring (North-Holland, Amsterdam) pp. 55-230.
- Kost, M.E. and V.I. Mikheeva, 1976, *Zh. Neorg. Khimii* **22**, 2910-2924.
- Kost, M.E. and A.L. Shilov, 1979, *Inorg. Mater.* **14**, 1270-1272.
- Kouvel, J.S., 1961, *J. Phys. Chem. Sol.* **21**, 57.
- Kübler, J., K.H. Bennemann, R. Lapka, F. Rösel, P. Oelhafen and H.J. Güntherodt, 1981, *Phys. Rev.* **B23**, 5176-5184.
- Kuijpers, F.A., 1972a, *Phys. Lett.* **39A**, 240-241.
- Kuijpers, F.A., 1972b, *Ber. Bunsenges. Phys. Chem.* **76**, 1220-1223.
- Kuijpers, F.A., 1973, *Philips Res. Repts. Suppl.* 1973 no. 2.
- Kuijpers, F.A. and B.O. Loopstra, 1971, *J. Physique* **32**, C1-657-658.
- Kuijpers, F.A., B.O. Loopstra, 1974, *J. Phys. Chem. Sol.* **35**, 301-306.
- Kuijpers, F.A. and H.H. van Mal, 1971, *J. Less-Common Met.* **23**, 395-398.
- Lacher, J.R., 1973, *Proc. Soc. (London) A* **161**, 525.
- Lakner, J.F., F.S. Uribe and S.A. Steward, 1980, *J. Less-Common Met.* **74**, 13.
- Landolt, M., F. Meier, P. Zürcher, H. Oesterreicher, K. Ensslen, J. Hoernigschmid and E. Bucker, 1979, *Solid State Commun.* **32**, 1009-1011.
- Larsen, J.W. and B.R. Livesay, 1978, *J. Appl. Phys.* **49**, 1506.
- Larsen, J.W. and B.R. Livesay, 1980, *J. Less-Common Met.* **73**, 79-88.
- Lebsanft, M., D. Richter and J. Töpler, 1979, *J. Phys. F: Metal Phys.* **9**, 1057-1065.
- Libowitz, G.G., 1972, *Inorg. Chem. Series*, Vol. 10, ed. E.J. Roberts (Butterworths, London) p. 79.
- Libowitz, G.G. and A.J. Maeland, 1978, in: *Handbook on the Physics and Chemistry of Rare Earths*, Vol. 3, eds. K.A. Gschneidner and L. Eyring (North-Holland, Amsterdam) pp. 299-336.



- Lindsay, R. and R.O. Moyer, 1981, *J. Less-Common Met.* **80**, 37-40.
- Lü Man-qi, Qi Zhen-Zhong and Wu Ping-sen, 1979, *Proc. 2nd Japan. Inst. Metals Symp. on Hydrogen in Metals* (Japan Inst. Metals, Minakami) p. 341.
- Lundin C.E. and F.E. Lynch, 1976, *Denver Research Inst. Rept. No. F44620-74-C-002 AF-OSR Contr.*
- Lundin, C.E. and F.E. Lynch, 1978, in: *Hydrides for Energy Storage*, eds. A.F. Andresen and A.J. Maeland (Pergamon, Oxford) pp. 395-403.
- Lundin, C.E., F.E. Lynch and C.B. Magee, 1977, *J. Less-Common Met.* **56**, 19-37.
- Lynch, F.E., 1980, *J. Less-Common Met.* **74**, 411-418.
- Maartense, I., 1973, *Can. J. Phys.* **51**, 2407-2414.
- Machida, Y., T. Yamadaya and M. Asanuma, 1978, in: *Hydrides for Energy Storage*, eds. A.F. Andresen and A.J. Maeland (Pergamon, Oxford) pp. 329-335.
- Maeland, A.J., A.F. Andresen and K. Videm, 1976, *J. Less-Common Met.* **45**, 347-350.
- Maeland, A.J., L.E. Tanner and G.G. Libowitz, 1978, *J. Less-Common Met.* **74**, 279-285.
- Magee, C.B., J. Liu and C.E. Lundin, 1981, *J. Less-Common Met.* **78**, 119-138.
- Malik, S.K. and W.E. Wallace, 1977, *Solid State Commun.* **24**, 283.
- Malik, S.K., T. Takeshita and W.E. Wallace, 1976, *Magn. Lett.* **1**, 33-39.
- Malik, S.K., F.J. Arlinghaus and W.E. Wallace, 1977a, *Phys. Rev. B* **16**, 1242-1248.
- Malik, S.K., T. Takeshita and W.E. Wallace, 1977b, *Solid State Commun.* **23**, 599-602.
- Malik, S.K., W.E. Wallace and T. Takeshita, 1978a, *Solid State Commun.* **28**, 359-360.
- Malik, S.K., W.E. Wallace and T. Takeshita, 1978b, *Solid State Commun.* **28**, 977-980.
- Malik, S.K., E.B. Boltich and W.E. Wallace, 1980, *Solid State Commun.* **33**, 921-923.
- Malik, S.K., E.B. Boltich and W.E. Wallace, 1981, *Solid State Commun.* **37**, 329-333.
- Markin, T.L., N.J. Bridger, R. Bennet and R.M. Dell, 1978, *Proc. 28th Power Source Symp.*, Atlanta City, NJ (1978), (The Electrochemical Society, Princeton, NJ) p. 139.
- McCue, J.C., 1980, *J. Less-Common Met.* **74**, 333-339.
- McHenry, E.J., 1977, *Fall Meeting, Atlanta (1977)*, *The Electrochem. Soc. Proc.* **77-2**, 98-100.
- Mendelsohn, M.H. and D.M. Gruen, 1980, *J. Less-Common Met.* **74**, 449-453.
- Mendelsohn, M.H., D.M. Gruen and A.E. Dwight, 1977, *Nature* **269**, 45.
- Mendelsohn, M., D. Gruen and A. Dwight, 1979, *Inorg. Chem.* **18**, 3343-3344.
- Meyer, C., F. Hartmann-Boutron and Y. Gros, 1981, *J. Appl. Phys.* **52**, 2116.
- Miedema, A.R., 1973, *J. Less-Common Met.* **32**, 117-136.
- Miedema, A.R., 1976, *J. Less-Common Met.* **46**, 167-173.
- Miedema, A.R., 1978, *Z. Metallkde* **69**, 455.
- Miedema, A.R., 1979, *Z. Metallkde* **70**, 345-352.
- Miedema, A.R. and F. van der Woude, 1980, *Physica* **100B**, 145.
- Miedema, A.R., K.H.J. Buschow and H.H. van Mal, 1976, *J. Less-Common Met.* **49**, 463.
- Miedema, A.R., K.H.J. Buschow and H.H. van Mal, 1977, *Proc. Symp. Electrode Mater.*, eds. J.D.E. McIntyre, S. Srinivasan and F.G. Wills, *The Electrochem. Soc. Proc.* **77-6**, 456.
- Miedema, A.R., P.F. de Châtel and F.R. de Boer, 1980, *Physica* **100B**, 1-28.
- Mikheeva, V.I., M.E. Kost and A.L. Shilov, 1978, *Russ. J. Inorg. Chem.* **23**, 657-661.
- Miyamoto, M., K. Yamaji and Y. Nakata, 1983, *J. Less-Common Met.* **89**, 111-116.
- Mueller, W.M., J.P. Blackledge and G.G. Libowitz, 1968, *Metal Hydrides* (Academic Press, New York).
- Murray, J.J., M.L. Post and J.B. Taylor, 1980, *J. Less-Common Met.* **73**, 33-40.
- Murray, J.J., M.L. Post and J.B. Taylor, 1981a, *J. Less-Common Met.* **80**, 201-209.
- Murray, J.J., M.L. Post and J.B. Taylor, 1981b, *J. Less-Common Met.* **80**, 211-219.
- Nacken, B. and W. Bronger, 1978, *Z. Anorg. Allg. Chem.* **439**, 29-34.
- Newkirk, H.W., 1972, *Lawrence Livermore Lab. Rept. UCRL-51244*, pp. 1-21.
- Niarchos, D., P.J. Viccaro, B.D. Dunlap and G.K. Shenoy, 1979, *J. Appl. Phys.* **50**, 7690-7692.
- Niarchos, D., P.J. Viccaro, G.K. Shenoy, B.D. Dunlap and A.T. Aldred, 1980a, *Proc. 5th Intern. Conf. Hyperfine Interactions*, Berlin (1980).
- Niarchos, D., P.J. Viccaro, B.D. Dunlap, G.K. Shenoy and A.T. Aldred, 1980b, *J. Less-Common Met.* **73**, 283-290.
- Nishimiya, N., A. Suzuki, T. Sekine, S. Ono and E. Asada, 1982, *J. Less-Common Met.* **88**, 263-268.
- Nomura, K., E. Akiba and S. Ono, 1983, *J. Less-Common Met.* **89**, 551-558.
- Noréus, D., L.G. Olsson and P.E. Werner, 1983, *J. Phys. F: Metal Phys.* **13**, 715-727.
- Northrup, C.J.M. and A.A. Heckes, 1980, *J. Less-Common Met.* **74**, 419-426.
- Oesterreicher, H., 1981, *Appl. Phys.* **24**, 169-186.
- Oesterreicher, H. and H. Bittner, 1977, *Phys. Stat. Sol. (a)* **41**, K101-102.
- Oesterreicher, H. and H. Bittner, 1980a, *J. Less-Common Met.* **73**, 339-344.
- Oesterreicher, H. and H. Bittner, 1980b, *J. Magn. Mater.* **15-18**, 1264-1266.
- Oesterreicher, H., J. Clinton and H. Bittner, 1976, *Mat. Res. Bull.* **11**, 1241-1248.
- Oesterreicher, H., H. Bittner and M. Misroch, 1977, *J. Less-Common Met.* **52**, 129-135.
- Oesterreicher, H., K. Ensslen and E. Bucher, 1980, *Mat. Res. Bull.* **15**, 275-283.
- Oesterreicher, H., K. Ensslen and E. Bucher, 1982, *Appl. Phys.* **22**, 303-306.
- Ohlendorf, D. and H.E. Flotow, 1980a, *J. Less-Common Met.* **73**, 25-32.
- Ohlendorf, D. and H.E. Flotow, 1980b, *J. Chem. Phys.* **73**, 2987.
- Okamoto, T., H. Fujii, S. Takeda and T. Hihara, 1982, *J. Less-Common Met.* **88**, 181-186.

- Oliver, F.W., K.H. West, R.L. Cohen and K.H.J. Buschow, 1978, *J. Phys. F: Metal Phys.* **8**, 701-707.
- Osumi, Y., H. Suzuki, A. Kato, K. Oguro and M. Nakane, 1980, *J. Less-Common Met.* **74**, 271-277.
- Palleau, J. and G. Chouteau, 1980, *J. Physique Lett.* **41**, L227-229.
- Parfenova, N.M., I.R. Konenko, A.L. Shilov, A.A. Tolstopyatova, E.I. Klabunovskii and M.E. Kost, 1979, *Inorg. Mater.* **14**, 1335-1336.
- Park, N.C. and J.Y. Lee, 1982, *J. Less-Common Met.* **83**, 39-48.
- Parker, F.T. and H. Oesterreicher, 1982, *Appl. Phys. A* **27**, 65-69.
- Parthé, E. and J.M. Moreau, 1977, *J. Less-Common Met.* **53**, 1-24.
- Percheron, A., F. Briancourt, H. Diaz, J.C. Achard, J. Sarradin and G. Bronoel, 1976, *Proc. 12th Rare Earth Conf.*, p. 300.
- Percheron-Guégan, A., J.C. Achard, J. Sarradin and G. Bronoel, 1978, in: *Hydrides for Energy Storage*, eds. A.F. Andresen and A.J. Maeland (Pergamon, Oxford) pp. 485-490.
- Percheron-Guégan, A., C. Lartigue, J.C. Archard, P. Germi and F. Tasset, 1980, *J. Less-Common Met.* **74**, 1-12.
- Pezat, M., B. Darriet and P. Hagenmuller, 1980, *J. Less-Common Met.* **74**, 427-434.
- Pourarian, F., E.B. Boltich, W.E. Wallace, R.S. Craig and S.K. Malik, 1980a, *J. Magn. Magn. Mater.* **21**, 128-132.
- Pourarian, F., E.B. Boltich, W.E. Wallace and S.K. Malik, 1980b, *J. Less-Common Met.* **74**, 153-160.
- Pourarian, F., W.E. Wallace, A. Elattar and J.F. Lakner, 1980c, *J. Less-Common Met.* **74**, 167-174.
- Pourarian, F., W.E. Wallace and S.K. Malik, 1982a, *J. Less-Common Met.* **83**, 95-103.
- Pourarian, F., W.E. Wallace and S.K. Malik, 1982b, *J. Magn. Magn. Mater.* **25**, 299-306.
- Powell, J.R., F.J. Salzano, Yu Wen-Shi and J.S. Milau, 1975, *USERDA Rept. BNL 50447 Brookhaven Nat. Lab.*
- Raichlen, J.S. and R.H. Doremus, 1971, *J. Appl. Phys.* **42**, 3166.
- Rees, A.L.G., 1954, *Trans. Faraday Soc.* **50**, 335.
- Reifenschweiler, O., 1972, *Proc. 1st Symp. on Neutron Dosimetry in Biology and Medicine*, Munich (1972); see also 1961, *Philips Res. Repts.* **16**, 401.
- Reilly, J.J., 1977, in: *Hydrogen, its Technology and Implications*, Vol. 2, eds. K.E. Cox and K.D. Williams (Chemical Rubber Co., Cleveland, OH) p. 13.
- Reilly, J.J., 1978a, in: *Hydrides for Energy Storage*, eds. A.F. Andresen and A.J. Maeland (Pergamon, Oxford) pp. 310-322.
- Reilly, J.J., 1978b, in: *Hydrides for Energy Storage*, eds. A.F. Andresen and A.J. Maeland (Pergamon, Oxford) pp. 527-550.
- Reilly, J.J. and R.H. Wiswall, 1972, *Brookhaven Nat. Lab. Rept. BLN-13136*.
- Rhyné, J.J., G.E. Fish, S.G. Sankar and W.E. Wallace, 1979, *J. Physique* **40**, C5-209-210.
- Richter, D., R. Hempelmann and L.A. Vinhas, 1982, *J. Less-Common Met.* **88**, 353-360.
- Ron, M., D. Gruen, M. Mendelsohn and I. Sheft, 1980, *J. Less-Common Met.* **74**, 445-448.
- Rudmann, P.S., J.J. Reilly and R.H. Wiswall, 1978, *Ber. Bunsenges. Phys. Chem.* **82**, 611-614.
- Rummel, H., R.L. Cohen, P. Gütlich and K.W. West, 1982, *Appl. Phys. Lett.* **40**, 477-479.
- Rush, J.J., J.M. Rowe and A.J. Maeland, 1980, *J. Phys. F: Metal Phys.* **10**, L283-285.
- Sandrock, G.D., 1978, in: *Hydrides for Energy Storage*, eds. A.F. Andresen and A.J. Maeland (Pergamon, Oxford) pp. 353-394.
- Sandrock, G.D. and P.D. Goodell, 1980, *J. Less-Common Met.* **73**, 161-168.
- Santoro, A., A.J. Maeland and J.J. Rush, 1978, *Acta Crystallogr. B* **34**, 3059.
- Sarynin, V.K., V.V. Burnasheva and K.N. Semenenko, 1977, *Russian Metall.* **4**, 54-55.
- Savitsky, E.M. and V.F. Terekhova, 1975, *Metallography of Rare Earths* (Nauka, Moscow).
- Schefer, J., P. Fischer, W. Hälgl, F. Stucki, L. Schlapbach, J.J. Didisheim, K. Yvon and A.F. Andresen, 1980, *J. Less-Common Met.* **74**, 65-73.
- Schlapbach, L., 1980, *J. Phys. F: Metal Phys.* **10**, 2477-2490.
- Schlapbach, L., A. Seiler and F. Stucki, 1978, *Mat. Res. Bull.* **13**, 697.
- Schlapbach, L., A. Seiler, H.C. Siegmann, T. von Waldkirch, P. Zürcher and C.R. Brundle, 1979, *Int. J. Hydr. Energy* **4**, 21-28.
- Schlapbach, L., A. Seiler, F. Stucki and H.C. Siegmann, 1980a, *J. Less-Common Met.* **73**, 145-160.
- Schlapbach, L., F. Stucki, A. Seiler and H.C. Siegmann, 1980b, *J. Magn. Magn. Mater.* **15-18**, 1271-1273.
- Schlapbach, L., C. Pina-Perez and T. Siegrist, 1982, *Solid State Commun.* **41**, 135-138.
- Scholtus, N.A. and W.K. Hail, 1963, *J. Chem. Phys.* **39**, 868.
- Semenenko, K.N. and V.V. Burnasheva, 1976, *Dokl. Akad. Nauk SSSR* **231**, 356-358.
- Semenenko, K.N., V.P. Malyshev, L.A. Petrova, V.V. Burnasheva and V.K. Sarynin, 1978, *Izv. Akad. Nauk SSSR, Neorg. Mater.* **13**, 2009-2013.
- Shaltiel, D., 1978, *J. Less-Common Met.* **62**, 407-408.
- Shaltiel, D., I. Jacob and D. Davidov, 1977, *J. Less-Common Met.* **53**, 117-131.
- Shaltiel, D., Th. von Waldkirch, F. Stucki and L. Schlapbach, 1981, *J. Phys. F: Metal Phys.* **11**, 471-485.
- Sheft, I., D.M. Gruen, G.J. Lamich, L.W. Carlson, A.E. Knox, J.M. Nixon and M.H. Mendelsohn, 1978, in: *Hydrides for Energy Storage*, eds. A.F. Andresen and A.J. Maeland (Pergamon, Oxford) pp. 551-568.
- Sheft, I., D.M. Gruen, G.J. Lamich, 1980, *J. Less-Common Met.* **74**, 401-409.
- Shenoy, G.K., D. Niarchos, P.J. Viccaro, B.D. Dunlap and A.T. Aldred, 1980, *J. Less-Common Met.* **73**, 171-173.

- Shinar, J., D. Shaltiel, D. Davidov and A. Gayevsky, 1978a, *J. Less-Common Met.* **60**, 209-219.
- Shinar, J., I. Jacob, D. Davidov and D. Shaltiel, 1978b, in: *Hydrides for Energy Storage*, eds. A.F. Andresen and A.J. Maeland (Pergamon, Oxford).
- Shinar, J., A. Malchin, D. Davidov and N. Kaplan, 1980, *J. Less-Common Met.* **73**, 255-260.
- Shinar, J., D. Davidov and R.D. Hogg, 1981, *Solid State Commun.* **37**, 175-178.
- Siegmann, H.C., L. Schlapbach and C.R. Brundle, 1978, *Phys. Rev. Lett.* **40**, 72.
- Skoskiewicz, T., 1972, *Phys. Stat. Sol. (a)* **11**, K-123.
- Smit, P.H. and K.H.J. Buschow, 1980, *Phys. Rev.* **21**, 3839-3843.
- Smit, P.H., H.C. Donkersloot and K.H.J. Buschow, 1982, *J. Appl. Phys.* **53**.
- Soga, K., H. Imamura and S. Ikeda, 1979, *J. Catal.* **56**, 119-126.
- Solov'ev, S.P., N.V. Fadeeva, V.A. Yarmys', V.V. Burnasheva and K.N. Semeneko, 1981, *Sov. Phys. Solid State* **23**, 721-723.
- Spit, F.H.M., J.W. Drijver and S. Radelaar, 1980, *Scripta Met.* **14**, 1071-1076.
- Stewart, G.A., J. Zukrowski and G. Wortmann, 1981a, *J. Magn. Magn. Mater.* **25**, 77-82.
- Stewart, G.A., J. Zukrowski and G. Wortmann, 1981b, *Solid State Commun.* **39**, 1017-1020.
- Stucki, F. and L. Schlapbach, 1980, *J. Less-Common Met.* **74**, 143-151.
- Suda, S., N. Kobayashi, K. Yoshida, Y. Ishido and S. Ono, 1980, *J. Less-Common Met.* **74**, 127.
- Suda, S., Y. Komazaki and N. Kobayashi, 1983a, *J. Less-Common Met.* **89**, 317-324.
- Suda, S., N. Kobayashi, E. Morishita and N. Takemoto, 1983b, *J. Less-Common Met.* **89**, 325-332.
- Suzuki, K., 1983, *J. Less-Common Met.* **89**, 183-195.
- Swartzendruber, L.J., L.H. Bennet and R.E. Watson, 1976, *J. Phys. F: Metal Phys.* **6**, L331.
- Swisher, J.H., 1980, *J. Less-Common Met.* **74**, 301-320.
- Switendick, A.C., 1978a, *Theoretical Studies of Hydrogen in Metals*, Rep. Sand-78-0250.
- Switendick, A.C., 1978b, in: *Hydrogen in Metals I*, eds. G. Alefeld and J. Völkl (Springer, Berlin) p. 101.
- Takehita, T., W.E. Wallace and R.S. Craig, 1974a, *Inorg. Chem.* **13**, 2282-2283.
- Takehita, T., W.E. Wallace and R.S. Craig, 1974b, *Inorg. Chem.* **13**, 2283-2284.
- Takehita, T., G. Dublon, O.D. McMasters and K.A. Gschneidner, 1980a, in: *Rare Earths in Modern Science and Technology*, Vol. 2, eds. G.J. McCarthy, J.J. Rhyne and H.B. Silber (Plenum, New York) p. 563.
- Takehita, T., K.A. Gschneidner, D.K. Thorne and O.D. McMasters, 1980b, *Phys. Rev.* **21**, 5636-5641.
- Takehita, T., K.A. Gschneidner and J.F. Lakner, 1981, *J. Less-Common Met.* **78**, 43-47.
- Tanaka, S., J.D. Clewley and T.B. Flanagan, 1977, *J. Less-Common Met.* **56**, 137-139.
- Tanaka, J., R.H. Wiswall and J.J. Reilly, 1978a, *Inorg. Chem.* **17**, 498.
- Tanada, S., J.D. Clewley and T.B. Flanagan, 1978b, *J. Catal.* **51**, 9.
- Tessema, G.X., J. Peyrand, A. Nemoz, J.P. Senaleus, A. Raoult and R. Fruchart, 1979, *J. Physique Lett.* **40**, L105-107.
- Thompson, J.S., R.O. Moyer and R. Lindsay, 1975, *Inorg. Chem.* **14**, 1866-1869.
- Thompson, P., J.J. Reilly, F. Reidinger, J.M. Hastings and L.M. Corliss, 1979, *J. Phys. F: Metal Phys.* **9**, L61-66.
- Töpler, J., E. Lebsanft and R. Schätzler, 1978, *J. Phys. F: Metal Phys.* **8**, L25-27.
- Töpler, J. O. Bernauer and H. Buchner, 1980a, *J. Mater. Energy Systems* **2**, 3-10.
- Töpler, J., O. Bernauer and H. Buchner, 1980b, *J. Less-Common Met.* **74**, 385-400.
- Van der Kraan, A.M. and K.H.J. Buschow, 1982, *Phys. Rev. B* **25**, 3311-3318.
- Van der Kraan, A.M. and K.H.J. Buschow, 1983, *Phys. Rev. B* **27**, 2693-2697.
- Van der Kraan, A.M., P.C.M. Gubbens and K.H.J. Buschow, 1982, in: *Proc. Intern. Conf. Mössbauer Spectroscopy*, Sunagar, India (1981).
- Van Diepen, A.M. and K.H.J. Buschow, 1977, *Solid State Commun.* **22**, 113.
- Van Dongen, J.C.M., T.T.M. Palstra, A.F.J. Morgownik, J.A. Mydosh, B.M. Geerken and K.H.J. Buschow, 1983, *Phys. Rev. B* **27**, 1887-1902.
- Van Essen, R.M. and K.H.J. Buschow, 1979, *J. Less-Common Met.* **64**, 277-284.
- Van Essen, R.M. and K.H.J. Buschow, 1980a, *Mat. Res. Bull.* **15**, 1149-1155.
- Van Essen, R.M. and K.H.J. Buschow, 1980b, *J. Less-Common Met.* **70**, 189-198.
- Van Mal, H.H., 1976, *Philips Res. Repts. Suppl.* 1976 no. 1.
- Van Mal, H.H., K.H.J. Buschow and A.R. Miedema, 1974, *J. Less-Common Met.* **35**, 65-76.
- Van Mal, H.H., K.H.J. Buschow and A.R. Miedema, 1976, *J. Less-Common Met.* **49**, 483-485.
- Van Mal, H.H., K.H.J. Buschow and F.A. Kuijpers, 1979, *J. Less-Common Met.* **32**, 289-296.
- Van Rijswijk, M.H.J., 1978, in: *Hydrides for Energy Storage*, eds. A.F. Andresen and A.J. Maeland (Pergamon, Oxford) p. 261.
- Van Vucht, J.H.N., 1963, *Philips Res. Repts. Suppl.* 1963 no. 1.
- Van Vucht, J.H.N. and K.H.J. Buschow, 1976, *J. Less-Common Met.* **46**, 133-138.
- Van Vucht, J.H.N., F.A. Kuijpers and H.C.A.M. Bruno, 1970, *Philips Res. Repts.* **25**, 133-140.
- Viccaro, P.J., G.K. Shenoy, B.D. Dunlap, D.G. Westlake and J.F. Miller, 1979a, *J. Physique* **40**, C2-198-201.
- Viccaro, P.J., J.M. Friedt, D. Niarchos, B.D. Dunlap, G.K. Shenoy, A.T. Aldred and D.G. Westlake, 1979b, *J. Appl. Phys.* **50**, 2051-2052.
- Viccaro, P.J., G.K. Shenoy, B.D. Dunlap, D.G. Westlake, S.K. Malik and W.G. Wallace, 1979c, *J. Physique* **40**, C2-157-158.

- Viccaro, P.J., G.K. Shenoy, D. Niarchos and B.D. Dunlap, 1980, *J. Less-Common Met.* **73**, 265-271.
- Videm, K., 1978, in: *Hydrides for Energy Storage*, eds. A.F. Andresen and A.J. Maeland (Pergamon, Oxford) pp. 463-484.
- Wagner, F.E. and G. Wortman, 1978, in: *Topics in Applied Physics*, Vol. 28, *Hydrogen in Metals I*, eds. G. Alefeld and J. Völkl (Springer, Berlin) pp. 131-153.
- Wakao, S., M. Sekine, H. Endo, T. Ito and H. Kanazawa, 1983, *J. Less-Common Met.* **89**, 341-350.
- Walker, L.R., G.K. Wertheim and V. Jaccarino, 1961, *Phys. Rev. Lett.* **6**, 98-101.
- Wallace, W.E., 1979, *Z. Phys. Chem. N.F.* **115**, 219-237.
- Wallace, W.E., R.F. Karliceck and H. Imamura, 1979a, *J. Phys. Chem.* **83**, 1708-1712.
- Wallace, W.E., R.F. Karliceck and H. Imamura, 1979b, *J. Phys. Chem.* **83**, 785.
- Wallace, W.E., R.S. Craig and V.U.S. Rao, 1980, *Advances in Chemistry*, Vol. **186**, eds. S.L. Holt, J.B. Milstein and M. Robins (Amer. Chem. Soc., Washington) pp. 207-240.
- Wallace, W.E., E.H. Flotow and D. Ohlendorf, 1981, *J. Less-Common Met.* **79**, 157-160.
- Wallace, W.E., 1982, *J. Less-Common Met.* **88**, 141-157.
- Walsh, W.M., L.W. Rupp, P.H. Schmidt and L.D. Longinotti, 1976, *AIP Conf. Proc.* **29**, 686-687.
- Wang, R., 1976, *Mat. Res. Bull.* **11**, 281-284.
- Weaver, J.H., J.A. Knapp, D.E. Eastman, D.T. Peterson and C.B. Satterthwaite, 1977, *Phys. Rev. Lett.* **39**, 639-642.
- Wemple, R.P. and C.J. Northrup, 1975, *Thermochim. Acta* **12**, 39-47.
- Wenzl, H., 1982, *Int. Met. Rev.* **27**, 140-169.
- Wenzl, H. and K.H. Klatt, 1978, in: *Hydrogen for Energy Storage*, eds. A.F. Andresen and A.J. Maeland (Pergamon, Oxford) pp. 323-327.
- Wenzl, H. and E. Lebsanft, 1980, *J. Phys. F: Metal Phys.* **10**, 2147-2156.
- Wenzl, H. and S. Pietz, 1980, *Solid State Commun.* **33**, 1163-1165.
- Wiswall, R.H., 1978, in: *Hydrogen in Metals II*, eds. G. Alefeld and J. Völkl (Springer, Berlin) pp. 201-242.
- Wiswall, R.H. and J.J. Reilly, 1972, *Inorg. Chem.* **11**, 1691-1693.
- Wiswall, R., J. Reilly, F. Bloch and E. Wirsing, 1977, Report BNL 50755 VC-22.
- Wohlfarth, E.P., 1979, *J. Phys. F: Metal Phys.* **9**, L123.
- Yajima, S. and H. Kayano, 1977, *J. Less-Common Met.* **55**, 139-141.
- Yamaguchi, M., S. Sasaki and T. Ohta, 1980, *J. Less-Common Met.* **73**, 201-206.
- Yamaguchi, M., T. Katamune and T. Ohta, 1982, *J. Less-Common Met.* **88**, 195-200.
- Yamaguchi, M., T. Ohta and T. Katayama, 1983, *J. Magn. Magn. Mater.* **31-34**, 221-222.
- Yamanaka, K., H. Saito and M. Someno, 1975, *Nippon Kagaku Kaishi (Tokyo)* **8**, 1267-1272.
- Yonezu, I., N. Nasako, N. Honda and T. Sakai, 1983, *J. Less-Common Met.* **89**, 351-358.
- Zijlstra H. and F.F. Westendorp, 1969, *Solid State Commun.* **7**, 857-859.

## Chapter 48

### CRYSTAL STRUCTURES AND CRYSTAL CHEMISTRY OF TERNARY RARE EARTH–TRANSITION METAL BORIDES, SILICIDES AND HOMOLOGUES

E. PARTHÉ and B. CHABOT

*Laboratoire de Cristallographie aux Rayons X, Université de Genève,  
 CH-1211 Geneva 4, Switzerland*

---

#### Contents

1. Introduction	114	3.4. Structural series of compounds having different composition	119
2. Survey of the compositions of ternary compounds	114	3.5. Classification of structures accord- ing to the type of homonuclear linkage of the M atoms	120
2.1. The four-digit composition code	115	3.6. Changes in structure type upon a systematic exchange of one of the component elements for a given composition	120
3. The different crystal chemical approaches to the classification of the ternary crystal structures	115	4. The structure types of the ternary phases in R–T–M systems	121
3.1. Classification according to the types of polyhedra around the smallest atoms	118	5. Recent structure determinations	285
3.2. Ternary structures interpreted as ordered derivatives of binary types	119	6. Survey of structures found in R–T–M compounds and concluding remarks	287
3.3. Interrelation of different crystal structures of the same composition which can be regarded as stacking variants of a common structure slab	119	Appendix. Atom coordinates for the structure types found in ternary R–T–M compounds	294
		References	326

---

#### Symbols

$a, b, c$	= lattice constants	T	= transition element from Ti to Ni group
$\Delta H$	= change in enthalpy	$V$	= unit cell volume
h.t.	= high temperature	$x, y, z$	= atom coordinates
LC	= linkage coefficient (see page 130)	$X^{[m+n]}$	= crystal-chemical formula (see page 122)
l.t.	= low temperature	□	= vacancy
M	= main group element from the boron or silicon group (carbon not included)	⋄	= part of crystal chemical formula (see page 122)
R	= rare earth element, Y, Sc	⊙	= part of crystal chemical formula (see page 122)
$r_{R^{3+}}$	= ionic radius of a trivalent rare earth atom		

---

## 1. Introduction

In a survey on the crystal structures of ternary metallic rare earth (including Sc, Y) compounds written 13 years ago (Parthé, 1970) the few known structures could be interpreted as ordered derivatives of well known binary structure types. Since that time phase diagram studies have shown that the number of ternary phases is surprisingly large (for example 21 phases in Ce–Ni–Si according to Bodak et al. (BoMTKG, 73)) and a large number of ternary structures are not derivatives of binary structure types. With a few notable exceptions most of the early structure determinations were made at Lvov University (USSR) under the guidance of Prof. Gladyshevskii, Prof. Kuzma and the late Prof. Kripyakevich. However, recently it was shown that some of these ternary rare earth compounds are superconductors (Matthias et al., 1977; Vandenberg and Matthias, 1977; Yvon, 1981; Braun and Segre, 1981; Johnston and Braun, 1982) which led to a wider interest in these compounds, and now a number of different laboratories are engaged in structure studies on metallic ternary rare earth compounds.

## 2. Survey of the compositions of ternary compounds

This survey is centered on the phases found in ternary R–T–M systems where

- R is a rare earth element including Y and Sc,
- T is a transition element from the Ti to the Ni group, and
- M is a main group element from the boron or silicon group (carbon not included).

These phases can be grouped into three categories:

a) Truly ternary stoichiometric phases  $R_xT_yM_z$ , where the different elements occupy different crystallographic sites. The structures of these phases are the main object of this paper. Frequently but not always they correspond to ternary derivatives of binary structure types.

b) Truly ternary phases, where certain crystallographic sites are occupied by different atoms at random. These phases can have extended homogeneity ranges. In nearly all the compounds of interest here, the content of rare earth element of a given ternary structure type is generally fixed; however, the ratio of the number of T atoms to the number of M atoms may vary. The composition given in the literature may correspond only to one point in the homogeneity domain in a ternary diagram. We shall denote these compositions by  $R_x(T_yM_z)$ . Here we are often confronted with insufficient data in the literature. In most cases the homogeneity ranges have not been investigated. Furthermore there is always the possibility that the phase studied was not in thermal equilibrium. A reinvestigation of certain supposedly disordered phases, allowing for a sufficient annealing time, has shown that these phases are fully ordered.

c) Extension of binary phases into the ternary phase diagram. These phases shall not be discussed here, except for the special case where, at special compositions, ternary ordering variants of the binary structures occur.

The compositions of all ternary  $R_xT_yM_z$  compounds which shall be discussed in this paper are plotted in the ternary diagram of fig. 1. There are about 80 composition points to be found in fig. 1. With this great number of different ternary compositions, we encountered difficulties finding enough space in fig. 1 to denote the complete chemical formulae and opted to write only  $x, y, z$  instead of  $R_xT_yM_z$ . This applies to compounds which are stoichiometric. In the case that a certain homogeneity range has been reported or that different atoms occupy a given crystallographic site at random the composition listed is that which has been found in the literature and for which the structure has been determined.

### 2.1. *The four-digit composition code*

We use, in this paper, a four-digit composition code to simplify the comparison between different formulae and as an aid in a quick search of a particular ternary compound in the ternary diagram. Since in nearly all compounds with variable composition the content of rare earth element is constant, it was found advantageous to characterize the composition of a given phase first with the content of non-rare-earth elements and secondly, with the M/T ratio or an equivalent value. In the proposed four-digit composition code the first two digits correspond to the (rounded-off) atomic percentage of non-rare-earth elements and the second two digits to the (round-off) atomic ratio, in per cent, of M element to the sum of T and M elements. Thus for a compound  $R_xT_yM_z$  the four-digit composition code is calculated as follows:

first two digits: rounded-off value of

$$\frac{y+z}{x+y+z} \times 100,$$

last two digits: rounded-off value of

$$\frac{z}{y+z} \times 100.$$

Examples of the composition code: 6750 for RTM, 9170 for  $RT_3M_7$ .

Fig. 2 corresponds to fig. 1 but with the composition points identified by the four-digit composition code. In the case of a compound where T and M atoms occupy a structure site at random the last two digits of the composition code have to be placed between parentheses. However, for simplicity these parentheses have been omitted in fig. 2.

### 3. **The different crystal chemical approaches to the classification of the ternary crystal structures**

Many of the composition points in figs. 1 and 2 correspond to two, in some cases even to six, structure types. There are more than 125 structure types for approximately 80 composition points. With this many crystal structures it becomes a

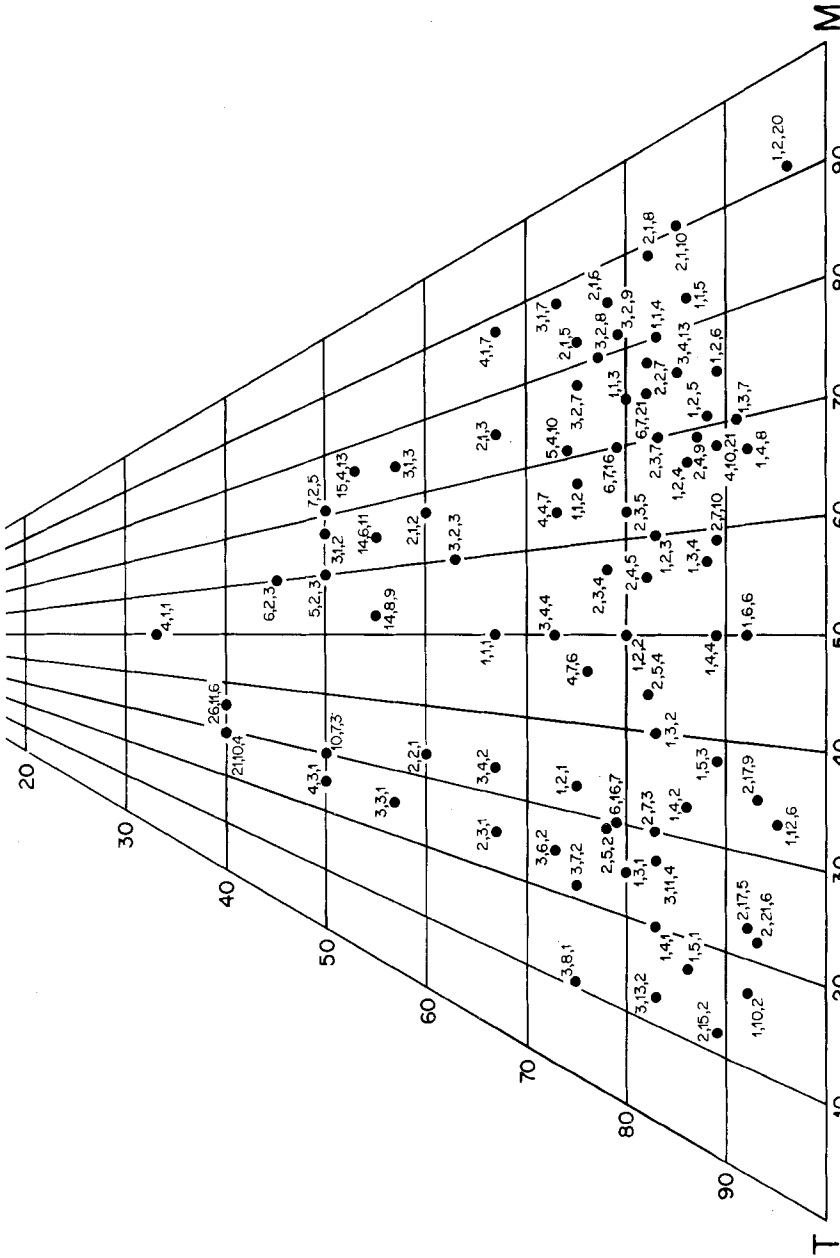


Fig. 1. The compositions of all  $R_xT_yM_z$  compounds discussed, plotted in a R-T-M ternary diagram. The composition points can be identified by means of the composition parameters  $x, y, z$ . Note that the grid refers to the atomic percentage of non-rare-earth atoms and the ratio, in percent, of the M atoms to the sum of all non-rare-earth atoms. Since there are no ternary compounds known with more than 70% at rare earth atoms, the upper part of the composition triangle has been left out.



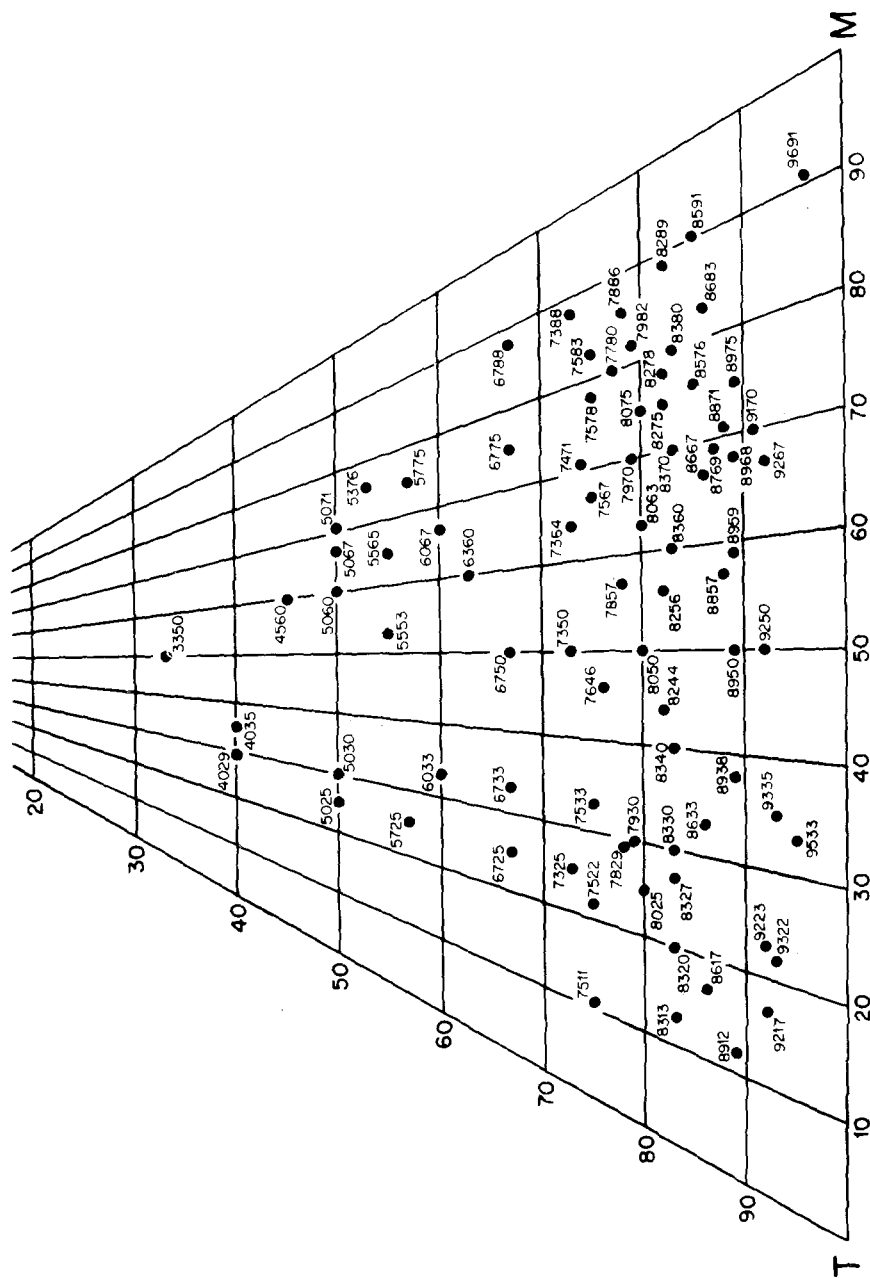


Fig. 2. The compositions of  $R_x T_y M_z$  compounds plotted in a R-T-M ternary diagram as in fig. 1 but denoted by the four-digit composition code. Note that as in fig. 1 the grid refers to the atomic percentage of non-rare-earth atoms and the ratio, in percent, of the M atoms to the sum of all non-rare-earth atoms.

challenging problem for the crystal chemist to classify these structures and to record their common structural features. Structures and stoichiometries appear in certain cases to be very complex; however, when “correctly” described, they are much easier to understand and to memorize. To systematize this wealth of crystal structures, a number of different approaches can be used.

### 3.1. Classification according to the types of polyhedra around the smallest atoms

This approach has been developed in particular by Kripyakevich (1963; 1974) and Gladyshevskii (1971). A great number of structures can be properly classified in this way. If the polyhedra are simple and if there are not too many different ones, structure drawings with drawn-in polyhedra are very useful to show geometrical relationships between different structures. The classification leads, in the case of R–T–M alloys, to the subdivision of the structures into three major groups:

- structures built up of only centred trigonal rare earth prisms  $R_6T$  and/or  $R_6M$  (see for example figs. 8, 9 and 10);
- structures with trigonal prisms and other polyhedra like octahedra, cubes, or Archimedean antiprisms (see for example fig. 6);
- structures without trigonal prisms (see for example fig. 5).

The number of structures with centred trigonal rare earth prisms is large. These structures can be further classified according to the number of directions of the prism axes and the type of linkage between the prisms. From the studies of binary structures

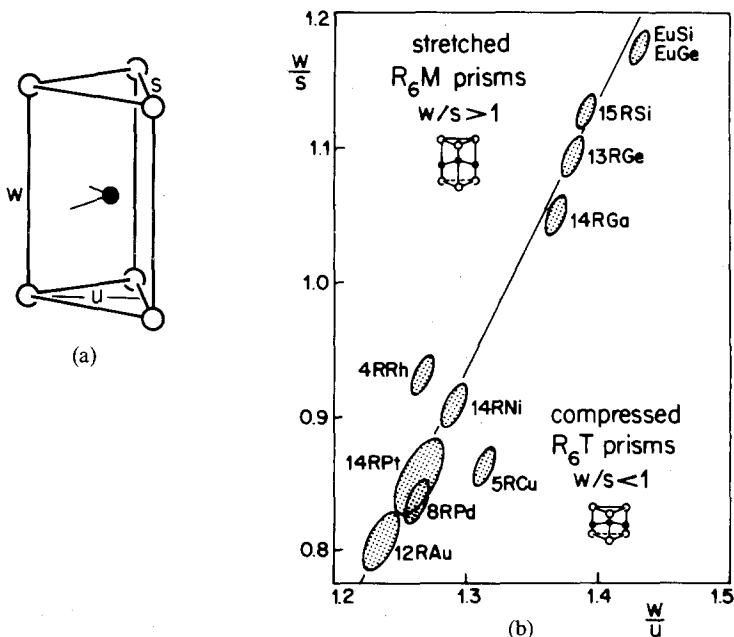


Fig. 3(a) Parameters used to characterize the shape of a trigonal prism. (b) The  $w/s$  and  $w/u$  ratios for the trigonal prisms in RT and RM compounds with FeB and/or CrB structure type.

with trigonal rare earth prisms (for example, structures of FeB and CrB type) it is known that the relative dimensions of the  $R_6T$  prisms are different from those of the  $R_6M$  prisms. If the relative dimensions of the prism are expressed by their  $w/s$  and  $w/u$  ratios as defined in fig. 3a, the data for binary compounds with CrB- or FeB-type, plotted in fig. 3b, indicate that  $R_6M$  prisms are stretched and  $R_6T$  prisms are compressed (Parthé, 1981). However, in ternary compounds stretched  $R_6T$  prisms can occur. In this case the T atoms in the prism centres cannot have an R atom in waist contact. Additional rules for atom ordering on the prism centre sites are based on the observation that certain transition elements prefer to have only Si or Ge atoms at their waist contacts. For a discussion, see 50(25):Gd<sub>4</sub>Ni<sub>3</sub>Cu.

### 3.2. Ternary structures interpreted as ordered derivatives of binary types

Here the structures which may be considered "filled-up" versions of binary structure types can be also included (see, for example, Gd<sub>3</sub>NiSi<sub>2</sub> shown in Fig. 9). There remain, however, many ternary structures for which no binary analogues can be found.

### 3.3. Interrelation of different crystal structures of the same composition which can be regarded as stacking variants of a common structure slab

The concept of structure slab shift has been used before to find geometrical relations between a number of different binary rare earth structures (Parthé and Moreau, 1977). The concept can also be applied to the structures of ternary compounds (see for example Figs. 10 and 73).

### 3.4. Structural series of compounds having different composition

The structures of structural series can be interpreted as a periodic intergrowth of different structure segments. Changing the proportions of the segments in a systematic manner leads to all possible members of a structural series. One can distinguish between intergrown two-dimensional slabs or intergrown one-dimensional columns. It is important how these segments are cut from the base structure, leading in certain cases to interfaces formed by rare earth atoms and in other cases to interfaces of other elements. Intergrowth between different structure segments is often possible only with a particular type of interface.

The crystal chemical concept of structural series has been used before to correlate the structures of certain binary rare earth compounds (see for example Parthé and Lemaire, 1975). For ternary structures the concept of intergrown structure segments is particularly useful (see for example tables 3, 10, 12, 13, 15, 16, 21).

### 3.5. Classification of structures according to the type of homonuclear linkage of the *M* atoms

This kind of classification has been used by Nowotny and Rogl (1977) and Rogl and Nowotny (1978) in a survey of ternary metal borides. The structures have been classified according to the occurrence of isolated *B* atoms, *B*-*B* dumbbells, *B* chains, or *B* nets and so on. A similar classification of binary transition metal borides had been proposed many years before by Kiessling (1950). The type of homonuclear boron linkage can be correlated with the metal to boron ratio of the compound (see table 20).

### 3.6. Changes in structure type upon a systematic exchange of one of the component elements for a given composition

We can consider here three possibilities.

(i) Changes in structure type within a series of rare earth compounds with *T* and *M* being the same may be due to a change in the electronic structure of a rare earth element or can be explained (not always) by the lanthanide contraction from La to Lu (the larger rare earth atom requiring a larger coordination polyhedron than the smaller rare earth atom). A conventional method to make these changes visible, for compounds of the same composition, consists of making diagrams with the length of the formula unit cube *L* plotted as ordinate\* and the trivalent ionic rare earth radii  $r_{R^{3+}}$  as abscissa (Parthé, 1967). Since a change of the electronic state of the rare earth element also changes its size, any abnormal behaviour of one rare earth as compared to the others can be easily detected in such *L* versus  $r_{R^{3+}}$  diagrams.

(ii) Changes in structure type for a series of ternary compounds with varying *T* can be explained by the increase of the *R*-*T* interactions with an increase of the group number of the *T* element. Predictions are shown in fig. 4 for the heat of formation of equi-atomic La*T* compounds (after Miedema, 1976). Positive  $\Delta H$  values indicate that binary compound formation is unlikely and vice versa. Similar curves can be

\* $L = (V/Z)^{1/3}$ , where *V* = volume of unit cell and *Z* = number of formula units in unit cell.

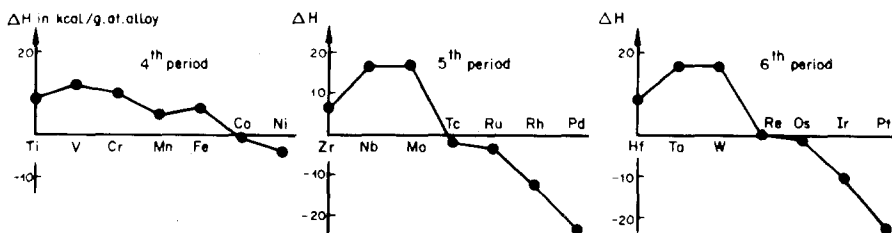


Fig. 4. Predictions for the heat of formation of equi-atomic La*T* compounds for *T* elements from the 4th, 5th and 6th periods, after Miedema (1976). When  $\Delta H$  is positive no compound will be formed; however, when  $\Delta H$  is negative compound formation is probable.

obtained for other rare earth elements. In ternary compounds with T elements of high group number strong R–T interactions are expected; however, if the T element has a low group number such interactions are weak if they occur at all. In this latter case the R–M and T–M interactions only are responsible for the formation of a compound and the R and T atoms are usually far apart.

In rare earth-rich ternary compounds the R–T interactions are not negligible for the formation of a compound and thus compounds are formed only if T is from the Fe, Co or Ni group. However, with small rare earth concentrations the other bonds are more important and compounds containing transition elements with smaller group number become stable.

(iii) Changes in structure type for a series of ternary compounds with the period of M increasing can be related to the decreasing tendency of the M atoms to form directed bonds. For example, with M elements of higher periods the rare earth elements do not form M-centred trigonal prisms.

#### 4. The structure types of the ternary phases in R–T–M systems

With the limited space available it is impossible to consider all these crystal-chemical view points for all structures in detail. The different crystal structures are presented in the order of their composition code. For compounds where the T and M atoms occupy certain structure sites at random the code represents one composition for one compound on which a structure determination has been made. Other isotypic phases may exist with different numerical values within the parentheses of the composition code.

For each type there will be given a heading with composition code, formula of R–T–M prototype\*, Pearson's classification symbol, space group, unit cell parameters of prototype (in Å), and the reference in an abbreviated form. (Only the first two letters of the first author and the first letters of all other authors are given together with the last two digits of the year of publication.) The complete reference can be obtained from the reference list at the end of this chapter. The lower part of the heading contains the name of the type (if it has been found before with other than R–T–M compounds) and/or the name of the binary structure type which is related to the ternary structure type. Below the heading there is to be found a list of isotypic compounds (only those containing R, T and 3B or 4B elements are given). A short crystal-chemical discussion follows if an easy interpretation, according to the outlines given above, is possible. Finally, a structure drawing\*\* is presented in the figures.

In the cases where it proves to be convenient, use of crystal-chemical formulae will be made (Parthé, 1980). The meanings of the most frequently encountered crystal

\*In most cases this corresponds to a compound on which a complete structure determination has been made.

\*\*In these structure drawings the choice of axes and of the origin of the unit cell does *not* necessarily correspond to the one given in the original literature.

chemical symbols are as follows:

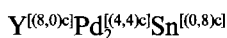
- $X^{[4c]}$ : tetrahedral coordination polyhedron around X;
- $X^{[6p]}$  or  $X^{[6o]}$ : trigonal prismatic or octahedral coordination of X atom;
- $X^{[8c]}$  or  $X^{[8a]}$ : the coordination polyhedron around X is a cube of an (Archimedean) antiprism,
- $X^{[12c]}$ : cubo-octahedral coordination;
- $\infty X$  or  $\infty X$ : X atoms form an infinite chain or a net;
- $\wedge [X_n]$ : X atoms form a limited chain of  $n$  atoms;
- $X^{[m+n]}$ : X has  $m + n$  nearest neighbours;  $m$  indicates the number of heteronuclear neighbours,  $n$  the number of homonuclear neighbours (always preceded by a + sign).

In the case of ternary compounds additional precision is necessary to distinguish between the two possible kinds of heteronuclear neighbours. This can be accomplished either by adding the chemical symbol or by use of the following convention:

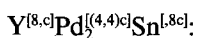
- $X^{[l,r+n]}$ : X has  $l + r + n$  neighbours, of which  $l, r$  are heteronuclear neighbours;  $l$  (on the left of the comma) refers to the number of heteronuclear elements at the left and  $r$  (on the right of the comma) to the number of heteronuclear elements at the right.

The terms left and right refer to the mutual positions of the heteronuclear elements in the chemical formula. If the heteronuclear coordination is formed by one kind of atom only, one of the values for  $l$  or  $r$  is zero and therefore left out. The position of the comma before or after the remaining number determines uniquely the kind of element forming the coordination polyhedron. If no comma is found the number corresponds to the total heteronuclear coordination. As described above, the number of atoms in the coordination polyhedron can be extended optionally by a small letter which characterizes the geometrical shape of the coordination polyhedron.

Example:



or more simply



Y surrounded by a cube of Pd atoms, Pd by a cube of four Y and four Sn atoms, Sn by a cube of Pd atoms.

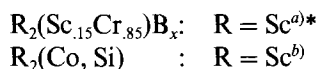
3333	$\text{Ho}_6\text{Co}_2\text{Ga}$	oI36 Immm	$a = 9.294$ $b = 9.370$ $c = 9.804$	GIGY, 83
------	-----------------------------------	--------------	---	----------

This structure is discussed in section 5.

33(50)	$\text{Sc}_4\text{CoSi}$ or $\text{Sc}_2(\text{Co, Si})$	cF96 Fd3m	$a = 12.099$	KoBG, 77
--------	--	--------------	--------------	----------

$\text{Ti}_2\text{Ni}$ -type with Co and Si atoms distributed at random on the Ni sites

Isotypic compounds:



\*This compound is stabilized by boron ( $x < 0.01$ ). Boron atoms are supposedly located in the octahedral voids present in the  $\text{Ti}_2\text{Ni}$  structure type as the oxygen atoms in  $\text{Ti}_4\text{Ni}_2\text{O}$ .

<sup>a)</sup>VaMCB, 76    <sup>b)</sup>KoBG, 77

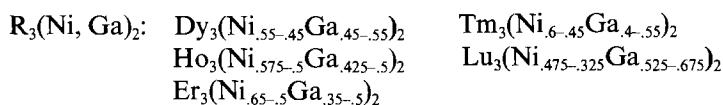
The  $\text{Ti}_2\text{Ni}$ -type can be described by an arrangement of linked, nested, polyhedral units (Chabot et al., ChCP, 81). It will be discussed together with the  $\text{Ca}_3\text{Ag}_8$ -type derivative 7325:  $\text{Ce}_3\text{Ni}_6\text{Si}_2$ .

4029	$\text{Er}_{21}\text{Ni}_{10}\text{Ga}_4$ or $\text{Er}_{21}\text{Ni}_y^{\text{[8, a]}}\text{Ni}_z^{\text{[8, c]}}\text{Ga}_4^{\text{[10, l]}}$ idealized formula	tI140 I4/mcm	$a = 11.42^*$ $c = 24.47$	GrYG, 80
------	--	-----------------	------------------------------	----------

$\text{Y}_3\text{Rh}_2$ -type (MoPP, 76) derivative

\*Corresponds to  $\text{Er}_{21}(\text{Ni}_{.875}\text{Ga}_{.125})_{10}\text{Ga}_4$  or  $\text{Er}_3(\text{Ni}_{.625}\text{Ga}_{.375})_2$ .

Isotypic compounds: All references GrYG, 80



$\text{Er}_3(\text{Ni}_{.625}\text{Ga}_{.375})_2$  has a  $\text{Y}_3\text{Rh}_2$ -type derivative structure where the characteristic ten-coordinated Rh sites are occupied by Ga atoms only. All other (eight-coordinated) Rh sites are occupied by a very Ni-rich mixture of Ni and Ga atoms. The correct formula for this compound is therefore  $\text{Er}_{21}(\text{Ni}_{.875}\text{Ga}_{.125})_{10}\text{Ga}_4$ . For all other isotypic compounds the occupation of the Ni/Ga sites has not been further studied. The idealized structure type formula corresponds to the case where all the Rh sites which are not ten-coordinated would be occupied by Ni atoms only. All phases have extended homogeneity ranges; however, surprisingly the idealized composition allowing perfect ordering of all Ni and Ga atoms  $\text{R}_{21}\text{Ni}_{10}\text{Ga}_4 \equiv \text{R}_3(\text{Ni}_{.715}\text{Ga}_{.285})_2$  has not yet been obtained.

The  $\text{Er}_{21}\text{Ni}_{10}\text{Ga}_4$ -type and the 4035:  $\text{Sm}_{26}\text{Co}_{11}\text{Ga}_6$ -type are ternary examples of the structure series  $\text{R}_{5n+6}\text{T}_{3n+5}$ , for binary structures, first reported by Le Roy et al. (LeMPP, 80), which interrelates the structure types of  $\text{W}_5\text{Si}_3$  ( $n = \infty$ ),  $\text{Pu}_{31}\text{Pt}_{20}$  or  $\text{Ca}_{31}\text{Sn}_{20}$  ( $n = 5$ ) and  $\text{Y}_3\text{Rh}_2$  ( $n = 3$ ). No binary example is known for  $n = 4$ , but  $\text{Sm}_{26}\text{Co}_{11}\text{Ga}_6$  [or  $\text{Sm}_{26}(\text{Co}, \text{Ga})_{17}$ ] represents a ternary example. The arrangements of the coordination polyhedra around the non-rare-earth elements in the different structures of the series are shown in fig. 5. The plane of projection for all five tetragonal structures is (110). The different coordination polyhedra have been shaded differently, except for the Archimedean antiprisms which have been left open. Only two types of polyhedra are found in the  $\text{W}_5\text{Si}_3$ -type of structure, but four types in all other structure types. In all structures, except in the  $\text{W}_5\text{Si}_3$ -type, horizontal slabs with cross-hatched cubes are found. The parameter  $n$  of the structural series formula indicates the number of horizontal slabs without cubes stacked between the slabs with cubes.

In fig. 5 all non-rare-earth positions are indicated by filled circles. In  $\text{Sm}_{26}\text{Co}_{11}\text{Ga}_6$  and  $\text{Er}_{21}\text{Ni}_{10}\text{Ga}_4$  the Ga atoms occupy the centres of the 10-atom polyhedra, which

TABLE I  
Structural data for the  $\text{R}_{5n+6}\text{T}_{3n+5}^{[8, a]}\text{M}_{2n-2}^{[10, c]}$  structural series.

$n$	Code	Composition	Structure type	Pearson's classif. symbol	Space group	Number of slabs stacked along $c$ axis/ unit cell
3	4029	$\text{R}_{21}\text{T}_{10}\text{M}_4$	$\text{Er}_{21}\text{Ni}_{10}\text{Ga}_4$ $\text{Y}_3\text{Rh}_2$ -type derivative	tI140	I4/mcm	8
4	4035	$\text{R}_{26}\text{T}_{11}\text{M}_6$	$\text{Sm}_{26}\text{Co}_{11}\text{Ga}_6$	tP86	P4/mbm	5
5	3940	$\text{R}_{31}\text{T}_{12}\text{M}_8$	$\text{Pu}_{31}\text{Pt}_{20}$ or $\text{Ca}_{31}\text{Sn}_{20}$ - type derivative, no ternary compounds known	tI204	I4/mcm	12
6	3943	$\text{R}_{36}\text{T}_{13}\text{M}_{10}$		tP118	P4/mbm	7
$\infty$	3867	$\text{R}_5\text{TM}_2$	$\text{W}_5\text{Si}_3$ -type derivative, no ternary compounds known	tI32	I4/mcm	2



Structure Series

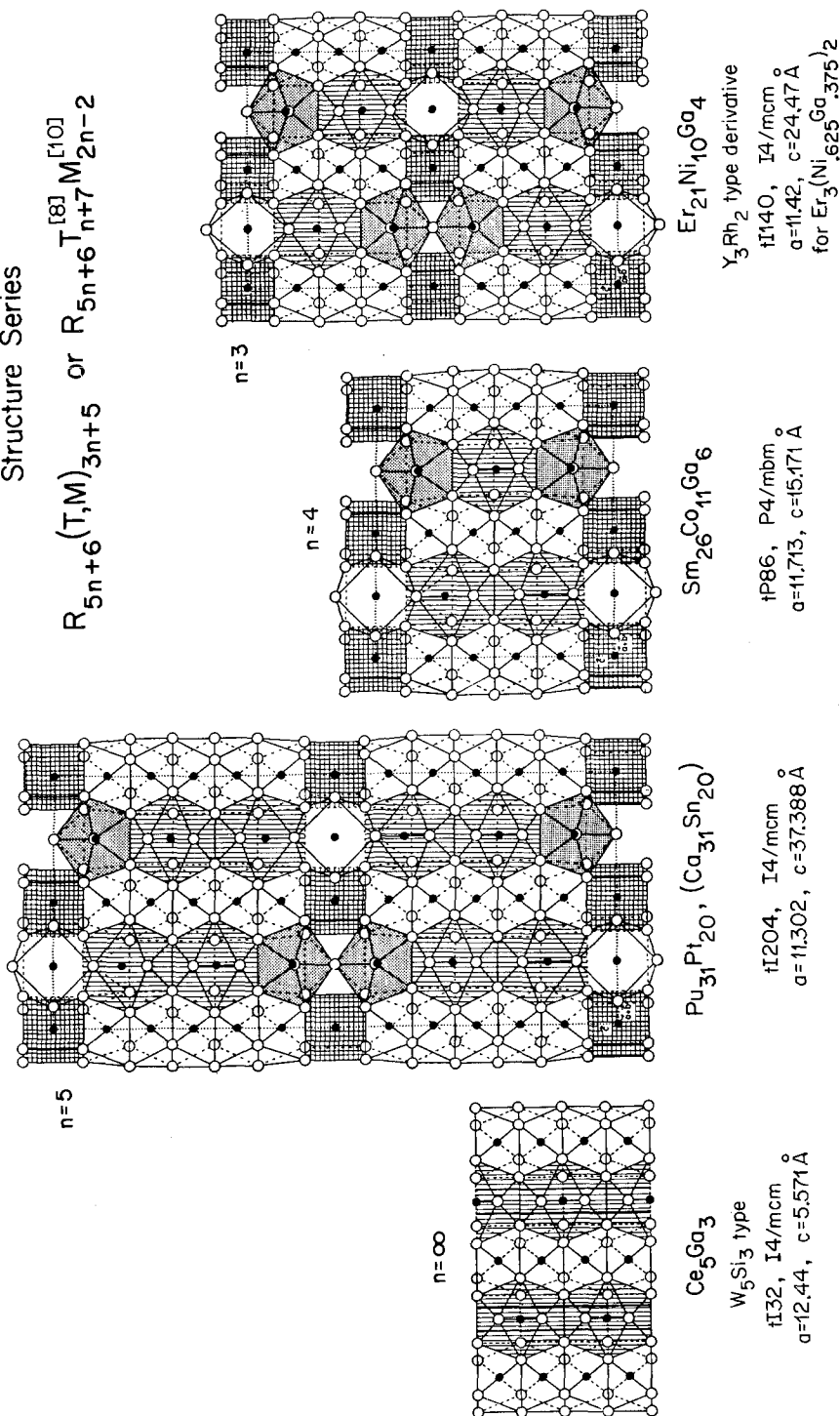
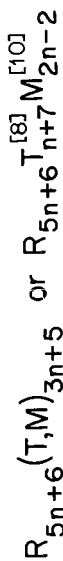


Fig. 5. The arrangements of the coordination polyhedra in the members of the  $R_{5n+6}(T, M)_{3n+5}$  or  $R_{5n+6}T_{n+7}M_{2n-2}^{[10]}$  structural series. The rare earth atoms are indicated with open circles and T and/or M atoms with filled ones. The plane of projection for all four structures is the (110) plane. In the  $W_5Si_3$  structure two types of coordination polyhedra occur, in all others four types. They have been shaded differently, except for the Archimedean antiprisms, which have been left open. The polyhedra, which in ternary structures are centred by Ga atoms, are hatched vertically.

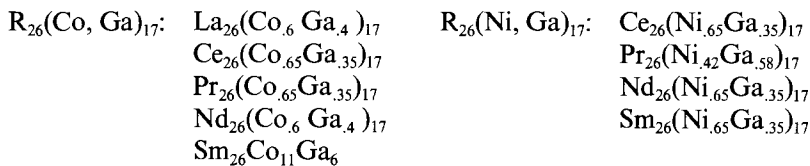
are vertically hatched, while all other filled circles correspond to Ni or Co atoms. In consideration of the different site occupation by T and M atoms in ternary compounds, the formula of the structural series can be rewritten as  $R_{5n+6}T_{n+6}^{[8,a]}T_{n+6}^{[8,c]}M_{2n-2}^{[10,l]}$  with  $n \geq 3$ . Compositions and space groups for known and hypothetical members of this structural series are compiled in table 1.

The centres of the 10-atom polyhedra can be also occupied by T atoms as for example in  $R_3Rh_2$  and  $R_3Ir_2$  compounds of  $Y_3Rh_2$ -type (MoPP, 76; LeMPP, 80). On the other hand, also the centres of the Archimedean antiprisms can be occupied by Ga atoms as, for example, in  $Ce_5Ga_3$  and  $Pr_5Ga_3$  of  $W_5Si_3$ -type (DzGK, 68).

The structural change of the ternary R-Ni-Ga compounds from  $n = 3$  to  $n = 4$  upon exchange of a larger R element by a smaller one is worth pointing out. It cannot be explained by size considerations.

4035	$Sm_{26}Co_{11}Ga_6$	tP86	$a = 11.713$	YaGO, 80
	or $Sm_{26}Co_{10}^{[8,a]}Co^{[8,c]}Ga_6^{[10,l]}$	P4/mbm	$c = 15.171$	

Isotypic compounds: All references YaGO, 80



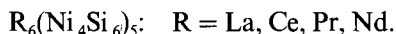
In the compound  $Sm_{26}Co_{11}Ga_6$  the Co and Ga atoms are strictly ordered and occupy different crystallographic sites. For the other compounds this has not yet been proven experimentally.

The  $Sm_{26}Co_{11}Ga_6$  structure, shown in fig. 5, together with the 4029:  $Er_{21}Ni_{10}Ga_4$ -type belongs to a structural series, which is discussed with the latter type.

45(60)	$Ce_6Ni_2Si_3$	hP22	$a = 12.112$	BoGK, 74
	or $Ce_6Ni^{[6,o]}(Ni_{.25}Si_{.75})_4^{[6,p]}$	P6 <sub>3</sub> /m	$c = 4.323$	
	or $Ce_6Ni(Ni_{.33}Si_{.67})_3Si$			

Filled-up variant of  $Ho_4Co_3$  ( $\equiv Ho_6Co_{4.5}\square_{.5}$ )-type (LeSY, 69), or filled-up variant of  $V_{12}P_7$  ( $\equiv V_6P_{3.5}\square_{1.5}$ )-type (OlG, 70)

Isotypic compounds: All references BoGK, 74



The  $Ce_6Ni_2Si_3$ , the 50(60): $Ce_5Ni_2Si_3$  and the 53(76): $Ce_{15}Ni_4Si_{13}$  structures constitute the members of the structure series  $R_{n^2/2+3n/2+1}T^{[6,ol](T,M)}_{n^2[p]}$  with  $n = 2, 3$  and 4, respectively, shown in fig. 6. All structures are characterized by centred rare earth octahedra (two per unit cell), which form infinite columns along the  $c$  axis and triangular columns of centred trigonal rare earth prisms, which share faces. The parameter  $n$  indicates the number of joined trigonal prisms along one of the basal edges of triangular columns. The centres of the octahedra are always occupied by T atoms, while the centres of the trigonal prisms are occupied in part by Si atoms alone and in part by a Ni/Si mixture.

The compositions, space groups and Pearson's classification symbols for the members of this series are listed in table 2. For  $n = \infty$  the octahedra are replaced by an infinite three-dimensional framework of centred trigonal prisms that is known as the  $Al_2B_2^{[6p+3]}$ -type. This type is found with 67(75): $Ce(Ni_{25}Si_{75})_2$  (GIB, 65) and many other  $R(T, Si)_2$  or  $R(T, Ge)_2$  compounds. Since, in the known examples of R-Ni-Si alloys, no regularity of the Ni/Si ratio at the prism centre sites is shown, and since the homogeneity ranges of these phases have not been investigated, the last two digits of the composition code have not been specified in table 2. Thus the compositions of the different members of this series can be correlated only by their content of rare earth (or non-rare-earth) element.

Binary analogues of these ternary structures are known only in the form of defect structures. There are two kinds of defect structures:

(1) Defects in the centres of the octahedra only. The  $Ho_4Co_3$  structure (LeSY, 69) corresponds to a structure of the ternary series  $R_6T^{[6,ol](T,M)}_4^{[6,p]}$  with  $n = 2$ , where, however, of every two octahedra only one is occupied. The formula can thus be rewritten as\*  $Ho_6(Co_{1/2}\square_{1/2})^{[6ol]}Co_4^{[6p]}$ . A ternary partially ordered derivative structure of  $Ho_4Co_3$  is found with  $Mg_{12-2x}Al_{2x}Cu_2Si_7$  (ArA, 80), for which the crystal chemical formula is  $Mg_{6-x}Al_x(Si_{1/2}\square_{1/2})^{[6ol]}Cu^{[6p]}Si_3^{[6p]}$ .

\*A new proposal for this structure, now shown to occur at  $Y_3Co_7$ , has recently been given by GrCSS, 82.

TABLE 2  
Structural data for the  $R_{n^2/2+3n/2+1}T^{[6,ol](T,M)}_{n^2[p]}$  structural series.

$n$	Code	Composition	Structure type	Pearson's classif. symbol	Space group
1	40(-)	$R_3T(T, M)_1$	—	hP10	
2	45(-)	$R_6T(T, M)_4$	$Ce_6Ni_2Si_3$	hP22	$P6_3/m$
3	50(-)	$R_{10}T(T, M)_9$	$Ce_5Ni_2Si_3$	hP40	$P6_3/m$
4	53(-)	$R_{15}T(T, M)_{16}$	$Ce_{15}Ni_4Si_{13}$	hP64	$P6_3/m$
5	55(-)	$R_{21}T(T, M)_{25}$	—	hP92	$P6_3/m$
$\infty$	67(-)	$R(T, M)_2$	$AlB_2$	hP3	$P6/mmm$

## STRUCTURE SERIES

$$R \frac{n^2}{2} + \frac{3}{2}n + 1 T^{[6\alpha]}(T, M)_{n^2}^{[6\beta]}$$

z=3/4 z=1/4  
and  
1/2

R

Ni

Si

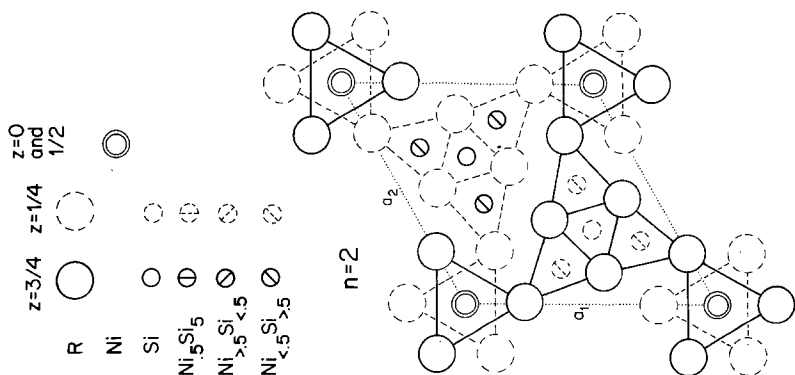
Ni<sub>5</sub>Si<sub>5</sub>Ni<sub>>5</sub>Si<sub><5</sub>Ni<sub><5</sub>Si<sub>>5</sub>

Fig. 6. Members of the structural series  $R_{n^2/2+3n/2+1}T^{[6\alpha]}(T, M)_{n^2}^{[6\beta]}$  with  $n = 2, 3$  and  $4$ , respectively.

Incidentally, in the  $Y(OH)_3$  type (ScS, 47) the O and Y sites correspond to R and  $(T, M)^{[6p]}$  sites, respectively, of the hypothetical structure of the ternary series with  $n = 1$ , where, however, all octahedra are unoccupied. Slight rotation of the trigonal prisms leads to the  $Re_3B$ -type found, for example, with  $Pu_3Co$  (LaCR, 63).

(2) Defects in the centres of the octahedra and the centres of the trigonal prisms.  $V_{12}P_7$  (OIG, 70) and  $Rh_{20}Si_{13}$  (En, 65) are members of a binary structural series (formed from transition and main group elements) with formula

$$T_{n^2/2 + 3n/2 + 1}(M_{1/2}^{[6o]} \square_{1/2})(M_{n^2 - [n^2/2 - n/2]}^{[6p]} \square_{n^2/2 - n/2})$$

for  $n = 2$  and  $n = 3$ , respectively. The mathematical expressions chosen for the indices permits a simple comparison with the formula for the ternary series (without defects) given above. The two binary structures resemble the ternary structures for  $n = 2$  and  $n = 3$  discussed above and shown in fig. 6. However, of every two octahedra per unit cell only one is occupied and certain trigonal prisms are empty. In detail, the maximum number of trigonal prisms is filled with the restriction that no two filled prisms have a common face (i.e. no short P-P or Si-Si contacts occur). The member of this binary series for  $n = \infty$  is also known; it is the  $WC^{[6p]}$ -type.

---

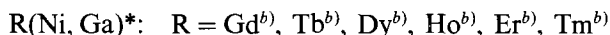
<b>50(25)</b>	<b>Er<sub>4</sub>Ni<sub>3</sub>Si</b>	<b>oC8</b>	<b>a = 3.735</b>	<b>Ra, 68</b>
	or	<b>Cmcm</b>	<b>b = 10.20</b>	
	<b>Er(Ni<sub>0.75</sub>Si<sub>0.25</sub>)<sup>[6, p]</sup></b>		<b>c = 4.082</b>	

---

CrB-type with statistical occupation of B sites by two kinds of atoms

---

Isotypic compounds:



\*Could be also a solid solution of Ga in the high temperature phase of RNi.

<sup>a</sup>Ra, 68    <sup>b</sup>GrY, 81

---

<b>50(25)</b>	<b>Gd<sub>4</sub>Ni<sub>3</sub>Cu</b>	<b>oP8</b>	<b>a = 7.033</b>	<b>Ra, 68</b>
	or	<b>Pnma</b>	<b>b = 4.230</b>	
	<b>Gd(Ni<sub>0.75</sub>Cu<sub>0.25</sub>)<sup>[6, p]</sup></b>		<b>c = 5.410</b>	

---

FeB-type with statistical occupation of B sites by two kinds of atoms

---

The CrB- and the FeB-types are found frequently in R-T and R-M binary phase diagrams and the homogeneity ranges of these phases extend into the ternary phase

diagram. However, the two phases mentioned here are truly ternary phases in the pseudo-binary system RT–RM.

The CrB-type occurs with ErSi and Er(Ni<sub>0.75</sub>Si<sub>0.25</sub>); however, in the binary compound the prisms are stretched and in the ternary one they are compressed. ErNi itself crystallizes with the FeB-type. In the case of Gd(Ni<sub>0.75</sub>Cu<sub>0.25</sub>) with FeB-type the binary end-members have different structures (GdNi with CrB-type and GdCu with CsCl-type, the latter type without trigonal prisms).

#### *The CrB- and FeB-types and the CrB–FeB stacking variants*

The CrB- and FeB-types, shown in fig. 7, can be considered as stacking variants of each other (Hohnke and Parthé, 1966; Parthé, 1976). In the case of certain ternary alloys it is possible to obtain hybrid structures containing CrB and FeB segments, the stacking of which can be systematically varied by a successive replacement of T atoms by M atoms. This gives rise to structures which can be considered as periodic intergrowths of FeB and CrB structure segments. For example, Gignoux and Gomez-Sal (1976) reported that GdNi with CrB type—after a 10% replacement of Ni by Cu atoms—changes its structure to a CrB/FeB stacking variant with 67% FeB stacking, called the TbNi, low temperature type. A 20% replacement of Ni atoms by Cu leads to the FeB-type. No detailed studies have been made on this system nor on any other RT–RM pseudobinary system. Probably more stacking variants exist. The other FeB–CrB stacking variants shown in fig. 7 have been found in R<sub>1-x</sub>R'<sub>x</sub>Ni systems (Klepp and Parthé, 1980) and with CaCu and SrAg compounds (Merlo and Fornasini, 1981). Detailed studies have been made of the homogeneity ranges of the different phases in pseudo-binary systems R<sub>1-x</sub>R'<sub>x</sub>Ni where RNi crystallizes with CrB- and R'Ni with FeB-type structure (Klepp and Parthé, 1982). It was found that stacking variants occur only in particular systems and that their compositions and homogeneity ranges vary in a systematic way depending on the kinds of participating rare earth atoms.

The CrB and FeB structures and the CrB–FeB stacking variants belong to the large group of structures where all R atoms participate in the formation of centred trigonal prisms and where all trigonal prismatic holes are occupied by T and/or M atoms. The known ternary structures of this group are listed in table 3.

#### *Classification according to linkage coefficient*

The structures containing trigonal prisms can be classified by means of the type of linkage of the centred trigonal prisms. The linkage coefficient LC denotes the average number of prisms in which the R atoms participate, assuming, as stated before, that all rare earths participate in the formation of such prisms (Parthé and Moreau, 1977; Parthé, 1981). LC corresponds to six times the ratio of the number of trigonal prisms to the number of R atoms in one unit cell. The composition of the compound is then directly related to the LC value according to R<sub>6</sub>(T, M)<sub>LC</sub>. The value of LC can vary from LC = 1 where only isolated trigonal prisms occur, to LC = 12 where the whole space is completely filled with trigonal prisms. An example of LC = 1 is the Pd<sub>6</sub>P structure type (AnKCR, 74) and examples of LC = 12 are the AlB<sub>2</sub> and ThSi<sub>2</sub> structure types. Ternary rare earth structures are found with 6 ≤ LC ≤ 12.

TABLE 3

Ternary  $R_6(T, M)_n^{(6,p)}$  or  $R_{m+n/2}(T, M)_n^{(6,p)}$  structures built up exclusively of T and/or M centred trigonal rare earth prisms arranged according to increasing LC value.

LC	Code	Ternary compound	Pearson's classif. symbol	Space group	Relation to binary types	Class*	m	n	$\frac{m}{n}$	number of slabs of type**		Hypothetical composition for order a)	Hypothetical composition for order a) and b)	Fig.
										W	AIB <sub>2</sub>			
6	50(25)	Er(Ni <sub>75</sub> Si <sub>25</sub> ) <sup>(6,p)</sup>	oC8	Cncc	CrB-type	I	2	4	$\frac{1}{2}$	2(1+1)	2(1+1)	—	—	7,8
6	50(25)	Gd(Ni <sub>75</sub> Cu <sub>25</sub> ) <sup>(6,p)</sup>	oP8	Pnma	FeB-type	IIb	2	4	$\frac{1}{2}$	—	—	—	—	7
6	50(30)	Y <sub>5</sub> Co <sub>3</sub> (Co <sub>25</sub> Ga <sub>75</sub> ) <sup>(6,p)</sup>	oP40	Pnma	filled-up	III	10	20	$\frac{1}{2}$	—	—	5060:R <sub>3</sub> T <sub>2</sub> M <sub>3</sub>	5080:R <sub>3</sub> TM <sub>4</sub>	9
6	5067	Gd <sub>3</sub> Ni <sup>(6,p)</sup> Si <sup>(6,p)</sup>	oP24	Pnma	filled-up Hf <sub>3</sub> P <sub>2</sub> -type	III	6	12	$\frac{1}{2}$	—	—	5067:R <sub>3</sub> TM <sub>2</sub>	5067:R <sub>3</sub> TM <sub>2</sub>	9
6	5071	Ce <sub>7</sub> Ni <sup>(6,p)</sup> Si <sup>(6,p)</sup>	oP56	Pnma		III	14	28	$\frac{1}{2}$	—	—	5071:R <sub>7</sub> T <sub>2</sub> M <sub>5</sub>	5071:R <sub>7</sub> T <sub>2</sub> M <sub>5</sub>	9
7 $\frac{1}{2}$	55-	R <sub>5</sub> (T, M) <sub>6</sub>	oC22	Cmcm	V <sub>3</sub> B <sub>6</sub> -type	I	4	12	$\frac{1}{3}$	4(1+1+1+1)	6(2+1+2+1)	5567:R <sub>5</sub> T <sub>2</sub> M <sub>4</sub>	5583:R <sub>5</sub> TM <sub>5</sub>	8
7 $\frac{2}{3}$	55(53)	Ce <sub>14</sub> (Ni <sub>49</sub> Si <sub>33</sub> ) <sup>(6,p)</sup>	mP62	P2 <sub>1</sub> /m		IIa	11	34	$\frac{11}{34}$	—	—	5553:R <sub>14</sub> T <sub>8</sub> M <sub>9</sub>	5565:R <sub>14</sub> T <sub>6</sub> M <sub>11</sub>	10
7 $\frac{2}{3}$	5565	Pr <sub>14</sub> Ni <sub>6</sub> Si <sub>11</sub>	mC124	C2/m		IIa	22	68	$\frac{11}{34}$	—	—	5553:R <sub>14</sub> T <sub>8</sub> M <sub>9</sub>	5565:R <sub>14</sub> T <sub>6</sub> M <sub>11</sub>	10
8	57(75)	Y <sub>3</sub> (Ni <sub>35</sub> Si <sub>20</sub> ) <sup>(6,p)</sup> Si <sup>(6,p)</sup>	oI14	Immm	Ta <sub>3</sub> B <sub>2</sub> -type derivative with partial disorder	I	2	8	$\frac{1}{4}$	2(1+1)	4(2+2)	5750:R <sub>3</sub> T <sub>2</sub> M <sub>2</sub>	5775:R <sub>3</sub> TM <sub>3</sub>	8
9	60-	R <sub>2</sub> (T, M) <sub>3</sub>	oC20	Cncc	V <sub>2</sub> B <sub>3</sub> -type	I	2	12	$\frac{1}{6}$	2(1+1)	6(3+3)	6033:R <sub>2</sub> T <sub>2</sub> M	6067:R <sub>2</sub> TM <sub>2</sub>	8
12	6750	LaPt <sup>(6,p)</sup> Si <sup>(6,p)</sup>	tI12	I4 <sub>1</sub> md	TiS <sub>2</sub> -type derivative or filled-up NbAs-type	IIa	0	8	0	—	—	—	6750:RTM	22
12	67(75)	Ce(Ni <sub>25</sub> Si <sub>75</sub> ) <sup>(6,p)</sup>	hP3	P6/mmm	AIB <sub>2</sub> -type	I	0	2	0	0	∞	—	6750:RTM	8

\*Classification according to number of directions of prism axes.

\*\*Only for structures which can be interpreted as intergrowths of W- and AIB<sub>2</sub>-type slabs.

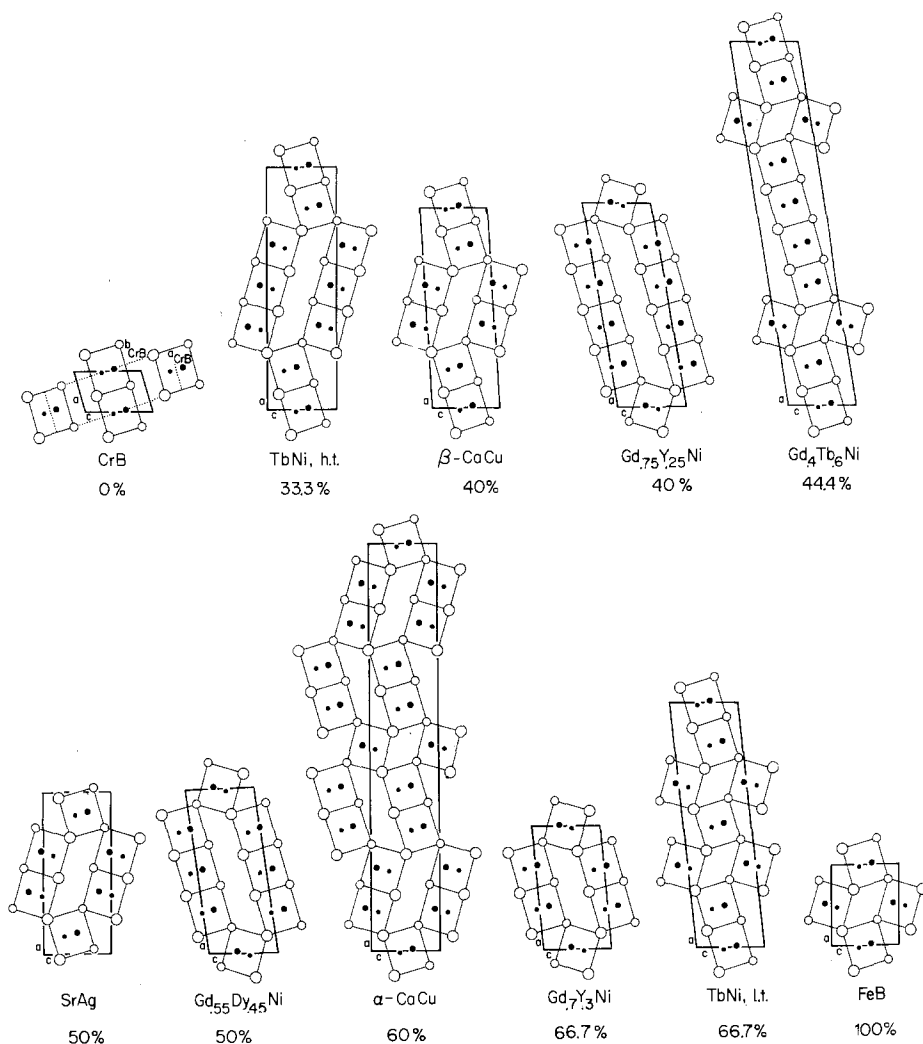


Fig. 7. The CrB-FeB stacking variants, arranged according to increasing percentage of FeB stacking. The open circles correspond to rare earth (or Cr, Ca, Sr, Fe) atoms. Large open or filled circles are at  $y = 3/4$ , all others at  $y = 1/4$ .

### *Subdivision according to the number of directions of the trigonal prism axes*

The structures built up exclusively of centred trigonal rare earth prisms can be subdivided according to the number of directions the trigonal prism axes assume.

I) Only one direction for the prism axes exists. Here all prisms are parallel. They are identical except for a rotation around the prism axis or a shift along it. The CrB structure belongs to this class.

II) There are two directions for the prism axes.

IIa) The two directions are perpendicular to each other as in the MoB structure.

IIb) The two directions are not perpendicular to each other as in the FeB structure and all FeB-CrB stacking variants.



III) More than two directions for the prism axes occur. Note that pairs of prisms with a common rectangular face must have their axes parallel or perpendicular.

The ternary R–T–M structures, built up exclusively of trigonal rare earth prisms, have nearly all one short unit cell dimension ( $\approx 4\text{\AA}$ ) which corresponds to the height of the trigonal prism and/or the length of its triangular base. It is convenient to present drawings of these structures in projection along this short axis.

The ternary structures of class I (all prism axes parallel) are shown in fig. 8 arranged in the order of increasing value of the linkage coefficient LC. Three examples for class III (three directions of the prism axes) with  $LC = 6$  are shown in fig. 9 and two examples for class IIa (two perpendicular directions for the prism axes) are presented in fig. 10.

*Structures interpreted as intergrowth of centred trigonal prisms with W structure type segments*

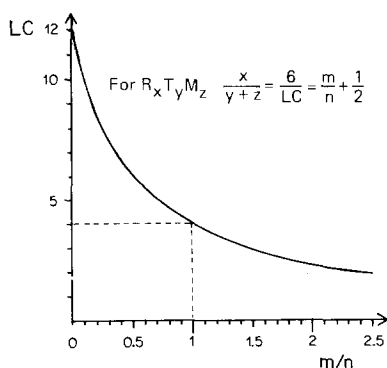
A study of the structures shown in figs. 8, 9 and 10 reveals that all atoms in the prism centres actually have nine neighbours. In addition to the six atoms of the surrounding R trigonal prism, there are three more atoms in the central plane perpendicular to the prism axis. In a prism with one (or two) unshared rectangular faces the central atom obtains its 9th (and 8th) neighbour by waist contact with a rare earth atom of a shifted, not connected, neighbouring trigonal prism (see for example fig. 9). The geometrical arrangement of the rare earth atoms at the interface corresponds to a (distorted) empty segment of the tungsten (A2) structure type. All structures can thus be considered as an intergrowth of centred trigonal prisms and W-type segments as shown in fig. 51. A W-type segment unit corresponds to half the unit cell of the W structure. The number of these segment units in a unit cell of a ternary structure,  $m$ , and the number of centred trigonal prisms per unit cell,  $n$ , can be related to the linkage coefficient LC (Grin' et al., GrYG, 79) according to:

$$LC = 6n / (m + \frac{1}{2}n).$$

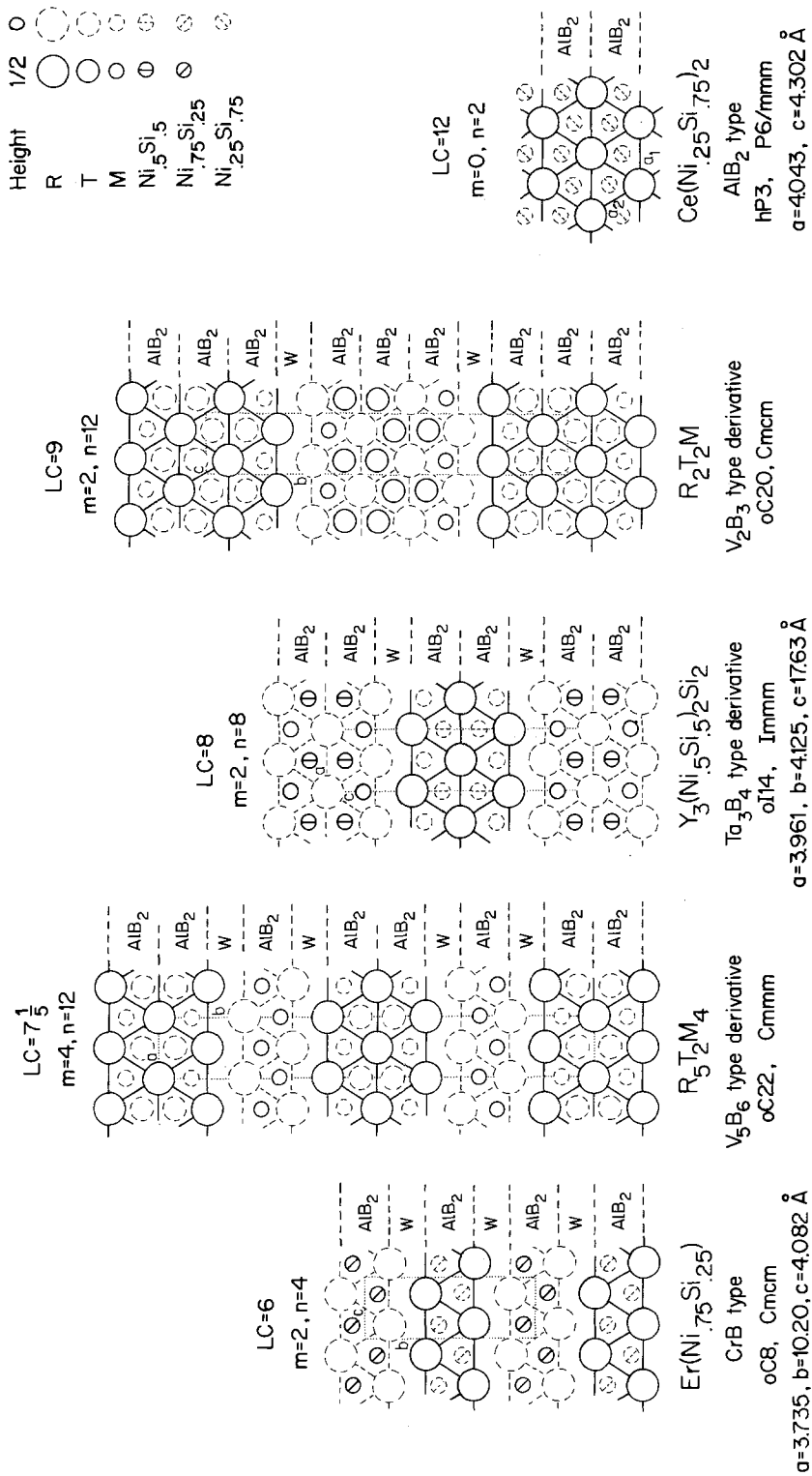
Expressed differently, the ratio  $m/n$  varies with LC according to

$$\frac{m}{n} = \frac{6}{LC} - \frac{1}{2}.$$

The variation of the ratio  $m/n$  with the LC value is graphically shown in the accompanying diagram.



$R_6(T,M)_{LC}^{[6p]}$  or  $R_{m+\frac{1}{2}n}(T,M)_{n}^{[6p]}$  structures with parallel prism axes



Height 1/2 ○  
 R ○  
 T ○  
 M ○  
 Ni<sub>.5</sub>Si<sub>.5</sub> ⊕  
 Ni<sub>.75</sub>Si<sub>.25</sub> ⊖  
 Ni<sub>.25</sub>Si<sub>.75</sub> ⊕

Fig. 8. Structures characterized by parallel centred trigonal rare earth prisms: the AIB<sub>2</sub>-type structure and four structures which can be interpreted as an intergrowth of W-type and AIB<sub>2</sub>-type slabs.

$R_6(T,M)_{LC}^{[6p]}$  or  $R_{m+\frac{1}{2}n}(T,M)_n^{[6p]}$  structures with  $LC=6$

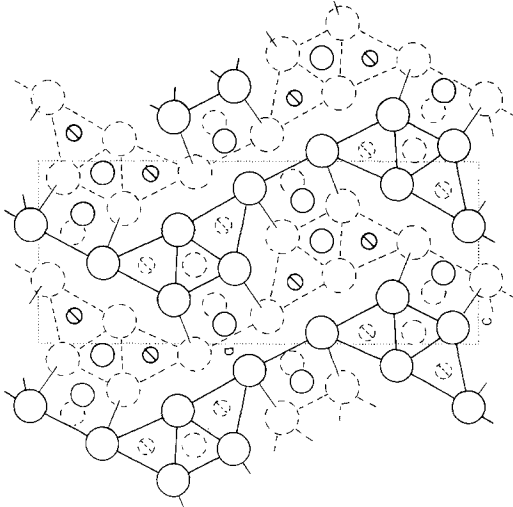
Height  
1/2    0

R    T    M     $Co_{25}Ga_{75}$

○    ○    ○    ⊙

○    ⊙    ⊙    ⊙

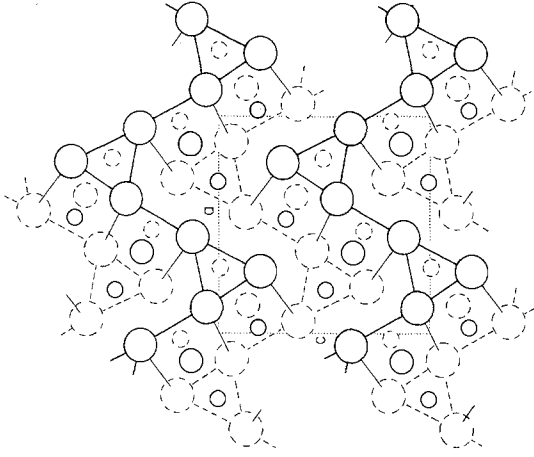
$m=10, n=20$



$Y_{10}Co_7Ga_3$

$\alpha P40, Pnma$   
 $a=23.558, b=3.9241, c=9.610 \text{ \AA}$   
for  $Y_5Co_3(Co_{25}Ga_{75})_2$

$m=6, n=12$



$Gd_3NiSi_2$

filled up  $Hf_3P_2$  type  
 $\alpha P24, Pnma$   
 $a=11.398, b=4.155, c=11.310 \text{ \AA}$

$m=14, n=28$



$Ce_7Ni_2Si_5$

$\alpha P56, Pnma$   
 $a=23.31, b=4.299, c=13.90 \text{ \AA}$

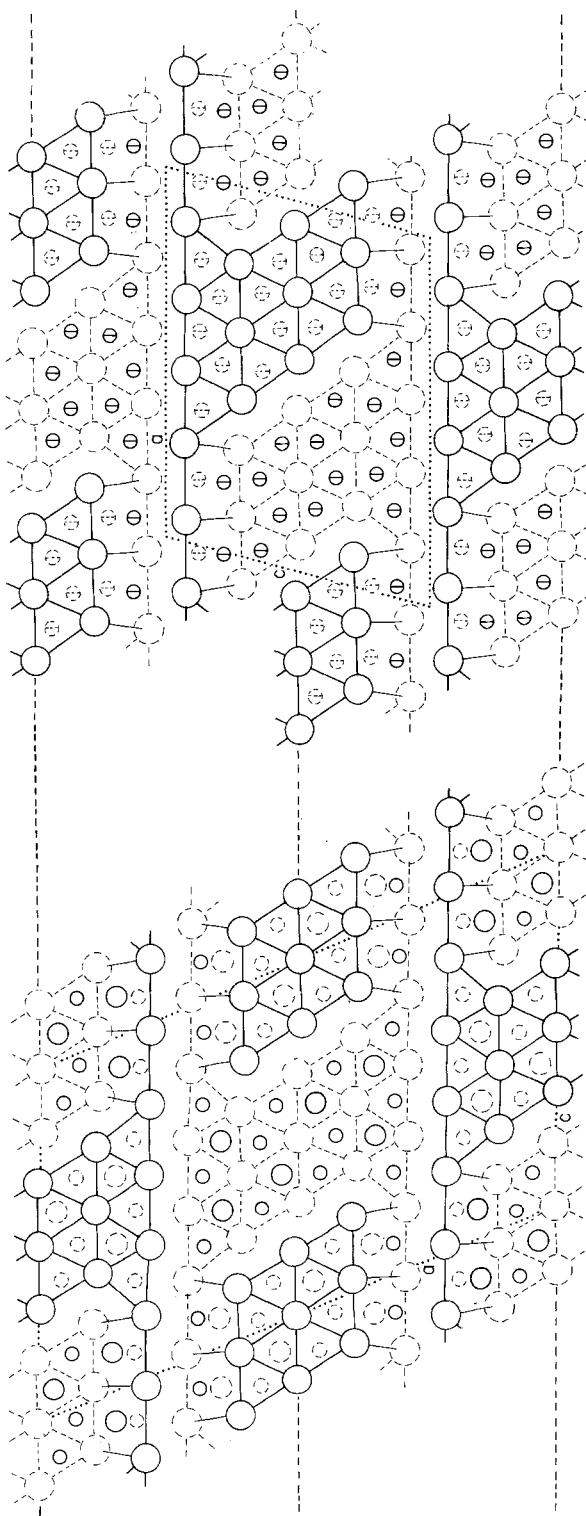
Fig. 9. Structures built up only of centred trigonal rare earth prisms with three different directions of the prism axes.

$R_6(T, M)_{LC}^{(6p)}$  or  $R_{m+\frac{1}{2}n}(T, M)_{n}^{(6p)}$  structures with  $LC=7^2/7$

Height R Ni Si Ni<sub>5</sub>Si<sub>5</sub>  
 1/2 ○ ○ ○ ○ ○  
 0 ○ ○ ○ ○ ○

$m=22, n=68$

$m=11, n=34$



$Pr_{14}Ni_6Si_{11}$

$mC124, C2/m$

$a=33.991, b=4.2328, c=21.330 \text{ \AA}, \beta=113.72^\circ$

$Ce_{14}(Ni,Si)_{17}$

$mP62, P2_1/m$

$a=21.79, b=4.290, c=16.43 \text{ \AA}, \beta=104.0^\circ$

for  $Ce_{14}(Ni_{.47}Si_{.53})_{17}$

Fig. 10. The  $Pr_{14}Ni_6Si_{11}$  and the  $Ce_{14}(Ni, Si)_{17}$  structures that are related as stacking variants. Both are built up of centred trigonal rare earth prisms only with  $LC = 7^2/7$  and only two perpendicular prism axis directions (class Ila). The  $Ce_{14}(Ni, Si)_{17}$  structure is obtained from the  $Pr_{14}Ni_6Si_{11}$  structure if the upper half of the drawing is shifted along the dashed line  $\frac{1}{2}c$  to the right and out of the plane of projection by  $\frac{1}{2}b$ .

The compositions of these structures can thus be denoted by  $R_{m/n+1/2}(T, M)$  or  $R_{m+n/2}(T, M)_n$  (GlG, 81 and PaCH, 83). The values of  $m$ ,  $n$  and  $m/n$  have been listed for all structures in table 3. These values can be verified by a careful study of the corresponding drawings in figs. 8, 9 and 10.

*Structures with parallel prisms described as an intergrowth of W-type and  $AlB_2$ -type slabs*

In the case that all trigonal prism axes are parallel, both the W-type segments and the  $AlB_2$ -type segments become slabs perpendicular to the longest cell axis and the structures can be described as an intergrowth of slabs of both types. The parameters  $m$  and  $n$  can now be related to the number of slabs per unit cell. The number of W-type slabs is designated  $m$ ; however, since to each unit of W-type segment in the W-type slab there corresponds two trigonal prisms in the  $AlB_2$ -type slab, the number of  $AlB_2$ -type slabs per unit cell is  $\frac{1}{2}n$ . In fig. 8 are shown an  $AlB_2$ -type structure and four structures which can be interpreted as intergrowths of W-type and  $AlB_2$ -type slabs. The ternary structures derived from  $V_2B_3$  and  $V_3B_6$  (SpG, 69)\* have not yet been found in R–T–M compounds. The compositions  $R_2T_2M$  and  $R_5T_2M_4$  given in fig. 8 and table 3 are in agreement with the general ordering rule discussed in the following subsection.

*Ordering of T and M atoms on the prism centres*

Concerning the order of the non-rare-earth atoms at the prism centres, the following observations have been made (Parthé et al., PaCH, 83):

(a) In 5067:Gd<sub>3</sub>NiSi<sub>2</sub>, 5071:Ce<sub>7</sub>Ni<sub>2</sub>Si<sub>5</sub>, 5565:Pr<sub>14</sub>Ni<sub>6</sub>Si<sub>11</sub> and 57(75):Y<sub>3</sub>(Ni<sub>5</sub>Si<sub>5</sub>)<sub>2</sub>Si<sub>2</sub> the Ni atoms occupy only those centre sites that in their waist contact have no rare earth atoms. The compositions for idealized order of T and M atoms, assuming that all prism centres without rare earth waist contacts are occupied by T atoms and the remaining prism centres by M atoms, are given under the heading "Composition for Order a)" in table 3. These are the most transition-metal-rich compositions which are possible if the T–R waist contact rule is fulfilled. The waist contact rule is well obeyed with R–Ni–Si compounds, but not with the ternary gallide 50(30):Y<sub>3</sub>Co<sub>3</sub>(Co<sub>0.25</sub>Ga<sub>0.75</sub>)<sub>2</sub>.

(b) In R–Ni–Si compounds, in addition to the T–R waist contact rule, an additional rule is observed that no T–T prism centre contacts should occur. The compositions obtained are listed in table 3 under the heading "Composition for order a) and b)". Both rules applied simultaneously allow one to derive correctly the compositions of the ordered ternary phases 5067:Gd<sub>3</sub>NiSi<sub>2</sub>, 5071:Ce<sub>7</sub>Ni<sub>2</sub>Si<sub>5</sub>, 5565:Pr<sub>14</sub>Ni<sub>6</sub>Si<sub>11</sub> and of the disordered phase 57(75):Y<sub>3</sub>(Ni<sub>5</sub>Si<sub>5</sub>)<sub>2</sub>Si<sub>2</sub>. In the last case an ordered arrangement should have a unit cell with an  $a$  lattice parameter twice as long.

(c) The T–R and T–T waist contact rules are valid only for those structures which have elongated  $R_6T$  prisms ( $w/s > 1$ , see fig. 3a).

\*In the paper by Spear and Gilles (1969) drawings of the  $V_2B_3$  and  $V_3B_6$  structures were presented but without numerical values of the adjustable atom coordinates. The  $V_2B_3$ -type has been found later for VCoB<sub>3</sub> (KuS, 73) and the  $V_3B_6$ -type for Cr<sub>2</sub>Ni<sub>3</sub>B<sub>6</sub> (CeKK, 72). For these ternary structures the atom coordinates were listed.

### Shape of the trigonal prisms

The tendency of the T atoms to form compressed  $R_6T$  prisms and of the M atoms to form stretched  $R_6M$  prisms leads to the deformation of the trigonal prisms as can be seen in fig. 9 in the drawings for 5067:Gd<sub>3</sub>NiSi<sub>2</sub> and 5071:Ce<sub>7</sub>Ni<sub>2</sub>Si<sub>5</sub>. That deformation is also observed with certain prisms in 55(53):Ce<sub>14</sub>Ni<sub>8</sub>Si<sub>9</sub> and could be an indication for an overlooked ordering of T and M atoms.

### Other possible ternary structures with centred trigonal prisms

To find other possible fully ordered ternary structures of the  $R_6(T, M)_{LC}$  family one can investigate other binary structures of the same kind which already have been found to be related to the ternary structures. There are two kinds of binary structures of interest:

– Many structures of the binary transition metal borides are characterized by B-centred trigonal prisms of the transition elements. Hypothetical ordered ternary structures derived from the  $R_6(T, M)_{LC}$  family are obtained by placing R atoms on the transition metal sites and by ordering T and M atoms on the B sites according to the principles outlined above. An example from table 3 is the partially ordered Y<sub>3</sub>NiSi<sub>3</sub> structure with a Ta<sub>3</sub>B<sub>4</sub>-type derivative structure, for which the expected composition, assuming complete ordering of type a), is R<sub>3</sub>T<sub>2</sub>M<sub>2</sub> and, with ordering of type a) and b), is R<sub>3</sub>TM<sub>3</sub>.

– Many structures of metal-rich binary transition metal phosphides and arsenides are built up in a systematic way of P (As)-centred and empty trigonal prisms of transition elements. Hypothetical ordered ternary structures of the  $R_6(T, M)_{LC}$  family are obtained by assuming the R atoms to occupy the transition metal sites. M atoms are assigned to the phosphorus (or arsenic) sites and the T atoms are placed at the centres of the empty trigonal prisms. Examples of such ordering from table 3 are 5067:Gd<sub>3</sub>NiSi<sub>2</sub> with filled-up Hf<sub>3</sub>P<sub>2</sub>-type, and 6750:LaPtSi, with filled-up NbAs type (BoP, 63) (this is a ThSi<sub>2</sub>-type derivative). The data for three hypothetical ternary structures derived from known binary types are given in table 4.

TABLE 4

Three hypothetical ternary structures of the  $R_6(T, M)_{LC}$  family derived from known binary transition metal boride and phosphide structure types.

Binary transition metal boride		Binary transition metal phosphide		LC	Code	Hypothetical formula	Pearson's classif. symbol	Space group	<i>m</i>	<i>n</i>
Ru <sub>11</sub> B <sub>8</sub>	(As, 60)	—	—	4 <sub>11</sub> <sup>4</sup>	4275	R <sub>11</sub> T <sub>2</sub> M <sub>6</sub>	oP38	Pbam	14	16
—	—	Mo <sub>8</sub> P <sub>5</sub>	(Jo, 72)	5 <sub>4</sub> <sup>1</sup>	4771	R <sub>8</sub> T <sub>2</sub> M <sub>5</sub>	mP15	Pm	4 <sub>2</sub> <sup>1</sup>	7
—	—	Mo <sub>4</sub> P <sub>3</sub>	(Ru, 65)	7 <sub>2</sub> <sup>1</sup>	5660	R <sub>4</sub> T <sub>2</sub> M <sub>3</sub>	oP72	Pnma	12	40

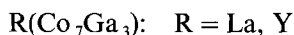
Data for hypothetical compound assuming ordering of type a) only

---

<b>50(30)</b>	$\text{Y}_{10}\text{Co}_7\text{Ga}_3$	oP40	$a = 23.558$	GrYG, 79
	or	Pnma	$b = 3.9241$	
	$\text{Y}(\text{Co}_{0.7}\text{Ga}_{0.3})^{[6, \text{pl}]}$		$c = 9.610$	
	or			
	$\text{Y}_5\text{Co}_3(\text{Co}_{0.25}\text{Ga}_{0.75})_2$			

---

Isotypic compounds: All references GrYG, 79



The  $\text{Y}_{10}\text{Co}_7\text{Ga}_3$  structure, shown in fig. 9, belongs to the  $\text{R}_6(\text{T}, \text{M})_{\text{LC}}$  family built up only of centred trigonal rare earth prisms. This structural family is discussed with the 50(25) compounds.

---

<b>50(60)</b>	$\text{Ce}_5\text{Ni}_2\text{Si}_3^*$	hP40	$a = 16.12$	BoGM, 72
	or	$\text{P6}_3/\text{m}$	$c = 4.309$	
	$\text{Ce}_{10}\text{Ni}^{[6, \text{ol}]}(\text{Ni}_{1.33}\text{Si}_{1.67})_3^{[6, \text{pl}]}$			
	or			
	$\text{Ce}_{10}\text{Ni}(\text{Ni}_{1.5}\text{Si}_{1.5})_6\text{Si}_3$			

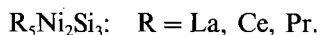
---

Filled-up variant of  $\text{Rh}_{20}\text{Si}_{13}$  ( $\equiv \text{Rh}_{20}\text{Si}_{13}\square_7$ )-type

---

\*In the publication incorrectly referred to as  $\text{Ce}_2\text{NiSi}$  compound.

Isotypic compounds: All references BoGM, 72



The crystal chemistry of this structure, shown in fig. 6, is discussed with the 45(60): $\text{Ce}_6\text{Ni}_2\text{Si}_3$  structure.

---

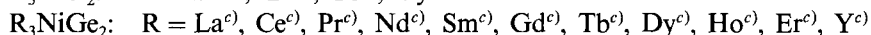
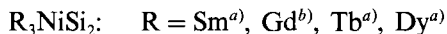
<b>5067</b>	$\text{Gd}_3\text{NiSi}_2$	oP24	$a = 11.398$	KIP, 81
	or	Pnma	$b = 4.155$	
	$\text{Gd}_3\text{Ni}^{[6, \text{pl}]}_2\text{Si}_2^{[6, \text{pl}]}$		$c = 11.310$	

---

Filled-up variant of  $\text{Hf}_3\text{P}_2$  ( $\equiv \text{Hf}_3\square_2\text{P}_2$ )-type (Lu, 68)

---

## Isotypic compounds:



<sup>a)</sup>KIP, 82a    <sup>b)</sup>KIP, 81    <sup>c)</sup>BoBP, 82

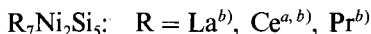
The  $Gd_3NiSi_2$  structure, which is shown in fig. 9, belongs to the  $R_6(T, M)_{LC}$  family built up only of centred rare earth prisms. This structural family is discussed with the 50(25) compounds.

---

5071	$Ce_7Ni_2Si_5$	oP56	$a = 23.31$	Mi, 74
	or	Pnma	$b = 4.299$	
	$Ce_7Ni_2^{[6, p]}Si_5^{[6, p]}$		$c = 13.90$	

---

## Isotypic compounds:



<sup>a)</sup>Mi, 74    <sup>b)</sup>MiBG, 74a

The  $Ce_7Ni_2Si_5$  structure, presented in fig. 9, belongs to the  $R_6(T, M)_{LC}$  family built up only of centred rare earth prisms. This structural family is discussed with the 50(25) compounds.

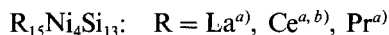
---

53(76)	$Ce_{15}Ni_4Si_{13}^*$	hP64	$a = 20.27$	MiBG, 74
	or	$P6_3/m$	$c = 4.306$	
	$Ce_{15}Ni^{[6, o]}(Ni_{19}Si_{.81})_{16}^{[6, p]}$			
	or $Ce_{15}Ni(Ni_{.5}Si_{.5})_6Si_{10}$			

---

\*R factor of this structure is 17%.

## Isotypic compounds:



<sup>a)</sup>Mi, 73    <sup>b)</sup>MiBG, 74

The crystal chemistry of this structure, shown in fig. 6, is discussed with the 45(60): $Ce_6Ni_2Si_3$  structure.

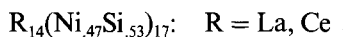


---

<b>55(53)</b>	<b>Ce<sub>14</sub>Ni<sub>8</sub>Si<sub>9</sub></b>	mP62	$a = 21.79$	Mi, 73
	or	P2 <sub>1</sub> /m	$b = 4.290$	
	Ce <sub>14</sub> (Ni <sub>4.7</sub> Si <sub>5.3</sub> ) <sub>17</sub> <sup>[6, p]</sup>		$c = 16.43$	
			$\beta = 104.0^\circ$	

---

Isotypic compounds: All references Mi, 73



The Ce<sub>14</sub>Ni<sub>8</sub>Si<sub>9</sub> structure, and a stacking variant of it, the 5565:Pr<sub>14</sub>Ni<sub>6</sub>Si<sub>11</sub> structure, are both shown in fig. 10. They belong to the R<sub>6</sub>(T, M)<sub>LC</sub> family built up only of centred rare earth prisms. This structural family is discussed with the 50(25) compounds.

---

<b>5565</b>	<b>Pr<sub>14</sub>Ni<sub>6</sub>Si<sub>11</sub></b>	mC124	$a = 33.991$	HoKP, 83
	or	C2/m	$b = 4.2328$	
	Pr <sub>14</sub> Ni <sub>6</sub> <sup>[6, p]</sup> Si <sub>11</sub> <sup>[6, p]</sup>		$c = 21.330$	
			$\beta = 113.72^\circ$	

---

No isotypic R<sub>14</sub>T<sub>6</sub>M<sub>11</sub> compounds are known.

The structure of Pr<sub>14</sub>Ni<sub>6</sub>Si<sub>11</sub>, shown in fig. 10, is characterized by Ni or Si centred trigonal rare earth prisms. The 55(53):Ce<sub>14</sub>(Ni<sub>4.7</sub>Si<sub>5.3</sub>)<sub>17</sub> structure as seen in fig. 10 is a stacking variant of the Pr<sub>14</sub>Ni<sub>6</sub>Si<sub>11</sub> structure. Both structures belong to the R<sub>6</sub>(T, M)<sub>LC</sub> structural family which is discussed with the 50(25) compounds.

---

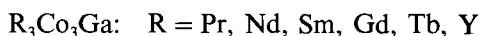
<b>5725</b>	<b>Y<sub>3</sub>Co<sub>3</sub>Ga</b>	oC28	$a = 4.098$	YaGG, 78
	or	Cmcm	$b = 10.11$	
	Y <sub>3</sub> ⊃[Co <sub>2</sub> <sup>[4, 2p]</sup> Co <sup>[6, p]</sup> ]Ga		$c = 13.01$	

---

Related to W<sub>3</sub>CoB<sub>3</sub>-type (JeBN, 69) with interchange of T and M atoms!

---

Isotypic compounds: All references YaGG, 78



According to Yarmolyuk, Grin' and Gladyshevskii (1978) the Y<sub>3</sub>Co<sub>3</sub>Ga structure can be considered as an intergrowth of 6033:Pr<sub>2</sub>Ni<sub>2</sub>Al and CrB-type segments as

shown in fig. 11. If the  $\text{Pr}_2\text{Ni}_2\text{Al}$  and the CrB structures are sliced into slabs as indicated by the dashed lines, the  $\text{Y}_3\text{Co}_3\text{Ga}$  can be described as a periodic stacking of two kinds of slabs,



Each Co atom in the  $\text{Y}_2\text{Co}_2\text{Ga}$  slab is in the centre of a trigonal prism of type  $\text{Y}_4\text{Ga}_2$  and forms bonds with the Co atom in the centre of a trigonal rare earth prism of the CrB slab. The crystal chemical formula for  $\text{Y}_3\text{Co}_3\text{Ga}$  is therefore  $\text{Y}_{3\frac{1}{2}}[\text{Co}_2^{[4, 2]p}\text{Co}^{[6, p]}]\text{Ga}$ .

We note that the three structure types which we correlated here are also found in transition metal borides not containing rare earth elements. In this case, the rare earth elements (R) are replaced by earlier transition elements (T'), the late transition elements (T) by boron atoms, and the main group elements (M) by late transition elements (T). The formulae of these compounds are compared in table 5.

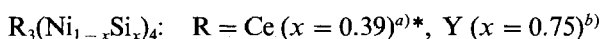
TABLE 5  
R-T-M and RT compounds compared with isotypic T'-T-B and T'B compounds having the atom arrangement of the  $\text{W}_2\text{CoB}_2$ ,  $\text{W}_3\text{CoB}_3$  and CrB structure types.

Structure type	Pearson's classif. symbol	Space group	R-T-M and RT	T'-T-B and T'B
$\text{W}_2\text{CoB}_2$	oI10	Immm	6033: $\text{R}_2\text{T}_2\text{M}$ $\text{Pr}_2\text{Ni}_2\text{Al}$	$\text{T}'_2\text{TB}_2$ $\text{W}_2\text{CoB}_2$
$\text{W}_3\text{CoB}_3$	oC28	Cmcm	5725: $\text{R}_3\text{T}_3\text{M}$ $\text{Y}_3\text{Co}_3\text{Ga}$	$\text{T}'_3\text{TB}_3$ $\text{W}_3\text{CoB}_3$
CrB	oC8	Cmcm	5000: RT PrNi	T'B WB, h.t.

57(75)	$\text{Y}_3\text{NiSi}_3$ or $\text{Y}_3(\text{Ni}_{1.5}\text{Si}_{1.5})_2^{[6, p]}\text{Si}_2^{[6, p]}$	oI14 Immm	$a = 3.9605$ $b = 4.125$ $c = 17.63$	KIP, 82b
--------	--	--------------	--	----------

$\text{Ba}_3\text{Al}_2\text{Ge}_2$ -type (WiEST, 76) with partial disorder  $\equiv \text{Ta}_3\text{B}_4$ -type (Ki, 49) derivative

Isotypic compounds:



\*From its space group and cell parameters, the Ce compound probably belongs to the  $\text{Y}_3\text{NiSi}_3$ -type.

<sup>a</sup>Mi, 73    <sup>b</sup>KIP, 82b

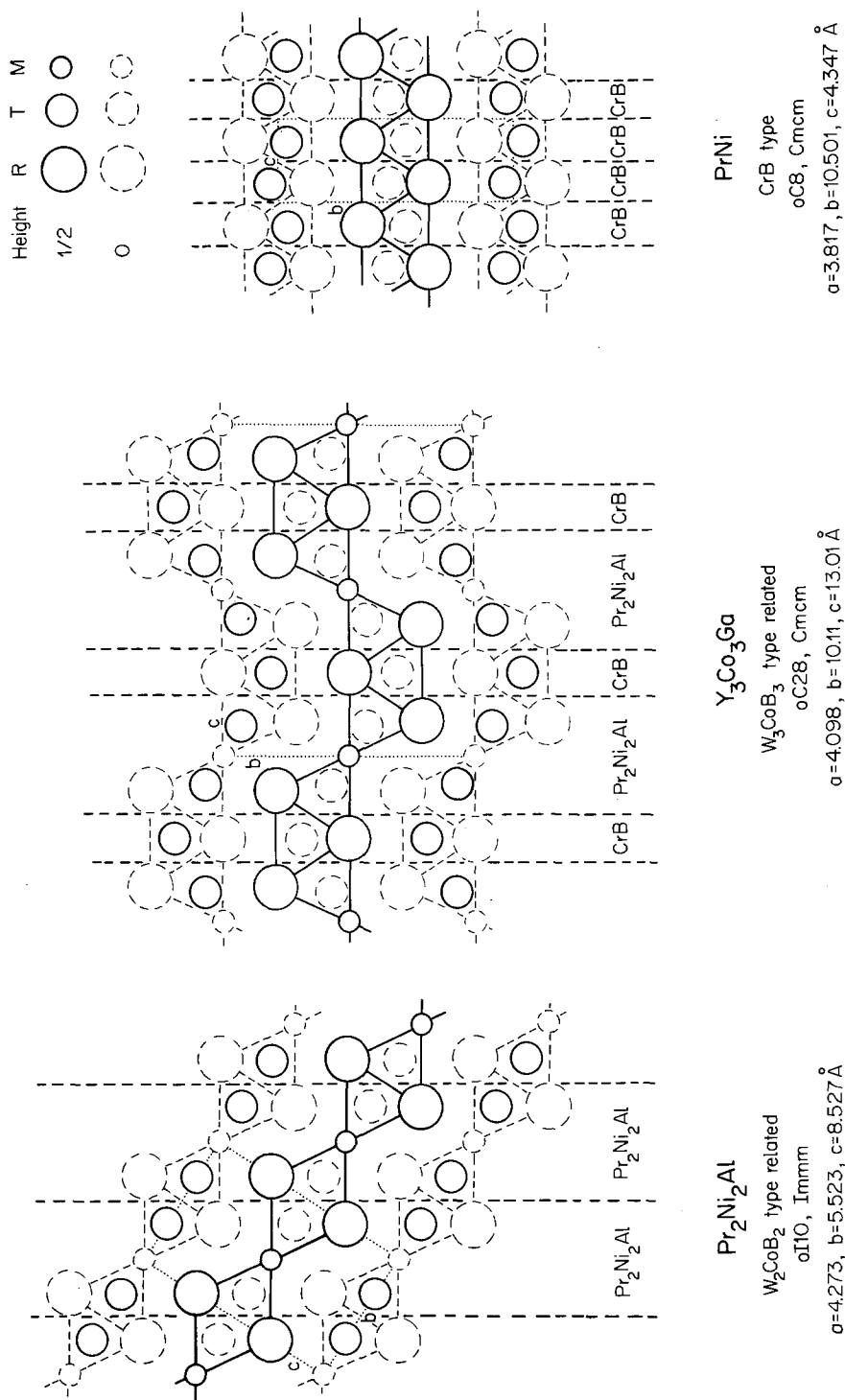


Fig. 11. The Y<sub>3</sub>Co<sub>3</sub>Ga structure type interpreted as intergrowth of Pr<sub>2</sub>Ni<sub>2</sub>Al and CrB structure type segments.

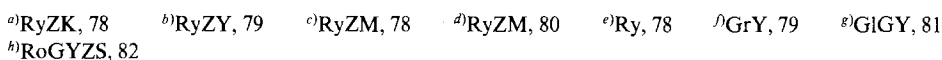
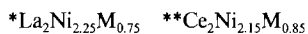
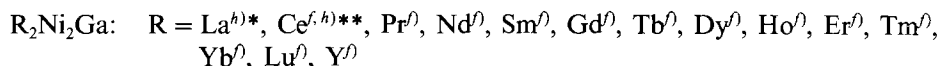
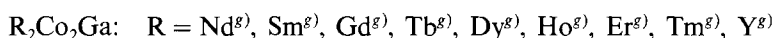
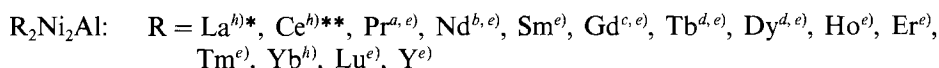
The  $Y_3NiSi_3$  structure, shown in fig. 8, belongs to the  $R_6(T, M)_{LC}$  family built up only of centred rare earth prisms. This structural family is discussed with the 50(25) compounds.

Two different structure types are found with composition 6033: the  $Pr_2Ni_2Al$ - and the  $Er_2Pd_2Si$ -types.

6033	$Pr_2Ni_2Al$	oI10	$a = 4.273$	RyZK, 78
	or	Immm	$b = 5.523$	Ry, 78
	$Pr_{2\frac{1}{2}}[Ni_{\frac{1}{2}}^{(4,2)p}]Al$		$c = 8.527$	

Related to  $W_2CoB_2$ -type (RiNB, 66) or  $Mo_2NiB_2$ -type (KuKS, 66) with interchange of T and M atoms!

Isotypic compounds:

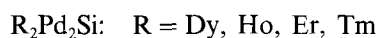


The  $Pr_2Ni_2Al$  structure is shown in figs. 11 and 18. Each Ni atom is in the centre of a trigonal prism formed of four Pr and two Al atoms and it forms a Ni–Ni dumbbell with the Ni atom of a face-joined trigonal prism.

Intergrowth of  $Pr_2Ni_2Al$  slabs with CrB-type slabs leads to the 5725:Y<sub>3</sub>Co<sub>3</sub>Ga structure and intergrowth with ThCr<sub>2</sub>Si<sub>2</sub>-type slabs to the 6733:La<sub>3</sub>Ni<sub>4</sub>Ga<sub>2</sub> structure.

60(33)	$Er_2Pd_2Si$	oP20	$a = 7.391$	KIHP, 83
	or	Pnnm	$b = 13.724$	
	$Er_2Pd^{[6,p]} \text{ } \textcircled{2} (Pd_{.5}Si_{.5})_2^{[+3]}$		$c = 4.281$	

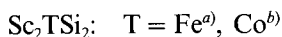
Isotypic compounds: All references KIHP, 83



The  $\text{Er}_2\text{Pd}_2\text{Si}$  structure can be considered as a periodic intergrowth of RTM and RT structure segments, as seen in fig. 12. The RTM segments correspond to the  $\text{CeCu}_2$ -type, discussed with the  $67(50):\text{Pr}(\text{Pt}_5\text{Ge}_5)_2$  compound, while the RT segments correspond to the atom arrangement of the MnP (B31)-type. The structure of the  $\text{ErPdSi}$  compound has not yet been studied; however,  $\text{Er}(\text{Pd}_5\text{Ge}_5)_2$  crystallizes with the  $\text{CeCu}_2$ -type. No rare earth compounds with MnP type are known.

6067	$\text{Sc}_2\text{CoSi}_2$	mC20	$a = 9.74$	GIK, 78
	or	C2/m	$b = 3.954$	
	$\text{Sc}_4\text{Co}_2\text{Si}_2^{\frac{1}{2}} [\text{Si}_2^{6, \text{pl}}]$		$c = 9.39$	
			$\beta = 118.27^\circ$	

Isotypic compounds:



<sup>a</sup>ChEP, 83    <sup>b</sup>GIK, 78

The  $\text{Sc}_2\text{CoSi}_2$  structure, the  $6360:\text{Sc}_3\text{Co}_2\text{Si}_3$  structure with  $\text{Hf}_3\text{Ni}_2\text{Si}_3$ -type and the  $6750:\text{ScCoSi}$  structure with TiNiSi-type, are members of the structural series  $\text{R}_{2+n}\text{T}_2\text{M}_2^{\frac{1}{2}} [\text{M}_n^{6, \text{pl}}]$  with  $n = 2, 1$  and  $0$ , respectively. Drawings of these three structures are presented in fig. 13. To this series belongs also, with  $n = \infty$ , the CrB-type shown in fig. 11 and reported for ScSi. The structural data for the members of this series are listed in table 6. Their compositions are located in the ternary diagram on the line between RTM and RM and correspondingly their structures can be considered as an intergrowth of RTM and RM structure elements as was noted first by Gladyshevskii and Kotur (1978).

TABLE 6  
Structural data for the  $\text{R}_{2+n}\text{T}_2\text{M}_2^{\frac{1}{2}} [\text{M}_n^{6, \text{pl}}]$  structural series.

$n$	Code	Composition	Structure type	Pearson's classif. symbol	Space group
0	6750	$\text{R}_2\text{T}_2\text{M}_2 \equiv \text{RTM}$	TiNiSi	oP12	Pnma
1	6360	$\text{R}_3\text{T}_2\text{M}_2\text{M}^{6, \text{pl}} \equiv \text{R}_3\text{T}_2\text{M}_3$	$\text{Hf}_3\text{Ni}_2\text{Si}_3$	oC32	Cmcm
2	6067	$\text{R}_4\text{T}_2\text{M}_2^{\frac{1}{2}} \text{M}_2^{6, \text{pl}} \equiv \text{R}_2\text{TM}_2$	$\text{Sc}_2\text{CoSi}_2$	mC20	C2/m
$\infty$	50100	$\text{R} \text{ } \infty \text{ } \text{M}^{6, \text{pl}} \equiv \text{RM}$	CrB	oC8	Cmcm

The members of this series belong to the general structural family which contains M-centred trigonal prisms with parallel trigonal axes. Whereas in the structural series

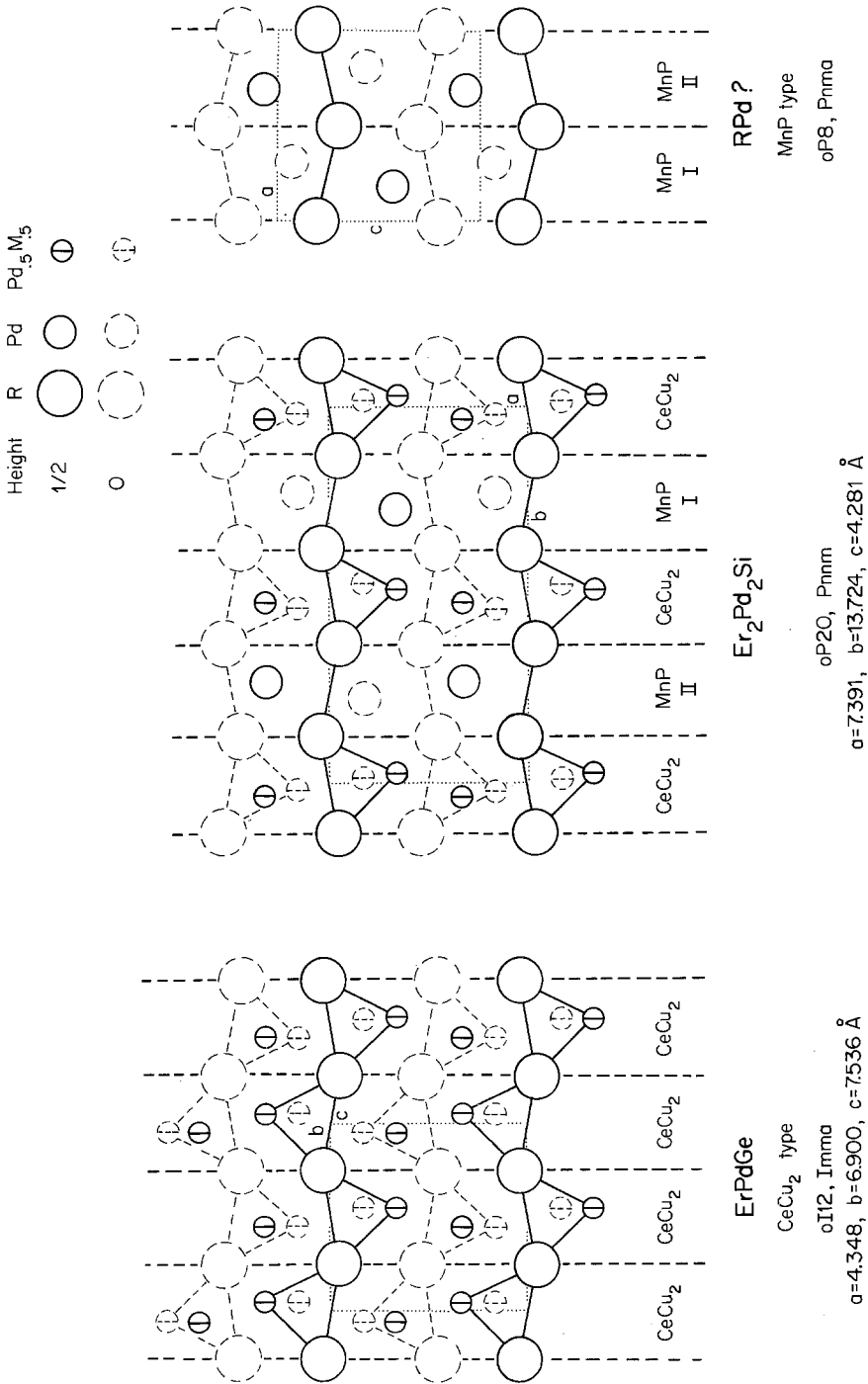
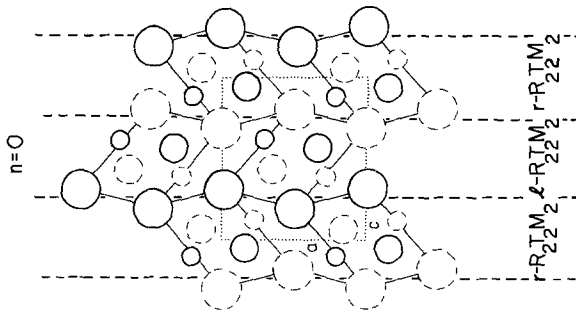
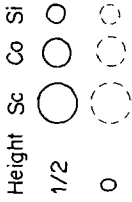


Fig. 12. The structure of Er<sub>2</sub>Pd<sub>2</sub>Si interpreted as periodic intergrowth of CeCu<sub>2</sub>- and MnP-type slabs.

$R_{2+n}T_2M_2\Delta[M_n^{(sp)}]$  structure series

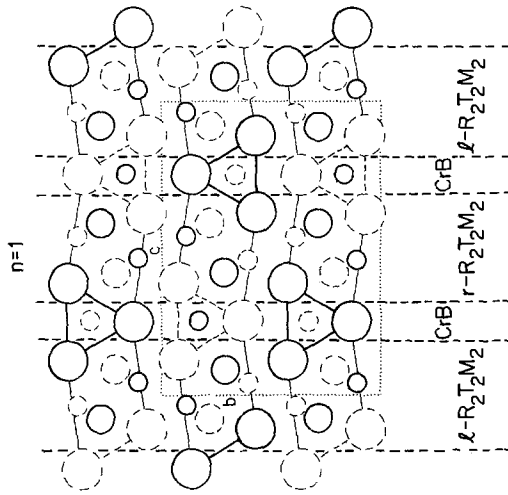


ScCoSi

TINISI type

$OP12$ ,  $Pnma$

$a=6.419$ ,  $b=3.953$ ,  $c=6.896 \text{ \AA}$

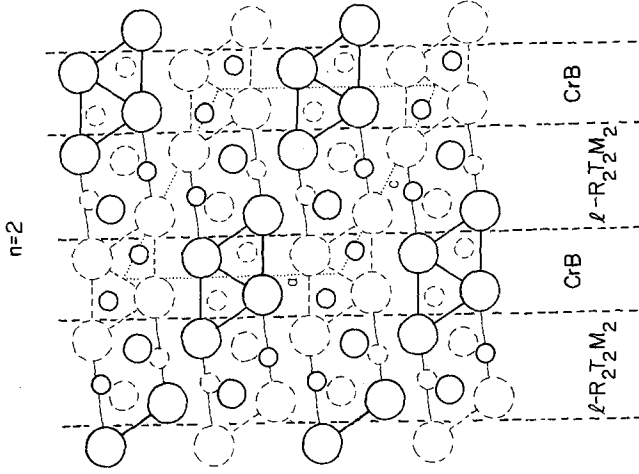


$Sc_3Co_2Si_3$

$Hf_3Ni_2Si_3$  type

$OC32$ ,  $Cmcm$

$a=3.996$ ,  $b=9.815$ ,  $c=12.67 \text{ \AA}$



$Sc_2CoSi_2$

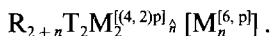
$Sc_2CoSi_2$  type

$mC20$ ,  $C2/m$

$a=9.74$ ,  $b=3.954$ ,  $c=9.39 \text{ \AA}$ ,  $\beta=118.27^\circ$

Fig. 13. Members of the structural series  $R_{2+n}T_2M_2\Delta[M_n^{(sp)}]$  with  $n = 0, 1$  and  $2$ , respectively. For the reservations regarding the link of the structure with  $n = 0$  to the other two structures, see text.

discussed under 45(60) *all* M atoms are at the centres of rare earth trigonal prisms, this is no longer true for the members of the structural series under discussion here. Some of the M atoms—or in case of TiNiSi all M atoms—are at the centres of  $R_4T_2$  prisms. Gladyshevskii and Kotur (1978) have pointed out that, going through the series  $ScCoSi \rightarrow Sc_3Co_2Si_3 \rightarrow Sc_2CoSi_2 \rightarrow ScSi$ , the ratio R/M remains constant, but the decrease in the number of T atoms leads to a decrease and eventual disappearance of the  $MR_4T_2$  prisms and their replacement by  $MR_6$  prisms. The crystal-chemical formula of this series can therefore be written as



To allow a comparison with other structure types, as for example the 7567:ScRhSi<sub>2</sub>, the 7567:YNiAl<sub>2</sub> and the 7350:Sc<sub>3</sub>Ni<sub>4</sub>Ge<sub>4</sub> structures, we place the emphasis of our description here on larger structural units which form infinite columns, rather than on the  $R_4T_2$  trigonal prisms. In fig. 13 the structures have been divided by dashed lines into different kinds of slabs. The parameter  $n$  of the formula for the series indicates the number of CrB-type slabs which are placed between slabs built up of TiNiSi structural elements or, expressed differently, the parameter  $n$  simply corresponds to the number of M-centred face-joined trigonal rare earth prism columns, which are to be found between the other slabs. A closer study of the TiNiSi structure itself reveals the presence of two kinds of enantiomorphic building columns of composition  $R_{4(-2)}T_2M_2$ , labelled  $\ell$  (left) and  $r$  (right), parallel to the  $b$  axis. They are shown in fig. 14 in a projection along their column axis. These columns will be found in a great number of other structures to be discussed later. Since the rare earth atoms at the corners participate in other columns or prisms, the composition of the columns in the TiNiSi structure and other structures of the structure series is  $R_{4-2}T_2M_2$ . The dashed lines in TiNiSi separate slabs which are built up of one kind of column only, but the complete structure is an intergrowth of slabs of  $\ell$ -type columns and slabs of  $r$ -type columns. The Hf<sub>3</sub>Ni<sub>2</sub>Si<sub>3</sub> and Sc<sub>2</sub>CoSi<sub>2</sub> structure types are built up of CrB slabs which alternate with slabs constructed of  $R_{4-2}T_2M_2$  columns of one kind only. These slabs correspond to a segment of a ThCr<sub>2</sub>Si<sub>2</sub>-type structure as can be seen by comparison with the structure of PrNi<sub>2</sub>Si<sub>2</sub>, shown in fig. 18. In Hf<sub>3</sub>Ni<sub>2</sub>Si<sub>3</sub> and Sc<sub>2</sub>CoSi<sub>2</sub> the dispositions of the columns in a  $R_2T_2M_2$  slab, with respect to each other, is different from that observed for the TiNiSi-type. In the segments

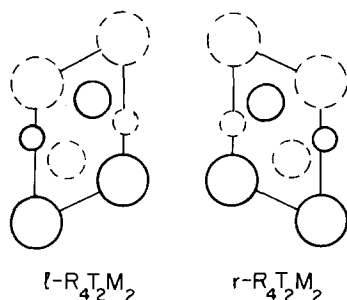


Fig. 14. The two kinds of characteristic columns of composition  $R_4T_2M_2$ .



of the latter type some of the columns have been displaced by one half in height and in a strict sense the TiNiSi-type cannot be linked to the other two structures in the form of a structure series. However, the surrounding of the T elements by the R, T and M elements remains the same in the three structure types. In first approximation, the coordination polyhedron of the T element is a deformed tetrahedron of four M elements. We shall see later that the same surrounding (R, T and M elements) is found around the T element in the  $Gd_3Cu_4Ge_4$ -type (7350:Sc<sub>3</sub>Ni<sub>4</sub>Ge<sub>4</sub>, see fig. 29).\*

Two different structure types are found with composition 6360: the Sc<sub>3</sub>Co<sub>2</sub>Si<sub>3</sub>- and Sc<sub>3</sub>Re<sub>2</sub>Si<sub>3</sub>-types.

6360	Sc <sub>3</sub> Co <sub>2</sub> Si <sub>3</sub>	oC32	$a = 3.996$	GIK, 78
	or	Cmcm*	$b = 9.815$	
	Sc <sub>3</sub> Co <sub>2</sub> Si <sub>2</sub> Si <sup>[6, p]</sup>		$c = 12.67$	

Hf<sub>3</sub>Ni<sub>2</sub>Si<sub>3</sub>-type (YaGG, 77)

\*For isotypic T<sub>3</sub>T<sub>2</sub>Si<sub>3</sub> compounds a reduction of symmetry from Cmcm to Pnma is probable according to YaGG, 77.

Isotypic compounds:

Sc<sub>3</sub>T<sub>2</sub>Si<sub>3</sub>: T = Fe<sup>a)</sup>, Co<sup>b)</sup>

Y<sub>3</sub>T<sub>2</sub>Si<sub>3</sub>: T = Rh<sup>c)</sup>, Pd<sup>c)</sup>

<sup>a)</sup>ChEP, 83    <sup>b)</sup>GIK, 78    <sup>c)</sup>PaLM, 82

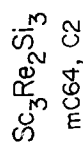
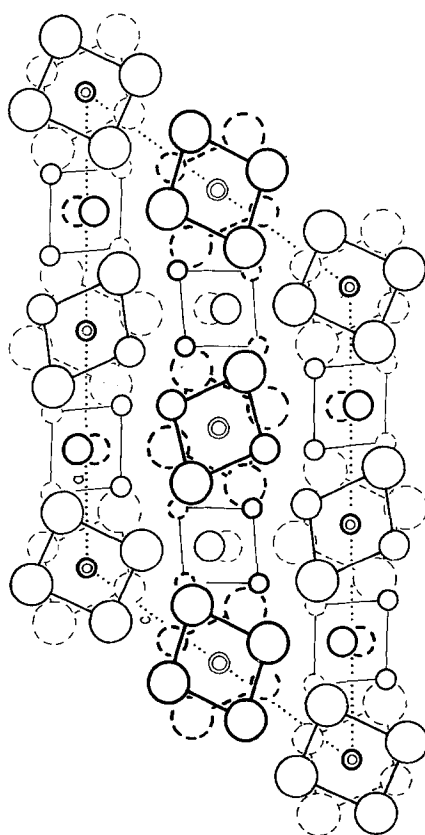
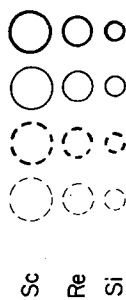
The Sc<sub>3</sub>Co<sub>2</sub>Si<sub>3</sub> structure with Hf<sub>3</sub>Ni<sub>2</sub>Si<sub>3</sub>-type shown in fig. 13, is a member of the R<sub>2+n</sub>T<sub>2</sub>M<sub>2</sub>[M<sub>n</sub><sup>[6, p]</sup>] structural series with  $n = 1$ . This series is discussed with the 6067:Sc<sub>2</sub>CoSi<sub>2</sub> structure.

6360	Sc <sub>3</sub> Re <sub>2</sub> Si <sub>3</sub>	mC64	$a = 19.604$	PeBG, 79
	or	C2	$b = 5.339$	
	Sc <sub>3</sub> Re <sub>2</sub> Si <sub>2</sub> Si <sup>[(6, 2)a]</sup>		$c = 13.741$	
			$\beta = 125.92^\circ$	

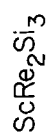
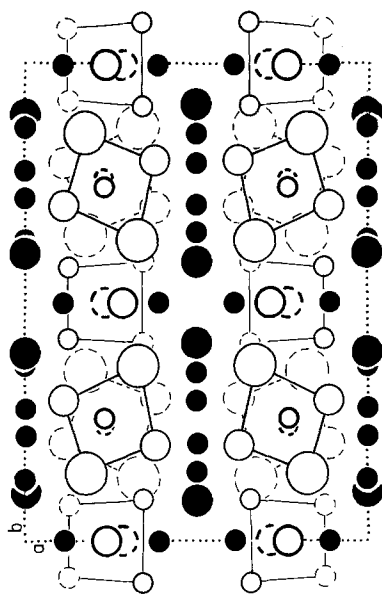
No isotypic R<sub>3</sub>T<sub>2</sub>M<sub>3</sub> compounds are known.

\*The deformed TM<sub>4</sub> tetrahedra are also found in the PbFCl-type (6750:CeFeSi) and in the ZrNiAl-type (6750:ScRuGe), as will be discussed with the TiNiSi-type (6750:ScRhSi).

Height 0 1/4 3/4 1/4+3/4 0+1/2 not indicated



$a=19.604$ ,  $b=5.339$ ,  $c=13.741$  Å,  $\beta=125.92^\circ$



oC96, Amm2

$a=14.486$ ,  $b=19.689$ ,  $c=5.2397$  Å

Fig. 15. Sc-Re silicides with columns of Si-centred antiprisms. For simplicity the height of the atoms in the extra layer in  $\text{ScRe}_2\text{Si}_3$ , indicated with filled circles, has been omitted.

The  $\text{Sc}_3\text{Re}_2\text{Si}_3$  structure together with that of 8360: $\text{ScRe}_2\text{Si}_3$  is shown in fig. 15. The common structural features are the occurrence of two types of infinite columns (perpendicular to the plane of projection) formed of

- Si-centred face-joined antiprisms built up of Sc and Re atoms,
- strongly deformed trigonal prisms of Si atoms with Re atoms in off-centre positions.

In  $\text{Sc}_3\text{Re}_2\text{Si}_3$  the antiprisms consist of six Sc and two Re, whereas in  $\text{ScRe}_2\text{Si}_3$  they consist of four Sc and four Re. In the second structure an extra layer of Re and Si atoms is found between the columns.

For a discussion of other structures with infinite columns of M-centred antiprisms, see 7567: $\text{ScFeSi}_2$ .

With compositions 67. . are found:

- ternary hexagonal Laves phases either ordered [6725: $\text{Sc}_2\text{Co}_3\text{Si}$ , hP12 and 6775: $\text{Sc}_2\text{RuAl}_3$ , hP12] or disordered [67(50): $\text{Sc}(\text{Ni}_{.5}\text{Al}_{.5})_2$ , hP12];
- 6733: $\text{La}_3\text{Ni}_4\text{Ga}_2$ -type, mC18;
- PbFCl-type, tP6 [see 6750: $\text{CeFeSi}$ ];
- ordered ZrNiAl-type, hP9 or disordered  $\text{Fe}_2\text{P}$ -type [see 6750: $\text{ScRuGe}$ ];
- ordered TiNiSi-type, oP12 [see 6750: $\text{ScRhSi}$ ] or disordered  $\text{CeCu}_2$ -type, oI12 [see 67(50): $\text{Pr}(\text{Pt}_{.5}\text{Ge}_{.5})_2$ ];
- ordered LaPtSi-type, tI12 or disordered  $\text{ThSi}_2$ -type [see 6750: $\text{LaPtSi}$ ];
- ordered ZrOS-type, cP12 [see 6750: $\text{LaIrSi}$ ];
- the TiFeSi-type, oI36 [see 6750: $\text{YMnGa}$ ];
- disordered  $\text{AlB}_2$ -type, hP3 [see 67(75): $\text{Ce}(\text{Ni}_{.25}\text{Si}_{.75})_2$ ];
- disordered  $\text{ZrSi}_2$ -type, oC12 [see 67(88): $\text{Sc}(\text{Co}_{.125}\text{Si}_{.875})_2$ ];
- disordered  $\text{CaIn}_2$ -type, hP6 [see 67(83): $\text{Sm}(\text{Mn}_{.17}\text{Ga}_{.83})_2$ ].

Several of these different structures may occur in one pseudobinary  $\text{RT}_2\text{-RM}_2$  system with different T/M ratio. See for example the results of Mayer and Felner (1973a) for the  $\text{RNi}_{2-x}\text{Si}_x$  systems. For a discussion of the structure type changes of equiatomic compounds with an increase of (a) the atomic number of the rare earth element, (b) the group number of the transition element, (c) the period of the transition element, (d) the group number of the M element, and (e) the period of the M element, the paper by Hovestreydt et al. (HoEKCP, 82) should be studied.

---

<b>6725</b>	<b><math>\text{Sc}_2\text{Co}_3\text{Si}</math></b>	hP12	$a = 4.95^*$	Ko, 77
		$\text{P6}_3/\text{mmc}$	$c = 7.90$	

---

$\text{Mg}_2\text{Cu}_3\text{Si}$ -type (Wi, 39)  $\equiv$   $\text{MgZn}_2$  (Laves phase)-type derivative

---

\*Cell parameters estimated from a diagram.

Isotypic compounds: All references Ko, 77

$\text{Sc}_2\text{T}_3\text{Si}$ : T = Fe, Co, Ni

Laves phases of the  $MgZn_2$  (C14)- and  $MgCu_2$  (C15)-types are found in many binary  $RT_2$  compounds and in certain cases their homogeneity ranges extend far into the ternary phase diagram. These results are beyond the scope of this paper. Only truly ternary phases should be mentioned here. Two kinds have to be distinguished:

(a) Laves phases with a random distribution of T and M atoms on the Zn or Cu sites having structures not found in the binary  $RT_2$  or  $RM_2$  compounds. These phases are listed with the 67(50): $Sc(Ni_5Al_5)_2$  compound.

(b) Laves phases with an ordered arrangement of T and M atoms.

The general possibility for complete ordering with ternary Laves phase structure has been studied by Teslyuk (1969). The crystallographic data for four ordered structure types, two derived from the  $MgZn_2$ - and two from the  $MgCu_2$ -type, are given in table 7.\* The arrangement of the atoms in and close to both sides of the  $(11\bar{2}0)$  plane of the hexagonal or triple hexagonal cells for these four ternary ordered Laves phase structure types is shown in fig. 16. The ternary ordered Laves phases in the R-T-M systems can thus be grouped into two categories:

b<sub>1</sub>) Laves phases derivatives (with code 67. .) where the A sites are fully occupied by rare earth atoms only and where the T and M atoms are distributed in an orderly fashion on the B sites.

Only a  $MgZn_2$ -type derivative is known. The  $Mg_2Cu_3Si$ -type (Wi, 39) occurs, however, with two compositions:  $R_2T_3M$  and  $R_2TM_3$ . Examples of the first can be found with the 6725: $Sc_2Co_3Si$  compound and of the latter with the 6775: $Sc_2RuAl_3$  compound. The structure of  $Sc_2Co_3Si$  is shown in the left hand part of fig. 17.  $Sc_2RuAl_3$  has the same structure but with T and M atoms interchanged.

\*For the notation of the structure types we follow Teslyuk here, but in the case of  $Mn_2Cu_3Al$  and  $MnInCu_4$  there is no complete proof that these compounds really have an ordered Laves phase structure. In the case of  $Mn_2Cu_3Al$ , there exists an independent investigation according to which Cu and Al are not ordered and the real structure is therefore cubic (JoH, 68).

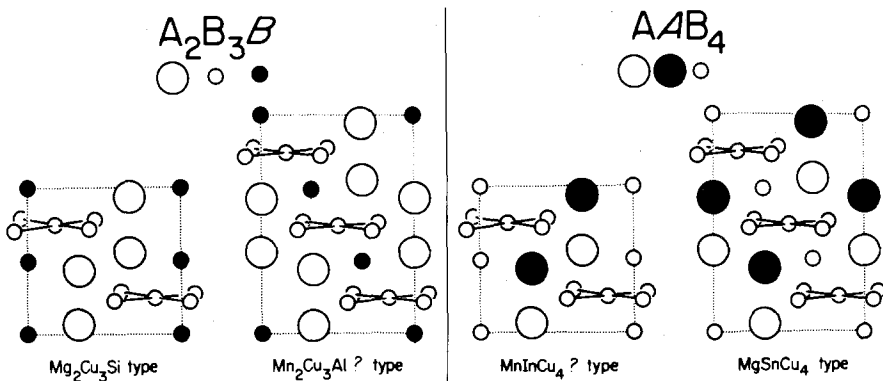


Fig. 16. The four ternary ordered Laves phase structure types showing the atom arrangement in or close to each side of the  $(11\bar{2}0)$  plane of the hexagonal or triple hexagonal cells. Of the atoms positioned away from the  $(11\bar{2}0)$  plane only B atoms are indicated which form a triangle with a B atom in the  $(11\bar{2}0)$  plane with the same  $z$  value.

TABLE 7

Crystallographic data for the  $\text{MgZn}_2$  and  $\text{MgCu}_2$  structure types and four ternary derivative types, after Teslyuk (1969). In the case of the  $\text{Mn}_2\text{Cu}_3\text{Al}$ - and  $\text{MnInCu}_4$ -types the experimental verification is incomplete.

$\text{AB}_2$	<u><math>\text{MgZn}_2</math>-type</u>	<u><math>\text{MgCu}_2</math>-type</u>
	$\text{hP12, P6}_3/\text{mmc}$	$\text{cF24, Fd}3\text{m}$ (origin away from symmetry centre)
	$c/a \approx 2\sqrt{2}/\sqrt{3}$	$(c/a = 3\sqrt{2}/\sqrt{3})$
	A in 4f) $z \approx 9/16$ B in 6h) $x \approx 1/6$ B in 2a)	A in 8a) B in 16a)
$\text{A}_2\text{B}_3\text{B}$	<u><math>\text{Mg}_2\text{Cu}_3\text{Si}</math>-type</u>	<u><math>\text{Mn}_2\text{Cu}_3\text{Al}^?</math>-type</u>
	$\text{hP12, P6}_3/\text{mmc}$	$\text{hR18, R}3\text{m}$
	$c/a \approx 2\sqrt{2}/\sqrt{3}$	$c/a \approx 3\sqrt{2}/\sqrt{3}$
	A in 4f) $z \approx 9/16$ B in 6h) $x \approx 1/6$ B in 2a)	A in 6c) $z \approx 5/8$ B in 9d) B in 3a)
$\text{AAB}_4$	<u><math>\text{MnInCu}_4</math>?-type</u>	<u><math>\text{MgSnCu}_4</math>-type*</u>
	$\text{hP12, P6}_3/\text{mc}$	$\text{cF24, F}43\text{m}$
	$c/a \approx 2\sqrt{2}/\sqrt{3}$	$(c/a = 3\sqrt{2}/\sqrt{3})$
	A in 2b) $z \approx 9/16$ A in 2b) $z \approx 15/16$ B in 6c) $x \approx 1/6$ B in 2a)	A in 4a) A in 4c) B in 16e) $x \approx 5/8$

\*Corresponds to a  $\text{AuBe}_3$ -type derivative (Mi, 35).

b<sub>2</sub>) Phases where the A sites are occupied by R and M atoms in an orderly fashion and with the T atoms only on the B sites.

Only a  $\text{MgCu}_2$ -type derivative is known. The  $\text{MgSnCu}_4$ -type (GlKT, 52), shown in the right hand part of fig. 17 is found with 8320:R $\text{Ni}_4\text{Au}$  compounds, where R = Gd, Tb, Dy, Ho, Er, Tm, Yb, Lu, Y and Sc (Dw, 75). However, since no compounds are known where the M element is from the boron or silicon group these compounds shall not be discussed further.

6733	$\text{La}_3\text{Ni}_4\text{Ga}_2$	$\text{mC18}$	$a = 10.273$	GrY, 80
	or	$\text{C2/m}$	$b = 4.225$	
	$\text{La}_3\text{Ni}_2^{\ddagger} [\text{Ni}_2^{(4, 2p)}]\text{Ga}_2$		$c = 8.357$	
			$\beta = 99.32^\circ$	

Isotypic compounds: All references GrY, 80

$\text{R}_3\text{Ni}_4\text{Ga}_2$ : R = La, Pr

## Ternary ordered Laves phase structures

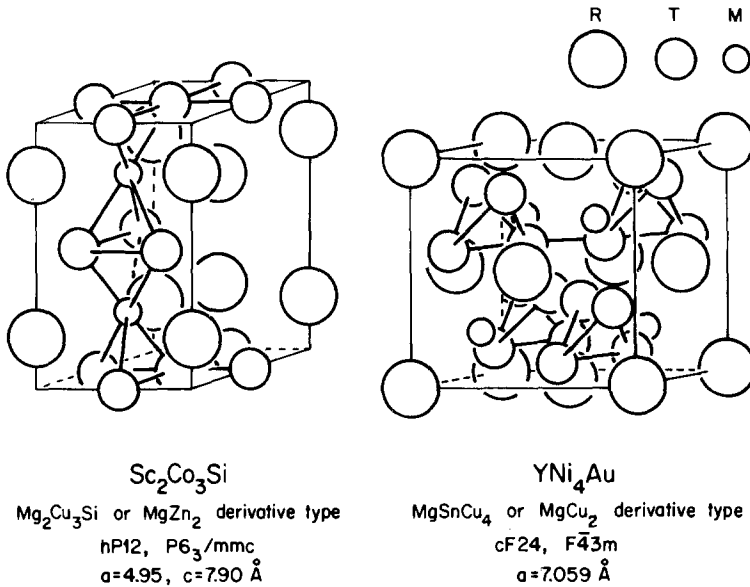


Fig. 17. Ternary ordered Laves phase structures.

The  $\text{La}_3\text{Ni}_4\text{Ga}_2$ -type can be considered as an intergrowth of  $6033:\text{Pr}_2\text{Ni}_2\text{Al}$  and  $8050:\text{ThCr}_2\text{Si}_2$  structural segments as shown in fig. 18. If the  $\text{Pr}_2\text{Ni}_2\text{Al}$  and the  $\text{ThCr}_2\text{Si}_2$  structures are sliced into slabs as indicated by the dashed lines, the  $\text{La}_3\text{Ni}_4\text{Ga}_2$  structure type can be described as a periodic stacking of two kinds of slabs:



Each Ni atom in  $\text{Pr}_2\text{Ni}_2\text{Al}$  and in the corresponding  $\text{La}_2\text{Ni}_2\text{Ga}$  slab is in the centre of a trigonal prism of type  $\text{R}_4\text{M}_2$  and forms Ni–Ni dumbbells with the Ni atoms of a similar (rectangular face-)joined trigonal prism. The crystal-chemical formula for  $\text{La}_3\text{Ni}_4\text{Ga}_2$  is therefore  $\text{La}_3\text{Ni}_2^{1/2} [\text{Ni}_2^{(4,2)\text{p}}] \text{Ga}_2$ .

6750	$\text{CeFeSi}$	tP6	$a = 4.062$	BoGK, 70
	or $\text{CeFe}^{[4\text{t}]} \text{Si}$	P4/nmm	$c = 6.752$	

PbFCl-type (ClFPb)  $\equiv$   $\text{Fe}_2\text{As}$ -type (FeFeAs) derivative

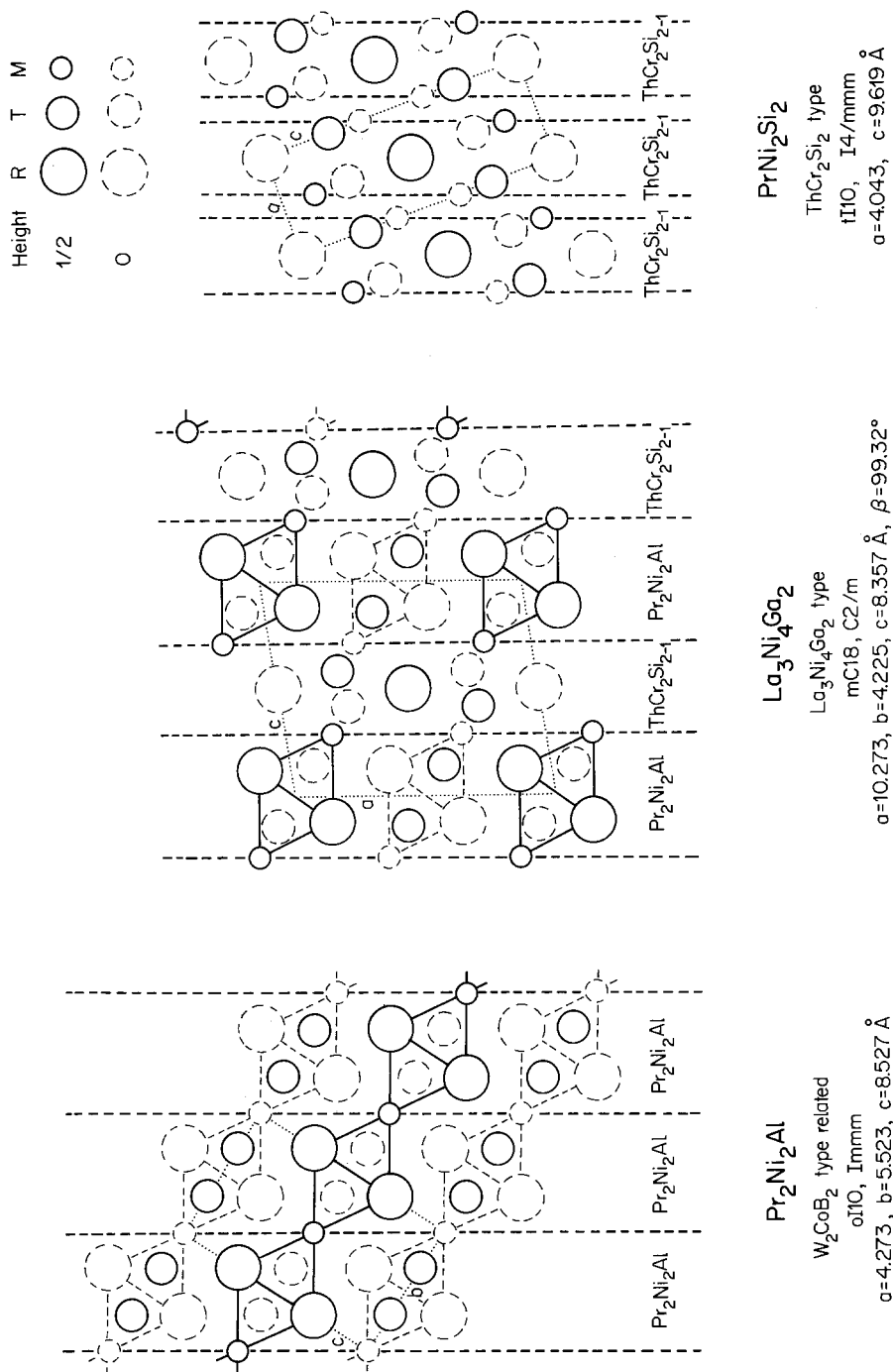


Fig. 18. The La<sub>3</sub>Ni<sub>4</sub>Ga<sub>2</sub> structure type interpreted as intergrowth of Pr<sub>2</sub>Ni<sub>2</sub>Al and ThCr<sub>2</sub>Si<sub>2</sub> structure type segments.

## Isotypic compounds:

RMnSi: R = La<sup>a,e</sup>, Ce<sup>a</sup>, Pr<sup>a</sup>, Nd<sup>a</sup>, Sm<sup>a</sup>, Gd<sup>e,f</sup>, Y<sup>e\*</sup>,

RFeSi: R = La<sup>b</sup>, Ce<sup>b</sup>, Pr<sup>b</sup>, Nd<sup>b</sup>\*\* , Sm<sup>b</sup>, Gd<sup>b,c</sup>, Tb<sup>b</sup>, Dy<sup>b</sup>, Ho<sup>b</sup>, Yb<sup>b</sup>, Y<sup>c</sup>

RCoSi: R = La<sup>b</sup>, Ce<sup>b</sup>, Pr<sup>b</sup>, Nd<sup>b,d</sup>, Sm<sup>b</sup>, Gd<sup>f</sup>

\*YMnSi also crystallizes with the TiNiSi-type (see 6750:ScRhSi).

\*\*According to MaF, 73a, the NdFeSi compound crystallizes in the TiNiSi structure type, but it should be noted that the cell parameters indicated in that paper are incompatible with this type of structure.

<sup>a</sup>KnMB, 77    <sup>b</sup>BoGK, 70    <sup>c</sup>BoGYDI, 78    <sup>d</sup>MaF, 73a    <sup>e</sup>Jo, 76    <sup>f</sup>KiSK, 82

The structure of CeFeSi is shown in fig. 19. There is a one-to-one site correspondence between the elements in CeFeSi and in PbFCl and Fe<sub>2</sub>As if the latter two are arranged as given in the formulae enclosed by round brackets in the lower part of the structure type heading. A discussion of the PbFCl-type and its different branches has been given recently by Hovestreydt et al. (HoEKCP, 82). The PbFCl structure may be considered as being built up of sheets perpendicular to the *c* direction, that is, one sheet per *c* translation period. As a general rule the two kinds of atoms which have only weak or no interaction will occupy the F and Cl sites with the larger one usually at the edges of the sheet. The CeFeSi-type is found with those RTM compounds where, according to Miedema's theory (see introduction), no or only weak R-T interactions occur. In agreement with what has been said above, each sheet consists of five layers with the sequence R-M-T<sub>2</sub>-M-R, the middle layer having a twice as high atom occupation. The sheets of the CeFeSi structure correspond to segments of the ThCr<sub>2</sub>Si<sub>2</sub> structure. This can be seen particularly well by a comparison of figs. 19 and 30. For a description of the CeFeSi structure as an intergrowth of BaAl<sub>4</sub> and W-type slabs see 8050:CeNi<sub>2</sub>Si<sub>2</sub>.

We note that in CeFeSi, as well as in 6750:ScRuGe with ZrNiAl-type and in 6750:ScRhSi with TiNiSi-type, the transition metal is tetrahedrally surrounded by Si or Ge atoms.

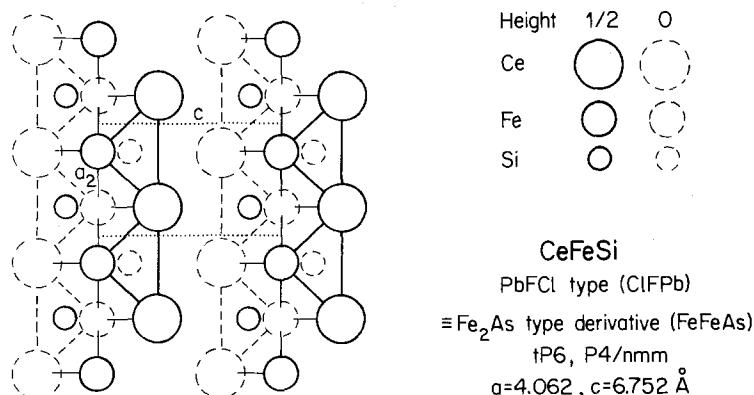
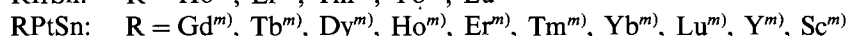
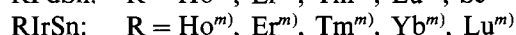
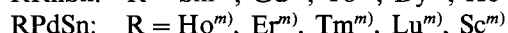
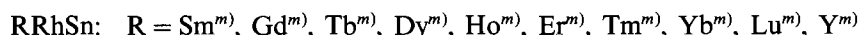
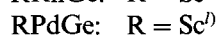
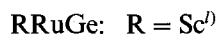
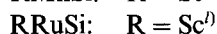
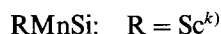
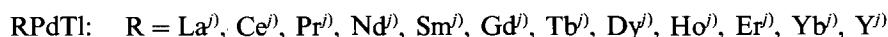
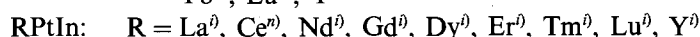
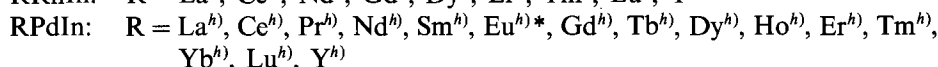
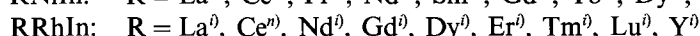
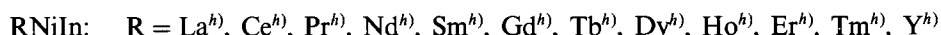
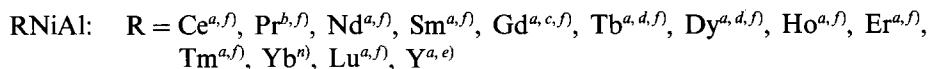


Fig. 19. CeFeSi with PbFCl-type, an Fe<sub>2</sub>As-type derivative.



6750	ScRuGe	hP9	$a = 6.962$	HoEKCP, 82
	or Sc <sub>3</sub> Ru <sub>3</sub> <sup>[4i]</sup> Ge <sub>2</sub> <sup>[6p, 3i]</sup> Ge <sup>[6p]</sup>	P $\bar{6}$ 2m	$a = 3.4683$	
ZrNiAl-type (ZrAlNi) (KrMM, 67) or HoNiAl-type (HoAlNi) (DwMCDK, 68) $\equiv$ Fe <sub>2</sub> P-type (FeFeP) derivative				

Isotypic compounds: All compounds are listed which were described as having ZrNiAl, HoNiAl, ordered Fe<sub>2</sub>P or simply Fe<sub>2</sub>P structure type



\*It is possible that for EuPdIn the true cell is a doubled one.

\*\*ScRhGe crystallizes also with the TiNiSi-type (see 6750:ScRhSi).

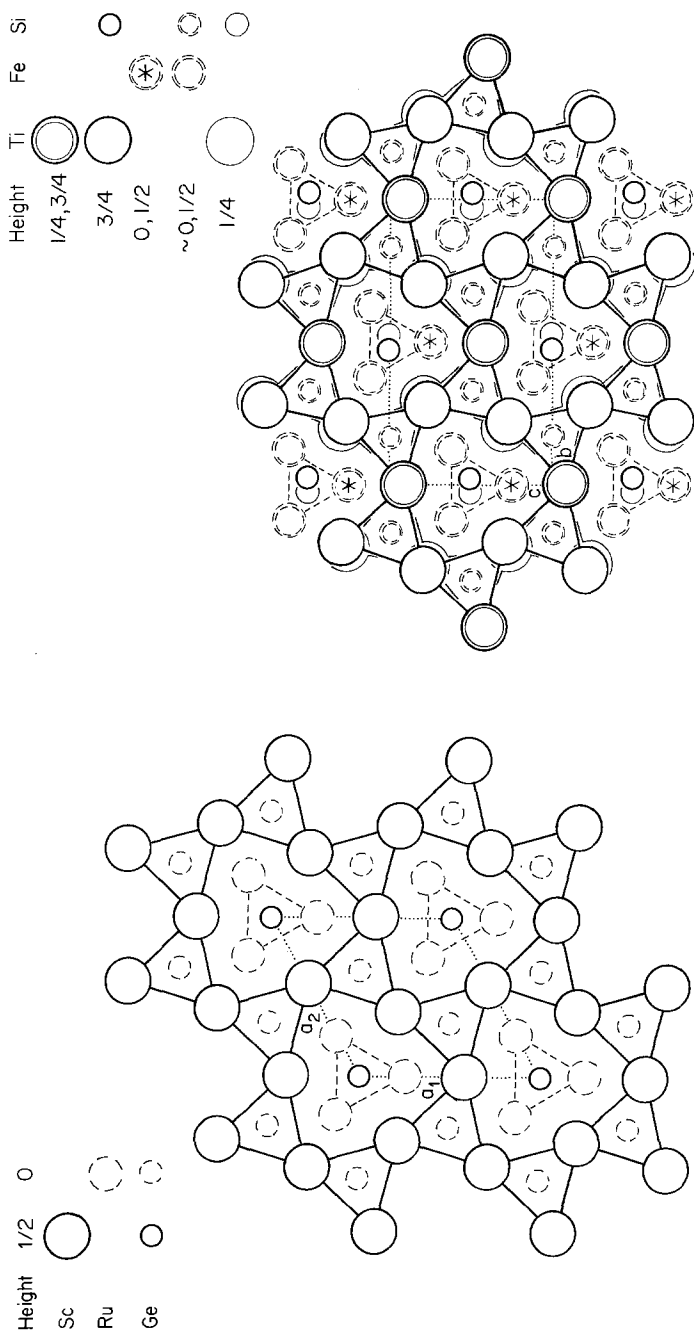
<sup>a</sup>)DwMCDK, 68      <sup>b</sup>)RyZK, 78      <sup>c</sup>)RyZM, 78      <sup>d</sup>)RyZM, 80

<sup>e</sup>)RyZ, 77      <sup>f</sup>)Oe, 73b      <sup>g</sup>)YaGG, 79      <sup>h</sup>)FeMR, 74

<sup>i</sup>)FeMR, 74a      <sup>j</sup>)FeMR, 74b      <sup>k</sup>)KoBK, 80      <sup>l</sup>)HoEKCP, 82

<sup>m</sup>)DwHK, 73      <sup>n</sup>)RoMMF, 83

The ScRuGe structure, shown in fig. 20, is a Fe<sub>2</sub>P-type derivative structure. The type name ZrNiAl or HoNiAl has been given to this arrangement of atom sites; however, to describe an isotypic crystal structure an additional precision is necessary concerning the kind of atoms which occupy the Ni and Al sites. As we shall see,



**ScRuGe**

ZrNiAl type (ZrAlNi)

$\equiv \text{Fe}_2\text{P}$  type derivative (FeFeP)

hP9,  $P\bar{6}2m$

$a=6.962$ ,  $c=3.4683 \text{ \AA}$

**TiFeSi**

TiFeSi type, a deformation variant of ZrNiAl type

$oI36$ ,  $Ima2$

$a=6.997$ ,  $b=10.830$ ,  $c=6.287 \text{ \AA}$

Fig. 20. Crystal structure of ScRuGe with ZrNiAl-type and of TiFeSi, a deformation variant of the ZrNiAl-type. YMnGa crystallizes in the TiFeSi-type but with a random distribution of Mn and Ga on the Fe and Si sites.

ZrNiAl-type phases are known where the Ni sites are occupied by M atoms and correspondingly the Al sites by T atoms. A study of fig. 20 reveals that Sc is surrounded by a tetragonal pyramid of five Ge atoms and the Ru by a tetrahedron of four Ge atoms. There are two kinds of Ge sites: one Ge is in the centre of a Sc prism with three extra Ru waist contacts and the second Ge, which occurs only half as often, is in the centre of a trigonal Ru prism. Thus the complete crystal chemical formula is



In all RTM compounds the pyramidal sites are occupied by rare earth (Y or Sc) atoms. However, the occupation of the tetrahedral and the trigonal prismatic sites is different in different compounds. In table 8 are listed the site occupations for a few selected RTM compounds where the site occupation has been studied.

It appears that in aluminides and gallides the prismatic sites are occupied by the T atoms, whereas in silicides and germanides they are occupied by M atoms.\* In the complete list of ZrNiAl-type compounds given below the type heading, all RTM compounds have been listed that were described in the literature as having ZrNiAl-type, ordered Fe<sub>2</sub>P-type, or simply Fe<sub>2</sub>P-type. In many cases the order has not been studied or a certain order was assumed without proof and without testing the other possibility for ordering of the T and M atoms.

There is a further reason to analyze critically the published ZrNiAl-type data, because there exists an orthorhombic deformation variant discussed with 6750:YMnGa.

It should be mentioned that another ternary Fe<sub>2</sub>P-type derivative structure has been found with Zr<sub>6</sub>CoGa<sub>2</sub> (hP9, P6̄2m) by Belyavina and Markiv (1982). In this case all trigonal prisms are formed by Zr atoms only. The centre of the isolated prism is occupied by a Co atom and the centres of the edge-linked prisms by Ga atoms.\*\* The crystal chemical formula is Zr<sub>6</sub>Co<sup>[6, p]</sup>Ga<sub>2</sub><sup>[6, p]</sup>. This atom arrangement corresponds to the β<sub>1</sub>-K<sub>2</sub>UF<sub>6</sub>-type (Br, 69).

\*This result has been found also with TT'M compounds (two transition elements without rare earth elements) by Jeitschko (1970).

\*\*The temperature factors are not in good agreement with the atomic numbers of the elements.

TABLE 8  
Site occupation in selected RTM compounds of the ZrNiAl-type.

Compound	Tetragonal pyramidal site	Tetrahedral site	Prismatic site	Ref.
CeNiAl	Ce	Al	Ni	DwMCDK, 68
HoNiAl	Ho	Al	Ni	DwMCDK, 68
CeNiGa	Ce	Ga	Ni	YaGG, 79
ScMnSi	Sc	Mn	Si	KoBK, 80
ScRuGe	Sc	Ru	Ge	HoEKCP, 82

6750	ScRhSi	oP12	$a = 6.4736$	HoEKCP, 82
	or	Pnma	$b = 4.0500$	
	ScRh <sup>[4]</sup> Si		$c = 7.2483$	
TiNiSi-type (ShS, 65) $\equiv$ PbCl <sub>2</sub> -type (ClClPb) derivative or CeCu <sub>2</sub> -type derivative				

## Isotypic compounds:

RCoGa:	R = Pr <sup>f</sup> , Nd <sup>j</sup> , Sm <sup>j</sup> , Gd <sup>j</sup> , Tb <sup>j</sup> , Dy <sup>j</sup> , Ho <sup>j</sup> , Er <sup>j</sup> , Y <sup>j</sup>
RNiGa:	R = Pr <sup>a</sup> , Nd <sup>a</sup> , Sm <sup>a</sup> , Gd <sup>a</sup> , Tb <sup>a</sup> , Dy <sup>a</sup> , Ho <sup>a</sup> , Er <sup>a</sup> , Tm <sup>a</sup> , Yb <sup>a</sup> , Lu <sup>a</sup> , Y <sup>a</sup> , Sc <sup>b</sup>
RRhGa:	R = Er <sup>c</sup> , Y <sup>c</sup>
RPdGa:	R = La <sup>c</sup> , Ce <sup>c</sup> , Pr <sup>c</sup> , Nd <sup>c</sup> , Sm <sup>c</sup> , Gd <sup>c</sup> , Tb <sup>c</sup> , Dy <sup>c</sup> , Ho <sup>c</sup> , Er <sup>c</sup> , Tm <sup>c</sup> , Yb <sup>k</sup> , Lu <sup>c</sup> , Y <sup>c</sup> , Sc <sup>c</sup>
RIrGa:	R = Er <sup>c</sup> , Y <sup>c</sup>
RPtGa:	R = La <sup>c</sup> , Ce <sup>c</sup> , Pr <sup>c</sup> , Nd <sup>c</sup> , Sm <sup>c</sup> , Gd <sup>c</sup> , Tb <sup>c</sup> , Dy <sup>c</sup> , Ho <sup>c</sup> , Er <sup>c</sup> , Tm <sup>c</sup> , Yb <sup>k</sup> , Lu <sup>c</sup> , Y <sup>c</sup> , Sc <sup>c</sup>
RMnSi:	R = Tm <sup>d</sup> , Y <sup>d</sup> *
RFeSi:	R = Nd <sup>**</sup> , Sc <sup>e</sup>
RCoSi:	R = Sc <sup>f</sup>
RNiSi:	R = Gd <sup>b</sup> , Tb <sup>b,h</sup> , Dy <sup>b,h</sup> , Ho <sup>b,h</sup> , Er <sup>b,h</sup> , Lu <sup>b</sup> , Y <sup>c,h</sup> , Sc <sup>f</sup>
RRhSi:	R = Gd <sup>g</sup> , Tb <sup>g</sup> , Dy <sup>g</sup> , Ho <sup>g</sup> , Er <sup>c,g</sup> , Y <sup>c,g</sup> , Sc <sup>c</sup>
RPdSi:	R = Sc <sup>c</sup>
RIrSi:	R = Gd <sup>c</sup> , Er <sup>c</sup> , Y <sup>c</sup> , Sc <sup>c</sup>
RPtSi:	R = Tb <sup>c</sup> , Dy <sup>c</sup> , Ho <sup>c</sup> , Er <sup>c</sup> , Tm <sup>c</sup> , Yb <sup>k</sup> , Lu <sup>c</sup> , Y <sup>c</sup> , Sc <sup>c</sup>
RCoGe:	R = Gd <sup>b</sup> , Ho <sup>b</sup> , Lu <sup>b</sup> , Sc <sup>b</sup>
RNiGe:	R = Gd <sup>b</sup> , Tb <sup>b</sup> , Ho <sup>b</sup> , Er <sup>b</sup> , Lu <sup>b</sup> , Y <sup>b</sup> , Sc <sup>b</sup>
RRhGe:	R = Ce <sup>c</sup> , Pr <sup>c</sup> , Nd <sup>c</sup> , Sm <sup>c</sup> , Gd <sup>c</sup> , Tb <sup>c</sup> , Dy <sup>c</sup> , Ho <sup>c</sup> , Er <sup>c</sup> , Tm <sup>c</sup> , Y <sup>c</sup> , Sc <sup>c</sup> ***
RIrGe:	R = Ce <sup>c</sup> , Pr <sup>c</sup> , Nd <sup>c</sup> , Sm <sup>c</sup> , Gd <sup>c</sup> , Tb <sup>c</sup> , Dy <sup>c</sup> , Ho <sup>c</sup> , Er <sup>c</sup> , Tm <sup>c</sup> , Y <sup>c</sup> , Sc <sup>c</sup>
RPtGe:	R = Sm <sup>c</sup> , Gd <sup>c</sup> , Tb <sup>c</sup> , Dy <sup>c</sup> , Ho <sup>c</sup> , Er <sup>c</sup> , Tm <sup>c</sup> , Y <sup>c</sup> , Sc <sup>c</sup>
RCoSn:	R = Tb <sup>i</sup> , Dy <sup>j</sup> , Ho <sup>j</sup> , Er <sup>j</sup> , Tm <sup>i</sup> , Lu <sup>i</sup> , Y <sup>i</sup>

\*YMnSi also crystallizes with the PbFCl-type (see 6750:CeFeSi).

\*\*MaF, 73a give cell parameters for the NdFeSi compound which are incompatible with a structure of the TiNiSi-type. According to BoGK, 70, the NdFeSi compound belongs to the 6750:CeFeSi-type.

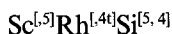
\*\*\*ScRhGe also crystallizes with the ZrNiAl-type (see 6750:ScRuGe).

<sup>a</sup> YaGG, 79	<sup>b</sup> Dw, 82	<sup>c</sup> HoEKCP, 82	<sup>d</sup> KnMB, 77	<sup>e</sup> ChEP, 83
<sup>f</sup> KoB, 77	<sup>g</sup> ChCLVEH, 82	<sup>h</sup> BoYG, 74	<sup>i</sup> SkKG, 82	<sup>j</sup> SiGGY, 82
<sup>k</sup> RoMMF, 83				

The TiNiSi-type (space group Pnma) is a ternary ordered derivative of the CeCu<sub>2</sub>-type (space group Imma), being reported for the 67(50):Pr(Pt<sub>5</sub>Ge<sub>5</sub>)<sub>2</sub> com-

pound. (Pnma is a class-equivalent maximal subgroup of Imma with index 2.) The structures can be compared in fig. 21. From a geometrical point of view the TiNiSi-type can also be considered as a ternary ordered derivative of the  $\text{PbCl}_2$  (or  $\text{Co}_2\text{P}$ )-type with the Pb sites in  $\text{PbCl}_2$  (or P sites of  $\text{Co}_2\text{P}$ ) corresponding to the Si sites in TiNiSi. For a discussion of the different branches of the TiNiSi-type see Hovestreydt et al. (HoEKCP, 82).

In ScRhSi the Sc atoms are in the centres of deformed tetragonal pyramids of Si atoms, the Rh atoms in the centres of Si tetrahedra and the Si atoms in the centres of tricapped trigonal prisms consisting of five Sc and four Rh atoms. The crystal chemical formula is thus



We note that the crystal-chemical formulae for the RTSi and RTGe compounds with  $\text{PbFCl}$ -type (6750:CeFeSi), the ZrNiAl-type (6750:ScRuGe) and the TiNiSi-type (6750:ScRhSi) are all equal—except for the coordination of the Si and Ge atoms. The geometrical similarity between the three corresponding binary types  $\text{Fe}_2\text{As}$ ,  $\text{Fe}_2\text{P}$  and  $\text{Co}_2\text{P}$  has been pointed out by Nylund et al. (NyRSF, 72).

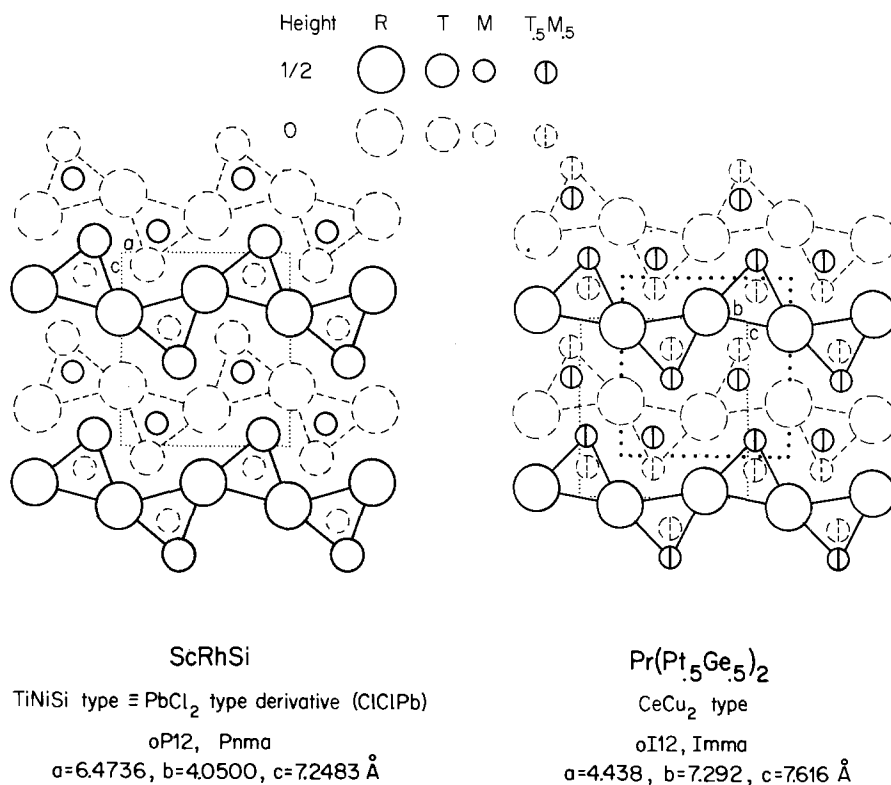


Fig. 21. ScRhSi with TiNiSi-type, a  $\text{PbCl}_2$ - or  $\text{CeCu}_2$ -type derivative and  $\text{Pr}(\text{Pt}_5\text{Ge}_5)_2$  with  $\text{CeCu}_2$ -type. In  $\text{CeCu}_2$  the unit cell indicated with extra heavy points corresponds to the unit cell for the TiNiSi- or  $\text{PbCl}_2$ -type.

Allowing for small shifts of the adjustable parameters of the T and M atom sites in the ScRhSi structure the coordination polyhedra of the T and M atoms become equal.\* In this case the M atom is no longer exactly in the centre of the trigonal prism  $R_4T_2$  nor is the coordination figure of M atoms around a T atom a perfect tetrahedron. This atom arrangement must still be called the TiNiSi-type, provided the T and M atoms are ordered. In the case that the T and M atoms are not ordered that atom arrangement—now body-centred orthorhombic—is called the CeCu<sub>2</sub>-type, for which examples are given with the 67(50):Pr(Pt<sub>5</sub>Ge<sub>5</sub>)<sub>2</sub> compound. Many ordered TiNiSi phases, where T and M atoms have similar X-ray scattering factors, have been erroneously classified as belonging to the CeCu<sub>2</sub>-type, because the extra diffraction lines, which distinguish the TiNiSi-type from the CeCu<sub>2</sub>-type, are weak and have been overlooked.

---

<b>6750</b>	<b>LaPtSi</b>	tI12	$a = 4.249$	KIP, 82c
	or	I4 <sub>1</sub> md	$c = 14.539$	
	LaPt <sup>[6p, 3]Si</sup> [6p, 3]			

---

ThSi<sub>2</sub>-type derivative

---

Isotypic compounds:

RNiSi\*: R = Ce<sup>a</sup>, Pr<sup>b</sup>, Nd<sup>b</sup>)

RPtSi: R = La<sup>c</sup>, Ce<sup>c</sup>, Pr<sup>c</sup>, Nd<sup>c</sup>, Sm<sup>c</sup>, Gd<sup>c</sup>.

RIrGe: R = La<sup>d</sup>)

RPtGe: R = La<sup>d</sup>)

\*Or R(Ni<sub>5</sub>Si<sub>5</sub>)<sub>2</sub>. For RNiSi compounds the order of Ni and Si atoms has not been investigated. The structures are described as corresponding to the ThSi<sub>2</sub>-type (space group I4<sub>1</sub>/amd).

<sup>a</sup>BoMTKG, 73    <sup>b</sup>MaF, 73a    <sup>c</sup>KIP, 82c    <sup>d</sup>HoEKCP, 82

The LaPtSi structure is an ordered ternary derivative of the ThSi<sub>2</sub> structure type. The geometrical relationship of the Th $\overset{\infty}{3}$ Si<sub>2</sub><sup>[6p+3]</sup>-type to the Al $\overset{\infty}{2}$ B<sub>2</sub><sup>[6p+3]</sup>-type is discussed with the 67(75):Ce(Ni<sub>25</sub>Si<sub>75</sub>)<sub>2</sub> compound. A drawing of the LaPtSi structure and of the LaIrSi structure, a Sr $\overset{\infty}{3}$ Si<sub>2</sub><sup>[6p+3]</sup>-type derivative, is shown in fig. 22.

A plot of the single-atom-cube length  $[(V/n)^{1/3}]$ , where  $V$  is the volume of the unit cell and  $n$  is the number of atoms per unit cell] of RPtSi and RPtGe compounds as a function of the ionic radii of the trivalent rare earth atoms is shown in fig. 23. Three structure types are found here: LaPtSi, TiNiSi and CeCu<sub>2</sub>. Silicides have a cell volume about 4% smaller than that of isotypic germanides. The data points for the CeCu<sub>2</sub> and TiNiSi-types with RPtGe compounds fall, as expected, on the same line;

\*For details see Hovestreydt et al. (HoEKCP, 82).

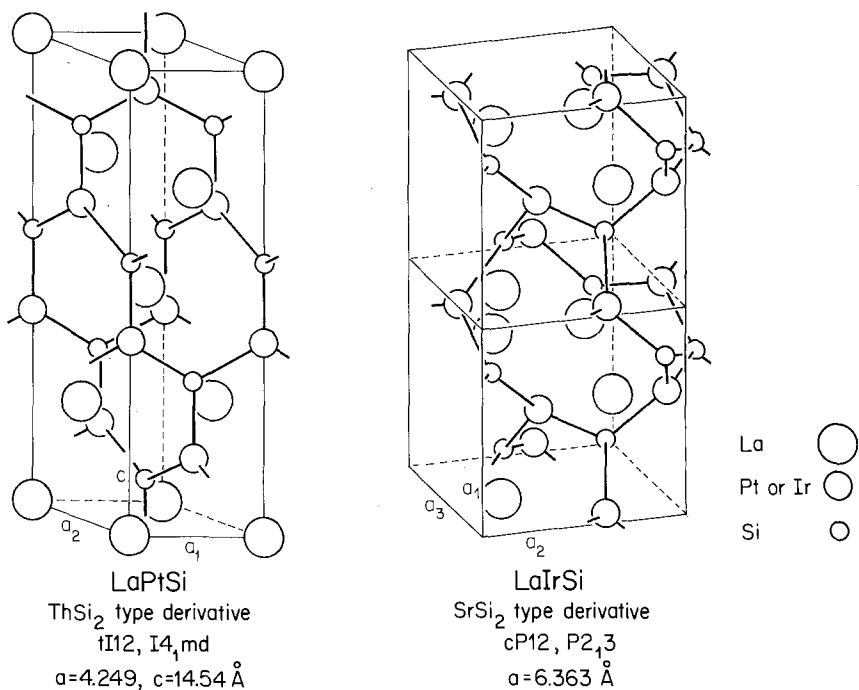


Fig. 22. The LaPtSi and LaIrSi structure types with their three-connected and three-dimensional Pt (or Ir)-Si framework.

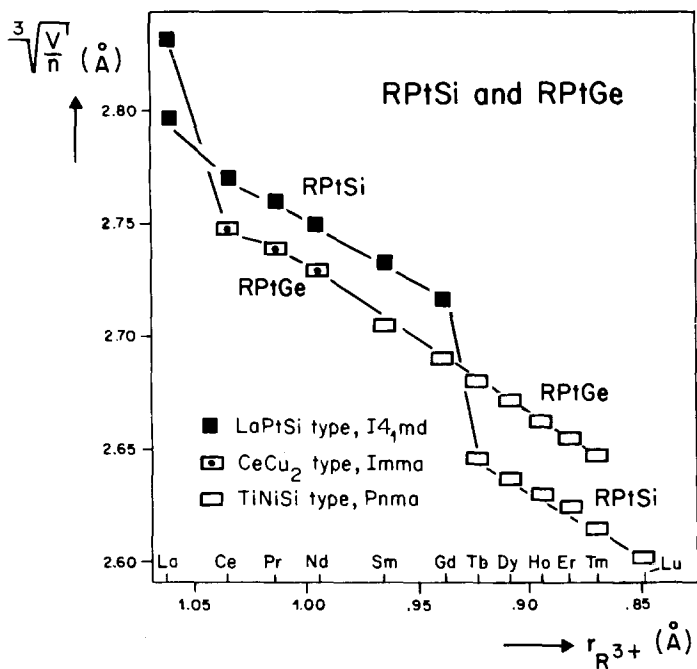


Fig. 23. A  $(V/n)^{1/3}$  versus  $r_{R^{3+}}$  diagram for RPtSi and RPtGe compounds (Hovestreydt et al., HoEKCP, 82).

however, the LaPtSi-type is less compact, leading to a volume about 7% larger than that of phases with the other two structure types.

---

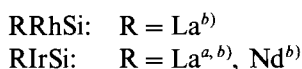
<b>6750</b>	<b>LaIrSi</b> or $\text{LaIr}^{[.3]}\text{Si}^{[.3]}$	cP12 P2 <sub>1</sub> 3	$a = 6.363$	KlP, 82d
-------------	---	---------------------------	-------------	----------

---

ZrOS-type (MccBB, 48)  $\equiv$  SrSi<sub>2</sub>-type (Pr, 72) derivative

---

Isotypic compounds:



<sup>a)</sup>KlP, 82d    <sup>b)</sup>ChLCVE, 82

The LaIrSi structure (space group P2<sub>1</sub>3) is an ordered ternary derivative of the SrSi<sub>2</sub>-type (space group P4<sub>3</sub>32). (P2<sub>1</sub>3 is a translation-equivalent maximal subgroup of P4<sub>3</sub>32 with index 2.) The LaIrSi structure together with the 6750:LaPtSi structure is shown in fig. 22. In both structures the Ir (or Pt)–Si atoms form a three-connected three-dimensional framework. Only in the LaPtSi structure are the Pt and Si atoms in the centres of trigonal rare earth prisms.

---

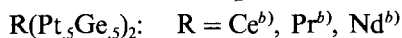
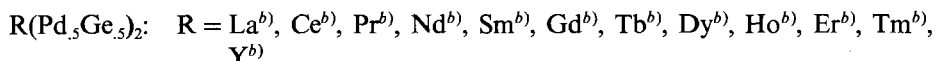
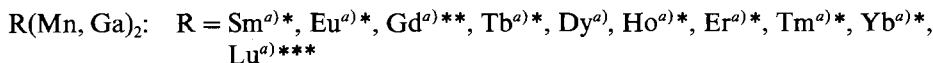
<b>67(50)</b>	<b>Pr(Pt<sub>5</sub>Ge<sub>5</sub>)<sub>2</sub></b>	oI12 Imma	$a = 4.438$ $b = 7.292$ $c = 7.616$	HoEKCP, 82
---------------	---	--------------	---	------------

---

CeCu<sub>2</sub>-type (LaC, 61)

---

Isotypic compounds:



\*R<sub>2</sub>MnGa<sub>3</sub>    \*\*RMn<sub>0.64</sub>Ga<sub>1.36</sub>    \*\*\*RMn<sub>0.34</sub>Ga<sub>1.66</sub>

<sup>a)</sup>MaBZB, 82    <sup>b)</sup>HoEKCP, 82



All the compounds listed are really  $\text{CeCu}_2$ -type compounds with a random distribution of T and M atoms on the Cu sites. Many of the  $\text{CeCu}_2$ -type compounds reported earlier are actually ordered  $\text{TiNiSi}$ -type compounds which are listed here with the 6750:ScRhSi compound. Under the same heading is to be found a drawing of a  $\text{CeCu}_2$ -type structure (fig. 21) and a discussion of the structure type.

---

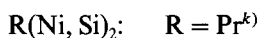
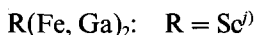
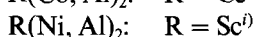
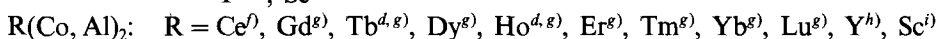
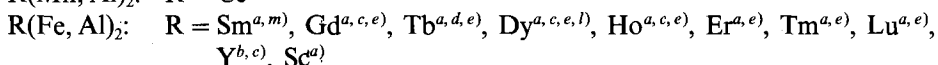
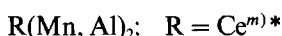
<b>67(50)</b> $\text{Sc}(\text{Ni}_5\text{Al}_5)_2$	hP12 $\text{P6}_3/\text{mmc}$	$a = 5.12$ $c = 8.20$	TeP, 65
---	----------------------------------	--------------------------	---------

---

MgZn<sub>2</sub> (Laves phase)-type

---

Isotypic compounds



\*Composition given as Ce<sub>2</sub>Mn<sub>3</sub>Al.

<sup>a</sup>)DwKPTW, 75

<sup>b</sup>)Bu, 75

<sup>c</sup>)GrS, 75

<sup>d</sup>)Oe, 73

<sup>e</sup>)Oe, 71

<sup>f</sup>)MaRH, 68

<sup>g</sup>)Oe, 71a

<sup>h</sup>)RyZ, 71

<sup>i</sup>)TeP, 65

<sup>j</sup>)GaM, 78

<sup>k</sup>)MaF, 73a

<sup>l</sup>)Oe, 73a

<sup>m</sup>)Dw, 68

All phases listed here are truly ternary phases. Most of the ternary hexagonal MgZn<sub>2</sub> Laves phases are formed in the pseudobinary systems between the two corresponding binary cubic MgCu<sub>2</sub> Laves phases. For the details concerning the homogeneity ranges of these phases and their eventual partial ordering the cited references should be studied. The Laves phase derivatives with full order are discussed with 6725:Sc<sub>2</sub>Co<sub>3</sub>Si and 6775:Sc<sub>2</sub>RuAl<sub>3</sub>.

---

<b>67(50)</b> YMnGa or Y(Mn, Ga) <sub>2</sub>	oI36 Ima2	$a = 8.592$ $b = 12.24$ $c = 7.067$	BeM, 82
---	--------------	---	---------

---

TiFeSi-type (Je, 70), a deformation variant of the ZrNiAl-type  $\equiv$  Fe<sub>2</sub>P-type derivative, but with Mn and Ga atoms (in the ratio 1:1) randomly distributed over Fe and Si sites

---

Isotypic compounds: All references BeM, 82

RMnGa: R = Gd, Tb, Dy, Ho, Er, Tm\*, Lu\*\*, Y

RCoGa: R = Sc\*\*\*

RNiGa: R = Sc\*\*\*

\*TmMn<sub>8</sub>Ga<sub>1.2</sub> \*\*LuMn<sub>64</sub>Ga<sub>1.36</sub> \*\*\*ScT<sub>35</sub>Ga<sub>1.65</sub>

Jeitschko (1970) has found an orthorhombic deformation variant of the ZrNiAl-type [ $a = 2c(\text{ZrNiAl})$ ,  $b = \sqrt{3} a(\text{ZrNiAl})$ ,  $c = a(\text{ZrNiAl})$ ] with the TiFeSi structure. This is shown on the right-hand side of fig. 20. In YMnGa the Fe and the Si sites are occupied randomly by Mn and Ga atoms. The differences in the X-ray diffraction patterns of the ZrNiAl- and the TiFeSi-type are small. The weak superstructure reflections can easily be overlooked in powder diagrams.

---

6775	<b>Sc<sub>2</sub>RuAl<sub>3</sub></b>	hP12 P6 <sub>3</sub> /mmc	$a = 5.27$ $c = 8.57$	KaBRS, 74
------	---------------------------------------	------------------------------	--------------------------	-----------

---

Mg<sub>2</sub>Cu<sub>3</sub>Si-type (Mg<sub>2</sub>SiCu<sub>3</sub>) (Wi, 39) ≡ MgZn<sub>2</sub> (Laves phase)-type derivative

---

Isotypic compounds:

R<sub>2</sub>TAl<sub>3</sub>: Lu<sub>2</sub>FeAl<sub>3</sub><sup>a)</sup>\*, Er<sub>2</sub>CoAl<sub>3</sub><sup>b)</sup>\*\* , Sc<sub>2</sub>RuAl<sub>3</sub><sup>c)</sup>\*\*

\*Composition for this compound should be written R<sub>2</sub>(Fe<sub>33</sub>Al<sub>67</sub>)<sub>3</sub>Al with Fe<sub>33</sub>Al<sub>67</sub> on the Co sites and Al on the Si sites of 6725:Sc<sub>2</sub>Co<sub>3</sub>Si.

\*\*Fully ordered structure as 6725:Sc<sub>2</sub>Co<sub>3</sub>Si but with T and M atoms interchanged.

<sup>a)</sup>DwKPTW, 75    <sup>b)</sup>Oe, 73a    <sup>c)</sup>KaBRS, 74

The ordered ternary Laves phases are discussed with the 6725:Sc<sub>2</sub>Co<sub>3</sub>Si structure. The disordered Laves phases can be found with the 67(50):Sc(Ni<sub>5</sub>Al<sub>5</sub>)<sub>2</sub> compound. A tendency toward a partial ordering of the non-rare-earth elements is found to be related to the T/M ratio. See for example Oesterreicher (1973a).

---

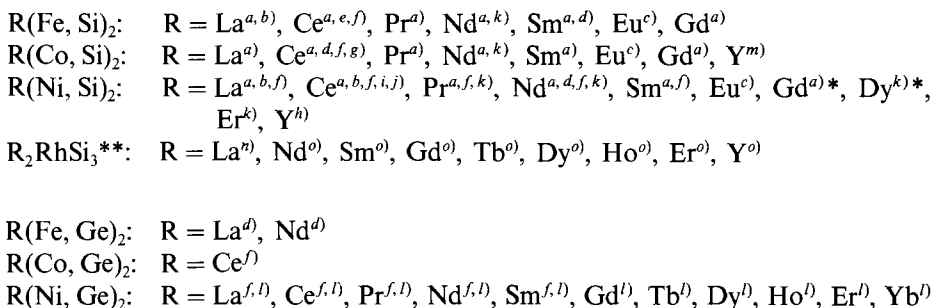
67(75)	<b>Ce(Ni<sub>25</sub>Si<sub>75</sub>)<sub>2</sub></b> or Ce Ⓞ (Ni, Si) <sub>2</sub> <sup>[6p+3]</sup>	hP3 P6/mmm	$a = 4.043$ $c = 4.302$	GIB, 65
--------	---	---------------	----------------------------	---------

---

AlB<sub>2</sub>-type with random distribution of the non-rare-earth elements on the B sites

---

## Isotypic compounds:



\*Might be a binary compound (GIKB, 66a).

\*\* $\text{R}_2\text{RhSi}_3$  with ordered ternary  $\text{AlB}_2$ -type derivative [ $a = 2a(\text{AlB}_2)$  and  $c = 2c(\text{AlB}_2)$ ].

<sup>a)</sup> MaT, 69	<sup>b)</sup> Ra, 67	<sup>c)</sup> MaF, 73	<sup>d)</sup> FeS, 73
<sup>e)</sup> BoGKC, 70	<sup>f)</sup> GIb, 65	<sup>g)</sup> BoG, 70	<sup>h)</sup> SkSG, 67
<sup>i)</sup> BoMTKG, 73	<sup>j)</sup> BoG, 69	<sup>k)</sup> MaF, 73a	<sup>l)</sup> CoFMR, 77
<sup>m)</sup> BoMMYSG, 74	<sup>n)</sup> ChLVEH, 82	<sup>o)</sup> ChLEVH, 82	

The  $\text{Al} \overset{3}{\text{B}}_2^{6p+3l}$ - and the  $\text{Th} \overset{3}{\text{Si}}_2^{6p+3l}$ -types are structure block shifted variants as shown in the upper part of fig. 24 (Parthé, 1967). For ternary equiatomic compounds an ordering of the non-rare-earth elements on the B or Si sites should lead to derivative structures having either larger unit cells or the same unit cells but then with lower symmetry.

The ternary derivative structure of the  $\text{AlB}_2$ -type having the same unit cell should have space group  $\text{P}\bar{6}\text{m}2$  instead of  $\text{P}6/\text{mmm}$  (KIP, 82c)\*. This structure has not yet been reported; however, a ternary  $\text{AlB}_2$  derivative structure with the  $c$  axis doubled is found, for example, with  $\text{RCuSi}$  compounds (Ia, 83). This atom arrangement ( $\text{hP}6$ ,  $\text{P}6_3/\text{mmc}$ ) is known as the  $\text{NaBeSb}$ -type (TiS, 77) or  $\text{MnCoGe}$ -type and corresponds to a ternary ordered  $\text{Ni}_2\text{In}$ -type. Recently a new ordered  $\text{AlB}_2$  derivative structure [ $\text{hP}24$ ,  $a = 2a(\text{AlB}_2)$  and  $c = 2c(\text{AlB}_2)$ ] has been found with  $\text{R}_2\text{RhSi}_3$  compounds (ChLEH, 83).

Two deformation variants of the  $\text{AlB}_2$ -type are known, where the atoms corresponding to the boron atoms are no longer in a plane parallel to (0001). The deviations from the plane are conveniently studied in the lower part of fig. 24, which shows the atom arrangement in the  $(11\bar{2}0)$  plane of the corresponding hexagonal unit cells. The trigonal  $\text{CdI}_2$ - or  $\text{CeCd}_2$ -type (IaF, 54) has been found with  $\text{EuGe}_2$  (Gl, 64). The hexagonal  $\text{CaIn}_2$ -type (Ia, 64) has been reported for  $67(83):\text{Sm}(\text{Mn}_{17}\text{Ga}_{83})_2$ .

A ternary derivative of the  $\text{ThSi}_2$ -type with the same unit cell is discussed with  $6750:\text{LaPtSi}$ . Here the symmetry is lowered from  $\text{I}4_1/\text{amd}$  to  $\text{I}4_1\text{md}$ \*\*.

\* $\text{P}\bar{6}\text{m}2$  is a translation equivalent maximal subgroup of  $\text{P}6/\text{mmm}$  with index 2.

\*\* $\text{I}4_1\text{md}$  is a translation equivalent maximal subgroup of  $\text{I}4_1/\text{amd}$  with index 2.

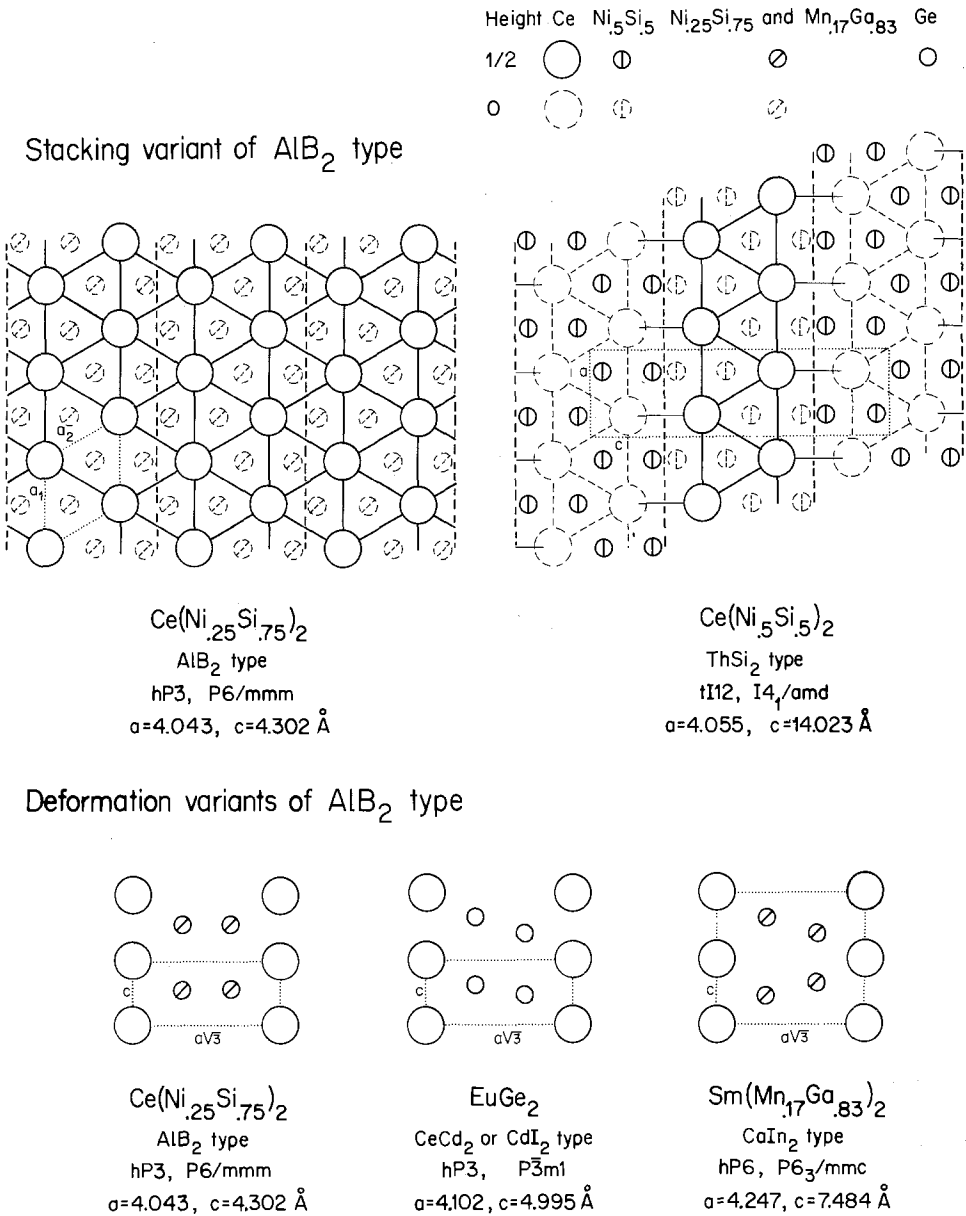


Fig. 24. Upper part: The AlB<sub>2</sub> and ThSi<sub>2</sub> structure types, found with Ce(Ni, Si)<sub>2</sub> compounds, interpreted as structure block shifted variants (Parthé, 1967). The Ce(Ni<sub>5</sub>Si<sub>5</sub>)<sub>2</sub> compound probably has an ordered arrangement of Ni and Si atoms and thus crystallizes in the 6750:LaPtSi-type with space group I4<sub>1</sub>md. Lower part: Arrangement of the atoms in the (11 $\bar{2}$ 0) plane for the AlB<sub>2</sub>-type and two deformation variants, the CeCd<sub>2</sub>- or CdI<sub>2</sub>-type and the CaIn<sub>2</sub>-type.

---

<b>67(83)</b>	<b>Sm(Mn<sub>17</sub>Ga<sub>83</sub>)<sub>2</sub></b>	hP6 P6 <sub>3</sub> /mmc	$a = 4.247$ $c = 7.484$	MaBZB, 82
---------------	---	-----------------------------	----------------------------	-----------

---

CaIn<sub>2</sub>-type (Ia, 64) \*

---

\*To the  $z$  parameter given in Structure Reports, Vol. 29, must be added  $\frac{1}{4}$ .

Isotypic compounds: All references MaBZB, 82

R(Mn, Ga)<sub>2</sub>: R = Sm \*, Gd \*, Tb \*, Dy \*\*, Ho \*\*, Er \*\*

\*RMn<sub>34</sub>Ga<sub>1.66</sub>    \*\*RMn<sub>2</sub>Ga<sub>1.8</sub>

The Sm(Mn<sub>17</sub>Ga<sub>83</sub>)<sub>2</sub> structure, shown in the lower part of fig. 24, crystallizes in the CaIn<sub>2</sub>-type, a hexagonal deformation variant of the AlB<sub>2</sub>-type, which is discussed with 67(75):Ce(Ni<sub>25</sub>Si<sub>75</sub>)<sub>2</sub>.

---

<b>67(88)</b>	<b>Sc<sub>4</sub>CoSi<sub>7</sub></b>	oC12 Cmcm	$a = 3.856$ $b = 14.54$ $c = 3.744$	KoB, 77
	or Sc $\frac{1}{2}$ (Co <sub>25</sub> Si <sub>75</sub> ) <sup>[6, p]</sup> $\frac{2}{3}$ Si <sup>[+4]</sup>			

---

ZrSi<sub>2</sub>-type (SchNK, 54) derivative with partial disorder of T and M atoms

---

Isotypic compounds: All references KoB, 77

Sc(T<sub>125</sub>Si<sub>875</sub>)<sub>2</sub>: T = Mn, Fe, Co, Ni

The Sc<sub>4</sub>CoSi<sub>7</sub> structure, shown in fig. 25, is a ZrSi<sub>2</sub>-type derivative structure with disorder of the T and M atoms on the trigonal prismatic Si sites, the other Si sites of ZrSi<sub>2</sub> being occupied by M atoms only in the ternary compounds. The atoms in the centres of the trigonal rare earth prisms form an infinite zig-zag chain. The arrangement of the centred prisms corresponds to a structure segment of the CrB-type with additional M atoms on the tetrahedral interstices of the W-type segments (see fig. 8).

---

<b>7325</b>	<b>Ce<sub>3</sub>Ni<sub>6</sub>Si<sub>2</sub></b>	cI44 Im3m	$a = 8.858$	GIKB, 66
-------------	---	--------------	-------------	----------

---

Ca<sub>3</sub>Ag<sub>8</sub>-type (CaR, 64) derivative

---

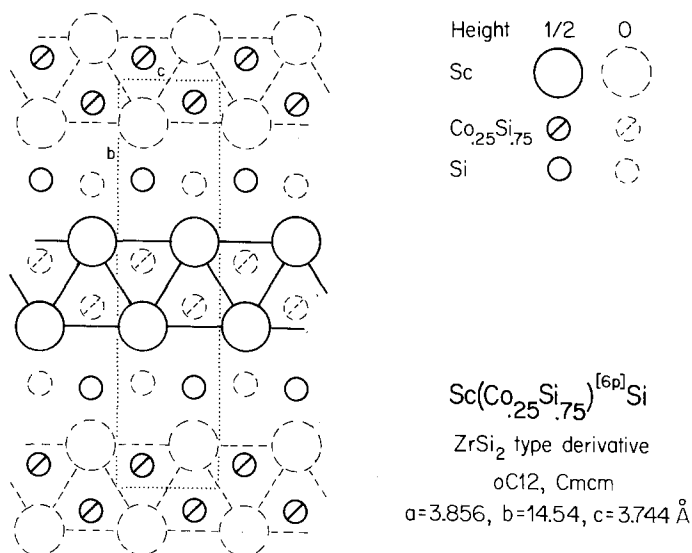
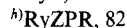
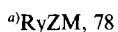
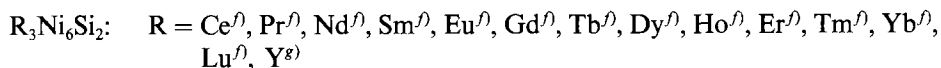
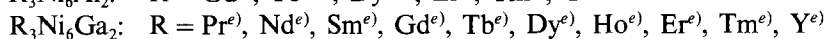
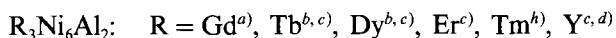


Fig. 25. The  $\text{Sc}_4\text{CoSi}_7$  structure, a  $\text{ZrSi}_2$ -type derivative with partial disorder of Co and Si atoms on the trigonal prismatic Si sites.

#### Isotypic compounds:



The  $\text{Ce}_3\text{Ni}_6\text{Si}_2$  structure, a  $\text{Ca}_3\text{Ag}_8$ -type derivative, is shown in the left hand part of fig. 26. The  $\text{Ca}_3\text{Ag}_8$  structure together with the other structures listed in table 9 belongs to the group of cubic structure with large unit cells which can be conveniently described with nested polyhedral units (Chabot et al., ChCP, 81)\*. Nested polyhedral units, discussed here, consist of various inscribed regular or semiregular polyhedra, the outermost polyhedron always being a cubo-octahedron, which are centred at points of high symmetry in the unit cell. One distinguishes between structures with isolated nested polyhedral units and those with linked units. All structures listed in table 9 are characterized by linked units. In one unit cell of  $\text{Ce}_3\text{Ni}_6\text{Si}_2$  there are two linked nested polyhedral units. Their spatial arrangement can be seen in the right-hand part of fig. 26, where only the outlines of the outer cubo-octahedra are shown and with dashed lines the outlines of inscribed cubes, which are linked with cubes of neighbouring nested polyhedral units.

\*Other descriptions have been proposed by Hellner and Koch (1981) and Nyman and Hyde (1981).

TABLE 9

List of structures which can be described with linked nested polyhedral units. The different units are made up of polyhedra as indicated by the capital letters given on top (for explanation see text). Below these symbols for the polyhedra are found the chemical symbols of the elements which occupy these sites in the different nested polyhedral units. Underlined element symbols indicate that this element on this particular site is shared by different units. For details see Chabot et al. (ChCP, 81).

Code	Compound	Structure type	Pearson's classif. symbol	Space group	$\alpha$ -Mn unit C + TT + T + CO	bcc unit C + CB + OH + CO	$\gamma$ -brass unit IT + OT + OH + CO	$\text{Ca}_3\text{Ag}_8$ unit OH + CB + CO	$\text{Ti}_2\text{Ni}$ unit OH + T + CO
33(50)	$\text{Sc}_2(\text{Co, Si})$	$\text{Ti}_2\text{Ni}$ -type	cF96	Fd3m			(Co, Si) + Sc + Sc + Sc	Ce + Si + Ni twice	Sc + (Co, Si) + Sc
7325	$\text{Ce}_3\text{Ni}_6\text{Si}_2$	$\text{Ce}_3\text{Ni}_6\text{Si}_2$ -type $\equiv \text{Ca}_3\text{Ag}_8$ derivative	cI44	Im3m					
7930	$\text{Sc}_6\text{Ni}_{16}\text{Si}_7$	$\left. \begin{array}{l} \text{MgCu}_4\text{Si}_7\text{-type} \\ \equiv \text{Th}_6\text{Mn}_{23} \text{ derivative} \end{array} \right\}$	cF116	Fm3m		Si + Ni + Sc + Si		Sc + Ni + Si	
7970	$\text{Sc}_6\text{Ni}_{17}\text{Al}_{16}$		cF116	Fm3m		Ni + Al + Sc + Ni		Sc + Al + Ni	
9322	$\text{Sc}_7\text{Co}_2\text{B}_6$	$\text{W}_2\text{Cr}_3\text{C}_6$ -type $\equiv \text{Cr}_3\text{C}_6$ derivative	cF116	Fm3m	Sc + Co + Co + B twice				
					also Co atom on interstitial sites				
9691	$\text{CeCr}_2\text{Al}_{30}$	$\text{CeCr}_2\text{Al}_{30}$ -type $\text{MgCr}_2\text{Al}_{18}$ -related $\equiv \text{ZrZn}_{22}$ derivative	cF184	Fd3m	Ce + Al + Al + Al				Al + Cr + Al

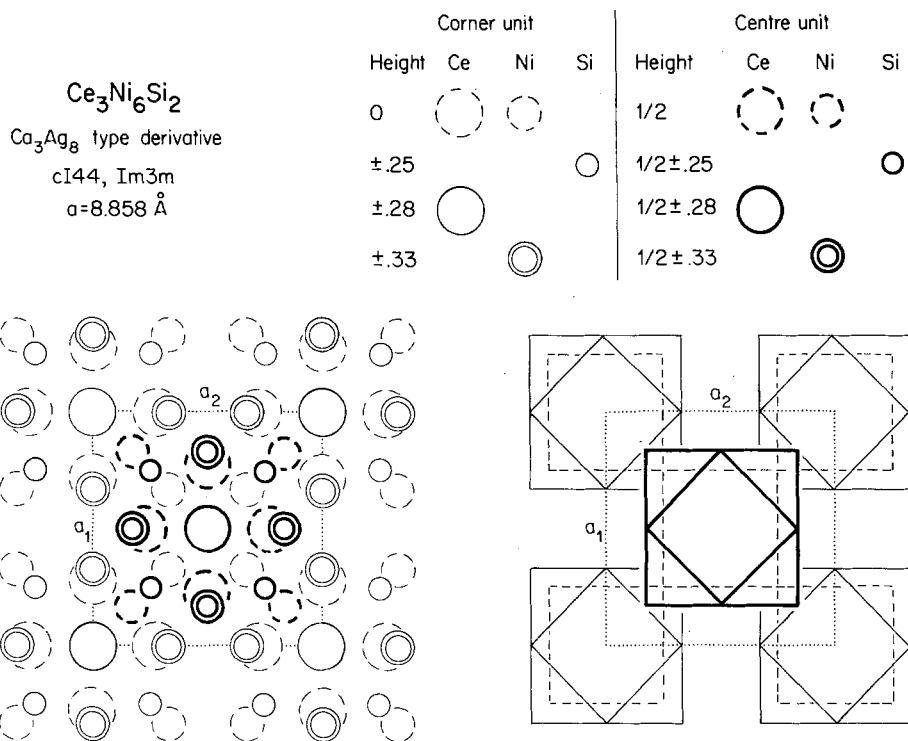


Fig. 26. Structure of  $\text{Ce}_3\text{Ni}_6\text{Si}_2$  with  $\text{Ca}_3\text{Ag}_8$ -type derivative. The atomic arrangement is shown on the left-hand side and the arrangement of linked nested polyhedral units in the drawing on the right-hand side. In the drawing on the left, outside the dotted unit cell, only atoms belong to the corner polyhedral units are indicated.

Five basic types of nested polyhedral units are shown in fig. 27. They are formed in different ways of a centre atom (C), a truncated tetrahedron (TT), a tetrahedron (T)—possibly subdivided in an inner tetrahedron (IT) and an outer tetrahedron (OT)—a cube (CB), an octahedron (OH), and in all cases an outer cubo-octahedron (CO). In the face-centred cubic structures listed in table 9 the linked nested polyhedral units are arranged as shown in fig. 28. In most cases there are two different

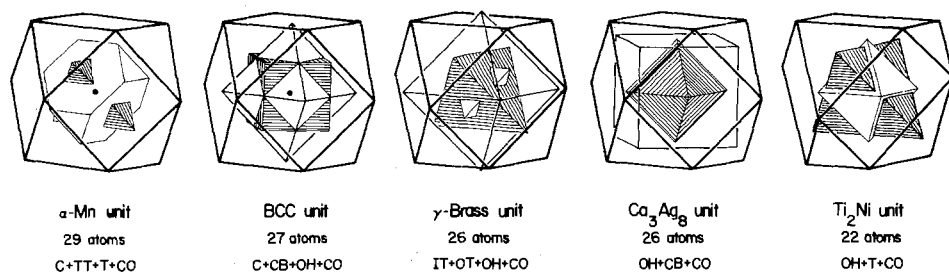


Fig. 27. The five basic types of nested polyhedral units.



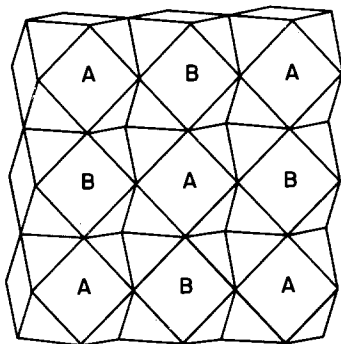


Fig. 28. Arrangement of linked nested polyhedral units in face-centred structures. Only the polyhedral units in the front half of the unit cell are shown.

kinds of polyhedral units, denoted A and B in the drawing. The different kinds of nested polyhedral units found in the different cubic structures and the individual occupation of the polyhedra by R, T or M atoms can be studied in the right hand part of table 9. Underlined chemical symbols indicate that these atoms on their particular polyhedral sites belong also to neighbouring nested polyhedral units. For details, the original paper (ChCP, 81) should be studied.

Two structure types occur with composition 7350: the  $Gd_3Cu_4Ge_4$ -type, found with  $Sc_3Ni_4Ge_4$ , and the  $U_3Ni_4Si_4$ -type, discussed with  $La_3Rh_4Ge_4$ .

7350	$Sc_3Ni_4Ge_4$	oI22	$a = 3.908$	KoS, 82
	or	Immm	$b = 6.598$	
	$Sc_3Ni_4Ge_2 \cdot 2[Ge_2^{6,p}]$		$c = 12.910$	

$Gd_3Cu_4Ge_4$ -type (Ri, 70) or  $Sr_3Li_4Sb_4$ -type (LiSW, 70)

Isotypic compounds:



<sup>a</sup>BoKG, 76    <sup>b</sup>KoS, 82

The  $Sc_3Ni_4Ge_4$  structure with  $Gd_3Cu_4Ge_4$ -type is presented in the right-hand part of fig. 29. It consists of pairs of columns of trigonal  $Sc_6Si$  prisms and of sheets, perpendicular to  $c$ , of characteristic columns of composition  $R_4T_2M_2$ , shown in fig. 14. In the  $TiNiSi$ -type (see fig. 13 and 6750:ScRhSi) these columns are edge-joined with other columns; however, in the sheets, in  $Sc_3Ni_4Ge_4$ , we find that  $l-R_4T_2M_2$  and  $r-R_4T_2M_2$  columns—positioned alternatively—are face-joined. For a further discussion see 6067:Sc<sub>2</sub>CoSi<sub>2</sub>.

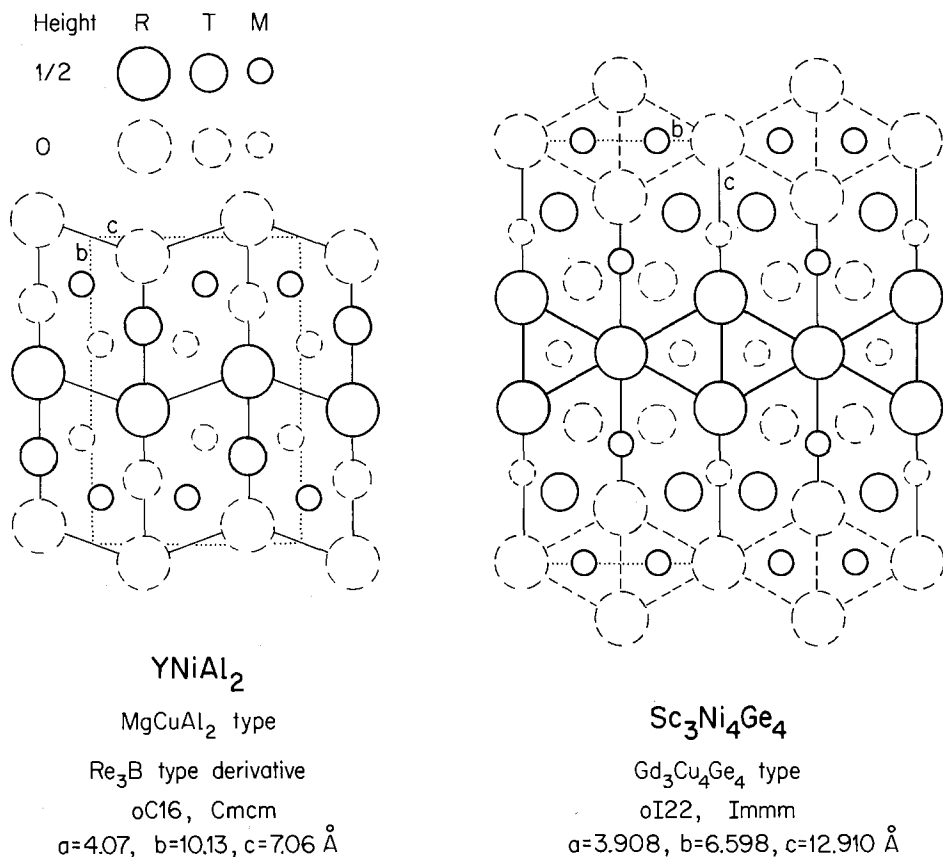


Fig. 29. The crystal structures of YNiAl<sub>2</sub> and Sc<sub>3</sub>Ni<sub>4</sub>Ge<sub>4</sub>.

The Sc<sub>3</sub>Ni<sub>4</sub>Ge<sub>4</sub> structure can also be compared with the 6360:Sc<sub>3</sub>Co<sub>2</sub>Si<sub>3</sub> structure. If one slices the Sc<sub>3</sub>Ni<sub>4</sub>Ge<sub>4</sub> structure parallel to (010) at  $y = 0$  and  $y = \frac{1}{2}$ , separates the slabs slightly, completes the atom halves ( $R_{3/2}T_2M_2 + R_{3/2}M = R_3T_2M_3$ ), and shifts the new slabs alternatively by  $c/2$ , an idealized model of the Sc<sub>3</sub>Co<sub>2</sub>Si<sub>3</sub> structure is obtained (see fig. 13).

It was shown above that the Sc<sub>3</sub>Ni<sub>4</sub>Ge<sub>4</sub> structure consists of trigonal prisms and sheets of face-joined R<sub>4</sub>T<sub>2</sub>M<sub>2</sub> columns. It is of interest to find out if a structure exists with only face-joined R<sub>4</sub>T<sub>2</sub>M<sub>2</sub> columns. Such a structure would have the composition 7533:RT<sub>2</sub>M and should have the MgCuAl<sub>2</sub>-type, a Re<sub>3</sub>B-type derivative. No 7533 compound of MgCuAl<sub>2</sub>-type exists but the aluminide 7567:YNiAl<sub>2</sub>, shown in the left-hand part of fig. 29, has this structure type. In this compound the T and M atoms in the characteristic columns have been interchanged. Here we have one other example of the unusual behaviour of Al as compared, for example, to Si and Ge in these compounds. Another example of site interchange has been discussed before with the ZrNiAl-type (see 6750:ScRuGe).

It should be mentioned that silicides and germanides with composition 7533 are

known. They crystallize with the  $\text{YPd}_2\text{Si}$ -type, a  $\text{Fe}_3\text{C}$ -type derivative. Geometrically, both binary types,  $\text{Fe}_3\text{C}$  and  $\text{Re}_3\text{B}$ , are closely related. Using the concept of periodic unit cell twinning they can be derived from base structures with different stackings (Chabot and Parthé, 1978).

7350	$\text{La}_3\text{Rh}_4\text{Ge}_4$	$\text{oI}22$	$a = 4.1746$	HoKP, 82
	or	$\text{Immm}$	$b = 4.2412$	
	$\text{La}_3\text{Rh}_2^{[6, \text{p}]} \text{Rh}_2^{[4\text{t}]}_2 [\text{Ge}_2^{[6, \text{p}]}] \text{Ge}_2$		$c = 25.234$	
$\text{U}_3\text{Ni}_4\text{Si}_4$ -type (YaAGFG, 79)				

#### Isotypic compounds:

$\text{Ce}_3\text{Ni}_4\text{Si}_4$ ?:  $\text{Ce}_6\text{Ni}_6\text{Si}_7$  has been reported with the same space group (BoG, 69). The similarity of composition and lattice parameters makes the isotypy with  $\text{La}_3\text{Rh}_4\text{Ge}_4$  likely.

$\text{La}_3\text{Rh}_4\text{Ge}_4$ : HoKP, 82

The structure of  $\text{La}_3\text{Rh}_4\text{Ge}_4$ , of  $\text{U}_3\text{Ni}_4\text{Si}_4$ -type, shown in fig. 30, can be considered as a periodic intergrowth of two kinds of slabs. One of these slabs with composition  $\text{LaRh}^{[6, \text{p}]} \text{Ge}^{[6, \text{p}]}$  is a segment of a ternary ordered  $\text{AlB}_2$ -type derivative structure [see 67(75): $\text{Ce}(\text{Ni}_{.25}\text{Si}_{.75})_2$ ] and the second with composition  $\text{LaRh}_2^{[4\text{t}]} \text{Ge}_2$  is a segment of the  $\text{ThCr}_2\text{Si}_2$  structure type, a ternary ordered  $\text{BaAl}_4$ -type derivative structure (see 8050: $\text{CeNi}_2\text{Si}_2$ ). The compound  $\text{LaRhGe}$  itself has not been studied, but  $\text{LaRh}_2\text{Ge}_2$  crystallizes with the  $\text{ThCr}_2\text{Si}_2$ -type with lattice constants as given in fig. 30 (Ho, 82).

According to Yarmolyuk et al. (YaAGFG, 79) the  $\text{U}_3\text{Ni}_4\text{Si}_4$ -type structure together with the 7567: $\text{CeNiSi}_2$  and 7780: $\text{Ce}_3\text{Ni}_2\text{Si}_8$  structures, the last two shown in fig. 31, are members of a structural series of formula  $\text{R}_{n+m}\text{T}_{2n}\text{M}_{4m}$ . The parameter  $n$  is the number of ordered  $\text{AlB}_2$  and  $m$  the number of ordered  $\text{BaAl}_4$  structure segments. The structural data for the members of this structural series and their  $n$  and  $m$  values are listed in table 10. We note that the two end-members of this

TABLE 10  
Structural data for the members of the structural series  $\text{R}_{n+m}\text{T}_{2n}\text{M}_{4m}$ , proposed by Yarmolyuk et al. (YaAGFG, 79).

$n$	$m$	Code	Composition	Structure type	Pearson's classif. symbol	Space group
$\infty$	0	6700	$\text{R T}_2$	$\text{AlB}_2$	hP3	P6/mmm
2	1	7350	$\text{R}_3\text{T}_4\text{M}_4$	$\text{U}_3\text{Ni}_4\text{Si}_4$	$\text{oI}22$	Immm
1	1	7567	$\text{R T M}_2$	$\text{CeNiSi}_2$	$\text{oC}16$	Cmcm
1	2	7780	$\text{R}_3\text{T}_2\text{M}_8$	$\text{Ce}_3\text{Ni}_2\text{Si}_8$	$\text{oC}26$	Cmmm
0	$\infty$	80100	$\text{R M}_4$	$\text{BaAl}_4$	tI10	I4/mmm

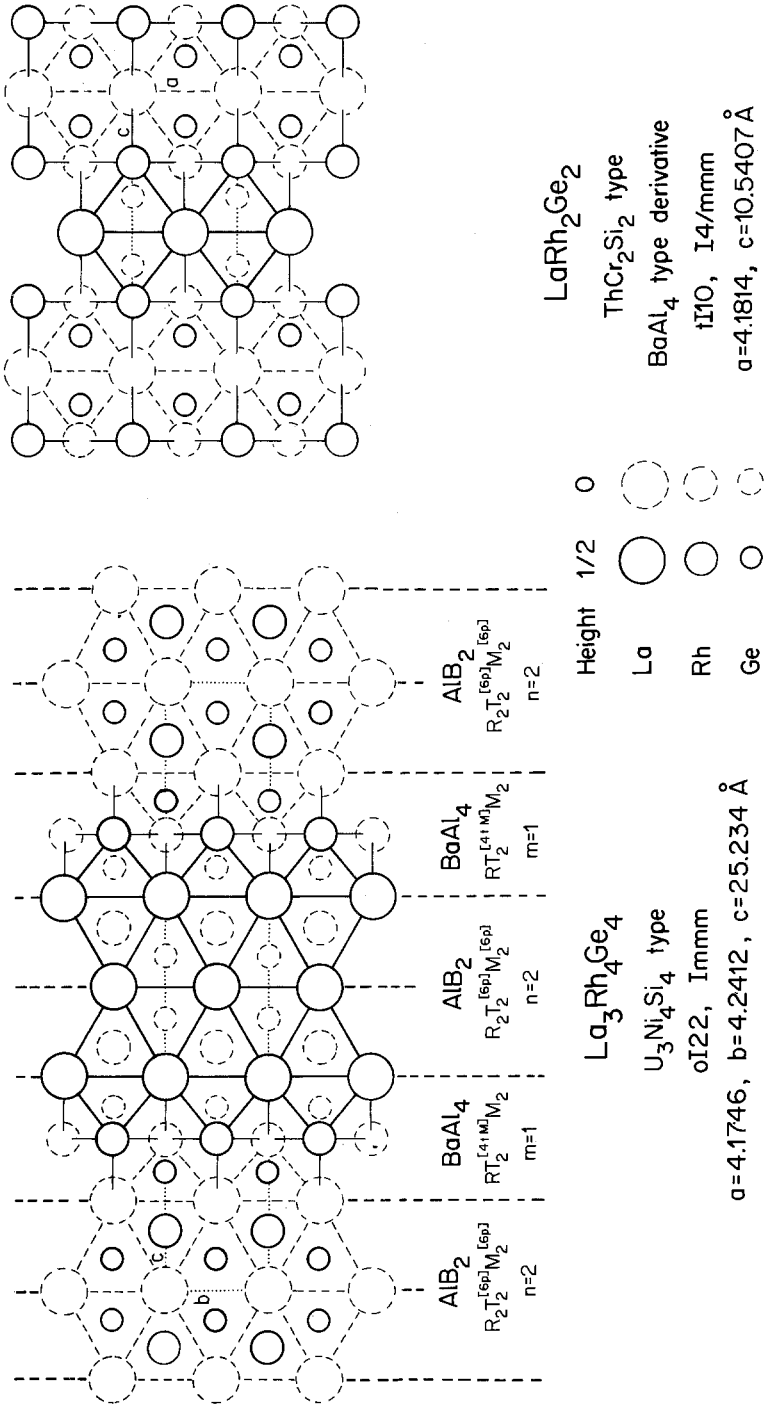


Fig. 30. The crystal structure of La<sub>3</sub>Rh<sub>4</sub>Ge<sub>4</sub>, compared with the structure of LaRh<sub>2</sub>Ge<sub>2</sub> having ThCr<sub>2</sub>Si<sub>2</sub>-type.

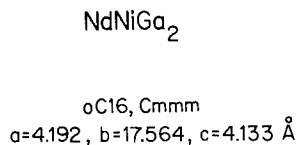
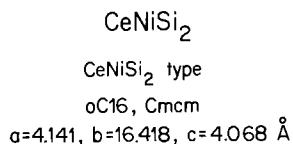
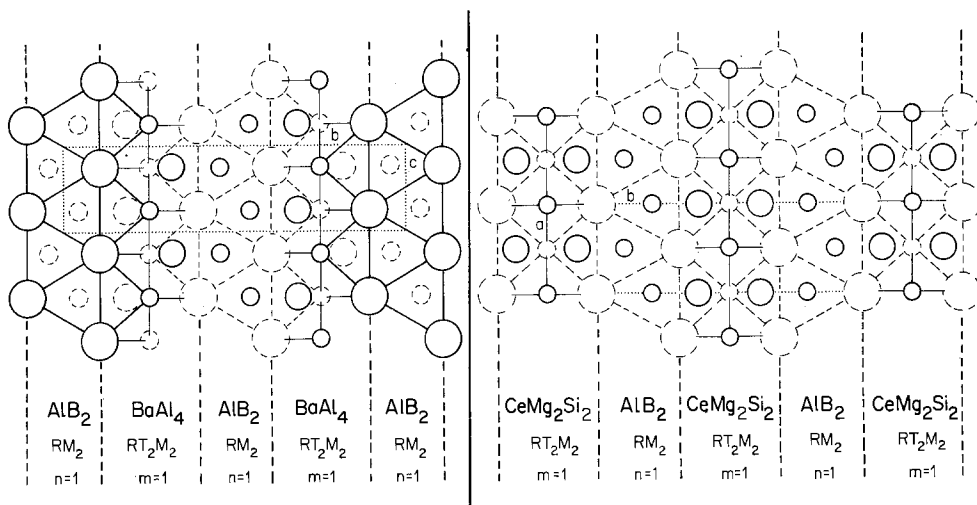
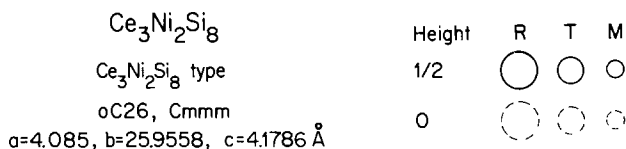
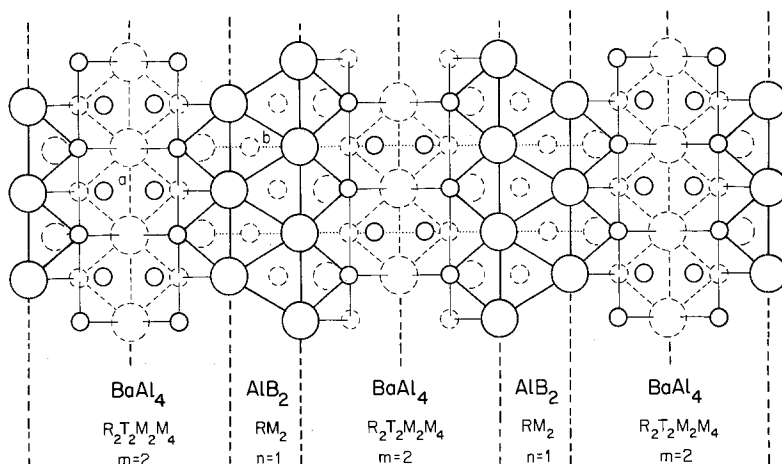


Fig. 31. The  $Ce_3Ni_2Si_8$  and  $CeNiSi_2$  structures together with the  $NdNiGa_2$  structure closely related to the latter.

structural series are  $RT_2$  with  $AlB_2$ -type ( $n = \infty, m = 0$ ) and  $RM_4$  with  $BaAl_4$ -type ( $n = 0, m = \infty$ ). Thus one might expect that in the structures of the members of this structural series all  $AlB_2$  slabs have composition  $RT_2$  and all  $BaAl_4$  slabs composition  $RM_4$ . This is, however, not the case. In  $CeNiSi_2$ , for example, the  $AlB_2$  slabs have composition  $RM_2$ . Similarly the Al sites in the  $BaAl_4$  slabs are not occupied by M atoms alone, but in the different structures by M and T atoms in different ratios. Nevertheless, in spite of these different site occupations, the overall chemical formula is correctly given by the structure series formula. We note that the trigonal rare earth prisms in  $La_3Rh_4Ge_4$  are compressed ( $a < b$ ) but stretched in  $CeNiSi_2$  ( $a > c$ ) and  $Ce_3Ni_2Si_8$  ( $c > a$ ). In the first case the prisms are centred by T and M atoms, in the last two compounds by M atoms only. It is known from studies of relative prism dimensions in binary RT and RM compounds that the prisms in the first are always compressed and in the latter always stretched.

For a more general discussion of structures which can be considered as an intergrowth of  $BaAl_4$  segments and segments of other simple structure types, see 8050:  $CeNi_2Si_2$ .

---

7364	$Sc_4Mn_4Si_7^*$ or $Sc_4Mn_4^{[60]}Si_6Si^{[8, a]}$	tI60 I4/mmm	$a = 13.06$ $c = 5.227$	KoBK, 80
------	--	----------------	----------------------------	----------

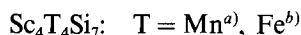
---

$Zr_4Co_4Ge_7$ -type (Je, 69) or V-phase type

---

\*In the publication on  $Sc_4Mn_4Si_7$  the Wyckoff position of the Si(2) is incorrectly given as 8j) instead of 8i). This probably explains why the  $R$  value would not go below 0.142.

Isotypic compounds:



<sup>a</sup>KoBK, 80    <sup>b</sup>B. Chabot, unpublished results [ $a = 13.099(4)$ ,  $c = 5.075(3)\text{Å}$ ]

The  $Sc_4Mn_4Si_7$  structure with  $Zr_4Co_4Ge_7$ -type together with the structures of  $Sc_2Cr_4Si_5$ ,  $ScFeSi_2$  and  $ZrMnSi_2$ , the last two having the same crystal-chemical formula, are shown in fig. 32.

All structures are characterized by two construction elements:

- parallel infinite rectilinear columns (perpendicular to the plane of projection) of Si-centred antiprisms,
- parallel infinite rectilinear columns (perpendicular to the plane of projection) of Cr, Mn, Fe-centred face-joined (deformed) octahedra formed by Si atoms.

The T atoms in the octahedron centres interact strongly with each other (more or less depending on the T element) through the common octahedron faces. The corresponding T–T distances are shorter than the sum of the metallic radii of the elements.

TABLE 11

Structural data for crystal structures characterized by infinite rectilinear columns of M-centred antiprisms and T-centred M octahedra.

Code	R-T-M compound	Structure type	Pearson's classif. symbol	Space group	Antiprism	Octahedron	Crystal-chemical formula
7364 (7567)	Sc <sub>4</sub> Mn <sub>4</sub> Si <sub>7</sub>	Zr <sub>4</sub> Co <sub>4</sub> Si <sub>7</sub>	tI60	I4/mmm	R <sub>8/2</sub> M <sup>[8a]</sup>	+ 4M <sub>6/4</sub> T <sup>[6a]</sup>	→ R <sub>4</sub> T <sub>4</sub> <sup>[6a]</sup> M <sub>6</sub> M <sup>[8, a]</sup>
		ZrMnSi <sub>2</sub>	oI48	Immm	R <sub>6/2</sub> T <sub>2/2</sub> M <sup>[(6, 2)a]</sup>	+ 2M <sub>4/4</sub> M <sub>2/2</sub> T <sup>[6a]</sup> + M→	R <sub>3</sub> T <sub>3</sub> <sup>[6a]</sup> M <sub>5</sub> M <sup>[(6, 2)a]</sup>
7567	ScFeSi <sub>2</sub>	ZrFeSi <sub>2</sub>	oC96	Cmca	R <sub>6/2</sub> T <sub>2/2</sub> M <sup>[(6, 2)a]</sup>	+ 2M <sub>4/4</sub> M <sub>2/2</sub> T <sup>[6a]</sup> + M→'	R <sub>3</sub> T <sub>3</sub> <sup>[6a]</sup> M <sub>5</sub> M <sup>[(6, 2)a]</sup>
8256	Sc <sub>2</sub> Cr <sub>4</sub> Si <sub>5</sub>	Nb <sub>2</sub> Cr <sub>4</sub> Si <sub>5</sub> V <sub>6</sub> Si <sub>5</sub> -type derivative	oI44	Ibam	R <sub>4/2</sub> T <sub>4/2</sub> M <sup>[(4, 4)a]</sup>	+ 2M <sub>4/4</sub> M <sub>2/2</sub> T <sup>[6a]</sup>	→ R <sub>2</sub> T <sub>2</sub> T <sub>2</sub> <sup>[6a]</sup> M <sub>4</sub> M <sup>[(4, 4)a]</sup>

The structural data and crystal-chemical formulae for all structures having those structural characteristics are given in table 11. The structures differ in the R/T ratio of the atoms which form the M-centred antiprisms and in the type of linkage of the centred octahedron columns with other octahedron columns (linkage by means of common octahedron edges). In ScFeSi<sub>2</sub> and ZrMnSi<sub>2</sub>, to complete the octahedral surrounding of those Fe or Mn atoms which participate in the formation of the antiprisms, extra Si atoms are positioned between the antiprism columns. Also the 7567:ScMnSi<sub>2</sub> structure with TiMnSi<sub>2</sub>-type is built up of M-centred antiprism columns and T-centred M octahedron columns (see fig. 44); however, the columns are not infinite; only column fragments of three joined polyhedra occur.

With the exception of Sc<sub>2</sub>Cr<sub>4</sub>Si<sub>5</sub> all T atoms which participate in the formation of the antiprisms are always octahedrally coordinated by Si atoms. This applies also to 8063:Sc<sub>2</sub>Fe<sub>3</sub>Si<sub>5</sub> (fig. 54).

7388	Y <sub>3</sub> ReB <sub>7</sub>	oC44	a = 3.525	KuM, 76
	or	Cmcm	b = 15.80	
	Y <sub>3</sub> Re ∞ (B <sub>6</sub> B <sup>[6, p]</sup> )		c = 9.366	

Isotypic compounds: All references KuM, 76

R<sub>3</sub>ReB<sub>7</sub>: R = Gd, Tb, Dy, Ho, Er, Tm, Y

The structure of Y<sub>3</sub>ReB<sub>7</sub>, shown in fig. 33, is characterized by a folded boron-boron chain, which extends infinitely in the [001] direction. The chain consists of fragments of a double chain connected by single boron atoms.

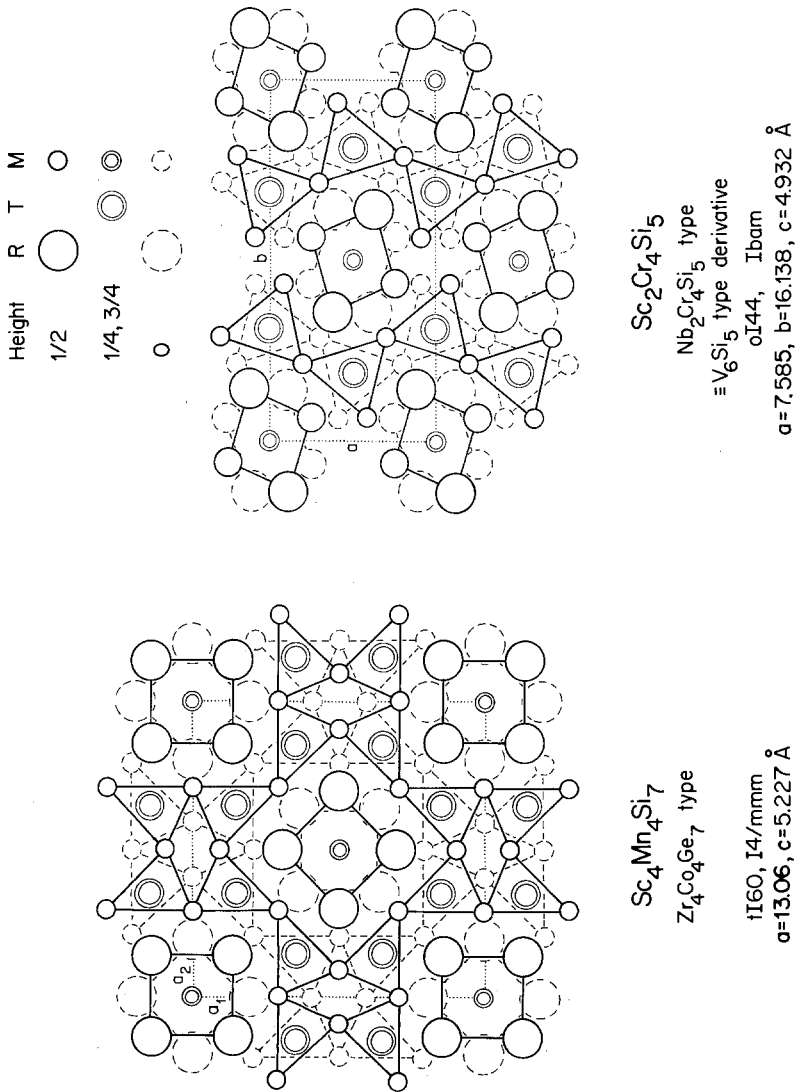


Fig. 32. The crystal structures of  $\text{Sc}_4\text{Mn}_4\text{Si}_7$ ,  $\text{Sc}_2\text{Cr}_4\text{Si}_5$  (above),  $\text{ScFeSi}_2$  and  $\text{ZrMnSi}_2$  (opposite page), all characterized by columns of T-centred Si-octahedra and columns of Si-centred antiprisms.



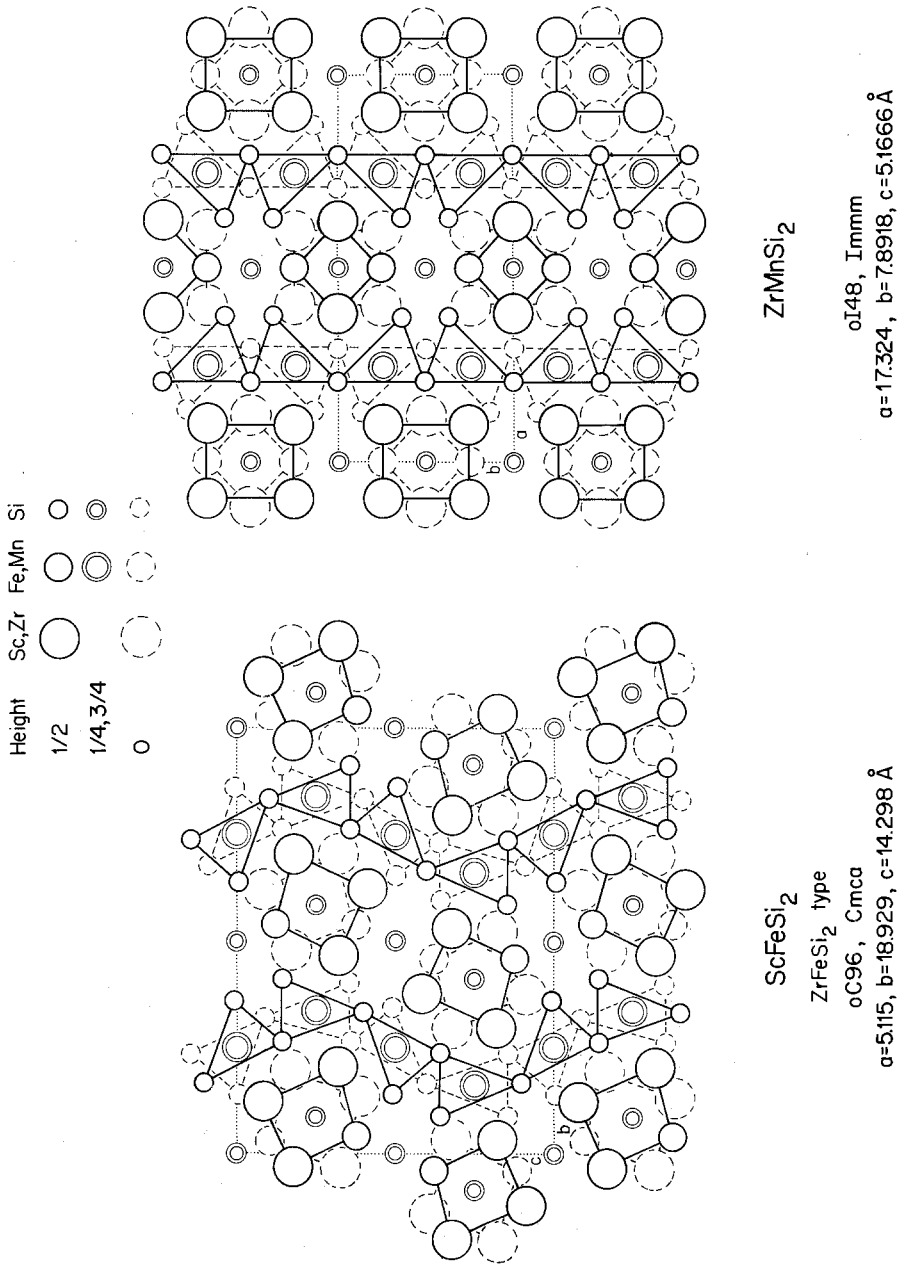


Fig. 32. continued.

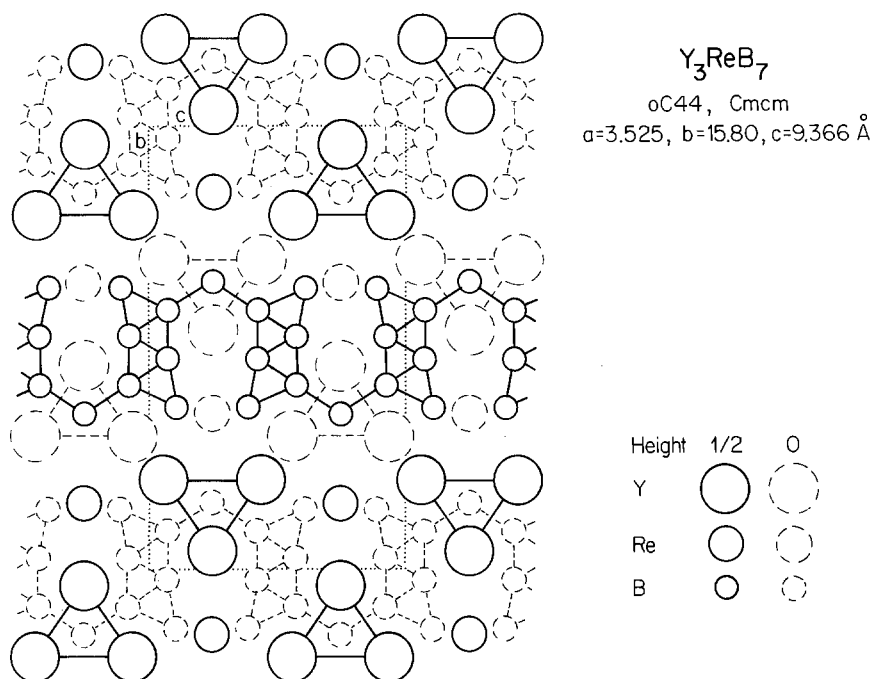


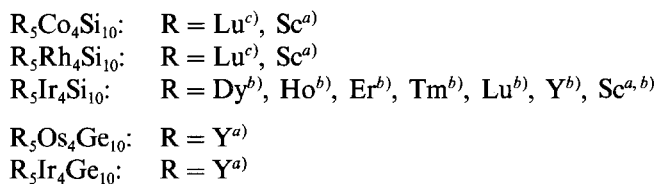
Fig. 33. The structure of  $Y_3ReB_7$ , with an infinite folded boron-boron chain.

---

<b>7471</b>	<b>Sc<sub>5</sub>Co<sub>4</sub>Si<sub>10</sub></b>	tP38	a = 12.01	<b>BrYB, 80</b>
	or	P4/mbm	c = 3.936	
	Sc <sub>5</sub> Co <sub>4</sub> Si <sub>8</sub> <sup>2</sup> [Si <sub>2</sub> <sup>6, p</sup> ]			

---

Isotypic compounds:



<sup>a</sup>)BrYB, 80    <sup>b</sup>)BrS, 81    <sup>c</sup>)Br, 82

The  $Sc_5Co_4Si_{10}$  structure and the geometrically related 7578:  $La_3Co_2Sn_7$  structure are shown in fig. 34. Both structures are built up of intergrown  $Cu_3Au$ -type segments and 7567:  $CeNiSi_2$ -type segments (see fig. 31). We note that the  $CeNiSi_2$  structure itself is built up of  $BaAl_4$ -type and  $AlB_2$ -type segments. In the  $La_3Co_2Sn_7$  structure

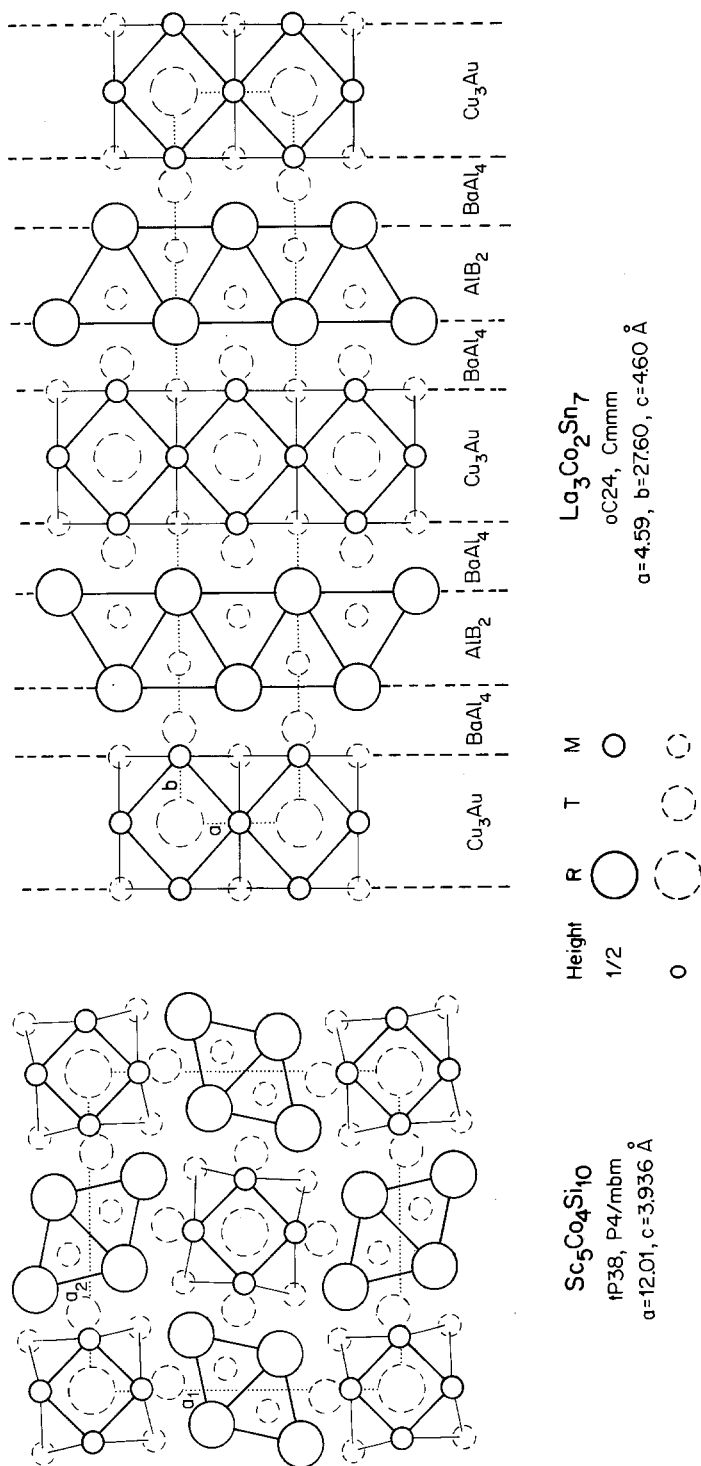


Fig. 34. The Sc<sub>5</sub>Co<sub>4</sub>Si<sub>10</sub> and the La<sub>3</sub>Co<sub>2</sub>Sn<sub>7</sub> structures, both built up of similar construction elements (segments of Cu<sub>3</sub>Au, BaAl<sub>4</sub> and AlB<sub>2</sub>).

there are intergrown slabs, in the  $\text{Sc}_5\text{Co}_4\text{Si}_{10}$  structure, however, intergrown columns. The composition of  $\text{La}_3\text{Co}_2\text{Sn}_7$  can be rationalized according to  $2\text{RTM}_2$  ( $\text{CeNiSi}_2$ -type slab) +  $\text{RM}_3$  ( $\text{Cu}_3\text{Au}$ -type slab) =  $\text{R}_3\text{T}_2\text{M}_7$ . For  $\text{Sc}_5\text{Co}_4\text{Si}_{10}$  we find  $\text{RM}_2$  ( $\text{AlB}_2$ -type column) +  $4\text{R}_{3/4}\text{TM}_{5/4}$  ( $\text{BaAl}_4$ -type column, edge-connected to four other columns) +  $\text{RM}_3$  ( $\text{Cu}_3\text{Au}$ -type column) =  $\text{R}_5\text{T}_4\text{M}_{10}$ .

7511	$\text{Ce}_3\text{Co}_8\text{Si}$	hP24 P6 <sub>3</sub> /mmc	$a = 4.960$ $c = 16.450$	Bo, 71
------	-----------------------------------	------------------------------	-----------------------------	--------

CeNi<sub>3</sub>-type (CrO, 59) derivative

Isotypic compounds:

R-Fe-Al: R = Tb<sup>g</sup>\*)

R<sub>3</sub>Ni<sub>8</sub>Al: R = Pr<sup>b,i</sup>, Nd<sup>c,i</sup>, Sm<sup>i</sup>, Gd<sup>d,i</sup>, Tb<sup>e,i</sup>, Dy<sup>e,i</sup>, Ho<sup>i</sup>, Er<sup>i</sup>, Tm<sup>i</sup>, Lu<sup>i</sup>, Yf<sup>i</sup>)

R<sub>3</sub>Co<sub>8</sub>Si: R = Ce<sup>a,h</sup>)

\*Composition is given as TbFe<sub>2</sub>Al.

<sup>a</sup>BoG, 70

<sup>b</sup>RyZK, 78

<sup>c</sup>RyZY, 79

<sup>d</sup>RyZM, 78

<sup>e</sup>RyZM, 80

<sup>f</sup>RyZ, 77

<sup>g</sup>Oe, 75

<sup>h</sup>Bo, 71

<sup>i</sup>Ry, 78

The  $\text{Ce}_3\text{Co}_8\text{Si}$  with CeNi<sub>3</sub> derivative structure is a member of the  $\text{R}_{2+n}\text{T}_{3+5n}\text{M}$  structural series (discussed below) with  $n = 1$ . It is composed of  $\text{CaCu}_5$ -type slabs and ordered ternary Laves-type slabs as found in 6725:  $\text{Sc}_2\text{Co}_3\text{Si}$  with  $\text{Mg}_2\text{Cu}_3\text{Si}$ -type (fig. 17). The atom arrangement in  $\text{Ce}_3\text{Co}_8\text{Si}$  can be conveniently compared with that of 7522:  $\text{Dy}_3\text{Ni}_7\text{B}_2$ , shown in fig. 38, another ternary ordered CeNi<sub>3</sub> derivative structure which belongs to another structural series  $\text{R}_{2+n}\text{T}_{4+3n}\text{M}_{2n}$  with  $n = 1$ . The CeNi<sub>3</sub>,  $\text{Ce}_3\text{Co}_8\text{Si}$  and  $\text{Dy}_3\text{Ni}_7\text{B}_2$  structures all have the same structure sites, but they differ in their occupation. In CeNi<sub>3</sub>, one finds intergrown  $\text{CaCu}_5$  and binary Laves-type slabs. In  $\text{Ce}_3\text{Co}_8\text{Si}$ , the Laves-type slab is replaced by an ordered ternary Laves-type slab; however, in  $\text{Dy}_3\text{Ni}_7\text{B}_2$  it is the  $\text{CaCu}_5$ -type slab which is replaced by a ternary ordered  $\text{CaCu}_5$ -type slab, i.e. a  $\text{CeCo}_3\text{B}_2$ -type slab.

For a better understanding of the  $\text{Ce}_3\text{Co}_8\text{Si}$  structure and the large group of ternary structures, all to be interpreted as intergrown (binary and/or ternary) Laves-type and/or  $\text{CaCu}_5$ -type slabs, it is useful to discuss first the corresponding binary structures.

In binary systems R-T several intermetallic compounds with composition between  $\text{RT}_2$  and  $\text{RT}_5$  are formed. These can be grouped in the structure series  $\text{R}_{2m+n}\text{T}_{4m+5n}$ . The parameter  $m$  indicates the number of Laves-type slabs  $\text{R}_2\text{T}_4$  and  $n$  the number of  $\text{CaCu}_5$ -type slabs  $\text{RT}_3$ . The structures can be conveniently presented if the hexagonal structure blocks are referred to orthohexagonal axes and projected along

the orthohexagonal axis (perpendicular to the  $(11\bar{2}0)$  plane of the hexagonal cell) as shown in fig. 35 (Parthé and Lemaire, 1975). The members of the  $R_{2m+n}T_{4m+5n}$  structural series are obtained by stacking  $n$   $RT_5$  blocks on top of  $m$   $R_2T_4$  blocks. However, so far only structures with  $m = 1$  or  $\infty$  are known and the formula of the series simplifies to  $R_{2+n}T_{4+5n}$ . One can distinguish two subseries depending on whether subsequent  $R_2T_4$  are stacked as in the hexagonal Laves phase (hexagonal subseries where all structures have space group  $P6_3/mmc$ ) or as in the cubic Laves phase (rhombohedral subseries with space group  $R\bar{3}m$ ). The block stacking for both binary subseries is shown in fig. 36.

All known ternary structures are derivatives of the structures of the hexagonal subseries. In the ternary structures we also find  $R_2T_4$  and  $RT_5$  blocks. However, some  $R_2T_4$  blocks may be replaced by  $R_2T_3M$  blocks and some  $RT_5$  blocks by  $RT_3M_2$  blocks.

The  $R_2T_3M$  block is identical to the  $R_2T_4$  block except that one T atom is replaced by an M atom. The atom arrangement in the  $R_2T_3M$  block, which corresponds to the  $Mg_2Cu_3Si$ -type, can be studied in the left hand part of fig. 17, a drawing of the  $6725:Sc_2Co_3Si$  structure with two  $R_2T_3M$  slabs per unit cell.

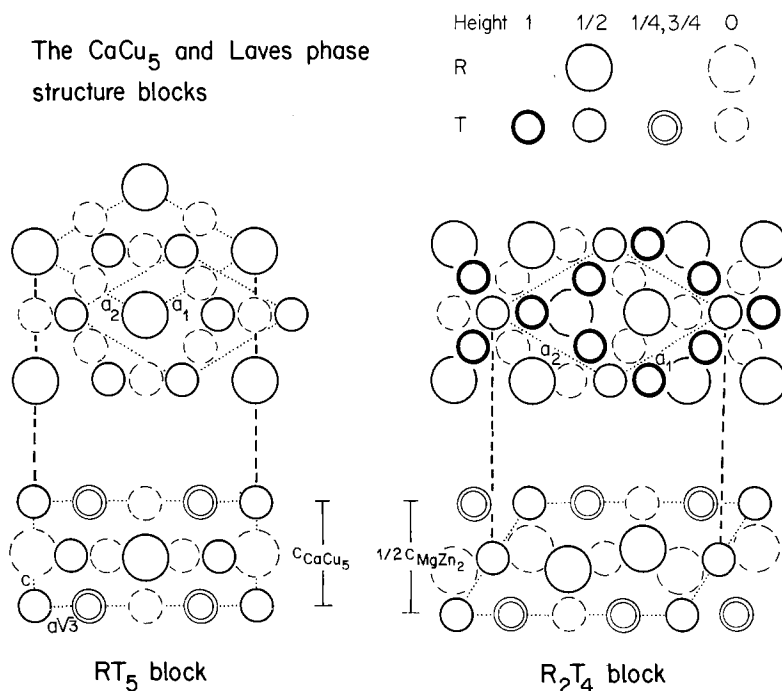


Fig. 35. The  $RT_5$  and  $R_2T_4$  structure blocks used in the binary  $R_{2+n}T_{4+5n}$  structural series, after Parthé and Lemaire (1975). The upper part shows the  $CaCu_5$  structure and one half of the unit cell of the  $MgZn_2$  structure in a projection along their hexagonal  $c$  axes. The lower part shows the structure blocks derived from the corresponding orthohexagonal unit cells projected along a short orthohexagonal axis. The  $RT_5$  block is a rectangular prism [ $\sqrt{3} a(CaCu_5) \times a(CaCu_5) \times c(CaCu_5)$ ], the  $R_2T_4$  block is a parallelepiped with two right angles [base:  $\sqrt{3} a(MgZn_2) \times a(MgZn_2)$ , height:  $\frac{1}{2}c(MgZn_2)$ ].

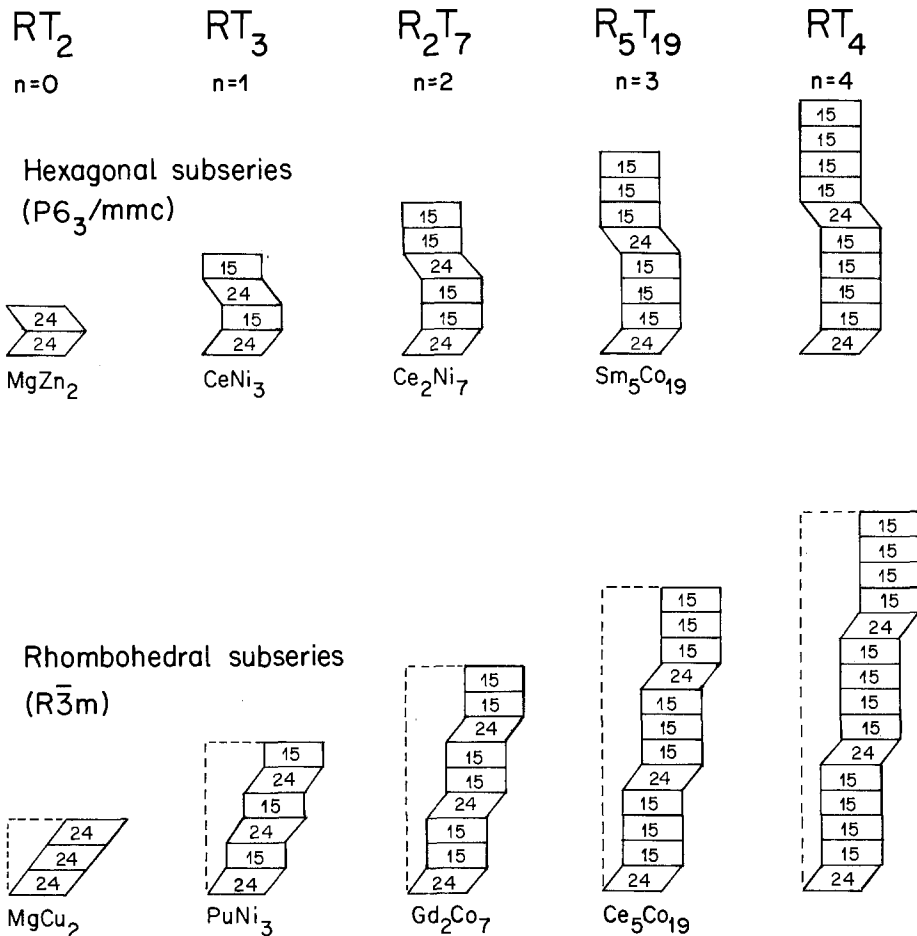


Fig. 36. Block stacking for the hexagonal and rhombohedral  $R_{2+n}T_{4+5n}$  structural series, after Parthé and Lemaire (1975). 24 denotes a  $R_2T_4$  block as found in the Laves phase structures and 15 a  $RT_3$  block with an atom arrangement as in the  $CaCu_5$ -type.

The  $RT_3M_2$  block is identical to the  $RT_5$  block, except that two T atoms are replaced by two M atoms, which leads, in the case of borides, to a small reduction of the height of the block. The  $RT_3M_2$  block can be seen in the last drawing of fig. 37. It corresponds to the 8340:  $CeCo_3B_2$  structure.

Slabs made of these different structure blocks can be intergrown in different ways, giving rise to three different ternary structural series:

(a) A  $R_{m+n}T_{5m+3n}M_{2n}$  structural series with intergrown  $CaCu_5$ -type and  $CeCo_3B_2$ -type slabs. The structures listed in table 12 and shown in fig. 37 all have composition code 83... and can be obtained by stacking  $m$   $CaCu_5$ -type slabs on top of  $n$   $CeCo_3B_2$ -type slabs. All structures are  $CaCu_5$ -type derivative structures.

TABLE 12

Structural data of the  $R_{m+n}T_{5m+3n}M_{2n}$  structural series, where the structures are built up of  $m$   $CaCu_5$ -type slabs and  $n$   $CeCo_3B_2$ -type slabs. All structures are  $CaCu_5$ -type derivatives.

$m$	$n$	Code	Structure type	Pearson's classif. symbol	Space group
$\infty$	0	8300	$CaCu_5$	hP6	P6/mmm
2	1	8313	$Nd_3Ni_{13}B_2$	hP18	P6/mmm
1	1	8320	$CeCo_4B$	hP12	P6/mmm
1	2	8327	$Ce_3Co_{11}B_4$	hP18	P6/mmm
1	3	8330	$Ce_2Co_7B_3$	hP24	P6/mmm
0	$\infty$	8340	$CeCo_3B_2$	hP6	P6/mmm

TABLE 13

Structural data for the binary structural series  $R_{2+n}T_{4+5n}$  ( $Mg_2Zn_4 + n CaCu_5$ ), the ternary structural series  $R_{2+n}T_{4+3n}M_{2n}$  ( $Mg_2Zn_4 + n CeCo_3B_2$ ) and ternary structural series  $R_{2+n}T_{3+5n}M$  ( $Mg_2Cu_3Si + n CaCu_5$ ). The classification symbol after Pearson and the space group are the same for corresponding structures of the binary and ternary structural series.

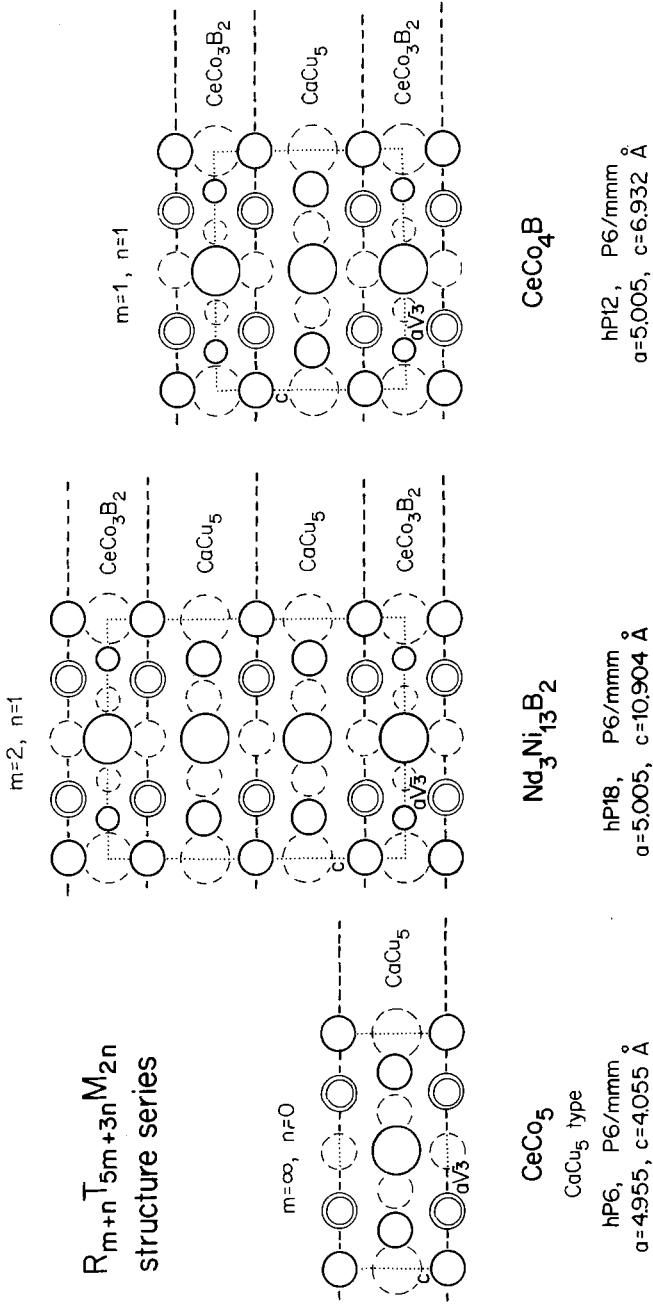
$n$	$R_{2+n}T_{4+5n}$			$R_{2+n}T_{4+3n}M_{2n}$		$R_{2+n}T_{3+5n}M$	
	Structure type	Pearson's classif. symbol	Space group	Code	Structure type	Code	Structure type
0	$MgZn_2$	hP12	$P6_3/mmc$	6700	$MgZn_2$	6725	$Sc_2Co_3Si$
1	$CeNi_3$	hP24	$P6_3/mmc$	7522	$Dy_3Ni_7B_2$	7511	$Ce_3Co_8Si$
2	$Ce_2Ni_7$	hP36	$P6_3/mmc$	7829	$Ce_3Co_3B_2$	7807	$R_4T_{13}M$
3	$Sm_5Co_{19}$	hP48	$P6_3/mmc$	7932	$R_5T_{13}M_6$		
4	$RT_4$	hP56	$P6_3/mmc$	8033	$R_3T_8M_4$		
$\infty$	$CaCu_5$	hP6	$P6/mmm$	8340	$CeCo_3B_2$	8300	$CaCu_5$

(b) A  $R_{2+n}T_{4+3n}M_{2n}$  structural series with intergrown  $MgZn_2$  and  $CeCo_3B_2$ -type slabs. In the structures listed in the middle of table 13 and shown in fig. 38 there are, stacked on top of every  $MgZn_2$ -type slab,  $n$   $CeCo_3B_2$ -type slabs. All structures are ternary derivatives of the structures of the binary  $R_{2+n}T_{4+5n}$  structural series.

(c) A  $R_{2+n}T_{3+5n}M$  structural series with intergrown  $Mg_2Cu_3Si$ -type slabs and  $CaCu_5$ -type slabs. The structures listed in the right-hand part of table 13 are composed of one ordered ternary Laves-type (i.e.  $Mg_2Cu_3Si$ -type) slab and  $n$   $CaCu_5$ -type slabs. All structures are ternary derivatives of the structures of the binary  $R_{2+n}T_{4+5n}$  structural series.

In fig. 39 an enlargement of the composition triangle shown in figs. 1 and 2 is given together with the composition lines of the one binary and three ternary structural series.

$R_{m+n}T_{5m+3n}M_{2n}$   
structure series





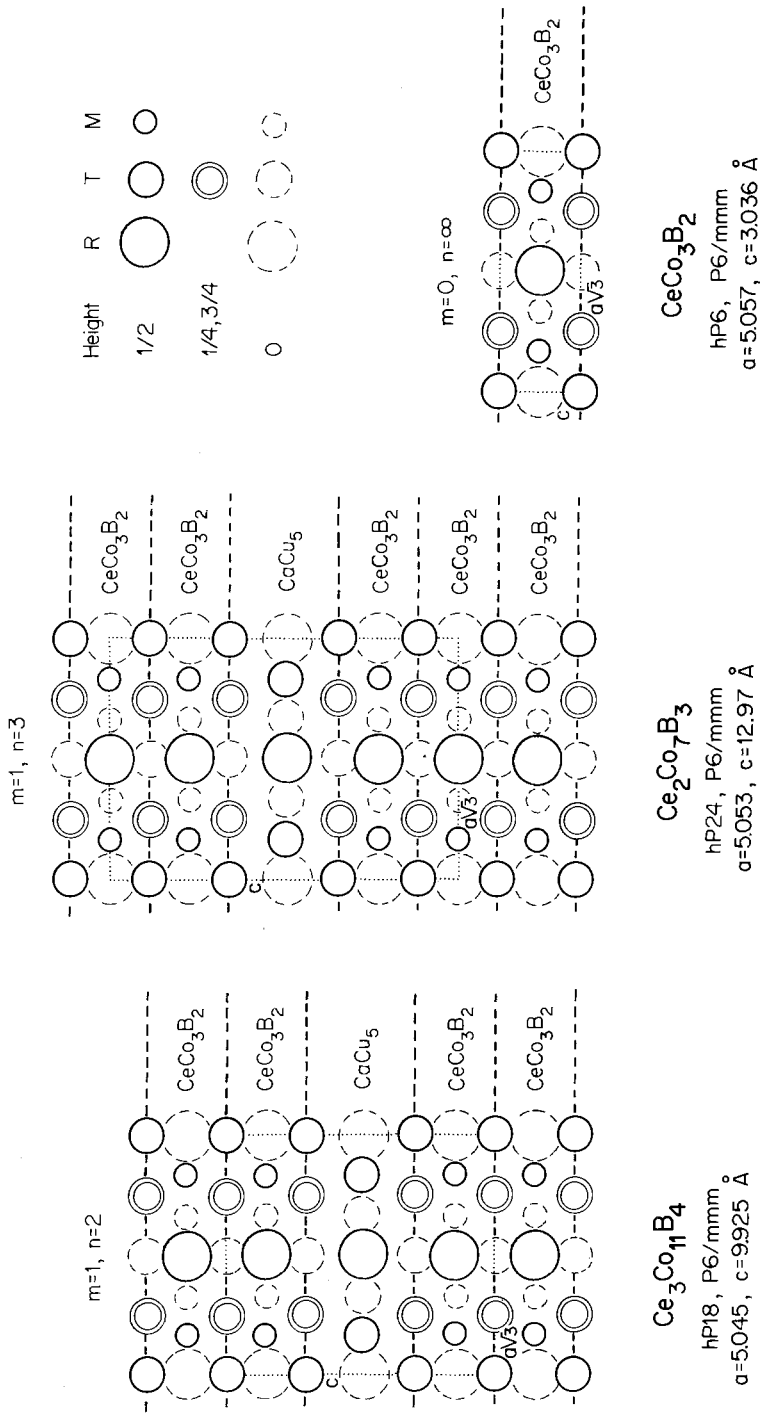


Fig. 37. The  $\text{CaCu}_5$ -type derivative structures of the  $\text{R}_{m+n}\text{T}_{3m+3n}\text{M}_{2n}$  structural series built up of  $\text{CaCu}_5$ - and  $\text{CeCo}_3\text{B}_2$ -type slabs. All structures are hexagonal. Here are shown orthohexagonal cells ( $a_0 = a_b\sqrt{3}, b_0 = a_b, c_0 = c_b$ ) in a projection along the  $b_0$  axis.

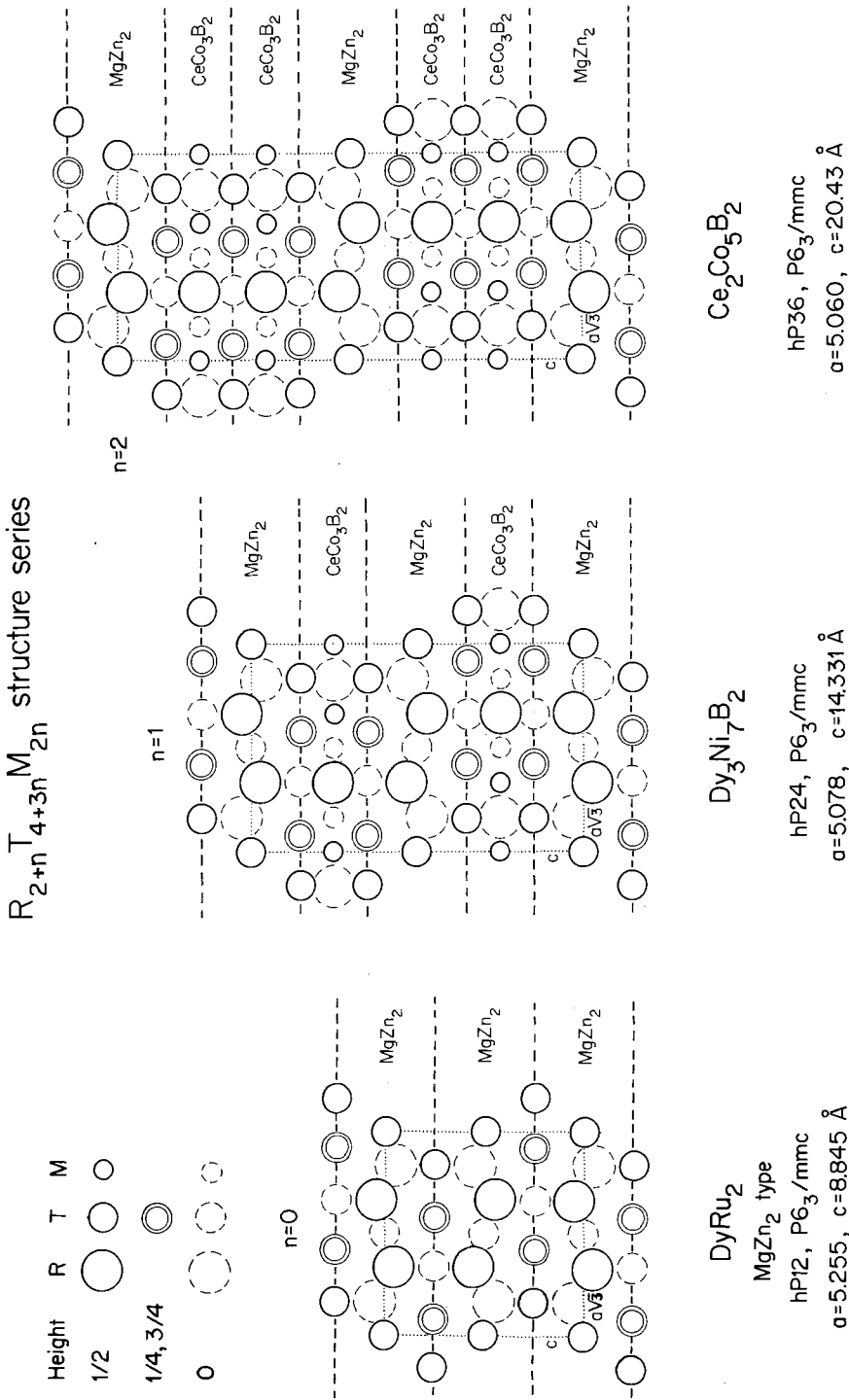


Fig. 38. The structures of the  $R_{2+n}T_{4+3n}M_{2n}$  structural series built up of  $R_2T_4$  blocks as found in Laves phases and of  $RT_3M_5$  blocks as in  $CeCo_3B_2$  with  $CaCu_5$  derivative structure. All structures are hexagonal. Here are shown orthohexagonal cells ( $a_0 = a_b\sqrt{3}$ ,  $b_0 = a_b$ ,  $c_0 = c_b$ ) in a projection along the  $b_0$  axis.

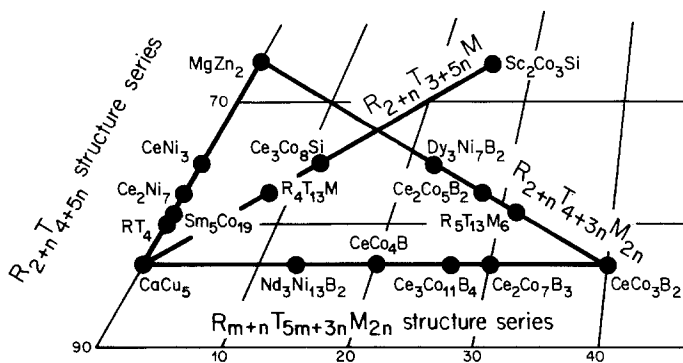


Fig. 39. Composition lines for four structural series, three of which are built up of binary or ternary Laves-type slabs ( $\text{MgZn}_2$ - or  $\text{Mg}_2\text{Cu}_3\text{Si}$ -type) and  $\text{CaCu}_5$ - or  $\text{CeCo}_3\text{B}_2$ -type slabs and one series of  $\text{CaCu}_5$ - and  $\text{CeCo}_3\text{B}_2$ -type slabs only.

7522	$\text{Dy}_3\text{Ni}_7\text{B}_2$	hP24	$a = 5.078$	KuC, 80
		$\text{P6}_3/\text{mmc}$	$c = 14.331$	

$\text{CeNi}_3$ -type (CrO, 59) derivative

Isotypic compounds:

$\text{R}_3\text{Ni}_7\text{B}_2$ : R =  $\text{Nd}^a$ ,  $\text{Sm}^b$ ,  $\text{Gd}^{a,b}$ ,  $\text{Tb}^{a,b}$ ,  $\text{Dy}^{a,b}$ ,  $\text{Ho}^{a,b}$ ,  $\text{Er}^{a,b}$ ,  $\text{Tm}^{a,b}$ ,  $\text{Lu}^{a,b}$ ,  $\text{Y}^{a,b}$

<sup>a</sup>KuBMS, 79

<sup>b</sup>KuC, 80

The  $\text{Dy}_3\text{Ni}_7\text{B}_2$  structure, shown in fig. 38, is a member of the  $\text{R}_{2+n}\text{T}_{4+3n}\text{M}_{2n}$  structural series with  $n = 1$  and is built up of Laves-type slabs and  $\text{CeCo}_3\text{B}_2$ -type slabs. It is discussed with the 7511: $\text{Ce}_3\text{Co}_8\text{Si}$  structure. The latter structure is also a  $\text{CeNi}_3$ -type derivative but constructed of intergrown  $\text{Mg}_2\text{Cu}_3\text{Si}$ -type slabs and  $\text{CaCu}_5$ -type slabs.

Three structure types are found with composition 7533: the  $\text{PrCo}_2\text{Ga}$ -type, oP8, the  $\text{YPd}_2\text{Si}$ -type, oP16, and the  $\text{MnCu}_2\text{Al}$  (Heusler phase)-type, cF16, discussed with  $\text{YPd}_2\text{Sn}$ .

7533	$\text{PrCo}_2\text{Ga}$	oP8	$a = 5.021$	YaK, 76
	or	Pmma	$b = 4.043$	
	$\text{PrCo}_2\text{Ga}^{[6p]}$		$c = 6.860$	

Isotypic compounds: All references YaK, 76



The  $\text{PrCo}_2\text{Ga}$  structure, shown in fig. 40, can be considered as an intergrowth of  $8340:\text{CeCo}_3\text{B}_2$ -type slabs (see fig. 58) and CsCl-type slabs according to

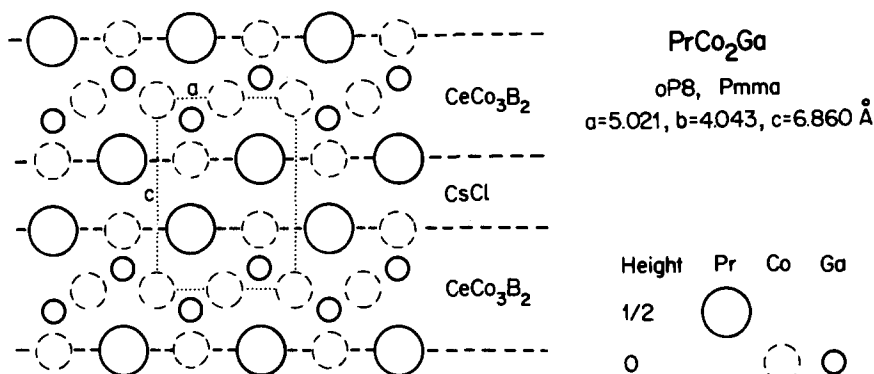
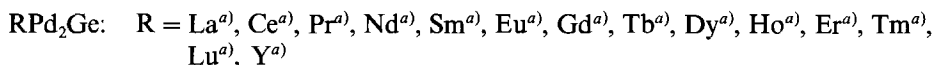
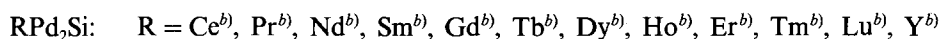
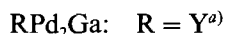


Fig. 40. The  $\text{PrCo}_2\text{Ga}$  structure, a periodic intergrowth of  $\text{CeCo}_3\text{B}_2$ - and CsCl-type slabs.

7533	$\text{YPd}_2\text{Si}$ or $\text{YPd}_2\text{Si}^{(2,4)\text{P}}$	oP16 Pnma	$a = 7.300$ $b = 6.927$ $c = 5.499$	MoLP, 82
------	--	--------------	---	----------

$\text{Fe}_3\text{C}$ -type ( $\text{D0}_{11}$ -type) derivative

Isotypic compounds:



<sup>a</sup>)JoIH, 83

<sup>b</sup>)MoLP, 82

The  $\text{YPd}_2\text{Si}$  structure, a segment of which ( $0 < y < \frac{1}{2}$ ) is shown in the left-hand part of fig. 41, is a  $\text{Fe}_3\text{C}$ -type derivative. Each Si (C) atom is in the centre of a trigonal

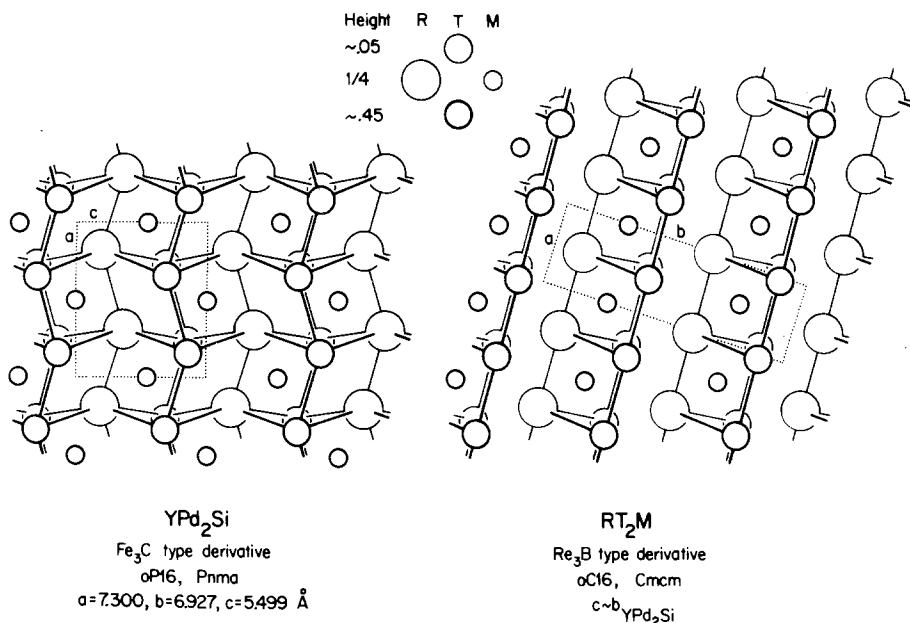


Fig. 41. Segments of YPd<sub>2</sub>Si structure ( $0 < y < \frac{1}{2}$ ) with Fe<sub>3</sub>C-type derivative and of hypothetical RT<sub>2</sub>M structure ( $0 < z < \frac{1}{2}$ ) with Re<sub>3</sub>B-type derivative. The latter structure with T and M sites interchanged is found with YNiAl<sub>2</sub>.

prism formed of two Y and four Pd atoms (six Fe atoms). The Fe<sub>3</sub>C-type is very common in binary R<sub>3</sub>T compounds (78 examples). Structurally related to the Fe<sub>3</sub>C-type is the Re<sub>3</sub>B-type (ArBR, 60) found, for example, with Pu<sub>3</sub>Co, Zr<sub>3</sub>Co and Ca<sub>3</sub>Zn. Both structure types are characterized by centred trigonal prisms and each atom forming a prism participates in two prisms [prism linkage coefficient LC = 2, see Parthé (1981) and Parthé and Moreau (1977)]. The two structures differ only in the way the prisms are linked. In Fe<sub>3</sub>C and YPd<sub>2</sub>Si the centred prisms are connected to form nets (two prism nets perpendicular to *b*, only one shown in fig. 41), but in Re<sub>3</sub>B they form isolated infinite columns of prisms. Using the concept of periodic unit cell twinning the Fe<sub>3</sub>C-type can be derived from a hexagonal close packed base structure and the Re<sub>3</sub>B-type from a cubic close packed base structure (Chabot and Parthé, 1978). The close relationship of the binary structure types suggests the possible existence of a ternary Re<sub>3</sub>B-type derivative RT<sub>2</sub>M, a segment of which ( $0 < z < \frac{1}{2}$ ) is shown in the right-hand part of fig. 41 (four columns parallel to *a* per unit cell, only two of which are shown in fig. 41). No silicide or germanide is known with this structure\*, but an aluminide exists. However, here the T sites are occupied by Al atoms and the M sites by T atoms. See 7567:YNiAl<sub>2</sub> and a further discussion with 7350:Sc<sub>3</sub>Ni<sub>4</sub>Ge<sub>4</sub>.

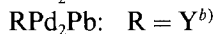
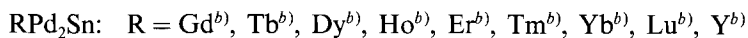
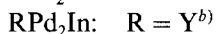
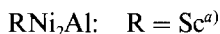
\*It should be mentioned, that a Re<sub>3</sub>B-type derivative structure has recently been found for TaCo<sub>2</sub>B (StRN, 79; NoRS, 82), however, as compared to the drawing given on the right of fig. 41, with the *a* and *b* axes doubled and space group Cm2m.

7533	<b>YPd<sub>2</sub>Sn</b> or Y <sup>[8, c]</sup> Pd <sub>2</sub> <sup>[(4, 4)c]</sup> Sn <sup>[, 8c]</sup>	cF16 Fm3m	$a = 6.720^*$	IsJJ, 82
------	---	--------------	---------------	----------

MnCu<sub>2</sub>Al (Heusler phase)-type  $\equiv$  CsCl-type derivative

\*From unpublished single crystal studies by K. Yvon.

Isotypic compounds:



<sup>a)</sup>GoR, 68    <sup>b)</sup>IsJJ, 82

The YPd<sub>2</sub>Sn structure with MnCu<sub>2</sub>Al (Heusler phase)-type is shown in fig. 42. This face-centred structure is a superstructure of the CsCl-type.

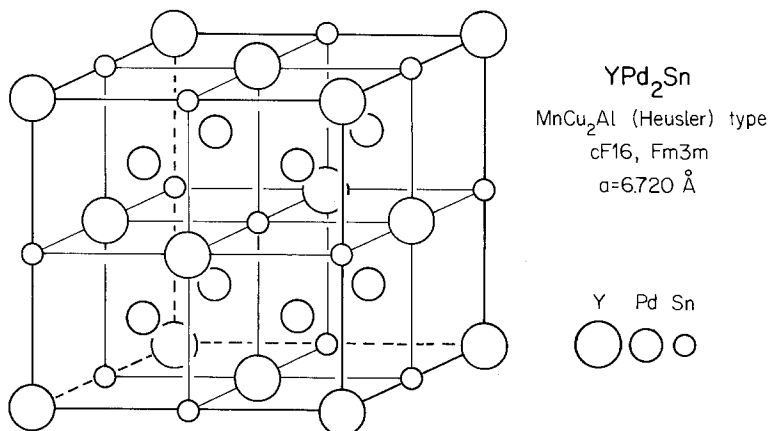


Fig. 42. The YPd<sub>2</sub>Sn structure with MnCu<sub>2</sub>Al (Heusler phase)-type.

Eight structure types are found with composition 7567:

- ScRhSi<sub>2</sub>-type, oP16,
- LuRuB<sub>2</sub>-type, oP16,
- CeNiSi<sub>2</sub> (or BaCuSn<sub>2</sub>)-type, oC16,
- TbFeSi<sub>2</sub>-type, oC16,
- NdNiGa<sub>2</sub>-type, oC16,
- MgCuAl<sub>2</sub>-type, oC16 (see YNiAl<sub>2</sub>),
- TiMnSi<sub>2</sub>-type, oP48 (see ScMnSi<sub>2</sub>),
- ZrFeSi<sub>2</sub>-type, oC96 (see ScFeSi<sub>2</sub>).

7567	ScRhSi <sub>2</sub>	oP16	<i>a</i> = 6.292	ChBYP, 81
	or	Pnma	<i>b</i> = 4.025	
	ScRh <sup>[4t]</sup> ⚬ Si <sub>2</sub> <sup>[+2]</sup>		<i>c</i> = 9.517	

Related to NbCoB<sub>2</sub>-type (Ku, 76), YZn<sub>3</sub>-type (MiR, 68) derivative\*

\*The NbNiP<sub>2</sub>-type (GhGPS, 81) has the same Pearson symbol, space group and Wyckoff positions, but is neither isotypic to ScRhSi<sub>2</sub> nor to NbCoB<sub>2</sub>.

No other isotypic RTM<sub>2</sub> compounds are known

The structure of ScRhSi<sub>2</sub>, a YZn<sub>3</sub>-type derivative, shown on the upper left of fig. 43, is composed of *l*-R<sub>4</sub>T<sub>2</sub>M<sub>2</sub> and *r*-R<sub>4</sub>T<sub>2</sub>M<sub>2</sub> columns which are presented in fig. 14 and discussed with 6067:Sc<sub>2</sub>CoSi<sub>2</sub>. These characteristic columns are identical with those found in 6750:ScRhSi with TiNiSi-type, where the Rh atoms are in the centres of silicon tetrahedra. In ScRhSi<sub>2</sub> the Si atoms form infinite Si-Si zig-zag chains parallel to *b*.

The ScRhSi<sub>2</sub> structure is related to the NbCoB<sub>2</sub> structure (Ku, 76), shown in the lower part of fig. 43, both having the same space group, the same equipoints and the same structural features. However, the much shorter B-B bonds in the zig-zag chains lead not only to different unit cell ratios, but also to considerable changes in the adjustable parameters of the atom positions. The axial ratios for the compounds of interest are as follows:

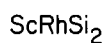
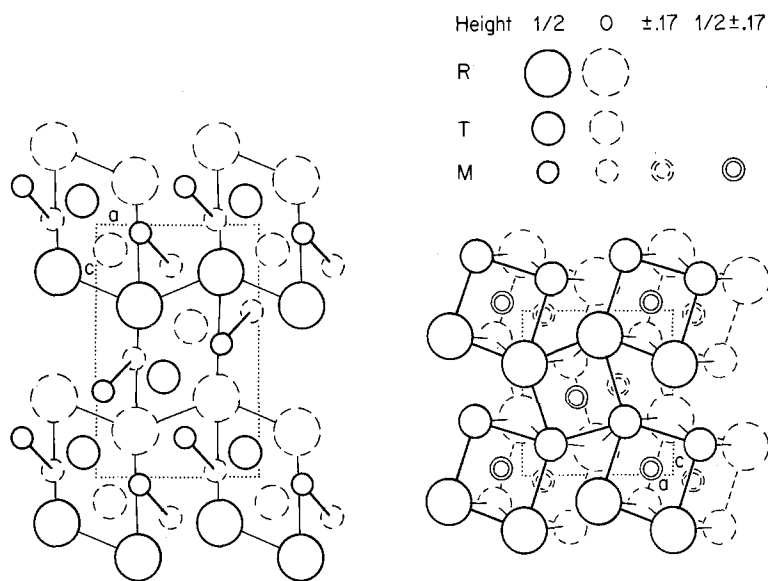
	ScRhSi <sub>2</sub>	YZn <sub>3</sub>	NbCoB <sub>2</sub>
<i>c/a</i>	1.512	1.51	1.356
<i>c/b</i>	2.364	2.30	2.627

A comparison of the ScRhSi<sub>2</sub> and NbCoB<sub>2</sub> drawings in fig. 43 indicates that in the boride the columns not only have a different shape but are also rotated with respect to each other. It appears therefore appropriate to call both structures not isotypic, but only geometrically related. Kuzma (1976) has described the NbCoB<sub>2</sub> structure as an arrangement of intergrown segments of CrB and FeB. In the right-hand part of the NbCoB<sub>2</sub> drawing the trigonal prisms are emphasized.

The third structure shown in fig. 43, the 7567:LuRuB<sub>2</sub> structure, differs from the first two in various aspects. The axial ratios are quite different (*c/a* = 1.082, *c/b* = 1.202) and the boron atoms now form dumbbells instead of zig-zag chains.

One recognizes boron-centred trigonal prisms formed of three Lu and three Ru atoms. The structure can be described as being built up of slabs of the FeB structure\* which are shifted with respect to each other.

\*To obtain a projection of the FeB structure similar to that of LuRuB<sub>2</sub> in fig. 43, the structure has to be projected approximately along <184>.



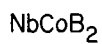
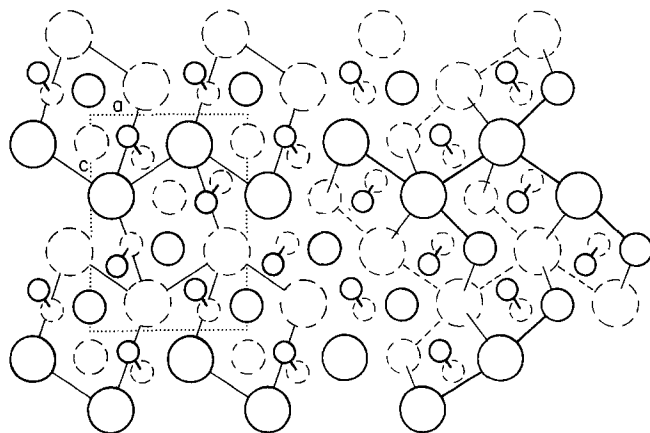
oP16, Pnma

$a=6.292$ ,  $b=4.025$ ,  $c=9.517 \text{ \AA}$



oP16, Pnma

$a=5.809$ ,  $b=5.229$ ,  $c=6.284 \text{ \AA}$



oP16, Pnma

$a=6.057$ ,  $b=3.127$ ,  $c=8.215 \text{ \AA}$

Fig. 43. The crystal structures of ScRhSi<sub>2</sub>, NbCoB<sub>2</sub> and LuRuB<sub>2</sub>, all having the same Pearson classification symbol and space group.



7567	<b>LuRuB<sub>2</sub></b>	oP16	$a = 5.809$	ShKPJK, 80
	or	Pnma	$b = 5.229$	
	LuRu <sub>2</sub> <sup>z</sup> [B <sub>2</sub> ]		$c = 6.284$	

Isotypic compounds: All references ShKPJK, 80

RRuB<sub>2</sub>: R = Tb, Dy, Ho, Er, Tm, Lu, Y

ROsB<sub>2</sub>: R = Tb, Dy, Ho, Er, Tm, Lu, Y, Sc

The LuRuB<sub>2</sub> structure, characterized by B–B dumbbells, is shown in fig. 43 and discussed with 7567:ScRhSi<sub>2</sub>.

7567	<b>CeNiSi<sub>2</sub></b>	oC16	$a = 4.141$	BoG, 70a
	or	Cmcm	$b = 16.418$	
	CeNiSi <sup>[4t]</sup> $\frac{1}{2}$ Si <sup>[6, p]</sup>		$c = 4.068$	

CeNiSi<sub>2</sub>-type (BoG, 70a) or BaCuSn<sub>2</sub>-type (MaS, 74)

Isotypic compounds:

RFeSi<sub>2</sub>: R = Ce<sup>a</sup>, Tb<sup>i</sup> \*

RCoSi<sub>2</sub>: R = Ce<sup>b, j</sup>, Nd<sup>j</sup>, Sm<sup>j</sup>, Gd<sup>j</sup>, Tb<sup>j</sup>, Dy<sup>j</sup>, Ho<sup>j</sup>, Er<sup>j</sup>, Tm<sup>j</sup>, Y<sup>f, l</sup>

RNiSi<sub>2</sub>: R = La<sup>c</sup>, Ce<sup>c</sup>, Pr<sup>c</sup>, Nd<sup>c</sup>, Sm<sup>c</sup>, Eu<sup>c</sup>, Gd<sup>c</sup>, Tb<sup>c</sup>, Dy<sup>c</sup>, Ho<sup>c</sup>, Er<sup>c</sup>, Tm<sup>c</sup>, Yb<sup>c</sup>, Lu<sup>c</sup>, Y<sup>f</sup>

RRhSi<sub>2</sub>: R = La<sup>g</sup>, Nd<sup>h</sup>, Gd<sup>h</sup>

RIrSi<sub>2</sub>: R = La<sup>h</sup>, Nd<sup>h</sup>, Gd<sup>h</sup>

RNiGe<sub>2</sub>: R = Ce<sup>c</sup>

RFeSn<sub>2</sub>: R = La<sup>d, e</sup> \*\*

RCoSn<sub>2</sub>: R = La<sup>d, e</sup> \*\*, Ce<sup>d</sup>

RNiSn<sub>2</sub>: R = La<sup>d, e</sup> \*\*, Ce<sup>d</sup>

\*Site occupation variant of the CeNiSi<sub>2</sub>-type with crystal-chemical formula RT<sup>[4t]</sup>M<sup>1</sup> $\frac{1}{2}$ M<sup>[6, p]</sup>, where T and M atoms in the "BaAl<sub>4</sub>-type" slab have been interchanged. See 7567:TbFeSi<sub>2</sub>.

\*\*According to DössS, 82 the compositions are LaFe<sub>0.34</sub>Sn<sub>2</sub>, LaCo<sub>0.52</sub>Sn<sub>2</sub>, and LaNi<sub>0.74</sub>Sn<sub>2</sub>.

<sup>a</sup>)BoGKC, 70

<sup>b</sup>)BoG, 70

<sup>c</sup>)BoG, 70a

<sup>d</sup>)Sk, 77

<sup>e</sup>)DössS, 82

<sup>f</sup>)BoMMYSG, 74

<sup>g</sup>)ChLVEH, 82

<sup>h</sup>)ChLEVH, 82

<sup>i</sup>)YaG, 81

<sup>j</sup>)PeBM, 82

The CeNiSi<sub>2</sub> structure, shown in fig. 31, belongs to the R<sub>n+m</sub>T<sub>2n</sub>M<sub>4m</sub> structural series. It is built up of AlB<sub>2</sub>- and BaAl<sub>4</sub>-type slabs and is discussed with 7350:La<sub>3</sub>Rh<sub>4</sub>Ge<sub>4</sub> and 8050:CeNi<sub>2</sub>Si<sub>2</sub>. For site exchange variant, see 7567:TbFeSi<sub>2</sub>.

7567	<b>TbFeSi<sub>2</sub></b>	oC16	<i>a</i> = 4.017	YaG, 81
	or	Cmcm	<i>b</i> = 16.308	
	TbFe <sup>[4t]</sup> Si $\oslash$ Si <sup>[6, p]</sup>		<i>c</i> = 3.933	
Site exchange variant of CeNiSi <sub>2</sub> -type				

Isotypic compounds:

TbFeSi<sub>2</sub> is the only compound for which this structure has been verified; however, after a careful restudy of the diffraction intensities some of the compounds listed as isotypic to 7567:CeNiSi<sub>2</sub> might be found to have actually an atom arrangement as in TbFeSi<sub>2</sub>.

The TbFeSi<sub>2</sub> structure is a site exchange variant of the 7567:CeNiSi<sub>2</sub>-type structure. The latter structure, which is shown in fig. 31, can be described as an intergrowth of AlB<sub>2</sub>- and BaAl<sub>4</sub>-type slabs. If the T and M atoms are interchanged in the BaAl<sub>4</sub>-type slabs the TbFeSi<sub>2</sub> structure is obtained. The atom arrangement of T and M atoms in the BaAl<sub>4</sub>-type slabs of TbFeSi<sub>2</sub> corresponds to the T and M atom arrangement in the ThCr<sub>2</sub>Si<sub>2</sub>-type (see 8050:CeNi<sub>2</sub>Si<sub>2</sub>), the most common ternary BaAl<sub>4</sub>-type derivative.

7567	<b>NdNiGa<sub>2</sub></b>	oC16	<i>a</i> = 4.192	GrY, 82
	or	Cmmm	<i>b</i> = 17.564	
	NdNiGa $\oslash$ Ga <sup>[6, p]</sup>		<i>c</i> = 4.1331	

Isotypic compounds: All references GrY, 82

RNiGa<sub>2</sub>: R = La, Ce, Pr, Nd, Sm, Gd

The NdNiGa<sub>2</sub> structure, shown in fig. 31, can be considered as an intergrowth of AlB<sub>2</sub>- and CeMg<sub>2</sub>Si<sub>2</sub>-type slabs. In contrast to the CeMg<sub>2</sub>Si<sub>2</sub> structure itself (see fig. 80), in NdNiGa<sub>2</sub> the Mg sites are occupied by Ga and the Si sites by Ni atoms. In fig. 80 it is demonstrated that the CeMg<sub>2</sub>Si<sub>2</sub> structure can be derived from the ThCr<sub>2</sub>Si<sub>2</sub> structure, a BaAl<sub>4</sub>-type derivative, by a simple shift. If a corresponding shift is applied to the CeMg<sub>2</sub>Si<sub>2</sub>-type slabs in NdNiGa<sub>2</sub> such that they become ThCr<sub>2</sub>Si<sub>2</sub>-type or BaAl<sub>4</sub>-type slabs the structure obtained is known as 7567:CeNiSi<sub>2</sub>-type.

The NdNiGa<sub>2</sub>-type is found only with the larger rare earth elements. With smaller ones the MgCuAl<sub>2</sub>-type (see 7567:YNiAl<sub>2</sub>) is formed.

7567	YNiAl <sub>2</sub>	oC16	<i>a</i> = 4.07	RyZY, 72
	or	Cmcm	<i>b</i> = 10.13	
	YNi <sup>[(2,4)B]Al<sub>2</sub></sup>		<i>c</i> = 7.06	

MgCuAl<sub>2</sub>-type (PeW, 43) ≡ Re<sub>3</sub>B-type derivative

#### Isotypic compounds

RCoAl<sub>2</sub>: R = Y<sup>a)</sup>

RNiAl<sub>2</sub>: R = Gd<sup>a,b)</sup>, Tb<sup>a,c)</sup>, Dy<sup>a,c)</sup>, Ho<sup>a)</sup>, Er<sup>a)</sup>, Tm<sup>a,e)</sup>, Yb<sup>f)</sup>, Lu<sup>e,f)</sup>, Y<sup>d)</sup>

RNiGa<sub>2</sub>: R = Tb<sup>g)</sup>, Dy<sup>g)</sup>, Ho<sup>g)</sup>, Er<sup>g)</sup>, Tm<sup>g)</sup>, Yb<sup>g)</sup>, Lu<sup>g)</sup>, Y<sup>g)</sup>

<sup>a)</sup>RyZP, 73

<sup>b)</sup>RyZM, 78

<sup>c)</sup>RyZM, 80

<sup>d)</sup>RyZY, 72

<sup>e)</sup>RyZPR, 82

<sup>f)</sup>RoZRYS, 82

<sup>g)</sup>YaG, 81

In the YNiAl<sub>2</sub> structure with MgCuAl<sub>2</sub>-type, a Re<sub>3</sub>B-type derivative, shown in fig. 29, every Ni (Cu) atom is in the centre of a trigonal prism formed of two Y and four Al atoms (two Mg and four Al atoms). The structure is discussed with 7350:Sc<sub>3</sub>Ni<sub>4</sub>Ge<sub>4</sub> and 7533:YPd<sub>2</sub>Si.

Ternary rare earth gallides with MgCuAl<sub>2</sub>-type are found only with smaller rare earth elements. For larger ones the 7567:NdNiGa<sub>2</sub> type is formed.

7567	ScMnSi <sub>2</sub>	oP48	<i>a</i> = 9.077	KoB, 80
	or	Pbam	<i>b</i> = 9.854	
	ScMn <sup>[60]Si<sub>2</sub></sup>		<i>c</i> = 7.928	

TiMnSi<sub>2</sub>-type (StVRECP, 82) or ZrCrSi<sub>2</sub>-type (YaSALG, 82)

#### Isotypic compounds:

ScTSi<sub>2</sub>: T = Mn<sup>a,b)</sup>, Fe<sup>a)</sup>\*

ScTGe<sub>2</sub>: T = Rh<sup>c)</sup>

\*ScFeSi<sub>2</sub> has a second orthorhombic modification with ZrFeSi<sub>2</sub>-type (see 7567:ScFeSi<sub>2</sub>).

<sup>a)</sup>KoB, 80

<sup>b)</sup>KoBK, 80

<sup>c)</sup>B. Chabot, unpublished results [*a* = 9.302(4), *b* = 10.359(5), *c* = 8.146(3) Å]

The ScMnSi<sub>2</sub> structure with TiMnSi<sub>2</sub>-type, shown in a projection along the *c* axis in the left-hand part of fig. 44, closely resembles the projection of a predicted pentagon-triangle analogue of the hexagon-triangle  $\sigma$ -phase with common second-

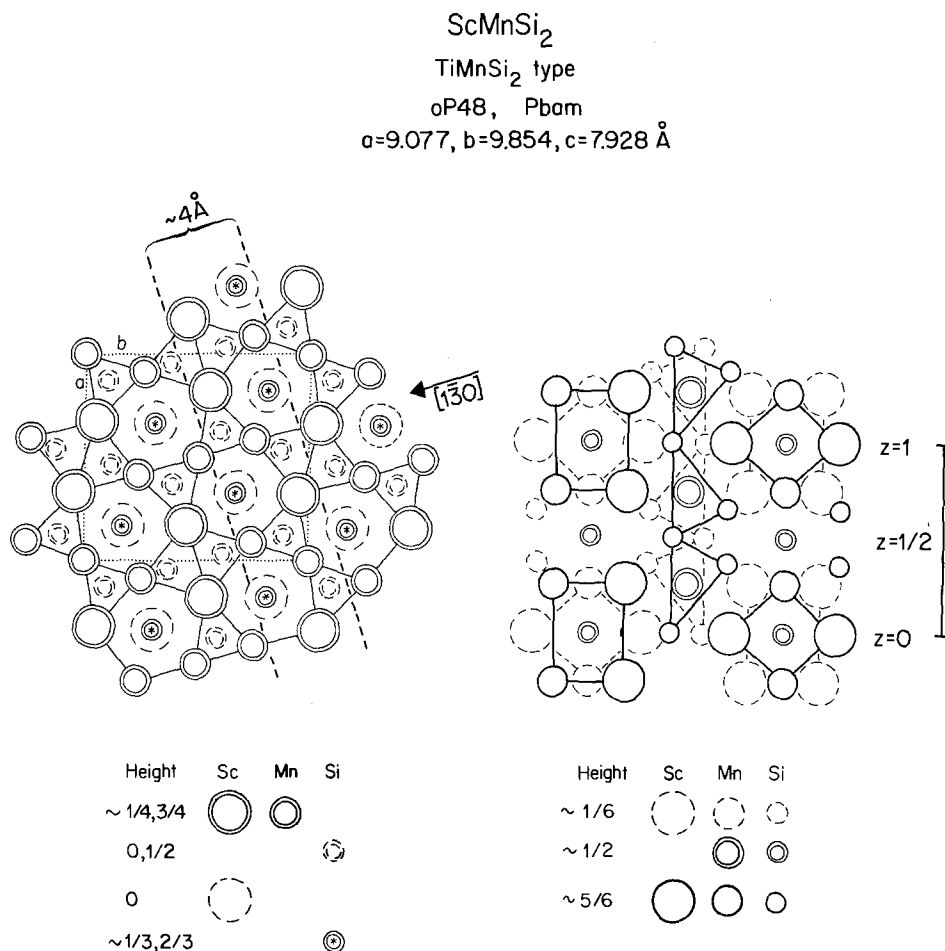


Fig. 44. The  $\text{ScMnSi}_2$  structure with TiMnSi<sub>2</sub>-type projected along the  $c$  axis (left) and projection of an  $\approx 4 \text{ \AA}$  thick slab along  $[1\bar{3}0]$ , after Steinmetz et al. (StVRECP; 82).

ary network of Schläfli-type  $4.3^2.4.3$  (see fig. 6b in Shoemaker and Shoemaker, 1969).\* However, for four main layers per unit cell ( $z = 0, \sim \frac{1}{4}, \frac{1}{2}, \sim \frac{3}{4}$ ) there are only three secondary layers ( $z = 0, \sim \frac{1}{3}, \sim \frac{2}{3}$ ). Thus the secondary layers are not half-way between the main layers.

In the  $\text{ScMnSi}_2$  structure all Mn atoms are in the centres of deformed Si octahedra. If the structure is projected along the  $[1\bar{3}0]$  direction, as shown for a  $4 \text{ \AA}$  thick slab in the right-hand part of fig. 44, one recognizes that chains of edge-connected  $\text{MnSi}_6$  octahedra and Si-centred antiprisms of Sc and Mn atoms are formed. Structures characterized by these two building blocks are discussed with  $7364:\text{Sc}_4\text{Mn}_4\text{Si}_7$ .

\*This structure has actually been found to exist in the W-Fe-Si system at approximate composition  $\text{W}_2\text{FeSi}$  (KrY, 74).

7567	ScFeSi <sub>2</sub> *	oC96	<i>a</i> = 5.115	YaKG, 80
	or	Cmca	<i>b</i> = 18.929	
	Sc <sub>3</sub> Fe <sub>3</sub> <sup>[60]</sup> Si <sub>5</sub> Si <sup>[(6, 2)a]</sup>		<i>c</i> = 14.298	

---

ZrFeSi<sub>2</sub>-type (YaKG, 80) \*

---

\*The single crystal study was undertaken on ScFeSi<sub>2</sub>, but since this compound crystallizes also with the TiMnSi<sub>2</sub>-type (see 7567:ScMnSi<sub>2</sub>) we prefer to call this atom arrangement the ZrFeSi<sub>2</sub>-type. ZrFeSi<sub>2</sub> was reported to be isotypic in the same paper.

No other isotypic RTM<sub>2</sub> compounds are known.

A projection of the ScFeSi<sub>2</sub> structure with ZrFeSi<sub>2</sub>-type along the *a* axis is shown together with the ZrMnSi<sub>2</sub> structure (VeSR, 82) in fig. 32. The ScFeSi<sub>2</sub> structure can be considered a variant of the ZrMnSi<sub>2</sub> structure. Both structures consist of infinite rectilinear columns (perpendicular to the plane of projection) of Si-centred antiprisms formed each by six Sc (Zr) and two Fe (Mn) atoms and parallel columns of T-centred face-joined (deformed) octahedra formed by M atoms only. Structures with these construction elements are discussed with 7364:Sc<sub>4</sub>Mn<sub>4</sub>Si<sub>7</sub>.

7578	La <sub>3</sub> Co <sub>2</sub> Sn <sub>7</sub> *	oC24	<i>a</i> = 4.59	DöS, 80
	or	Cmmm	<i>b</i> = 27.60	
	La <sub>3</sub> Co <sub>2</sub> Sn <sub>5</sub> ♂ Sn <sub>2</sub> <sup>[6, p]</sup>		<i>c</i> = 4.60	

\*Note that the point position for La(1) should be 2c) and not 2e) as printed by mistake in the paper by Dörrscheidt and Schäfer (1980).

No isotypic R<sub>3</sub>T<sub>2</sub>M<sub>7</sub> compounds are known; however, U<sub>3</sub>Fe<sub>2</sub>Si<sub>7</sub> and U<sub>3</sub>Co<sub>2</sub>Si<sub>7</sub> have the same structure (AkYRG, 81).

The La<sub>3</sub>Co<sub>2</sub>Sn<sub>7</sub> structure, shown in fig. 34, consists of intergrown CeNiSi<sub>2</sub>(≡ BaAl<sub>4</sub> + AlB<sub>2</sub> + BaAl<sub>4</sub> slabs) and Cu<sub>3</sub>Au-type layers. The different kinds of intergrown structures are discussed with 8050:CeNi<sub>2</sub>Si<sub>2</sub>. The La<sub>3</sub>Co<sub>2</sub>Sn<sub>7</sub> structure is also geometrically related to the 7471:Sc<sub>5</sub>Co<sub>4</sub>Si<sub>10</sub> structure and more discussion is found with the latter.

---

<b>75(83)</b>	<b>Y<sub>2</sub>MnGa<sub>5</sub>*</b> or Y(Mn <sub>.17</sub> Ga <sub>.83</sub> ) <sub>3</sub>	cP4 Pm3m	<i>a</i> = 4.296	MaBZB, 82
---------------	---	-------------	------------------	-----------

---

Cu<sub>3</sub>Au-type

---

\*Order has not been determined.

No other R<sub>2</sub>TM<sub>5</sub> compounds are known.

Y<sub>2</sub>MnGa<sub>5</sub> is the only R–T–M compound known with Cu<sub>3</sub>Au-type. Intergrown segments with the Cu<sub>3</sub>Au-type are found in many gallides as for example in 8275:Ho<sub>6</sub>Co<sub>7</sub>Ga<sub>21</sub> (fig. 56) and 79(82):Ho<sub>3</sub>Ni<sub>2</sub>Ga<sub>9</sub> (fig. 49). For a discussion of R–T–M structures with intergrown Cu<sub>3</sub>Au-type segments see 8289:Ho<sub>2</sub>CoGa<sub>8</sub>.

---

<b>7646</b>	<b>Sc<sub>4</sub>Rh<sub>7</sub>Ge<sub>6</sub></b> or Sc <sub>4</sub> <sup>[(6,6)c]</sup> Rh <sub>6</sub> <sup>[(4,4+4)c]</sup> Rh <sup>[(6o)]</sup> Ge <sub>6</sub>	cI34 Im3m	<i>a</i> = 8.1255	EnCP, 83
-------------	---	--------------	-------------------	----------

---

U<sub>4</sub>Re<sub>7</sub>Si<sub>6</sub>-type (AkYG, 78), filled-up Cu<sub>3</sub>Au-type

---

Isotypic compounds: All references EnCP, 83

Sc<sub>4</sub>T<sub>7</sub>Si<sub>6</sub>: T = Ir

Sc<sub>4</sub>T<sub>7</sub>Ge<sub>6</sub>: T = Ru, Rh, Os, Ir

The atom arrangement in one unit cell of Sc<sub>4</sub>Rh<sub>7</sub>Ge<sub>6</sub> with U<sub>4</sub>Re<sub>7</sub>Si<sub>6</sub>-type, shown on the right-hand side of fig. 45, corresponds to eight (2 × 2 × 2) unit cells of the Cu<sub>3</sub>Au structure, an ordered variant of the Cu structure. Sc is found on the Au sites and Rh and Ge are arranged in orderly fashion on the Cu sites. There are two extra Rh atoms positioned in the centres of the octahedral interstices created by the Ge atoms. The insertion of these Rh atoms requires the Ge atoms to make small shifts away from their ideal Cu<sub>3</sub>Au positions. We note that the binary Cu<sub>3</sub>Au-type occurs in ScRh<sub>3</sub> and RSn<sub>3</sub> compounds.

In Sc<sub>4</sub>Rh<sub>7</sub>Ge<sub>6</sub> there is one extra atom in one octahedral void for four Cu<sub>3</sub>Au unit cells. The atom arrangement with one extra atom for each Cu<sub>3</sub>Au cell is known as perovskite-type, shown on the left-hand side of fig. 45. This type is found with 8025:LaPd<sub>3</sub>B.

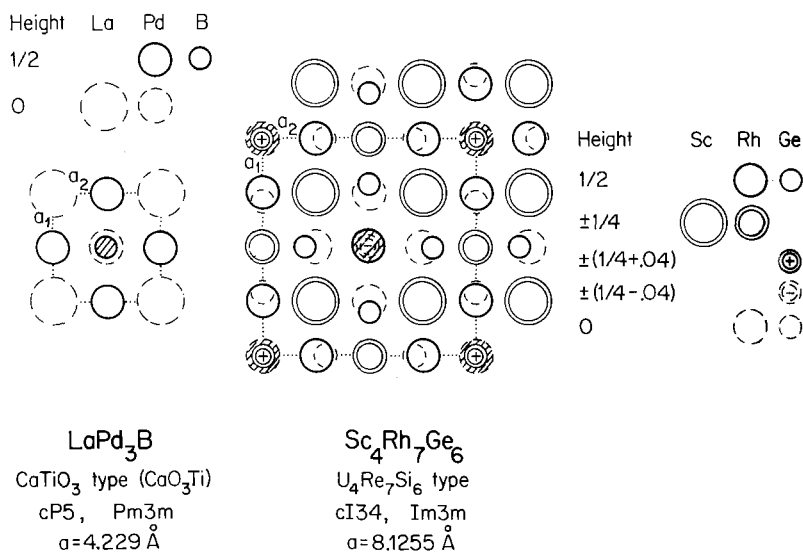


Fig. 45. Two filled-up Cu<sub>3</sub>Au-type structures, the LaPd<sub>3</sub>B structure with perovskite-type and the Sc<sub>4</sub>Rh<sub>7</sub>Ge<sub>6</sub> structure with U<sub>4</sub>Re<sub>7</sub>Si<sub>6</sub>-type. The extra atoms which are inserted in the octahedral interstices are shaded.

<b>7780</b>	<b>Ce<sub>3</sub>Ni<sub>2</sub>Si<sub>8</sub>*</b>	<b>oC26</b>	$a = 4.085$	<b>StLGB, 72</b>
	or	<b>Cmmm</b>	$b = 25.9558$	
	Ce <sub>3</sub> Ni <sub>2</sub> Si <sub>2</sub> Si <sub>4</sub> <sup>[(2+2)t]</sup> ∞ Si <sub>2</sub> <sup>[6, p]</sup>		$c = 4.1786$	

\*This compound was formulated before as CeNiSi<sub>4</sub>.

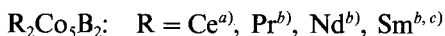
No isotypic R<sub>3</sub>T<sub>2</sub>M<sub>8</sub> compounds are known.

The Ce<sub>3</sub>Ni<sub>2</sub>Si<sub>8</sub> structure, shown in fig. 31, consists of intergrown BaAl<sub>4</sub> and AlB<sub>2</sub> slabs. It belongs to the R<sub>n+m</sub>T<sub>2n</sub>M<sub>4m</sub> structural series, which is discussed with 7350: La<sub>3</sub>Rh<sub>4</sub>Ge<sub>4</sub>.

<b>7829</b>	<b>Ce<sub>2</sub>Co<sub>3</sub>B<sub>2</sub></b>	<b>hP36</b>	$a = 5.060$	<b>Ku, 79</b>
		<b>P6<sub>3</sub>/mmc</b>	$c = 20.43$	

Ce<sub>2</sub>Ni<sub>7</sub>-type (CrL, 59) derivative

Isotypic compounds:



<sup>a)</sup>Ku, 79    <sup>b)</sup>KuBCC, 81    <sup>c)</sup>BiKP, 80

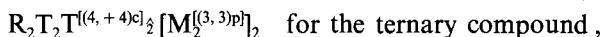
The  $Ce_2Co_5B_2$  structure, shown in fig. 38, is a member of the  $R_{2+n}T_{4+3n}M_{2n}$  structural series with  $n = 2$  and is built up of Laves-type slabs and  $CeCo_3B_2$ -type slabs. It is discussed with the 7511: $Ce_3Co_8Si$  structure.

7857	$Sc_2Re_3Si_4$	tP36	$a = 6.619$	PeBG, 78
	or	P4 <sub>1</sub> 2,2	$c = 12.36$	
	$Sc_2Re_2Re^{[(4,+4)c]_{\frac{1}{2}}}[Si_2^{[(3,3)p]}]_2$			

$Zr_5Si_4$ -type (PfS, 66) derivative

No isotypic  $R_2T_3M_4$  compounds are known.

One half of the unit cell of the  $Sc_2Re_3Si_4$  structure with  $Zr_5Si_4$ -type derivative is shown on the left-hand side of fig. 46. The structure is characterized by pairs of M-centred trigonal prisms and T-centred cubes. All prisms are constructed of three R and three T atoms and all cubes of four R and four T atoms. Each group of four atoms at the cube corners and the T atom in the cube centre are on a diagonal cube plane. The crystal-chemical formula is



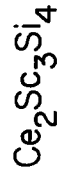
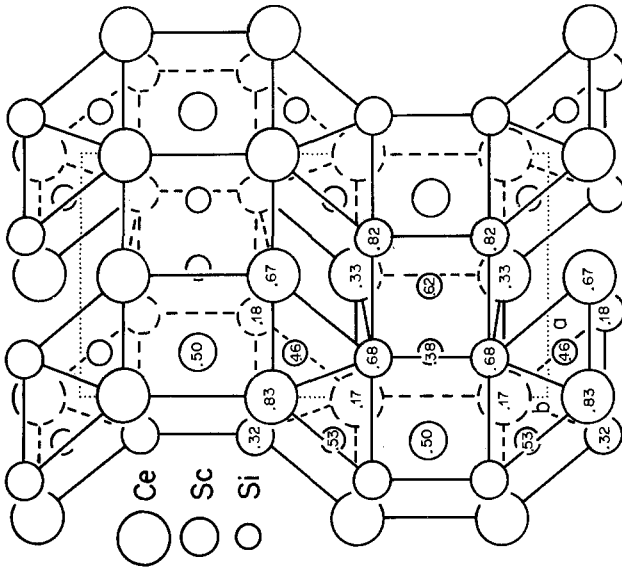
and



The orthorhombic  $Sm_5Ge_4$  structure (SmJT, 67) has the same structural features as  $Zr_5Si_4$  and the same crystal-chemical formula. A ternary structure with  $Sm_5Ge_4$ -type derivative is found with  $Ce_2Sc_3Si_4$  (MoBG, 79), of which half of one unit cell is shown on the right-hand side of fig. 46. The positional coordinates inscribed in the circles for both ternary structures agree well with those of the corresponding binary compounds, as can be seen by comparing fig. 46 with the corresponding drawings for the binary structures in the paper by Le Roy et al. (LeMPP, 78). In the same article some comments on the branches of the  $Sm_5Ge_4$ -type can be found.

Many Sc compounds are known, where Sc behaves more like a transition element of the 4th group, than a rare earth element. To interpret the structural similarities between the  $Sc_2Re_3Si_4$  and the  $Ce_2Sc_3Si_4$  structure we shall—for this discussion only—consider the latter compound as a  $R_2$ “ $T_3$ ” $M_4$  compound. Then one finds in  $Ce_2Sc_3Si_4$  the same pairs of M-centred trigonal prisms and the “T”-centred cubes.

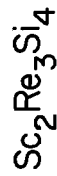
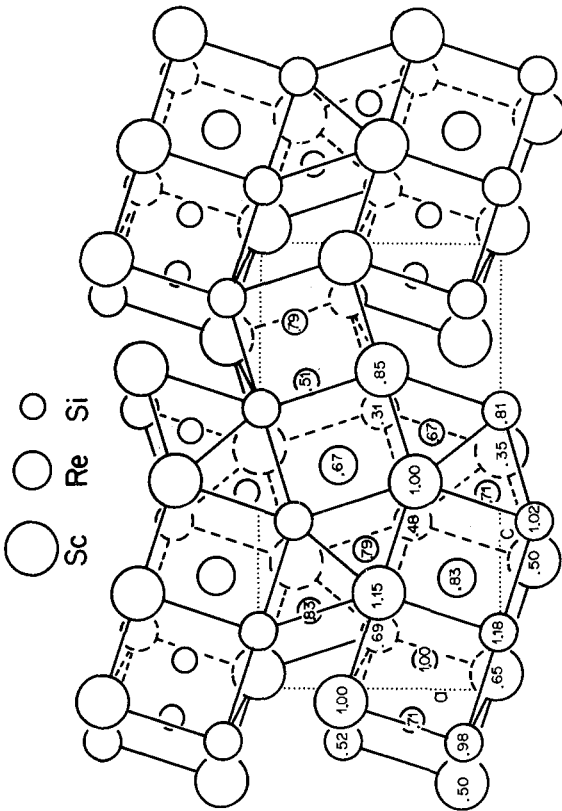




$\text{Sm}_5\text{Ge}_4$  type derivative

$\text{oP}36, \text{Pnma}$

$a=7.248, b=14.255, c=7.551 \text{ \AA}$



$\text{Zr}_5\text{Si}_4$  type derivative

$\text{tP}36, \text{P}4_12_12$

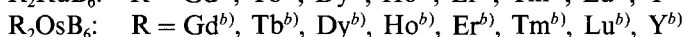
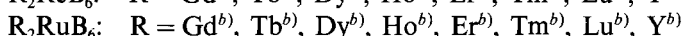
$a=6.619, c=12.36 \text{ \AA}$

Fig. 46. Arrangement of Si-centred double prisms and of the centred cubes in  $\text{Sc}_2\text{Re}_3\text{Si}_4$  and  $\text{Ce}_2\text{Sc}_3\text{Si}_4$ . Only the polyhedra with their centres at  $y \approx \frac{1}{2}$  and at  $z \approx \frac{1}{2}$ , respectively, are shown, which corresponds to one half of the unit cell content for both structures.

However, according to the structure proposed by Mokraya et al. (MoBG, 79) with space group Pnma, the trigonal prisms are not equal. Those with their centres at  $y \approx 0$  are formed of three R and three "T" atoms, while those at  $y \approx \frac{1}{2}$  have either four R and two "T" or two R and four "T" atoms. To avoid this we have to assume that in the trigonal prisms with their centres at  $y \approx \frac{1}{2}$  the R sites are occupied by "T" atoms and vice versa. In this case the space group of  $\text{Ce}_2\text{Sc}_3\text{Si}_4$  would be centrosymmetric  $P2_1/c$  (or  $P2_1/b$  with the  $c$  axis unique and  $\gamma = 90^\circ$ , assuming equal unit cell setting) and all structural features and the crystal-chemical formula would be identical to that given for  $\text{Sc}_2\text{Re}_3\text{Si}_4$ .

7886	$\text{Y}_2\text{ReB}_6$	$\text{oP}36$	$a = 9.175$	KuS, 72
	or	$\text{Pbam}$	$b = 11.55$	
	$\text{Y}^{[.14]}\text{Y}^{[.12]}\text{Re}^{[.10]} \infty \text{B}_6^{[6p+3]}$		$c = 3.673$	

Isotypic compounds:



<sup>a</sup>KuS, 72

<sup>b</sup>RoN, 82

The  $\text{Y}_2\text{ReB}_6$  structure is shown in fig. 47 together with the  $\text{ScB}_2$  structure with  $\text{AlB}_2$ -type. The structural features of  $\text{Y}_2\text{ReB}_6$  are conveniently discussed together with those of the 8380:  $\text{YCrB}_4$  structure and its structure block shifted variant, the  $\text{ThMoB}_4$  structure (RoN, 75). The last two structures, which have the same crystal-chemical formula, are presented in fig. 48. The structural data of all four structures are given in table 14. The ternary structures can be interpreted as modifications of the  $\text{AlB}_2$  structure to accommodate different boron partners of different size. All compounds have 67 at % boron—and thus are on the line between  $\text{RB}_2$  and  $\text{TB}_2$ —and their structures are all characterized by two-dimensional planar boron nets. All boron atoms are in the centres of trigonal prisms formed by R and T atoms and form three homonuclear bonds with boron atoms in the centres of (rectangular) face-joined trigonal prisms. The structures differ from  $\text{AlB}_2$  in the number of nearest boron neighbours of the R and T atoms.

In  $\text{ScB}_2$  with  $\text{AlB}_2$ -type all Sc atoms are surrounded by a hexagonal prism of boron atoms (twelve boron neighbours). If the Sc atoms are partially replaced by a transition element of the same size there is no reason why the  $\text{AlB}_2$ -type (or an ordering variant of it) should not be retained as structure type for the ternary compound.\* However, in  $\text{YCrB}_4$ , with the non-negligible size difference between the

\*Unfortunately no experimental data are available. We note that  $\text{ScB}_2$  ( $a = 3.146$ ,  $c = 3.517$  Å) and  $\text{HfB}_2$  ( $a = 3.141$ ,  $c = 3.470$  Å) are isotypic and have nearly the same lattice constants. It can be predicted that in the system  $\text{ScB}_2$ - $\text{HfB}_2$  the formation of the  $\text{Y}_2\text{ReB}_6$ - or  $\text{YCrB}_4$ -type is unlikely.

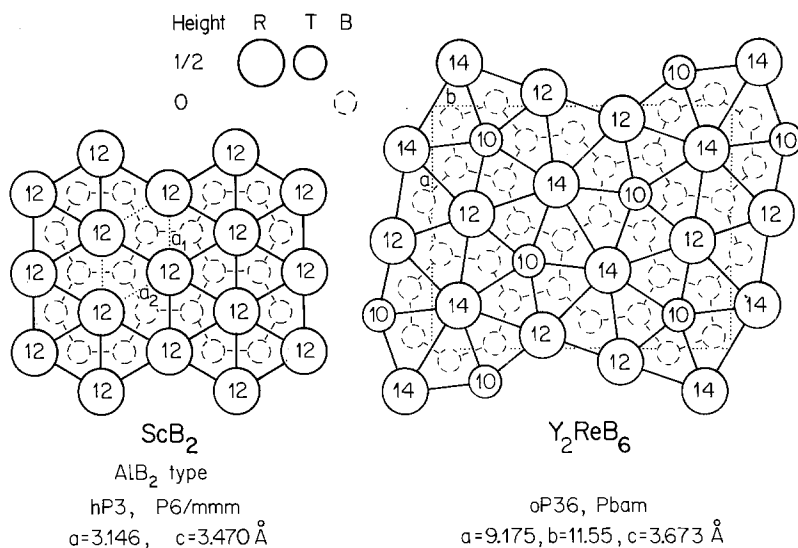


Fig. 47. The crystal structure of ScB<sub>2</sub> with AlB<sub>2</sub>-type and of Y<sub>2</sub>ReB<sub>6</sub>, with a structure related to the AlB<sub>2</sub>-type, where the Y atoms are surrounded by 14 or 12 and the Re atoms by 10 boron neighbours. The numbers inscribed in the circles correspond to the boron coordination of these atoms.

TABLE 14

Structural data for the AlB<sub>2</sub>-type and AlB<sub>2</sub>-related ternary structures which can accommodate different boron partners of different sizes.

Boron coordination of boron partners	Code	Compound and type	Pearson's classif. symbol	Space group	crystal-chemical formula
12	67100	ScB <sub>2</sub> (AlB <sub>2</sub> -type)	hP3	P6/mmm	Sc <sup>[12]</sup> B <sub>2</sub> <sup>[6p+3]</sup>
14,12,10	7886	Y <sub>2</sub> ReB <sub>6</sub>	oP36	Pbam	Y <sup>[14]</sup> Y <sup>[12]</sup> Re <sup>[10]</sup> B <sub>6</sub> <sup>[6p+3]</sup>
14,10	8380	YCrB <sub>4</sub>	oP24	Pbam	Y <sup>[14]</sup> Cr <sup>[10]</sup> B <sub>4</sub> <sup>[6p+3]</sup>
14,10	(8380)	ThMoB <sub>4</sub>	oC24	Cmmm	Th <sup>[14]</sup> Mo <sup>[10]</sup> B <sub>4</sub> <sup>[6p+3]</sup>

Y and Cr atoms, the B–B distances become more equal if the boron atoms form a heptagonal prism around Y and a pentagonal prism around Cr.

For Y<sub>2</sub>ReB<sub>6</sub> one might thus expect both Y atoms to have 14 B neighbours and for Re ten B neighbours. However, with composition R<sub>2</sub>TB<sub>6</sub> it is geometrically impossible to form a structure with B-centred trigonal prisms, where the boron partners have these coordination numbers. Since the total number of B–R and B–T contacts must be equal to the total number of R–B and T–B bonds, the latter sum must be a multiple of 6 (2 × 14 + 1 × 10 = 38 ≠ 6N). In Y<sub>2</sub>ReB<sub>6</sub> half of the Y atoms are in the centre of a heptagonal prism and the other half in a trigonal prism, while the Re atoms centre a pentagonal boron prism (1 × 14 + 1 × 12 + 1 × 10 = 36 = 6N).

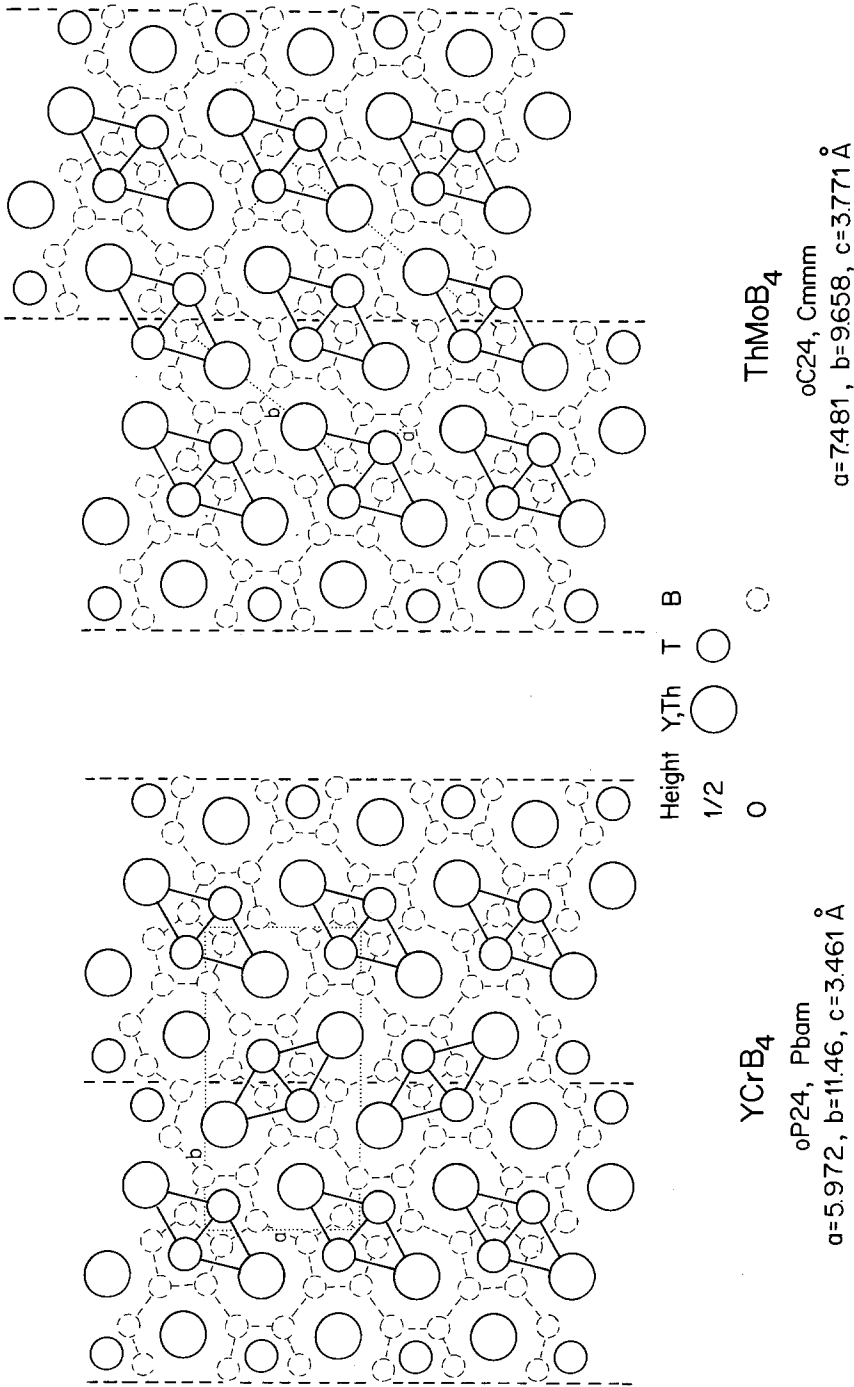


Fig. 48. The  $\text{YCrB}_4$  and the  $\text{ThMoB}_4$  structures, two  $\text{AlB}_2$ -related structures, which can be interpreted as structure block shifted variants. Y and Th have 14 boron neighbours, but Cr and Mo only 10. Only those trigonal prisms are indicated which are formed of two Y (Th) and four Cr (Mo) atoms.

---

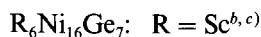
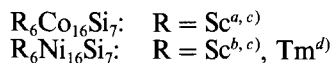
<b>7930</b>	<b>Sc<sub>6</sub>Ni<sub>16</sub>Si<sub>7</sub></b>	cF116 Fm3m	$a = 11.46$	GIMK, 62
-------------	--	---------------	-------------	----------

---

**Mg<sub>6</sub>Cu<sub>16</sub>Si<sub>7</sub>-type (BeW, 56)  $\equiv$  Th<sub>6</sub>Mn<sub>23</sub>-type derivative**

---

Isotypic compounds:



<sup>a</sup>KoBG, 77      <sup>b</sup>GIMK, 62      <sup>c</sup>DwCD, 63      <sup>d</sup>GIKB, 66

The Mg<sub>6</sub>Cu<sub>16</sub>Si<sub>7</sub>-type of Sc<sub>6</sub>Ni<sub>16</sub>Si<sub>7</sub> is found also with aluminides but now with T and M atoms interchanged and the composition is then 7970:Sc<sub>6</sub>Ni<sub>7</sub>Al<sub>16</sub>. The Mg<sub>6</sub>Cu<sub>16</sub>Si<sub>7</sub> structure belongs to those with large cubic unit cells, conveniently described with nested polyhedral units and treated here with 7325:Ce<sub>3</sub>Ni<sub>6</sub>Si<sub>2</sub>.

---

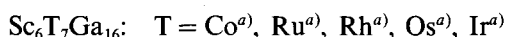
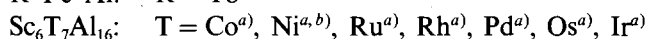
<b>7970</b>	<b>Sc<sub>6</sub>Ni<sub>7</sub>Al<sub>16</sub></b>	cF116 Fm3m	$a = 12.16$	MaS, 73
-------------	--	---------------	-------------	---------

---

**Mg<sub>6</sub>Cu<sub>16</sub>Si<sub>7</sub>-related type (BeW, 56)  $\equiv$  Th<sub>6</sub>Mn<sub>23</sub>-type derivative**

---

Isotypic compounds:



<sup>a</sup>MaS, 73      <sup>b</sup>MaB, 69      <sup>c</sup>Oe, 75      <sup>d</sup>OeP, 72

\*This compound appears at the unusual composition Tb<sub>0.167</sub>Fe<sub>0.633</sub>Al<sub>0.20</sub>.

The Mg<sub>6</sub>Cu<sub>16</sub>Si<sub>7</sub>-type of Sc<sub>6</sub>Ni<sub>7</sub>Al<sub>16</sub> is found also with silicides and germanides but now with T and M atoms interchanged and the composition is then 7930:Sc<sub>6</sub>Ni<sub>16</sub>Si<sub>7</sub>. The Mg<sub>6</sub>Cu<sub>16</sub>Si<sub>7</sub> structure has a large cubic unit cell and is conveniently described with nested polyhedral units. These are treated here with 7325:Ce<sub>3</sub>Ni<sub>6</sub>Si<sub>2</sub>.

79(82) $\text{Ho}_3\text{Ni}_2\text{Ga}_9$ or $\text{Ho}_2(\text{Ni}_5\text{Ga}_5)_4\text{Ga}_4$ <sup>[(4Ho, 4Ga)]Ga<sub>6</sub>Ga<sup>[(4, + 8)c]</sup></sup>	oI28	$a = 4.142^*$	Gr, 82
	Immm	$b = 9.608$	
		$c = 12.34$	

$\text{La}_3\text{Al}_{11}$ -type (GoB, 67) derivative with partial disorder on one Al site

\*Corresponds to  $\text{Ho}_3\text{Ni}_{1.8}\text{Ga}_{9.2}$ .

Isotypic compounds: All references Gr, 82

$\text{R}_3(\text{Ni, Ga})_{11}$ : R = Ho, Er, Tm, Lu, Y

The  $\text{Ho}_3\text{Ni}_2\text{Ga}_9$  structure with  $\text{La}_3\text{Al}_{11}$ -type derivative is shown in fig. 49. The  $\text{La}_3\text{Al}_{11}$  structure can be considered as a periodic intergrowth of  $\text{Cu}_3\text{Au}$ -type columns and  $\text{BaAl}_4$ -type columns. We note that  $\text{LaAl}_4$  itself crystallizes with the  $\text{BaAl}_4$ -type. The formula of  $\text{La}_3\text{Al}_{11}$  can be rationalized according to  $\text{LaAl}_3 + 2 \text{LaAl}_4 = \text{La}_3\text{Al}_{11}$ . In fig. 49 the outlines of the two different construction elements are indicated with thin lines. In the ternary compound they have the compositions  $\text{HoGa}_3$  and  $\text{Ho}_2(\text{Ni}_5\text{Ga}_5)_4\text{Ga}_4$ .

We note that one modification of the binary compound  $\text{HoGa}_3$  crystallizes in the  $\text{Cu}_3\text{Au}$ -type. Further the  $\text{R}(\text{Ni, Ga})_4$  compounds adopt the 8050: $\text{ThCr}_2\text{Si}_2$ -type, a  $\text{BaAl}_4$ -type derivative, but with statistical distribution of Ni and Ga atoms on one structure site.

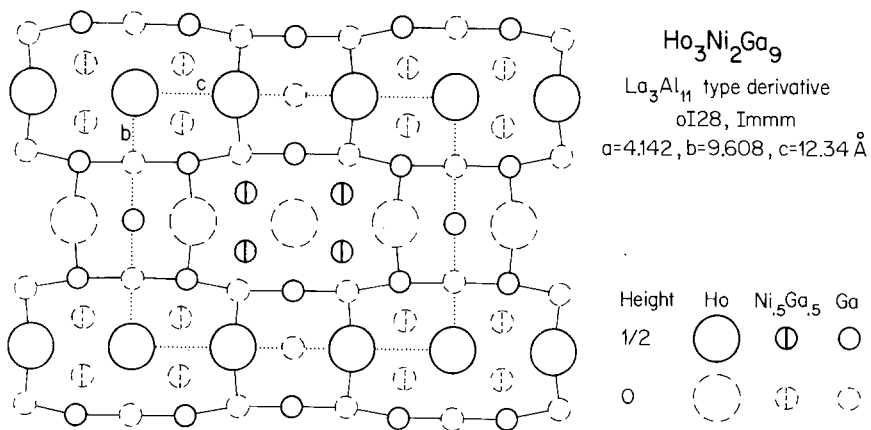


Fig. 49. The  $\text{Ho}_3\text{Ni}_2\text{Ga}_9$  structure interpreted as intergrowth of two construction elements corresponding to the  $\text{Cu}_3\text{Au}$ -type (square outline) and the  $\text{BaAl}_4$ -type (rectangular outline).

---

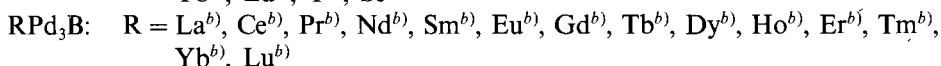
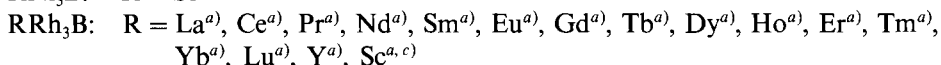
<b>8025</b>	<b>LaPd<sub>3</sub>B</b> or La <sup>[12, c]</sup> Pd <sub>3</sub> B <sup>[60]</sup>	cP5 Pm3m	$a = 4.229$	DhMV, 81
-------------	---	-------------	-------------	----------

---

Perovskite CaTiO<sub>3</sub>-type (CaO<sub>3</sub>Ti)

---

Isotypic compounds:



<sup>a</sup>Ho, 73

<sup>b</sup>DhMV, 81

<sup>c</sup>Ho, 77

<sup>d</sup>StK, 81

The LaPd<sub>3</sub>B structure with perovskite CaTiO<sub>3</sub>-type is shown on the left-hand side of fig. 45. This structure can be considered as a filled-up Cu<sub>3</sub>Au-type. The binary RPd<sub>3</sub> compounds, also CeRh<sub>3</sub> and ScRh<sub>3</sub>, all crystallize with the Cu<sub>3</sub>Au-type. Boron atoms can be inserted in the T<sub>6</sub> octahedra of the binary RT<sub>3</sub> compounds, giving rise to a continuous solid solution of composition RTB<sub>x</sub> with 0 ≤ x ≤ 1 when T = Pd. For some of the Rh-containing compounds a binary Cu<sub>3</sub>Au phase is unknown. In CePd<sub>3</sub> and EuPd<sub>3</sub> the addition of boron causes a change in the valence state of the rare earth ion (Ce<sup>4+</sup> → Ce<sup>3+</sup> and Eu<sup>3+</sup> → Eu<sup>2+</sup>).

For another structure which can also be described as filled-up Cu<sub>3</sub>Au-type see 7646:Sc<sub>4</sub>Rh<sub>7</sub>Ge<sub>6</sub>.

Four structure types are found with composition 8050: ThCr<sub>2</sub>Si<sub>2</sub>, tI10 (see CeNi<sub>2</sub>Si<sub>2</sub>), CaBe<sub>2</sub>Ge<sub>2</sub>, tP10 (see LaIr<sub>2</sub>Si<sub>2</sub>), HfFe<sub>2</sub>Si<sub>2</sub>, oP20 (see ScFe<sub>2</sub>Si<sub>2</sub>) and LaRe<sub>2</sub>Si<sub>2</sub>, oI20.

---

<b>8050</b>	<b>CeNi<sub>2</sub>Si<sub>2</sub></b> or CeNi <sub>2</sub> <sup>[4t]</sup> Si <sub>2</sub> <sup>[(4, 4)a]</sup>	tI10 I4/mmm	$a = 4.027$ $c = 9.557$	BoGK, 66
-------------	---	----------------	----------------------------	----------

---

ThCr<sub>2</sub>Si<sub>2</sub>-type (BaS, 65) or CeAl<sub>2</sub>Ga<sub>2</sub>-type (ZaKG, 65) ≡ BaAl<sub>4</sub>-type (D1<sub>3</sub>-type) derivative

---

## Isotypic compounds:

RFe <sub>2</sub> B <sub>2</sub> :	R = Gd <sup>a</sup> , Tb <sup>a</sup> , Dy <sup>a</sup> , Ho <sup>a</sup> , Er <sup>a</sup> , Tm <sup>a</sup> , Lu <sup>a</sup> , Y <sup>a</sup> )
RCO <sub>2</sub> B <sub>2</sub> :	R = La <sup>c</sup> , Pr <sup>b</sup> , Nd <sup>c</sup> , Sm <sup>b,c</sup> , Gd <sup>b,c</sup> , Tb <sup>b,c</sup> , Dy <sup>b,c</sup> , Ho <sup>b</sup> , Y <sup>b,c,d,β</sup> )
R(Ni, Ga) <sub>4</sub> *:	R = La <sup>w</sup> , Ce <sup>w</sup> , Pr <sup>w</sup> , Nd <sup>w</sup> , Sm <sup>w</sup> , Gd <sup>w</sup> , Tb <sup>w</sup> , Dy <sup>w</sup> )
RCr <sub>2</sub> Si <sub>2</sub> :	R = Gd <sup>k</sup> , Y <sup>e</sup> )
RMn <sub>2</sub> Si <sub>2</sub> :	R = La <sup>h,f</sup> , Ce <sup>g,h</sup> , Pr <sup>f</sup> , Nd <sup>f</sup> , Sm <sup>f</sup> , Gd <sup>f</sup> , Tb <sup>f</sup> , Dy <sup>f</sup> , Ho <sup>f</sup> , Er <sup>f</sup> , Tm <sup>a</sup> , Yb <sup>f</sup> , Lu <sup>a</sup> , Y <sup>f</sup> )
RFe <sub>2</sub> Si <sub>2</sub> :	R = La <sup>i</sup> , Ce <sup>h,k</sup> , Pr <sup>i</sup> , Nd <sup>i,j,l,x</sup> ** <sup>†</sup> , Sm <sup>z</sup> , Eu <sup>l,m</sup> , Gd <sup>k</sup> , Dy <sup>i,l</sup> , Ho <sup>n</sup> , Yb <sup>i</sup> , Y <sup>i</sup> )
RCO <sub>2</sub> Si <sub>2</sub> :	R = La <sup>i</sup> , Ce <sup>h,k,θ</sup> ***, Pr <sup>i</sup> , Nd <sup>i</sup> , Sm <sup>i</sup> , Eu <sup>m</sup> , Gd <sup>k</sup> , Tb <sup>i</sup> , Dy <sup>i</sup> , Ho <sup>i</sup> , Er <sup>i</sup> , Yb <sup>i</sup> , Y <sup>i</sup> , Sc <sup>n</sup> )
RNi <sub>2</sub> Si <sub>2</sub> :	R = La <sup>h</sup> , Ce <sup>h,k</sup> , Pr <sup>h</sup> , Nd <sup>h</sup> , Sm <sup>h</sup> , Eu <sup>h,m</sup> †, Gd <sup>h</sup> , Tb <sup>h</sup> , Dy <sup>h</sup> , Ho <sup>h</sup> , Er <sup>h</sup> , Tm <sup>h</sup> , Yb <sup>h</sup> , Lu <sup>h</sup> , Y <sup>k,o</sup> , Sc <sup>k,p</sup> )
RRu <sub>2</sub> Si <sub>2</sub> :	R = La <sup>q,c</sup> , Ce <sup>q,c</sup> , Pr <sup>c</sup> , Nd <sup>q,c</sup> , Sm <sup>q,c</sup> , Eu <sup>z</sup> , Gd <sup>δ,c</sup> , Tb <sup>q,c</sup> , Dy <sup>q,δ,c</sup> , Ho <sup>δ,c</sup> , Er <sup>q,δ,c</sup> , Tm <sup>c</sup> , Yb <sup>q,c</sup> , Lu <sup>c</sup> , Y <sup>c</sup> )
RRh <sub>2</sub> Si <sub>2</sub> :	R = La <sup>s</sup> , Ce <sup>s</sup> , Pr <sup>s</sup> , Nd <sup>s</sup> , Sm <sup>s</sup> , Eu <sup>s,δ</sup> , Gd <sup>s,δ</sup> , Tb <sup>s</sup> , Dy <sup>s,δ</sup> , Ho <sup>s,δ</sup> , Er <sup>s</sup> , Yb <sup>r</sup> , Y <sup>s</sup> )
RPd <sub>2</sub> Si <sub>2</sub> :	R = La <sup>s</sup> , Ce <sup>r,s</sup> , Pr <sup>s</sup> , Nd <sup>s</sup> , Sm <sup>s</sup> , Eu <sup>s</sup> , Gd <sup>r,s,δ</sup> , Tb <sup>s</sup> , Dy <sup>s,δ</sup> , Ho <sup>s,δ</sup> , Er <sup>s,δ</sup> , Yb <sup>r</sup> , Y <sup>s</sup> )
ROs <sub>2</sub> Si <sub>2</sub> :	R = La <sup>e</sup> , Ce <sup>z</sup> , Pr <sup>e</sup> , Nd <sup>e</sup> , Sm <sup>e</sup> , Gd <sup>e</sup> , Tb <sup>e</sup> , Dy <sup>e</sup> , Ho <sup>e</sup> , Er <sup>e</sup> , Tm <sup>e</sup> , Yb <sup>e</sup> , Lu <sup>e</sup> , Y <sup>e</sup> )
RIr <sub>2</sub> Si <sub>2</sub> :	R = La <sup>z</sup> ††, Gd <sup>r,δ</sup> , Er <sup>δ</sup> )
RPt <sub>2</sub> Si <sub>2</sub> †††:	R = La <sup>r,t</sup> , Ce <sup>r,q</sup> , Nd <sup>r,t,q</sup> , Sm <sup>q</sup> , Eu <sup>t</sup> , Gd <sup>r,t,q</sup> , Dy <sup>r,t,q</sup> , Er <sup>t,q</sup> , Tm <sup>t</sup> , Yb <sup>r</sup> , Lu <sup>t</sup> , Y <sup>q</sup> )
RMn <sub>2</sub> Ge <sub>2</sub> :	R = La <sup>f,u</sup> , Ce <sup>f,u</sup> , Pr <sup>f,u</sup> , Nd <sup>f,u</sup> , Sm <sup>f</sup> , Gd <sup>f,u</sup> , Tb <sup>f,u</sup> , Dy <sup>f,u</sup> , Ho <sup>f,u</sup> , Er <sup>f,u</sup> , Yb <sup>f</sup> , Y <sup>f</sup> )
RFe <sub>2</sub> Ge <sub>2</sub> :	R = La <sup>i</sup> , Ce <sup>k</sup> , Pr <sup>i</sup> , Nd <sup>i</sup> , Gd <sup>k</sup> , Dy <sup>i</sup> , Yb <sup>i</sup> )
RCO <sub>2</sub> Ge <sub>2</sub> :	R = La <sup>v</sup> , Ce <sup>k,v</sup> , Pr <sup>v</sup> , Nd <sup>v</sup> , Sm <sup>v</sup> , Gd <sup>k,v</sup> , Tb <sup>v</sup> , Dy <sup>v</sup> , Ho <sup>v</sup> , Er <sup>v</sup> , Tm <sup>v</sup> , Yb <sup>v</sup> , Lu <sup>v</sup> , Y <sup>v</sup> )
RNi <sub>2</sub> Ge <sub>2</sub> :	R = La <sup>k</sup> , Ce <sup>h,k</sup> , Pr <sup>k</sup> , Nd <sup>k</sup> , Sm <sup>k</sup> , Eu <sup>h,m</sup> , Gd <sup>k</sup> , Tb <sup>k</sup> , Dy <sup>k</sup> , Ho <sup>k</sup> , Er <sup>k</sup> , Tm <sup>k</sup> , Yb <sup>k</sup> , Lu <sup>k</sup> , Y <sup>k</sup> )
RRh <sub>2</sub> Ge <sub>2</sub> :	R = La <sup>v</sup> , Gd <sup>r</sup> )
RPd <sub>2</sub> Ge <sub>2</sub> :	R = La <sup>r</sup> , Ce <sup>r</sup> , Nd <sup>r</sup> , Eu <sup>z</sup> , Gd <sup>r</sup> , Dy <sup>r</sup> , Yb <sup>r</sup> )
RPt <sub>2</sub> Ge <sub>2</sub> <sup>x</sup> :	R = La <sup>r</sup> , Ce <sup>r</sup> , Nd <sup>r</sup> , Gd <sup>r</sup> , Dy <sup>r</sup> )
RNi <sub>2</sub> Sn <sub>2</sub> :	R = La <sup>k</sup> , Ce <sup>k</sup> , Pr <sup>k</sup> , Nd <sup>k</sup> , Sm <sup>k</sup> )

\*Composition is close to RNiGa<sub>3</sub>. See 80(75):PrNiGa<sub>3</sub>.

\*\*According to Pinto and Shaked (1973) the *R* value can be slightly lowered if 9.8% of the Fe atoms are on the antiprismatic Si sites and vice versa.

\*\*\*Bodak and Gladyshevskii (1970) give two compositions: CeCo<sub>2</sub>Si<sub>2</sub> and CeCoSi<sub>3</sub>. According to B. Chabot (unpublished results) CeCoSi<sub>3</sub> has the BaNiSn<sub>3</sub>-type (see 8075:LaIrSi<sub>3</sub>).

†MaF, 77 give two compositions: EuNi<sub>2</sub>Si<sub>2</sub> and EuNiSi<sub>3</sub>, BoGK, 66 give only the 1:1:3 composition. See 80(75):PrNiGa<sub>3</sub>.

††Low-temperature modification. High-temperature modification with CaBe<sub>2</sub>Ge<sub>2</sub>-type.



<sup>†††</sup>According to Mayer and Yetor (1977) and Rossi et al. (RoMF, 79) Pt and Si atoms are randomly distributed on the Al sites of the BaAl<sub>4</sub>-type. According to Ballestracci and Astier (1978) the lattice is tetragonal primitive (CaBe<sub>2</sub>Ge<sub>2</sub>-type?).

\* BaAl<sub>4</sub>-type variant. Order of Pt and Ge atoms on Al sites needs further investigation.

<sup>a)</sup> StKC, 78	<sup>b)</sup> Ro, 73	<sup>c)</sup> NiSY, 73	<sup>d)</sup> NiSY, 71
<sup>e)</sup> SoBG, 71	<sup>f)</sup> RoMMF, 78	<sup>g)</sup> SiSL, 78	<sup>h)</sup> BoGK, 66
<sup>i)</sup> RoMF, 78	<sup>j)</sup> MaF, 72	<sup>k)</sup> RiP, 69	<sup>l)</sup> FeM, 73
<sup>m)</sup> MaF, 77	<sup>n)</sup> KoBG, 77	<sup>o)</sup> SkSG, 67	<sup>p)</sup> BoKG, 76
<sup>q)</sup> BaA, 78	<sup>r)</sup> RoMF, 79	<sup>s)</sup> Ba, 76	<sup>t)</sup> MaY, 77
<sup>u)</sup> NaRBW, 75	<sup>v)</sup> MccNB, 73	<sup>w)</sup> Gr, 82	<sup>x)</sup> PiS, 73
<sup>y)</sup> E. Hovestreydt, unpublished results (LaRh <sub>2</sub> Ge <sub>2</sub> : <i>a</i> = 4.1814, <i>c</i> = 10.5407 Å)			
<sup>z)</sup> FeMGS, 75	<sup>aa)</sup> SzS, 81	<sup>ab)</sup> KuS, 74	<sup>ac)</sup> BrEP, 83
<sup>ad)</sup> SiS, 82	<sup>ae)</sup> HiHRS, 83	<sup>af)</sup> SaGVGPD, 81	<sup>ag)</sup> SkGBY, 80
<sup>ah)</sup> BoG, 70	<sup>ai)</sup> SkMGT, 81	<sup>aj)</sup> HoR, 83	

The ThCr<sub>2</sub>Si<sub>2</sub>-type, a BaAl<sub>4</sub>-type derivative, shown in fig. 50a, is the most frequent structure type found in R–T–B, R–T–Si and R–T–Ge systems. It is also found with phosphides and related compounds. For a recent literature survey see Jeitschko and Jaberg (1980).

#### BaAl<sub>4</sub>-type derivatives with tetragonal unit cell as BaAl<sub>4</sub>

In the BaAl<sub>4</sub> structure with crystal-chemical formula BaAl<sub>2</sub><sup>[2+4c]</sup>Al<sub>2</sub><sup>[(4+4a)]</sup> there are two crystallographically different Al sites, i.e., four tetrahedral sites and four antiprismatic sites per tetragonal unit cell. In the BaAl<sub>4</sub>-type derivatives the Al

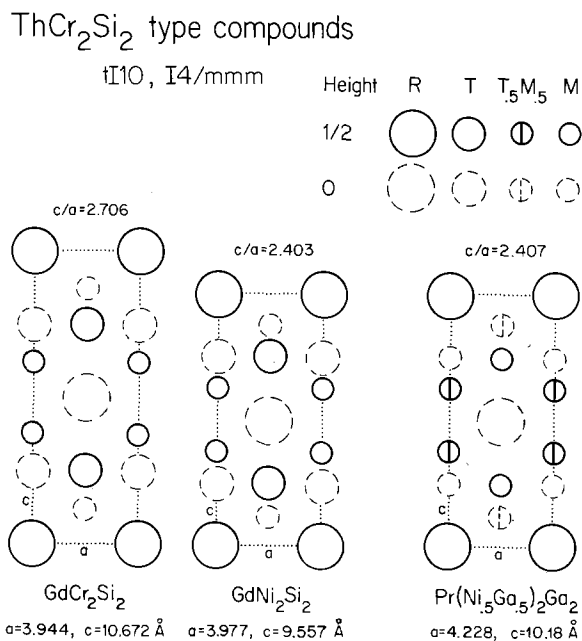


Fig. 50a. Examples of compounds with the ThCr<sub>2</sub>Si<sub>2</sub>-type, a BaAl<sub>4</sub>-type derivative.

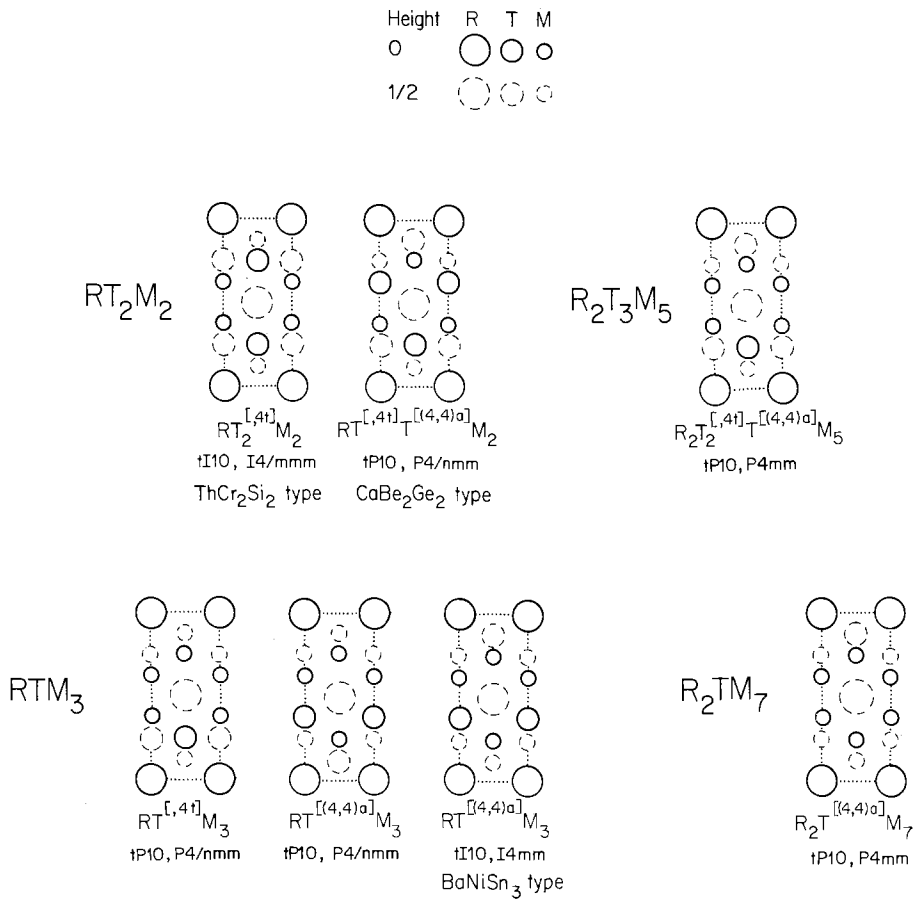


Fig. 50b. The seven possible ordered ternary  $BaAl_4$  derivative structures with tetragonal symmetry and the same unit cell as  $BaAl_4$  and without short T-T contacts.

sites are occupied in ordered fashion by T and M atoms. Limiting ourselves to those hypothetical derivative structures which have the same tetragonal unit cell as  $BaAl_4$  there are 22 possibilities of arranging T and M atoms on the available eight Al sites per unit cell (Parthé et al., PaCBE, 83). However, a comparative study of all known  $BaAl_4$ -type derivative structures and also of the intergrowth structures with ternary ordered  $BaAl_4$ -type derivative segments makes it evident, that only those  $BaAl_4$ -type derivative structures or segments are formed where no short T-T contacts occur. Then only seven hypothetical  $BaAl_4$ -type derivative structures remain (shown in fig. 50b), of which three have already been confirmed experimentally.

– $ThCr_2Si_2$ -type ( $tI10, I4/mmm$ ). The crystal-chemical formula is



i.e., transition metals are on tetrahedral sites. The site exchange variant  $RT_2^{[(4,4)a]}M_2^{[4t]}$  with transition elements on the antiprismatic sites is not included in fig. 50b, because

in this case T atoms are in close contact along the [001] direction, and no compounds have been found with this less probable structure.

–CaBe<sub>2</sub>Ge<sub>2</sub>-type (tP10, P4/nmm; EiMMS, 72). For the same composition RT<sub>2</sub>M<sub>2</sub> there is the further ordering possibility of arrangement of the T and M atoms such that both species have both coordinations, tetrahedral and antiprismatic, according to



This is, however, possible only with a change of symmetry to a tetragonal primitive lattice. The corresponding atom arrangement is called CaBe<sub>2</sub>Ge<sub>2</sub>-type. It is found, for example, with 8050:LaIr<sub>2</sub>Si<sub>2</sub> (high-temperature modification) and LaCu<sub>2</sub>Sn<sub>2</sub> (DöSSS, 82). With rare earth–nickel (palladium) pnictides both structure types occur, the ThCr<sub>2</sub>Si<sub>2</sub>- and the CaBe<sub>2</sub>Ge<sub>2</sub>-types. Phosphides and arsenides crystallize with the first and antimonides and bismuthides with the second type (HoJ, 83).

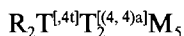
–BaNiSn<sub>3</sub> type (tI10, I4mm; DöS, 78). In this structure with crystal-chemical formula



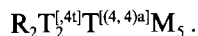
half of the antiprismatic sites are occupied by Ni atoms, the other antiprismatic sites and all tetrahedral sites by Sn atoms. This structure has been found with 8075:LaIrSi<sub>3</sub>.

#### *Other BaAl<sub>4</sub>-type derivatives*

–U<sub>2</sub>Co<sub>3</sub>Si<sub>5</sub> type (oI40, Ibam; KoB, 80). This more complicated arrangement of T and M atoms on the Al sites of BaAl<sub>4</sub> and crystal-chemical formula



is shown in fig. 55 and discussed with 8063:Sc<sub>2</sub>Co<sub>3</sub>Si<sub>5</sub>. The orthorhombic unit cell has a volume which is four times as large as that of the corresponding tetragonal BaAl<sub>4</sub> cell. A possible atom arrangement with the same composition R<sub>2</sub>T<sub>3</sub>M<sub>5</sub> is also shown in fig. 50b, but with less T atoms in antiprismatic coordination according to the crystal chemical formula



For completeness we should also mention an orthorhombic deformation of the BaAl<sub>4</sub>-type (with unit cell dimensions similar to the BaAl<sub>4</sub>-type unit cell) found with Ce(Ni, Sb)<sub>4</sub> (PePB, 82). No R–T–M compounds with this structure type are known.

A stacking variant of the ThCr<sub>2</sub>Si<sub>2</sub>-type is the CeMg<sub>2</sub>Si<sub>2</sub>-type shown in fig. 80 and discussed with 9267:CeMn<sub>4</sub>Al<sub>8</sub>.

#### *Variation of the axial ratio of the ThCr<sub>2</sub>Si<sub>2</sub>-type compounds*

The *c/a* ratios of the ThCr<sub>2</sub>Si<sub>2</sub>-type phases vary from 2.35 to 2.7. The change of *c/a* from 2.7 for GdCr<sub>2</sub>Si<sub>2</sub> to 2.4 for GdNi<sub>2</sub>Si<sub>2</sub>, both shown in fig. 50a, is obviously due to the larger R–T interactions and required shorter R–T distances in the case of GdNi<sub>2</sub>Si<sub>2</sub> as compared to GdCr<sub>2</sub>Si<sub>2</sub>. This is in complete agreement with the

predictions of Miedema concerning the heat of formation of RT compounds, discussed in the introduction.

### *Intergrowth structures with BaAl<sub>4</sub>-type segments*

A great number of different ternary structure types can be interpreted as an intergrowth of BaAl<sub>4</sub>-type (or BaAl<sub>4</sub>-type derivative) segments with segments of another simple structure type. These other segments are of the following structure types: Cu, Po, W, AlB<sub>2</sub>, ZrSi<sub>2</sub>, CaF<sub>2</sub> and Cu<sub>3</sub>Au.

The AlB<sub>2</sub> type is shown in fig. 24 and the ZrSi<sub>2</sub> type in fig. 25. The Cu, Po, W and CaF<sub>2</sub> types are presented in fig. 51, projected along particular directions which should allow easy recognition of these types in the corresponding drawings of the composite structures. The 79(82):Ho<sub>3</sub>Ni<sub>2</sub>Ga<sub>9</sub> structure, shown in fig. 49, is an example of intergrown columns of the BaAl<sub>4</sub>- and CuAu<sub>3</sub>-types; however, in the other structures to be discussed below no columns but slabs are intergrown. What kind of slabs can be intergrown depends on the interface of the BaAl<sub>4</sub>-type slab. If the BaAl<sub>4</sub> slab interface consists of a layer of rare earth atoms, intergrowth is possible only with a W-, an AlB<sub>2</sub>- or a ZrSi<sub>2</sub>-type slab. However, if the BaAl<sub>4</sub>-type slab has as interface a non-rare-earth layer, intergrowth is possible with a Cu-, Po-, CaF<sub>2</sub>- or Cu<sub>3</sub>Au-type slab.

We shall now consider the different kinds of intergrowth structures. If the kind and the number of segments are known, the rare earth content of the compound (100

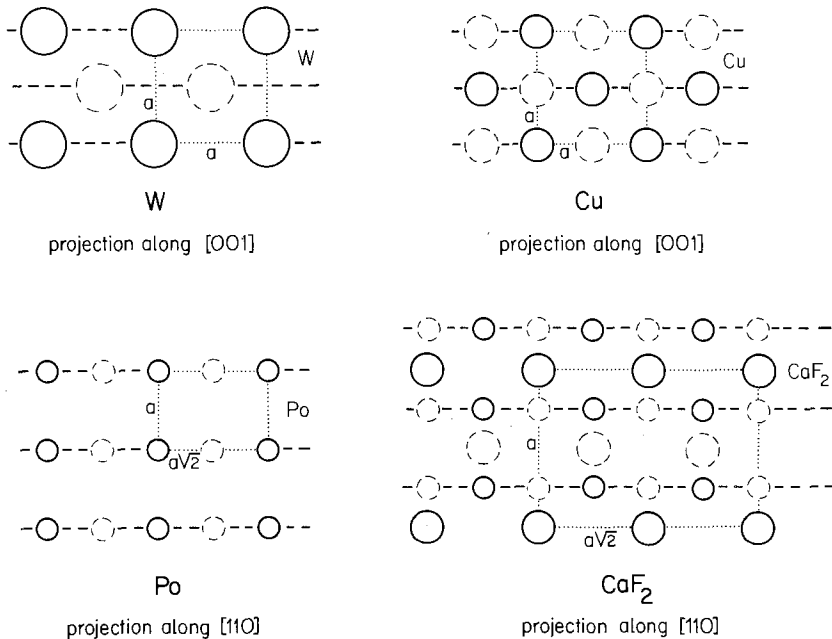


Fig. 51. Segments of simple structure types which can be intergrown with BaAl<sub>4</sub>- or CeNiSi<sub>2</sub>-type segments. Fully drawn circles at height  $\frac{1}{2}$  above the plane of projection and dashed circles in the plane of projection.

minus the first two digits of the composition code) is uniquely determined\*. However, the distribution of the T and M atoms on the Al sites of the  $BaAl_4$ -type segments varies; thus the last two figures of the composition code cannot be determined in advance, but there are never close T–T contacts.

(a) *Intergrowth structures with  $BaAl_4$ -type slabs having a rare earth interface.\*\**

$BaAl_4 + W$ -type slab intergrowth results in a compound of predicted composition  $R(\underline{T}, M)_2$ . Such a structure is found with 6750:CeFeSi, which crystallizes with the PbFCl-type and is shown in fig. 19.

$m BaAl_4 + n AlB_2$ -type slab intergrowth gives the three structures of the  $R_{m+n}\underline{T}_{2n}\underline{M}_{4m}$  structural series 7350:La<sub>3</sub>Rh<sub>4</sub>Ge<sub>4</sub> ( $m = 1, n = 2$ ), 7567:CeNiSi<sub>2</sub> ( $m = 1, n = 1$ ) and 7780:Ce<sub>3</sub>Ni<sub>2</sub>Si<sub>8</sub> ( $m = 2, n = 1$ ), which are shown in figs. 30 and 31 and which are discussed with 7350:La<sub>3</sub>Rh<sub>4</sub>Ge<sub>4</sub>.

$BaAl_4 + ZrSi_2$ -type slab intergrowth should give a compound  $R(T, M)_3$ . A corresponding structure has not yet been found with R–T–M compounds, but exists with CaMnBi<sub>2</sub>, tP8, P4/nmm (BrCS, 80) and SrZnSb<sub>2</sub> oP16, Pnma (BrCS, 79), a deformation variant of the CaMnBi<sub>2</sub> structure. A quaternary CaMnBi<sub>2</sub>-type derivative is the structure of ZrCuSiAs, tP8, P4/nmm (JoJ, 74) which was originally described as “filled” PbFCl-type. In this case the ZrSi<sub>2</sub>-type slab is actually formed by Zr and Si atoms.

(b) *Intergrowth structures with  $BaAl_4$ -type slabs without rare earth interface.*

Four R–T–M structures belong to this category: CeRe<sub>4</sub>Si<sub>2</sub>, ScNi<sub>2</sub>Si<sub>3</sub>, LaNi<sub>0.6</sub>Ga<sub>6</sub> and Ce<sub>2</sub>NiGa<sub>10</sub>. Their structural data are listed in the upper part of table 15 and their drawings are given in figs. 52a and 85. The slabs intergrown with the  $BaAl_4$ -type slabs are of the Cu-, Po- and CaF<sub>2</sub>-type, respectively. These slabs contain no rare earth elements.

(c) *Intergrowth structures with CeNiSi<sub>2</sub>-type slabs without rare earth interface.*

A series of more complicated structures can be obtained if a CeNiSi<sub>2</sub>-type slab is substituted for every  $BaAl_4$ -type slab. The 7567:CeNiSi<sub>2</sub> structure, shown in fig. 31, is itself already an intergrowth structure consisting of  $BaAl_4$ - and  $AlB_2$ -type slabs. Three intergrowth structures with CeNiSi<sub>2</sub>-type slabs, the LaRe<sub>2</sub>Si<sub>2</sub>, ScNiSi<sub>3</sub> and the U<sub>2</sub>Ni<sub>2</sub>Si<sub>7</sub> structures, are shown in fig. 52b and their structural data are listed in the lower part of table 15. The structure types of the slabs intergrown with the CeNiSi<sub>2</sub>-type slabs are, as above, of the Cu-, Po- and CaF<sub>2</sub>-type, respectively. Thus to each drawing in fig. 52a corresponds a drawing in fig. 52b. One should note that the term CeNiSi<sub>2</sub>-type slab refers to an arrangement where the Ce sites are always occupied by R atoms, but where the distribution of the T and M atoms on the Ni and Si sites varies and does not necessarily correspond to that in CeNiSi<sub>2</sub>. Thus, as above, if the kind and number of slabs are known only the content of rare earth element can be stated beforehand. In the lower part of table 15 are also given the

\*In the  $BaAl_4$ -,  $AlB_2$ -,  $ZrSi_2$ -, W- and Cu<sub>3</sub>Au-type slabs the Ba, Al, Zr, W and Au sites are occupied by rare earth atoms. The Cu-, Po- and CaF<sub>2</sub>-type slabs do not contain rare earth atoms.

\*\*The structural sites of the underlined elements are occupied by rare earth atoms.

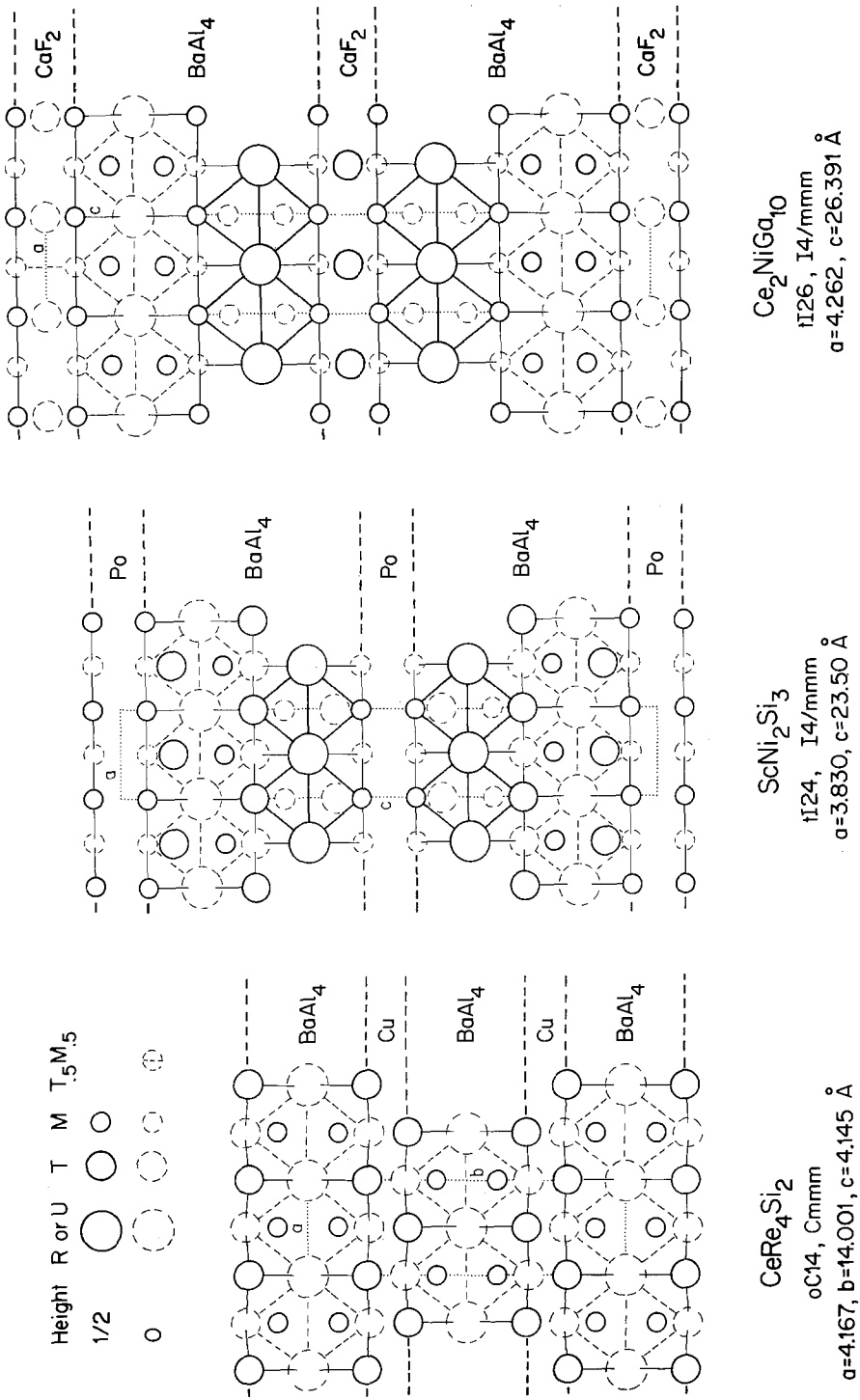
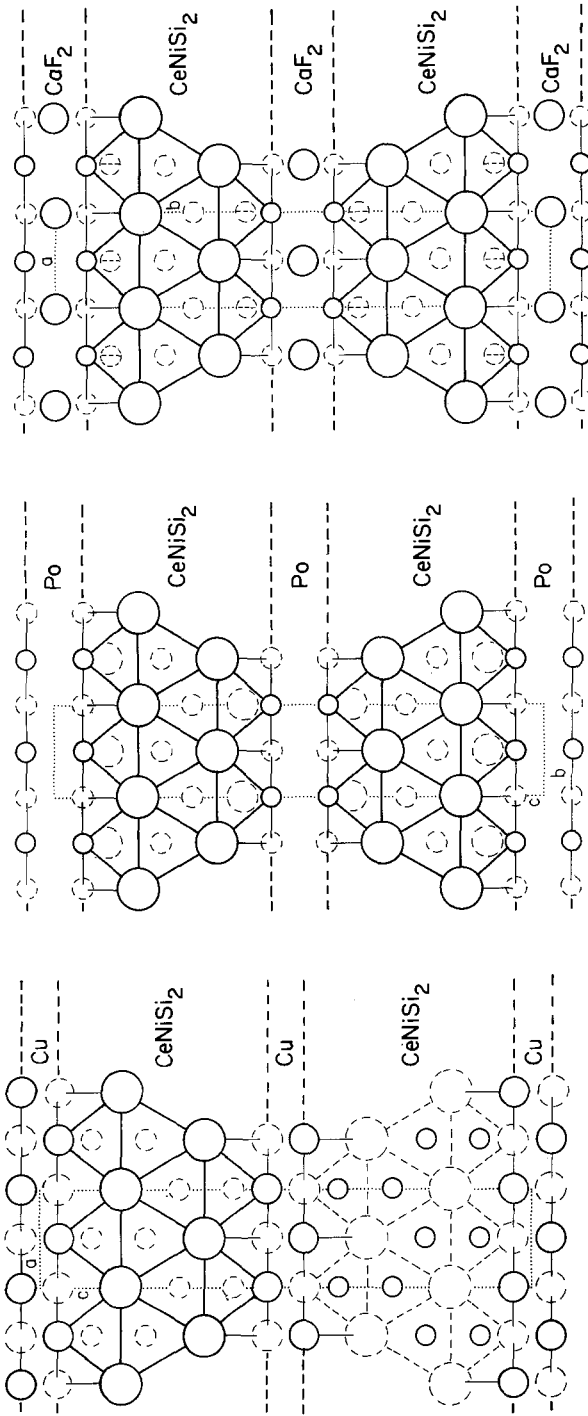


Fig. 52a. Intergrowth structures containing BaAl<sub>4</sub>-type slabs without rare earth atoms on the interface.



$\text{LaRe}_2\text{Si}_2$   
 $\text{oI}20, \text{I}mmma$   
 $a=4.116, b=4.206, c=20.89 \text{ \AA}$

$\text{ScNiSi}_3$   
 $\text{oC}20, \text{A}mm2$   
 $a=3.815, b=3.825, c=20.62 \text{ \AA}$

$\text{U}_2\text{Ni}_2\text{Si}_7$   
 $\text{oC}22, \text{C}mmm$   
 $a=3.964, b=20.85, c=3.964 \text{ \AA}$

Fig. 52b. Intergrowth structures containing  $\text{CeNiSi}_2$ -type slabs without rare earth atoms on the interface.

TABLE 15

Structural data for intergrowth structures containing  $BaAl_4$ -type (or  $BaAl_4$ -type derivative) slabs or  $CeNiSi_2$ -type slabs without rare earth atoms on the interface. The structural sites of the underlined elements in the first column are occupied by rare earth atoms.

Structure type and composition of slabs	Predicted stoichiometry	Composition code for known compound*	Compound formula	Pearson's classif. symbol	Space group	Fig.
<i>BaAl<sub>4</sub>-type slabs</i>						
<u>Ba</u> Al <sub>4</sub> + 2 Cu	R(T, M) <sub>6</sub>	8633	CeRe <sub>4</sub> Si <sub>2</sub>	oC14	Cmmm	52a
2 <u>Ba</u> Al <sub>4</sub> + 2 Cu	R(T, M) <sub>5</sub>	—				
2 <u>Ba</u> Al <sub>4</sub> + 2 Po	R(T, M) <sub>5</sub>	8360	ScNi <sub>2</sub> Si <sub>3</sub>	tI24	I4/mmm	52a
1 <u>Ba</u> Al <sub>4</sub> + CaF <sub>2</sub>	R(T, M) <sub>7</sub>	8791	LaNi <sub>0.6</sub> Ga <sub>6</sub>	tP16(−0.8)	P4/mmm	85
2 <u>Ba</u> Al <sub>4</sub> + CaF <sub>2</sub>	R <sub>2</sub> (T, M) <sub>11</sub>	8591	Ce <sub>2</sub> NiGa <sub>10</sub>	tI26	I4/mmm	52a
2 <u>Ba</u> Al <sub>4</sub> + Cu <sub>3</sub> Au	R <sub>3</sub> (T, M) <sub>11</sub>	**				
<i>CeNiSi<sub>2</sub>-type slabs</i>						
<u>Ce</u> NiSi <sub>2</sub> + 2 Cu	R(T, M) <sub>5</sub>	—				
2 <u>Ce</u> NiSi <sub>2</sub> + 2 Cu	R(T, M) <sub>4</sub>	8050	LaRe <sub>2</sub> Si <sub>2</sub>	oI20	Imma	52b
2 <u>Ce</u> NiSi <sub>2</sub> + 2 Po	R(T, M) <sub>4</sub>	8075	ScNiSi <sub>3</sub>	oC20	Amm2	52b
2 <u>Ce</u> NiSi <sub>2</sub> + CaF <sub>2</sub>	R <sub>2</sub> (T, M) <sub>9</sub>	(8278)	U <sub>2</sub> Ni <sub>2</sub> Si <sub>7</sub>	oC22	Cmmm	52b
2 <u>Ce</u> NiSi <sub>2</sub> + 2 CaF <sub>2</sub>	R(T, M) <sub>6</sub>	(8650)	EuMg <sub>3</sub> Ge <sub>3</sub>	oC28	Cmcm	—
2 <u>Ce</u> NiSi <sub>2</sub> + Cu <sub>3</sub> Au	R(T, M) <sub>3</sub>	7578	La <sub>3</sub> Co <sub>2</sub> Sn <sub>7</sub>	oC24	Cmmm	34

\*Parentheses around the composition code indicate that the compound is not a R–T–M compound.

\*\*79(82):Ho<sub>3</sub>Ni<sub>2</sub>Ga<sub>9</sub> has intergrown columns of  $BaAl_4$ - and  $Cu_3Au$ -type.

structural data for the  $EuMg_3Ge_3$  structure (ZmGB, 73) not yet found with R–T–M compounds. This structure corresponds to the structure of  $U_2Ni_2Si_7$  (AkYG, 75), shown in fig. 52b, except that the  $CaF_2$  slab is twice as thick. The last entry concerns the 7578:La<sub>3</sub>Co<sub>2</sub>Sn<sub>7</sub> structure, shown in fig. 34, which consists of intergrown  $CeNiSi_2$ - and  $Cu_3Au$ -type slabs.

Concerning a special notation for and the symmetry of these intergrowth structures see Grin et al. (GrYG, 77, 82).

8050	<u>La</u> Ir <sub>2</sub> Si <sub>2</sub> *	tP10	$a = 4.1909$	BrEP, 83
		P4/nmm	$c = 9.944$	

CaBe<sub>2</sub>Ge<sub>2</sub>-type (EiMMS, 72) ≡  $BaAl_4$ -type (Dl<sub>3</sub>) derivative

\*High-temperature modification. Low-temperature modification with ThCr<sub>2</sub>Si<sub>2</sub>-type.



No isotypic  $RT_2M_2$  compounds are known.

The  $LaIr_2Si_2$  structure with the  $CaBe_2Ge_2$ -type is shown in fig. 50b. It is a variant of the  $ThCr_2Si_2$ -type and is discussed with 8050: $CeNi_2Si_2$ .

8050	$ScFe_2Si_2$	$oP20$ $Pbcm$	$a = 7.263$ $b = 7.076$ $c = 5.009$	GIKBS, 77
------	--------------	------------------	---	-----------

$HfFe_2Si_2$ -type (YaLG, 76)

No isotypic  $RT_2M_2$  compounds are known.

The  $ScFe_2Si_2$  structure with  $HfFe_2Si_2$  type is shown in fig. 53. The characteristic surrounding of the T elements by square pyramids of M elements suggests some structural similarities with the  $CaBe_2Ge_2$ -type (see 8050: $LaIr_2Si_2$ , h.t.). Comparison of  $ScFe_2Si_2$  (fig. 53) with the  $CaBe_2Ge_2$ -type, projected along [110] (fig. 55) shows that effectively the lower part of  $ScFe_2Si_2$  (as delimited by dashed lines on the drawing) is similar to the lower part of  $CaBe_2Ge_2$ . The upper segment of  $ScFe_2Si_2$  differs from the upper part of  $CaBe_2Ge_2$  by a shift of the T elements outside the M tetrahedra, changing the tetrahedral coordination into an approximately pyramidal coordination.

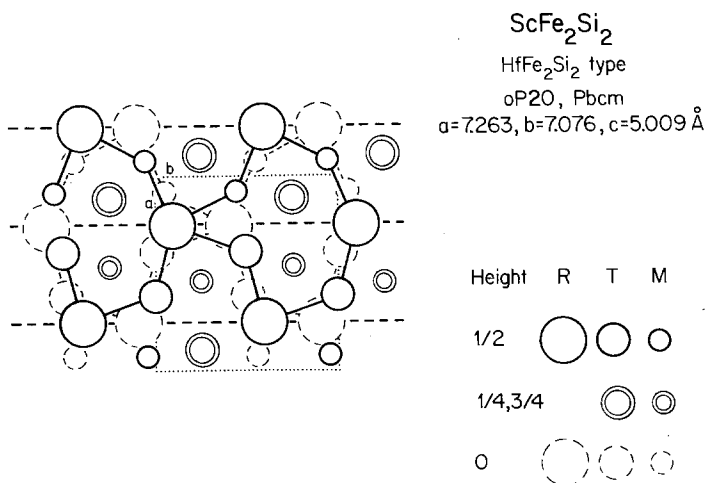


Fig. 53. The crystal structure of  $ScFe_2Si_2$  with  $HfFe_2Si_2$ -type.

8050	$\text{LaRe}_2\text{Si}_2$	$\text{oI}20$	$a = 4.116$	PeBG, 77
	or	Imma	$b = 4.206$	
	$\text{LaRe}_2\text{Si} \oplus \text{Si}^{[6, \text{p}]}$		$c = 20.89$	

No isotypic  $\text{RT}_2\text{M}_2$  compounds are known.

The  $\text{LaRe}_2\text{Si}_2$  structure, shown in fig. 52b, can be considered as an intergrowth of  $\text{CeNiSi}_2$ - and Cu-type slabs. The intergrowth structures are discussed in detail with 8050:  $\text{CeNi}_2\text{Si}_2$ .

Two structure types are found with composition 8063:  $\text{Sc}_2\text{Fe}_3\text{Si}_5$ , tP40 and  $\text{U}_2\text{Co}_3\text{Si}_5$ , oI40 (see  $\text{Sc}_2\text{Co}_3\text{Si}_5$ ).

8063	$\text{Sc}_2\text{Fe}_3\text{Si}_5$	tP40	$a = 10.225^*$	BoKYG, 77
	or	P4/mnc	$c = 5.275$	
	$\text{Sc}_2\text{Fe}_2^{[6\text{o}]} \text{Fe}^{[4\text{t}]} \text{Si}_4\text{Si}^{[(4, 4)\text{a}]}$			

$\text{Sc}_2\text{Fe}_3\text{Si}_5$ -type (BoKYG, 77) or  $\text{U}_2\text{Mn}_3\text{Si}_5$ -type (YaAG, 77)

\*Lattice parameters are those given by Braun (1980).

Isotypic compounds:

$\text{R}_2\text{Mn}_3\text{Si}_5$ :	$\text{R} = \text{Tb}^f, \text{Dy}^f, \text{Ho}^f, \text{Er}^f, \text{Tm}^f, \text{Lu}^f, \text{Y}^f$
$\text{R}_2\text{Fe}_3\text{Si}_5$ :	$\text{R} = \text{Sm}^{c, d}, \text{Gd}^{c, d}, \text{Tb}^{c, d}, \text{Dy}^{a, c, d}, \text{Ho}^{c, d}, \text{Er}^{c, d}, \text{Tm}^{c, d}, \text{Yb}^{c, d}, \text{Lu}^{b, c, d},$ $\text{Y}^{b, c, d}, \text{Sc}^{a, b, c, d}$
$\text{R}_2\text{Ru}_3\text{Si}_5$ :	$\text{R} = \text{Lu}^{d, f}, \text{Y}^{d, f}$
$\text{R}_2\text{Re}_3\text{Si}_5$ :	$\text{R} = \text{La}^f, \text{Ce}^e, \text{Pr}^e, \text{Nd}^e, \text{Sm}^e, \text{Gd}^e, \text{Tb}^e, \text{Dy}^e, \text{Ho}^e, \text{Er}^e, \text{Tm}^e, \text{Y}^{e, d}$
$\text{R}_2\text{Os}_3\text{Si}_5$ :	$\text{R} = \text{Lu}^{d, f}, \text{Y}^{d, f}$
<sup>a</sup> )BoKYG, 77	<sup>b</sup> )Br, 80
<sup>c</sup> )BrAS, 80	<sup>d</sup> )JoB, 82
<sup>e</sup> )BoPG, 78	<sup>f</sup> )Se, 81

The  $\text{Sc}_2\text{Fe}_3\text{Si}_5$  structure, shown in fig. 54, can be considered as a periodic intergrowth of columns of two types. The column with rhombic cross section corresponds to a segment of the  $\text{U}_2\text{Co}_3\text{Si}_5$ -type found with 8063:  $\text{Sc}_2\text{Co}_3\text{Si}_5$  (fig. 55) and the columns with square cross section are of the  $\text{CeMg}_2\text{Si}_2$ -type (fig. 80), discussed with 9267:  $\text{CeMn}_4\text{Al}_8$ . It should be remarked that the  $\text{U}_2\text{Co}_3\text{Si}_5$ -type is a  $\text{BaAl}_4$ -type deformation derivative and  $\text{CeMg}_2\text{Si}_2$  is a  $\text{BaAl}_4$ -type stacking variant. One third of the T elements—those in the columns with rhombic cross section—are tetrahedrally, all others octahedrally surrounded by Si atoms. The  $\text{Sc}_2\text{Fe}_3\text{Si}_5$ -type is found only with transition elements of the Mn and Fe group. With transition elements of the Co and Ni group the related 8063:  $\text{Sc}_2\text{Co}_3\text{Si}_5$  structure is formed.

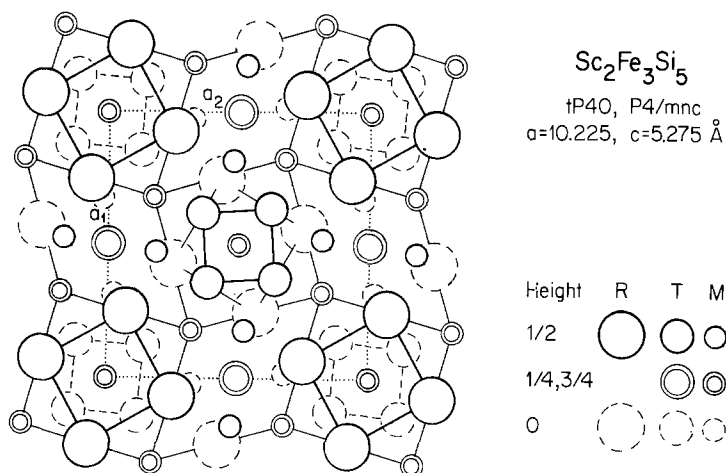
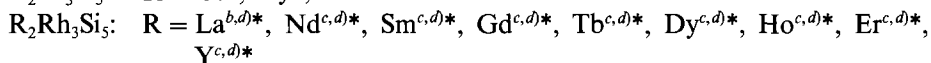
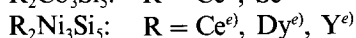
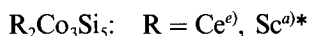


Fig. 54. The crystal structure of  $\text{Sc}_2\text{Fe}_3\text{Si}_5$ , built up of  $\text{U}_2\text{Co}_3\text{Si}_5$ -type columns (rhombic cross section) and  $\text{CeMg}_2\text{Si}_2$ -type columns (square cross section).

8063	$\text{Sc}_2\text{Co}_3\text{Si}_5$	$\text{oI}40$	$a = 9.206$	KoB, 80
	or	$\text{Ibam}$	$b = 11.30$	
	$\text{ScCo}_2\text{Co}^{[4i]}\text{Si}_2\text{Si}_2^{[(2+2)j]}\text{Si}^{[4i]}$		$c = 5.348$	

$\text{U}_2\text{Co}_3\text{Si}_5$ -type (AkYG, 77)  $\equiv$   $\text{BaAl}_4$ -type ( $\text{D1}_3$ -type) derivative

Isotypic compounds:



\*With the same T elements are found  $\text{RT}_2\text{M}_2$  compounds which crystallize with the  $\text{ThCr}_2\text{Si}_2$ -type (see 8050:  $\text{CeNi}_2\text{Si}_2$ ).

<sup>a</sup>KoB, 80

<sup>b</sup>ChLVEH, 82

<sup>c</sup>ChLEVH, 82

<sup>d</sup>ChLEVH, 82a

<sup>e</sup>ChP, 83a

The  $\text{Sc}_2\text{Co}_3\text{Si}_5$  structure with  $\text{U}_2\text{Co}_3\text{Si}_5$  type is shown on the left-hand side of fig. 55. It is a derivative of the tetragonal  $\text{BaAl}_4$ -type (see discussion with 8050:  $\text{CeNi}_2\text{Si}_2$ ). Co and Si atoms occupy the Al sites in an ordered fashion, which leads to an orthorhombic unit cell with a volume four times as large [ $a = c(\text{BaAl}_4)$ ,  $b = 2\sqrt{2}a(\text{BaAl}_4)$ ,  $c = \sqrt{2}a(\text{BaAl}_4)$ ]. The  $\text{Sc}_2\text{Co}_3\text{Si}_5$  structure can be considered as an intergrowth of  $\text{CaBe}_2\text{Ge}_2$ -type slabs (right-hand side of fig. 55; see 8050:  $\text{LaIr}_2\text{Si}_2$ ) with slabs of composition  $\text{RTM}_3$ . The atom arrangement of the latter corresponds

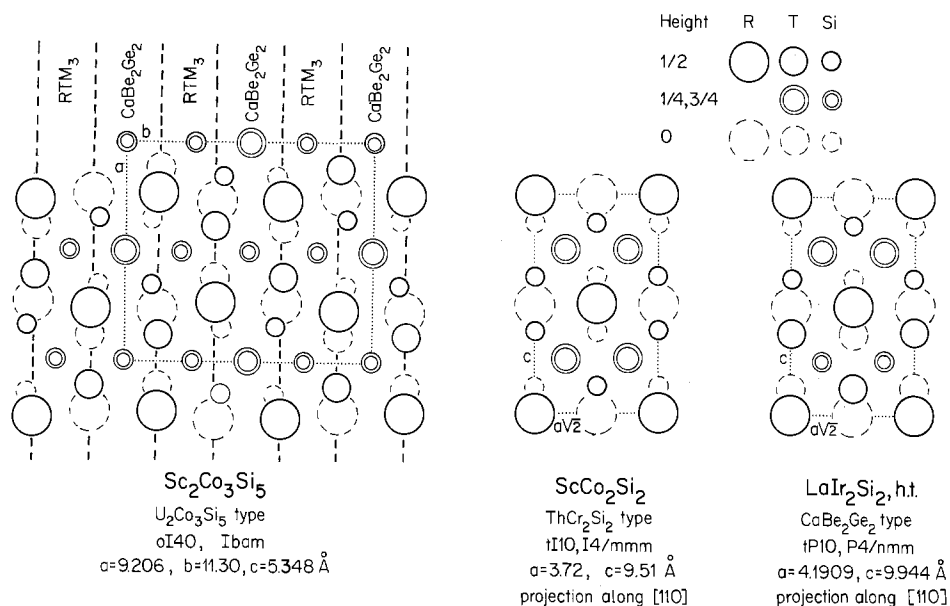


Fig. 55. A projection of the Sc<sub>2</sub>Co<sub>3</sub>Si<sub>5</sub> (U<sub>2</sub>Co<sub>3</sub>Si<sub>5</sub>-type) along [001] compared with the ScCo<sub>2</sub>Si<sub>2</sub> structure (ThCr<sub>2</sub>Si<sub>2</sub>-type) and the LaIr<sub>2</sub>Si<sub>2</sub> structure (CaBe<sub>2</sub>Ge<sub>2</sub>-type), both projected along [110]. The three structures are BaAl<sub>4</sub>-type derivative structures with a different arrangement of T and M elements on the Al sites of BaAl<sub>4</sub>.

to an unknown BaAl<sub>4</sub>-type derivative structure. For structural similarities with 8063: Sc<sub>2</sub>Fe<sub>3</sub>Si<sub>5</sub> see the latter type.

Three structure types are found with composition 8075 or 80(75): ScNiSi<sub>3</sub>, oC20; BaNiSn<sub>3</sub>, tI10 (see LaIrSi<sub>3</sub>) and PrNiGa<sub>3</sub>, tI10, the last two being BaAl<sub>4</sub>-type derivatives.

<b>8075</b>	ScNiSi <sub>3</sub>	oC20	a = 3.815	KoBMG, 77
	or	Amm2	b = 3.825	
	ScNiSi <sub>2</sub> ∞ Si <sup>[6,p]</sup>		c = 20.62	

#### Isotypic compounds:

RNiSi<sub>3</sub>\*: R = Gd<sup>(c)</sup>, Tb<sup>(c)</sup>, Dy<sup>(c)</sup>, Ho<sup>(c)</sup>, Er<sup>(c)</sup>, Tm<sup>(c)</sup>, Yb<sup>(c)</sup>, Lu<sup>(c,d)</sup>, Y<sup>(a,c)</sup>, Sc<sup>(b)</sup>

\*It should be noted that for ScNiSi<sub>3</sub> a < b, but for YNiSi<sub>3</sub> a > b. No cell parameters were given for the other compounds.

<sup>a)</sup>Ya, 77      <sup>b)</sup>KoBMG, 77      <sup>c)</sup>GoBGY, 77

<sup>d)</sup>B. Chabot, unpublished results [LuNiSi<sub>3</sub>: a = 3.891(1), b = 3.889(1), c = 20.834(6) Å]

The  $\text{ScNiSi}_3$  structure, shown in fig. 52b, can be interpreted as an intergrowth of  $\text{CeNiSi}_2$ - and Po-type slabs. For a detailed discussion of these intergrowth structures see 8050: $\text{CeNi}_2\text{Si}_2$ .

---

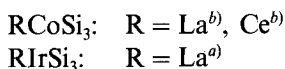
<b>8075</b>	<b>LaIrSi<sub>3</sub></b>	tI10	$a = 4.282$	EnBP, 83
	or	I4mm	$c = 9.838$	
	$\text{LaIr}^{[(4,4)a]}_2\text{Si}_2^{[4t]}\text{Si}^{[(4,4)a]}$			

---

$\text{BaNiSn}_3$ -type (DöS, 78)  $\equiv$   $\text{BaAl}_4$ -type ( $\text{D1}_3$ -type) derivative

---

Isotypic compounds:



<sup>a</sup>EnBP, 83

<sup>b</sup>B. Chabot, unpublished results [ $\text{LaCoSi}_3$ ;  $a = 4.1868(8)$ ,  $c = 9.654(2)$  Å and  $\text{CeCoSi}_3$ ;  $a = 4.1344(8)$ ,  $c = 9.561(3)$  Å]

It is probable that some of the compounds listed under 80(75): $\text{PrNiGa}_3$  have the  $\text{BaNiSn}_3$ -type.

The  $\text{BaNiSn}_3$ -type is a  $\text{BaAl}_4$ -type derivative structure, which is shown in fig. 50b and discussed with 8050: $\text{CeNi}_2\text{Si}_2$ .

---

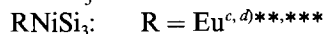
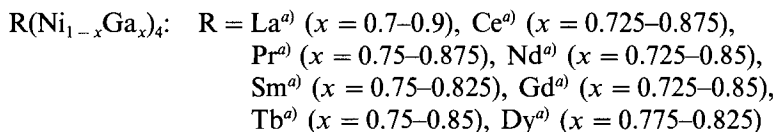
<b>80(75)</b>	<b>PrNiGa<sub>3</sub></b>	tI10	$a = 4.228$	Gr, 82
	or	I4/mmm	$c = 10.18$	
	$\text{Pr}(\text{Ni}_{.5}\text{Ga}_{.5})_2^{[(4\text{Pr},4\text{Ga})a]}\text{Ga}_2^{[4(\text{Ni}_{.5}\text{Ga}_{.5})t]}$			

---

$\text{BaAl}_4$  ( $\text{D1}_3$ )-type derivative with mixed Ni and Ga atom occupation on the antiprismatic Al sites

---

Isotypic compounds:



\*According to BoG, 70 there exists a  $\text{CeCo}_2\text{Si}_2$  phase with  $\text{ThCr}_2\text{Si}_2$ -type (ordered  $\text{BaAl}_4$ -type derivative) and a  $\text{CeCoSi}_3$  phase with  $\text{BaAl}_4$ -type or a superstructure of it. See also 8075:LaIrSi<sub>3</sub>.

\*\*Distribution of atoms on the tetrahedral and antiprismatic sites has not been determined.

\*\*\*According to MaF, 77 this structure also exists with composition 1:2:2. See 8050:CeNi<sub>2</sub>Si<sub>2</sub>.

<sup>a</sup>Gr, 82      <sup>b</sup>BoG, 70      <sup>c</sup>BoGK, 66      <sup>d</sup>MaF, 77

The structure of  $\text{Pr}(\text{Ni}_{.5}\text{Ga}_{.5})_2\text{Ga}_2$ , a  $\text{BaAl}_4$ -related structure where Ni and Ga atoms are distributed at random on the antiprismatic Al sites, is shown in fig. 50a. One should note that Ni and Ga differ by only three electrons and consequently it is difficult to determine any possible atom ordering. Assuming full order the compounds should crystallize with the  $\text{BaNiSn}_3$ -type (see 8075:LaIrSi<sub>3</sub>) discussed with the  $\text{ThCr}_2\text{Si}_2$ -type compounds (see 8050:CeNi<sub>2</sub>Si<sub>2</sub>). At a slightly different composition another ordered  $\text{BaAl}_4$ -type derivative is known for 8063:Sc<sub>2</sub>Co<sub>3</sub>Si<sub>5</sub> with orthorhombic  $\text{U}_2\text{Co}_3\text{Si}_5$ -type.

<b>8244</b>	<b>Sc<sub>2</sub>Ru<sub>5</sub>B<sub>4</sub></b>	mP22	$a = 8.452$	Ro, 83
	or	P2/m	$b = 3.004$	
	Sc <sub>2</sub> Ru <sub>5</sub> [B <sub>2</sub> <sup>[6p]</sup> ]B <sub>2</sub> <sup>[6p]</sup>		$c = 9.953$	
			$\beta = 90.01^\circ$	

Isotypic compounds: All references Ro, 83

Sc<sub>2</sub>T<sub>5</sub>B<sub>4</sub>: T = Ru, Os

The projection along  $b$  of the pseudo-orthorhombic structure of Sc<sub>2</sub>Ru<sub>5</sub>B<sub>4</sub> is presented in fig. 75. The arrangement of the B-centred trigonal prisms and R-centred pentagonal prisms resembles the corresponding projection of 7567:ScMnSi<sub>2</sub> (fig. 44). The structure can be described as an intergrowth of deformed CeCo<sub>3</sub>B<sub>2</sub>-type columns (see fig. 58) and columns of the W<sub>2</sub>CoB<sub>2</sub>-type (also shown in fig. 75), however, with different atom distribution.

<b>8256</b>	<b>Sc<sub>2</sub>Cr<sub>4</sub>Si<sub>5</sub></b>	oI44	$a = 7.585$	KoS, 82a
	or	Ibam	$b = 16.138$	
	Sc <sub>2</sub> Cr <sub>2</sub> Cr <sub>2</sub> <sup>[60]</sup> Si <sub>4</sub> Si <sub>1</sub> <sup>[(4,4)a]</sup>		$c = 4.932$	

Nb<sub>2</sub>Cr<sub>4</sub>Si<sub>5</sub>-type (KrYG, 69) ≡ V<sub>6</sub>Si<sub>5</sub>-type (SpFH, 70) derivative

No isotypic R<sub>2</sub>T<sub>4</sub>M<sub>5</sub> compounds are known.

The Sc<sub>2</sub>Cr<sub>4</sub>Si<sub>5</sub> structure with Nb<sub>2</sub>Cr<sub>4</sub>Si<sub>5</sub>-type, a V<sub>6</sub>Si<sub>5</sub>-type derivative, is shown in fig. 32. It is discussed with 7364:Sc<sub>4</sub>Mn<sub>4</sub>Si<sub>7</sub>.

---

<b>8275</b>	<b>Ho<sub>6</sub>Co<sub>7</sub>Ga<sub>21</sub></b>	tP68 P4/mbm*	$a = 16.687$ $c = 4.134$	YaGG, 81
-------------	--	-----------------	-----------------------------	----------

---

\*Co(2) is in equipoint 8i) and not 8g) as stated erroneously in YaGG, 81.

Isotypic compounds: All references YaGG, 81

R<sub>6</sub>Co<sub>7</sub>Ga<sub>21</sub>: R = Sm, Gd, Tb, Dy, Ho, Er, Tm, Lu, Y

The Ho<sub>6</sub>Co<sub>7</sub>Ga<sub>21</sub> structure, shown on the left-hand side of fig. 56, can be interpreted in simple terms as an intergrowth of Cu<sub>3</sub>Au- and CeCo<sub>3</sub>B<sub>2</sub>-type columns (see 8340:CeCo<sub>3</sub>B<sub>2</sub> and fig. 58). In fig. 56 the outlines of these columns are indicated with thin lines. However, to have complete agreement with the Cu<sub>3</sub>Au and the CeCo<sub>3</sub>B<sub>2</sub> structures it would be necessary to interchange the Co atom in the centre of Cu<sub>3</sub>Au block with the Ga atom in the centre of the CeCo<sub>3</sub>B<sub>2</sub> block of Ho<sub>6</sub>Co<sub>7</sub>Ga<sub>21</sub>. Since Co and Ga atoms differ only by four electrons their differentiation by X-ray diffraction methods is difficult and a structure with "pure" Cu<sub>3</sub>Au and CeCo<sub>3</sub>B<sub>2</sub> columns is not fully excluded. We note that the binary compound HoGa<sub>3</sub> crystallizes in the Cu<sub>3</sub>Au-type.

The Ho<sub>6</sub>Co<sub>7</sub>Ga<sub>21</sub> structure can be compared with the Ti<sub>3</sub>Co<sub>3</sub>B<sub>2</sub> structure (KuY, 71), shown on the right-hand side of fig. 56, which also has intergrown Cu<sub>3</sub>Au- and CeCo<sub>3</sub>B<sub>2</sub>-type columns; however, both columns have a smaller cross section.

---

<b>82(78)</b>	<b>U<sub>2</sub>Ni<sub>2</sub>Si<sub>7</sub></b>	oC22 Cmmm	$a = 3.964$ $b = 20.85$ $c = 3.964$	AkYG, 75
	or U <sub>2</sub> Ni <sup>[1,8c]</sup> (Ni <sub>5</sub> Si <sub>5</sub> ) <sub>2</sub> Si <sub>4</sub> ∞ Si <sub>2</sub> <sup>[6, p]</sup>			

---

The U<sub>2</sub>Ni<sub>2</sub>Si<sub>7</sub> structure has not yet been found with R-T-M compounds, but its occurrence in R-T-M systems seems likely. The structure is shown in fig. 52b. It can be interpreted as an intergrowth of CeNiSi<sub>2</sub>- and CaF<sub>2</sub>-type slabs. These kinds of intergrowth structures are discussed with 8050:CeNi<sub>2</sub>Si<sub>2</sub>.

---

<b>8289</b>	<b>Ho<sub>2</sub>CoGa<sub>8</sub></b>	tP11 P4/mmm	$a = 4.217$ $c = 10.97$	GrYG, 79a
	or Ho <sub>2</sub> <sup>[12c]</sup> Co <sup>[8c]</sup> Ga <sub>8</sub>			

---

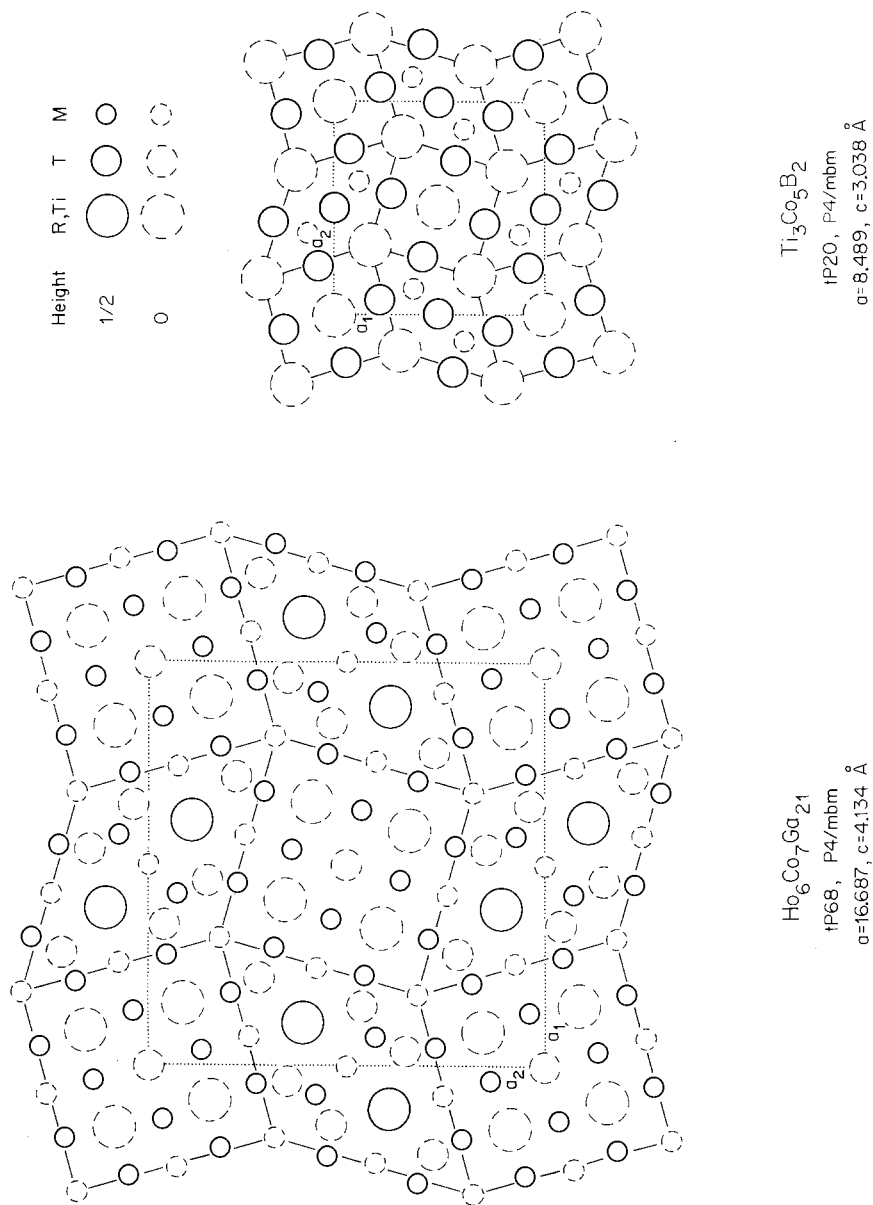


Fig. 56. The crystal structures of  $\text{Ho}_6\text{Co}_7\text{Ga}_{21}$  and  $\text{Ti}_3\text{Co}_5\text{B}_2$ , both built up of intergrown  $\text{Cu}_3\text{Au}$ - and  $\text{CeCo}_3\text{B}_2$ -type columns.



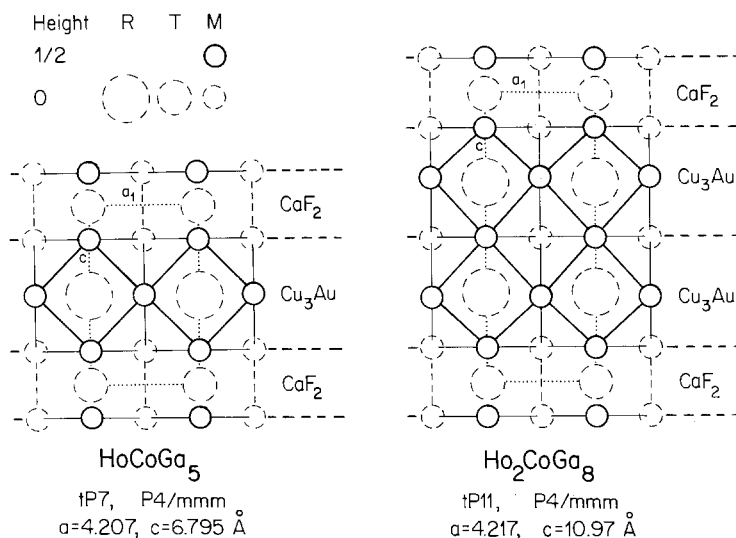
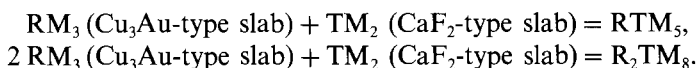


Fig. 57. The HoCoGa<sub>5</sub> and the Ho<sub>2</sub>CoGa<sub>8</sub> structures, both constructed of intergrown Cu<sub>3</sub>Au- and CaF<sub>2</sub>-type slabs.

Isotypic compounds: All references GrYG, 79a

R<sub>2</sub>CoGa<sub>8</sub>: R = Sm, Gd, Tb, Dy, Ho, Er, Tm, Lu, Y.

The Ho<sub>2</sub>CoGa<sub>8</sub> structure is presented in fig. 57 together with the 8683:HoCoGa<sub>5</sub> structure. Both structures can be interpreted as an intergrowth of Cu<sub>3</sub>Au-type slabs with CaF<sub>2</sub>-type slabs. In HoCoGa<sub>5</sub> there is one Cu<sub>3</sub>Au-type slab for every CaF<sub>2</sub>-type slab; in Ho<sub>2</sub>CoGa<sub>8</sub>, however, there are double slabs of Cu<sub>3</sub>Au-type. The compositions of both compounds can be rationalized according to



The structures with intergrown Cu<sub>3</sub>Au-type segments are conveniently classified according to the structure type of the other segment and according to the geometrical form of the segment. One finds intergrown slabs and intergrown columns. The structures one finds with R-T-M compounds are listed in table 16.

8313	Nd <sub>3</sub> Ni <sub>13</sub> B <sub>2</sub>	hP18	a = 5.005	KuB, 81
		P6/mmm	c = 10.904	

CaCu<sub>5</sub>-type derivative

Isotypic compounds:

R<sub>3</sub>Ni<sub>13</sub>B<sub>2</sub>: R = La<sup>a</sup>, Ce<sup>a</sup>, Pr<sup>a</sup>, Nd<sup>a</sup>, Sm<sup>a</sup>, Gd<sup>a</sup>, Tb<sup>b</sup>, Dy<sup>b</sup>, Ho<sup>b</sup>, Er<sup>b</sup>, Tm<sup>b</sup>, Y<sup>a</sup>

<sup>a</sup>KuB, 81    <sup>b</sup>KuBCC, 83

TABLE 16  
R-T-M structures with intergrown  $\text{Cu}_3\text{Au}$ -type segments.

Structure types of segments	Intergrown slabs				Intergrown columns				
	Code	Compound	Pearson's classif. symbol	Space group	Fig.	Code	Compound	Pearson's classif. symbol	Space group
$\text{Cu}_3\text{Au} + \text{CaF}_2$	8289	$\text{Ho}_2\text{CoGa}_8$	tP11	P4/mmm	57				
	8683	$\text{HoCoGa}_5$	tP7	P4/mmm	57				
$\text{Cu}_3\text{Au} + \text{BaAl}_4$						79(82)	$\text{Ho}_3\text{Ni}_2\text{Ga}_9$	oI28	Immm
$\text{Cu}_3\text{Au} + \text{CeNiSi}_2^*$	7578	$\text{La}_3\text{Co}_2\text{Sn}_7$	oC24	Cmmm	34	7471	$\text{Sc}_5\text{Co}_4\text{Si}_{10}$	tP38	P4/mbm
$\text{Cu}_3\text{Au} + \text{CeCo}_3\text{B}_2$						8275	$\text{Ho}_6\text{Co}_7\text{Ga}_{21}$	tP68	P4/mbm
$\text{Cu}_3\text{Au} + \text{MgCuAl}_2$	8380	$\text{YNiAl}_4$	oC24	Cmcm	59				

\* $\text{CeNiSi}_2 \equiv \text{BaAl}_4 + \text{AlB}_2$  (see fig. 31).

The  $\text{Nd}_3\text{Ni}_{13}\text{B}_2$  structure, shown in fig. 37, is a member of the  $\text{R}_{m+n}\text{T}_{5m+3n}\text{M}_{2n}$  structural series with  $m = 2$  and  $n = 1$ , and is built up of  $\text{CaCu}_5$ - and  $\text{CeCo}_3\text{B}_2$ -type slabs. It is discussed with the  $7511:\text{Ce}_3\text{Co}_8\text{Si}$  structure.

---

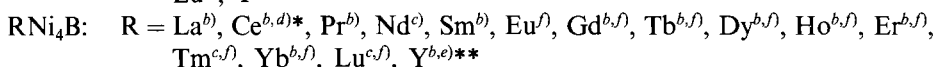
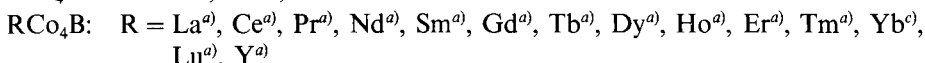
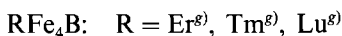
<b>8320</b>	<b>CeCo<sub>4</sub>B</b>	hP12 P6/mmm	$a = 5.005$ $c = 6.932$	KuB, 74
-------------	--------------------------	----------------	----------------------------	---------

---

CaCu<sub>5</sub>-type derivative

---

Isotypic compounds:



\*According to KuB, 71 a superstructure of the CeCo<sub>4</sub>B-type with  $a = 8a(\text{CeCo}_4\text{B})$  and  $c = c(\text{CeCo}_4\text{B})$ .

\*\*According to KuK, 75 a superstructure of the CeCo<sub>4</sub>B-type with  $a = 3a(\text{CeCo}_4\text{B})$  and  $c = c(\text{CeCo}_4\text{B})$ .

<sup>a</sup>KuB, 74    <sup>b</sup>NiKY, 73    <sup>c</sup>KuBCC, 81    <sup>d</sup>KuB, 71    <sup>e</sup>KuK, 75    <sup>f</sup>ChCK, 82

<sup>g</sup>KuBCC, 83

The CeCo<sub>4</sub>B structure, shown in fig. 37, is a member of the  $\text{R}_{m+n}\text{T}_{5m+3n}\text{M}_{2n}$  structural series with  $m = 1$  and  $n = 1$  and is built up of  $\text{CaCu}_5$ - and  $\text{CeCo}_3\text{B}_2$ -type slabs. It is discussed with the  $7511:\text{Ce}_3\text{Co}_8\text{Si}$  structure.

---

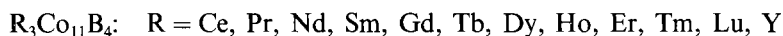
<b>8327</b>	<b>Ce<sub>3</sub>Co<sub>11</sub>B<sub>4</sub></b>	hP18 P6/mmm	$a = 5.045$ $c = 9.925$	KuB, 74
-------------	---	----------------	----------------------------	---------

---

CaCu<sub>5</sub>-type derivative

---

Isotypic compounds: All references KuB, 74



The Ce<sub>3</sub>Co<sub>11</sub>B<sub>4</sub> structure, shown in fig. 37, is a member of the  $\text{R}_{m+n}\text{T}_{5m+3n}\text{M}_{2n}$  structural series with  $m = 1$  and  $n = 2$  and is built up of  $\text{CaCu}_5$ - and  $\text{CeCo}_3\text{B}_2$ -type slabs. It is discussed with the  $7511:\text{Ce}_3\text{Co}_8\text{Si}$  structure.

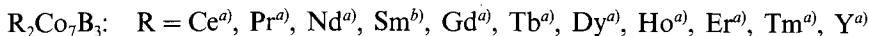
<b>8330</b>	<b>Ce<sub>2</sub>Co<sub>7</sub>B<sub>3</sub></b>	hP24 P6/mmm	$a = 5.053$ $c = 12.97$	KuB, 74
-------------	--	----------------	----------------------------	---------

---

CaCu<sub>5</sub>-type derivative

---

Isotypic compounds:



<sup>a)</sup>KuB, 74

<sup>b)</sup>BiKP, 80

The Ce<sub>2</sub>Co<sub>7</sub>B<sub>3</sub> structure, shown in fig. 37, is a member of the R<sub>m+n</sub>T<sub>5m+3n</sub>M<sub>2n</sub> structural series with  $m = 1$  and  $n = 3$  and is built up of CaCu<sub>5</sub>- and CeCo<sub>3</sub>B<sub>2</sub>-type slabs. It is discussed with the 7511:Ce<sub>3</sub>Co<sub>8</sub>Si structure.

Six structure types are found with composition 8340, all related to the CaCu<sub>5</sub>-type and listed with CeCo<sub>3</sub>B<sub>2</sub>.

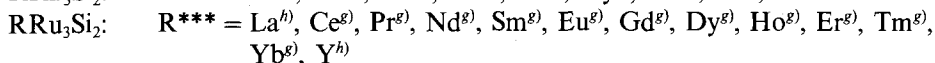
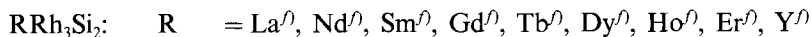
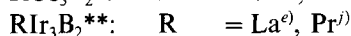
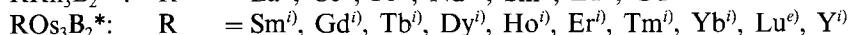
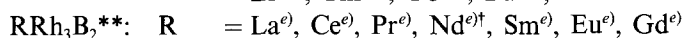
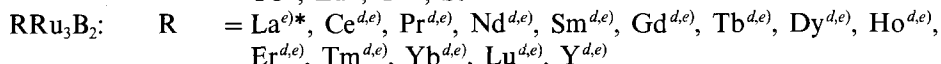
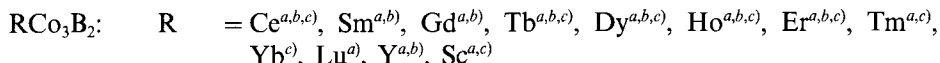
<b>8340</b>	<b>CeCo<sub>3</sub>B<sub>2</sub></b> or <b>CeCo<sub>3</sub>B<sub>2</sub><sup>[6p]</sup></b>	hP6 P6/mmm	$a = 5.057$ $c = 3.036$	KuKB, 69
-------------	---	---------------	----------------------------	----------

---

CaCu<sub>5</sub>-type derivative

---

Isotypic compounds:



\*All RO<sub>3</sub>B<sub>2</sub> compounds (except for LuOs<sub>3</sub>B<sub>2</sub>) and one other modification of LaRu<sub>3</sub>B<sub>2</sub> crystallize in a not fully determined orthorhombic deformation variant of the CeCo<sub>3</sub>B<sub>2</sub>-type, the so-called YO<sub>3</sub>B<sub>2</sub>-type (Ku, 80).

\*\*See also 8340:ErIr<sub>3</sub>B<sub>2</sub>.

\*\*\*For LaRu<sub>3</sub>Si<sub>2</sub> and YRu<sub>3</sub>Si<sub>2</sub>, Vandenberg and Barz (1980) have proposed a hexagonal structure

with  $c = 2c(\text{CeCo}_3\text{B}_2)$ , which is very close to the  $\text{CeCo}_3\text{B}_2$ -type. The other  $\text{RRu}_3\text{Si}_2$  compounds have not yet been properly identified. No lattice constants have been published. Some alloys were prepared with the composition  $\text{RRu}_{3.5}\text{Si}_2$ .

<sup>f</sup>For  $\text{Nd}_{0.71}\text{Rh}_{3.29}\text{B}_2$ , VIOCE, 83 report a mixed Nd and Rh occupancy of the Ce sites and a symmetry reduction to  $\text{P62m}$ .

<sup>a</sup>KuKB, 69    <sup>b</sup>NiY, 73    <sup>c</sup>Ro, 73    <sup>d</sup>HiRUS, 80    <sup>e</sup>KuMAJ, 80    <sup>f</sup>ChCLE, 81  
<sup>g</sup>Ba, 80    <sup>h</sup>VaB, 80    <sup>i</sup>Ku, 80    <sup>j</sup>KuM, 81

The  $\text{CeCo}_3\text{B}_2$  structure, shown in fig. 37 and in fig. 58, is a  $\text{CaCu}_5$ -type derivative, with Co and B atoms, respectively, replacing the Ca atoms on two crystallographically distinct structure sites. Some of the  $\text{CeCo}_3\text{B}_2$ -type phases are deformed and do not have hexagonal symmetry and/or the same small unit cell. The following deformation variants are known:

- monoclinic  $\text{ErIr}_3\text{B}_2$ -type (mC12, C2/m), shown in fig. 58 (see 8340:  $\text{ErIr}_3\text{B}_2$ );
- rhombohedral  $\text{ZrCo}_3\text{B}_2$ -type (hR54, R3) (VoKK, 71), not yet found with  $\text{RT}_3\text{M}_2$  compounds;
- orthorhombic  $\text{YOs}_3\text{B}_2$ -type with  $a \approx a(\text{CeCo}_3\text{B}_2)$ ,  $b \approx \sqrt{3} a(\text{CeCo}_3\text{B}_2)$  and  $c \approx 6c(\text{CeCo}_3\text{B}_2)$ , for which, however, structural details have not been given (Ku, 80);
- hexagonal  $\text{LaRu}_3\text{Si}_2$ -type (hP12,  $\text{P6}_3/\text{m}$ ), where  $a \approx a(\text{CeCo}_3\text{B}_2)$  and  $c \approx 2c(\text{CeCo}_3\text{B}_2)$  (VaB, 80);
- trigonal  $\text{URu}_3\text{B}_2$ -type (hP48,  $\text{P}\bar{3}$ ), where  $a \approx 2a(\text{CeCo}_3\text{B}_2)$  and  $c \approx 2c(\text{CeCo}_3\text{B}_2)$  (Ro, 80a).

For a detailed discussion see Johnston and Braun (1982).

For completeness one can mention the  $\text{Ba}_2\text{Ni}_9\text{B}_6$ -type (JuQ, 80a) with rhombohedral cell (hR102,  $\text{R}\bar{3}\text{c}$ ), and the  $\text{CaRh}_2\text{B}_2$ -type (SchJ, 78), an orthorhombic defect variant (oF40, Fddd), which both can also be derived from the  $\text{CeCo}_3\text{B}_2$ -type.

In the binary  $\text{RT}_5$  phases with  $\text{CaCu}_5$ -type the T element can be partly substituted by Al and the solid solution  $\text{RT}_{5-x}\text{Al}_x$  approaches in certain cases the composition  $\text{RT}_3\text{Al}_2$ . However, since these phases are not truly ternary phases they will not be discussed here. A ternary aluminide with a  $\text{CeCo}_3\text{B}_2$ -related structure is, however, found with 8360:  $\text{PrNi}_2\text{Al}_3$ , a site exchange variant of  $\text{CeCo}_3\text{B}_2$ -type, shown in fig. 58. With smaller rare earth elements the 8360:  $\text{YNi}_2\text{Al}_3$ -type is formed (also shown in fig. 58), where the z coordinate of one rare earth atom differs by one half.

The  $\text{CeCo}_3\text{B}_2$  structure is the end member of two structural series:  $\text{R}_{m+n}\text{T}_{5m+3n}\text{M}_{2n}$  and  $\text{R}_{2+n}\text{T}_{4+3n}\text{M}_{2n}$ , which are discussed with 7511:  $\text{Ce}_3\text{Co}_8\text{Si}$ .

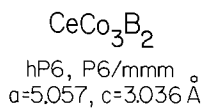
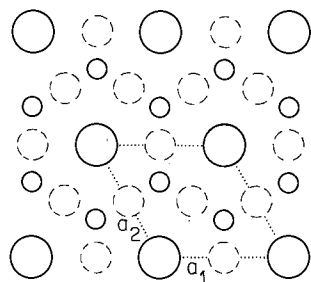
---

8340	$\text{ErIr}_3\text{B}_2$ or $\text{ErIr}_3\text{B}_2^{[6p]}$	mC12 C2/m	$a = 5.409$ $b = 9.379$ $c = 3.101$ $\beta = 91.2^\circ$	KuM, 81
------	---	--------------	---	---------

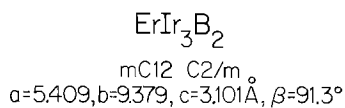
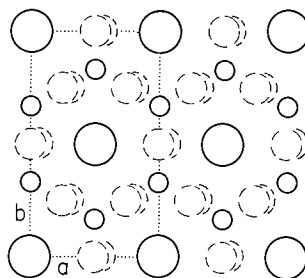
---

Monoclinic deformation variant of  $\text{CeCo}_3\text{B}_2$ -type  $\equiv$   $\text{CaCu}_5$ -type derivative

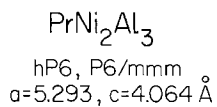
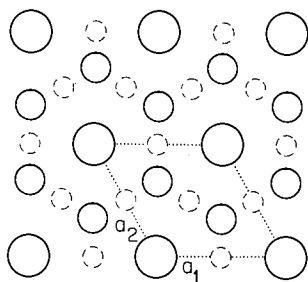
---



Deformation variant



Site exchange variant



Height	R	T	M
1/2			
0			
1,0			

Related structure

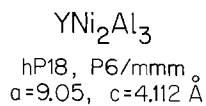
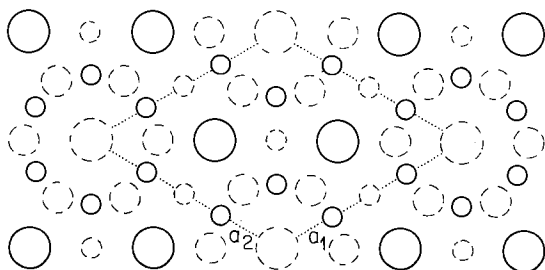


Fig. 58. The  $\text{CeCo}_3\text{B}_2$ -type and three of its variants.

Isotypic compounds: All references KuM, 81

$\text{RRh}_3\text{B}_2$ : R = Tb, Dy, Ho, Er, Tm, Yb, Lu, Y

$\text{RIr}_3\text{B}_2$ : R = Ce, Nd, Sm, Gd, Tb, Dy, Ho, Er, Tm, Yb, Lu, Y, Sc

The  $\text{ErIr}_3\text{B}_2$  structure is a monoclinic deformation variant of the  $\text{CeCo}_3\text{B}_2$ -type with  $a = a(\text{CeCo}_3\text{B}_2)$ ,  $b = \sqrt{3} a(\text{CeCo}_3\text{B}_2)$ ,  $c \approx c(\text{CeCo}_3\text{B}_2)$  and  $\beta > 90^\circ$ . A drawing of the  $\text{ErIr}_3\text{B}_2$  and  $\text{CeCo}_3\text{B}_2$  structures is given in fig. 58. For a discussion of other deformation variants see 8340: $\text{CeCo}_3\text{B}_2$  and Johnston and Braun (1982).

Four structure types are found with composition 8360: the  $\text{PrNi}_2\text{Al}_3$ -type, hP6; the  $\text{YNi}_2\text{Al}_3$ -type, hP18; the  $\text{ScNi}_2\text{Si}_3$ -type, tI24 and the  $\text{ScRe}_2\text{Si}_3$  type, oC96.

8360	$\text{PrNi}_2\text{Al}_3^*$	hP6	$a = 5.293$	RyZK, 78
	or $\text{PrNi}_2^{[6p]}\text{Al}_3$	P6/mmm	$c = 4.064$	

$\text{CeCo}_3\text{B}_2$ -type related with T and M sites interchanged  $\equiv$   $\text{CaCu}_5$ -type derivative

\*Error in the position published for Ni. It has to be in equipoint 2c) to be consistent with the  $\text{CaCu}_5$ -type of the structure.

Isotypic compounds:

$\text{RNi}_2\text{Al}_3$ : R = Pr<sup>a)</sup>, Nd<sup>b)</sup>

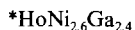
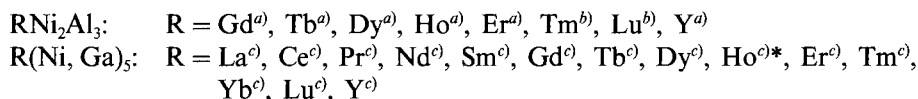
<sup>a)</sup>RyZK, 78      <sup>b)</sup>RyZY, 79

The  $\text{PrNi}_2\text{Al}_3$  structure, presented in fig. 58, is closely related to the  $\text{CeCo}_3\text{B}_2$ -type with T and M sites interchanged. For a discussion of the latter type see 8340: $\text{CeCo}_3\text{B}_2$ .

8360	$\text{YNi}_2\text{Al}_3$	hP18	$a = 9.05$	ZaR, 81
		P6/mmm	$c = 4.112$	

Also called  $\text{HoNi}_{2.6}\text{Ga}_{2.4}$ -type (YaG, 79), but in the latter case no complete atom ordering

## Isotypic compounds:



The YNi<sub>2</sub>Al<sub>3</sub> structure, shown in fig. 58, is related to the 8340:CeCo<sub>3</sub>B<sub>2</sub>-type. The unit cell dimensions are related to the latter as  $a = \sqrt{3} a(\text{CeCo}_3\text{B}_2)$  and  $c = c(\text{CeCo}_3\text{B}_2)$ ; also the atom coordinates agree approximately except for the  $z$  coordinate of one of the three rare earth atoms per unit cell, which has been shifted by  $\frac{1}{2}$ . The coordination of the rare earth atom at the origin of the unit cell is identical to the rare earth coordination in 8360:PrNi<sub>2</sub>Al<sub>3</sub>, the site exchange variant of the CeCo<sub>3</sub>B<sub>2</sub>-type.

---

<b>8360</b>	<b>ScNi<sub>2</sub>Si<sub>3</sub></b>	tI24 I4/mmm	$a = 3.830$ $c = 23.50$	KoBG, 78
-------------	---------------------------------------	----------------	----------------------------	----------

---

No isotypic RT<sub>2</sub>M<sub>3</sub> compounds are known.

The ScNi<sub>2</sub>Si<sub>3</sub> structure, which is presented in fig. 52a, can be interpreted as an intergrowth of BaAl<sub>4</sub>- and Po-type slabs. For a detailed discussion on these intergrowth structures see 8050:CeNi<sub>2</sub>Si<sub>2</sub>.

---

<b>8360</b>	<b>ScRe<sub>2</sub>Si<sub>3</sub></b> or <b>Sc<sub>2</sub>Re<sub>4</sub>Si<sub>5</sub>Si<sup>[(4,4)a]</sup></b>	oC96 Amm2	$a = 14.486$ $b = 19.689$ $c = 5.2397$	PeBG, 79
-------------	---	--------------	--	----------

---

No isotypic RT<sub>2</sub>M<sub>3</sub> compounds are known.

The ScRe<sub>2</sub>Si<sub>3</sub> structure, shown in fig. 15, has features in common with the 6360:Sc<sub>3</sub>Re<sub>2</sub>Si<sub>3</sub> structure and is discussed with the latter.



8370	$\text{La}_2\text{Re}_3\text{B}_7$	oP48	$a = 7.681$	KuMKY, 82
		Pcca	$b = 6.773$	
			$c = 11.658$	

No isotypic  $\text{R}_2\text{T}_3\text{M}_7$  compounds are known.

In the  $\text{La}_2\text{Re}_3\text{B}_7$  structure the boron atoms are either in the centres of deformed trigonal prisms formed of La and Re atoms or in the centre of an octahedron. The boron atoms form infinite, branched chains as shown in fig. 84.

Three structure types are found with composition 8380:  $\text{LaCoAl}_4$ , oP12;  $\text{YCrB}_4$ , oP24 and  $\text{YNiAl}_4$ , oC24.

8380	$\text{LaCoAl}_4$	oP12	$a = 7.701$	RyZY, 77
	or	Pmma	$b = 4.082$	
	$\text{LaCo}^{[6p]}\text{Al}_3\text{Al}^{[+8c]}$		$c = 7.023$	

Isotypic compounds: All references RyZY, 77

$\text{RCoAl}_4$ : R = La, Ce, Pr.

The structures of  $\text{LaCoAl}_4$  and 8380:  $\text{YNiAl}_4$  are both built up of  $\text{MgCuAl}_2$ -type slabs. The  $\text{MgCuAl}_2$ -type, demonstrated on 7567:  $\text{YNiAl}_2$ , and the two other structures are shown in fig. 59. The slabs of the  $\text{MgCuAl}_2$ -type are cut differently, such that in  $\text{YNiAl}_4$  there are R atoms at the interface, and in  $\text{LaCoAl}_4$ , T atoms. Layers of Al atoms are found between the  $\text{MgCuAl}_2$  slabs in both structures. In  $\text{YNiAl}_4$  the slab intergrown with the  $\text{MgCuAl}_2$ -type slab corresponds to a segment of (deformed)  $\text{Cu}_3\text{Au}$ -type [cut parallel to the (110) plane]. This type is found with  $\text{RAl}_3$  compounds ( $\text{TmAl}_3$ ,  $\text{YbAl}_3$ ,  $\text{LuAl}_3$ ,  $\text{ScAl}_3$ ). In  $\text{LaCoAl}_4$  the atom arrangement of the other intergrown slab should correspond to a structure which occurs with Al-rich transition metal aluminides.

In all three structures shown in fig. 59 the T atoms are in the centres of trigonal prisms which, in both  $\text{YNiAl}_2$  and  $\text{YNiAl}_4$ , have the formula  $(\text{R}_2\text{M}_4)\text{T}$ , but  $(\text{M}_6)\text{T}$  in  $\text{LaCoAl}_4$ . An example of a structure where both kinds of trigonal prisms occur is 8968:  $\text{Ho}_4\text{Ni}_{10}\text{Ga}_{21}$  (fig. 74).

The geometrical relationship between the  $\text{LaCoAl}_4$  and the 8871:  $\text{PrNi}_2\text{Al}_5$  structure is discussed with the latter one (see fig. 67).

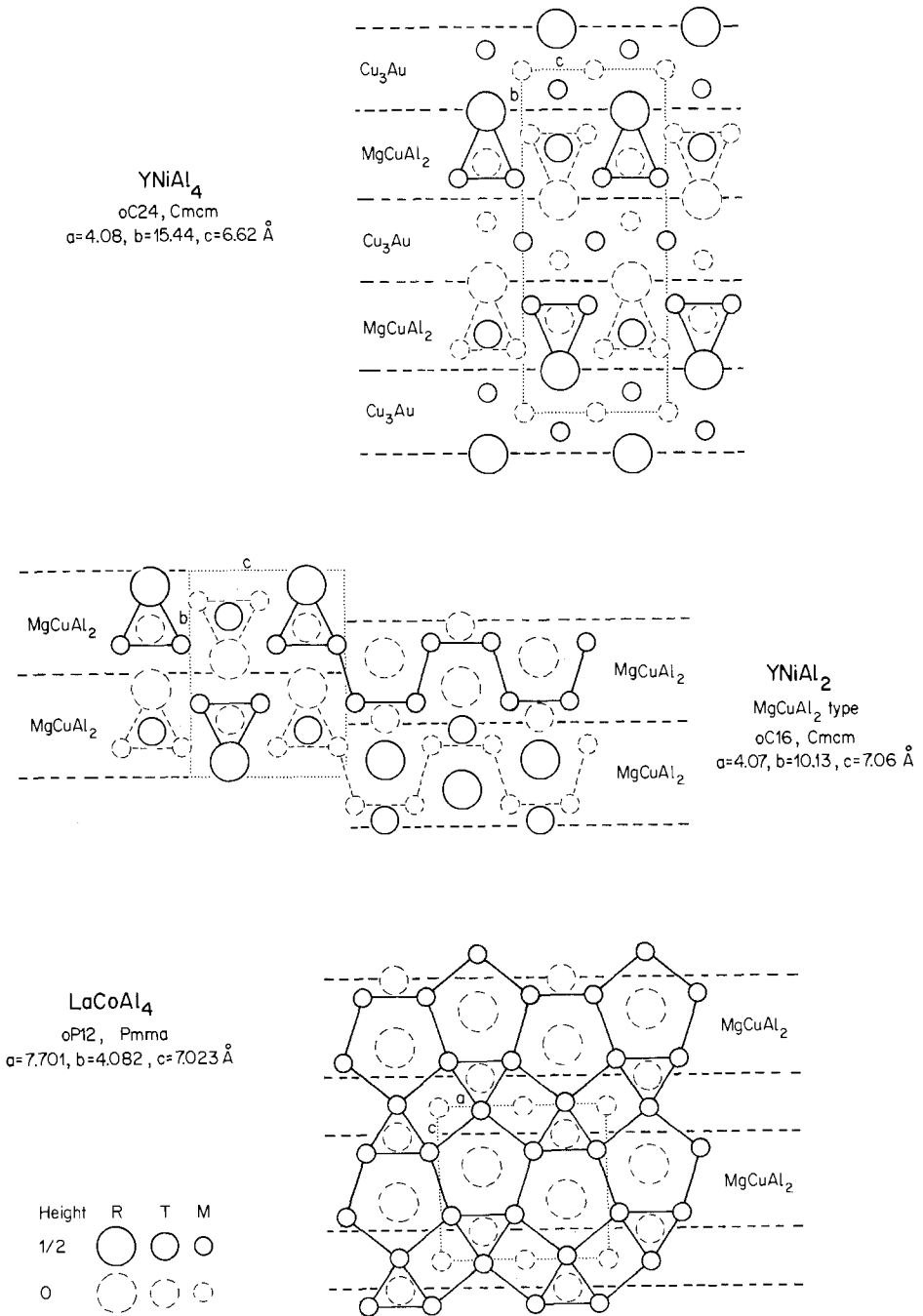


Fig. 59. The YNiAl<sub>4</sub> and the LaCoAl<sub>4</sub> structures, both built up of MgCuAl<sub>2</sub>-type slabs intergrown with Al-rich slabs having another structure.

8380	<b>YCrB<sub>4</sub></b>	oP24	$a = 5.972$	Ku, 70
	or	Pbam	$b = 11.46$	
	$\text{Y}^{[1,14]}\text{Cr}^{[1,10]}\infty\text{B}_4^{[6p+3]}$		$c = 3.461$	

## Isotypic compounds:

RVB <sub>4</sub> :	R = Gd <sup>a</sup> , Tb <sup>a</sup> , Dy <sup>a</sup> , Ho <sup>a</sup> , Er <sup>a</sup> , Y <sup>a,f</sup> )
RCrB <sub>4</sub> :	R = Ce <sup>e</sup> , Pr <sup>d</sup> , Nd <sup>d</sup> , Sm <sup>d</sup> , Gd <sup>b</sup> , Tb <sup>b</sup> , Dy <sup>b</sup> , Ho <sup>b</sup> , Er <sup>b</sup> , Tm <sup>c</sup> , Lu <sup>b</sup> , Y <sup>b</sup> )
RMnB <sub>4</sub> :	R = Ce <sup>p</sup> , Gd <sup>a</sup> , Tb <sup>a</sup> , Dy <sup>a</sup> , Ho <sup>a</sup> , Er <sup>a</sup> , Y <sup>a</sup> )
RFeB <sub>4</sub> :	R = Ce <sup>g</sup> , Sm <sup>h</sup> , Gd <sup>g,i,j</sup> , Tb <sup>g</sup> , Dy <sup>g</sup> , Ho <sup>g</sup> , Er <sup>g</sup> , Tm <sup>g</sup> , Lu <sup>g</sup> , Y <sup>g</sup> )
RCoB <sub>4</sub> :	R = Ce <sup>l</sup> , Gd <sup>g,k</sup> , Tb <sup>g</sup> , Dy <sup>g</sup> , Ho <sup>g</sup> , Er <sup>g</sup> , Tm <sup>g</sup> , Lu <sup>g,l</sup> , Y <sup>g</sup> )
RNiB <sub>4</sub> :	R = Er <sup>l</sup> , Tm <sup>l</sup> , Lu <sup>l</sup> )
RMoB <sub>4</sub> :	R = Gd <sup>c</sup> , Tb <sup>c</sup> , Dy <sup>c</sup> , Ho <sup>c</sup> , Er <sup>c</sup> , Y <sup>c,m</sup> )
RRuB <sub>4</sub> :	R = Gd <sup>n</sup> , Tb <sup>n</sup> , Dy <sup>n</sup> , Ho <sup>n</sup> , Er <sup>n</sup> , Tm <sup>n</sup> , Yb <sup>i</sup> , Lu <sup>q</sup> , Y <sup>n</sup> )
RWB <sub>4</sub> :	R = Gd <sup>c</sup> , Tb <sup>c</sup> , Dy <sup>c</sup> , Ho <sup>c</sup> , Er <sup>c</sup> , Y <sup>c,m</sup> )
RReB <sub>4</sub> :	R = Gd <sup>c</sup> , Tb <sup>c</sup> , Dy <sup>c</sup> , Ho <sup>c</sup> , Er <sup>c</sup> , Tm <sup>o</sup> , Y <sup>c</sup> )
ROsB <sub>4</sub> :	R = Gd <sup>n</sup> , Tb <sup>n</sup> , Dy <sup>n</sup> , Ho <sup>n</sup> , Er <sup>n</sup> , Tm <sup>n</sup> , Yb <sup>i</sup> , Lu <sup>q</sup> , Y <sup>n</sup> )

<sup>a</sup>Ku, 70a<sup>b</sup>Ku, 70<sup>c</sup>KuS, 72a<sup>d</sup>MiK, 77<sup>e</sup>KuSF, 73<sup>f</sup>KuSF, 70<sup>g</sup>StK, 77<sup>h</sup>BrY, 80<sup>i</sup>SoR, 79<sup>j</sup>ChKBKP, 79<sup>k</sup>ChK, 77<sup>l</sup>KuBCC, 81<sup>m</sup>KuSS, 73<sup>n</sup>Ro, 78<sup>o</sup>Mi, 74<sup>p</sup>KuBMSC, 79<sup>q</sup>RoD, 83

The YCrB<sub>4</sub> structure is presented in fig. 48 together with a structure block shifted variant, the ThMoB<sub>4</sub> structure (RoN, 75). Both structures, together with 7886:Y<sub>2</sub>ReB<sub>6</sub>, can be considered as modifications of the AlB<sub>2</sub>-type and all these related structures are discussed in more detail with the Y<sub>2</sub>ReB<sub>6</sub> structure.

8380	<b>YNiAl<sub>4</sub></b>	oC24	$a = 4.08$	RyZY, 72
	or	Cmcm	$b = 15.44$	
	$\text{YNi}^{[(2,4)p]}\text{Al}_4$		$c = 6.62$	

## Isotypic compounds:

RNiAl <sub>4</sub> :	R = Pr <sup>a</sup> , Nd <sup>b</sup> , Tb <sup>c</sup> , Dy <sup>c</sup> , Ho <sup>c</sup> , Er <sup>c</sup> , Tm <sup>c</sup> , Lu <sup>c</sup> , Y <sup>d</sup> )
RNiGa <sub>4</sub> :	R = Sm <sup>e</sup> , Gd <sup>e</sup> , Tb <sup>e</sup> , Dy <sup>e</sup> , Ho <sup>e</sup> , Er <sup>e</sup> , Tm <sup>e</sup> , Yb <sup>e</sup> , Lu <sup>e</sup> , Y <sup>e</sup> )

<sup>a</sup>RyZK, 78<sup>b</sup>RyZY, 79<sup>c</sup>RyZP, 73<sup>d</sup>RyZY, 72<sup>e</sup>YaG, 81

The YNiAl<sub>4</sub> structure shown in fig. 59 can be considered as an intergrowth of MgCuAl<sub>2</sub>-type and Cu<sub>3</sub>Au-type slabs [with interface (110)]. For a further discussion see 8380:LaCoAl<sub>4</sub>. A list of all the different R-T-M structures which contain intergrown Cu<sub>3</sub>Au-type segments (slabs or columns) is given with 8289:Ho<sub>2</sub>CoGa<sub>8</sub>.

8576	$\text{Yb}_3\text{Rh}_4\text{Sn}_{13}$ or $\text{Yb}_3^{[12c]}\text{Rh}_4^{[6p]}\text{Sn}_{12}\text{Sn}^{[+12]}$	cP40 Pm3n	$a = 9.676$	HoCMR, 80
------	--	--------------	-------------	-----------

Previously called  $\text{Pr}_3\text{Rh}_4\text{Sn}_{13}$ -type (Va, 80), but according to HoMRC, 82, this compound crystallizes with a superstructure having a larger unit cell

### Isotypic compounds:

According to Hodeau et al. (HoMR, 82a) one should distinguish, in the case of R–Rh–Sn phases, between four different structures, which are all characterized by Rh-centred trigonal prisms of Sn atoms. All structures have (not necessarily equal but at least) similar compositions and related unit cell parameters, which stand in a simple relationship to those of the  $\text{Yb}_3\text{Rh}_4\text{Sn}_{13}$ -type structures (the so-called Phase I compounds).

Phase I:  $\text{R}_3\text{Rh}_4\text{Sn}_{13}$ , cP40, Pm3n;

Phase I': distortion of phase I structure, tP80, P4<sub>2</sub>22 with  $a = \sqrt{2} a_1$ ,  $c = a_1$  or larger cubic cell;

Phase II:  $(\text{R}_{1-x}\text{Sn}_x)\text{R}_4\text{Rh}_6\text{Sn}_{18}$ , tI232, I4<sub>1</sub>/acd with  $a = \sqrt{2} a_1$ ,  $c = 2\sqrt{2} a_1$ ;

Phase III: Disordered phase II,  $\text{XX}_4\text{Rh}_6\text{X}_4\text{Sn}_{14}$  with  $\text{X} = \text{R}_{1-x}\text{Sn}_x$ , cF116, F43m with  $a = \sqrt{2} a_1$ .

In many cases the compositions and the crystal structures of these phases are only poorly defined. Single crystal structure determinations have been made on  $\text{Y}_3\text{Ru}_4\text{Ge}_{13}^c$ ,  $\text{Lu}_3\text{Os}_4\text{Ge}_{13}^c$ ,  $\text{Yb}_3\text{Rh}_4\text{Sn}_{13}^b$ , and  $\text{Er}_{2.8/9}\text{Rh}_4\text{Sn}_{12.4/9}^h$  [=  $(\text{Er}_{.32}\text{Sn}_{.68})\text{Er}_4\text{Rh}_6\text{Sn}_{18}$ ]. For reasons of simplicity all these different phases are listed under the heading 8576:  $\text{Yb}_3\text{Rh}_4\text{Sn}_{13}$ .

$\text{R}_3\text{Ru}_4\text{Ge}_{13}$ : R = Ce<sup>c</sup>, Pr<sup>c</sup>, Nd<sup>c</sup>, Sm<sup>c</sup>, Gd<sup>c</sup>, Tb<sup>c</sup>, Dy<sup>c</sup>, Ho<sup>c</sup>, Er<sup>c</sup>, Tm<sup>c</sup>, Yb<sup>c</sup>, Lu<sup>c</sup>, Y<sup>c</sup>\*

$\text{R}_3\text{Os}_4\text{Ge}_{13}$ : R = Ce<sup>c</sup>, Pr<sup>c</sup>, Nd<sup>c</sup>, Sm<sup>c</sup>, Eu<sup>c</sup>, Gd<sup>c</sup>, Tb<sup>c</sup>, Dy<sup>c</sup>, Ho<sup>c</sup>, Er<sup>c</sup>, Tm<sup>c</sup>, Yb<sup>c</sup>, Lu<sup>c</sup>, Y<sup>c</sup>

$\text{R}_3\text{Co}_4\text{Sn}_{13}$ : R = Er<sup>g</sup>\*\* , Yb<sup>g</sup>

$\text{R}_3\text{Ru}_4\text{Sn}_{13}$ : R = La<sup>f</sup>, Er<sup>f,g</sup>\*\*\*, Lu<sup>g</sup>\*\* , Y<sup>f</sup>\*\*\*

$\text{R}_3\text{Rh}_4\text{Sn}_{13}$ : R = La<sup>a</sup>††, Ce<sup>a</sup>††, Pr<sup>a</sup>††, Nd<sup>a</sup>††, Sm<sup>a</sup>††, Eu<sup>a</sup>†, Gd<sup>a</sup>††, Tb<sup>d,e,g,h</sup>‡, Dy<sup>e,g,h</sup>‡, Ho<sup>e,g,h</sup>‡,††, Er<sup>e,g,h</sup>‡,†††, Tm<sup>e,g,h</sup>‡,†††, Yb<sup>a,b</sup>†, Lu<sup>e,g,h</sup>†††, Y<sup>e,g,h</sup>†††, Sc<sup>e,g,h</sup>†††

$\text{R}_3\text{Os}_4\text{Sn}_{13}$ : R = Er<sup>f</sup>\*\*\*, Y<sup>f</sup>\*\*\*

$\text{R}_3\text{Ir}_4\text{Sn}_{13}$ : R = La<sup>g</sup>, Ce<sup>g</sup>, Pr<sup>g</sup>, Nd<sup>g</sup>, Sm<sup>g</sup>, Gd<sup>g</sup>\*\*\*, Tb<sup>g</sup>\*\*\*, Dy<sup>g</sup>\*\*\*, Ho<sup>g</sup>\*\*\*, Er<sup>g</sup>\*\* , Tm<sup>g</sup>\*\* , Yb<sup>g</sup> also \*\*\*, Lu<sup>g</sup>\*\* , Y<sup>g</sup>\*\*\*, Sc<sup>g</sup>\*\*

\*Electron density maps suggest that the true symmetry is lower than cubic.

\*\*Not resolved tetragonal structure, which is supposedly closely related to  $\text{Yb}_3\text{Rh}_4\text{Sn}_{13}$ -type [ $a = \sqrt{2} a(\text{Yb}_3\text{Rh}_4\text{Sn}_{13}\text{-type})$ ,  $c = na(\text{Yb}_3\text{Rh}_4\text{Sn}_{13}\text{-type})$ ].

\*\*\*Not resolved face-centred cubic structure, which is supposedly closely related to  $\text{Yb}_3\text{Rh}_4\text{Sn}_{13}$ -type.

†Phase I ††Phase I' †††Phase II ‡Phase III

<sup>a)</sup>HoMRC, 82    <sup>b)</sup>HoCMR, 80    <sup>c)</sup>SeBY, 81    <sup>d)</sup>Va, 80    <sup>e)</sup>ReECBRMVMFWMST, 80  
<sup>f)</sup>EsCBR, 80    <sup>g)</sup>Co, 80    <sup>h)</sup>HoMR, 82

In the  $\text{Yb}_3\text{Rh}_4\text{Sn}_{13}$  structure there are two crystallographically different Sn sites, which allows the formula to be written as  $\text{Yb}_3\text{SnRh}_4\text{Sn}_{12}$ . For a geometrical interpretation of this structure it is convenient to consider separately the atom arrangement in the  $\text{Yb}_3\text{Sn}$  and the  $\text{Rh}_4\text{Sn}_{12}$  part. As shown in fig. 60, the disposition of the atoms in the  $\text{Yb}_3\text{Sn}$  part corresponds to the  $\text{Cr}_3\text{Si}$  ( $\beta\text{W}$ )-type, while the  $\text{Rh}_4\text{Sn}_{12}$  part is a three-dimensional array of corner-shared trigonal Sn prisms whose centres are occupied by Rh atoms. The Sn and Yb atoms of the  $\text{Yb}_3\text{Sn}$  part occupy the icosahedral and cubo-octahedral holes, respectively, of the Sn prism array.

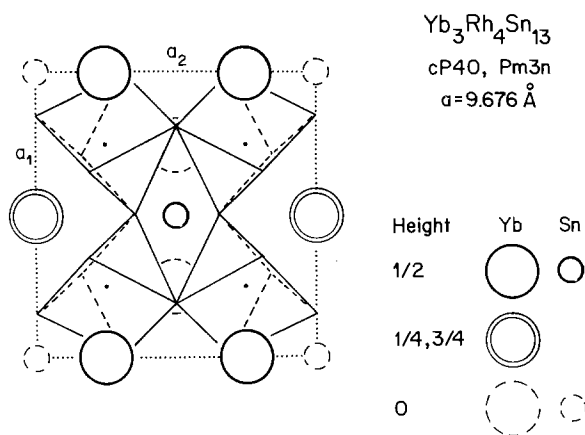


Fig. 60. The structure of  $\text{Yb}_3\text{Rh}_4\text{Sn}_{13}$  projected along [001]. The atoms of the  $\text{Yb}_3\text{Sn}$  part with the  $\text{Cr}_3\text{Si}$  ( $\beta\text{W}$ ) arrangement are indicated with circles. For the  $\text{Rh}_4\text{Sn}_{12}$  part only the outlines of the Rh-centred trigonal Sn prisms with centres of  $z = \frac{1}{4}$  are shown.

8591	$\text{Ce}_2\text{NiGa}_{10}$	tI26	$a = 4.262$	YaGUKRBG, 81
	or	I4/mmm	$c = 26.391$	YaGRUKBG, 82
	$\text{Ce}_2\text{Ni}^{[8c]}\text{Ga}_{10}$			

Isotypic compounds: All references YaGUKRBG, 81 and YaGRUKBG, 82

$\text{R}_2\text{NiGa}_{10}$ : R = La, Ce

The  $\text{Ce}_2\text{NiGa}_{10}$  structure, shown in fig. 52a, can be interpreted as an intergrowth of  $\text{BaAl}_4$ - and  $\text{CaF}_2$ -type slabs. It is closely related to the 8791:  $\text{La}_2\text{Ni}_{1.2}\square_{0.8}\text{Ga}_{12}$  structure, where the  $\text{BaAl}_4$ -type slab is only half as thick and where the Ni site in one  $\text{CaF}_2$ -type slab is only partially occupied. For a detailed discussion of these intergrowth structures see 8050:  $\text{CeNi}_2\text{Si}_2$ .

8617	CeNi <sub>5</sub> Sn	hP28	$a = 4.9049$	SkMA, 81
		P6 <sub>3</sub> /mmc	$c = 19.731$	

No isotypic RT<sub>3</sub>M compounds are known.

The structure of CeNi<sub>5</sub>Sn, projected along [11 $\bar{2}$ 0], is compared with the structure of CeCu<sub>6</sub> (CrLR, 60) in fig. 61. Both can be considered as an intergrowth of two structure segments. One has been cut from a CaCu<sub>5</sub>-type structure (see fig. 35) and the second from a yet unknown binary structure with composition R(T/M)<sub>7</sub>. In CeNi<sub>5</sub>Sn, layers of segments of one kind are intergrown with layers of segments of the other kind. In CeCu<sub>6</sub>, however, there are intergrown columns.

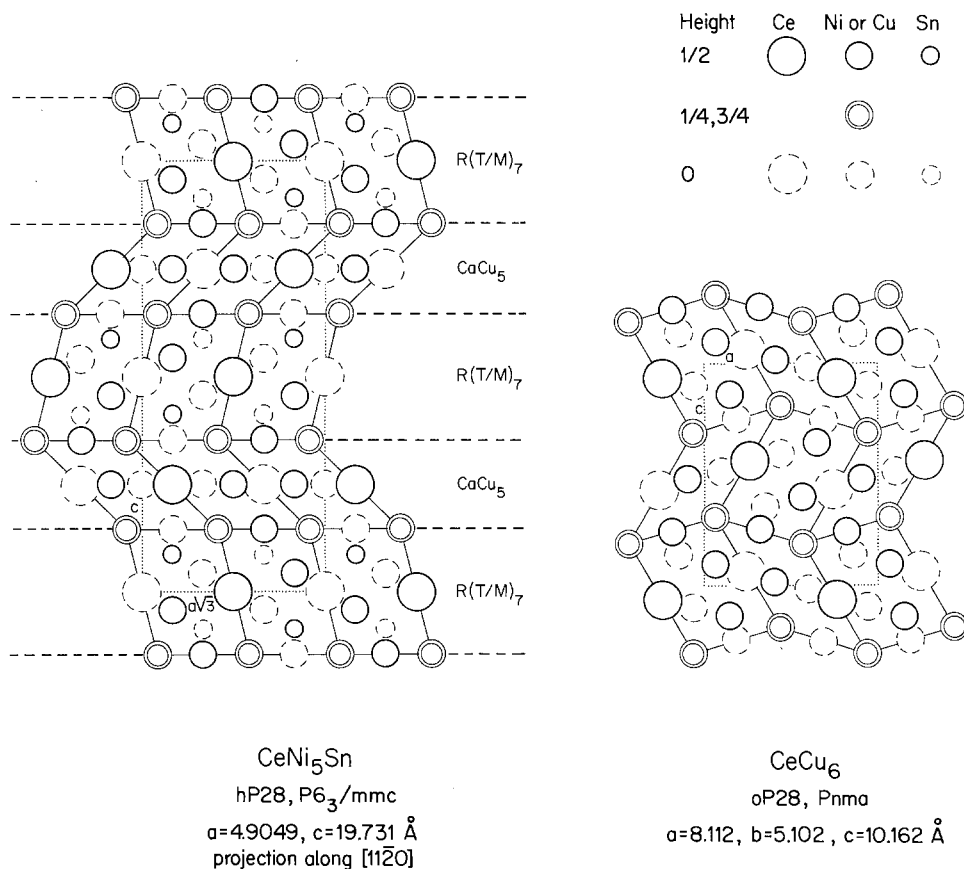


Fig. 61. The CeNi<sub>5</sub>Sn and the CeCu<sub>6</sub> structures, both built up of CaCu<sub>5</sub>-type and R(T/M)<sub>7</sub> segments. The first structure consists of intergrown layers and the second of intergrown columns.

Three structure types are found with composition 8633:  $\text{CeRe}_4\text{Si}_2$ , oC14;  $\text{ZrFe}_4\text{Si}_2$ , tP14 (see  $\text{YRe}_4\text{Si}_2$ ) and  $\text{NdRe}_4\text{Si}_2$ , oP28.

8633	$\text{CeRe}_4\text{Si}_2$	oC14	$a = 4.167$	BoGP, 77
	or	Cmmm	$b = 14.001$	
	$\text{CeRe}_4\text{Si}_2^{[(4,2)p]}$		$c = 4.145$	

Isotypic compounds: All references BoGP, 77

$\text{RRe}_4\text{Si}_2$ : R = Ce, Pr

The  $\text{CeRe}_4\text{Si}_2$  structure, shown in fig. 52a, can be interpreted as an intergrowth of  $\text{BaAl}_4$ - and Cu-type slabs. For a more general discussion of these intergrowth structures see 8050:  $\text{CeNi}_2\text{Si}_2$ . As shown in fig. 62 slabs of the  $\text{CeRe}_4\text{Si}_2$  structure, cut parallel to the (110) plane, can be intergrown with  $\text{ZrFe}_4\text{Si}_2$ -type slabs (see 8633:  $\text{YRe}_4\text{Si}_2$ ) to form the 8633:  $\text{NdRe}_4\text{Si}_2$  structure.

8633	$\text{YRe}_4\text{Si}_2$	tP14	$a = 7.321$	BoPG, 78
	or	$\text{P4}_2/\text{mnm}$	$c = 4.113$	
	$\text{YRe}_4\text{Si}_2^{[(2,4)p]}$			

$\text{ZrFe}_4\text{Si}_2$ -type (YaLG, 75)\*

\*Si atoms are in position 4g)  $x\bar{x}0$  and not  $xx0$  as stated erroneously in the original publication.

Isotypic compounds:

$\text{RFe}_4\text{Si}_2$ : R =  $\text{Y}^a$ ,  $\text{Sc}^b$ )

$\text{RRe}_4\text{Si}_2$ : R =  $\text{Sm}^c$ ,  $\text{Gd}^c$ ,  $\text{Y}^c$ )

<sup>a)</sup>BoGYDI, 78

<sup>b)</sup>GIKBS, 77

<sup>c)</sup>BoPG, 78

The  $\text{YRe}_4\text{Si}_2$  structure with  $\text{ZrFe}_4\text{Si}_2$ -type is shown in the lower part of fig. 62. The structure is characterized by infinite double columns of triangular-face-joined trigonal prisms, each built of two R and four T atoms and centred by a Si atom. The two columns which constitute a double column share the prism edges occupied by the R atoms. Further, every T atom participates on parallel Cu-type columns, each formed by the T atoms of four neighbouring prism columns.

Infinite columns of triangular-face-joined centred prisms, each built up by two kinds of atoms in the ratio 4:2, are common with R-T-M structures. In rare-earth-rich compounds there are four R atoms per prism, in compounds with smaller rare

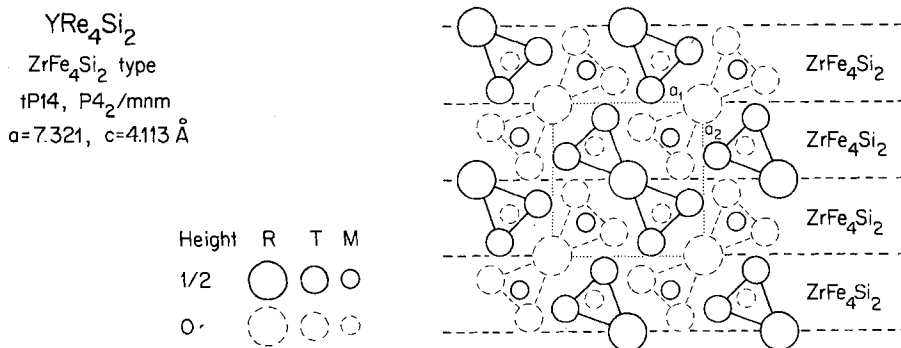
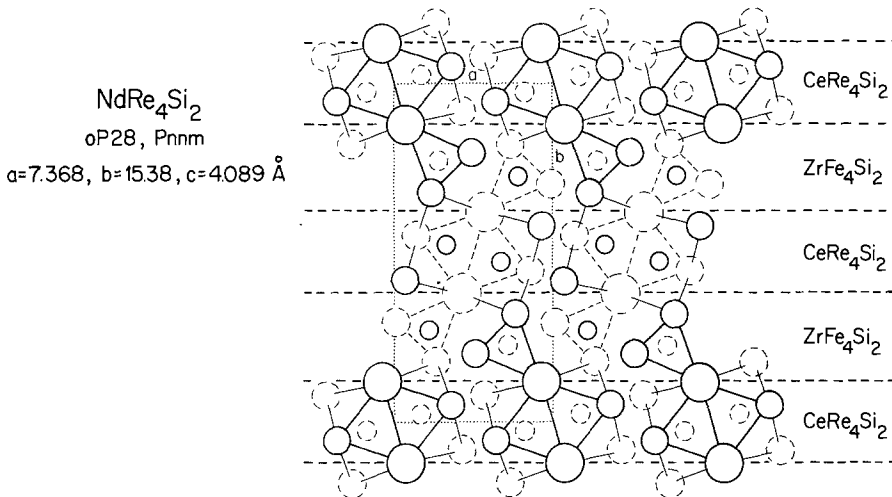
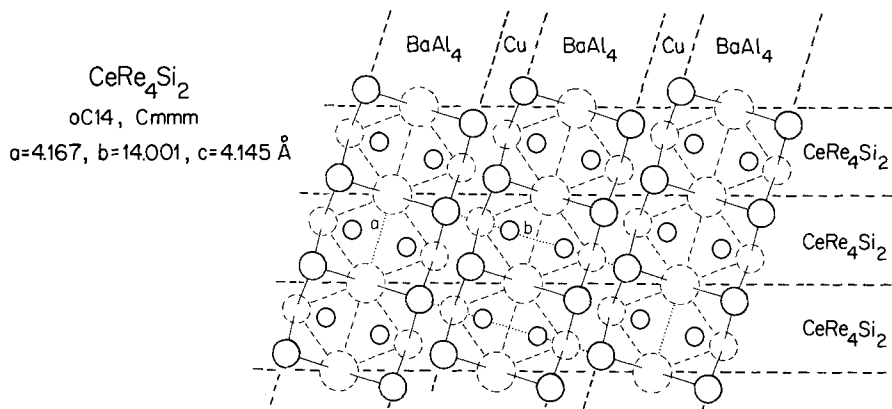


Fig. 62. The structural relationships between the  $\text{CeRe}_4\text{Si}_2$ ,  $\text{NdRe}_4\text{Si}_2$  and  $\text{YRe}_4\text{Si}_2$  structure types.



earth content only two. However, the composition of the prism also differs depending on whether one has ternary aluminides and gallides or ternary silicides and germanides. In the case of aluminides (or gallides) the prism is preferentially centred by T atoms and the composition of the centred prism is  $(R_4M_2)T^{[6p]}$  or  $(R_2M_4)T^{[6p]}$ . In the case of silicides (or germanides) the M atom is in the prism centre and the centred prism has the composition  $(R_4T_2)M^{[6p]}$  or  $(R_2T_4)M^{[6p]}$ . Examples of structures with columns of prisms having different compositions are listed in table 17.

8633	$NdRe_4Si_2$	oP28	$a = 7.368$	PeBG, 78a
	or	Pnnm	$b = 15.38$	
	$NdRe_4Si^{[(4,2)p]}Si^{[(2,4)p]}$		$c = 4.089$	

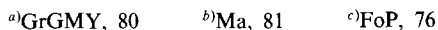
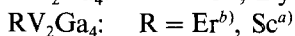
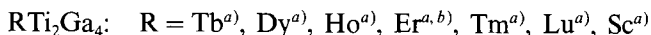
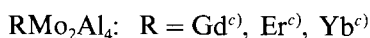
No isotypic  $RT_4M_2$  compounds are known.

The  $NdRe_4Si_2$  structure, shown in fig. 62, can be interpreted as an intergrowth of 8633:CeRe<sub>4</sub>Si<sub>2</sub>-type slabs with slabs of ZrFe<sub>4</sub>Si<sub>2</sub>-type (see 8633:YRe<sub>4</sub>Si<sub>2</sub>).

The Cu-type segments formed by T elements have different shapes in the three structures. The two-dimensional Cu-type slabs in CeRe<sub>4</sub>Si<sub>2</sub> are split up in NdRe<sub>4</sub>Si<sub>2</sub> into one-dimensional Cu-type ribbons (ribbon axes perpendicular to the plane of projection with the ribbon cross section characterized by eight (four plus four) T atoms). In YRe<sub>4</sub>Si<sub>2</sub>, finally, there are only one-dimensional Cu-type columns (also perpendicular to the plane of projection) represented in the cross section by four (two plus two) T atoms.

8667	$YbMo_2Al_4$	tI14	$a = 6.717$	FoP, 76
		I4/mmm	$c = 5.312$	

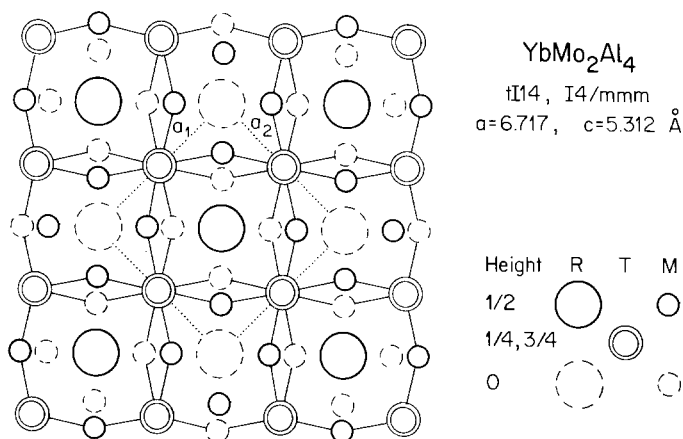
Isotypic compounds:



The  $YbMo_2Al_4$  structure, shown in fig. 63, can be interpreted as a checker-board arrangement of intergrown columns of the CeMg<sub>2</sub>Si<sub>2</sub>-type (see fig. 80). Neighbouring columns are displaced with respect to each other over half a translation period in the *c* direction. For other structures with CeMg<sub>2</sub>Si<sub>2</sub>-type segments, see 9267:CeMn<sub>4</sub>Al<sub>8</sub> (fig. 79) and 8063:Sc<sub>2</sub>Fe<sub>3</sub>Si<sub>5</sub> (fig. 54).

TABLE 17  
 Examples of structures with isolated or linked infinite columns of triangular-face-centred prisms, each built up of two kinds of atoms in the ratio 4:2. There may also be other structure segments present, which are not considered here.

Columns of $(R_4M_2)T^{(6p)}$ prisms					Columns of $(R_2M_4)T^{(6p)}$ prisms						
Code	Compound	Structure type	Pearson's classif. symbol	Space group	Fig.	Code	Compound	Structure type	Pearson's classif. symbol	Space group	Fig.
5725	$Y_3Co_3Ga$	$W_3CoB_3$	oC28	Cmcm	11	7567	$YNiAl_2$	$MgCuAl_2$	oC16	Cmcm	29
6033	$Pt_2Ni_2Al$	$W_2CoB_2$	oI10	Immm	11	8380	$YNiAl_4$	$YNiAl_4$	oC24	Cmcm	59
6733	$La_3Ni_4Ga_2$	$La_3Ni_4Ga_2$	mC18	$C2/m$	18	8871	$PrNi_2Al_5$	$PrNi_2Al_5$	oI16	Immm	67
						8968	$Ho_4Ni_{10}Ga_{21}$	$Ho_4Ni_{10}Ga_{21}$	mC70	$C2/m$	74
Columns of $(R_4T_2)M^{(6p)}$ prisms					Columns of $(R_2T_4)M^{(6p)}$ prisms						
6067	$Se_2CoSi_2$	$Se_2CoSi_2$	mC20	$C2/m$	13	7350	$Sc_3Ni_4Ge_4$	$Gd_3Cu_4Ge_4$	oI22	Immm	29
6360	$Se_3Co_2Si_3$	$Hf_3Ni_5Si_3$	oC32	Cmcm	13	8633	$YRe_6Si_2$	$ZrFe_6Si_2$	tP14	$P4_2/mnm$	62
8050	$LaRe_2Si_2$	$LaRe_2Si_2$	oI20	Imma	52b	8633	$NdRe_6Si_2$	$NdRe_6Si_2$	oP24	Pnmm	62
						8938	$YNi_5Si_3$	$YNi_5Si_3$	oP36	Pnma	69

Fig. 63. The YbMo<sub>2</sub>Al<sub>4</sub> structure built up of intergrown CeMg<sub>2</sub>Si<sub>2</sub>-type columns.

---

<b>8683</b>	<b>HoCoGa<sub>5</sub></b> or Ho <sup>[.12c]</sup> Co <sup>[.8c]</sup> Ga <sub>5</sub>	tP7 P4/mmm	a = 4.207 c = 6.795	GrYG, 79a
-------------	---	---------------	------------------------	-----------

---

Isotypic compounds:

RFeGa<sub>5</sub>: R = Sc<sup>b)</sup>\*RCoGa<sub>5</sub>: R = Gd<sup>a)</sup>, Tb<sup>a)</sup>, Dy<sup>a)</sup>, Ho<sup>a)</sup>, Er<sup>a)</sup>, Tm<sup>a)</sup>, Yb<sup>c)</sup>, Lu<sup>a)</sup>, Y<sup>a)</sup>, Sc<sup>b)</sup>RNiGa<sub>5</sub>: R = Sc<sup>b)</sup>\*

\*No unit cell parameters are given.

<sup>a)</sup>GrYG, 79a<sup>b)</sup>BeM, 78<sup>c)</sup>YaG, 79

The HoCoGa<sub>5</sub> structure, shown in fig. 57, can be interpreted as intergrown Cu<sub>3</sub>Au- and CaF<sub>2</sub>-type slabs and is discussed with 8289:Ho<sub>2</sub>CoGa<sub>8</sub>.

---

<b>8769</b>	<b>Y<sub>2</sub>Fe<sub>4</sub>Si<sub>9</sub></b> * or Y <sup>[.6p]</sup> Fe <sub>2</sub> Si <sub>4</sub> Si <sub>1/2</sub> □ <sub>1/2</sub>	hP16(-1) P6 <sub>3</sub> /mmc	a = 3.928 c = 15.44	GIBYGS, 78
-------------	---	----------------------------------	------------------------	------------

---

\*The formula would be 8871:YFe<sub>2</sub>Si<sub>5</sub> if the half-filled Si site would be fully occupied.

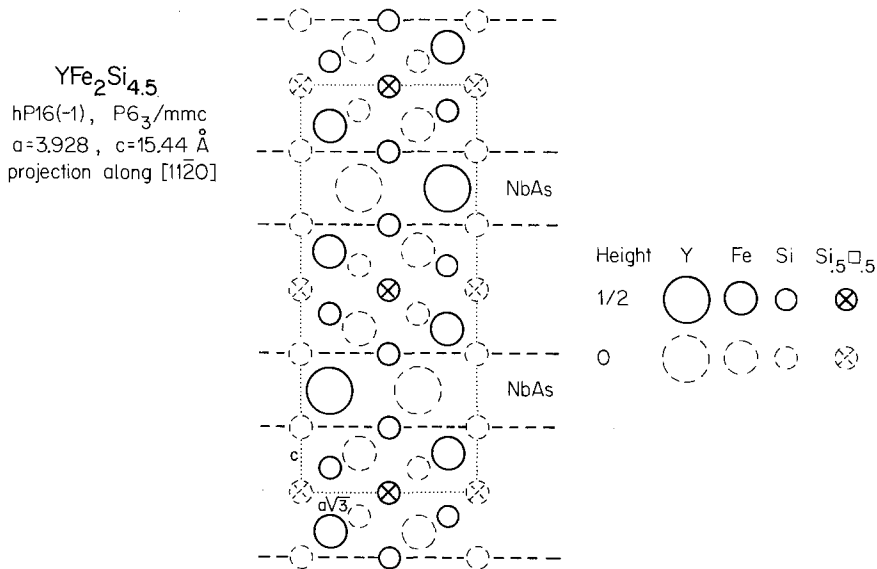


Fig. 64. The crystal structure of  $\text{YFe}_2\text{Si}_{5-x}$  with  $x = \frac{1}{2}$  in a projection along  $[11\bar{2}0]$ .

Isotypic compounds\*\*: All references GIBYGS, 78



\*\*BoGYDI, 78 have first indicated the existence of two phases with slightly different composition  $\text{R}_2\text{Fe}_5\text{Si}_8$  for R = Gd, Y. These phases, which have not been structurally analysed, were said to crystallize in space group  $P6_3/mcm$  instead of  $P6_3/mmc$ . However, from the composition and the cell parameters they should be identical with the phases  $\text{Gd}_2\text{Fe}_4\text{Si}_9$  and  $\text{Y}_2\text{Fe}_4\text{Si}_9$  reported later by GIBYGS, 78.

The structure of  $\text{Y}_2\text{Fe}_4\text{Si}_9$  is shown in fig. 64. It may be considered as an intergrowth of two kinds of slabs. One consists of an arrangement of Y-centred edge-connected (compressed) trigonal prisms of Si atoms as found, for example, in the NbAs-type (BoP, 63) or WC-type. Assuming the half-filled Si sites to be fully occupied, the second slab has the composition  $\text{TM}_3$ . The atom arrangement in this slab is best understood if we concentrate first on the atoms located in a plane that is perpendicular to the plane of projection and intersects the drawing of the slab in a diagonal direction. One finds a close-packed rectangular  $\text{TM}_3$  layer (two-dimensional space group pmm) as observed, for example, in  $\text{Ti}_3\text{Cu}$  (oP8) or  $\text{TiAl}_3$  (tI8). These layers are stacked in the slab with the sequence AB. The superposition of these layers is, however, not as with close-packed structures ( $\text{Ti}_3\text{Cu}$ -type), but as in the  $\text{MoSi}_2$ -type. No binary compound is known which has this simple atom arrangement.

---

<b>8791</b>	<b>LaNi<sub>0.6</sub>Ga<sub>6</sub></b>	tP16(−0.8)	<i>a</i> = 4.300	GrYRG, 82
	or	P4/mmm	<i>c</i> = 15.632	
	La <sub>2</sub> Ni <sub>1.2</sub> □ <sub>0.8</sub> Ga <sub>12</sub>			

---

Isotypic compounds: All references GrYRG, 82



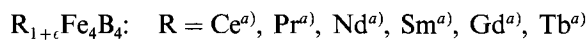
The LaNi<sub>0.6</sub>Ga<sub>6</sub> structure, shown in fig. 85, can be interpreted as an intergrowth of BaAl<sub>4</sub>-type and CaF<sub>2</sub>-type slabs with the nickel sites in the centre in one of two CaF<sub>2</sub>-type slabs only partially occupied. The structure is closely related to the 8591:Ce<sub>2</sub>NiGa<sub>10</sub> structure, shown in fig. 52a, but has a BaAl<sub>4</sub>-type slab which is only half as thick. These intergrowth structures are discussed in detail with 8050:CeNi<sub>2</sub>Si<sub>2</sub>.

---

<b>8850</b>	<b>Sm<sub>17</sub>(Fe<sub>4</sub>B<sub>4</sub>)<sub>15</sub></b>	tP274	<i>a</i> = 7.098	BrPY, 82
	or	P4 <sub>2</sub> /n	<i>c</i> = 58.69	
	( $\frac{1}{\infty}$ Sm) <sub>17</sub> (Fe <sub>4</sub> [B <sub>2</sub> ] <sub>2</sub> ) <sub>15</sub>			

---

Isotypic compounds:



<sup>a</sup>BrPY, 82

<sup>b</sup>Yvon, K., private communication (1982)

The structure of Sm<sub>17</sub>(Fe<sub>4</sub>B<sub>4</sub>)<sub>15</sub>, which is shown in fig. 65, is an example of the R<sub>1+ $\epsilon$</sub> T<sub>4</sub>B<sub>4</sub> structures, which can all be related to the 8950:NdCo<sub>4</sub>B<sub>4</sub> structure. In the discussion of the latter structure it is shown that one finds a framework of linked T<sub>4</sub> tetrahedra with inserted B<sub>2</sub> dumbbells. In the octagonal tubular holes of this framework linear infinite R–R chains are inserted. In the NdCo<sub>4</sub>B<sub>4</sub> structure the translation period of the metal framework *t*<sub>Co</sub> agrees with the translation period of the R–R chains in the *c* direction *t*<sub>Nd</sub>. The NdCo<sub>4</sub>B<sub>4</sub> structure can thus be described with the small tetragonal unit cell. In the R<sub>1+ $\epsilon$</sub> T<sub>4</sub>B<sub>4</sub> structures these two translation periods no longer agree or can be made commensurable only if one assumes very large unit cells. For example, in the case of Sm<sub>17</sub>(Fe<sub>4</sub>B<sub>4</sub>)<sub>15</sub> the length of 17 Sm chain translation units (17*t*<sub>Sm</sub>) corresponds to 15 Fe framework translation units (15*t*<sub>Fe</sub>). The composition of the compounds R<sub>1+ $\epsilon$</sub> T<sub>4</sub>B<sub>4</sub> is thus related to the ratio of the metal framework translation period to the chain translation period according to

$$\epsilon = t_T/t_R - 1.$$

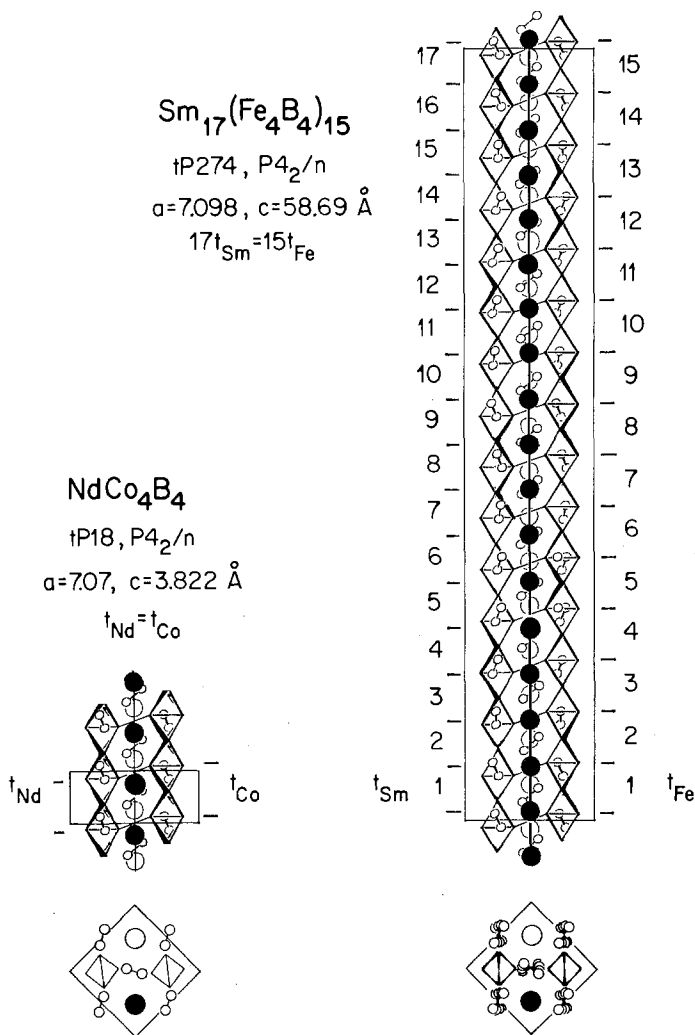


Fig. 65. The structure of  $\text{NdCo}_4\text{B}_4$  and of  $\text{Sm}_{17}(\text{Fe}_4\text{B}_4)_{15}$  approximated in the centrosymmetric space group  $P4_2/n$ . Shown are the chains of transition metal tetrahedra, the rare earth atoms (large circles) and the boron pairs (small circles), as viewed along  $[110]$  (top) and  $[001]$  (bottom). Courtesy of H. F. Braun, M. Pelizzone and K. Yvon.

Fig. 65 shows that in  $\text{Sm}_{17}(\text{Fe}_4\text{B}_4)_{15}$  there is a twist modulation of the Fe tetrahedral chains and of the B atom pairs around the tetragonal axis.

Selected values of the compositions and the large unit cells of  $\text{R}_{1+\epsilon}\text{T}_4\text{B}_4$  compounds are given in table 18. However, each of these phases has a certain "homogeneity" range which, for example in the case of  $\text{Gd}_{1+\epsilon}\text{Fe}_4\text{B}_4$ , lies between  $0.13 \leq \epsilon \leq 0.15$ . Within this composition range the Fe and B partial structure is (practically) unchanged, but the translation period of the Gd chain decreases with  $\epsilon$  increasing.

TABLE 18  
Selected values of the compositions and tetragonal lattice constants of  $R_{1+\epsilon}T_4B_4$  compounds.

Code	$\epsilon$	Compound	Pearson's classif. symbol	Space group	$a$ (Å)	$c$ (Å)
8850	0.1212	$Ce_{37}(Fe_4B_4)_{33}$	tP602	$P4_2/n$	7.090	129.04
8850	0.1053	$Pr_{21}(Fe_4B_4)_{19}$	tP346	$P4_2/n$	7.158	74.18
8850	0.1081	$Nd_{41}(Fe_4B_4)_{37}$	tP674	$P4_2/n$	7.141	144.57
8850	0.1333	$Sm_{17}(Fe_4B_4)_{15}$	tP274	$P4_2/n$	7.098	58.69
8850	0.1379	$Gd_{33}(Fe_4B_4)_{29}$	tP530	$P4_2/n$	7.073	113.73
8750	0.1481	$Tb_{31}(Fe_4B_4)_{27}$	tP494	$P4_2/n$	7.049	105.81
8950	0	Nd $Co_4B_4$	tP18	$P4_2/n$	7.07	3.822

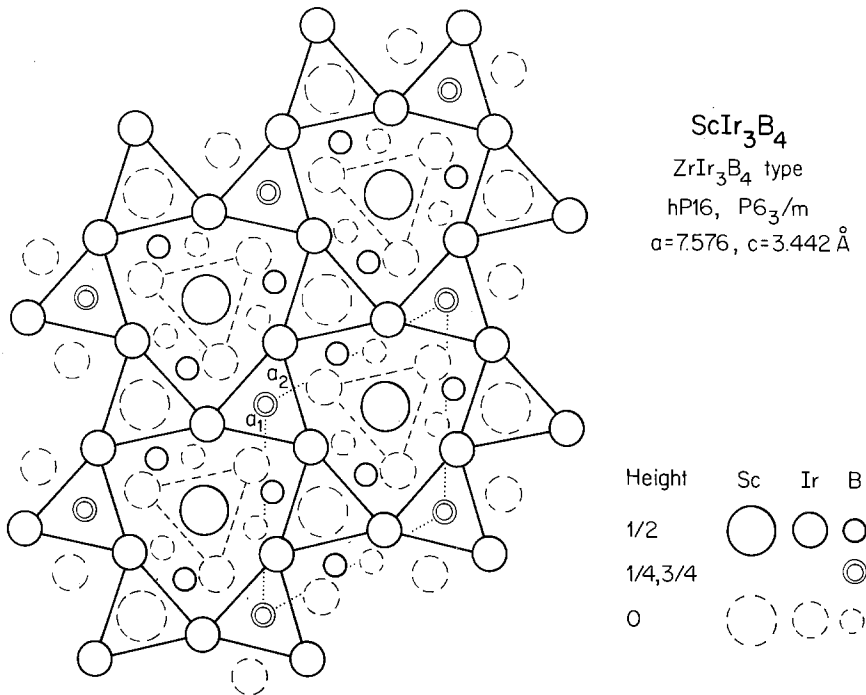
Thus for a composition other than that given in table 18 the commensurability between  $t_{Gd}$  and  $t_{Fe}$  can be reached only with other multiples and consequently the tetragonal unit cell has a different  $c$  value.

<b>8857</b>	<b>ScIr<sub>3</sub>B<sub>4</sub></b> or Sc <sup>[6,p]</sup> Ir <sub>3</sub> B <sub>3</sub> ∞ B <sup>[6o]</sup>	hP16 P6 <sub>3</sub> /m	$a = 7.576$ $c = 3.442$	<b>RoN, 79</b>
ZrIr <sub>3</sub> B <sub>4</sub> -type (Ro, 78).				

No isotypic  $RT_3M_4$  compounds are known.

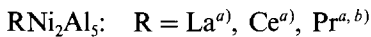
The ScIr<sub>3</sub>B<sub>4</sub> structure with ZrIr<sub>3</sub>B<sub>4</sub>-type, which is presented in fig. 66, can be considered in first approximation as a stuffed version of the ZrNiAl-type (see 6750:ScRuGe and fig. 20). The boron atoms in the centres of the Ir octahedra form infinite linear chains perpendicular to the plane of projection. However, the other B atoms, inserted between the columns (formed of trigonal-face-joined Sc-centred trigonal prisms of Ir atoms), are so far apart from each other that they have to be considered as isolated.

Two structure types occur with composition 8871: PrNi<sub>2</sub>Al<sub>5</sub>, oI16 and YFe<sub>2</sub>Si<sub>5</sub>, hP16. In structures with the latter type one site is supposedly only partially filled. These structures are correspondingly treated here under the heading 8769: Y<sub>2</sub>Fe<sub>4</sub>Si<sub>9</sub>.

Fig. 66. The crystal structure of  $\text{ScIr}_3\text{B}_4$ .

8871	$\text{PrNi}_2\text{Al}_5$ or $\text{PrNi}_2^{[(2,4)p]}\text{Al}_4\text{Al}^{[+8c]}$	oI16 Immm	$a = 3.979$ $b = 7.024$ $c = 9.562$	YaRAZ, 81
------	--	--------------	---	-----------

Isotypic compounds:



<sup>a)</sup>YaRAZ, 81

<sup>b)</sup>RyZK, 78

The  $\text{PrNi}_2\text{Al}_5$  structure and the 8380:  $\text{LaCoAl}_4$  structure are both presented in fig. 67. They are built up of the same construction elements, rectilinear columns (perpendicular to the plane of projection) of rhombic cross section with R and T atoms at the corners. Inscribed in the rhombic column is a square column formed of face-joined  $\text{AlAl}_8$  cubes. The contour lines of the rhombic columns are indicated in fig. 67 by thin lines. The  $\text{PrNi}_2\text{Al}_5$  structure differs from the  $\text{LaCoAl}_4$  structure by the way these columns are joined. In  $\text{LaCoAl}_4$  slabs are formed, each column having



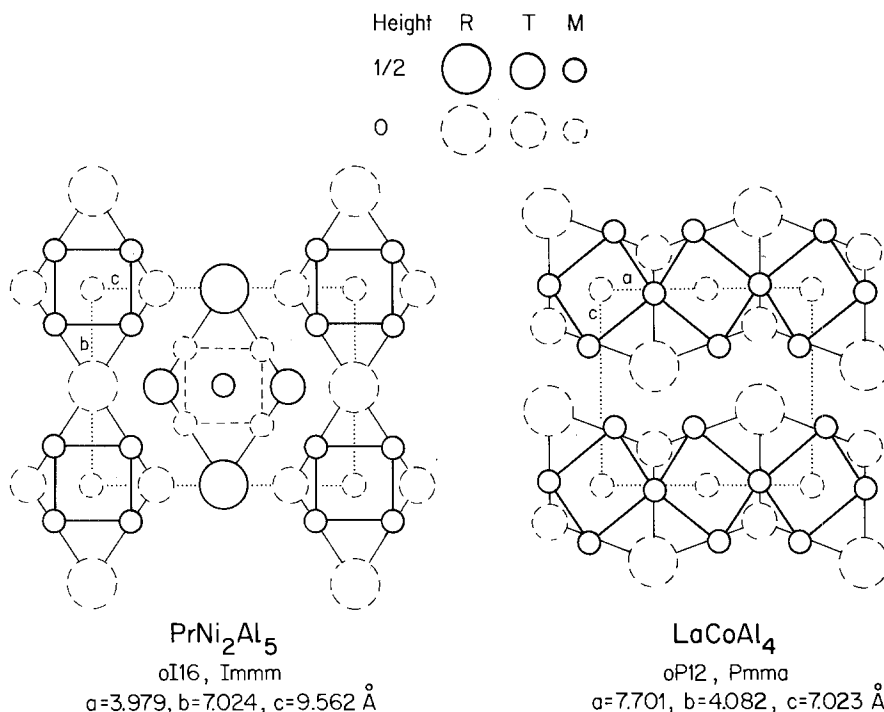


Fig. 67. The PrNi<sub>2</sub>Al<sub>5</sub> and the LaCoAl<sub>4</sub> structures, both built up of identical construction elements but connected in a different way.

two faces in common with two neighbouring columns. In PrNi<sub>2</sub>Al<sub>5</sub>, however, each column is joined to two others by two common edges.

In both structures the T atoms are in the centres of trigonal prisms but with different formula. In PrNi<sub>2</sub>Al<sub>5</sub> there are (R<sub>2</sub>M<sub>4</sub>)T prisms, but (M<sub>6</sub>)T prisms in LaCoAl<sub>4</sub>.

Two structure types occur with composition 8912: Ce<sub>2</sub>Ni<sub>15</sub>Si<sub>2</sub>, hP38 and Ce<sub>2</sub>Co<sub>15</sub>Al<sub>2</sub>, hR57.

<b>8912</b>	Ce <sub>2</sub> Ni <sub>15</sub> Si <sub>2</sub> *	hP38	a = 8.289	GIKB, 67
and	or	P6 <sub>3</sub> /mmc	c = 8.085	
<b>89(-)</b>	Ce <sub>2</sub> Ni <sub>9</sub> Ni <sub>6</sub> <sup>6pl</sup> <sub>2</sub> [Si <sub>2</sub> ]			

Th<sub>2</sub>Ni<sub>17</sub>-type (FIBR, 56) derivative\*

\*Ordering of T and M atoms was difficult to determine because only powder diffraction data were available. It is assumed here that the order in the slabs is identical to that found in 8912: Ce<sub>2</sub>Co<sub>15</sub>Al<sub>2</sub>.

## Isotypic compounds:

The following list includes all ternary  $\text{Th}_2\text{Ni}_{17}$ -type derivative phases regardless of the M/T ratio. Ordering of T and M atoms is possible for the compositions 8912:  $\text{R}_2\text{T}_{15}\text{M}_2$ , 8947:  $\text{R}_2\text{T}_9\text{M}_8$  and 8965:  $\text{R}_2\text{T}_6\text{M}_{11}$  but has not been experimentally verified.

R-Fe-Al: R = Tb<sup>a)</sup> ( $\text{Tb}_2\text{Fe}_{17-13.2}\text{Al}_{0-3.8}$ ), Dy<sup>b)</sup>\* ( $\text{Dy}_2\text{Fe}_{17-12}\text{Al}_{0-5}$ )

R-Co-Al: R = Y<sup>c)</sup> ( $\text{Y}_2\text{Co}_{17-15}\text{Al}_{0-2}$ )

R-Ni-Al: R = Gd<sup>d)</sup> ( $\text{Gd}_2\text{Ni}_{17-0}\text{Al}_{0-17}$ )

R-Ni-Si: R = Ce<sup>e,f,g,h)</sup> ( $\text{Ce}_2\text{Ni}_{15.1-14.5}\text{Si}_{1.9-2.5}$ ), Nd<sup>e,h)</sup>\*\* , Pr<sup>e,h)</sup>\*\*

\* $\text{Dy}_2\text{Fe}_{9-11}\text{Al}_{8-6}$  phases crystallize with the  $\text{Th}_2\text{Zn}_{17}$ -type (see 8912:  $\text{Ce}_2\text{Co}_{15}\text{Al}_2$ ).

\*\* $\text{R}_2(\text{Ni}, \text{Si})_{17}$ .

<sup>a)</sup>Oe, 75

<sup>b)</sup>ViZR, 73

<sup>c)</sup>RyZ, 71

<sup>d)</sup>PoDCH, 79

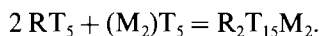
<sup>e)</sup>GIKB, 66a

<sup>f)</sup>BoG, 69

<sup>g)</sup>BoMTKG, 73

<sup>h)</sup>GIKB, 67

The  $\text{Ce}_2\text{Ni}_{15}\text{Si}_2$  structure with hexagonal  $\text{Th}_2\text{Ni}_{17}$ -type derivative and the 8912:  $\text{Ce}_2\text{Co}_{15}\text{Al}_2$  structure with rhombohedral  $\text{Th}_2\text{Zn}_{17}$ -type derivative are closely related. Both can be considered as intergrowth variants of a common structural slab of composition  $\text{R}_2\text{T}_{15}\text{M}_2$ , which is shown in the upper part of fig. 68.\* This slab itself can be described as an intergrowth of two different kinds of structure blocks, the outlines of which are indicated in fig. 68 by thin lines. The intergrown structure block containing the rare earth element has the composition  $\text{RT}_5$ . It occurs twice as often as the other block and corresponds to a segment of the hexagonal  $\text{CaCu}_5$ -type structure (compare with the upper left drawing in fig. 35). The second block with the same size has the composition  $\text{T}_5\text{M}_2$ . It may be described as a  $\text{CaCu}_5$ -type block where the rare earth atom has been replaced by a pair of M atoms (dumbbell axis perpendicular to the plane of projection). The structure sites in this block correspond to the structure sites in the hexagonal  $\text{Zr}_4\text{Al}_3$ -type (WiTS, 60) (compare with the left-hand side drawing in fig. 80). The composition of the slab can thus be derived from



The intergrown blocks are arranged in such a manner that the slab has hexagonal symmetry with a translation period corresponding to  $\sqrt{3}a(\text{CaCu}_5)$ . The height of the slab is  $c(\text{CaCu}_5)$ . In the  $\text{Th}_2\text{Ni}_{17}$ - and  $\text{Th}_2\text{Zn}_{17}$ -type derivative structures the slabs are intergrown with each other. Referring to the slab translation period in the plane and denoting the positions  $00$ ,  $\frac{1}{3}\frac{2}{3}$  and  $\frac{2}{3}\frac{1}{3}$  by A, B and C, respectively, the intergrown slabs are stacked one above the next such that the M atom pairs of successive slabs assume positions

\*In this discussion the compositions of the slabs and blocks always refer to intergrown slabs and blocks. For example, the drawing of the  $\text{R}_2\text{T}_{15}\text{M}_2$  slab actually shows a  $\text{R}_2\text{T}_{24}\text{M}_2$  slab; however, since per slab unit cell 18 T atoms at the interface are shared with intergrown slabs (9 with the slab above and 9 with the slab below), the composition given is  $\text{R}_2\text{T}_6\text{T}_{18/2}\text{M}_2 = \text{R}_2\text{T}_{15}\text{M}_2$ .

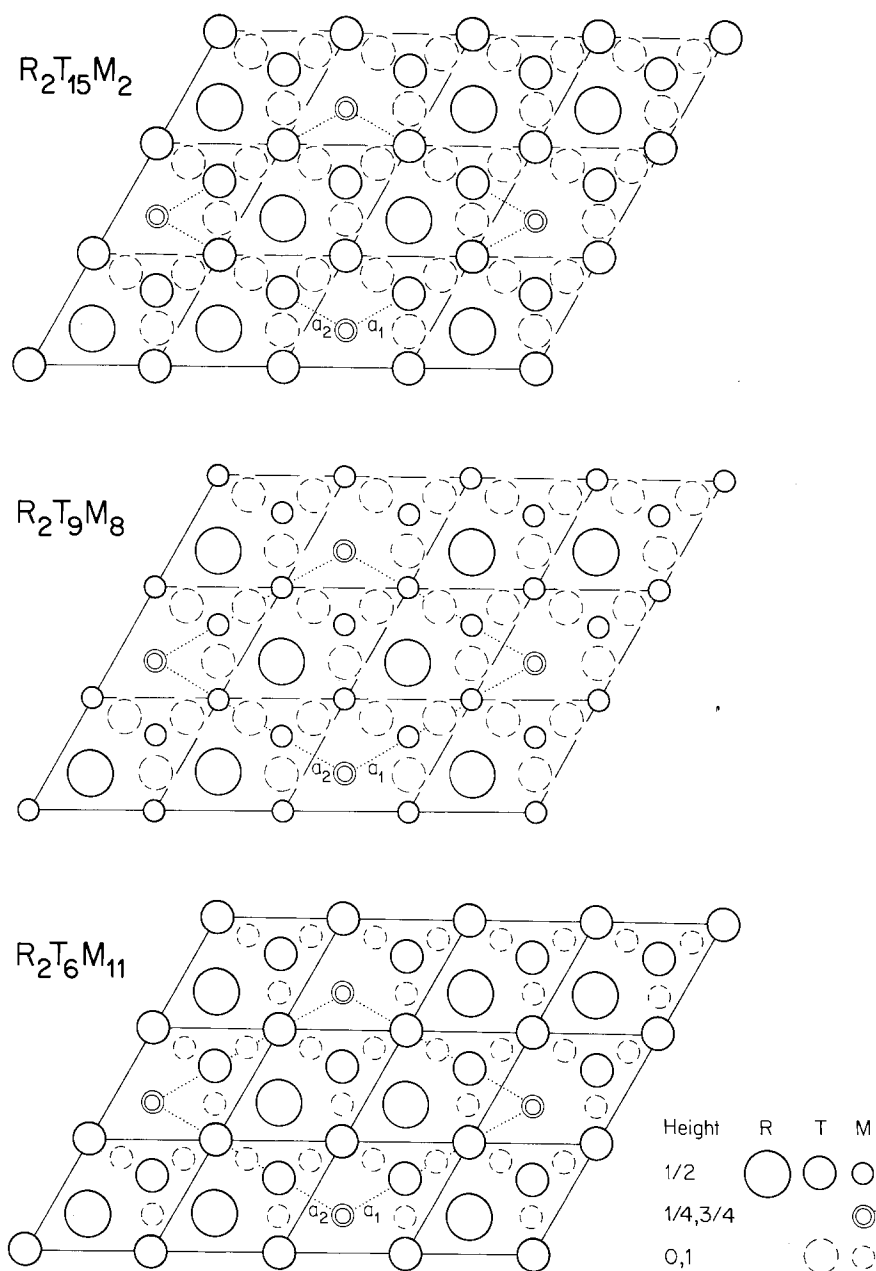


Fig. 68. Three different ordering variants of the structural slab which, when stacked in the sequence AB or ABC, result in a  $Th_2Ni_{17}$ - or  $Th_2Zn_{17}$ -type derivative structure, respectively. The slabs are intergrown of differently ordered  $CaCu_5$ -type and  $Zr_4Al_3$ -type blocks in the ratio 2:1. The contour lines of the structure blocks are indicated with thin lines. The values for the height of the atoms are normalized to the thickness of one slab. The middle of the slab is at height  $\frac{1}{2}$ . The atoms at height 0 and 1 are shared in the structures when the slabs are stacked.

A B A B . . . in the hexagonal  $\text{Th}_2\text{Ni}_{17}$ -type derivative,  
 A B C A B C . . . in the rhombohedral  $\text{Th}_2\text{Zn}_{17}$ -type derivative.

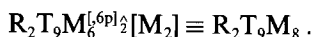
The hexagonal axial ratios of the  $\text{Th}_2\text{Ni}_{17}$ - and  $\text{Th}_2\text{Zn}_{17}$ -type phases are thus related according to

$$\begin{aligned} \text{Th}_2\text{Ni}_{17}: \quad \frac{c}{a} &= \frac{2c(\text{CaCu}_5)}{\sqrt{3} a(\text{CaCu}_5)} \approx 0.975, \\ \text{Th}_2\text{Zn}_{17}: \quad \frac{c}{a} &= \frac{3c(\text{CaCu}_5)}{\sqrt{3} a(\text{CaCu}_5)} \approx 1.460. \end{aligned}$$

The extreme constancy of the axial ratios for various  $\text{Th}_2\text{Zn}_{17}$ -type structures has been the subject of intensive study (Pearson, 1979).

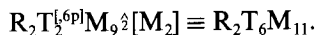
Some of the phases with hexagonal  $\text{Th}_2\text{Ni}_{17}$ -type derivative structure and particularly the more numerous phases with rhombohedral  $\text{Th}_2\text{Zn}_{17}$ -type derivative phases have more M-rich compositions, which deviate considerably from  $\text{R}_2\text{T}_{15}\text{M}_2$ . One can mention here, for example, the  $\text{Th}_2\text{Zn}_{17}$ -type derivative phases 8947:  $\text{Y}_2\text{Mn}_9\text{Al}_8$  (RyZG, 71) without a homogeneity range and 8965:  $\text{La}_2\text{Fe}_6\text{Al}_{11}$  (ZaERD, 68). The compositions  $\text{R}_2\text{T}_9\text{M}_8$  and  $\text{R}_2\text{T}_6\text{M}_{11}$  can be derived theoretically if one assumes that the  $\text{RT}_5$  blocks with  $\text{CaCu}_5$ -type and the  $\text{T}_5\text{M}_2$  blocks with  $\text{Zr}_4\text{Al}_3$ -type are replaced by blocks where the sites are occupied by the atoms in a different order.

Assuming that in the slabs described above all  $\text{RT}_5$  blocks are replaced by  $\text{RT}_3\text{M}_2^{[6pl]}$  blocks as in 8340:  $\text{CeCo}_3\text{B}_2$  (see fig. 58) and the intergrown  $\text{T}_5\hat{\Delta}[\text{M}_2]$  blocks correspondingly by  $\text{T}_3\text{M}_2^{[6pl]\hat{\Delta}}[\text{M}_2]$ , the slab changes its composition to



The atom ordering in the slab is shown in the middle part of fig. 68.

If, however, the  $\text{RT}_5$  blocks are replaced by  $\text{RT}_2\text{M}_3^{[6pl]}$  blocks as found in 8360:  $\text{PrNi}_2\text{Al}_3$  and correspondingly the  $\text{T}_5\hat{\Delta}[\text{M}_2]$  blocks by  $\text{T}_2^{[6pl]}\text{M}_3\hat{\Delta}[\text{M}_2]$ , the slab looks as shown in the lower part of fig. 68. The composition of the slab is then



Unfortunately the structures of 8947:  $\text{Y}_2\text{Mn}_9\text{Al}_8$  and 8965:  $\text{La}_2\text{Fe}_6\text{Al}_{11}$  have not been investigated for the order of the T and M atoms. Even in the case of  $\text{Y}_2\text{Mn}_9\text{Al}_8$  no lattice constants have been published. The only thoroughly studied structure of a  $\text{Th}_2\text{Zn}_{17}$ -type derivative with a M-rich composition is the one of 8959:  $\text{Ce}_2\text{Mn}_7\text{Al}_{10}$  (ZaK, 63). Here one finds essentially  $\text{R}_2\text{T}_9\text{M}_8$  slabs, where, however, on some of the T sites the Mn atoms are partially replaced by Al atoms. The formation of a  $\text{R}_2\text{T}_9\text{M}_8$  slab with an aluminide is somewhat surprising. Previous results on  $\text{CeCo}_3\text{B}_2$ -type aluminides have shown, that the Al atoms do not prefer to be in the centres of trigonal prisms. For example, the  $\text{CeCo}_3\text{B}_2$ -type aluminides differ from other compounds in having the composition  $\text{RT}_2\text{M}_3$  and the corresponding crystal chemical formula  $\text{RT}_2^{[6pl]}\text{Al}_3$ . For the ternary  $\text{Th}_2\text{Zn}_{17}$ -type derivative structures one might thus have predicted the formation of a  $\text{R}_2\text{T}_6\text{Al}_{11}$  slab where the transition element is in the centre of the trigonal Al prisms.

Up to now we considered structures formed by the intergrowth of identical slabs, each slab being built up of two kinds of structure blocks. Now we want to consider structures formed by intergrowth of different slabs, each slab formed by one kind of structure block only. If one uses, for example, the  $RT_3M_2^{[6p]}$  and  $T_3M_2^{[6p]} [M_2]$  blocks (which were used in the construction of the  $R_2T_9M_8$  slab shown in the middle part of fig. 68) and constructs one kind of slab from the  $RT_3M_2$  blocks and the other from the other block, which are then intergrown (with T atoms at the interface shared) one obtains:

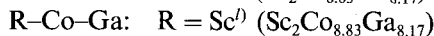
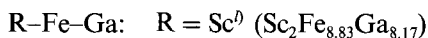
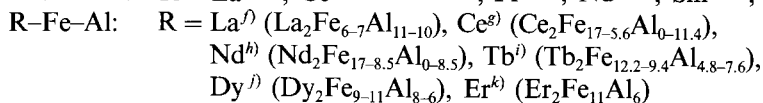
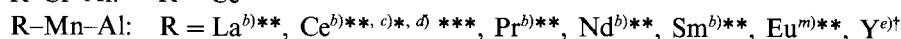
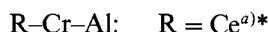


The structure with these features is found with 9250:ScFe<sub>6</sub>Ge<sub>6</sub> having the HfFe<sub>6</sub>Ge<sub>6</sub>-type (see fig. 78).

<b>8912</b>	<b>Ce<sub>2</sub>Co<sub>15</sub>Al<sub>2</sub></b>	<b>hR57</b>	<b>a = 8.44</b>	<b>ZaK, 63</b>
and	or	<b>R<math>\bar{3}</math>m</b>	<b>c = 12.30</b>	
<b>89(-)</b>	<b>Ce<sub>2</sub>Co<sub>9</sub>Co<sub>6</sub><sup>[+6p]</sup><sub>2</sub> [Al<sub>2</sub>]</b>			
Th <sub>2</sub> Zn <sub>17</sub> -type (MaV, 56; JoSW, 69) derivative				

### Isotypic compounds:

The following list includes all ternary Th<sub>2</sub>Zn<sub>17</sub>-type derivative phases regardless of the M/T ratio. Ordering of T and M atoms is possible for the compositions 8912:R<sub>2</sub>T<sub>15</sub>M<sub>2</sub>, 8947:R<sub>2</sub>T<sub>9</sub>M<sub>8</sub> and 8965:R<sub>2</sub>T<sub>6</sub>M<sub>11</sub> and was experimentally verified with Ce<sub>2</sub>Co<sub>15</sub>Al<sub>2</sub>.



\*R<sub>2</sub>T<sub>7</sub>Al<sub>10</sub> partially ordered [see 89(59):Ce<sub>2</sub>Mn<sub>7</sub>Al<sub>10</sub>].

\*\*Composition is given as RMn<sub>6</sub>Al<sub>6</sub>. Result is unexpected. A reinvestigation might be appropriate.

\*\*\*Composition not specified.

†R<sub>2</sub>T<sub>6</sub>Al<sub>8</sub>.

††R<sub>2</sub>T<sub>15</sub>Al<sub>2</sub>, order verified experimentally.

<sup>a)</sup>ZaR, 74

<sup>b)</sup>Fe, 80

<sup>c)</sup>ZaK, 63

<sup>d)</sup>ZaKT, 63

<sup>e)</sup>RyZG, 71

<sup>f)</sup>ZaERD, 68

<sup>g)</sup>ZaMR, 69

<sup>h)</sup>ViZR, 70

<sup>i)</sup>Oe, 75

<sup>j)</sup>ViZR, 73

<sup>k)</sup>ZaVR, 72

<sup>l)</sup>BeM, 82a

<sup>m)</sup>FeN, 82

The  $\text{Ce}_2\text{Co}_{15}\text{Al}_2$  structure, a  $\text{Th}_2\text{Zn}_{17}$ -type derivative, is discussed with the 8912: $\text{Ce}_2\text{Ni}_{15}\text{Si}_2$  structure, a  $\text{Th}_2\text{Ni}_{17}$ -type derivative. There also the other possibilities for ordering the T and M atoms are treated. Beside  $\text{Ce}_2\text{Co}_{15}\text{Al}_2$  the only other exact structure determination of a (partially) ordered ternary  $\text{Th}_2\text{Zn}_{17}$ -type derivative was made on 89(59): $\text{Ce}_2\text{Mn}_7\text{Al}_{10}$ .

8938	$\text{YNi}_5\text{Si}_3$ or $\text{YNi}_5\text{Si}_3^{[(2,4)p]}$	oP36 Pnma	$a = 18.787^*$ $b = 3.795$ $c = 6.587$	BoYG, 74
------	---	--------------	--	----------

\*Cell parameters from AkYBYG, 76.

#### Isotypic compounds:



<sup>a</sup>)BoYG, 74      <sup>b</sup>)AkYBYG, 76

The  $\text{YNi}_5\text{Si}_3$  structure is shown on the left-hand side of fig. 69. The characteristic construction elements are columns of (trigonal-face-joined) M-centred trigonal prisms, each formed of two R and four T elements. Other structures with such columns are listed in table 17 and discussed with 8633: $\text{YRe}_4\text{Si}_2$ . A particular feature of the  $\text{YNi}_5\text{Si}_3$  structure is the linkage of the trigonal prism columns. Some column edges are shared between three, some between two columns and some are not shared at all. The rare earth atoms are always and only found on the edges common to three columns, all other edges being occupied by T atoms. Thus all R atoms participate in the formation of six centred trigonal prisms, but T atoms only in the formation of four or two centred trigonal prisms. If one denotes pictorially the three joined centred prisms with the common edge as a *prism propeller*, the  $\text{YNi}_5\text{Si}_3$  structure can now be described as an infinite planar sheet of joined prism propeller columns. Each prism propeller column is joined to two neighbouring propeller columns by a shared outer prism edge occupied by T atoms. Two kinds of equivalent sheets are stacked along the [100] direction, the two sheets being displaced with respect to each other by half a translation period perpendicular to the plane of projection.

A number of different structures are known, all of or close to composition 1:5:3, which are characterized by joined prism propeller columns. In all cases the rare earth or uranium atoms are exclusively on the propeller axes and the  $\text{R}_2\text{T}_4$  prisms are always centred by M or phosphorus atoms.

The structure of  $\text{LaCo}_5\text{P}_3$  (DaK, 81), which is shown on the right-hand side of fig. 69\* is closely related to  $\text{YNi}_5\text{Si}_3$ . Here we find the same kind of sheets of joined prism

\*The interatomic distances for  $\text{LaCo}_5\text{P}_3$  listed do not agree with the distances calculated from the given atomic coordinates.

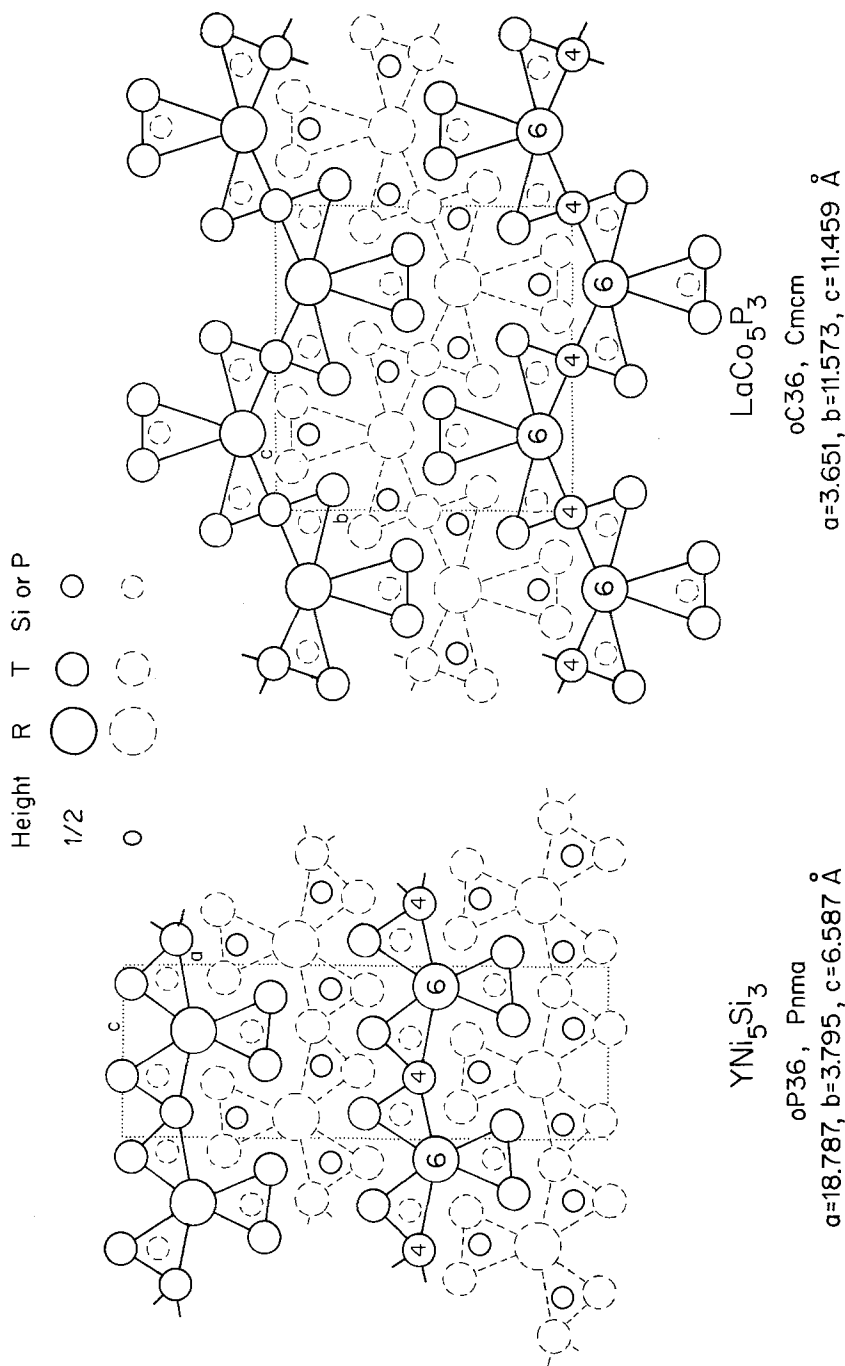


Fig. 69. The  $\text{YNi}_5\text{Si}_3$  and the  $\text{LaCo}_5\text{P}_3$  structures, both characterized by slabs of joined prism propeller columns. In both structures two propeller blades of each prism propeller are connected to neighbouring prism propellers. In  $\text{YNi}_5\text{Si}_3$ , the non-connected blades of neighbouring prism propellers stand in *cis*, in  $\text{LaCo}_5\text{P}_3$ , however, in *trans* position. The numbers inscribed in the circles correspond to the number of centred trigonal prisms in which a particular atom participates.

propeller columns; however, in  $\text{YNi}_3\text{Si}_3$  neighbouring prism propellers are in the *cis* position but in  $\text{LaCo}_5\text{P}_3$  in the *trans* position.

The structure of  $\text{UCo}_5\text{Si}_3$  (YaAG, 78) has not yet been found with rare earth compounds; however, its occurrence is probable, just as  $\text{UNi}_5\text{Si}_3$  was found to adopt the  $\text{YNi}_5\text{Si}_3$ -type. As can be seen on the left-hand side of fig. 70, the same prism propeller columns are found but instead of an infinite sheet they close on themselves and form a triple propeller column. There are two kinds of equivalent triple propeller columns in the structure, which are displaced with respect to each other by half a translation unit perpendicular to the plane of projection.

The triple propeller column can be joined with three more propeller columns to form the more complicated triangular propeller column arrangement found in  $\text{U}_6\text{Co}_{30}\text{Si}_{19}$  (YaAFG, 80) and shown in the middle part of fig. 70. Finally, if ten propeller columns are joined to form a super column also with triangular cross section, one obtains the column arrangement observed in the structure of  $\text{U}_{10}\text{Co}_{51}\text{Si}_{33}$  (AkYG, 80), which is presented on the right-hand side of fig. 70. In the last two structures, by joining three triple propeller columns, a space is generated between them which is occupied by simple columns of face-joined Si-centred trigonal prisms formed by T atoms only.

The three structures with (simple or joined) triple propeller columns can be grouped into a structural series. We denote by  $n$  the number of prism propeller columns at the edge of the triangular cross section of the super columns shown in fig. 70. The formula of the joined prism propeller arrangement is then

$$\text{R}_{(n/2)(n+1)}\text{T}_{3(n^2+1)}\text{M}_{2n^2+1}.$$

The  $\frac{1}{2}(n-2)(n-1)$  interstices of this prism propeller arrangement are occupied by simple prism columns of composition  $\text{T}_3\text{M}$ . The sum gives the final formula of this structural series:

$$\text{R}_{(n/2)(n+1)}\text{T}_{3(n^2+1)}\text{M}_{2n^2+1}.$$

The structural data for members of this series are listed in table 19. We note that the compositions of the members of this series are all very close to  $\text{RT}_5\text{M}_3$ . For phase diagram studies it is therefore particularly important to investigate this region with a very fine composition mesh.

TABLE 19  
The structural data for the  $\text{R}_{(n/2)(n+1)}\text{T}_{3(n^2+1)}\text{M}_{2n^2+1}$  structural series.

$n$	Code	Calculated composition	Structure type	Pearson's classif. symbol	Space group	Number of joined propeller columns	Number of inserted simple prism columns
2	8938	$\text{RT}_5\text{M}_3$	$\text{UCo}_5\text{Si}_3$	hP54	$\text{P6}_3/\text{m}$	3	0
3	8938	$\text{R}_6\text{T}_{30}\text{M}_{19}$	$\text{U}_6\text{Co}_{30}\text{Si}_{19}$	hP110	$\text{P6}_3/\text{m}$	6	1
4	8939	$\text{R}_{10}\text{T}_{51}\text{M}_{33}$	$\text{U}_{10}\text{Co}_{51}\text{Si}_{33}$	hP188	$\text{P6}_3/\text{m}$	10	3
5	9040	$\text{R}_5\text{T}_{26}\text{M}_{17}$		hP288	$\text{P6}_3/\text{m}$	15	6



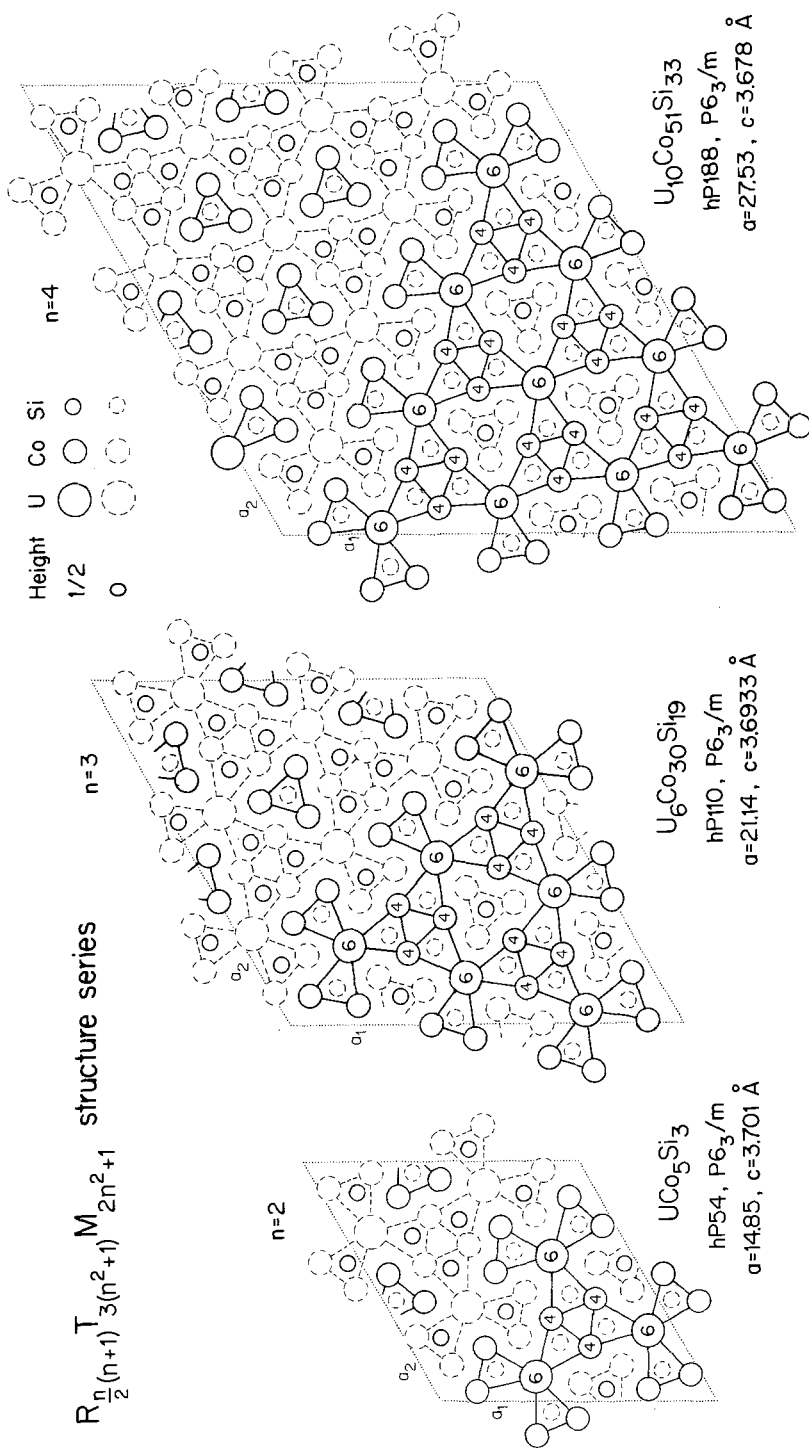


Fig. 70. The three structures of the  $R_{\frac{n}{2}(n+1)} T_{3(n^2+1)} M_{2n^2+1}$  structural series, all built up of triple propeller prism columns. The numbers inscribed in the circles indicate the number of centred prisms in which the particular atom participates. Uranium atoms are exclusively found on the propeller axes.

Four structure types occur with composition 8950:  $\text{NdCo}_4\text{B}_4$ , tP18;  $\text{CeCo}_4\text{B}_4$ , tP18;  $\text{LuRu}_4\text{B}_4$ , tI72, and  $\text{LuRh}_4\text{B}_4$ , oC108. A very similar composition is found in the  $\text{R}_{1+c}\text{T}_4\text{B}_4$  phases discussed with 8850:  $\text{Sm}_{17}(\text{Fe}_4\text{B}_4)_{15}$ .

<b>8950</b>	<b><math>\text{NdCo}_4\text{B}_4</math></b>	tP18	$a = 7.07$	KuB, 78
	or	$\text{P4}_2/\text{n}$	$c = 3.822$	
	$\text{NdCo}_4[\text{B}_2]_2$			

Isotypic compounds:

$\text{RCo}_4\text{B}_4$ : R =  $\text{La}^a$ ,  $\text{Pr}^a$ ,  $\text{Nd}^a$ ,  $\text{Sm}^a$ )

$\text{RRu}_4\text{B}_4$ : R =  $\text{La}^b$ )

$\text{ROs}_4\text{B}_4$ : R =  $\text{La}^c$ \*,  $\text{Ce}^d$ \*,  $\text{Pr}^c$ \*,  $\text{Nd}^c$ ),  $\text{Sm}^{c,d}$ \*,  $\text{Eu}^d$ ),  $\text{Gd}^g$ \*\*\*,  $\text{Tb}^g$ \*\*\*,  $\text{Dy}^g$ \*\*\*,  
 $\text{Ho}^g$ \*\*\*,  $\text{Er}^g$ \*\*\*,  $\text{Tm}^g$ \*\*\*,  $\text{Yb}^g$ \*\*\*,  $\text{Y}^g$ \*\*\*)

$\text{RIr}_4\text{B}_4$ : R =  $\text{La}^{c,e}$ \*,  $\text{Ce}^c$ \*,  $\text{Pr}^c$ \*,  $\text{Nd}^e$ ),  $\text{Sm}^c$ \*,  $\text{Eu}^d$ ),  $\text{Gd}^c$ ),  $\text{Tb}^c$ ),  $\text{Dy}^f$ ),  $\text{Y}^c$ )

\*For pseudo-ternary systems  $\text{R}(\text{Os}_{1-x}\text{Ir}_x)_4\text{B}_4$  with R = La, Ce, Pr and Sm, see HiRS, 82.

\*\*Superstructure of  $\text{NdCo}_4\text{B}_4$  ( $\text{YOs}_4\text{B}_4$ -type). According to Yvon (private communication, 1982) the compounds with R = Gd and Y belong to the  $\text{R}_{1+c}\text{T}_4\text{B}_4$  structures described under the heading 8850:  $\text{Sm}_{17}(\text{Fe}_4\text{B}_4)_{15}$ .

<sup>a</sup>KuB, 78    <sup>b</sup>GrY, 79    <sup>c</sup>Ro, 79    <sup>d</sup>HiRS, 82    <sup>e</sup>Ro, 80    <sup>f</sup>JoB, 82    <sup>g</sup>RoN, 80

The  $\text{NdCo}_4\text{B}_4$  structure, shown in fig. 71, as well as the three other boride structures with the same composition  $\text{CeCo}_4\text{B}_4$ ,  $\text{LuRu}_4\text{B}_4$  and  $\text{LuRh}_4\text{B}_4$  (fig. 73), are all characterized by  $\text{B}_2$  dumbbells and  $\text{T}_4$  tetrahedra. The characteristic difference between the four structure types is the different mode of linkage of the  $\text{T}_4$  tetrahedra.

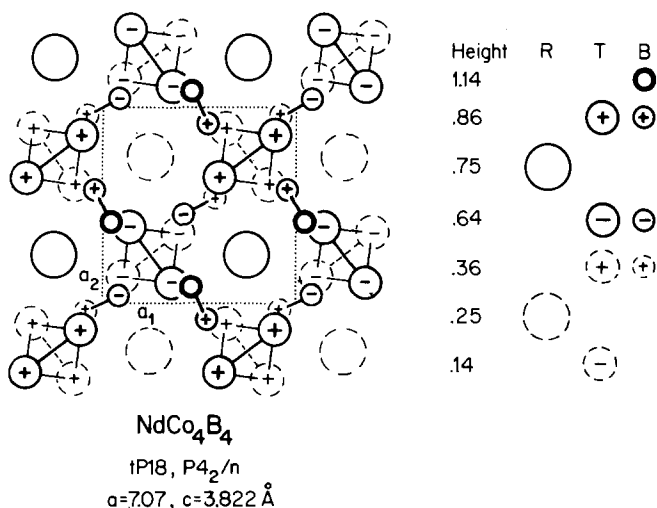


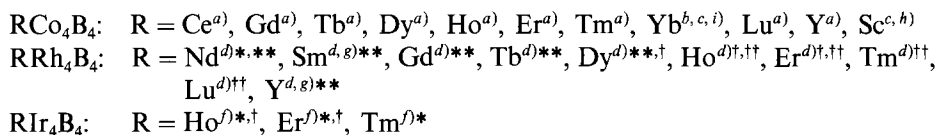
Fig. 71. The crystal structure of  $\text{NdCo}_4\text{B}_4$ . The heights are rounded values.

In  $\text{NdCo}_4\text{B}_4$  the tetrahedra share two of their edges with neighbouring tetrahedra forming tetrahedral chains parallel to the  $c$  axis. The tetrahedral chains are sufficiently close to each other that one must assume bonds between T atoms of one chain with T atoms of a neighbouring chain. Thus one actually has a T metal framework which, together with the imbedded boron dumbbells, leaves free octagonal tubes which are occupied by infinite linear R–R chains parallel to [001]. The  $\text{R}_{1-c}\text{T}_c\text{B}_4$  structures discussed with 8850:  $\text{Sm}_{17}(\text{Fe}_4\text{B}_4)_{15}$  present a modification of the  $\text{NdCo}_4\text{B}_4$ -type where the translation period in the  $c$  direction of the R–R chain does not fully agree with the translation period of the transition metal framework (see fig. 65).

In the three other boride structures the T tetrahedra share no edges with other tetrahedra. There are no tetrahedral chains and no rare earth chains. These structures are discussed in detail with 8950:  $\text{CeCo}_4\text{B}_4$ .

8950	$\text{CeCo}_4\text{B}_4$ or $\text{CeCo}_4[\text{B}_2]_2$	tP18 $\text{P4}_2/\text{nmc}$	$a = 5.059$ $c = 7.063$	KuB, 72
------	--	----------------------------------	----------------------------	---------

#### Isotypic compounds:



\*Metastable.

\*\*Exists also with  $\text{LuRu}_4\text{B}_4$ -type.

†For studies on  $\text{R}(\text{Ir}_x\text{Rh}_{1-x})_4\text{B}_4$  compounds with R = Dy, Ho, Er having the  $\text{CeCo}_4\text{B}_4$ -type, see for example KuMB, 79 and KuA, 80. More references are found in JoB, 82.

‡Exists also with  $\text{LuRu}_4\text{B}_4$ - and  $\text{LuRh}_4\text{B}_4$ -type.

<sup>a)</sup>KuB 72    <sup>b)</sup>KuBCC, 81    <sup>c)</sup>KuBMSC, 79    <sup>d)</sup>VaM, 77    <sup>e)</sup>MyCK, 81    <sup>f)</sup>KuMB, 79  
<sup>g)</sup>YvG, 80    <sup>h)</sup>St, 79    <sup>i)</sup>Ch, 81

The  $\text{CeCo}_4\text{B}_4$  structure, shown in fig. 73, and all other boride structure types of the same composition:  $\text{LuRu}_4\text{B}_4$ ,  $\text{LuRh}_4\text{B}_4$  and  $\text{NdCo}_4\text{B}_4$ , are characterized by  $\text{B}_2$  dumbbells and transition metal tetrahedra. The  $\text{NdCo}_4\text{B}_4$  structure is the only structure where the tetrahedra, by sharing edges, form infinite tetrahedron chains, and this structure is discussed separately under its own heading. In the three structure types mentioned first the tetrahedra do not share edges or corners with other tetrahedra; however, the tetrahedra are so close together that bonding between T atoms of different tetrahedra must be assumed. Thus we find here a transition metal tetrahedral framework in the holes of which the  $\text{B}_2$  pairs and the R atoms are located.

*The three  $RT_4B_4$  structure types described as stacking variants*

The  $CeCo_4B_4$ ,  $LuRu_4B_4$  and  $LuRh_4B_4$  structures can be described from a geometrical point of view as stacking variants of a common structural slab, shown in fig. 72 in two different projections. The slab consists of  $T_4$  tetrahedra, R atoms and has near the interface "isolated" B atoms which, by stacking of the slabs, form dumbbells with "isolated" B atoms from the next slab. The slab has a thickness  $w$  and a two-dimensional translation period denoted in fig. 72 by  $u$  and  $v$ . The values of  $u$ ,  $v$  and  $w$  are related to the translation periods of the three structures as follows:

$$u = a'_1(CeCo_4B_4) = c(LuRh_4B_4) = a_2(LuRu_4B_4),$$

$$v = c(CeCo_4B_4) = a(LuRh_4B_4) = a_1(LuRu_4B_4),$$

$$w = \frac{1}{2}a'_2(CeCo_4B_4) = \frac{1}{6}b(LuRh_4B_4) = \frac{1}{4}c(LuRu_4B_4).$$

Note that in order to compare the tetragonal primitive  $CeCo_4B_4$  structure with the two other structures and in order to define the slab, a non-conventional unit cell has

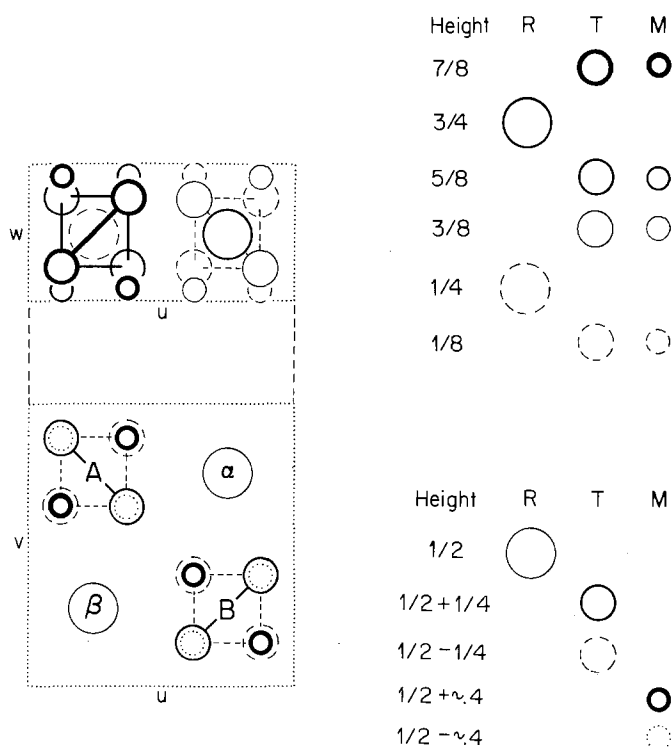
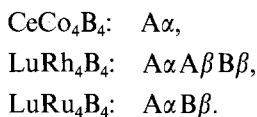


Fig. 72. Atom arrangement in the slab, common to the  $CeCo_4B_4$ ,  $LuRh_4B_4$  and  $LuRu_4B_4$  structures. Lower drawing: One repeat unit of the infinite slab, parallel to the plane of projection, with an indication of the four possible stacking positions. The values for the height of the atoms are normalized to the thickness of one slab. The middle of the slab is at height  $\frac{1}{2}$ . The B atoms at height  $\frac{1}{2} \pm \approx 0.4$  form dumbbells with boron atoms of slabs stacked above or below. Upper drawing: Projection of the same slab segment but perpendicular to the plane of projection. The height of the atoms refers to one slab repeat unit indicated in the drawing below.

to be used, which is a base-centred tetragonal cell with  $a' \approx \sqrt{2} a$ . The (010) plane of this cell is parallel with the slab.

The slab has four stacking positions denoted by A,  $\alpha$ , B and  $\beta$  (see fig. 72). Slabs can be stacked only in such a way that a Roman letter slab is followed by a Greek letter slab and vice versa. For the three structures, shown in fig. 73, the stacking sequence of the slabs is as follows:



The LuRh<sub>4</sub>B<sub>4</sub> structure thus has a stacking which is intermediate between the CeCo<sub>4</sub>B<sub>4</sub>- and LuRu<sub>4</sub>B<sub>4</sub>-type.

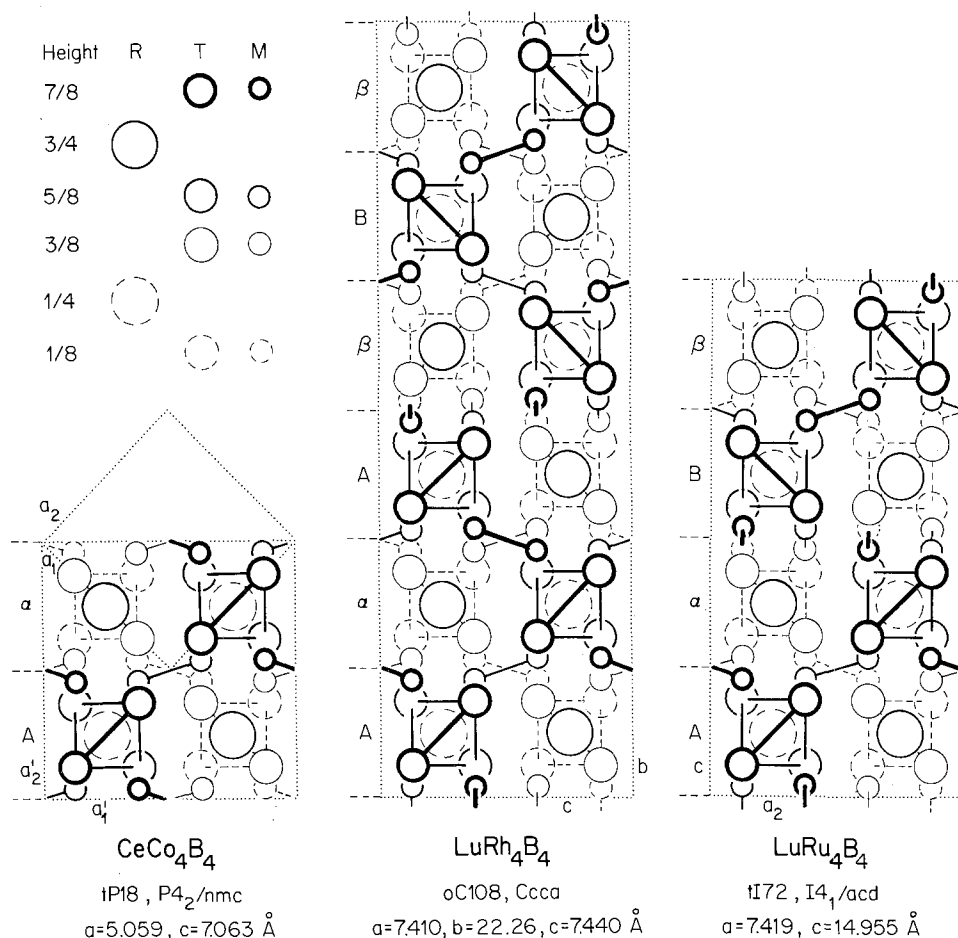


Fig. 73. Idealized versions of the crystal structures of CeCo<sub>4</sub>B<sub>4</sub>, LuRh<sub>4</sub>B<sub>4</sub> and LuRu<sub>4</sub>B<sub>4</sub>, which can be interpreted as stacking variations of a common structural slab. In the case of CeCo<sub>4</sub>B<sub>4</sub>, both the conventional primitive tetragonal unit cell ( $a_1$ ,  $a_2$ ) and the base-centred tetragonal unit cell ( $a'_1$ ,  $a'_2$ ) are indicated.

*The boron–boron linkage in ternary boride structures as a function of the metal:boron ratio*

Rogl and Nowotny (1978) have observed that the type of homonuclear linkage in borides can be correlated in simple form with the metal:boron ratio of the compound. All ternary rare earth–transition metal borides are listed in table 20, arranged according to decreasing metal:boron ratio, and the observed homonuclear linkage of the B atoms. One notes that if the ratio is larger than 1.75 only isolated B atoms occur. Boron dumbbells are found with values between 1.3 and 1.0. Two homonuclear bonds occur first with a metal to boron ratio of 1 and three

TABLE 20  
The boron–boron linkage in rare earth–transition metal borides, arranged according to decreasing metal:boron ratio.

Metal: boron ratio	Code	Boride	Pearson's classif. symbol	Space group	Type of boron linkage	Fig.
8.0	8313	Nd <sub>3</sub> Ni <sub>13</sub> B <sub>2</sub>	hP18	P6/mmm	B <sup>[+0]</sup>	37
5.0	7522	Dy <sub>3</sub> Ni <sub>7</sub> B <sub>2</sub>	hP24	P6 <sub>3</sub> /mmc	B <sup>[+0]</sup>	38
	8320	CeCo <sub>4</sub> B	hP12	P6/mmm	B <sup>[+0]</sup>	37
4.0	8025	LaPd <sub>3</sub> B	cP5	Pm3m	B <sup>[+0]</sup>	45
3.8	9322	Sc <sub>2</sub> Co <sub>21</sub> B <sub>6</sub>	cF116	Fm3m	B <sup>[+0]</sup>	—
3.5	7829	Ce <sub>2</sub> Co <sub>5</sub> B <sub>2</sub>	hP36	P6 <sub>3</sub> /mmc	B <sup>[+0]</sup>	38
	8327	Ce <sub>3</sub> Co <sub>11</sub> B <sub>4</sub>	hP18	P6/mmm	B <sup>[+0]</sup>	37
3.0	8330	Ce <sub>2</sub> Co <sub>7</sub> B <sub>3</sub>	hP24	P6/mmm	B <sup>[+0]</sup>	37
2.2	9533	EuNi <sub>12</sub> B <sub>6</sub>	hR57	R3m	B <sup>[+0]</sup>	82
2.0	8340	CeCo <sub>3</sub> B <sub>2</sub>	hP6	P6/mmm	B <sup>[+0]</sup>	37, 58
		ErIr <sub>3</sub> B <sub>2</sub>	mC12	C2/m	B <sup>[+0]</sup>	58
1.75	8244	Sc <sub>2</sub> Ru <sub>5</sub> B <sub>4</sub>	mP22	P2/m	B <sup>[+0]</sup> , [B <sub>2</sub> <sup>[+1]</sup> ]	75
1.5	8050	LaCo <sub>2</sub> B <sub>2</sub>	tI10	I4/mmm	B <sup>[+0]</sup>	50
1.28	8850	Sm <sub>17</sub> (Fe <sub>4</sub> B <sub>4</sub> ) <sub>15</sub>	tP274	P4 <sub>2</sub> /n	[B <sub>2</sub> <sup>[+1]</sup> ]	65
1.25	8950	NdCo <sub>4</sub> B <sub>4</sub>	tP18	P4 <sub>2</sub> /n	[B <sub>2</sub> <sup>[+1]</sup> ]	65, 71
		CeCo <sub>4</sub> B <sub>4</sub>	tP18	P4 <sub>2</sub> /nmc	[B <sub>2</sub> <sup>[+1]</sup> ]	73
		LuRu <sub>4</sub> B <sub>4</sub>	tI72	I4 <sub>1</sub> /acd	[B <sub>2</sub> <sup>[+1]</sup> ]	73
		LuRh <sub>4</sub> B <sub>4</sub>	oC108	Ccca	[B <sub>2</sub> <sup>[+1]</sup> ]	73
1.0	7567	LuRuB <sub>2</sub>	oP16	Pnma	[B <sub>2</sub> <sup>[+1]</sup> ]	43
	8857	ScIr <sub>3</sub> B <sub>4</sub>	hP16	P6 <sub>3</sub> /m	∞ B <sup>[+2]</sup> , B <sup>[+0]</sup>	66
0.71	8370	La <sub>2</sub> Re <sub>3</sub> B <sub>7</sub>	oP48	Pcca	∞ (2B <sup>[+1]</sup> , 1B <sup>[+2]</sup> , 4B <sup>[+3]</sup> )	84
0.57	7388	Y <sub>3</sub> ReB <sub>7</sub>	oC44	Cmcm	∞ (3B <sup>[+2]</sup> , 4B <sup>[+4]</sup> )	33
0.50	7886	Y <sub>2</sub> ReB <sub>6</sub>	oP36	Pbam	∞ B <sup>[+3]</sup>	47
	8380	YCrB <sub>4</sub>	oP24	Pbam	∞ B <sup>[+3]</sup>	48
	8975	CeCr <sub>2</sub> B <sub>6</sub>	oI18	Immm	2B <sup>[+3]</sup> , 4B <sup>[+(+2)]</sup>	75

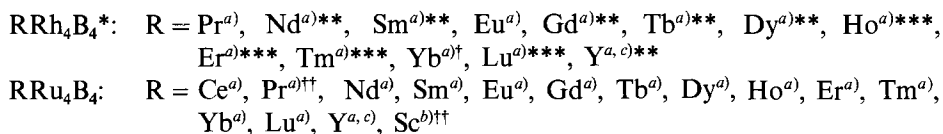
homonuclear bonds with a value of 0.71. It should be noted, that in contrast to the silicides and aluminides the ternary borides are always fully ordered, and a random occupation of structure sites by T and B atoms is unknown.

---

<b>8950</b>	<b>LuRu<sub>4</sub>B<sub>4</sub></b>	tI72	$a = 7.419$	Jo, 77
	or	I4 <sub>1</sub> /acd	$c = 14.955$	
	LuRu <sub>4</sub> [B <sub>2</sub> ] <sub>2</sub>			

---

Isotypic compounds:



\*RRh<sub>4</sub>B<sub>4</sub> compounds with LuRu<sub>4</sub>B<sub>4</sub>-type are stable at high temperatures only and in most cases change to the CeCo<sub>4</sub>B<sub>4</sub>-type at lower temperatures. In the case of YbRh<sub>4</sub>B<sub>4</sub> (see YvJ, 82) and YRh<sub>4</sub>B<sub>4</sub> (Jo, 77) it is possible to quench the LuRu<sub>4</sub>B<sub>4</sub>-type (but not as a single phase). In the other cases this type can be stabilized if Rh is replaced in small amounts by Ru (Jo, 77; YvG, 80).

\*\*Exists also with CeCo<sub>4</sub>B<sub>4</sub>-type.

\*\*\*Exists also with CeCo<sub>4</sub>B<sub>4</sub>- and LuRh<sub>4</sub>B<sub>4</sub>-type.

†Exists also with LuRh<sub>4</sub>B<sub>4</sub>-type.

††Metastable.

<sup>a)</sup>Jo, 77      <sup>b)</sup>KuJMBBR, 79      <sup>c)</sup>YvG, 80

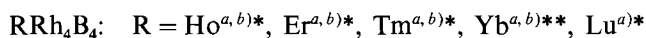
The LuRu<sub>4</sub>B<sub>4</sub> structure, shown in fig. 73, can be related to the 8950:CeCo<sub>4</sub>B<sub>4</sub> and 8950:LuRh<sub>4</sub>B<sub>4</sub> structures. All three structures can be built up by stacking of a common slab in different ways. For a discussion see CeCo<sub>4</sub>B<sub>4</sub>.

---

<b>8950</b>	<b>LuRh<sub>4</sub>B<sub>4</sub></b>	oC108	$a = 7.410$	YvJ, 82
	or	Ccca	$b = 22.26$	
	LuRh <sub>4</sub> [B <sub>2</sub> ] <sub>2</sub>		$c = 7.440$	

---

Isotypic compounds:



\*Exists also with CeCo<sub>4</sub>B<sub>4</sub>- and LuRu<sub>4</sub>B<sub>4</sub>-type. The LuRh<sub>4</sub>B<sub>4</sub>-type corresponds to the low temperature modification.

\*\*Exists also with LuRu<sub>4</sub>B<sub>4</sub>-type.

<sup>a)</sup>YvJ, 82      <sup>b)</sup>JoM, 79

The  $\text{LuRh}_4\text{B}_4$  structure, shown in fig. 73, is a stacking variant of the 8950: $\text{CeCo}_4\text{B}_4$  and the 8950: $\text{LuRu}_4\text{B}_4$  structures. It is discussed with  $\text{CeCo}_4\text{B}_4$ .

---

<b>89(59)</b>	$\text{Ce}_2\text{Mn}_7\text{Al}_{10}$ or $\text{Ce}_2\text{Mn}_3(\text{Mn}_{.67}\text{Al}_{.33})_6\text{Al}_6^{[6p]2}[A]_2$	hR57 $R\bar{3}m$	$a = 9.04$ $c = 13.17$	ZaK, 63
---------------	--	---------------------	---------------------------	---------

---

$\text{Th}_2\text{Zn}_{17}$ -type (MaV, 56; JoSW, 69) derivative with partial disorder of the Mn and Al atoms on one of the Zn sites

---

For isotypic compounds, see 8912: $\text{Ce}_2\text{Co}_{15}\text{Al}_2$ .

Besides 8912: $\text{Ce}_2\text{Co}_{15}\text{Al}_2$  the only other exact structure determination of a ternary  $\text{Th}_2\text{Zn}_{17}$ -type derivative was made on this compound. For a discussion of the structural features see 8912: $\text{Ce}_2\text{Ni}_{15}\text{Si}_2$  and fig. 68.

---

<b>8968</b>	$\text{Ho}_4\text{Ni}_{10}\text{Ga}_{21}$ * or $\text{Ho}_4\text{Ni}_8^{(2,4)p}\text{Ni}_2^{[6p]}\text{Ga}_{21}$	mC70 C2/m	$a = 20.802$ $b = 4.0736$ $c = 15.346$ $\beta = 125.80^\circ$	GrYG, 79b
-------------	--	--------------	--	-----------

---

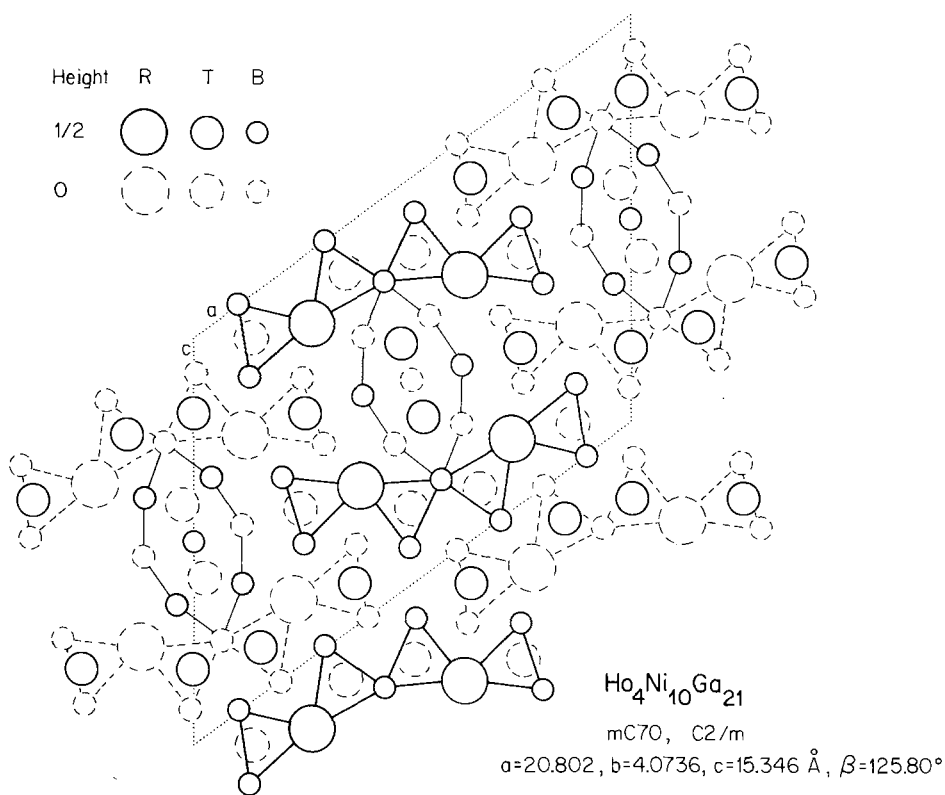
\*The  $x$  parameter for Ho(1) is misprinted. It should probably be 0.2376 instead of 0.2776.

Isotypic compounds: All references GrYG, 79b

$\text{R}_4\text{Ni}_{10}\text{Ga}_{21}$ : R = Tb, Dy, Ho, Er, Tm, Yb, Lu, Y

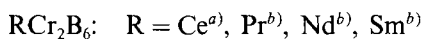
In the  $\text{Ho}_4\text{Ni}_{10}\text{Ga}_{21}$  structure, shown in fig. 74, all Ni atoms are in the centres of (deformed) trigonal prisms, formed either of two Ho and four Ga atoms or of six Ga atoms alone. The prisms are joined with neighbouring prisms by their triangular faces. The formation of columns of  $(\text{R}_2\text{M}_4)\text{T}$  prisms is common with aluminides and gallides with only small rare earth content. They occur for example in 7567: $\text{YNiAl}_2$  (fig. 59) and 8380: $\text{YNiAl}_4$  (fig. 59). For a more detailed discussion on the different kinds of prism columns see 8633: $\text{YRe}_4\text{Si}_2$ . In  $\text{Ho}_4\text{Ni}_{10}\text{Ga}_{21}$  every four  $(\text{Ho}_{2/2}\text{Ga}_{4/2})\text{Ni}$  columns share one or two of their column edges and thus create a column ribbon. The  $(\text{Ga}_{6/2})\text{Ni}$  columns form part of an atom arrangement found in 8360: $\text{PrNi}_2\text{Al}_3$  except that the rare earth atoms are substituted by Ga atoms.  $\text{PrNi}_2\text{Al}_3$  crystallizes in the 8340: $\text{CeCo}_3\text{B}_2$  structure (fig. 58), a  $\text{CaCu}_5$ -type derivative, but with T and M atoms interchanged. In this case the T, and not the M atoms, are positioned at the centres of the trigonal prisms.



Fig. 74. The crystal structure of  $\text{Ho}_4\text{Ni}_{10}\text{Ga}_{21}$ .

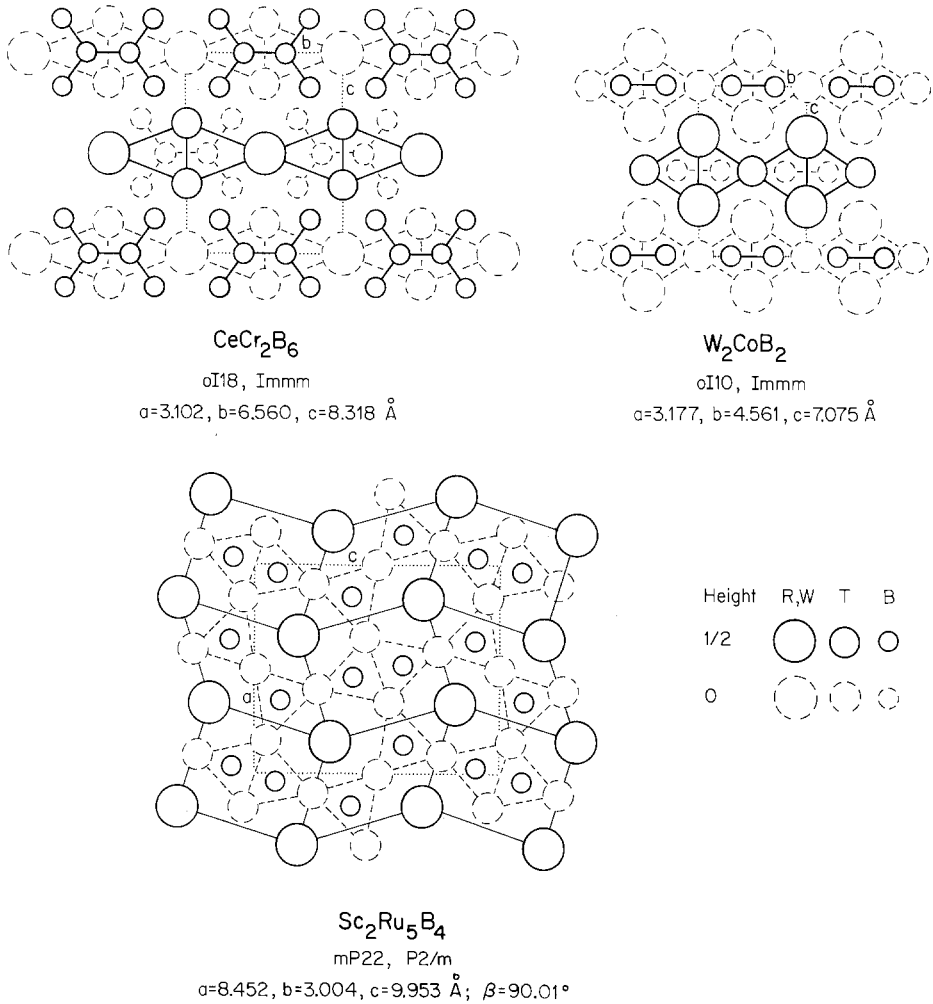
<b>8975</b>	<b>CeCr<sub>2</sub>B<sub>6</sub></b>	<b>oI18</b>	$a = 3.102$	<b>KuS, 73</b>
	or	<b>Immm</b>	$b = 6.560$	
	$\text{CeCr}_2\text{B}_2^{[(2,4)p+3]}\text{B}_4^{[+1(+2)]}$		$c = 8.318$	

Isotypic compounds:



<sup>a)</sup>KuS, 73      <sup>b)</sup>MiK, 75

The  $\text{CeCr}_2\text{B}_6$  structure, shown on the top left of fig. 75, can be considered as a filled-up version of the  $\text{W}_2\text{CoB}_2$ -type ( $\text{RiNB}$ , 66) or  $\text{Mo}_2\text{NiB}_2$ -type ( $\text{KuKS}$ , 66), presented on the top right of fig. 75. The rare earth atom sites correspond to the Co sites and the Cr sites to the W atom sites. Every six boron atoms are linked in a planar group parallel to the (100) plane. Each planar group is connected by longer B–B bonds to eight other planar groups, displaced by  $a/2$ . Thus every boron atom has in first approximation three homonuclear bonds.

Fig. 75. The crystal structures of CeCr<sub>2</sub>B<sub>6</sub>, W<sub>2</sub>CoB<sub>2</sub> and Sc<sub>2</sub>Ru<sub>5</sub>B<sub>4</sub>.

9170	ScRh <sub>3</sub> Si <sub>7</sub>	hR66	$a = 7.5056$	ChEP, 81
	or Sc <sup>[6,o]</sup> Rh <sub>3</sub> Si <sub>7</sub> <sup>[3p]</sup>	R $\bar{3}$ c	$c = 19.691$	

Isotopic compounds: All references ChEP, 81

RRh<sub>3</sub>Si<sub>7</sub>: R = Sc

RIr<sub>3</sub>Si<sub>7</sub>: R = Sc

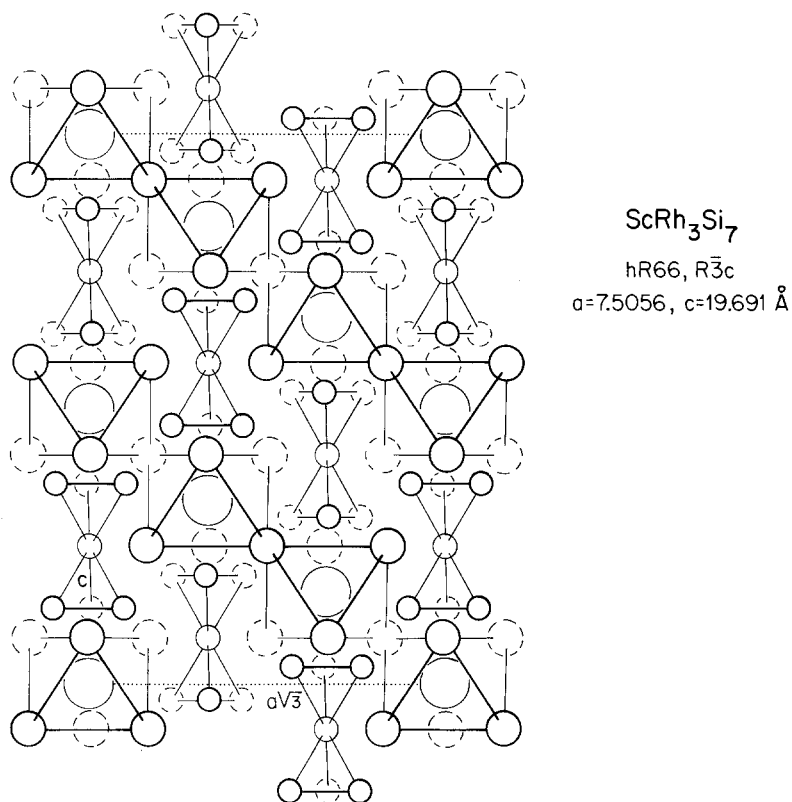


Fig. 76. A segment of the  $\text{ScRh}_3\text{Si}_7$  structure showing the arrangement of  $(\text{Rh}_6)\text{Sc}$  octahedra and  $(\text{Si}_7)$  double tetrahedra which are centred on the  $(11\bar{2}0)$  plane. Sc: large circles, Rh: medium circles, Si: small circles.

The rhombohedral  $\text{ScRh}_3\text{Si}_7$  structure is characterized by Sc-centred Rh octahedra and Si double tetrahedra. The arrangement of these polyhedra, centred on the  $(11\bar{2}0)$  plane, is shown in fig. 76. Every Si atom is in the centre of a Rh triangle. The structure is stabilized by strong T–M interactions. The contractions in the Rh–Si distances amount to 0.25 Å with respect to the sum of the metallic radii.

---

92(17)	$\text{YNi}_{10}\text{Si}_2$ or $\text{Y}^{[20]}\text{Ni}_8(\text{Ni}_5\text{Si}_5)_4$	tI26 I4/mmm	$a = 8.207$ $c = 4.677$	Ya, 78
--------	--	----------------	----------------------------	--------

---

$\text{CeMn}_4\text{Al}_8$ -type (ZaK, 63) with different atom occupation and partial disorder  $\equiv$   $\text{ThMn}_{12}$ -type (FeRS, 52) derivative

---

Isotypic compounds: All references Ya, 78

$RNi_{10}Si_2$ : R = Gd, Tb, Dy, Ho, Er, Tm, Yb, Lu, Y

The  $YNi_{10}Si_2$  structure with a  $ThMn_{12}$ -type derivative is discussed with  $9267:CeMn_4Al_8$ .

92(23)	$Ce_2Ni_{17}Si_5^*$	tI48	$a = 9.799^{**}$	BoG, 69a
	or $Ce^{[22]}Ni_8(Ni_{.5}Si_{.5})Si_2$	$I4_1/amd$	$c = 6.249$	

$BaCd_{11}$ -type (SaB, 53) derivative with partial disorder of the Ni and Si atoms on one of the Cd sites

\*Depending on the occupation of the mixed site by T or M atoms there are two hypothetical compositions for full order:  $9218:RT_8M_2$  and  $9227:RT_8M_3$ . However, ordering has not been verified experimentally.

\*\*Unit cell data for  $CeNi_{8.6}Si_{2.4}$ .

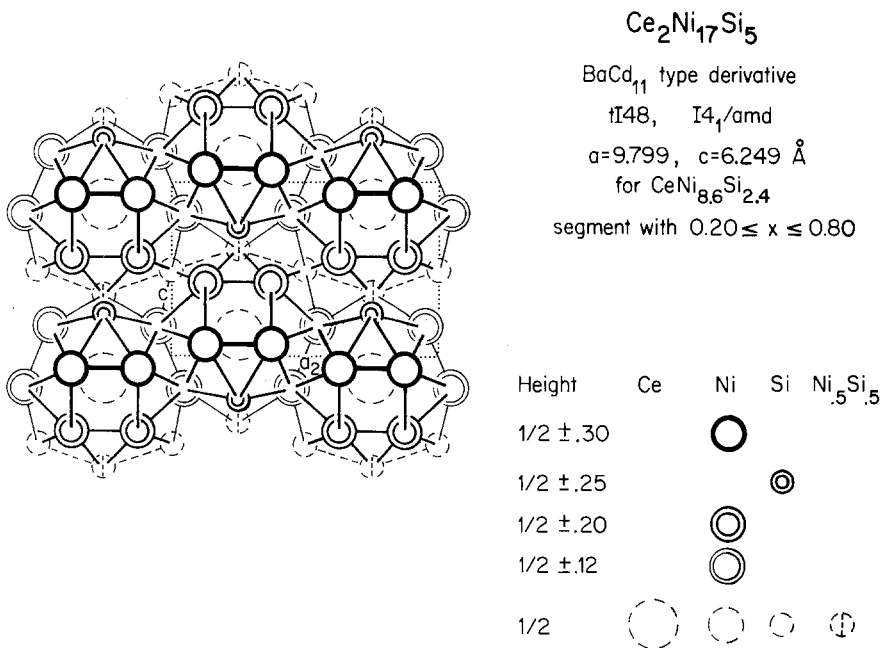
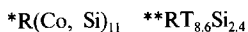
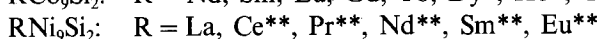
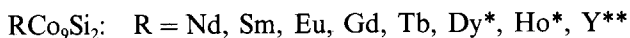


Fig. 77. A crystal structure segment ( $0.20 \leq x \leq 0.80$ ) of the  $Ce_2Ni_{17}Si_5$  structure with  $BaCd_{11}$ -type derivative.

Isotypic compounds: All references BoG, 69a



In the  $\text{Ce}_2\text{Ni}_{17}\text{Si}_5$  structure with BaCd<sub>11</sub>-type derivative the Ce atoms are arranged as the atoms in  $\beta$ -tin. Each Ce atom is surrounded by a polyhedron of 22 atoms, i.e. 16 Ni, 4 Si and 2 atoms which may be Ni or Si. The arrangement of the Ce-centred 22-atom polyhedra with their centres on the (200) plane is shown in fig. 77. An even larger rare-earth-centred coordination polyhedron with 24 atoms is found in 93(35): $\text{Ce}_2\text{Ni}_{17}\text{Si}_9$ , having a NaZn<sub>13</sub>-type derivative structure.

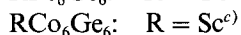
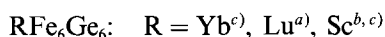
Another possible R(T, M)<sub>11</sub> structure, not yet found with R–T–M compounds, is the tetragonal U(Ni<sub>68</sub>Si<sub>1,32</sub>)<sub>11</sub> structure discussed with 9267:CeMn<sub>4</sub>Al<sub>8</sub>.

With composition 9250 need to be considered the HfFe<sub>6</sub>Ge<sub>6</sub>-type, hP13 (see ScFe<sub>6</sub>Ge<sub>6</sub>) with its two variants: YCo<sub>6</sub>Ge<sub>6</sub>, hP6<sup>1</sup>/<sub>2</sub> and ScNi<sub>6</sub>Ge<sub>6</sub>, hP52, and further the two types related to ThMn<sub>12</sub>:ScFe<sub>6</sub>Ga<sub>6</sub>, oI26 and partially disordered DyFe<sub>6</sub>Al<sub>6</sub>, tI26.

9250	ScFe <sub>6</sub> Ge <sub>6</sub>	hP13	$a = 5.069$	OIAY, 81
	or ScFe <sub>6</sub> <sup>[6o]</sup> Ge <sub>4</sub> <sup>[6p]</sup> <sub>2</sub> [Ge <sub>2</sub> ]	P6/mmm	$c = 8.077$	

HfFe<sub>6</sub>Ge<sub>6</sub>-type (OIAY, 81) or ZrCo<sub>6</sub>Ge<sub>6</sub>-type (BuS, 81)

Isotypic compounds:



<sup>a</sup>ChP, 83

<sup>b</sup>OIAY, 81

<sup>c</sup>BuS, 81

The ScFe<sub>6</sub>Ge<sub>6</sub> structure with HfFe<sub>6</sub>Ge<sub>6</sub>-type is shown in fig. 78a. It can be considered as an intergrowth of two slabs. One has the atom arrangement of the 8340:CeCo<sub>3</sub>B<sub>2</sub> structure, a CaCu<sub>5</sub>-type derivative. A corresponding projection of the CeCo<sub>3</sub>B<sub>2</sub> structure along the [11 $\bar{2}$ 0] direction is shown in fig. 37. The second slab has the composition T<sub>6,2</sub>M<sub>4</sub> = T<sub>3</sub>M<sub>4</sub> and has atom sites as found in the Zr<sub>4</sub>Al<sub>3</sub>-type (see fig. 80). Segments with Zr<sub>4</sub>Al<sub>3</sub>-type and segments with CoCo<sub>3</sub>B<sub>2</sub>- or CaCu<sub>5</sub>-type intergrown in a different way lead to the Th<sub>2</sub>Ni<sub>17</sub> and Th<sub>2</sub>Zn<sub>17</sub> structures and their derivative structures. For a detailed discussion see 8912:Ce<sub>2</sub>Ni<sub>15</sub>Si<sub>2</sub>.

One should note that all Fe atoms are in the centres of Ge octahedra, which form a framework. This framework can be obtained from the structure of ZrMnSi<sub>2</sub> (fig. 32) by the condensation of the octahedron slabs.

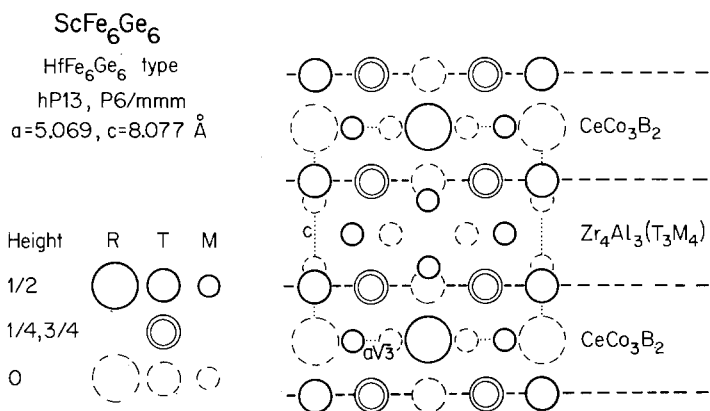


Fig. 78a. Structure of ScFe<sub>6</sub>Ge<sub>6</sub> with HfFe<sub>6</sub>Ge<sub>6</sub>-type (projection along [11 $\bar{2}$ 0]).

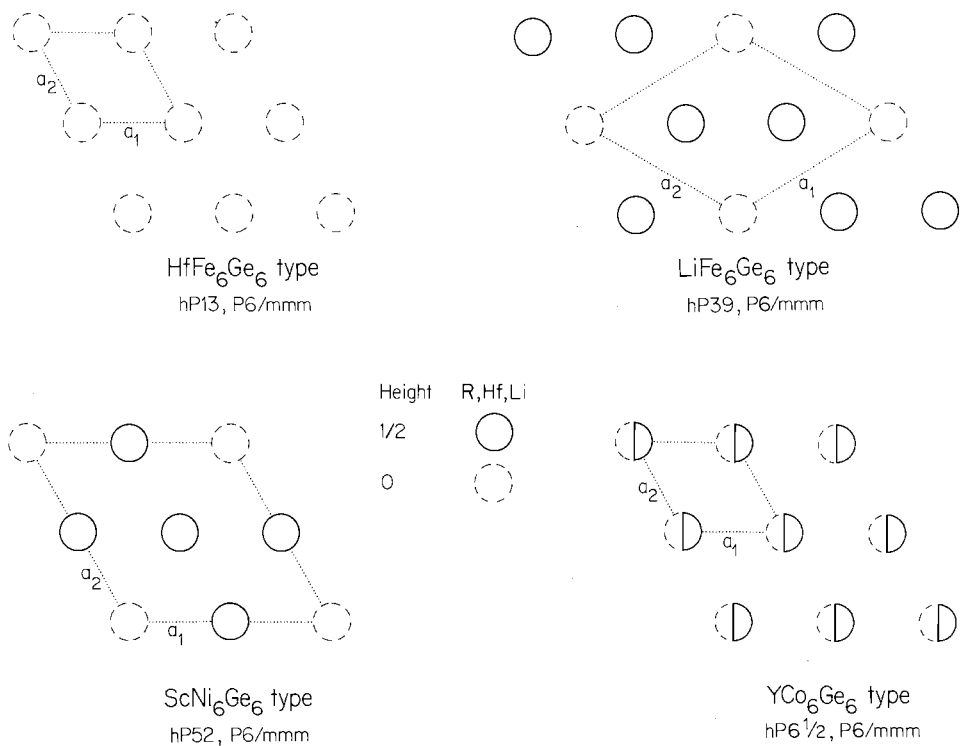


Fig. 78b. R(Hf or Li) atom arrangement in the HfFe<sub>6</sub>Ge<sub>6</sub>-type and its variants in a projection along [0001] (after Buchholz and Schuster, 1981). LiFe<sub>6</sub>Ge<sub>6</sub> and ScNi<sub>6</sub>Ge<sub>6</sub> have the same *c* translation as HfFe<sub>6</sub>Ge<sub>6</sub>. However, in YCo<sub>6</sub>Ge<sub>6</sub> the random distribution of the R atoms on the available sites leads to a unit cell of half the height with only 6½ atoms per unit cell.

*Variants of the HfFe<sub>6</sub>Ge<sub>6</sub>-type*

The two intergrown slabs which build up the HfFe<sub>6</sub>Ge<sub>6</sub>-type are not too different. All T sites and the larger part of the M sites are identical. However, the R atoms in the CeCo<sub>3</sub>B<sub>2</sub>-type slabs are replaced by M<sub>2</sub> dumbbells in the Zr<sub>4</sub>Al<sub>3</sub>-type slabs. Variants of the HfFe<sub>6</sub>Ge<sub>6</sub>-type are obtained if the R atoms and M<sub>2</sub> dumbbells are partially interchanged. Two ordered variants are known: the LiFe<sub>6</sub>Ge<sub>6</sub>-type [hP39, P6/mmm,  $a = \sqrt{3} a(\text{HfFe}_6\text{Ge}_6)$ ,  $c = c(\text{HfFe}_6\text{Ge}_6)$ ], determined by Welk and Schuster (1976) (not yet found with R-T-M compounds), and the ScNi<sub>6</sub>Ge<sub>6</sub>-type [hP52, P6/mmm,  $a = 2a(\text{HfFe}_6\text{Ge}_6)$ ,  $c = c(\text{HfFe}_6\text{Ge}_6)$ ], reported by Buchholz and Schuster (1981). These variants can be compared with the HfFe<sub>6</sub>Ge<sub>6</sub>-type in a simplified way (as shown in fig. 78b) by indicating only the positions and the height of the R atoms in a projection along [0001]. Half a translation unit above the R atom the M<sub>2</sub> dumbbell is always found, all other atoms being identical to the atoms in the HfFe<sub>6</sub>Ge<sub>6</sub> type. The fourth drawing in fig. 78b corresponds to the so-called YCo<sub>6</sub>Ge<sub>6</sub>-type [hP6 $\frac{1}{2}$ , P6/mmm,  $a = a(\text{HfFe}_6\text{Ge}_6)$  but  $c = \frac{1}{2}c(\text{HfFe}_6\text{Ge}_6)$ ], a HfFe<sub>6</sub>Ge<sub>6</sub>-type variant with R atoms and M<sub>2</sub> dumbbells arranged at random on the possible structure sites.

---

9250	YCo <sub>6</sub> Ge <sub>6</sub>	hP6 $\frac{1}{2}$	$a = 5.074$	BuS, 81
		P6/mmm	$c = 3.908$	

---

YCo<sub>6</sub>Ge<sub>6</sub>-type

Isotypic compounds: All determined by BuS, 81

RCo<sub>6</sub>Ge<sub>6</sub>: R = Gd, Tb, Dy, Ho, Er, Tm, Yb, Lu, Y

The YCo<sub>6</sub>Ge<sub>6</sub> structure, which is a partially disordered HfFe<sub>6</sub>Ge<sub>6</sub>-type structure, is discussed with 9250:ScFe<sub>6</sub>Ge<sub>6</sub>.

---

9250	ScNi <sub>6</sub> Ge <sub>6</sub>	hP52	$a = 10.152$	BuS, 81
		P6/mmm	$c = 7.813$	

---

ScNi<sub>6</sub>Ge<sub>6</sub>-type

No isotypic RT<sub>6</sub>M<sub>6</sub> compounds are known.

The ScNi<sub>6</sub>Ge<sub>6</sub> structure, for which the Sc atom arrangement is shown in fig. 78b, is a HfFe<sub>6</sub>Ge<sub>6</sub>-type variant, which is discussed with 9250:ScFe<sub>6</sub>Ge<sub>6</sub>.

9250	ScFe <sub>6</sub> Ga <sub>6</sub>	oI26	<i>a</i> = 5.009	BeM, 82a
		Immm	<i>b</i> = 8.431	
			<i>c</i> = 8.613	

ThMn<sub>12</sub>-type (FIRS, 52) derivative

ScFe<sub>6</sub>Ga<sub>6</sub> is the only representative known; however, it is probable that some of the compounds listed under 92(50):DyFe<sub>6</sub>Al<sub>6</sub> actually crystallize with this ordered structure type.

The orthorhombic pseudotetragonal ScFe<sub>6</sub>Ga<sub>6</sub> structure, a fully ordered ternary ThMn<sub>12</sub>-type derivative, has an atom arrangement similar to the tetragonal 92(50):DyFe<sub>6</sub>Al<sub>6</sub> structure shown on the left-hand side of fig. 79. However, all former mixed sites at  $x = 0$  and  $x = \frac{1}{2}$  are occupied by Fe atoms only and the remaining mixed sites by Ga atoms only. For a more detailed discussion see 9267:CeMn<sub>4</sub>Al<sub>8</sub>.

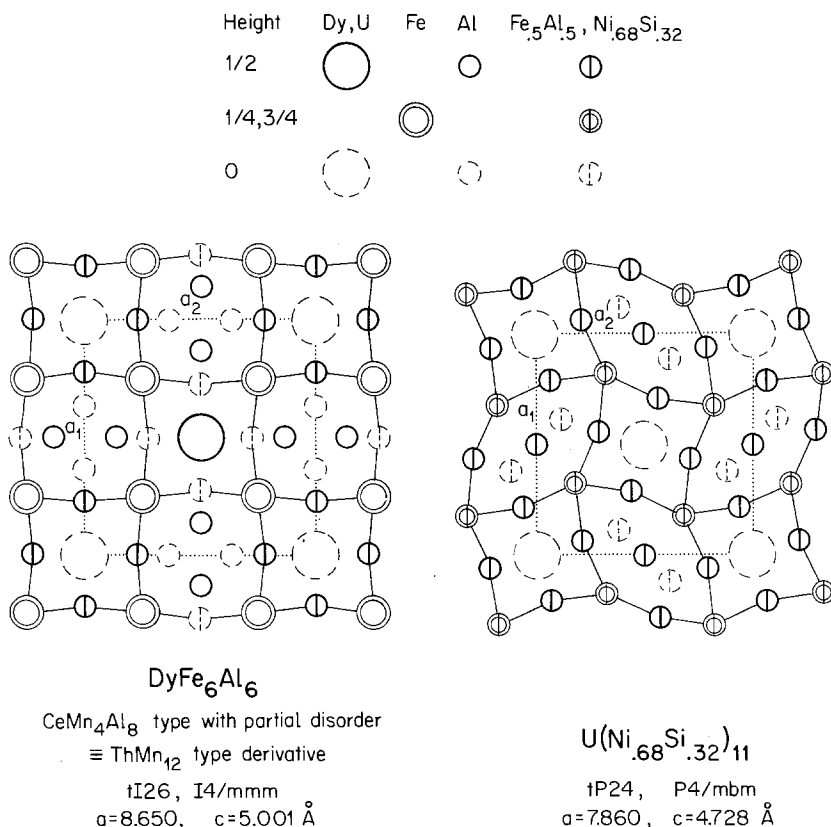


Fig. 79. The DyFe<sub>6</sub>Al<sub>6</sub> structure with partially disordered CeMn<sub>4</sub>Al<sub>8</sub>-type and the U(Ni<sub>.68</sub>Si<sub>.32</sub>)<sub>11</sub> structure, both constructed from segments of the Zr<sub>4</sub>Al<sub>3</sub>- and the CeMg<sub>2</sub>Si<sub>2</sub>-type.



---

<b>92(50)</b>	<b>DyFe<sub>6</sub>Al<sub>6</sub></b>	tI26	$a = 8.650$	Fe, 80
	or	I4/mmm	$c = 5.001$	
	Dy <sup>[20]</sup> Fe <sub>4</sub> (Fe <sub>2</sub> Al <sub>2</sub> ) <sub>4</sub> Al <sub>4</sub>			

---

CeMn<sub>4</sub>Al<sub>8</sub>-type (ZaK, 63) with partial disorder of Fe and Al atoms on one Al site  $\equiv$  ThMn<sub>12</sub>-type (FIRS, 52) derivative

---

Isotypic compounds:

RCr <sub>6</sub> Al <sub>6</sub> :	R = Gd <sup>a</sup> , Dy <sup>a</sup> , Er <sup>a</sup> , Tm <sup>a</sup> , Lu <sup>a</sup>
RMn <sub>6</sub> Al <sub>6</sub> :	R = Gd <sup>a</sup> , Tb <sup>a</sup> , Dy <sup>a</sup> , Ho <sup>a</sup> , Er <sup>a</sup> , Tm <sup>a</sup> , Yb <sup>a</sup> , Lu <sup>a</sup> , Y <sup>a</sup>
RFe <sub>6</sub> Al <sub>6</sub> :	R = Pr <sup>a</sup> , Eu <sup>a</sup> , Gd <sup>a</sup> , Tb <sup>a</sup> , Dy <sup>a</sup> , Ho <sup>a</sup> , Er <sup>a</sup> , Tm <sup>a</sup> , Yb <sup>a</sup> , Y <sup>a</sup> , Sc <sup>b</sup> *)
RRh <sub>6</sub> Al <sub>6</sub> :	R = Gd <sup>c</sup>
R(Fe, Ga) <sub>12</sub> :	R = Ce <sup>e</sup> , Pr <sup>e</sup> , Nd <sup>e</sup> , Sm <sup>e</sup> , Gd <sup>e</sup> , Tb <sup>e</sup> , Dy <sup>e</sup> , Ho <sup>e</sup> , Er <sup>e</sup> , Tm <sup>e</sup> , Yb <sup>e</sup> , Y <sup>e</sup> , Sc <sup>d,f</sup> **)
R(Co, Ga) <sub>12</sub> :	R = Sc <sup>f</sup>

\*No indications on the atom site occupation are given.

\*\*According to BeM, 82a ScFe<sub>6</sub>Ga<sub>6</sub> crystallizes with an orthorhombic fully ordered variant of the ThMn<sub>12</sub> structure (see 9250:ScFe<sub>6</sub>Ga<sub>6</sub>).

<sup>a</sup>)Fe, 80    <sup>b</sup>)MaB, 69    <sup>c</sup>)FeSN, 81    <sup>d</sup>)GrM, 78    <sup>e</sup>)GrGLGY, 83    <sup>f</sup>)BeM, 82a

The DyFe<sub>6</sub>Al<sub>6</sub> structure, shown on the left-hand side of fig. 79, crystallizes in the CeMn<sub>4</sub>Al<sub>8</sub>-type with partial disorder of Fe and Al atoms on certain structure sites common to the Zr<sub>4</sub>Al<sub>3</sub>- and the CeMg<sub>2</sub>Si<sub>2</sub>-type columns. It is probable that some of the compounds listed as isotypic have only pseudotetragonal symmetry and crystallize with the ordered 9250:ScFe<sub>6</sub>Ga<sub>6</sub>-type. For a more detailed discussion see 9267:CeMn<sub>4</sub>Al<sub>8</sub>.

---

<b>9267</b>	<b>CeMn<sub>4</sub>Al<sub>8</sub></b>	tI26	$a = 8.89$	ZaK, 63
	or	I4/mmm	$c = 5.17$	
	Ce <sup>[20]</sup> Mn <sub>4</sub> Al <sub>8</sub>			

---

ThMn<sub>12</sub>-type (FIRS, 52) derivative

---

Isotypic compounds:

RCr <sub>4</sub> Al <sub>8</sub> :	R = La <sup>a,b</sup> , Ce <sup>a,b,c</sup> , Pr <sup>a,b</sup> , Nd <sup>b</sup> , Sm <sup>b</sup> , Gd <sup>a,b</sup> , Tb <sup>b</sup> , Dy <sup>b</sup> , Ho <sup>b</sup> , Er <sup>a,b</sup> , Tm <sup>b</sup> , Yb <sup>a,b</sup> , Lu <sup>b</sup> , Y <sup>a,b,d</sup>
RMn <sub>4</sub> Al <sub>8</sub> :	R = La <sup>a,b</sup> , Ce <sup>a,b</sup> , Pr <sup>a,b</sup> , Nd <sup>b</sup> , Sm <sup>b</sup> , Eu <sup>b</sup> , Gd <sup>a,b</sup> , Tb <sup>b</sup> , Dy <sup>b</sup> , Ho <sup>b</sup> , Er <sup>a,b</sup> , Tm <sup>b</sup> , Yb <sup>a,b</sup> , Lu <sup>b</sup> , Y <sup>a,b,d</sup>
RFe <sub>4</sub> Al <sub>8</sub> :	R = La <sup>a,h</sup> , Ce <sup>a,e,h</sup> , Pr <sup>a,h</sup> , Nd <sup>a,g,h</sup> , Sm <sup>a,h</sup> , Eu <sup>h</sup> , Gd <sup>a,h</sup> , Tb <sup>a,h</sup> , Dy <sup>a,h</sup> , Ho <sup>a,h</sup> , Er <sup>e,h</sup> , Tm <sup>a,h</sup> , Yb <sup>h</sup> , Lu <sup>a,h</sup> , Y <sup>a,d,h</sup> , Sc <sup>f</sup>

<sup>a</sup>)BuVV, 76    <sup>b</sup>)FeN, 79    <sup>c</sup>)ZaR, 74    <sup>d</sup>)Za, 66    <sup>e</sup>)ZaK, 63    <sup>f</sup>)ZaVR, 70    <sup>g</sup>)ViZR, 70    <sup>h</sup>)FeN, 78

The  $\text{CeMn}_4\text{Al}_8$  structure is one of the two fully ordered  $\text{ThMn}_{12}$ -type derivatives.  $\text{ThMn}_{12}$ -type derivative structures are found with aluminides, gallides and silicides, which, however, have different site occupations and different compositions. There are four structure sites in the  $\text{ThMn}_{12}$  structure which are occupied in the three tetragonal and the one pseudotetragonal orthorhombic  $\text{ThMn}_{12}$ -type derivative structures as follows:

	Equipoints of space group I4/mmm			
	2(a) 000	8(f) $\frac{111}{444}$	8(j) $x_2^10$	8(i) $x00$
92(17): $\text{YNi}_{10}\text{Si}_2$	2 Y	8 Ni	8 Ni	8(Ni <sub>5</sub> Si <sub>5</sub> )
92(50): $\text{DyFe}_6\text{Al}_6$	2 Dy	8 Fe	8(Fe <sub>5</sub> Al <sub>5</sub> )	8 Al
9267: $\text{CeMn}_4\text{Al}_8$	2 Ce	8 Mn	8 Al	8 Al
9250: $\text{ScFe}_6\text{Ga}_6$	2 Sc	8 Fe	4 Fe + 4 Ga	4 Ga + 4 Ga

The  $\text{DyFe}_6\text{Al}_6$  structure is shown on the left-hand side of fig. 79. In the  $\text{CeMn}_4\text{Al}_8$  structure the mixed sites are occupied by Al atoms only. In the silicide, however, all mixed sites in  $\text{DyFe}_6\text{Al}_6$  are occupied by Ni atoms and the Al sites by a mixture of Ni and Si atoms. In the ordered orthorhombic  $\text{ScFe}_6\text{Ga}_6$  structure, the former Wyckoff sets 8(j) and 8(i) are both split into two independent Wyckoff sets of multiplicity 4, which permits an ordered arrangement of Fe and Ga atoms on sites which are mixed in tetragonal structures.

The  $\text{CeMn}_4\text{Al}_8$  structure can be interpreted as an intergrowth of two columns, one with  $\text{CeMg}_2\text{Si}_2$ -type and the other with  $\text{Zr}_4\text{Al}_3$ -type.

The  $\text{CeMg}_2\text{Si}_2$  structure (ZmG, 71), shown on the right-hand side of fig. 80, can be regarded as intergrown slabs of silicon-centred tetragonal antiprisms ( $\text{Ce}_4\text{Mg}_4$ )Si with the slab normal parallel to *c*. A comparison of fig. 80 with fig. 50 makes it evident that the  $\text{CeMg}_2\text{Si}_2$  structure can be considered as a stacking variant of the  $\text{ThCr}_2\text{Si}_2$ -type (see 8050: $\text{CeNi}_2\text{Si}_2$ ). The intergrown  $\text{CeMg}_2\text{Si}_2$ -type segments in the R-T-M structures always have an R atom on the Ce sites. In ordered ternary aluminides the Si sites are occupied by T atoms and the Mg sites by Al atoms.

The  $\text{Zr}_4\text{Al}_3$  structure (WiTS, 60), shown on the left-hand side of fig. 80, has been postulated by Frank and Kasper (1958, 1959) on the basis of sphere-packing considerations. It represents a modification of the  $\text{CaCu}_5$  structure (see fig. 35) where the Ca atom has been replaced by a pair of atoms. In the ternary R-T-M structures the intergrown  $\text{Zr}_4\text{Al}_3$  segment never has a rare earth element. It occurs with T atoms on Al and M atoms on Zr sites in 9250: $\text{ScFe}_6\text{Ge}_6$ . In  $\text{CeMn}_4\text{Al}_8$  the corners of the  $\text{Zr}_4\text{Al}_3$ -type columns are occupied by T elements and all other sites by Al atoms.

There are two structures which can be considered as an intergrowth of  $\text{CeMg}_2\text{Si}_2$ -type and  $\text{Zr}_4\text{Al}_3$ -type columns: the  $\text{CeMn}_4\text{Al}_8$  structure (type shown on the left-hand side of fig. 79) and the tetragonal  $\text{U}(\text{Ni}_{.68}\text{Si}_{.32})_{11}$  structure (KaAYBG, 76), shown on the right-hand side of fig. 79. The column axis of the  $\text{CeMg}_2\text{Si}_2$ -type column always corresponds to the [001] direction of the  $\text{CeMg}_2\text{Si}_2$  cell. The column axis of the  $\text{Zr}_4\text{Al}_3$ -type column is, however, the [11 $\bar{2}$ 0] direction of the  $\text{Zr}_4\text{Al}_3$  cell in the  $\text{CeMn}_4\text{Al}_8$  structure but the [0001] direction in  $\text{U}(\text{Ni}_{.68}\text{Si}_{.32})_{11}$ .  $\text{Zr}_4\text{Al}_3$  type segments

TABLE 21  
The different intergrowth structures containing  $Zr_4Al_3$ -type and/or  $CeMg_2Si_2$ -type segments.

Code	Compound	Ternary structure type	Related binary structure type	Pearson's classif. symbol	Space group	Orientation of intergrown structure segments*			Fig.
						$Zr_4Al_3$ segment (fig. 80)	$CaCu_5$ (or $CeCo_3B_2$ ) segment (figs. 35, 37, 58)	$CeMg_2Si_2$ segment (fig. 80)	
<b>Structures of intergrown columns</b>									
8667	$YbMo_2Al_4$	$YbMo_2Al_4$	—	tI14	I4/mmm	—	—	[001]	63
(92(32))	$U(Ni_{.68}Si_{.32})_{11}$	$U(Ni_{.68}Si_{.32})_{11}$	—	tP24	P4/mbm	[0001]	—	[001]	79
9250	$ScFe_6Ga_6$	$ScFe_6Ga_6$	$ThMn_{12}$	oI26	Immm	[1120]	—	[001]	(79)
9267	$CeMn_4Al_8$	$CeMn_4Al_8$	$ThMn_{12}$	tI26	I4/mmm	[1120]	—	[001]	(79)
<b>Structures of intergrown slabs</b>									
8912	$Ce_2Ni_{15}Si_2$	$Ce_2Ni_{15}Si_2$	$Th_2Ni_{17}$	hP38	$P6_3/mmc$	[0001]**	[0001]**	—	68
8912	$Ce_2Co_{15}Al_2$	$Ce_2Co_{15}Al_2$	$Th_2Zn_{17}$	hR57	$R\bar{3}m$	[0001]**	[0001]**	—	68
9250	$ScFe_6Ge_6$	$HfFe_6Ge_6$	—	hP13	$P6/mmm$	[0001]	[0001]	—	78

\*The direction is indicated here, referred to the unit cell of the structure defining the structure segment, which coincides with the column axis or the slab normal of the intergrown structures.

\*\*One kind of slab only, which is built up of intergrown  $Zr_4Al_3$ - and  $CaCu_5$ - (or  $CeCo_3B_2$ -)type blocks in the ratio 1:2.

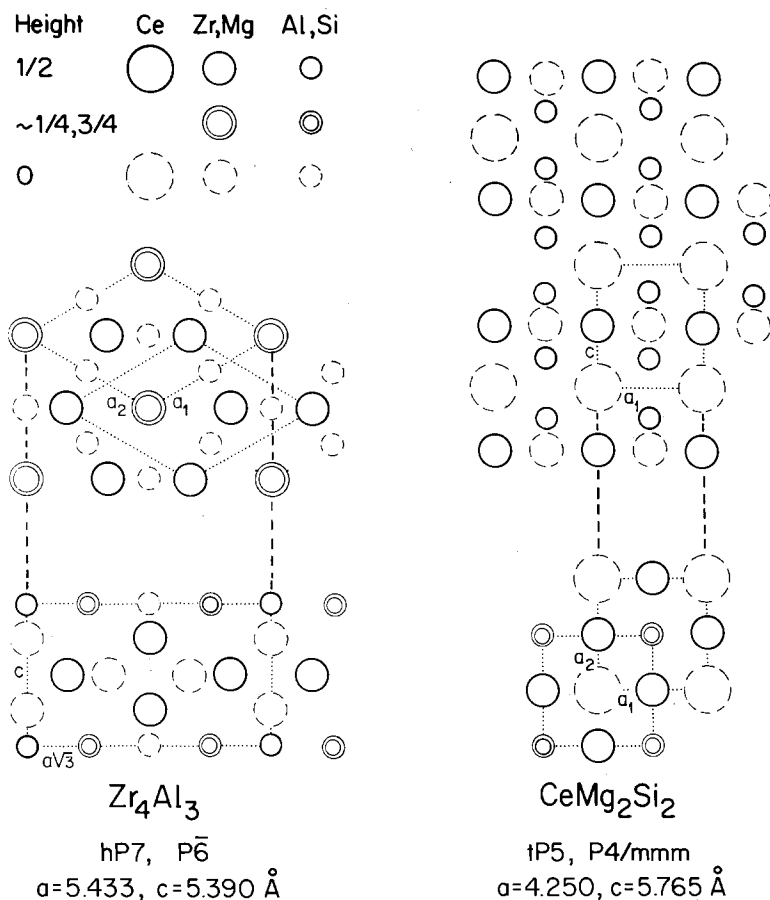


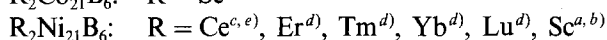
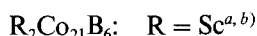
Fig. 80. The Zr<sub>4</sub>Al<sub>3</sub> and CeMg<sub>2</sub>Si<sub>2</sub> structures. Segments of these two structures (with different atom occupations on the given sites) occur as intergrowth blocks in different ternary R-T-M structures. The upper part shows the Zr<sub>4</sub>Al<sub>3</sub> structure in a projection along [0001], the lower along [1120]. The CeMg<sub>2</sub>Si<sub>2</sub> structure is presented in projection along [010] in the upper part and along [001] in the lower part. Note that in CeMg<sub>2</sub>Si<sub>2</sub> the *z* parameter of the Si atoms is  $\pm 0.226$ .

can also be intergrown with CaCu<sub>5</sub> (or CeCo<sub>3</sub>B<sub>2</sub>)-type segments. The different kinds of intergrowth structures containing Zr<sub>4</sub>Al<sub>3</sub>-type segments and/or CeMg<sub>2</sub>Si<sub>2</sub>-type segments are listed in table 21.

9322	Sc <sub>2</sub> Co <sub>21</sub> B <sub>6</sub>	cF116 Fm3m	$a = 10.54$	GaNb, 66 KuV, 67
------	---	---------------	-------------	---------------------

W<sub>2</sub>Cr<sub>21</sub>C<sub>6</sub>-type (WeP, 25)  $\equiv$  Cr<sub>23</sub>C<sub>6</sub>-type (BoASN, 72) derivative

Isotypic compounds:



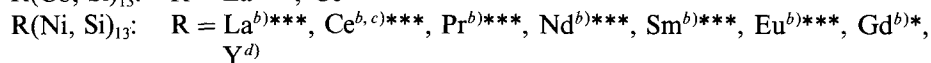
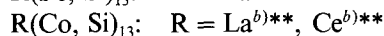
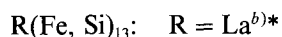
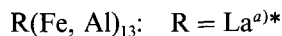
The  $Sc_2Co_{21}B_6$  structure with  $Cr_{23}C_6$ -type derivative belongs to the cubic structures with large unit cells, which are conveniently described with nested polyhedral units and which are treated here with 7325:  $Ce_3Ni_6Si_2$ .

93(35)	$Ce_2Ni_{17}Si_9$	tI56	$a = 7.857$	Bo, 79
	or	I4/mcm	$c = 11.503$	
	$Ce_2^{[24]}Ni_{16}(Ni_5Si_5)_2Si_8$			

NaZn<sub>13</sub>-type (ZiH, 38) derivative

Isotypic compounds:

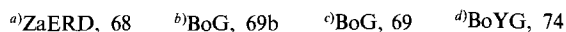
The only complete structure determination was made on  $Ce_2Ni_{17}Si_9$ . For all others the order of the T and M atoms needs to be investigated. For studies of the large homogeneity ranges, see BoG, 69b.



\*Cubic NaZn<sub>13</sub>-type [cF112, Fm3c with  $a_{cubic} \approx c(Ce_2Ni_{17}Si_9)$ ].

\*\*Tetragonal  $Ce_2Ni_{17}Si_9$ -type,  $c/a \approx \sqrt{2}$ .

\*\*\*NaZn<sub>13</sub>- and  $Ce_2Ni_{17}Si_9$ -type.



The body-centred tetragonal  $Ce_2Ni_{17}Si_9$  structure, for which a segment with  $-\frac{1}{4} \leq z \leq \frac{1}{4}$  is shown in fig. 81, is a ternary derivative of the face-centred cubic NaZn<sub>13</sub>-type (cF112, Fm3c) with  $a(Ce_2Ni_{17}Si_9) \approx \frac{1}{2}\sqrt{2}a(NaZn_{13})$ ,  $c(Ce_2Ni_{17}Si_9) \approx a(NaZn_{13})$ ,  $c/a \approx \sqrt{2}$  and  $V(Ce_2Ni_{17}Si_9) \approx \frac{1}{2}V(NaZn_{13})$ . Some of the R(T, M)<sub>13</sub> phases have been given in the literature with the small tetragonal cell, some with the larger cubic NaZn<sub>13</sub> cell, some have been listed as a tetragonal deformation of the cubic NaZn<sub>13</sub> cell ( $c/a \approx 1$ ). This is crystallographically incorrect, since a face-centred tetragonal cell must be transformed into the smaller body-centred tetragonal cell with  $c/a \approx \sqrt{2}$ . Referring to the correct description with the body-centred tetragonal unit

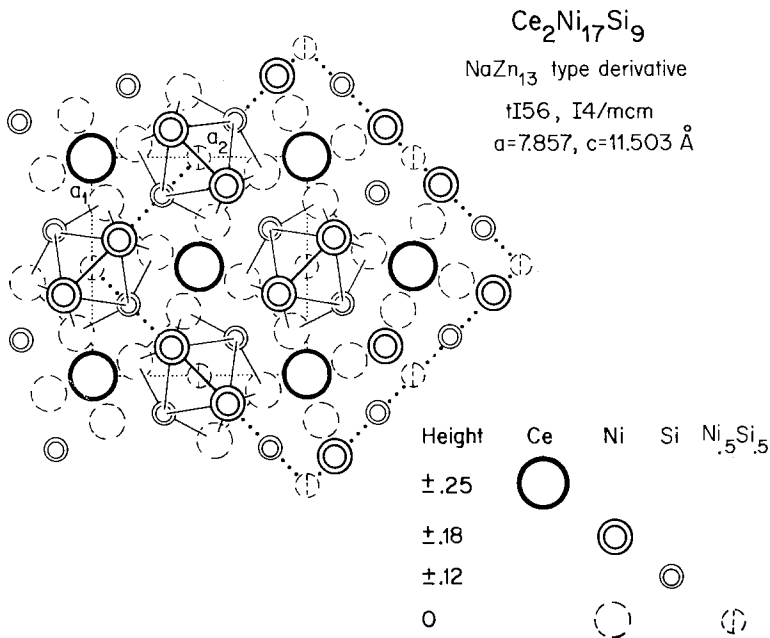
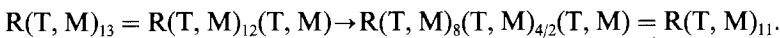


Fig. 81. A crystal structure segment with  $-\frac{1}{4} \leq z \leq +\frac{1}{4}$  of the tetragonal body-centred  $\text{Ce}_2\text{Ni}_{17}\text{Si}_9$  structure, a  $\text{NaZn}_{13}$ -type derivative. The base of the face-centred cubic  $\text{NaZn}_{13}$  cell has an area twice as large and is rotated with respect to the base of the  $\text{Ce}_2\text{Ni}_{17}\text{Si}_9$  cell by  $45^\circ$ .

cell, it appears that some  $\text{R}(\text{T}, \text{M})_{13}$  phases, depending on the T/M ratio, have domains where  $c/a \leq \sqrt{2}$  ( $\Omega_1$  phases) and other domains where  $c/a > \sqrt{2}$  ( $\Omega_2$  phases). The ordered  $\text{Ce}_2\text{Ni}_{17}\text{Si}_9$ -type is found with  $c/a = 1.466$  ( $\Omega'$  phases). For details see Bodak and Gladyshevskii (1969b).

A characteristic feature of the  $\text{Ce}_2\text{Ni}_{17}\text{Si}_9$  (or  $\text{NaZn}_{13}$ ) structure is the large coordination polyhedron of 24 atoms around the R atom. In fig. 81, however, thin lines have been used to emphasize instead the icosahedra of eight Ni and four Si atoms, in the centre of which is found the site on which Ni and Si atoms are randomly distributed. The projection of the  $\text{Ce}_2\text{Ni}_{17}\text{Si}_9$  structure segment shown in fig. 81 can be compared with the projection along [001] of the  $\text{U}(\text{Ni}_{.68}\text{Si}_{.32})_{11}$  structure shown in fig. 79. The drawings, except for the thin lines connecting atoms, appear identical, both structures having R atoms and centred icosahedra aligned in an identical way on a (001) plane. The difference is found in the way the icosahedra are connected in the [001] direction. In  $\text{NaZn}_{13}$  (or  $\text{Ce}_2\text{Ni}_{17}\text{Si}_9$ ) they are isolated, but in  $\text{U}(\text{Ni}_{.68}\text{Si}_{.32})_{11}$  they share edges and thus form chains of centred icosahedra parallel to [001]. This condensation of the centred icosahedra  $(\text{T}/\text{M})_{12}(\text{T}/\text{M})$  leads to a change of the composition according to



The three binary structure types  $\text{Na}^{[24]}\text{Zn}_{13}$ ,  $\text{Ba}^{[22]}\text{Cd}_{11}$  and  $\text{Th}^{[20]}\text{Mn}_{12}$  differ in the number of atoms in the coordination polyhedron around the minority component.

TABLE 22

The R-Fe-Al and R-Co-Si compounds formed with structures having large coordination polyhedra around the R atoms.

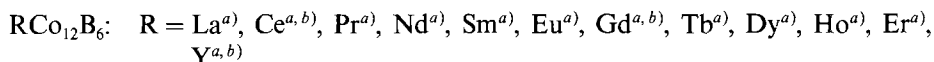
Binary structure type	Code of ternary compound	Compound	Pearson's classif. symbol	Space group	R-Fe-Al	R-Co-Si
Na <sup>[24]</sup> Zn <sub>13</sub>	93(35)	Ce <sub>5</sub> <sup>[24]</sup> Ni <sub>17</sub> Si <sub>9</sub>	tI56	I4/mcm	La	La, Ce
Ba <sup>[22]</sup> Cd <sub>11</sub>	92(23)	Ce <sub>5</sub> <sup>[22]</sup> Ni <sub>17</sub> Si <sub>5</sub>	tI48	I4 <sub>1</sub> /amd	—	Nd, Sm, Eu, Gd, Tb, Dy, Ho, Y
Th <sup>[20]</sup> Mn <sub>12</sub>	92(50)	Dy <sup>[20]</sup> Fe <sub>6</sub> Al <sub>6</sub>	tI26	I4/mmm	Pr, Eu, Gd, Tb, Dy, Ho, Er, Tm, Yb, Y, Sc	
Th <sup>[20]</sup> Mn <sub>12</sub>	9267	Ce <sup>[20]</sup> Mn <sub>4</sub> Al <sub>8</sub>	tI26	I4/mmm	La, Ce, Pr, Nd, Sm, Eu, Gd, Tb, Dy, Ho, Er, Tm, Yb, Lu, Y, Sc	

It is to be expected that structures with very large coordination polyhedra are formed only with the very large rare earth elements. In table 22 are listed the R-Fe-Al and R-Co-Si compounds which are formed with Na<sup>[24]</sup>Zn<sub>13</sub>, Ba<sup>[22]</sup>Cd<sub>11</sub> and Th<sup>[20]</sup>Mn<sub>12</sub>-type derivative structures. Not every type is formed with aluminides and silicides for reasons which are not geometrical in origin. However, the NaZn<sub>13</sub>-type occurs only with La (and Ce) while types with smaller polyhedra may also accommodate smaller rare earth elements.

9533	EuNi <sub>12</sub> B <sub>6</sub>	hR57 R $\bar{3}$ m	$a = 9.551$ $c = 7.408$	KuCC, 81
------	-----------------------------------	-----------------------	----------------------------	----------

SrNi<sub>12</sub>B<sub>6</sub>-type (JuQ, 80)

Isotypic compounds\*:



\*KuCC, 81 state that the compounds CeCo<sub>8</sub>B<sub>3</sub> (BiK, 74), YNi<sub>8</sub>B<sub>3</sub> (KuK, 75), LaCo<sub>12</sub>B<sub>6</sub> (StK, 76) and YCo<sub>8</sub>B<sub>3</sub> (KuS, 74), previously given as monoclinic, belong in fact to the SrNi<sub>12</sub>B<sub>6</sub>-type. Further, the compounds GdCo<sub>12</sub>B<sub>6</sub> (ChK, 77) and YNi<sub>12</sub>B<sub>6</sub> (KuK, 75), previously reported with an orthorhombic cell, and the compounds YCo<sub>12</sub>B<sub>6</sub> and CeCo<sub>12</sub>B<sub>6</sub> (NiY, 72) with R $\bar{3}$ m symmetry, all crystallize in the rhombohedral SrNi<sub>12</sub>B<sub>6</sub>-type.

\*\*Indicated as orthorhombic but probably also belongs to the SrNi<sub>12</sub>B<sub>6</sub>-type structure family.

<sup>a</sup>KuCG, 81    <sup>b</sup>NiY, 72    <sup>c</sup>KuBN, 73

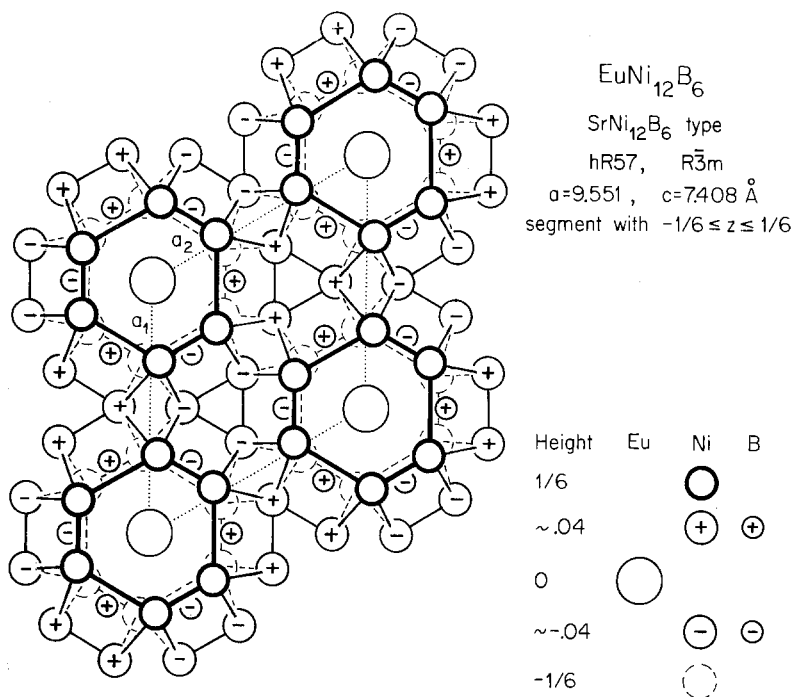


Fig. 82. A crystal structure segment ( $-\frac{1}{6} \leq z \leq +\frac{1}{6}$ ) of the rhombohedral  $\text{EuNi}_{12}\text{B}_6$  structure with  $\text{SrNi}_{12}\text{B}_6$ -type.

A segment of the  $\text{EuNi}_{12}\text{B}_6$  structure with  $\text{SrNi}_{12}\text{B}_6$ -type with  $-\frac{1}{6} \leq z \leq +\frac{1}{6}$  is shown in fig. 82. All B atoms are in the centres of deformed trigonal prisms of Ni atoms. The prisms share two edges of a rectangular prism face with two neighbouring prisms and form a six-membered prism ring around every R atom. Ni atoms form prism rings above and below the R atom and surround it in the form of an octahedron. The structure is characterized by T-B and R-T interactions and the absence of R-B interactions.

---

<b>9691</b>	<b>CeCr<sub>2</sub>Al<sub>20</sub></b>	cF184 Fd3m	$a = 14.44$	KrZ, 68
-------------	--	---------------	-------------	---------

---

$\text{Mg}_3\text{Cr}_2\text{Al}_{18}$ -related-type (Sa, 58)  $\equiv$   $\text{ZrZn}_{22}$ -type derivative

---

Isotypic compounds:

$\text{RV}_2\text{Al}_{20}$ :  $\text{R}^* = \text{La}^a, \text{Ce}^a, \text{Pr}^a, \text{Nd}^a, \text{Gd}^a, \text{Dy}^b, \text{Y}^a$   
 $\text{RCr}_2\text{Al}_{20}$ :  $\text{R} = \text{La}^a, \text{Ce}^a, \text{Pr}^a, \text{Nd}^a, \text{Gd}^a, \text{Dy}^b, \text{Ho}^a, \text{Er}^a, \text{Y}^a$



\*These compounds may represent true ternary compounds or solid solutions of the binary compound  $\text{VA}_{10}$ , which has the same structure as  $\text{CeCr}_2\text{Al}_{20}$  but with the Ce sites unoccupied (Br, 57).

<sup>a</sup>KrZ, 68    <sup>b</sup>RyZM, 79

The  $\text{CeCr}_2\text{Al}_{20}$  structure, a  $\text{ZrZn}_{22}$ -type derivative, has a very large cubic unit cell. The structure is conveniently described with nested polyhedral units which are treated here with 7325:  $\text{Ce}_3\text{Ni}_6\text{Si}_2$ .

## 5. Recent structure determinations

As far as possible data on recently determined isotypic phases have been inserted into the main text and table 23. For new structure types at least the heading can be found in section 4. Here are given only a few complementary drawings and structure comments which for editorial reasons could not be incorporated in the main text. For all three structures listed below the corresponding entry in section 4 should be consulted first.

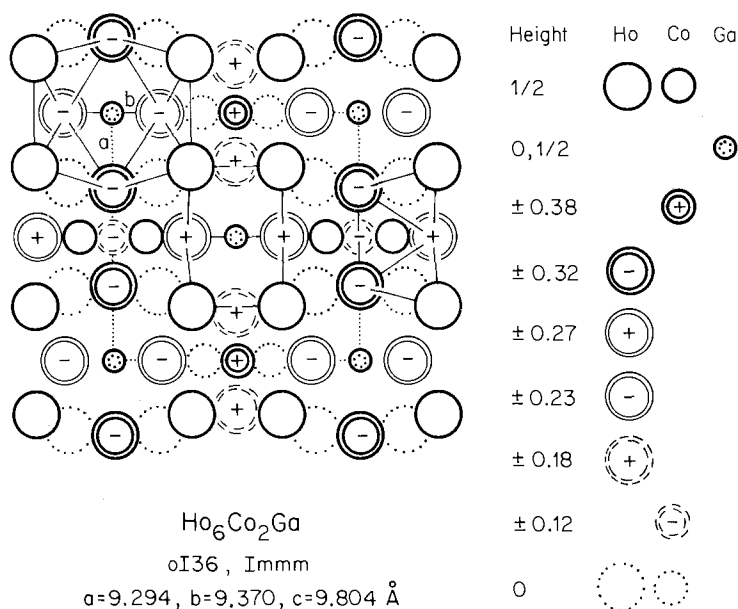
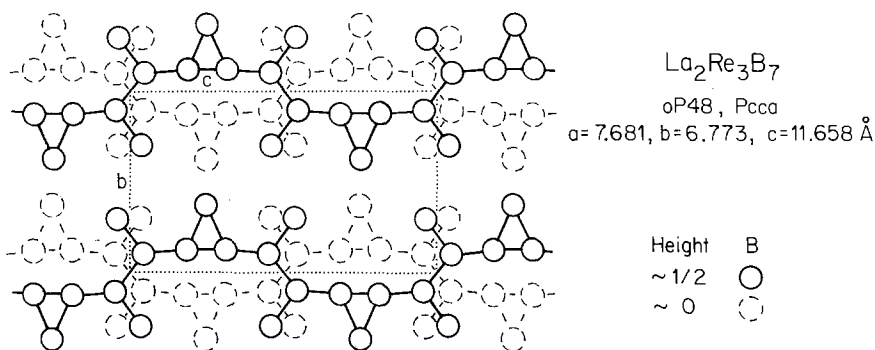


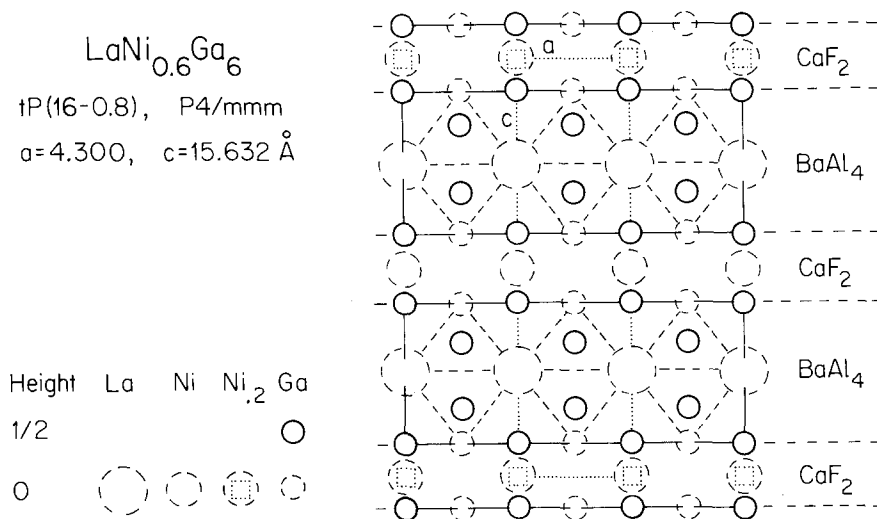
Fig. 83. Projection of the  $\text{Ho}_6\text{Co}_2\text{Ga}$  structure along  $c$ . The Ho atom polyhedra formed around a Co atom at  $z = \frac{1}{2}$  (deformed Archimedean antiprism) and two crystallographically different Ga atoms, both at  $z = \frac{1}{2}$  (icosahedron and cube), are indicated (only the lower halves of the polyhedra are shown).

**3333:** The  $\text{Ho}_6\text{Co}_2\text{Ga}$  structure has been found with seven  $\text{R}_6\text{Co}_2\text{Ga}$  compounds, where  $\text{R} = \text{Tb}, \text{Dy}, \text{Ho}, \text{Er}, \text{Tm}, \text{Lu}$  and  $\text{Y}$  (GIGY, 83). The  $\text{Ho}_6\text{Co}_2\text{Ga}$  structure is shown in fig. 83 in a projection along  $c$ . The Co atoms are in the centres of deformed Archimedean antiprisms of Ho atoms, the Ga atoms occupy the icosahedral and the cubical voids in the Ho atom framework. Transition-metal centred Archimedean

Fig. 84. The infinite boron chains in  $\text{La}_2\text{Re}_3\text{B}_7$ .

antiprisms of rare earth atoms occur also in 4029: $\text{Er}_{21}\text{Ni}_{10}\text{Ga}_4$  and 4035: $\text{Sm}_{26}\text{Co}_{11}\text{Ga}_6$ ; however, Ga-centred icosahedra and cubes have not yet been found with the other ternary gallides.

**8370:** The infinite boron atom chains formed in  $\text{La}_2\text{Re}_3\text{B}_7$  are shown in fig. 84. From the relation between the metal:boron ratio and the type of boron–boron linkage established with other boride structures (table 20), the formation of boron–boron chains in  $\text{La}_2\text{Re}_3\text{B}_7$  with metal:boron ratio of 0.71 is not unexpected. The boron chain has branches and the average number of boron–boron bonds is 2.28. Infinite boron–boron chains are also formed in 7388: $\text{Y}_3\text{ReB}_7$  (see fig. 33). However, with a metal:boron ratio of 0.57 the average number of boron–boron bonds should be

Fig. 85. The  $\text{LaNi}_{0.6}\text{Ga}_6$  structure with intergrown  $\text{BaAl}_4$ - and  $\text{CaF}_2$ -type slabs.

higher than in  $\text{La}_2\text{Re}_3\text{B}_7$ . This is actually the case. In  $\text{Y}_3\text{ReB}_7$  there are on the average 3.14 homonuclear boron–boron bonds per boron atom.

**8791:** The  $\text{LaNi}_{0.6}\text{Ga}_6$  structure is shown in fig. 85. If the defect sites in the  $\text{CaF}_2$ -type slabs would be fully occupied by Ni atoms the composition would be 8886:  $\text{LaNiGa}_6$  and a smaller unit cell with half the  $c$  axis could be used.

## 6. Survey of structures found with R–T–M compounds and concluding remarks

By the end of 1982 we know more than 1650 R–T–M compounds, which crystallize with more than 120 structure types. Less than half of these types can be described as ternary derivatives of binary structure types. The number of R–T–M compounds known for each structure type and a simple classification of the elements present in these compounds is given in condensed form in table 23.

With few exceptions boride structures are different from the structures of aluminides, silicides, and germanides. Aluminides often have the same structures as the silicides and germanides, but with T and M elements interchanged on their crystallographic sites. Ternary phases containing Sc generally crystallize in structure types which differ from those found with the other rare earths. Due to its relatively small size the element Sc behaves rather more similar to Zr and Hf in its ternary structures.

This study shows that a great effort has already been made, since the seventies, in the exploration of the R–T–M phases, in particular by the Russian scientists. Nevertheless, a lot of work needs to be done to study the still unknown ternary phases and to further characterize those already known. In the course of this study, we have been hampered by the lack of accurate structural data. As an example we may mention the case of the  $\text{ThCr}_2\text{Si}_2$ -type, which was mostly presumed a priori without testing for the  $\text{CaBe}_2\text{Ge}_2$ -type, or the similar case of the  $\text{CeNiSi}_2$ -type and its site exchange variant, the  $\text{TbFeSi}_2$ -type. Structures refined from single crystal data are a minority, most of them having been refined, if at all, from powder diffraction data with frequently no information about the relative errors on the structural parameters. Furthermore, in many cases structure refinements from powder data are not appropriate to analyze the atom ordering on the crystallographic sites of a given structure. Thus the affirmative way in which the atom ordering has been stated in certain papers does not necessarily appear justified.

We have presented here the structural relationships between the R–T–M compounds without giving particular attention to such problems as the link between structures and physical properties. This we had to do in part because of the limited space available for this chapter, in part because the uncertainty and lack of precision of the structural data makes any effort to correlate properties with structures of doubtful value.

The reader should note that the majority of the structures have been described, for simplicity and in order to facilitate the structural comparison, with the help of

TABLE 23  
 Survey of structures found with R-T-M compounds.

Code	R-T-M compound discussed in the text	Ternary structure type	Related binary structure type	Pearson's†t classif. symbol	Space group	R elements			
						early rare earth	late rare earth	Y	Sc
3333	Ho <sub>6</sub> Co <sub>2</sub> Ga	Ho <sub>6</sub> Co <sub>2</sub> Ga	—	oI36	Immm	.	*	*	.
33(50)	Sc <sub>7</sub> (Co, Si)	—	Ti <sub>2</sub> Ni	cF96	Fd3m	.	.	.	*
4029	Er <sub>21</sub> Ni <sub>10</sub> Ga <sub>4</sub>	Er <sub>21</sub> Ni <sub>10</sub> Ga <sub>4</sub>	Y <sub>3</sub> Rh <sub>2</sub>	tI140	I4/mcm	.	*	.	.
4035	Sm <sub>26</sub> Co <sub>11</sub> Ga <sub>6</sub>	Sm <sub>26</sub> Co <sub>11</sub> Ga <sub>6</sub>	—	tP86	P4/mbm	*	.	.	.
45(60)	Ce <sub>6</sub> Ni <sub>2</sub> Si <sub>3</sub>	Ce <sub>6</sub> Ni <sub>2</sub> Si <sub>3</sub>	—	hP22	P6 <sub>3</sub> /m	*	.	.	.
50(25)	Er(Ni, Si)	—	CrB	oC8	Cmcm	.	*	.	.
50(30)	Y <sub>10</sub> Co <sub>7</sub> Ga <sub>3</sub>	Y <sub>10</sub> Co <sub>7</sub> Ga <sub>3</sub>	—	oP40	Pnma	*	.	*	.
50(60)	Ce <sub>5</sub> Ni <sub>2</sub> Si <sub>3</sub>	Ce <sub>5</sub> Ni <sub>2</sub> Si <sub>3</sub>	—	hP40	P6 <sub>3</sub> /m	*	.	.	.
5067	Gd <sub>3</sub> NiSi <sub>2</sub>	Gd <sub>3</sub> NiSi <sub>2</sub>	—	oP24	Pnma	*	*	*	.
5071	Ce <sub>7</sub> Ni <sub>2</sub> Si <sub>5</sub>	Ce <sub>7</sub> Ni <sub>2</sub> Si <sub>5</sub>	—	oP56	Pnma	*	.	.	.
53(76)	Ce <sub>15</sub> Ni <sub>4</sub> Si <sub>13</sub>	Ce <sub>15</sub> Ni <sub>4</sub> Si <sub>13</sub>	—	hP64	P6 <sub>3</sub> /m	*	.	.	.
55(53)	Ce <sub>14</sub> Ni <sub>8</sub> Si <sub>9</sub>	Ce <sub>14</sub> Ni <sub>8</sub> Si <sub>9</sub>	—	mP62	P2 <sub>1</sub> /m	*	.	.	.
5565	Pr <sub>14</sub> Ni <sub>6</sub> Si <sub>11</sub>	Pr <sub>14</sub> Ni <sub>6</sub> Si <sub>11</sub>	—	mC124	C2/m	*	.	.	.
5725	Y <sub>3</sub> Co <sub>3</sub> Ga	"W <sub>3</sub> CoB <sub>3</sub> "	—	oC28	Cmcm	*	*	*	.
57(75)	Y <sub>3</sub> NiSi <sub>3</sub>	Ba <sub>3</sub> Al <sub>2</sub> Ge <sub>2</sub>	Ta <sub>3</sub> B <sub>4</sub>	oI14	Immm	*	.	*	.
6033	Pr <sub>2</sub> Ni <sub>2</sub> Al	"W <sub>2</sub> CoB <sub>2</sub> "	—	oI10	Immm	*	*	*	.
( )	Er <sub>2</sub> Pd <sub>2</sub> Si	Er <sub>2</sub> Pd <sub>2</sub> Si	—	oP20	Pnmm	.	*	.	.
6067	Sc <sub>2</sub> CoSi <sub>2</sub>	Sc <sub>2</sub> CoSi <sub>2</sub>	—	mC20	C2/m	.	.	.	*
6360	Sc <sub>3</sub> Co <sub>2</sub> Si <sub>3</sub>	Hf <sub>3</sub> Ni <sub>2</sub> Si <sub>3</sub>	—	oC32	Cmcm	.	.	*	*
	Sc <sub>3</sub> Re <sub>2</sub> Si <sub>3</sub>	Sc <sub>3</sub> Re <sub>2</sub> Si <sub>3</sub>	—	mC64	C2	.	.	.	*
6725	Sc <sub>2</sub> Co <sub>3</sub> Si	Mg <sub>2</sub> Cu <sub>3</sub> Si	MgZn <sub>2</sub>	hP12	P6 <sub>3</sub> /mmc	.	.	.	*
6733	La <sub>3</sub> Ni <sub>4</sub> Ga <sub>2</sub>	La <sub>3</sub> Ni <sub>4</sub> Ga <sub>2</sub>	—	mC18	C2/m	*	.	.	.
6750	CeFeSi	PbFCl	Fe <sub>2</sub> As	tP6	P4/nmm	*	*	*	.
	ScRuGe	ZrNiAl	Fe <sub>2</sub> P	hP9	P6 <sub>2</sub> m	*	*	*	*
	ScRhSi	TiNiSi	PbCl <sub>2</sub>	oP12	Pnma	*	*	*	*
	LaPtSi	LaPtSi	ThSi <sub>2</sub>	tI12	I4 <sub>1</sub> md	*	.	.	.
	LaIrSi	ZrOS	SrSi <sub>2</sub>	cP12	P2 <sub>1</sub> 3	*	.	.	.
( )	Pr(Pt <sub>3</sub> Ge <sub>5</sub> ) <sub>2</sub>	—	CeCu <sub>2</sub>	oI12	Imma	*	*	*	.
( )	Sc(Ni <sub>5</sub> Al <sub>3</sub> ) <sub>2</sub>	—	MgZn <sub>2</sub>	hP12	P6 <sub>3</sub> /mmc	*	*	*	*
( )	Y(Mn <sub>5</sub> Ga <sub>3</sub> ) <sub>2</sub>	TiFeSi	Fe <sub>2</sub> P	oI36	Ima2	.	*	*	*
6775	Sc <sub>2</sub> RuAl <sub>3</sub>	Mg <sub>2</sub> Cu <sub>3</sub> Si	MgZn <sub>2</sub>	hP12	P6 <sub>3</sub> /mmc	.	*	.	*
( )	Ce(Ni, Si) <sub>2</sub>	—	AlB <sub>2</sub>	hP3	P6/mmm	*	*	*	.
67(83)	Sm(Mn <sub>17</sub> Ga <sub>83</sub> ) <sub>2</sub>	—	CaIn <sub>2</sub>	hP6	P6 <sub>3</sub> /mmc	.	*	.	.
67(88)	Sc <sub>4</sub> CoSi <sub>7</sub>	Sc <sub>4</sub> CoSi <sub>7</sub>	ZrSi <sub>2</sub>	oC12	Cmcm	.	.	.	*
7325	Ce <sub>3</sub> Ni <sub>6</sub> Si <sub>2</sub>	Ce <sub>3</sub> Ni <sub>6</sub> Si <sub>2</sub>	Ca <sub>3</sub> Ag <sub>8</sub>	cI44	Im3m	*	.	*	.
7350	Sc <sub>3</sub> Ni <sub>4</sub> Ge <sub>4</sub>	Gd <sub>3</sub> Cu <sub>4</sub> Ge <sub>4</sub>	—	oI22	Immm	.	.	.	*
	La <sub>3</sub> Rh <sub>4</sub> Ge <sub>4</sub>	U <sub>3</sub> Ni <sub>4</sub> Si <sub>4</sub>	—	oI22	Immm	*	.	.	.
7364	Sc <sub>4</sub> Mn <sub>4</sub> Si <sub>7</sub>	Zr <sub>4</sub> Co <sub>4</sub> Ge <sub>7</sub>	—	tI60	I4/mmm	.	.	.	*

†In this chapter, in the case of rhombohedral structures the number of atoms/cell always refers to the triple hexagonal unit cell.

T elements								M elements						Number of R-T-M compounds	Code
Ti group	V Group	Cr group	Mn group	Fe group	Co group	Ni group	B	Al	Ga	In	Si	Ge	Sn		
.	.	.	.	.	*	.	.	.	*	.	.	.	.	7	3333
.	.	*	.	.	*	.	.	.	*	.	*	.	.	2	33(50)
.	.	.	.	.	.	*	.	.	*	.	.	.	.	5	4029
.	.	.	.	.	*	*	.	.	*	.	.	.	.	9	4035
.	.	.	.	.	.	*	.	.	*	.	*	.	.	4	45(60)
.	.	.	.	.	.	*	.	.	*	.	*	.	.	7	50(25)
.	.	.	.	.	*	.	.	.	*	.	*	.	.	2	50(30)
.	.	.	.	.	.	*	.	.	*	.	*	.	.	3	50(60)
.	.	.	.	.	.	*	.	.	.	.	*	*	.	15	5067
.	.	.	.	.	.	*	.	.	.	.	*	.	.	3	5071
.	.	.	.	.	.	*	.	.	.	.	*	.	.	3	53(76)
.	.	.	.	.	.	*	.	.	.	.	*	.	.	2	55(53)
.	.	.	.	.	.	*	.	.	.	.	*	.	.	1	5565
.	.	.	.	.	*	.	.	.	*	.	.	.	.	6	5725
.	.	.	.	.	.	*	.	.	.	.	*	.	.	2	57(75)
.	.	.	.	.	*	*	.	*	*	.	.	.	.	37	6033
.	.	.	.	.	.	*	.	.	.	.	*	.	.	4	( )
.	.	.	.	*	*	*	.	.	.	.	*	.	.	2	6067
.	.	.	.	*	*	*	.	.	.	.	*	.	.	4	6360
.	.	.	*	.	.	.	.	.	.	.	*	.	.	1	
.	.	.	.	*	*	*	.	.	.	.	*	.	.	3	6725
.	.	.	.	.	.	*	.	.	*	.	.	.	.	2	6733
.	.	.	*	*	*	.	.	.	.	.	*	.	.	24	6750
.	.	.	*	*	*	*	.	*	*	*	*	*	*	107	
.	.	.	*	*	*	*	.	.	*	.	*	*	*	141	
.	.	.	.	.	*	.	.	.	.	.	*	.	.	11	
.	.	.	.	.	*	.	.	.	.	.	*	.	.	3	
.	.	.	*	.	.	*	.	.	*	.	.	*	.	25	( )
.	.	.	*	*	*	*	.	*	*	.	*	.	.	25	( )
.	.	.	*	.	*	*	.	.	*	.	.	.	.	10	( )
.	.	.	.	*	*	*	.	*	.	.	.	.	.	3	6775
.	.	.	.	*	*	*	.	.	.	.	*	*	.	48	( )
.	.	.	*	.	.	.	.	.	*	.	.	.	.	6	67(83)
.	.	.	*	*	*	*	.	.	.	.	*	.	.	4	67(88)
.	.	.	.	.	.	*	.	*	*	.	*	.	.	30	7325
.	.	.	.	.	.	*	.	.	.	.	*	*	.	2	7350
.	.	.	.	.	*	*	.	.	.	.	*	*	.	2	
.	.	.	*	*	*	*	.	.	.	.	*	.	.	2	7364

TABLE 23 (cont'd)

Code	R-T-M compound discussed in the text	Ternary structure type	Related binary structure type	Pearson's classif. symbol	Space group	R elements			
						RE <sub>c</sub>	RE <sub>t</sub>	Y	Sc
7388	Y <sub>3</sub> ReB <sub>7</sub>	Y <sub>3</sub> ReB <sub>7</sub>	—	oC44	Cmcm	*	*	*	*
7471	Sc <sub>2</sub> Co <sub>4</sub> Si <sub>10</sub>	Sc <sub>2</sub> Co <sub>4</sub> Si <sub>10</sub>	—	tP38	P4/mbm	*	*	*	*
7511	Ce <sub>3</sub> Co <sub>8</sub> Si	Ce <sub>3</sub> Co <sub>8</sub> Si	CeNi <sub>3</sub>	hP24	P6 <sub>3</sub> /mmc	*	*	*	*
7522	Dy <sub>3</sub> Ni <sub>7</sub> B <sub>2</sub>	Dy <sub>3</sub> Ni <sub>7</sub> B <sub>2</sub>	CeNi <sub>3</sub>	hP24	P6 <sub>3</sub> /mmc	*	*	*	*
7533	PrCo <sub>2</sub> Ga	PrCo <sub>2</sub> Ga	—	oP8	Pmma	*	*	*	*
	YPd <sub>2</sub> Si	YPd <sub>2</sub> Si	Fe <sub>3</sub> C	oP16	Pnma	*	*	*	*
	YPd <sub>2</sub> Sn	MnCu <sub>2</sub> Al	CsCl	cF16	Fm3m	*	*	*	*
7567	ScRhSi <sub>2</sub>	ScRhSi <sub>2</sub>	YZn <sub>3</sub>	oP16	Pnma	*	*	*	*
	LuRuB <sub>2</sub>	LuRuB <sub>2</sub>	—	oP16	Pnma	*	*	*	*
	CeNiSi <sub>2</sub>	CeNiSi <sub>2</sub>	—	oC16	Cmcm	*	*	*	*
	TbFeSi <sub>2</sub>	TbFeSi <sub>2</sub>	—	oC16	Cmcm	*	*	*	*
	NdNiGa <sub>2</sub>	NdNiGa <sub>2</sub>	—	oC16	Cmmm	*	*	*	*
	YNiAl <sub>2</sub>	MgCuAl <sub>2</sub>	Re <sub>3</sub> B	oC16	Cmcm	*	*	*	*
	ScMnSi <sub>2</sub>	TiMnSi <sub>2</sub>	—	oP48	Pbam	*	*	*	*
	ScFeSi <sub>2</sub>	ZrFeSi <sub>2</sub>	—	oC96	Cmca	*	*	*	*
7578	La <sub>3</sub> Co <sub>2</sub> Sn <sub>7</sub>	La <sub>3</sub> Co <sub>2</sub> Sn <sub>7</sub>	—	oC24	Cmmm	*	*	*	*
75(83)	Y <sub>2</sub> MnGa <sub>5</sub>	—	Cu <sub>3</sub> Au	cP4	Pm3m	*	*	*	*
7646	Sc <sub>4</sub> Rh <sub>7</sub> Ge <sub>6</sub>	U <sub>4</sub> Re <sub>7</sub> Si <sub>6</sub>	—	cI34	Im3m	*	*	*	*
7780	Ce <sub>3</sub> Ni <sub>7</sub> Si <sub>8</sub>	Ce <sub>3</sub> Ni <sub>7</sub> Si <sub>8</sub>	—	oC26	Cmmm	*	*	*	*
7829	Ce <sub>2</sub> Co <sub>5</sub> B <sub>2</sub>	Ce <sub>2</sub> Co <sub>5</sub> B <sub>2</sub>	Ce <sub>2</sub> Ni <sub>7</sub>	hP36	P6 <sub>3</sub> /mmc	*	*	*	*
7857	Sc <sub>2</sub> Re <sub>3</sub> Si <sub>4</sub>	Sc <sub>2</sub> Re <sub>3</sub> Si <sub>4</sub>	Zr <sub>3</sub> Si <sub>4</sub>	tP36	P4 <sub>1</sub> 2 <sub>1</sub> 2	*	*	*	*
7886	Y <sub>2</sub> ReB <sub>6</sub>	Y <sub>2</sub> ReB <sub>6</sub>	—	oP36	Pbam	*	*	*	*
7930	Sc <sub>6</sub> Ni <sub>16</sub> Si <sub>7</sub>	Mg <sub>6</sub> Cu <sub>16</sub> Si <sub>7</sub>	Th <sub>6</sub> Mn <sub>23</sub>	cF116	Fm3m	*	*	*	*
7970	Sc <sub>6</sub> Ni <sub>7</sub> Al <sub>16</sub>	"Mg <sub>6</sub> Cu <sub>16</sub> Si <sub>7</sub> "	Th <sub>6</sub> Mn <sub>23</sub>	cF116	Fm3m	*	*	*	*
79(82)	Ho <sub>3</sub> Ni <sub>7</sub> Ga <sub>9</sub>	Ho <sub>3</sub> Ni <sub>7</sub> Ga <sub>9</sub>	La <sub>3</sub> Al <sub>11</sub>	oI28	Immm	*	*	*	*
8025	LaPd <sub>3</sub> B	CaTiO <sub>3</sub>	Fe <sub>4</sub> N	cP5	Pm3m	*	*	*	*
8050	CeNi <sub>2</sub> Si <sub>2</sub>	ThCr <sub>2</sub> Si <sub>2</sub>	BaAl <sub>4</sub>	tI10	I4/mmm	*	*	*	*
	LaIr <sub>2</sub> Si <sub>2</sub>	CaBe <sub>2</sub> Ge <sub>2</sub>	BaAl <sub>4</sub>	tP10	P4/nmm	*	*	*	*
	ScFe <sub>2</sub> Si <sub>2</sub>	HfFe <sub>2</sub> Si <sub>2</sub>	—	oP20	Pbcm	*	*	*	*
	LaRe <sub>2</sub> Si <sub>2</sub>	LaRe <sub>2</sub> Si <sub>2</sub>	—	oI20	Imma	*	*	*	*
8063	Sc <sub>2</sub> Fe <sub>3</sub> Si <sub>5</sub>	Sc <sub>2</sub> Fe <sub>3</sub> Si <sub>5</sub>	—	tP40	P4/mnc	*	*	*	*
	Sc <sub>2</sub> Co <sub>3</sub> Si <sub>5</sub>	U <sub>2</sub> Co <sub>3</sub> Si <sub>5</sub>	BaAl <sub>4</sub>	oI40	Ibam	*	*	*	*
8075	ScNiSi <sub>3</sub>	ScNiSi <sub>3</sub>	—	oC20	Amm2	*	*	*	*
	LaIrSi <sub>3</sub>	BaNiSn <sub>3</sub>	BaAl <sub>4</sub>	tI10	I4mm	*	*	*	*
( )	PrNiGa <sub>3</sub>	PrNiGa <sub>3</sub>	BaAl <sub>4</sub>	tI10	I4/mmm	*	*	*	*
8244	Sc <sub>2</sub> Ru <sub>2</sub> B <sub>4</sub>	Sc <sub>2</sub> Ru <sub>2</sub> B <sub>4</sub>	—	mP22	P2/m	*	*	*	*
8256	Sc <sub>2</sub> Cr <sub>4</sub> Si <sub>5</sub>	Nb <sub>2</sub> Cr <sub>4</sub> Si <sub>5</sub>	V <sub>6</sub> Si <sub>5</sub>	oI44	Ibam	*	*	*	*
8275	Ho <sub>3</sub> Co <sub>7</sub> Ga <sub>21</sub>	Ho <sub>3</sub> Co <sub>7</sub> Ga <sub>21</sub>	—	tP68	P4/mbm	*	*	*	*
82(78)	U <sub>2</sub> Ni <sub>2</sub> Si <sub>7</sub>	U <sub>2</sub> Ni <sub>2</sub> Si <sub>7</sub>	—	oC22	Cmmm	*	*	*	*
8289	Ho <sub>2</sub> CoGa <sub>8</sub>	Ho <sub>2</sub> CoGa <sub>8</sub>	—	tP11	P4/mmm	*	*	*	*
8313	Nd <sub>3</sub> Ni <sub>13</sub> B <sub>2</sub>	Nd <sub>3</sub> Ni <sub>13</sub> B <sub>2</sub>	CaCu <sub>5</sub>	hP18	P6/mmm	*	*	*	*
8320	CeCo <sub>4</sub> B	CeCo <sub>4</sub> B	CaCu <sub>5</sub>	hP12	P6/mmm	*	*	*	*
8327	Ce <sub>3</sub> Co <sub>11</sub> B <sub>4</sub>	Ce <sub>3</sub> Co <sub>11</sub> B <sub>4</sub>	CaCu <sub>5</sub>	hP18	P6/mmm	*	*	*	*
8330	Ce <sub>2</sub> Co <sub>7</sub> B <sub>3</sub>	Ce <sub>2</sub> Co <sub>7</sub> B <sub>3</sub>	CaCu <sub>5</sub>	hP24	P6/mmm	*	*	*	*
8340	CeCo <sub>3</sub> B <sub>2</sub>	CeCo <sub>3</sub> B <sub>2</sub>	CaCu <sub>5</sub>	hP6	P6/mmm	*	*	*	*
	ErIr <sub>3</sub> B <sub>2</sub>	ErIr <sub>3</sub> B <sub>2</sub>	CaCu <sub>5</sub>	mC12	C2/m	*	*	*	*



TABLE 23 (cont'd)

Code	R-T-M compound discussed in the text	Ternary structure type	Related binary structure type	Pearson's classif. symbol	Space group	R elements			
						RE <sub>c</sub>	RE <sub>r</sub>	Y	Sc
8360	PrNi <sub>2</sub> Al <sub>3</sub>	CeCo <sub>3</sub> B <sub>2</sub>	CaCu <sub>5</sub>	hP6	P6/mmm	*	.	.	.
	YNi <sub>2</sub> Al <sub>3</sub>	YNi <sub>2</sub> Al <sub>3</sub>	—	hP18	P6/mmm	*	*	*	.
	ScNi <sub>2</sub> Si <sub>3</sub>	ScNi <sub>2</sub> Si <sub>3</sub>	—	tI24	I4/mmm	.	.	.	*
	ScRe <sub>2</sub> Si <sub>3</sub>	ScRe <sub>2</sub> Si <sub>3</sub>	—	oC96	Amm2	.	.	.	*
8370	La <sub>2</sub> Re <sub>3</sub> B <sub>7</sub>	La <sub>2</sub> Re <sub>3</sub> B <sub>7</sub>	—	oP48	Pcca	*	.	.	.
8380	LaCoAl <sub>4</sub>	LaCoAl <sub>4</sub>	—	oP12	Pmma	*	.	.	.
	YCrB <sub>4</sub>	YCrB <sub>4</sub>	—	oP24	Pbam	*	*	*	.
	YNiAl <sub>4</sub>	YNiAl <sub>4</sub>	—	oC24	Cmcm	*	*	*	.
8576	Yb <sub>3</sub> Rh <sub>4</sub> Sn <sub>13</sub>	Yb <sub>3</sub> Rh <sub>4</sub> Sn <sub>13</sub>	—	cP40	Pm3n	*	*	*	*
8591	Ce <sub>2</sub> NiGa <sub>10</sub>	Ce <sub>2</sub> NiGa <sub>10</sub>	—	tI26	I4/mmm	*	.	.	.
8617	CeNi <sub>5</sub> Sn	CeNi <sub>5</sub> Sn	—	hP28	P6 <sub>3</sub> /mmc	*	.	.	.
8633	CeRe <sub>4</sub> Si <sub>2</sub>	CeRe <sub>4</sub> Si <sub>2</sub>	—	oC14	Cmmm	*	.	.	.
	YRe <sub>4</sub> Si <sub>2</sub>	ZrFe <sub>4</sub> Si <sub>2</sub>	—	tP14	P4 <sub>2</sub> /mnm	.	*	*	*
	NdRe <sub>4</sub> Si <sub>2</sub>	NdRe <sub>4</sub> Si <sub>2</sub>	—	oP28	Pnmm	*	.	.	.
8667	YbMo <sub>2</sub> Al <sub>4</sub>	YbMo <sub>2</sub> Al <sub>4</sub>	—	tI14	I4/mmm	.	*	.	*
8683	HoCoGa <sub>5</sub>	HoCoGa <sub>5</sub>	—	tP7	P4 <sub>1</sub> /mmm	.	*	*	*
8769	Y <sub>2</sub> Fe <sub>4</sub> Si <sub>9</sub>	Y <sub>2</sub> Fe <sub>4</sub> Si <sub>9</sub>	—	hP16(-1)	P6 <sub>3</sub> /mmc	.	*	*	.
8791	LaNi <sub>0.6</sub> Ga <sub>6</sub>	LaNi <sub>0.6</sub> Ga <sub>6</sub>	—	tP16(-0.8)	P4 <sub>1</sub> /mmm	*	.	.	.
8850	Sm <sub>17</sub> (Fe <sub>4</sub> B <sub>4</sub> ) <sub>15</sub>	Sm <sub>17</sub> (Fe <sub>4</sub> B <sub>4</sub> ) <sub>15</sub>	—	tP274	P4 <sub>2</sub> /n	*	*	*	.
8857	ScIr <sub>3</sub> B <sub>4</sub>	ZrIr <sub>3</sub> B <sub>4</sub>	—	hP16	P6 <sub>3</sub> /m	*	.	.	*
8871	PrNi <sub>2</sub> Al <sub>5</sub>	PrNi <sub>2</sub> Al <sub>5</sub>	—	oI16	Immm	*	.	.	.
8912	Ce <sub>2</sub> Ni <sub>15</sub> Si <sub>2</sub>	Ce <sub>2</sub> Ni <sub>15</sub> Si <sub>2</sub>	Th <sub>2</sub> Ni <sub>17</sub>	hP38	P6 <sub>3</sub> /mmc	*	*	*	.
	Ce <sub>2</sub> Co <sub>15</sub> Al <sub>2</sub>	Ce <sub>2</sub> Co <sub>15</sub> Al <sub>2</sub>	Th <sub>2</sub> Zn <sub>17</sub>	hR57	R3m	*	*	*	*
8938	YNi <sub>5</sub> Si <sub>3</sub>	YNi <sub>5</sub> Si <sub>3</sub>	—	oP36	Pnma	.	*	*	.
8950	NdCo <sub>4</sub> B <sub>4</sub>	NdCo <sub>4</sub> B <sub>4</sub>	—	tP18	P4 <sub>2</sub> /n	*	*	*	.
	CeCo <sub>4</sub> B <sub>4</sub>	CeCo <sub>4</sub> B <sub>4</sub>	—	tP18	P4 <sub>2</sub> /nmc	*	*	*	*
	LuRu <sub>4</sub> B <sub>4</sub>	LuRu <sub>4</sub> B <sub>4</sub>	—	tI72	I4 <sub>1</sub> /acd	*	*	*	*
	LuRh <sub>4</sub> B <sub>4</sub>	LuRh <sub>4</sub> B <sub>4</sub>	—	oC108	Ccca	.	*	.	.
8968	Ho <sub>4</sub> Ni <sub>10</sub> Ga <sub>21</sub>	Ho <sub>4</sub> Ni <sub>10</sub> Ga <sub>21</sub>	—	mC70	C2/m	.	*	*	.
8975	CeCr <sub>2</sub> B <sub>6</sub>	CeCr <sub>2</sub> B <sub>6</sub>	—	oI18	Immm	*	.	.	.
9170	ScRh <sub>3</sub> Si <sub>7</sub>	ScRh <sub>3</sub> Si <sub>7</sub>	—	hR66	R3c	.	.	.	*
92(17)	YNi <sub>10</sub> Si <sub>2</sub>	CeMn <sub>4</sub> Al <sub>8</sub>	ThMn <sub>12</sub>	tI26	I4/mmm	.	*	*	.
92(23)	Ce <sub>2</sub> Ni <sub>17</sub> Si <sub>5</sub>	Ce <sub>2</sub> Ni <sub>17</sub> Si <sub>5</sub>	BaCd <sub>11</sub>	tI48	I4 <sub>1</sub> /amd	*	*	*	.
9250	ScFe <sub>6</sub> Ge <sub>6</sub>	HfFe <sub>6</sub> Ge <sub>6</sub>	—	hP13	P6/mmm	.	*	.	*
	YCo <sub>6</sub> Ge <sub>6</sub>	YCo <sub>6</sub> Ge <sub>6</sub>	—	hP6 <sub>2</sub> <sup>1</sup>	P6/mmm	.	*	*	.
	ScNi <sub>6</sub> Ge <sub>6</sub>	ScNi <sub>6</sub> Ge <sub>6</sub>	—	hP52	P6/mmm	.	.	.	*
	ScFe <sub>6</sub> Ga <sub>6</sub>	ScFe <sub>6</sub> Ga <sub>6</sub>	ThMn <sub>12</sub>	oI26	Immm	.	.	.	*
( )	DyFe <sub>6</sub> Al <sub>6</sub>	CeMn <sub>4</sub> Al <sub>8</sub>	ThMn <sub>12</sub>	tI26	I4/mmm	*	*	*	*
9267	CeMn <sub>4</sub> Al <sub>8</sub>	CeMn <sub>4</sub> Al <sub>8</sub>	ThMn <sub>12</sub>	tI26	I4/mmm	*	*	*	*
9322	Sc <sub>2</sub> Co <sub>21</sub> B <sub>6</sub>	W <sub>2</sub> Cr <sub>21</sub> C <sub>6</sub>	Cr <sub>23</sub> C <sub>6</sub>	cF116	Fm3m	*	*	.	*
93(35)	Ce <sub>2</sub> Ni <sub>17</sub> Si <sub>9</sub>	Ce <sub>2</sub> Ni <sub>17</sub> Si <sub>9</sub>	NaZn <sub>13</sub>	tI56	I4/mcm	*	.	*	.
9533	EuNi <sub>12</sub> B <sub>6</sub>	SrNi <sub>12</sub> B <sub>6</sub>	—	hR57	R3m	*	*	*	.
9691	CeCr <sub>2</sub> Al <sub>20</sub>	Mg <sub>3</sub> Cr <sub>2</sub> Al <sub>18</sub>	ZrZn <sub>22</sub>	cF184	Fd3m	*	*	*	.



T elements							M elements						No.	Code	
Ti	V	Cr	Mn	Fe	Co	Ni	B	Al	Ga	In	Si	Ge			Sn
.	.	.	.	.	.	*	.	*	.	.	.	.	.	2	8360
.	.	.	.	.	.	*	.	*	*	.	.	.	.	22	
.	.	.	.	.	.	*	.	.	.	.	*	.	.	1	
.	.	.	*	.	.	.	.	.	.	.	*	.	.	1	
.	.	.	*	.	.	.	*	.	.	.	.	.	.	1	8370
.	.	.	.	.	*	.	.	*	.	.	.	.	.	3	8380
.	*	*	*	*	*	*	*	*	*	.	.	.	.	84	
.	.	.	.	.	*	*	*	*	*	.	.	.	.	19	
.	.	.	.	*	*	*	.	.	.	.	.	*	*	66	8576
.	.	.	.	.	.	*	.	.	*	.	.	.	.	2	8591
.	.	.	.	.	.	*	.	.	.	.	.	.	*	1	8617
.	.	.	*	.	.	.	.	.	.	.	*	.	.	2	8633
.	.	.	*	*	.	.	.	.	.	.	*	.	.	5	
.	.	.	*	.	.	.	.	.	.	.	*	.	.	1	
*	*	*	.	.	.	.	.	*	*	.	.	.	.	12	8667
.	.	.	.	*	*	*	.	.	*	.	.	.	.	12	8683
.	.	.	.	*	.	.	.	.	.	.	*	.	.	9	8769
.	.	.	.	.	.	*	.	.	*	.	.	.	.	2	8791
.	.	.	.	*	.	.	*	.	.	.	.	.	.	8	8850
.	.	.	.	.	*	.	*	.	.	.	.	.	.	1	8857
.	.	.	.	.	.	*	.	*	.	.	.	.	.	3	8871
.	.	.	.	*	*	*	.	*	.	.	*	.	.	7	8912
.	.	*	*	*	*	.	.	*	*	.	.	.	.	17	
.	.	.	.	.	.	*	.	.	.	.	*	.	.	5	8938
.	.	.	.	*	*	.	*	.	.	.	.	.	.	29	8950
.	.	.	.	.	*	.	*	.	.	.	.	.	.	24	
.	.	.	.	*	*	.	*	.	.	.	.	.	.	28	
.	.	.	.	.	*	.	*	.	.	.	.	.	.	5	
.	.	.	.	.	.	*	.	.	*	.	.	.	.	8	8968
.	.	*	.	.	.	.	*	.	.	.	.	.	.	4	8975
.	.	.	.	.	*	.	.	.	.	.	*	.	.	2	9170
.	.	.	.	.	.	*	.	.	.	.	*	.	.	9	92(17)
.	.	.	.	.	*	*	.	.	.	.	*	.	.	14	92(23)
.	.	.	.	*	*	.	.	.	.	.	.	*	.	4	9250
.	.	.	.	.	*	.	.	.	.	.	.	*	.	9	
.	.	.	.	.	.	*	.	.	.	.	.	*	.	1	
.	.	.	.	*	.	.	.	.	*	.	.	.	.	1	
.	.	*	*	*	*	.	.	*	*	.	.	.	.	40	( )
.	.	*	*	*	.	.	.	*	.	.	.	.	.	45	9267
.	.	.	.	.	*	*	*	*	.	.	.	.	.	7	9322
.	.	.	.	*	*	*	.	*	.	.	*	.	.	12	93(35)
.	.	.	.	.	*	*	*	*	.	.	.	.	.	18	9533
.	*	*	.	.	.	.	.	*	.	.	.	.	.	16	9691

simple polyhedra (trigonal prisms, tetragonal antiprisms etc.) surrounding the T and/or M elements. Coordination polyhedra so defined are only a crude approximation of the true coordination polyhedra found in a structure. For example, atoms in the centres of the trigonal prisms mostly have more than six close neighbours, the other neighbours capping the rectangular prism faces. For the tricapped trigonal prism the coordination number of the prism centre atom is nine instead of six.

In this study we have frequently given a personal point of view on the crystal chemistry of the R–T–M compounds. Deliberately, we have not examined in detail the coordination of the atoms; instead we have attempted, in an as systematic way as possible, to correlate structures by emphasizing simple structural slabs and columns which are common to a number of different structures. The intergrowth concept, i.e., the interpretation of structures as an intergrowth of different simple structural segments, we found to be the most successful crystal-chemical concept for the understanding of the ternary crystal structures and their compositions.

### Acknowledgement

We would like to thank Dr. K.A. Gschneidner (Ames) and Dr. T. Lundström (Uppsala) for help with the Russian literature. This work would have been impossible without the devoted participation of Birgitta Künzler, who made the complicated drawings, and Ilse Jequier, who typed the difficult manuscript. Furthermore, we would like to thank Dr. Louise Gelato for the great help with the standardization of the crystal structure data and the search for the best representation of the crystal structures using computer plots.

This study was supported by the Swiss National Science Foundation under Contract No. 2.416-0.82.

### Appendix: Atom coordinates for the structure types found in ternary R–T–M compounds

In the following list the atom coordinates of the structure types apply to the R–T–M compounds found in the headings of the text. The types are ordered according to the composition code of the R–T–M compounds (see also table 23).

One should take note that the structural data given here have been standardized (Parthé, E. and L. Gelato, 1983, *Acta Crystallogr.*, in print) and that the unit cell setting, the unit cell origin and/or the numbering of the atoms do not necessarily correspond to the data given in the original papers. However, unit cell axes given in the structure type headings in the text always correspond to the structure description used in this appendix. Footnotes indicate how the original axes and/or atom coordinates have been interchanged and by what amount, if any, the origin has been shifted. For certain structures, to the right of the atom coordinates are given, the numbering of the atoms in the original publication and/or the site occupation in the prototype. To obtain the literature references one is referred to the corresponding pages in the text.

3333 : Ho<sub>6</sub>Co<sub>2</sub>Ga

oI36

Immm

8 Ho 1	in 8(n)	0.2806	0.1836	0	Ho1
8 Ho 2	in 8(m)	0.3032	0	0.3210	Ho3
8 Ho 3	in 8(l)	0	0.1971	0.2332	Ho2
4 Co 1	in 4(j) 1/2	0	0	0.1160	Co2
4 Co 2	in 4(g) 0	0	0.3660	0	Co1
2 Ga 1	in 2(c) 1/2	1/2	1/2	0	Ga1
2 Ga 2	in 2(a) 0	0	0	0	Ga2

Origin shifted by 0 1/2 1/2

33(50) : Sc<sub>4</sub>CoSi (Type Ti<sub>2</sub>Ni)

cF96

Fd3m

48 Sc 1	in 48(f)	0.436	1/8	1/8	Ti 2
32 X	in 32(e)	0.213	0.213	0.213	Ni
16 Sc 2	in 16(c)	0	0	0	Ti 1

X = 1/2Co + 1/2Si

We used the atom positions of Ti<sub>2</sub>Ni.4029 : Er<sub>21</sub>Ni<sub>10</sub>Ga<sub>4</sub>

tI140

I4/mcm

32 Er 1	in 32(m)	0.081	0.211	0.188	Er 2
32 Er 2	in 32(m)	0.210	0.089	0.080	Er 1
16 Ga	in 16(l)	0.166	0.666	0.197	Ga
16 X 1	in 16(l)	0.653	0.153	0.098	X 1
8 X 2	in 8(h)	0.120	0.620	0	X 2
8 Er 3	in 8(h)	0.652	0.152	0	Er 3
8 Er 4	in 8(g)	0	1/2	0.118	Er 4
8 X 3	in 8(f)	0	0	0.130	X 3
4 X 4	in 4(c)	0	0	0	X 5
4 Er 5	in 4(b)	0	1/2	1/4	Er 5
4 X 5	in 4(a)	0	0	1/4	X 4

X = 0.1Ga + 0.9Ni

For idealized formula given X = 1Ni.

4035 : Sm<sub>26</sub>Co<sub>11</sub>Ga<sub>6</sub>

tP86

P4/mbm

16 Sm 1	in 16(l)	0.0731	0.2070	0.1192	Sm 1
16 Sm 2	in 16(l)	0.2083	0.0806	0.3147	Sm 2
8 Co 1	in 8(k)	0.192	0.692	0.180	Co 1
8 Ga 1	in 8(k)	0.662	0.162	0.292	Ga 1
8 Sm 3	in 8(j)	0.0864	0.2121	1/2	Sm 3
4 Ga 2	in 4(h)	0.151	0.651	1/2	Ga 2
4 Sm 4	in 4(g)	0.160	0.660	0	Sm 4
4 Co 2	in 4(g)	0.592	0.092	0	Co 2
4 Sm 5	in 4(f)	0	1/2	0.1635	Sm 6
4 Sm 6	in 4(f)	0	1/2	0.3855	Sm 5
4 Co 3	in 4(e)	0	0	0.226	Co 4
4 Co 4	in 4(e)	0	0	0.411	Co 3
2 Co 5	in 2(a)	0	0	0	Co 5

Origin shifted by 1/2 1/2 0

45(60) : Ce<sub>6</sub>Ni<sub>2</sub>Si<sub>3</sub>

hP22

P63/m

6 X	in	6(h)	.165	.456	1/4	X
6 Ce 1	in	6(h)	.236	.231	1/4	Ce 2
6 Ce 2	in	6(h)	.521	.142	1/4	Ce 1
2 Si	in	2(c)	1/3	2/3	1/4	Si
2 Ni	in	2(b)	0	0	0	Ni

$$X = 1/3\text{Ni} + 2/3\text{Si}$$

x,y,z changed to y,x,-z

50(25) : Er<sub>4</sub>Ni<sub>3</sub>Si (Type CrB)

oC8

Cmcm

4 X	in	4(c)	0	0.06	1/4	B
4 Er	in	4(c)	0	0.354	1/4	Cr

$$X = 3/4\text{Ni} + 1/4\text{Si}$$

Origin shifted by 1/2 1/2 1/2

We used atom positions of CrB.

50(30) : Y<sub>10</sub>Co<sub>7</sub>Ga<sub>3</sub>

oP40

Pnma

4 Y 1	in	4(c)	0.0195	1/4	0.6499	Y 1
4 Y 2	in	4(c)	0.0549	1/4	0.0888	Y 4
4 Co 1	in	4(c)	0.0775	1/4	0.3901	Co 3
4 Y 3	in	4(c)	0.1834	1/4	0.8764	Y 3
4 Y 4	in	4(c)	0.1923	1/4	0.2588	Y 5
4 X 1	in	4(c)	0.2459	1/4	0.5642	X 1
4 Y 5	in	4(c)	0.3546	1/4	0.0584	Y 2
4 Co 2	in	4(c)	0.3549	1/4	0.5654	Co 1
4 Co 3	in	4(c)	0.4000	1/4	0.7866	Co 2
4 X 2	in	4(c)	0.4187	1/4	0.3477	X 2

$$X = 1/4\text{Co} + 3/4\text{Ga}$$

Origin shifted by 0 0 1/2

50(60) : Ce<sub>5</sub>Ni<sub>2</sub>Si<sub>3</sub>

hP40

P63/m

6 Ce 1	in	6(h)	0.0117	0.1795	1/4	Ce 1
6 Si 1	in	6(h)	0.1672	0.5472	1/4	Si 1
6 X 1	in	6(h)	0.2416	0.3333	1/4	X 1
6 X 2	in	6(h)	0.2834	0.5021	1/4	X 2
6 Ce 2	in	6(h)	0.3978	0.2618	1/4	Ce 2
6 Ce 3	in	6(h)	0.4542	0.0671	1/4	Ce 3
2 Ce 4	in	6(d)	2/3	1/3	1/4	Ce 4
2 Ni	in	2(b)	0	0	0	Ni

$$X1 = 0.3\text{Ni} + 0.7\text{Si} \quad X2 = 0.7\text{Ni} + 0.3\text{Si}$$

x,y,z changed to y,x,-z and origin shifted by 0 0 1/2

5067 : Gd<sub>3</sub>NiSi<sub>2</sub>

oP24

Pnma

4	Gd 1	in	4(c)	0.0576	1/4	0.3750	Gd 2
4	Ni	in	4(c)	0.1285	1/4	0.1334	Ni
4	Gd 2	in	4(c)	0.2137	1/4	0.6976	Gd 3
4	Si 1	in	4(c)	0.303	1/4	0.005	Si 2
4	Gd 3	in	4(c)	0.3814	1/4	0.4403	Gd 1
4	Si 2	in	4(c)	0.473	1/4	0.685	Si 1

5071 : Ce<sub>7</sub>Ni<sub>2</sub>Si<sub>5</sub>

oP56

Pnma

4	Ni 1	in	4(c)	0.018	1/4	0.248	Ni 1
4	Ce 1	in	4(c)	0.021	1/4	0.614	Ce 1
4	Ce 2	in	4(c)	0.067	1/4	0.043	Ce 5
4	Si 1	in	4(c)	0.069	1/4	0.385	Si 2
4	Si 2	in	4(c)	0.159	1/4	0.685	Si 5
4	Si 3	in	4(c)	0.187	1/4	0.383	Si 3
4	Ce 3	in	4(c)	0.227	1/4	0.899	Ce 4
4	Ni 2	in	4(c)	0.230	1/4	0.530	Ni 2
4	Ce 4	in	4(c)	0.234	1/4	0.168	Ce 7
4	Si 4	in	4(c)	0.334	1/4	0.532	Si 4
4	Ce 5	in	4(c)	0.366	1/4	0.028	Ce 2
4	Ce 6	in	4(c)	0.384	1/4	0.750	Ce 3
4	Ce 7	in	4(c)	0.396	1/4	0.313	Ce 6
4	Si 5	in	4(c)	0.499	1/4	0.658	Si 1

Origin shifted by 0 1/2 1/2

53(76) : Ce<sub>15</sub>Ni<sub>4</sub>Si<sub>13</sub>

hP64

P63/m

6	Si 1	in	6(h)	0.079	0.285	1/4	Si 1
6	X 1	in	6(h)	0.103	0.477	1/4	X 1
6	Ce 1	in	6(h)	0.143	0.144	1/4	Ce 1
6	X 2	in	6(h)	0.172	0.417	1/4	X 2
6	Si 4	in	6(h)	0.203	0.611	1/4	Si 3
6	Si 5	in	6(h)	0.302	0.422	1/4	Si 2
6	Ce 2	in	6(h)	0.317	0.112	1/4	Ce 2
6	Ce 3	in	6(h)	0.355	0.325	1/4	Ce 4
6	Ce 4	in	6(h)	0.496	0.074	1/4	Ce 3
6	Ce 5	in	6(h)	0.537	0.290	1/4	Ce 5
2	Si 4	in	2(c)	1/3	2/3	1/4	Si 4
2	Ni	in	2(b)	0	0	0	Ni

X = 1/2Ni + 1/2Si for all X

x,y,z changed to y,x,-z and origin shifted by 0 0 1/2

55(53) : Ce14Ni8Si9

mP62

P21/m

2 X 1	in	2(e)	0.0	1/4	0.212	X 2
2 X 2	in	2(e)	0.012	1/4	0.360	X 4
2 Ce 1	in	2(e)	0.041	1/4	0.928	Ce14
2 X 3	in	2(e)	0.076	1/4	0.125	X 3
2 Ce 2	in	2(e)	0.077	1/4	0.712	Ce13
2 X 4	in	2(e)	0.139	1/4	0.430	X 8
2 X 5	in	2(e)	0.170	1/4	0.565	X 9
2 X 6	in	2(e)	0.183	1/4	0.203	X 6
2 X 7	in	2(e)	0.222	1/4	0.360	X 7
2 Ce 3	in	2(e)	0.236	1/4	0.931	Ce12
2 X 8	in	2(e)	0.270	1/4	0.134	X 5
2 X 9	in	2(e)	0.278	1/4	0.645	X 15
2 X 10	in	2(e)	0.316	1/4	0.780	X 16
2 X 11	in	2(e)	0.323	1/4	0.430	X 13
2 X 12	in	2(e)	0.362	1/4	0.569	X 14
2 Ce 4	in	2(e)	0.424	1/4	0.289	Ce 8
2 Ce 5	in	2(e)	0.443	1/4	0.925	Ce11
2 X 13	in	2(e)	0.470	1/4	0.639	X 12
2 X 14	in	2(e)	0.477	1/4	0.124	X 10
2 X 15	in	2(e)	0.508	1/4	0.780	X 11
2 Ce 6	in	2(e)	0.572	1/4	0.509	Ce 9
2 Ce 7	in	2(e)	0.602	1/4	0.281	Ce10
2 Ce 8	in	2(e)	0.639	1/4	0.926	Ce 4
2 X 16	in	2(e)	0.675	1/4	0.123	X 17
2 Ce 9	in	2(e)	0.717	1/4	0.724	Ce 5
2 Ce10	in	2(e)	0.750	1/4	0.501	Ce 6
2 Ce11	in	2(e)	0.781	1/4	0.273	Ce 7
2 Ce12	in	2(e)	0.844	1/4	0.926	Ce 1
2 X 17	in	2(e)	0.863	1/4	0.137	X 1
2 Ce13	in	2(e)	0.899	1/4	0.717	Ce 2
2 Ce14	in	2(e)	0.929	1/4	0.495	Ce 3

$$X = 1/2Ni + 1/2Si$$

Axes changed to a-cb . Rounded values for atom positions.

5565 : Pr<sub>14</sub>Ni<sub>6</sub>Si<sub>11</sub>

mC124

C2/m

4	Pr 1	in	4(i)	0.0050	0	0.1827
4	Ni 1	in	4(i)	0.0325	0	0.4209
4	Si 1	in	4(i)	0.0440	0	0.621
4	Si 2	in	4(i)	0.0683	0	0.345
4	Si 3	in	4(i)	0.0741	0	0.534
4	Pr 2	in	4(i)	0.1059	0	0.7831
4	Pr 3	in	4(i)	0.1135	0	0.1461
4	Ni 2	in	4(i)	0.1449	0	0.3856
4	Ni 3	in	4(i)	0.1501	0	0.5832
4	Si 4	in	4(i)	0.1812	0	0.3050
4	Si 5	in	4(i)	0.1850	0	0.707
4	Si 6	in	4(i)	0.1879	0	0.5105
4	Si 7	in	4(i)	0.1915	0	0.111
4	Pr 4	in	4(i)	0.2857	0	0.3738
4	Pr 5	in	4(i)	0.2889	0	0.5749
4	Pr 6	in	4(i)	0.2902	0	0.1765
4	Ni 4	in	4(i)	0.3563	0	0.1152
4	Pr 7	in	4(i)	0.3857	0	0.3537
4	Pr 8	in	4(i)	0.3910	0	0.5375
4	Si 8	in	4(i)	0.4328	0	0.155
4	Ni 5	in	4(i)	0.4673	0	0.0793
4	Pr 9	in	4(i)	0.4959	0	0.3187
4	Si 9	in	4(i)	0.5457	0	0.125
4	Si10	in	4(i)	0.5737	0	0.034
4	Pr10	in	4(i)	0.6083	0	0.2838
4	Ni 6	in	4(i)	0.6509	0	0.0855
4	Pr11	in	4(i)	0.7107	0	0.2280
4	Pr12	in	4(i)	0.7117	0	0.0233
4	Si11	in	4(i)	0.8142	0	0.089
4	Pr13	in	4(i)	0.8914	0	0.0377
2	Pr14	in	2(d)	0	1/2	1/2
2	Pr15	in	2(a)	0	0	0

5725 : Y<sub>3</sub>Co<sub>3</sub>Ga ( related to W<sub>3</sub>CoB<sub>3</sub> type)

oC28

Cmcm

8	Y 1	in	8(f)	0	0.2890	0.1041	W
8	Co 1	in	8(f)	0	0.5714	0.0886	B
4	Y 2	in	4(c)	0	0.0017	1/4	W
4	Co 2	in	4(c)	0	0.6912	1/4	B
4	Ga	in	4(a)	0	0	0	Co

57(75) : Y<sub>3</sub>NiSi<sub>3</sub>

oI14

Immm

4	Y 1	in	4(j)	1/2	0	0.18307	Y 2
4	Si	in	4(j)	1/2	0	0.35990	Si
4	X	in	4(i)	0	0	0.4349	X
2	Y 2	in	2(a)	0	0	0	Y 1

$$X = 1/2\text{Ni} + 1/2\text{Si}$$

6033 : Pr<sub>2</sub>Ni<sub>2</sub>Al ( related to W<sub>2</sub>CoB<sub>2</sub> type)

oI10

Immm

4	Pr	in	4(j)	1/2	0	0.300	W
4	Ni	in	4(h)	0	0.224	1/2	B
2	Al	in	2(a)	0	0	0	Co

Axes changed to cab

60(33) : Er<sub>2</sub>Pd<sub>2</sub>Si

oP20

Pnnm

4	X	1	in	4(g)	0.164	0.5325	0
4	X	2	in	4(g)	0.167	0.0168	0
4	Pd	in	4(g)	0.172	0.2262	0	0
4	Er	1	in	4(g)	0.4590	0.3723	0
4	Er	2	in	4(g)	0.5462	0.1264	0

$$X1 = 0.58Pd + 0.42Si$$

$$X2 = 0.57Pd + 0.43Si$$

6067 : Sc<sub>2</sub>CoSi<sub>2</sub>

mC20

C2/m

4	Sc	1	in	4(i)	0.0016	0	0.3266
4	Sc	2	in	4(i)	0.1869	0	0.1030
4	Co	in	4(i)	0.2752	0	0.6278	
4	Si	1	in	4(i)	0.3560	0	0.4316
4	Si	2	in	4(i)	0.4868	0	0.1259

Axes changed to -ac(a+b) and origin shifted by 0 1/2 0

6360 : Sc<sub>3</sub>Co<sub>2</sub>Si<sub>3</sub> ( Type Hf<sub>3</sub>Ni<sub>2</sub>Si<sub>3</sub>)

oC32

Cmcm

8	Sc	1	in	8(f)	0	0.0781	0.1149
8	Co	1	in	8(f)	0	0.2119	0.5845
8	Si	1	in	8(f)	0	0.3860	0.0384
4	Sc	2	in	4(c)	0	0.3589	1/4
4	Si	2	in	4(c)	0	0.6618	1/4

Origin shifted by 0 1/2 1/2



6360 : Sc<sub>3</sub>Re<sub>2</sub>Si<sub>3</sub>

mC64

C2

4	Re 1	in	4(c)	0.0238	0.017	0.1654	Re 1
4	Re 2	in	4(c)	0.0257	0.250	0.6752	Re 2
4	Si 1	in	4(c)	0.119	0.253	0.374	Si 1
4	Sc 1	in	4(c)	0.1219	0.512	0.2092	Sc 1
4	Sc 2	in	4(c)	0.1587	0.285	0.6019	Sc 3
4	Sc 3	in	4(c)	0.1705	0.029	0.1255	Sc 5
4	Si 2	in	4(c)	0.225	0.532	0.131	Si 4
4	Re 3	in	4(c)	0.2631	0.060	0.5322	Re 4
4	Re 4	in	4(c)	0.2634	0.243	0.0320	Re 3
4	Si 3	in	4(c)	0.268	0.284	0.347	Si 2
4	Sc 4	in	4(c)	0.3812	0.266	0.3113	Sc 2
4	Si 4	in	4(c)	0.396	0.508	0.135	Si 3
4	Sc 5	in	4(c)	0.4215	0.008	0.0916	Sc 6
4	Sc 6	in	4(c)	0.5807	0.247	0.3987	Sc 4
2	Si 5	in	2(b)	0	0.001	1/2	Si 8
2	Si 6	in	2(b)	0	0.500	1/2	Si 7
2	Si 7	in	2(a)	0	0.242	0.0	Si 6
2	Si 8	in	2(a)	0	0.781	0.0	Si 5

Axes changed to a-cb and origin shifted by 0 0.255 0

6725 : Sc<sub>2</sub>Co<sub>3</sub>Si ( Type Mg<sub>2</sub>Cu<sub>3</sub>Si ; ternary Laves phase)

hP12

P63/mmc

6	Co	in	6(h)	1/6	1/3	1/4	
4	Sc	in	4(f)	1/3	2/3	9/16	
2	Si	in	2(a)	0	0	0	

Idealized point positions.

6733 : La<sub>3</sub>Ni<sub>4</sub>Ga<sub>2</sub>

mC18

C2/m

4	Ni 1	in	4(i)	0.0856	0.	0.1401	Ni 2
4	Ni 2	in	4(i)	0.2605	0	0.4157	Ni 1
4	La 1	in	4(i)	0.3761	0	0.121	La 2
4	Ga	in	4(i)	0.6787	0	0.286	Ga
2	La 2	in	2(c)	0	0	1/2	La 1

Axes changed to a-cb and origin shifted by 0 0 1/2

6750 : CeFeSi ( Type PbFC1)

tP6

P4/nmm

2	Si	in	2(c)	1/4	1/4	0.175	Pb
2	Ce	in	2(c)	1/4	1/4	0.672	Cl
2	Fe	in	2(a)	3/4	1/4	0	F

6750 : ScRuGe ( Type ZrNiAl)  
 hP9  
 P-62m

3 Ru	in	3(g)	0.2535	0	1/2	Al
3 Sc	in	3(f)	0.599	0	0	Zr
2 Ge 1	in	2(d)	1/3	2/3	1/2	Ni
1 Ge 2	in	1(a)	0	0	0	Ni

6750 : ScRhSi ( Type TiNiSi)  
 oP12  
 Pnma

4 Sc	in	4(c)	0.0094	1/4	0.6893	Ti
4 Rh	in	4(c)	0.1568	1/4	0.0620	Ni
4 Si	in	4(c)	0.2857	1/4	0.3851	Si

6750 : LaPtSi  
 tI12  
 I41md

4 Si	in	4(a)	0	0	0.0
4 Pt	in	4(a)	0	0	0.1660
4 La	in	4(a)	0	0	0.581

Origin shifted by 0 0 0.419

6750 : LaIrSi ( ZrOS-type )  
 cP12  
 P213

4 Ir	in	4(a)	0.0770	0.0770	0.0770	0
4 La	in	4(a)	0.3675	0.3675	0.3675	Zr
4 Si	in	4(a)	0.661	0.661	0.661	S

x,y,z changed to -x,-y,-z and origin shifted by 1/2 1/2 1/2

67(50) : Pr(Pt0.5Ge0.5)2 ( Type CeCu2)  
 oI12  
 Imma

8 X	in	8(h)	0	0.0449	0.1666
4 Pr	in	4(e)	0	1/4	0.5417

$$X = 1/2Pt + 1/2Ge$$

67(50) : Sc(Ni0.5Al0.5)2 ( Type MgZn2 ; Laves phase)  
 hP12  
 P63/mmc

6 X 1	in	6(h)	1/6	1/3	1/4	X 2
4 Sc	in	4(f)	1/3	2/3	9/16	Sc
2 X 2	in	2(a)	0	0	0	X 1

$$X = 1/2Ni + 1/2Al$$

Origin shifted by 0 0 1/2

67(50) :  $\text{Y}(\text{Mn}_{0.5}\text{Ga}_{0.5})_2$  (TiFeSi-type with partial disorder)

oI36

Ima2

8 X	1	in	8(c)	0.003	0.326	0.020	X	3
8 X	2	in	8(c)	0.006	0.620	0.342	X	1
4 X	3	in	4(b)	1/4	0.001	0.000	X	4
4 Y	1	in	4(b)	1/4	0.200	0.245	Y	2
4 Y	2	in	4(b)	1/4	0.501	0.045	Y	3
4 Y	3	in	4(b)	1/4	0.810	0.196	Y	1
4 X	4	in	4(a)	0	0	0.223	X	2

$$X = 1/2\text{Mn} + 1/2\text{Ga}$$

$x, y, z$  changed to  $-x, y, -z$  and origin shifted by 0 0 0.477

6775 :  $\text{Sc}_2\text{RuAl}_3$  (Type  $\text{Mg}_2\text{Cu}_3\text{Si}$ ; ternary Laves phase)

hP12

P63/mmc

6 Al		in	6(h)	1/6	1/3	1/4	Cu
4 Sc		in	4(f)	1/3	2/3	9/16	Mg
2 Ru		in	2(a)	0	0	0	Si

Origin shifted by 0 0 1/2. Idealized point positions

67(75) :  $\text{Ce}(\text{Ni}, \text{Si})_2$  (Type AlB<sub>2</sub>)

hP3

P6/mmm

2 X		in	2(d)	1/3	2/3	1/2
1 Ce		in	1(a)	0	0	0

$$X = 1/4\text{Ni} + 3/4\text{Si}$$

67(83) :  $\text{Sm}(\text{Mn}_{0.17}\text{Ga}_{0.83})_2$  (Type  $\text{CaIn}_2$ )

hP6

P63/mmc

4 X		in	4(f)	1/3	2/3	0.205
2 Sm		in	2(b)	0	0	1/4

$$X = 0.17\text{Mn} + 0.83\text{Ga}$$

Atom positions of  $\text{CaIn}_2$ .

67(88) :  $\text{Sc}_4\text{CoSi}_7$  (Type  $\text{ZrSi}_2$  but with partial disorder)

oC12

Cmcm

4 X		in	4(c)	0	0.055	1/4
4 Sc		in	4(c)	0	0.396	1/4
4 Si		in	4(c)	0	0.755	1/4

$$X = 1/4\text{Co} + 3/4\text{Si}$$

Origin shifted by 0 1/2 1/2

7325 : Ce<sub>3</sub>Ni<sub>6</sub>Si<sub>2</sub>

cI44

Im $\bar{3}$ m

24 Ni	in 24(h)	0	0.330	0.330
12 Ce	in 12(e)	0.280	0	0
8 Si	in 8(c)	1/4	1/4	1/4

7350 : Sc<sub>3</sub>Ni<sub>4</sub>Ge<sub>4</sub> ( Gd<sub>3</sub>Cu<sub>4</sub>Ge<sub>4</sub>- or Sr<sub>3</sub>Li<sub>4</sub>Sb<sub>4</sub>-type )

oI22

Immm

8 Ni	in 8(l)	0	0.3040	0.3231	Ni	Cu
4 Sc 1	in 4(j)	1/2	0	0.3734	Sc 2	Gd
4 Ge 1	in 4(i)	0	0	0.2189	Ge 1	Ge
4 Ge 2	in 4(h)	0	0.1941	1/2	Ge 2	Ge
2 Sc 2	in 2(a)	0	0	0	Sc 1	Gd

Axes changed to -cba and origin shifted by 0 1/2 0

7350 : La<sub>3</sub>Rh<sub>4</sub>Ge<sub>4</sub> ( Type U<sub>3</sub>Ni<sub>4</sub>Si<sub>4</sub> )

oI22

Immm

4 Rh 1	in 4(j)	1/2	0	0.10010
4 Ge 1	in 4(j)	1/2	0	0.1984
4 La 1	in 4(j)	1/2	0	0.35455
4 Rh 2	in 4(i)	0	0	0.24976
4 Ge 2	in 4(i)	0	0	0.4502
2 La 2	in 2(a)	0	0	0

7364 : Sc<sub>4</sub>Mn<sub>4</sub>Si<sub>7</sub> ( Type Zr<sub>4</sub>Co<sub>4</sub>Ge<sub>7</sub> )

tI60

I4/mmm

16 Mn	in 16(k)	0.150	0.650	1/4	Mn
8 Si 1	in 8(j)	0.215	1/2	0	Si 2
8 Sc 1	in 8(i)	0.194	0	0	Sc 1
8 Si 2	in 8(i)	0.408	0	0	Si 1
8 Si 3	in 8(h)	0.204	0.204	0	Si 3
8 Sc 2	in 8(h)	0.363	0.363	0	Sc 1
4 Si 4	in 4(e)	0	0	0.250	Si 4

Error in published position of Si(2)  
Origin shifted by 0 0 1/2

7388 : Y3ReB7

oC44

Cmcm

8 B	1	in	8(f)	0	0.025	0.075	B	2
8 B	2	in	8(f)	0	0.085	0.575	B	1
8 B	3	in	8(f)	0	0.135	0.110	B	3
8 Y	1	in	8(f)	0	0.300	0.061	Y	1
4 Y	2	in	4(c)	0	0.460	1/4	Y	2
4 Re		in	4(c)	0	0.648	1/4	Re	
4 B	4	in	4(c)	0	0.850	1/4	B	4

Origin shifted by 0 1/2 0

7471 : Sc5Co4Si10

tP38

P4/mbm

8 Si	1	in	8(j)	0.1638	0.0031	1/2	Si	3
8 Si	2	in	8(i)	0.1575	0.1985	0	Si	2
8 Co		in	8(i)	0.2460	0.0240	0	Co	
4 Sc	1	in	4(h)	0.1756	0.6756	1/2	Sc	2
4 Sc	2	in	4(h)	0.6118	0.1118	1/2	Sc	3
4 Si	3	in	4(g)	0.0679	0.5679	0	Si	1
2 Sc	3	in	2(a)	0	0	0	Sc	1

7511 : Ce3Co8Si

hP24

P63/mmc

12 Co	1	in	12(k)	0.167	0.334	0.127	Co	1
4 Ce	1	in	4(f)	1/3	2/3	0.5418	Ce	2
2 Co	2	in	2(d)	1/3	2/3	3/4	Co	3
2 Ce	2	in	2(c)	1/3	2/3	1/4	Ce	1
2 Co	3	in	2(b)	0	0	1/4	Co	2
2 Si		in	2(a)	0	0	0	Si	

Atom positions of CeNi3; the ordering has been tested.

Origin shifted by 0 0 1/2

7522 : Dy3Ni7B2

hP24

P63/mmc

12 Ni	1	in	12(k)	0.161	0.322	0.149	Ni	2
4 Dy	1	in	4(f)	1/3	2/3	0.529	Dy	2
2 Dy	2	in	2(d)	1/3	2/3	3/4	Dy	1
2 B	1	in	2(c)	1/3	2/3	1/4	B	2
2 B	2	in	2(b)	0	0	1/4	B	1
2 Ni	2	in	2(a)	0	0	0	Ni	1

Origin shifted by 0 0 1/2

7533 : PrCo<sub>2</sub>Ga

oP8

Pmma

2 Ga	in	2(f)	1/4	1/2	0.108
2 Pr	in	2(f)	1/4	1/2	0.683
2 Co 1	in	2(e)	1/4	0	0.315
2 Co 2	in	2(a)	0	0	0

Origin shifted by 1/2 1/2 0

7533 : YPd<sub>2</sub>Si

oP16

Pnma

8 Pd	in	8(d)	0.1767	0.0517	0.0928
4 Y	in	4(e)	0.0303	1/4	0.644
4 Si	in	4(e)	0.362	1/4	0.353

Origin shifted by 0 0 1/2

7533 : YPd<sub>2</sub>Sn ( Type MnCu<sub>2</sub>Al)

cF16

Fm $\bar{3}$ m

8 Pd	in	8(c)	1/4	1/4	1/4	Cu
4 Sn	in	4(b)	1/2	1/2	1/2	Mn
4 Y	in	4(a)	0	0	0	Al

7567 : ScRhSi<sub>2</sub>

oP16

Pnma

4 Rh	in	4(c)	0.0832	1/4	0.5992
4 Si 1	in	4(c)	0.2318	1/4	0.0282
4 Sc	in	4(c)	0.2385	1/4	0.3181
4 Si 2	in	4(c)	0.4573	1/4	0.6587

7567 : LuRuB<sub>2</sub>

oP16

Pnma

8 B	in	8(d)	0.358	0.084	0.464
4 Lu	in	4(c)	0.0105	1/4	0.6648
4 Ru	in	4(c)	0.1816	1/4	0.1824

Origin shifted by 0 0 1/2

7567 : CeNiSi<sub>2</sub>  
 oC16  
 Cmcm  
 4 Si 1 in 4(c) 0 0.043 1/4  
 4 Ni in 4(c) 0 0.1842 1/4  
 4 Ce in 4(c) 0 0.3930 1/4  
 4 Si 2 in 4(c) 0 0.7508 1/4

Origin shifted by 0 1/2 1/2

7567 : TbFeSi<sub>2</sub> (Site exchange variant of the CeNiSi<sub>2</sub> Type)  
 oC16  
 Cmcm  
 4 Si 1 in 4(c) 0 0.0459 1/4  
 4 Si 2 in 4(c) 0 0.1872 1/4  
 4 Tb in 4(c) 0 0.3955 1/4  
 4 Fe in 4(c) 0 0.7514 1/4

Origin shifted by 0 1/2 1/2

7567 : NdNiGa<sub>2</sub>  
 oC16  
 Cmmm  
 4 Nd in 4(j) 0 0.364 1/2  
 4 Ni in 4(i) 0 0.084 0  
 4 Ga 1 in 4(i) 0 0.212 0  
 2 Ga 2 in 2(d) 0 0 1/2  
 2 Ga 3 in 2(b) 1/2 0 0

Origin shifted by 0 1/2 1/2

7567 : YNiAl<sub>2</sub> ( Type MgCuAl<sub>2</sub>)  
 oC16  
 Cmcm  
 8 Al in 8(f) 0 0.152 0.044 Al  
 4 Y in 4(c) 0 0.439 1/4 Mg  
 4 Ni in 4(c) 0 0.713 1/4 Cu

Origin shifted by 0 1/2 1/2

7567 : ScMnSi<sub>2</sub> ( Type TiMnSi<sub>2</sub>)  
 oP48  
 Pbam

8 Mn	in	8(i)	0.0849	0.2536	0.2476	Mn 1
8 Sc	in	8(i)	0.3289	0.0468	0.2404	Ti 1
8 Si	in	8(i)	0.3325	0.3177	0.3479	Si 1
4 Si	in	4(h)	0.0371	0.3773	1/2	Si 2
4 Si	in	4(h)	0.1270	0.0967	1/2	Si 3
4 Si	in	4(g)	0.0379	0.3803	0	Si 4
4 Si	in	4(g)	0.1307	0.1040	0	Si 5
4 Sc	in	4(g)	0.3320	0.3204	0	Ti 2
4 Mn	in	4(e)	0	0	0.2425	Mn 2

We used the atom positions of TiMnSi<sub>2</sub>.

7567 : ScFeSi<sub>2</sub> ( ZrFeSi<sub>2</sub>-type )  
 oC96  
 Cmca

8 Fe 1	in	8(f)	0	0.0411	0.1230	Fe 2
8 Sc 1	in	8(f)	0	0.1231	0.4152	Sc 3
8 Si 1	in	8(f)	0	0.1397	0.0068	Si 5
8 Sc 2	in	8(f)	0	0.2042	0.1802	Sc 1
8 Si 2	in	8(f)	0	0.2635	0.3567	Si 4
8 Si 3	in	8(f)	0	0.3338	0.0998	Si 1
8 Si 4	in	8(f)	0	0.4127	0.3568	Si 2
8 Sc 3	in	8(f)	0	0.4677	0.1777	Sc 2
8 Si 5	in	8(e)	1/4	0.0866	1/4	Si 6
8 Fe 2	in	8(e)	1/4	0.3383	1/4	Fe 1
8 Si 6	in	8(d)	0.256	0	0	Si 3
8 Fe 3	in	8(c)	1/4	1/4	0	Fe 3

Origin shifted by 0 1/2 1/2

7578 : La<sub>3</sub>Co<sub>2</sub>Sn<sub>7</sub>  
 oC24  
 Cmmm

4 Sn 1	in	4(j)	0	0.0905	1/2	Sn 2
4 La 1	in	4(j)	0	0.3155	1/2	La 2
4 Co	in	4(i)	0	0.1283	0	Co
4 Sn 2	in	4(i)	0	0.2178	0	Sn 4
4 Sn 3	in	4(i)	0	0.4093	0	Sn 3
2 Sn 4	in	2(c)	1/2	0	1/2	Sn 1
2 La 2	in	2(a)	0	0	0	La 1

Origin shifted by 0 1/2 1/2

Error in published position of La 1



75(83) : Y<sub>2</sub>MnGa<sub>5</sub> ( Type Cu<sub>3</sub>Au)

cP4

Pm $\bar{3}$ m

3 X	in	3(c)	0	1/2	1/2	Cu
1 Y	in	1(a)	0	0	0	Au

X = 1/6Mn + 5/6Ga

7646 : Sc<sub>4</sub>Rh<sub>7</sub>Ge<sub>6</sub> ( Type U<sub>4</sub>Re<sub>7</sub>Si<sub>6</sub>)

cI34

Im $\bar{3}$ m

12 Ge	in	12(e)	0.3128	0	0
12 Rh 1	in	12(d)	1/4	0	1/2
8 Sc	in	8(c)	1/4	1/4	1/4
2 Rh 2	in	2(a)	0	0	0

7780 : Ce<sub>3</sub>Ni<sub>2</sub>Si<sub>8</sub>

oC26

Cmmm

4 Si 1	in	4(j)	0	0.0941	1/2	Si 3
4 Ce 1	in	4(j)	0	0.3162	1/2	Ce 2
4 Si 2	in	4(j)	0	0.4534	1/2	Si 4
4 Ni	in	4(i)	0	0.1335	0	Ni
4 Si 3	in	4(i)	0	0.2240	0	Si 2
4 Si 4	in	4(i)	0	0.4077	0	Si 1
2 Ce 2	in	2(a)	0	0	0	Ce 1

7829 : Ce<sub>2</sub>Co<sub>5</sub>B<sub>2</sub>

hP36

P6 $\bar{3}$ /mmc

12 Co 1	in	12(k)	0.176	0.352	0.103	Co 3
6 Co 2	in	6(h)	0.189	0.378	1/4	Co 2
4 B 1	in	4(f)	1/3	2/3	0.177	B 2
4 Ce 1	in	4(f)	1/3	2/3	0.522	Ce 1
4 Ce 2	in	4(f)	1/3	2/3	0.670	Ce 2
4 B 2	in	4(e)	0	0	0.177	B 1
2 Co 3	in	2(a)	0	0	0	Co 1

Origin shifted by 0 0 1/2

7857 : Sc<sub>2</sub>Re<sub>3</sub>Si<sub>4</sub>

tP36

P41212

8 Sc	in	8(b)	0.003	0.350	0.2230	Sc
8 Re 1	in	8(b)	0.186	0.019	0.3851	Re 1
8 Si 1	in	8(b)	0.290	0.008	0.199	Si 2
8 Si 2	in	8(b)	0.329	0.288	0.301	Si 1
4 Re 2	in	4(a)	0.168	0.168	0	Re 2

Origin shifted by 1/2 1/2 1/2

7886 : Y2ReB6

oP36

Pbam

4	Re	in	4(h)	0.138	0.178	1/2	Re	
4	Y	1	in	4(h)	0.323	0.413	1/2	Y
4	Y	2	in	4(h)	0.445	0.131	1/2	Y
4	B	1	in	4(g)	0.050	0.060	0	B
4	B	2	in	4(g)	0.110	0.470	0	B
4	B	3	in	4(g)	0.140	0.310	0	B
4	B	4	in	4(g)	1/4	0.075	0	B
4	B	5	in	4(g)	0.300	0.240	0	B
4	B	6	in	4(g)	0.480	0.290	0	B

Origin shifted by 0 0 1/2

7930 : Sc6Ni16Si7 ( Type Mg6Cu16Si7)

cF116

Fm3m

32	Ni	1	in	32(f)	0.1230	0.1230	0.1230	Cu
32	Ni	2	in	32(f)	0.3316	0.3316	0.3316	Cu
24	Sc		in	24(e)	0.3176	0	0	Mg
24	Si	1	in	24(d)	0	1/4	1/4	Si
4	Si	2	in	4(b)	0	0	0	Si

Origin shifted by 1/2 1/2 1/2

We used the atom positions of Mg6Cu16Si7

7970 : Sc6Ni7Al16 ( Type Mg6Cu16Si7)

cF116

Fm3m

32	Al		in	32(f)	0.1230	0.1230	0.1230	Cu
32	Al		in	32(f)	0.3316	0.3316	0.3316	Cu
24	Sc		in	24(e)	0.3176	0	0	Mg
24	Ni		in	24(d)	0	1/4	1/4	Si
4	Ni		in	4(b)	0	0	0	Si

Origin shifted by 1/2 1/2 1/2

We used the atom positions of Mg6Cu16Si7

79(82) : Ho3Ni2Ga9

oI28

Immm

8	Ga	1	in	8(1)	0	0.271	0.169	Ga
8	X		in	8(1)	0	0.364	0.350	X
4	Ho	1	in	4(i)	0	0	0.315	Ho
4	Ga	2	in	4(h)	0	0.228	1/2	Ga
2	Ga	3	in	2(d)	1/2	0	1/2	Ga
2	Ho	2	in	2(a)	0	0	0	Ho

$$X = 0.54\text{Ga} + 0.46\text{Ni}$$

Axes changed to a-cb

For idealized formula given  $X = 1/2\text{Ga} + 1/2\text{Ni}$

8025 : LaPd3B ( Type CaTiO3)

cP5

Pm3m

3 Pd	in	3(c)	1/2	0	0	0
1 La	in	1(b)	1/2	1/2	1/2	Ca
1 B	in	1(a)	0	0	0	Ti

Origin shifted by 1/2 1/2 1/2

8050 : CeNi2Si2 ( Type ThCr2Si2)

tI10

I4/mmm

4 Si	in	4(e)	0	0	0.350
4 Ni	in	4(d)	0	1/2	1/4
2 Ce	in	2(a)	0	0	0

8050 : LaIr2Si2 h.t. ( CaBe2Ge2-type )

tP10

P4/nmm

2 Si 1	in	2(c)	1/4	1/4	0.1262
2 Ir 1	in	2(e)	1/4	1/4	0.3745
2 La	in	2(c)	1/4	1/4	0.7447
2 Si 2	in	2(b)	3/4	1/4	1/2
2 Ir 2	in	2(a)	3/4	1/4	0

8050 : ScFe2Si2 ( Type HfFe2Si2)

oP20

Pbcm

4 Si 1	in	4(d)	0.0830	0.0510	1/4
4 Sc	in	4(d)	0.2518	0.4019	1/4
4 Fe 1	in	4(d)	0.3824	0.0105	1/4
4 Si 2	in	4(c)	0.5507	1/4	0
4 Fe 2	in	4(c)	0.8827	1/4	0

Origin shifted by 1/2 1/2 1/2

8050 : LaRe2Si2

oI20

Imma

4 Re 1	in	4(e)	0	1/4	0.0371	Re 2
4 Si 1	in	4(e)	0	1/4	0.284	Si 2
4 Si 2	in	4(e)	0	1/4	0.394	Si 1
4 Re 2	in	4(e)	0	1/4	0.5381	Re 1
4 La	in	4(e)	0	1/4	0.835	La

Axes changed to ba-c and origin shifted by 3/4 1/4 3/4

8063 : Sc<sub>2</sub>Fe<sub>3</sub>Si<sub>5</sub>

tP40

P4/mnc

8	Si 1	in	8(h)	0.0239	0.3201	0	Si 3
8	Fe 1	in	8(h)	0.1399	0.1210	0	Fe 1
8	Sc	in	8(h)	0.25	0.4299	0	Sc
8	Si 2	in	8(g)	0.1779	0.6779	1/4	Si 1
4	Si 3	in	4(e)	0	0	0.2472	Si 2
4	Fe 2	in	4(d)	0	1/2	1/4	Fe 2

Origin shifted by 0 0 1/2

8063 : Sc<sub>2</sub>Co<sub>3</sub>Si<sub>5</sub> ( Type U<sub>2</sub>Co<sub>3</sub>Si<sub>5</sub> )

oI40

Ibam

8	Co 1	in	8(j)	0.1150	0.1374	0	Co 2
8	Sc	in	8(j)	0.2668	0.3672	0	U
8	Si 1	in	8(j)	0.3467	0.1073	0	Si 3
8	Si 2	in	8(g)	0	0.2747	1/4	Si 2
4	Co 2	in	4(b)	1/2	0	1/4	Co 1
4	Si 3	in	4(a)	0	0	1/4	Si 1

Origin shifted by 0 1/2 1/2

We used the atom positions of U<sub>2</sub>Co<sub>3</sub>Si<sub>5</sub>.8075 : ScNiSi<sub>3</sub>

oC20

Amm2

2	Sc 1	in	2(b)	1/2	0	0.1129	Sc 2
2	Si 1	in	2(b)	1/2	0	0.3856	Si 4
2	Si 2	in	2(b)	1/2	0	0.5016	Si 3
2	Sc 2	in	2(b)	1/2	0	0.7750	Sc 1
2	Si 3	in	2(a)	0	0	0.0000	Si 6
2	Si 4	in	2(a)	0	0	0.2245	Si 2
2	Ni 1	in	2(a)	0	0	0.3273	Ni 2
2	Ni 2	in	2(a)	0	0	0.5502	Ni 1
2	Si 5	in	2(a)	0	0	0.6601	Si 1
2	Si 6	in	2(a)	0	0	0.8862	Si 5

x,y,z changed to -x,y,-z and origin shifted by 1/2 0 0.062

8075 : LaIrSi<sub>3</sub> ( BaNiSn<sub>3</sub>-type )

tI10

I4mm

4	Si 1	in	4(b)	0	1/2	0.1088	
2	Ir	in	2(a)	0	0	0.0	
2	La	in	2(a)	0	0	0.3455	
2	Si 2	in	2(a)	0	0	0.7599	

80(75) : PrNiGa<sub>3</sub>

tI10

I4/mmm

4 X	in	4(e)	0	0	0.389
4 Ga	in	4(d)	0	1/2	1/4
2 Pr	in	2(a)	0	0	0

Idealized formula for X = 1/2Ni + 1/2Ga

Structure refinement for X = 1/4Ni + 3/4Ga

8244 : Sc<sub>2</sub>Ru<sub>5</sub>B<sub>4</sub>

mP22

P2/m

2 B 1	in	2(n)	0.0340	1/2	0.4097	B 4
2 B 2	in	2(n)	0.1538	1/2	0.0989	B 3
2 Sc 1	in	2(n)	0.1582	1/2	0.8187	Sc 1
2 Sc 2	in	2(n)	0.3423	1/2	0.3186	Sc 2
2 B 3	in	2(n)	0.3493	1/2	0.6030	B 1
2 B 4	in	2(n)	0.5315	1/2	0.0893	B 2
2 Ru 1	in	2(m)	0.0960	0	0.2614	Ru 4
2 Ru 2	in	2(m)	0.1606	0	0.5477	Ru 1
2 Ru 3	in	2(m)	0.3397	0	0.0474	Ru 2
2 Ru 4	in	2(m)	0.5956	0	0.2381	Ru 3
1 Ru 5	in	1(g)	1/2	0	1/2	Ru 5
1 Ru 6	in	1(a)	0	0	0	Ru 6

Axes changed to bca and origin shifted by 0 0 1/2

8256 : Sc<sub>2</sub>Cr<sub>4</sub>Si<sub>5</sub> ( Type Nb<sub>2</sub>Cr<sub>4</sub>Si<sub>5</sub>)

oI44

Ibam

8 Si 1	in	8(j)	0.0777	0.4362	0	Si 2
8 Si 2	in	8(j)	0.2053	0.2112	0	Si 1
8 Cr 1	in	8(j)	0.2540	0.0620	0	Cr 1
8 Sc	in	8(j)	0.3819	0.3579	0	Sc
8 Cr 2	in	8(g)	0	0.3093	1/4	Cr 2
4 Si 3	in	4(a)	0	0	1/4	Si 3

Origin shifted by 0 0 1/2

8275 : Ho6Co7Ga21

tP68

P4/mbm

8 Ga 1	in	8(j)	0.0464	0.2738	1/2	Ga 7
8 Ga 2	in	8(j)	0.2072	0.1829	1/2	Ga 6
8 Ga 3	in	8(j)	0.3527	0.0376	1/2	Ga 5
8 Co 1	in	8(i)	0.0388	0.3512	0	Co 2
8 Ho 1	in	8(i)	0.0867	0.1565	0	Ho 2
8 Ga 4	in	8(i)	0.2557	0.0743	0	Ga 4
4 Ho 2	in	4(h)	0.1090	0.6090	1/2	Ho 1
4 Ga 5	in	4(h)	0.5730	0.0730	1/2	Ga 3
4 Co 2	in	4(g)	0.2200	0.7200	0	Co 1
4 Ga 6	in	4(g)	0.6800	0.1800	0	Ga 2
2 Ga 7	in	2(d)	0	1/2	0	Ga 1
2 Co 3	in	2(a)	0	0	0	Co 3

Co 2 in publication should be on equipoint 8(i) and not 8(g)

82(78) : U2Ni2Si7

oC22

Cmmm

4 Si 1	in	4(j)	0	0.063	1/2	Si 2
4 Si 2	in	4(j)	0	0.278	1/2	Si 3
4 X	in	4(j)	0	0.386	1/2	X
4 U	in	4(i)	0	0.170	0	U
4 Si 4	in	4(i)	0	0.437	0	Si 1
2 Ni	in	2(a)	0	0	0	Ni

$$X = 1/2Ni + 1/2Si$$

8289 : Ho2CoGa8

tP11

P4/mmm

4 Ga 1	in	4(i)	0	1/2	0.1189	Ga 1
2 Ga 2	in	2(h)	1/2	1/2	0.2933	Ga 3
2 Ho	in	2(g)	0	0	0.3093	Ho
2 Ga 3	in	2(e)	0	1/2	1/2	Ga 2
1 Co	in	1(a)	0	0	0	Co

8313 : Nd3Ni13B2

hP18

P6/mmm

6 Ni 1	in	6(i)	1/2	0	0.134
4 Ni 2	in	4(h)	1/3	2/3	0.323
3 Ni 3	in	3(g)	1/2	0	1/2
2 Nd 1	in	2(e)	0	0	0.328
2 B	in	2(c)	1/3	2/3	0
1 Nd 2	in	1(a)	0	0	0

8320 : CeCo<sub>4</sub>B

hP12

P6/mmm

6 Co 1	in 6(i)	1/2	0	0.213	Co 2
2 Co 2	in 2(d)	1/3	2/3	1/2	Co 1
2 B	in 2(c)	1/3	2/3	0	B
1 Ce 1	in 1(b)	0	0	1/2	Ce 1
1 Ce 2	in 1(a)	0	0	0	Ce 2

Origin shifted by 0 0 1/2

8327 : Ce<sub>3</sub>CollB<sub>4</sub>

hP18

P6/mmm

6 Co 1	in 6(i)	1/2	0	0.200	Co 3
4 B	in 4(h)	1/3	2/3	0.350	B
3 Co 2	in 3(g)	1/2	0	1/2	Co 2
2 Ce 1	in 2(e)	0	0	0.333	Ce 2
2 Co 3	in 2(c)	1/3	2/3	0	Co 1
1 Ce 2	in 1(a)	0	0	0	Ce 1

8330 : Ce<sub>2</sub>Co<sub>7</sub>B<sub>3</sub>

hP24

P6/mmm

6 Co 1	in 6(i)	1/2	0	0.125	Co 3
6 Co 2	in 6(i)	1/2	0	0.350	Co 2
4 B 1	in 4(h)	1/3	2/3	0.238	B 2
2 Ce 1	in 2(e)	0	0	0.25	Ce 3
2 Co 3	in 2(d)	1/3	2/3	1/2	Co 1
2 B 2	in 2(c)	1/3	2/3	0	B 1
1 Ce 2	in 1(b)	0	0	1/2	Ce 1
1 Ce 3	in 1(a)	0	0	0	Ce 2

Origin shifted by 0 0 1/2

8340 : CeCo<sub>3</sub>B<sub>2</sub>

hP6

P6/mmm

3 Co	in 3(g)	1/2	0	1/2
2 B	in 2(c)	1/3	2/3	0
1 Ce	in 1(a)	0	0	0

8340 : ErIr<sub>3</sub>B<sub>2</sub>

mC12

C2/m

4 B	in 4(h)	0	0.167	1/2	B
4 Ir 1	in 4(e)	1/4	1/4	0	Ir 2
2 Er	in 2(d)	0	1/2	1/2	Er
2 Ir 2	in 2(a)	0	0	0	Ir 1

Origin shifted by 0 1/2 1/2

8360 : PrNi<sub>2</sub>Al<sub>3</sub> ( Type CeCo<sub>3</sub>B<sub>2</sub>)

hP6

P6/mmm

3 Al	in	3(g)	1/2	0	1/2	Co
2 Ni	in	2(c)	1/3	2/3	0	B
1 Pr	in	1(a)	0	0	0	Ce

Error in published position of Ni; Ni is now on equipoint 2(c)

8360 : YNi<sub>2</sub>Al<sub>3</sub>

hP18

P6/mmm

6 Ni	in	6(l)	0.188	0.376	0	Ni
6 Al 1	in	6(k)	0.287	0	1/2	Al 2
3 Al 2	in	3(f)	1/2	0	0	Al 1
2 Y 1	in	2(d)	1/3	2/3	1/2	Y 2
1 Y 2	in	1(a)	0	0	0	Y 1

8360 : ScNi<sub>2</sub>Si<sub>3</sub>

tI24

I4/mmm

8 Si 1	in	8(g)	0	1/2	0.0488	Si 2
4 Ni 1	in	4(e)	0	0	0.0983	Ni 2
4 Si 2	in	4(e)	0	0	0.1935	Si 1
4 Sc	in	4(e)	0	0	0.3512	Sc
4 Ni 2	in	4(d)	0	1/2	1/4	Ni 1

Origin shifted by 0 0 1/2

8360 : ScRe<sub>2</sub>Si<sub>3</sub>

oC96

Am<sub>2</sub>

8 Re 1	in	8(f)	0.1221	0.2992	0.008	Re 2
8 Si 1	in	8(f)	0.157	0.413	0.004	Si 2
8 Sc 1	in	8(f)	0.171	0.1312	0.012	Sc 1
8 Si 2	in	8(f)	0.269	0.257	0.263	Si 3
8 Sc 2	in	8(f)	0.324	0.3575	0.003	Sc 2
8 Si 3	in	8(f)	0.373	0.075	0.000	Si 1
8 Re 2	in	8(f)	0.3877	0.2049	0.014	Re 1
4 Si 4	in	4(e)	1/2	0.1310	0.210	Si 5
4 Si 5	in	4(e)	1/2	0.279	0.166	Si 7
4 Re 3	in	4(e)	1/2	0.3956	0.256	Re 4
4 Re 4	in	4(d)	0	0.0848	0.247	Re 3
4 Si 6	in	4(d)	0	0.206	0.135	Si 6
4 Si 7	in	4(d)	0	0.3544	0.283	Si 4
4 Si 8	in	4(c)	0.112	0	0.161	Si 8
4 Re 5	in	4(c)	0.2165	0	0.782	Re 6
4 Re 6	in	4(c)	0.2653	0	0.289	Re 5
4 Si 9	in	4(c)	0.390	0	0.588	Si 9

x,y,z changed to -x,y,-z and origin shifted by 0 0 0.500



8370 : La<sub>2</sub>Re<sub>3</sub>B<sub>7</sub>

oP48

Pcca

8 B 1	in 8(f)	0.034	0.102	0.454
8 B 2	in 8(f)	0.040	0.125	0.186
8 Re 1	in 8(f)	0.0912	0.3950	0.0806
8 La	in 8(f)	0.3220	0.2883	0.3226
8 B 3	in 8(f)	0.371	0.299	0.038
4 Re 2	in 4(d)	1/4	0	0.0683
4 B 4	in 4(c)	0	0.370	1/4

8380 : LaCoAl<sub>4</sub>

oP12

Pmma

4 Al 1	in 4(j)	0.561	1/2	0.292
2 Al 2	in 2(f)	1/4	1/2	0.022
2 La	in 2(e)	1/4	0	0.388
2 Co	in 2(e)	1/4	0	0.813
2 Al 3	in 2(a)	0	0	0

8380 : YCrB<sub>4</sub>

oP24

Pbam

4 Y	in 4(h)	0.375	0.350	1/2	Y
4 Cr	in 4(h)	0.375	0.081	1/2	Cr
4 B 1	in 4(g)	0.015	0.320	0	B 4
4 B 2	in 4(g)	0.115	0.450	0	B 3
4 B 3	in 4(g)	0.160	0.035	0	B 2
4 B 4	in 4(g)	0.220	0.185	0	B 1

Origin shifted by 1/2 1/2 1/2

8380 : YNiAl<sub>4</sub>

oC24

Cmcm

8 Al 1	in 8(f)	0	0.186	0.054
4 Y	in 4(c)	0	0.379	1/4
4 Al 2	in 4(c)	0	0.557	1/4
4 Ni	in 4(c)	0	0.729	1/4
4 Al 3	in 4(a)	0	0	0

Origin shifted by 0 1/2 1/2

8576 : Yb<sub>3</sub>Rh<sub>4</sub>Sn<sub>13</sub> ( Previously called Pr<sub>3</sub>Rh<sub>4</sub>Sn<sub>13</sub>-type )

cP40

Pm<sub>3</sub>n

24 Sn 1	in 24(k)	0	0.15333	0.30570	Sn 2
8 Rh	in 8(e)	1/4	1/4	1/4	Rh
6 Yb	in 6(c)	1/4	0	1/2	Yb
2 Sn 2	in 2(a)	0	0	0	Sn 1

Origin shifted by 1/2 1/2 1/2

8591 : Ce<sub>2</sub>NiGa<sub>10</sub>

tI26

I4/mmm

8 Ga 1	in	8(g)	0	1/2	0.0491	Ga 2
4 Ce	in	4(e)	0	0	0.1461	Ce
4 Ga 2	in	4(e)	0	0	0.3032	Ga 4
4 Ga 3	in	4(e)	0	0	0.3935	Ga 3
4 Ga 4	in	4(d)	0	1/2	1/4	Ga 1
2 Ni	in	2(a)	0	0	0	Ni

Origin shifted by 0 0 1/2

8617 : CeNi<sub>5</sub>Sn

hP28

P63/mmc

12 Ni 1	in	12(k)	0.1690	0.3380	0.1458
4 Ni 2	in	4(f)	1/3	2/3	0.0425
4 Sn	in	4(f)	1/3	2/3	0.5873
2 Ce 1	in	2(d)	1/3	2/3	3/4
2 Ni 3	in	2(c)	1/3	2/3	1/4
2 Ni 4	in	2(b)	0	0	1/4
2 Ce 2	in	2(a)	0	0	0

Origin shifted by 0 0 1/2

8633 : CeRe<sub>4</sub>Si<sub>2</sub>

oC14

Cmmm

4 Re 1	in	4(j)	0	0.1855	1/2
4 Si	in	4(j)	0	0.405	1/2
4 Re 2	in	4(i)	0	0.3058	0
2 Ce	in	2(a)	0	0	0

8633 : YRe<sub>4</sub>Si<sub>2</sub> (Type ZrFe<sub>4</sub>Si<sub>2</sub>)

tP14

P42/mmm

8 Re	in	8(i)	0.151	0.599	0
4 Si	in	4(f)	0.289	0.289	0
2 Y	in	2(a)	0	0	0

Origin shifted by 0 0 1/2

8633 : NdRe4Si2

oP28

Pnnm

4	Re 1	in	4(g)	0.0136	0.2959	0	Re 4
4	Re 2	in	4(g)	0.1400	0.5519	0	Re 1
4	Si 1	in	4(g)	0.172	0.025	0	Si 1
4	Re 3	in	4(g)	0.2650	0.1788	0	Re 2
4	Nd	in	4(g)	0.4255	0.3797	0	Nd
4	Re 4	in	4(g)	0.5706	0.0807	0	Re 3
4	Si 2	in	4(g)	0.719	0.227	0	Si 2

Origin shifted by 0 1/2 0

8667 : YbMo2Al4

tI14

I4/mmm

8	Al	in	8(h)	0.303	0.303	0	
4	Mo	in	4(d)	0	1/2	1/4	
2	Yb	in	2(a)	0	0	0	

8683 : HoCoGa5

tP7

P4/mmm

4	Ga 1	in	4(i)	0	1/2	0.3120	Ga 2
1	Ga 2	in	1(c)	1/2	1/2	0	Ga 1
1	Co	in	1(b)	0	0	1/2	Co
1	Ho	in	1(a)	0	0	0	Ho

8769 : Y2Fe4Si9

hP(16-1)

P63/mmc

4	Si 1	in	4(f)	1/3	2/3	0.0596	
4	Fe	in	4(f)	1/3	2/3	0.5966	
4	Si 2	in	4(e)	0	0	0.1598	
2	Y	in	2(c)	1/3	2/3	1/4	
1	Si 3	in	2(a)	0	0	0	

Position 2(a) only half occupied

8791 : LaNi0.6Ga6

tP(16-0.8)

P4/mmm

4	Ga 1	in	4(i)	0	1/2	0.078	Ga 4
4	Ga 2	in	4(i)	0	1/2	0.4179	Ga 2
2	Ga 3	in	2(h)	1/2	1/2	0.161	Ga 3
2	Ga 4	in	2(h)	1/2	1/2	0.321	Ga 1
2	La	in	2(g)	0	0	0.2534	La
1	Ni 1	in	1(b)	0	0	1/2	Ni 1
1	Ni 2	in	1(a)	0	0	0	Ni 2

The Ni2 position is only 1/5 filled

8857 : ScIr<sub>3</sub>B<sub>4</sub> ( ZrIr<sub>3</sub>B<sub>4</sub>-type )

hP16

P63/m

6 B	1	in	6(h)	0.054	0.460	1/4
6 Ir		in	6(h)	0.2520	0.3273	1/4
2 Sc		in	2(d)	2/3	1/3	1/4
2 B	2	in	2(b)	0	0	0

x,y,z changed to y,x,-z

8871 : PrNi<sub>2</sub>Al<sub>5</sub>

oI16

Immm

8 Al	1	in	8(l)	0	0.310	0.354
4 Ni		in	4(i)	0	0	0.242
2 Pr		in	2(d)	1/2	0	1/2
2 Al	2	in	2(a)	0	0	0

Axes changed to bca and origin shifted by 0 1/2 0

89(12) : Ce<sub>2</sub>Ni<sub>15</sub>Si<sub>2</sub>

hP38

P63/mmc

12 X	1	in	12(k)	0.166	0.332	0.0	X	4
12 X	2	in	12(j)	0.371	0.038	1/4	X	3
6 X	3	in	6(g)	1/2	0	0	X	2
4 X	4	in	4(f)	1/3	2/3	0.610	X	1
2 Ce	1	in	2(c)	1/3	2/3	1/4	Ce	2
2 Ce	2	in	2(b)	0	0	1/4	Ce	1

X = 15/17Ni + 2/17Si for all X

Origin shifted by 0 0 1/2

Atom positions of Th<sub>2</sub>Ni<sub>17</sub>

A complete ordering could be possible with the 2:15:2 composition

8912 : Ce<sub>2</sub>Co<sub>15</sub>Al<sub>2</sub>

hR57

R-3m

18 Co	1	in	18(h)	1/2	1/2	1/6
18 Co	2	in	18(f)	1/3	0	0
9 Co	3	in	9(d)	1/2	0	1/2
6 Al		in	6(c)	0	0	0.097
6 Ce		in	6(c)	0	0	0.333

Atom positions of Th<sub>2</sub>Zn<sub>17</sub>; the ordering has been tested.

8938 : YNi<sub>5</sub>Si<sub>3</sub>

oP36

Pnma

4 Ni 1	in	4(c)	0.0129	1/4	0.1124	Ni 2
4 Si 1	in	4(c)	0.0898	1/4	0.0694	Si 1
4 Ni 2	in	4(c)	0.1142	1/4	0.8602	Ni 5
4 Y	in	4(c)	0.1532	1/4	0.3696	Y
4 Si 2	in	4(c)	0.2364	1/4	0.8850	Si 2
4 Ni 3	in	4(c)	0.2939	1/4	0.5696	Ni 3
4 Ni 4	in	4(c)	0.2995	1/4	0.1899	Ni 4
4 Si 3	in	4(c)	0.4295	1/4	0.1681	Si 3
4 Ni 5	in	4(c)	0.4955	1/4	0.8635	Ni 1

Origin shifted by 1/2 1/2 0

8950 : NdCo<sub>4</sub>B<sub>4</sub>

tP18

P42/n

8 B	in	8(g)	0.025	0.600	0.125
8 Co	in	8(g)	0.625	0.107	0.362
2 Nd	in	2(a)	1/4	1/4	1/4

x,y,z changed to y,x,-z and origin shifted by 1/2 1/2 1/2

8950 : CeCo<sub>4</sub>B<sub>4</sub>

tP18

P42/nmc

8 B	in	8(g)	1/4	0.08	0.10
8 Co	in	8(g)	1/4	0.503	0.384
2 Ce	in	2(b)	3/4	1/4	1/4

8950 : LuRu<sub>4</sub>B<sub>4</sub>

tI72

I41/acd

32 B	in	32(g)	0.139	0.068	0.289
32 Ru	in	32(g)	0.350	0.138	3/16
8 Lu	in	8(b)	0	1/4	1/8

Origin shifted by 0 0 1/2

8950 : LuRh<sub>4</sub>B<sub>4</sub>

oC108

Ccca

16 Rh 1	in	16(i)	0.1180	0.0417	0.0955
16 B 1	in	16(i)	0.13	0.147	0.07
16 Rh 2	in	16(i)	0.1530	0.1245	0.3670
16 B 2	in	16(i)	0.19	0.023	0.40
16 Rh 3	in	16(i)	0.3531	0.2065	0.1272
16 B 3	in	16(i)	0.36	0.318	0.09
8 Lu 1	in	8(f)	0	0.5824	1/4
4 Lu 2	in	4(a)	0	1/4	1/4

89(59) : Ce<sub>2</sub>Mn<sub>7</sub>Al<sub>10</sub>

hR57

R-3m

18 X	in 18(h)	1/2	1/2	1/6	X
18 Al 1	in 18(f)	1/3	0	0	Al 2
9 Mn	in 9(d)	1/2	0	1/2	Mn
6 Al 2	in 6(c)	0	0	0.097	Al 1
6 Ce	in 6(c)	0	0	0.333	Ce

$$X = 2/3\text{Mn} + 1/3\text{Al}$$

Atom positions of Th<sub>2</sub>Zn<sub>17</sub>; the ordering has been tested.8968 : Ho<sub>4</sub>Ni<sub>10</sub>Ga<sub>21</sub>.

mC70

C2/m

4 Ga 1	in 4(i)	0.0059	0	0.0915	Ga 6
4 Ni 1	in 4(i)	0.0250	0	0.6101	Ni 2
4 Ga 2	in 4(i)	0.0647	0	0.7951	Ga 4
4 Ga 3	in 4(i)	0.1125	0	0.5501	Ga 2
4 Ho 1	in 4(i)	0.1195	0	0.3341	Ho 2
4 Ni 2	in 4(i)	0.1331	0	0.1050	Ni 4
4 Ga 4	in 4(i)	0.2004	0	0.0030	Ga10
4 Ni 3	in 4(i)	0.2447	0	0.6131	Ni 1
4 Ga 5	in 4(i)	0.2487	0	0.2952	Ga 7
4 Ga 6	in 4(i)	0.2978	0	0.4974	Ga11
4 Ni 4	in 4(i)	0.3477	0	0.1144	Ni 3
4 Ga 7	in 4(i)	0.3883	0	0.3052	Ga 8
4 Ga 8	in 4(i)	0.3968	0	0.0011	Ga 9
4 Ni 5	in 4(i)	0.5019	0	0.1867	Ni 5
4 Ga 9	in 4(i)	0.5401	0	0.3743	Ga 3
4 Ga10	in 4(i)	0.6273	0	0.1963	Ga 5
4 Ho 2	in 4(i)	0.7224	0	0.1791	Ho 1
2 Ga11	in 2(d)	0	1/2	1/2	Ga 1

Axes changed to a-cb and origin shifted by 0 0 1/2

The x-parameter for Ho1, in the publication, should probably be 0.2376 instead of 0.2776; value given here corresponds to 0.2376

8975 : CeCr<sub>2</sub>B<sub>6</sub>

oI18

Immm

8 B 1	in 8(l)	0	0.290	0.330	B 2
4 Cr	in 4(j)	1/2	0	0.348	Cr
4 B 2	in 4(h)	0	0.135	1/2	B 1
2 Ce	in 2(a)	0	0	0	Ce

Axes changed to cab and origin shifted by 0 1/2 0

9170 : ScRh<sub>3</sub>Si<sub>7</sub>

hR66

R-3c

36 Si 1	in 36(f)	0.0119	0.2047	0.1365	
18 Rh	in 18(e)	0.3223	0	1/4	
6 Sc	in 6(b)	0	0	0	
6 Si 2	in 6(a)	0	0	1/4	

92(17) : YNi<sub>10</sub>Si<sub>2</sub> ( Type CeMn<sub>4</sub>Al<sub>8</sub> with partial disorder)

tI26

I4/mmm

8 Ni 1	in 8(j)	0.2847	1/2	0	Ni 2	Al
8 X	in 8(i)	0.3706	0	0	X	Al
8 Ni 2	in 8(f)	1/4	1/4	1/4	Ni 1	Mn
2 Y	in 2(a)	0	0	0	Y	Ce

$$X = 1/2\text{Ni} + 1/2\text{Si}$$

92(23) : Ce<sub>2</sub>Ni<sub>17</sub>Si<sub>5</sub>

tI48

I41/amd

32 Ni	in 32(i)	0.2006	0.1266	0.0722	
8 Si	in 8(d)	0	0	0	
4 Ce	in 4(b)	0	1/4	3/8	
4 X	in 4(a)	0	3/4	1/8	

$$X = 0.6\text{Ni} + 0.4\text{Si}$$

Origin shifted by 0 0 1/2

9250 : ScFe<sub>6</sub>Ge<sub>6</sub> ( Type HfFe<sub>6</sub>Ge<sub>6</sub>)

hP13

P6/mmm

6 Fe	in 6(i)	1/2	0	0.2531	Fe
2 Ge 1	in 2(e)	0	0	0.3438	Ge 3
2 Ge 2	in 2(d)	1/3	2/3	1/2	Ge 1
2 Ge 3	in 2(c)	1/3	2/3	0	Ge 2
1 Sc	in 1(a)	0	0	0	Hf

Origin shifted by 0 0 1/2

We used the atom positions of HfFe<sub>6</sub>Ge<sub>6</sub>.9250 : YCo<sub>6</sub>Ge<sub>6</sub>

hP6 1/2

P6/mmm

3 Co	in 3(g)	1/2	0	1/2	Co
2 Ge 1	in 2(e)	0	0	0.307	Ge 2
2 Ge 2	in 2(c)	1/3	2/3	0	Ge 1
1 Y	in 1(a)	0	0	0	Y

For the idealized formula the population is 1/2 for Ge 1 and Y

9250 : ScNi<sub>6</sub>Ge<sub>6</sub>

hP52

P6/mmm

12 Ni 1	in 12(o)	0.246	0.493	1/4	Ni 2
12 Ni 2	in 12(n)	0.238	0	0.258	Ni 1
6 Ge 1	in 6(m)	0.162	0.324	1/2	Ge 2
6 Ge 2	in 6(l)	0.160	0.320	0	Ge 1
6 Ge 3	in 6(i)	1/2	0	0.158	Ge 6
3 Sc 1	in 3(g)	1/2	0	1/2	Sc 2
2 Ge 4	in 2(e)	0	0	0.340	Ge 5
2 Ge 5	in 2(d)	1/3	2/3	1/2	Ge 4
2 Ge 6	in 2(c)	1/3	2/3	0	Ge 3
1 Sc 2	in 1(a)	0	0	0	Sc 1

9250 : ScFe<sub>6</sub>Ga<sub>6</sub>

oI26

Immm

8 Fe 1	in 8(k)	1/4	1/4	1/4	Fe 1
4 Ga 1	in 4(j)	1/2	0	0.165	Ga 3
4 Ga 2	in 4(i)	0	0	0.345	Ga 2
4 Fe 2	in 4(h)	0	0.257	1/2	Fe 2
4 Ga 3	in 4(g)	0	0.336	0	Ga 1
2 Sc	in 2(a)	0	0	0	Sc

Axes changed to cab.

92(50) : DyFe<sub>6</sub>Al<sub>6</sub> (Type CeMn<sub>4</sub>Al<sub>8</sub> with partial disorder)

tI26

I4/mmm

8 X	in 8(j)	0.282	1/2	0	Al
8 Al	in 8(i)	0.343	0	0	Al
8 Fe	in 8(f)	1/4	1/4	1/4	Mn
2 Dy	in 2(a)	0	0	0	Ce

$$X = 1/2\text{Fe} + 1/2\text{Al}$$

9267 : CeMn<sub>4</sub>Al<sub>8</sub>

tI26

I4/mmm

8 Al 1	in 8(j)	0.275	1/2	0	Al 2
8 Al 2	in 8(i)	0.365	0	0	Al 1
8 Mn	in 8(f)	1/4	1/4	1/4	Mn
2 Ce	in 2(a)	0	0	0	Ce



9322 : Sc<sub>2</sub>Co<sub>2</sub>1B<sub>6</sub> ( Type W<sub>2</sub>Cr<sub>2</sub>1C<sub>6</sub>)

cF116

Fm $\bar{3}$ m

48 Co	in 48(h)	0	0.1699	0.1699		Cr 3
32 Co	in 32(f)	0.3809	0.3809	0.3809		Cr 4
24 B	in 24(e)	0.2765	0	0		C
8 Sc	in 8(c)	1/4	1/4	1/4		Cr 2
4 Co	in 4(a)	0	0	0		Cr 1

We used the atom positions of Cr<sub>2</sub>3C<sub>6</sub>.93(35) : Ce<sub>2</sub>Ni<sub>17</sub>Si<sub>9</sub>

tI56

I4/mcm

16 Si 1	in 16(l)	0.1700	0.6700	0.1180	
16 Ni 1	in 16(l)	0.6294	0.1294	0.1832	
16 Ni 2	in 16(k)	0.0691	0.2024	0	
4 X	in 4(d)	0	1/2	0	
4 Ce	in 4(a)	0	0	1/4	

$$X = 1/2\text{Ni} + 1/2\text{Si}$$

Origin shifted by 0 0 1/2

9533 : EuNi<sub>12</sub>B<sub>6</sub> ( Type SrNi<sub>12</sub>B<sub>6</sub>)

hR57

R- $\bar{3}$ m

18 Ni 1	in 18(h)	0.426	0.574	0.047		Ni 2
18 B	in 18(h)	0.476	0.524	0.291		B
18 Ni 2	in 18(g)	0.368	0	1/2		Ni 1
3 Eu	in 3(a)	0	0	0		Eu

9691 : CeCr<sub>2</sub>Al<sub>12</sub>O ( related to type Mg<sub>3</sub>Cr<sub>2</sub>Al<sub>18</sub>)

cF184

Fd $\bar{3}$ m

96 Al 1	in 96(g)	0.0584	0.0584	0.3252		Al 3	Al
48 Al 2	in 48(f)	0.4843	1/8	1/8		Al 2	Al
16 Cr	in 16(d)	1/2	1/2	1/2		Cr	Cr
16 Al 3	in 16(c)	0	0	0		Al 1	Mg
8 Ce	in 8(a)	1/8	1/8	1/8		Ce	Mg

Origin shifted by 5/8 5/8 5/8

Atom positions of Mg<sub>3</sub>Cr<sub>2</sub>Al<sub>18</sub>; the ordering has been tested.

## References

- Akselrud, L.G., Ya.P. Yarmolyuk and E.I. Gladyshevskii, 1975, *Dopov. Akad. Nauk Ukr. RSR, Ser. A*(7), 643-645.
- Akselrud, L.G., Ya.P. Yarmolyuk and E.I. Gladyshevskii, 1977, *Sov. Phys. Crystallogr.* **22**, 492-493.
- Akselrud, L.G., Ya.P. Yarmolyuk and E.I. Gladyshevskii, 1978, *Dopov. Akad. Nauk Ukr. RSR, Ser. A*, 359-362.
- Akselrud, L.G., Ya.P. Yarmolyuk and E.I. Gladyshevskii, 1980, *Dopov. Akad. Nauk Ukr. RSR, Ser. A*(5), 79-81.
- Akselrud, L.G., Ya.P. Yarmolyuk, I.V. Rozhdestvenskaya and E.I. Gladyshevskii, 1981, *Sov. Phys. Crystallogr.* **26**, 103-104.
- Akselrud, L.G., V.I. Yarovets, O.I. Bodak, Ya.P. Yarmolyuk and E.I. Gladyshevskii, 1976, *Sov. Phys. Crystallogr.* **21**, 210-211.
- Andersson, Y., V. Kaechansilp, M. Casteleiro Soto and S. Rundqvist, 1974, *Acta Chem. Scand.* **A28**, 797-802.
- Arnberg, L. and B. Aurivillius, 1980, *Acta Chem. Scand.* **A34**, 1-5.
- Aronsson, B., M. Backman and S. Rundqvist, 1960, *Acta Chem. Scand.* **14**, 733-741.
- Åselius, J., 1960, *Acta Chem. Scand.* **14**, 2169-2178.
- Ballestracci, R., 1976, *C.R. Acad. Sci. Paris, Ser. B* **282**, 291-292.
- Ballestracci, R. and G. Astier, 1978, *C.R. Acad. Sci. Paris, Ser. B* **286**, 109-112.
- Ban, Z. and M. Sikirica, 1965, *Acta Crystallogr.* **18**, 594-599.
- Barz, H., 1980, *Mater. Res. Bull.* **15**, 1489-1491.
- Belyavina, N.M. and V.Ya. Markiv, 1978, 3rd All-Union Conf. on the Crystal Chemistry of Intermetallic Compounds, Lvov, Collected Abstracts, pp. 26-27.
- Belyavina, N.M. and V.Ya. Markiv, 1982, *Dopov. Akad. Nauk Ukr. RSR, Ser. B*(5), 39-42.
- Belyavina, N.M. and V.Ya. Markiv, 1982a, *Dopov. Akad. Nauk Ukr. RSR, Ser. B*(12), 30-33.
- Bergman, G. and J.L.T. Waugh, 1956, *Acta Crystallogr.* **9**, 214-217.
- Bilonizhko, N.S. and Yu.B. Kuzma, 1974, *Inorg. Mater.* **10**, 227-230.
- Bilonizhko, N.S., Yu.B. Kuzma and L.D. Polyanskaya, 1980, *Inorg. Mater.* **16**, 575-578.
- Bodak, O.I., 1971, *Visn. L'vivsk. Univ., Ser. Khim.* **12**, 22-25.
- Bodak, O.I., 1979, *Sov. Phys. Crystallogr.* **24**, 732-734.
- Bodak, O.I., V.A. Bruskov and V.K. Pecharskii, 1982, *Sov. Phys. Crystallogr.* **27**, 538-540.
- Bodak, O.I. and E.I. Gladyshevskii, 1969, *Inorg. Mater.* **5**, 1754-1758.
- Bodak, O.I. and E.I. Gladyshevskii, 1969a, *Dopov. Akad. Nauk Ukr. RSR, Ser. A*, 452-455.
- Bodak, O.I. and E.I. Gladyshevskii, 1969b, *Dopov. Akad. Nauk Ukr. RSR, Ser. A*, 1125-1129.
- Bodak, O.I. and E.I. Gladyshevskii, 1970, *Inorg. Mater.* **6**, 1037-1040.
- Bodak, O.I. and E.I. Gladyshevskii, 1970a, *Sov. Phys. Crystallogr.* **14**, 859-862.
- Bodak, O.I., E.I. Gladyshevskii, A.V. Kardash and E.E. Cherkashin, 1970, *Inorg. Mater.* **6**, 935-938.
- Bodak, O.I., E.I. Gladyshevskii and O.I. Kharченко, 1974, *Sov. Phys. Crystallogr.* **19**, 45-46.
- Bodak, O.I., E.I. Gladyshevskii and P.I. Kripyakevich, 1966, *Inorg. Mater.* **2**, 1861-1864.
- Bodak, O.I., E.I. Gladyshevskii and P.I. Kripyakevich, 1970, *J. Struct. Chem.* **11**, 283-288.
- Bodak, O.I., E.I. Gladyshevskii and M.G. Mis'kiv, 1972, *Sov. Phys. Crystallogr.* **17**, 439-441.
- Bodak, O.I. E.I. Gladyshevskii and V.K. Pecharskii, 1977, *Sov. Phys. Crystallogr.* **22**, 100-103.
- Bodak, O.I., E.I. Gladyshevskii, V.I. Yarovets, V.N. Davydov and T.V. Il'chuk, 1978, *Inorg. Mater.* **14**, 366-369.
- Bodak, O.I., B.Ya. Kotur and E.I. Gladyshevskii, 1976, *Dokl. Akad. Nauk Ukr. SSR, Ser. A*, 656-659.
- Bodak, O.I., B.Ya. Kotur, V.I. Yarovets and E.I. Gladyshevskii, 1977, *Sov. Phys. Crystallogr.* **22**, 217-219.
- Bodak, O.I., M.G. Mis'kiv, A.T. Tyvanchuk, O.I. Kharchenko and E.I. Gladyshevskii, 1973, *Inorg. Mater.* **9**, 777-779.
- Bodak, O.I., L.A. Muratova, I.R. Mokra, V.I. Yarovets, A.S. Sobolev and E.I. Gladyshevskii, 1974, in: *Strukt. Faz. Fazovye Prevrashch. Diagr. Sostoyaniya Met. Sist.*, eds. O.S. Ivanov and Z.M. Alekseeva, pp. 182-186.
- Bodak, O.I., V.K. Pecharskii and E.I. Gladyshevskii, 1978, *Inorg. Mater.* **14**, 188-192.
- Bodak, O.I., V.I. Yarovets and E.I. Gladyshevskii, 1974, *Tesizy Dokl. Vses. Konf. Kristalloghim. Internet. Soedin*, 2nd Ed., ed. R.M. Rykhal, (L'vov Gos. Univ., Lvov, USSR) pp. 32-33.
- Boller, H. and E. Parthé, 1963, *Acta Crystallogr.* **16**, 1095-1101.
- Bowman, A.L., G.P. Arnold, E.K. Storms and N.G. Nereson, 1972, *Acta Crystallogr.* **B28**, 3102-3103.
- Braun, H.F., 1980, *Phys. Lett.* **75A**, 386-388.
- Braun, H.F., 1982, private communication.
- Braun, H.F., F. Acker and C.U. Segre, 1980, *Bull. Am. Phys. Soc.* **25**, 232.
- Braun, H.F. N. Engel and E. Parthé, 1983, *Phys. Rev.* **B28** (3), 1389-1395.
- Braun, H.F., M. Pelizzone and K. Yvon, 1982, VIIth Intern. Conf. on Solid Compounds of Transition Elements, Grenoble (June 1982).
- Braun, H.F. and C.U. Segre, 1981, in: *Ternary Superconductors, Proc. Conf. on Ternary Superconductors, Lake Geneva, WI, USA (24-26 Sept. 1980)*, eds. G.K. Shenoy, B.D. Dunlap and F.Y. Fradin, (Elsevier-North-Holland, Amsterdam) pp. 239-242.

- Braun, H.F. and K. Yvon, 1980, *Acta Crystallogr.* **B36**, 2400–2402.
- Braun, H.F., K. Yvon and R.M. Braun, 1980, *Acta Crystallogr.* **B36**, 2397–2399.
- Brechtel, E., G. Cordier and H. Schäfer, 1979, *Z. Naturforsch.* **34B**, 251–255.
- Brechtel, E., G. Cordier and H. Schäfer, 1980, *Z. Naturforsch.* **35B**, 1–3.
- Brown, P.J., 1957, *Acta Crystallogr.* **10**, 133–135.
- Brunton, G., 1969, *Acta Crystallogr.* **B25**, 2163–2164.
- Buchholz, W. and H.U. Schuster, 1981, *Z. Anorg. Allg. Chem.* **482**, 40–48.
- Buschow, K.H.J., 1975, *J. Less-Common Metals* **40**, 361–363.
- Buschow, K.H.J., J.H.N. van Vucht and W.W. van der Hoogenhof, 1976, *J. Less-Common Metals* **50**, 145–150.
- Calvert, L.D. and C. Rand, 1964, *Acta Cryst.* **17**, 1175–1176.
- Cëpiga, M.V., V.P. Krivuckii and Yu.B. Kuzma, 1972, *Inorg. Mater.* **8**, 928–932.
- Chaban, N.F., 1981, *Vestn. L'vovsk. Univ., Ser. Khim.* **23**, 43–45.
- Chaban, N.F. and Yu.B. Kuzma, 1977, *Inorg. Mater.* **13**, 757–758.
- Chaban, N.F., Yu.B. Kuzma, N.S. Bilonizhko, O.O. Kachmar and N.V. Petriv, 1979, *Dopov. Akad. Nauk Ukr. RSR, Ser. A*, 875–877.
- Chaban, N.F., Yu.B. Kuzma and L.D. Kotovskaya, 1980, *Dopov. Akad. Nauk. Ukr. RSR, Ser. A(6)*, 88–90.
- Chabot, B., 1982, unpublished results.
- Chabot, B., H.F. Braun, K. Yvon and E. Parthé, 1981, *Acta Crystallogr.* **B37**, 668–671.
- Chabot, B., K. Cenzual and E. Parthé, 1981, *Acta Crystallogr.* **A37**, 6–11.
- Chabot, B., N. Engel and E. Parthé, 1981, *Acta Crystallogr.* **B37**, 671–673.
- Chabot, B., N. Engel and E. Parthé, 1983, *J. Less-Common Metals* **96**, 331–339.
- Chabot, B. and E. Parthé, 1978, *Acta Crystallogr.* **B34**, 3173–3177.
- Chabot, B. and E. Parthé, 1983, *J. Less-Common Metals* **93**, L9–11.
- Chabot, B. and E. Parthé, 1983a, *J. Less-Common Metals*, submitted.
- Chernyak, G.V., N.F. Chaban and Yu.B. Kuzma, 1982, *Inorg. Mater.* **18**, 590–592.
- Chevalier, B., A. Cole, P. Lejay and J. Etourneau, 1981, *Mater. Res. Bull.* **16**, 1067–1075.
- Chevalier, B., A. Cole, P. Lejay, M. Vlasse, J. Etourneau and P. Hagenmuller, 1982, *Mater. Res. Bull.* **17**, 251–258.
- Chevalier, B., P. Lejay, A. Cole, M. Vlasse and J. Etourneau, 1982, *Solid State Commun.* **41**, 801–804.
- Chevalier, B., P. Lejay, J. Etourneau and P. Hagenmuller, 1983, *Mater. Res. Bull.* **18**, 315–330.
- Chevalier, B., P. Lejay, J. Etourneau, M. Vlasse and P. Hagenmuller, 1982, VIIIth Intern. Conf. on Solid Compounds of Transition Elements, Grenoble, Abstract II B 16.
- Chevalier, B., P. Lejay, J. Etourneau, M. Vlasse and P. Hagenmuller, 1982a, *Mater. Res. Bull.* **17**, 1211–1220.
- Chevalier, B., P. Lejay, M. Vlasse, J. Etourneau and P. Hagenmuller, 1982, *Solid State Chem. Conf., Veldhoven, The Netherlands, Paper FII 19*.
- Contardi, V., R. Ferro, R. Marazza and D. Rossi, 1977, *J. Less-Common Metals* **51**, 277–281.
- Cooper, A.S., 1980, *Mater. Res. Bull.* **15**, 799–805.
- Cromer, D.T. and A.C. Larson, 1959, *Acta Crystallogr.* **12**, 855–859.
- Cromer, D.T., A.C. Larson and R.B. Roof, 1960, *Acta Crystallogr.* **13**, 913–918.
- Cromer, D.T. and C.E. Olsen, 1959, *Acta Crystallogr.* **12**, 689–694.
- Davidov, V.M. and Yu.B. Kuzma, 1981, *Dopov. Akad. Nauk Ukr. RSR, Ser. A(1)*, 81–84.
- Dhar, S.K., S.K. Malik and R. Vijayaraghavan, 1981, *Mater. Res. Bull.* **16**, 1557–1560.
- Dörrscheidt, W., G. Savelsberg, J. Stöhr and H. Schäfer, 1982, *J. Less-Common Metals* **83**, 269–278.
- Dörrscheidt, W. and H. Schäfer, 1978, *J. Less-Common Metals* **58**, 209–216.
- Dörrscheidt, W. and H. Schäfer, 1980, *J. Less-Common Metals* **70**, P1–P10.
- Dwight, A.E., 1968, *Proc. 7th Rare Earth Research Conf., Coronado, CA, USA (October 28–30)*.
- Dwight, A.E., 1975, *J. Less-Common Metals* **43**, 117–120.
- Dwight, A.E., 1982, private communication.
- Dwight, A.E., R.A. Conner and J.W. Downey, 1963, *Nature (London)* **197**, 587.
- Dwight, A.E., W.C. Harper and C.W. Kimball, 1973, *J. Less-Common Metals* **30**, 1–8.
- Dwight, A.E., C.W. Kimball, R.S. Preston, S.P. Taneja and L. Weber, 1975, *J. Less-Common Metals* **40**, 285–291.
- Dwight, A.E., M.H. Mueller, R.A. Conner Jr., J.W. Downey and H. Knott, 1968, *Trans. Met. Soc. AIME* **242**, 2075–2080.
- Dzyana, D.I., E.I. Gladyshevskii and P.I. Kripyakevich, 1968, *Dopov. Akad. Nauk Ukr. RSR, Ser. A* **30(3)**, 282–284.
- Eisenmann, B., N. May, W. Müller and H. Schäfer, 1972, *Z. Naturforsch.* **27b**, 1155–1157.
- Engel, N., H.F. Braun and E. Parthé, 1983, *J. Less-Common Metals* **95(2)**, 309–315.
- Engel, N., B. Chabot and E. Parthé, 1983, *J. Less-Common Metals* **96**, 291–296.
- Engström, I., 1965, *Acta Chem. Scand.* **19**, 1924–1932.
- Espinosa, G.P., A.S. Cooper, H. Barz and J.P. Remeika, 1980, *Mater. Res. Bull.* **15**, 1635–1641.
- Felner, I., 1980, *J. Less-Common Metals* **72**, 241–249.
- Felner, I. and I. Mayer, 1973, *Mater. Res. Bull.* **8**, 1317–1320.
- Felner, I., I. Mayer, A. Grill and M. Schieber, 1975, *Solid State Commun.* **16**, 1005–1009.
- Felner, I. and I. Nowik, 1978, *J. Phys. Chem. Solids* **39**, 951–956.
- Felner, I. and I. Nowik, 1979, *J. Phys. Chem. Solids* **40**, 1035–1044.
- Felner, I. and I. Nowik, 1982, *J. Phys. Chem. Solids* **43**, 463–465.

- Felner, I. and M. Schieber, 1973, *Solid State Commun.* **13**, 457–461.
- Felner, I., M. Sch and I. Nowik, 1981, *J. Phys. Chem. Solids* **42**, 1091–1095.
- Ferro, R., R. Marazza and G. Rambaldi, 1974, *Z. Metallkde* **65**, 37–39.
- Ferro, R., R. Marazza and G. Rambaldi, 1974a, *Z. Anorg. Allg. Chem.* **410**, 219–224.
- Ferro, R., R. Marazza and G. Rambaldi, 1974b, *Z. Metallkde* **65**, 40–41.
- Florio, J.V., N.C. Baenziger and R.E. Rundle, 1956, *Acta Crystallogr.* **9**, 367–372.
- Florio, J.V., R.E. Rundle and A.I. Snow, 1952, *Acta Crystallogr.* **5**, 449–457.
- Fornasini, M.L. and A. Palenzona, 1976, *J. Less-Common Metals* **45**, 137–141.
- Frank, F.C. and J.S. Kasper, 1958, *Acta Crystallogr.* **11**, 184–190.
- Frank, F.C. and J.S. Kasper, 1959, *Acta Crystallogr.* **12**, 483–499.
- Ganglberger, E., H. Nowotny and F. Benesovsky, 1966, *Monatsh. Chem.* **97**, 101–102.
- Gavrilenko, I.S. and V.Ya. Markiv, 1978, *Dopov. Akad. Nauk Ukr. RSR, Ser. A*, 271–274.
- Ghadraoui, E.H.E., R. Guérin, M. Potel and M. Sergeant, 1981, *Mater. Res. Bull.* **16**, 933–941.
- Gignoux, D. and J.C. Gomez-Sal, 1976, *J. Magn. Mater.* **1**, 203–213.
- Gladyshevskii, E.I., 1971, *Crystal Chemistry of Silicides and Germanides (Metallurgia, Moscow)* (in Russian).
- Gladyshevskii, E.I., 1964, *Dopov. Akad. Nauk Ukr. RSR, Ser. A*, 209–212.
- Gladyshevskii, E.I. and O.I. Bodak, 1965, *Dopov. Akad. Nauk Ukr. RSR, Ser. A*, 601–604.
- Gladyshevskii, E.I., O.I. Bodak, V.I. Yarovets, Yu.K. Gorelenko and R.V. Skolozdra, 1978, *Ukr. Fiz. Zh.* **23**, 77–82.
- Gladyshevskii, E.I. and Yu.N. Grin', 1981, *Sov. Phys. Crystallogr.* **26**, 683–689.
- Gladyshevskii, E.I., Yu.N. Grin' and Ya.P. Yarmolyuk, 1981, *Vestn. L'vovsk. Univ., Ser. Khim.* **23**, 26–30.
- Gladyshevskii, E.I., Yu.N. Grin' and Ya.P. Yarmolyuk, 1983, *Dopov. Akad. Nauk Ukr. RSR, Ser. A(2)*, 67–70.
- Gladyshevskii, E.I. and B.Ya. Kotur, 1978, *Sov. Phys. Crystallogr.* **23**, 533–535.
- Gladyshevskii, E.I., B.Ya. Kotur, O.I. Bodak and V.P. Skvorchuk, 1977, *Dokl. Akad. Nauk Ukr. SSR, Ser. A*, 751–754.
- Gladyshevskii, E.I., P.I. Kripyakevich and O.I. Bodak, 1966, *Z. Anorg. Allg. Chem.* **344**, 95–101.
- Gladyshevskii, E.I., P.I. Kripyakevich and O.I. Bodak, 1966a, *Acta Crystallogr.* **21**, A80–A81.
- Gladyshevskii, E.I., P.I. Kripyakevich and O.I. Bodak, 1967, *Visn. L'vivsk. Univ., Ser. Khim.* **9**, 34–39.
- Gladyshevskii, E.I., P.I. Kripyakevich and M.Yu. Teslyuk, 1952, *Dokl. Akad. Nauk SSSR* **85**, 81–84.
- Gladyshevskii, E.I., V.J. Markiv and Yu.B. Kuzma, 1962, *Dopov. Akad. Nauk Ukr. RSR, Ser. A*, 481–483.
- Goebel, J.A. and S. Rosen, 1968, *J. Less-Common Metals* **16**, 441–446.
- Gomes de Mesquita, A.H. and K.H.J. Buschow, 1967, *Acta Crystallogr.* **22**, 497–501.
- Gorelenko, Yu.K., O.I. Bodak, E.I. Gladyshevskii and V.I. Yarovets, 1977, *Ukr. Fiz. Zh.* **22**, 1020–1022.
- Grin', Yu.N., 1982, *Dopov. Akad. Nauk Ukr. RSR, Ser. A(2)*, 76–79.
- Grin', Yu.N., I.S. Gavrilenko, V.Ya. Markiv and Ya.P. Yarmolyuk, 1980, *Dopov. Akad. Nauk Ukr. RSR, Ser. A(8)*, 73–76.
- Grin', Yu.N. and Ya.P. Yarmolyuk, 1979, *Vestn. L'vovsk. Univ., Ser. Khim.* **21**, 13–17.
- Grin', Yu.N. and Ya.P. Yarmolyuk, 1980, *Sov. Phys. Crystallogr.* **25**, 353–355.
- Grin', Yu.N. and Ya.P. Yarmolyuk, 1981, *Vestn. L'vovsk. Univ., Ser. Khim.* **23**, 30–33.
- Grin', Yu.N. and Ya.P. Yarmolyuk, 1982, *Dopov. Akad. Nauk Ukr. RSR, Ser. A(3)*, 69–72.
- Grin', Yu.N., Ya.P. Yarmolyuk and E.I. Gladyshevskii, 1977, *Theoretical and Experimental Chemistry, Vestn. L'vovsk. Univ., Ser. Khim.* **19**, 14–21.
- Grin', Yu.N., Ya.P. Yarmolyuk and E.I. Gladyshevskii, 1979, *Sov. Phys. Crystallogr.* **24**, 263–266.
- Grin', Yu.N., Ya.P. Yarmolyuk and E.I. Gladyshevskii, 1979a, *Sov. Phys. Crystallogr.* **24**, 137–139.
- Grin', Yu.N., Ya.P. Yarmolyuk and E.I. Gladyshevskii, 1979b, *Sov. Phys. Dokl.* **24**, 228–230.
- Grin', Yu.N., Ya.P. Yarmolyuk and E.I. Gladyshevskii, 1980, *Dokl. Akad. Nauk Ukr. SSR, Ser. A(1)*, 80–85.
- Grin', Yu.N., Ya.P. Yarmolyuk and E.I. Gladyshevskii, 1982, *Sov. Phys. Crystallogr.* **27**, 413–417.
- Griniv, I.A., O.I. Golovanets, R.V. Labunova, Yu.N. Grin' and Ya.P. Yarmolyuk, 1983, *Dopov. Akad. Nauk Ukr. RSR, Ser. A(1)*, 74–77.
- Grössinger, R. and W. Steiner, 1975, *Phys. Stat. Sol.* **28a**, K135–K138.
- Grover, A.K., B.R. Coles, B.V.B. Sarkissian and H.E.N. Stone, 1982, *J. Less-Common Metals* **86**, 29–36.
- Grüttner, A. and K. Yvon, 1979, *Acta Crystallogr.* **B35**, 451–453.
- Hellner, E. and E. Koch, 1981, *Acta Crystallogr.* **A37**, 1–6.
- Hiebl, K., C. Horvath, P. Rogl and M.J. Sienko, 1983, *J. Magn. Mater.* **37**, 287–296 and *Solid State Commun.* **48**, 211–215.
- Hiebl, K., P. Rogl and M.J. Sienko, 1982, *Inorg. Chem.* **21**, 1128–1133.
- Hiebl, K., P. Rogl, E. Uhl and M.J. Sienko, 1980, *Inorg. Chem.* **19**, 3316–3320.
- Hodeau, J.L., J. Chenavas, M. Marezio and J.P. Remeika, 1980, *Solid State Commun.* **36**, 839–845.
- Hodeau, J.L., M. Marezio and J.P. Remeika, 1982, *VIIth Intern. Conf. on Solid Compounds of Transition Elements, Grenoble, Abstract II B 15*.
- Hodeau, J.L., M. Marezio and J.P. Remeika, 1982a, *Solid State Chem. Conf., Veldhoven, The Netherlands, Paper FV 63*.

- Hodeau, J.L., M. Marezio, J.P. Remeika and C.H. Chen, 1982, *Solid State Commun.* **42**, 97-102.
- Hofmann, W. and W. Jeitschko, 1983, in: *Solid State Chemistry 1982, Proc. 2nd Europ. Conf., Veldhoven, The Netherlands (7-9 June 1982)*, Studies in Inorganic Chemistry, Vol. 3, eds. R. Metselaar, H.J.M. Heijligers and J. Schoonman (Elsevier, Amsterdam) pp. 711-712.
- Hohnke, D. and E. Parthé, 1966, *Acta Crystallogr.* **20**, 572-582.
- Holleck, H., 1973, IVth Intern. Conf. on Solid Compounds of Transition Elements, Geneva, Switzerland, Collected Abstracts, pp. 210-212.
- Holleck, H., 1977, *J. Less-Common Metals* **52**, 167-172.
- Horvath, C. and P. Rogl, 1983, *Mater. Res. Bull.* **18**, 443-448.
- Hovestreydt, E., N. Engel, K. Klepp, B. Chabot and E. Parthé, 1982, *J. Less-Common Metals* **86**, 247-274.
- Hovestreydt, E., K. Klepp and E. Parthé, 1982, *Acta Crystallogr.* **B38**, 1803-1805.
- Hovestreydt, E., K. Klepp and E. Parthé, 1983, *Acta Crystallogr.* **C39**, 422-425.
- Iandelli, A., 1964, *Z. Anorg. Allg. Chem.* **330**, 221-232.
- Iandelli, A., 1983, *J. Less-Common Metals* **90**, 121-126.
- Iandelli, A. and R. Ferro, 1954, *Gazz. Chim. Ital.* **84**, 463-478.
- Ishikawa, M., J.L. Jorda and A. Junod, 1982, in: *Superconductivity in d- and f-Band Metals 1982, Proc. IVth Conf., Kernforschungszentrum Karlsruhe, Karlsruhe (June 28-30, 1982)* eds. W. Buckel and W. Weber, pp. 141-144.
- Jedlicka, H., F. Benesovsky and H. Nowotny, 1969, *Monatsh. Chem.* **100**, 844-850.
- Jeitschko, W., 1969, *Acta Crystallogr.* **B25**, 557-564.
- Jeitschko, W., 1970, *Acta Crystallogr.* **B26**, 815-822.
- Jeitschko, W. and B. Jaberg, 1980, *J. Solid State Chem.* **35**, 312-317.
- Johnson, V., 1976, *C.A.* **85**, No. 115903; also cited in: *Gmelin Handbook of Inorganic Chemistry*, 8th Ed., Ch. 8, Manganese (Springer, Berlin, 1982) p. 115.
- Johnson, V. and W. Jeitschko, 1974, *J. Solid State Chem.* **11**, 161-166.
- Johnson, Qu., G.S. Smith and D.H. Wood, 1969, *Acta Crystallogr.* **B25**, 464-469.
- Johnssen, T., 1972, *Acta Chem. Scand.* **26**, 365-382.
- Johnston, D.C., 1977, *Solid State Commun.* **24**, 699-702.
- Johnston, D.C. and H.F. Braun, 1982, in: *Superconductivity in Ternary Compounds II*, eds. M.B. Maple and Ø. Fischer, Topics in Current Physics, Vol. 34 (Springer, Berlin) pp. 11-55.
- Johnston, G.B. and E.O. Hall, 1968, *J. Phys. Chem. Solids* **29**, 201-207.
- Johnston, D.C. and H.B. MacKay, 1979, *Bull. Amer. Phys. Soc.* **24**, 390.
- Jorda, J.L., M. Ishikawa and E. Hovestreydt, 1983, *J. Less-Common Metals* **92**, 155-161.
- Jung, W. and D. Quentmeier, 1980, *Z. Kristallogr.* **151**, 121-128.
- Jung, W. and D. Quentmeier, 1980a, *Z. Kristallogr.* **151**, 172-174.
- Kalychak, Ya.M., L.G. Akselrud, Ya.P. Yarmolyuk, O.I. Bodak and E.I. Gladyshevskii, 1975, *Sov. Phys. Crystallogr.* **20**, 639-640.
- Karatygina, E.P., V.V. Burnasova, M.V. Raevskaja and E.M. Sokolovskaja, 1974, *Metallofiz.* **52**, 105-109.
- Kido, H., M. Shimada and M. Koizumi, 1982, *Phys. Stat. Sol.* **A70**, K23-26.
- Kiessling, R., 1949, *Acta Chem. Scand.* **3**, 603-615.
- Kiessling, R., 1950, *Acta Chem. Scand.* **4**, 209-227.
- Klepp, K., E. Hovestreydt and E. Parthé, 1983, *Acta Crystallogr.* **C39**, 662-664.
- Klepp, K. and E. Parthé, 1980, *Acta Crystallogr.* **B36**, 774-782.
- Klepp, K. and E. Parthé, 1981, *Acta Crystallogr.* **B37**, 1500-1504.
- Klepp, K. and E. Parthé, 1982, *J. Less-Common Metals* **85**, 181-194.
- Klepp, K. and E. Parthé, 1982a, *J. Less-Common Metals* **83**, L33-L35.
- Klepp, K. and E. Parthé, 1982b, *Acta Crystallogr.* **B38**, 2026-2028.
- Klepp, K. and E. Parthé, 1982c, *Acta Crystallogr.* **B38**, 1105-1108.
- Klepp, K. and E. Parthé, 1982d, *Acta Crystallogr.* **B38**, 1541-1544.
- Knigenko, L.D., I.R. Mokra and O.I. Bodak, 1977, *Theoretical and Experimental Chemistry, Vestn. L'vovsk. Univ., Ser. Khim.* **19**, 68-71.
- Kotur, B.Ya., 1977, *Dopov. Akad. Nauk Ukr. RSR, Ser. A*, 164-165.
- Kotur, B.Ya. and O.I. Bodak, 1977, *Sov. Phys. Crystallogr.* **22**, 687-689.
- Kotur, B.Ya. and O.I. Bodak, 1980, *Inorg. Mater.* **16**, 308-311.
- Kotur, B.Ya., O.I. Bodak and E.I. Gladyshevskii, 1977, *Dopov. Akad. Nauk Ukr. RSR, Ser. A*, 664-666.
- Kotur, B.Ya., O.I. Bodak and E.I. Gladyshevskii, 1978, *Sov. Phys. Crystallogr.* **23**, 101-102.
- Kotur, B.Ya., O.I. Bodak and B.Ya. Kotur, 1980, *Dopov. Akad. Nauk Ukr. RSR, Ser. A(8)*, 80-83.
- Kotur, B.Ya., O.I. Bodak, M.G. Mis'kiv and E.I. Gladyshevskii, 1977, *Sov. Phys. Crystallogr.* **22**, 151-153.
- Kotur, B.Ya. and M. Sikirica, 1982, *Acta Crystallogr.* **B38**, 917-918.
- Kotur, B.Y. and M. Sikirica, 1982a, *J. Less-Common Metals* **83**, L29-L31.
- Kripyakevich, P.I., 1963, *J. Struct. Chem.* **4**, 103-121; 257-274.
- Kripyakevich, P.I., 1977, *Structure Types of Intermetallic Compounds (Nauka, Moscow) (in Russian)*.
- Kripyakevich, P.I., Y.Ya Markiv and E.V. Melnik, 1967, *Dopov. Akad. Nauk Ukr. RSR, Ser. A(8)*, 750-753.
- Kripyakevich, P.I. and Ya.P. Yarmolyuk, 1974, *Dopov. Akad. Nauk Ukr. RSR, Ser. A*, 460-463.
- Kripyakevich, P.I., Ya.P. Yarmolyuk and E.I. Gladyshevskii, 1969, *Sov. Phys. Crystallogr.* **13**, 677-681.

- Kripyakevich, P.I. and O.S. Zarechnyuk, 1968, *Dopov. Akad. Nauk Ukr. RSR, Ser. A*, 364-367.
- Ku, H.C., 1980, Ph.D. Thesis, Univ. of California at San Diego.
- Ku, H.C. and F. Acker, 1980, *Solid State Commun.* **35**, 937-943.
- Ku, H.C., D.C. Johnston, B.T. Matthias, H. Barz, G. Burri and L. Rinderer, 1979, *Mater. Res. Bull.* **14**, 1591-1599.
- Ku, H.C., B.T. Matthias and H. Barz, 1979, *Solid State Commun.* **32**, 937-944.
- Ku, H.C. and G.P. Meisner, 1981, *J. Less-Common Metals* **78**, 99-107.
- Ku, H.C. G.P. Meisner, F. Acker and D.C. Johnston, 1980, *Solid State Commun.* **35**, 91-96.
- Kuzma, Yu.B., 1970, *Sov. Phys. Crystallogr.* **15**, 312-314.
- Kuzma, Yu.B., 1970a, *Dopov. Akad. Nauk Ukr. RSR, Ser. A*, 756-758.
- Kuzma, Yu.B., 1976, *Sov. Phys. Crystallogr.* **20**, 636-638.
- Kuzma, Yu.B., 1979, *Dopov. Akad. Nauk Ukr. RSR, Ser. A*, 146-151.
- Kuzma, Yu.B. and N.S. Bilonizhko, 1971, *Inorg. Mater.* **7**, 542-544.
- Kuzma, Yu.B. and N.S. Bilonizhko, 1972, *Sov. Phys. Crystallogr.* **16**, 897-898.
- Kuzma, Yu.B. and N.S. Bilonizhko, 1974, *Sov. Phys. Crystallogr.* **18**, 447-449.
- Kuzma, Yu.B. and N.S. Bilonizhko, 1978, *Dopov. Akad. Nauk Ukr. RSR, Ser. A*, 275-277.
- Kuzma, Yu.B. and N.S. Bilonizhko, 1981, *Dopov. Akad. Nauk Ukr. RSR, Ser. A*(10), 87-90.
- Kuzma, Yu.B., N.S. Bilonizhko, N.F. Chaban and G.V. Chernyak, 1981, *J. Less-Common Metals* **82**, 364.
- Kuzma, Yu.B., N.S. Bilonizhko, S.I. Mykhailenko, G.F. Stepanchikova and N.F. Chaban, 1979, *J. Less-Common Metals* **67**, 51-57.
- Kuzma, Yu.B., N.S. Bilonizhko and E.M. Nimkovich, 1973, *Dopov. Akad. Nauk Ukr. RSR, Ser. A*(10), 939-941.
- Kuzma, Yu.B. and N.F. Chaban, 1980, *Dokl. Akad. Nauk Ukr. SSR, Ser. A*, 88-91.
- Kuzma, Yu.B., G.V. Chernyak and N.F. Chaban, 1981, *Dopov. Akad. Nauk Ukr. RSR, Ser. A*(12), 80-83.
- Kuzma, Yu.B. and M.P. Khaburskaya, 1975, *Inorg. Mater.* **11**, 1625-1626.
- Kuzma, Yu.B., P.I. Kripyakevich and N.S. Bilonizhko, 1969, *Dopov. Akad. Nauk Ukr. RSR, Ser. A*, 939-941.
- Kuzma, Yu.B., P.I. Kripyakevich and R.V. Skolozdra, 1966, *Dopov. Akad. Nauk Ukr. RSR*, 1290-1293
- Kuzma, Yu.B. and S.I. Mikhalenko, 1976, *Dopov. Akad. Nauk Ukr. RSR, Ser. A*, 1029-1031.
- Kuzma, Yu.B., S.I. Mikhalenko, B.Ya. Kotur and Ya.P. Yarmolyuk, 1982, *Dopov. Akad. Nauk Ukr. RSR, Ser. B*(3), 24-27.
- Kuzma, Yu.B., A.S. Sobolev and M.P. Furtak, 1970, *Inorg. Mater.* **6**, 1936-1937.
- Kuzma, Yu.B. and P.K. Starodub, 1973, *Inorg. Mater.* **9**, 337-340.
- Kuzma, Yu.B. and G.F. Stepanchikova, 1974, *Inorg. Mater.* **10**, 1905-1906.
- Kuzma, Yu.B. and S.I. Svarichevskaya, 1972, *Sov. Phys. Crystallogr.* **17**, 569-571.
- Kuzma, Yu.B. and S.I. Svarichevskaya, 1972a, *Dopov. Akad. Nauk Ukr. RSR, Ser. A*, 166-169.
- Kuzma, Yu.B. and S.I. Svarichevskaya, 1973, *Sov. Phys. Crystallogr.* **17**, 830-832.
- Kuzma, Yu.B., S.I. Svarichevskaya and V.N. Fomenko, 1973, *Inorg. Mater.* **9**, 1372-1374.
- Kuzma, Yu.B., S.I. Svarichevskaya and A.S. Sobolev, 1973, *Inorg. Mater.* **9**, 1512-1516.
- Kuzma, Yu.B. and Yu.V. Voroshilov, 1967, *Sov. Phys. Crystallogr.* **12**, 297-298.
- Kuzma, Yu.B. and Ya.P. Yarmolyuk, 1971, *J. Struct. Chem.* **12**, 422-424.
- Larson, A.C. and D.T. Cromer, 1961, *Acta Crystallogr.* **14**, 73-74.
- Larson, A.C., D.T. Cromer and R.B. Roof Jr., 1963, *Acta Crystallogr.* **16**, 835-836.
- Lemaire, R., J. Schweizer and J. Yakinthos, 1969, *Acta Crystallogr.* **B32**, 2697-2699.
- Le Roy, J., J.M. Moreau, D. Paccard and E. Parthé, 1978, *Acta Crystallogr.* **B34**, 3315-3318.
- Le Roy, J., J.M. Moreau, D. Paccard and E. Parthé, 1980, *J. Less-Common Metals* **76**, 131-135.
- Liebrich, O., H. Schäfer and A. Weiss, 1970, *Z. Naturforsch.* **25B**, 650-651.
- Lundström, T., 1968, *Acta Chem. Scand.* **22**, 2191-2199.
- Makarov, E.S. and S.I. Vinogradov, 1956, *Sov. Phys. Crystallogr.* **1**, 499-505.
- Mansey, R.C., G.V. Raynor and I.R. Harris, 1968, *J. Less-Common Metals* **14**, 337-347.
- Markiv, V.Ya., 1981, *Dopov. Akad. Nauk Ukr. RSR, Ser. A*(4), 86-89.
- Markiv, V.Ya., N.M. Belyavina, T.I. Zhunkivska and O.A. Babenko, 1982, *Dopov. Akad. Nauk Ukr. Ser. A*(4), 73-76.
- Markiv, V.Ya. and V.V. Burnashova, 1969, *Dopov. Akad. Nauk Ukr. RSR, Ser. A*, 463-464.
- Markiv, V.Ya. and A.I. Storozhenko, 1973, *Dopov. Akad. Nauk Ukr. RSR, Ser. A*, 941-943.
- Matthias, B.T., E. Corenzwit, J.M. Vandenberg and H.E. Barz, 1977, *Proc. Natl. Acad. Sci. USA* **74**, 1334-1335.
- May, N. and H. Schäfer, 1974, *Z. Naturforsch.* **29B**, 20-23.
- Mayer, I. and I. Felner, 1972, *J. Less-Common Metals* **29**, 25-31.
- Mayer, I. and I. Felner, 1973, *J. Solid State Chem.* **8**, 355-356.
- Mayer, I. and I. Felner, 1973a, *J. Solid State Chem.* **7**, 292-296.
- Mayer, I. and I. Felner, 1977, *J. Phys. Chem. Solids* **38**, 1031-1034.
- Mayer, I. and M. Tassa, 1969, *J. Less-Common Metals* **19**, 173-177.
- Mayer, I. and P.D. Yetor, 1977, *J. Less-Common Metals* **55**, 171-176.

- McCall, W.M., K.S.V.L. Narasimhan and R.A. Butera, 1973, *J. Appl. Crystallogr.* **6**, 301-303.
- McCullough, J.D., L. Brewer and L.A. Bromley, 1948, *Acta Crystallogr.* **1**, 287-289.
- Merlo, F. and M. Fornasini, 1981, *Acta Crystallogr.* **B37**, 500-503.
- Michel, D.J. and E. Riba, 1968, *Acta Crystallogr.* **B24**, 1267-1269.
- Miedema, A.R., 1976, *J. Less-Common Metals* **46**, 67-83.
- Mikhailenko, S.I., 1974, *Visn. L'vivsk. Univ., Ser. Khim.* **16**, 58-59.
- Mikhailenko, S.I., N.F. Chaban and Yu.B. Kuzma, 1981, *J. Less-Common Metals* **82**, 365.
- Mikhailenko, S.I. and Yu.B. Kuzma, 1975, *Dopov. Akad. Nauk Ukr. RSR, Ser. A*, 465-466.
- Mikhailenko, S.I. and Yu.B. Kuzma, 1977, *Dopov. Akad. Nauk Ukr. RSR, Ser. A*, 951-955.
- Misch, L., 1935, *Metallwirtsch.* **14**, 897-899.
- Mis'kiv, M.G., 1973, Thesis, Ivan Frank Univ., Lvov, USSR.
- Mis'kiv, M.G., 1974, *Visn. L'vivsk. Univ., Ser. Khim.* **15**, 17-21 [see *Structure Repts.* **41**, 44].
- Mis'kiv, M.G., P.I. Bodak and E.I. Gladyshevskii, 1974, *Sov. Phys. Crystallogr.* **18**, 450-453.
- Mis'kiv, M.G., O.I. Bodak and E.I. Gladyshevskii, 1974a, *Tezisy. Dokl. Vses. Konf. Kristalloghim. Internet. Soedin.*, 2nd Ed., ed. R.M. Rykhal (L'vov Gos. Univ., Lvov, USSR) pp. 31-32.
- Mokraya, I.R., O.I. Bodak and E.I. Gladyshevskii, 1979, *Sov. Phys. Crystallogr.* **24**, 729-730.
- Moreau, J.M., J. Le Roy and D. Paccard, 1982, *Acta Crystallogr.* **B38**, 2446-2448.
- Moreau, J.M., D. Paccard and E. Parthé, 1976, *Acta Crystallogr.* **B32**, 1767-1771.
- Narasimhan, K.S.V.L., V.U.S. Rao, R.L. Bergner and W.E. Wallace, 1975, *J. Appl. Phys.* **46**, 4957-4960.
- Niihara, K., Y. Katayama and S. Yajima, 1973, *Chem. Lett.* 613-614.
- Niihara, K., T. Shishido and S. Yajima, 1971, *Bull. Chem. Soc. Jpn.* **44**, 3214.
- Niihara, K., T. Shishido and S. Yajima, 1973, *Bull. Chem. Soc. Jpn.* **46**, 1137-1140.
- Niihara, K. and S. Yajima, 1972, *Chem. Lett.* 875-876.
- Niihara, K. and S. Yajima, 1973, *Bull. Chem. Soc. Jpn.* **46**, 770-774.
- Nowotny, H. and P. Rogl, 1977, in: *Boron and Refractory Borides*, ed. V.I. Matkovich (Springer, Berlin) Ch. C-XII.
- Nowotny, H., P. Rogl and J.C. Schuster, 1982, *J. Solid State Chem.* **44**, 126-133.
- Nylund, A., A. Roger, J.P. Sénateur and R. Fruchart, 1972, *J. Solid State Chem.* **4**, 115-122.
- Nyman, H. and B.G. Hyde, 1981, *Acta Crystallogr.* **A37**, 11-17.
- Oesterreicher, H., 1971, *J. Less-Common Metals* **25**, 341-342.
- Oesterreicher, H., 1971a, *J. Less-Common Metals* **25**, 228-230.
- Oesterreicher, H., 1973, *J. Phys. Chem. Solids* **34**, 1267-1280.
- Oesterreicher, H., 1973a, *J. Less-Common Metals* **33**, 25-41.
- Oesterreicher, H., 1973b, *J. Less-Common Metals* **30**, 225-236.
- Oesterreicher, H., 1975, *J. Less-Common Metals* **40**, 207-219.
- Oesterreicher, H. and R. Pitts, 1972, *J. Less-Common Metals* **29**, 100-103.
- Olenitch, R.R., L.G. Akselrud and Ya.P. Yarmolyuk, 1981, *Dopov. Akad. Nauk Ukr. RSR, Ser. A(2)*, 84-88.
- Olofsson, O. and E. Ganglberger, 1970, *Acta Chem. Scand.* **24**, 2389-2396.
- Paccard, D., J. Le Roy and J.M. Moreau, 1982, *Acta Crystallogr.* **B38**, 2448-2449.
- Parthé, E., 1967, *Colloq. Int. Centre Nat. Rech. Sci.* **157**, 195-205.
- Parthé, E., 1970, *Colloq. Int. Centre Nat. Rech. Sci.* **180**, 61-79.
- Parthé, E., 1976, *Acta Crystallogr.* **B32**, 2813-2818.
- Parthé, E., 1980, *Acta Crystallogr.* **B36**, 1-7.
- Parthé, E. 1981, in: *Structure and Bonding in Crystals*, eds. M. O'Keeffe and A. Navrotsky, Vol. II, Ch. 25 (Academic Press, New York) pp. 256-296.
- Parthé, E., B. Chabot, H.F. Braun and N. Engel, 1983, *Acta Crystallogr.* **B39**, 588-595.
- Parthé, E., B. Chabot and E. Hovestreydt, 1983, *Acta Crystallogr.* **B39**, 596-603.
- Parthé, E. and L. Gelato, 1983, *Acta Crystallogr. A*, in press.
- Parthé, E. and R. Lemaire, 1975, *Acta Crystallogr.* **B31**, 1879-1889.
- Parthé, E. and J.M. Moreau, 1977, *J. Less-Common Metals* **53**, 1-24.
- Pearson, W.B., 1979, *Acta Crystallogr.* **B35**, 1329-1333.
- Pecharskii, V.K., O.I. Bodak and E.I. Gladyshevskii, 1977, *Sov. Phys. Crystallogr.* **22**, 359-361.
- Pecharskii, V.K., O.I. Bodak and E.I. Gladyshevskii, 1978, *Dopov. Akad. Nauk Ukr. RSR, Ser. A*, 755-759.
- Pecharskii, V.K. O.I. Bodak and E.I. Gladyshevskii, 1978a, *Sov. Phys. Crystallogr.* **23**, 22-24.
- Pecharskii, V.K., O.I. Bodak and E.I. Gladyshevskii, 1979, *Sov. Phys. Crystallogr.* **24**, 433-438.
- Pecharskii, V.K., Yu.V. Pankevich and O.I. Bodak, 1982, *Dopov. Akad. Nauk Ukr. RSR, Ser. B(4)*, 44-48.
- Pelizzone, M., H.F. Braun and J. Muller, 1982, *J. Magn. Magn. Mater.* **30**, 33-36.
- Perlitz, H. and A. Westgren, 1943, *Ark. Kemi Min. Geol.* **16B(13)**, 5.
- Pfeifer, H.U. and K. Schubert, 1966, *Z. Metallkde.* **57**, 884-888.
- Pinto, H. and H. Shaked, 1973, *Phys. Rev.* **B7**, 3261-3266.
- Pop, I., N. Dihoin, M. Coldea and C. Hagan, 1979, *J. Less-Common Metals* **64**, 63-67.
- Pringle, G.E., 1972, *Acta Crystallogr.* **B28**, 2326-2328.
- Raman, A., 1967, *Naturwiss.* **54**, 560.

- Raman, A., 1968, *Inorg. Chem.* **7**, 973-976.
- Remeika, J.P., G.P. Espinosa, A.S. Cooper, H. Barz, J.M. Rowell, D.B. McWhan, J.M. Vandenberg, D.E. Moncton, Z. Fisk, L.D. Woolf, H.C. Hamaker, M.B. Maple, G. Shirane and W. Thomlinson, 1980, *Solid State Commun.* **34**, 923-926.
- Rieger, W., 1970, *Monatsh. Chem.* **101**, 449-462.
- Rieger, W., H. Nowotny and F. Benesovsky, 1966, *Monatsh. Chem.* **97**, 378-382.
- Rieger, W. and E. Parthé, 1969, *Monatsh. Chem.* **100**, 444-454.
- Rogl, P., 1973, *Monatsh. Chem.* **104**, 1623-1631.
- Rogl, P., 1978, *Mater. Res. Bull.* **13**, 519-523.
- Rogl, P., 1978a, *Acta Crystallogr.* **B34**, 721-724.
- Rogl, P., 1979, *Monatsh. Chem.* **110**, 235-243.
- Rogl, P., 1980, *Monatsh. Chem.* **111**, 517-527.
- Rogl, P., 1980a, *J. Nucl. Mater.* **92**, 292-298.
- Rogl, P., 1983, *J. Less-Common Metals*, in press.
- Rogl, P. and L. Delong, 1983, *J. Less-Common Metals* **91**, 97-106.
- Rogl, P. and H. Nowotny, 1975, *Monatsh. Chem.* **106**, 381-387.
- Rogl, P. and H. Nowotny, 1978, *J. Less-Common Metals* **61**, 39-45.
- Rogl, P. and H. Nowotny, 1979, *J. Less-Common Metals* **67**, 41-50.
- Rogl, P. and H. Nowotny, 1980, in: *The Rare Earths in Modern Science and Technology*, eds. G.J. McCarthy, J.J. Rhyne and H.B. Silber, Vol. 2 (Plenum, New York/London) pp. 173-179.
- Rogl, P. and H. Nowotny, 1982, in: *The Rare Earths in Modern Science and Technology*, eds. G.J. McCarthy, H.B. Silber and J.J. Rhyne, Vol. 3 (Plenum, New York/London) pp. 353-356.
- Romaka, V.A., Yu.N. Grin', Ya.P. Yarmolyuk, O.S. Zarechnyuk and R.V. Skolozdra, 1982, *Fiz. Metall. Metalloved. (USSR)* **54**, 691-696.
- Romaka, V.A., O.S. Zarechnyuk, R.M. Rykhal, Ya.P. Yarmolyuk and R.V. Skolozdra, 1982, *Fiz. Metall. Metalloved. (USSR)* **54**, 410-412 [English Transl. in *Phys. Metals Metallogr.*].
- Rossi, D., R. Marazza and R. Ferro, 1978, *J. Less-Common Metals* **58**, 203-207.
- Rossi, D., R. Marazza and R. Ferro, 1979, *J. Less-Common Metals* **66**, P17-P25.
- Rossi, D., R. Marazza, D. Mazzone and R. Ferro, 1978, *J. Less-Common Metals* **59**, 79-83.
- Rossi, D., D. Mazzone, R. Marazza and R. Ferro, 1983, *Z. Anorg. Allg. Chemie*, in press.
- Rundqvist, S., 1965, *Acta Chem. Scand.* **19**, 393-400.
- Rykhal, R.M., 1977, *Theoretical and Experimental Chemistry*, *Vestn. L'vovsk. Univ.*, Ser. *Khim.* **19**, 36-37.
- Rykhal, R.M., 1978, 3rd All-Union Conf. on the Crystal Chemistry of Intermetallic Compounds, Lvov, *Collected Abstracts*, p. 17.
- Rykhal, R.M. and O.S. Zarechnyuk, 1971, *Dopov. Akad. Nauk Ukr. RSR*, Ser. A, 854-856.
- Rykhal, R.M. and O.S. Zarechnyuk, 1977, *Dopov. Akad. Nauk Ukr. RSR*, Ser. A, 375-377.
- Rykhal, R.M., O.S. Zarechnyuk and N.V. German, 1971, *Russ. Metall.* **6**, 144-146.
- Rykhal, R.M., O.S. Zarechnyuk and Ya.I. Kuten, 1978, *Dopov. Akad. Nauk Ukr. RSR*, Ser. A, 1136-1138.
- Rykhal, R.M., O.S. Zarechnyuk and V.M. Mandzin, 1980, *Dopov. Akad. Nauk Ukr. RSR*, Ser. A(12), 77-79.
- Rykhal, R.M., O.S. Zarechnyuk and O.M. Marich, 1978, *Dopov. Akad. Nauk Ukr. RSR*, Ser. A, 853-855.
- Rykhal, R.M., O.S. Zarechnyuk and O.P. Matz'kiv, 1979, *Vestn. L'vovsk. Univ.*, Ser. *Khim.* **21**, 46-49.
- Rykhal, R.M., O.S. Zarechnyuk and G.V. Pishchik, 1973, *Dopov. Akad. Nauk Ukr. RSR*, Ser. A, 568-570.
- Rykhal, R.M., O.S. Zarechnyuk, V.S. Protasov and V.A. Romaka, 1982, *Dopov. Akad. Nauk Ukr. RSR*, Ser. B(3), 41-44.
- Rykhal, R.M., O.S. Zarechnyuk and T.I. Yanson, 1979, *Dokl. Akad. Nauk Ukr. SSR*, Ser. A, 1057-1059.
- Rykhal, R.M., O.S. Zarechnyuk and Ya.P. Yarmolyuk, 1972, *Sov. Phys. Crystallogr.* **17**, 453-455.
- Rykhal, R.M., O.S. Zarechnyuk and Ya.P. Yarmolyuk, 1977, *Dopov. Akad. Nauk Ukr. RSR*, Ser. A, 265-268.
- Sampathkumaran, E.V., L.C. Gupta, R. Vijayaraghavan, K.V. Gopalakrishnan, R.G. Pillay and H.G. Devare, 1981, *J. Phys. C: Solid State Phys.* **14**, L237-L241.
- Samson, S., 1958, *Acta Crystallogr.* **11**, 851-857.
- Sanderson, M.J. and N.C. Baenziger, 1953, *Acta Crystallogr.* **6**, 627-631.
- Schachner, H., H. Nowotny and H. Kudielka, 1954, *Monatsh. Chem.* **85**, 1140-1153.
- Schmidt, B. and W. Jung, 1978, *Z. Naturforsch.* **33b**, 1430-1433.
- Schubert, K. and A. Seitz, *Z. Anorg. Allg. Chemie* **254**, 116-125.
- Segre, C.U., 1981, Ph.D. Thesis, Univ. of California at San Diego, USA.
- Segre, C.U., H.F. Braun and K. Yvon, 1981, in: *Ternary Superconductors*, Proc. Conf. on Ternary Superconductors, Lake Geneva, WI, USA (24-26 Sept. 1980), eds. G.K. Shenoy, B.D. Dunlap and F.Y. Fradin (Elsevier-North-Holland, Amsterdam) pp. 243-246.
- Shelton, R.N., B.A. Karcher, D.R. Powell, R.A. Jacobson and H.C. Ku, 1980, *Mater. Res. Bull.* **15**, 1445-1452.
- Shoemaker, C.B. and D.P. Shoemaker, 1965, *Acta Crystallogr.* **18**, 900-905.
- Shoemaker, C.B. and D.P. Shoemaker, 1969, in: *Developments in the Structural Chemistry of Alloy Phases*, ed. B.C. Giessen (Plenum, New York) pp. 107-137.
- Sichevich, O.M., R.E. Gladyshevskii, Yu.N. Grin' and Ya.P. Yarmolyuk, 1982, *Dopov. Akad. Nauk Ukr. RSR*, Ser. B(11), 57-59.
- Siek, S., A. Szytula and J. Leciejewicz, 1978, *Phys. Stat. Sol.* **A46**, K101-K105.
- Skolozdra, R.V., 1977, *Theoretical and Experimental Chemistry*, *Vestn. L'vovsk. Univ.*, Ser. *Khim.* **19**, 40-42.



- Skolozdra, R.V., Yu.K. Gorenko, O.I. Bodak and V.I. Yarovets, 1980, *Ukr. Fiz. Zh.* **25**(10), 1683-1687.
- Skolozdra, R.V., O.E. Koretskaya and Yu.K. Gorenko, 1982, *Ukr. Fiz. Zh.* **27**, 263-266.
- Skolozdra, R.V., V.M. Mandzyk and L.G. Akselrud, 1981, *Sov. Phys. Crystallogr.* **26**, 272-274.
- Skolozdra, R.V., V.M. Mandzyk, Yu.K. Gorenko and V.D. Tkachuk, 1981, *Fiz. Metall. Metalloved.* **52**, 966-970.
- Skolozdra, O.E., R.V. Skolozdra and E.I. Gladyshevskii, 1967, *Inorg. Mater.* **3**, 727-729.
- Slaski, M. and A. Szytula, 1982, *J. Less-Common Metals* **87**, L1-L3.
- Smith, G.S., Q. Johnson and A.G. Tharp, 1967, *Acta Crystallogr.* **23**, 269-272.
- Sobczak, R. and P. Rogl, 1979, *J. Solid State Chem.* **27**, 343-348.
- Sobolev, A.S., O.I. Bodak and E.I. Gladyshevskii, 1971, *Inorg. Mater.* **7**, 37-40.
- Spear, K.E. and P.W. Gilles, 1969, *High Temp. Sci.* **1**, 86-97.
- Spinat, P., R. Fruchart and P. Herpin, 1970, *Bull. Soc. Fr. Mineral. Cristallogr.* **93**, 23-36.
- Steinmetz, J. and B. Roques, 1977, *J. Less-Common Metals* **32**, 247-258.
- Steinmetz, J., G. Venturini, B. Roques, N. Engel, B. Chabot and E. Parthé, 1982, *Acta Crystallogr.* **B38**, 2103-2108.
- Stepanchikova, G.F., 1979, *Visn. L'vivsk. Politekh. Inst.* **130**, 58-61.
- Stepanchikova, G.F. and Yu.B. Kuzma, 1976, *Visn. L'vivsk. Univ., Ser. Khim.* **18**, 16-19.
- Stepanchikova, G.F. and Yu.B. Kuzma, 1977, *Theoretical and Experimental Chemistry, Vestn. L'vovsk. Univ., Ser. Khim.* **19**, 37-40.
- Stepanchikova, G.F. and Yu.B. Kuzma, 1981, *Vestn. L'vovsk. Univ., Ser. Khim.* **23**, 48-51.
- Stepanchikova, G.F., Yu.B. Kuzma and B.I. Chernyak, 1978, *Dopov. Akad. Nauk Ukr. RSR, Ser. A*, 950-953.
- Stepien, J.A., K. Lukaszewicz, E.I. Gladyshevskii and O.I. Bodak, 1972, *Bull. Acad. Pol. Sci., Ser. Sci. Chim.* **20**, 1029-1036.
- Steurer, W., P. Rogl and H. Nowotny, 1979, 6th Intern. Conf. on Solid Compounds of Transition Elements, Stuttgart (June 12-16, 1979), *Collected Abstracts*, pp. 93-95.
- Szytula, A. and I. Szott, 1981, *Solid State Commun.* **40**, 199-202.
- Teslyuk, M.Yu., 1969, *Metallic Compounds with Laves Phase Structure (Nauka, Moscow) (in Russian)*.
- Teslyuk, M.Yu. and V.S. Protasov, 1965, *Dopov. Akad. Nauk Ukr. RSR, Ser. A*, 599-601.
- Tiburtius, C. and H.U. Schuster, 1977, *Z. Naturforsch.* **32b**, 1133-1138.
- Vandenberg, J.M., 1980, *Mater. Res. Bull.* **15**, 835-847.
- Vandenberg, J.M. and H. Barz, 1980, *Mater. Res. Bull.* **15**, 1493-1498.
- Vandenberg, J.M. and B.T. Matthias, 1977, *Proc. Natl. Acad. Sci. USA* **74**, 1336-1337.
- Vandenberg, J.M., B.T. Matthias, E. Corenzwit and H. Barz, 1976, *J. Solid State Chem.* **18**, 395-396.
- Venturini, G., J. Steinmetz and B. Roques, 1982, *J. Less-Common Metals* **87**, 21-30.
- Vivchar, O.I., O.S. Zarechnyuk and V.R. Ryabov, 1970, *Russ. Metall.* **1**, 140-143.
- Vivchar, O.I., O.S. Zarechnyuk and V.R. Ryabov, 1973, *Dopov. Akad. Nauk Ukr. RSR, Ser. A*(2), 159-161.
- Vlasse, M., T. Ohtani, B. Chevalier and J. Etourneau, 1983, *J. Solid State Chem.* **46**, 188-192.
- Voroshilov, Yu.V., P.I. Kripyakevich and Yu.B. Kuzma, 1971, *Sov. Phys. Crystallogr.* **15**, 813-816.
- Welk, E. and H.U. Schuster, 1976, *Z. Anorg. Allg. Chem.* **424**, 193-197.
- Westgren, A. and G. Phragmén, 1925, *K. Sven. Vetensk. Akad. Handl.* **2**, 1.
- Widera, A., B. Eisenmann, H. Schäfer and K. Turban, 1976, *Z. Naturforsch.* **31b**, 1592-1595.
- Wilson, C.G., D.K. Thomas and F.J. Spooner, 1960, *Acta Crystallogr.* **13**, 56-57; 358-359.
- Witte, H., 1939, *Metallwirtschaft* **18**, 459-463.
- Yarmolyuk, Ya.P., L.G. Akselrud, V.S. Fundamenskii and E.I. Gladyshevskii, 1980, *Sov. Phys. Crystallogr.* **25**, 97-98.
- Yarmolyuk, Ya.P., L.G. Akselrud and E.I. Gladyshevskii, 1977, *Sov. Phys. Crystallogr.* **22**, 358-359.
- Yarmolyuk, Ya.P., L.G. Akselrud and E.I. Gladyshevskii, 1978, *Sov. Phys. Crystallogr.* **23**, 531-533.
- Yarmolyuk, Ya.P., L.G. Akselrud, Yu.N. Grin', V.S. Fundamenskii and E.I. Gladyshevskii, 1979, *Sov. Phys. Crystallogr.* **24**, 332-333.
- Yarmolyuk, Ya.P. and Yu.N. Grin', 1979, IIIrd Interunion Seminar for Young Scientists, General Problems of Crystal Chemistry, *Tezisy Dokl., Lvov*, pp. 69-70.
- Yarmolyuk, Ya.P. and Yu.N. Grin', 1981, *Russ. Metall.* **81**(5), 179-183.
- Yarmolyuk, Ya.P., Yu.N. Grin' and E.I. Gladyshevskii, 1977, *Sov. Phys. Crystallogr.* **22**, 416-419.
- Yarmolyuk, Ya.P., Yu.N. Grin' and E.I. Gladyshevskii, 1978, *Dopov. Akad. Nauk Ukr. RSR, Ser. A*, 855-858.
- Yarmolyuk, Ya.P., Yu.N. Grin' and E.I. Gladyshevskii, 1978a, *Dopov. Akad. Nauk Ukr. RSR, Ser. A*, 759-763.
- Yarmolyuk, Ya.P., Yu.N. Grin' and E.I. Gladyshevskii, 1979, *Dopov. Akad. Nauk Ukr. RSR, Ser. A*, 771-775.
- Yarmolyuk, Ya.P., Yu.N. Grin' and E.I. Gladyshevskii, 1981, *Dokl. Akad. Nauk SSSR* **260**, 1139-1143.
- Yarmolyuk, Ya.P., Yu.N. Grin' and O.M. Olesh, 1980, *Sov. Phys. Crystallogr.* **25**, 143-146.
- Yarmolyuk, Ya.P., Yu.N. Grin', I.V. Rozhdestvenskaya, O.A. Usov, A.M. Kuzmin, V.A. Bruskov and E.I. Gladyshevskii, 1982, *Sov. Phys. Crystallogr.* **27**, 599-600.
- Yarmolyuk, Ya.P., Yu.N. Grin', O.A. Usov, A.M. Kuzmin, I.V. Rozhdestvenskaya, V.A. Bruskov and E.I. Gladyshevskii, 1981, *Acta Crystallogr.* **37A**, Suppl. C-183, Paper 08.3-05.
- Yarmolyuk, Ya.P., B.Ya. Kotur and Yu.N.

- Grin', 1980, *Dopov. Akad. Nauk Ukr. RSR, Ser. B*(11), 68-72.
- Yarmolyuk, Ya.P. and P.I. Kripyakevich, 1976, *Dopov. Akad. Nauk Ukr. RSR, Ser. A*, 86-88; *Dokl. Akad. Nauk Ukr. SSR, Ser A*(1), 88-91.
- Yarmolyuk, Ya.P., L.A. Lysenko and E.I. Gladyshevskii, 1975, *Dopov. Akad. Nauk Ukr. RSR, Ser. A*, 279-282.
- Yarmolyuk, Ya.P., L.A. Lysenko and E.I. Gladyshevskii, 1976, *Sov. Phys. Crystallogr.* **21**, 473-475.
- Yarmolyuk, Ya.P., R.M. Rykhal, L.G. Akselrud and O.S. Zarechnyuk, 1981, *Dopov. Akad. Nauk Ukr. RSR, Ser. A*(9), 86-90.
- Yarmolyuk, Ya.P., M. Sikiritsa, L.G. Akselrud, L.A. Lysenko and E.I. Gladyshevskii, 1982, *Sov. Phys. Crystallogr.* **27**, 1090-1093.
- Yarovets, V.I., 1977, *Theoretical and Experimental Chemistry, Vestn. L'vovsk. Univ., Ser. Khim.* **19**, 30-34.
- Yarovets, V.I., 1978, 3rd All-Union Conf. on the Crystal Chemistry of Intermetallic Compounds, Lvov, Collected Abstracts, p. 124.
- Yarovets, V.I. and Yu.K. Gorelenko, 1981, *Vestn. L'vovsk. Univ., Ser. Khim.* **23**, 20-23.
- Yvon, K., 1981, in: *Ternary Superconductors, Proc. Conf. on Ternary Superconductors, Lake Geneva, WI, USA (24-26 Sept. 1980)*, eds. G.K. Shenoy, B.D. Dunlap and F.Y. Fradin (Elsevier-North-Holland, Amsterdam) pp. 15-20.
- Yvon, K. and A. Grüttner, 1980, in: *Superconductivity in d- and f-band Metals*, eds. H. Suhl and M.B. Maple (Academic Press, New York) pp. 515-519.
- Yvon, K. and D.C. Johnston, 1982, *Acta Crystallogr.* **B38**, 247-250.
- Zarechnyuk, O.S., 1966, *Dopov. Akad. Nauk Ukr. RSR, Ser. A*, 767-769.
- Zarechnyuk, O.S., E.I. Emes-Misenko and V.R. Ryabov, 1968, *Russ. Metall.* **3**, 133-134.
- Zarechnyuk, O.S., E.I. Emes-Misenko, V.R. Ryabov and I.I. Dikiy, 1968, *Russ. Metall.* **3**, 152-154.
- Zarechnyuk, O.S., I.F. Kolobnev and M.Yu. Teslyuk, 1963, *Russ. J. Inorg. Chem.* **8**, 868-870.
- Zarechnyuk, O.S. and P.I. Kripyakevich, 1963, *Sov. Phys. Crystallogr.* **7**, 436-446.
- Zarechnyuk, O.S., P.I. Kripyakevich and E.I. Gladyshevskii, 1965, *Sov. Phys. Crystallogr.* **9**, 706-708.
- Zarechnyuk, O.S., M.G. Mis'kiv and V.R. Ryabov, 1969, *Russ. Metall.* **2**, 133-135.
- Zarechnyuk, O.S. and R.M. Rykhal, 1974, *Visn. L'vivsk. Univ., Ser. Khim.* **16**, 5-8.
- Zarechnyuk, O.S. and R.M. Rykhal, 1981, *Vestn. L'vovsk. Univ., Ser. Khim.* **23**, 45-47.
- Zarechnyuk, O.S., R.M. Rykhal and V.V. Korin, 1980, *Dopov. Akad. Nauk Ukr. RSR, Ser. A*(1), 84-86.
- Zarechnyuk, O.S., O.I. Vivchar and V.R. Ryabov, 1970, *Dopov. Akad. Nauk Ukr. RSR, Ser. A*, 943-945.
- Zarechnyuk, O.S., O.I. Vivchar and V.R. Ryabov, 1972, *Visn. L'vivsk. Univ., Ser. Khim.* **14**, 16-19.
- Zintl, E. and W. Hauke, 1938, *Z. Elektrochem.* **44**, 104-111.
- Zmii, O.F. and E.I. Gladyshevskii, 1971, *Sov. Phys. Crystallogr.* **15**, 817-819.
- Zmii, O.F., E.I. Gladyshevskii and V.S. Bulov, 1973, *Sov. Phys. Crystallogr.* **18**, 171-172.

## Chapter 49

# PHASE EQUILIBRIA IN TERNARY AND HIGHER ORDER SYSTEMS WITH RARE EARTH ELEMENTS AND BORON

Peter ROGL

*Institut für Physikalische Chemie, Universität Wien, Währingerstrasse 42,  
A-1090 Vienna, Austria*

---

### Contents

1. Introduction	336
2. Ternary systems	338
3. Quaternary and higher order systems	482
4. Notes added in proof	505

---

### Symbols and abbreviations

$a, b, c$	unit cell dimensions in Å (for rhombohedral symmetry denoted as $a_R$ ; for the equivalent triple-primitive hexagonal cell indicated as $a_H, c_H$ )
a/o	composition in atomic percentage
AM(Zr)	A(arc) M(melting) under Zr-gettered argon atmosphere
CP	powder mixtures were cold pressed
HT(Ar)	heat treatment under argon atmosphere
HV	high vacuum, $\approx 10^{-4}$ Pa
ME	metallographic analysis
mol%	composition in molar percentage
PXD	powder X-ray diffraction analysis
QE	samples radiation quenched
Qu(Mo)	samples wrapped in Mo foil and sealed in evacuated silica (quartz) tubes for heat treatment
$R$	reliability factor of crystal structure determination, defined as $\Sigma \Delta F /\Sigma F_{\text{obs}} $
$T_c$	superconducting transition temperature, in K
$T_m$	magnetic ordering temperature, in K
$T_N$	Néel temperature, in K
$T_n$	sample remained normal (with respect to superconductivity) down to $T$ , in K
w/o	composition in weight percentage
$\alpha, \beta, \gamma$	unit cell angles in degrees
$\rho_E$	measured density (kg/dm <sup>3</sup> )
$\rho_x$	calculated density (kg/dm <sup>3</sup> ); theoretical density, corresponding to the composition and parameters obtained from X-ray data, atomic weight based on <sup>12</sup> C, $N = 6.022 \times 10^{23}$ atoms/gmol

---

## 1. Introduction

The present status of information about phase equilibria and formation of ternary metal borides with R elements (R = Sc, Y, and the lanthanides) is summarized in fig. 1. Only a small number of the possible ternary combinations R-M-B have been investigated by now and for a larger number only a few compounds have been identified. Little information is available involving main group elements.

Most of the ternary phase diagram studies (isothermal sections) have been carried out by Kuz'ma and coworkers at Lvov University, USSR. Only recently the interesting interplay of superconducting and magnetic properties, first discovered by Matthias and coworkers (Bell Laboratories and University of California at San Diego), has stimulated a world-wide activity in low-temperature investigations of primarily R-Platinum metal-boron alloys. Comprehensive reviews on electrical and magnetic properties of these materials can be found in recent articles written by Maple (1981) and Johnston and Braun (1982). Whereas most binary boride phase diagrams are now well established, for a number of systems careful revisions seem to be necessary.

For binary R-B systems an excellent compilation has recently been presented by Spear (1976).

As far as the present compilation of phase diagram data of R-M-B systems is concerned, no efforts have been made to recompile data on the binary systems involved—and thus for details the reader is referred to the well-known handbooks on binary diagrams by Hansen (1958), Ageev (1959), Elliott (1965), Shunk (1969), Gschneidner and Verkade (1974), Spear (1976), Moffatt (1976), and Spear (1978). Therefore binary phase diagrams are rather briefly discussed, but it was the general

B	Ti	Zr	Hf	V	Nb	Ta	Cr	Mo	W	Mn	Tc	Re	Fe	Ru	Os	Co	Rh	Ir	Ni	Pd	Pt	Cu	Ag	Au	Zn	Cd	Hg	Al	Ga	In	Tl	C	Si	Ge	Sn	Pb		
Sc							1						0	3	3	4		2	1												1	1	3		0	1	1	
Y				1			1	1	1			5	6	5	5	10	5	2	11									0						0	4	0	0	
La							0	0	0			3	3	2	2	6	1	2	6															3	0	0	0	
Ce				0	0		2	1	0		1	2	3	2	2	13	1	2	6			0							0					3	0	0	0	
Pr							2	1	0				2	2	6	2	2	2																	3			
Nd							2						3	2	2	6	2	2	6																3			
Pm																																						
Sm								2					4	2	1	13	2	2	3																	3		
Eu				0					0				2	1		2	1	1	1																	2		
Gd	0	0	0	0	0	0	1	1	1	1	1	5	5	4	4	9	2	2	4				0												5			
Tb							1	1	1	1	1	3	3	5	5	7	2	2	3																	5		
Dy							1	1	1	1	1	4	3	5	5	7	2	1	3																	5		
Ho							1	1	1	1	1	4	3	5	5	7	2	2	2																	5		
Er							1	1	1	1	1	3	3	5	5	7	4	2	4																	5		
Tm							1					3	1	5	5	6	3	2	4																	5		
Yb													4	3	2	2	1	2																	2		1	
Lu							1					1	2	5	5	5	4	1	4															1			5	

Fig. 1. Existence of ternary borides and phase equilibria in ternary boride systems of the type R-M-B. (R = rare earth element, M = element as indicated, B = boron). ■ complete isothermal section has been established, ▣ partial isothermal section established. The numbers in the squares correspond to the number of ternary compounds observed for each particular elemental combination.

intention to incorporate the most recent results and to point out those problems where further investigations will have to clarify points still in question.

Hardly any phase diagram studies were found to concentrate on the boron-rich corner of multicomponent systems and many confusing results exist about boron-rich transition metal borides, which more recently turned out to merely represent a solid solution of metal atoms in  $\beta$ -rhombohedral boron. Only few reliable data exist on the solubility limits of metals in the different boron modifications as a function of temperature as well as on the (stabilizing) influence of T metals on the polymorphic transition itself. Thus metal solubilities in B indicated throughout this publication are the "ss of M in  $\beta$ -rh. B".

Furthermore, mutual solubilities of the binary phases—and the same holds for the homogeneity ranges of ternary compounds—have been determined in exceptionally few cases with a higher degree of reliability. Therefore the solubilities indicated ( $\leq 0.5$  a/o) are schematic in all cases not especially specified and should serve as a guideline only. From the various influences of the factors responsible for the stability of a crystal structure of a given composition (geometrical, electrochemical, and energy band factor), complete or extended solid solutions can be expected to form between isotypic binary borides of the same or neighboring group numbers. From the well-known similarity in the alloying behavior of the R members, in those cases where exact phase equilibria have not been determined the known phase equilibria of one of the neighboring R may serve as a first order approximation for the phase diagram. However, exchange of the non-R metal constituent by one of the homologous elements (or even changing to a neighboring group number) in general causes a considerable change in phase equilibria.

All data used in this chapter were obtained from a manual collection of the author compiled over the last 15 years as well as from a computerized literature search consulting CAC (Chemical Abstracts Condensates), and METADEX (Metals Abstracts—Alloys Index) services up to July 1982.

No attempt however has been made to include papers concerning numerous technical alloys (i.e., much has been said about physical properties of R hexaborides), unless they revealed valuable information on phase equilibria, solid solubilities, lattice parameters or crystal structure data.

The "short" Hermann Mauguin symbol (according to the International Tables for X-ray Crystallography, 1974) has been used to characterize the crystal structure of each ternary compound in combination with its formula and the name of the structure type (representative substance).

Whenever information on atomic parameters or metal ordering—deviating from the general description of the structure type concerned—was available it has been included; however, for a more detailed description of the crystallographic structure types, the reader is referred to Parthé and Chabot's contribution to this volume of the Handbook, ch. 48.

Rare earth-metal-boron ternary phase diagrams are listed in alphabetical order of the chemical symbol of the rare earth element (Sc, Y, La, Ce, . . . , Lu). Under each rare earth the systems are listed alphabetically by the chemical symbol of the non-rare-earth element. After the ternary systems, higher order systems are presented following the same scheme.

### References

- Ageev, N.V., 1959, Phase Diagrams of Metallic Systems (Viniti Press, Acad. Sci. USSR, Moscow) (in Russian); regularly updated.
- Elliott, R.P., 1965, Constitution of Binary Alloys, First Supplement (McGraw-Hill, New York).
- Gschneidner Jr., K.A. and M.E. Verkade, 1974, Selected Cerium Phase Diagrams, Document IS-RIC-7, Rare Earth Information Center, Iowa State Univ., Ames, IA, USA.
- Hansen, M., 1958, Constitution of Binary Alloys, 2nd Ed. (McGraw-Hill, New York).
- Johnston, D.C. and H.F. Braun, 1982, Systematics of Superconductivity in Ternary Compounds, in: Superconductivity in Ternary Compounds, eds. Ø. Fischer and M.B. Maple (Springer, Berlin).
- Maple, B., 1981, Superconductivity and magnetism of rare earth rhodium boride compounds, in: Ternary Superconductors, Proc. Intern. Conf. on Ternary Superconductors, Lake Geneva, WI, USA (1980), eds. G.K. Shenoy, B.D. Dunlap and F.Y. Fradin (North-Holland, Amsterdam) pp. 131–139.
- Moffatt, W.G., 1976, The Handbook of Binary Phase Diagrams (General Electric Comp., Schenectady, NY), updating service.
- Shunk, F.A., 1969, Constitution of Binary Alloys, Second Supplement, (McGraw-Hill, New York).
- Spear, K.E., 1976, Phase Behavior and Related Properties of Rare Earth Borides, in: Phase Diagrams in Materials Science and Technology, ed. A.M. Alper (Academic Press, New York).
- Spear, K.E., 1978, Correlations and Predictions of Metal-Boron Phase Equilibria, in: Applications of Phase Diagrams in Metallurgy and Ceramics, NBS Special Publ. NBS-496, Vol. 2, pp. 744–762.

## 2. Ternary systems

### *R-Pd-B*

Dhar et al. (1981) studied the stabilizing influence of boron fill-up in the binary phases  $RPd_3$  with  $Cu_3Au$ -type,  $Pm\bar{3}m$ . Samples were prepared by arc melting of the constituents under Ar. Alloys with intermediate compositions were arc melted from  $RPd_3$  and  $RPd_3B$  master alloys. Samples obtained for  $YbPd_3B$  as well as  $CePd_3B_x$  ( $x > 1.5$ ) were multiphase. Lattice parameters (X-ray powder diffraction of as-cast alloys) as a function of R in  $RPd_3$  and  $RPd_3B_x$ , as well as the variation of lattice parameter with boron concentration  $x$  in  $RPd_3B_x$  are represented in fig. 2. Samples obtained were claimed to be single phase for  $x \leq 1$  from X-ray powder diffraction

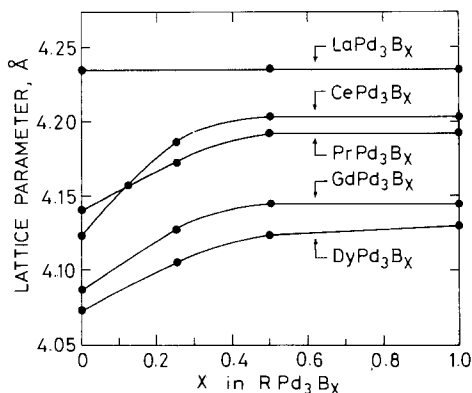


Fig. 2. The variation of lattice parameters with boron concentration  $x$  in  $RPd_3B_x$  compounds ( $R = La, Ce, Pr, Gd$  and  $Dy$ ); after Dhar et al. (1981).

analysis. However, no metallographic analysis or/and detailed determination of the final boron content has been carried out. As seen from the graph, the lattice parameter of  $\text{LaPd}_3\text{B}_x$  stays constant for  $0 < x \leq 1$  (boron fill-up?). Similarly the constant lattice parameters for  $\text{RPd}_3\text{B}_x$  ( $\text{R} = \text{Ce}, \text{Pr}, \text{Gd}, \text{Dy}$ ) with  $x > 0.5$  possibly indicate a rather incomplete (50%) filling of the octahedral voids. The lattice parameter variation of  $(\text{Ce}, \text{Eu})\text{Pd}_3\text{B}_x$  with increasing boron content was interpreted from susceptibility measurements as a valence change of the R-ion from a higher to a lower valence state.

### Reference

Dhar, S.K., S.K. Malik and R. Vijayaraghavan, 1981, *Mater. Res. Bull.* **16**, 1557.

### R-Rh-B

Pressure dependencies up to 21 kbar of the superconducting and magnetic transition temperatures of  $\text{RRh}_4\text{B}_4$  borides were studied by Shelton and Johnston (1978), for  $\text{R} = \text{Nd}, \text{Sm}, \text{Gd}, \text{Tb}, \text{Dy}, \text{Ho}, \text{Er}, \text{Tm}, \text{Lu}, \text{Y}$ . No structural details were given, but from  $T_c$  values the  $\text{CeCo}_4\text{B}_4$ -type of structure,  $\text{P4}_2/\text{nmc}$ , can be inferred.

X-ray magnetization and Mössbauer studies were performed on hexagonal compounds  $\text{RRh}_6\text{B}_4$  by Felner and Nowik (1980). Samples were prepared from elements (99.9% R, 99.999% Rh, B) by melting in an induction furnace. The new ternary compounds were reported to be "stable and well defined" for all the R elements, with a hexagonal unit cell  $a \approx 5.65$ ,  $c \approx 17.1$ ,  $\rho_{\text{exp}} \approx 10.2 \text{ kg/dm}^3$ . Relatively large single crystals were obtained from the melt and X-ray powder patterns of  $\text{EuRh}_6\text{B}_4$  were said to be indexed completely with the hexagonal unit cell; the crystal structure is unsolved. Magnetic data were presented for  $\text{R} = \text{Y}, \text{La}, \text{Ce}, \text{Eu}^{3+}, \text{Lu}$ .

Boron was found to stabilize ternary compounds  $\text{RRh}_3\text{B}_{1-x}$  with perovskite-type structure ( $\text{Cu}_3\text{Au}$ -type),  $\text{Pm}3\text{m}$ . Samples were prepared by arc melting and subsequent homogenization in a high vacuum at  $1300^\circ\text{C}$  and were investigated by chemical, X-ray and metallographic analysis. Lattice parameter ranges are shown in fig. 3.  $\text{ScRh}_3$  and  $\text{CeRh}_3$  are the only binary  $\text{Cu}_3\text{Au}$ -type phases reported (Iandelli and Palenzona, 1979).

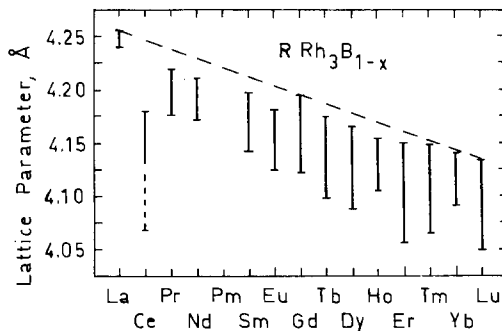


Fig. 3. Lattice parameter ranges of perovskite borides  $\text{RRh}_3\text{B}_{1-x}$  as a function of the atomic number of R; after Holleck (1973).

An excellent review comprising superconductivity and magnetism of  $RRh_4B_4$  borides can be found in the articles by Maple (1981) and Johnston and Braun (1982).

From  $^{155}\text{Gd}$  Mössbauer experiments Shenoy et al. (1982) measured the quadruple interaction in  $\text{GdRh}_4\text{B}_4$  and from this they were able to deduce the crystalline electric field Hamiltonian terms for the  $RRh_4B_4$  compounds with  $R = \text{Gd, Tb, Dy, Ho, Er}$  and  $\text{Tm}$ . For  $R = \text{Pr, Nd, Tb, Dy, Ho, Er, Tm}$  see also Dunlap and Niarchos (1982).

### References

- Dunlap, B.D. and D. Niarchos, 1982, *Solid State Commun.* **44**(12), 1577.  
 Felner, I. and I. Nowik, 1980, *Phys. Rev. Lett.* **45**(26), 2128.  
 Holleck, H., 1973, *Perovskite Carbides and Borides of the Transition Metals*, paper presented at the 4th Intern. Conf. on Solid Compounds of Transition Elements, Geneva.  
 Iandelli, A. and A. Palenzona, 1979, *Crystal chemistry of intermetallic compounds*, in: *Handbook on the Physics and Chemistry of Rare Earths*, Vol. 2, eds. K.A. Gschneidner, Jr. and L. Eyring (North-Holland, Amsterdam) pp. 1–54.  
 Johnston, D.C. and H.F. Braun, 1982, *Systematics of superconductivity in ternary compounds*, in: *Superconductivity in Ternary Compounds*, Vol. 2, eds. Ø. Fischer and M.B. Maple (Springer, Berlin).  
 Maple, M.B., 1981, *Superconductivity and magnetism of rare earth rhodium boride compounds*, in: *Ternary Superconductors*, Proc. Intern. Conf. on Ternary Superconductors, Lake Geneva, WI, USA (1980), eds. G.K. Shenoy, B.D. Dunlap and F.Y. Fradin (North-Holland, Amsterdam) pp. 131–139.  
 Shelton, R.N. and D.C. Johnston, 1978, *Pressure dependencies of the superconducting and magnetic critical temperatures of ternary rhodium borides*, in: *High Pressure and Low Temperature Physics*, eds. C.W. Chu and J.A. Wollam (Plenum, New York) pp. 409–417.  
 Shenoy, G.K., D.R. Noakes and D.G. Hinks, 1982, *Solid State Commun.* **42**(6), 411.

### Ce–Al–B

Chaban and Kuz'ma (1971) reported a partial isothermal section at  $500^\circ\text{C}$  (fig. 4). Phase equilibria within the region  $\text{Ce–Al–CeB}_6$  were derived from X-ray and

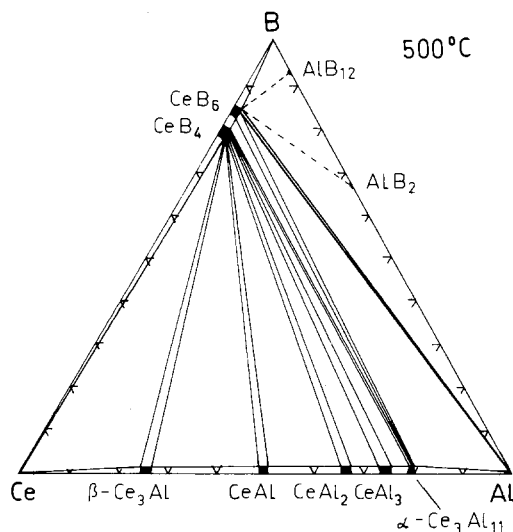


Fig. 4. Ce–Al–B, isothermal section at  $500^\circ\text{C}$ ; region  $\text{CeB}_6\text{–B–Al}$  is proposed.



metallographic analysis of arc melted and subsequently heat treated samples (500°C, 400 h in evacuated quartz capsules). Starting materials were: Ce ingot 99.56%, B powder 99.3% and Al powder 99.997%.

No ternary compounds were reported, mutual solid solubilities of Ce-B and Ce-Al alloys were negligible. Phase equilibria within the region B-Al-CeB<sub>6</sub> are proposed. The Ce-Al binary system [ $\beta$ -Ce<sub>3</sub>Al (Cu<sub>3</sub>Au-type), CeAl, CeAl<sub>2</sub> (MgCu<sub>2</sub>-type), CeAl<sub>3</sub> (Ni<sub>3</sub>Sn-type), Ce<sub>3</sub>Al<sub>11</sub> (La<sub>3</sub>Al<sub>11</sub>-type)] has been revised according to a recent critical assessment by Gschneidner (1981).

*References*

Chaban, N.F. and Yu.B. Kuz'ma, 1971, *Dopov. Akad. Nauk Ukr. RSR, Ser. A* **11**, 1048.  
 Gschneidner Jr., K.A., 1981, *Bulletin of Alloy Phase Diagrams* **2**(2), 224.

*Ce-Co-B*

Using X-ray and metallographic analysis, Bilonishko and Kuz'ma (1974) investigated the phase equilibria within the Ce-Co-B system in two isothermal sections at 800°C (region 0-33 a/o Ce) and at 400°C for the region 33.3-100 a/o Ce (fig. 5). 189 samples were prepared from elemental powder mixtures (Ce ingot 98.9%, Co 99.87% and B 99.3% powders) by arc melting and subsequent annealing in evacuated quartz capsules for 330 h at 800°C or 500 h at 400°C (quenched in water). According to a recent survey of Ce phase diagrams by Gschneidner and Verkade (1974) Ce<sub>5</sub>Co<sub>19</sub> has been included among the binary Ce-Co compounds observed (fig. 5): Ce<sub>2</sub>Co<sub>17</sub>

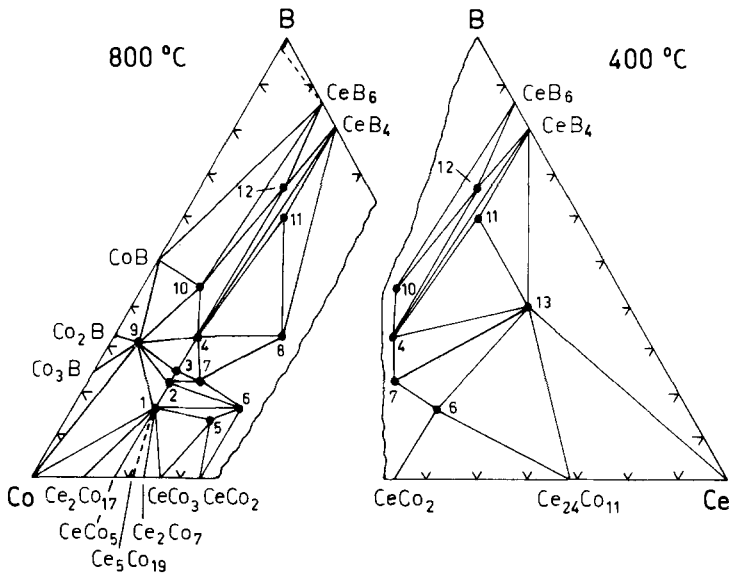


Fig. 5. Ce-Co-B, partial isothermal sections at 800°C (0-33 a/o Ce), and at 400°C (33-100 a/o Ce). 1: CeCo<sub>4</sub>B, 2: Ce<sub>3</sub>Co<sub>11</sub>B<sub>4</sub>, 3: Ce<sub>2</sub>Co<sub>7</sub>B<sub>3</sub>, 4: CeCo<sub>3</sub>B<sub>2</sub>, 5: Ce<sub>2</sub>Co<sub>4</sub>B, 6: Ce<sub>2</sub>Co<sub>3</sub>B, 7: Ce<sub>2</sub>Co<sub>5</sub>B<sub>2</sub> (earlier CeCo<sub>2</sub>B), 8: CeCoB, 9: CeCo<sub>12</sub>B<sub>6</sub> (earlier CeCo<sub>8</sub>B<sub>3</sub>), 10: CeCo<sub>4</sub>B<sub>4</sub>, 11: CeCoB<sub>3</sub>, 12: CeCoB<sub>4</sub>, 13: Ce<sub>2</sub>CoB<sub>2</sub>.

TABLE 1  
Formation and structural data of ternary compounds Ce-Co-B.

Compound	Structure type Space group	Lattice parameters, Density	Preparation, Characterization	Refs.	Purity	
CeCoB <sub>4</sub>	YCrB <sub>4</sub> Pbam		AM, Qu		Ce 98.9	
			800°C, 330 h, PXD	BiK, 74	Co 99.87	
			400°C, 330 h, PXD	KuBCC, 81	B 99.3	
CeCoB <sub>3</sub>	unknown		AM, Qu		Ce 98.9	
			800°C, 330 h, PXD	BiK, 74	Co 99.87	
			400°C, 330 h, PXD		B 99.3	
Ce <sub>2</sub> CoB <sub>2</sub>	unknown		Am, Qu		Ce 98.9	
			400°C, 330 h, PXD	BiK, 74	Co 99.87	
					B 99.3	
Ce <sub>2</sub> Co <sub>3</sub> B	unknown		AM, Qu		Ce 98.9	
			800°C, 400°C, 330 h, PXD	BiK, 74	Co 99.87	
					B 99.3	
Ce <sub>2</sub> Co <sub>4</sub> B	unknown		AM, Qu		Ce 98.9	
			800°C, 330 h, PXD	BiK, 74	Co 99.87	
					B 99.3	
CeCoB <sup>(†)</sup>	P $\bar{3}$ 1m, P312, P31m, P $\bar{3}$ m1, P321, P3m1	$a = 8.61(5)$ $c = 5.54(2)$	AM, Qu		Ce 98.9	
			800°C, 330 h, PXD, ME	BiK, 74	Co 99.87	
					B 99.3	
CeCo <sub>3</sub> B <sub>2</sub> <sup>(††)</sup>	CeCo <sub>3</sub> B <sub>2</sub> P6/mmm	$a = 5.057(3), \rho_E = 8.24$ $c = 3.036(2), \rho_X = 8.36$	AM, Qu			
			800°C, 50 h,	KuKB, 69		
			$a = 5.058(2), \rho_E = 4.96$ $c = 3.040(2), \rho_X = 8.34$	AM, Qu(Ta)		Ce 99.8
			1150°C, 96 h, PXD	NiY, 73	Co 99.99	
					B 99.9	
			$a = 5.061(4)$ $c = 3.038(2)$	AM, Qu(Mo)		Ce 98.8
800°C, 50 h, PXD	Ro, 73	Co 99.5				
			B 99.0			
CeCo <sub>4</sub> B <sup>(*)</sup>	CeCo <sub>4</sub> B P6/mmm	$a = 5.005(3), \rho_E = 8.37$ $c = 6.932(4), \rho_X = 8.49$	AM, Qu		Ce 99	
			800°C, 50 h	KuB, 73	Co 99.87	
					B 99.3	
Ce <sub>3</sub> Co <sub>11</sub> B <sub>4</sub> <sup>(**)</sup>	Ce <sub>3</sub> Co <sub>11</sub> B <sub>4</sub> P6/mmm	$a = 5.045(3), \rho_E = 8.32$ $c = 9.925(6), \rho_X = 8.39$	AM, Qu		Ce 99	
			800°C, 50 h	KuB, 73	Co 99.87	
					B 99.3	
Ce <sub>2</sub> Co <sub>7</sub> B <sub>3</sub> <sup>(+)</sup>	Ce <sub>2</sub> Co <sub>7</sub> B <sub>3</sub> P6/mmm	$a = 5.053(3), \rho_E = 8.18$ $c = 12.97(2), \rho_X = 8.35$	obtained at 25 a/o B after prolonged heat treatment, PXD		Ce 99	
				KuB, 73	Co 99.87	
					B 99.3	
CeCo <sub>4</sub> B <sub>4</sub> <sup>(+++)</sup>	CeCo <sub>4</sub> B <sub>4</sub> P4 <sub>2</sub> /nmc	$a = 5.059(3), \rho_E = 7.49$ $c = 7.063(5), \rho_X = 7.65$	single crystals were obtained from slowly cooled melt CeCo <sub>4</sub> B <sub>5</sub>			
				KuB, 72		
			$a = 5.042(3)$ $c = 7.081(5)$	AM, Qu		Ce 98.9
			800°C, 330 h, PXD	BiK, 74	Co 99.87	
					B 99.3	

TABLE 1 (contd.)

Compound	Structure type Space group	Lattice parameters, Density	Preparation, Characterization	Refs.	Purity
Ce <sub>2</sub> Co <sub>3</sub> B <sub>2</sub> denoted as CeCo <sub>2</sub> B by BiK, 74	Ce <sub>2</sub> Co <sub>3</sub> B <sub>2</sub> P6 <sub>3</sub> /mmc	$a = 5.060(3)$ $c = 20.43(2)$	AM, Qu 800°C, 330 h, PXD refinement	Ku, 78	Ce 98.9 Co 99.87 B 99.3
		$a = 5.08$ $c = 20.50$	no details given	KuC, 78	
CeCo <sub>12</sub> B <sub>6</sub> <sup>(*)</sup>	SrNi <sub>12</sub> B <sub>6</sub> R $\bar{3}$ m	$a_H = 9.511(6)$ $c_H = 7.486(6)$	AM, Qu 800°C, 270 h, PXD	KuCC, 81	Ce 99.5 Co 99.9 B 99.3
		$a_H = 9.469(6), \rho_E = 7.81$ $c_H = 7.433(5), \rho_x = 7.87$	AM + M in Al <sub>2</sub> O <sub>3</sub> (Ar) PXD	NiY, 72	Ce 99.9 Co 99.99 B 99.9
		$a_R = 6.002, \alpha = 104.16^\circ$	suscept. data, 5–8 kOe, 80–300 K		

<sup>(†)</sup>CeCoB, stable at 800°C, decomposes at lower temperatures into Ce<sub>2</sub>CoB<sub>2</sub> and Ce<sub>2</sub>Co<sub>3</sub>B<sub>2</sub> (formerly CeCo<sub>2</sub>B).

<sup>(††)</sup>The crystal structure has been refined from single crystal photographs,  $R_{hko} = 0.115$ ,  $R_{0kl} = 0.173$ .

<sup>(\*)</sup>The crystal structure has been refined from single crystal X-ray photographs,  $R_{hol} = 0.136$ ,  $R_{hll} = 0.114$ .

<sup>(\*\*)</sup>The crystal structure has been refined from single crystal X-ray photographs,  $R_{hol} = 0.138$ ,  $R_{hll} = 0.141$ .

<sup>(+)</sup>No single crystals were available, thus the structure was refined from X-ray powder photographs on the assumption of a CaCu<sub>5</sub>–CeCo<sub>3</sub>B<sub>2</sub> intermediate;  $R = 0.159$  for all 68 reflections (CrK $\alpha$ ).

<sup>(++)</sup>The structure was refined from single crystal X-ray photographs,  $R_{hol} = 0.088$ ,  $R_{hll} = 0.126$ .

<sup>(\*)</sup>CeCo<sub>12</sub>B<sub>6</sub> was earlier formulated as CeCo<sub>8</sub>B<sub>3</sub> by Bilonishko et al. (1974), and from rotating crystal photographs a monoclinic symmetry was assigned, C2/c or Cc,  $a = 11.84(1)$ ,  $b = 9.47(5)$ ,  $c = 7.69(5)$ ,  $\beta = 106.5(5)^\circ$ .

(Th<sub>2</sub>Zn<sub>17</sub>-type), CeCo<sub>5</sub> (CaCu<sub>5</sub>-type), Ce<sub>2</sub>Co<sub>7</sub> (Ce<sub>2</sub>Ni<sub>7</sub>-type), CeCo<sub>3</sub> (PuNi<sub>3</sub>-type), CeCo<sub>2</sub> (MgCu<sub>2</sub>-type), Ce<sub>24</sub>Co<sub>11</sub>. For the system Co–B, see Sc–Co–B.

Mutual solid solubility of the binary compounds was found to be small; 13 ternary compounds were observed (table 1) and the crystal structures of most of them were determined from single crystal photographs (Laue, rotation and reciprocal lattice photography).

The crystal structures of CeCo<sub>4</sub>B, Ce<sub>3</sub>Co<sub>11</sub>B<sub>4</sub>, Ce<sub>2</sub>Co<sub>7</sub>B<sub>3</sub> and CeCo<sub>3</sub>B<sub>2</sub> form a homologous series  $R_{m+n}Co_{5m+3n}B_{2n}$ , from which the existence of compounds with  $m = 2$ ,  $n = 1$ , Ce<sub>3</sub>Co<sub>13</sub>B<sub>2</sub>, and  $m = 1$ ,  $n = 4$ , Ce<sub>5</sub>Co<sub>17</sub>B<sub>8</sub> was expected (Kuz'ma and Bilonishko, 1973).

The two ternary borides CeCoB<sub>3</sub> (unknown structure type) and CeCoB<sub>4</sub> (YCrB<sub>4</sub>-type) could not be obtained in homogeneous form and a peritectic or peritectoid type of formation was suggested by Bilonishko and Kuz'ma (1974).

### References

- Bilonishko, N.S. and Yu.B. Kuz'ma, 1974, *Izv. Akad. Nauk SSSR, Neorg. Mater.* **10**(2), 265.  
 Gschneidner Jr., K.A. and M.E. Verkade, 1974, *Selected Cerium Phase Diagrams*, Document IS-RIC-7, Iowa State Univ., Ames, IA, USA, p. 14.  
 Kuz'ma, Yu.B., 1978, *Dopov. Akad. Nauk Ukr. RSR, Ser. A*, 147.  
 Kuz'ma, Yu.B. and N.S. Bilonishko, 1972, *Sov. Phys. Crystallogr.* **16**(5), 897.  
 Kuz'ma, Yu.B. and N.S. Bilonishko, 1973, *Kristallografiya* **18**, 710.  
 Kuz'ma, Yu.B. and N.F. Chaban, 1978, New structure types in the homologous series of  $MgZn_2$ - and  $CeCo_3B_2$ -types, in: *Tret. Vses. Konf. Kristalloghim. Intermet. Soedin. Tezisy Dokl.*, Lvov, eds. I. Franko and D.I. Medvedeva (Vyscha Shkola, Lvov) p. 83.  
 Kuz'ma, Yu.B., P.I. Kripyakevich and N.S. Bilonishko, 1969, *Dopov. Akad. Nauk. Ukr. RSR, Ser. A* **10**, 939.  
 Kuz'ma, Yu.B., N.S. Bilonishko, N.F. Chaban and G.V. Chernjak, 1981, *J. Less-Common Metals* **82**, 364.  
 Kuz'ma, Yu.B., G.V. Chernjak and N.F. Chaban, 1981, *Dopov. Akad. Nauk Ukr. RSR, Ser. A* **12**, 80.  
 Niihara, K. and S. Yajima, 1972, *Chem. Lett. (Chem. Soc. Jpn)*, 875.  
 Niihara, K. and S. Yajima, 1973, *Bull. Chem. Soc. Jpn.* **46**, 770.  
 Rogl, P., 1973, *Monatsh. Chem.* **104**, 1623.

### Ce-Cr-B

Two ternary compounds were characterized by Kuz'ma et al. (1973) during a phase diagram study (X-ray and metallographic analysis) of arc melted and subsequently annealed alloys, sealed in quartz capsules for 360 h at 800°C and 600°C (45–100 a/o Ce), respectively (fig. 6). Starting materials were Cr powder 99.5%, B powder 99.3%, Ce ingot 99.5%. Practically no mutual solid solubility of binary phases was observed. For the Cr-B binary system, see Y-Cr-B. Structural data of the two ternary compounds were determined from single crystal X-ray photographs.  $CeCrB_4$  has the  $YCrB_4$ -type of structure, Pbam;  $a = 5.974(5)$ ,  $b = 11.53(1)$ ,

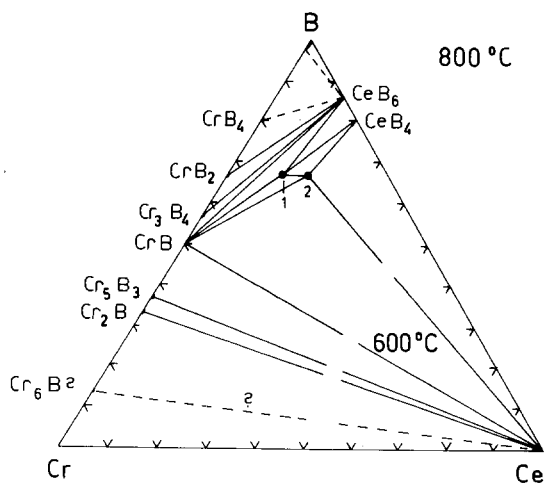


Fig. 6. Ce-Cr-B, partial isothermal sections at 800°C (0–40 a/o Ce), and at 600°C (40–100 a/o Ce). 1:  $CeCr_2B_6$ , 2:  $CeCrB_4$ .

$c = 3.536(4)$  (Kuz'ma et al., 1973). Atom parameters of  $\text{CeCr}_2\text{B}_6$  were refined from single crystal data:  $\text{CeCr}_2\text{B}_6$ -type, Immm;  $a = 6.560(4)$ ,  $b = 8.318(5)$ ,  $c = 3.102(3)$ ,  $\rho_{\text{exp}} = 6.606$ ,  $\rho_{\text{theor}} = 6.10 \text{ kg/dm}^3$  (Kuz'ma and Svarichevskaya, 1973).  $R_{hk0} = 0.132$ ,  $R_{hkl} = 0.079$ : Ce in 2b) 0, 1/2, 1/2; Cr in 4g) 0, 0.152, 0; B in 4f) 0.365, 1/2, 0; B in 8n) 0.210, 0.330, 0. The short Ce–Ce distances (3.10 Å) obtained suggest Ce to be in the tetravalent state.

### References

- Kuz'ma, Yu.B. and S.I. Svarichevskaya, 1973, *Kristallografiya* 17(5), 939.  
 Kuz'ma, Yu.B., S.I. Svarichevskaya and V.N. Fomenko, 1973, *Izv. Akad. Nauk SSSR, Neorg. Mater.* 9(9), 1542.

### Ce–Cu–B

Two partial isothermal sections were derived for the system Ce–Cu–B by Bilonishko (1977) from a röntgenographic study of 50 arc melted alloys at 600°C (region 0–33 a/o Ce) and at 400°C (region 33–100 a/o Ce). Annealing was performed in evacuated silica tubes for 200 h at 600°C and 300 h at 400°C; starting materials were 99.5% Cu and 99.3% B powders and Ce ingot 99.5%. Mutual solid solubilities of Ce–B and Ce–Cu alloys [ $\text{CeCu}_6$ ,  $\text{CeCu}_5$  (CaCu<sub>5</sub>-type),  $\text{CeCu}_4$ ,  $\text{CeCu}_2$ , CeCu (FeB-type)] were found to be negligible; no ternary compounds were observed (fig. 7). The solid solubility of Cu in  $\beta$ -rh. B (retrograde at  $T > T_E$ ) has been extensively studied by Lundström and Tergenius (1975). At 600°C the solid solubility of Cu will be less than the value of  $\text{CuB}_{34.4}$ , which was obtained by Rexer and Petzow (1970) at 950°C.

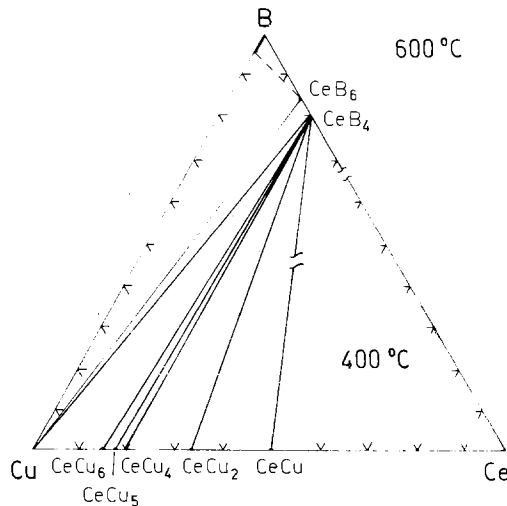


Fig. 7. Ce–Cu–B, partial isothermal sections at 600°C (0–33 a/o Ce), and at 400°C (33–100 a/o Ce); region  $\text{CeB}_6$ –Cu–B is proposed.

### References

- Bilonishko, N.S., 1977, Vestn. Lvov Univ., Ser. Khim. **19**, 56.  
 Lundström, T. and L.E. Terenius, 1975, Univ. of Uppsala Rept UIIC-B18-39, Uppsala, Sweden; see also 1974, C.R. Acad. Sci. (Paris) **278C**, 1495.  
 Rexer, J. and G. Petzow, 1970, Metall **24**, 1083.

### Ce–Eu–B

The magnetic susceptibility of solid solutions  $\text{Ce}_x^3+\text{Eu}_{1-x}^{2+}\text{B}_6$ ,  $\text{CaB}_6$ -type,  $\text{Pm}3m$ , was studied by Aivazov et al. (1978) within the temperature range of 80–1000 K. Lattice parameters were:  $\text{EuB}_{6,1}$ :  $a = 4.1852$ ;  $\text{Ce}_{0.22}\text{Eu}_{0.78}\text{B}_{6,1}$ :  $a = 4.171$ ;  $\text{Ce}_{0.43}\text{Eu}_{0.57}\text{B}_{6,2}$ :  $a = 4.162$ ;  $\text{Ce}_{0.6}\text{Eu}_{0.4}\text{B}_{6,1}$ :  $a = 4.151$ ;  $\text{Ce}_{0.83}\text{Eu}_{0.17}\text{B}_{5,9}$ :  $a = 4.147$ ;  $\text{CeB}_{6,0}$ :  $a = 4.1408$ .

### Reference

- Aivazov, M.I., S.V. Aleksandrovski and V.S. Mkrtychyan, 1978, Fiz. Tverd. Tela **20**(11), 3446.

### Ce–Fe–B

Bilonishko and Kuz'ma (1972) investigated the phase equilibria of the system Ce–Fe–B by means of X-ray and metallographic analysis of 93 specimens, prepared by arc melting of Ce ingots (99.56%), carbonyl-iron powder (99.98%) and B powder (99.4%). Annealing was performed in evacuated quartz capsules at 700°C, 300 h for alloys containing 0–33.3 a/o Ce and at 500°C, 500 h for alloys with 33–100 a/o Ce. All samples were quenched in cold water. The Ce–Fe binary system, containing the two compounds  $\alpha\text{-Ce}_2\text{Fe}_{17}$  ( $\text{Th}_2\text{Ni}_{17}$ -type) and  $\text{CeFe}_2$  ( $\text{MgCu}_2$ -type), is in good accord with a recent compilation of binary Ce systems by Gschneidner and Verkade (1974); see also Kubaschewski-von Goldbeck (1982). For Fe borides, see Y–Fe–B.

Mutual solid solubility of the binary compounds is small and three ternary compounds were observed in both the as-cast and the annealed alloys (fig. 8).

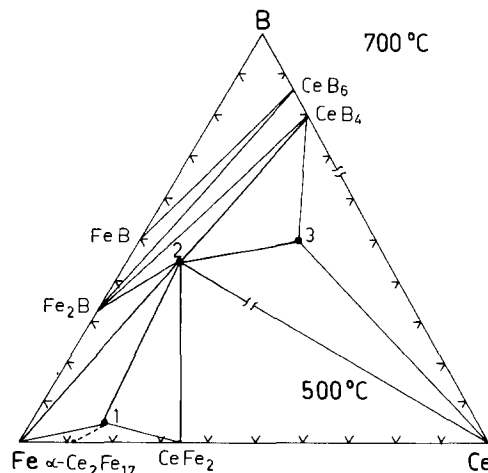


Fig. 8. Ce–Fe–B, partial isothermal sections at 700°C (0–33 a/o Ce) and at 500°C (33–100 a/o Ce). 1:  $\text{Ce}_3\text{Fe}_{16}\text{B}$ , 2:  $\text{Ce}_{1+x}\text{Fe}_4\text{B}_4$  (earlier  $\text{CeFe}_2\text{B}_2$ ), 3:  $\text{Ce}_2\text{FeB}_3$ . At 800°C the compound  $\text{CeFeB}_4$  was said to be in equilibrium with  $\text{CeB}_4$ ,  $\text{CeFe}_4\text{B}_4$  and  $\text{Ce}_2\text{FeB}_3$  (StK, 77).

TABLE 2

Lattice parameters and repeat units of the Fe and R sublattices (in Å) in  $R_{1+x}Fe_4B_4$ , as obtained from single crystal X-ray data; after Braun et al. (1982).

R	Ce	Pr	Nd	Sm	Gd	Tb
$a$	7.090 (1)	7.158 (1)	7.141 (3)	7.098 (1)	7.073 (3)	7.049 (1)
$c_{Fe}$	3.9102(3)	3.9042(5)	3.9073(7)	3.9124(5)	3.9217(4)	3.919 (1)
$c_R$	3.4889(4)	3.5301(2)	3.5241(7)	3.4574(2)	3.442 (1)	3.4109(4)
$c_{Fe}/c_R$	1.1208(5)	1.1060(5)	1.1087(11)	1.1316(6)	1.1394(12)	1.1490(12)
$m = 1, n =$	8	10	9	8	7	7
$(n + m)/n$	1.1250	1.1000	1.1111	1.1250	1.1429	1.1429
$m = 2, n =$	17	19	19	15	15	13
$(n + m)/n$	1.1176	<u>1.1053</u>	1.1053	<u>1.1333</u>	1.1333	1.1538
$m = 3, n =$	25	28	28	23	22	20
$(n + m)/n$	1.1200	1.1071	1.1071	1.1304	1.1364	1.1500
$m = 4, n =$	33	39	37	31	29	27
$(n + m)/n$	<u>1.1212</u>	1.1026	<u>1.1081</u>	1.1290	<u>1.1379</u>	<u>1.1481</u>
$c$	129.04	74.18	144.57	58.69	113.73	105.81

The numbers in parentheses correspond to 1 e.s.d. (estimated standard deviation), except those for the  $c_{Fe}/c_R$  ratio, which correspond to 3 e.s.d. The values of  $n$  and  $m$  shown are the smallest integers for which the ratio  $(n + m)/n$  lies within the experimental error limits of the measured axial ratio  $c_{Fe}/c_R$  ( $\pm 1 + \epsilon$ ). The  $c$  parameters in the bottom line refer to the supercells corresponding to the underlined  $(n + m)/n$  values.

$CeFe_4B_4$  with  $YCrB_4$ -type,  $Pb_{am}$ ,  $a = 5.934(10)$ ,  $b = 11.50(2)$ ,  $c = 3.511(5)$ , was obtained by Stepanchikova and Kuz'ma (1977) from arc melted compacts (Ce ingots 99%, Fe 99.9% and B 99.3% powders) and subsequent annealing at 800°C, 340 h in evacuated quartz capsules. The crystal structure of  $Ce_{\sim 3}Fe_{\sim 16}B_{\sim 1}$  is unknown.  $CeFe_{\sim 2}B_{\sim 2}$  was later corrected to its actual composition of  $CeFe_4B_4$ ; single crystals were obtained from a slowly cooled melt of composition (in a/o): Ce(19)Fe(41)B(40). The space group as derived from rotation photographs was claimed to be  $P4/ncc$ ,  $a = 7.07(2)$ ,  $c = 27.6(1)$ , revealing an eight-fold superstructure along the  $c$ -axis:  $c = 8c_0$ . In this context a series of superstructures  $Ce_{n+m}(Fe_4B_4)_n$ , whose crystal structures derive from the  $NdCo_4B_4$ -type of structure and are either incommensurate or have unusually large repeat units along the  $c$ -axis, have been described by Braun et al. (1982) (see table 2); for sample preparation, see  $Gd_{1+x}Fe_4B_4$ .

### References

- Bilonishko, N.S. and Yu.B. Kuz'ma, 1972, *Izv. Akad. Nauk SSSR, Neorg. Mater.* **8**(1), 183.  
 Braun, H.F., M. Pelizzone and K. Yvon, 1982, Ferromagnetic borides with incommensurate R- and Fe-sublattices:  $R_{1+x}Fe_4B_4$ , paper presented at the 7th Intern. Conf. on Solid Compounds of Transition Elements, Grenoble (June 21-26), Proceedings, II B11.  
 Gschneidner Jr., K.A. and M.E. Verkade, 1974, Selected Cerium Phase Diagrams, Document IS-RIC-7, Iowa State Univ., Ames, IA, USA, p. 20.  
 Kubaschewski-von Goldbeck, O., 1982, Iron-Binary Phase Diagrams, (Springer, Berlin) p. 97.  
 Stepanchikova, G.F. and Yu.B. Kuz'ma, 1977, *Vestn. Lvov Univ., Ser. Khim.* **19**, 37.

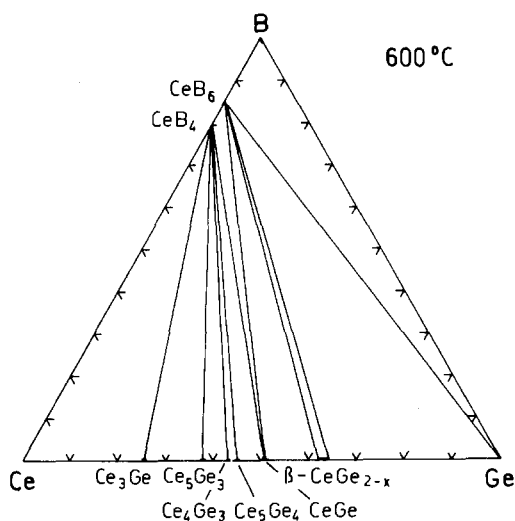


Fig. 9. Ce-Ge-B, isothermal section at 600°C.

### Ce-Ge-B

Phase equilibria of the system Ce-Ge-B at 600°C (fig. 9) have been studied by Marko and Kuz'ma (1979), using X-ray and metallographic analysis of arc melted samples, prepared from 99.3% B powder, 99.99% Ge ingot and 99.56% Ce ingot. The samples were homogenized in evacuated quartz capsules at 600°C for 480 h. No ternary compounds were observed. For the Ge-B binary system, see Y-Ge-B. Cerium germanides observed were:  $\text{Ce}_3\text{Ge}$ ,  $\text{Ce}_5\text{Ge}_3$  ( $\text{Mn}_5\text{Si}_3$ -type),  $\text{Ce}_4\text{Ge}_3$  ( $\text{Th}_3\text{P}_4$ -type),  $\text{Ce}_5\text{Ge}_4$  ( $\text{Sm}_5\text{Ge}_4$ -type),  $\text{CeGe}$  (FeB-type),  $\text{CeGe}_{2-x}$  ( $0.3 \leq x \leq 0.4$ , GdSi<sub>2</sub>-type).

#### Reference

Marko, M.A. and Yu.B. Kuz'ma, 1979, *Izv. Akad. Nauk SSSR, Neorg. Mater.* **15**(11).

### Ce-Hf-B

On the basis of measurements of hexaboride lattice parameters, microhardness, metallographic and X-ray analysis, the solubility of Hf in  $\text{CeB}_6$  was shown to be  $\leq 0.5$  a/o Hf (Bondarenko et al., 1971).

#### Reference

Bondarenko, V.P., V.V. Morozov and L.V. Chernjak, 1971, *Poroshk. Metall.* **97**(1), 73.

### Ce-Ir-B

At least two ternary phases exist in the Cr-Ir-B system. Congruent melting behavior was reported by Rogl (1979) for  $\text{CeIr}_4\text{B}_4$  (metallographic and X-ray



analysis),  $\text{NdCo}_4\text{B}_4$ -type,  $\text{P4}_2/\text{n}$ ,  $a = 7.642(3)$ ,  $c = 3.970(2)$ . For sample preparation, see  $\text{LaOs}_4\text{B}_4$ . Magnetic behavior was studied by Hiebl et al. (1982),  $T_n = 1.5$  K.

$\text{CeIr}_3\text{B}_2$  crystallizes with  $\text{ErIr}_3\text{B}_2$ -type (possible space group  $\text{C2/m}$ ),  $a = 5.502(6)$ ,  $b = 9.526(9)$ ,  $c = 3.090(4)$ ,  $\beta = 90.8(1)^\circ$  (Ku and Meisner, 1981; X-ray powder diffractometry of arc melted samples).

### References

- Hiebl, K., P. Rogl and M.J. Sienko, 1982, *Inorg. Chem.* **21**, 1128.  
 Ku, H.C. and G.P. Meisner, 1981, *J. Less-Common Metals* **78**, 99.  
 Rogl, P., 1979, *Monatsh. Chem.* **110**, 235.

### Ce-La-B

Sato et al. (1981) investigated the effects of La substitution on the Kondo state in a  $\text{Ce}_{0.75}\text{La}_{0.25}\text{B}_6$  alloy ( $\text{CaB}_6$ -type; no crystallographic details given).

### Reference

- Sato, N., T. Komatsubara, S. Kunii, T. Suzuki and T. Kasuya, 1981, Effects of La-substitution on the Kondo state in  $\text{CeB}_6$ , in: *Valence Fluctuations in Solids*, eds. L.M. Falicov, W. Hanke and M.B. Maple (North-Holland, Amsterdam) pp. 259–262.

### Ce-Mn-B

The phase diagram presented in fig. 10 is primarily based on the work of Kuz'ma and Romashov (1975) (X-ray and metallographic analysis). Samples were prepared by arc melting compacts of Ce ingot 99.5%, and Mn 99.5% and B 99.3% powders, and subsequent heat treatment in evacuated silica tubes for 400 h. The region 0–33 a/o Ce was investigated at 800°C, the section containing 33–100 a/o Ce at

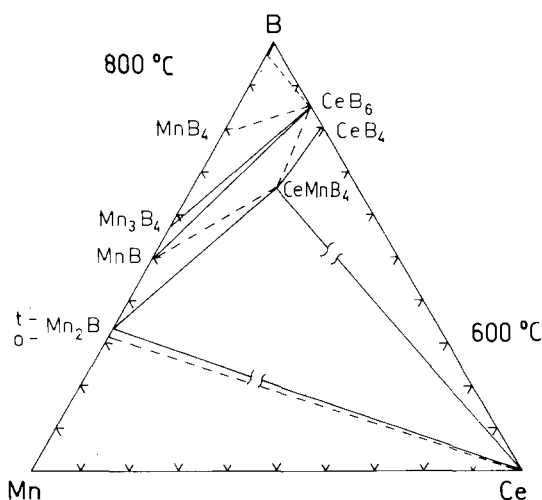


Fig. 10. Ce-Mn-B, partial isothermal sections at 800°C (0–40 a/o Ce) and at 600°C (40–100 a/o Ce).

600°C. Solid solubilities of the binary compounds were negligible;  $\text{CeMnB}_4$  with  $\text{YCrB}_4$ -type, Pbam,  $a = 5.977(5)$ ,  $b = 11.53(1)$ ,  $c = 3.571(4)$  is the only ternary compound.

No details were reported by Kuz'ma and Romashov (1975) concerning the existence and crystal structures of the binary phases.  $\text{MnB}_2$  ( $\text{AlB}_2$ -type) was confirmed to be a high-temperature phase and according to Andersson and Carlsson (1970) decomposes eutectoidically into  $\text{Mn}_3\text{B}_4$  ( $\text{Ta}_3\text{B}_4$ -type) and  $\text{MnB}_4$  ( $\text{MnB}_4$ -type) at  $T \approx 1050\text{--}1100^\circ\text{C}$  (see also Papesch and Nowotny, 1973). Furthermore, Papesch and Nowotny (1973) obtained at 51–55 a/o B and  $\approx 1000^\circ\text{C}$ , besides MnB with FeB-type, a new low-temperature(?) phase, whose structure is closely related to the CrB-type. Kanaizuka (1982) confirmed the solid state transition FeB-type  $\rightleftharpoons$  CrB-type at  $T \approx 1050^\circ\text{C}$ ; however, at slightly lower temperatures ( $T \lesssim 900^\circ\text{C}$ ) the diffraction patterns were said to be due to the CrB-type phase plus another phase for which the low-temperature modification of FeB was suggested (see Y–Fe–B).

At variance with earlier phase diagram data concerning the orthorhombic compound " $\text{Mn}_{\sim 4}\text{B}$ " (see e.g. Moffatt, 1976), Tergenius (1981) was able to precisely determine, from a single crystal X-ray refinement study, a practically complete boron occupation of 98.2% yielding an actual metal to boron ratio of  $\approx 2$  (space group: Fddd,  $R = 0.029$ ). Thus the notation o- $\text{Mn}_2\text{B}$  was suggested in order to distinguish this phase from the tetragonal phase t- $\text{Mn}_2\text{B}$  ( $\text{CuAl}_2$ -type). Samples of a nominal composition of  $\text{Mn}_{0.81}\text{B}_{0.19}$ , prepared by arc melting and after prolonged heat treatment at  $1000^\circ\text{C}$  in vacuum, contained o- $\text{Mn}_2\text{B}$  in equilibrium with  $\alpha$ -Mn. No two-phase sample revealing the two structure types o,t- $\text{Mn}_2\text{B}$  could be obtained and no transformation between the two types has been observed. Indication of a higher B content for " $\text{Mn}_4\text{B}$ " was also given by Papesch and Nowotny (1973).

The maximum solubility of Mn in  $\beta$ -rhombohedral boron as determined by Andersson and Callmer (1974) by single crystal diffractometry is  $\text{MnB}_{\sim 23}$ . The crystals investigated [ $R\bar{3}m$ ,  $a = 10.9875(8)$ ,  $c = 23.9937(28)$ ] were taken from samples with initial composition " $\text{MnB}_{9.2}$ ", prepared by arc melting under argon (B 99.8%, Mn 99.99%). From powder photographs, Carlsson and Lundström (1970) reported  $a = 10.9907(8)$ ,  $c = 23.9964(24)$ .

### References

- Andersson, S. and B. Callmer, 1974, *J. Solid State Chem.* **10**, 219.  
 Andersson, S. and J.O. Carlsson, 1970, *Acta Chem. Scand.* **24**, 1791.  
 Carlsson, J.O. and T. Lundström, 1970, *J. Less-Common Metals* **22**, 317.  
 Kanaizuka, T., 1982, *J. Solid State Chem.* **41**, 195.  
 Kuz'ma, Yu. B. and V.E. Romashov, 1975, *Visn. L'vivsk. Derzh. Univ., Ser. Khim.* **17**, 26.  
 Moffatt, W.G., 1976, *The Handbook of Binary Phase Diagrams* (General Electric Comp., Schenectady, NY), updating service.  
 Papesch, G. and H. Nowotny, 1973, *Monatsh. Chem.* **104**, 933.  
 Tergenius, L.E., 1981, *J. Less-Common Metals* **82**, 335.

### Ce–Mo–B

Using X-ray analysis the phase equilibria of the system Ce–Mo–B were investigated by Mikhalenko and Kuz'ma (1976) at  $800^\circ\text{C}$  for the region 0–67 a/o Ce

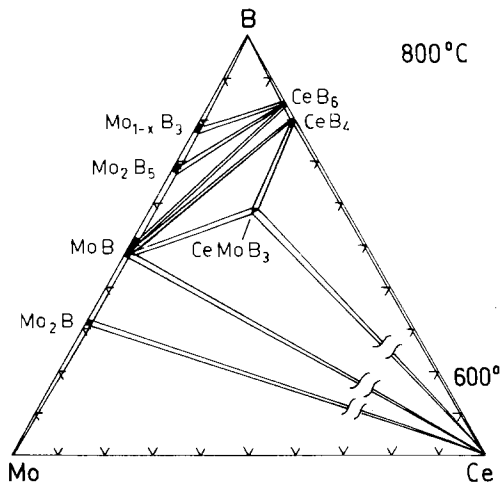


Fig. 11. Ce-Mo-B, partial isothermal sections at 800°C (0-67 a/o Ce), and at 600°C (67-100 a/o Ce).

and at 600°C for the region 67-100 a/o Ce (fig. 11); a ternary compound  $Ce_{\sim 1}Mo_{\sim 1}B_{\sim 3}$  with unknown structure type was observed. For the Mo-B binary system, see Y-Mo-B.

*Reference*

Mikhaleiko, S.I. and Yu.B. Kuz'ma, 1976, Poroshk. Metall. **158**(2), 56.

*Ce-Nb-B*

Phase equilibria within an isothermal section of the system Ce-Nb-B at 800°C, as presented in fig. 12, were established by Mikhaleiko and Bilensh (1979) by means

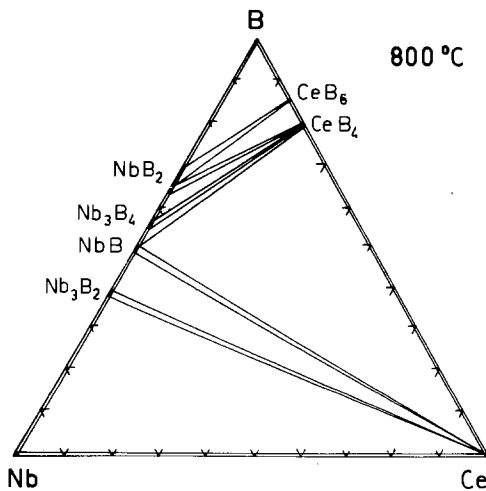


Fig. 12. Ce-Nb-B, isothermal section at 800°C.

of X-ray analysis of 40 alloys, which were arc melted and subsequently heat treated in evacuated silica tubes for 800 h at 800°C. Starting materials were of 99.9% min. purity. Mutual solid solubilities of binary compounds were negligible and no ternary compounds were observed. The binary niobium borides are in good accord with phase diagram data by Rudy and Windisch (1965):  $\text{Nb}_3\text{B}_2$  ( $\text{U}_3\text{Si}_2$ -type),  $\text{NbB}$  ( $\text{CrB}$ -type),  $\text{Nb}_3\text{B}_4$  ( $\text{Ta}_3\text{B}_4$ -type),  $\text{Nb}_{1-x}\text{B}_2$  ( $\text{AlB}_2$ -type).

The variation of the microhardness of  $\text{NbB}_2$  was measured by Lundström et al. (1982) as a function of the boron content of its homogeneous range:  $1830 \times 10^7 \text{ N/m}^2$  at 66 a/o B and  $2090 \times 10^7 \text{ N/m}^2$  at 70 a/o B.  $\text{NbB}_2$  crystallizes with the  $\text{AlB}_2$ -type of structure and is likely to exhibit defects on the metal sublattice.

### References

- Lundström, T., B. Lönnberg and I. Westman, 1982, The microhardness of  $\text{NbB}_2$  and  $\text{TaB}_2$  within the homogeneity range, paper presented at the 7th Intern. Conf. on Solid Compounds of Transition Elements, Grenoble (June 21–25), Proceedings II B10.  
 Mikhalenko, S.I. and O.I. Bilensh, 1979, Vestn. Lvov Univ. Ser. Khim. **21**, 42.  
 Rudy, E. and St. Windisch, 1965, Air Force Materials Laboratory, Technical Report 65-2, Part I, Vol. IX.

### Ce–Ni–B

Phase equilibria were investigated (Kuz'ma and Bilonishko, 1971) (fig. 13) by X-ray analysis of 133 alloys prepared from Ni 99.98% and B 99.3% powders and Ce 98.9% ingot by arc melting and subsequent annealing in evacuated quartz capsules at 800°C, 700 h and for the region Ce– $\text{CeNi}_2$ – $\text{CeB}_4$  at 400°C, 500 h. Ce–Ni compounds:  $\text{CeNi}_5$  ( $\text{CaCu}_5$ -type),  $\text{Ce}_2\text{Ni}_7$ ,  $\text{CeNi}_3$ ,  $\text{CeNi}_2$  ( $\text{MgCu}_2$ -type),  $\text{CeNi}$  ( $\text{CrB}$ ),  $\text{Ce}_7\text{Ni}_3$  ( $\text{Th}_7\text{Fe}_6$ -type) are in agreement with a recent phase diagram compilation by

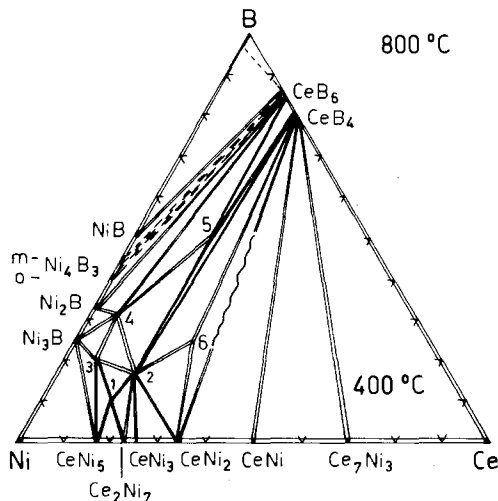


Fig. 13. Ce–Ni–B partial isothermal sections at 800°C (0–33 a/o Ce), and at 400°C (33–100 a/o Ce). 1:  $\text{Ce}_3\text{Ni}_{13}\text{B}_2$  (earlier  $\text{CeNi}_3\text{B}$ ), 2:  $\text{CeNi}_4\text{B}$ , 3:  $\text{Ce}_2\text{Ni}_{21}\text{B}_6$ , 4:  $\text{CeNi}_{12}\text{B}_6$ , 5:  $\text{CeNi}_2\text{B}_3$ , 6:  $\text{CeNi}_2\text{B}$ .

TABLE 3  
Formation and structural data of ternary compounds Ce-Ni-B.

Compound	Structure type, Space Group	Lattice parameters, Density	Preparation, Characterization	Refs.	Purity
Ce <sub>2</sub> Ni <sub>21</sub> B <sub>6</sub> <sup>(*)</sup>	Cr <sub>23</sub> C <sub>6</sub> Fm3m	$a = 10.678(6)$	AM, Qu 800°C, 700 h, PXD	KuB, 71	Ce 98.9 Ni 99.98 B 99.3
CeNi <sub>12</sub> B <sub>6</sub>	Cmcm, Cmc2 <sub>1</sub> Ama2	$a = 9.63(2), \rho_E = 7.73$ $b = 7.39(2), \rho_x = 7.67$ $c = 11.13(3)$	AM, Qu 800°C, 700 h, PXD small region of homogeneity	KuB, 71	Ce 98.9 Ni 99.98 B 99.3
Ce <sub>3</sub> Ni <sub>13</sub> B <sub>2</sub> <sup>(**)</sup>	Nd <sub>3</sub> Ni <sub>13</sub> B <sub>2</sub> P6/mmm	$a = 4.954(3)$ $c = 10.972(13)$	Am, Qu 800°C, 700 h, PXD	KuB, 81	Ce 99.07 Ni 99.22 B 99.3
CeNi <sub>4</sub> B	P6/mmm, P622 P6 mm, P6m2 or P62m	$a' = 40.0(1), \rho_E = 8.46$ $c = 6.98(1), \rho_x = 8.48$ $a' = 8a_0$	AM, Qu 800°C, 700 h, Single crystal rotation photographs	KuB, 71	Ce 99.07 Ni 99.22 B 99.3
CeNi <sub>2</sub> B <sub>3</sub>	I4/mmm I4m2, I42m I4mm or I42	$a = 7.62(2)$ $c = 8.63(2)$	AM, Qu 800°C, 700 h PXD	KuB, 71	Ce 99.07 Ni 99.22 B 99.3
CeNi <sub>2</sub> B	unknown		AM, Qu 800°C, 700 h PXD	KuB, 71	Ce 99.07 Ni 99.22 B 99.3

(\*)X-ray intensities were calculated for Ce in 8c), Ni in 4a), 32f)  $x = 0.385$ , 48h)  $x = 0.165$ , B in 24e)  $x = 0.275$ ; agreement was satisfactory.

(\*\*)This compound probably corresponds to CeNi<sub>6</sub>B, earlier reported with pseudohexagonal cell:  $a = 34.70(5)$ ,  $b = 4.96(1)$ ,  $c = 11.00(2)$ ,  $\beta = 90.0(1)^\circ$ , P2<sub>1</sub>/m or P2<sub>1</sub> (Kuz'ma and Bilonishko, 1971).

Gschneidner and Verkade (1974). For nickel borides see Y-Ni-B. From lattice parameter changes the mutual solubilities of binary compounds were found to be insignificant. Six ternary compounds were observed from both the as-cast and heat treated alloys (table 3).

From a preliminary single crystal X-ray study of the ternary phase CeNi<sub>4</sub>B Kuz'ma and Bilonishko (1971) derived a hexagonal symmetry for a subcell  $a_0 = 5.00(1)$ ,  $c_0 = 6.98(1)$ , which is likely to correspond to a CeCo<sub>4</sub>B-type atomic arrangement. The presence of weak reflection-layer lines on the X-ray single crystal photographs, however, revealed an eight-fold superstructure in the direction of the  $a$ -axis,  $a = 8a_0$ ; the complete unit cell thus consists of 64 subcells.

### References

- Gschneidner Jr., K.A. and M.E. Verkade, 1974, Selected Cerium Phase Diagrams, Document IS-RIC-7, Iowa State Univ., Ames, IA, USA, p. 28.  
Kuz'ma, Yu.B. and N.S. Bilonishko, 1971, Izv. Akad. Nauk SSSR, Neorg. Mater. 7(4), 620.  
Kuz'ma, Yu.B. and N.S. Bilonishko, 1981, Dopov. Akad. Nauk Ukr. RSR, Ser. A 10, 88.

*Ce-Os-B*

$\text{CeOs}_4\text{B}_4$ ,  $\text{NdCo}_4\text{B}_4$ -type,  $\text{P4}_2/\text{n}$ ,  $a = 7.538(3)$ ,  $c = 4.005(2)$ , forms congruently from the melt (Rogl, 1979; X-ray and metallographic analysis). For sample preparation, see  $\text{LaOs}_4\text{B}_4$ . Magnetic properties were investigated by Rupp et al. (1979) and Hiebl et al. (1982);  $T_n = 1.5$  K.

*References*

- Hiebl, K., P. Rogl and M.J. Sienko, 1982, *Inorg. Chem.* **21**, 1128.  
 Rogl, P., 1979, *Monatsh. Chem.* **110**, 232.  
 Rupp, B., R. Rogl and R. Sobczak, 1979, *Mater. Res. Bull.* **14**, 1301.

*Ce-Re-B*

The existence of two ternary compounds in the Ce-Re-B system has been mentioned:  $\text{CeReB}_4$  with  $\text{YCrB}_4$ -type,  $\text{P6mm}$  (Kuz'ma and Svarichevskaya 1974) and  $\text{CeRe}_2\text{B}_4$  (unknown structure type; Mikhalenko et al., 1977).

Using X-ray, metallographic and microhardness analysis, the solubility of Re in  $\text{CeB}_6$  was found to be  $\leq 0.5$  a/o Re (Bondarenko et al., 1971).

*References*

- Bondarenko, V.P., V.V. Morozov and L.V. Chernjak, 1971, *Poroshk. Metall.* **97**(1), 73.  
 Kuz'ma, Yu.B. and S.I. Svarichevskaya, 1974, in: *Bor. Pluch. Strukt. Svoistva, Mater. Mezunar. Simp. Boru 4*, Tiflis, USSR, Vol. 2, eds. F.N. Tavazde and V. Metsniereba, p. 124.  
 Mikhalenko, S.I., Yu.B. Kuz'ma and A.S. Sobolev, 1977, *Poroshk. Metall.* **169**(1), 48.

*Ce-Rh-B*

Ku et al. (1980) investigated the crystal structure (powder X-ray analysis) as well as magnetic and superconducting properties of arc melted alloys of composition  $\text{CeRh}_3\text{B}_2$  ( $\text{CeCo}_3\text{B}_2$ -type,  $\text{P6}/\text{mmm}$ ),  $a = 5.474(6)$ ,  $c = 3.085(4)$ ,  $T_n = 1.2$  K. Dhar et al. (1981) gave  $a = 5.477$ ,  $c = 3.091$ ; magnetic properties were measured within 77–500 K, alloys were arc melted.

For the perovskite-type boride  $\text{CeRh}_3\text{B}_{1-x}$  with  $\text{Cu}_3\text{Au}$ -type,  $a = 4.096$ ,  $x = 0.45(?)$ , see also R-Rh-B.

*References*

- Dhar, S.K., S.K. Malik and R. Vijayaraghavan, 1981, *J. Phys. C: Solid State Phys.* **14**, L321; *J. Appl. Phys.* **53**, 8074.  
 Ku, H.C., G.P. Meisner, F. Acker and D.C. Johnston, 1980, *Solid State Commun.* **35**, 91.

*Ce-Ru-B*

No phase diagram is available yet for the Ce-Ru-B system. From X-ray powder diffractometry of arc melted samples, Johnston (1977) found that  $\text{CeRu}_4\text{B}_4$  adopts the  $\text{LuRu}_4\text{B}_4$ -type of structure,  $\text{I4}_1/\text{acd}$ ,  $a = 7.470(5)$ ,  $c = 15.085(10)$ ;  $T_n = 1.5$  K.

The crystal structure of  $\text{CeRu}_3\text{B}_2$  ( $\text{CeCo}_3\text{B}_2$ -type,  $\text{P6}/\text{mmm}$ ) was determined from

X-ray powder data by Hiebl et al. (1980),  $a = 5.523(4)$ ,  $c = 2.991(2)$ , and the melting behavior was found to be congruent; accordingly Ku et al. (1980) reported  $a = 5.527(6)$ ,  $c = 2.991(4)$ . For sample preparations, see  $\text{YRu}_3\text{B}_2$ . In a study of the magnetic properties (77–400 K) of the compound  $\text{CeRu}_3\text{B}_2$ , Dhar et al. (1981) confirmed the structure but gave slightly larger lattice parameters:  $a = 5.534$ ,  $c = 2.999$  (X-ray powder diffraction, samples were arc melted).

### References

- Dhar, S.K., S.K. Malik and R. Vijayaraghavan, 1981, *J. Phys. C: Solid State Phys.* **14**, L321.  
 Hiebl, K., P. Rogl, E. Uhl and M.J. Sienko, 1980, *Inorg. Chem.* **19**(11), 3316.  
 Johnston, D.C., 1977, *Solid State Commun.* **24**(10), 699.  
 Ku, H.C., G.P. Meisner, F. Acker and D.C. Johnston, 1980, *Solid State Commun.* **35**, 91.

### Ce–Si–B

Phase equilibria at 800°C (partial isothermal section  $\text{CeB}_6$ –Si–Ce) were investigated by Chaban and Kuz'ma (1971) by means of X-ray and metallographic analysis of arc melted and subsequently annealed specimens (500 h at 800°C in evacuated silica tubes). Materials used were Ce ingot, 99.56%, B powder 99.3%, Si powder 99.99%.

No ternary compounds were observed and mutual solid solubilities of binary phases were negligible. Cerium silicides observed:  $\text{Ce}_5\text{Si}_3$  ( $\text{Cr}_3\text{B}_3$ -type),  $\text{Ce}_3\text{Si}_2$  ( $\text{U}_3\text{Si}_2$ -type),  $\text{Ce}_5\text{Si}_4$  ( $\text{Zr}_5\text{Si}_4$ -type),  $\text{CeSi}$  (FeB-type),  $\text{Ce}_3\text{Si}_5$  ( $\text{GdSi}_2$ -type),  $\text{CeSi}_2$  ( $\text{ThSi}_2$ -type) are in agreement with a recent compilation by Gschneidner and Verkade (1974). According to the melting point of Ce (795°C), the Ce-rich corner is liquid at 800°C (fig. 14). See Y–Si–B for the B–Si binary system.

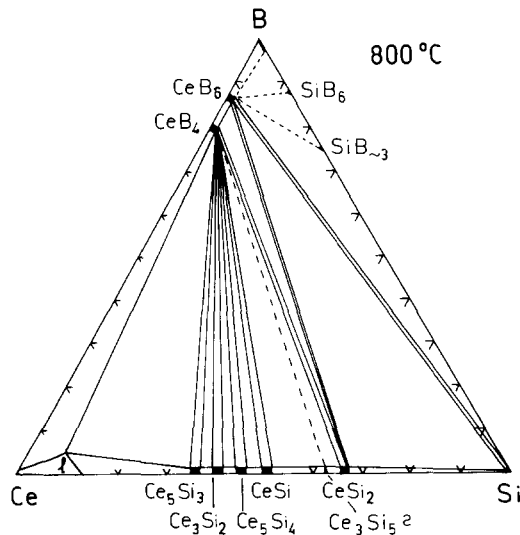


Fig. 14. Ce–Si–B, isothermal section at 800°C; region B–Si– $\text{CeB}_6$  is proposed. The Ce-rich region is liquid (l) at 800°C.

### References

- Chaban, N.F. and Yu.B. Kuz'ma, 1971, *Dopov. Akad. Nauk Ukr. RSR, Ser. A* **11**, 1048.  
 Gschneidner Jr., K.A. and M.E. Verkade, 1974, *Selected Cerium Phase Diagrams*, Document IS-RIC-7, Iowa State Univ., Ames, IA, USA, p. 36.

### Ce-Sm-B

Structural and physical properties of solid solutions  $Ce_{1-x}Sm_xB_6$  were studied by Aivazov et al. (1980) on a series of samples prepared by borothermal reduction of the mixed oxides at 1700°C in vacuum. X-ray and chemical analysis revealed a continuous solid solubility of  $SmB_{5.7}$  to  $CeB_{6.1}$ ,  $CaB_6$ -type, Pm3m (table 4). Magnetic susceptibilities (80–1000 K; 3, 5, 10 kOe) revealed Sm-ions to be present in different valence states. Hall emf, electrical conductivity and thermo-emf were also measured on specimens obtained by hotpressing at 1900–2000°C, 500 kg/cm<sup>2</sup> in vacuum.

TABLE 4  
 Lattice parameters and physical properties of  $Ce_{1-x}Sm_xB_6$ -alloys; after Aivazov et al. (1980).

Chemical composition	Lattice constant $a$ (Å)	Hall coefficient $R_H \times 10^4$ (cm <sup>3</sup> /C) ( $T = 295$ K)	Magnetic susceptibility $\chi \times 10^6$ (cm <sup>3</sup> /g) ( $T = 80$ K)
$CeB_{6.1}$	$4.1408 \pm 3$	-4.3	25.0
$Sm_{0.08}Ce_{0.92}B_{5.95}$	$4.1412 \pm 3$	-4.2	25.4
$Sm_{0.18}Ce_{0.82}B_{6.0}$	$4.1418 \pm 2$	-5.4	26.8
$Sm_{0.25}Ce_{0.75}B_{5.9}$	$4.1424 \pm 2$	-5.2	28.0
$Sm_{0.35}Ce_{0.65}B_{5.7}$	$4.1421 \pm 3$	-6.0	26.2
$Sm_{0.50}Ce_{0.50}B_{5.0}$	$4.1418 \pm 2$	-6.5	24.0
$Sm_{0.62}Ce_{0.38}B_{5.7}$	$4.1403 \pm 3$	-6.2	23.3
$Sm_{0.68}Ce_{0.34}B_{5.9}$	$4.1399 \pm 3$	-6.5	21.1
$Sm_{0.78}Ce_{0.22}B_{5.7}$	$4.1378 \pm 3$	-3.5	19.0
$Sm_{0.89}Ce_{0.11}B_{5.9}$	$4.1358 \pm 2$	-1.0	17.7
$SmB_{5.7}$	$4.1334 \pm 2$	+2.5	15.3

### Reference

- Aivazov, M.I., S.V. Aleksandrovich, B.A. Evseev, A.Yu. Koropova and V.S. Mkrtchyan, 1980, *Izv. Akad. Nauk SSSR, Neorg. Mater.* **16**(3), 450; see also 1982, *Fiz. Tverd. Tela* **24**(9), 2667.

### Ce-Ta-B

On the basis of measurements of hexaboride lattice parameters, microhardness, metallographic and X-ray analysis, the solubility of Ta in  $CeB_6$  was shown to be  $\leq 0.5$  a/o Ta (Bondarenko et al., 1971).

### Reference

- Bondarenko, V.P., V.V. Morozov and L.V. Chernjak, 1971, *Poroshk. Metall.* **97**(1), 73.



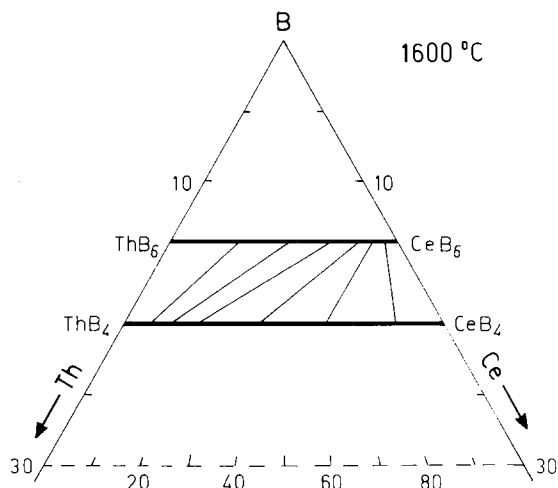


Fig. 15. Ce-Th-B, partial isothermal section ( $\geq 75$  a/o B) at 1600°C.

### Ce-Th-B

A partial Ce-Th-B phase diagram at 1600°C for the boron-rich region containing 70–85 a/o B (fig. 15) has been proposed by Stecher et al. (1965) and Benesovsky et al. (1967) on the basis of X-ray analysis on sintered specimens produced from powdered cerium hydride containing 0.5% O, Th powder containing 0.4% O and B powder with a purity of 96.5% B. A typical oxygen content of the sintered alloys was 0.3–0.8 a/o O (10 h in high vacuum). Continuous solid solutions were observed for  $\text{CeB}_4$ - $\text{ThB}_4$  as well as for  $\text{CeB}_6$ - $\text{ThB}_6$ . The concentration dependence of lattice parameters indicates different valence states for Ce in the solid solutions  $\text{Ce}_{1-x}\text{Th}_x\text{B}_4$  and  $\text{Ce}_{1-x}\text{Th}_x\text{B}_6$ . From tie line positions the thermodynamic interaction parameters of the tetraboride and hexaboride solutions were calculated on the basis of a regular solution model:  $\epsilon(\text{Th}_{1-x}\text{Ce}_x\text{B}_4) = 4500$  cal/mole and  $\epsilon(\text{Th}_{1-x}\text{Ce}_x\text{B}_6) = 3800$  cal/mole.

According to a more recent careful X-ray and neutron diffraction and density study by Etourneau et al. (1971) the homogeneous range of  $\text{Th}_{1-x}\text{Ce}_x\text{B}_6$  at 1300°C was determined to be within  $x = 0$  ( $a = 4.1105$ ) and  $x = 0.22$  ( $a = 4.1125$ ). From this a similar situation is likewise to be found at higher temperatures.

### References

- Benesovsky, F., P. Stecher, H. Nowotny and W. Rieger, 1967, Collog. Int. CNRS (Paris) **157**, 419.  
 Etourneau, J., R. Naslain and S. La Placa, 1971, J. Less-Common Metals **24**, 183.  
 Stecher, P., F. Benesovsky and H. Nowotny, 1965, Planseeberichte für Pulvermetallurgie **13**(1), 37.

### Ce-U-B

Partial phase diagrams at 1600°C and 1900°C for the boron-rich region of the system Ce-U-B containing 75–100 a/o B have been determined by Benesovsky et al. (1967) and Stecher et al. (1965) by means of X-ray analysis of sintered specimens,

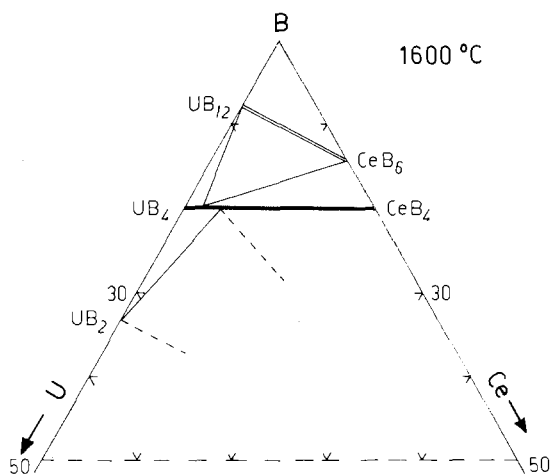


Fig. 16. Ce-U-B, partial isothermal section ( $\geq 67$  a/o B) at 1600°C.

produced from powdered cerium hydride (0.5% O), U powder (0.25% O) and boron (96.5% B). A typical oxygen content of the reaction products was 0.3–0.8 a/o O. Due to the sluggish reaction kinetics, samples of the section  $\text{CeB}_4$ – $\text{UB}_4$  were additionally annealed for 15–20 h at 1900–2000°C.  $(\text{Ce}_{1-x}\text{U}_x)\text{B}_4$  forms a continuous solid solution with negative deviation of lattice parameters from Vegard's rule. Ternary solubility of  $\text{UB}_2$ ,  $\text{CeB}_6$ ,  $\text{UB}_{12}$  was found to be negligible. Phase equilibria at 1600°C and at 1900°C were found to be identical; see fig. 16.

### References

- Benesovsky, F., P. Stecher, H. Nowotny and W. Rieger, 1967, *Colloq. Int. CNRS (Paris)* **157**, 419.  
 Stecher, P., F. Benesovsky and H. Nowotny, 1965, *Planseeberichte für Pulvermetallurgie* **13**(1), 37.

### Ce-V-B

Phase equilibria in the Ce-V-B system at 800°C (fig. 17) were established by X-ray analysis of 40 arc melted and subsequently heat treated (in evacuated silica tubes, 800°C, 800 h) alloys (Mikhaleenko and Bilensh, 1979). Starting materials were of 99.9 min. purity. Solid solubilities of binary compounds were negligible and no ternary compounds were found to exist. The vanadium borides observed:  $\text{V}_2\text{B}_3$  ( $\text{U}_3\text{Si}_2$ -type), VB (CrB-type),  $\text{V}_3\text{B}_6$  ( $\text{V}_5\text{B}_6$ -type),  $\text{V}_3\text{B}_4$  ( $\text{Ta}_3\text{B}_4$ -type),  $\text{V}_2\text{B}_3$  ( $\text{V}_2\text{B}_3$ -type) and  $\text{VB}_2$  with  $\text{AlB}_2$ -type are in good accordance with a recent critical assessment of the V-B binary by Spear et al. (1981).

### References

- Mikhaleenko, S.I and O.I. Bilensh, 1979, *Vestn. Lvov Univ., Ser. Khim.* **21**, 42.  
 Spear, K.E., J.H. Blanks and M.S. Wang, 1981, *J. Less-Common Metals* **82**, 237.

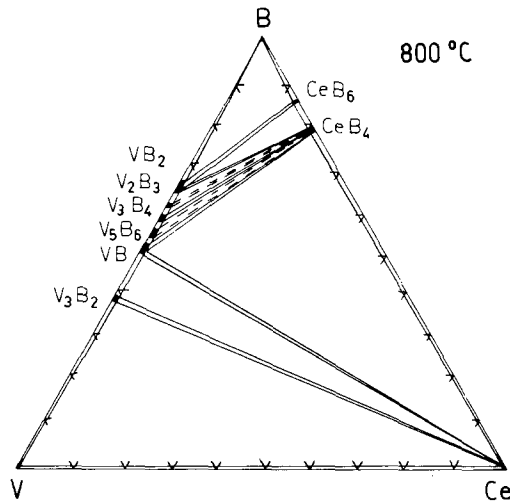


Fig. 17. Ce-V-B, isothermal section at 800°C.

*Ce-W-B*

Phase equilibria of the system Ce-W-B, as presented in fig. 18, were investigated by Mikhalenko and Kuz'ma (1976) by means of X-ray analysis at 800°C for the region 0-67 a/o Ce and at 600°C for the region 67-100 a/o Ce. Mutual solubilities of Ce and W borides were found to be small; no ternary compounds were observed. For the W-B binary system, see La-W-B. Using X-ray, metallographic and microhardness analysis, the solubility of W in CeB<sub>6</sub> was observed to be less than 0.5 a/o W (Bonderenko et al., 1971).

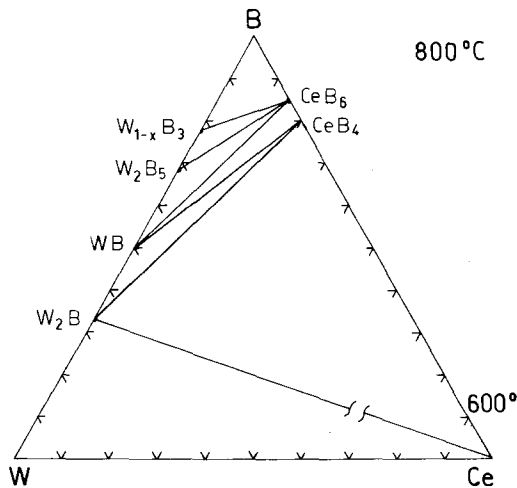


Fig. 18. Ce-W-B, partial isothermal sections at 800°C (0-67 a/o Ce), and at 600°C (67-100 a/o Ce).

## References

- Bonderenko, V.P., V.V. Morozov and L.V. Chernjak, 1971, Poroshk. Metall. **97**(1), 73.  
 Mikhaleiko, S.K. and Yu.B. Kuz'ma, 1976, Poroshk. Metall. **158**(2), 56.

## Dy-Co-B

Eight ternary compounds have been established in the Dy-Co-B system. The experimental details and results of X-ray studies are summarized in table 5.

TABLE 5  
 Formation and structural data of ternary compounds Dy-Co-B.

Compound	Structure type, Space group	Lattice parameters, Density	Preparation, Characterization	Refs.	Purity
DyCo <sub>4</sub> B <sub>4</sub>	YCrB <sub>4</sub> Pbam	$a = 5.885(10)$ $b = 11.40(2)$ $c = 3.403(5)$	AM, Qu 800°C, 340 h, PXD	StK, 77	Dy 99.0 Co 99.9 B 99.3
DyCo <sub>4</sub> B <sub>4</sub>	CeCo <sub>4</sub> B <sub>4</sub> P4 <sub>2</sub> /nmc	$a = 5.026(3)$ $c = 7.014(5)$	no details given, PXD	KuB, 72	
DyCo <sub>2</sub> B <sub>2</sub>	ThCr <sub>2</sub> Si <sub>2</sub> I4/mmm	$a = 3.546(4), \rho_E = 8.50$ $c = 9.354(6), \rho_X = 8.53$	AM, Qu (Ta) 800°C, 150 h, PXD	NiSY, 73	Dy 99.5 Co 99.99 B 99.9
		$a = 3.558$ $c = 9.327$	AM, Qu(Mo) 800°C, 50 h, PXD	Ro, 73	Dy 99.7 Co 99.5 B 99.0
DyCo <sub>3</sub> B <sub>2</sub>	CeCo <sub>3</sub> B <sub>2</sub> P6/mmm	$a = 5.028(3)$ $c = 3.015(2)$	AM, Qu 800°C, 50 h, PXD	KuKB, 69	
		$a = 5.031(3), \rho_E = 5.45$ $c = 3.021(2), \rho_X = 9.05$	AM, Qu(Ta) 1150°C, 96 h, PXD	NiY, 73	Dy 99.8 Co 99.99 B 99.9
		$a = 5.033(4)$ $c = 3.015(1)$	AM, Qu 800°C, 50 h, PXD	Ro, 73	Dy 99.7 Co 99.5 B 99.0
DyCo <sub>4</sub> B	CeCo <sub>4</sub> B P6/mmm	$a = 4.991(3)$ $c = 6.863(4)$	AM, Qu 800°C, 50 h, PXD	KuB, 73	Dy 99 Co 99.87 B 99.3
Dy <sub>3</sub> Co <sub>11</sub> B <sub>2</sub>	Ce <sub>3</sub> Co <sub>11</sub> B <sub>2</sub> P6/mmm	$a = 5.048(3)$ $c = 9.839(6)$	AM, Qu 800°C, 50 h, PXD	KuB, 73	Dy 99 Co 99.87 B 99.3
Dy <sub>2</sub> Co <sub>7</sub> B <sub>3</sub>	Ce <sub>2</sub> Co <sub>7</sub> B <sub>3</sub> P6/mmm	$a = 5.046(3)$ $c = 12.84(2)$	AM, Qu 800°C, 50 h, PXD	KuB, 73	Dy 99 Co 99.87 B 99.3
DyCo <sub>12</sub> B <sub>6</sub>	SrNi <sub>12</sub> B <sub>6</sub> R $\bar{3}$ m	$a_H = 9.452(3)$ $c_H = 7.451(4)$	AM, Qu 800°C, 270 h, PXD	KuCC, 81	Dy 99.5 Co 99.95 B 99.4

*References*

- Kuz'ma, Yu.B. and N.S. Bilonishko, 1972, *Sov. Phys. Crystallogr.* **16**(5), 897.  
 Kuz'ma, Yu.B. and N.S. Bilonishko, 1973, *Kristallografiya* **18**(4), 710.  
 Kuz'ma, Yu.B., P.I. Kripyakevich and N.S. Bilonishko, 1969, *Dopov. Akad. Nauk Ukr. RSR, Ser. A* **10**, 939.  
 Kuz'ma, Yu.B., G.V. Chernjak and N.F. Chaban, 1981, *Dopov. Akad. Nauk Ukr. RSR, Ser. A* **12**, 80.  
 Niihara, K.S. and S. Yajima, 1973, *Bull. Chem. Soc. Jpn* **46**, 770.  
 Niihara, K.S., T. Shishido and S. Yajima, 1973, *Bull. Chem. Soc. Jpn* **46**, 1137.  
 Rogl, P., 1973, *Monatsh. Chem.* **104**, 1623.  
 Stepanchikova, G.F. and Yu.B. Kuz'ma, 1977, *Vestn. Lvov Univ., Ser. Khim.* **19**, 37.

*Dy-Cr-B*

Kuz'ma (1970), using X-ray powder analysis, found that DyCrB<sub>4</sub> crystallizes with the YCrB<sub>4</sub>-type of structure, Pbam,  $a = 5.792(5)$ ,  $b = 11.48(1)$ ,  $c = 3.451(4)$ .

*Reference*

- Kuz'ma, Yu.B., 1970, *Kristallografiya* **15**(2), 372.

*Dy-Fe-B*

DyFeB<sub>4</sub>, as characterized by Stepanchikova and Kuz'ma (1977), has the YCrB<sub>4</sub>-type of structure, Pbam,  $a = 5.885(10)$ ,  $b = 11.38(2)$ ,  $c = 3.403(5)$ ; for alloy preparation, see YFeB<sub>4</sub>.

Dy<sub>3</sub>FeB<sub>7</sub> crystallizes with the Y<sub>3</sub>ReB<sub>7</sub>-type of structure, Cmc<sub>2</sub>m,  $a = 3.375$ ,  $b = 15.54$ ,  $c = 9.403$  (Stepanchikova and Kuz'ma, 1980). For sample preparation, see Y<sub>3</sub>FeB<sub>7</sub>.

DyFe<sub>2</sub>B<sub>2</sub> was characterized by Stepanchikova et al. (1979) with the ThCr<sub>2</sub>Si<sub>2</sub>-type of structure, I4/mmm,  $a = 3.537(5)$ ,  $c = 9.441(10)$ , from X-ray powder analysis of arc melted alloys, which subsequently have been annealed in evacuated quartz capsules at 800°C for 720 h.

*References*

- Stepanchikova, G.F. and Yu.B. Kuz'ma, 1977, *Vestn. Lvov Univ., Ser. Khim.* **19**, 37.  
 Stepanchikova, G.F. and Yu.B. Kuz'ma, 1980, *Poroshk. Metall.* **214**(10), 44.  
 Stepanchikova, G.F., Yu.B. Kuz'ma and B.I. Chernjak, 1979, *Dopov. Akad. Nauk Ukr. RSR, Ser. A*, 950.

*Dy-Ge-B*

The influence of boron additions to R<sub>5</sub>Ge<sub>3</sub> compounds was studied (X-ray analysis) by Mayer and Felner (1974) on a series of samples with a nominal boron content according to the formula: Dy<sub>5</sub>Ge<sub>3</sub>, Dy<sub>5</sub>Ge<sub>3</sub>B<sub>0.5</sub>, Dy<sub>5</sub>Ge<sub>3</sub>B<sub>1.0</sub>, Dy<sub>5</sub>Ge<sub>3</sub>B<sub>1.5</sub> and Dy<sub>5</sub>Ge<sub>3</sub>B<sub>2.0</sub>. Alloys were prepared by heating (melting) elemental mixtures of a min. purity of 99.9% in Ta crucibles to 1600°C under He atmosphere. Mayer and Felner (1974) claim the Mn<sub>5</sub>Si<sub>3</sub>-type phase to be stable up to a composition of Dy<sub>5</sub>Ge<sub>3</sub>B<sub>2</sub>; lattice parameters are listed in table 6. Boron solubility (filling of octahedral voids) in Mn<sub>5</sub>Si<sub>3</sub>-type phases, however, is limited to a formula R<sub>5</sub>Ge<sub>3</sub>B<sub>1.0</sub>. For higher boron concentrations the boron solubility might be accompanied by simultaneous substi-

TABLE 6  
Lattice parameters of boron-containing  $M_5X_3$  compounds; after Mayer and Felner (1974).

	X = Si		X = Ge	
	a (Å)	c (Å)	a (Å)	c (Å)
$La_5X_3$	—	—	8.95	6.90
$La_5X_2B_{0.5}$	—	—	8.96	6.89
$La_5X_3B_{1.0}$	—	—	8.95	6.88
$La_5X_3B_{1.5}$	—	—	8.96	6.89
$La_5X_3B_2$	—	—	8.95	6.89
$Nd_5X_3B_{0.5}$	8.71	6.61	—	—
$Nd_5X_3B_{1.0}$	8.68	6.60	—	—
$Nd_5X_3B_{1.5}$	8.65	6.59	—	—
$Nd_5X_3B_2$	8.65	6.57	—	—
$Gd_5X_3$	8.52	6.39	8.57	6.43
$Gd_5X_3B_{0.5}$	8.50	6.39	8.57	6.43
$Gd_5X_3B_{1.0}$	8.50	6.38	8.57	6.43
$Gd_5X_3B_{1.5}$	8.47	6.40	8.56	6.43
$Gd_5X_3B_2$	8.50	6.40	8.56	6.42
$Tb_5X_3$	8.43	6.30	8.49	6.37
$Tb_5X_3B_{0.5}$	8.44	6.32	8.49	6.37
$Tb_5X_3B_{1.0}$	8.45	6.33	8.49	6.37
$Tb_5X_3B_{1.5}$	8.44	6.33	8.47	6.36
$Tb_5X_3B_2$	8.44	6.33	8.51	6.38
$Dy_5X_3$	8.40	6.28	8.44	6.33
$Dy_5X_3B_{0.5}$	8.40	6.30	8.44	6.33
$Dy_5X_3B_{1.0}$	8.40	6.30	8.42	6.32
$Dy_5X_3B_{1.5}$	8.40	6.30	8.42	6.32
$Dy_5X_3B_2$	8.37	6.28	8.46	6.35

tution Ge/B, which probably could explain the irregular variation of lattice parameters (see table 6); a reinvestigation seems to be necessary.

#### Reference

Mayer, I. and I. Felner, 1974, *J. Less-Common Metals* **37**, 171.

#### Dy-Ir-B

From an X-ray analysis of arc melted samples Ku and Meisner (1981) found that  $DyIr_3B_2$  is isostructural with  $ErIr_3B_2$  (possible space group  $C2/m$ ),  $a = 5.437(6)$ ,  $b = 9.393(9)$ ,  $c = 3.106(4)$ ,  $\beta = 91.1(1)^\circ$ ; and that  $T_m = 17.7$  K.

$DyIr_4B_4$  with a  $NdCo_4B_4$ -type subcell was found to be metastable by Rogl (1979) (X-ray analysis of as-cast as well as alloys annealed at  $1400^\circ\text{C}$ , 24 h in high vacuum, BN substrate).

#### References

Ku, H.C. and G.P. Meisner, 1981, *J. Less-Common Metals* **78**, 99.

Rogl, P., 1979, *Monatsh. Chem.* **110**, 235.

*Dy-La-B*: see notes added in proof

*Dy-Mn-B*

The crystal structure of  $\text{DyMnB}_4$ ,  $\text{YCrB}_4$ -type,  $\text{Pbam}$ ,  $a = 5.897(5)$ ,  $b = 11.39(1)$ ,  $c = 3.439(5)$ , was characterized by Kuz'ma (1970) from X-ray powder diffraction; for sample preparation, see  $\text{GdMnB}_4$ .

*Reference*

Kuz'ma, Yu.B., 1970, *Dopov. Akad. Nauk Ukr. RSR, Ser. A* **32**(8), 756.

*Dy-Mo-B*

Kuz'ma and Svarichevskaya (1972), who used X-ray powder diffraction, found  $\text{DyMoB}_4$  to be isotypic with the  $\text{YCrB}_4$ -type of structure,  $\text{Pbam}$ ,  $a = 6.033(5)$ ,  $b = 11.64(1)$ ,  $c = 3.596(5)$ ; for sample preparation, see  $\text{GdMoB}_4$ .

*Reference*

Kuz'ma, Yu.B. and S.I. Svarichevskaya, 1972, *Dopov. Akad. Nauk Ukr. RSR, Ser. A* **34**(2), 166.

*Dy-Ni-B* (see also notes added in proof)

No ternary phase diagram exists for the  $\text{Dy-Ni-B}$  system.

Niihara et al. (1973) mentioned the occurrence of a ternary  $\text{DyNi}_4\text{B}$  with presumably the  $\text{YNi}_4\text{B}$ -type structure; Kuz'ma et al. (1981a) confirmed the  $\text{CeCo}_4\text{B}$ -type of structure and reported  $a = 4.977(1)$ ,  $c = 6.940(3)$ ,  $\text{P6}/\text{mmm}$ ; see also  $\text{YNi}_4\text{B}$ .

From arc melted and annealed alloys (800°C, 360 h in evacuated silica tubes) Kuz'ma and Chaban (1979) observed by X-ray and metallographic analysis the formation of a compound  $\text{Dy}_3\text{Ni}_7\text{B}_2$ . Starting materials were Dy ingots 99.5%, B powder 99.3%, Ni powder 99.98%; the crystal structure was refined from single crystal photographs,  $R = 0.122$ . The crystal structure of  $\text{Dy}_3\text{Ni}_7\text{B}_2$  ( $\text{Dy}_3\text{Ni}_7\text{B}_2$ -type,  $\text{P6}_3/\text{mmc}$ ,  $a = 5.078(2)$ ,  $c = 14.331(10)$ ,  $\rho_{\text{exp}} = 9.44$ ,  $\rho_{\text{theor}} = 9.54 \text{ kg}/\text{dm}^3$ ) is a member of the homologous series based on the structure types of  $\text{MgZn}_2$  and  $\text{CeCo}_3\text{B}_2$ .

$\text{DyNi}_{12}\text{B}_6$  has the  $\text{SrNi}_{12}\text{B}_6$ -type of structure,  $\text{R}\bar{3}\text{m}$ ,  $a_{\text{H}} = 9.520(6)$ ,  $c_{\text{H}} = 7.410(6)$  (Kuz'ma et al., 1981b). For sample preparation, see  $\text{YCo}_{12}\text{B}_6$ .

*References*

Kuz'ma, Yu.B. and N.F. Chaban, 1979, *Dopov. Akad. Nauk Ukr. RSR, Ser. A*, 88.

Kuz'ma, Yu.B., N.S. Bilonishko, N.F. Chaban and G.V. Chernjak, 1981a, *J. Less-Common Metals* **82**, 364; see also 1982, *Izv. Akad. Nauk SSSR, Neorg. Mater.* **18**, 691.

Kuz'ma, Yu.B., G.V. Chernjak and N.F. Chaban, 1981b, *Dopov. Akad. Nauk Ukr. RSR, Ser. A* **12**, 80. Niihara, K., Y. Katayama and S. Yajima, 1973, *Chem. Lett. (Chem. Soc. Jpn)* 613.

*Dy-Os-B*

Five ternary  $\text{Dy-Os-B}$  compounds have been identified; see table 7 for experimental procedures and the results of X-ray studies.

TABLE 7  
 Formation and structural data of ternary compounds Dy–Os–B.

Compound	Structure type, Space group	Lattice parameters, Density	Preparation, Characterization	Refs.	Purity
DyOsB <sub>4</sub>	YCrB <sub>4</sub> Pbam	$a = 5.954$ (3) $b = 11.527$ (6) $c = 3.553$ (2)	AM, HT, 1600°C, 12 h HV, W substrate, QE congruent melting ME, PXD suscept., 80–300 K	Ro, 78 SoR, 79	Dy 99.9 Os 99.9 B 99.0
Dy <sub>2</sub> OsB <sub>6</sub>	Y <sub>2</sub> ReB <sub>6</sub> Pbam	$a = 9.1542$ (26) $b = 11.5211$ (51) $c = 3.6435$ (2)	AM, HT, 1600°C, 12 h HV, W substrate, QE PXD	RoN, 82	Dy 99.9 Os 99.9 B 99.7
DyOsB <sub>2</sub>	LuRuB <sub>2</sub> Pnma	$a = 5.869$ (6) $b = 5.297$ (5) $c = 6.369$ (7)	AM(Zr), Ta tubes 1250°C, 24 h 800°C, 9 d PXD, $T_m = 25.3$ K	ShKPKJ, 80 KuS, 80	99.9
DyOs <sub>4</sub> B <sub>4</sub>	YOs <sub>4</sub> B <sub>4</sub> tetragonal	$a = 7.4559$ (7) $c = 32.7264$ (56)	AM, HT, 1400°C, 12 h HV, BN substrate PXD, $T_m = 4.7$ K	RoHS, 82	Dy 99.9 Os 99.9 B 99.7
DyOs <sub>3</sub> B <sub>2</sub>	YOs <sub>3</sub> B <sub>2</sub> (?) orthorh. (?)	$a \approx 5.5$ $b \approx 9.5$ $c \approx 18$	AM(Zr) PXD, $T_m = 24.9$ K	Ku, 80	99.9

### References

- Ku, H.C., 1980, Thesis, Univ. of California at San Diego, USA.  
 Ku, H.C. and R.N. Shelton, 1980, Mater. Res. Bull. **15**(10), 1441.  
 Rogl, P., 1978, Mater. Res. Bull. **13**, 519.  
 Rogl, P. and H. Nowotny, 1982, Crystal structures and phase relationships within ternary systems: rare earth metal–noble metal–boron, in: The Rare Earths in Science and Technology, Vol. 3, eds. J. McCarthy, B. Silber and J.J. Rhyne (Plenum, New York, London) pp. 353–356.  
 Rogl, P., K. Hiebl and M.J. Sienko, 1982, Structural chemistry and magnetic behavior of RM<sub>4</sub>B<sub>4</sub> borides, paper presented at the 7th Intern. Conf. on Solid Compounds of Transition Elements, Grenoble (June 21–25), Proceedings, II A4.  
 Shelton, R.N., B.A. Karcher, D.R. Powell, R.A. Jacobson and H.C. Ku, 1980, Mater. Res. Bull. **15**, 1445.  
 Sobczak, R. and P. Rogl, 1979, J. Solid State Chem. **27**, 343.

*Dy–Re–B* (see also notes added in proof)

DyReB<sub>4</sub> with YCrB<sub>4</sub>-type, Pbam,  $a = 5.977$ (5),  $b = 11.55$ (1),  $c = 3.572$ (5), was prepared by Kuz'ma and Svarichevskaya (1972a) from arc melted alloys annealed at 1000°C, 360 h in evacuated quartz capsules (Dy ingot 98%, Re 99.5% and B 99.3% powders).

Dy<sub>2</sub>ReB<sub>6</sub> is isostructural with Y<sub>2</sub>ReB<sub>6</sub>-type, Pbam,  $a = 9.157$ (5),  $b = 11.54$ (1),  $c = 3.672$ (4) (Kuz'ma and Svarichevskaya, 1972b).



$\text{Dy}_3\text{ReB}_7$  crystallizes with  $\text{Y}_3\text{ReB}_7$ -type,  $\text{Cmcm}$ ,  $a = 3.513(2)$ ,  $b = 15.78(1)$ ,  $c = 9.358(4)$  (Kuz'ma and Mikhalenko, 1976).

$\text{DyRe}_{11}\text{B}$  is cubic, crystal structure unsolved (Mikhalenko et al., 1981).

### References

- Kuz'ma, Yu.B. and S.I. Mikhalenko, 1976, *Dopov. Akad. Nauk Ukr. RSR*, Ser. A **11**, 1029.  
 Kuz'ma, Yu.B. and S.I. Svarichevskaya, 1972a, *Dopov. Akad. Nauk Ukr. RSR*, Ser. A **2**, 166.  
 Kuz'ma, Yu.B. and S.I. Svarichevskaya, 1972b, *Kristallografiya* **17**(3), 658.  
 Mikhalenko, S.F., N.F. Chaban and Yu.B. Kuz'ma, 1981, *J. Less-Common Metals* **82**, 365.

### Dy-Rh-B

Ku and Meisner (1981) investigated the crystal structure of  $\text{DyRh}_3\text{B}_2$  by means of X-ray powder diffractometry of arc melted alloys:  $\text{ErIr}_3\text{B}_2$ -type of structure, possible space group  $\text{C2/m}$ ,  $a = 5.379(6)$ ,  $b = 9.331(9)$ ,  $c = 3.093(4)$ ,  $\beta = 90.9(1)^\circ$ ;  $T_m = 38.0$  K.

$\text{DyRh}_4\text{B}_4$  has the  $\text{CeCo}_4\text{B}_4$ -type of structure,  $\text{P4}_2/\text{nmc}$ ,  $a = 5.302(3)$ ,  $c = 7.395(2)$  (Vandenberg and Matthias, 1977; X-ray powder diffractometry); for sample description and preparation, see  $\text{YRh}_4\text{B}_4$ .  $T_m = 12.03$  K (Matthias et al., 1977). The magnetic order was said to appear unstable and its ferromagnetic nature was put into question by Acker and Ku (1981).

For the existence of a perovskite-type phase  $\text{DyRh}_3\text{B}_{1-x}$  with  $\text{AuCu}_3$ -type,  $a = 4.159$ ,  $x = 0.1$ , see also R-Rh-B.

### References

- Acker, F. and H.C. Ku, 1981, *J. Magn. Magn. Mater.* **24**, 47.  
 Ku, H.C. and G.P. Meisner, 1981, *J. Less-Common Metals* **78**, 99.  
 Matthias, B.T., E. Corenzwit, J.M. Vandenberg and H.E. Barz, 1977, *Proc. Nat'l Acad. Sci. US* **74**(4), 1334.  
 Vandenberg, J.M. and B.T. Matthias, 1977, *Proc. Nat'l Acad. Sci. US* **74**(4), 1336.

### Dy-Ru-B

No ternary phase diagram exists for the Dy-Ru-B system, but the X-ray crystallographic data for five ternary compounds are summarized in table 8.

### References

- Hiebl, K., P. Rogl, E. Uhl and M.J. Sienko, 1980, *Inorg. Chem.* **19**(11), 3316.  
 Johnston, D.C., 1977, *Solid State Commun.* **24**(10), 699.  
 Ku, H.C. and R.N. Shelton, 1980, *Mater. Res. Bull.* **15**(10), 1441.  
 Ku, H.C., G.P. Meisner, F. Acker and D.C. Johnston, 1980, *Solid State Commun.* **35**, 91.  
 Rogl, P., 1978, *Mater. Res. Bull.* **13**, 519.  
 Rogl, P. and H. Nowotny, 1982, Crystal structures and phase relationships within ternary systems: rare earth metal-noble metal-boron, in: *The Rare Earths in Science and Technology*, Vol. 3, eds J. McCarthy, B. Silber and J.J. Rhyne (Plenum, New York, London) pp. 353-356).  
 Shelton, R.N., B.A. Karcher, D.R. Powell, R.A. Jacobson and H.C. Ku, 1980, *Mater. Res. Bull.* **15**, 1445.  
 Sobczak, R. and P. Rogl, 1979, *J. Solid State Chem.* **27**, 343.

TABLE 8  
Formation and structural data of ternary compounds Dy–Ru–B.

Compound	Structure type, Space group	Lattice parameters, Density	Preparation, Characterization	Refs.	Purity
DyRuB <sub>4</sub>	YCrB <sub>4</sub> Pbam	$a = 5.948(3)$ $b = 11.513(6)$ $c = 3.541(2)$	AM, HT, 1600°C, 12 h HV, W substrate congruent melting, PXD, ME suscept., 80–300 K	Ro, 78  SoR, 79	Dy 99.9 Ru 99.9 B 99.0
Dy <sub>2</sub> RuB <sub>6</sub>	Y <sub>2</sub> ReB <sub>6</sub> Pbam	$a = 9.1433(23)$ $b = 11.5067(18)$ $c = 3.6489(2)$	AM, HT, 1600°C, 12 h HV, W substrate, PXD	RoN, 82	Dy 99.9 Ru 99.9 B 99.0
DyRuB <sub>2</sub>	LuRuB <sub>2</sub> Pnma	$a = 5.886(6)$ $b = 5.300(5)$ $c = 6.352(7)$	AM(Zr), HT, Ta tubes 1250°C, 24 h, 800°C 9 d, PXD $T_m = 21.9$ K	ShKPJK, 80 KuS, 80	99.9
DyRu <sub>4</sub> B <sub>4</sub>	LuRu <sub>4</sub> B <sub>4</sub> I4 <sub>1</sub> /acd	$a = 7.453(5)$ $c = 14.983(10)$	AM(Zr), PXD $T_m = 2.65$ K	Jo, 77	high purity
DyRu <sub>3</sub> B <sub>2</sub>	CeCo <sub>3</sub> B <sub>2</sub> P6/mmm	$a = 5.474(4)$ $c = 3.016(2)$	AM, HT, 1400°C, 24 h BN substrate PXD, ME, congr. melting $T_m = 50$ K	HiRUS, 80	Dy 99.9 Ru 99.9 B 99.7
		$a = 5.485(6)$ $c = 3.011(4)$	AM(Ar), PXD $T_m = 40.1$ K	KuMAJ, 80	99.9

### Dy–Si–B

The influence of boron additions to R<sub>5</sub>Si<sub>3</sub> compounds was studied (X-ray analysis) by Mayer and Felner (1974) on a series of samples with a nominal boron content according to the formulas: Dy<sub>5</sub>Si<sub>3</sub>, Dy<sub>5</sub>Si<sub>3</sub>B<sub>0.5</sub>, Dy<sub>5</sub>Si<sub>3</sub>B<sub>1.0</sub>, Dy<sub>5</sub>Si<sub>3</sub>B<sub>1.5</sub> and Dy<sub>5</sub>Si<sub>3</sub>B<sub>2.0</sub>. Alloys were prepared by heating (melting) elemental mixtures of a min. purity of 99.9% in Ta crucibles to 1600°C under He atmosphere. Mayer and Felner (1974) claim the Mn<sub>5</sub>Si<sub>3</sub>-type phase to be stable up to a composition of Dy<sub>5</sub>Si<sub>3</sub>B<sub>2</sub>; lattice parameters are listed in table 6. Boron solubility (filling of octahedral voids) in Mn<sub>5</sub>Si<sub>3</sub>-type phase, however, is limited to a formula R<sub>5</sub>Si<sub>3</sub>B<sub>1.0</sub>. For higher boron concentrations the boron solubility might be accompanied by simultaneous substitution Si/B, which probably would explain the irregular variation of lattice parameters (see table 6); a reinvestigation seems to be necessary.

### Reference

Mayer, I. and I. Felner, 1974, *J. Less-Common Metals* **37**, 171.

### Dy–U–B

Alizade et al. (1972) reported a shift of the magnetic ordering temperature within the solid solution (Dy<sub>x</sub>U<sub>1-x</sub>)B<sub>4</sub>.

*Reference*

Alizade, N.Kh., M.G. Ramazanzade, V.I. Chechernikov, N.G. Guseinov and V.K. Slovianskii, 1972, Uch. Zap. Azerb. Inst. Nefti Khim 9(8), 54

*Dy-V-B*

Kuz'ma (1970) reported the existence of the ternary compound DyVB<sub>4</sub> with the YCrB<sub>4</sub>-type of structure [Pbam,  $a = 5.966(5)$ ,  $b = 11.58(1)$ ,  $c = 3.475(5)$ ] from X-ray powder photographs; for sample preparation, see GdMnB<sub>4</sub>.

*Reference*

Kuz'ma, Yu.B., 1970, Dopov. Akad. Nauk Ukr. RSR, Ser. A 32(8), 756.

*Dy-W-B*

The crystal structure of DyWB<sub>4</sub>, YCrB<sub>4</sub>-type, Pbam,  $a = 6.033(5)$ ,  $b = 11.65(1)$ ,  $c = 3.598(5)$ , was characterized by Kuz'ma and Svarichevskaya (1972) by means of X-ray powder analysis; for sample preparation, see GdWB<sub>4</sub>.

*Reference*

Kuz'ma, Yu.B. and S.I. Svarichevskaya, 1972, Dopov. Akad. Nauk Ukr. RSR, Ser. A 34(2), 166.

*Er-Ca-B*

Calcium was found to stabilize the "ErB<sub>6</sub>-phase" with CaB<sub>6</sub>-type, Pm3m (Nichols et al., 1973). A sample of bulk composition ErB<sub>8</sub> was melted in a BN crucible under 10 psi Ar at 2200°C and then slowly cooled ( $\approx 20^\circ\text{C}/\text{min}$ ). Starting materials were Er sponge (impurities in ppm: R: < 400, Ca: < 200, C: 4000–7000, O:  $\approx 300$ , Fe: 100–200, as claimed by the manufacturer) and B powder (5–10 ppm Ca). From metallographic and electron microprobe examination large grains of "ErB<sub>6</sub>" and ErB<sub>4</sub> in a matrix of ErB<sub>12</sub> were found. Depending on the grain examined, the Ca contents were: 1–4 w/o Ca in ErB<sub>6</sub>, no Ca in ErB<sub>12</sub>, 0.2 w/o Ca in ErB<sub>4</sub>. Large dark blue crystals, obtained from the melt, revealed the CaB<sub>6</sub>-type of structure, Pm3m,  $a = 4.098(1)$ . In accordance with the microprobe results, X-ray single crystal refinement postulated a Ca concentration of 20 a/o ( $\approx 4$  w/o Ca),  $R = 0.036$ ; Er in 0,0,0; 6 B in 6f) 0.198(7), 1/2, 1/2. When 10 w/o of Ca was added to the starting materials, the hexaboride phase could be stabilized single phase directly by arc melting; thus an extended solid solution Er<sub>x</sub>Ca<sub>1-x</sub>B<sub>6</sub> can be concluded for values of  $x \leq 0.8$ . From Vegard's law a lattice parameter of  $a = 4.090$  was extrapolated for a hypothetical "ErB<sub>6</sub>".

From a comprehensive literature survey and a detailed experimental study of Ca<sub>x</sub>Er<sub>1-x</sub>B<sub>6</sub> alloys (X-ray, electromicroprobe analysis) Imperato (1976) confirmed the nonexistence of "ErB<sub>6</sub>" reported by earlier investigators. Samples were prepared by arc melting and subsequent annealing in a covered Ta crucible with a black-body hole at 1800–1850°C, 30 min. The measured lattice parameters (X-ray powder

TABLE 9  
Lattice parameters for phases in samples of nominal<sup>a)</sup> composition  $\text{Er}_{1-x}\text{R}_x\text{B}_6$ ,  
R = Ca, La, Ho, Yb; after Imperato (1976).

R	Nominal <sup>a)</sup> value of $x$	(Er, R)B <sub>4</sub>		(Er, R)B <sub>6</sub>	(Er, R)B <sub>12</sub>
		$a_0$ (Å)	$c_0$ (Å)	$a_0$ (Å)	$a_0$ (Å)
Ca	0.34	7.0713(8) <sup>b)</sup>	3.9996(6)	4.098 (1)	7.4798(7)
La	0.20	7.070 (1)	4.0000(7)	4.104 (2)	7.482 (1)
Ho	0.75	7.0795(6)	4.0056(4)	c)	7.4856(9)
Yb	0.17	7.0689(7)	3.9966(5)	4.0971(9)	7.477 (1)
Er <sup>d)</sup>	0.0	7.0684	3.9935(2)		7.4802(4)

<sup>a)</sup>Before arc melting.

<sup>b)</sup>The number in parentheses is the standard deviation in the last significant figure.

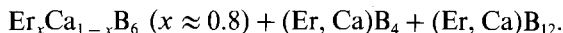
<sup>c)</sup>The hexaboride X-ray pattern was weak and diffuse.

<sup>d)</sup>Values for pure, approximately stoichiometric erbium borides.

analysis) and Vegard's law were used to determine the Ca, Er distribution (see table 9).

A sample of nominal composition  $(\text{Er}_{0.66}\text{Ca}_{0.34})\text{B}_6$  consisted of  $(\text{Er}_{0.82}\text{Ca}_{0.18})\text{B}_6$ :  $a = 4.098(1)$ ,  $(\text{Er, Ca})\text{B}_{12}$ :  $a = 7.4798(7)$  and  $(\text{Er, Ca})\text{B}_4$ :  $a = 7.0713(8)$ .

Solid state phase equilibria in the Er-Ca-B system are thus characterized by a limited solid solution of  $\text{Er}_x\text{Ca}_{1-x}\text{B}_6$ , terminating at the vertex of a three-phase equilibrium:



### References

- Imperato, E.G., 1976, Thesis, Univ. of Pennsylvania, Philadelphia, USA.  
Nichols, M.C., R.W. Mar and Q. Johnson, 1973, J. Less-Common Metals **33**, 317.

### Er-Co-B

Seven ternary compounds in the Er-Co-B system have been characterized (table 10).

### References

- Kuz'ma, Yu.B. and N.S. Bilonishko, 1972, Sov. Phys. Crystallogr. **16**(5), 897.  
Kuz'ma, Yu.B. and N.S. Bilonishko, 1973, Kristallografiya **18**(4), 710.  
Kuz'ma, Yu.B., P.I. Kripyakevich and N.S. Bilonishko, 1969, Dopov. Akad. Nauk Ukr. RSR, Ser. A **10**, 939.  
Kuz'ma, Yu.B., G.V. Chernjak and N.F. Chaban, 1981, Dopov. Akad. Nauk Ukr. RSR, Ser. A **12**, 80.  
Niihara, K. and S. Yajima, 1973, Bull. Chem. Soc. Jpn **46**, 770.  
Rogl, P., 1973, Monatsh. Chem. **104**, 1623.  
Stepanchikova, G.F. and Yu.B. Kuz'ma, 1977, Vestn. Lvov Univ., Ser. Khim. **19**, 37.

TABLE 10  
Formation and structural data of ternary compounds Er-Co-B.

Compound	Structure type, Space group	Lattice parameters, Density	Preparation, Characterization	Refs.	Purity
ErCoB <sub>4</sub>	YCrB <sub>4</sub> Pbam	$a = 5.869(10)$ $b = 11.34 (2)$ $c = 3.353(5)$	AM, Qu 800°C, 340 h, PXD	StK, 77	Er 99% Co 99.9 B 99.3
ErCo <sub>4</sub> B <sub>4</sub>	CeCo <sub>4</sub> B <sub>4</sub> P4 <sub>2</sub> /nmc	$a = 5.016(3)$ $c = 6.989(5)$	no details given, PXD	KuB, 72	
ErCo <sub>3</sub> B <sub>2</sub>	CeCo <sub>3</sub> B <sub>2</sub> P6/mmm	$a = 5.003(3)$ $c = 3.024(2)$ $a = 5.006(3), \rho_E = 5.57$ $c = 3.024(2), \rho_X = 9.25$	AM, Qu 800°C, 50 h, PXD AM, Qu(Ta) 1150°C, 96 h, PXD	KuKB, 69 NiY, 73	Er 99.8 Co 99.99 B 99.9
		$a = 5.005(5)$ $c = 3.029(2)$	CP, Qu(Mo) 800°C, 50 h, PXD	Ro, 73	Er 99.7 Co 99.5 B 99.0
ErCo <sub>4</sub> B	CeCo <sub>4</sub> B P6/mmm	$a = 4.968(3)$ $c = 6.858(4)$	AM, Qu 800°C, 50 h, PXD	KuB, 73	Er 99 Co 99.87 B 99.3
Er <sub>3</sub> Co <sub>11</sub> B <sub>4</sub>	Ce <sub>3</sub> Co <sub>11</sub> B <sub>4</sub> P6/mmm	$a = 5.022(3)$ $c = 9.845(6)$	AM, Qu 800°C, 50 h, PXD	KuB, 73	Er 99 Co 99.87 B 99.3
Er <sub>2</sub> Co <sub>7</sub> B <sub>3</sub>	Ce <sub>2</sub> Co <sub>7</sub> B <sub>3</sub> P6/mmm	$a = 5.006(3)$ $c = 12.87 (2)$	AM, Qu 800°C, 50 h, PXD	KuB, 73	Er 99 Co 99.87 B 99.3
ErCo <sub>12</sub> B <sub>6</sub>	SrNi <sub>12</sub> B <sub>6</sub> R3m	$a_H = 9.448(5)$ $c_H = 7.432(5)$	AM, 800°C, 270 h, PXD	KuCC, 81	Er 99.5 Co 99.95 B 99.4

### Er-Cr-B

ErCrB<sub>4</sub> with YCrB<sub>4</sub>-type, Pbam,  $a = 5.774(5)$ ,  $b = 11.44(1)$ ,  $c = 3.433(4)$ , has been observed by Kuz'ma (1970) from X-ray powder diffraction.

### Reference

Kuz'ma, Yu.B., 1970, Kristallografiya **15**(2), 372.

### Er-Fe-B (see also notes added in proof)

There exist at least three ternary compounds in the Er-Fe-B system. Stepanchikova and Kuz'ma (1977) characterized ErFeB<sub>4</sub> with YCrB<sub>4</sub>-type, Pbam,  $a = 5.861(10)$ ,  $b = 11.34(2)$ ,  $c = 3.377(5)$  (X-ray powder analysis); for alloy preparation, see CeFeB<sub>4</sub>.

$\text{Er}_3\text{FeB}_7$  crystallizes with the  $\text{Y}_3\text{ReB}_7$ -type of structure,  $\text{Cmcm}$ ,  $a = 3.363$ ,  $b = 15.34$ ,  $c = 9.350$  (Stepanchikova and Kuz'ma, 1980). For sample preparation, see  $\text{Y}_3\text{FeB}_7$ .

Stepanchikova et al. (1979) found  $\text{ErFe}_2\text{B}_2$  to be tetragonal with  $\text{ThCr}_2\text{Si}_2$ -type,  $\text{I4/mmm}$ ,  $a = 3.515(5)$ ,  $c = 9.387(10)$ . The alloys were arc melted and annealed in evacuated quartz capsules at  $800^\circ\text{C}$ , 720 h.

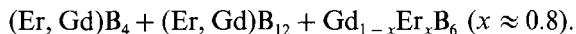
### References

- Stepanchikova, G.F. and Yu.B. Kuz'ma, 1977, *Vestn. Lvov Univ.*, Ser. Khim. **19**, 37.  
 Stepanchikova, G.F. and Yu.B. Kuz'ma, 1980, *Poroshk. Metall.* **214**(10), 44.  
 Stepanchikova, G.F., Yu.B. Kuz'ma and B.I. Chernjak, 1979, *Dopov. Akad. Nauk Ukr. RSR*, Ser. A, 950.

### Er-Gd-B

From a comprehensive literature survey and a detailed experimental study of  $\text{Gd}_x\text{Er}_{1-x}\text{B}_6$  alloys Imperato (1976) confirmed the nonexistence of " $\text{ErB}_6$ " reported by earlier investigators. For experimental details, see Er-Ca-B.

Thus solid state phase equilibria within the ternary system Er-Gd-B are characterized by a continuous solid solution of tetraborides  $\text{Er}_x\text{Gd}_{1-x}\text{B}_4$  and, due to the slight instability of  $\text{ErB}_6$ , by a limited solid solution of  $\text{Gd}_{1-x}\text{Er}_x\text{B}_6$  with  $0 \leq x \lesssim 0.8$ . The hexaboride solid solution finally terminates at the vertex of a three-phase equilibrium:



### Reference

- Imperato, E.G., 1976, Thesis, Univ. of Pennsylvania, Philadelphia, USA.

### Er-Ho-B

From a detailed experimental study of  $\text{Ho}_x\text{Er}_{1-x}\text{B}_6$  alloys Imperato (1976) confirmed the nonexistence of " $\text{ErB}_6$ ", reported by earlier investigators (see table 9). For experimental details and methods, see Er-Ca-B. Samples with a nominal composition of  $x = 0.75$  were reported to mainly consist of  $(\text{Ho, Er})\text{B}_4$  and  $(\text{Ho, Er})\text{B}_{12}$ ; a "hexaboride pattern" was claimed to be "very weak and diffuse". See Ho-La-B for the "instability of a  $\text{HoB}_6$ " phase.

### Reference

- Imperato, E.G., 1976, Thesis, Univ. of Pennsylvania, Philadelphia, USA.

### Er-Ir-B

The crystal structure of  $\text{ErIr}_3\text{B}_2$  has been derived by Ku and Meisner (1981) from X-ray powder diffraction data of arc melted samples;  $R = 0.10$  for the first 22 reflections ( $\text{Cu K}_\alpha$ ).  $\text{ErIr}_3\text{B}_2$  is monoclinic,  $a = 5.409(6)$ ,  $b = 9.379(9)$ ,  $c = 3.101(4)$ ,  $\beta = 91.3(1)^\circ$ , possible space group is  $\text{C2/m}$ , 2 Er in 2a), 2 Ir in 2d), 4 Ir in 4f), 4 B

in 4g)  $y = 0.333$ . The structure proposed is a distortion derivative of the  $\text{CeCo}_3\text{B}_2$ -type of structure;  $T_m = 11.9$  K.

From arc melted alloys, Ku et al. (1979) were able to isolate a metastable phase  $\text{ErIr}_4\text{B}_4$  with  $\text{CeCo}_4\text{B}_4$ -type of structure:  $\text{P}4_2/\text{nmc}$ ,  $a = 5.408(4)$ ,  $c = 7.278(6)$ , from refinement of X-ray powder data.  $T_c = 2.34\text{--}1.88$  K. The phase disappears after heat treatment.

### References

- Ku, H.C. and G.P. Meisner, 1981, *J. Less-Common Metals* **78**, 99.  
 Ku, H.C., B.T. Matthias and H. Barz, 1979, *Solid State Commun.* **32**(1), 937.

### Er-La-B

From a comprehensive literature survey and a detailed experimental study of  $\text{La}_x\text{Er}_{1-x}\text{B}_6$  alloys ( $x = 0.20$ ) Imperato (1976) confirmed the nonexistence of "ErB<sub>6</sub>" reported by earlier investigators (see table 9). The annealing temperature for the (Er, La)B<sub>6</sub> alloys was 1650°C. For experimental details and methods, see Er-Ca-B.

### Reference

- Imperato, E.G., 1976, Thesis, Univ. of Pennsylvania, Philadelphia, USA.

### Er-Mn-B

By using X-ray powder data Kuz'ma (1970) found  $\text{ErMnB}_4$  to be isostructural with the  $\text{YCrB}_4$ -type,  $\text{Pb}am$ ,  $a = 5.868(5)$ ,  $b = 11.40(1)$ ,  $c = 3.424(5)$ . For sample preparation, see  $\text{GdMnB}_4$ .

### Reference

- Kuz'ma, Yu.B., 1970, *Dopov. Akad. Nauk Ukr. RSR, Ser. A* **32**(8), 756.

### Er-Mo-B

From an X-ray powder analysis Kuz'ma and Svarichevskaya (1972) found  $\text{ErMoB}_4$  to have the  $\text{YCrB}_4$ -type of structure,  $\text{Pb}am$ ,  $a = 6.010(5)$ ,  $b = 11.59(1)$ ,  $c = 3.579(5)$ . For sample preparation, see  $\text{GdMoB}_4$ .

### Reference

- Kuz'ma, Yu.B. and S.I. Svarichevskaya, 1972, *Dopov. Akad. Nauk Ukr. RSR, Ser. A* **34**(2), 166.

### Er-Ni-B (see also notes added in proof)

Four ternary compounds have been characterized in the Er-Ni-B system.  $\text{Er}_3\text{Ni}_7\text{B}_2$  with  $\text{Dy}_3\text{Ni}_7\text{B}_2$ -type [ $\text{P}6_3/\text{mmc}$ ,  $a = 5.060(2)$ ,  $c = 14.276(10)$ ] was determined by Kuz'ma and Chaban (1979) from arc melted alloys (99.5% Er ingot, 99.3% B powder, 99.98% Ni powder), which were annealed at 800°C, 360 h, in sealed quartz capsules.

$\text{ErNiB}_4$ ,  $\text{YCrB}_4$ -type,  $\text{Pb}am$ ,  $a = 5.792(7)$ ,  $b = 11.544(11)$ ,  $c = 3.435(6)$  was ob-

served by Chaban et al. (1981) in as-cast and annealed (1070 K, 720 h, evacuated silica tubes) alloys in equilibrium with  $\text{ErB}_4$ .

$\text{Er}_2\text{Ni}_{21}\text{B}_6$ ,  $\text{Cr}_{23}\text{C}_6$ -type,  $\text{Fm}\bar{3}\text{m}$ ,  $a = 10.640(5)$ , has been prepared by Chaban et al. (1980) by arc melting mixtures with 5–10 a/o Er ingots (99.5%), 20 a/o B (99.3%) and Ni (99.98%) powders. Satisfactory agreement was obtained for calculated X-ray powder intensities with 8 Er in 8c), Ni in 4a); in 48h)  $x = 0.165$ ; in 32f)  $x = 0.385$  and 24 B in 24e)  $x = 0.275$ .

$\text{ErNi}_4\text{B}$  was claimed by Kuz'ma et al. (1981) to be of  $\text{CeCo}_4\text{B}$ -type ( $a = 4.949(4)$ ,  $c = 6.931(11)$ ,  $\text{P6}/\text{mmm}$ ).

### References

- Chaban, N.F., Yu.B. Kuz'ma and P.L. Kotovskaya, 1980, *Dopov. Akad. Nauk Ukr. RSR, Ser. A*, 88.  
 Chaban, N.F., G.V. Chernjak and Yu.B. Kuz'ma, 1981, *Izv. Akad. Nauk SSSR, Neorg. Mater.* 17(8), 1494.  
 Kuz'ma, Yu.B. and N.F. Chaban, 1979, *Dopov. Akad. Nauk Ukr. RSR, Ser. A*, 88.  
 Kuz'ma, Yu.B., N.S. Bilonishko., N.F. Chaban and G.V. Chernjak, 1981, *J. Less-Common Metals* 82, 364; see also 1982, *Izv. Akad. Nauk SSSR, Neorg. Mater.* 18, 691.

### Er–Os–B

No phase diagram exists for the Er–Os–B system. The X-ray data for the five known compounds are summarized in table 11.

TABLE 11  
Formation and structural data of ternary compounds Er–Os–B.

Compound	Structure type, Space group	Lattice parameters, Density	Preparation, Characterization	Refs.	Purity
$\text{ErOsB}_4$	$\text{YCrB}_4$ $\text{Pbam}$	$a = 5.928(3)$ $b = 11.482(6)$ $c = 3.539(2)$	AM, HT, 1600°C, 12 h HV, W substrate, QE congruent melting, ME PXD, suscept., 80–300 K	Ro, 78   SoR, 79	Er 99.9 Os 99.9 B 99.0
$\text{Er}_2\text{OsB}_6$	$\text{Y}_2\text{ReB}_6$ $\text{Pbam}$	$a = 9.0973(21)$ $b = 11.4644(21)$ $c = 3.6169(3)$	AM, HT, 1600°C, 12 h HV, W substrate, QE PXD	RoN, 82	Er 99.9 Os 99.9 B 99.7
$\text{ErOsB}_2$	$\text{LuRuB}_2$ $\text{Pnma}$	$a = 5.834(6)$ $b = 5.274(5)$ $c = 6.341(7)$	AM(Zr), Ta tubes 1250°C, 24 h, 800°C, 9d PXD, $T_m = 3.80$ K	ShKPJK, 80 KuS, 80	99.9
$\text{ErOs}_4\text{B}_4$	$\text{YO}_4\text{B}_4$ tetragonal	$a = 7.4317(10)$ $c = 32.7448(56)$ $c = 8c_0$	AM, HT, 1400°C, 12 h HV, BN substrate PXD, $T_m = 1.8$ K	RoHS, 82	Er 99.9 Os 99.9 B 99.7
$\text{ErOs}_3\text{B}_2$	$\text{YO}_3\text{B}_2(?)$ orthorh.(?)	$a \approx 5.5$ $b \approx 9.5$ $c \approx 18$	AM(Zr) PXD, $T_m = 16.0$ K	Ku, 80	99.9



*References*

- Ku, H.C., 1980, Thesis, Univ. of California at San Diego, USA.  
 Ku, H.C. and R.N. Shelton, 1980, *Mater. Res. Bull.* **15**(10), 1441.  
 Rogl, P., 1978, *Mater. Res. Bull.* **13**, 519.  
 Rogl, P. and H. Nowotny, 1982, Crystal structures and Phase relationships within ternary systems: rare earth metal-noble metal-boron, in: *The Rare Earths in Science and Technology*, Vol. 3, eds. J. McCarthy, B. Silber and J.J. Rhyne (Plenum, New York, London) pp. 353-356.  
 Rogl, P., K. Hiebl and M.J. Sienko, 1982, Structural chemistry and magnetic behavior of  $RM_4B_4$ -borides, paper presented at the 7th Intern. Conf. on Solid Compounds of Transition Elements, Grenoble (June 21-25), Proceedings, II A4.  
 Shelton, R.N., B.A. Karcher, D.R. Poweil, R.A. Jacobson and H.C. Ku, 1980, *Mater. Res. Bull.* **15**, 1445.  
 Sobczak R. and P. Rogl, 1979, *J. Solid State Chem.* **27**, 343.

*Er-Re-B*

Three ternary compounds in the Er-Re-B system have been characterized by means of X-ray powder analysis.

$ErReB_4$  is  $YCrB_4$ -type, Pbam,  $a = 5.952(5)$ ,  $b = 11.50(1)$ ,  $c = 3.560(5)$  (Kuz'ma and Svarichevskaya, 1972a); for sample preparation, see  $GdReB_4$ .

$Er_2ReB_6$  is isostructural with the  $Y_2ReB_6$ -type, Pbam,  $a = 9.128(5)$ ,  $b = 11.49(1)$ ,  $c = 3.634(4)$  (Kuz'ma and Svarichevskaya, 1972b).

$Er_3ReB_7$ ,  $Y_3ReB_7$ -type, Cmcm,  $a = 3.486(2)$ ,  $b = 15.63(1)$ ,  $c = 9.308(5)$  (Kuz'ma and Mikhaleiko, 1976).

*References*

- Kuz'ma, Yu.B. and S.I. Mikhaleiko, 1976, *Dopov. Akad. Nauk Ukr. RSR*, Ser. A **11**, 1029.  
 Kuz'ma, Yu.B. and S.I. Svarichevskaya, 1972a, *Dopov. Akad. Nauk Ukr. RSR*, Ser. A **2**, 166.  
 Kuz'ma, Yu.B. and S.I. Svarichevskaya, 1972b, *Kristallografiya* **17**(3), 658.

*Er-Rh-B* (see also notes added in proof)

$ErRh_3B_2$  crystallizes with the  $ErIr_3B_2$ -type of structure [possible space group  $C2/m$ ,  $a = 5.362(6)$ ,  $b = 9.288(9)$ ,  $c = 3.099(4)$ ,  $\beta = 90.9(1)^\circ$ ] (Ku and Meisner, 1981; X-ray powder diffractometry of arc melted samples);  $T_m = 20.4$  K.

Vandenberg and Matthias (1977) reported the crystal structure of  $ErRh_4B_4$  to be isostructural with the  $CeCo_4B_4$ -type of structure,  $P4_2/nmc$ ,  $a = 5.292(2)$ ,  $c = 7.374(3)$  (X-ray powder methods); for sample preparation, see  $YRh_4B_4$ . Matthias et al. (1977) reported that  $ErRh_4B_4$  becomes superconducting at  $T_{c1} = 8.55-8.49$  K, followed by a return to a normal but ferromagnetic state at  $T_{c2} = 0.9$  K. From neutron scattering experiments, Moncton et al. (1977) observed that the Er moments are aligned in the basal plane of the unit cell, with an effective moment of  $5.67 \mu_B$ . The neutron scattering experiments indicated that the magnetic ordering at  $T_{c2}$  is ferromagnetic and thermodynamically of second order. A much larger Er moment of  $8.3(2) \mu_B$  was obtained from Mössbauer-effect measurements and this indicates that about 68% of the moments show long-range magnetic order (Shenoy et al., 1980). NMR ( $^{11}B$ ) measurements suggest a possible phase change from type II/2 to type II/1 super-

conductor as well as the possible coexistence of the ferromagnetically ordered and the superconducting state (Kumagai et al., 1980); see also measurements of the hyperfine magnetic field by Cort et al. (1981). The values of the thermodynamic critical field  $H_c(T)$  of  $\text{ErRh}_4\text{B}_4$  were obtained by Behroozi et al. (1981). More recent investigations of physical properties comprise ultrasonic attenuation studies of the lower critical field by Schneider et al. (1981) as well as electron tunneling experiments by Umbach et al. (1981) and Poppe (1981). The low temperature thermal conductivity was studied by Odoni et al. (1981).

The puzzling physico-chemical properties of  $\text{ErRh}_4\text{B}_4$  at low temperatures have stimulated quite a large number of papers—for a comprehensive review, see the articles by Maple (1981) and by Johnston and Braun (1982).

By arc melting samples of  $\text{ErRh}_4\text{B}_4$  with a slight excess of Rh and subsequent annealing at 1420–1520 K for 125 h in a Ta tube sealed under Ar, Yvon and Johnston (1982) obtained a new structure type (probably a low-temperature phase):  $\text{LuRh}_4\text{B}_4$ -type,  $Ccca$ ,  $a = 7.444\text{--}7.439(6)$ ,  $b = 22.30(2)$ ,  $c = 7.465\text{--}7.460(9)$ . The structure is closely related (shift) to the structure types of  $\text{CeCo}_4\text{B}_4$  and  $\text{LuRu}_4\text{B}_4$ . Arc melted samples  $\text{ErRh}_4\text{B}_4$  in as-cast condition were said to mainly consist of  $\text{CeCo}_4\text{B}_4$ -type and  $\text{LuRu}_4\text{B}_4$ -type (metastable?) phases.

For the existence of a  $\text{Cu}_3\text{Au}$ -type phase  $\text{ErRh}_3\text{B}_{1-x}$  ( $a = 4.142$ ,  $x = 0.02$ ), see R–Rh–B.

### References

- Behroozi, R., M. Levy, D.C. Johnston and B.T. Matthias, 1981, *Solid State Commun.* **38**, 515.  
 Cort, G., R.D. Taylor and J.O. Willis, 1981, *Physica* **108B**, 809.  
 Johnston, D.C. and H.F. Braun, 1982, Systematics of Superconductivity in Ternary Compounds, in: Superconductivity in Ternary Compounds, eds. Ø. Fischer and M.B. Maple (Springer, Berlin).  
 Ku, H.C. and G.P. Meisner, 1981, *J. Less-Common Metals* **78**, 99.  
 Kumagai, K., Y. Inoue and K. Asayama, 1980, *Solid State Commun.* **35**, 531.  
 Maple, B., 1981, Superconductivity and magnetism of rare earth rhodium boride compounds, in: Ternary Superconductors, Proc. Intern. Conf. on Ternary Superconductors, Lake Geneva, WI, USA (1980), eds. G.K. Shenoy, B.D. Dunlap and F.Y. Fradin (North-Holland, Amsterdam) pp. 131–139.  
 Matthias, B.T., E. Corenzwit, J.M. Vandenberg and H.E. Barz, 1977, *Proc. Nat'l Acad. Sci. US* **74(4)**, 1334.  
 Moncton, D.E., D.B. McWhan, J. Eckert, G. Shirane and W. Thomlinson, 1977, *Phys. Rev. Lett.* **39**, 1164.  
 Odoni, W., G. Keller, H.R. Ott, H.C. Hamaker, D.C. Johnston and M.B. Maple, 1981, *Physica* **B108**, 1227.  
 Poppe, U., 1981, *Physica* **108B**, 805.  
 Schneider, S.C., M. Levy, M. Tachiki and D.C. Johnston, 1981, *Physica* **108B**, 807.  
 Shenoy, G.K., B.D. Dunlap, F.Y. Fradin, S.K. Sinha, C.W. Kimball, W. Potzel, F. Pröbst and G.M. Kalvius, 1980, *Phys. Rev.* **21B**, 3886.  
 Umbach, C.P., L.E. Toth, E.D. Dahlberg, and A.M. Goldman, 1981, *Physica* **108B**, 803.  
 Vandenberg, J.M. and B.T. Matthias, 1977, *Proc. Nat'l Acad. Sci. US* **74(4)**, 1336.  
 Yvon, K. and D.C. Johnston, 1982, *Acta Crystallogr.* **B38**, 247.

### Er–Ru–B

Five ternary compounds have been characterized in the Er–Ru–B system (see table 12).

TABLE 12  
Formation and structural data of ternary compounds Er–Ru–B.

Compound	Structure type, Space group	Lattice parameters, Density	Preparation, Characterization	Refs.	Purity
ErRuB <sub>4</sub>	YCrB <sub>4</sub> Pbam	$a = 5.930(3)$ $b = 11.481(6)$ $c = 3.536(2)$	AM, HT, 1600°C, 12 h HV, W substrate congruent melting, PXD, ME suscept., 80–300 K	Ro, 78 SoR, 79	Er 99.9 Ru 99.9 B 99.0
Er <sub>2</sub> RuB <sub>6</sub>	Y <sub>2</sub> ReB <sub>6</sub> Pbam	$a = 9.0822(31)$ $b = 11.4439(56)$ $c = 3.6266(4)$	AM, HT, 1600°C, 12 h HV, W substrate PXD	RoN, 82	Er 99.9 Ru 99.9 B 99.0
ErRuB <sub>2</sub>	LuRuB <sub>2</sub> Pnma	$a = 5.868(6)$ $b = 5.262(5)$ $c = 6.323(7)$	AM(Zr), HT, Ta tubes 1250°C, 24 h 800°C, 9 d, PXD $T_m = 5.21$ K	ShKPJK, 80 KuS, 80	99.9
ErRu <sub>4</sub> B <sub>4</sub>	LuRu <sub>4</sub> B <sub>4</sub> I4 <sub>1</sub> /acd	$a = 7.438(5)$ $c = 14.972(10)$	AM(Zr), PXD $T_m = 2.16$ K	Jo, 77	high purity
ErRu <sub>3</sub> B <sub>2</sub>	CeCo <sub>3</sub> B <sub>2</sub> P6/mmm	$a = 5.461(4)$ $c = 3.016(2)$ (*)	AM, HT, 1400°C, 24 h BN substrate PXD, ME, congr. melting $T_m = 32$ K	HiRUS, 80	Er 99.9 Ru 99.9 B 99.7
		$a = 5.467(6)$ $c = 3.017(4)$	AM(Zr), PXD $T_m = 27.3$ K	KuMAJ, 80	99.9

(\*)Laue symmetry was checked from single crystal Weissenberg photographs to be 6/mmm without superstructure reflections.

### References

- Hiebl, K., P. Rogl, E. Uhl and M.J. Sienko, 1980, *Inorg. Chem.* **19**(11), 3316.  
 Johnston, D.C., 1977, *Solid State Commun.* **24**(10), 699.  
 Ku, H.C. and R.N. Shelton, 1980, *Mater. Res. Bull.* **15**(10), 1441.  
 Ku, H.C., G.P. Meisner, F. Acker and D.C. Johnston, 1980, *Solid State Commun.* **35**, 91.  
 Rogl, P., 1978, *Mater. Res. Bull.* **13**, 519.  
 Rogl, P. and H. Nowotny, 1982, Crystal structures and phase relationships within ternary systems: rare earth metal–noble metal–boron, in: *The Rare Earths in Science and Technology*, Vol. 3, eds. J. McCarthy, B. Silber and J.J. Rhyne (Plenum, New York, London) pp. 353–356.  
 Shelton, R.N., B.A. Karcher, D.R. Powell, R.A. Jacobson and H.C. Ku, 1980, *Mater. Res. Bull.* **15**, 1445.  
 Sobczak, R. and P. Rogl, 1979, *J. Solid State Chem.* **27**, 343.

### Er–U–B

Alizade et al. (1972) reported a shift of the magnetic ordering temperature within the solid solution (Er<sub>1-x</sub>U<sub>x</sub>)B<sub>4</sub>.

### Reference

- Alizade, N.Kh., M.G. Ramazanzade, V.I. Cherchernikov, N.G. Guseinov and V.K. Slovianskii, 1972, *Uch. Zap. Azerb. Inst. Nefti Khim.* **9**(8), 54.

*Er-V-B*

Kuz'ma (1970), using X-ray powder techniques, found that  $\text{ErVB}_4$  has the  $\text{YCrB}_4$ -type of structure, Pbam,  $a = 5.961(5)$ ,  $b = 11.55(1)$ ,  $c = 3.448(5)$ . For sample preparation, see  $\text{GdMnB}_4$ .

*Reference*

Kuz'ma, Yu.B., 1970, *Dopov. Akad. Nauk Ukr. RSR, Ser. A* **32**(8), 756.

*Er-W-B*

Kuz'ma and Svarichevskaya (1972) determined the crystal structure of  $\text{ErWB}_4$  [ $\text{YCrB}_4$ -type, Pbam,  $a = 6.014(5)$ ,  $b = 11.61(1)$ ,  $c = 3.582(5)$ ] from X-ray powder photographs; for sample preparation, see  $\text{GdWB}_4$ .

*Reference*

Kuz'ma, Yu.B. and S.I. Svarichevskaya, 1972, *Dopov. Akad. Nauk Ukr. RSR, Ser. A* **34**(2), 166.

*Er-Yb-B*

From a detailed experimental study of  $\text{Yb}_x\text{Er}_{1-x}\text{B}_6$  alloys with  $x = 0.17$  (X-ray, electronmicroprobe, metallographic analysis) Imperato (1976) confirmed the non-existence of " $\text{ErB}_6$ ", reported by earlier investigators; the annealing temperature was  $1650^\circ\text{C}$ . For experimental details and methods, see  $\text{Er-Ca-B}$ .

*Reference*

Imperato, E.G., 1976, Thesis, Univ. of Pennsylvania, Philadelphia, USA.

*Eu-Co-B*

Hardly any information exists on the  $\text{Eu-Co-B}$  ternary system. Attempts to prepare  $\text{EuCo}_4\text{B}$  ( $\text{CeCo}_4\text{B}$ -type),  $\text{Eu}_3\text{Co}_{11}\text{B}_4$  ( $\text{Ce}_3\text{Co}_{11}\text{B}_4$ -type) and  $\text{Eu}_2\text{Co}_7\text{B}_3$  ( $\text{Ce}_2\text{Co}_7\text{B}_3$ -type) were unsuccessful (Kuz'ma and Bilonishko, 1973).  $\text{EuCo}_{12}\text{B}_6$  has the  $\text{SrNi}_{12}\text{B}_6$ -type of structure,  $R\bar{3}m$ ,  $a_H = 9.472(2)$ ,  $c_H = 7.456(2)$  (Kuz'ma et al., 1981). The samples were arc melted and annealed in evacuated quartz tubes for 270 h at  $800^\circ\text{C}$ .

*References*

Kuz'ma, Yu.B. and N.S. Bilonishko, 1973, *Kristallografiya* **18**(4), 710.

Kuz'ma, Yu.B., G.V. Chernjak and N.F. Chaban, 1981, *Dopov. Akad. Nauk Ukr. RSR, Ser. A* **12**, 80.

*Eu-Gd-B*

Raman spectra of the hexaboride solid solution  $\text{Eu}_x\text{Gd}_{1-x}\text{B}_6$  have been measured by Ishii et al. (1976). Samples were prepared by borothermal reduction of oxide mixtures. Lattice parameters obtained from powder X-ray methods confirmed the

CaB<sub>6</sub>-type, Pm3m: GdB<sub>6</sub>:  $a = 4.110$ ; Gd<sub>0.8</sub>Eu<sub>0.2</sub>B<sub>6</sub>:  $a = 4.118$ ; Gd<sub>0.6</sub>Eu<sub>0.4</sub>B<sub>6</sub>:  $a = 4.127$ ; Gd<sub>0.5</sub>Eu<sub>0.5</sub>B<sub>6</sub>:  $a = 4.132$ ; Gd<sub>0.4</sub>Eu<sub>0.6</sub>B<sub>6</sub>:  $a = 4.138$ ; Gd<sub>0.2</sub>Eu<sub>0.8</sub>B<sub>6</sub>:  $a = 4.157$ ; EuB<sub>6</sub>:  $a = 4.178$ .

### Reference

Ishii, M., M. Aono, S. Muranaka and S. Kawai, 1976, Solid State Commun. **20**, 437.

### Eu-Hf-B

Bakarinoва et al. (1970) studied the reaction of EuB<sub>6</sub> (contained 0.5 w/o C) and Hf from powder mixtures (25 mole% EuB<sub>6</sub>), heat treated in two different ways: a) temperature range 800–2100°C, 1 h, vacuum ( $1 \times 10^{-4}$  Torr); b) temperature range 1300–2000°C, 1–30 min, 1.2 atm He (Ar + H<sub>2</sub> + O<sub>2</sub> ≤ 0.0025 rel%). The degree of reaction  $\text{EuB}_6 + 3 \text{Hf} \rightarrow 3 \text{HfB}_2 + \text{Eu}\uparrow$  was assessed from results of chemical, X-ray, metallographic and gravimetric analysis. Coinciding results were obtained for the chemical as well as the gravimetric analysis of the Eu content of samples a) and b). The reaction vigorously starts at 800°C and at 1900°C the Eu content falls from 20.3 to 1.7%. Change of weight of specimens versus time is given for different temperatures (1350°C, 1500°, 1700°, 2000°C). Samples subjected to a 1 h heat treatment at 2770°C contained solely HfB<sub>2</sub>.

Alloys with concentration EuB<sub>6</sub> > 25 mol% were two-phase: HfB<sub>2</sub> + EuB<sub>6</sub>. As a result the Hf-Eu-B ternary system seems to be characterized by a series of two-phase equilibria: Eu + HfB<sub>2</sub>, EuB<sub>6</sub> + HfB<sub>2</sub>. According to the well-established Hf monoboride (FeB-type, Rudy and Windisch, 1965) a two-phase equilibrium Eu-HfB is likely for temperatures  $1250^\circ\text{C} < T \leq 2100^\circ\text{C}$ ; see also the system Gd-HfB.

### References

Bakarinoва, V.I., E.M. Savitskii, B.G. Arabci and S.E. Salibekov, 1970, Izv. Akad. Nauk SSSR, Neorg. Mater. **6**(11), 2071.  
Rudy, E. and St. Windisch, 1965, Air Force Materials Laboratory, Technical Report 65-2, Part I, Vol. IX.

### Eu-Ir-B

EuIr<sub>4</sub>B<sub>4</sub> has the NdCo<sub>4</sub>B<sub>4</sub>-type of structure, P4<sub>2</sub>/n,  $a = 7.6219(9)$ ,  $c = 3.9771(5)$  (Hiebl et al., 1982). The structure was examined by X-ray powder photographs; atomic positions were 2 Eu in 2b); 8 Ir in 8g) 0.5937, 0.1397, 0.1441; 8 B in 8g) 0.531, 0.409, 0.136. For sample preparation, see EuOs<sub>4</sub>B<sub>4</sub>; samples contained small amounts of IrB<sub>0.9</sub> and IrB<sub>1.1</sub>. Magnetic data were presented by Hiebl et al. (1982),  $T_N = 1.5$  K.

### Reference

Hiebl, K., P. Rogl and M.J. Sienko, 1982, Inorg. Chem. **21**, 1128.

### Eu-La-B

Electric and magnetic properties of the hexaboride solid solution La<sub>x</sub>Eu<sub>1-x</sub>B<sub>6</sub> have been investigated by Mercurio et al. (1974). Samples were prepared by borothermic

reduction of the mixed oxides (99.9% min. pur.) at 1600°C, 1 h, 1800°C. From X-ray and fluorescence analysis a complete solid solubility,  $\text{CaB}_6$ -type,  $\text{Pm}\bar{3}\text{m}$ , was observed:  $\text{EuB}_6$ :  $a = 4.184$ ;  $\text{La}_{0.04}\text{Eu}_{0.957}\text{B}_6$ :  $a = 4.183$ ;  $\text{La}_{0.09}\text{Eu}_{0.91}\text{B}_6$ :  $a = 4.179$ ;  $\text{La}_{0.2}\text{Eu}_{0.8}\text{B}_6$ :  $a = 4.173$ ;  $\text{La}_{0.51}\text{Eu}_{0.49}\text{B}_6$ :  $a = 4.165$ ,  $\text{La}_{0.74}\text{Eu}_{0.26}\text{B}_6$ :  $a = 4.162$ ; boron concentration was determined to a precision of  $\pm 0.3\%$  and La/Eu concentration to  $\pm 1\%$ .

The existence of a continuous series of solid solutions  $\text{La}_{1-x}\text{Eu}_x\text{B}_6$ ,  $\text{CaB}_6$ -type,  $\text{Pm}\bar{3}\text{m}$ , was confirmed by Aivazov et al. (1979), who used various physico-chemical methods. Samples were synthesized by borothermal reduction of the corresponding oxides (1900–2000°C). On the basis of the electrophysical properties a supposition is made on an increase of the ionic component in the Me–B bond when Eu is substituted for La. Boron and metal defects were determined from density and lattice parameter measurements (small negative deviation from Vegard's rule). Their X-ray results essentially agree with the data by Mercurio et al. (1974).

The nature of the exchange interaction in solid solutions  $\text{La}_x\text{Eu}_{1-x}\text{B}_6$  was investigated by Mercurio et al. (1979). Samples were prepared by borothermal reduction of mixed oxides at 1550°C in high vacuum (X-ray and chemical analysis). No lattice parameter data were given.

### References

- Aivazov, M.I., V.A. Bashilov, K.A. Zinchenko and R.R. Kagramanova, 1979, *Poroshk. Metall.* **193**(1), 46.  
 Mercurio, J.P., J. Etourneau, R. Naslain, P. Hagenmuller and J.B. Goodenough, 1974, *Solid State Chem.* **9**, 37.  
 Mercurio, J.P., S. Angelov and J. Etourneau, 1979, *J. Less-Common Metals* **67**, 257.

### *Eu–Ni–B*

The crystal structure of  $\text{EuNi}_{12}\text{B}_6$  ( $\text{SrNi}_{12}\text{B}_6$ -type),  $\text{R}\bar{3}\text{m}$ ,  $a_{\text{H}} = 9.551(3)$ ,  $c_{\text{H}} = 7.408(3)$ , has been refined from X-ray powder analysis (Kuz'ma et al., 1981; Eu in 3a); Ni in 18g) 0.368, 0, 1/2; 18h) 0.426, 0.426, 0.047 and B in 18h) 0.191, 0.191, 0.042. For sample preparation, see  $\text{YCo}_{12}\text{B}_6$ ;  $R = 0.134$ .

$\text{EuNi}_4\text{B}$  adopts the  $\text{CeCo}_4\text{B}$ -type,  $\text{P6}/\text{mmm}$ ,  $a = 4.989(6)$ ,  $c = 6.947(16)$  (Chernjak et al., 1982).

### Reference

- Kuz'ma, Yu.B., G.V. Chernjak and N.F. Chaban, 1981, *Dopov. Akad. Nauk Ukr. RSR, Ser. A* **12**, 80.  
 Chernjak, G.V., N.F. Chaban and Yu.B. Kuz'ma, 1982, *Izv. Akad. Nauk SSSR, Neorg. Mater.* **18**, 691.

### *Eu–Os–B*

By means of X-ray and metallographic analysis  $\text{EuOs}_4\text{B}_4$  was shown, by Hiebl et al. (1982) to crystallize with  $\text{NdCo}_4\text{B}_4$ -type,  $\text{P4}_2/\text{n}$ ,  $a = 7.5262(9)$ ,  $c = 4.0159(6)$ . Samples were prepared by sintering compacts of Eu filings,  $\text{EuB}_6$  and Os powders of 99.9% min. purity in a vapor-tight assembly of an internal BN crucible within a tightly screwed Ta container (1400°C, 2 h and after regrinding and recompacting for 24 h at 1400°C, under Ar). Samples contained small amounts of  $\text{OsB}_{1.1}$ ;  $T_{\text{n}} = 1.5$  K.

### Reference

- Hiebl, K., P. Rogl and M.J. Sienko, 1982, *Inorg. Chem.* **21**, 1128.

*Eu-Pd-B*

$\text{EuPd}_6\text{B}_4$  was claimed by Felner and Nowik (1982) to be isostructural with the  $\text{RRh}_6\text{B}_4$  compounds. The crystal structure is unknown, but for the  $\text{RRh}_6\text{B}_4$  compounds a hexagonal unit cell  $a \approx 5.65$ ,  $c \approx 17.1$  was proposed from X-ray analysis by Felner and Nowik (1980). Mössbauer and magnetic susceptibility data were presented for the region 4.1–600 K.

Boron changes the valence state of Eu in  $\text{EuPd}_3\text{B}_x$  alloys,  $0 \leq x \leq 1$ , as reported by Dhar et al. (1982) from  $^{151}\text{Eu}$  Mössbauer studies, 88–300 K. Samples were prepared by arc melting the constituents under Ar. The alloys with intermediate boron concentration were arc melted from  $\text{EuPd}_3$  and  $\text{EuPd}_3\text{B}$  master alloys. The lattice parameters were obtained from X-ray powder diffraction data and as read from a diagram possibly indicate incomplete B occupation (75%) of the  $\text{Cu}_3\text{Au}$ -type metal host lattice (Pm3m):  $\text{EuPd}_3$ :  $a = 4.102$ ,  $\text{EuPd}_3\text{B}_{0.25}$ :  $a = 4.140$ ,  $\text{EuPd}_3\text{B}_{0.5}$ :  $a = 4.160$ ,  $\text{EuPd}_3\text{B}_{0.75}$ :  $a = 4.195$ ,  $\text{EuPd}_3\text{B}$ :  $a = 4.195$ .

*References*

- Dhar, S.K., S.K. Malik, D. Rambabu and R. Vijayaraghavan, 1982, J. Appl. Phys. **53**(11), 8077.  
 Felner, I. and I. Nowik, 1980, Phys. Rev. Lett. **45**, 2128.  
 Felner, I. and I. Nowik, 1982, Solid State Commun. **39**, 61.

*Eu-Rh-B*

Ku et al. (1980) investigated the crystal structure (X-ray powder methods) as well as magnetic and superconducting properties of  $\text{EuRh}_3\text{B}_2$ ,  $\text{CeCo}_3\text{B}_2$ -type,  $a = 5.601(6)$ ,  $c = 2.906(4)$ . Due to the vigorous boil-off of Eu during the arc melting process, the Eu content was compensated for by adding an excess beforehand; samples obtained were multiphase;  $T_m = 41.7$  K. The magnetic ordering was confirmed at 40 K and concluded to be of the itinerant type from a  $^{151}\text{Eu}$  Mössbauer study (Dhar et al., 1981). Dhar et al. (1981) found  $a = 5.574$ ,  $c = 2.856$  for a sample prepared in the same manner as that of Ku et al. (1980).

The existence of a new unique, but unknown structure type  $\text{EuRh}_4\text{B}_4$  has been claimed by Ku and Barz (1981).

See RE-Rh-B for the perovskite-type phase  $\text{EuRh}_3\text{B}_{1-x}$  ( $\text{AuCu}_3$ -type,  $a = 4.187$ ,  $x = 0.1$ ).

*References*

- Dhar, S.K., R. Nagarajan, S.K. Malik and R. Vijayaraghavan, 1981, Intern. Conf. on the Applications of the Mössbauer Effect, Jaipur, India; see also 1982, Solid State Commun. **43**(6), 461.  
 Ku, H.C. and H. Barz, 1981, Superconductivity in pseudoternary compounds  $\text{R}(\text{Ir}_x\text{Rh}_{1-x})_4\text{B}_4$ , in: Ternary Superconductors, Proc. Intern. Conf. on Ternary Superconductors, Lake Geneva, WI, USA (1980), eds. G.K. Shenoy, B.D. Dunlap and F.Y. Fradin (North-Holland, Amsterdam) pp. 209–212.  
 Ku, H.C., G.P. Meisner, F. Acker and D.C. Johnston, 1980, Solid State Commun. **35**, 91.

*Eu-Ru-B*

$\text{EuRu}_6\text{B}_4$  was claimed by Felner and Nowik (1981) to be isostructural with the

RRh<sub>6</sub>B<sub>4</sub> compounds. The crystal structure is unknown, but for RRh<sub>6</sub>B<sub>4</sub> a hexagonal unit cell,  $a \approx 5.65$ ,  $c \approx 17.1$ , was proposed from X-ray analysis by Felner and Nowik (1980).

The crystal structure of EuRu<sub>4</sub>B<sub>4</sub> has been analysed by Johnston (1977) by means of X-ray powder diffractometry: EuRu<sub>4</sub>B<sub>4</sub> adopts the LuRu<sub>4</sub>B<sub>4</sub>-type structure, I4<sub>1</sub>/acd,  $a = 7.477(5)$ ,  $c = 15.035(10)$ . Samples prepared by arc melting were multiphase.

### References

- Felner, I. and I. Nowik, 1980, Phys. Rev. Lett. **45**, 2128.  
 Felner, I. and I. Nowik, 1981, Solid State Commun. **39**, 61.  
 Johnston, D.C., 1977, Solid State Commun. **24**(10), 699.

*Eu-Sm-B*: see notes added in proof

### *Eu-Sr-B*

Mercurio et al. (1979) studied the nature of the exchange interaction in solid solutions Eu<sub>1-x</sub>Sr<sub>x</sub>B<sub>6</sub>. Samples were prepared by borothermal reduction of mixed oxides at 1550°C in high vacuum (X-ray and chemical analysis). No lattice parameter data were reported.

### Reference

- Mercurio, J.P., S. Angelov and J. Etourneau, 1979, J. Less-Common Metals **67**, 257.

### *Eu-Ta-B*

Bakarinoва et al. (1970) studied the reaction of EuB<sub>6</sub> (containing 0.5 w/o C) and Ta powder mixtures, heat treated in two different ways: a) temperature range 800–2100°C, 1 h, vacuum 10<sup>-4</sup> Torr; b) temperature range 1300–2000°C, 1–30 min, 1.2 atm He (Ar + H<sub>2</sub> + O<sub>2</sub> ≤ 0.0025 rel%). The degree of reaction EuB<sub>6</sub> +  $m$  Ta → Ta <sub>$m$</sub> B <sub>$n$</sub>  + Eu was assessed from the results of chemical, X-ray, metallographic and gravimetric analysis. TaB<sub>2</sub> and free Eu were obtained as end products of the reaction with lower Ta borides in the intermediate reaction stages.

### Reference

- Bakarinoва, V.I., E.M. Savitskii, B.G. Arabei and S.E. Salibekov, 1970, Izv. Akad. Nauk SSSR, Neorg. Mater. **6**(11), 2071.

### *Eu-W-B*

Bakarinoва et al. (1970) studied the reaction of EuB<sub>6</sub> (C content 0.5 w/o) and W (99.85%) powder mixtures, heat treated in two different ways: a) temperature range 800–2100°C, 1 h, vacuum 10<sup>-4</sup> Torr; b) temperature range 1300–2000°C, 1–30 min, 1.2 atm He (Ar + H<sub>2</sub> + O<sub>2</sub> ≤ 0.0025 rel%). The degree of reaction EuB<sub>6</sub> +  $m$  W → W <sub>$m$</sub> B <sub>$n$</sub>  + Eu was assessed from the results of chemical, X-ray, metallographic and gravimetric analysis. W<sub>2</sub>B<sub>3</sub> and free Eu were obtained as end products of the reaction with lower W borides for the intermediate reaction stages.



*Reference*

Bakarionova, V.I., E.M. Savitskii, B.G. Arabei and S.E. Salibekov, 1970, *Izv. Akad. Nauk SSSR, Neorg. Mater.* 6(11), 2071.

*Eu–Yb–B*

Exchange interactions in the hexaboride solid solution  $\text{Eu}_x\text{Yb}_{1-x}\text{B}_6$  have been investigated by the EPR technique at 296 K. Samples were prepared by borothermal reduction of the mixed oxides with 5% excess boron (materials were 99.9% pure) in a  $\text{ZrB}_2$  crucible at 1800°C under Ar, 15 min. The samples were remixed and reheated for another 15 min. The lattice parameters of  $\text{EuB}_6$ ,  $\text{YbB}_6$  (X-ray powder analysis) were reported to be in good agreement with previous work, and those of the solid solution obeyed Vegard's law ( $\text{CaB}_6$ -type, Pm3m) (Glaunsinger, 1975). Magnetic susceptibilities have been reported for  $\text{Eu}_x\text{Yb}_{1-x}\text{B}_6$  solid solutions for  $x = 0.1, 0.2, 0.3, 0.4, 0.6, 0.8$  by Krause and Sienko (1973).

*Reference*

Glaunsinger, W.S., 1975, *J. Magn. Res.* 18, 265.

Krause, J.L. and M.J. Sienko, 1973, *J. Solid State Chem.* 6, 590.

*Gd–Co–B*

Two phase diagrams of the system Gd–Co–B have been presented, at 800°C by Stadelmaier and Lee (1978) and at 600°C by Chaban and Kuz'ma (1977) (figs. 19a, b). Except for the compound  $\text{GdCoB}_4$  both investigations agree on the phase relations. In both cases samples were prepared by arc melting Co, B powders and Gd ingots of comparable purity (see table 13) with subsequent heat treatment in evacuated Vycor capsules ( $800 \pm 10^\circ\text{C}$ , 300 h, Stadelmaier and Lee) or in quartz capsules (600°C, 800 h, Chaban and Kuz'ma), respectively. To avoid boron losses in the arc melting process, boron was introduced by Stadelmaier and Lee from a CoB master alloy. X-ray and metallographic (Chaban and Kuz'ma, Stadelmaier and Lee) as well as electron microprobe analysis (Stadelmaier and Lee) were employed to determine the phase equilibria.  $\text{Gd}_{12}\text{Co}_7$  ( $\text{Ho}_{12}\text{Co}_7$ -type), recently characterized by Adams et al. (1976), has been incorporated in fig. 19b among gadolinium–Cobalt phases observed:  $\text{Gd}_2\text{Co}_{17}$  ( $\text{Th}_2\text{Zn}_{17}$ -type),  $\text{GdCo}_5$  ( $\text{CaCu}_5$ -type),  $\text{Gd}_2\text{Co}_7$  ( $\text{Ce}_2\text{Ni}_7$ - or  $\text{Gd}_2\text{Co}_7$ -type),  $\text{GdCo}_3$  ( $\text{PuNi}_3$ -type),  $\text{GdCo}_2$  ( $\text{MgCu}_2$ -type),  $\text{Gd}_4\text{Co}_3$  ( $\text{Ho}_4\text{Co}_3$ -type). For Co borides, see Sc–Co–B. According to data by Blanks and Spear (1974) and Spear and Petsinger (1972)  $\text{GdB}_2$  ( $\text{AlB}_2$ -type) was shown to be a high-temperature phase and to decompose at  $T \approx 1280^\circ\text{C}$  into  $\text{Gd} + \text{Gd}_2\text{B}_5$ .  $\text{Gd} + \text{Gd}_2\text{B}_5$  from a eutectic at 1180°C.

Table 14 lists the four-phase reactions according to the liquidus projection (fig. 19c) as determined by Stadelmaier and Lee (1978).  $\text{Gd}_2\text{CoB}_3$  is the only ternary phase without a field of primary crystallization. Some controversy exists about the existence of  $\text{GdCoB}_4$ . Whereas Stadelmaier and Lee (1978) reported the absence of a compound  $\text{GdCoB}_4$  with  $\text{YCrB}_4$ -type, Pbam, in annealed (800°C) as well as in as-cast alloys, Chaban and Kuz'ma (1977) found  $\text{GdCoB}_4$  in alloys annealed at 600°C and Sobczak and Rogl (1979) measured magnetic susceptibilities (800–300 K) of  $\text{GdCoB}_4$ .

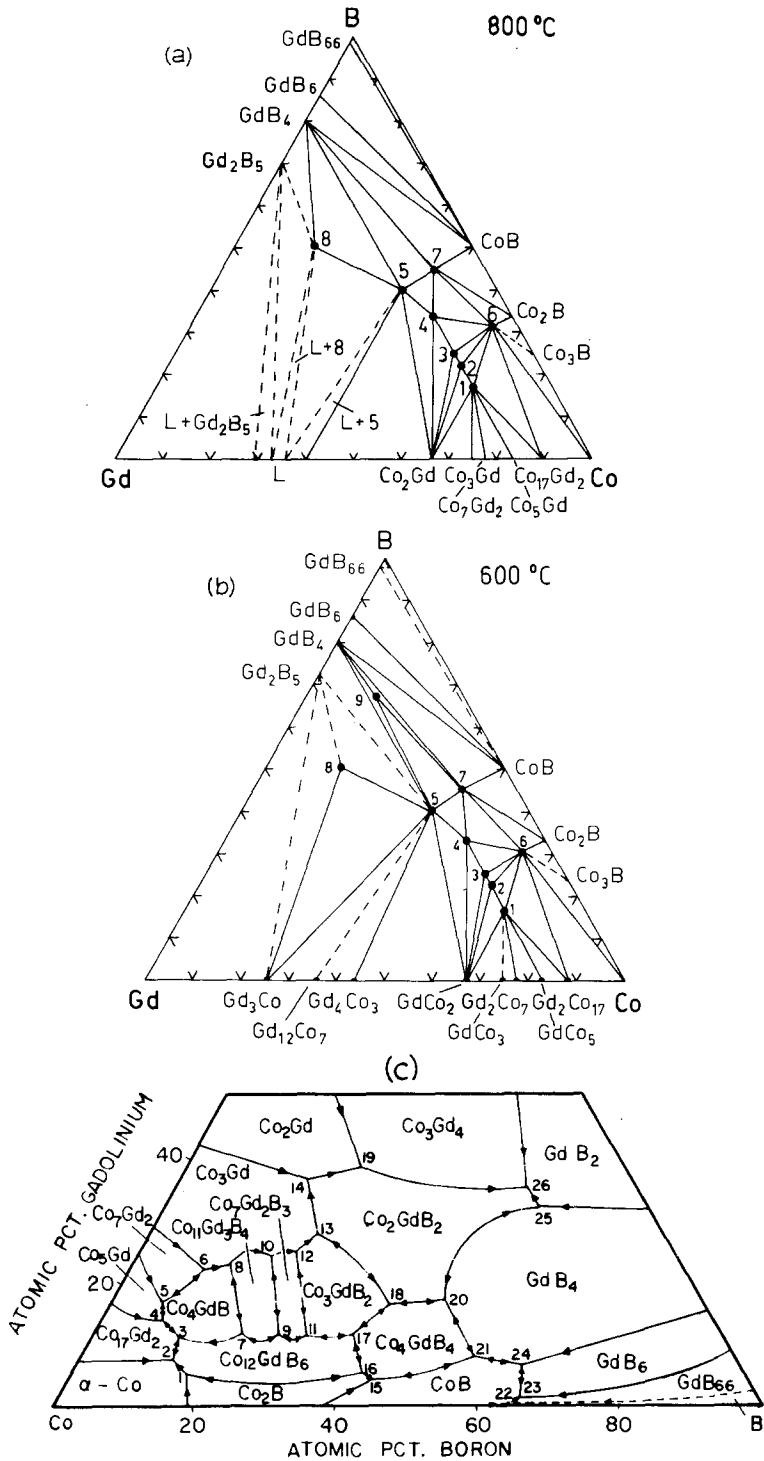


Fig. 19. Gd-Co-B, isothermal sections (a) at 800°C, and (b) at 600°C. 1:  $\text{GdCo}_5\text{B}$ , 2:  $\text{Gd}_3\text{Co}_{11}\text{B}_4$ , 3:  $\text{Gd}_2\text{Co}_7\text{B}_3$ , 4:  $\text{GdCo}_3\text{B}_2$ , 5:  $\text{GdCo}_2\text{B}_2$ , 6:  $\text{GdCo}_{12}\text{B}_6$ , 7:  $\text{GdCo}_4\text{B}_4$ , 8:  $\text{Gd}_2\text{CoB}_3$ , 9:  $\text{GdCoB}_4$ . (c) Gd-Co-B, liquidus projection, see table 14; after Stadelmaier and Lee (1978).

TABLE 13  
Formation and structural data of ternary compounds Gd-Co-B

Compound	Structure type, Space Group	Lattice parameters, Density	Preparation, Characterization	Refs.	Purity
GdCoB <sub>4</sub>	YCrB <sub>4</sub> Pbam	$a = 5.887(5)$ $b = 11.56(1)$ $c = 3.406(4)$	AM, Qu 600°C, 800 h, PXD	ChK, 77	Gd 98.5 Co 99.90 B 99.3
		$a = 5.924(3)$ $b = 11.472(6)$ $c = 3.453(2)$ homogeneous range?	AM HT, 1600°C, 12 h in vacuum, PXD	SoR, 79	Gd 99.9 Co 99.5 B 99.0
Gd <sub>2</sub> CoB <sub>3</sub> <sup>(*)</sup>	hexagonal	$a = 3.130$ $c = 7.894$	AM, Vycor 800°C, 300 h, QE, PXD	StL, 78	Gd 99.9 Co 99.75 B 99.4
			AM, Qu 600°C, 800 h, PXD	ChK, 77	Gd 98.5 Co 99.90 B 99.3
GdCo <sub>4</sub> B <sub>4</sub>	CeCo <sub>4</sub> B <sub>4</sub> P4 <sub>2</sub> /nmc	$a = 5.043(3)$ $c = 7.049(5)$	no details given, PXD	KuB, 71	
GdCo <sub>2</sub> B <sub>2</sub>	ThCr <sub>2</sub> Si <sub>2</sub> I4/mmm	$a = 3.573(3), \rho_E = 8.02$ $c = 9.540(5), \rho_x = 8.09$	AM, Qu(Ta) 800°C, 150 h, PXD	NiSY, 73	Gd 99.9 Co 99.99 B 99.3
		$a = 3.574$ $c = 9.555$	AM, Qu(Mo) 800°C, 50 h, PXD	Ro, 73	Gd 99.9 Co 99.5 B 99.0
GdCo <sub>12</sub> B <sub>6</sub>	SrNi <sub>12</sub> B <sub>6</sub> R $\bar{3}m$	$a_H = 9.474(2)$ $c_H = 7.450(2)$	AM, Qu 800°C, 270 h, PXD	KuCC, 81	Gd 99.5 Co 99.95 B 99.4
		$a_H = 9.353$ $c_H = 7.410$ homogeneous range?	AM, Qu, 600°C, 800 h PXD	ChK, 77	Gd 98.5 Co 99.9 B 99.3
GdCo <sub>3</sub> B <sub>2</sub> <sup>(**)</sup>	CeCo <sub>3</sub> B <sub>2</sub> P6/mmm	$a = 5.059(3)$ $c = 3.019(2)$	AM, Qu 800°C, 50 h, PXD	KuKB, 69	
		$a = 5.066(3), \rho_E = 5.25$ $c = 3.022(2), \rho_x = 8.79$	AM, Qu(Ta) 1150°C, 96 h PXD refinement, $R = 0.13$	NiY, 73	Gd 99.8 Co 99.99 B 99.9
GdCo <sub>4</sub> B <sup>(**)</sup>	CeCo <sub>4</sub> B P6/mmm	$a = 5.053(3)$ $c = 6.854(4)$	AM, Qu 800°C, 50 h, PXD	KuB, 73	Gd 99 Co 99.87 B 99.3
Gd <sub>3</sub> Co <sub>11</sub> B <sub>4</sub> <sup>(**)</sup>	Ce <sub>3</sub> Co <sub>11</sub> B <sub>4</sub> P6/mmm	$a = 5.079(3)$ $c = 9.842(6)$	AM, Qu 800°C, 50 h, PXD	KuB, 73	Gd 99 Co 99.87 B 99.3
Gd <sub>2</sub> Co <sub>7</sub> B <sub>3</sub> <sup>(**)</sup>	Ce <sub>2</sub> Co <sub>7</sub> B <sub>3</sub> P6/mmm	$a = 5.078(3)$ $c = 12.85(2)$	AM, Qu 800°C, 50 h, PXD	KuB, 73	Gd 99 Co 99.87 B 99.3

<sup>(\*)</sup>Close resemblance was observed for the subsystem of strong X-ray intensities corresponding to an AlB<sub>2</sub>-type subcell.

<sup>(\*\*)</sup>The magnetic moments at 77 K, the coercive forces and the Curie temperatures were reported by EISSJ, 83: GdCo<sub>3</sub>B<sub>2</sub>:  $T_m = 58$  K; GdCo<sub>4</sub>B:  $T_m = 321$  K; Gd<sub>3</sub>Co<sub>11</sub>B<sub>4</sub>:  $T_m = 293$  K; Gd<sub>2</sub>Co<sub>7</sub>B<sub>3</sub>:  $T_m = 287$  K.

TABLE 14  
Four-phase reactions in Gd-Co-B, see fig. 19c; after Stadelmaier and Lee (1978).

1. $L + Co_2B \rightarrow Co + Co_{12}GdB_6$	14. $L + Co_3Gd \rightarrow Co_2GdB_2 + Co_2Gd$
2. $L \rightarrow Co + Co_{17}Gd_2 + Co_{12}GdB_6$	15. $L \rightarrow Co_2B + Co_4GdB_4 + CoB$
3. $L \rightarrow Co_{17}Gd_2 + Co_4GdB + Co_{12}GdB_6$	16. $L + Co_{12}GdB_6 \rightarrow Co_2B + Co_4GdB_4$
4. $L \rightarrow Co_{17}Gd_2(+Co_3Gd) + Co_4GdB$	17. $L \rightarrow Co_{12}GdB_6 + Co_3GdB_2 + Co_4GdB_4$
5. $L \rightarrow Co_3Gd + Co_7Gd_2 + Co_4GdB$	18. $L \rightarrow Co_3GdB_2 + Co_2GdB_2 + Co_4GdB_4$
6. $L + Co_7Gd_2 \rightarrow Co_3Gd + Co_4GdB$	19. $L + Co_2Gd \rightarrow Co_2GdB_2 + Co_3Gd_4$
7. $L + Co_{11}Gd_3B_4 \rightarrow Co_4GdB + Co_{12}GdB_6$	20. $L \rightarrow Co_4GdB_4 + Co_2GdB_2 + GdB_4$
8. $L + Co_4GdB \rightarrow Co_{11}Gd_3B_4 + Co_3Gd$	21. $L \rightarrow Co_4GdB_4 + CoB + GdB_4$
9. $L \rightarrow Co_{11}Gd_3B_4 + Co_{12}GdB_6 + Co_7Gd_2B_3$	22. $L + B \rightarrow CoB + GdB_{66}$
10. $L + Co_{11}Gd_3B_4 \rightarrow Co_7Gd_2B_3 + Co_3Gd$	23. $L \rightarrow CoB + GdB_{66} + GdB_6$
11. $L \rightarrow Co_7Gd_2B_3 + Co_3GdB_2 + Co_{12}GdB_6$	24. $L \rightarrow CoB + GdB_6 + GdB_4$
12. $L + Co_7Gd_2B_3 \rightarrow Co_3GdB_2 + Co_3Gd$	25. $L + GdB_4 \rightarrow Co_2GdB_2 + GdB_2$
13. $L + Co_3GdB_2 \rightarrow Co_2GdB_2 + Co_3Gd$	26. $L \rightarrow Co_2GdB_2 + Co_3Gd_4 + GdB_2$

with quite different lattice parameters, see table 13. The lattice parameters and other crystallographic data for the ternary Gd-Co-B alloys are given in table 13.

Maximum solubilities of cobalt in the gadolinium borides at 800°C as determined by microprobe analysis were given by Stadelmaier and Lee (1978) in a/o:  $GdB_2(?)$ : 0.1,  $GdB_4$ : 1.9,  $GdB_6$ : 0.1 and  $GdB_{66}$ : 1.0 a/o Co.

The magnetic properties of amorphous thin films of GdCoB were investigated by Taylor and Gangulee (1982) (magnetization versus temperature).

### References

- Adams, W., J.M. Moreau, E. Parthé and J. Schweitzer, 1976, *Acta Crystallogr.* **B32**(9), 2697.  
 Blanks, J.H. and K.E. Spear, 1974, paper presented at 76th Annual Meeting of the Amer. Ceram. Soc., Chicago, IL, USA.  
 Chaban, N.F. and Yu.B. Kuz'ma, 1977, *Izv. Akad. Nauk SSSR, Neorg. Mater.* **13**(5), 923.  
 ElMasry, N.A., H.H. Stadelmaier, C.J. Shahwan and L.T. Jordan, 1983, *Z. Metallkde* **74**(1), 33.  
 Kuz'ma, Yu.B. and N.S. Bilonishko, 1971, *Kristallografiya* **16**, 1030.  
 Kuz'ma, Yu.B. and N.S. Bilonishko, 1973, *Kristallografiya* **18**, 710.  
 Kuz'ma, Yu.B., P.I. Kripyakevich and N.S. Bilonishko, 1969, *Dopov. Akad. Nauk Ukr. RSR, Ser. A* **10**, 939.  
 Kuz'ma, Yu.B., G.V. Chernjak and N.F. Chaban, 1981, *Dopov. Akad. Nauk Ukr. RSR, Ser. A* **12**, 80.  
 Niihara, K. and S. Yajima, 1972, *Chem. Lett. (Chem. Soc. Jpn)*, 875.  
 Niihara, K. and S. Yajima, 1973, *Bull. Chem. Soc. Jpn* **46**, 770.  
 Niihara, K., T. Shishido and S. Yajima, 1973, *Bull. Chem. Soc. Jpn* **46**, 1137.  
 Rogl, P., 1973, *Monatsh. Chem.* **104**, 1623.  
 Spear, K.E. and D.W. Petsinger, 1972, Paper presented at the 14th Annual Meeting of the Amer. Ceram. Soc., Washington, DC, USA.  
 Sobczak, R. and P. Rogl, 1979, *J. Solid State Chem.* **27**, 343.  
 Stadelmaier, H.H. and H.J. Lee, 1978, *Z. Metallkde* **69**(11), 685.  
 Taylor, R.C. and A. Gangulee, 1982, *J. Appl. Phys.* **53**(3), 2341.

*Gd-Cr-B* (see also notes added in proof)

The crystal structure of  $GdCrB_4$  [ $YCrB_4$ -type, 5.953(3),  $b = 11.527(6)$ ,  $c = 3.493(2)$ ] was confirmed by Sobczak and Rogl (1979) by X-ray powder methods. Samples were prepared by arc melting compacts of Gd ingots 99.9%, and B 99% and

Cr 99.5% pure powders, followed by heat treatment at 1400°C, 5 h on a BN substrate under argon. Kuz'ma (1970) reported  $a = 5.872(5)$ ,  $b = 11.55(1)$ ,  $c = 3.485(4)$  for this phase.

### References

- Kuz'ma, Yu.B., 1970, *Kristallografiya* **15**(2), 372.  
 Sobczak, R. and P. Rogl, 1979, *J. Solid State Chem.* **27**, 343.

### Gd-Cu-B

Two partial isothermal sections of the system Gd-Cu-B (region 33–100 a/o Gd at 400°C; region 0–33 a/o Gd at 600°C) were analyzed by Chaban (1979) using röntgenographic as well as metallographic methods. 46 samples were prepared from powder compacts (B 99.3%, Cu 99.5%) and Gd ingots (98.5%) by arc melting and subsequent annealing in evacuated silica tubes for 1000 h. The boron-rich section B-Cu-GdB<sub>6</sub>, including the compounds GdB<sub>66</sub> and CuB<sub>~26</sub>, was not investigated and is tentative (fig. 20).

Mutual solid solubilities of binary Gd-Cu alloys, GdCu<sub>6</sub> (CeCu<sub>6</sub>-type), GdCu<sub>5</sub> (CaCu<sub>5</sub>-type), GdCu<sub>2</sub> (CeCu<sub>2</sub>-type), GdCu (CsCl-type), and Gd-B alloys were negligible; no ternary compounds form; for the solid solubility of Cu in β-rh. B, see Ce-Cu-B. "Gd<sub>2</sub>B<sub>5</sub>" was observed with unknown structure type, but likely is isostructural with Sm<sub>2</sub>B<sub>5</sub>, for which a structure proposal by La Placa is still unpublished.

### References

- Chaban, N.F., 1979, *Vestn. Lvov Univ., Ser. Khim.* **21**, 44.  
 La Placa, S., unpublished results.

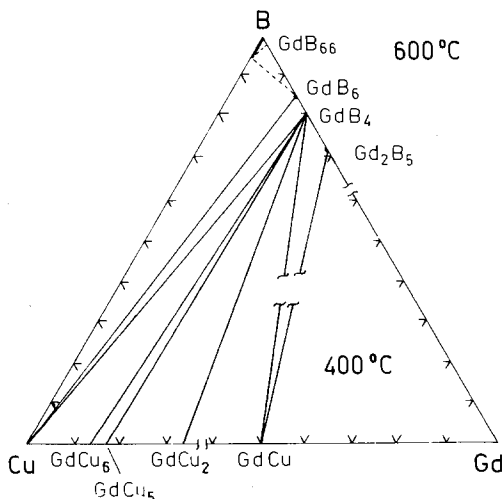


Fig. 20. Gd-Cu-B, partial isothermal sections at 600°C (0–33 a/o Gd), and at 400°C (33–100 a/o Gd); region GdB<sub>6</sub>-Cu-B is proposed.

*Gd-Fe-B*

Chaban et al. (1980) investigated the phase equilibria at 800°C by means of X-ray and metallographic analysis of 130 arc melted and annealed alloys (800°C, 700 h). Starting materials were Gd ingot 98.5%, and Fe 99.9% and B 99.3% powders. The compounds of the binary system Gd-Fe are in basic agreement with a recent compilation by Kubaschewski-von Goldbeck (1982):  $\text{Gd}_2\text{Fe}_{17}$ ,  $\text{Gd}_2\text{Fe}_{17-x}$  ( $\text{Th}_2\text{Zn}_{17}$ ,  $\text{Th}_2\text{Ni}_{17}$ -type);  $\text{GdFe}_3$  ( $\text{PuNi}_3$ -type),  $\text{GdFe}_2$  ( $\text{MgCu}_2$ -type); the phase  $\text{Gd}_6\text{Fe}_{23}$  was not observed at 800°C (see also, e.g., Moffatt, 1976). For the Fe borides, see Y-Fe-B, and for the Gd borides, see Gd-Ti-B. Mutual solid solubilities were found to be negligible; at least five ternary compounds were observed (fig. 21).

$\text{GdFeB}_4$  has been confirmed to crystallize with the  $\text{YCrB}_4$ -type, Pbam; Sobczak and Rogl (1979) gave  $a = 5.918(3)$ ,  $b = 11.456(6)$ ,  $c = 3.457(2)$  and accordingly Stepanchikova and Kuz'ma (1977) measured  $a = 5.911(10)$ ,  $b = 11.50(2)$ ,  $c = 3.436(5)$ . Magnetic susceptibility (80–300 K) of  $\text{GdFeB}_4$  was investigated by Sobczak and Rogl (1979).

$\text{GdFe}_2\text{B}_2$  has the  $\text{ThCr}_2\text{Si}_2$ -type of structure  $I4/mmm$ ,  $a = 3.558(5)$ ,  $c = 9.507(10)$  (Stepanchikova et al., 1978).

The compound  $\text{GdFe}_4\text{B}_4$ , first observed by Chaban et al. (1980), was reported to be isostructural with  $\text{CeFe}_4\text{B}_4$ ,  $a = 7.05$ ,  $c = 27.42 \text{ \AA}$ , with an eight-fold superstructure along the  $c$ -axis:  $c = 8c_0$ . In this context quite recently a series of superstructures  $\text{Gd}_{n+m}(\text{Fe}_4\text{B}_4)_n$ , whose crystal structures were claimed to derive from the  $\text{NdCo}_4\text{B}_4$ -type and are either incommensurate or have unusually long repeat units along their  $c$ -axis, have been described by Braun et al. (1982); see table 2. Samples of composition  $\text{Gd}_x\text{Fe}_4\text{B}_4$ ,  $0.95 \leq x \leq 1.35$ , which were arc melted and annealed at 1000°C for 10–14 days, indicated a small but significant homogeneous range (?) insofar as the Gd subcellparameter changes within  $3.40 \leq c_{\text{Gd}} \leq 3.48 \text{ \AA}$  and decreases with increasing content of Gd.

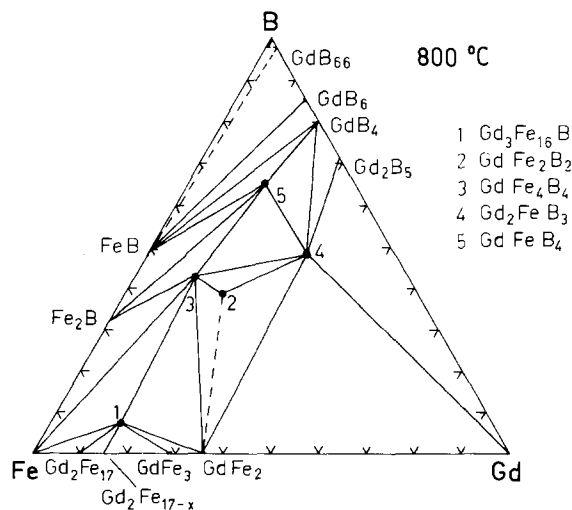


Fig. 21. Gd-Fe-B, isothermal section at 800°C.

$Gd_{\sim 2}FeB_{\sim 3}$ , whose structure is still unknown, probably is isostructural with  $Gd_2CoB_3$ ; the structure type of  $Gd_3Fe_{16}B_1$  is unknown.

The magnetic properties of amorphous thin films of  $GdFeB$  have been investigated by Taylor and Gangulee (1982) (magnetization as a function of temperature and the high field volume susceptibility as a function of the boron concentration).

### References

- Braun, H.F., M. Pelizzone and K. Yvon, 1982, Ferromagnetic borides with incommensurate rare earth and iron sublattices:  $R_{1+\epsilon}Fe_4B_4$ , paper presented at the 7th Intern. Conf. on Solid Compounds of Transition Elements, Grenoble (June 21–26), Proceedings, II B11.
- Chaban, N.F., Yu.B. Kuz'ma, N.S. Bilonishko, O.O. Kachmar and N.V. Petriv, 1980, Dopov. Akad. Nauk Ukr. RSR, Ser. A, 875.
- Kubaschewski-von Goldbeck, O., 1982, Iron-binary phase diagrams (Springer, Berlin) pp. 106–107.
- Moffatt, W.G., 1976, The Handbook of Binary Phase Diagrams (General Electric Comp., Schenectady, NY), updating service.
- Sobczak, R. and P. Rogl, 1979, J. Solid State Chem. **27**, 343.
- Stepanchikova, G.F. and Yu.B. Kuz'ma, 1977, Vestn. Lvov Univ., Ser. Khim. **19**, 37.
- Stepanchikova, G.F., Yu.B. Kuz'ma and B.I. Chernjak, 1978, Dopov. Akad. Nauk Ukr. RSR, Ser. A **10**, 951.
- Taylor, R.C. and A. Gangulee, 1982, J. Appl. Phys. **53**(3), 2341.

### *Gd-Ge-B*

The influence of boron additions to  $R_5Ge_3$  compounds was studied (X-ray analysis) by Mayer and Felner (1974) on a series of samples with a nominal boron content according to the formulas:  $Gd_5Ge_3$ ,  $Gd_5Ge_3B_{0.5}$ ,  $Gd_5Ge_3B_{1.0}$ ,  $Gd_5Ge_3B_{1.5}$  and  $Gd_5Ge_3B_{2.0}$ . Alloys were prepared by heating (melting) elemental mixtures of a min. purity of 99.9% in Ta crucibles to 1600°C under He atmosphere. Mayer and Felner (1974) claim the  $Mn_5Si_3$ -type phase to be stable up to a composition of  $Gd_5Ge_3B_2$ ; lattice parameters are listed in table 6. Boron solubility (filling of octahedral voids) in  $Mn_5Si_3$ -type phases, however, is limited to a formula  $R_5Ge_3B_{1.0}$ . For higher boron concentrations the boron solubility might be accompanied by simultaneous substitution Ge/B, which probably would explain the irregular variation of lattice parameters (see table 6); a reinvestigation seems to be necessary.

### Reference

- Mayer, I. and I. Felner, 1974, J. Less-Common Metals **37**, 171.

### *Gd-Hf-B*

An isothermal section of the system  $Gd-Hf-B$  was determined at 800°C by Chaban et al. (1978) by means of X-ray analysis of arc melted samples (Hf powder 99.0%, B powder 99.3%, Gd ingot 98.5%), which have been annealed for 500 h at 800°C in evacuated silica tubes.

At variance with earlier papers (Glaser et al., 1953) dealing with the formation of a NaCl-type hafnium monoboride, Rudy and Windisch (1965), in a detailed investigation of the Hf-B system, established the existence of the binary compound

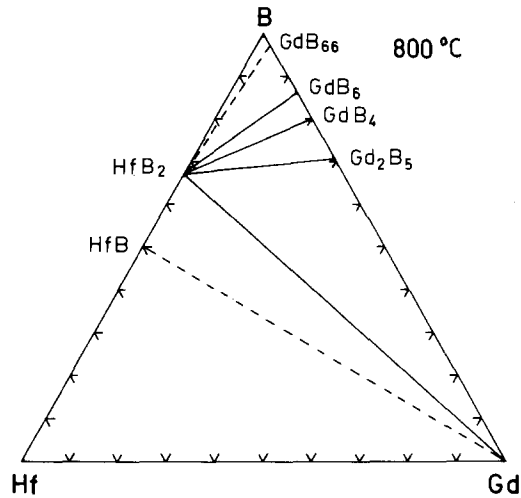


Fig. 22. Gd-Hf-B, isothermal section at 800°C.

HfB with FeB-type of structure stable at temperatures  $T \leq 2100$  ( $\pm 20$ )°C. The nucleation reaction  $L + \text{HfB}_2 \rightleftharpoons \text{HfB}$  was observed to be slow at temperatures below  $\approx 1650$ °C. Although not specifically investigated (and therefore unproven) Rudy and Windisch (1965) reported about indications that HfB might be unstable below  $\approx 1250$ °C, decomposing in an extremely slow reaction into  $\alpha\text{-Hf} + \text{HfB}_2$ . Although not specifically stated, HfB was not observed by Chaban et al. (1978) at 800°C. Therefore the two-phase equilibrium:  $\text{HfB} + \text{Gd}$  (dashed line in fig. 22) is tentative.

### References

- Chaban, N.F., Yu.B. Kuz'ma and I.D. Gerasim, 1978, *Poroshk. Metall.* **188**(8), 24.  
 Glaser, F.W., D. Moskowitz and B.W. Post, 1953, *J. Metals* **5**, 1119.  
 Rudy, E. and St. Windisch, 1965, *Air Force Materials Laboratory, Technical Report 65-2, Part I, Vol. IX.*

### Gd-Ir-B

$\text{GdIr}_4\text{B}_4$  forms congruently from the melt (X-ray and metallographic analysis; Rogl, 1979);  $\text{NdCo}_4\text{B}_4$ -type,  $\text{P4}_2/\text{n}$ ,  $a = 7.571(3)$ ,  $c = 3.979(2)$ . For preparation techniques, see  $\text{LaOs}_4\text{B}_4$ . Magnetic data were presented by Rupp et al. (1979).

$\text{GdIr}_3\text{B}_2$  was reported to be isostructural with  $\text{ErIr}_3\text{B}_2$  (possible space group  $\text{C2/m}$ ),  $a = 5.466(6)$ ,  $b = 9.473(9)$ ,  $c = 3.092(4)$ ,  $\beta = 91.0(1)^\circ$ . (Ku and Meisner, 1981; X-ray powder analysis of arc melted samples);  $T_m = 29.8$  K.

### References

- Ku, H.C. and G.B. Meisner, 1981, *J. Less-Common Metals* **78**, 99.  
 Rogl, P., 1979, *Monatsh. Chem.* **110**, 235.  
 Rupp, B., P. Rogl and R. Sobczak, 1979, *Mater. Res. Bull.* **14**, 1301.



TABLE 15

Lattice parameters and physical properties of  $Gd_xLa_{1-x}B_6$  alloys; after Aivazov et al. (1980).  $\rho_x$  is the X-ray density, calculated for a defect-free lattice,  $\rho_{pyc}$  is the pycnometric density,  $n$  is the number of conduction electrons per unit cell, determined from Hall effect measurements.

Chemical composition	$a$ (Å)	$\rho_x$ (kg/dm <sup>3</sup> )	$\rho_{pyc}$	$n$	$\mu_{eff}$ ( $\mu_B$ )	$\theta$ (K)
$La_{0.97}B_6$	$4.1563 \pm 2$	4.711	4.62	0.96		
$Gd_{0.09}La_{0.82}B_6$	$4.1518 \pm 3$	4.770	4.47	—	2.7	0
$Gd_{0.18}La_{0.73}B_6$	$4.1470 \pm 3$	4.828	4.52	0.89	3.6	0
$Gd_{0.36}La_{0.54}B_6$	$4.1384 \pm 3$	4.945	4.61	0.89	4.9	-5
$Gd_{0.48}La_{0.41}B_6$	$4.1319 \pm 3$	5.028	4.66	0.86	5.6	-15
$Gd_{0.60}La_{0.28}B_6$	$4.1258 \pm 4$	5.112	4.68	—	6.6	-20
$Gd_{0.72}La_{0.15}B_6$	$4.1187 \pm 3$	5.203	4.71	0.82	6.9	-30
$Gd_{0.78}La_{0.09}B_6$	$4.1154 \pm 2$	5.246	4.76	—	7.3	-30
$Gd_{0.91}B_6$	$4.1111 \pm 2$	5.307	4.98	0.99	7.9	-30

### Gd-La-B

A continuous solid solution  $Gd_xLa_{1-x}B_6$  was reported by Samsonov et al. (1951), Sperlich et al. (1973) and Kunitzkii et al. (1977). A structural and magnetochemical study of this system was carried out by Aivazov et al. (1980). Specimens were obtained from borothermal reduction of the mixed oxides in vacuum at 1600°C (8 h). X-ray combined with chemical analysis proved that the alloys form a continuous series of solid solutions with  $CaB_6$ -type, Pm3m, obeying Vegard's rule. Pycnometric densities, measured in toluene, revealed an increasing metal deficiency for intermediate alloys and furthermore increasing deficiency with increasing Gd content (table 15). Magnetic susceptibilities (80–1000 K) indicate Gd to be trivalent ( $^8S_{7/2}$ ) in these alloys. Spin-glass behavior was reported by Ali and Woods (1983).

### References

- Aivazov, M.I., S.V. Aleksandrovich, B.A. Evseev, V.N. Sorokin and O.M. Tsarev, 1980, *Izv. Akad. Nauk SSSR, Neorg. Mater.* **16**(9), 1556.  
 Ali, N. and S.B. Woods, 1983, *Solid State Commun.* **45**(6), 471.  
 Kunitzkii, Yu.A., V.V. Morozov and V.Ya. Shlyuko, 1977, *High. Temp. Electronic Materials (Vyshcha Shkola, Kiev)*.  
 Samsonov, G.V., V.S. Nespor and T.I. Serebryakova, 1951, *Inzh. Fiz. Zh.* **2**, 118.  
 Sperlich, G., K.H. Janneck and K.H.J. Buschow, 1973, *Phys. Stat. Sol.* **57B**, 701.

### Gd-Mn-B

Kuz'ma (1970) reported the existence of the ternary compound  $GdMnB_4$  with the  $YCrB_4$ -type of structure, Pbam,  $a = 5.944(5)$ ,  $b = 11.51(1)$ ,  $c = 3.464(5)$ , from X-ray powder analysis. Samples were prepared by arc melting powder compacts of 98% Gd, 99.4% B and 95.5% Mn with subsequent heat treatment at 800°C for 240 h in evacuated silica tubes.

Magnetic susceptibility data (80–300 K) of  $GdMnB_4$  [ $YCrB_4$ -type, Pbam,  $a = 5.922(3)$ ,  $b = 11.466(6)$ ,  $c = 3.451(2)$ ] were measured by Sobczak and Rogl

(1979). Samples were prepared by reacting  $GdB_4$  and Mn powder compacts, wrapped in Mo foil and sealed in evacuated quartz tubes, 48 h at  $900^\circ C$  and 12 h at  $1200^\circ C$ . The pellets were reground, recompact and finally heat treated for 5 h at  $1400^\circ C$  on a BN substrate under argon.

### References

- Kuz'ma, Yu.B., 1970, Dopov. Akad. Nauk Ukr. RSR, Ser. A 32(8), 756.  
 Sobczak, R. and P. Rogl, 1979, J. Solid State Chem. 27, 343.

### Gd-Mo-B (see also notes added in proof)

The crystal structure of  $GdMoB_4$ ,  $YCrB_4$ -type, Pbam,  $a = 6.059(5)$ ,  $b = 11.70(1)$ ,  $c = 3.619(5)$ , has been characterized by Kuz'ma and Svarichevskaya (1972) from X-ray powder photographs. Samples were prepared by arc melting of powder compacts (98% Gd, 99.9% Mo, 99.3% B) and subsequent annealing at  $1000^\circ C$  for 360 h in evacuated silica tubes.

### Reference

- Kuz'ma, Yu.B. and S.I. Svarichevskaya, 1972, Dopov. Akad. Nauk Ukr. RSR, Ser. A. 34(2), 166.

### Gd-Ni-B (see also notes added in proof)

No ternary phase diagram exists for the Gd-Ni-B system.

Niihara et al. (1973) mentioned the existence of a  $GdNi_4B$  compound presumably isostructural with  $YNi_4B$ ; Kuz'ma and Bilonishko (1981) confirmed a  $CeCo_4B$ -type (see also  $YNi_4B$ ).

$Gd_2Ni_{13}B_2$  was reported to adopt the  $Nd_3Ni_{13}B_2$ -type structure,  $P6/mmm$ ,  $a = 4.976(4)$ ,  $c = 10.878(15)$  (Kuz'ma and Bilonishko, 1981).

The compound  $Gd_3Ni_7B_2$  [ $Dy_3Ni_7B_2$  type,  $P6_3/mmc$ ,  $a = 5.115(2)$ ,  $c = 14.342(10)$ ] was prepared by Kuz'ma and Chaban (1979) by arc melting compacted elemental mixtures (Gd ingot 99.5%, Ni powder 99.98%, B powder 99.3%) and subsequent annealing at  $800^\circ C$ , 360 h in evacuated quartz capsules. Lattice parameters as derived by Kuz'ma and Chaban (1978) were  $a = 5.118$ ,  $c = 14.33$ .

$GdNi_{12}B_6$  crystallizes with the  $SrNi_{12}B_6$ -type of structure,  $R\bar{3}m$ ,  $a_H = 9.523(6)$ ,  $c_H = 7.419(5)$  (Kuz'ma et al., 1981); for sample preparation, see  $YCo_{12}B_6$ .

### References

- Kuz'ma, Yu.B. and N.S. Bilonishko, 1981, Dopov. Akad. Nauk Ukr. RSR, Ser. A 10, 88.  
 Kuz'ma, Yu.B. and N.F. Chaban, 1978, New crystal structures of the homologous series based on the structure types of  $MgZn_2$  and  $CeCo_3B_2$ , in: Tret. Vses. Konf. Kristalloghim. Internet. Soedin, Tezisy Dokl., Lvov, eds. I. Franko and D.I. Medvedeeva (Vyscha Shkola, Lvov) p. 83.  
 Kuz'ma, Yu.B. and N.F. Chaban, 1979, Dopov. Akad. Nauk Ukr. RSR, Ser. A, 88.  
 Kuz'ma, Yu.B., G.V. Chernjak and N.F. Chaban, 1981, Dopov. Akad. Nauk Ukr. RSR, Ser. A 12, 80.  
 Niihara, K., Y. Katayama and S. Yajima, 1973, Chem. Lett. (Chem. Soc. Jpn) 613.

### Gd-Os-B

At least four ternary compounds exist in the Gd-Os-B system (table 16).

TABLE 16  
Formation and structural data of ternary compounds Gd–Os–B.

Compound	Structure type, Space group	Lattice, parameters, Density	Preparation, Characterization	Refs.	Purity
GdOsB <sub>4</sub>	YCrB <sub>4</sub> Pbam	$a = 5.988(3)$ $b = 11.587(6)$ $c = 3.572(2)$	AM, HT, 1600°C, 12 h HV, W substrate, QE congruent melting ME, PXD suscept., 80–300 K	Ro, 78 SoR, 79	Gd 99.9 Os 99.9 B 99.0
Gd <sub>2</sub> OsB <sub>6</sub>	Y <sub>2</sub> ReB <sub>6</sub> Pbam	$a = 9.2425(36)$ $b = 11.5912(41)$ $c = 3.6814(3)$	AM, HT, 1600°C, 12 h HV, BN substrate, QE PXD	RoN, 82	Gd 99.9 Os 99.9 B 99.7
GdOs <sub>4</sub> B <sub>4</sub>	YOs <sub>4</sub> B <sub>4</sub> tetragonal	$a = 7.4878(8)$ $c = 32.6128(24)$ $c = 8c_0$	AM, HT, 1400°C, 12 h HV, BN substrate PXD, $T_n = 11.0$ K	RoHS, 82	Gd 99.9 Os 99.9 B 99.7
GdOs <sub>3</sub> B <sub>2</sub>	YOs <sub>3</sub> B <sub>2</sub> (?) orthorh. (?)	$a \approx 5.5$ $b \approx 9.5$ $c \approx 18$	AM(Zr) PXD, $T_m > 45$ K	Ku, 80	99.9

### References

- Ku, H.C., 1980, Thesis, Univ. of California at San Diego, USA.  
 Rogl, P., 1978, Mater. Res. Bull. **13**, 519.  
 Rogl, P. and H. Nowotny, 1982, Crystal structures and phase relationships within ternary systems: rare earth metal–noble metal–boron, in: *The Rare Earths in Science and Technology*, Vol. 3, eds. J. McCarthy, B. Silber and J.J. Rhyne (Plenum, New York, London) pp. 353–356.  
 Rogl, P., K. Hiebl and M.J. Sienko, 1982, Structural chemistry and magnetic behavior of RM<sub>4</sub>B<sub>4</sub> borides, paper presented at the 7th Intern. Conf. on Solid Compounds of Transition Elements, Grenoble (June 21–25), Proceedings, II A4.  
 Sobczak, R. and P. Rogl, 1979, J. Solid State Chem. **27**, 343.

### Gd–Re–B

No phase diagram exists for the Gd–Re–B system, but five ternary phases have been identified from independent investigations.

GdReB<sub>4</sub> has the YCrB<sub>4</sub>-type of structure, Pbam,  $a = 6.003(5)$ ,  $b = 11.59(1)$ ,  $c = 3.592(5)$  (Kuz'ma and Svarichevskaya, 1972a), determined from arc melted alloys annealed at 1000°C, 360 h, in evacuated silica tubes; purity of starting materials was: Gd ingot 98%, 99.5% Re and 99.3% B powders.

Gd<sub>2</sub>ReB<sub>6</sub> was characterized from X-ray powder analysis by Kuz'ma and Svarichevskaya (1972b) to be Y<sub>2</sub>ReB<sub>6</sub>-type, Pbam,  $a = 9.187(5)$ ,  $b = 11.61(1)$ ,  $c = 3.691(4)$ .

Gd<sub>3</sub>ReB<sub>7</sub> crystallizes with Y<sub>3</sub>ReB<sub>7</sub>-type, Cmcm,  $a = 3.558(2)$ ,  $b = 15.97(1)$ ,  $c = 9.427(5)$  (Kuz'ma and Mikhalenko, 1976).

Furthermore the existence of ternary compounds with approximate formulas "GdReB<sub>2</sub>" and "GdReB" and with unknown structure type was reported by Mikhalenko et al. (1981).

## References

- Kuz'ma, Yu.B. and S.I. Mikhailenko, 1976, *Dopov. Akad. Nauk Ukr. RSR, Ser. A* **11**, 1029.  
 Kuz'ma, Yu.B. and S.I. Svarichevskaya, 1972a, *Dopov. Akad. Nauk Ukr. RSR, Ser. A* **2**, 166.  
 Kuz'ma, Yu.B. and S.I. Svarichevskaya, 1972b, *Kristallografiya*, **17**(3), 658.  
 Mikhailenko, S.I., N.F. Chaban and Yu.B. Kuz'ma, 1981, *J. Less-Common Metals* **82**, 365.

*Gd-Rh-B*

Ku et al. (1980) investigated the crystal structure as well as magnetic and superconducting properties of the arc melted alloy  $GdRh_3B_2$  with the  $CeCo_3B_2$ -type,  $P6/mmm$ ,  $a = 5.404(6)$ ,  $c = 3.115(4)$ ;  $T_m > 45$  K; see also Malik et al. (1982).

$GdRh_4B_4$  has the  $CeCo_4B_4$ -type of structure,  $P4_2/nmc$ ,  $a = 5.309(2)$ ,  $c = 7.417(2)$  (Vandenberg and Matthias, 1977; X-ray powder methods); for sample preparation, see  $YRh_4B_4$ . Magnetic ordering was observed at  $T_m = 5.62$  K as measured by Matthias et al. (1977).

For the perovskite-type phase  $GdRh_3B_{1-x}$  ( $Cu_3Au$ -type,  $a = 4.178$ ,  $x = 0.15$ ), see  $R-Rh-B$ .

## References

- Ku, H.C., C.P. Meisner, F. Acker and D.C. Johnston, 1980, *Solid State Commun.* **35**, 91.  
 Malik, S.K., S.K. Dhar, R. Vijayaraghavan and W.E. Wallace, 1982, *J. Appl. Phys.* **53**, 8074.  
 Matthias, B.T., E. Corenzwit, J.M. Vandenberg and E. Barz, 1977, *Proc. Nat'l Acad. Sci. US* **74**(4), 1334.  
 Vandenberg, J.M. and B.T. Matthias, 1977, *Proc. Nat'l Acad. Sci. US* **74**(4), 1336.

*Gd-Ru-B*

Four ternary compounds were identified in the  $Gd-Ru-B$  system (table 17).

TABLE 17  
 Formation and structural data of ternary compounds  $Gd-Ru-B$ .

Compound	Structure type, Space group	Lattice parameters, Density	Preparation, Characterization	Refs.	Purity
$GdRuB_4$	$YCrB_4$	$a = 5.973(3)$	AM, HT, 1600°C, 12 h		Gd 99.9
	Pbam	$b = 11.568(6)$ $c = 3.570(2)$	HV, W substrate congruent melting, ME suscept., 80–300 K	Ro, 78 RoR, 79	Ru 99.9 B 99.0
$Gd_2RuB_6$	$Y_2ReB_6$	$a = 9.2323(30)$	AM, HT, 1600°C, 12 h		Gd 99.9
	Pbam	$b = 11.5843(36)$ $c = 3.6902(3)$	HV, W substrate PXD	RoN, 82	Ru 99.9 B 99.0
$GdRu_4B_4$	$LuRu_4B_4$	$a = 7.470(5)$	AM(Ar)		high
	$I4_1/acd$	$c = 15.009(10)$	PXD, $T_m = 4.55$ K	Jo, 77	purity
$GdRu_3B_2$	$CeCo_3B_2$ $P6/mmm$	$a = 5.493-5.505(4)$	AM, HT, 1400°C		Gd 99.9
		$c = 3.024-3.015(2)$	24 h, BN substrate PXD, congr. melting, ME $T_m = 10$ K	HiRUS, 80	Ru 99.9 B 99.0
		$a = 5.508(6)$ $c = 3.018(4)$	AM(Ar) PXD $T_m > 45$ K	KuMAJ, 80	99.9

*References*

- Hiebl, K., P. Rogl, E. Uhl and M.J. Sienko, 1980, *Inorg. Chem.* **19**(11), 3316.  
 Johnston, D.C., 1977, *Solid State Commun.* **24**(10), 699.  
 Ku, H.C., G.P. Meisner, F. Acker and D.C. Johnston, 1980, *Solid State Commun.* **35**, 91.  
 Rogl, P., 1978, *Mater. Res. Bull.* **13**, 519.  
 Rogl, P. and H. Nowotny, 1982, Crystal structures and phase relationships within ternary systems: rare earth metal-noble metal-boron, in: *The Rare Earths in Science and Technology*, Vol. 3, eds. J. McCarthy, B. Silber and J.J. Rhyne (Plenum, New York, London) pp. 353-356.  
 Sobczak, R. and P. Rogl, 1979, *J. Solid State Chem.* **27**, 343.

*Gd-Si-B*

The influence of boron additions to  $R_5Si_3$  compounds was studied (X-ray analysis) by Mayer and Felner (1974) on a series of samples with a nominal boron content according to the formulas:  $Gd_5Si_3$ ,  $Gd_5Si_3B_{0.5}$ ,  $Gd_5Si_3B_{1.0}$ ,  $Gd_5Si_3B_{1.5}$  and  $Gd_5Si_3B_{2.0}$ . Alloys were prepared by heating (melting) elemental mixtures of a min. purity of 99.9% in Ta crucibles to 1600°C under He atmosphere. Mayer and Felner (1974) claim the  $Mn_5Si_3$ -type phase to be stable up to a composition of  $Gd_5Si_3B_2$ ; lattice parameters are listed in table 6. Boron solubility (filling of octahedral voids) in  $Mn_5Si_3$ -type phases, however, is limited to a formula  $R_5Si_3B_{1.0}$ . For higher boron concentrations the boron solubility might be accompanied by simultaneous substitution Si/B, which probably would explain the irregular variation of lattice parameters (see table 6); a reinvestigation seems to be necessary.

*Reference*

- Mayer, I. and I. Felner, 1974, *J. Less-Common Metals* **37**, 171.

*Gd-Sm-B*: see notes added in proof under *Sm-M-B*

*Gd-Ti-B*

An isothermal section of the system Gd-Ti-B (fig. 23) was determined by Chaban

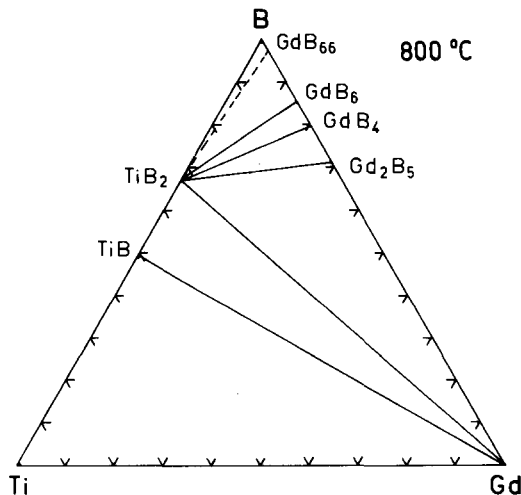


Fig. 23. Gd-Ti-B, isothermal section at 800°C.

et al. (1978) at 800°C by means of X-ray analysis of arc melted samples (Ti powder 99.7%, B powder 99.3%, Gd ingot 98.5%) which have been annealed for 500 h at 800°C in evacuated silica tubes. The Gd–B binary system was reinvestigated. GdB<sub>2</sub> [AlB<sub>2</sub>-type,  $a = 3.314(3)$ ,  $c = 3.934(3)$ ] was not obtained at 800°C in accord with recent data by Blanks (1980). Gd<sub>2</sub>B<sub>5</sub> was observed with unknown structure type, but probably is isostructural with Sm<sub>2</sub>B<sub>5</sub>, for which a structure proposal by La Placa is still unpublished. Vapor composition and chemical activity within the Gd–B binary have recently been investigated by Storms and Mueller (1981). In accordance with a phase diagram study by Rudy (1969), TiB (FeB-type) and TiB<sub>2</sub> (AlB<sub>2</sub>-type) were the only binary titanium borides observed. Mutual solid solubilities of Ti and Gd borides were found to be small and no ternary compounds are formed.

### References

- Blanks, C.E., 1980, Thesis, Univ. of Pennsylvania, Philadelphia, USA.  
 Chaban, N.F., Yu.B. Kuz'ma and I.D. Gerasim, 1978, Poroshk. Metall. **188**(8), 24.  
 La Placa, S., unpublished results.  
 Rudy, E., 1969, Compendium of Phase Diagram Data, Air Force Materials Laboratory, Technical Report 65-2, 5.  
 Storms, E.K. and B.A. Mueller, 1981, J. Appl. Phys. **52**(4), 2966.

### Gd–V–B

GdVB<sub>4</sub> has the YCrB<sub>4</sub>-type of structure, Pbam,  $a = 6.022(5)$ ,  $b = 11.66(1)$ ,  $c = 3.504(5)$  (Kuz'ma, 1970, X-ray powder diffraction); for sample preparation, see GdMnB<sub>4</sub>.

### Reference

- Kuz'ma, Yu.B., 1970, Dopov. Akad. Nauk Ukr. RSR, Ser. A **32**(8), 756.

### Gd–W–B (see also notes added in proof)

GdWB<sub>4</sub> was prepared by Kuz'ma and Svarichevskaya (1972) by arc melting powder compacts of 98% pure Gd, 99.99% W and 99.4% B, followed by heat treatment at 1000°C, 360 h in evacuated silica tubes. From X-ray powder analysis GdWB<sub>4</sub> is isotypic with the YCrB<sub>4</sub>-type of structure, Pbam,  $a = 6.066(5)$ ,  $b = 11.71(1)$ ,  $c = 3.618(5)$ .

### Reference

- Kuz'ma, Yu.B. and S.I. Svarichevskaya, 1972, Dopov. Akad. Nauk Ukr. RSR, Ser. A **34**(9), 166.

### Gd–Zr–B

An isothermal section at 800°C (fig. 24) was determined by Chaban et al. (1978) by means of X-ray analysis of arc melted samples (Zr powder 99.5%, B powder

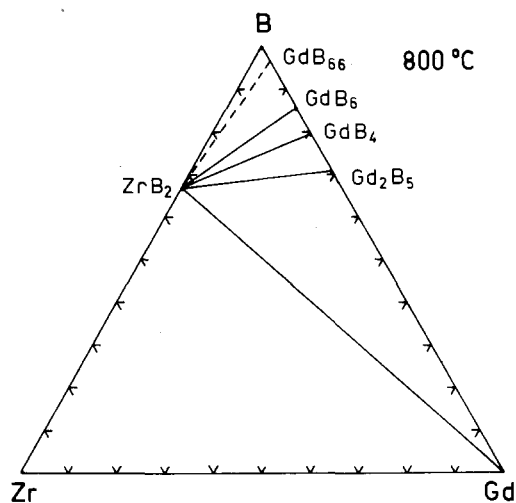


Fig. 24. Gd-Zr-B, isothermal section at 800°C.

99.3%, Gd ingot 98.5%) which have been annealed for 500 h at 800°C in evacuated silica tubes. For details on the binary system Gd-B, see Gd-Ti-B. The Zr-B binary system ( $ZrB_2$  with  $AlB_2$ -type) is in accord with a phase diagram study by Rudy (1969). No ternary compounds and solid solutions are formed.

### References

- Chaban, N.F., Yu.B. Kuz'ma and I.D. Gerasim, 1978, *Poroshk. Metall.* **188**(8), 24.  
 Rudy, E., 1969, *Compendium of Phase Diagram Data*, Air Force Materials Laboratory, Technical Report 65-2, 5.

### Ho-Co-B

Eight ternary compounds have been identified in the Ho-Co-B system. The preparation and crystallographic characteristics of these ternary compounds are listed in table 18.

### References

- Kuz'ma, Yu.B. and N.S. Bilonishko, 1972, *Sov. Phys. Crystallogr.* **16**(5), 897.  
 Kuz'ma, Yu.B. and N.S. Bilonishko, 1973, *Kristallografiya* **18**(4), 710.  
 Kuz'ma, Yu.B., P.I. Kripyakevich and N.S. Bilonishko, 1969, *Dopov. Akad. Nauk Ukr. RSR, Ser. A* **10**, 939.  
 Kuz'ma, Yu.B., G.V. Chernjak and N.F. Chaban, 1981, *Dopov. Akad. Nauk Ukr. RSR, Ser. A* **12**, 80.  
 Niihara, K. and S. Yajima, 1973, *Bull. Chem. Soc. Jpn* **46**, 770.  
 Rogl, P., 1973, *Monatsh. Chem.* **104**, 1623.  
 Stepanchikova, G.F. and Yu.B. Kuz'ma, 1977, *Vestn. Lvov Univ., Ser. Khim.* **19**, 37.

TABLE 18  
Formation and Structural data of ternary compounds Ho-Co-B.

Compound	Structure type, Space group	Lattice parameters Density	Preparation, Characterization	Refs.	Purity	
HoCoB <sub>4</sub>	YCrB <sub>4</sub> Pbam	$a = 5.879(10)$ $b = 11.36(2)$ $c = 3.375(5)$	AM, Qu 800°C, 340 h, PXD	StK, 77	Ho 99.0 Co 99.9 B 99.3	
HoCo <sub>4</sub> B <sub>4</sub>	CeCo <sub>4</sub> B <sub>4</sub> P4 <sub>2</sub> /nmc	$a = 5.020(3)$ $c = 7.003(5)$	no details given, PXD	KuB, 72		
HoCo <sub>2</sub> B <sub>2</sub>	ThCr <sub>2</sub> Si <sub>2</sub> I4/mmm	$a = 3.551$ $c = 9.245$	AM, Qu(Mo) 800°C, 50 h, PXD	Ro, 73	Ho 99.9 Co 99.5 B 99.0	
HoCo <sub>3</sub> B <sub>2</sub>	CeCo <sub>3</sub> B <sub>2</sub> P6/mmm	$a = 5.026(3)$ $c = 3.029(2)$	AM, Qu 800°C, 50 h, PXD	KuKB, 69		
		$a = 5.018(3), \rho_E = 5.50$ $c = 3.023(2), \rho_X = 9.15$	AM, Qu(Ta) 1150°C, 96 h, PXD		NiY, 73	Ho 99.8 Co 99.99 B 99.9
		$a = 5.017(5)$ $c = 3.024(2)$	AM, Qu(Mo) 800°C, 50 h, PXD		Ro, 73	Ho 99.9 Co 99.5 B 99.0
HoCo <sub>4</sub> B	CeCo <sub>4</sub> B P6/mmm	$a = 4.976(3)$ $c = 6.873(4)$	AM, Qu 800°C, 50 h, PXD	KuB, 73	Ho 99 Co 99.87 B 99.3	
Ho <sub>3</sub> Co <sub>11</sub> B <sub>4</sub>	Ce <sub>3</sub> Co <sub>11</sub> B <sub>4</sub> P6/mmm	$a = 5.030(3)$ $c = 9.846(6)$	AM, Qu 800°C, 50 h, PXD	KuB, 73	Ho 99 Co 99.87 B 99.3	
Ho <sub>2</sub> Co <sub>7</sub> B <sub>3</sub>	Ce <sub>2</sub> Co <sub>7</sub> B <sub>3</sub> P6/mmm	$a = 5.033(3)$ $c = 12.88(2)$	AM, Qu 800°C, 50 h, PXD	KuB, 73	Ho 99 Co 99.87 B 99.3	
HoCo <sub>12</sub> B <sub>6</sub>	SrNi <sub>12</sub> B <sub>6</sub> R3m	$a_H = 9.459(3)$ $c_H = 7.439(3)$	AM, Qu 800°C, 270 h, PXD	KuCC, 81	Ho 99.5 Co 99.95 B 99.4	

### Ho-Cr-B

Using X-ray powder diffraction, Kuz'ma (1970) characterized the crystal structure of HoCrB<sub>4</sub>, YCrB<sub>4</sub>-type,  $a = 5.774(5)$ ,  $b = 11.48(1)$ ,  $c = 3.444(4)$ .

### Reference

Kuz'ma, Yu.B., 1970, *Kristallografiya* **15**(2), 372.

### Ho-Fe-B

HoFeB<sub>4</sub> is isostructural with the YCrB<sub>4</sub>-type of structure, Pbam,  $a = 5.871(10)$ ,  $b = 11.36(2)$ ,  $c = 3.391(5)$  (Stepanchikova and Kuz'ma, 1977); for alloy preparation, see YFeB<sub>4</sub>.



$\text{Ho}_3\text{FeB}_7$  was found to crystallize with the  $\text{Y}_3\text{ReB}_7$ -type, Cmcm,  $a = 3.369$ ,  $b = 15.50$ ,  $c = 9.358$  (Stepanchikova and Kuz'ma, 1980); for sample preparation, see Y-Fe-B.

$\text{HoFe}_2\text{B}_2$  with the  $\text{ThCr}_2\text{Si}_2$ -type of structure, I4/mmm,  $a = 3.527(5)$ ,  $c = 9.425(10)$ , has been characterized by Stepanchikova et al. (1979); alloys were arc melted and annealed in evacuated quartz capsules at  $800^\circ\text{C}$  for 720 h; X-ray powder analysis.

### References

- Stepanchikova, G.F. and Yu.B. Kuz'ma, 1977, Vestn. Lvov Univ., Ser. Khim. **19**, 37.  
 Stepanchikova, G.F. and Yu.B. Kuz'ma, 1980, Poroshk. Metall. **214**(10), 44.  
 Stepanchikova, G.F., Yu.B. Kuz'ma and B.I. Chernjak, 1979, Dopov. Akad. Nauk Ukr. RSR, Ser. A, 950.

### Ho-Ir-B

From X-ray powder analysis of arc melted alloys,  $\text{HoIr}_3\text{B}_2$  crystallizes with  $\text{ErIr}_3\text{B}_2$ -type (possible space group C2/m),  $a = 5.420(6)$ ,  $b = 9.393(9)$ ,  $c = 3.107(4)$ ,  $\beta = 91.2(1)^\circ$ ;  $T_m = 12.9$  K (Ku and Meisner, 1981).

Ku et al. (1979) reported the existence of a metastable compound  $\text{HoIr}_4\text{B}_4$  from arc melted samples; the phase disappears after heat treatment ( $T_c = 2.12$ – $1.88$  K). Despite the fact that the amount of this phase present in the X-ray sample was too low ( $< 10\%$ ) to measure reliable lattice parameters, the authors believed that the  $\text{HoIr}_4\text{B}_4$  phase had a  $\text{CeCo}_4\text{B}_4$ -type of structure.

### References

- Ku, H.C. and G.P. Meisner, 1981, J. Less-Common Metals **78**, 99.  
 Ku, H.C., B.T. Matthias and H. Barz, 1979, Solid State Commun. **32**, 937.

### Ho-La-B

Berrada et al. (1976) studied crystal- and magnetochemistry within the section  $\text{LaB}_6$ -“ $\text{HoB}_6$ ”. Samples were prepared by borothermal reduction of the mixed oxides  $\text{R}_2\text{O}_3$  (99.9%) in a tantalum crucible at  $1800^\circ\text{C}$ , 2 h,  $10^{-4}$  Pa, and were then analysed by X-ray diffraction, X-ray fluorescence and chemical analysis. The binary holmium hexaboride could not be obtained and was considered to be unstable due to the small  $\text{Ho}^{3+}$  radius. Accordingly solid solutions  $\text{La}_x\text{Ho}_{1-x}\text{B}_6$  were single phase for  $x \geq 0.2$  ( $\text{CaB}_6$ -type, Pm3m), but for smaller La concentrations the (La, Ho) $\text{B}_6$  phase was found to be in equilibrium with  $\text{HoB}_4$  and  $\text{HoB}_{12}$ ; lattice parameters of  $\text{La}_x\text{Ho}_{1-x}\text{B}_6$  varied as a linear function of  $x$ .  $\text{LaB}_6$ :  $a = 4.156$ ,  $\text{La}_{0.033}\text{Ho}_{0.967}\text{B}_6$ :  $a = 4.154$ ,  $\text{La}_{0.9}\text{Ho}_{0.1}\text{B}_6$ :  $a = 4.150$ ,  $\text{La}_{0.8}\text{Ho}_{0.2}\text{B}_6$ :  $a = 4.144$ ,  $\text{La}_{0.76}\text{Ho}_{0.24}\text{B}_6$ :  $a = 4.141$ ,  $\text{La}_{0.5}\text{Ho}_{0.5}\text{B}_6$ :  $a = 4.127$ ,  $\text{La}_{0.4}\text{Ho}_{0.6}\text{B}_6$ :  $a = 4.120$ ,  $\text{La}_{0.2}\text{Ho}_{0.8}\text{B}_6$ :  $a = 4.108$ , as read from the diagram. The extrapolated lattice parameter of a hypothetical “ $\text{HoB}_6$ ” was  $a = 4.096$ .

### Reference

- Berrada, A., J.P. Mercurio, J. Etourneau and P. Hagenmuller, 1976, Mater. Res. Bull. **11**, 947.

*Ho-Mn-B*

HoMnB<sub>4</sub> crystallizes with the YCrB<sub>4</sub>-type of structure, Pbam,  $a = 5.901(5)$ ,  $b = 11.38(1)$ ,  $c = 3.428(5)$  (Kuz'ma, 1970; X-ray powder analysis); for sample preparation, see GdMnB<sub>4</sub>.

*Reference*

Kuz'ma, Yu.B., 1970, Dopov. Akad. Nauk Ukr. RSR, Ser. A **32**(8), 756.

*Ho-Mo-B*

The crystal structure of HoMoB<sub>4</sub>, YCrB<sub>4</sub>-type, Pbam,  $a = 6.019(5)$ ,  $b = 11.62(1)$ ,  $c = 3.589(5)$ , has been established by Kuz'ma and Svarichevskaya (1972) from X-ray powder photographs; for sample preparation, see GdMoB<sub>4</sub>.

*Reference*

Kuz'ma, Yu.B. and S.I. Svarichevskaya, 1972, Dopov. Akad. Nauk Ukr. RSR, Ser. A **34**(2), 166.

*Ho-Ni-B* (see also notes added in proof)

Niihara et al. (1973) claimed the existence of a HoNi<sub>4</sub>B phase with presumably YNi<sub>4</sub>B-type structure. Kuz'ma et al. (1981) confirmed the CeCo<sub>4</sub>B-type and gave  $a = 4.962(4)$ ,  $c = 6.935(11)$ , P6/mmm; see also YNi<sub>4</sub>B.

The existence of the compound Ho<sub>3</sub>Ni<sub>7</sub>B<sub>2</sub> with Dy<sub>3</sub>Ni<sub>7</sub>B<sub>2</sub>-type, P6<sub>3</sub>/mmc,  $a = 5.063(2)$ ,  $c = 14.285$  was observed by Kuz'ma and Chaban (1979) by X-ray and metallographic analysis of arc melted and subsequently annealed alloys (360 h, 800°C, in evacuated silica tubes). Starting materials were Ho ingots 99.5%, B powder 99.3%, Ni powder 99.98%.

*References*

- Kuz'ma, Yu.B. and N.F. Chaban, 1979, Dopov. Akad. Nauk Ukr. RSR, Ser. A, 88.  
 Kuz'ma, Yu.B., N.S. Bilonishko, N.F. Chaban and G.V. Chernjak, 1981, J. Less-Common Metals **82**, 364; see also 1982, Izv. Akad. Nauk SSSR, Neorg. Mater. **18**, 691.  
 Niihara, K., Y. Katayama and S. Yajima, 1973, Chem. Lett. (Chem. Soc. Jpn) 613.

*Ho-Os-B*

The crystallographic data and methods of preparation of the five ternary compounds in the Ho-Os-B system are summarized in table 19.

*References*

- Ku, H.C., 1980, Thesis, Univ. of California at San Diego, USA.  
 Ku, H.C. and R.N. Shelton, 1980, Mater. Res. Bull. **15**(10), 1441.  
 Rogl, P., 1978, Mater. Res. Bull. **13**, 519.  
 Rogl, P. and H. Nowotny, 1982, Crystal structures and phase relationships within ternary systems: rare earth metal-noble metal-boron, in: The Rare Earths in Science and Technology, Vol. 3, eds. J. McCarthy, B. Silber and J.J. Rhyne (Plenum, New York, London) pp. 353-356.

TABLE 19  
Formation and structural data of ternary compounds Ho-Os-B.

Compound	Structure type, Space group	Lattice parameters, Density	Preparation, Characterization	Refs.	Purity
HoOsB <sub>4</sub>	YCrB <sub>4</sub> Pbam	$a = 5.943(3)$ $b = 11.495(6)$ $c = 3.548(2)$	AM, HT, 1600°C, 12 h HV, W substrate, QE congruent melting, ME, PXD suscept., 80–300 K	Ro, 78 SoR, 79	Ho 99.9 Os 99.9 B 99.0
Ho <sub>2</sub> OsB <sub>6</sub>	Y <sub>2</sub> ReB <sub>6</sub> Pbam	$a = 9.1229(15)$ $b = 11.4909(35)$ $c = 3.6320(2)$	AM, HT, 1600°C, 12 h HV, W substrate, QE PXD	RoN, 82	Ho 99.9 Os 99.9 B 99.7
HoOsB <sub>2</sub>	LuRuB <sub>2</sub> Pnma	$a = 5.850(6)$ $b = 5.286(5)$ $c = 6.355(7)$	AM(Zr), Ta tubes 1250°C, 24 h 800°C, 9 d PXD, $T_m = 14.2$ K	ShKPJK, 80 KuS, 80	99.9
HoOs <sub>4</sub> B <sub>4</sub>	YOs <sub>4</sub> B <sub>4</sub> tetragonal	$a = 7.4415(9)$ $c = 32.7240(40)$ $c = 8c_0$	AM, HT, 1400°C, 12 h HV, BN substrate, PXD, $T_m = 4.5$ K	RoHS, 82	Ho 99.9 Os 99.9 B 99.7
HoOs <sub>3</sub> B <sub>2</sub>	YOs <sub>3</sub> B <sub>2</sub> (?) orthorh. (?)	$a \approx 5.5$ $b \approx 9.5$ $c \approx 18$	AM(Zr) PXD, $T_m = 9.91$ K	Ku, 80	99.9

Rogl, P., K. Hiebl and M.J. Sienko, 1982, paper presented at the 7th Intern. Conf. on Solid Compounds of Transition Elements, Grenoble (June 21–25), Proceedings, II A4.

Shelton, R.N., B.A. Karcher, D.R. Powell, R.A. Jacobson and H.C. Ku, 1980, Mater. Res. Bull. **15**, 1445.  
Sobczak, R. and P. Rogl, 1979, J. Solid State Chem. **27**, 343.

### Ho-Re-B

Four ternary compounds have been identified.

HoReB<sub>4</sub>, YCrB<sub>4</sub>-type, Pbam,  $a = 5.964(5)$ ,  $b = 11.53(1)$ ,  $c = 3.565(5)$  (Kuz'ma and Svarichevskaya, 1972a); for preparation techniques, see GdReB<sub>4</sub>.

Ho<sub>2</sub>ReB<sub>6</sub> is isostructural with Y<sub>2</sub>ReB<sub>6</sub>-type, Pbam,  $a = 9.151(5)$ ,  $b = 11.52(1)$ ,  $c = 3.648(4)$  (Kuz'ma and Svarichevskaya, 1972b).

Ho<sub>3</sub>ReB<sub>7</sub> crystallizes with Y<sub>3</sub>ReB<sub>7</sub>-type, Cmcn,  $a = 3.500(2)$ ,  $b = 15.70(1)$ ,  $c = 9.332(5)$  (Kuz'ma and Mikhalenko, 1976).

Furthermore HoRe<sub>11</sub>B with cubic lattice, structure unsolved, was observed by Mikhalenko et al. (1981).

### References

- Kuz'ma, Yu.B. and S.I. Mikhalenko, 1976, Dopov. Akad. Nauk Ukr. RSR, Ser. A **11**, 1029.  
Kuz'ma, Yu.B. and S.I. Svarichevskaya, 1972a, Dopov. Akad. Nauk Ukr. RSR, Ser. A **2**, 166.  
Kuz'ma, Yu.B. and S.I. Svarichevskaya, 1972b, Kristallografiya, **17**(3), 658.  
Mikhalenko, S.I., N.F. Chaban and Yu.B. Kuz'ma, 1981, J. Less-Common Metals **82**, 365.

*Ho-Rh-B*

HoRh<sub>3</sub>B<sub>2</sub> was reported to crystallize with the ErIr<sub>3</sub>B<sub>2</sub>-type of structure, possible space group C2/m,  $a = 5.366(6)$ ,  $b = 9.307(9)$ ,  $c = 3.100(4)$ ,  $\beta = 91.0(1)^\circ$  (Ku and Meisner, 1981; X-ray powder analysis of arc melted samples);  $T_m = 24.2$  K.

HoRh<sub>4</sub>B<sub>4</sub> adopts the CeCo<sub>4</sub>B<sub>4</sub> type of structure, P4<sub>2</sub>/nmc,  $a = 5.293(3)$ ,  $c = 7.379(2)$  (Vandenberg and Matthias, 1977; X-ray powder data); for sample preparation, see YRh<sub>4</sub>B<sub>4</sub>.  $T_m = 6.56$  K (Matthias et al., 1977). HoRh<sub>4</sub>B<sub>4</sub> orders ferromagnetically due to a spontaneous alignment of the localized 4f electron magnetic moments of the Ho<sup>3+</sup> ions along the tetragonal axis (Lander et al., 1979, from neutron diffraction experiments). A helical or sinusoidal antiferromagnetism was suggested for the order of the normal compound HoRh<sub>4</sub>B<sub>4</sub> by Acker and Ku (1981).

For the existence of a perovskite-type phase HoRh<sub>3</sub>B<sub>1-x</sub> with Cu<sub>3</sub>Au-type,  $a = 4.148$ ,  $x = 0.05$ , see also R-Rh-B.

*References*

- Acker, F. and H.C. Ku, 1981, *J. Low Temp. Phys.* **42**, 516.  
 Ku, H.C. and G.P. Meisner, 1981, *J. Less-Common Metals* **78**, 99.  
 Lander, G.H., S.K. Sinha and F.Y. Fradin, 1979, *J. Appl. Phys.* **50**, 1990.  
 Matthias, B.T., E. Corenzwit, J.M. Vandenberg and H.E. Barz, 1977, *Proc. Nat'l Acad. Sci. US* **74**(4), 1334.  
 Vandenberg, J.M. and B.T. Matthias, 1977, *Proc. Nat'l Acad. Sci. US* **74**(4), 1336.

TABLE 20  
 Formation and structural data of ternary compounds Ho-Ru-B.

Compound	Structure type, Space group	Lattice parameters, Density	Preparation, Characterization	Refs.	Purity
HoRuB <sub>4</sub>	YCrB <sub>4</sub> Pbam	$a = 5.933(3)$ $b = 11.480(6)$ $c = 3.533(2)$	AM, HT, 1600°C, 12 h HV, W substrate congruent melting, PXD, ME suscept., 80-300 K	Ro, 78 SoR, 79	Ho 99.9 Ru 99.9 B 99.0
Ho <sub>2</sub> RuB <sub>6</sub>	Y <sub>2</sub> ReB <sub>6</sub> Pbam	$a = 9.1083(24)$ $b = 11.4666(19)$ $c = 3.6407(3)$	AM, HT, 1600°C, 12 h HV, W substrate PXD	RoN, 82	Ho 99.9 Ru 99.9 B 99.0
HoRuB <sub>2</sub>	LuRuB <sub>2</sub> Pnma	$a = 5.875(6)$ $b = 5.287(5)$ $c = 6.332(7)$	AM(Zr), HT, Ta tubes 1250°C, 24 h 800°C, 9 d, PXD $T_m = 15.5$ K	ShKPJK, 80 KuS, 80	99.9
HoRu <sub>4</sub> B <sub>4</sub>	LuRu <sub>4</sub> B <sub>4</sub> I4 <sub>1</sub> /acd	$a = 7.442(5)$ $c = 14.975(10)$	AM(Zr), PXD $T_m = 2.58$ K	Jo, 77	high purity
HoRu <sub>3</sub> B <sub>2</sub>	CeCo <sub>3</sub> B <sub>2</sub> P6/mmm	$a = 5.466(4)$ $c = 3.017(2)$	AM, HT, 1400°C, 24 h BN substrate PXD, ME, congr. melting $T_m = 25$ K	HiRUS, 80	Ho 99.9 Ru 99.9 B 99.7
		$a = 5.474(6)$ $c = 3.017(4)$	AM(Zr), PXD $T_m = 16.1$ K	KuMAJ, 80	99.9

*Ho-Ru-B*

No ternary phase diagram has been established yet for the Ho-Ru-B system, but five ternary compounds have been characterized (see table 20).

*References*

- Hiebl, K., P. Rogl, E. Uhl and M.J. Sienko, 1980, *Inorg. Chem.* **19**(11), 3316.  
Johnston, D.C., 1977, *Solid State Commun.* **24**(10), 699.  
Ku, H.C. and R.N. Shelton, 1980, *Mater. Res. Bull.* **15**(10), 1441.  
Ku, H.C., G.P. Meisner, F. Acker and D.C. Johnston, 1980, *Solid State Commun.* **35**, 91.  
Rogl, P., 1978, *Mater. Res. Bull.* **13**, 519.  
Rogl, P. and H. Nowotny, 1982, Crystal structures and phase relationships within ternary systems: rare earth metal-noble metal-boron, in: *Rare Earths in Science and Technology*, Vol. 3, eds. J. McCarthy, B. Silber and J.J. Rhyne (Plenum, New York, London) pp. 353-356.  
Shelton, R.N., B.A. Karcher, D.R. Powell, R.A. Jacobson and H.C. Ku, 1980, *Mater. Res. Bull.* **15**, 1445.  
Sobczak, R. and P. Rogl, 1979, *J. Solid State Chem.* **27**, 343.

*Ho-V-B*

HoVB<sub>4</sub> is isostructural with the structure type of YCrB<sub>4</sub>, Pbam,  $a = 5.968(5)$ ,  $b = 11.56(1)$ ,  $c = 3.462(5)$  (Kuz'ma, 1970; X-ray powder diffraction); for sample preparation, see GdMnB<sub>4</sub>.

*Reference*

- Kuz'ma, Yu.B., 1970, *Dopov. Akad. Nauk Ukr. RSR, Ser. A* **32**(8), 756.

*Ho-W-B*

HoWB<sub>4</sub> has the YCrB<sub>4</sub>-type of structure, Pbam,  $a = 6.029(5)$ ,  $b = 11.63(1)$ ,  $c = 3.591(5)$  (Kuz'ma and Svarichevskaya, 1972; X-ray analysis). For sample preparation, see GdWB<sub>4</sub>.

*Reference*

- Kuz'ma, Yu.B. and S.I. Svarichevskaya, 1972, *Dopov. Akad. Nauk Ukr. RSR, Ser. A* **34**(2), 166.

*Ho-Y-B*

Single crystals of Ho<sub>0.85</sub>Y<sub>0.15</sub>B<sub>4</sub> were grown from molten Al and investigated for their magnetic properties: UB<sub>4</sub>-type structure, P4/mbm (Fisk et al., 1981). No lattice parameter data were given.

*Reference*

- Fisk, Z., M.B. Maple, D.C. Johnston and L.D. Woolf, 1981, *Solid State Commun.* **39**, 1189.

*La-Al-B*

Chaban and Kuz'ma (1971) investigated the phase equilibria at 600°C by X-ray and metallographic analysis. Samples were prepared by arc melting (La ingot 98.48%,

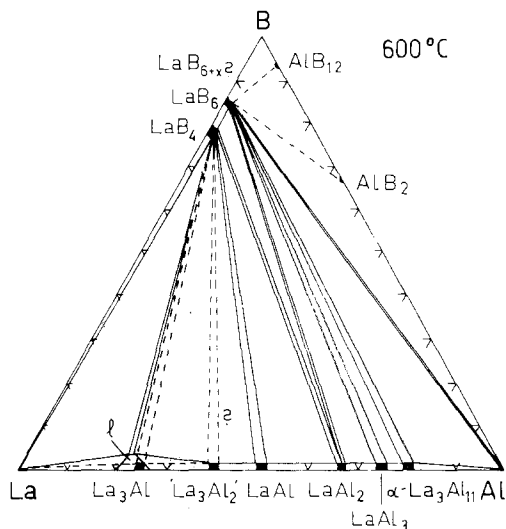


Fig. 25. La–Al–B, isothermal section at 600°C; region LaB<sub>6</sub>–B–Al is proposed. The existence of “La<sub>3</sub>Al<sub>2</sub>” is in doubt; the region near La<sub>3</sub>Al is liquid ( $\rho$ ) at 600°C.

B powder 99.3%, Al powder 99.997%) and subsequent heat treatment in evacuated silica tubes at 600°C for 350 h.

No samples were prepared for the boron-rich region: B–LaB<sub>6</sub>–Al, and no ternary borides were observed; mutual solid solubilities were found to be negligible. Thus phase equilibria within the region B–Al–LaB<sub>6</sub> are proposed. The La–Al binary system, La<sub>3</sub>Al (Ni<sub>3</sub>Sn-type), LaAl (CeAl-type), LaAl<sub>2</sub> (MgCu<sub>2</sub>-type), LaAl<sub>3</sub> (Ni<sub>3</sub>Sn-type),  $\alpha$ -La<sub>3</sub>Al<sub>11</sub>, has been revised according to a recent critical assessment by Elliott and Shunk (1981). Accordingly the compound “La<sub>3</sub>Al<sub>2</sub>”, reported by Chaban and Kuz'ma (1971), seems to be in doubt and furthermore due to the low eutectic  $L \rightleftharpoons La + LaAl$  at  $T_E = 550^\circ\text{C}$ , the vicinity of La<sub>3</sub>Al (fig. 25) will be liquid at 600°C. The solid state phase equilibria in the La-rich region ( $T < 550^\circ\text{C}$ ) are shown in broken lines (according to Chaban and Kuz'ma, 1971).

### References

- Chaban, N.F. and Yu.B. Kuz'ma, 1971, Dopov. Akad. Nauk Ukr. RSR, Ser. A **11**, 1048.  
 Elliott, R.P. and F.A. Shunk, 1981, Bulletin of Alloy Phase Diagrams **2**(2), 219.

### La–Co–B

Stepanchikova and Kuz'ma (1976) studied the phase equilibria of the La–Co–B system within isothermal sections at 600°C (0–40 a/o La) and at 400°C (40–100 a/o La) by means of X-ray analysis of 118 samples, which were prepared by arc melting and subsequent annealing for 600 h (La ingot 98.48%, and Co 99.87% and B 99.4% powders).

La–Co compounds, LaCo<sub>13</sub> (NaZn<sub>13</sub>-type), LaCo<sub>5</sub> (CaCu<sub>5</sub>-type), La<sub>2</sub>Co<sub>7</sub> (Ce<sub>2</sub>Ni<sub>7</sub>-type), La<sub>2</sub>Co<sub>3</sub> (La<sub>2</sub>Ni<sub>3</sub>-type), La<sub>4</sub>Co<sub>3</sub> (Pr<sub>2</sub>Co<sub>1.7</sub>-type) and La<sub>3</sub>Co (Fe<sub>3</sub>C-type),

correspond to a phase diagram study by Buschow and Velge (1967). For binary Co borides, see Sc-Co-B; for La borides, see La-Cr-B. Six ternary compounds were found to exist (table 21, fig. 26); however, attempts to prepare  $\text{La}_3\text{Co}_{11}\text{B}_4$  with  $\text{Ce}_3\text{Co}_{11}\text{B}_4$ -type and  $\text{La}_2\text{Co}_7\text{B}_3$  with  $\text{Ce}_2\text{Co}_7\text{B}_3$ -type were reported to be unsuccessful (Kuz'ma and Bilonishko, 1973). The crystal structure of  $\text{La}_{\sim 3}\text{Co}_{\sim 14}\text{B}$  is unsolved.

The actual composition of the compound  $\text{LaCo}_{\sim 2}\text{B}_{\sim 3}$ , first observed by Stepanchikova and Kuz'ma (1976), was later corrected by Kuz'ma and Bilonishko (1978) to a more precise formula of  $\text{LaCo}_4\text{B}_4$ , as derived from structural (X-ray) data. The type of phase equilibria in fig. 26 remained unaffected by this compositional change.

The wetting and contact reactions of a  $\text{LaB}_6$  substrate with molten Co were studied in the temperature range of 1100–1675°C under He, using X-ray, metallographic and

TABLE 21  
Formation and structural data of ternary compounds La-Co-B.

Compound	Structure type, Space group	Lattice parameters, Density	Preparation, Characterization	Refs.	Purity
$\text{LaCo}_2\text{B}_2$	$\text{ThCr}_2\text{Si}_2$ I4/mmm	$a = 3.641(3)$ $c = 10.200(5)$	AM, Qu 600°C, 600 h, PXD	StK, 76	La 98.48 Co 99.87 B 99.4
		$a = 3.616(3), \rho_E = 6.88$ $c = 10.215(5), \rho_X = 6.92$	AM, Qu(Ta) 800°C, 150 h, PXD <sup>(*)</sup>	NiSY, 73	La 99.5 Co 99.99 B 99.9
		$a = 3.617$ $c = 10.225$	AM, Qu(Mo) 800°C, 50 h, PXD	Ro, 73	La 99.5 Co 99.5 B 99.0
$\text{LaCo}_4\text{B}_4^{(**)}$	$\text{NdCo}_4\text{B}_4$ $\text{P4}_2/\text{n}$	$a = 7.151(4)$ $c = 3.811(2)$	no details given, PXD	KuB, 78	
$\text{LaCo}_{12}\text{B}_6$	$\text{SrNi}_{12}\text{B}_6$ $\text{R}\bar{3}\text{m}$	$a_H = 9.533(3)$ $c_H = 7.498(3)$	AM, Qu 800°C, 270 h, PXD	KuCC, 81	La 99.5 Co 99.95 B 99.4
		$a_H = 9.500(5)$ $c_H = 7.495(5)$	AM, Qu 600°C, 600 h, PXD	StK, 76	La 98.48 Co 99.87 B 99.4
$\text{LaCo}_4\text{B}$	$\text{CeCo}_4\text{B}$ $\text{P6}/\text{mmm}$	$a = 5.172(3)$ $c = 6.860(4)$	AM, Qu 800°C, 50 h, PXD	KuB, 73	La 99.0 Co 99.87 B 99.3
$\text{La}_2\text{CoB}_2$	unknown $\text{R}\bar{3}\text{m}, \text{R}32, \text{R}3\text{m}$	$a_H = 5.48(2)$ $c_H = 25.31(3)$	AM, Qu 600°C, 600 h, PXD	StK, 76	La 98.48 Co 99.87 B 99.4
$\text{La}_3\text{Co}_{14}\text{B}$	unknown		AM, Qu 600°C, 600 h, PXD	StK, 76	La 98.48 Co 99.87 B 99.4

(\*)Agreement between observed and calculated powder intensities was stated to be excellent.

(\*\*)First observed as  $\text{LaCo}_{\sim 2}\text{B}_{\sim 3}$  (Stepanchikova and Kuz'ma, 1976).

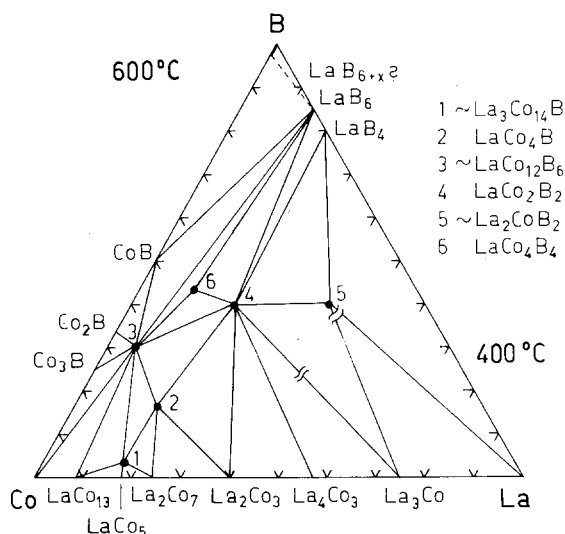


Fig. 26. La-Co-B, partial isothermal sections at 600°C (0–40 a/o La), and at 400°C (40–100 a/o La). Ray (1974) observed indications for the existence of  $\text{La}_5\text{Co}_{19}$  ( $\text{Ce}_5\text{Co}_{19}$ -type?) which in this case is likely to enter a two-phase equilibrium:  $\text{La}_5\text{Co}_{19} + \text{La}_3\text{Co}_{14}\text{B}$ .

electron microprobe analysis (Yupko et al., 1981).  $\text{LaCo}_{12}\text{B}_6$  was encountered among the reaction products. The lattice parameter of  $\text{LaB}_6$  was practically unchanged,  $a = 4.152$ .

### References

- Buschow, K.H.J. and W.A.J.J. Velge, 1967, *J. Less-Common Metals* **13**, 11.  
 Kuz'ma, Yu.B. and N.S. Bilonishko, 1973, *Kristallografiya* **18**(4), 710.  
 Kuz'ma, Yu.B. and N.S. Bilonishko, 1978, *Dopov. Akad. Nauk Ukr. RSR, Ser. A* **3**, 275.  
 Kuz'ma, Yu.B., G.V. Chernjak and N.F. Chaban, 1981, *Dopov. Akad. Nauk Ukr. RSR, Ser. A* **12**, 80.  
 Niihara, K., T. Shishido and S. Yajima, 1973, *Bull. Chem. Soc. Jpn* **46**, 1137.  
 Ray, A.E., 1974, *Cobalt* **1**, 13.  
 Rogl, P., 1973, *Monatsh. Chem.* **104**, 1623.  
 Stepanchikova, G.F. and Yu.B. Kuz'ma, 1976, *Vestn. Lvov Univ., Ser. Khim.* **18**, 16.  
 Yupko, V.P., P.A. Verkhovodov, V.V. Morosov, A.V. Besov and V.Ya. Shlyuko, 1981, *Poroshk. Metall.* **219**(3), 64.

### La-Cr-B

No ternary compounds have been observed during a phase equilibrium study (X-ray, metallographic analysis) of the system La-Cr-B at 800°C (fig. 27, Kuz'ma et al., 1973). Samples were prepared by arc melting of compacted powders (B 99.3%, Cr 99.5%) and La ingots (98.6%) and subsequent annealing in evacuated quartz capsules (800°C, 360 h). The mutual solid solubility of the binary compounds was found to be negligible; the existence of "La<sub>2</sub>B", as claimed by Markovsky and Vekshina (1967), was not confirmed; for the Cr-B binary system, see Y-Cr-B.

With respect to resent results by Storms and Mueller, (1978) and McKelvy (1981) about the phase  $\text{LaB}_{6+x}$ , a closer inspection of the ternary boron-rich region seems to be necessary.



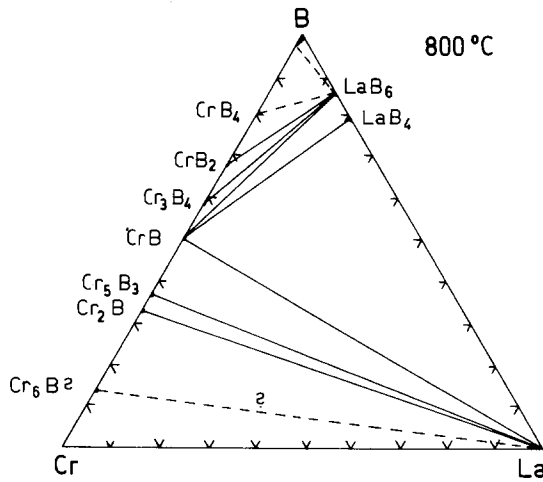


Fig. 27. La-Cr-B, isothermal section at 800°C.

*References*

- Kuz'ma, Yu.B., S.I. Svarichevskaya and V.N. Fomenko, 1973, *Izv. Akad. Nauk SSSR, Neorg. Mater.* 9(9), 1542.  
 Markovsky, L.Ya. and N.V. Vekshina, 1967, *Zh. Prikl. Khim.* 38, 1945.  
 McKelvy, M.J., 1981, Thesis, Arizona State Univ., Tempe, USA.  
 Storms, E. and B. Mueller, 1978, *J. Phys. Chem.* 82, 51.

*La-Fe-B*

In a review article, Kuz'ma et al. (1977) presented a tentative partial isothermal section at 800°C of the La-poor region of the La-Fe-B system containing 0-40 a/o La (fig. 28). Three ternary phases were observed;  $La_{\sim 3}Fe_{\sim 13}B_{\sim 1}$  and

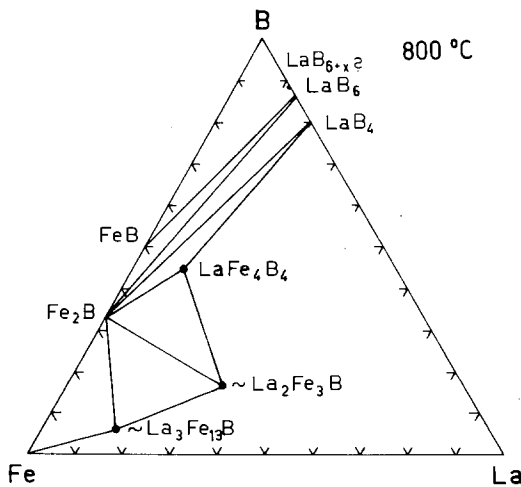


Fig. 28. La-Fe-B, partial isothermal section at 800°C (0-40 a/o La).

$\text{La}_{\sim 2}\text{Fe}_{\sim 3}\text{B}_{\sim 1}$  have unknown structure types and  $\text{LaFe}_{\sim 2}\text{B}_{\sim 2}$  probably is isostructural with the compound  $\text{CeFe}_4\text{B}_4$  crystallizing with a  $\text{NdCo}_4\text{B}_4$ -derivative type of structure.

### Reference

Kuz'ma, Yu.B., N.S. Bilonishko and S.I. Svarichevskaya, 1977, in: *Tugoplavkije Boridi e Silizidi*, ed. G.V. Samsonov (Akad. Nauk Ukr. SSR, Nauka Dumka, Kiev).

### La-Ge-B

Phase equilibria in the La-Ge-B system at 700°C (fig. 29) were derived by X-ray phase analysis from 52 samples (B powder 99.3%, La ingot 99.7%, Ge ingot 99.999%), which were arc melted and subsequently heat treated in evacuated quartz capsules (700°C, 480 h, quenched in ice water, Marko et al., 1978).

According to Muratova et al. (1974) the homogeneity range of  $\text{LaGe}_2$  was obtained for 35–39 a/o La. For the Ge-B binary system, see Y-Ge-B, and for La borides, see La-Cr-B. Practically no mutual solubility was observed at 700°C between La borides and La germanides:  $\text{La}_3\text{Ge}$  (tetragonal?)  $\text{La}_5\text{Ge}_3$  ( $\text{Mn}_5\text{Si}_3$ -type),  $\text{La}_4\text{Ge}_3$  ( $\text{Th}_3\text{P}_4$ -type),  $\text{La}_5\text{Ge}_4$  ( $\text{Sm}_5\text{Ge}_4$ -type)  $\text{LaGe}$  (FeB-type),  $\text{LaGe}_2$  ( $\text{GdSi}_2$ -type?). This was particularly claimed for  $\text{La}_5\text{Ge}_3$  with  $\text{Mn}_5\text{Si}_3$ -type, whereas in alloys heat treated at higher temperature Mayer and Felner (1974) claimed the  $\text{Mn}_5\text{Si}_3$ -type phase to be stable up to  $\text{La}_5\text{Ge}_3\text{B}_2$  (metastable phases?).

Mayer and Felner (1974) studied the influence of boron additions to  $\text{R}_5\text{Ge}_3$  compounds in a series of samples with a nominal boron content corresponding to formulas  $\text{La}_5\text{Ge}_3$ ,  $\text{La}_5\text{Ge}_3\text{B}_{0.5}$ ,  $\text{La}_5\text{Ge}_3\text{B}_{1.0}$ ,  $\text{La}_5\text{Ge}_3\text{B}_{1.5}$  and  $\text{La}_5\text{Ge}_3\text{B}_{2.0}$ . Alloys were prepared by heating (melting) elemental mixtures (min. purity 99.9%) in Ta crucibles

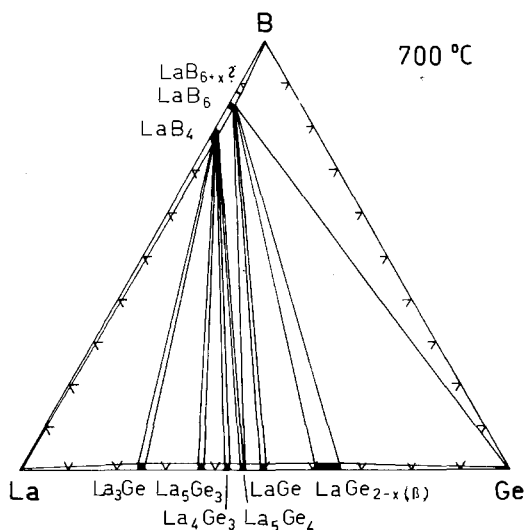


Fig. 29. La-Ge-B, isothermal section at 700°C.

to 1600°C under He atmosphere. Boron solubility (filling of octahedral voids) in  $Mn_5Si_3$ -type phases, however, is limited to a formula  $R_5Ge_3B_{1.0}$ , thus for higher boron concentrations the boron solubility might be accompanied by a simultaneous substitution Ge/B, which probably would explain the irregular variation of lattice parameters (table 6).

### References

- Marko, M.A., M.S. Nalyvaiko and Yu.B. Kuz'ma, 1978, *Izv. Akad. Nauk SSSR, Neorg. Mater.* **14**(7), 1350.  
Mayer, I. and I. Felner, 1974, *J. Less-Common Metals* **37**, 171.  
Muratova, L.O., O.I. Bodak and E.I. Gladyshevskii, 1974, *Vestn. L'vov Univ., Ser. Khim.* **15**, 28.

### La-Hf-B

On the basis of measurements of hexaboride lattice parameters, microhardness, metallographic, and X-ray analysis, the solubility of Hf in  $LaB_6$  was shown to be  $\leq 0.5$  a/o Hf (Bondarenko et al., 1971).

### Reference

- Bondarenko, V.P., V.V. Morozov and L.V. Chernjak, 1971, *Poroshk. Metall.* **97**(1), 73.

### La-Ir-B

On the basis of X-ray and metallographic analysis, Rogl (1979) derived congruent melting behavior of  $LaIr_4B_4$ . For experimental details, see  $LaOs_4B_4$ . The crystal structure has been refined (Rogl, 1980) from single crystal automatic diffractometer data,  $R = 0.039$ .  $LaIr_4B_4$  is  $NdCo_4B_4$ -type,  $P4_2/n$ ,  $a = 7.6719(4)$ ,  $c = 3.9739(2)$ ,  $\rho_{calc} = 13.5$  kg/dm<sup>3</sup>; atomic parameters were: 2 La in 2b); 8 Ir in 8g) 0.5937(1), 0.1397(1), 0.1441(2); 8 B in 8g) 0.529(2), 0.405(4), 0.142(6). Magnetic properties were reported by Rupp et al. (1979) and Hiebl et al. (1981);  $T_n = 1.5$  K.

$LaIr_3B_2$  adopts the  $CeCo_3B_2$ -type of structure,  $P6/mmm$ ,  $a = 5.543(6)$ ,  $c = 3.116(4)$ , as reported by Ku et al. (1980) from X-ray powder diffraction of arc melted alloys;  $T_c = 1.65$ – $1.38$  K.

### References

- Hiebl, K., M.J. Sienko and P. Rogl, 1981, *J. Less-Common Metals* **82**, 21.  
Ku, H.C., G.P. Meisner, F. Acker and D.C. Johnston, 1980, *Solid State Commun.* **35**, 91.  
Rogl, P., 1979, *Monatsh. Chem.* **110**, 235.  
Rogl, P., 1980, *Monatsh. Chem.* **111**, 517.  
Rupp, B., P. Rogl and R. Sobczak, 1979, *Mater. Res. Bull.* **14**, 1301.

### La-Mo-B

Mikhalenko and Kuz'ma (1976) presented the phase equilibria of the system La-Mo-B in two partial isothermal sections at 800°C (for the region 0–67 a/o La)

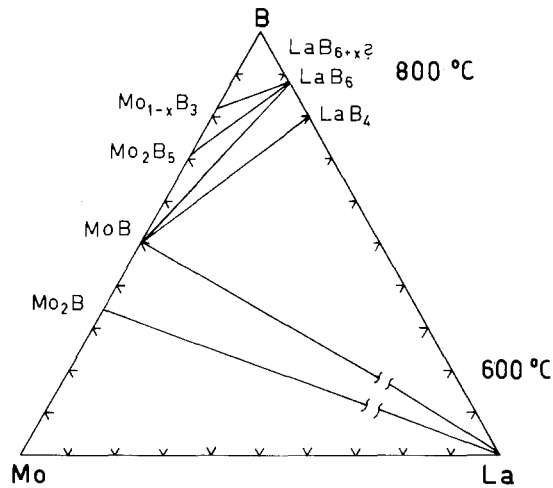


Fig. 30. La-Mo-B, partial isothermal sections at 800°C (0-67 a/o La), and at 600°C (67-100 a/o La).

and at 600°C (for the region 67-100 a/o La), see fig. 30. For Mo borides, see Y-Mo-B, and for the La-B binary, see La-Cr-B. From the röntgenographic analysis solid solubilities of La and Mo borides were found to be small. No two-phase equilibrium  $\text{LaB}_6 + \text{Mo}$  exists and no ternary compounds are formed.

#### Reference

Mikhaleiko, S.I. and Yu.B. Kuz'ma, 1976, Poroshk. Metall. **158**(2), 56.

#### La-Nd-B

A complete solid solution  $\text{Nd}_x\text{La}_{1-x}\text{B}_6$  with  $\text{CaB}_6$ -type, Pm3m, has been obtained by Aivazov et al. (1981) from borothermal reduction of mixed oxides. Lattice parameters (X-ray powder diffraction data) were:  $\text{LaB}_{6.0}$ : 4.1563(2),  $\text{Nd}_{0.1}\text{La}_{0.9}\text{B}_{6.0}$ : 4.1536(2),  $\text{Nd}_{0.2}\text{La}_{0.8}\text{B}_{6.1}$ : 4.1501(2),  $\text{Nd}_{0.3}\text{La}_{0.7}\text{B}_{5.9}$ : 4.1473(2),  $\text{Nd}_{0.4}\text{La}_{0.6}\text{B}_{6.0}$ : 4.1447(2),  $\text{Nd}_{0.5}\text{La}_{0.5}\text{B}_{6.2}$ : 4.1407(2),  $\text{Nd}_{0.6}\text{La}_{0.4}\text{B}_{6.1}$ : 4.1380(2),  $\text{Nd}_{0.7}\text{La}_{0.3}\text{B}_{6.1}$ : 4.1354(3),  $\text{Nd}_{0.8}\text{La}_{0.2}\text{B}_{6.2}$ : 4.1320(3),  $\text{Nd}_{0.9}\text{La}_{0.1}\text{B}_{6.0}$ : 4.1297(2),  $\text{NdB}_{6.1}$ : 4.1268(1). From magnetic susceptibility measurements Nd was found to be trivalent ( $^4I_{9/2}$ ) throughout the entire range.

#### Reference

Aivazov, M.I., S.V. Aleksandrovich, B.A. Evseev, V.S. Mkrtchyan and V.N. Sorokin, 1981, Izv. Akad. Nauk SSSR, Neorg. Mater. **17**(2), 248.

#### La-Ni-B

Kuz'ma et al. (1972) investigated two partial isothermal sections of the La-Ni-B system at 800°C (0-33 a/o La) and at 400°C (33-100 a/o La) by means of X-ray and

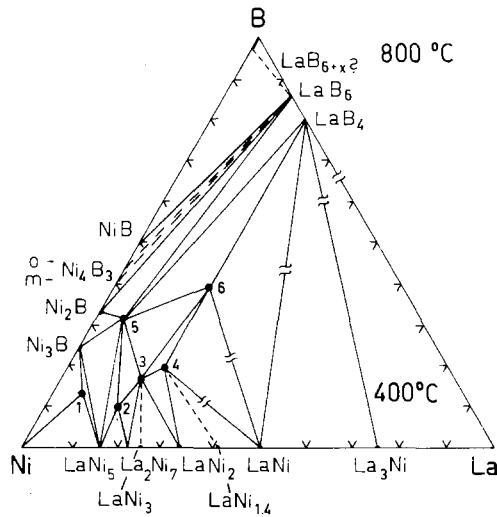


Fig. 31. La-Ni-B, partial isothermal sections at 800°C (0-33 a/o La), and at 400°C (33-100 a/o La). 1:  $\text{LaNi}_{12}\text{B}_2$ , 2:  $\text{La}_3\text{Ni}_{13}\text{B}_2$  (earlier  $\text{LaNi}_3\text{B}$ ), 3:  $\text{LaNi}_4\text{B}$ , 4:  $\text{LaNi}_3\text{B}$ , 5:  $\text{LaNi}_{12}\text{B}_6$ , 6:  $\text{LaNi}_2\text{B}_2$ .

metallographic analysis of 107 arc melted and subsequent annealed alloys (800°C, 400 h; 400°C, 600 h), see fig. 31. Starting materials were 98.48% La ingot, and 99.98% Ni and 99.3% B powders. Mutual solid solubilities of binary compounds were reported to be negligible and six ternary compounds have been identified (table 22). The binary system La-Ni, comprising the following compounds:  $\text{LaNi}_5$  (CaCu<sub>5</sub>-type),  $\text{La}_2\text{Ni}_7$  (Ce<sub>2</sub>Ni<sub>7</sub>-type),  $\text{LaNi}_3$  (PuNi<sub>3</sub>-type),  $\text{LaNi}_2$  (MgCu<sub>2</sub>-type),  $\text{LaNi}_{1.4}$  ( $\text{La}_2\text{Ni}_3$ -type),  $\text{LaNi}$  (CrB-type),  $\text{La}_3\text{Ni}$  (Fe<sub>3</sub>C-type), has been modified on the basis of a recent phase diagram study by van Vucht and Buschow (1976). For Ni borides, see Y-Ni-B, and for La borides, see La-Cr-B.

The wetting and contact reactions of  $\text{LaB}_6$  substrates with molten Ni were studied in the temperature range of 1100-1675°C under He, using X-ray, metallographic and electron microprobe analysis (Yupko et al., 1981).  $\text{LaNi}_{12}\text{B}_6$  was encountered among the reaction products.

The enthalpy and entropy of transition of an  $\text{LaNi}_{4.4}\text{B}_{0.6}$  alloy to the hydride phase was measured by Mendelson et al. (1980). The lattice parameter of La hexaboride remained practically unchanged,  $a \approx 4.150$ .

### References

- Kuz'ma, Yu.B. and N.S. Bilonishko, 1972, *Sov. Phys. Crystallogr.* **16**(5), 897.  
 Kuz'ma, Yu.B. and N.S. Bilonishko, 1981, *Dopov. Akad. Nauk Ukr. RSR, Ser. A* **10**, 88.  
 Kuz'ma, Yu.B., N.S. Bilonishko and E.M. Nimkovich, 1972, *Dopov. Akad. Nauk Ukr. RSR., Ser. A*, 939.  
 Kuz'ma, Yu.B., N.S. Bilonishko, N.F. Chaban and G.V. Chernjak, 1983, *J. Less-Common Metals* **90**, 217.  
 Mendelson, M.L., D.M. Gruen and G.D. Sandroock, 1980, *J. Less-Common Metals* **70**, 273.  
 Spada, F. and H. Oesterreicher, 1983, *J. Less-Common Metals* **90**, L1.  
 Van Vucht, J.H.N. and K.H.J. Buschow, 1976, *J. Less-Common Metals* **46**, 133.

TABLE 22  
 Formation and structural data of ternary compounds La-Ni-B.

Compound	Structure type, Space group	Lattice parameters, Density	Preparation, Characterization	Refs.	Purity
La <sub>3</sub> Ni <sub>13</sub> B <sub>2</sub> <sup>(*)</sup>	Nd <sub>3</sub> Ni <sub>13</sub> B <sub>2</sub> P6/mmm	$a = 5.072(2)$ $c = 10.942(8)$	AM, Qu 800°C, 400 h, PXD	KuB, 81	La 98.48 Ni 99.98 B 99.3
LaNi <sub>4</sub> B	CeCo <sub>4</sub> B <sub>4</sub> P6/mmm	$a' = 5.122(4)$ $c = 6.990(9)$	AM, Qu 800°C, 400 h, PXD	KuB, 72 KuBCC, 83	La 98.48 Ni 99.98 B 99.3
LaNi <sub>3</sub> B	mmmPna-	$a = 12.35(2)$ $b = 10.80(2)$ $c = 9.68(2)$	AM, Qu 800°C, 400 h, PXD	KuB, 72	La 98.48 Ni 99.98 B 99.3
LaNi <sub>12</sub> B <sub>6</sub>	mmmC-c-	$a = 9.85(2)$ $b = 7.31(2)$ $c = 11.11(2)$	AM, Qu 800°C, 400 h, PXD	KuB, 72	La 98.48 Ni 99.98 B 99.3
LaNi <sub>2</sub> B <sub>2</sub>	2/mC-c	$a = 9.65(2)$ $b = 5.16(1)$ $c = 11.31(2)$ $\beta = 103.75(1)^\circ$	Am, Qu 800°C, 400 h, PXD	KuB, 72	La 98.48 Ni 99.98 B 99.3
LaNi <sub>12</sub> B <sub>2</sub>	unknown		AM, Qu 800°C, 400 h, PXD	KuB, 72	La 98.48 Ni 99.98 B 99.3

(\*) This compound probably corresponds to LaNi<sub>5</sub>B, earlier reported with diffraction symbol 2/mP2<sub>1</sub>/-,  $a = 35.20(5)$ ,  $b = 5.11(1)$ ,  $c = 11.03(2)$ ,  $\beta = 90.0(1)^\circ$  (Kuz'ma et al., 1972). Furthermore it seems to correspond to the ternary phase LaNi<sub>4.4</sub>B<sub>0.6</sub> whose hydrogen absorption properties were studied by Mendelson et al. (1980). The latter fact has recently been confirmed by a detailed investigation of the characteristics of hydrogen absorption in La<sub>3</sub>Ni<sub>13</sub>B<sub>2</sub> by Spada and Oesterreicher (1983). According to their work, this compound [ $a = 5.094(6)$ ,  $c = 10.986(21)$ ] at 800°C is in equilibrium with LaNi<sub>5</sub> and possibly LaNi<sub>4</sub>B; at 8 atm H<sub>2</sub>, 23°C the hydrogen take up was La<sub>3</sub>Ni<sub>13</sub>B<sub>2</sub>H<sub>~10</sub>.

Yupko, V.P., P.A. Verkhovodov, V.V. Morosov, A.V. Besov and V.Ya. Shlyuko, 1981, Poroshk. Metall. 219(3), 64.

### La-Os-B

One ternary compound has been characterized in the La-Os-B system.

LaOs<sub>4</sub>B<sub>4</sub> [NdCo<sub>4</sub>B<sub>4</sub>-type, P4<sub>2</sub>/n,  $a = 7.611(3)$ ,  $c = 3.988(2)$ ] was prepared by arc melting compacts of 99.9% La ingots, and 99.9% Os and 99.0% B powders, and annealing at 1400°C, 12 h in high vacuum on a boronitride substrate. Os atom parameters were calculated from single crystal Weissenberg photographs:  $x_{Os} = 0.605$ ,  $y_{Os} = 0.140$ ,  $z_{Os} = 0.140$  (Rogl, 1979); magnetic properties were studied by Hiebl et al. (1981);  $T_n = 1.5$  K.

A compound LaOs<sub>~2</sub>B<sub>~2</sub> was observed by Rogl (unpublished) from arc melted alloys.

## References

- Hiebl, K., M.J. Sienko and P. Rogl, 1981, *J. Less-Common Metals* **82**, 21.  
 Rogl, P., 1979, *Monatsh. Chem.* **110**, 235.

## La-Re-B

The La-Re-B ternary system has been investigated by Mikhailenko et al. (1977) by means of X-ray and metallographic analysis, and two partial isothermal sections were established (fig. 32). Samples were prepared from 98.48% La ingots, and Re 99.7% and B 99.4% powders by arc melting and subsequent annealing in evacuated quartz capsules at 800°C (0–45 at% La), and 600°C (45–100% La) for 360 h.

Solid solubilities of binary compounds were found to be negligible; La and Re are practically immiscible. As far as the rhenium borides are concerned ( $\text{Re}_3\text{B}$ ,  $\text{Re}_7\text{B}_3$ ,  $\text{ReB}_{2+x}$ ), the homogeneous range of  $\text{ReB}_{2+x}$  has not yet been investigated in detail (i.e., as a function of temperature, see La Placa and Post, 1962; Portnoi and Romashov, 1968); for the lanthanum borides, see La-Cr-B. Using X-ray, microhardness, and metallographic analysis the solubility of Re in  $\text{LaB}_6$  was reported to be less than 0.5 a/o Re (Bondarenko et al., 1971).

Ternary equilibria are characterized by three compounds. The crystal structure of  $\text{La}_2\text{Re}_3\text{B}_7$  has recently been derived by Kuz'ma et al. (1982) from single crystal counter data:  $\text{La}_2\text{Re}_3\text{B}_7$ -type,  $a = 7.681(3)$ ,  $b = 6.773(2)$ ,  $c = 11.658(4)$ ,  $Pcca$ ,  $R = 0.074$ ,  $\rho_{\text{exp}} = 9.62$ ,  $\rho_{\text{theor}} = 10.05 \text{ kg/dm}^3$ . Originally a formula  $\text{La}_2\text{Re}_3\text{B}_8$  was assigned by Mikhailenko et al. (1977) with lattice parameters  $a = 7.71$ ,  $b = 6.76$ ,  $c = 11.5$ .  $\text{LaRe}_4\text{B}_4$  is tetragonal  $a = 7.40$ ,  $c = 10.60$  and was claimed to be isostructural to  $\text{CeRe}_4\text{B}_4$  (structure unsolved). The crystal structure of  $\text{La}_{\sim 3}\text{Re}_{\sim 3}\text{B}_{\sim 4}$  is unknown (tetragonal symmetry?).

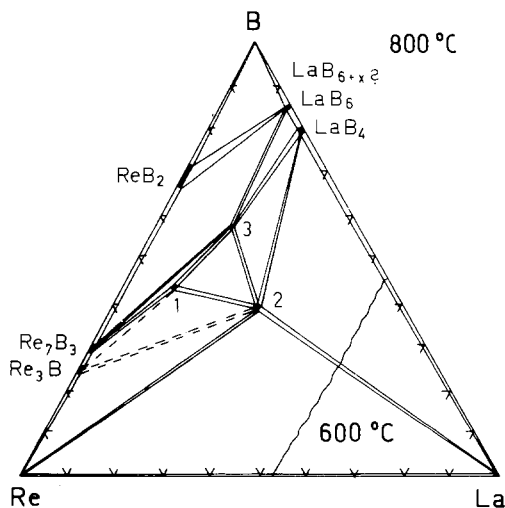


Fig. 32. La-Re-B, partial isothermal sections at 800°C (0–55 a/o La), and at 600°C (55–100 a/o La). 1:  $\text{LaRe}_4\text{B}_4$ , 2:  $\text{La}_3\text{Re}_3\text{B}_4$ , 3:  $\text{La}_2\text{ReB}_7$  (earlier  $\text{La}_2\text{ReB}_8$ ).

*References*

- Bondarenko, V.P., V.V. Morozov and L.V. Chernjak, 1971, Poroshk. Metall. **97**(1), 73.  
 Kuz'ma, Yu.B., S.I. Mikhaleiko and B.Ya. Kotyr, 1982, Dopov. Akad. Nauk Ukr. RSR, Ser. B **3**, 25.  
 La Placa, S. and B. Post, 1962, Acta Crystallogr. **15**, 97.  
 Mikhaleiko, S.I., Yu.B. Kuz'ma and A.S. Sobolev, 1977, Poroshk. Metall. **169**(1), 48.  
 Portnoi, K.I. and V.M. Romashov, 1968, Poroshk. Metall. **2**, 41.

*La-Rh-B*

The crystal structure of  $\text{LaRh}_3\text{B}_2$  (CeCo<sub>3</sub>B<sub>2</sub>-type, P6/mmm) has been analyzed by Ku et al. (1980) using X-ray powder diffraction of arc melted samples;  $a = 5.480(6)$ ,  $c = 3.137(4)$ ;  $T_c = 2.82\text{--}2.60$  K.

For the perovskite-type boride  $\text{LaRh}_3\text{B}_{1-x}$  with Cu<sub>3</sub>Au-type,  $a = 4.244$ ,  $x = 0.2$ ; see also R-Rh-B.

*Reference*

- Ku, H.C., G.P. Meisner, F. Acker and D.C. Johnston, 1980, Solid State Commun. **35**, 91.

*La-Ru-B*

$\text{LaRu}_4\text{B}_4$  has the NdCo<sub>4</sub>B<sub>4</sub>-type of structure,  $a = 7.541(3)$ ,  $c = 4.012(1)$ , P4<sub>2</sub>/n,  $\rho_{\text{theor}} = 8.54$  kg/dm<sup>3</sup> (Grüttner and Yvon, 1979); the structure was examined from single crystal counter data,  $R = 0.05$ ; atom parameters were 2 La in 2b); 8 Ru in 8g) 0.6074(1), 0.1413(1), 0.1410(3); 8 B in 8g) 0.543(2), 0.417(2), 0.144(4).

$\text{La}_{1-0.9}\text{Ru}_3\text{B}_2$  with the CeCo<sub>3</sub>B<sub>2</sub>-type structure was reported by Ku et al. (1980), from X-ray analysis of arc melted samples:  $a = 5.605(6)$ ,  $c = 3.006(4)$ ;  $\rho_{\text{exp}} = 9.5(1)$  in methylene diiodide,  $\rho_{\text{calc}} = 9.55$  kg/dm<sup>3</sup>. The structure was said to exhibit defects on the La sites.

$\text{LaRu}_{3-x}\text{B}_2$  at  $x \approx 0.25$  was claimed by Ku (1980) to crystallize with the YO<sub>3</sub>B<sub>2</sub>-type (orthorhombically distorted CeCo<sub>3</sub>B<sub>2</sub>-type with a sixfold superstructure along the  $c$ -axis,  $c = 6c_0$ ?);  $T_c = 3.95\text{--}3.72$  K.

*References*

- Grüttner, A. and K. Yvon, 1979, Acta Crystallogr. **B35**, 451.  
 Ku, H.C., 1980, Thesis, Univ. of California at San Diego, USA.  
 Ku, H.C., G.P. Meisner, F. Acker and D.C. Johnston, 1980, Solid State Commun. **35**, 91.

*La-Si-B*

Chaban and Kuz'ma (1971) presented the LaB<sub>6</sub>-La-Si partial isothermal section at 800°C (fig. 33), based on X-ray and metallographic analysis of arc melted and heat treated alloys (800°C, 500 h in evacuated silica tubes). Starting materials were: La ingot 98.48%, B powder 99.3%, Si powder 99.99%.

No ternary compounds were reported and mutual solid solubilities were found to be negligible. The lanthanum silicides reported: La<sub>5</sub>Si<sub>3</sub> (Cr<sub>5</sub>B<sub>3</sub>-type), La<sub>3</sub>Si<sub>2</sub> (U<sub>3</sub>Si<sub>2</sub>-type), La<sub>5</sub>Si<sub>4</sub> (Zr<sub>5</sub>Si<sub>4</sub>-type), LaSi (FeB-type), LaSi<sub>2</sub> (GdSi<sub>2</sub>-type), are in agree-



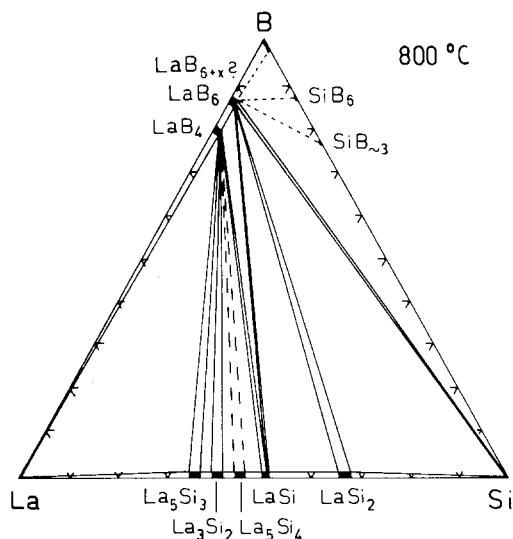


Fig. 33. La-Si-B, isothermal section at 800°C; region LaB<sub>6</sub>-Si-B is proposed.

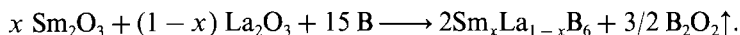
ment with the compilation by Iandelli and Palenzona (1979). For the Si-B system, see Y-Si-B, and for La borides, see La-Cr-B.

### References

- Chaban, N.F. and Yu.B. Kuz'ma, 1971, *Dopov. Akad. Nauk Ukr. RSR, Ser. A* **11**, 1048.  
 Iandelli, A. and A. Palenzona, 1979, *Crystal chemistry of intermetallic compounds*, in: *Handbook on the Physics and Chemistry of Rare Earths*, Vol. 2, eds. K.A. Gschneidner, Jr. and L. Eyring (North-Holland, Amsterdam) pp. 1-54.

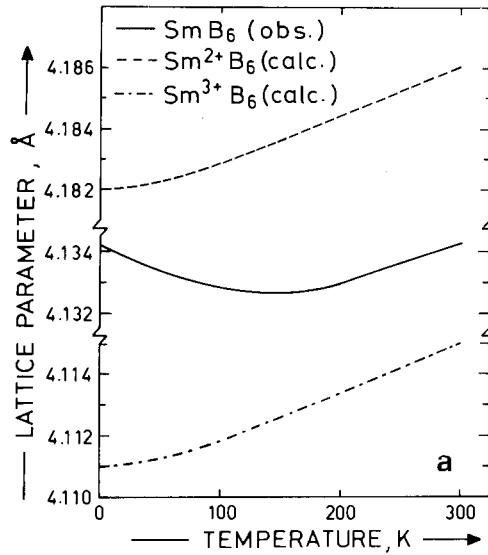
### La-Sm-B

Aivazov et al. (1979) investigated phase equilibria and magnetic properties within the section LaB<sub>6</sub>-SmB<sub>6</sub>. Alloys were prepared by borothermal reduction at 1700°C in vacuum:

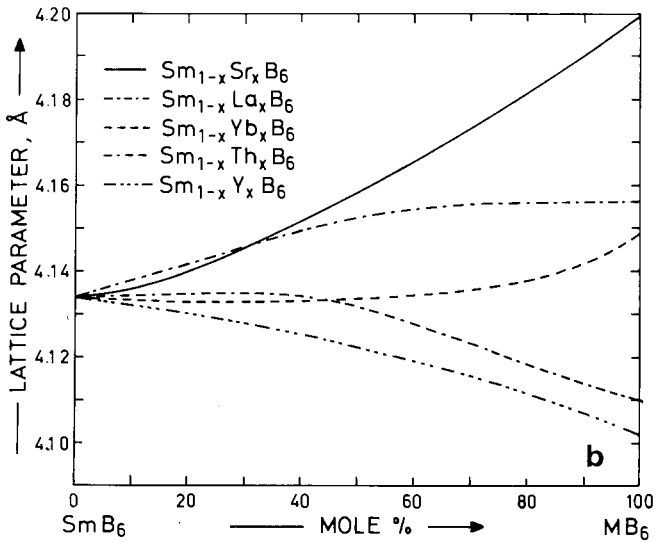


From chemical, gravimetric and X-ray structural analysis a complete solid solution La<sub>1-x</sub>Sm<sub>x</sub>B<sub>6-y</sub> was found, usually deviating from stoichiometry towards boron defects. Comparison of pycnometric (measured in toluene) and X-ray densities revealed the existence of metal vacancies. Due to the change in the proportion of the Sm<sup>2+</sup> and Sm<sup>3+</sup> ions the magnetic susceptibility depends nonlinearly on the La concentration (30% Sm<sup>2+</sup> in SmB<sub>6</sub> to 50% Sm<sup>2+</sup> for 80% LaB<sub>6</sub>).

Tarascon et al. (1980) independently studied the valence transition of Sm as well as the temperature dependence of the Sm oxidation state in Sm<sub>1-x</sub>La<sub>x</sub>B<sub>6</sub> solid solutions, CaB<sub>6</sub>-type, Pm3m. Samples were prepared by borothermal reduction of the mixed oxides under vacuum and high temperatures. The exact values of *x* have been



(a)



(b)

Fig. 34. (a) Temperature dependence of lattice parameter of  $\text{SmB}_6$  (experimental) and of hypothetical calculated  $\text{Sm}^{2+}\text{B}_6$ ,  $\text{Sm}^{3+}\text{B}_6$ . (b)  $\text{Sm}_{1-x}\text{La}_x\text{B}_6$ ,  $\text{Sm}_{1-x}\text{Sr}_x\text{B}_6$ ,  $\text{Sm}_{1-x}\text{Yb}_x\text{B}_6$ ,  $\text{Sm}_{1-x}\text{Th}_x\text{B}_6$  and  $\text{Sm}_{1-x}\text{Y}_x\text{B}_6$ , lattice parameters versus composition. After Tarascon et al. (1980).

determined by X-ray fluorescence analysis and checked by density measurements. Density measurements, X-ray and chemical analysis of  $\text{SmB}_6$  indicate an atomic ratio B/Sm of  $\approx 6$ . From the temperature dependence of the  $\text{SmB}_6$  lattice parameters as well as the X-ray absorption measurement at the  $L_{\text{III}}$  edge between 4.2 and 300 K, Tarascon et al. (1980) were able to propose the variation of the average Sm valence from 2.6 (300 K) to 2.53 at 4.2 K (corresponding to an increase of 17.5% of  $\text{Sm}^{2+}$  ions). A similar result was obtained from  $\text{Sm}_{0.75}\text{La}_{0.25}\text{B}_6$ . Substitution Sm/La involves a decrease of the average samarium valence to a much higher extent than reported by Aivazov et al. (1980). Figure 34 represents the lattice parameter dependence of  $\text{SmB}_6$ , for  $\text{Sm}_{1-x}^{2+}\text{Sm}_x^{3+}\text{B}_6$ ,  $\text{Sm}_{0.75}\text{La}_{0.25}\text{B}_6$  and for  $\text{Sm}_{1-x}\text{La}_x\text{B}_6$ . Due to the valence change of Sm a remarkable deviation from Vegard's law is observed (Kasaya et al., 1980).

The work functions of lanthanum, samarium and ytterbium hexaborides and  $(\text{La}_x\text{Sm}_{1-x})\text{B}_6$  alloys were obtained from secondary ion-ion emission during 8 keV argon ion bombardment at  $10^{-3}$  A/cm<sup>2</sup> current density (Cherepin et al., 1977). The experimental results were used to estimate qualitatively the energy of the atomic bond on the alloy surface. Replacement of lanthanum atoms by samarium causes an increase in metal-boron and metal-metal bond strength.

### References

- Aivazov, M.I., S.V. Aleksandrovich, B.A. Evseev, K.A. Zinchenko and V.S. Mkrtchyan, 1979, *Izv. Akad. Nauk SSSR, Neorg. Mater.* **15**(1), 61; 1982, *Fiz. Tverd. Tela* **24**(9), 2667.  
 Cherepin, V.T., M.A. Vasil'ev, A.A. Kosjuchkov, V.V. Morozov, V.Ja. Shljuko and V.S. Kresanov, 1977, *Poroshk. Metall.* **178**(10), 22.  
 Kasaya, M., J.M. Tarascon and J. Etourneau, 1980, *Solid State Commun.* **33**, 1005.  
 Tarascon, J.M., Y. Isikawa, B. Chevalier, J. Etourneau and P. Hagenmuller, 1980, *J. Physique* **41**, 1135 and 1141.

### La-Ta-B

On the basis of measurements of hexaboride lattice parameters, microhardness, metallographic and X-ray analysis, the solubility of Ta in  $\text{LaB}_6$  was shown to be  $\leq 0.5$  a/o Ta (Bondarenko et al., 1971).

### Reference

- Bondarenko, V.P., V.V. Morozov and L.V. Chernjak, 1971, *Poroshk. Metall.* **97**(1), 73.

*La-Tm-B*: see notes added in proof

### La-U-B

Hill et al. (1974) investigated alloys of the form  $(\text{U}_{1-x}\text{La}_x)\text{B}_4$  with respect to their magnetic properties (ferromagnetic ordering of U) in the as-cast condition after arc melting, and after heat treatment for 2.5 h at 1450°C. From X-ray powder diffraction the samples contained  $\text{LaB}_6$  as the second phase, its amount increasing with increasing La concentration. Due to the preponderance of the  $\text{LaB}_6$  phase no lattice parameters

were determined. The magnetic ordering temperature  $T_m(x) \approx 31$  K was constant for  $x = 0.4$  to  $0.8$  and from data of  $(Y, La, U)B_4$  alloys was extrapolated to be appropriate to the tetraboride phase,  $ThB_4$ -type,  $P4/mbm$  (see also figs. 54 and 55).

#### Reference

Hill, H., A.L. Giorgi, E.G. Szklarz and J.L. Smith, 1974, *J. Less-Common Metals* **38**, 239.

#### La-W-B

Phase equilibria in the La-W-B system at  $800^\circ\text{C}$  (0–67 a/o La) and  $600^\circ\text{C}$  (67–100 a/o La) were presented by Mikhaleiko and Kuz'ma (1976) on the basis of X-ray data (fig. 35). For La borides, see La-Cr-B; for W borides, see Y-W-B. Mutual solid solubilities of La and W borides were found to be small. Due to the high thermodynamic stability of W borides no two-phase equilibrium exists between W and  $LaB_6$ . Using X-ray, metallographic and microhardness analysis, the solubility of W in  $LaB_6$  was shown to be  $\leq 0.5$  a/o W (Bondarenko et al., 1971). Some ambiguity exists concerning the two competing tie-lines  $W_2B + LaB_4$  and  $WB + La$ .

#### References

Bondarenko, V.P., V.V. Morozov and L.V. Chernjak, 1971, *Poroshk. Metall.* **97**(1), 73.

Mikhaleiko, S.I. and Yu.B. Kuz'ma, 1976, *Poroshk. Metall.* **158**(2), 56; see also 1972, *Vestn. Lvov Univ., Ser. Khim.* **14**, 24.

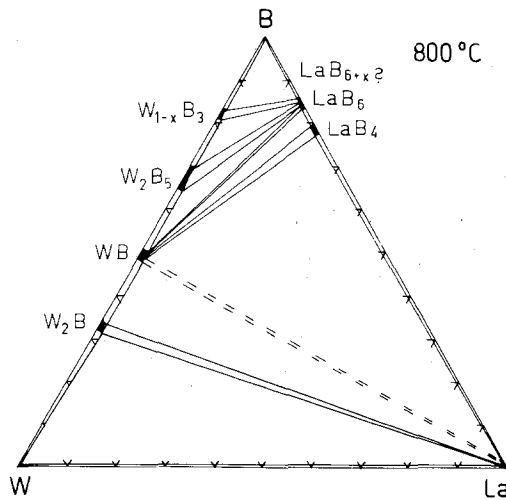
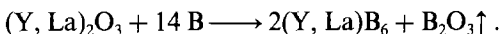


Fig. 35. La-W-B, isothermal section at  $800^\circ\text{C}$ .

#### La-Y-B

Fisk et al. (1974) investigated the mutual solubility of  $LaB_6$  and  $YB_6$  by X-ray analysis as well as electron microscope data on a) arc melted alloys and b) specimens prepared from mixed oxides and boron at  $1600^\circ\text{C}$  in vacuum:



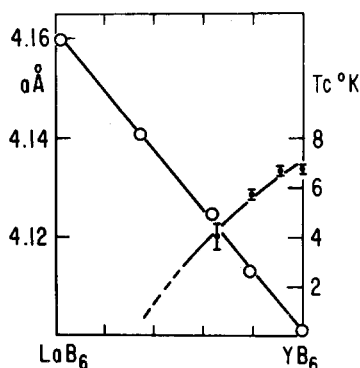


Fig. 36. Lattice parameters and superconducting transition temperatures of  $\text{La}_{1-x}\text{Y}_x\text{B}_6$  solid solutions; after Fisk et al. (1974).

A continuous solid solution  $(\text{Y}, \text{La})\text{B}_6$  with  $\text{CaB}_6$ -type of structure,  $\text{Pm}3\text{m}$ , was found from specimens b), but a restricted solid solution appears from alloys a), due to the different melting behavior of  $\text{YB}_6$  (incongruent) and  $\text{LaB}_6$  (congruent), which results in a nearly complete fractional crystallization of the two hexaborides. At variance with the results obtained by Bondarenko et al. (1966) on samples prepared by borothermal reduction, lattice parameters of specimens b) closely obey Vegard's rule and are shown in fig. 36 including superconductivity data.

### References

- Bondarenko, V.P., I.I. Bilyk and V.Ya. Shlyuko, 1966, *Poroshk. Metall.* **45**(9), 43.  
 Fisk, Z., A.C. Lawson and R.W. Fitzgerald, 1974, *Mater. Res. Bull.* **9**, 633.

### La-Yb-B

The work functions of lanthanum, samarium and ytterbium hexaborides and  $(\text{La}_x\text{Sm}_{1-x})\text{B}_6$  alloys were obtained from secondary ion-ion emission during 8 keV argon ion bombardment at  $10^{-3}$  A/cm<sup>2</sup> current density (Cherepin et al., 1977). The experimental results were used to estimate qualitatively the energy of the atomic bond on the alloy surface. Replacement of lanthanum atoms by samarium causes an increase in metal-boron and metal-metal bond strength.

### Reference

- Cherepin, V.T., M.A. Vasil'ev, A.A. Kosjuchkov, V.V. Morozov, V.Ja. Shljuko and V.S. Kresanov, 1977, *Poroshk. Metall.* **178**(10), 22.

### Lu-Al-B

Using the aluminum metal flux technique, Mikhalenko et al. (1980) obtained single crystals of  $\text{LuAlB}_4$  when cooling melts with a Lu:B ratio ranging from 1:6 to 1:12 from 1523 K. Specimens were prepared by heating charges of amorphous boron

(>99%), Lu 99.9%, Al granules in an alundum crucible under a stream of purified argon at 1523 K for 6 h followed by slow cooling (100 K/h). Excess Al was dissolved in dilute HCl (1:3). LuAlB<sub>4</sub> has the YCrB<sub>4</sub>-type of structure, Pbam;  $a = 5.906(2)$ ,  $b = 11.44(1)$ ,  $c = 3.480(1)$ ; metal atom parameters were refined to  $R = 0.112$  from X-ray diffractometer data (microdensitometer): 4 Lu in 4g) 0.132(1), 0.149(1), 0; Al in 4g) 0.129(1), 0.413(1), 0; boron atoms in 4h) were determined from geometrical considerations: B(1) 0.305, 0.300, 0.5; B(2) 0.370, 0.465, 0.5; B(3) 0.385, 0.050, 0.5 and B(4) 0.470, 0.195, 0.5.

### Reference

Mikhaleiko, S.I., Yu.B. Kuz'ma, M.M. Korsukova and V.N. Gurin, 1980, *Izv. Akad. Nauk SSSR, Neorg. Mater.* **16**(11), 1941.

### Lu-Co-B

No phase diagram exists for the Lu-Co-B system, but five ternary compounds have been characterized (table 23).

### References

Kuz'ma, Yu.B. and N.S. Bilonishko, 1973, *Kristallografiya* **18**(4), 710.

Kuz'ma, Yu.B., P.I. Kripyakevich and N.S. Bilonishko, 1969, *Dopov. Akad. Nauk Ukr. RSR, Ser. A* **10**, 939.

Kuz'ma, Yu.B. and N.S. Bilonishko, 1972, *Sov. Phys. Crystallogr.* **16**(5), 897.

Stepanchikova, G.F. and Yu.B. Kuz'ma, 1977, *Vestn. Lvov Univ., Ser. Khim.* **19**, 37.

TABLE 23  
Formation and structural data of ternary compounds Lu-Co-B.

Compound	Structure type, Space group	Lattice parameters, Density	Preparation Characterization	Refs.	Purity
LuCoB <sub>4</sub>	YCrB <sub>4</sub> Pbam	$a = 5.827(10)$ $b = 11.28(2)$ $c = 3.327(5)$	AM, Qu 800°C, 340 h, PXD	StK, 77	Lu 99.0 Co 99.9 B 99.3
LuCo <sub>4</sub> B <sub>4</sub>	CeCo <sub>4</sub> B <sub>4</sub> P4 <sub>2</sub> /nmc	$a = 4.998(3)$ $c = 6.947(5)$	no details given PXD	KuB, 72	
LuCo <sub>3</sub> B <sub>2</sub>	CeCo <sub>3</sub> B <sub>2</sub> P6/mmm	$a = 4.959(3)$ $c = 3.035(2)$	AM, Qu 800°C, 50 h, PXD	KuKB, 69	
LuCo <sub>4</sub> B	CeCo <sub>4</sub> B P6/mmm	$a = 4.940(3)$ $c = 6.867(4)$	AM, Qu 800°C, 50 h, PXD	KuB, 73	Lu 99. Co 99.87 B 99.3
Lu <sub>3</sub> Co <sub>11</sub> B <sub>4</sub>	Ce <sub>3</sub> Co <sub>11</sub> B <sub>4</sub> P6/mmm	$a = 4.982(3)$ $c = 9.867(6)$	AM, Qu 800°C, 50 h, PXD	KuB, 73	Lu 99. Co 99.87 B 99.3

*Lu-Cr-B*

The crystal structure of LuCrB<sub>4</sub> [YCrB<sub>4</sub>-type, Pbam,  $a = 5.726(5)$ ,  $b = 11.38(1)$ ,  $c = 3.404(4)$ ] has been determined by Kuz'ma (1970) by X-ray diffraction methods.

*Reference*

Kuz'ma, Yu.B., 1970, *Kristallografiya* **15**(2), 312.

*Lu-Fe-B*

Three ternary compounds have been characterized in the Lu-Fe-B system.

LuFeB<sub>4</sub>, YCrB<sub>4</sub>-type, Pbam,  $a = 5.832(10)$ ,  $b = 11.29(2)$ ,  $c = 3.353(5)$ , as derived from X-ray powder analysis by Stepanchikova and Kuz'ma (1977); for sample preparation, see CeFeB<sub>4</sub>.

LuFe<sub>2</sub>B<sub>2</sub> crystallizes with the ThCr<sub>2</sub>Si<sub>2</sub>-type of structure, I4/mmm,  $a = 3.499(5)$ ,  $c = 9.288(10)$  (Stepanchikova et al., 1979); for sample preparation, see TmFe<sub>2</sub>B<sub>2</sub>.

LuFe<sub>4</sub>B is CeCo<sub>4</sub>B-type [P6/mmm,  $a = 5.007(2)$ ,  $c = 6.966(6)$ ] (Chernjak, 1983); for sample preparation, see ErFe<sub>4</sub>B.

*References*

Chernjak, G.V., 1983, *Izv. Akad. Nauk SSSR, Neorg. Mater.* **19**(3), 485.

Stepanchikova, G.F. and Yu.B. Kuz'ma, 1977, *Vestn. Lvov Univ., Ser. Khim.* **19**, 37.

Stepanchikova, G.F., Yu.B. Kuz'ma and B.I. Chernjak, 1979, *Dopov. Akad. Nauk Ukr. RSR, Ser. A*, 950.

*Lu-Ir-B*

LuIr<sub>3</sub>B<sub>2</sub> is isostructural with the ErIr<sub>3</sub>B<sub>2</sub>-type of structure (possible space group C2/m),  $a = 5.394(6)$ ,  $b = 9.354(9)$ ,  $c = 3.080(4)$ ,  $\beta = 91.4(1)^\circ$  (Ku and Meisner, 1981; from X-ray powder analysis of arc melted alloys);  $T_n = 1.2$  K (see also Lu-Y-Ir-B).

*Reference*

Ku, H.C. and G.P. Meisner, 1981, *J. Less-Common Metals* **78**, 99.

*Lu-Ni-B*

No ternary phase diagram has been reported for the Lu-Ni-B system.

Lu<sub>3</sub>Ni<sub>7</sub>B<sub>2</sub> has the Dy<sub>3</sub>Ni<sub>7</sub>B<sub>2</sub>-type, P6<sub>3</sub>/mmc,  $a = 5.015(2)$ ,  $c = 14.180(10)$  (Kuz'ma and Chaban, 1979). Samples were arc melted and annealed for 360 h at 800°C in evacuated silica tubes. Starting materials were Lu ingot 99.5%, Ni powder 99.98%, B powder 99.3%.

Lu<sub>2</sub>Ni<sub>21</sub>B<sub>6</sub> with Cr<sub>23</sub>C<sub>6</sub>-type, Fm3m,  $a = 10.632(5)$ , was reported by Chaban et al. (1980) from arc melted alloys.

LuNi<sub>4</sub>B was claimed by Kuz'ma et al. (1981) to crystallize with CeCo<sub>4</sub>B-type structure  $a = 4.934(3)$ ,  $c = 6.918(8)$ , P6/mmm.

LuNiB<sub>4</sub> has YCrB<sub>4</sub>-type, Pbam,  $a = 5.789(24)$ ,  $b = 11.340(71)$ ,  $c = 3.469(25)$  (Chaban et al., 1981). Arc melted and annealed alloys (800°C, 720 h in evacuated silica capsules) contained small amounts of LuB<sub>4</sub> (equilibrium with LuB<sub>4</sub>?).

## References

- Chaban, N.F., Yu.B. Kuz'ma and P.L. Kotovskaya, 1980, *Dopov. Akad. Nauk Ukr. RSR, Ser. A*, 88.  
 Chaban, N.F., G.V. Chernjak and Yu.B. Kuz'ma, 1981, *Izv. Akad. Nauk SSSR, Neorg. Mater.* **17**(8), 1494.  
 Kuz'ma, Yu.B. and N.F. Chaban, 1979, *Dopov. Akad. Nauk Ukr. RSR, Ser. A*, 88.  
 Kuz'ma, Yu.B., N.S. Bilonishko, N.F. Chaban and G.V. Chernjak, 1981, *J. Less-Common Metals* **82**, 364; see also 1982, *Izv. Akad. Nauk SSSR, Neorg. Mater.* **18**, 691.

## Lu–Os–B

Five ternary compounds have been identified in the Lu–Os–B system. The methods of preparation and the crystallographic data are presented in table 24.

## References

- Ku, H.C. and R.N. Shelton, 1980, *Mater. Res. Bull.* **15**(10), 1441.  
 Ku, H.C., G.P. Meisner, F. Acker and D.C. Johnston, 1980, *Solid State Commun.* **35**, 91.  
 Rogl, P. and L. DeLong, 1983, *J. Less-Common Metals*, **91**, 97.  
 Rogl, P. and H. Nowotny, 1982, Crystal structures and phase relationships within ternary systems: rare earth metal–noble metal–boron, in: *The Rare Earths in Science and Technology*, Vol. 3, eds. J. McCarthy, B. Silber and J.J. Rhyne (Plenum, New York, London) pp. 353–356.  
 Rogl, P., K. Hiebl and M.J. Sienko, 1982, Structural chemistry and magnetic behavior of  $RM_4B_4$ -borides, paper presented at the 7th Intern. Conf. on Solid Compounds of Transition Elements, Grenoble (June 21–25), Proceedings, II A4.  
 Shelton, R.N., B.A. Karcher, D.R. Powell, R.A. Jacobson and H.C. Ku, 1980, *Mater. Res. Bull.* **15**, 1445.

TABLE 24  
 Formation and structural data of ternary compounds Lu–Os–B.

Compound	Structure type, Space group	Lattice parameters, Density	Preparation, Characterization	Refs.	Purity
LuOsB <sub>4</sub>	YCrB <sub>4</sub> Pbam	$a = 5.9232(41)$ $b = 11.4496(73)$ $c = 3.5284(9)$	AM, HT, 1300°C, 12 h HV, W substrate $T_n = 1.5$ K, PXD	RoD, 83	Lu 99.9 Os 99.9 B 99.7
Lu <sub>2</sub> OsB <sub>6</sub>	Y <sub>2</sub> ReB <sub>6</sub> Pbam	$a = 9.0331(35)$ $b = 11.4113(29)$ $c = 3.5842(5)$	AM, HT, 1300°C, 12 h HV, W substrate $T_n = 1.5$ K, PXD	RoN, 82	Lu 99.9 Os 99.9 B 99.7
LuOsB <sub>2</sub>	LuRuB <sub>2</sub> Pnma	$a = 5.809(6)$ $b = 5.231(5)$ $c = 6.318(7)$	AM(Zr), Ta tubes 1250°C, 24 h 800°C, 9 d PXD, $T_c = 2.66$ – $2.14$ K	ShKPJK, 80 KuS, 80	99.9
LuOs <sub>4</sub> B <sub>4</sub>	YOs <sub>4</sub> B <sub>4</sub> tetragonal	$a = 7.4154(7)$ $c = 32.6224(16)$ $c = 8c_0$	AM, HT, 1400°C, 12 h HV, BN substrate PXD, $T_n = 1.5$ K	RoHS, 82	Lu 99.9 Os 99.9 B 99.7
LuOs <sub>3</sub> B <sub>2</sub>	CeCo <sub>3</sub> B <sub>2</sub> P6/mmm	$a = 5.457(6)$ $c = 3.052(4)$	AM(Zr) PXD $T_c = 4.62$ – $4.45$ K	KuMAJ, 80	99.9



*Lu-Re-B*

$\text{Lu}_2\text{ReB}_6$  has been characterized with  $\text{Y}_2\text{ReB}_6$ -type, Pbam,  $a = 9.075(5)$ ,  $b = 11.41(1)$ ,  $c = 3.600(4)$  by Kuz'ma and Svarichevskaya (1972) from X-ray powder analysis.

*Reference*

Kuz'ma, Yu.B. and S.I. Svarichevskaya, 1972, *Kristallografiya* 17(3), 658.

*Lu-Rh-B*

$\text{LuRh}_3\text{B}_2$  adopts the  $\text{ErIr}_3\text{B}_2$ -type of structure (possible space group C2/m),  $a = 5.353(6)$ ,  $b = 9.276(9)$ ,  $c = 3.089(4)$ ,  $\beta = 90.9(1)^\circ$  (Ku and Meisner, 1981; X-ray powder analysis of arc melted samples);  $T_n = 1.2$  K.

$\text{LuRh}_4\text{B}_4$  was reported to crystallize with the  $\text{CeCo}_4\text{B}_4$ -type,  $\text{P4}_2/\text{nmc}$ ,  $a = 5.294(2)$ ,  $c = 7.359(3)$  by Vandenberg and Matthias (1977) from X-ray powder analysis; for sample preparation, see  $\text{YRh}_4\text{B}_4$ .  $T_c = 11.76\text{--}11.54$  K (Matthias et al., 1977). Arc melted samples containing excess Rh were said to mainly consist of  $\text{CeCo}_4\text{B}_4$ -type and (metastable?)  $\text{LuRu}_4\text{B}_4$ -type phases (Yvon and Johnston, 1982).

After annealing arc melted samples at the composition  $\text{LuRh}_{4.05}\text{B}_4$  at  $1200^\circ\text{C}$  for 125 h in a sealed Ta tube (finally quenched into cold water), Yvon and Johnston (1982) obtained a new low-temperature phase with the  $\text{LuRh}_4\text{B}_4$ -type of structure,  $\text{Ccca}$ ,  $a = 7.410(3)$ ,  $b = 22.26(1)$ ,  $c = 7.440(3)$ ,  $\rho_{\text{theor}} = 10.22$ ,  $\rho_{\text{exp}} = 10.19(2)$   $\text{kg}/\text{dm}^3$ . The crystal structure has been refined from single crystal diffractometer data,  $R = 0.05$ . The  $\text{LuRh}_4\text{B}_4$ -type phase was found to be in equilibrium with RhB,  $\text{LuRh}_4\text{B}_4$  (unknown structure),  $\text{LuRh}_3\text{B}_2$  and  $\text{LuRh}_4\text{B}_4$  with the  $\text{CeCo}_4\text{B}_4$ -type; at lower temperatures the phase was reported to decompose (Johnston and Braun, 1982). A DTA signal at  $1300 \pm 5^\circ\text{C}$ , indicating a solid state transition, was recorded for a sample  $\text{LuRh}_4\text{B}_4$  by Rogl (1982).

From an unusual nonlinear pressure dependence of  $T_c$ , a pressure-induced phase transformation was suggested for  $\text{LuRh}_4\text{B}_4$  at  $\approx 6.6$  kbar (Shelton and Johnston, 1978).

For the existence of a  $\text{LuRh}_3\text{B}_{1-x}$  phase with  $\text{Cu}_3\text{Au}$ -type structure,  $a = 4.132$ ,  $x \approx 0.2$ , see R-Rh-B.

Thermal conductivity measurements for  $\text{LuRh}_4\text{B}_4$  between 0.05 and 15 K were reported by Odoni et al. (1982).

*References*

- Johnston, D.C. and H.F. Braun, 1982, Systematics of superconductivity in ternary compounds, in: *Superconductivity in Ternary Compounds*, Vol. 2, eds. Ø. Fischer and M.B. Maple (Springer, Berlin).  
 Ku, H.C. and G.P. Meisner, 1981, *J. Less-Common Metals* 78, 99.  
 Matthias, B.T., E. Corenzwit, J.M. Vandenberg and H.E. Barz, 1977, *Proc. Nat'l Acad. Sci. US* 74(4), 1334.  
 Odoni, W., G. Keller, H.R. Ott, H.C. Hamaker, D.C. Johnston and M.B. Maple, 1982, *Physica* 108B, 1227.  
 Rogl, P., 1982, Univ. of Vienna, Austria, unpublished results.

TABLE 25  
Formation and structural data of ternary compounds Lu-Ru-B.

Compound	Structure type, Space group	Lattice parameters, Density	Preparation, Characterization	Refs.	Purity
LuRuB <sub>4</sub>	YCrB <sub>4</sub> Pbam	$a = 5.8996(35)$ $b = 11.4299(58)$ $c = 3.5270(11)$	AM, HT, 1300°C, 12 h HV, W substrate congruent melting PXD, ME, $T_n = 1.5$ K	RoD, 83	Lu 99.9 Ru 99.9 B 99.7
Lu <sub>3</sub> RuB <sub>6</sub>	Y <sub>2</sub> ReB <sub>6</sub> Pbam	$a = 9.0138(39)$ $b = 11.3880(17)$ $c = 3.5826(8)$	AM, HT, 1600°C, 12 h HV, W substrate PXD, $T_n = 1.5$ K	RoN, 82	Lu 99.9 Ru 99.9 B 99.7
LuRuB <sub>2</sub> <sup>(*)</sup>	LuRuB <sub>2</sub> Pnma	$a = 5.809(2)$ , $\rho_E = 10.27$ $b = 5.229(2)$ , $\rho_x = 10.36$ $c = 6.284(2)$	AM(Zr) HT, Ta tubes 1250°C, 24 h 800°C, 9 d, PXD $T_c = 9.99-9.86$ K	ShKPJK, 80 KuS, 80	99.9
LuRu <sub>4</sub> B <sub>4</sub> <sup>(**)</sup>	LuRu <sub>4</sub> B <sub>4</sub> I4 <sub>1</sub> /acd	$a = 7.419(5)$ , $\rho_E = 10.03$ $c = 14.955(10)$ , $\rho_x = 10.04$	AM(Zr) PDX refinement $T_c = 1.77-1.70$ K	Jo, 77	high purity
LuRu <sub>3</sub> B <sub>2</sub>	CeCo <sub>3</sub> B <sub>2</sub> P6/mmm	$a = 5.439(4)$ $c = 3.016(2)$	AM, HT, 1400°C, 24 h BN substrate PXD, ME, congr. melting	HiRUS, 80	Lu 99.9 Ru 99.9 B 99.7
		$a = 5.454(6)$ $c = 3.004(4)$	AM(Zr), PXD $T_n = 1.2$ K	KuMAJ, 80	99.9

<sup>(\*)</sup>The crystal structure has been refined from single crystal counter data; atomic parameters were Lu in 4c) 0.0105(4), 1/4, 0.1648(3); Ru in 4c) 0.1816(9), 1/4, 0.6824(6); B in 8d) 0.358(7), 0.084(9), 0.964(7),  $R = 0.085$ ; occupancy in all cases was 100%.

<sup>(\*\*)</sup>The crystal structure has been refined from X-ray powder diffractometer data,  $R = 0.065$ ; atomic parameters were Ru in 32g) 0.112, 0.100, 15/16; B in 32g) 0.818, 0.111, 0.961, Lu in 8b).

- Shelton, R.N. and D.C. Johnston, 1978, Pressure dependencies of the superconducting and magnetic critical temperatures of ternary rhodium borides, in: High Pressure and Low Temperature Physics, eds. C.W. Chu and J.A. Wollam (Plenum, New York) pp. 409–417.
- Vandenberg, J.M. and B.T. Matthias, 1977, Proc. Nat'l Acad. Sci. US **74**(4), 1336.
- Yvon, K. and D.C. Johnston, 1982, Acta Crystallogr. **B38**, 247.

### *Lu–Ru–B*

No ternary phase diagram exists for the Lu–Ru–B system, but five ternary compounds have been identified, see table 25.

### *References*

- Hiebl, K., P. Rogl, E. Uhl and M.J. Sienko, 1980, Inorg. Chem. **19**(11), 3316.
- Johnston, D.C., 1977, Solid State Commun. **24**(10), 699.
- Ku, H.C. and R.N. Shelton, 1980, Mater. Res. Bull. **15**(10), 1441.
- Ku, H.C., G.P. Meisner, F. Acker and D.C. Johnston, 1980, Solid State Commun. **35**, 91.
- Rogl, P. and L. DeLong, 1983, J. Less-Common Metals, **91**, 97.
- Rogl, P. and H. Nowotny, 1982, Crystal structures and phase relationships within ternary systems: rare earth metal–noble metal–boron, in: The Rare Earths in Science and Technology, Vol. 3, eds. J. McCarthy, B. Silber and J.J. Rhyne (Plenum, New York, London) pp. 353–356.
- Shelton, R.N., B.A. Karcher, D.R. Powell, R.A. Jacobson and H.C. Ku, 1980, Mater. Res. Bull. **15**, 1445.

### *Lu–U–B*

Hill et al. (1974) investigated alloys of the form  $(U_{1-x}Lu_x)B_4$  with respect to their magnetic properties (ferromagnetic ordering of U) in the as-cast condition after arc melting, and after heat treatment for 2.5 h at 1450°C. From X-ray powder diffraction analysis samples were found to be homogeneous  $ThB_4$ -type, P4/mbm. Lattice parameters as a function of  $x$  reveal irregular variation. The extrapolated unit-cell dimensions for a hypothetical (ferromagnetic)  $UB_4$  were given as  $a_0 = 7.092$ ,  $c_0 = 3.997$ ; see figs. 54 and 55.

### *Reference*

- Hill, H., A.L. Giorgi, E.G. Szklarz and J.L. Smith, 1974, J. Less-Common Metals **38**, 239.

### *Nd–Co–B* (see notes added in proof)

Ten ternary compounds have been reported. The structural details and preparative methods are summarized in table 26; see also notes added in proof.

### *References*

- Kuz'ma, Yu.B. and N.S. Bilonishko, 1973, Kristallografiya **18**(4), 710.
- Kuz'ma, Yu.B. and N.S. Bilonishko, 1978, Dopov. Akad. Nauk Ukr. RSR, Ser. A **3**, 275.
- Kuz'ma, Yu.B., N.S. Bilonishko, N.F. Chaban and G.V. Chernjak, 1981, J. Less-Common Metals **82**, 364.
- Kuz'ma, Yu.B., G.V. Chernjak and N.F. Chaban, 1981, Dopov. Akad. Nauk Ukr. RSR, Ser. A **12**, 80.
- Niihara, K., T. Shishido and S. Yajima, 1973, Bull. Chem. Soc. Jpn **46**, 1137.

TABLE 26  
Formation and structural data of ternary compounds Nd–Co–B.

Compound	Structure type, Space group	Lattice parameters, Density	Preparation, Characterization	Refs.	Purity
NdCo <sub>4</sub> B <sub>4</sub> <sup>(*)</sup>	NdCo <sub>4</sub> B <sub>4</sub> P4 <sub>2</sub> /n	$a = 7.070(4), \rho_E = 7.31$ $c = 3.822(2), \rho_x = 7.30$	AM, alloy Nd <sub>0.13</sub> Co <sub>0.37</sub> B <sub>0.50</sub> congruent melting(?)	KuB, 78	Nd 99.07 Co 99.9 B 99.3
NdCo <sub>2</sub> B <sub>2</sub>	ThCr <sub>2</sub> Si <sub>2</sub> I4/mmm	$a = 3.586(5), \rho_E = 7.49$ $c = 9.747(7), \rho_x = 7.52$	AM, Qu(Ta) 800°C, 150 h, PXD	NiSY, 73	Nd 99.5 Co 99.99 B 99.9
NdCo <sub>4</sub> B	CeCo <sub>4</sub> B P6/mmm	$a = 5.102(3)$ $c = 6.788(4)$	AM, Qu 800°C, 50 h, PXD	KuB, 73	Nd 99% Co 99.87 B 99.3
Nd <sub>3</sub> Co <sub>11</sub> B <sub>4</sub>	Ce <sub>3</sub> Co <sub>11</sub> B <sub>4</sub> P6/mmm	$a = 5.132(3)$ $c = 9.808(6)$	AM, Qu 800°C, 50 h, PXD	KuB, 73	Nd 99% Co 99.87 B 99.3
Nd <sub>2</sub> Co <sub>7</sub> B <sub>3</sub>	Ce <sub>2</sub> Co <sub>7</sub> B <sub>3</sub> P6/mmm	$a = 5.134(3)$ $c = 12.78(2)$	AM, Qu 800°C, 50 h, PXD	KuB, 73	Nd 99% Co 99.87 B 99.3
NdCo <sub>12</sub> B <sub>6</sub>	SrNi <sub>12</sub> B <sub>6</sub> R $\bar{3}m$	$a_H = 9.502(1)$ $c_H = 7.471(1)$	AM, Qu 800°C, 270 h, PXD	KuCC, 81	Nd 99.5 Co 99.95 B 99.4
Nd <sub>2</sub> Co <sub>5</sub> B <sub>2</sub>	Ce <sub>2</sub> Co <sub>5</sub> B <sub>2</sub> P6 <sub>3</sub> /mmc	$a = 5.115(11)$ $c = 20.56(5)$	no details given	KuBCC, 81	

<sup>(\*)</sup>The crystal structure was refined from single crystal X-ray photographs,  $R_{hk0} = 0.097$ ,  $R_{hk1} = 0.074$ . Nd in 2b), Co in 8g) 0.607, 0.125, 0.138; B in 8g) 0.525, 0.400, 0.125.

### Nd–Cr–B

Phase equilibria of the system Nd–Cr–B at 800°C, as presented in fig. 37, are primarily based on the work by Mikhaleiko and Kuz'ma (1977), who used X-ray and metallographic analysis of 30 alloys, which were prepared in the same way as described for the systems (La, Ce)–Cr–B. Solid solubility of binary compounds was reported to be negligible. The boron-rich region CrB<sub>4</sub>–B–NdB<sub>6</sub>, including the well established compound NdB<sub>66</sub> (Spear, 1976), was not considered in detail and phase equilibria furthermore did not include the binary compound Nd<sub>2</sub>B<sub>5</sub>, which, according to La Placa, is structurally closely related (lower symmetry) to the structure type of Sm<sub>2</sub>B<sub>5</sub>. The homogeneity range of NdB<sub>6</sub> in the range of 1600 to 2000 K (Nd vacancy formation) has recently been investigated by Storms (1981) and the existence of a "random Nd vacancy" phase NdB<sub>6+x</sub> similar to "LaB<sub>9</sub>" was suggested (also see La–Mo–B). For the Cr–B binary system, see Y–Cr–B.

Two ternary compounds were characterized. NdCrB<sub>4</sub> has the YCrB<sub>4</sub>-type of structure, Pbam,  $a = 6.025(5)$ ,  $b = 11.69(1)$ ,  $c = 3.547(4)$ , and NdCr<sub>2</sub>B<sub>6</sub> was confirmed to be isostructural with CeCr<sub>2</sub>B<sub>6</sub>, Immm,  $a = 6.597(4)$ ,  $b = 8.319(5)$ ,  $c = 3.113(3)$  (Mikhaleiko and Kuz'ma 1975).

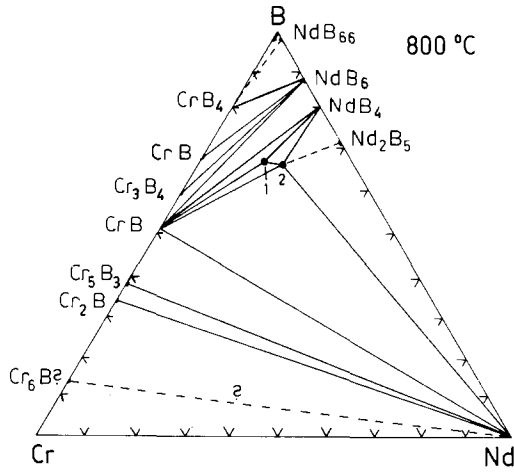


Fig. 37. Nd-Cr-B, isothermal section at 800°C. 1:  $\text{NdCr}_2\text{B}_6$ , 2:  $\text{NdCr}_4\text{B}_4$ .

*References*

La Placa, S., unpublished results.  
 Mikhalenko, S.I. and Yu.B. Kuz'ma, 1977, *Dopov. Akad. Nauk Ukr. RSR, Ser. A*, 951; see also 1975, *Dopov. Akad. Nauk Ukr. RSR, Ser. A* 5, 465.  
 Spear, K.E., 1976, Phase behavior and related properties of rare earth borides in: *Phase Diagrams in Science and Technology*, Vol. 6, ed. A.M. Alper (Academic Press, New York) pp. 91-159.  
 Storms, E.K., 1981, *J. Phys. Chem.* **85**, 1536 and *J. Appl. Phys.* **52**(4), 2961.

*Nd-Fe-B*

Phase equilibria in the Nd-Fe-B system as shown in fig. 38 were determined by Chaban et al. (1980) by means of X-ray and metallographic analysis of arc melted

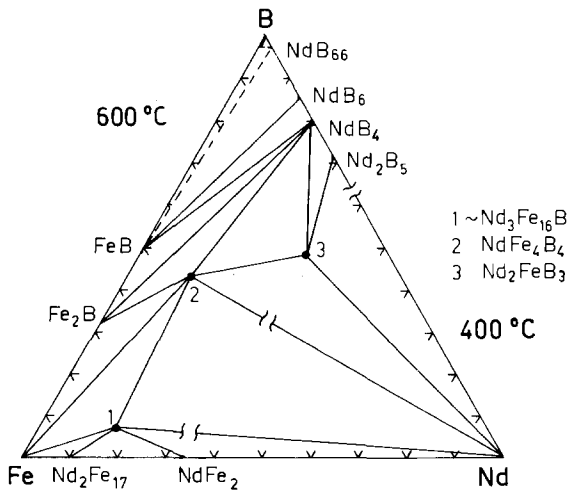


Fig. 38. Nd-Fe-B, partial isothermal sections at 600°C (0-33 a/o Nd) and at 400°C (33-100 a/o Nd).

and heat treated alloys prepared from Nd ingot 99.07%, and Fe 99.9% and B 99.3% powders. Annealing conditions were 700 h at 600°C for the region containing 0–33 a/o Nd and 700 h at 400°C for alloys containing 33–100 a/o Nd. Two binary Nd–Fe compounds were reported: Nd<sub>2</sub>Fe<sub>17</sub> (Th<sub>2</sub>Zn<sub>17</sub>-type) and NdFe<sub>2</sub> (Laves phase ?). The phase diagram of Fe–Nd was recently discussed by Kubaschewski-von Goldbeck (1982). For Fe borides, see Y–Fe–B; for Nd borides, see Nd–Cr–B.

Mutual solid solubilities of binary compounds were found to be negligible. Three ternary compounds were observed, of which Nd<sub>~3</sub>Fe<sub>~16</sub>B<sub>~1</sub> and Nd<sub>~2</sub>FeB<sub>~3</sub> have not yet been characterized.

NdFe<sub>4</sub>B<sub>4</sub> was claimed to be isostructural with CeFe<sub>4</sub>B<sub>4</sub>; the possible space group is P4/ncc(?),  $a = 7.09$ ,  $c = 27.56$ , with an eight-fold superstructure along the  $c$ -axis:  $c = 8c_0$ . Quite recently, however, a series of superstructures Nd <sub>$n+m$</sub> (Fe<sub>4</sub>B<sub>4</sub>) <sub>$n$</sub> , whose crystal structures derive from the NdCo<sub>4</sub>B<sub>4</sub>-type of structure and are either incommensurate or have unusually large repeat units along the  $c$ -axis, have been described by Braun et al. (1982); see table 2 and for sample preparation, see Gd<sub>1+x</sub>Fe<sub>4</sub>B<sub>4</sub>.

### References

- Braun, H.F., M. Pelizzone and K. Yvon, 1982, Ferromagnetic borides with incommensurate rare earth and iron sublattices: R<sub>1+c</sub>Fe<sub>4</sub>B<sub>4</sub>, paper presented at the 7th Intern. Conf. on Solid Compounds of Transition Elements, Grenoble (June 21–26), Proceedings, II B11.  
 Chaban, N.F., Yu.B. Kuz'ma, N.S. Bilonishko, O.O. Kachmar and N.V. Petriv, 1980, Dopov. Akad. Nauk Ukr. RSR, Ser. A, 875.  
 Kubaschewski-von Goldbeck, O., 1982, Iron-binary phase diagrams (Springer, Berlin) pp. 101–102.

### Nd–Ir–B

NdIr<sub>4</sub>B<sub>4</sub> with NdCo<sub>4</sub>B<sub>4</sub>-type, P4<sub>2</sub>/n,  $a = 7.616(3)$ ,  $c = 3.974(2)$ , was shown to form congruently from the melt (X-ray and metallographic analysis, Rogl, 1979). For sample preparation, see LaOs<sub>4</sub>B<sub>4</sub>. Magnetic data were presented by Rupp et al. (1979) and Hiebl et al. (1981);  $T_N = 1.5$  K.

From X-ray powder diffraction data of arc melted alloys Ku and Meisner (1981) found the crystal structure of NdIr<sub>3</sub>B<sub>2</sub> to be isostructural with the ErIr<sub>3</sub>B<sub>2</sub>-type of structure, possible space group C2/m,  $a = 5.513(6)$ ,  $b = 9.540(9)$ ,  $c = 3.084(4)$ ,  $\beta = 90.8(1)^\circ$ ;  $T_m = 4.72$  K.

### References

- Hiebl, K., M.J. Sienko and P. Rogl, 1981, J. Less-Common Metals **82**, 21.  
 Ku, H.C. and G.P. Meisner, 1981, J. Less-Common Metals **78**, 99.  
 Rogl, P., 1979, Monatsh. Chem. **110**, 235.  
 Rupp, B., P. Rogl and R. Sobczak, 1979, Mater. Res. Bull. **14**, 1301.

### Nd–Ni–B

The phase equilibria within two partial isothermal sections of the system Nd–Ni–B are presented in fig. 39 and are primarily based on the work of Bilonishko et al. (1982). 160 samples were prepared by arc melting compacts of Nd ingot (99.07% pure) and Ni (99.98%) and B (99.5%) powders and subsequent annealing in

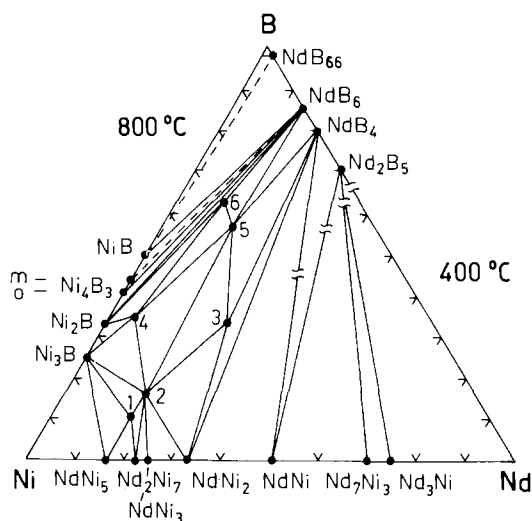


Fig. 39. Nd-Ni-B, partial isothermal sections at 800°C (region 0–30 a/o Nd) and at 400°C (region 30–100 a/o Nd). 1:  $\text{Nd}_3\text{Ni}_{13}\text{B}_2$  (earlier  $\text{NdNi}_5\text{B}$ ), 2:  $\text{NdNi}_4\text{B}$ , 3:  $\text{Nd}_3\text{Ni}_5\text{B}_4$  (earlier  $\text{NdNi}_2\text{B}_2$ ?), 4:  $\text{NdNi}_{12}\text{B}_7$ , 5:  $\text{NdNi}_2\text{B}_4$ , 6:  $\text{NdNi}_3\text{B}_7$ .

evacuated silica tubes. Heating conditions were 500 h at 800°C for alloys containing 0–33 a/o Nd and 700 h at 400°C for alloys with 33–100 a/o Nd.

The Nd-Ni binary system is in good accord with a recent compilation by Iandelli and Palenzona (1979):  $\text{NdNi}_5$  (CaCu<sub>5</sub>-type),  $\text{Nd}_2\text{Ni}_7$  ( $\text{Gd}_2\text{Ni}_7$ -,  $\text{Ce}_2\text{Ni}_7$ -type; both structure types were observed at 800°C, equilibrium?, see also Virkar and Raman, 1969),  $\text{NdNi}_3$  ( $\text{PuNi}_3$ -type),  $\text{NdNi}_2$  ( $\text{MgCu}_2$ -type),  $\text{NdNi}$  ( $\text{CrB}$ -type),  $\text{Nd}_7\text{Ni}_3$  ( $\text{Th}_7\text{Fe}_3$ -type) and  $\text{Nd}_3\text{Ni}$  ( $\text{Fe}_3\text{C}$ -type).  $\text{Nd}_2\text{Ni}_{17}$  with  $\text{Th}_2\text{Ni}_{17}$ -type was not observed at 800°C (unstable).

The mutual solid solubilities of the binary compounds were reported to be insignificant; six ternary borides have been identified by X-ray and metallographic analysis.

The crystal structure of  $\text{Nd}_3\text{Ni}_{13}\text{B}_2$  has been refined by Kuz'ma and Bilonishko (1981) from X-ray powder photographs:  $\text{Nd}_3\text{Ni}_{13}\text{B}_2$ -type, CaCu<sub>5</sub>-type derivative,  $P6/mmm$ ,  $a = 5.005(3)$ ,  $c = 10.904(9)$ ,  $\rho_{\text{exp}} = 8.41$ ,  $\rho_{\text{theor}} = 8.54 \text{ kg/dm}^3$ ;  $R = 0.125$ . Atom positions derived were as follows: Nd in 1a), 2e) and 3g); Ni in 4h) 1/3, 2/3, 0.323; Ni in 6i) 1/2, 0, 0.134 and B in 2c). Kuz'ma et al. (1981) reported  $a = 5.011$ ,  $c = 10.87$ . In a review article by Kuz'ma et al. (1979)  $\text{Nd}_3\text{Ni}_7\text{B}_2$  was reported to crystallize with the  $\text{Dy}_3\text{Ni}_7\text{B}_2$ -type ( $P6_3/mmc$ ), but this was not confirmed by Kuz'ma and Chaban (1980) and not observed by Bilonishko et al. (1982).

The crystal structure of  $\text{NdNi}_4\text{B}$ , earlier reported by Kuz'ma and Bilonishko (1981), has been refined from single crystal X-ray counter data:  $\text{NdNi}_4\text{B}$  is isostructural with  $\text{CeCo}_4\text{B}$ ,  $P6/mmm$ ,  $a = 5.043(2)$ ,  $c = 6.941(6)$ ;  $R = 0.126$ . The atom parameters derived were: Nd in 1a, 1b; Ni in 2c and 6i [ $z = 0.280(3)$ ]; B in 2d (Bilonishko et al., 1982).

From a preliminary single crystal X-ray study of  $\text{Nd}_3\text{Ni}_5\text{B}_4$  a monoclinic symmetry was found; the possible space groups are  $C2/c$  and  $Cc$ ,  $a = 9.52(4)$ ,  $b = 5.13(2)$ ,  $c = 10.82(4)$  and  $\beta = 100.0(5)^\circ$  (Bilonishko et al., 1982). The phase  $\text{Nd}_3\text{Ni}_5\text{B}_4$  is likely to be identical with  $\text{NdNi}_{\sim 2}\text{B}_{\sim 2}$  reported earlier by Kuz'ma and Bilonishko (1981). The crystal structure types of the new borides  $\text{NdNi}_{12}\text{B}_7$ ,  $\text{NdNi}_2\text{B}_4$  and  $\text{NdNi}_3\text{B}_7$  have not yet been determined.

### References

- Bilonishko, N.S., B.I. Krik and Yu.B. Kuz'ma, 1982, *Dopov. Akad. Nauk Ukr. RSR, Ser. A* **4**, 22.  
 Iandelli, A. and A. Palenzona, 1979, *Crystal chemistry of intermetallic compounds*, in: *Handbook on the Physics and Chemistry of Rare Earths*, Vol. 2, eds. K.A. Gschneidner and L. Eyring (North-Holland, Amsterdam) pp. 1-54.  
 Kuz'ma, Yu.B. and N.S. Bilonishko, 1981, *Dopov. Akad. Nauk Ukr. RSR, Ser. A* **10**, 88.  
 Kuz'ma, Yu.B. and N.F. Chaban, 1980, *Dopov. Akad. Nauk Ukr. RSR, Ser. A*, 88.  
 Kuz'ma, Yu.B., N.S. Bilonishko, S.F. Mikhalenko, G.F. Stepanchikova and N.F. Chaban, 1979, *J. Less-Common Metals* **67**, 51.  
 Kuz'ma, Yu.B., N.S. Bilonishko, N.F. Chaban and G.V. Chernjak, 1981, *J. Less-Common Metals* **82**, 364.  
 Virkar, A.V. and A. Raman, 1969, *J. Less-Common Metals* **18**(1), 59.

### Nd-Os-B

One ternary phase has been identified in the Nd-Os-B system.

$\text{NdOs}_4\text{B}_4$  [ $\text{NdCo}_4\text{B}_4$ -type,  $P4_2/n$ ,  $a = 7.552(3)$ ,  $c = 4.003(2)$ ] forms congruently from the melt (Rogl, 1979; X-ray and metallographic analysis). For sample preparation, see  $\text{LaOs}_4\text{B}_4$ . Atom parameters were refined from single crystal automatic diffractometer data:  $a = 7.5591(13)$ ,  $c = 4.0026(9)$ ,  $R = 0.08$ ; 2 Nd in 2b); 8 Os in 8g) 0.6061(2), 0.1418(2), 0.1372(3); 8 B in 8g) 0.532(6), 0.415(5), 0.150(8) (Hiebl et al., 1981). Magnetic behavior was studied by Rupp et al. (1979) and Hiebl et al. (1981);  $T_n = 1.5$  K.

### References

- Hiebl, K., M.J. Sienko and P. Rogl, 1981, *J. Less-Common Metals* **82**, 21.  
 Rogl, P., 1979, *Monatsh. Chem.* **110**, 235.  
 Rupp, B., P. Rogl and R. Sobczak, 1979, *Mater. Res. Bull.* **14**, 1301.

### Nd-Rh-B (see also notes added in proof)

Ku et al. (1980) analysed the crystal structure as well as superconducting and magnetic properties of arc melted alloys  $\text{NdRh}_3\text{B}_2$  with  $\text{CeCo}_3\text{B}_2$ -type of structure,  $P6/mmm$ ,  $a = 5.466(6)$ ,  $c = 3.109(4)$ ;  $T_m = 13.5$  K; see also Malik et al. (1982).

$\text{NdRh}_4\text{B}_4$  has the  $\text{CeCo}_4\text{B}_4$ -type of structure,  $P4_2/nmc$ ,  $a = 5.333(2)$ ,  $c = 7.468(2)$ , from X-ray powder analysis by Vandenberg and Matthias (1977); for sample preparation, see  $\text{YRh}_4\text{B}_4$ ;  $T_c = 5.36-5.26$  K (Matthias et al., 1977). From unpublished data by MacKay et al., as quoted by Ku et al. (1979),  $\text{NdRh}_4\text{B}_4$  was claimed to be a metastable compound. Features in the upper critical field and heat capacity data at 1.31 K and 0.89 K (two magnetic transitions) suggested the occurrence of long-range magnetic order in the superconducting state (Hamaker et al., 1979).



For the perovskite boride  $\text{NdRh}_3\text{B}_{1-x}$  with  $\text{Cu}_3\text{Au}$ -type,  $a = 4.195$ ,  $x = 0.1$ , see also R–Rh–B.

### References

- Hamaker, H.C., L.D. Woolf, H.B. MacKay, Z. Fisk and M.B. Maple, 1979, *Solid State Commun.* **31**, 139.  
 Ku, H.C., D.C. Johnston, B.T. Matthias, H. Barz, G. Burri and L. Rinderer, 1979, *Mater Res. Bull.* **14**, 1591.  
 Ku, H.C., G.P. Meisner, F. Acker and D.C. Johnston, 1980, *Solid State Commun.* **35**, 91.  
 Malik, S.K., S.K. Dhar, R. Vijayaraghavan and W.E. Wallace, 1982, *J. Appl. Phys.* **53**(1), 8074.  
 Matthias, B.T., E. Corenzwit, J.M. Vandenberg and H.E. Barz, 1977, *Proc. Nat'l Acad. Sci. US* **74**(4), 1334.  
 Vandenberg, J.M. and B.T. Matthias, 1977, *Proc. Nat'l Acad. Sci. US* **74**(4), 1336.

### Nd–Ru–B

The crystal structure of congruently melted  $\text{NdRu}_3\text{B}_2$  ( $\text{CeCo}_3\text{B}_2$ -type,  $P6/mmm$ ) was determined from X-ray powder data by Hiebl et al. (1980):  $a = 5.538(4)$ ,  $c = 3.010(2)$ , ferromagnetic transition at  $T_m = 39$  K. Data by Ku et al. (1980) confirm  $a = 5.544(6)$ ,  $c = 3.010(4)$ ,  $T_m = 33.2$  K. For sample preparation, see  $\text{YRu}_3\text{B}_2$ .

$\text{NdRu}_4\text{B}_4$  has the  $\text{LuRu}_4\text{B}_4$ -type of structure,  $I4_1/acd$ ,  $a = 7.502(5)$ ,  $c = 15.053(10)$ , as determined by Johnston (1977) by X-ray powder analysis of arc melted samples;  $T_m = 1.62$  K.

### References

- Hiebl, K., P. Rogl, E. Uhl and M.J. Sienko, 1980, *Inorg. Chem.* **19**(11), 3316.  
 Johnston, D.C., 1977, *Solid State Commun.* **24**(10), 699.  
 Ku, H.C., G.P. Meisner, F. Acker and D.C. Johnston, 1980, *Solid State Commun.* **35**, 91.

### Nd–Si–B

The influence of boron additions to  $\text{R}_5\text{Si}_3$  compounds was studied (X-ray analysis) by Mayer and Felner (1974) on a series of samples with a nominal boron content according to the formulas:  $\text{Nd}_5\text{Si}_3$ ,  $\text{Nd}_5\text{Si}_3\text{B}_{0.5}$ ,  $\text{Nd}_5\text{Si}_3\text{B}_{1.0}$ ,  $\text{Nd}_5\text{Si}_3\text{B}_{1.5}$  and  $\text{Nd}_5\text{Si}_3\text{B}_{2.0}$ . Alloys were prepared by heating (melting) elemental mixtures of a 99.9% min. purity in Ta crucibles at  $1600^\circ\text{C}$  under He atmosphere.

At a nominal composition of  $\text{Nd}_5\text{Si}_3\text{B}_{1.5}$  the  $\text{Cr}_5\text{B}_3$ -type of structure of  $\text{Nd}_5\text{Si}_3$  was observed to transform into a  $\text{Mn}_5\text{Si}_3$ -type and for lower boron contents the two structure types were reported to coexist. Mayer and Felner (1974) claim the  $\text{Mn}_5\text{Si}_3$ -type phase to be stable up to a composition of  $\text{Nd}_5\text{Si}_3\text{B}_2$ ; lattice parameters are listed in table 6. Boron solubility (filling of octahedral voids) in  $\text{Mn}_5\text{Si}_3$ -type phases, however, is limited to a formula  $\text{R}_5\text{Si}_3\text{B}_{1.0}$ . For higher boron concentrations the boron solubility might be accompanied by simultaneous substitution Si/B, which probably would explain the irregular variation of lattice parameters.

### Reference

- Mayer, I. and I. Felner, 1974, *J. Less-Common Metals* **37**, 171.

*Nd–Sm–B*: see notes added in proof under *Sm–M–B*

TABLE 27  
Formation and structural data of ternary compounds Pr-Co-B.

Compound	Structure type, Space group	Lattice parameters, Density	Preparation, Characterization	Refs.	Purity
PrCo <sub>4</sub> B <sub>4</sub>	NdCo <sub>4</sub> B <sub>4</sub> F4 <sub>2</sub> /n	$a = 7.085(4)$ $c = 3.815(2)$	no details given, PXD	KuB, 78	
PrCo <sub>2</sub> B <sub>2</sub>	ThCr <sub>2</sub> Si <sub>2</sub> I4/mmm	$a = 3.599(3)$ $c = 9.932(5)$	AM, Qu(Mo), 900°C, 70 h	Ro, 73	Pr 99.9 Co 99.5 B 99.0
PrCo <sub>4</sub> B	CeCo <sub>4</sub> B P6/mmm	$a = 5.100(3)$ $c = 6.777(4)$	AM, Qu 800°C, 50 h, PXD	KuB, 73	Pr 99 Co 99.87 B 99.3
Pr <sub>3</sub> Co <sub>11</sub> B <sub>4</sub>	Ce <sub>3</sub> Co <sub>11</sub> B <sub>4</sub> P6/mmm	$a = 5.145(3)$ $c = 9.784(6)$	AM, Qu 800°C, 50 h, PXD	KuB, 73	Pr 99 Co 99.87 B 99.3
Pr <sub>2</sub> Co <sub>7</sub> B <sub>3</sub>	Ce <sub>2</sub> Co <sub>7</sub> B <sub>3</sub> P6/mmm	$a = 5.150(3)$ $c = 12.75(2)$	AM, Qu 800°C, 50 h, PXD	KuB, 73	Pr 99 Co 99.87 B 99.3
Pr <sub>2</sub> Co <sub>5</sub> B <sub>2</sub>	Ce <sub>2</sub> Co <sub>5</sub> B <sub>2</sub> P6 <sub>3</sub> /mmc		no details given	KuBCC, 81	
PrCo <sub>12</sub> B <sub>6</sub>	SrNi <sub>12</sub> B <sub>6</sub> R $\bar{3}$ m	$a_H = 9.506(3)$ $c_H = 7.477(3)$	AM, Qu 800°C, 270 h PXD	KuCC, 81	Pr 99.5 Co 99.95 B 99.4

### Pr-Co-B

No ternary phase diagram exists for the Pr-Co-B system, but seven ternary compounds have been characterized by X-ray powder analysis (table 27).

### References

- Kuz'ma, Yu.B. and N.S. Bilonishko, 1973, *Kristallografiya* **18**(4), 710.  
 Kuz'ma, Yu.B. and N.S. Bilonishko, 1978, *Dopov. Akad. Nauk Ukr. RSR, Ser. A* **3**, 275.  
 Kuz'ma, Yu.B., N.S. Bilonishko, N.F. Chaban and G.V. Chernjak, 1981, *J. Less-Common Metals* **82**, 364.  
 Kuz'ma, Yu.B., G.V. Chernjak and N.F. Chaban, 1981, *Dopov. Akad. Nauk Ukr. RSR, Ser. A* **12**, 80.  
 Rogl, P., 1973, *Monatsh. Chem.* **104**, 1623.

### Pr-Cr-B

The phase equilibria within the 800°C isothermal section of the Pr-Cr-B system are primarily based on the investigation by Mikhalenko and Kuz'ma (1977). The results of X-ray and metallographic analysis of 30 alloys is shown in fig. 40. Sample preparation is the same as described for (La, Ce)-Cr-B. Mutual solid solubilities of binary compounds were found to be negligible. Two ternary compounds have been

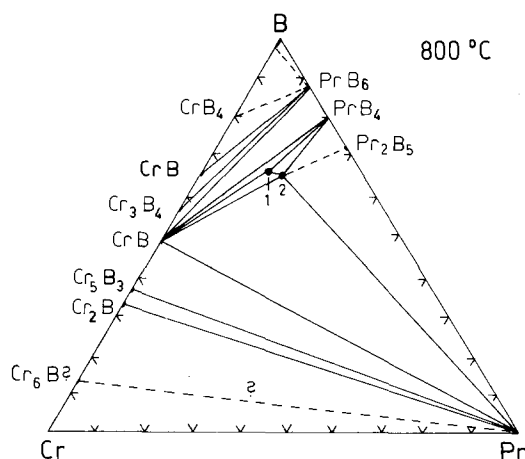


Fig. 40. Pr-Cr-B, isothermal section at 800°C. 1:  $\text{PrCr}_2\text{B}_6$ , 2:  $\text{PrCrB}_4$ .

characterized:  $\text{PrCrB}_4$  with  $\text{YCrB}_4$ -type,  $\text{Pbam}$ ,  $a = 6.058(5)$ ,  $b = 11.72(1)$ ,  $c = 3.563(4)$  (Mikhaleiko and Kuz'ma, 1977), and  $\text{PrCr}_2\text{B}_6$  with  $\text{CeCr}_2\text{B}_6$ -type,  $\text{Immm}$ ,  $a = 6.611(4)$ ,  $b = 8.325(5)$ ,  $c = 3.136(3)$  (Mikhaleiko and Kuz'ma, 1975). Phase equilibria after Mikhaleiko and Kuz'ma (1977) did not include the binary phase  $\text{Pr}_2\text{B}_5$ , which according to La Placa is structurally closely related (lower symmetry) to the structure type of  $\text{Sm}_2\text{B}_5$ . For the Cr-B binary system, see Y-Cr-B.

### References

- La Placa, S., unpublished results.  
 Mikhaleiko, S.I. and Yu.B. Kuz'ma, 1975, *Dopov. Akad. Nauk Ukr. RSR, Ser. A* 5, 465.  
 Mikhaleiko, S.I. and Yu.B. Kuz'ma, 1977, *Dopov. Akad. Nauk Ukr. RSR, Ser. A*, 951.

### Pr-Fe-B

A series of superstructures  $\text{Pr}_{n+m}(\text{Fe}_4\text{B}_4)_n$  have recently been observed by Braun et al. (1982) in the Pr-Fe-B system (table 2). Their crystal structures derive from the  $\text{NdCo}_4\text{B}_4$ -type of structure and are either incommensurate or have unusual large repeat units along the  $c$ -axis. Samples were prepared by arc melting  $\text{Pr}_{1.1}\text{Fe}_4\text{B}_4$  alloys with subsequent heat treatment at 1000°C, 10–14 days.

The addition of Pr to iron-boron melts,  $\text{Pr}_x(\text{Fe}_{0.8}\text{B}_{0.2})_{1-x}$ , was observed to stabilize the glassy structure. At  $x = 0.1$  and  $T = 899$  K a maximum appeared in the crystallization onset temperature, measured at a heating rate of 20 K/min (Kabacoff et al., 1982).

### References

- Braun, H.F., M. Pelizzone and K. Yvon, 1982, Ferromagnetic borides with incommensurate rare earth and iron sublattices:  $\text{R}_{1+\epsilon}\text{Fe}_4\text{B}_4$ , paper presented at the 7th Intern. Conf. on Solid Compounds of Transition Elements, Grenoble (June 21–26), Proceedings, II B11.  
 Kabacoff, L., S. Dallek, C. Modzelewski and W. Krull, 1982, *J. Appl. Phys.* 53(3), 2255.

*Pr-Ir-B*

$\text{PrIr}_4\text{B}_4$ ,  $\text{NdCo}_4\text{B}_4$ -type,  $\text{P4}_2/\text{n}$ ,  $a = 7.629(3)$ ,  $c = 3.974(2)$ , forms congruently from the melt (X-ray and metallographic analysis, Rogl, 1979); for sample preparation, see  $\text{LaOs}_4\text{B}_4$ . Magnetic data were presented by Rupp et al. (1979) and Hiebl et al. (1981);  $T_n = 1.5$  K;  $T_m < 1$  K.

Ku and Meisner (1981), mentioned the existence of a compound  $\text{PrIr}_3\text{B}_2$  with the  $\text{CeCo}_3\text{B}_2$ -type of structure; no further details were given.

*References*

- Hiebl, K., M.J. Sienko and P. Rogl, 1981, *J. Less-Common Metals* **82**, 21.  
 Ku, H.C. and G.P. Meisner, 1981, *J. Less-Common Metals* **78**, 99.  
 Rogl, P., 1979, *Monatsh. Chem.* **110**, 235.  
 Rupp, B., Rogl and R. Sobczak, 1979, *Mater. Res. Bull.* **14**, 1301.

*Pr-Ni-B*

No ternary phase diagram is available for the Pr-Ni-B system.

Niihara et al. (1973) mentioned the existence of a ternary compound  $\text{PrNi}_4\text{B}$ , presumably isostructural with  $\text{YNi}_4\text{B}$ ; Kuz'ma et al. (1981) in a review article confirmed the  $\text{CeCo}_4\text{B}$ -type;  $a = 5.063(2)$ ,  $c = 6.951(5)$ ,  $\text{P6}/\text{mmm}$ .

$\text{Pr}_3\text{Ni}_{13}\text{B}_2$  has been characterized with the  $\text{Nd}_3\text{Ni}_{13}\text{B}_2$ -type of structure,  $\text{P6}/\text{mmm}$ ,  $a = 5.019(1)$ ,  $c = 10.929(5)$  (Kuz'ma and Bilonishko, 1981, X-ray powder analysis).

*References*

- Kuz'ma, Yu.B. and N.S. Bilonishko, 1981, *Dopov. Akad. Nauk Ukr. RSR, Ser. A* **10**, 88.  
 Kuz'ma, Yu.B., N.S. Bilonishko, N.F. Chaban and G.V. Chernjak, 1981, *J. Less-Common Metals* **82**, 364; see also 1983, *J. Less-Common Metals* **90**, 219.  
 Niihara, K., Y. Katayama and S. Yajima, 1973, *Chem. Lett (Chem. Soc. Jpn)* 613.

*Pr-Os-B*

Metallographic and X-ray powder data of arc melted as well as heat treated alloys revealed congruent melting behavior for  $\text{PrOs}_4\text{B}_4$ ,  $\text{NdCo}_4\text{B}_4$ -type,  $\text{P4}_2/\text{n}$ ,  $a = 7.567(3)$ ,  $c = 4.002(2)$  (Rogl, 1979); for sample preparation, see  $\text{LaOs}_4\text{B}_4$ . Magnetic data were presented by Hiebl et al. (1981);  $T_n = 1.5$  K.

$\text{PrOs}_{\sim 2}\text{B}_{\sim 2}$  with unknown structure type was observed by Rogl (1981, unpublished data) in arc melted alloys.

*References*

- Hiebl, K., M.J. Sienko and P. Rogl, 1981, *J. Less-Common Metals* **82**, 21.  
 Rogl, P., 1979, *Monatsh. Chem.* **110**, 235.

*Pr-Rh-B*

Ku et al. (1980) investigated the crystal structure (powder X-ray analysis) as well as magnetic and superconducting properties of arc melted alloys  $\text{PrRh}_3\text{B}_2$  with  $\text{CeCo}_3\text{B}_2$ -type,  $\text{P6}/\text{mmm}$ ,  $a = 5.461(6)$ ,  $c = 3.105(4)$ ;  $T_m = 1.68$  K; see also Malik et al. (1982).

Matthias et al. (1977) mentioned the existence of a metastable compound  $\text{PrRh}_4\text{B}_4$  ( $\text{CeCo}_4\text{B}_4$ -type?) from arc melted alloys, containing excess RhB. No details were given.

For the perovskite-type boride  $\text{PrRh}_3\text{B}_{1-x}$  with  $\text{Cu}_3\text{Au}$ -type,  $a = 4.213$ ,  $x = 0.25$ , see also R-Rh-B.

### References

- Ku, H.C., G.P. Meisner, F. Acker and D.C. Johnston, 1980, *Solid State Commun.* **35**, 91.  
 Malik, S.K., S.K. Dhar, R. Vijayaraghavan and W.E. Wallace, 1982, *J. Appl. Phys.* **53**(11), 8076.  
 Matthias, B.T., E. Corenzwit, J.M. Vandenberg and E. Barz, 1977, *Proc. Nat'l Acad. Sci. US* **74**(4), 1334.

### Pr-Ru-B

Two compounds were identified in the Pr-Ru-B system.

The crystal structure of  $\text{PrCo}_3\text{B}_2$  ( $\text{CeCo}_3\text{B}_2$ -type, P6/mmm) has been analysed from X-ray powder data (Hiebl et al., 1980):  $a = 5.532(4)$ ,  $c = 3.015(2)$ , congruent melting, ferromagnetic transition at  $T_m = 5$  K. Ku et al. (1980) reported  $a = 5.554(6)$ ,  $c = 3.006(4)$  and  $T_m = 6.85$  K. For sample preparation techniques, see  $\text{YRu}_3\text{B}_2$ .

Johnston (1977) established the  $\text{LuRu}_4\text{B}_4$ -type of structure for  $\text{PrRu}_4\text{B}_4$  by X-ray powder methods:  $I4_1/acd$ ,  $a = 7.505(5)$ ,  $c = 15.066(10)$ ; samples were arc melted, but due to possible instability or metastability of  $\text{PrRu}_4\text{B}_4$  the alloys obtained were multiphase.

### References

- Hiebl, K., P. Rogl, E. Uhl and M.J. Sienko, 1980, *Inorg. Chem.* **19**(11), 3316.  
 Johnston, D.C., 1977, *Solid State Commun.* **24**(10), 699.  
 Ku, H.C., G.P. Meisner, F. Acker and D.C. Johnston, 1980, *Solid State Commun.* **35**, 91.

*Pr-Sm-B*: see notes added in proof under Sm-M-B

### Sc-Co-B

Using X-ray and metallographic analysis, Stepanchikova (1979) established the phase equilibria of the Sc-Co-B system within two partial isothermal sections: for 0-33 a/o Sc at 800°C, and for 33-100 a/o Sc at 600°C (fig. 41). Samples were prepared by arc melting compacts of Sc ingot (99.84% Sc) and 99.4% Co and 99.4% B powders, followed by heat treatment for 600 h. The boron-rich region B- $\text{ScB}_{12}$ -CoB has not been investigated and is proposed (fig. 41).

According to earlier results by Peshev et al. (1970)  $\text{ScB}_2$  and  $\text{ScB}_{12}$  are the only binary compounds in equilibrium. The solid solubility of Sc in  $\beta$ -boron at elevated temperatures was established to be  $\text{ScB}_{\sim 28}$  from a single crystal study,  $a = 10.966$ ,  $c = 24.088$  (arc melted, quenched; Callmer, 1978). Furthermore from single crystal data a tetragonal symmetry  $a = 5.22$ ,  $c = 7.40$  was confirmed for  $\text{ScB}_{12}$  (Callmer, 1978; Stepanchikova, 1979).  $\text{Sc}_2\text{Co}$  ( $\text{CuAl}_2$ -type),  $\text{ScCo}$  ( $\text{CsCl}$ -type) and  $\text{ScCo}_2$  ( $\text{MgCu}_2$ -type) were confirmed. " $\text{Sc}_2\text{Co}$ " with  $\text{Ti}_2\text{Ni}$ -type (Gladyshevskii et al., 1964) probably is impurity (C, N, O)-stabilized. The crystal structure of  $\text{Sc}_3\text{Co}$  ( $\text{Sc}_3\text{Co}$ -type, Pnma,  $a = 13.102(9)$ ,  $b = 8.624(6)$ ,  $c = 5.829(3)$ ,  $\rho_{\text{theor}} = 3.913$  kg/dm<sup>3</sup>) has recently been established by Chabot and Parthé (1978). According to Schöbel and Stadelmaier (1966) the Co-B system:  $\text{Co}_3\text{B}$  ( $\text{Fe}_3\text{C}$ -type),  $\text{Co}_2\text{B}$  ( $\text{Al}_2\text{Cu}$ -type), and CoB

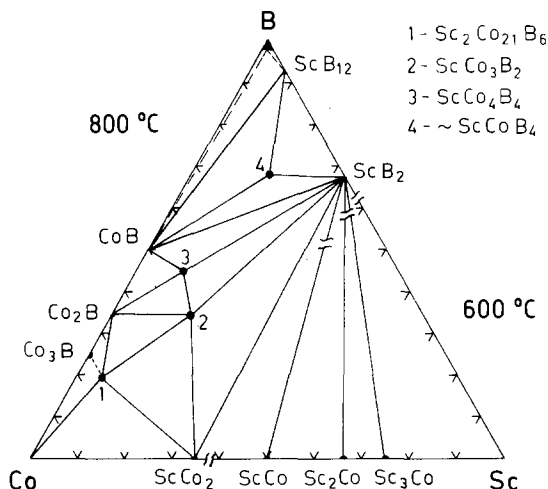


Fig. 41. Sc-Co-B, partial isothermal sections at 800°C (0–33 a/o Sc), and at 600°C (33–100 a/o Sc).

(FeB-type), exhibits a metastable eutectic  $L \rightleftharpoons \text{Co}_2\text{B} + (\text{Co})$ ; thus solidification of stable  $\text{Co}_3\text{B}$  is frequently suppressed. Considerable doubt exists about the formation of a compound  $\text{CoB}_n$ ,  $n \geq 12$  (Avlokhashvili et al., 1979), which rather seems to belong to the solid solution of Co in  $\beta$ -rh. B (Carlsson and Lundström, 1970).

Solid solubilities of binary compounds obviously were considered to be negligible. The existence of the  $\text{ScCo}_3\text{B}_2$  and  $\text{Sc}_2\text{Co}_{21}\text{B}_6$  phases (see below) was confirmed and two more compounds were observed. The structure type of  $\text{ScCoB}_{\sim 4}$  is unknown and  $\text{ScCo}_4\text{B}_4$  has the  $\text{CeCo}_4\text{B}_4$ -type of structure,  $P4_2/nmc$ ,  $a = 4.902(5)$ ,  $c = 6.961(5)$ . From powder X-ray analysis a sample of  $\text{ScCo}_4\text{B}_4$  contained small amounts of  $\text{CoB}$  and  $\text{Co}_2\text{B}$ ; atom positions were found to be: Sc in 2b), Co in 8g)  $1/4$ ,  $-0.003$ ,  $0.384$  and B in 8g)  $1/4$ ,  $0.08$ ,  $0.10$ .

Kuz'ma and Voroshilov (1967) obtained the  $\tau$ -phase  $\text{Sc}_2\text{Co}_{21}\text{B}_6$ ,  $\text{Cr}_{23}\text{C}_6$ -type,  $\text{Fm}3m$ ,  $a = 10.537(5)$ , by reacting compacted powder mixtures (Sc, Co: 99.9%; B amorphous: 99.5%) at 1200°C for 2 h in vacuum, followed by a heat treatment at 800°C, 120 h in evacuated silica tubes. From X-ray intensities Sc was proposed to occupy the 8c sites.

$\text{ScCo}_3\text{B}_2$  with  $\text{CeCo}_3\text{B}_2$ -type of structure,  $P6/mmm$ ,  $a = 4.889(3)$ ,  $c = 2.977(2)$  was first obtained by Kuz'ma et al. (1969) from powder X-ray analysis; for sample preparation, see  $\text{YCo}_3\text{B}_2$ . Rogl (1973), from Debye-Scherrer photographs, confirmed the structure type, but unit cell dimensions  $a = 4.864(5)$ ,  $c = 2.997(1)$  were found to be considerably different from those reported by Kuz'ma et al. (1969); for sample preparation, see  $\text{YCo}_3\text{B}_2$ .

Attempts to prepare  $\text{ScCo}_4\text{B}$  ( $\text{CeCo}_4\text{B}$ -type),  $\text{Sc}_3\text{Co}_{11}\text{B}_4$  ( $\text{Ce}_3\text{Co}_{11}\text{B}_4$ -type) and  $\text{Sc}_2\text{Co}_7\text{B}_3$  ( $\text{Ce}_2\text{Co}_7\text{B}_3$ -type) were unsuccessful (Kuz'ma and Bilonishko 1974).

### References

- Avlokhashvili, J.A., F.N. Tavadze, G.F. Tavadze, D.N. Tsikaridze, D.L. Gabunia and K.P. Tsomaya, 1979, *J. Less-Common Metals* **67**, 367.  
Callmer, B., 1978, *J. Solid State Chem.* **23**, 391.

- Carlsson, J.O. and T. Lundström, 1970, *J. Less-Common Metals* **22**, 317.  
 Chabot, B. and E. Parthé, 1978, *Acta Crystallogr.* **B34**, 3173.  
 Gladyshevskii, E.I., E.M. Savitskii and V.F. Tereskhova, eds., 1964, *Voprosy Teorii i Primeneniya Redkozemelnykh Metallov* (Akad. Nauk SSSR, Moscow) pp. 153–154.  
 Kuz'ma, Yu.B. and N.S. Bilonishko, 1974, *Kristallografiya* **18**(4), 710.  
 Kuz'ma, Yu.B. and Yu.V. Voroshilov, 1967, *Sov. Phys. Crystallogr.* **12**(2), 297.  
 Kuz'ma, Yu.B., P.I. Kripyakevich and N.S. Bilonishko, 1969, *Dopov. Akad. Nauk Ukr. RSR, Ser. A* **10**, 939.  
 Peshev, P., J. Etourneau and R. Naslain, 1970, *Mater. Res. Bull.* **5**, 323.  
 Rogl, P., 1973, *Monatsh. Chem.* **104**, 1623.  
 Schöbel, J.D. and H.H. Stadelmaier, 1966, *Z. Metallkde* **57**, 323.  
 Stepanchikova, G.F., 1979, *Visn. L'vov Politekh. Inst.* **130**, 58.

### *Sc-Cr-B*

Specific heat anomaly was observed by Vandenberg et al. (1976) in an arc melted sample  $\text{Sc}_{0.75}\text{Cr}_{0.1875}\text{B}_{0.0625}$  confirming earlier indications (Arrhenius et al., 1964) of a superconducting Sc-Cr-B compound. Superconductivity (6.4 K) was considerably reduced on annealing at lower temperatures (500–650°C). By metallographic and X-ray analysis the superconducting phase (estimated content 15–20%) was identified as a metastable, boron-stabilized  $\text{Ti}_2\text{Ni}$ -type structure:  $\text{Sc}_{2.15}\text{Cr}_{0.85}\text{B}_x$ ,  $x < 0.01$ , Fd3m,  $a = 12.33 \text{ \AA}$ .

### *References*

- Arrhenius, O., T.H. Geballe and B.T. Matthias, 1964, *Bull. Amer. Phys. Soc. Ser. 8* II(4), 294.  
 Vandenberg, J.M., B.T. Matthias, E. Corenzwit and H. Barz, 1976, *J. Solid State Chem.* **18**, 395.

### *Sc-Fe-B*

The investigation of an isothermal section of the system, Sc-Fe-B revealing no ternary compounds, was mentioned by Kuz'ma et al. (1979); however, no detailed information has yet been published; see notes added in proof.

### *Reference*

- Kuz'ma, Yu.B., N.S. Bilonishko, S.I. Mikhaleiko, G.F. Stepanchikova and N.F. Chaban, 1979, *J. Less-Common Metals* **67**, 51.

### *Sc-In-B*

The stabilizing influence of boron atoms as filler atoms in the octahedral sites of the perovskite metal host lattice structure ( $\text{Cu}_3\text{Au}$ -type, Pm3m) was demonstrated by Holleck (1977) by means of X-ray and metallographic analysis of arc melted alloys, homogenized at 800°C. The lattice parameter for  $\text{Sc}_3\text{InB}_{1-x}$  was  $a = 4.560(2)$ ;  $x$  was not specified. But for the alloy  $\text{Sc}_3\text{In}$  no  $\text{Cu}_3\text{Au}$  lattice was observed, which is in agreement with Compton and Matthias (1962), who report a hexagonal  $\text{Ni}_3\text{Sn}$ -type structure for this phase,  $a = 6.421$  and  $c = 5.183$ .

*References*

- Compton, V.B. and B.T. Matthias, 1962, *Acta Crystallogr.* **15**, 94.  
 Holleck, H., 1977, *J. Less-Common Metals* **52**, 167.

*Sc-Ir-B*

At least two ternary compounds exist in the Sc-Ir-B system.

ScIr<sub>3</sub>B<sub>4</sub> was characterized by Rogl and Nowotny (1979) by X-ray analysis of arc melted and homogenized alloys (1100°C, 48 h, BN substrate, 10<sup>-4</sup> Pa). Starting materials were presintered compacts of Sc filings 99.9%, and Ir 99.9% and B 99.0% powders. ScIr<sub>3</sub>B<sub>4</sub> is isostructural with ZrIr<sub>3</sub>B<sub>4</sub>, P6<sub>3</sub>/m,  $a = 7.576(2)$ ,  $c = 3.442(1)$ ; practically no homogeneous range exists (1100°C, quench). The atomic positions were refined from X-ray powder intensities: 2 Sc in 2d), 6 Ir in 6h) 0.0753, 0.3273, 1/4; 6 B in 6h) 0.406, 0.460, 1/4; 2 B in 2a);  $T_n = 1.5$  K.

The crystal structure of ScIr<sub>3</sub>B<sub>2</sub> was found to be isostructural with the structure type of ErIr<sub>3</sub>B<sub>2</sub>, possible space group C2/m,  $a = 5.344(6)$ ,  $b = 9.307(9)$ ,  $c = 3.062(4)$ ,  $\beta = 92.1(1)^\circ$ , from powder X-ray analysis of arc melted samples (Ku and Meisner, 1981).

The stabilizing influence of boron atoms in the octahedral sites of the perovskite metal host lattice structure was investigated by Holleck (1977) for ScIr<sub>3</sub>B<sub>1-x</sub>,  $a = 3.999(2)$ , Pm3m, Cu<sub>3</sub>Au-type, by X-ray and metallographic analysis of arc melted alloys, homogenized at 1300°C.

*References*

- Holleck, H., 1977, *J. Less-Common Metals* **52**, 167.  
 Ku, H.C. and G.P. Meisner, 1981, *J. Less-Common Metals* **78**, 99.  
 Rogl, P. and H. Nowotny, 1979, *J. Less-Common Metals* **67**, 41.

*Sc-Ni-B* (see also notes added in proof)

Kuz'ma and Voroshilov (1967) obtained a  $\tau$ -phase Sc<sub>3</sub>Ni<sub>20</sub>B<sub>6</sub> by reacting powder compacts at 1200°C, 12 h in vacuum and subsequent homogenizing in evacuated silica tubes, 800°C, 120 h [Cr<sub>23</sub>C<sub>6</sub>-type, Fm3m,  $a = 10.585(5)$ ]. From X-ray powder data Sc atoms were proposed to fill the 8c sites, the rest being statistically distributed with Ni atoms in the 4a, 32f and 48h sites.

*Reference*

- Kuz'ma, Yu.B. and Yu.V. Voroshilov, 1967, *Sov. Phys. Crystallogr.* **12**(2), 297.

*Sc-Os-B*

The crystal structure of ScOsB<sub>2</sub> has been established by Shelton et al. (1980) by means of X-ray powder diffractometry: LuRuB<sub>2</sub>-type, Pnma,  $a = 5.647(6)$ ,  $b = 5.178(5)$ ,  $c = 6.184(7)$ . Samples were prepared by arc melting compacts of elemental powder mixtures with subsequent annealing at 1250°C for 24 h, followed by heat treatment at 800°C for 9 days in Ta crucibles sealed under Ar. Powder



patterns also contained an unidentified second phase.  $T_c = 1.34\text{--}1.22$  K (Ku and Shelton, 1980).

$\text{Sc}_2\text{Os}_5\text{B}_4$  is isostructural with the crystal structure of  $\text{Sc}_2\text{Ru}_5\text{B}_4$ , P2/m (Rogl, 1983; X-ray powder analysis of arc melted alloys).

$\text{ScOsB}_4$  with unknown structure type has been observed from arc melted samples (Rogl, 1983).

### References

Ku, H.C. and R.N. Shelton, 1980, *Mater. Res. Bull.* **15**(10), 1441.

Rogl, P., 1983, *J. Less-Common Metals*, to be published.

Shelton, R.N., B.A. Karcher, D.R. Powell, R.A. Jacobson and H.C. Ku, 1980, *Mater. Res. Bull.* **15**, 1445.

### Sc-Pb-B

The stabilizing influence of boron atoms as filler atoms in the octahedral sites of the Perovskite metal host lattice structure ( $\text{Cu}_3\text{Au}$ -type, Pm3m) was demonstrated by Holleck (1977) by means of X-ray and metallographic analysis of arc melted alloys, homogenized at  $800^\circ\text{C}$ . The lattice parameter for  $\text{Sc}_3\text{PbB}_{1-x}$  was  $a = 4.622(2)$ ;  $x$  was not specified, but for the alloy  $\text{Sc}_3\text{Pb}$  no  $\text{Cu}_3\text{Au}$  lattice was observed.

### Reference

Holleck, H., 1977, *J. Less-Common Metals* **52**, 167.

### Sc-Rh-B

The stabilizing influence of boron as filler atom in the octahedral sites of the perovskite metal host lattice structure ( $\text{Cu}_3\text{Au}$ -type, Pm3m) was investigated by Holleck (1977) by means of X-ray and metallographic analysis of arc melted alloys, homogenized at  $1300^\circ\text{C}$ . Lattice parameters, as read from a graph, change from binary  $\text{ScRh}_3$ :  $a = 3.900$ , to  $\text{ScRh}_3\text{B}_{0.25}$ :  $a = 3.94$ ,  $\text{ScRh}_3\text{B}_{0.5}$ :  $a = 3.98$ ,  $\text{ScRh}_3\text{B}_{0.75}$ :  $a = 4.03$  and  $\text{ScRh}_3\text{B}$ :  $a = 4.078(2)$ .

### Reference

Holleck, H., 1977, *J. Less-Common Metals* **52**, 167.

### Sc-Ru-B

Some information about phase equilibria in the monoboride region of the Sc-Ru-B system is found from an investigation of superconductivity by Ku et al. (1979). Samples were arc melted and annealed below  $1300^\circ\text{C}$ , wrapped in Ta foils and then sealed under Ar in quartz tubes or sealed under Ar in Ta tubes. One sample  $\text{ScRu}_4\text{B}_4$  has been annealed at  $1400^\circ$  in a Ta tube furnace under Ar and quenched to room temperature in a Ga-In eutectic solution. Compositions were checked by electronmicroprobe analysis. From this  $\text{ScRuB}_4$  and " $\text{ScRu}_2\text{B}_2$ " were reported as two nonsuperconducting single-phase compounds with unknown structure type.

$\text{ScRu}_4\text{B}_4$  with the  $\text{LuRu}_4\text{B}_4$ -type of structure ( $I4_1/acd$ ,  $a = 7.346$ ,  $c = 14.895$ ) was

claimed to be metastable with  $T_c = 7.23\text{--}6.30$  K. On annealing at  $800\text{--}1300^\circ\text{C}$  the phase disappears. The crystal structure has been analysed by means of X-ray powder diffractometry. Electron microprobe analysis of an arc melted sample  $\text{ScRu}_6\text{B}_6$  revealed four areas of different composition:  $\text{Sc}_{0.96}\text{Ru}_{4.00}\text{B}_{3.83}$ ,  $\text{Sc}_{1.03}\text{Ru}_{4.00}\text{B}_{3.83}$ , a fine mixture of phases with overall composition  $\text{Sc}_{0.09}\text{Ru}_{1.00}\text{B}_{0.92}$ , and  $\text{Sc}_{1.01}\text{Ru}_{2.00}\text{B}_{2.96}$  ( $\text{Sc}_{0.96}\text{Ru}_{4.00}\text{B}_{3.83}$  corresponds to  $\text{ScRu}_4\text{B}_4$  and indicates small boron deficiency).

According to Ku et al. (1979) the following two-phase equilibria were observed:  $\text{RuB}\text{--}\text{ScRuB}_4$ , “ $\text{ScRu}_2\text{B}_2$ ”– $\text{ScRuB}_4$ , “ $\text{ScRu}_2\text{B}_2$ ”– $\text{Ru}_7\text{B}_3$  and metastable equilibria for  $\text{ScRu}_4\text{B}_4$  with each of the phases  $\text{ScRuB}_4$ , “ $\text{ScRu}_2\text{B}_2$ ”,  $\text{RuB}$ ,  $\text{Ru}_7\text{B}_3$ . “ $\text{ScRu}_2\text{B}_2$ ” was shown quite recently to correspond to a correct formula of  $\text{Sc}_2\text{Ru}_5\text{B}_4$  ( $\text{Sc}_2\text{Ru}_5\text{B}_4$ -type, P2/m):  $a = 9.953$ ,  $b = 8.452$ ,  $c = 3.004$ ,  $\beta = 90.0(1)^\circ$  (Rogl, 1983).

### References

- Ku, H.C., D.C. Johnston, B.T. Matthias, H. Barz, G. Burri and L. Rinderer, 1979, *Mater. Res. Bull.* **14**, 1591.  
 Rogl, P., 1983, *J. Less-Common Metals*, to be published.

### Sc–Sn–B

The stabilizing influence of boron atoms as filler atoms in the octahedral sites of the perovskite metal host lattice structure ( $\text{Cu}_3\text{Au}$ -type, Pm3m) was demonstrated by Holleck (1977) by means of X-ray and metallographic analysis of arc melted alloys, homogenized at  $800^\circ\text{C}$ . The lattice parameter for  $\text{Sc}_3\text{SnB}_{1-x}$  was  $a = 4.571(2)$ ;  $x$  was not specified, but for the alloy  $\text{Sc}_3\text{Sn}$  no  $\text{Cu}_3\text{Au}$  lattice was observed.

### Reference

- Holleck, H., 1977, *J. Less-Common Metals* **52**, 167.

### Sc–Ti–B

The stabilizing influence of boron atoms as filler atoms in the octahedral sites of the perovskite metal host lattice structure ( $\text{Cu}_3\text{Au}$ -type, Pm3m) was demonstrated by Holleck (1977) by means of X-ray and metallographic analysis of arc melted alloys, homogenized at  $800^\circ\text{C}$ . The lattice parameter for  $\text{Sc}_3\text{TiB}_{1-x}$  was  $a = 4.520(2)$ ;  $x$  was not specified, but for the alloy  $\text{Sc}_3\text{Ti}$  no  $\text{Cu}_3\text{Au}$  lattice was observed.

### Reference

- Holleck, H., 1977, *J. Less-Common Metals* **52**, 167.

*Sm–Ba,Ca–B*: see notes added in proof under *Sm–M–B*

### Sm–Co–B

The phase equilibria within partial isothermal sections at  $600^\circ\text{C}$  (0–33.3 a/o Sm) and  $400^\circ\text{C}$  (33.3–100 a/o Sm) of the *Sm–Co–B* system are presented in fig. 42. Data in fig. 42 and table 28 (Bilonishko et al., 1980) are based on X-ray and metallographic analysis of 147 samples, which were arc melted and subsequently annealed in evacuated quartz capsules (600 h) and then quenched in water. Starting materials

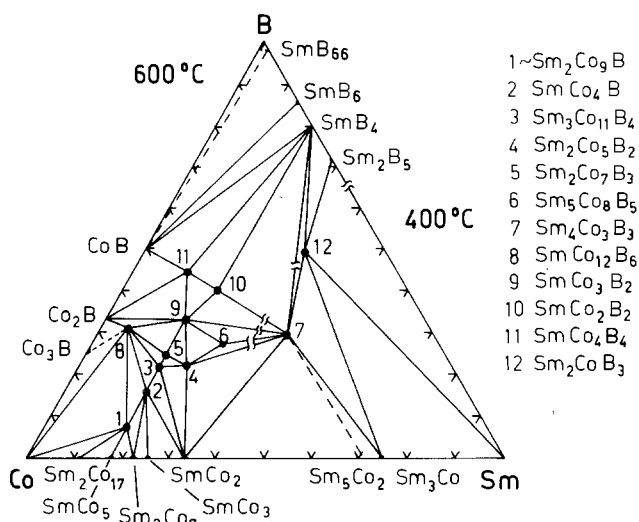


Fig. 42. Sm-Co-B, partial isothermal sections at 600°C (0–30 a/o Sm), and at 400°C (30–100 a/o Sm). (See text for discussion concerning “Sm<sub>2</sub>Co<sub>3</sub>B<sub>2</sub>”, unstable at  $T < 800^\circ\text{C}$ .)

were Sm ingots 97.7%, and Co 99.9% and B 99.3% powders. Samarium cobalt compounds observed: Sm<sub>2</sub>Co<sub>17</sub> (Th<sub>2</sub>Zn<sub>17</sub>-type), SmCo<sub>5</sub> (CaCu<sub>5</sub>-type), Sm<sub>2</sub>Co<sub>7</sub> (Ce<sub>2</sub>Ni<sub>7</sub>-type), SmCo<sub>3</sub> (PuNi<sub>3</sub>-type), SmCo<sub>2</sub> (MgCu<sub>2</sub>-type), Sm<sub>5</sub>Co<sub>2</sub> (Mn<sub>5</sub>C<sub>2</sub>-type), Sm<sub>3</sub>Co (Fe<sub>3</sub>C-type) are in good agreement with recent phase diagram work by Buschow and van der Groot (1968), Buschow and den Broeder (1973), and Moreau and Paccard (1976). For Co borides, see Sc-Co-B.

Mutual solid solubilities were found to be negligible; five ternary borides, mentioned in earlier papers, were confirmed and a total of 12 ternary phases were identified. The crystal structure of the compounds Sm<sub>2</sub>Co<sub>9</sub>B, Sm<sub>5</sub>Co<sub>8</sub>B<sub>5</sub>, Sm<sub>4</sub>Co<sub>3</sub>B<sub>3</sub> and Sm<sub>2</sub>CoB<sub>3</sub> remained unsolved. The Sm-rich part of the diagram (0–33 a/o Sm) has also been investigated at 800°C. An additional phase was identified near the composition “Sm<sub>2</sub>Co<sub>3</sub>B<sub>2</sub>” and all the 13 ternary borides were reported to be stable at 800°C. Within the 800°C partial isothermal section the phase “Sm<sub>2</sub>Co<sub>3</sub>B<sub>2</sub>” was observed in equilibria with Sm<sub>4</sub>Co<sub>3</sub>B<sub>3</sub> and SmCo<sub>3</sub>B<sub>2</sub>, but at temperatures  $T < 800^\circ\text{C}$  “Sm<sub>2</sub>Co<sub>3</sub>B<sub>2</sub>” was found to decompose (Bilonishko et al., 1980). As “Sm<sub>2</sub>Co<sub>3</sub>B<sub>2</sub>” is unstable at 600°C, its location is not shown in fig. 42; its composition, however, would be extremely close to the compound Sm<sub>5</sub>Co<sub>8</sub>B<sub>5</sub> claimed at 600°C.

### References

- Bilonishko, N.S., Yu.B. Kuz'ma and L.D. Polyanskaya, 1980, *Izv. Akad. Nauk SSSR, Neorg. Mater.* **16**(5), 832.
- Buschow, K.H. and F.J.A. den Broeder, 1973, *J. Less-Common Metals* **33**, 191.
- Buschow, K.H. and A.S. van der Groot, 1968, *J. Less-Common Metals* **14**, 323.
- ElMasry, N.A., H.H. Stadelmaier, C.J. Shahwan and L.T. Jordan, 1983, *Z. Metallkde* **74**(1), 33.
- Kuz'ma, Yu.B. and N.S. Bilonishko, 1973, *Kristallografiya* **18**, 710.
- Kuz'ma, Yu.B. and N.S. Bilonishko, 1978, *Dopov. Akad. Nauk Ukr. RSR, Ser. A* **3**, 275.
- Kuz'ma, Yu.B., P.I. Kripyakevich and N.S. Bilonishko, 1969, *Dopov. Akad. Nauk Ukr. RSR, Ser. A* **10**, 939.

TABLE 28  
Formation and structural data of ternary compounds Sm-Co-B.

Compound	Structure type, Space group	Lattice parameters, Density	Preparation, Characterization	Refs.	Purity
SmCo <sub>2</sub> B <sub>2</sub>	ThCr <sub>2</sub> Si <sub>2</sub> I4/mmm	$a = 3.563(3), \rho_E = 7.70$	AM, Qu(Ta)	NiSY, 73	Sm 99.5
		$c = 9.630(7), \rho_x = 7.83$	800°C, 150 h, PXD		Co 99.99
					B 99.9
SmCo <sub>4</sub> B <sub>4</sub>	NdCo <sub>4</sub> B <sub>4</sub> P4 <sub>2</sub> /h	$a = 3.580$	AM, Qu(Mo)	Ro, 73	Sm 99.7
		$c = 9.671$	800°C, 50 h, PXD		Co 99.5
					B 99.0
SmCo <sub>3</sub> B <sub>2</sub> <sup>(*)</sup>	CeCo <sub>3</sub> B <sub>2</sub> P6/mmm	$a = 7.037(4)$	no details given, PXD	KuB, 78	
		$c = 3.824(2)$			
		$a = 5.101(3)$	AM, Qu		
$c = 2.991(2)$	800°C, 50 h, PXD				
$a = 5.079(3), \rho_E = 5.20$	AM, Qu(Ta)	NiY, 73			
$c = 3.031(2), \rho_x = 8.55$	1150°C, 96 h, PXD				
SmCo <sub>4</sub> B <sup>(*)</sup>	CeCo <sub>4</sub> B P6/mmm	$a = 5.078(3)$	AM, Qu	KuB, 73	Sm 99
		$c = 6.871(4)$	800°C, 50 h, PXD		Co 99.87
					B 99.3
Sm <sub>3</sub> Co <sub>11</sub> B <sub>4</sub> <sup>(*)</sup>	Ce <sub>3</sub> Co <sub>11</sub> B <sub>4</sub> P6/mmm	$a = 5.092(3)$	AM, Qu	KuB, 73	Sm 99
		$c = 9.799(6)$	800°C, 50 h, PXD		Co 99.99
					B 99.3
SmCo <sub>12</sub> B <sub>6</sub>	SrNi <sub>10</sub> B <sub>6</sub> R3m	$a_H = 9.432(6)$	AM, Qu, 600°C, 800 h	BIKP, 80	Sm 99.7
		$c_H = 7.482(5)$	PXD		Co 99.9
					B 99.3
		$a_H = 9.473(4)$	AM, Qu, 800°C, 270 h	KuCC, 81	Sm 99.5
		$c_H = 7.461(4)$	PXD		Co 99.95
					B 99.3

$\text{Sm}_2\text{Co}_3\text{B}_2$	$\text{Ce}_2\text{Co}_3\text{B}_2$ $\text{P6}_3/\text{mmc}$	$a = 5.098(3)$ $c = 20.61(3)$	AM, Qu 600°C, 800 h, PXD, QE	BiKP, 80	Sm 97.7 Co 99.9 B 99.3
$\text{Sm}_2\text{Co}_7\text{B}_3^{(*)}$	$\text{Ce}_2\text{Co}_7\text{B}_3$ $\text{P6}/\text{mmm}$	$a = 5.088(2)$ $c = 12.79(3)$	AM, Qu 600°C, 800 h, PXD, QE	BiKP, 80	Sm 97.7 Co 99.9 B 99.3
$\text{Sm}_2\text{Co}_9\text{B}$	unknown		AM, Qu 600°C, 800 h, PXD, QE	BiKP, 80	Sm 97.7 Co 99.9 B 99.3
$\text{Sm}_3\text{Co}_8\text{B}_3$	unknown		AM, Qu 600°C, 800 h, PXD, QE	BiKP, 80	Sm 97.7 Co 99.9 B 99.3
$\text{Sm}_2\text{CoB}_3$	unknown		AM, Qu 400°C, 800 h, PXD, QE	BiKP, 80	Sm 97.7 Co 99.9 B 99.3
$\text{Sm}_2\text{Co}_3\text{B}_2$	unknown		AM, Qu 600°C, 800 h, PXD, QE	BiKP, 80	Sm 97.7 Co 99.9 B 99.3
$\text{Sm}_4\text{Co}_3\text{B}_3$	tetragonal $4/\text{mmm}1\text{-}/\text{-}$	$a = 7.04(2)$ $c = 17.55(3)$ $c = 5c_0$	single crystal photographs AM, Qu 400°C, 800 h, PXD, QE	BiKP, 80	Sm 97.7 Co 99.9 B 99.3

(\*)The magnetic moments (77 K) and the coercive forces have been measured; the Curie temperatures were given as follows (EISSJ, 83):  $\text{SmCo}_3\text{B}_2$ ,  $T_m = 40$  K;  $\text{SmCo}_4\text{B}$ ,  $T_m = 498$  K;  $\text{Sm}_3\text{Co}_{11}\text{B}_4$ ,  $T_m = 448$  K;  $\text{Sm}_2\text{Co}_7\text{B}_3$ ,  $T_m = 402$  K.

Kuz'ma, Yu.B., G.V. Chernjak and N.F. Chaban, 1981, *Dopov. Akad. Nauk Ukr. RSR, Ser. A* **12**, 80.  
 Moreau, J.M. and D. Paccard, 1976, *Acta Crystallogr.* **B32**, 1654.  
 Niihara, K. and S. Yajima, 1973, *Bull. Chem. Soc. Jpn* **46**, 770.  
 Niihara, K., T. Shishido and S. Yajima, 1973, *Bull. Chem. Soc. Jpn* **46**, 1137.  
 Rogl, P., 1973, *Monatsh. Chem.* **104**, 1623.

### *Sm-Cr-B*

Mikhaleiko and Kuz'ma (1977) presented an isothermal section of the Sm-Cr-B system at 800°C as based on X-ray and metallographic data of  $\approx 30$  alloys. Sample preparation as described for (La, Ce)-Cr-B. Mutual solid solubilities of binary compounds were observed to be negligible. Two ternary compounds have been characterized:  $\text{SmCrB}_4$  with  $\text{YCrB}_4$ -type, Pbam,  $a = 5.993(5)$ ,  $b = 11.61(1)$ ,  $c = 3.511(4)$  (Mikhaleiko and Kuz'ma, 1977), and  $\text{SmCr}_2\text{B}_6$  with  $\text{CeCr}_2\text{B}_6$ -type, Immm,  $a = 6.571(4)$ ,  $b = 8.306(5)$ ,  $c = 3.102(3)$  (Mikhaleiko and Kuz'ma, 1975). Phase equilibria after Mikhaleiko and Kuz'ma (1977) did not include the well established  $\text{Sm}_2\text{B}_5$  binary for which a structure proposal exists (La Placa, unpublished). From this a two-phase equilibrium  $\text{Sm}_2\text{B}_5$ - $\text{SmCrB}_4$  is likely (fig. 43). For the Cr-B binary system, see Y-Cr-B.

### *References*

La Placa, S., unpublished results.  
 Mikhaleiko, S.I. and Yu.B. Kuz'ma, 1975, *Dopov. Akad. Nauk Ukr. RSR, Ser. A* **5**, 465.  
 Mikhaleiko, S.I. and Yu.B. Kuz'ma, 1977, *Dopov. Akad. Nauk. Ukr. RSR, Ser. A*, 951.

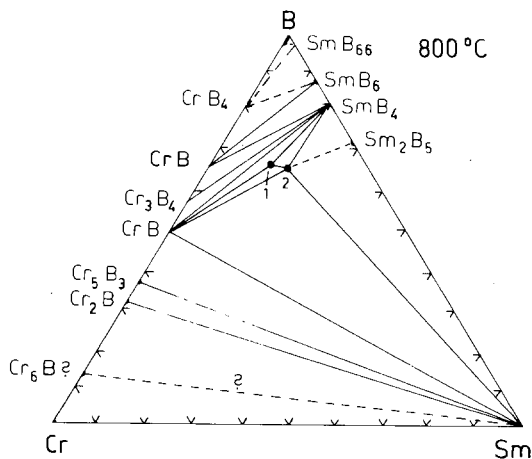


Fig. 43. Sm-Cr-B, isothermal section at 800°C. 1:  $\text{SmCr}_2\text{B}_6$ , 2:  $\text{SmCrB}_4$ .

### *Sm-Fe-B*

Phase diagram data for the Sm-Fe-B system shown in fig. 44 are primarily based on the X-ray and metallographic analysis of arc melted samples annealed at 600°C for 700 h in evacuated quartz capsules (Chaban et al., 1980). Starting materials were Sm ingot 99.7%, and Fe 99.9% and B 99.3% powders. The binary Sm-Fe compounds

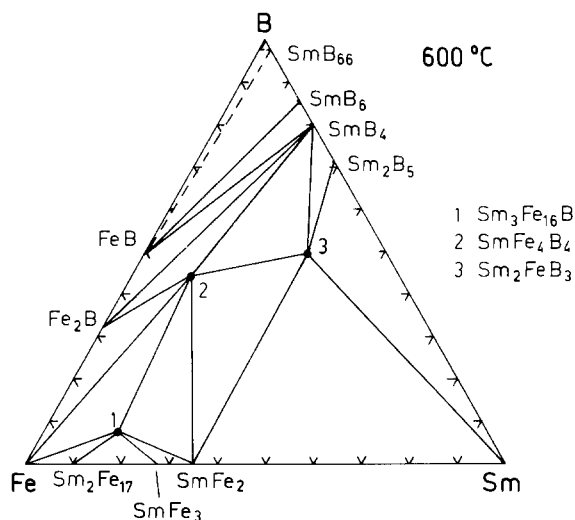


Fig. 44. Sm-Fe-B, isothermal section at 600°C.

observed are in agreement with recent compilations by Iandelli and Palenzona (1979) and Kubaschewski-von Goldbeck (1982):  $\text{Sm}_2\text{Fe}_{17}$  ( $\text{Th}_2\text{Zn}_{17}$ -type),  $\text{SmFe}_3$  ( $\text{PuNi}_3$ -type) and  $\text{SmFe}_2$  ( $\text{MgCu}_2$ -type).

Mutual solid solubilities of the binary compounds at 600°C were observed to be negligible; three ternary compounds were reported from the isothermal section at 600°C.

$\text{SmFe}_4\text{B}_4$  was claimed to be isostructural with  $\text{CeFe}_4\text{B}_4$ , the possible space group is  $\text{P4/ncc}(\?)$ ,  $a = 7.07$ ,  $c = 27.50 \text{ \AA}$ , with an eight-fold superstructure along the  $c$ -axis:  $c = 8c_0$ ; in this context a series of superstructures  $\text{Sm}_{n+m}(\text{Fe}_4\text{B}_4)_n$ , whose crystal structures derive from the  $\text{NdCo}_4\text{B}_4$ -type and are either incommensurate or have unusual repeat units along their  $c$ -axis, have been described quite recently by Braun et al. (1982), see table 2. Atomic positions were refined from single crystal data for  $\text{Sm}_{17}(\text{Fe}_4\text{B}_4)_{15}$  (approximated space group  $\text{P4}_2/\text{n}$ ). For sample preparation, see  $\text{Gd}_{1+x}\text{Fe}_4\text{B}_4$ .

The crystal structures of the compounds  $\text{Sm}_{\sim 3}\text{Fe}_{\sim 16}\text{B}_{\sim 1}$  and  $\text{Sm}_{\sim 2}\text{FeB}_{\sim 3}$ , reported by Chaban et al. (1980), are not yet solved.

From arc melted samples, Braun and Yvon (1980) were able to isolate a single crystal of  $\text{SmFeB}_4$  with  $\text{YCrB}_4$ -type,  $\text{Pbam}$ ,  $a = 5.958(5)$ ,  $b = 11.53(1)$ ,  $c = 3.465(4)$ ,  $\rho_{\text{theor}} = 6.96 \text{ kg/dm}^3$ . Atomic parameters were refined to  $R = 0.04$ . In this context it is reasonable to assume the compound  $\text{SmFeB}_4$  to be either metastable or a high-temperature phase stable at temperatures  $T > 600^\circ\text{C}$  with congruent (?) melting behavior.

### References

- Braun, H.F. and K. Yvon, 1980, *Acta Crystallogr.* **B36**, 2400.  
 Braun, H.F., M. Pelizzone and K. Yvon, 1982, Ferromagnetic borides with incommensurate rare earth and iron sublattices:  $\text{R}_{1+x}\text{Fe}_4\text{B}_4$ , paper presented at the 7th Intern. Conf. on Solid Compounds of Transition Elements, Grenoble (June 21-26), Proceedings, II B11.

Chaban, N.F., Yu.B. Kuz'ma, N.S. Bilonishko, O.O. Kachmar and N.V. Petriv, 1980, *Dopov. Akad. Nauk Ukr. RSR, Ser. A*, 875.

Iandelli, A. and A. Palenzona, 1979, Crystal chemistry of intermetallic compounds, in: *Handbook on the Physics and Chemistry of Rare Earths, Vol. 2*, eds. K.A. Gschneidner, Jr. and L. Eyring (North-Holland, Amsterdam) pp. 1-54.

Kubaschewski-von Goldbeck, O., 1982, *Iron-binary phase diagrams* (Springer, Berlin) pp. 104-105.

### *Sm-Ir-B*

No phase diagram for the Sm-Ir-B system has yet been established.

$\text{SmIr}_4\text{B}_4$ ,  $\text{NdCo}_4\text{B}_4$ -type,  $\text{P4}_2/\text{n}$ ,  $a = 7.590(3)$ ,  $c = 3.976(2)$ , forms congruently from the melt (X-ray and metallographic analysis; Rogl, 1979). For experimental details, see  $\text{LaOs}_4\text{B}_4$ . Magnetic behavior was studied by Rupp et al. (1979) and Hiebl et al. (1982);  $T_n = 1.5$  K.

From X-ray powder diffractometer analysis of arc melted alloys Ku and Meisner (1981) characterized the crystal structure of  $\text{SmIr}_3\text{B}_2$  with  $\text{ErIr}_3\text{B}_2$ -type,  $a = 5.492(6)$ ,  $b = 9.506(9)$ ,  $c = 3.076(4)$ ,  $\beta = 90.8(1)^\circ$ ; possible space group  $\text{C2/m}$ ;  $T_m = 12.6$  K.

### *References*

Hiebl, K., P. Rogl and M.J. Sienko, 1982, *Inorg. Chem.* **21**, 1128.

Ku, H.C. and G.P. Meisner, 1981, *J. Less-Common Metals* **78**, 99.

Rogl, P., 1979, *Monatsh. Chem.* **110**, 235.

Rupp, B., P. Rogl and R. Sobczak, 1979, *Mater. Res. Bull.* **14**, 1301.

### *Sm-Ni-B*

No ternary phase diagram exists for the Sm-Ni-B system.

Romashov et al. (1970) studied the interaction of  $\text{SmB}_6$  with Ni by thermal, X-ray, metallographic and local röntgen-spectral analysis.  $\text{SmB}_6$  was prepared by borothermal reduction of 99.7% pure  $\text{Sm}_2\text{O}_3$  and 99.5% B at  $\approx 1600^\circ\text{C}$ . No two-phase equilibrium exists for the pair Ni- $\text{SmB}_6$ ; the two-phase equilibria observed were:  $\text{SmB}_6$ - $\text{NiB}_{\sim 20}$  (ss. of Ni in  $\beta$ -rh, B),  $\text{SmB}_6$ -NiB,  $\text{SmB}_6$ -o- $\text{Ni}_4\text{B}_3$ ,  $\text{SmB}_4$ -o- $\text{Ni}_4\text{B}_3$ ,  $\text{SmB}_4$ - $\text{Ni}_2\text{B}$ , and Sm- $\text{Ni}_2\text{B}$ .

Niihara et al. (1973) reported the existence of a compound  $\text{SmNi}_4\text{B}$ , presumably isostructural with  $\text{YNi}_4\text{B}$ ; Kuz'ma et al. (1979) confirmed  $\text{SmNi}_4\text{B}$  with  $\text{CeCo}_4\text{B}$ -type:  $a = 5.029(3)$ ,  $c = 6.956(9)$ ,  $\text{P6}/\text{mmm}$ .

$\text{Sm}_3\text{Ni}_{13}\text{B}_2$  crystallizes with the  $\text{Nd}_3\text{Ni}_{13}\text{B}_2$ -type of structure,  $\text{P6}/\text{mmm}$ ,  $a = 4.990(2)$ ,  $c = 10.885(8)$  (Kuz'ma and Bilonishko, 1981).

Kuz'ma and Chaban (1979) observed the existence of the compound  $\text{Sm}_3\text{Ni}_7\text{B}_2$  with  $\text{Dy}_3\text{Ni}_7\text{B}_2$ -type [ $\text{P6}_3/\text{mmc}$ ,  $a = 5.142(2)$ ,  $c = 14.348(10)$ ], from arc melted powder mixtures (Sm ingot, 99.5%, Ni powder 99.98%, B powder 99.3%), heat treated at  $800^\circ\text{C}$  for 360 h in evacuated silica tubes.

### *References*

Kuz'ma, Yu.B. and N.S. Bilonishko, 1981, *Dopov. Akad. Nauk Ukr. RSR, Ser. A* **10**, 88.

Kuz'ma, Yu.B. and N.F. Chaban, 1979, *Dopov. Akad. Nauk Ukr. RSR, Ser. A*, 88.



Kuz'ma, Yu.B., N.S. Bilonishko, S.I. Mikhalenko, G.F. Stepanchikova and N.F. Chaban, 1979, *J. Less-Common Metals* **67**, 51; see also 1983, *J. Less-Common Metals* **90**, 219.  
 Niihara, K., Y. Katayama and S. Yajima, 1973, *Chem. Lett. (Chem. Soc. Jpn)* 613.  
 Romashov, V.M., N.I. Timofeeva, K.I. Frolova and I.V. Romanovich, 1970, *Poroshk. Metall.* **93**(9), 80.

### *Sm-Os-B*

$\text{SmOs}_4\text{B}_4$  has the  $\text{NdCo}_4\text{B}_4$ -type of structure [ $\text{P4}_2/\text{n}$ ,  $a = 7.526(3)$ ,  $c = 4.009(2)$ ] and forms congruently from the melt (Rogl, 1979; X-ray and metallographic analysis); for sample preparation, see  $\text{LaOs}_4\text{B}_4$ . Magnetic behavior was investigated by Rupp et al. (1979) and Hiebl et al. (1982);  $T_N = 1.5$  K.

$\text{SmOs}_3\text{B}_2$  with unknown structure (orthorhombic distortion of  $\text{CeCo}_3\text{B}_2$ -type (?),  $c = 6c_0$ ) has been reported by Ku (1980);  $T_M > 45$  K.

### *References*

Hiebl, K., P. Rogl and M.J. Sienko, 1982, *Inorg. Chem.* **21**, 1128.  
 Ku, H.C., 1980, Thesis, Univ. of California at San Diego, USA.  
 Rogl, P., 1979, *Monatsh. Chem.* **110**, 235.  
 Rupp, B., P. Rogl and R. Sobczak, 1979, *Mater. Res. Bull.* **14**, 1301.

*Sm-Re-B*: see notes added in proof

### *Sm-Rh-B*

The crystal structure of  $\text{SmRh}_3\text{B}_2$ ,  $\text{CeCo}_3\text{B}_2$ -type,  $\text{P6}/\text{mmm}$ ,  $a = 5.437(6)$ ,  $c = 3.090(4)$ , has been established by means of X-ray powder methods (Ku et al., 1980);  $T_m > 45$  K; samples were arc melted; according to Malik et al. (1982)  $T_m = 89$  K.

$\text{SmRh}_4\text{B}_4$  is isostructural with  $\text{CeCo}_4\text{B}_4$ -type,  $\text{P4}_2/\text{nmc}$ ,  $a = 5.312(2)$ ,  $c = 7.430(2)$  (Vandenberg and Matthias, 1977; powder X-ray analysis); for sample preparation, see  $\text{YRh}_4\text{B}_4$ . Precise atom parameters were refined by Yvon and Grüttner (1980) by single crystal X-ray diffraction analysis (see table 29).  $T_c = 2.51\text{--}2.45$  K (Matthias et al., 1977). Specific heat and upper critical field anomalies in  $\text{SmRh}_4\text{B}_4$ ,  $T_i = 0.87$  K, indicated the occurrence of antiferromagnetic(?) ordering without destruction of superconductivity (Ott et al., 1980). See *R-Rh-B* for the perovskite-type boride  $\text{SmRh}_3\text{B}_{1-x}$  ( $\text{Cu}_3\text{Au}$ -type,  $a = 4.192$ ,  $x = 0.2$ ).

### *References*

Ku, H.C., G.P. Meisner, F. Acker and D.C. Johnston, 1980, *Solid State Commun.* **35**, 91.  
 Matthias, B.T., E. Corenzwit, J.M. Vandenberg and H.E. Barz, 1977, *Proc. Nat'l Acad. Sci. US* **74**(4), 1334.  
 Malik, S.K., S.K. Dhar, R. Vijayaraghavan and W.E. Wallace, 1982, *J. Appl. Phys.* **53**(11), 8076.  
 Ott, H.R., W. Odoni, H.C. Hamaker and M.B. Maple, 1980, *Phys. Lett.* **75A**, 243.  
 Vandenberg, J.M. and B.T. Matthias, 1977, *Proc. Nat'l Acad. Sci. US* **74**(4), 1336.  
 Yvon, K. and A. Grüttner, 1980, The influence of the formal electric charge on the size of the transition metal atom cluster in  $\text{YRh}_4\text{B}_4$ ,  $\text{YRu}_4\text{B}_4$  and  $\text{PbMo}_6\text{S}_8$  related compounds, in: *Superconductivity of d- and f-band metals*, eds. H. Suhl and M.B. Maple (Academic Press, New York) pp. 516-519.

TABLE 29

Structural data for  $RT_4B_4$  compounds (R = Y, Sm, Th; T = Ru, Rh) at 293 K. Standard deviations are in parentheses, point positions are according to International Tables (1969), centre at origin of unit cell. The Y, Sm and Th atoms occupy the special equipoints 2b ( $P4_2/nmc$ ); 8b ( $I4_1/acd$ ).

After Yvon and Grüttner (1980).

Compound	Space group	<i>a</i> <i>c</i>	<i>x</i> <i>y</i> (Rh, Ru) <i>z</i>	<i>x</i> <i>y</i> (B) <i>z</i>
YRh <sub>4</sub> B <sub>4</sub>	P4 <sub>2</sub> /nmc (No. 137)	5.310(2)	0.25	0.25
		7.402(3)	0.9988(1)	0.080(1)
SmRh <sub>4</sub> B <sub>4</sub>	P4 <sub>2</sub> /nmc	5.324(2)	0.25	0.25
		7.449(3)	0.9989(1)	0.076(1)
			0.3935(1)	0.101(1)
ThRh <sub>4</sub> B <sub>4</sub>	P4 <sub>2</sub> /nmc	5.356(2)	0.25	0.25
		7.538(3)	0.0006(4)	0.071(5)
			0.3934(3)	0.099(4)
YRu <sub>4</sub> B <sub>4</sub>	I4 <sub>1</sub> /acd (No. 142)	7.443(3)	0.1159(2)	0.832(3)
		14.990(7)	0.1023(2)	0.106(2)
			0.9369(1)	0.957(1)
Y(Ru <sub>0.7</sub> Rh <sub>0.3</sub> ) <sub>4</sub> B <sub>4</sub>	I4 <sub>1</sub> /acd	7.452(3)	0.1145(1)	0.834(1)
		14.961(7)	0.1019(1)	0.107(1)
			0.9370(1)	0.961(1)
Y(Ru <sub>0.5</sub> Rh <sub>0.5</sub> ) <sub>4</sub> B <sub>4</sub>	I4 <sub>1</sub> /acd	7.459(3)	0.1152(2)	0.828(5)
		14.941(7)	0.1016(2)	0.111(5)
			0.9375(1)	0.971(2)
Y(Ru <sub>0.4</sub> Rh <sub>0.6</sub> ) <sub>4</sub> B <sub>4</sub>	I4 <sub>1</sub> /acd	7.471(5)	0.1155(3)	0.850(5)
		14.903(9)	0.1002(3)	0.109(5)
			0.9377(2)	0.962(3)
Y(Ru <sub>0.15</sub> Rh <sub>0.85</sub> ) <sub>4</sub> B <sub>4</sub>	I4 <sub>1</sub> /acd	7.478(3)	0.1165(3)	0.827(3)
		14.887(7)	0.0999(3)	0.106(3)
			0.9383(2)	0.950(2)

### Sm–Ru–B

At least two ternary compounds exist in the Sm–Ru–B system.

The crystal structure of SmRu<sub>3</sub>B<sub>2</sub> (CeCo<sub>3</sub>B<sub>2</sub>-type, P6/mmm) has been confirmed from X-ray powder data by Hiebl et al. (1980);  $a = 5.514(4)$ ,  $c = 3.010(2)$ ; congruent melting behavior. Ku et al. (1980) reported  $a = 5.536(6)$ ,  $c = 2.997(4)$ ,  $T_m > 45$  K. For sample preparation, see YRu<sub>3</sub>B<sub>2</sub>.

SmRu<sub>4</sub>B<sub>4</sub> is isostructural with the LuRu<sub>4</sub>B<sub>4</sub>-type, I4<sub>1</sub>/acd,  $a = 7.482(5)$ ,  $c = 15.049(10)$ , as determined by Johnston (1977) by X-ray powder diffraction of arc melted alloys;  $T_n = 1.5$  K.

*References*

- Johnston, D.C., 1977, *Solid State Commun.* **24**(10), 699.  
 Hiebl, K., P. Rogl, E. Uhl, M.J. Sienko, 1980, *Inorg. Chem.* **19**(11), 3316.  
 Ku, H.C., G.P. Meisner, F. Acker and D.C. Johnston, 1980, *Solid State Commun.* **35**, 91.

*Sm-Sr-B*

The valence transition of Sm in the  $\text{Sm}_{1-x}\text{Sr}_x\text{B}_6$  hexaboride solution (Pm3m) was investigated by Tarascon et al. (1980). For sample preparation and methods of experimental investigation, see  $\text{Sm}_{1-x}\text{Y}_x\text{B}_6$ .  $\text{Sr}^{2+}$  substitution of Sm was found to increase the average Sm valence towards  $\text{Sm}^{3+}$ . Lattice parameters are shown in fig. 34b.

*Reference*

- Tarascon, J.M., Y. Isikawa, B. Chevalier, J. Etourneau and P. Hagemuller, 1980, *J. Physique (Paris)* **41**, 1135.

*Sm-Th-B*

Tarascon et al. (1980) investigated the valence transition of Sm in the  $\text{Sm}_{1-x}\text{Th}_x\text{B}_6$  hexaboride solid solution (Pm3m). For sample preparation as well as methods of investigation employed, see  $\text{Sm}_{1-x}\text{Y}_x\text{B}_6$ .  $\text{Th}^{4+}$  substitution of Sm was found to decrease the average Sm valence more rapidly than  $\text{La}^{3+}$  or  $\text{Y}^{3+}$ . The variation of lattice parameters (pronounced positive deviation of Vegard's rule) is presented in fig. 34c.

*Reference*

- Tarascon, J.M., Y. Isikawa, B. Chevalier, J. Etourneau and P. Hagemuller, 1980, *J. Physique (Paris)* **41**, 1135.

*Sm-Y-B*

Tarascon et al. (1980) investigated the valence transition of Sm in the hexaboride solid solutions  $\text{Sm}_{1-x}\text{M}_x\text{B}_6$  ( $\text{M} = \text{Yb}^{2+}, \text{Sr}^{2+}, \text{La}^{3+}, \text{Y}^{3+}, \text{Th}^{4+}$ ). Samples were prepared by borothermal reduction of the mixed oxides under vacuum and high temperatures. The exact values of  $x$  have been determined by  $x$ -ray fluorescence analysis and checked by density measurements. Density measurements, X-ray and chemical analysis of  $\text{SmB}_6$  indicate an atomic ratio  $\text{B}/\text{Sm} \approx 6$ . From X-ray absorption measurements at the  $\text{L}_{\text{III}}$  edge at 300 K the  $\text{Sm}^{2+}:\text{Sm}^{3+}$  atomic ratio was obtained as a function of  $x$ . (The  $\text{L}_{\text{III}}$  absorption spectrum of  $\text{Eu}^{2+}$  in  $\text{EuB}_6$  was used as reference.)  $\text{Y}^{3+}$  substitution of Sm decreases the average Sm valence towards  $\text{Sm}^{2+}$  in accordance with estimations of the average Sm valence in the hexaborides  $(\text{Sm}_z^{2+}\text{Sm}_y^{3+})_{1-x}\text{M}_x\text{B}_6$  from lattice parameter measurements, fig. 34c. Lattice parameters of " $\text{Sm}^{2+}\text{B}_6$ ":  $a = 4.186$ , and " $\text{Sm}^{3+}\text{B}_6$ ":  $a = 4.115$ , were derived from interpolations of neighboring divalent and trivalent rare earth hexaborides.

TABLE 30  
Formation and structural data of ternary compounds Tb-Co-B.

Compound	Structure type, Space group	Lattice parameters Density	Preparation, Characterization	Refs.	Purity
TbCoB <sub>4</sub>	YCrB <sub>4</sub> Pbam	$a = 5.899(10)$ $b = 11.43(2)$ $c = 3.421(5)$	AM, Qu 800°C, 340 h, PXD	SuK, 77	Tb 99% Co 99.9 B 99.3
TbCo <sub>3</sub> B <sub>4</sub>	CeCo <sub>3</sub> B <sub>4</sub> P4 <sub>2</sub> /mnc	$a = 5.038(3)$ $c = 7.030(5)$	no details given, PXD	KuB, 72	
TbCo <sub>2</sub> B <sub>2</sub>	TbCr <sub>2</sub> Si <sub>2</sub> I4/mmm	$a = 3.557(4), \rho_E = 8.25$ $c = 9.419(7), \rho_A = 8.31$	AM, Qu(Ta) 800°C, 150 h, PXD	NiSY, 73	Tb 99.5 Co 99.99 B 99.9
TbCo <sub>2</sub> B <sub>2</sub>	CeCo <sub>3</sub> B <sub>2</sub> P6/mmm	$a = 3.561$ $c = 9.416$	AM, Qu(Mo) 800°C, 50 h, PXD	Ro, 73	Tb 99.7 Co 99.5 B 99.0
TbCo <sub>2</sub> B <sub>2</sub>	CeCo <sub>3</sub> B <sub>2</sub> P6/mmm	$a = 5.048(3)$ $c = 3.005(2)$	AM, Qu 800°C, 50 h, PXD	KuKB, 69	
TbCo <sub>2</sub> B <sub>2</sub>	CeCo <sub>3</sub> B <sub>2</sub> P6/mmm	$a = 5.050(3), \rho_E = 5.32$ $c = 3.009(2), \rho_A = 8.93$	AM, Qu(Ta) 1150°C, 96 h, PXD	NiY, 73	Tb 99.8 Co 99.99 B 99.9
TbCo <sub>2</sub> B	CeCo <sub>3</sub> B P6/mmm	$a = 5.048(5)$ $c = 3.010(2)$	AM, Qu(Mo) 800°C, 50 h, PXD	Ro, 73	Tb 99.7 Co 99.5 B 99.0
TbCo <sub>2</sub> B	CeCo <sub>3</sub> B P6/mmm	$a = 4.998(3)$ $c = 6.864(4)$	AM, Qu 800°C, 50 h, PXD	KuB, 73	Tb 99.0 Co 99.87 B 99.3
Tb <sub>3</sub> Co <sub>11</sub> B <sub>4</sub>	Ce <sub>3</sub> Co <sub>11</sub> B <sub>4</sub> P6/mmm	$a = 5.058(3)$ $c = 9.823(6)$	AM, Qu 800°C, 50 h, PXD	KuB, 73	Tb 99.0 Co 99.87 B 99.3
Tb <sub>2</sub> Co <sub>3</sub> B <sub>3</sub>	Ce <sub>2</sub> Co <sub>3</sub> B <sub>3</sub> P6/mmm	$a = 5.061(3)$ $c = 12.83(2)$	AM, Qu 800°C, 50 h, PXD	KuB, 73	Tb 99.0 Co 99.87 B 99.3
TbCo <sub>10</sub> B <sub>6</sub>	SrNi <sub>12</sub> B <sub>6</sub> R3m	$a_H = 9.454(3)$ $c_H = 7.453(3)$	AM, Qu 800°C, 270 h, PXD	KuCC, 81	Tb 99.5 Co 99.95 B 99.4

*Reference*

Tarascon, J.M., Y. Isikawa, B. Chevalier, J. Etourneau and P. Hagenmuller, 1980, *J. Physique (Paris)* **41**, 1135.

*Sm-Yb-B*

Substitution of Sm by  $\text{Yb}^{2+}$  in  $\text{SmB}_6$  was found to increase the Sm valence (Kasaya et al., 1980; Tarascon et al., 1980; from X-ray and magnetochemical analysis). Samples were prepared by borothermal reduction of mixed oxides (4-N  $\text{Sm}_2\text{O}_3$ ; 5-N  $\text{Yb}_2\text{O}_3$ ) at 1500°C, 5 h in a Ta crucible and slowly cooled (see also  $\text{Sm}_{1-x}\text{Y}_x\text{B}_6$ ). A complete solid solution  $\text{Sm}_{1-x}\text{Y}_x\text{B}_6$ ,  $\text{CaB}_6$ -type, Pm3m, is formed with lattice parameters strongly deviating from Vegard's rule (fig. 34b), thus reflecting the change of Sm valence.

*References*

Kasaya, M., J.M. Tarascon, J. Etourneau, 1980, *Solid State Commun.* **33**, 1005.

Tarascon, J.M., Y. Isikawa, B. Chevalier, J. Etourneau and P. Hagenmuller, 1980, *J. Physique (Paris)* **41**, 1135.

*Tb-Co-B*

No phase diagram for the Tb-Co-B system is yet available, but a close resemblance with the Gd-Co-B system is likely. Eight ternary compounds have been identified (table 30).

*References*

Kuz'ma, Yu.B. and N.S. Bilonishko, 1972, *Sov. Phys. Crystallogr.* **16**(5), 897.

Kuz'ma, Yu.B. and N.S. Bilonishko, 1973, *Kristallografiya* **18**(4), 710.

Kuz'ma, Yu.B., P.I. Kripyakevich and N.S. Bilonishko, 1969, *Dopov. Akad. Nauk Ukr. RSR, Ser. A* **10**, 939.

Kuz'ma, Yu.B., G.V. Chernjak and N.F. Chaban, 1981, *Dopov. Akad. Nauk Ukr. RSR, Ser. A* **12**, 80.

Niihara, K. and S. Yajima, 1973, *Bull. Chem. Soc. Jpn* **46**, 770.

Niihara, K., T. Shishido and S. Yajima, 1973, *Bull. Chem. Soc. Jpn* **46**, 1137.

Rogl, P., 1973, *Monatsh. Chem.* **104**, 1623.

Stepanchikova, G.F. and Yu.B. Kuz'ma, 1977, *Vestn. Lvov Univ., Ser. Khim.* **19**, 37.

*Tb-Cr-B*

$\text{TbCrB}_4$  was found to be isostructural with the  $\text{YCrB}_4$ -type of structure, Pbam,  $a = 5.832(5)$ ,  $b = 11.51(1)$ ,  $c = 3.463(4)$  (Kuz'ma, 1970; X-ray powder analysis).

*Reference*

Kuz'ma, Yu.B., 1970, *Kristallografiya* **15**(2), 372.

*Tb-Fe-B*

$\text{TbFeB}_4$  crystallizes with  $\text{YCrB}_4$ -type, Pbam,  $a = 5.900(10)$ ,  $b = 11.41(2)$ ,  $c = 3.418(5)$  (X-ray powder analysis; Stepanchikova and Kuz'ma, 1977). For sample preparation, see  $\text{YFeB}_4$ .

$\text{Tb}_3\text{FeB}_7$  is orthorhombic,  $\text{Y}_3\text{ReB}_7$ -type,  $\text{Cmcm}$ ,  $a = 3.397$ ,  $b = 15.64$ ,  $c = 9.413$  (Stepanchikova and Kuz'ma, 1980); for sample preparation, see  $\text{Y}_3\text{FeB}_7$ .

$\text{TbFe}_2\text{B}_2$  with  $\text{ThCr}_2\text{Si}_2$ -type has been obtained by Stepanchikova et al. (1979) from arc melted alloys, annealed at  $800^\circ\text{C}$ , 720 h in evacuated quartz capsules;  $I4/mmm$ ,  $a = 3.544(5)$ ,  $c = 9.473(10)$ .

A series of superstructures  $\text{Tb}_{n+m}(\text{Fe}_4\text{B}_4)_n$  have recently been observed by Braun et al. (1982), (table 2). Their crystal structures derive from the  $\text{NdCo}_4\text{B}_4$ -type of structure and are either incommensurate or have unusual large repeat units along the  $c$ -axis. For sample preparation, see  $\text{Gd}_{1+x}\text{Fe}_4\text{B}_4$ .

### References

- Braun, H.F., M. Pelizzone and K. Yvon, 1982, Ferromagnetic borides with incommensurate rare earth and iron sublattices:  $\text{R}_{1+c}\text{Fe}_4\text{B}_4$ , paper presented at the 7th Intern. Conf. on Solid Compounds of Transition Elements, Grenoble (June 21–26), Proceedings II B11.
- Stepanchikova, G.F. and Yu.B. Kuz'ma, 1977, Vestn. Lvov Univ., Ser. Khim. **19**, 37.
- Stepanchikova, G.F. and Yu.B. Kuz'ma, 1980, Poroshk. Metall. **214**(10), 44.
- Stepanchikova, G.F., Yu.B. Kuz'ma and B.I. Chernjak, 1979, Dopov. Akad. Nauk Ukr. RSR, Ser. A, 950.

### *Tb-Ge-B*

The influence of boron additions to  $\text{R}_5\text{Ge}_3$  compounds was studied (X-ray analysis) by Mayer and Felner (1974) on a series of samples with a nominal boron content according to the formulas:  $\text{Tb}_5\text{Ge}_3$ ,  $\text{Tb}_5\text{Ge}_3\text{B}_{0.5}$ ,  $\text{Tb}_5\text{Ge}_3\text{B}_{1.0}$ ,  $\text{Tb}_5\text{Ge}_3\text{B}_{1.5}$  and  $\text{Tb}_5\text{Ge}_3\text{B}_{2.0}$ . Alloys were prepared by heating (melting) elemental mixtures of a min. purity of 99.9% in Ta crucibles to  $1600^\circ\text{C}$  under He atmosphere. Mayer and Felner (1974) claim the  $\text{Mn}_5\text{Si}_3$ -type phase to be stable up to a composition of  $\text{Tb}_5\text{Ge}_3\text{B}_2$ ; lattice parameters are listed in table 6. Boron solubility (filling of octahedral voids) in  $\text{Mn}_5\text{Si}_3$ -type phases, however, is limited to a formula  $\text{R}_5\text{Ge}_3\text{B}_{1.0}$ . For higher boron concentrations the boron solubility might be accompanied by simultaneous substitution Ge/B, which probably would explain the irregular variation of lattice parameters (see table 6); a reinvestigation seems to be necessary.

### Reference

- Mayer, I. and I. Felner, 1974, J. Less-Common Metals **37**, 171.

### *Tb-Ir-B*

$\text{TbIr}_4\text{B}_4$  has  $\text{NdCo}_4\text{B}_4$ -type,  $\text{P4}_2/\text{n}$ ,  $a = 7.557(3)$ ,  $c = 3.979(2)$  and forms congruently from the melt (Rogl, 1979; X-ray and metallographic analysis, magnetochemical data).

$\text{TbIr}_3\text{B}_2$  adopts the  $\text{ErIr}_3\text{B}_2$ -type of structure (possible space group  $\text{C2/m}$ ),  $a = 5.459(6)$ ,  $b = 9.464(9)$ ,  $c = 3.084(4)$ ,  $\beta = 91.1(1)^\circ$  (Ku and Meisner, 1981; X-ray powder analysis of arc melted alloys);  $T_m = 6.10$  K.

### References

- Ku, H.C. and G.P. Meisner, 1981, J. Less-Common Metals **78**, 99.
- Rogl, P., 1979, Monatsh. Chem. **110**, 235.

*Tb-Mn-B*

TbMnB<sub>4</sub> has the YCrB<sub>4</sub>-type of structure, Pbam,  $a = 5.928(5)$ ,  $b = 11.46(1)$ ,  $c = 3.448(5)$  (Kuz'ma, 1970; X-ray powder analysis); for sample preparation, see GdMnB<sub>4</sub>.

*Reference*

Kuz'ma, Yu.B., 1970, Dopov. Akad. Nauk Ukr. RSR, Ser. A **32**(8), 756.

*Tb-Mo-B*

TbMoB<sub>4</sub> has the YCrB<sub>4</sub>-type of structure, Pbam,  $a = 6.044(5)$ ,  $b = 11.67(1)$ ,  $c = 3.607(5)$  (Kuz'ma and Svarichevskaya, 1972; X-ray powder analysis); for sample preparation, see GdMoB<sub>4</sub>.

*Reference*

Kuz'ma, Yu.B. and S.I. Svarichevskaya, 1972, Dopov. Akad. Nauk Ukr. RSR, Ser. A **34**(9), 166.

*Tb-Ni-B* (see also notes added in proof)

Niihara et al. (1973) mentioned the occurrence of a ternary TbNi<sub>4</sub>B phase with presumably YNi<sub>4</sub>B-type structure; Kuz'ma et al. (1981a) reported the CeCo<sub>4</sub>B-type (see also YNi<sub>4</sub>B):  $a = 4.979(1)$ ,  $c = 6.941(4)$ , P6/mmm.

The existence of Tb<sub>3</sub>Ni<sub>7</sub>B<sub>2</sub> with Dy<sub>3</sub>Ni<sub>7</sub>B<sub>2</sub>-type structure, P6<sub>3</sub>/mmc,  $a = 5.097(2)$ ,  $c = 14.335(10)$ , was observed by Kuz'ma and Chaban (1979) in arc melted elemental mixtures (Tb ingot 99.5%, B powder 99.3%, Ni powder 99.98%), which were subsequently annealed at 800°C, 360 h in evacuated silica tubes.

TbNi<sub>12</sub>B<sub>6</sub> has the SrNi<sub>12</sub>B<sub>6</sub>-type of structure, R $\bar{3}$ m,  $a_H = 9.518(5)$ ,  $c_H = 7.411(5)$  (Kuz'ma et al., 1981b); for sample preparation, see YCo<sub>12</sub>B<sub>6</sub>.

*References*

Kuz'ma, Yu.B. and N.F. Chaban, 1979, Dopov. Akad. Nauk Ukr. RSR, Ser. A, 88.

Kuz'ma, Yu.B., N.S. Bilonishko, N.F. Chaban and G.V. Chernjak, 1981a, J. Less-Common Metals **82**, 364; see also 1982, Izv. Akad. Nauk SSSR, Neorg. Mater. **18**, 691.

Kuz'ma, Yu.B., G.V. Chernjak and N.F. Chaban, 1981b, Dopov. Akad. Nauk Ukr. RSR, Ser. A **12**, 80. Niihara, K., Y. Katayama and S. Yajima, 1973, Chem. Lett (Chem. Soc. Jpn) 613.

*Tb-Os-B*

No phase diagram exists for the Tb-Os-B system, but five ternary phases are known, see table 31.

*References*

Ku, H.C., 1980, Thesis, Univ. of California at San Diego, USA.

Ku, H.C. and R.N. Shelton, 1980, Mater. Res. Bull. **15**(10), 1441.

Rogl, P., 1978, Mater. Res. Bull. **13**, 519.

TABLE 31  
Formation and structural data of ternary compounds Tb-Os-B.

Compound	Structure type, Space group	Lattice parameters, Density	Preparation, Characterization	Refs.	Purity
TbOs <sub>4</sub> B <sub>4</sub>	YCrB <sub>4</sub> Pbam	$a = 5.966(3)$ $b = 11.553(6)$ $c = 3.561(2)$	AM, HT, 1600°C, 12 h HV, W substrate, QE congruent melting, ME, PXD suscept., 80–300 K	Ro, 78  SoR, 79	Tb 99.9 Os 99.9 B 99.0
Tb <sub>2</sub> OsB <sub>6</sub>	Y <sub>2</sub> ReB <sub>6</sub> Pbam	$a = 9.1889(19)$ $b = 11.5612(43)$ $c = 3.6567(2)$	AM, HT, 1600°C, 12 h HV, W substrate, QE PXD	RoN, 82	Tb 99.9 Os 99.9 B 99.7
TbOsB <sub>2</sub>	LuRuB <sub>2</sub> Pnma	$a = 5.885(6)$ $b = 5.309(5)$ $c = 6.392(7)$	AM(Zr), Ta tubes 1250°C, 24 h 800°C, 9 d PXD, $T_m = 39.2$ K	ShKPJK, 80 KuS, 80	99.9
TbOs <sub>4</sub> B <sub>4</sub>	YOs <sub>4</sub> B <sub>4</sub> tetragonal	$a = 7.4683(10)$ $c = 32.7112(32)$ $c = 8c_0$	AM, HT, 1400°C, 12 h HV, W substrate, PXD, $T_m = 0.5$ K	RoHS, 82	Tb 99.9 Os 99.9 B 99.7
TbOs <sub>3</sub> B <sub>2</sub>	YOs <sub>3</sub> B <sub>2</sub> (?) orthorh. (?)	$a \approx 5.5$ $b \approx 9.5$ $c \approx 18$	AM(Zr) PXD, $T_m = 34.5$	Ku, 80	99.9

Rogl, P. and H. Nowotny, 1982, Crystal structures and phase relationships within ternary systems: rare earth metal-noble metal-boron, in: Rare Earths in Science and Technology, Vol. 3, eds. J. McCarthy, B. Silber and J.J. Rhyne (Plenum, New York, London) pp. 353–356.

Rogl, P., K. Hiebl and M.J. Sienko, 1982, Structural chemistry and magnetic behavior of RM<sub>4</sub>B<sub>4</sub>-borides, paper presented at the 7th Intern. Conf. on Solid Compounds of Transition Elements, Grenoble (June 21–25), Proceedings, II A4.

Shelton, R.N., B.A. Karcher, D.R. Powell, R.A. Jacobson and H.C. Ku, 1980, Mater. Res. Bull. **15**, 1445.  
Sobczak, R. and P. Rogl, 1979, J. Solid State Chem. **27**, 343.

### Tb-Re-B

Kuz'ma and Svarichevskaya (1972a) prepared TbReB<sub>4</sub> with YCrB<sub>4</sub>-type, Pbam,  $a = 5.978(5)$ ,  $b = 11.56(1)$ ,  $c = 3.582(5)$ , from arc melted compacts (Y ingot 98%, Re 99.5% and B 99.3% powders) and subsequent annealing at 1000°C, 360 h in evacuated silica capsules.

Tb<sub>2</sub>ReB<sub>6</sub> crystallizes with Y<sub>2</sub>ReB<sub>6</sub>-type, Pbam,  $a = 9.177(5)$ ,  $b = 11.56(1)$ ,  $c = 3.677(4)$  (Kuz'ma and Svarichevskaya, 1972b; X-ray powder analysis).

Tb<sub>3</sub>ReB<sub>7</sub> has Y<sub>3</sub>ReB<sub>7</sub>-type, Cmc<sub>m</sub>,  $a = 3.534(2)$ ,  $b = 15.83(1)$ ,  $c = 9.377(5)$  (Kuz'ma and Mikhalevko, 1976).

### References

- Kuz'ma, Yu.B. and S.I. Mikhalevko, 1976, Dopov. Akad. Nauk Ukr. RSR, Ser. A **11**, 1029.  
Kuz'ma, Yu.B. and S.I. Svarichevskaya, 1972a, Dopov. Akad. Nauk Ukr. RSR, Ser. A **2**, 166.  
Kuz'ma, Yu.B. and S.I. Svarichevskaya, 1972b, Kristallografiya **17**(3), 658.



*Tb-Rh-B*

From X-ray powder diffraction of arc melted alloys  $\text{TbRh}_3\text{B}_2$  was established to be isostructural with  $\text{ErIr}_3\text{B}_2$  (possible space group  $\text{C}2/m$ ),  $a = 5.390(6)$ ,  $b = 9.335(9)$ ,  $c = 3.100(4)$ ,  $\beta = 91.0(1)^\circ$  (Ku and Meisner, 1981);  $T_m = 45$  K.

$\text{TbRh}_4\text{B}_4$  is isostructural with the structure type of  $\text{CeCo}_4\text{B}_4$ ,  $\text{P}4_2/nmc$ ,  $a = 5.303(2)$ ,  $c = 7.404(2)$  (Vandenberg and Matthias, 1977; X-ray powder analysis); for sample preparation, see  $\text{YRh}_4\text{B}_4$ .  $T_m = 7.08$  K (Matthias et al., 1977).

For the existence of a perovskite-type phase  $\text{TbRh}_3\text{B}_{1-x}$  with  $\text{Cu}_3\text{Au}$ -type,  $a = 4.165$ ,  $x = 0.1$ , see also *R-Rh-B*.

*References*

- Ku, H.C. and G.P. Meisner, 1981, *J. Less-Common Metals* **78**, 99.  
 Matthias, B.T., E. Corenzwit, J.M. Vandenberg and H.E. Barz, 1977, *Proc. Nat'l Acad. Sci. US* **74**(4), 1334.  
 Vandenberg, J.M. and B.T. Matthias, 1977, *Proc. Nat'l Acad. Sci. US* **74**(4), 1336.

*Tb-Ru-B*

No phase diagram exists for the *Tb-Ru-B* system, but five ternary compounds have been characterized (see table 32).

TABLE 32  
 Formation and structural data of ternary compounds *Tb-Ru-B*.

Compound	Structure type, Space group	Lattice parameters, Density	Preparation, Characterization	Refs.	Purity
$\text{TbRuB}_4$	$\text{YCrB}_4$ $\text{Pb}am$	$a = 5.958(3)$ $b = 11.532(6)$ $c = 3.551(2)$	AM, HT, $1600^\circ\text{C}$ , 12 h HV, W substrate congruent melting, PXD, Me suscept., 80–300 K	Ro, 78  SoR, 79	Tb 99.9 Ru 99.9 B 99.0
$\text{Tb}_2\text{RuB}_6$	$\text{Y}_2\text{ReB}_6$ $\text{Pb}am$	$a = 9.1796(20)$ $b = 11.5407(19)$ $c = 3.6650(2)$	AM, HT, $1600^\circ\text{C}$ , 12 h HV, W substrate, PXD	RoN, 82	Tb 99.9 Ru 99.9 B 99.0
$\text{TbRuB}_2$	$\text{LuRuB}_2$ $\text{Pn}ma$	$a = 5.897(6)$ $b = 5.311(5)$ $c = 6.367(7)$	AM(Zr), HT, Ta tubes $1250^\circ\text{C}$ , 24 h $800^\circ\text{C}$ , 9 d, PXD $T_m = 45.6$ K	ShKPJK, 80 KuS, 80	99.9
$\text{TbRu}_4\text{B}_4$	$\text{LuRu}_4\text{B}_4$ $\text{I}4_1/acd$	$a = 7.456(5)$ $c = 14.995(10)$	AM(Zr), PXD $T_m = 4.30$ K	Jo, 77	high purity
$\text{TbRu}_3\text{B}_2$	$\text{CeCo}_3\text{B}_2$ $\text{P}6/mmm$	$a = 5.485(4)$ $c = 3.014(2)$	AM, HT, $1400^\circ\text{C}$ 24 h, BN substrate PXD, congr. melting, ME $T_m = 83$ K	HiRUS, 80	Tb 99.9 Ru 99.9 B 99.7
		$a = 5.495(6)$ $c = 3.010(4)$	AM(Ar), PXD $T_m > 45$ K	KuMAJ, 80	99.9

*References*

- Hiebl, K., P. Rogl, E. Uhl and M.J. Sienko, 1980, *Inorg. Chem.* **19**(11), 3316.  
 Johnston, D.C., 1977, *Solid State Commun.* **24**(10), 699.  
 Ku, H.C. and R.N. Shelton, 1980, *Mater. Res. Bull.* **15**(10), 1441.  
 Ku, H.C., G.P. Meisner, F. Acker and D.C. Johnston, 1980, *Solid State Commun.* **35**, 91.  
 Rogl, P., 1978, *Mater. Res. Bull.* **13**, 519.  
 Rogl, P. and H. Nowotny, 1982, Crystal structures and phase relationships within ternary systems: rare earth metal-noble metal-boron, in: *Rare Earths in Science and Technology*, Vol. 3, eds. J. McCarthy, B. Silber and J.J. Rhyne (Plenum, New York, London) pp. 353-356.  
 Shelton, R.N., B.A. Karcher, D.R. Powell, R.A. Jacobson and H.C. Ku, 1980, *Mater. Res. Bull.* **15**, 1445.  
 Sobczak, R. and P. Rogl, 1979, *J. Solid State Chem.* **27**, 343.

*Tb-Si-B*

The influence of boron additions to  $R_5Si_3$  compounds was studied (X-ray analysis) by Mayer and Felner (1974) on a series of samples with a nominal boron content according to the formulas:  $Tb_5Si_3$ ,  $Tb_5Si_3B_{0.5}$ ,  $Tb_5Si_3B_{1.0}$ ,  $Tb_5Si_3B_{1.5}$  and  $Tb_5Si_3B_{2.0}$ . Alloys were prepared by heating (melting) elemental mixtures of a min. purity of 99.9% in Ta crucibles to 1600°C under He atmosphere. Mayer and Felner (1974) claim the  $Mn_5Si_3$ -type phase to be stable up to a composition of  $Tb_5Si_3B_2$ ; lattice parameters are listed in table 6. Boron solubility (filling of octahedral voids) in  $Mn_5Si_3$ -type phases, however, is limited to a formula  $R_5Si_3B_{1.0}$ . For higher boron concentrations the boron solubility might be accompanied by simultaneous substitution Si/B, which probably would explain the irregular variation of lattice parameters (see table 6); a reinvestigation seems to be necessary.

*Reference*

- Mayer, I. and I. Felner, 1974, *J. Less-Common Metals* **37**, 171.

*Tb-V-B*

The crystal structure of  $TbVB_4$  [ $YCrB_4$ -type, Pbam,  $a = 5.970(5)$ ,  $b = 11.60(1)$ ,  $c = 3.475(5)$ ] has been characterized by Kuz'ma (1970) by means of X-ray powder diffraction; for sample preparation, see  $GdMnB_4$ .

*Reference*

- Kuz'ma, Yu.B., 1970, *Dopov. Akad. Nauk Ukr. RSR, Ser. A* **32**(8), 756.

*Tb-W-B*

$TbWB_4$  is isostructural with the  $YCrB_4$ -type, Pbam,  $a = 6.047(5)$ ,  $b = 11.69(1)$ ,  $c = 3.606(5)$  (Kuz'ma and Svarichevskaya, 1972; X-ray powder diffraction); for sample preparation, see  $GdWB_4$ .

*Reference*

- Kuz'ma, Yu.B. and S.I. Svarichevskaya, 1972, *Dopov. Akad. Nauk Ukr. RSR, Ser. A* **34**(9), 166.

*Tb-Y-B*

Single crystals of  $Tb_{0.79}Y_{0.21}B_4$  were grown from molten Al and investigated for their magnetic properties:  $UB_4$ -type structure,  $P4/mbm$  (Fisk et al., 1981). No lattice parameter data were given.

*Reference*

Fisk, Z., M.B. Maple, D.C. Johnston and L.D. Woolf, 1981, *Solid State Commun.* **39**, 1189.

*Tm-Co-B*

No ternary phase diagram exists for the Tm-Co-B system, but six ternary compounds were observed (table 33).

*References*

Kuz'ma, Yu.B. and N.S. Bilonishko, 1972, *Sov. Phys. Crystallogr.* **16**(5), 897.

Kuz'ma, Yu.B. and N.S. Bilonishko, 1973, *Kristallografiya* **18**(4), 710.

Kuz'ma, Yu.B., P.I. Kripyakevich and N.S. Bilonishko, 1969, *Dopov. Akad. Nauk Ukr. RSR, Ser. A* **10**, 939.

Rogl, P., 1973, *Monatsh. Chem.* **104**, 1623.

Stepanchikova, G.F. and Yu.B. Kuz'ma, 1977, *Vestn. Lvov Univ. Ser. Khim.* **19**, 37.

TABLE 33  
Formation and structural data of ternary compounds Tm-Co-B.

Compound	Structure type, Space group	Lattice parameters, Density	Preparation, Characterization	Refs.	Purity
$TmCo_4B_4$	$YCrB_4$ $Pbam$	$a = 5.858(10)$ $b = 11.31(2)$ $c = 3.342(5)$	AM, Qu 800°C, 340 h, PXD	Stk, 77	Tm 99% Co 99.9 B 99.3
$TmCo_4B_4$	$CeCo_4B_4$ $P4_2/nmc$	$a = 5.009(3)$ $c = 6.980(5)$	no details given, PXD	KuB, 72	
$TmCo_3B_2$	$CeCo_3B_2$ $P6/mmm$	$a = 4.991(3)$ $c = 3.019(2)$	AM, Qu 800°C, 50 h, PXD	KuKB, 69	
		$a = 4.999(5)$ $c = 3.019(1)$	AM, Qu(Mo), PXD 900°C, 70 h CP, Qu(Mo), 800°C, 100 h	Ro, 73	Tm 99.9 Co 99.5 B 99.0
$TmCo_4B$	$CeCo_4B$ $P6/mmm$	$a = 4.948(3)$ $c = 6.862(4)$	AM, Qu 800°C, 50 h, PXD	KuB, 73	Tm 99.0 Co 99.87 B 99.3
$Tm_3Co_{11}B_4$	$Ce_3Co_{11}B_4$ $P6/mmm$	$a = 5.004(3)$ $c = 9.853(6)$	AM, Qu 800°C, 50 h, PXD	KuB, 73	Tm 99.0 Co 99.87 B 99.3
$Tm_2Co_7B_3$	$Ce_2Co_7B_3$ $P6/mmm$	$a = 5.002(3)$ $c = 12.85(2)$	AM, Qu 800°C, 50 h, PXD	KuB, 73	Tm 99.0 Co 99.87 B 99.3

*Tm-Cr-B*

The existence of the ternary compound  $\text{TmCrB}_4$  with the  $\text{YCrB}_4$ -type of structure [Pbam,  $a = 5.732(5)$ ,  $b = 11.43(1)$ ,  $c = 3.419(5)$ ] has been observed by Kuz'ma and Svarichevskaya (1972) from X-ray powder diffraction analysis.

*Reference*

Kuz'ma, Yu.B. and S.I. Svarichevskaya, 1972, *Dopov. Akad. Nauk Ukr. RSR, Ser. A* **2**, 166.

*Tm-Fe-B* (see also notes added in proof)

$\text{TmFeB}_4$  crystallizes with  $\text{YCrB}_4$ -type, Pbam,  $a = 5.850(10)$ ,  $b = 11.32(2)$ ,  $c = 3.365(5)$  (X-ray powder analysis; Stepanchikova and Kuz'ma, 1977); for sample preparation, see  $\text{CeFeB}_4$ .

$\text{TmFe}_2\text{B}_2$  is tetragonal with  $\text{ThCr}_2\text{Si}_2$ -type,  $I4/mmm$ ,  $a = 3.507(5)$ ,  $c = 9.342(10)$  (Stepanchikova et al., 1979). Samples were arc melted and annealed (720 h,  $800^\circ\text{C}$ ) in evacuated quartz capsules.

*References*

Stepanchikova, G.F. and Yu.B. Kuz'ma, 1977, *Vestn. Lvov Univ., Ser. Khim.* **19**, 37.

Stepanchikova, G.F., Yu.B. Kuz'ma and B.I. Chernjak, 1979, *Dopov. Akad. Nauk Ukr. RSR, Ser. A*, 950.

*Tm-Ir-B*

$\text{TmIr}_3\text{B}_2$  adopts the  $\text{ErIr}_3\text{B}_2$ -type of structure (possible space group  $C2/m$ ),  $a = 5.404(6)$ ,  $b = 9.371(9)$ ,  $c = 3.097(4)$ ,  $\beta = 91.3(1)^\circ$  (Ku and Meisner, 1981; X-ray powder data of arc melted alloys);  $T_m = 5.69$  K.

From arc melted alloys, Ku et al. (1979) were able to isolate a metastable phase  $\text{TmIr}_4\text{B}_4$  with the  $\text{CeCo}_4\text{B}_4$ -type of structure:  $P4_2/nmc$ ,  $a = 5.404(4)$ ,  $c = 7.281(6)$ ;  $T_c = 1.75\text{--}1.34$  K. The phase disappears after heat treatment.

*References*

Ku, H.C. and G.P. Meisner, 1981, *J. Less-Common Metals* **78**, 99.

Ku, H.C., B.T. Matthias and H. Barz, 1979, *Solid State Commun.* **32**(1), 937.

*Tm-Ni-B* (see also notes added in proof)

At least four ternary compounds exist in the  $\text{Tm-Ni-B}$  system.

$\text{Tm}_3\text{Ni}_7\text{B}_2$  [ $\text{Dy}_3\text{Ni}_7\text{B}_2$ -type,  $P6_3/mmc$ ,  $a = 5.013(2)$ ,  $c = 14.231(10)$ ] was observed by Kuz'ma and Chaban (1979) from arc melted alloys (Tm ingot 99.5%, B powder 99.3%, Ni powder 99.98%), which were annealed at  $800^\circ\text{C}$ , 360 h in evacuated silica tubes.

$\text{Tm}_2\text{Ni}_{21}\text{B}_6$  is  $\text{Cr}_{23}\text{C}_6$ -type,  $Fm3m$ ,  $a = 10.633(5)$  Å (Chaban et al., 1980; arc melted alloys).

$\text{TmNiB}_4$  [ $\text{YCrB}_4$ -type, Pbam,  $a = 5.793(24)$ ,  $b = 11.456(71)$ ,  $c = 3.457(25)$ ] was observed by Chaban et al. (1981) in arc melted and annealed alloys ( $800^\circ\text{C}$ , 720 h,

evacuated silica capsules) containing additionally small amounts of  $\text{TmB}_4$  (equilibrium with  $\text{TmB}_4$ ?).

$\text{TmNi}_4\text{B}$  was reported by Kuz'ma et al. (1981) to crystallize with the  $\text{CeCo}_4\text{B}$ -type of structure:  $a = 4.960(2)$ ,  $c = 6.917(5)$ ,  $P6/mmm$ ; from a refinement of powder X-ray data ( $R = 0.13$ ) the atomic parameters were derived as follows: Tm in 1a, 1b; Ni in 2c and 6i ( $z = 0.281$ ); B in 2d.

### References

- Chaban, N.F., Yu.B. Kuz'ma and P.L. Kotovskaya, 1980, *Dopov. Akad. Nauk Ukr. RSR, Ser. A*, 88.  
 Chaban, N.F., G.V. Chernjak and Yu.B. Kuz'ma, 1981, *Izv. Akad. Nauk SSSR, Neorg. Mater.* 17(8), 1494.  
 Kuz'ma, Yu.B. and N.F. Chaban, 1979, *Dopov. Akad. Nauk Ukr. RSR, Ser. A*, 88.  
 Kuz'ma, Yu.B., N.S. Bilonishko, N.F. Chaban and G.V. Chernjak, 1981, *J. Less-Common Metals* 82, 364; see also 1982, *Izv. Akad. Nauk SSSR, Neorg. Mater.* 18, 691.

### Tm-Os-B

Four ternary phases have been identified in the Tm-Os-B system (table 34).

### References

- Ku, H.C., 1980, Thesis, Univ. of California at Dan Diego, USA.  
 Ku, H.C. and R.N. Shelton, 1980, *Mater. Res. Bull.* 15(10), 1441.  
 Rogl, P., 1978, *Mater. Res. Bull.* 13, 519.

TABLE 34  
 Formation and structural data of ternary compounds Tm-Os-B.

Compound	Structure type, Space group	Lattice parameters, Density	Preparation, Characterization	Refs.	Purity
$\text{TmOsB}_4$	$\text{YCrB}_4$ Pbam	$a = 5.919(3)$ $b = 11.461(6)$ $c = 3.532(2)$	AM, HT, 1600°C, 12 h HV, W substrate, QE congruent melting, ME, PXD suscept., 80–300 K	Ro, 78  SoR, 79	Tm 99.9 Os 99.9 B 99.0
$\text{Tm}_2\text{OsB}_6$	$\text{Y}_2\text{ReB}_6$ Pbam	$a = 9.0677(29)$ $b = 11.4336(36)$ $c = 3.6037(3)$	AM, HT, 1600°C, 12 h HV, W substrate, QE PXD	RoN, 82	Tm 99.9 Os 99.9 B 99.7
$\text{TmOsB}_2$	$\text{LuRuB}_2$ Pnma	$a = 5.817(6)$ $b = 5.258(5)$ $c = 6.328(7)$	AM(Zr), Ta tubes 1250°C, 24 h 800°C, 9 d PXD, $T_m = 2.26$ K	ShKPJK, 80 KuS, 80	99.9
$\text{TmOs}_4\text{B}_4$	$\text{YO}_4\text{B}_4$ tetragonal	$a = 7.4231(5)$ $c = 32.7520(48)$ $c = 8c_0$	AM, HT, 1400°C, 12 h HV, BN substrate PXD, $T_m = 3.9$ K	RoHS, 82	Tm 99.9 Os 99.9 B 99.7
$\text{TmOs}_3\text{B}_2$	$\text{YO}_3\text{B}_2(?)$ orthorh.(?)	$a \approx 5.5$ $b \approx 9.5$ $c \approx 18$	AM(Zr) PXD, $T_m = 10.2$ K	Ku, 80	99.9

- Rogl, P. and H. Nowotny, 1982, Crystal structures and phase relationships within ternary systems: rare earth metal-noble metal-boron, in: *The Rare Earths in Science and Technology*, Vol. 3, eds. J. McCarthy, B. Silber and J.J. Rhine (Plenum, New York, London) pp. 353-356.
- Rogl, P., K. Hiebl and M.J. Sienko, 1982, Structural chemistry and magnetic behavior of  $RM_4B_4$ -borides, paper presented at the 7th Intern. Conf. on Solid Compounds of Transition Elements, Grenoble (June 21-25), Proceedings, II A4.
- Shelton, R.N., B.A. Karcher, D.R. Powell, R.A. Jacobson and H.C. Ku, 1980, *Mater. Res. Bull.* **15**, 1445.
- Sobczak, R. and P. Rogl, 1979, *J. Solid State Chem.* **27**, 343.

### *Tm-Re-B*

No ternary phase diagram has been derived for the Tm-Re-B system, but three compounds were established by means of X-ray powder analysis.

$TmReB_4$  with  $YCrB_4$ -type [Pbam,  $a = 5.945(5)$ ,  $b = 11.49(1)$ ,  $c = 3.553(5)$ ] has been observed by Mikhalenko (1974) from arc melted and annealed alloys, 800°C, 360 h in evacuated silica tubes. Starting materials were 99.5% Tm ingots, 99.5% Re and 99.3% B powders.

$Tm_2ReB_6$  crystallizes with  $Y_2ReB_6$ -type, Pbam,  $a = 9.102(5)$ ,  $b = 11.46(1)$ ,  $c = 3.622(4)$  (Kuz'ma and Svarichevskaya, 1972).

$Tm_3ReB_7$  was characterized with  $Y_3ReB_7$ -type, Cmc $m$ ,  $a = 3.474(2)$ ,  $b = 15.58(1)$ ,  $c = 9.307(5)$  (Kuz'ma and Mikhalenko, 1976).

### *References*

- Kuz'ma, Yu.B. and S.I. Mikhalenko, 1976, *Dopov. Akad. Nauk Ukr. RSR, Ser. A* **11**, 1029.
- Kuz'ma, Yu.B. and S.I. Svarichevskaya, 1972, *Kristallografiya* **17**(3), 658.
- Mikhalenko, S.I. 1974, *Vestn. Lvov Univ., Ser. Khim.* **16**, 58.

### *Tm-Rh-B* (see also notes added in proof)

From powder X-ray analysis of arc melted alloys, Ku and Meisner (1981) found  $TmRh_3B_2$  to crystallize with the  $ErIr_3B_2$ -type of structure, possible space group  $C2/m$ ,  $a = 5.357(6)$ ,  $b = 9.285(9)$ ,  $c = 3.091(4)$ ,  $\beta = 90.8(1)^\circ$ ;  $T_m = 11.8$  K.

$TmRh_4B_4$  was reported by Vandenberg and Matthias (1977) to adopt the  $CeCo_4B_4$ -type of structure,  $P4_2/nmc$ ,  $a = 5.287(2)$ ,  $c = 7.359(3)$  (X-ray powder diffraction); for sample preparation, see  $YRh_4B_4$ .  $T_c = 9.86-9.73$  K (Matthias et al., 1977). Heat capacity data and anomalies in the thermal expansion coefficient indicate a phase transition below 0.5 K (Hamaker et al., 1981). Antiferromagnetic ordering at  $T_m \approx 0.7$  K (Majkrzak et al., as quoted in Maple, 1981).

Yvon and Johnston (1982) obtained  $TmRh_4B_4$  with the  $LuRh_4B_4$ -type of structure, Ccca (low-temperature phase?):  $a = 7.432-7.433(6)$ ,  $b = 22.28-22.31(2)$ ,  $c = 7.455-7.453(6)$ , from arc melted alloys containing excess Rh after annealing at 1420-1520 K, 125 h, in Ta tubes, sealed under Ar. Arc melted alloys were said to mainly consist of  $CeCo_4B_4$ -type and (metastable?)  $LuRu_4B_4$ -type phases.

For the existence of a  $Cu_3Au$ -type phase  $TmRh_3B_{1-x}$ ,  $a = 4.146$ ,  $x = 0.02$ , see also R-Rh-B.

*References*

- Hamaker, H.C., H.B. MacKay, L.D. Woolf, M.B. Maple, W. Odoni and H.R. Ott, 1981, *Phys. Lett.* **81A**, 91.
- Ku, H.C. and G.P. Meisner, 1981, *J. Less-Common Metals* **78**, 99.
- Maple, M.B., 1981, Superconductivity and magnetism of rare earth rhodium boride compounds, in: Ternary Superconductors, Proc. Intern. Conf. on Ternary Superconductors, Lake Geneva, WI, USA (1980), eds. G.K. Shenoy, B.D. Dunlap and F.Y. Fradin (North-Holland, Amsterdam) pp. 131–139.
- Matthias, B.T., E. Corenzwit, J.M. Vandenberg and H.E. Barz, 1977, *Proc. Nat'l Acad. Sci. US* **74**(4), 1334.
- Vandenberg, J.M. and B.T. Matthias, 1977, *Proc. Nat'l Acad. Sci. US* **74**(4), 1336.
- Yvon, K. and D.C. Johnston, 1982, *Acta Crystallogr.* **B38**, 247.

*Tm–Ru–B*

Ternary phase equilibria for the Tm–Ru–B system have not been established, but the existence of five ternary compounds is known (see table 35).

*References*

- Hiebl, K., P. Rogl, E. Uhl and M.J. Sienko, 1980, *Inorg. Chem.* **19**(11), 3316.
- Johnston, D.C., 1977, *Solid State Commun.* **24**(10), 699.

TABLE 35  
Formation and structural data of ternary compounds Tm–Ru–B.

Compound	Structure type, Space group	Lattice parameters, Density	Preparation, Characterization	Refs.	Purity
TmRuB <sub>4</sub>	YCrB <sub>4</sub> Pbam	$a = 5.913(3)$ $b = 11.440(6)$ $c = 3.511(2)$	AM, HT, 1600°C, 12 h HV, W substrate congruent melting PXD, ME suscept., 80–300 K	Ro, 78  SoR, 79	Tm 99.9 Ru 99.9 B 99.0
Tm <sub>2</sub> RuB <sub>6</sub>	Y <sub>2</sub> ReB <sub>6</sub> Pbam	$a = 9.0605(28)$ $b = 11.4203(31)$ $c = 3.6091(3)$	AM, HT, 1600°C, 12 h HV, W substrate PXD	RoN, 82	Tm 99.9 Ru 99.9 B 99.0
TmRuB <sub>2</sub>	LuRuB <sub>2</sub> Pnma	$a = 5.831(6)$ $b = 5.254(5)$ $c = 6.299(7)$	AM(Zr), HT, Ta tubes 1250°C, 24 h 800°C, 9 d, PXD, $T_m = 4.07$ K	ShKPJK, 80 KuS, 80	99.9
TmRu <sub>4</sub> B <sub>4</sub>	LuRu <sub>4</sub> B <sub>4</sub> I4 <sub>1</sub> /acd	$a = 7.429(5)$ $c = 14.965(10)$	AM(Zr), PXD $T_n = 1.5$ K	Jo, 77	high purity
TmRu <sub>3</sub> B <sub>2</sub>	CeCo <sub>3</sub> B <sub>2</sub> P6/mmm	$a = 5.454(4)$ $c = 3.010(2)$	AM, HT, 1400°C, 24 h BN substrate PXD, ME, congr. melting $T_m = 27$ K	HiRUS, 80	Tm 99.9 Ru 99.9 B 99.7
		$a = 5.461(6)$ $c = 3.012(4)$	AM(Zr), PXD $T_m = 18.3$ K	KuMAJ, 80	99.9

Ku, H.C. and R.N. Shelton, 1980, *Mater. Res. Bull.* **15**(10), 1441.

Ku, H.C., G.P. Meisner, F. Acker and D.C. Johnston, 1980, *Solid State Commun.* **35**, 91.

Rogl, P., 1978, *Mater. Res. Bull.* **13**, 519.

Rogl, P. and H. Nowotny, 1982, Crystal structures and phase relationships within ternary systems: rare earth metal-noble metal-boron, in: *The Rare Earths in Science and Technology*, Vol. 3, eds. J. McCarthy, B. Silber and J.J. Rhyne (Plenum, New York, London) pp. 353-356.

Shelton, R.N., B.A. Karcher, D.R. Powell, R.A. Jacobson and H.C. Ku, 1980, *Mater. Res. Bull.* **15**, 1445.

Sobczak, R. and P. Rogl, 1979, *J. Solid State Chem.* **27**, 343.

*Tm-Yb-B*: see notes added in proof

### *Y-Al-B*

Chaban and Kuz'ma (1971) studied the phase equilibria in an isothermal section at 600°C of the Y-Al-B system by means of X-ray and metallographic analysis. Equilibria within the boron-rich section B-YB<sub>12</sub>-Al were not investigated and are tentative, fig. 45. Samples were arc melted (Y ingot 99.9%, B powder 99.3%, Al powder 99.997%) and subsequently annealed in evacuated silica capsules at 600°C, 350 h.

No ternary compounds were observed, mutual solid solubilities of binary phases were negligible. The binary Y-Al compounds Y<sub>2</sub>Al (PbCl<sub>2</sub>-type), Y<sub>3</sub>Al<sub>2</sub> (Zr<sub>3</sub>Al<sub>2</sub>-type), YAl (CrB-type), YAl<sub>2</sub> (MgCu<sub>2</sub>-type), YAl<sub>3</sub> (Ni<sub>3</sub>Sn-type) are in agreement with the compilation of Iandelli and Palenzona (1979).

### *References*

Chaban, N.F. and Yu.B. Kuz'ma, 1971, *Dopov. Akad. Nauk Ukr. RSR, Ser. A* **11**, 1048.

Iandelli, A. and A. Palenzona, 1979, Crystal chemistry of intermetallic compounds, in: *Handbook on the Physics and Chemistry of Rare Earths*, Vol. 2, eds. K.A. Gschneidner Jr. and L. Eyring (North-Holland, Amsterdam) pp. 1-54.

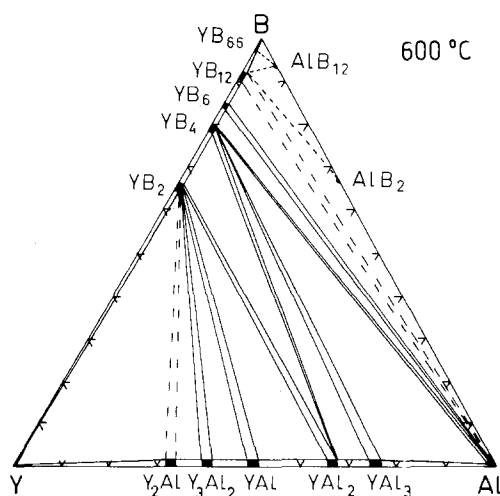


Fig. 45. Y-Al-B, isothermal section at 600°C; region B-YB<sub>12</sub>-Al is proposed.



*Y-Ca-B*

A sample with composition  $Y_{0.85}Ca_{0.15}B_6$ , prepared by borothermal reduction of the mixed oxides, was found to be homogeneous with  $CaB_6$ -type,  $Pm\bar{3}m$ ,  $a = 4.1069(10)$  (Hiebl and Sienko, 1980; X-ray powder analysis); for details of sample preparation, see *Yb-Y-B*.

*Reference*

Hiebl, K. and M.J. Sienko, 1980, *Inorg. Chem.* **19**, 2179.

*Y-Co-B*

Using X-ray and metallographic analysis Kuz'ma and Stepanchikova (1974) have determined the isothermal section of the Y-Co-B system at 800°C (region 0–33 a/o Y) and at 600°C for the region 33–100 a/o Y (fig. 46). 125 specimens were arc melted and then annealed in evacuated quartz capsules for 340 h and quenched (Co 99.8% and B 99.3% powders, and Y ingot 99.5%). The Y-Co binary system  $Y_2Co_{17}$  ( $Th_2Zn_{17}$ -type),  $YCo_5$  ( $CaCu_5$ -type),  $Y_2Co_7$  ( $Gd_2Co_7$ -type),  $YCo_3$  ( $PuNi_3$ -type),  $YCo_2$  ( $MgCu_2$ -type),  $Y_4Co_3$  ( $Ho_4Co_3$ -type),  $Y_3Co$  ( $Fe_3C$ -type), has been modified to include  $Y_3Co_2$  and  $Y_8Co_5$ , recently characterized by Moreau et al. (1975, 1976). For Co borides, see *Sc-Co-B*.

Mutual solubilities of binary compounds were found to be negligible. Nine ternary phases were observed, confirming earlier results (table 36).

The compound  $Y_4Co_3B_3$ , whose structure is still unknown, is a low-temperature

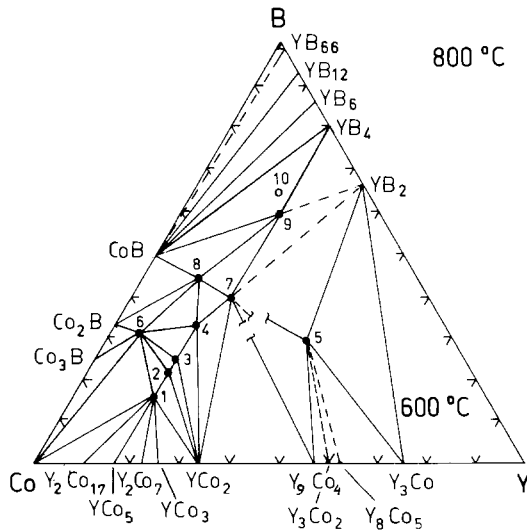


Fig. 46. Y-Co-B, partial isothermal sections at 800°C (0–33 a/o Y), and at 600°C (33–100 a/o Y). 1:  $YCo_4B$ , 2:  $Y_3Co_{11}B_4$ , 3:  $Y_2Co_7B_3$ , 4:  $YCo_3B_2$ , 5:  $Y_4Co_3B_3$ , 6:  $YCo_{12}B_6$  (earlier  $YCo_8B_3$ ), 7:  $YCo_2B_2$ , 8:  $YCo_4B_4$ , 9:  $YCoB_3$ , 10:  $YCoB_4$ .

TABLE 36  
 Formation and structural data of ternary compounds Y-Co-B.

Compound	Structure type, Space group	Lattice parameters Density	Preparation, Characterization	Refs.	Purity
YCo <sub>4</sub> B	CeCo <sub>4</sub> B P6/mmm	$a = 5.005(3)$ $c = 6.864(4)$	AM, Qu 800°C, 50 h, PXD	KuB, 73	
Y <sub>3</sub> Co <sub>11</sub> B <sub>4</sub>	Ce <sub>3</sub> Co <sub>11</sub> B <sub>4</sub> P6/mmm	$a = 5.086(3)$ $c = 9.810(6)$	AM, Qu 800°C, 50 h, PXD	KuB, 73	Y 99 Co 99.87 B 99.3
Y <sub>2</sub> Co <sub>7</sub> B <sub>3</sub>	Ce <sub>2</sub> Co <sub>7</sub> B <sub>3</sub> P6/mmm	$a = 5.045(3)$ $c = 12.88(2)$	AM, Qu 800°C, 50 h, PXD	KuB, 73	
YCo <sub>3</sub> B <sub>2</sub>	CeCo <sub>3</sub> B <sub>2</sub> P6/mmm	$a = 5.033(3)$ $c = 3.038(2)$	AM, Qu 800°C, 50 h, PXD	KuKB, 69	
		$a = 5.020(2), \rho_E = 4.29$ $c = 3.027(2), \rho_X = 7.22$	AM, Qu(Ta) 1150°C, 96 h, PXD refinement. $R = 0.122$	NiY, 73	Y 99.8 Co 99.99 B 99.9
Y <sub>4</sub> Co <sub>3</sub> B <sub>3</sub>	unknown		AM, Qu 800°C, 340 h, QE PXD	KuS, 74	Y 99.5 Co 99.8 B 99.3
YCo <sub>12</sub> B <sub>6</sub> <sup>(**)</sup>	SrNi <sub>12</sub> B <sub>6</sub> R $\bar{3}m$	$a_H = 9.435(6), \rho_E = 7.48$ $c_H = 7.435(5), \rho_X = 7.52$ $a_R = 5.985, \alpha = 104.05^\circ$	AM + M in Al <sub>2</sub> O <sub>3</sub> (Ar) PXD	NiY, 72	Y 99.9 Co 99.99 B 99.9
		$a_H = 9.441(3)$ $c_H = 7.457(3)$	AM, Qu 800°C, 270 h, PXD	KuCC, 81	Y 99.5 Co 99.95 B 99.4
YCo <sub>2</sub> B <sub>2</sub>	ThCr <sub>2</sub> Si <sub>2</sub> I4/mmm	$a = 3.561(3), \rho_E = 6.30$ $c = 9.358(5), \rho_X = 6.39$	AM, Qu 800°C, 150 h PXD, $R = 0.16^{(*)}$	NiSY, 73 NiSY, 71	Y 99.9 Co 99.99 B 99.9
		$a = 3.565$ $c = 9.338$	AM, Qu 800°C, 340 h, PXD	KuS, 74	Y 99.5 Co 99.8 B 99.3
		$a = 3.561(3)$ $c = 9.353(5)$	AM, Qu(Mo) 800°C, 50 h, PXD	Ro, 73	Y 99.9 Co 99.5 B 99.0
YCo <sub>4</sub> B <sub>4</sub>	CeCo <sub>4</sub> B <sub>4</sub> P4 <sub>2</sub> /nmc	$a = 5.028(3)$ $c = 7.015(5)$	no details given, PXD	KuB, 71	
		$a = 5.07$ $c = 7.13$	AM, Qu(Ta) 800°C, 150 h, PXD	NiSY, 73	Y 99.5 Co 99.9 B 99.9
YCoB <sub>4</sub> <sup>(†)</sup>	YCrB <sub>4</sub> Pbam	$a = 5.878$ $b = 11.48$ $c = 3.410$	AM, Qu 800°C, 340 h, PXD	StK, 77	Y 99.8 Co 99.9 B 99.3

<sup>(\*)</sup>Atomic parameters were refined from Debye-Scherrer photographs,  $R = 0.16$ , and in a following paper (Niihara et al., 1973) including anomalous dispersion:  $R = 0.14$ ; Y in 2a); Co in 4d) 0, 1/2, 0.125; B in 4e) 0, 0, 0.378.

<sup>(\*\*)</sup>YCo<sub>12</sub>B<sub>6</sub> originally was observed with formula YCo<sub>8</sub>B<sub>3</sub> by Kuz'ma and Stepanchikova (1974).

<sup>(†)</sup>YCoB<sub>4</sub> corresponds to the earlier denoted "YCoB<sub>3</sub>" (Kuz'ma and Stepanchikova, 1974).

phase, formed after annealing at 600°C; as-cast alloys of this composition were observed to consist of  $YB_2$ ,  $Y_3Co$  and  $YCo_2B_2$ .

In the original paper by Kuz'ma and Stepanchikova (1974) a compound with the approximate formula of " $YCo_8B_3$ " was observed, whose crystal structure was recognized to be monoclinic and isotypic with the structure of " $CeCo_8B_3$ ". The actual crystal structure of " $CeCo_8B_3$ " was quite recently assigned by Kuz'ma et al. (1981) to be isotypic with the rhombohedral structure of  $SrNi_{12}B_6$ . Similarly for " $YCo_8B_3$ " the proper representation was mentioned to be the correct formula  $YCo_{12}B_6$  with the  $SrNi_{12}B_6$ -type of structure.

Some ambiguity exists concerning the compounds " $YCoB_3$ " and  $YCoB_4$ . The existence of " $YCoB_3$ " was derived by Kuz'ma and Stepanchikova (1974) from the isothermal section at 800°C. In a later paper by Stepanchikova and Kuz'ma (1977) the crystal structure of  $YCrB_4$  was attributed to a compound  $YCoB_4$  observed in arc melted alloys which subsequently were heat treated at 800°C. At present it is unclear whether  $YCoB_4$  is a new ternary compound or more likely corresponds to the earlier observed " $YCoB_3$ ". Even boron defects, which are not likely and not especially mentioned by Stepanchikova and Kuz'ma (1977), cannot be ruled out completely. Thus phase equilibria in fig. 46 concerning this area are as reported by Kuz'ma and Stepanchikova (1974); the composition of  $YCoB_4$ , however, is presented by a small open circle.

The microhardness of ternary borides with a boron content of 0–50 a/o B was found to range between 650 to 950 kg/mm<sup>2</sup> (Kuz'ma and Stepanchikova, 1974).

### References

- Kuz'ma, Yu.B. and N.S. Bilonishko, 1971, *Kristallografiya* **16**, 1030.  
 Kuz'ma, Yu.B. and N.S. Bilonishko, 1973, *Kristallografiya* **18**(4), 710.  
 Kuz'ma, Yu.B. and G.F. Stepanchikova, 1974, *Izv. Akad. Nauk SSSR, Neorg. Mater.* **10**(12), 2223.  
 Kuz'ma, Yu.B., P.I. Kripyakevich and N.S. Bilonishko, 1969, *Dopov. Akad. Nauk Ukr. RSR, Ser. A* **10**, 939.  
 Kuz'ma, Yu.B., G.V. Chernjak and N.F. Chaban, 1981, *Dopov. Akad. Nauk Ukr. RSR, Ser. A* **12**, 80.  
 Moreau, J.M., E. Parthé and D. Paccard, 1975, *Acta Crystallogr.* **B31**, 747.  
 Moreau, J.M., D. Paccard and E. Parthé, 1976, *Acta Crystallogr.* **B32**, 496.  
 Niihara, K. and S. Yajima, 1972, *Chem. Lett. (Chem. Soc. Jpn)* 875.  
 Niihara, K. and S. Yajima, 1973, *Bull. Chem. Soc. Jpn* **46**, 770.  
 Niihara, K., T. Shishido and S. Yajima, 1971, *Bull. Chem. Soc. Jpn* **44**, 3214.  
 Niihara, K., T. Shishido and S. Yajima, 1973, *Bull. Chem. Soc. Jpn* **46**, 1137.  
 Rogl, P., 1973, *Monatsh. Chem.* **104**, 1623.  
 Stepanchikova, G.F. and Yu.B. Kuz'ma, 1977, *Vestn. Lvov Univ., Ser. Khim.* **19**, 37.

### Y–Cr–B

Kuz'ma et al. (1970) determined the phase equilibria in the Y–Cr–B system at 800°C (fig. 47) by X-ray and metallographic analysis; samples were prepared by arc melting compacts of B (99.3%) and Cr (99.5%) powders and Y ingots (99.5%) followed by a heat treatment in vacuum sealed quartz capsules at 800°C for 300 h.

Mutual solid solubility of Y and Cr borides was found to be small. Ternary phase equilibria are characterized by one ternary compound  $YCrB_4$ . The crystal structure

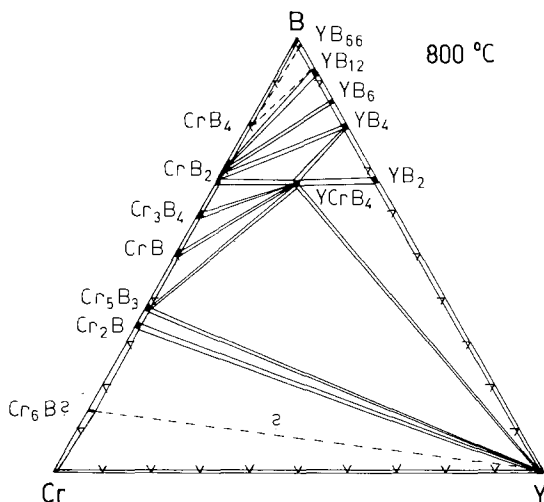


Fig. 47. Y-Cr-B, isothermal section at 800°C.

( $\text{YCrB}_4$ -type, Pbam,  $a = 5.972(5)$ ,  $b = 11.46(1)$ ,  $c = 3.461(4)$ ,  $\rho_{\text{exp}} = 5.14$ ,  $\rho_{\text{theor}} = 5.19 \text{ kg/dm}^3$ ) has been refined from single crystal Laue, rotation and reciprocal lattice photographs:  $R_{hk0} = 0.088$  (Kuz'ma, 1970). Microhardness of  $\text{YCrB}_4$  at a load of 200 g was 2060 kg/mm<sup>2</sup> (Kuz'ma et al., 1970). Concerning the binary Cr-B system controversial reports exist about the crystal structure of the compound " $\text{Cr}_{\sim 6}\text{B}$ " (Epelbaum et al., 1957; Borlera and Pradelli, 1971; Papesch et al., 1973).  $\text{Cr}_2\text{B}$  with filled  $\text{Mn}_4\text{B}$ -type (see also Ce-Mn-B) has been confirmed (Bolera and Pradelli, 1971; Papesch et al., 1973; Kuz'ma et al., 1970).  $\text{Cr}_3\text{B}_4$  is orthorhombic  $\text{Ta}_3\text{B}_4$ -type,  $\text{CrB}_2$  hexagonal,  $\text{AlB}_2$ -type. Papesch et al. (1973) observed a low-temperature modification of CrB with the  $\alpha$ -MoB-type of structure (I4/amd) for  $T \leq 1000^\circ\text{C}$  (transition-shift structures). The solid state transformation in CrB was recently confirmed by Kanaizuka (1982), who reported a transition temperature of  $T \approx 1120^\circ\text{C}$ . In the boron-rich corner of the ternary Y-Cr-B system a more detailed investigation will be necessary concerning the phase equilibria among the well established compounds:  $\text{CrB}_4$ ,  $\text{CrB}_4$ -type (Andersson and Lundström, 1968),  $\text{CrB}_{\sim 41}$  (ss of Cr in  $\beta$ -rh B) (Andersson and Lundström, 1970), and  $\text{YB}_{\sim 66}$ ,  $\text{YB}_{66}$ -type (Richards and Kaspar, 1969).

### References

- Andersson, S. and T. Lundström, 1968, *Acta Chem. Scand.* **22**, 3103.  
 Andersson, S. and T. Lundström, 1970, *J. Solid State Chem.* **2**, 603.  
 Borlera, M.L. and G. Pradelli, 1971, *La Metallurgia Italiana* **2**, 61.  
 Epelbaum, V.A., N.G. Sevastyanov, M.A. Gurevich, B.F. Ormont and G.S. Zhdanov, 1957, *Zh. Neorg. Khim.* **8**, 1848.  
 Kanaizuka, T., 1982, *J. Solid State Chem.* **41**, 195.  
 Kuz'ma, Yu.B., 1970, *Kristallografiya* **15**(2), 372.  
 Kuz'ma, Yu.B., A.S. Sobolev and M.P. Furta, 1970, *Izv. Akad. Nauk SSSR, Neorg. Mater.* **6**(12), 2205.  
 Papesch, G., H. Nowotny and F. Benesovsky, 1973, *Monatsh. Chem.* **104**, 933.  
 Richards, S.M. and J.S. Kaspar, 1969, *Acta Crystallogr.* **B25**, 237.

*Y-Fe-B*

Stepanchikova and Kuz'ma (1980) determined the phase equilibria in the Y-Fe-B system within an isothermal section at 800°C, fig. 48, by means of X-ray analysis of 105 arc melted and annealed samples (800°C, 720 h, Y ingot: 99.3%, Fe powder: 99.99%, B powder: 99.4%). Yttrium-iron compounds observed at 800°C:  $\alpha$ -Y<sub>2</sub>Fe<sub>17</sub> (Th<sub>2</sub>Zn<sub>17</sub>-type), Y<sub>6</sub>Fe<sub>23</sub> (Th<sub>6</sub>Fe<sub>23</sub>-type), YFe<sub>3</sub> (PuNi<sub>3</sub>-type), YFe<sub>2</sub> (MgCu<sub>2</sub>-type), are in agreement with the recent compilation by Iandelli and Palenzona (1979) and by Kubaschewski-von Goldbeck (1982). As far as the Fe-B binary system is concerned, a critical assessment of the phase diagram and thermodynamic data has recently been published by Chart (1981). Fe<sub>2</sub>B (CuAl<sub>2</sub>-type) and FeB are the only two compounds in equilibrium. Earlier findings (Fruchart, 1959) concerning an orthorhombic low-temperature modification of FeB at  $T < 740^\circ\text{C}$  have been confirmed quite recently by Kanaizuka (1982), who also presented a structural model for the low-temperature form based on the random stacking of CrB- and FeB-type layers. Samples with composition FeB annealed at lower temperatures  $T < 650^\circ\text{C}$  were reported to decompose into Fe<sub>2</sub>B + B (Kanaizuka, 1982). All investigators agree on the FeB-type high-temperature modification. There is some doubt about the existence of (metastable?) "FeB<sub>2</sub>" with AlB<sub>2</sub>-type, claimed by Voroshnin et al. (1970) (rather poor agreement between observed and calculated X-ray powder intensities). Similarly a compound claimed at composition FeB<sub>n</sub>,  $n \geq 19$  (see, e.g., Portnoi and Romashov, 1972) rather seems to belong to the ss of Fe in  $\beta$ -rh. B (FeB<sub>~49</sub>, Callmer and Lundström, 1976). For the metastable phases Fe<sub>3</sub>B (and various structure types), and Fe<sub>23</sub>B<sub>6</sub> with Cr<sub>23</sub>C<sub>6</sub>-type, see Herold and Köster (1978). According to a recent investigation by Kahn et al. (1982) Fe<sub>3</sub>B is believed to be in thermodynamic equilibrium with two modifications stable for  $1150^\circ\text{C} < T < 1250^\circ\text{C}$ .

Solid solubilities of binary compounds were found to be negligible, and six ternary compounds were observed.

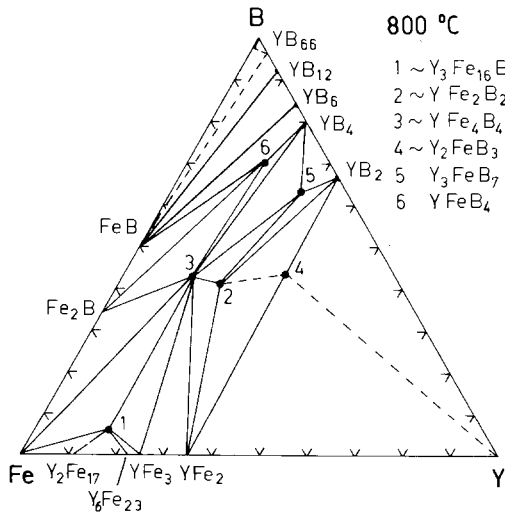


Fig. 48. Y-Fe-B, isothermal section at 800°C.

$Y_3FeB_7$  has the  $Y_3ReB_7$ -type of structure, Cmc $m$ ,  $a = 3.422$ ,  $b = 15.64$ ,  $c = 9.327$ .  $YFeB_4$  crystallizes with  $YCrB_4$ -type, Pbam,  $a = 5.906$ ,  $b = 11.398$ ,  $c = 3.407$  (Stepanchikova and Kuz'ma, 1977; 99.0% Y, 99.9% Fe, 99.3% B, arc melted and annealed at 800°C, 340 h in silica tubes).  $YFe_2B_2$  with  $ThCr_2Si_2$ -type [I4/mmm,  $a = 3.546(5)$ ,  $c = 9.555(10)$ ] has been analyzed by Stepanchikova et al. (1978) from X-ray powder photographs.  $YFe_4B_4$  was claimed to be isostructural with  $CeFe_4B_4$ , P4/nnc(?), structure unsolved.  $Y_{\sim 2}FeB_{\sim 3}$  is hexagonal,  $a = 3.13$ ,  $c = 7.69$ , and isostructural with  $Gd_2FeB_3$ (?). The structure type of  $Gd_2FeB_3$  is unknown but likely derives from the  $AlB_2$ -type (see also  $Gd_2CoB_3$ ). The crystal structure of  $Y_{\sim 3}Fe_{\sim 16}B_{\sim 1}$  is unknown.

### References

- Callmer, B. and T. Lundström, 1976, *J. Solid State Chem.* **17**, 165.  
 Chart, G.T., 1981, Commission des Communautés Européennes, CECA No. 7210-CA/3/303.  
 Fruchart, R., 1959, *Ann. Chem.* **4**, 1247.  
 Herold, U. and U. Köster, 1978, *Z. Metallkde* **69**, 326.  
 Iandelli, A. and A. Palenzona, 1979, in: *Handbook on the Physics and Chemistry of Rare Earths*, Vol. 2, eds. K.A. Gschneidner Jr. and L. Eyring (North-Holland, Amsterdam) pp. 1-54.  
 Kahn, Y., E. Kneller and M. Sostarich, 1982, *Z. Metallkde* **73**(10), 624.  
 Kanaizuka, T., 1982, *J. Solid State Chem.* **41**, 195.  
 Kubaschewski-von Goldbeck, O., 1982, *Iron-binary phase diagrams* (Springer, Berlin) p. 168.  
 Portnoi, K.I. and V.M. Romashov, 1972, *Poroshk. Metall.* **113**(5), 48.  
 Stepanchikova, G.F. and Yu.B. Kuz'ma, 1977, *Vestn. Lvov Univ.*, Ser. Khim. **19**, 37.  
 Stepanchikova, G.F. and Yu.B. Kuz'ma, 1980, *Poroshk. Metall.* **214**(10), 44.  
 Stepanchikova, G.F., Yu.B. Kuz'ma and B.I. Chernjak, 1978, *Dopov. Akad. Nauk Ukr. RSR*, Ser. A **10**, 951.  
 Voroshnin, L.G., L.S. Lyakhovich, G.G. Panich and G.F. Protasevich, 1970, *Metalloved. Term. Obrab. Metal.* **9**, 14.

### Y-Ge-B

Phase equilibria in the Y-Ge-B system at 800°C (fig. 49) were derived by X-ray phase analysis from 53 arc melted alloys (B powder 99.3%, Y ingot 99.9%, Ge ingot 99.999%), which were subsequently heat treated in evacuated quartz capsules (800°C, 360 h) and quenched in ice water (Marko et al., 1978). The  $AlB_2$ -type structure was confirmed for  $Y_2Ge_3$  (Gladyshevskii, 1971), but a composition of  $YGe_2$  was claimed for the  $\alpha$ - $ThSi_2$ -type structure (which disagrees with the results obtained by Schmidt et al., 1972). Mutual solubility of Y germanides:  $Y_5Ge_3$  ( $Mn_5Si_3$ -type),  $Y_3Ge_4$  ( $Sm_3Ge_4$ -type),  $Y_{11}Ge_{10}$  ( $Ho_{11}Ge_{10}$ -type),  $YGe$  (CrB-type),  $Y_2Ge_3$  (defect  $AlB_2$ -type),  $YGe_{1.7}$  (defect  $ThSi_2$ -type ?),  $YGe_2$  (orthorhombic,  $ZrSi_2$ -related),  $YGe_{3.5}$  (orthorhombic), and Y borides was found to be insignificant at 800°C and due to the high thermodynamic stability of  $YB_4$  no equilibrium and no Ge/B exchange is found for the pair of isostructural phases  $Y_2Ge_3$  and  $YB_2$ . The solid solubility of Ge in  $\beta$ -rh. B was recently determined from single crystal counter data to be  $GeB_{\sim 90}$  from an arc melted sample finally heat treated at 925°C (25 h):  $a = 10.9588(8)$ ,  $c = 23.8622(11)$  (Lundström and Terjenius, 1981).

### References

- Gladyshevskii, E.I., 1971, *Crystal Chemistry of Silicides and Germanides* (Izdat. Metallurgiya, Moscow).  
 Lundström, T. and L.E. Terjenius, 1981, *J. Less-Common Metals* **82**, 341.

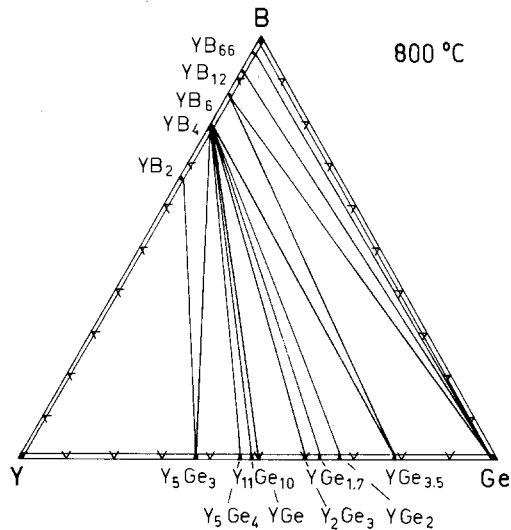


Fig. 49. Y-Ge-B, isothermal section at 800°C.

Marko, M.A., M.S. Nalyvaiko and Yu.B. Kuz'ma, 1978, *Izv. Akad. Nauk SSSR, Neorg. Mater.* **14**(7), 1350.

Schmidt, F.A., O.D. McMasters and N. Carlson, 1972, *J. Less-Common Metals* **26**, 53.

### Y-Ir-B

No phase diagram is available for the Y-Ir-B system, but two ternary compounds are known.

From X-ray and metallographic analysis  $\text{YIr}_4\text{B}_4$  crystallizes congruently from the melt:  $\text{NdCo}_4\text{B}_4$ -type,  $\text{P4}_2/\text{n}$ ,  $a = 7.547(3)$ ,  $c = 3.980(2)$  (Rogl, 1979); for sample preparation, see  $\text{LaOs}_4\text{B}_4$ . Magnetic data were derived by Rupp et al. (1979).

From X-ray powder methods,  $\text{YIr}_3\text{B}_2$  was found to be isostructural with the structure type of  $\text{ErIr}_3\text{B}_2$ ; possible space group  $\text{C2}/\text{m}$ ;  $a = 5.428(6)$ ,  $b = 9.406(9)$ ,  $c = 3.107(4)$ ,  $\beta = 92.8(1)^\circ$  (Ku and Meisner, 1981; samples were arc melted);  $T_n = 1.2$  K.

### Reference

Ku, H.C. and G.P. Meisner, 1981, *J. Less-Common Metals* **78**, 99.

Rogl, P., 1979, *Monatsh. Chem.* **110**, 235.

Rupp, B., P. Rogl and R. Sobczak, 1979, *Mater. Res. Bull.* **14**, 1301.

### Y-Mn-B

$\text{YMnB}_4$  is orthorhombic,  $\text{YCrB}_4$ -type,  $\text{Pbam}$ ,  $a = 5.913(5)$ ,  $b = 11.42(1)$ ,  $c = 3.439(5)$  (Kuz'ma, 1970; X-ray powder analysis); for sample preparation, see  $\text{GdMnB}_4$ .

### Reference

Kuz'ma, Yu.B., 1970, *Dopov. Akad. Nauk Ukr. RSR, Ser. A* **32**(8), 756.

## Y–Mo–B

Phase equilibria in the Y–Mo–B system at 1000°C (fig. 50) were investigated (X-ray and metallographic analysis) by Kuz'ma et al. (1973) and independently (?) reinvestigated by Mikhaleiko and Kuz'ma (1976). In both cases samples were prepared by arc melting and subsequent heat treatment in evacuated silica tubes for 360 h and finally quenched. Starting materials were Y ingot 99.5%, and Mo 99.98% and B 99.3% powders. The Mo–B binary system,  $\text{Mo}_2\text{B}$  (CuAl<sub>2</sub>-type), MoB ( $\alpha$ -MoB-type),  $\text{Mo}_2\text{B}_5$  ( $\text{Mo}_2\text{B}_5$ -type),  $\text{Mo}_{1-x}\text{B}_3$  ( $\text{Mo}_{1-x}\text{B}_3$ -type), is in agreement with a recent critical thermodynamic assessment of phase diagram data by Spear and Wang (1981). For high-temperature phase boundaries, see also Storms and Mueller (1977). There is some inconsistency in the literature about the compound  $\text{Mo}_{1-x}\text{B}_3$  (earlier also referred to as  $\text{MoB}_n$ ,  $\text{MoB}_{12}$ ,  $\text{Mo}_2\text{B}_9$  or  $\text{MoB}_4$ ). Most references agree on  $x$  close to 0.20, which was also derived from a single crystal refinement by Lundström and Rosenberg (1972). Mutual solid solubilities of Mo and Y borides were found to be negligible except for  $\text{YB}_2$  ( $\text{AlB}_2$ -type), which was reported to dissolve up to 5 a/o Mo with a change of lattice parameters from  $\text{YB}_2$ :  $a = 3.298$ ,  $c = 3.843$ , to  $(\text{Y}, \text{Mo})\text{B}_2$ :  $a = 3.302$ ,  $c = 3.773$  Å.  $\text{YMoB}_4$  with  $\text{YCrB}_4$ -type [Pbam,  $a = 6.016(5)$ ,  $b = 11.65(1)$ ,  $c = 3.598(4)$ ] is the only ternary compound (Kuz'ma et al., 1973). Metal-atom parameters were refined from single crystal X-ray photographs: Y in 4g) 0.129, 0.150, 0; Mo in 4g) 0.131, 0.416, 0; boron parameters were taken from  $\text{YCrB}_4$  (Kuz'ma, 1970).

Yttrium was found to exert a retarding effect on the solid state phase transformations: a) the decomposition of h-Mo(Y)B<sub>2</sub>, b) the transformation of h,ℓ-MoB. Whereas in binary alloys the eutectoid decomposition of  $\text{MoB}_2$  is complete at 1000°C, Kuz'ma et al. (1973) reported the presence of the  $\text{AlB}_2$ -type phase  $\text{Mo}(\text{Y})\text{B}_2$  with 5 a/o Y dissolved (1000°C):  $a = 3.036$ ,  $c = 3.062$ . Similarly at 1000°C a specimen  $\text{Y}_{0.20}\text{Mo}_{0.30}\text{B}_{0.50}$  contained the high-temperature CrB-type phase with lattice param-

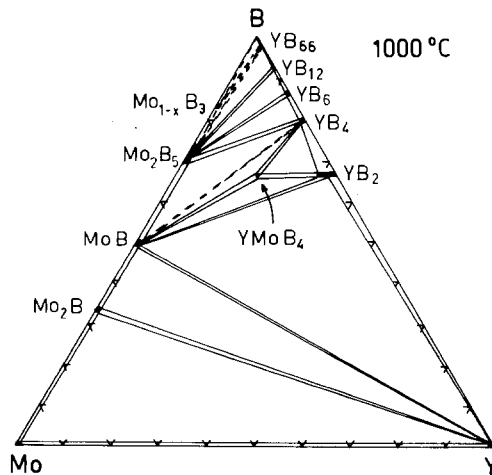


Fig. 50. Y–Mo–B, isothermal section at 1000°C.



ters  $a = 3.140$ ,  $b = 8.46$ ,  $c = 3.075$ . Again the polymorphic transition of monoborides is complete within the binary. On further annealing of the samples for 800 h at  $1000^\circ\text{C}$ , both high-temperature phases disappeared (non-equilibrium phases). A single crystal study of a fragment obtained from a  $\text{Y}_{0.25}\text{Mo}_{0.25}\text{B}_{0.50}$  melt revealed a similar system of diffuse and sharp X-ray reflections as described by Boller et al. (1964) for the shift-like transition of tungsten monoboride.

### References

- Boller, H., W. Rieger and H. Nowotny, 1964, *Monatsh. Chem.* **95**, 1497.  
 Kuz'ma, Yu.B., 1970, *Kristallografiya* **15**, 372.  
 Kuz'ma, Yu.B., S.I. Svarichevskaya and A.S. Sobolev, 1973, *Izv. Akad. Nauk SSSR, Neorg. Mater.* **9**(10), 1697.  
 Lundström, T. and I. Rosenberg, 1972, *J. Solid State Chem.* **6**, 299.  
 Mikhalenko, S.I. and Yu.B. Kuz'ma, 1976, *Poroshk. Metall.* **158**(2), 56.  
 Spear, K.E. and M.S. Wang, 1981, *Calphad* **5**(2), 109.  
 Storms, E. and B. Mueller, 1977, *J. Phys. Chem.* **81**, 318.

### Y-Ni-B

The Y-Ni-B phase diagram at  $700^\circ\text{C}$  was derived by Kuz'ma and Khaburshaya (1973) by means of X-ray analysis as well as metallography of 216 arc melted and subsequently annealed alloys ( $700^\circ\text{C}$ , 500 h in evacuated silica tubes). Starting materials were Y ingots 99.5%, and B 99.3% and Ni 99.98% powders. The Y-Ni binary compounds:  $\text{Y}_3\text{Ni}$  ( $\text{Fe}_3\text{C}$ -type),  $\text{YNi}$  ( $\text{FeB}$ -type),  $\text{YNi}_2$  ( $\text{MgCu}_2$ -type),  $\text{YNi}_3$  ( $\text{PuNi}_3$ -type),  $\text{Y}_2\text{Ni}_7$  ( $\text{Gd}_2\text{Co}_7$ -type),  $\text{YNi}_5$  ( $\text{CaCu}_5$ -type),  $\text{Y}_2\text{Ni}_{17}$  ( $\text{Th}_2\text{Ni}_{17}$ -type), are in agreement with the compilation by Iandelli and Palenzona (1979). Besides the well established nickel borides,  $\text{Ni}_3\text{B}$  ( $\text{Fe}_3\text{C}$ -type),  $\text{Ni}_2\text{B}$  ( $\text{CuAl}_2$ -type) *m*, *o*- $\text{Ni}_4\text{B}_3$ ,  $\text{NiB}$  ( $\text{CrB}$ -type), some ambiguity exists about a compound  $\text{NiB}_n$ ,  $n \geq 12$  (e.g. Portnoi et al., 1967), which was not found in a detailed investigation by Lundström (1969). A considerable solid solubility of Ni in  $\beta$ -rh. B, however, seems to exist (Carlsson and Lundström, 1970).

Solid solubilities of binary compounds were found to be negligible; eleven ternary compounds were observed (see fig. 51); the crystal structures of several of them:  $\text{Y}_2\text{Ni}_2\text{B}$ ,  $\text{Y}_2\text{Ni}_4\text{B}_3$ ,  $\text{Y}_1\text{Ni}_4\text{B}_3$ ,  $\text{Y}_1\text{Ni}_3\text{B}_2$  and  $\text{Y}_1\text{Ni}_4\text{B}_7$ , have not been characterized.

Niihara et al. (1973) obtained  $\text{YNi}_4\text{B}$  by arc melting an elemental mixture of  $\text{Y}_{0.167}\text{Ni}_{0.667}\text{B}_{0.167}$  and from X-ray powder data a hexagonal unit cell was proposed:  $\text{P6/mmm}$ ,  $a = 4.977(4)$ ,  $c = 6.942(5)$ ,  $\rho_{\text{exp}} = 7.38$ ,  $\rho_{\text{theor}} = 7.46 \text{ kg/dm}^3$ ,  $Z = 2$ . With a reliability factor of  $R = 0.148$  the atomic parameters [Y in 1a) 0, 0, 0; 1b) 0, 0, 1/2; Ni in 2c) 1/3, 2/3, 0; Ni in 6i) 1/2, 0, 0.29 and B in 2d) 1/3, 2/3, 1/2] were claimed to indicate isostructural behavior with the structure type of  $\text{CeCo}_4\text{B}$  (Kuz'ma and Bilonishko, 1973). In a more detailed X-ray study of  $\text{YNi}_4\text{B}$  single crystal photographs Kuz'ma and Khaburskaya (1973) were able to detect a three-fold superstructure confirming the  $\text{CeCo}_4\text{B}$  subcell, according to  $a = 14.89(5) = 3a_0$  and  $c = 6.91(2)$ . As stated by Kuz'ma and Khaburskaya (1973), the superstructure reflections are too weak to be discernible from X-ray powder data. A complete crystal structure analysis, however, is still lacking.

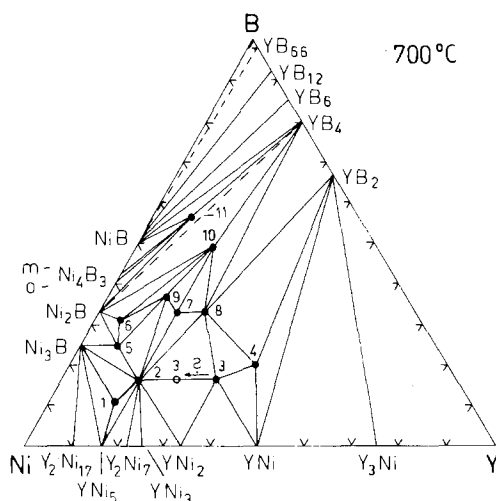


Fig. 51. Y-Ni-B, isothermal section at 700°C. 1:  $Y_3Ni_{13}B_2$ , 2:  $YNi_4B$ , 3:  $Y_2Ni_3B$  ( $Dy_3Ni_7B_2$ -type (?), see also text), 4:  $Y_2Ni_{12}B$ , 5:  $YNi_8B_3$  ( $SrNi_{12}B_6$ -type), 6:  $YNi_{12}B_6$  (?), 7:  $Y_2Ni_4B_3$ , 8:  $YNi_3B_2$ , 9:  $YNi_4B_3$ , 10:  $YNi_2B_3$ , 11:  $YNi_4B_7$ .

$YNi_2B_3$  is isostructural with  $CeNi_2B_3$ , tetragonal, structure unsolved (Kuz'ma and Khaburskaya, 1973).

" $YNi_8B_3$ " was first claimed to be monoclinic and isostructural to  $CeCo_8B_3$  (Kuz'ma and Khaburskaya, 1973), but later revised to crystallize with the  $SrNi_{12}B_6$ -type,  $R\bar{3}m$ ,  $a_H = 9.525(3)$ ,  $c_H = 7.421(3)$  (Kuz'ma et al., 1981); for sample preparation, see  $YCo_{12}B_6$ . However, some conflict now exists with the orthorhombic compound,  $a = 9.71(2)$ ,  $b = 7.26(2)$ ,  $c = 11.52(3)$ , claimed to be isostructural with  $CeNi_{12}B_6$ , whose structure is still unsolved (Kuz'ma and Khaburskaya, 1973).

Kuz'ma and Chaban (1979) prepared  $Y_3Ni_7B_2$  with  $Dy_3Ni_7B_2$ -type structure,  $P6_3/mmc$ ,  $a = 5.128(2)$ ,  $c = 14.343(10)$ , by arc melting elemental mixtures (Y ingot 99.5%, B powder 99.3%, Ni powder 99.98%) and subsequent annealing in evacuated silica capsules at 800°C for 360 h. At present it is not clear, whether  $Y_3Ni_7B_2$  is a high-temperature phase or corresponds to the yttrium-rich phase  $Y_{\sim 2}Ni_{\sim 3}B$ , earlier reported by Kuz'ma and Khaburskaya (1973). Y/Ni substitution, although less likely, cannot be ruled out completely.

$Y_3Ni_{13}B_2$  with the  $Nd_3Ni_{13}B_2$ -type of structure,  $P6/mmm$ ,  $a = 4.942(3)$ ,  $c = 10.886(11)$ , has been characterized by Kuz'ma and Bilonishko (1981) (this compound was first referred to as  $YNi_{\sim 5}B$  with monoclinic symmetry; Kuz'ma and Khaburskaya, 1973).

### References

- Carlsson, J.O. and T. Lundström, 1970, *J. Less-Common Metals* **22**, 317.  
 Iandelli, A. and A. Palenzona, 1979, in: *Handbook on the Physics and Chemistry of Rare Earths*, Vol. 2, eds. K.A. Gschneidner Jr. and L. Eyring (North-Holland, Amsterdam) pp. 1-54.  
 Kuz'ma, Yu.B. and N.S. Bilonishko, 1973, *Kristallografiya* **18**, 710.  
 Kuz'ma, Yu.B. and N.S. Bilonishko, 1981, *Dopov. Akad. Nauk Ukr. RSR, Ser. A* **10**, 88.

- Kuz'ma, Yu.B. and N.F. Chaban, 1979, *Dopov. Akad. Nauk Ukr. RSR, Ser. A*, 88.  
 Kuz'ma, Yu.B. and M.P. Khaburskaya, 1973, *Izv. Akad. Nauk SSSR, Neorg. Mater.* **11**(10), 1893.  
 Kuz'ma, Yu.B., G.V. Chernjak and N.F. Chaban, 1981, *Dopov. Akad. Nauk Ukr. RSR, Ser. A* **12**, 80.  
 Lundström, T., 1969, *Arkiv Kemi* **31**, 227.  
 Niihara, K., Y. Katayama and S. Yajima, 1973, *Chem. Lett. (Chem. Soc. Jpn)* 613.  
 Portnoi, K.I., V.M. Romashov, V.M. Chubarov, M.K. Levinskaya and S.E. Salibekov, 1967, *Poroshk. Metall.* **50**(2), 15.

*Y–Os–B*

No ternary phase diagram is available for the Y–Os–B system. The crystallographic data and methods of preparation of five ternary phases are given in table 37.

*References*

- Ku, H.C., 1980, Thesis, Univ. of California at San Diego, USA.  
 Ku, H.C. and R.N. Shelton, 1980, *Mater. Res. Bull.* **15**(10), 1441.  
 Rogl, P., 1978, *Mater. Res. Bull.* **13**, 519.  
 Rogl, P., 1979, *Monatsh. Chem.* **110**, 235.

TABLE 37  
 Formation and structural data of ternary compounds Y–Os–B.

Compound	Structure type, Space group	Lattice parameters, Density	Preparation, Characterization	Refs.	Purity
YOsB <sub>4</sub>	YCrB <sub>4</sub> Pbam	$a = 5.955(3)$ $b = 11.527(6)$ $c = 3.556(2)$	AM, HT, 1600°C, 12 h HV, W substrate, QE congruent melting, ME PXD suscept., 80–300 K, $T_c = 1.40$	Ro, 78 SoR, 79 KuS, 80	Y 99.9 Os 99.9 B 99.0
Y <sub>2</sub> OsB <sub>6</sub>	Y <sub>2</sub> ReB <sub>6</sub> Pbam	$a = 9.1592(10)$ $b = 11.5311(25)$ $c = 3.6473(2)$	AM, HT, 1600°C, 12 h HV, W substrate, QE PXD	RoN, 82	Y 99.9 Os 99.9 B 99.7
YOsB <sub>2</sub>	LuRuB <sub>2</sub> Pbam	$a = 5.905(6)$ $b = 5.299(5)$ $c = 6.391(7)$	AM(Zr), Ta tubes, 1250°C, 24 h, 800°C, 9 d PXD, $T_c = 2.22$ –1.60 K	ShKPJK, 80 KuS, 80	99.9
YOs <sub>4</sub> B <sub>4</sub>	YOs <sub>4</sub> B <sub>4</sub> tetragonal	$a = 7.4650(5)$ $c = 32.8160(32)$ $c = 8c_0$	AM, HT, 1400°C, 12 h HV, BN substrate PXD $T_n = 1.2$ K	Ro, 79 Ku, 80	Y 99.9 Os 99.9 B 99.7
YOs <sub>3</sub> B <sub>2</sub>	YOs <sub>3</sub> B <sub>3</sub> (?) orthorh. (?) related to CeCo <sub>3</sub> B <sub>2</sub>	$a \approx 5.5$ $b \approx 9.5$ $c \approx 18$ $a = a_H$ $b = \sqrt{3} a_H$ $c = 6c_H$	AM(Zr), PXD $T_c = 6.00$ –4.97 K	Ku, 80	99.9

Rogl, P. and H. Nowotny, 1982, Crystal structures and phase relationships within ternary systems: rare earth metal-noble metal-boron, in: Rare Earths in Science and Technology, Vol. 3, eds. J. McCarthy, B. Silber and J.J. Rhyne (Plenum, New York, London) pp. 353-356.

Shelton, R.N., B.A. Karcher, D.R. Powell, R.A. Jacobson and H.C. Ku, 1980, Mater. Res. Bull. **15**, 1445.  
Sobczak, R. and P. Rogl, 1979, J. Solid State Chem. **27**, 343.

### Y-Re-B

An isothermal section of the Y-Re-B system at 1000°C was presented by Mikhailenko et al. (1977) (fig. 52), based on X-ray and metallographic analysis of heat treated alloys (360 h in evacuated silica capsules). Starting materials were Y ingots 99.3%, and Re 99.7% and B 99.4% powders. Mutual solid solubilities of binary phases were negligible.  $YRe_2$  is  $MgZn_2$ -type; for La borides, see La-Cr-B, and for Re borides, see La-Re-B. Earlier data on  $YReB_4$ ,  $Y_2ReB_6$  and  $Y_3ReB_7$  were confirmed and two new ternary compounds  $YRe_{\sim 4}B_{\sim 4}$  and  $YRe_{\sim 11}B$  were identified.  $YReB_4$  is orthorhombic  $YCrB_4$ -type,  $Pbam$ ,  $a = 6.000(5)$ ,  $b = 11.48(1)$ ,  $c = 3.577(5)$  (Kuz'ma and Svarichevskaya, 1972a).  $Y_2ReB_6$  with  $Y_2ReB_6$ -type ( $Pbam$ ,  $a = 9.175(5)$ ,  $b = 11.55(1)$ ,  $c = 3.673(4)$ ,  $\rho_{exp} = 7.23 \text{ kg/dm}^3$ ,  $\rho_{theor} = 7.35 \text{ kg/dm}^3$ ) was characterized by Kuz'ma and Svarichevskaya (1972b); atom parameters were refined from single crystal photographs:  $R_{hk0} = 0.129$ ,  $R_{hkl} = 0.116$ . Atom parameters of  $Y_3ReB_7$  ( $Y_3ReB_7$ -type,  $Cmcm$ ,  $a = 3.525(2)$ ,  $b = 15.80(1)$ ,  $c = 9.366(5)$ ,  $\rho_{exp} = 6.14$ ,  $\rho_{theor} = 6.77 \text{ kg/cm}^3$ ) were refined from crystal photographs by Kuz'ma and Mikhailenko (1976)  $R_{0kl} = 0.185$ ,  $R_{hkl} = 0.209$ .

$YRe_{\sim 4}B_{\sim 4}$  is tetragonal,  $a = 7.40$ ,  $c = 10.58$ , and was claimed to be isostructural with  $CeRe_{\sim 4}B_{\sim 4}$  (structure unsolved).

$YRe_{\sim 11}B$  is cubic,  $a = 10.66$ ; its crystal structure is unsolved.

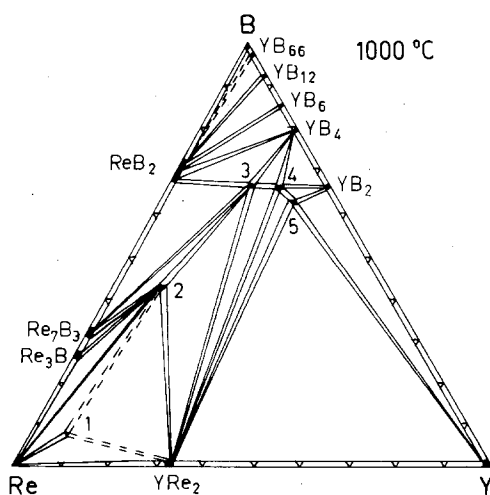


Fig. 52. Y-Re-B, isothermal section at 1000°C. 1:  $YRe_{\sim 11}B$ , 2:  $YRe_{\sim 4}B_{\sim 4}$ , 3:  $YReB_4$ , 4:  $Y_2ReB_6$ , 5:  $Y_3ReB_7$ .

*References*

- Kuz'ma, Yu.B. and S.I. Mikhalenko, 1976, *Dopov. Akad. Nauk Ukr. RSR, Ser. A* **11**, 1029.  
 Kuz'ma, Yu.B. and S.I. Svarichevskaya, 1972a, *Dopov. Akad. Nauk Ukr. RSR, Ser A* **34**(2), 166.  
 Kuz'ma, Yu.B. and S.I. Svarichevskaya, 1972b, *Kristallografiya* **17**(3), 658.  
 Mikhalenko, S.I., Yu.B. Kuz'ma and A.S. Sobolev, 1977, *Poroshk. Metall* **169**(1), 48.

*Y-Rh-B*

Vandenberg and Matthias (1977) established the crystal structure of  $YRh_4B_4$  to be isostructural with the  $CeCo_4B_4$ -type of structure ( $P4_2/nmc$ ):  $a = 5.308(2)$ ,  $c = 7.403(3)$  (X-ray powder diffraction). Samples were prepared by arc melting with excess of Rh and B and finally contained  $YRh_4B_4 + RhB$ ;  $\rho_{exp} = 8.55 \text{ kg/dm}^3$ . Precise atom parameters were refined by Yvon and Grüttner (1980) by single crystal X-ray diffraction analysis (see table 29).  $T_c = 11.34\text{--}11.26 \text{ K}$ , as reported by Matthias et al. (1977) for a sample  $YRh_4B_4 + 2 RhB$ .

The only information concerning phase equilibria in the Y-Rh-B system near the composition  $YRh_4B_4$  has been reported by Johnston (1977). At  $800\text{--}1200^\circ\text{C}$   $YRh_4B_4$  was found to be of  $CeCo_4B_4$ -type and in equilibrium with  $RhB$  (NiAs-type?),  $YRh_3B_2$  ( $ErIr_3B_2$ -type),  $YRhB_4$  (structure unknown) and  $YRh_6B_4$  (structure unknown). Arc melted samples of  $YRh_4B_4$  were, on the basis of an X-ray powder analysis, said to melt incongruently and arc melted samples within the region  $YRh_4B_4\text{--}YRh_6B_4\text{--}RhB$  contained primarily the  $LuRu_4B_4$ -type phase (high-temperature phase, metastable?,  $T_c = 9\text{--}10 \text{ K}$ ). See also  $Y(Rh, Ru)_4B_4$ .

From X-ray powder analysis of arc melted samples,  $YRh_3B_2$  was found to crystallize with the  $ErIr_3B_2$ -type of structure (possible space group  $C2/m$ ):  $a = 5.377(6)$ ,  $b = 9.325(9)$ ,  $c = 3.102(4)$ ,  $\beta = 90.9(1)^\circ$  (Ku and Meisner, 1981);  $T_n = 1.2 \text{ K}$ .

The boron solubility in  $YRh_3B_{1-x}$ ,  $Cu_3Au$ -type,  $Pm3m$ , was found to extend from  $x = 0.6$  to  $x = 1.0$  (Rogl and DeLong, 1983; X-ray powder analysis of arc melted samples annealed at  $1400^\circ\text{C}$ , 24 h, HV, BN substrate). Lattice parameters were as follows:  $YRh_3B$ :  $a = 4.1656(3)$ ,  $YRh_3B_{0.85}$ :  $a = 4.1392(8)$ ;  $YRh_3B_{0.65}$ :  $a = 4.1011(8)$ ,  $YRh_3B_{0.6}$ :  $a = 4.0840(5)$ ;  $T_n = 1.5 \text{ K}$ .

*References*

- Johnston, D.C., 1977, *Solid State Commun.* **24**, 699.  
 Ku, H.C. and G.P. Meisner, 1981, *J. Less-Common Metals* **78**, 99.  
 Matthias, B.T., E. Corenzwit, J.M. Vandenberg and H.E. Barz, 1977, *Proc. Nat'l Acad. Sci. US* **74**(4), 1334.  
 Rogl, P. and L. DeLong, 1983, *J. Less-Common Metals*, in press.  
 Vandenberg, J.M. and B.T. Matthias, 1977, *Proc. Nat'l Acad. Sci. US* **74**(4), 1336.  
 Yvon, K. and A. Grüttner, 1980, The influence of the formal electric charge on the size of the transition metal atom cluster in  $YRh_4B_4$ ,  $YRu_4B_4$  and  $PbMo_6S_8$  related compounds, in: *Superconductivity in d- and f-band metals*, eds. H. Suhl and M.B. Maple (Academic Press, New York) pp. 515–519.

*Y-Ru-B*

Five ternary compounds have been identified in the Y-Ru-B system.

YRuB<sub>4</sub> has the YCrB<sub>4</sub>-type of structure, Pbam,  $a = 5.954(3)$ ,  $b = 11.524(6)$ ,  $c = 3.559(2)$  and forms congruently from the melt (Rogl, 1978); X-ray and metallographic analysis of as-cast as well as annealed alloys (1600°C, 12 h, high vacuum, tungsten substrate, radiation quench). Starting materials were R filings 99.9%, Ru 99.9% and B 99.0% powders. Magnetic behavior was investigated by Sobczak and Rogl (1979); the superconducting transition temperature was  $T_c = 1.38\text{--}1.29$  K, as measured by Ku and Shelton (1980).

Using the same preparation techniques as for YRuB<sub>4</sub>, Rogl and Nowotny (1982) determined the structure of Y<sub>2</sub>RuB<sub>6</sub> from X-ray powder data: Y<sub>2</sub>ReB<sub>6</sub>-type, Pbam,  $a = 9.1498(16)$ ,  $b = 11.5139(32)$ ,  $c = 3.6501(2)$ .

YRu<sub>3</sub>B<sub>2</sub> with a CeCo<sub>3</sub>B<sub>2</sub>-type of structure [P6/mmm,  $a = 5.471(4)$ ,  $c = 3.027(2)$ ] is confirmed by Hiebl et al. (1980) from X-ray powder analysis of arc melted alloys annealed at 1400°C, 24 h in high vacuum on a BN substrate; starting materials were 99.9% pure, B 99.7%. In agreement with them Ku et al. (1980) gave  $a = 5.481(6)$ ,  $c = 3.028(4)$ , from arc melted alloys; the X-ray powder pattern has been refined to  $R = 0.12$ ;  $T_n = 1.2$  K.

The crystal structure (X-ray powder diffraction) as well as superconducting and magnetic properties of arc melted alloys YRu<sub>4</sub>B<sub>4</sub> were analysed by Johnston (1977): YRu<sub>4</sub>B<sub>4</sub> adopts the LuRu<sub>4</sub>B<sub>4</sub>-type of structure, I4<sub>1</sub>/acd,  $a = 7.454(5)$ ,  $c = 14.994(10)$ . The crystal structure was refined by Yvon and Grüttner (1980) by single crystal X-ray diffraction (table 29);  $T_c = 1.40\text{--}1.38$  K (Matthias et al., unpublished).

YRuB<sub>2</sub> crystallizes with the LuRuB<sub>2</sub>-type of structure, Pnma,  $a = 5.918(6)$ ,  $b = 5.297(5)$ ,  $c = 6.377(7)$  (X-ray powder methods; Shelton et al., 1980); for sample preparation, see ScOsB<sub>2</sub>.  $T_c = 7.80\text{--}7.68$  K as reported by Ku and Shelton (1980).

### References

- Hiebl, K., P. Rogl, E. Uhl and M.J. Sienko, 1980, *Inorg. Chem.* **19**, 3316.  
 Johnston, D.C., 1977, *Solid State Commun.* **24**, 699.  
 Ku, H.C. and R.N. Shelton, 1980, *Mater. Res. Bull.* **15**(10), 1441.  
 Ku, H.C., G.P. Meisner, F. Acker and D.C. Johnston, 1980, *Solid State Commun.* **35**, 91.  
 Matthias, B.T., E. Corenzwit and H. Barz, unpublished data, as quoted by Ku and Shelton (1980).  
 Rogl, P., 1978, *Mater. Res. Bull.* **13**, 519.  
 Rogl, P. and H. Nowotny, 1982, Crystal structures and phase relationships within ternary systems: rare earth metal-noble metal-boron, in: *Rare Earths in Science and Technology*, Vol. 3, eds. J. McCarthy, B. Silber and J.J. Rhyne (Plenum, New York, London) pp. 353–356.  
 Shelton, R.N., B.A. Karcher, D.R. Powell, R.A. Jacobson and H.C. Ku, 1980, *Mater. Res. Bull.* **15**, 1445.  
 Sobczak, R. and P. Rogl, 1979, *J. Solid State Chem.* **27**, 343.  
 Yvon, K. and A. Grüttner, 1980, The influence of the formal electric charge on the size of the transition metal atom cluster in YRh<sub>4</sub>B<sub>4</sub>, YRu<sub>4</sub>B<sub>4</sub> and PbMo<sub>6</sub>S<sub>8</sub> related compounds, in: *Superconductivity in d- and f-band metals*, eds. H. Suhl and M.B. Maple (Academic Press, New York) pp. 515–519.

### Y–Si–B

Chaban and Kuz'ma (1971) investigated the phase equilibria of the system Y–Si–B in an isothermal section at 800°C by means of X-ray and metallographic analysis of arc melted and subsequently annealed alloys (480 h in evacuated quartz tubes, quenched in cold water). Starting materials were: Y ingots 99.90%, B powder 99.3%

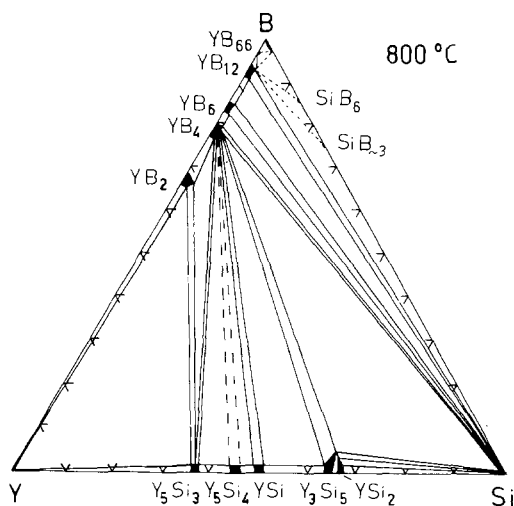


Fig. 53. Y-Si-B, isothermal section at 800°C; region  $YB_{12}$ -Si-B is proposed.

and Si powder 99.99%. Yttrium silicides reported,  $Y_5Si_3$  ( $Mn_5Si_3$ -type),  $Y_5Si_4$  ( $Sm_5Ge_4$ -type), YSi (CrB-type),  $Y_3Si_5$  (defect  $AlB_2$ -type),  $YSi_2$  ( $GdSi_2$ -type?), are in good agreement with the compilation of Iandelli and Palenzona (1979).

Concerning the B-Si binary system, at least two compounds seem to be well established (Lugscheider et al., 1979; Salanoubat, 1980; Vlasse and Viala, 1981). The solid solubility of Si in  $\beta$ -rh. B has been studied recently by Vlasse and Viala (1981); from samples which were reacted for 1 h in BN crucibles at 1660°C and quenched in argon the solubility limit found was  $SiB_{\sim 36}$ ,  $a = 11.01(1)$ ,  $c = 23.90(2)$ ,  $R\bar{3}m$ . The starting materials were 99.7% B and 99.9% Si.

Mutual solid solubilities at 800°C were found to be negligible, except for  $Y_3Si_5$  and  $YB_2$ .  $Y_3Si_5$  is  $AlB_2$ -type with  $a = 3.842$ ,  $c = 4.140$  and dissolves up to 3 a/o B, changing its lattice parameters to  $a = 3.842$ ,  $c = 4.096$ .  $YB_2$  ( $AlB_2$ -type,  $a = 3.298$ ,  $c = 3.843$ ) dissolves up to 2 a/o Si ( $a = 3.323$ ,  $c = 3.863$ ). The boron-rich region B-Si- $YB_{12}$  has not been studied and is tentative (fig. 53).

### References

- Chaban, N.F. and Yu.B. Kuz'ma, 1971, *Dopov. Akad. Nauk Ukr. RSR, Ser. A* **11**, 1048.  
 Iandelli, A. and A. Palenzona, 1979, *Crystal chemistry of intermetallic compounds*, in: *Handbook on the Physics and Chemistry of Rare Earths*, Vol. 2, eds. K.A. Gschneidner Jr. and L. Eyring (North-Holland, Amsterdam) pp. 1-54.  
 Lugscheider, E., H. Reimann and W.J. Quadakker, 1979, *Ber. Deutsch. Keram. Ges.* **59**(10), 301.  
 Salanoubat, D., 1980, Thesis, Univ. of Perpignan, France.  
 Vlasse, M. and J.C. Viala, 1981, *J. Solid State Chem.* **37**, 181.

### Y-Th-B

Superconductivity in hexaboride solid solutions  $Y_xTh_{1-x}B_6$  was studied by Hiebl and Sienko (1980) on samples prepared by borothermal reduction of the mixed

oxides ( $Y_2O_3$ , 99.9999%;  $ThO_2$ , 99.95%; B, 99.999%) in  $ZrB_2$  crucibles at  $\approx 1700^\circ C$  in vacuum. The samples were reground, reheated and finally analysed by X-ray diffraction as well as atomic absorption spectroscopy.

Lattice parameters of homogeneous solid solutions (CaB<sub>6</sub>-type, Pm3m) were:  $YB_6$ :  $a = 4.0994(10)$ ;  $Y_{0.88}Th_{0.12}B_6$ :  $a = 4.1009(10)$ ;  $Y_{0.70}Th_{0.30}B_6$ :  $a = 4.1023(10)$ ;  $Y_{0.41}Th_{0.59}B_6$ :  $a = 4.1051(10)$ ;  $Y_{0.35}Th_{0.65}B_6$ :  $a = 4.1057(10)$ ;  $Y_{0.28}Th_{0.72}B_6$ :  $a = 4.1062(10)$ ;  $ThB_6$ :  $a = 4.1099(10)$ .

### Reference

Hiebl, K. and M.J. Sienko, 1980, *Inorg. Chem.* **19**, 2179.

### Y-U-B

Giorgi et al. (1974) studied the onset of ferromagnetic ordering in  $(Y_xU_{1-x})B_4$  alloys in the as-cast condition (arc melted) and after heat treatment for 7 h at  $1400^\circ C$ . From X-ray powder diffraction analysis samples were found to be homogeneous ThB<sub>4</sub>-type, P4/mbm. Lattice parameters are presented in fig. 54. The relationship between the lattice parameters of the  $(Y_xU_{1-x})B_4$  phases and its Curie temperature are shown in fig. 55.

### References

Giorgi, A.L., E.G. Szklarz, R.W. White and H.H. Hill, 1974, *J. Less-Common Metals* **34**, 348.

Hill, H., A.L. Giorgi, E.G. Szklarz and J.L. Smith, 1974, *J. Less-Common Metals* **38**, 239.

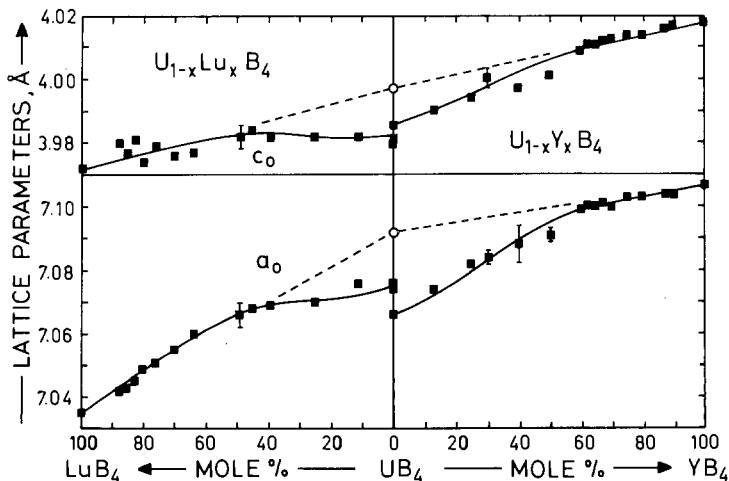


Fig. 54. Lattice parameters as a function of  $x$  for the solid solutions  $U_{1-x}Lu_xB_4$  and  $U_{1-x}Y_xB_4$  (values of  $x$  are nominal values). Different parameters of  $UB_4$  were claimed to suggest a small homogeneous region. Dashed lines are linear extrapolations to a hypothetical magnetic  $UB_4$  ( $a = 7.092$ ,  $c = 3.997$ ). Solid curves represent theoretical dependences based on a statistical dilution model incorporating two different sizes of U atoms. (After Giorgi et al. 1974.)



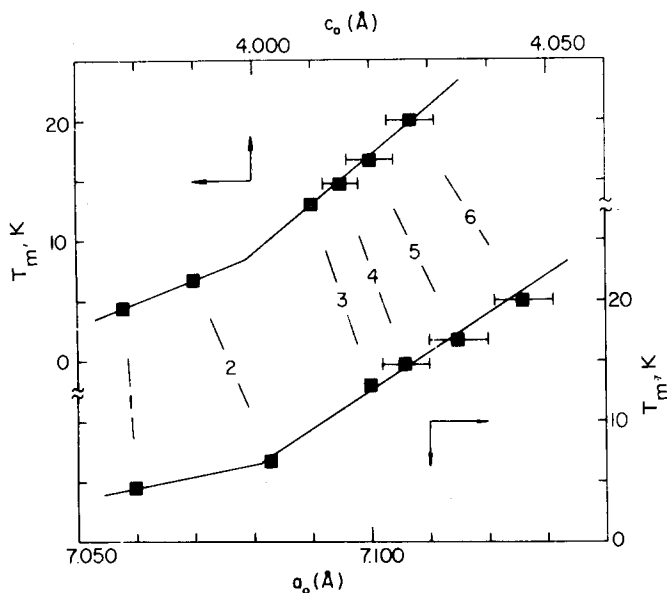


Fig. 55. Curie temperatures versus lattice parameters for 1:  $(\text{Lu}_{0.64}\text{U}_{0.36})\text{B}_4$ ; 2:  $(\text{U}_{0.40}\text{Lu}_{0.30}\text{Y}_{0.30})\text{B}_4$ ; 3:  $(\text{U}_{0.40}\text{Y}_{0.60})\text{B}_4$ ; 4:  $(\text{U}_{0.39}\text{Y}_{0.49}\text{La}_{0.12})\text{B}_4$ ; 5:  $(\text{U}_{0.39}\text{Y}_{0.42}\text{La}_{0.19})\text{B}_4$ ; 6:  $(\text{U}_{0.39}\text{Y}_{0.37}\text{La}_{0.24})\text{B}_4$  (all concentrations nominal); after Hill et al. (1974).

#### Y-V-B

$\text{YVB}_4$  is isotypic with the crystal structure of  $\text{YCrB}_4$ ,  $\text{Pbam}$ ,  $a = 5.975(5)$ ,  $b = 11.60(1)$ ,  $c = 3.485(5)$  (Kuz'ma, 1970; X-ray powder diffraction); for sample preparation (V 95.5% powder), see  $\text{GdMnB}_4$ .

#### Reference

Kuz'ma, Yu.B., 1970, *Dopov. Akad. Nauk Ukr. RSR, Ser. A* **32**(8), 756.

#### Y-W-B

Phase equilibria in the Y-W-B system at  $1000^\circ\text{C}$  (fig. 56) were investigated (X-ray and metallographic analysis) by Kuz'ma et al. (1973) and independently(?) reinvestigated by Mikhaleenko and Kuz'ma (1976). In both cases samples were prepared by arc melting and subsequent heat treatment in evacuated silica tubes (360 h) and finally quenched. Starting materials were Y ingots 99.5%, and W 99.98% and B 99.3% powders. The tungsten-boron binary system at  $1000^\circ\text{C}$ :  $\text{W}_2\text{B}$  ( $\text{CuAl}_2$ -type),  $\text{WB}$  ( $\alpha$ - $\text{MoB}$ -type),  $\text{W}_2\text{B}_5$  ( $\text{W}_2\text{B}_5$ -type),  $\text{W}_{1-x}\text{B}_3$  ( $\text{Mo}_{1-x}\text{B}_3$ -type), is in agreement with earlier phase diagram studies, e.g., by Rudy and Windisch (1965). The exact temperature and nature of a polymorphic transition of  $\text{W}_2\text{B}_5$  (low-temperature form with  $\text{Mo}_2\text{B}_5$ -type, claimed by Kuz'ma et al., 1967) has not been determined yet.  $\text{W}_{1-x}\text{B}_3$  ( $x \approx 0.2$ , earlier described as  $\text{W}_2\text{B}_9$ ,  $\text{WB}_{\sim 12}$ ,  $\text{WB}_4$ ) probably is isotypic with  $\text{Mo}_{1-x}\text{B}_3$  (Lundström and Rosenberg, 1973; Nowotny et al., 1967). Mutual solid

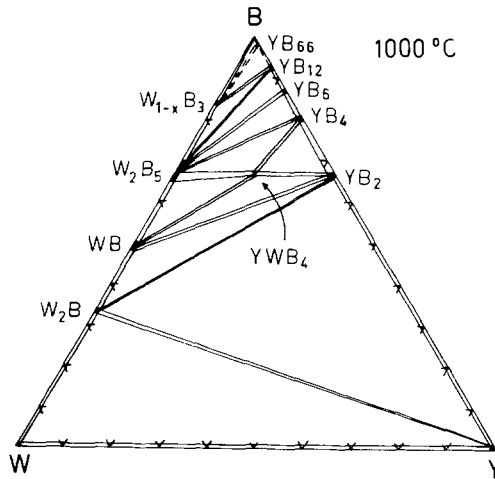


Fig. 56. Y-W-B, isothermal section at 1000°C.

solubilities of W and Y borides were found to be negligible.  $YWB_4$  with  $YCrB_4$ -type, Pbam,  $a = 6.037(5)$ ,  $b = 11.66(1)$ ,  $c = 3.598(4)$ , is the only ternary compound (Kuz'ma et al., 1973).

Yttrium exerts a retarding effect on the solid state transition of tungsten monoboride. At 1000°C a specimen  $Y_{0.10}W_{0.40}B_{0.50}$  still contained the high-temperature CrB-type phase:  $a = 3.132$ ,  $b = 8.45$ ,  $c = 3.073$ , whereas the transition to the low-temperature phase with MoB-type is complete in the W-B binary. Further annealing for 800 h at 1000°C completed the transformation. A single crystal X-ray study of a fragment obtained from a  $Y_{0.10}W_{0.33}B_{0.57}$  melt revealed a similar system of diffuse and sharp reflections as described by Boller et al. (1964), thus confirming the shift like transition of tungsten monoboride.

Kudintseva et al. (1970) studied the work function and electric resistance of W- $YB_6$  alloys.

### References

- Boller, H., W. Rieger and H. Nowotny, 1964, *Monatsh. Chem.* **95**, 1497.  
 Kudintseva, G.A., I.Ya. Kondratov and G.M. Kuznetsova, 1970, *Izv. Akad. Nauk SSSR, Neorg. Mater.* **6(7)**, 1335.  
 Kuz'ma, Yu.B., T.I. Serebryakova and A.M. Plakhina, 1967, *Zh. Neorg. Khim.* **12**, 559.  
 Kuz'ma, Yu.B., S.I. Svarichevskaya and A.S. Sobolev, 1973, *Izv. Akad. Nauk SSSR, Neorg. Mater.* **9(10)**, 1697.  
 Lundström, T. and I. Rosenberg, 1973, *J. Solid State Chem.* **6**, 299.  
 Mikhalenko, S.I. and Yu.B. Kuz'ma, 1976, *Poroshk. Metall.* **158(2)**, 56.  
 Nowotny, H., H. Haschke and F. Benesovsky, 1967, *Monatsh. Chem.* **98**, 547.  
 Rudy, E. and St. Windisch, 1965, Air Force Materials Laboratory, Technical Report 65-2, Part I, Vol. II.

### Y-Yb-B

Superconductivity in hexaboride solid solutions  $Y_{1-x}Yb_xB_6$  ( $x < 0.3$ ) was studied by Hiebl and Sienko (1980) on samples prepared by borothermal reduction of the

mixed oxides (min. purity 99.99%, B: 99.999%) in ZrB<sub>2</sub> crucibles,  $\approx 1700^\circ\text{C}$ , vacuum. The samples were reground, reheated and finally analysed by X-ray diffraction as well as atomic absorption spectroscopy.

Lattice parameters of the homogeneous solid solutions (CaB<sub>6</sub>-type, Pm3m) closely follow Vegard's law: YB<sub>6</sub>:  $a = 4.0994(10)$ ; Y<sub>0.96</sub>Yb<sub>0.04</sub>B<sub>6</sub>:  $a = 4.1012(10)$ ; Y<sub>0.91</sub>Yb<sub>0.09</sub>B<sub>6</sub>:  $a = 4.1036(10)$ ; Y<sub>0.84</sub>Yb<sub>0.16</sub>B<sub>6</sub>:  $a = 4.1063(10)$ ; Y<sub>0.72</sub>Yb<sub>0.28</sub>B<sub>6</sub>:  $a = 4.1121(10)$ ; YbB<sub>6</sub>:  $a = 4.1450(10)$ .

### Reference

Hiebl, K. and M.J. Sienko, 1980, *Inorg. Chem.* **19**, 2179.

### Yb-Al-B

Using the aluminum metal flux technique Mikhaleiko et al. (1980) prepared two ternary borides YbAlB<sub>4</sub> and Yb<sub>2</sub>AlB<sub>6</sub>. YbAlB<sub>4</sub> was obtained on cooling a mixture Yb : B  $\approx 1:2$  to  $1:4$  from  $1200^\circ\text{C}$ . Specimens were prepared by heating charges of amorphous boron ( $> 99\%$ ), Yb 99.9% and Al granules in an alundum crucible under a stream of purified Ar at  $1100\text{--}1200^\circ\text{C}$  for 6 h, followed by slow cooling ( $100^\circ\text{C}/\text{h}$ ). Excess Al was dissolved in dilute HCl (1:3). Yb<sub>2</sub>AlB<sub>6</sub> was obtained on cooling mixtures Yb : B  $\approx 1:2$  from  $1100^\circ\text{C}$ . The crystal structures of both compounds were determined by single crystal Laue rotation and reciprocal lattice photography.

YbAlB<sub>4</sub> has the YCrB<sub>4</sub>-type, Pbam,  $a = 5.927(2)$ ,  $b = 11.47(1)$ ,  $c = 3.492(1)$  and golden brown color. With a similar preparation technique (Al flux method to prepare YbB<sub>4</sub>) Fisk et al. (1981) obtained the compound YbAlB<sub>4</sub> with intermediate valence behavior,  $a = 5.921$ ,  $b = 11.424$ ,  $c = 3.507$  (structure refinement, YCrB<sub>4</sub>-type was proposed). Electrical resistivity, magnetic susceptibility and specific heat data were reported.

Yb<sub>2</sub>AlB<sub>6</sub> has the Y<sub>2</sub>ReB<sub>6</sub>-type, Pbam,  $a = 9.127(5)$ ,  $b = 11.46(1)$ ,  $c = 3.584(4)$  and dark color; metal atom parameters were refined from X-ray powder data (microdensitometer),  $R = 0.085$ : Yb(1) in 4g) 0.822(1), 0.086(1), 0; Yb(2) in 4g) 0.444(1), 0.133(1), 0; Al in 4g) 0.148(1), 0.192(1), 0; boron parameters were taken from Kuz'ma and Svarichevskaya (1972).

### References

- Fisk, Z., K.N. Yang, M.B. Maple and H.R. Ott, 1981, A new intermediate valence compound YbAlB<sub>4</sub>, in: Valence fluctuations in solids, eds. L.M. Falicov, W. Hanke and M.B. Maple (North-Holland, Amsterdam) pp. 345-348.
- Kuz'ma, Yu.B. and S.I. Svarichevskaya, 1972, *Kristallografiya* **17**, 658.
- Mikhaleiko, S.I., Yu.B. Kuz'ma, M.M. Korsukova and V.N. Gurin, 1980, *Izv. Akad. Nauk SSSR, Neorg. Mater.* **16**(3), 1941.

### Yb-Co-B (see also notes added in proof)

The structure of YbCo<sub>3</sub>B<sub>2</sub> has been analyzed by Rogl (1973) by means of X-ray powder methods, CeCo<sub>3</sub>B<sub>2</sub>-type, P6/mmm,  $a = 4.985(5)$ ,  $c = 3.020(2)$ . Powder mixtures were compacted, wrapped in Mo foil, sealed in evacuated quartz capsules and

heated at 800°C for 50 h; after grinding and recompacting the pellets were reheated at 800°C for 70 h.

YbCo<sub>4</sub>B<sub>4</sub> with a CeCo<sub>4</sub>B<sub>4</sub>-type of structure was mentioned by Kuz'ma et al. (1981) and in the same paper YbCo<sub>4</sub>B was claimed to be CeCo<sub>4</sub>B-type, P6/mmm. Attempts to prepare Yb<sub>3</sub>Co<sub>11</sub>B<sub>4</sub> with Ce<sub>3</sub>Co<sub>11</sub>B<sub>4</sub>-type or Yb<sub>2</sub>Co<sub>7</sub>B<sub>3</sub> with Ce<sub>2</sub>Co<sub>7</sub>B<sub>3</sub>-type were unsuccessful (Kuz'ma and Bilonishko, 1973).

### References

- Kuz'ma, Yu.B. and N.S. Bilonishko, 1973, *Kristallografiya* **18**(4), 710.  
 Kuz'ma, Yu.B., N.S. Bilonishko, N.F. Chaban and G.V. Chernjak, 1981, *J. Less-Common Metals* **82**, 364.  
 Rogl, P., 1973, *Monatsh. Chem.* **104**, 1623.

### Yb-Ir-B

From X-ray powder diffraction data of arc melted alloys Ku and Meisner (1981) characterized the structure type of YbIr<sub>3</sub>B<sub>2</sub> to be isostructural with ErIr<sub>3</sub>B<sub>2</sub>, possible space group C2/m,  $a = 5.401(6)$ ,  $b = 9.353(9)$ ,  $c = 3.099(4)$ ,  $\beta = 91.3(1)^\circ$ ,  $T_n = 1.2$  K.

### Reference

- Ku, H.C. and G.P. Meisner, 1981, *J. Less-Common Metals* **78**, 99.

### Yb-Ni-B

No data on ternary phase equilibria exist for the Yb-Ni-B system.

Niihara et al. (1973) claimed the existence of a YbNi<sub>4</sub>B phase with presumably the YNi<sub>4</sub>B-type structure, Kuz'ma et al. (1981) mentioned the CeCo<sub>4</sub>B-type,  $a = 4.938(4)$ ,  $c = 6.929(10)$ , P6/mmm.

Chaban et al. (1980) observed a  $\tau$ -phase Yb<sub>2</sub>Ni<sub>21</sub>B<sub>6</sub> in arc melted alloys [Cr<sub>23</sub>C<sub>6</sub>-type, Fm3m,  $a = 10.636(5)$ ]. Starting materials were Yb ingots 99.5%, and B 99.3% and Ni 99.98% powders.

### References

- Chaban, N.F., Yu.B. Kuz'ma and P.L. Kotovskaya, 1980, *Dopov. Akad. Nauk Ukr. RSR, Ser. A*, 88.  
 Kuz'ma, Yu.B., N.S. Bilonishko, N.F. Chaban and G.V. Chernjak, 1981, *J. Less-Common Metals* **82**, 364; see also 1982, *Izv. Akad. Nauk SSSR, Neorg. Mater.* **18**, 691.  
 Niihara, K., Y. Katayama and S. Yajima, 1973, *Chem. Lett. (Chem. Soc. Jpn)* 613.

### Yb-Os-B

At least two ternary compounds exist in the Yb-Os-B system.

YbOsB<sub>4</sub> adopts the YCrB<sub>4</sub>-type of structure, Pbam,  $a = 5.911(3)$ ,  $b = 11.449(6)$ ,  $c = 3.535(5)$ , as found from X-ray analysis by Sobczak and Rogl (1979); for sample preparation, see YbRuB<sub>4</sub>.

YbOs<sub>4</sub>B<sub>4</sub> is tetragonal, YOs<sub>4</sub>B<sub>4</sub>-type,  $a = 7.4154(7)$ ,  $c = 32.7430(40)$ , with a superstructure of the NdCo<sub>4</sub>B<sub>4</sub>-type;  $c = 8c_0$ ; magnetic data were presented by Rogl et al. (1982);  $T_n = 1.5$  K (Ku, 1980). For sample preparation, see YbRuB<sub>4</sub>.

$\text{YbOs}_3\text{B}_2$  with an unknown structure type (described as orthorhombically distorted  $\text{CeCo}_3\text{B}_2$ -type with a sixfold superstructure along the  $c$ -axis,  $c = 6c_0$ ) has been observed by Ku (1980);  $T_n = 1.2$  K.

### References

- Ku, H.C., 1980, Thesis, Univ. of California at San Diego, USA.  
 Rogl, P., K. Hiebl and M.J. Sienko, 1982, Structural chemistry and magnetic behavior of  $\text{RM}_4\text{B}_4$ -borides, paper presented at the 7th Intern. Conf. on Solid Compounds of Transition Elements, Grenoble (June 21–25), Proceedings, II A4.  
 Sobczak, R. and P. Rogl, 1979, J. Solid State Chem. **27**, 343.

### *Yb–Rh–B*

Ku and Meisner (1981) found  $\text{YbRh}_3\text{B}_2$  to be isostructural with the crystal structure of  $\text{ErIr}_3\text{B}_2$ , possible space group  $\text{C2/m}$ ,  $a = 5.355(6)$ ,  $b = 9.280(9)$ ,  $c = 3.090(4)$ ,  $\beta = 90.9(1)^\circ$  (X-ray powder analysis of arc melted (?) samples);  $T_N = 1.2$  K.

Yvon and Johnston (1982) characterized the compound  $\text{YbRh}_4\text{B}_4$  with the  $\text{LuRh}_4\text{B}_4$ -type of structure,  $\text{Ccca}$ ,  $a = 7.424(6)$ ,  $b = 22.26(2)$ ,  $c = 7.458(6)$ . The new phase was obtained from arc melted alloys containing excess Rh, which were subsequently annealed in Ta tubes sealed under Ar at 1150–1250°C for 125 h. Arc melted alloys were said to mainly consist of  $\text{CeCo}_4\text{B}_4$ - and (metastable)  $\text{LuRu}_4\text{B}_4$ -type phases.

For the existence of the  $\text{Cu}_3\text{Au}$ -type phase  $\text{YbRh}_3\text{B}_{1-x}$ ,  $a = 4.137$ ,  $x = 0.15$ , see also R–Rh–B.

### References

- Ku, H.C. and G.P. Meisner, 1981, J. Less-Common Metals **78**, 99.  
 Yvon, K. and D.C. Johnston, 1982, Acta Crystallogr. **B38**, 247.

### *Yb–Ru–B*

At least three ternary compounds exist in the Yb–Ru–B system.

$\text{YbRuB}_4$  with  $\text{YCrB}_4$ -type structure has been analysed by X-ray powder methods by Sobczak and Rogl (1979);  $\text{Pbam}$ ,  $a = 5.907(3)$ ,  $b = 11.429(6)$ ,  $c = 3.502(2)$ ; magnetic susceptibility data were presented within the temperature range of 80–300 K. Samples were prepared by sintering compacts of Yb (99.9%) fillings, and Ru (99.9%) and B (99.0%) powders, wrapped in Mo foil and sealed in evacuated silica tubes for 48 h at 900°C and additionally for 12 h at 1200°C. After grinding and recompacting the samples were finally heat treated for 5 h at 1400°C under argon on a boronitride substrate. Samples contained small amounts of  $\text{YbB}_4$ .

The crystal structure of  $\text{YbRu}_3\text{B}_2$  with  $\text{CeCo}_3\text{B}_2$ -type of structure,  $\text{P6/mmm}$ , has been confirmed from powder X-ray-diffraction. Hiebl et al. (1980) reported  $a = 5.454(4)$ ,  $c = 3.003(2)$ ; magnetic measurements indicate trivalency of Yb. Samples were prepared by reacting compacts of Yb fillings (99.9%) and Ru 99.9% and B 99.7% powders, wrapped in Mo foil and sealed in evacuated quartz tubes (two times 24 h at 1200°C). In good accord Ku et al. (1980) observed  $a = 5.464(6)$ ,

$c = 3.006(4)$  and trivalency of Yb from magnetic susceptibility data; compacts of Yb filings, and Ru and B powders of high purity were sealed in Ta tubes under Ar and reacted at  $1250^\circ\text{C}$  for 24 h. Alloys were obtained in multiphase condition (no details given).

$\text{YbRu}_4\text{B}_4$  is isostructural with the structure type of  $\text{LuRu}_4\text{B}_4$ ,  $I4_1/acd$ ,  $a = 7.427(5)$ ,  $c = 14.962(10)$ , as derived by Johnston (1977) from X-ray powder diffractometry. Samples were prepared by firing compacts of Yb filings, and RuB, Ru and B powders of high purity in Ta tubes under Ar at  $1200^\circ\text{C}$  for 24 h; the alloys obtained were multiphase.

### References

- Hiebl, K., P. Rogl, E. Uhl and M.J. Sienko, 1980, *Inorg. Chem.* **19**(11), 3316.  
 Johnston, D.C., 1977, *Solid State Commun.* **24**(10), 699.  
 Ku, H.C., G.P. Meisner, F. Acker and D.C. Johnston, 1980, *Solid State Commun.* **35**, 91.  
 Sobczak, R. and P. Rogl, 1979, *J. Solid State Chem.* **27**, 343.

## Quarternary and higher order systems

### *Ce-Ir-Os-B*

Magnetism and structure of  $\text{CeIr}_{4-x}\text{Os}_x\text{B}_4$  alloys were investigated by Hiebl et al. (1982). For sample preparation, see  $\text{SmIr}_{4-x}\text{Os}_x\text{B}_4$ . X-ray and metallographic analysis proved for all values of  $x$  congruent melting behavior with  $\text{NdCo}_4\text{B}_4$ -type structure,  $P4_2/n$ . Lattice parameters of pseudobinary alloys show a remarkable positive deviation from Vegard's rule, according to a valence transition  $\text{Ce}^{3+} \rightarrow \text{Ce}^{4+}$ ; lattice parameters were:  $\text{CeOs}_3\text{IrB}_4$ :  $a = 7.5764(8)$ ,  $c = 3.9930(3)$ ;  $\text{CeOs}_{2.67}\text{Ir}_{1.33}\text{B}_4$ :  $a = 7.5865(20)$ ,  $c = 3.9874(13)$ ;  $\text{CeOs}_{2.5}\text{Ir}_{1.5}\text{B}_4$ :  $a = 7.5905(14)$ ,  $c = 3.9860(9)$ ;  $\text{CeOs}_{2.2}\text{Ir}_{1.8}\text{B}_4$ :  $a = 7.6001(19)$ ,  $c = 3.9842(7)$ ;  $\text{CeOs}_2\text{Ir}_2\text{B}_4$ :  $a = 7.6055(5)$ ,  $c = 3.9815(3)$ ;  $\text{CeOs}_{1.52}\text{Ir}_{2.48}\text{B}_4$ :  $a = 7.6190(9)$ ,  $c = 3.9786(4)$ ;  $\text{CeOsIr}_3\text{B}_4$ :  $a = 7.6304(10)$ ,  $c = 3.9789(7)$ .

### Reference

- Hiebl, K., P. Rogl and M.J. Sienko, 1982, *Inorg. Chem.* **21**, 1128.

### *Dy-Ir-Rh-B*

Ku (1980) investigated the magnetic, superconducting and structural behavior in the  $\text{Dy}(\text{Ir}_x\text{Rh}_{1-x})_4\text{B}_4$  phase diagram for  $x < 0.9$  within the  $\text{CeCo}_4\text{B}_4$ -type region ( $P4_2/nmc$ ), using arc melted and annealed samples (fig. 57). The sharp drop of  $T_c$  around  $x = 0.5-0.6$  was interpreted to coincide with a change in the variation of lattice parameters with composition (ordering of platinum metal atoms?, see fig. 58). The magnetic behavior for  $x \leq 0.15$  is not simple ferromagnetic and similarly the nature of the magnetic transition at  $x \geq 0.55$  is unclear.

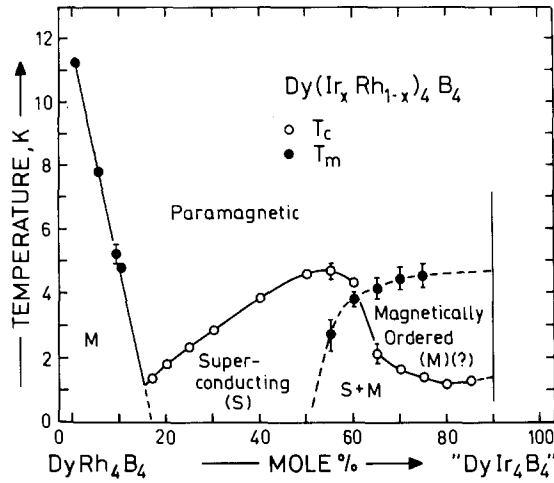


Fig. 57.  $\text{Dy}(\text{Ir}_x\text{Rh}_{1-x})_4\text{B}_4$ ; low-temperature phase diagram. The  $\text{CeCo}_4\text{B}_4$ -type phase does not exist for a " $\text{DyIr}_4\text{B}_4$ ". After Ku (1980).  $T_m$  = magnetic ordering temperature ( $\bullet$ ),  $T_c$  = superconducting transition temperature ( $\circ$ ).

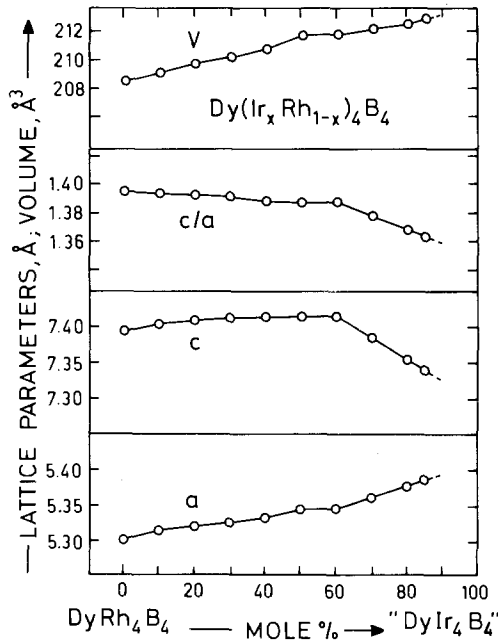


Fig. 58.  $\text{Dy}(\text{Ir}_x\text{Rh}_{1-x})_4\text{B}_4$ ; lattice parameters ( $\text{\AA}$ ) and volume ( $\text{\AA}^3$ ) versus concentration; after Ku (1980).

### Reference

Ku, H.C., 1980, Thesis, Univ. of California at San Diego, USA.

### Dy-Rh-Ru-B

Hamaker and Maple (1981) presented the low-temperature phase diagram of the system  $\text{Dy}(\text{Ru}_x\text{Rh}_{1-x})_4\text{B}_4$  ( $0.1 < x \leq 1$ ) from ac magnetic susceptibility and heat capacity measurements (fig. 59). For  $x = 0.154$  and below  $T_m = 1.5$  K superconductivity and magnetic order were found to coexist. Samples were prepared by arc melting under argon and subsequent annealing at  $1200^\circ\text{C}$  for 2 days, at  $1000^\circ\text{C}$  for 2 days and at  $800^\circ\text{C}$  for 3 days. No structural details have been given ( $\text{LuRu}_4\text{B}_4$ -type,  $I4_1/acd$ ).

### Reference

Hamaker, H.C. and M.B. Maple, 1981, Interaction of superconductivity and magnetism in  $\text{Dy}(\text{Ru}_x\text{Rh}_{1-x})_4\text{B}_4$ , in: Ternary Superconductors, Proc. Intern. Conf. on Ternary Superconductors, Lake Geneva, WI, USA (1980), eds. G.K. Shenoy, B.D. Dunlap and F.Y. Fradin (North-Holland, Amsterdam) pp. 201-204.

*Er-Co-Rh-B*: see notes added in proof

### Er-Gd-Rh-B

The low-temperature magnetic and superconducting behavior in the  $\text{Gd}_x\text{Er}_{1-x}\text{Rh}_4\text{B}_4$  system was established by Wang et al. (1978) by means of four-probe electrical resistance and ac-susceptibility techniques; see fig. 60. Samples were prepared by arc melting in a Zr-gettered Ar atmosphere and subsequently annealed

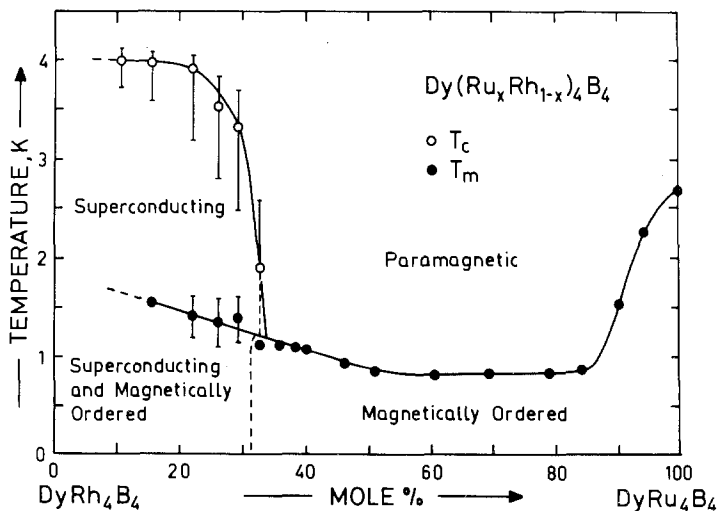


Fig. 59.  $\text{Dy}(\text{Rh}_{1-x}\text{Ru}_x)_4\text{B}_4$ ; low-temperature phase diagram. Error bars represent temperatures at which the transition is ten and ninety percent complete, and the dashed error bar for  $x = 0.327$  indicates the transition was less than 90% complete. After Hamaker and Maple (1981).  $T_m$  = magnetic ordering temperature (●),  $T_c$  = superconducting transition temperature (○).



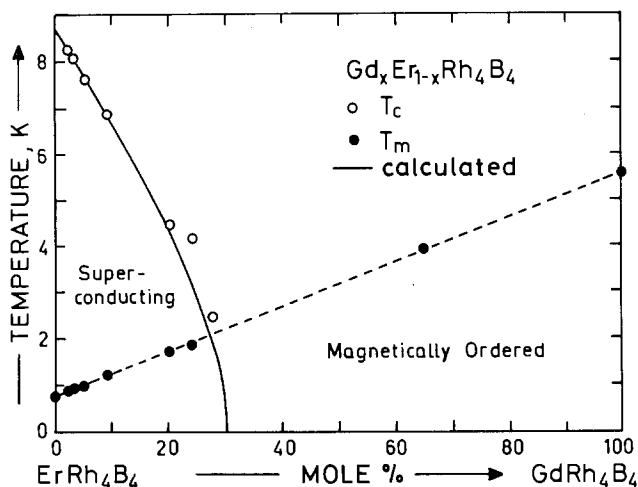


Fig. 60.  $\text{Er}_{1-x}\text{Gd}_x\text{Rh}_4\text{B}_4$ ; low-temperature phase diagram; after Wang et al. (1978).  $T_m$  = magnetic ordering temperature (●),  $T_c$  = superconducting transition temperature (○), solid line: depression of  $T_c$  calculated using the Abrikosov-Gorkov theory.

at 1000°C for 1 to 14 days. The  $\text{CeCo}_4\text{B}_4$ -type of structure,  $\text{P4}_2/\text{nmc}$ , was checked by powder X-ray diffraction. No lattice parameters were given. Heat capacity data confirm the ferromagnetic transitions for  $x = 0.09, 0.28$  and  $0.65$  (Ho et al., 1978). The superconducting transition temperature  $T_c$  remains unchanged under hydrostatic pressures (up to 19 kbar for  $x = 0.24, 0.26$  and  $0.28$ ); the magnetic transition temperature  $T_m$  is enhanced linearly by pressure but at an increased rate as  $x$  approaches the critical concentration  $x_c \approx 0.28$  (Chu et al., 1978).

### References

- Chu, C.W., C.Y. Huang, S. Kohn and J.L. Smith, 1978, *J. Less-Common Metals* **62**, 245.  
 Ho, J.C., C.Y. Huang and J.L. Smith, 1978, *J. Physique (Paris)* **C6**, 386.  
 Wang, R.H., R.J. Laskowski, C.Y. Huang, J.L. Smith and C.W. Chu, 1978, *J. Appl. Phys.* **49**(3), 1392; see also *J. Appl. Phys.* **50**(3), 1862.

### *Er-Ho-Rh-B*

The boundaries between the normal paramagnetic, superconducting and normal magnetically ordered phases in the alloy system  $(\text{Er}_{1-x}\text{Ho}_x)\text{Rh}_4\text{B}_4$  have been established by Johnston et al. (1978) by means of ac-susceptibility measurements as low as 0.07 K (see fig. 61). Samples were synthesized by arc melting (Ar) and subsequent heat treatment at 1200°C for 1 week and then at 900°C for 3 weeks. From X-ray powder diffraction tetragonal symmetry was mentioned, but no lattice parameters given,  $\text{CeCo}_4\text{B}_4$ -type,  $\text{P4}_2/\text{nmc}$ .

The minimum in the ferromagnetic transition temperatures at  $\text{Ho}_{\sim 0.25}\text{Er}_{\sim 0.75}\text{Rh}_4\text{B}_4$  was identified as a "decoupled" tetracritical point by Maekawa and Huang (1980).

Using powder neutron scattering techniques, Mook et al. (1982) examined the magnetic transition and found a complicated magnetic behavior with more than one

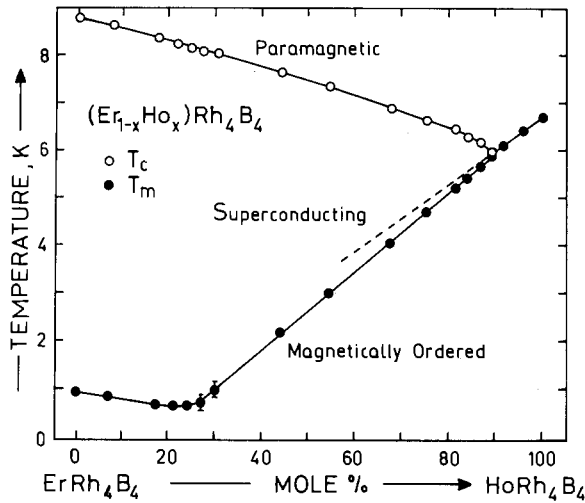


Fig. 61.  $(\text{Er}_{1-x}\text{Ho}_x)\text{Rh}_4\text{B}_4$ ; low-temperature phase diagram; after Johnston et al. (1978).  $T_m$  = magnetic ordering temperature ( $\bullet$ ),  $T_c$  = superconducting transition temperature ( $\circ$ ), ( $T_{c1}$  = normal to superconducting transition,  $T_{c2}$  = transition of superconducting into magnetically ordered state).

type of ordering for  $\text{Ho}_{0.3}\text{Er}_{0.7}\text{Rh}_4\text{B}_4$ . Ho orders along the  $c$  axis with nearly its free-ion moment, Er independently orders in the basal plane with a moment reduced from the free-ion value. Long range ferromagnetic order is observed at the lowest temperatures for all values of  $x$ . Er-rich materials reveal ordering in a sinusoidally modulated state in which ferromagnetism and superconductivity might coexist.

At variance with Ishikawa (1979), Adrian et al. (1980) suggested from magnetization measurements a transition from type II to type I superconductivity in the vicinity of the lower critical temperature  $T_{c2}$ . The reentrant transition from the superconducting to the ferromagnetic state was claimed from specific heat data to be a first order transition (MacKay et al. 1979). Both the superconducting and magnetic interactions are strengthened by external pressure (up to 21 kbar; Shelton et al., 1980); samples investigated near the tricritical point at  $x \approx 0.89$  show the disappearance of superconductivity in favor of ferromagnetic order.

### References

- Adrian, H., K. Müller and G. Saemann-Ischenko, 1980, Phys. Rev. B **22**(9), 4424.  
 Ishikawa, M., 1979, Phys. Lett. **74A**, 263.  
 Johnston, D.C., W.A. Fertig, M.B. Maple and B.T. Matthias, 1978, Solid State Commun. **26**, 141.  
 MacKay, H.B., L.D. Woolf, M.B. Maple and D.C. Johnston, 1979, Phys. Rev. Lett. **42**, 918.  
 Maekawa, S. and C.Y. Huang, 1980, Roles of crystal field in magnetic superconducting rare earth rhodium borides, in: Crystalline Electric Field and Structural Effects in f-electron Systems, eds. J. Crow, R.P. Guertin and T.W. Mihalasin (Plenum, New York) p. 561.  
 Mook, H.A., W.C. Koehler, M.B. Maple, Z. Fisk, D.C. Johnston and L.D. Woolf, 1982, Phys. Rev. B **25**(1), 372; see also J. Appl. Phys. **53**(3), 2614.  
 Shelton, R.N., C.U. Segre and D.C. Johnston, 1980, Solid State Commun. **33**, 843.

### Er-Ir-Rh-B

Ku et al. (1979) investigated the crystal structure and superconductivity of arc melted alloys  $\text{Er}(\text{Ir}_x\text{Rh}_{1-x})_4\text{B}_4$ . From X-ray powder analysis a  $\text{CeCo}_4\text{B}_4$ -type of

structure,  $P4_2/nmc$ , was claimed for all values of  $x$ . The sharp, nearly discontinuous drop of the superconducting transition  $T_c$  at  $x \approx 0.5$  (fig. 62) is reflected by an irregular variation of the lattice parameters (fig. 63) and was speculated to be due to a complicated Rh–Ir atom ordering on the tetrahedral sites. During heat treatment (1200°C, 3 d and 900°C, 10 d in quartz tubes; samples wrapped in Ta foil) the amount

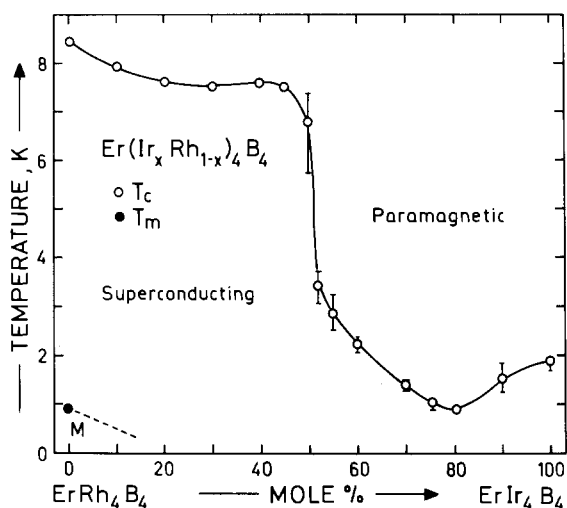


Fig. 62.  $Er(Ir_xRh_{1-x})_4B_4$ ; low-temperature phase diagram; after Ku et al. (1979).  $T_m$  = magnetic ordering temperature (●),  $T_c$  = superconducting transition temperature (○).

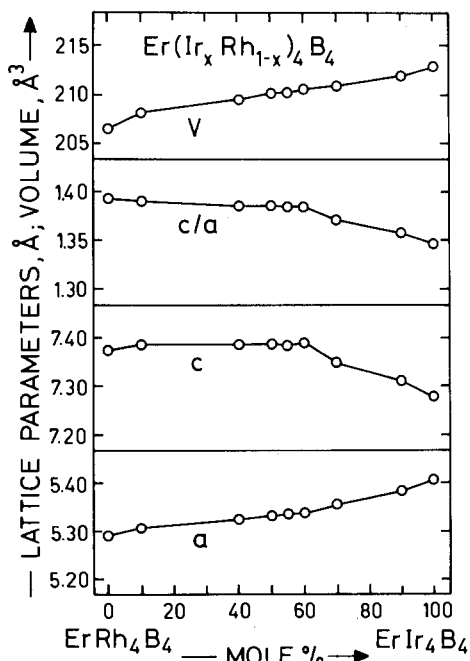


Fig. 63.  $Er(Ir_xRh_{1-x})_4B_4$ ; lattice parameters versus composition; after Ku et al. (1979).

of this phase which had the  $\text{CeCo}_4\text{B}_4$ -type structure rapidly decreased from  $\approx 95\%$  ( $0 \leq x \leq 0.7$ ) to  $10\%$  at  $x \approx 0.9$ ; at  $x = 1.0$  the phase essentially disappeared (metastability).

### Reference

Ku, H.C., B.T. Matthias and H. Barz, 1979, Solid State Commun. **32**(11), 937.

### *Er-Rh-Ru-B*

The interplay of long-range magnetic order and superconductivity within the alloy system  $\text{Er}(\text{Rh}_{1-x}\text{Ru}_x)_4\text{B}_4$  has been investigated by Hornig and Shelton (1981) (fig. 64). Two different processes were employed to synthesize the samples. In all cases, the melting steps were performed on a water cooled copper hearth in a Zr gettered argon arc furnace and mass losses were  $< 0.1\%$ . Method 1 consisted of three separate steps. First the Rh:Ru ratio was fixed by melting the appropriate amounts of these elements together into one ingot. Secondly the correct mass of boron was carefully melted into this ingot, followed by the final step of melting in a stoichiometric amount of Er. The final product was remelted several times to promote homogeneity. This method was successful for all samples except those with compositions  $0.40 < x < 0.75$ . Method 2 consisted of first making two samples via method 1, one with  $x < 0.40$  and a second with  $x \geq 0.80$ . These homogeneous compounds were then combined in correct proportion to produce the desired ternary boride. The only impurity phase present in specimens prepared by method 2 was a small amount ( $< 3\%$ ) of RhB. Additionally, for some of the high Rh concentration samples, X-ray

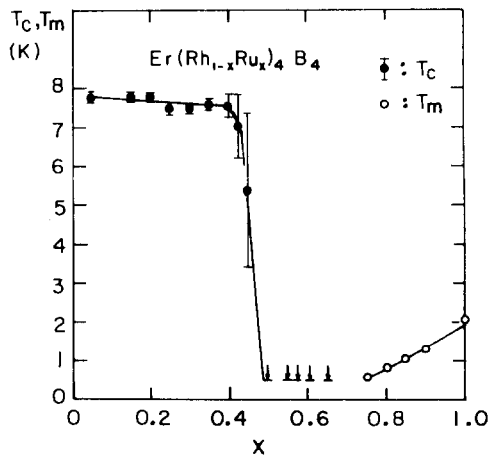


Fig. 64.  $\text{Er}(\text{Rh}_{1-x}\text{Ru}_x)_4\text{B}_4$ ; low-temperature phase diagram. Error bars on the superconducting transition temperatures  $T_c$  (●) indicate the width of the transition into the superconducting state. ↓ indicates a transition into an ordered magnetic state had begun, but was not completed upon reaching a minimum temperature of 0.5 K. After Hornig and Shelton (1981).  $T_m$  = magnetic ordering temperature (○),  $T_c$  = superconducting transition temperature (●).

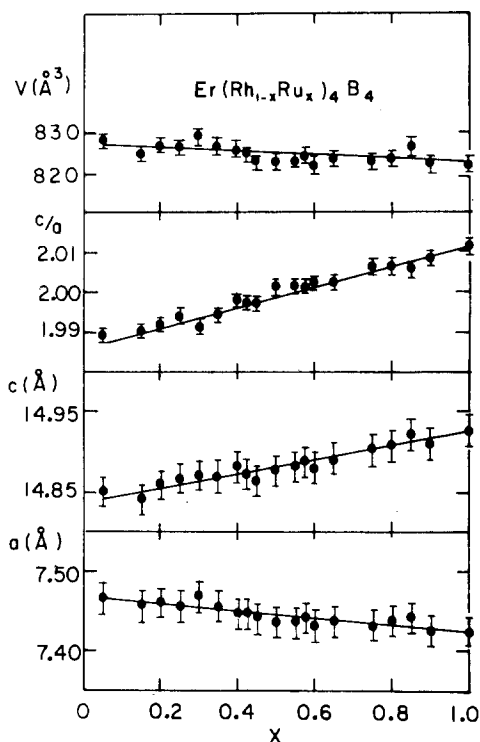


Fig. 65.  $\text{Er}(\text{Rh}_{1-x}\text{Ru}_x)_4\text{B}_4$ ; lattice parameters versus concentration; after Horng and Shelton (1981).

data indicated the presence of a few percent of an unidentified ternary phase. The variation of unit cell dimensions for  $\text{Er}(\text{Rh}_{1-x}\text{Ru}_x)_4\text{B}_4$  alloys with the  $\text{LuRu}_4\text{B}_4$ -type of structure,  $I4_1/acd$ , is presented in fig. 65.

### Reference

Horng, H.E. and R.N. Shelton, 1981, Superconductivity and long range magnetic order in the body centered tetragonal system  $\text{Er}(\text{Rh}_{1-x}\text{Ru}_x)_4\text{B}_4$  in: Ternary Superconductors, Proc. Intern. Conf. on Ternary Superconductors, Lake Geneva, WI, USA (1980), eds. E.K. Shenoy, B.D. Dunlap and F.Y. Fradin (North-Holland, Amsterdam) pp. 213–216.

### *Er-Sm-Rh-B*

Woolf and Maple (1981) derived the low-temperature phase diagram for the system  $(\text{Sm}_{1-x}\text{Er}_x)\text{Rh}_4\text{B}_4$ , using ac magnetic susceptibility and heat capacity measurements. Antiferromagnetic ordering was observed for  $x < 0.15$  (fig. 66) and complicated ordering exists around the minimum in  $T_m$ . Ferromagnetic ordering was observed for  $x > 0.3$ . Samples were prepared by arc melting; intermediate concentrations were obtained from  $\text{SmRh}_4\text{B}_4$  and  $\text{ErRh}_4\text{B}_4$  master alloys. No structural details were given ( $\text{CeCo}_4\text{B}_4$ -type,  $P4_2/nmc$ ).

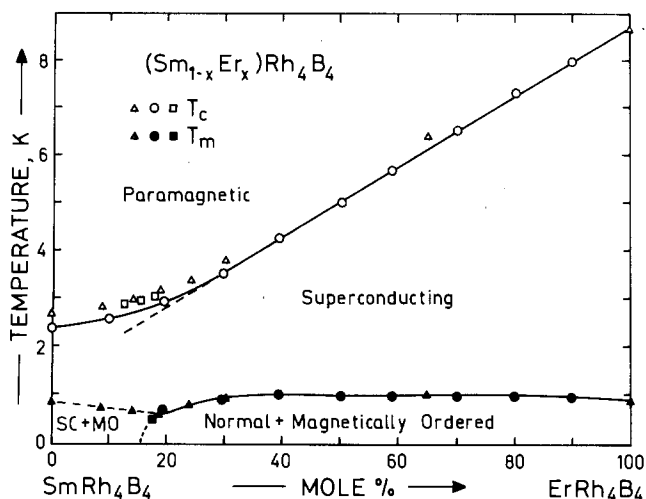


Fig. 66.  $\text{Er}_x\text{Sm}_{1-x}\text{Rh}_4\text{B}_4$ ; low temperature phase diagram; after Woolf and Maple (1981).  $T_m$  = magnetic ordering temperature (filled symbols),  $T_c$  = superconducting transition temperature (open symbols) (triangles were from heat capacity data; circles and squares represent ac magnetic susceptibility data).

### Reference

Woolf, L.D. and M.B. Maple, 1981, Transition from antiferromagnetism to ferromagnetism in the superconducting pseudoternary system  $(\text{Sm}_{1-x}\text{Er}_x)\text{Rh}_4\text{B}_4$ , in: Ternary Superconductors, Proc. Intern. Conf. on Ternary Superconductors, Lake Geneva, WI, USA (1980), eds. G.K. Shenoy, B.D. Dunlap and F.Y. Fradin (North-Holland, Amsterdam) pp. 181–184.

### Er–Tm–Rh–B

From ac-susceptibility measurements Maekawa et al. (1980) determined the superconducting and magnetic transformations in the  $(\text{Er}_{1-x}\text{Tm}_x)\text{Rh}_4\text{B}_4$  system, see

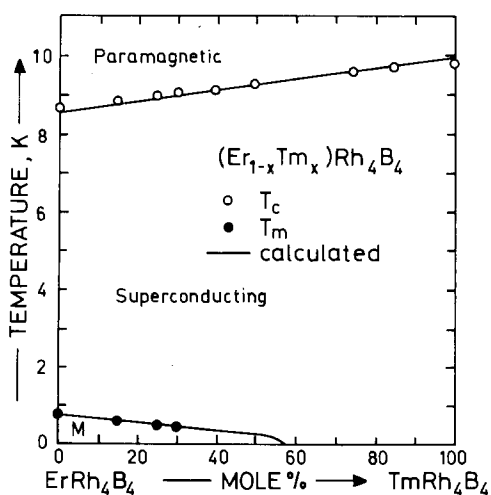


Fig. 67.  $\text{Er}_{1-x}\text{Tm}_x\text{Rh}_4\text{B}_4$ ; low-temperature phase diagram; after Maekawa et al. (1980).  $T_m$  = magnetic ordering temperature (●),  $T_c$  = superconducting transition temperature (○).

fig. 67. Neither preparative nor structural details were given (probably  $\text{CeCo}_4\text{B}_4$ -type,  $\text{P4}_2/\text{nmc}$ ).

*Reference*

Maekawa, S., J.L. Smith and C.Y. Huang, 1980, Phys. Rev. B **22**(1), 164.

*Er-Y-Rh-B*

Okuda et al. (1980) established the superconducting and magnetic transition temperatures in the  $\text{Er}_x\text{Y}_{1-x}\text{Rh}_4\text{B}_4$  system by means of four-probe electrical resistance measurements as low as 0.08 K, see fig. 68. No structural details were presented (probably  $\text{CeCo}_4\text{B}_4$ -type,  $\text{P4}_2/\text{nmc}$ ).

*Reference*

Okuda, K., Y. Nakakura and K.T. Kadowaki, 1980, J. Magn. Magn. Mater. **15-18**, 1575.

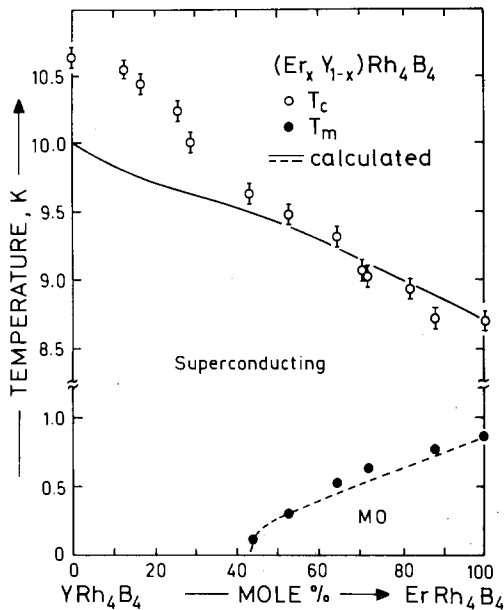


Fig. 68.  $\text{Er}_x\text{Y}_{1-x}\text{Rh}_4\text{B}_4$ ; low-temperature phase diagram; after Okuda et al. (1980).  $T_{c1}$  = superconducting to normal transition (○),  $T_{c2}$  = transition temperature from superconducting to magnetically ordered state ( $T_m$ ) (●).

*Gd-Y-Rh-B*

Wang et al. (1978) investigated the low-temperature behavior of  $\text{Gd}_x\text{Y}_{1-x}\text{Rh}_4\text{B}_4$  ( $\text{CeCo}_4\text{B}_4$ -type,  $\text{P4}_2/\text{nmc}$ ) by means of four-probe electrical resistance and ac-susceptibility techniques. Huang et al. (1979) found that the magnetic structure is of spin glass type for  $x = 0.1$  and ferromagnetic for  $x \geq 0.2$ . For sample preparation, see  $\text{Er}_{1-x}\text{Gd}_x\text{Rh}_4\text{B}_4$ .

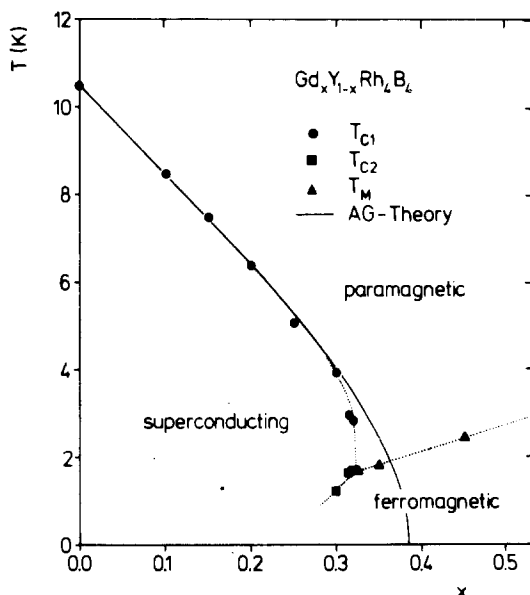


Fig. 69. Gd-Y-Rh-B; low-temperature phase diagram; after Adrian et al. (1981).  $T_m$  = magnetic ordering temperature,  $T_c$  = superconducting transition temperature.

The low-temperature phase diagram of the system  $Gd_xY_{1-x}Rh_4B_4$  was established by Adrian et al. (1981); see fig. 69. For alloys with  $x \geq 0.2$  a transition from type II to type I superconductivity was indicated and a reentrant behavior was observed in alloys with  $x \geq 0.30$ .

### References

- Adrian, H., R. Müller, R. Behrle, G. Saemann-Ischenko and G. Voit, 1981, *Physica* **108B**, 1281.  
 Huang, C.Y., S.E. Kohn, S. Maekawa and J.L. Smith, 1979, *Solid State Commun.* **32**, 929.  
 Wang, R.H., R.J. Laskowski, C.Y. Huang, J.L. Smith and C.W. Chu, 1978, *J. Appl. Phys.* **49**(3), 1392.

### Ho-Ir-Rh-B

Ku (1980) determined the low-temperature magnetic and superconducting transitions in the system  $Ho(Ir_xRh_{1-x})_4B_4$  from ac-susceptibility measurements (as low as 1.2 K) on as-cast as well as annealed alloys (1150°C, 5 d; 900°C, 2 weeks). Néel temperatures were obtained by means of static susceptibility measurements (vibrating sample magnetometer). Phase equilibria are characterized by the existence of a superconducting phase between two different, magnetically ordered phases and a region where antiferromagnetism and superconductivity seems to coexist (fig. 70). The magnetic and superconducting transition temperatures  $T_{c1}$ ,  $T_{c2}$  and  $T_m$  appeared to be slightly increased by annealing.  $T_{c1}$  shows a minimum at  $x \approx 0.8$ . Comparison



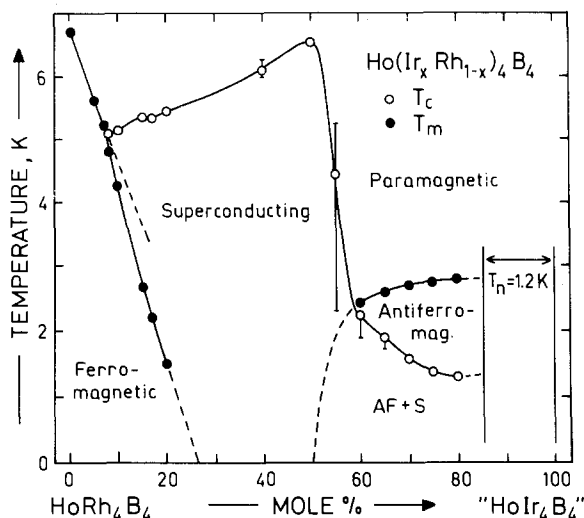


Fig. 70.  $\text{Ho}(\text{Ir}_x\text{Rh}_{1-x})_4\text{B}_4$ ; low-temperature phase diagram. No  $\text{CeCo}_4\text{B}_4$ -type phase is observed for a “ $\text{HoIr}_4\text{B}_4$ ”; alloys for more than 95 mole%  $\text{HoIr}_4\text{B}_4$  were normal down to  $T_n = 1.2\text{ K}$ . After Ku (1980).  $T_m$  = magnetic transition temperature (●),  $T_c$  = superconducting transition temperature:  $T_{c1}$  = normal to superconducting transition (○),  $T_{c2}$  = transition temperature of superconducting to magnetically ordered state ( $T_m$ ).

is made with the system  $\text{Er}(\text{Ir}_x\text{Rh}_{1-x})_4\text{B}_4$  insofar as the spectacular drop in  $T_c$  for both systems was claimed to indicate a partial Rh/Ir order in the sites 8g of the  $\text{CeCo}_4\text{B}_4$ -type structure,  $\text{P4}_2/\text{nmc}$ . No lattice parameters were given. For a neutron diffraction study of  $\text{Ho}(\text{Rh}_{0.3}\text{Ir}_{0.7})_4\text{B}_4$ , see Hamaker et al. (1982).

### Reference

Hamaker, H.C., H.C. Ku, M.B. Maple and H.A. Mook, 1982, *Solid State Commun.* **43**(6), 45.  
 Ku, H.C., 1980, Thesis, Univ. of California at San Diego, USA.

### Ho-Lu-Rh-B

Maple et al. (1978) established the magnetic and superconducting transition temperatures  $T_{c1}$ ,  $T_{c2}$  and  $T_m$  in the system  $(\text{Lu}_{1-x}\text{Ho}_x)\text{Rh}_4\text{B}_4$  by means of low frequency ac-susceptibility measurements on powdered samples (fig. 71) as low as 0.07 K.  $T_{c1}$ ,  $T_{c2}$  and  $T_m$  become identical at  $x = 0.92$ . Samples were synthesized by arc melting (Ar) and subsequent annealing in sealed Ta tubes at 1150°C for 2 weeks, then at 900°C for 1 week, finally at 800°C for 1 week. No structural details were given ( $\text{CeCo}_4\text{B}_4$ -type,  $\text{P4}_2/\text{nmc}$ ).

### Reference

Maple, M.B., H.C. Hamaker, D.C. Johnston, H.B. MacKay and L.D. Woolf, 1978, *J. Less-Common Metals* **62**, 251.

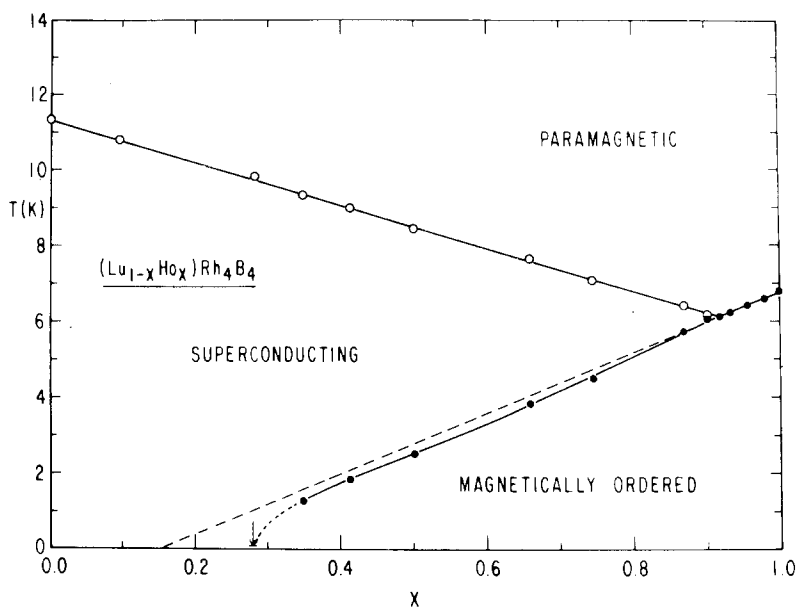


Fig. 71.  $(\text{Ho}_x\text{Lu}_{1-x})\text{Rh}_4\text{B}_4$ ; low-temperature phase diagram; after Maple et al. (1978).  $T_m$  = magnetic ordering temperature ( $\bullet$ ),  $T_c$  = superconducting transition temperature ( $\circ$ ) [ $T_{c1}$  = superconducting to normal transition,  $T_{c2}$  = transition temperature of superconducting to magnetically ordered state ( $T_m$ )], broken line = linear extrapolation of  $T_m$  versus  $x$ .

### La-Ir-Os-B

The pseudobinary system  $\text{LaOs}_4\text{B}_4$ - $\text{LaIr}_4\text{B}_4$  has been investigated with respect to superconducting and magnetic properties by Hiebl et al. (1981). A continuous solid solution  $\text{LaIr}_{4-x}\text{Os}_x\text{B}_4$  with  $\text{NdCo}_4\text{B}_4$ -type ( $\text{P4}_2/\text{n}$ ) and with congruent melting behavior was derived from X-ray and metallographic analysis of arc melted and subsequently annealed alloys (1200°C, 12 h, high vacuum on a boronitride substrate). Lattice parameters show a small negative deviation from Vegard's rule:  $\text{LaOs}_2\text{Ir}_2\text{B}_4$ :  $a = 7.6380(10)$ ,  $c = 3.9782(4)$ ;  $\text{LaOs}_1\text{Ir}_3\text{B}_4$ :  $a = 7.6528(10)$ ,  $c = 3.9738(4)$ ;  $\text{LaOs}_3\text{Ir}_1\text{B}_4$ :  $a = 7.6241(16)$ ,  $c = 3.9880(5)$ . Atom parameters were refined for  $\text{LaOs}_2\text{Ir}_2\text{B}_4$  from powder diffraction intensity data: 2 La in 2b; random distribution of 4 Os + 4 Ir in 8g) 0.5999, 0.1408, 0.1408; 8 B in 8g) 0.5250, 0.4080, 0.1371.

### Reference

Hiebl, K., M.J. Sienko and P. Rogl, 1981, *J. Less-Common Metals* **82**, 21.

### La-Lu-Rh-Ru-B

The variation of the superconducting transition  $T_c$  as a function of the rare earth ion exchange has been investigated by Johnston (1981) for the system  $\text{La}_{1-x}\text{Lu}_x(\text{Rh}_{0.85}\text{Ru}_{0.15})_4\text{B}_4$ . Samples were prepared by arc melting the high-purity

elements under argon. Consistently with the earlier observation about the non-existence of a  $\text{La}(\text{Rh}_{0.85}\text{Ru}_{0.15})_4\text{B}_4$  phase with  $\text{LuRu}_4\text{B}_4$ -type of structure (see R–Rh–Ru–B, table 41), the amount of second phases continuously increased towards the La-rich concentrations (decreasing values of  $x$ ).  $T_c$  decreased, linearly with decreasing  $x$ ,  $0.5 < x < 1$ . For  $0.1 < x < 0.3$  the value  $T_c \approx 5$  K becomes independent of composition; for  $x < 0.1$  the samples remained normal down to  $T_n = 1.5$  K. The extrapolated superconducting transition for a hypothetical “ $\text{La}(\text{Rh}_{0.85}\text{Ru}_{0.15})_4\text{B}_4$ ” was obtained to be  $T_c \approx 2\text{--}4$  K. From this quite a large contribution of the nonmagnetic factors (size factor) to the depression of  $T_c$  values was concluded.

#### Reference

Johnston, D.C., 1981, *Physica* **108B**, 755.

#### La–Y–Rh–B

Ku et al. (1980) studied structural as well as superconducting and magnetic properties of an arc melted alloy  $\text{Y}_{0.5}\text{La}_{0.5}\text{Rh}_3\text{B}_2$ . From X-ray powder analysis a  $\text{CeCo}_3\text{B}_2$ -type of structure was derived,  $P6/mmm$ ,  $a = 5.434(6)$ ,  $c = 3.127(4)$ ; superconducting transition range  $T_c = 1.88\text{--}1.56$  K.

#### Reference

Ku, H.C., G.P. Meisner, F. Acker and D.C. Johnston, 1980, *Solid State Commun.* **35**, 91.

#### La–Y–U–B

Hill et al. (1974) investigated structural and magnetic properties of quaternary alloys of the form  $(\text{La}, \text{Y}, \text{U})\text{B}_4$  with a constant ratio  $\text{U}:(\text{Y} + \text{La}) = 0.4:0.6$ . For sample preparation, see  $(\text{La}, \text{U})\text{B}_4$ . Magnetic ordering temperatures  $T_m$  are shown in fig. 55 as a function of the unit cell parameters; X-ray powder analysis;  $\text{ThB}_4$ -type,  $P4/mbm$ .

#### Reference

Hill, H., A.L. Giorgi, E.G. Szklarz and J.L. Smith, 1974, *J. Less-Common Metals* **38**, 239.

#### Lu–Y–Ir–B

Ku et al. (1979) investigated structural and superconducting properties of  $\text{Y}_x\text{Lu}_{1-x}\text{Ir}_4\text{B}_4$  alloys. Despite the fact that  $\text{YIr}_4\text{B}_4$  forms the  $\text{NdCo}_4\text{B}_4$ -type structure and that no trace of a  $\text{CeCo}_4\text{B}_4$ -type structure could be detected for  $\text{LuIr}_4\text{B}_4$ , a metastable solid solution which has the  $\text{CeCo}_4\text{B}_4$ -type structure is observed for  $0.1 < x < 0.7$ . Lattice parameters and superconducting transition temperatures are listed in table 38. The concentration of the superconducting  $\text{CeCo}_4\text{B}_4$  phase in the arc melted samples was estimated from powder X-ray and ac magnetic susceptibility measurements to be near or below 10%. After heat treatment this superconducting phase disappears. The majority of phases was identified with the  $\text{NdCo}_4\text{B}_4$ - and the  $\text{ErIr}_3\text{B}_2$ -type structure.

TABLE 38  
Superconducting transition temperature  $T_c$  and lattice parameters of the  $\text{CeCo}_4\text{B}_4$ -type phase ( $\text{P4}_2/\text{nmc}$ ) in the ternary  $\text{Y}_x\text{Lu}_{1-x}\text{Ir}_4\text{B}_4$  system. (After Ku et al., 1979).

Alloy composition	$T_c$ (K)	$a$ (Å) ( $\pm 0.004$ )	$c$ (Å) ( $\pm 0.006$ )	$c/a$
$(\text{Y}_{0.2}\text{Lu}_{0.8})\text{Ir}_4\text{B}_4$	3.04–1.44	5.400	7.251	1.343
$(\text{Y}_{0.3}\text{Lu}_{0.7})\text{Ir}_4\text{B}_4$	2.98–2.02	5.402	7.272	1.346
$(\text{Y}_{0.4}\text{Lu}_{0.6})\text{Ir}_4\text{B}_4$	3.07–2.70	5.403	7.268	1.345
$(\text{Y}_{0.5}\text{Lu}_{0.5})\text{Ir}_4\text{B}_4$	3.21–3.00	5.408	7.280	1.346
$(\text{Y}_{0.6}\text{Lu}_{0.4})\text{Ir}_4\text{B}_4$	3.06–1.50	(*)	(*)	(*)

(\*) Concentration of the phase was too low to determine lattice parameters.

### Reference

Ku, H.C., B.T. Matthias and H. Barz, 1979, Solid State Commun. **32**(11), 937.

### *Lu–R–Ru–B*

Superconducting transition temperatures have been measured for the compounds  $(\text{R}_{1-x}\text{Lu}_x)\text{RuB}_2$  with  $\text{LuRuB}_2$ -type ( $\text{Pnma}$ ) for  $x = 0.8$  and  $0.9$ ,  $\text{R} = \text{Gd}, \text{Tb}, \text{Dy}, \text{Ho}, \text{Er}, \text{Tm}$ , by Ku and Shelton (1981), who also made an X-ray analysis of arc melted samples (no structural details were given).

Pressure dependence of  $T_c$  of dilute  $(\text{Lu}, \text{R})\text{Rh}_4\text{B}_4$  alloys was investigated by DeLong (1981).

### References

- DeLong, L.E., 1981, Pressure dependence of the superconducting transition temperature of dilute  $(\text{Lu}, \text{R})\text{Rh}_4\text{B}_4$  alloys, in: Ternary Superconductors, Proc. Intern. Conf. on Ternary Superconductors, Lake Geneva, WI, USA (1980), eds. G.K. Shenoy, B.D. Dunlap and F.Y. Fradin (North-Holland, Amsterdam) pp. 193–196.
- Ku, H.C. and R.N. Shelton, 1981, Solid State Commun. **40**, 237.

### *Lu–Sc–Ru–B*

Ku et al. (1979) investigated the crystal structure and superconductivity of arc melted samples  $\text{Lu}_{1-x}\text{Sc}_x\text{Ru}_4\text{B}_4$ ; for sample preparation and heat treatment, see *Sc–Ru–B*. From powder X-ray analysis a  $\text{LuRu}_4\text{B}_4$ -type of structure,  $\text{I4}_1/\text{acd}$ , was derived, see table 39.

### Reference

Ku, H.C., D.C. Johnston, B.T. Matthias, H. Barz, G. Burri and L. Rinderer, 1979, Mater. Res. Bull. **14**, 1591.

TABLE 39  
Lattice parameters and superconducting transition temperatures for arc melted samples of  $(\text{Lu}_{1-x}\text{Sc}_x)\text{Ru}_4\text{B}_4$ .  
(After Ku et al., 1979.)

Compound	$a$ (Å) ( $\pm 0.007$ )	$c$ (Å) ( $\pm 0.015$ )	$T_c$ (K)
$\text{LuRu}_4\text{B}_4$	7.419	14.955	2.06–2.00
$(\text{Lu}_{0.9}\text{Sc}_{0.1})\text{Ru}_4\text{B}_4$	7.420	14.943	3.26–2.30
$(\text{Lu}_{0.7}\text{Sc}_{0.3})\text{Ru}_4\text{B}_4$	7.417	14.936	3.77–3.20
$(\text{Lu}_{0.5}\text{Sc}_{0.5})\text{Ru}_4\text{B}_4$	7.408	14.916	4.96–4.05
$(\text{Lu}_{0.3}\text{Sc}_{0.7})\text{Ru}_4\text{B}_4$	7.389	14.908	5.99–5.22
$(\text{Lu}_{0.1}\text{Sc}_{0.9})\text{Ru}_4\text{B}_4$	7.361	14.871	6.95–6.54
$\text{ScRu}_4\text{B}_4$	7.346	14.895	7.23–6.30

*Lu-Th-Rh-B*

Matthias et al. (1977) measured the superconducting transition temperature range  $T_c = 11.93\text{--}11.3\text{ K}$  for a  $\text{Lu}_{0.75}\text{Th}_{0.25}\text{Rh}_4\text{B}_4$  alloy with  $\text{CeCo}_4\text{B}_4$ -type,  $\text{P4}_2/\text{nmc}$ ; no lattice parameters were given; for sample preparation, see  $\text{YRh}_4\text{B}_4$ .

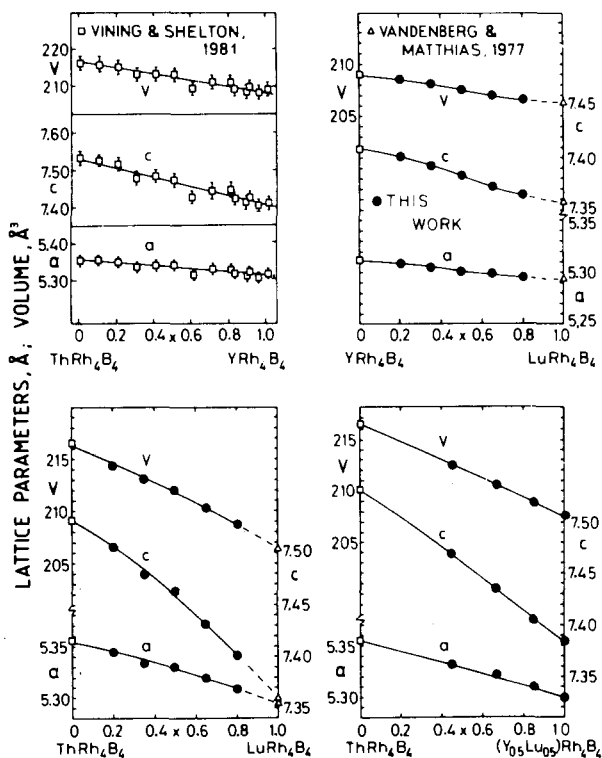


Fig. 72. Lattice parameters versus concentration;  $\text{Lu}_x\text{Y}_{1-x}\text{Rh}_4\text{B}_4$ ,  $\text{Lu}_x\text{Th}_{1-x}\text{B}_4$  and  $(\text{Lu}_{0.5}\text{Y}_{0.5})_x\text{Th}_{1-x}\text{Rh}_4\text{B}_4$  after Hiebl et al. (1981);  $\text{Y}_x\text{Th}_{1-x}\text{Rh}_4\text{B}_4$  after Vining and Shelton (1981).

Hiebl et al. (1981) confirmed the existence of a  $\text{CeCo}_4\text{B}_4$ -type solid solution  $\text{Lu}_x\text{Th}_{1-x}\text{Rh}_4\text{B}_4$  from X-ray and metallographic analysis (fig. 72); superconducting transition temperatures were slightly less than the values reported by Matthias et al. (1977). For sample preparation and Lu-rich region, see  $(\text{Lu}, \text{Th}, \text{Y})\text{Rh}_4\text{B}_4$ .

### References

- Hiebl, K., P. Rogl and M.J. Sienko, 1981, *J. Less-Common Metals* **82**, 201.  
 Matthias, B.T., E. Corenzwit, J.M. Vandenberg and H.E. Barz, 1977, *Proc. Nat'l Acad. Sci. US* **74**(4), 1334.  
 Vining, C.B. and R.N. Shelton (1981), Pressure dependence of the superconducting transition temperature of  $(\text{Th}_{1-x}\text{Y}_x)\text{Rh}_4\text{B}_4$ , in: *Ternary Superconductors, Proc. Intern. Conf. on Ternary Superconductors, Lake Geneva, WI, USA eds. G.K. Shenoy, B.D. Dunlap and F.Y. Fradin (1980), (North-Holland, Amsterdam) pp. 189-192.*

### *Lu-Tm-Ru-B*

The boundaries between the paramagnetic, superconducting and magnetically ordered phases of the solid solution  $\text{Lu}_x\text{Tm}_{1-x}\text{RuB}_2$  ( $\text{LuRuB}_2$ -type of structure,  $\text{Pnma}$ ) have been established by Ku and Shelton (1981), who also made an X-ray analysis on arc melted samples, annealed at  $1000^\circ\text{C}$  for 1 week; no lattice parameters were presented. Reentrant superconductivity was observed for  $x = 0.52$  to  $x = 0.68$ ; long-range magnetic ordering (probably ferromagnetic) was found for  $x < 0.52$ , see fig. 73.

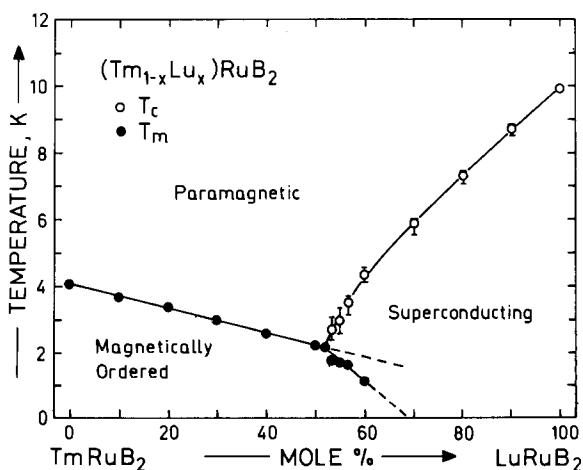


Fig. 73.  $(\text{Lu}_x\text{Tm}_{1-x})\text{RuB}_2$ ; low-temperature phase diagram; after Ku and Shelton (1981).  $T_m$  = magnetic ordering temperature ( $\bullet$ ),  $T_c$  = superconducting transition temperature ( $T_{c1}$  = superconducting to normal transition ( $\circ$ ),  $T_{c2}$  = transition temperature of superconducting to magnetically ordered state).

*Reference*

Ku, H.C. and R.N. Shelton, 1981, Solid State Commun. **40**, 237.

*Lu–Y–Rh–B*

A minimum in the superconducting transition temperature was found for the pseudobinary system  $Y_xLu_{1-x}Rh_4B_4$  at 10.1 K  $x = 0.5$  (Hiebl et al., 1981; X-ray powder analysis). Lattice parameters of the continuous solid solution with  $CeCo_4B_4$ -type ( $P4_2/nmc$ ) are shown in fig. 72. For sample preparation and Lu-rich region, see (Lu, Th, Y) $Rh_4B_4$ .

*Reference*

Hiebl, K., P. Rogl and M.J. Sienko, 1981, J. Less-Common Metals **82**, 201.

*Lu–Y–U–B*

Hill et al. (1974) investigated the magnetic properties of quaternary alloys of the form (Lu, Y, U) $B_4$  with a constant ratio  $U:(Y + Lu) \approx 0.4:0.6$ . For sample preparation, see (La, U) $B_4$ . Magnetic ordering temperatures  $T_m$  are shown in fig. 55 as a function of the unit cell parameters (Th $B_4$ -type,  $P4/mbm$ , X-ray powder diffraction).

*Reference*

Hill, H., A.L. Giorgi, E.G. Szklarz and J.L. Smith, 1974, J. Less-Common Metals **38**, 239.

*Lu–Y–Th–Rh–B*

Hiebl et al. (1981) studied the superconducting behavior for  $T \geq 1.5$  K in the pseudoternary system  $YRh_4B_4$ – $LuRh_4B_4$ – $ThRh_4B_4$  on 30 samples in as-cast as well as annealed condition (1250°C, 48 h, radiation quench).

Congruent melting behavior in the Th-rich region as well as complete solid solubility  $> 1250^\circ C$  ( $CeCo_4B_4$ -type,  $P4_2/nmc$ ) was observed from X-ray and metallographic analysis. Isocritical temperatures and isochores were determined (see fig. 74) and the influence on the superconducting transition temperature in the absence of magnetic ordering was studied with respect to a changing unit cell volume at constant electron density as well as a changing electron density at constant unit cell volume. In the  $LuRh_4B_4$ -rich region a solid state transition (at  $\approx 1300^\circ C$ ) was observed from samples annealed at temperatures lower than 1250°C.

*Reference*

Hiebl, K., P. Rogl and M.J. Sienko, 1981, J. Less-Common Metals **82**, 201.

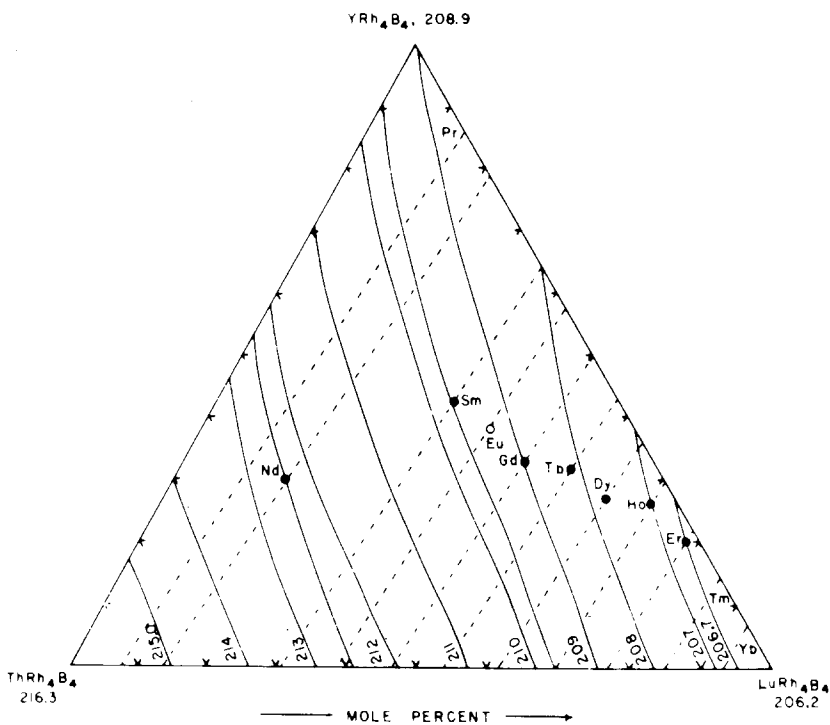


Fig. 74. Isochores of the ternary system  $YRh_4B_4$ - $LuRh_4B_4$ - $ThRh_4B_4$ . — isochore line (constant volume); --- concentrations isoelectronic with lanthanide atoms as indicated; ● intersections of isochores and isoelectronic curves. After Hiebl et al. (1981).

### *Pr-Ir-Os-B*

Hiebl et al. (1982) have investigated magnetism and structure of a  $PrIr_2Os_2B_4$  alloy. For sample preparation, see  $SmIr_{4-x}Os_xB_4$ . From X-ray and metallographic analysis  $PrIr_2Os_2B_4$  melts congruently and crystallizes with  $NdCo_4B_4$ -type of structure,  $P4_2/n$ ,  $a = 7.5991(12)$ ,  $c = 3.9835(5)$ .

### *Reference*

Hiebl, K., P. Rogl and M.J. Sienko, 1982, *Inorg. Chem.* **21**, 1128.

### *Sm-Ir-Os-B*

Hiebl et al. (1982) have investigated the magnetic properties as well as the structural chemistry of  $SmIr_{4-x}Os_xB_4$  alloys. Samples, prepared by arc melting of elemental mixtures (min. purity 99.9%, B 99.3%) and analysed by X-ray and metallography, proved in all cases congruent melting behavior as well as complete solid solubility with a  $NdCo_4B_4$ -type of structure,  $P4_2/n$  (also found after heat treatment at 1200°C, 12 h). Lattice parameters of pseudobinary alloys show small



negative deviation from Vegard's rule:  $\text{SmOs}_3\text{IrB}_4$ :  $a = 7.5406(8)$ ,  $c = 3.9949(6)$ ;  $\text{SmOs}_2\text{Ir}_2\text{B}_4$ :  $a = 7.5538(6)$ ,  $c = 3.9860(4)$ ;  $\text{SmOsIr}_3\text{B}_4$ :  $a = 7.5742(7)$ ,  $c = 3.9822(4)$ .

### Reference

Hiebl, K., P. Rogl and M.J. Sienko, 1982, *Inorg. Chem.* **21**, 1128.

### R-Ir-Rh-B

Ku and Barz (1981) established the phase boundaries between the  $\text{CeCo}_4\text{B}_4$ -type compounds and compounds of other structural types in the systems  $\text{R}(\text{Ir}_x\text{Rh}_{1-x})_4\text{B}_4$ . Samples were prepared by arc melting under Zr-gettered Ar. The boil-off of Sm, Eu was compensated by adding an excess beforehand. For the Yb compounds compacted mixtures of Yb filings and Rh, Ir and B powders were sintered at 800–1250°C, 24 h, in sealed Ta tubes within sealed quartz tubes. For heat treatments the samples were wrapped in Ta foils and sealed under Ar in quartz tubes. Phase boundaries of the  $\text{CeCo}_4\text{B}_4$ -type structure in the  $\text{R}(\text{Ir}_x\text{Rh}_{1-x})_4\text{B}_4$  compounds are presented in fig. 75, differentiating also metastable regions. From powder X-ray diffraction Rh and Ir atoms were statistically distributed in the 8g sites of  $\text{P4}_2/\text{nmc}$ ,  $\text{CeCo}_4\text{B}_4$ -type. No detailed lattice parameters were presented; see also Ku et al. (1979).

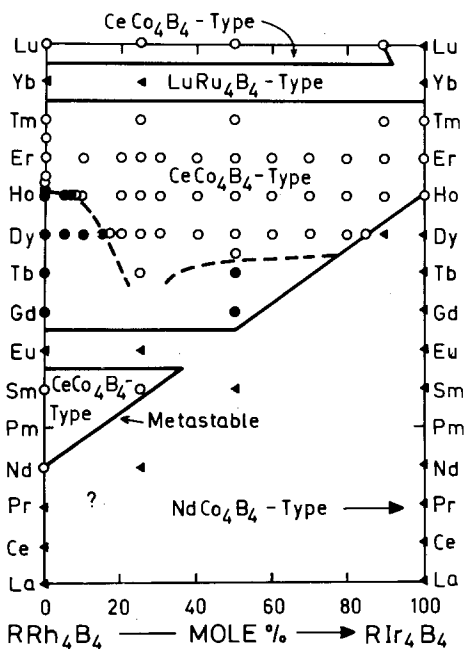


Fig. 75. Phase boundaries of the  $\text{CeCo}_4\text{B}_4$ -type structure in the compounds  $\text{R}(\text{Ir}_x\text{Rh}_{1-x})_4\text{B}_4$ . Metastable phase boundaries are indicated by thick solid lines. Open circles: occurrence of superconductivity, filled circles:  $T_n = 1.2$  K (for  $\text{CeCo}_4\text{B}_4$ -type phases), filled triangles:  $T_n = 1.2$  K, for other types of phases. After Ku and Barz (1981).

### References

- Ku, H.C. and H. Barz, 1981, Superconductivity in pseudoternary compounds  $R(\text{Ir}_x\text{Rh}_{1-x})_4\text{B}_4$ , in: Ternary Superconductors, Proc. Intern. Conf. on Ternary Superconductors, Lake Geneva, WI, USA (1980), eds. G.K. Shenoy, B.D. Dunlap and F.Y. Fradin (North-Holland, Amsterdam) pp. 209-212.
- Ku, H.C., B.T. Matthias and H. Barz, 1979, Solid State Commun. **32**(1), 937.

### *R-Sc-Rh-B*

Whereas Sc itself has not been reported to form a  $\text{ScRh}_4\text{B}_4$ -type phase, Sc substitution for R by  $\approx 30\%$  reveals a  $\text{R}_{0.7}\text{Sc}_{0.3}\text{Rh}_4\text{B}_4$  phase with either a  $\text{CeCo}_4\text{B}_4(\text{hT})$ - or  $\text{LuRh}_4\text{B}_4(?,\text{IT})$ -type of structure; see table 40 (Matthias et al., 1978; samples were arc melted).

TABLE 40  
Transition temperatures (in K) of scandium substituted ternary borides.

Sc	R	$T_c$	Modification <sup>(*)</sup>
30%	La	will not form	will not form
30%	Ce	3.3	hT
30%	Pr	5.15	hT
30%	Nd	4.7	hT
30%	Sm	4.9	hT + IT
30%	Gd	3.2	IT
30%	Tb	4.3	hT
30%	Dy	4.7	hT
30%	Ho	1.3	IT
40%	Ho	6.4	hT
20%	Er	7.8	hT
30%	Er	7.6	
30%	Tm	7.9	hT

<sup>(\*)</sup>hT = high-temperature modification, IT = low-temperature modification.

### Reference

- Matthias, B.T., C.K.N. Patel, H. Barz, E. Corenzwit and J.M. Vandenberg, 1978, Phys. Lett. **68A**(1), 119.

### *R-Rh-Ru-B*

With the exception of La, Ce and Sc, all R members were observed to stabilize the  $\text{LuRu}_4\text{B}_4$ -type of structure ( $I4_1/\text{acd}$ ) for a composition of  $\text{R}(\text{Rh}_{0.85}\text{Ru}_{0.15})_4\text{B}_4$  (Johnston, 1977; X-ray powder diffraction). Unit cell dimensions and superconducting transition and magnetic ordering temperatures are presented in table 41. Samples were synthesized by arc melting under Zr-gettered Ar. The boil-off of Sm, Eu was compensated by adding an excess beforehand. For the Yb member well-mixed powders of (Ru, Rh)B and Yb filings were compacted, sealed in Ta tubes under Ar and sintered at  $1200^\circ\text{C}$  for 24 h. Samples generally were found to be single phase except for the Pr, Eu, and Yb members.

TABLE 41  
Superconducting and magnetic transition temperatures ( $T_c$  and  $T_m$ ) and lattice parameters for  $R(\text{Rh}_{0.85}\text{Ru}_{0.15})_4\text{B}_4$  borides (LuRu<sub>4</sub>B<sub>4</sub>-type, I4<sub>1</sub>/acd); after Johnston (1977).

<i>R</i>	<i>a</i> (Å) (± 0.005)	<i>c</i> (Å) (± 0.010)	$T_c$ (K)	$T_m$ (K)
Pr	7.543	14.995	2.41–2.10	
Nd	7.537	14.969	(*)	(*)
Sm	7.516	14.945	(*)	(*)
Eu	7.505	14.932	2.0 –1.5	
Gd	7.502	14.916	(*)	(*)
Tb	7.490	14.898	(*)	(*)
Dy	7.479	14.885	4.08–3.91	
Ho	7.476	14.872	6.45–6.23	
Er	7.468	14.862	8.02–7.83	
Tm	7.458	14.853	8.38–8.25	
Yb	7.449	14.851	(*)	(*)
Lu	7.445	14.837	9.16–8.74	
Y	7.484	14.895	9.56–9.22	

(\*)No transition observed down to  $T = 1.2$  K.

The effects of hydrostatic pressure (21 kbar) on the superconducting and magnetic critical temperatures have been investigated by Shelton et al. (1981) for  $R(\text{Rh}_{0.85}\text{Ru}_{0.15})_4\text{B}_4$  as well as for  $\text{RRu}_4\text{B}_4$  phases ( $R = \text{Pr, Nd, Gd, Tb, Dy, Ho, Er, Tm, Lu}$ ) which have the LuRu<sub>4</sub>B<sub>4</sub>-type (I4<sub>1</sub>/acd), as determined from X-ray powder analysis of arc melted alloys, prepared by Johnston (1977).  $dT_c/dp$  and  $dT_m/dp$  both change sign between the Dy and Ho compounds. The nonmagnetic contributions (size factor) to the depression of  $T_c$  as a function of the R element in  $R(\text{Rh, Ru})_4\text{B}_4$  compounds has been analyzed by Johnston (1981) in comparison with the predictions using the Abrikosov–Goerkov theory. The role of boron on the superconducting behavior of  $R(\text{Ru, Rh})_4\text{B}_4$  borides was discussed by Johnston (1982).

### References

- Johnston, D.C., 1977, Solid State Commun. **24**, 699; see also: 1981, Physica **108B**, 755.  
 Johnston, D.C., 1982, Solid State Commun. **42**(6), 453.  
 Shelton, R.N., C.U. Segre and D.C. Johnston, 1981, Effect of pressure on the superconducting and magnetic critical temperatures of bct ternary ruthenium borides, in: Ternary Superconductors, Proc. Intern. Conf. on Ternary Superconductors, Lake Geneva, WI, USA (1980), eds G.K. Shenoy, B.D. Dunlap and F.Y. Fradin (North-Holland, Amsterdam) pp. 205–208.

### Sc–Ca–Rh–B

Neither Ca nor Sc form a  $\text{RRh}_4\text{B}_4$ -type phase, but on substitution of 30% Ca for Sc a high- and a low-temperature modification (probably  $\text{CeCo}_4\text{B}_4$ - or LuRu<sub>4</sub>B<sub>4</sub>-type) was reported to exist by Matthias et al. (1978).

*Reference*

Matthias, B.T., C.K.N. Patel, H. Barz, E. Corenzwit and J.M. Vandenberg, 1978, Phys. Lett. **68A**(1), 119.

*Sc-Th-Rh-B*

Vandenberg and Matthias (1977) analysed the crystal structure and superconductivity of two homogeneous, pseudoternary alloys with  $\text{CeCo}_4\text{B}_4$ -type of structure,  $\text{P4}_2/\text{nmc}$ :  $\text{Sc}_{0.65}\text{Th}_{0.35}\text{Rh}_4\text{B}_4$ ,  $a = 5.317(2)$ ,  $c = 7.422(3)$  and  $\text{Sc}_{0.5}\text{Th}_{0.5}\text{Rh}_4\text{B}_4$ ,  $a = 5.322(2)$ ,  $c = 7.453(3)$ ; X-ray powder diffraction; for sample preparation, see  $\text{YRh}_4\text{B}_4$ .

Matthias et al. (1977) measured the superconducting transition temperature range for  $\text{Sc}_{0.75}\text{Th}_{0.25}\text{Rh}_4\text{B}_4$  with  $\text{CeCo}_4\text{B}_4$ -type:  $T_c = 8.74\text{--}8.49$  K; no lattice parameters were given. Thus an extended solid solution  $\text{Sc}_x\text{Th}_{1-x}\text{Rh}_4\text{B}_4$  is conceivable for  $x \lesssim 0.80$ ; " $\text{ScRh}_4\text{B}_4$ " does not form (Vandenberg and Matthias, 1977).

*References*

Matthias, B.T., E. Corenzwit, J.M. Vandenberg and H.E. Barz, 1977, Proc. Nat'l Acad. Sci. US **74**(4), 1334.

Vandenberg, J.M. and B.T. Matthias, 1977, Proc. Nat'l Acad. Sci. US **74**(4), 1336.

*Sc-Y-Ru-B*

Ku and Shelton (1980) characterized the crystal structure of a sample  $\text{Y}_{0.8}\text{Sc}_{0.2}\text{RuB}_2$  as  $\text{LuRuB}_2$ -type,  $\text{Pnma}$ ; no lattice parameters were given; the superconducting transition is at  $T_c = 8.10\text{--}7.73$  K. A ternary  $\text{ScRuB}_2$ -alloy appeared to be multiphase with no  $\text{LuRuB}_2$ -type phase; see also  $\text{Sc-Ru-B}$ . For sample preparation, see  $\text{ScOsB}_2$ .

*Reference*

Ku, H.C. and R.N. Shelton, 1980, Mater. Res. Bull. **15**(10), 1441.

*Sc-Y-Ir-Rh-B*

Ku et al. (1979) investigated the crystal structure and superconducting properties of arc melted alloys  $(\text{Sc}_x\text{Y}_{1-x})(\text{Ir}_{0.9}\text{Rh}_{0.1})_4\text{B}_4$ . From X-ray powder analysis a  $\text{CeCo}_4\text{B}_4$ -type of structure was observed for  $x = 0.1, 0.2, 0.25, 0.3$  and  $0.5$  with assumed random distribution of Rh, Ir atoms in the tetrahedral sites. Superconducting transition temperatures range from 2.13 to 3.45 K; no lattice parameters were given.

*Reference*

Ku, H.C., B.T. Matthias and H. Barz, 1979, Solid State Commun. **32**(1), 937.

*Y-Th-Rh-B*

Vining and Shelton (1981) investigated the pressure dependence of the superconducting transition temperature of  $\text{Th}_{1-x}\text{Y}_x\text{Rh}_4\text{B}_4$  up to 21 kbar. Samples were prepared by arc melting under Zr-gettered Ar and contained less than ten percent

of an unidentified impurity phase (from X-ray powder analysis). Lattice parameters linearly decrease with  $x$ ,  $\text{CeCo}_4\text{B}_4$ -type,  $\text{P4}_2/\text{nmc}$ ; see fig. 72.

#### Reference

Vining, C.B. and R.N. Shelton, 1981, Pressure dependence of the superconducting transition temperature of  $(\text{Th}_{1-x}\text{Y}_x)\text{Rh}_4\text{B}_4$ , in: Ternary Superconductors, Proc. Intern. Conf. on Ternary Superconductors, Lake Geneva, WI, USA (1980), eds. G.K. Shenoy, B.D. Dunlap and F.Y. Fradin (North-Holland, Amsterdam) pp. 189–192.

#### *Y-Th-Ru-B*

Ku et al. (1980) studied structural, superconducting and magnetic properties of an arc melted alloy  $\text{Y}_{0.5}\text{Th}_{0.5}\text{Ru}_3\text{B}_2$ . From X-ray powder analysis a  $\text{CeCo}_3\text{B}_2$ -type of structure was derived,  $\text{P6}/\text{mmm}$ ,  $a = 5.499(6)$ ,  $c = 3.048(4)$ ;  $T_c = 1.53\text{--}1.40$  K.

#### Reference

Ku, H.C., G.P. Meisner, F. Acker and D.C. Johnston, 1980, Solid State Commun. **35**, 91.

#### *Y-Rh-Ru-B*

From arc melted ingots within the region  $\text{RhB}$ ,  $\text{YRh}_6\text{B}_4$  and  $\text{YRh}_4\text{B}_4$  Johnston (1977) observed a high-temperature modification  $\text{YRh}_4\text{B}_4$  (metastable ?) with  $\text{LuRu}_4\text{B}_4$ -type structure. Substitution of as little as 4% of Rh by Ru resulted in stabilizing the high-temperature form ( $\text{LuRu}_4\text{B}_4$ -type) to room temperature with negligible amounts of second phases;  $T_c = 9.3$  K; thus a complete superconducting solid solution  $\text{Y}(\text{Ru}_{1-x}\text{Rh}_x)_4\text{B}_4$  is conceivable if the metastable alloys are quenched from high temperatures. The  $\text{LuRu}_4\text{B}_4$ -type of structure,  $\text{I4}/\text{acd}$ , has been confirmed from single crystal X-ray diffraction analysis of compositions  $x = 0.3, 0.5, 0.6$  and  $0.8$  (Yvon and Grüttner, 1980). Structural parameters are listed in table 29. Samples were prepared by Johnston (1977); see *Y-Rh-B*.

#### References

Johnston, D.C., 1977, Solid State Commun. **24**, 699.

Yvon, K. and A. Grüttner, 1980, The influence of the formal electric charge on the size of the transition metal atom cluster in  $\text{YRh}_4\text{B}_4$ ,  $\text{YRu}_4\text{B}_4$  and  $\text{PbMo}_6\text{S}_8$  related compounds, in: Superconductivity in d- and f-band metals, eds. H. Suhl and M.B. Maple (Academic Press, New York) pp. 515–519.

## 4. Notes added in proof

#### *Dy-La-B*

Polycrystalline alloys of the solid solution  $\text{La}_{1-x}\text{Dy}_x\text{B}_6$  ( $0.03 \leq x \leq 0.08$ ) have been investigated with respect to electrical resistance and absolute thermoelectric power (2–30 K); their behaviour resembles that of a spin glass. The alloys were reported to crystallize with the  $\text{CaB}_6$ -type of structure ( $\text{Pm}3\text{m}$ ); however, no lattice parameter data have been given.

*Reference*

Ali, N. and S.B. Woods, 1983, *Solid State Commun.* **45**(6), 471.

*Dy-Ni-B*

$\text{Dy}_3\text{Ni}_{13}\text{B}_2$  is isostructural with the  $\text{Nd}_3\text{Ni}_{13}\text{B}_2$ -type:  $P6/mmm$ ,  $a = 4.949(2)$ ,  $c = 10.909(7)$ . Refinement of X-ray powder data was as good as  $R = 0.120$  (Kuz'ma et al., 1983).

*Reference*

Kuz'ma, Yu.B., N.S. Bilonishko, N.F. Chaban and G.V. Chernjak, 1983, *J. Less-Common Metals* **90**, 217.

*Dy-Re-B*

The phase equilibria of the system Dy-Re-B as presented in fig. 76 have been derived by Mikhalenko (1981) and reveal the existence of five ternary compounds in an isothermal section at  $1000^\circ\text{C}$ . 93 alloys prepared by arc-melting and heat treatment in evacuated silica tubes (1200 h at  $1000^\circ\text{C}$ ) have been investigated by means of X-ray diffraction and metallographic analysis. Starting materials were 99.98% pure ingots of Dy and 99.98% Re and 99.4% B powders.

The binary systems are in agreement with literature data and mutual solid solubilities were observed to be very small (no details presented).

The existence of the ternary borides,  $\text{DyReB}_4$ ,  $\text{Dy}_2\text{ReB}_6$  and  $\text{Dy}_3\text{ReB}_7$ , as reported earlier was confirmed (see Dy-Re-B); furthermore, compound formation was also

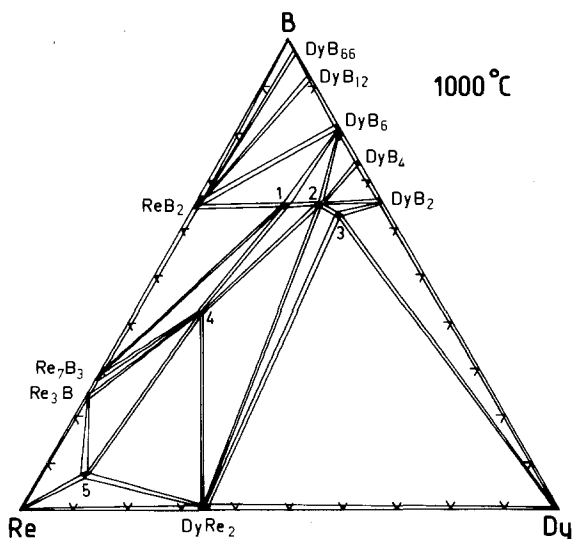


Fig. 76. Dy-Re-B, isothermal section at  $1000^\circ\text{C}$ . 1:  $\text{DyReB}_4$ , 2:  $\text{Dy}_2\text{ReB}_6$ , 3:  $\text{Dy}_3\text{ReB}_7$ , 4:  $\text{DyRe}_4\text{B}_4$ , 5:  $\text{DyRe}_{11}\text{B}$ .

observed for  $\text{DyRe}_4\text{B}_4$  and  $\text{DyRe}_{11}\text{B}$ . The crystal structures of the latter two phases have not yet been evaluated; however, from preliminary X-ray studies  $\text{DyRe}_4\text{B}_4$  was indicated to be tetragonal ( $a = 7.408$ ,  $c = 10.51$ ) and isostructural with  $\text{CeRe}_4\text{B}_4$ . Similarly,  $\text{DyRe}_{11}\text{B}$  is cubic ( $a = 10.62$ ) and presumably isotypic with  $\text{YRe}_{11}\text{B}$ .

#### Reference

Mikhaleiko, S.N., 1981, Vestn. Lvov Univ., Ser. Khim. **23**, 52.

#### Er-Fe-B

The formation of the compound  $\text{ErFe}_4\text{B}$  was quite recently reported by Chernjak (1983).  $\text{ErFe}_4\text{B}$  was prepared by arc-melting and subsequent annealing in evacuated silica tubes at  $800^\circ\text{C}$  for 240 h. Refinement of X-ray powder data indicated a  $\text{CeCo}_4\text{B}$ -type of structure with  $a = 5.033(1)$ ,  $c = 6.985(3)$ , and Er in 1a, b; Fe in 2c and 6i ( $z = 0.287$ ), and B in the 2d site of the space group  $\text{P6}/\text{mmm}$ ;  $R = 0.12$ .

#### Reference

Chernjak, G.V., 1983, Izv. Akad. Nauk SSSR, Neorg. Mater. **19**(3), 485.

#### Er-Ni-B

Confirming the similar alloying behaviour among the rare earth metal-Ni-B combinations,  $\text{Er}_3\text{Ni}_{13}\text{B}_2$  was observed with the  $\text{Nd}_3\text{Ni}_{13}\text{B}_2$ -type:  $\text{P6}/\text{mmm}$ ,  $a = 4.938(2)$ ,  $c = 10.90(1)$  (Kuz'ma et al., 1983).

#### Reference

Kuz'ma, Yu.B., N.S. Bilonishko, N.F. Chaban and G.V. Chernjak, 1983, J. Less-Common Metals **90**, 217.

#### Er-Rh-B

According to Christner et al. (1979), who investigated the optimal conditions for the preparation of thin films of  $\text{ErRh}_4\text{B}_4$  by means of sputter deposition from an arc melted target, the thin films of  $\text{ErRh}_4\text{B}_4$  are reentrant superconductors with slightly reduced values of  $T_c$ . The reduction was suspected to be due to disorder effects. Similarly radiation damage in thin films of  $\text{ErRh}_4\text{B}_4$  (1.8 MeV  $\alpha$ -particles) was found to quench both the superconduction and more drastically the ferromagnetic transition temperature (Rowell et al., 1979).

Confirming earlier indications by Johnston (1977), and Yvon and Johnston (1982),  $\text{ErRh}_4\text{B}_4$  with the  $\text{LuRu}_4\text{B}_4$ -type ( $\text{I4}_1/\text{acd}$ ) has recently been obtained from arc melted alloy buttons which subsequently were wrapped in Ta-foils sealed in silica tubes and heat treated for 10 days at  $1050^\circ\text{C}$  (Iwasaki et al., 1983). Boron deficiency was claimed with respect to a quantitative analysis, but no details were given and no lattice parameter data were presented. From magnetic measurements  $\text{ErRh}_4\text{B}_4$  exhibits a superconducting transition at  $T_c = 7.15$  K and antiferromagnetic ordering below  $T_N \sim 0.4$  K.

Employing single crystal studies Behroozi et al. (1983) were able to detect a first-order phase transition at  $H_{c2}$  for  $1.4 \text{ K} \lesssim T < 3.3 \text{ K}$  in case the magnetic field is  $\parallel$  to the  $a$ -axis (easy axis of magnetization), whereas in the  $c$ -direction ordinary type-II behaviour is revealed from the superconducting and magnetization curves.

In accordance with the earlier neutron scattering data (polycrystalline samples, Moncton et al., 1980), Sinha et al. (1982), from single crystal neutron diffraction and electrical resistivity data, concluded to the coexistence of superconductivity and long-range ferromagnetic order in a spatially inhomogeneous manner (0.71–1.2 K) and with a transverse, linearly polarized, sinusoidally modulated magnetic structure ( $\lambda = 100 \text{ \AA}$ ) along [010] (the propagation directions are at  $45^\circ$  to [001] and [100]).

### References

- Behroozi, F., G.W. Crabtree, S.A. Campbell and D.G. Hinks, 1983, Phys. Rev. B **27**(11), 6849.  
 Christner, G.L., B. Bradford, L.E. Toth, R. Cantor, E.D. Dahlberg, A.M. Goldman and C.Y. Huang, 1979, J. Appl. Phys. **50**(9), 5820.  
 Iwasaki, H., M. Isino, K. Tsunokuni and Y. Muto, 1983, J. Magn. Magn. Mater. **31–34**, 521.  
 Johnston, D.C., 1977, Solid State Commun. **24**(10), 699.  
 Moncton, D.E., D.B. McWhan, P.H. Schmidt, G. Shirane, W. Thomlinson, M.B. Maple, H.B. MacKay, L.D. Woolf, Z. Fisk and D.C. Johnston, 1980, Phys. Rev. Lett. **45**, 2060.  
 Rowell, J.M., R.C. Dynes and P.H. Schmidt, 1979, Solid State Commun. **30**, 191.  
 Sinha, S.K., G.W. Crabtree, D.G. Hinks and H.A. Mook, 1982, Phys. Rev. Lett. **48**, 950.  
 Yvon, K. and D.C. Johnston, 1982, Acta Crystallogr. **B38**, 247.

### Eu–Sm–B

A complete solid solubility with a slight negative deviation from Vegard's rule is reported for the concentrational section  $\text{Sm}_{1-x}\text{Eu}_x\text{B}_6$ , revealing the  $\text{CaB}_6$ -type (Pm3m) (Konovalova et al., 1982). Samples were prepared by borothermal reduction of oxide mixtures in vacuum. Monitored by X-ray  $L_{\text{III}}$  absorption spectroscopy the Sm-valence was found to increase on Sm/Eu substitution from 2.52 ( $\text{SmB}_6$ ) to 3.0 in  $\text{Sm}_{0.3}\text{Eu}_{0.7}\text{B}_6$ .

### Reference

- Konovalova, E.S., Yu.B. Paderno, T. Lundström, L.D. Finkelshtein, N.N. Efremova and E.M. Dudnik, 1982, Poroshk. Metall. **238**(10), 78.

### Gd–Cr–B

Fig. 77 represents the phase equilibria of an isothermal section of the Gd–Cr–B system at  $1000^\circ\text{C}$ . The metal-rich region up to 85 a/o boron has been investigated by Chaban (1982) by means of X-ray diffraction analysis of arc melted alloys annealed at  $1000^\circ\text{C}$  for 1000 h in evacuated silica tubes. The starting materials were powders of Cr (99.98%) and B (99.5%) and ingots of Gd (98.5%). Samples in the region of chromium monoboride were subjected to a prolonged heat treatment. The binary boundary systems are in essential agreement with literature data (see also Gd–Co–B and Y–Cr–B). Mutual solid solubility of Cr- and Gd-borides was claimed to be negligible at  $1000^\circ\text{C}$  and phase equilibria are dominated by the existence of one



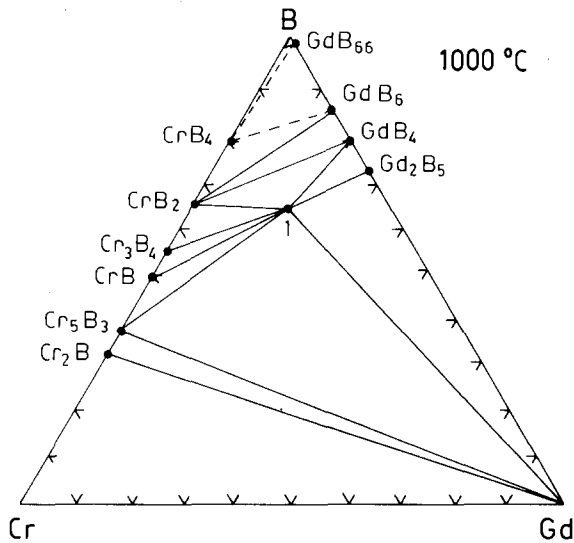


Fig. 77. Gd-Cr-B, isothermal section at 1000°C, 1: GdCrB<sub>4</sub>.

ternary compound GdCrB<sub>4</sub>, earlier observed by Kuz'ma (1970). The boron-rich region has not been investigated and is proposed including a two-phase equilibrium CrB<sub>4</sub> + GdB<sub>66</sub> and a three-phase equilibrium CrB<sub>4</sub> + GdB<sub>66</sub> + B(Gd,  $\lesssim 2$  a/o Cr). Despite the fact that the existence of a 'Cr<sub>6</sub>B'-phase is still dubious a closer inspection of the Cr-rich region will be necessary.

#### Reference

Chaban, N.F., 1982, Poroshk. Metall. **229**(1), 61.

#### Gd-Mo-B

The existence of the ternary compound GdMoB<sub>4</sub> (YCrB<sub>4</sub>-type), earlier observed by Kuz'ma and Svarichevskaya (1972), has recently been confirmed by a study of the ternary phase equilibria at 1000°C in the metal-rich region (0–85% B) of the system Gd-Mo-B by Chaban (1982); see fig. 78. Alloys have been prepared by arc melting compacts of Gd ingot (98.5%) and B (99.5%) and Mo (99.98%) powders and subsequent annealing in evacuated silica tubes for more than 1000 h at 1000°C. Due to the sluggish solid state transition of Mo-monoborides, samples near MoB have been subjected to a prolonged heat treatment. From X-ray analysis a second ternary compound, Gd<sub>3</sub>MoB<sub>7</sub>, has been observed, whose crystal structure was suggested to be of the Y<sub>3</sub>ReB<sub>7</sub>-type (no details were given). The phase equilibria in the boron-rich region of fig. 78 are proposed, including the three-phase equilibria Mo<sub>1-x</sub>B<sub>3</sub> + GdB<sub>6</sub> + GdB<sub>66</sub> and Mo<sub>1-x</sub>B<sub>3</sub> + GdB<sub>66</sub> + B(Mo, Gd).

#### Reference

Chaban, N.F., 1982, Poroshk. Metall. **229**(1), 61.

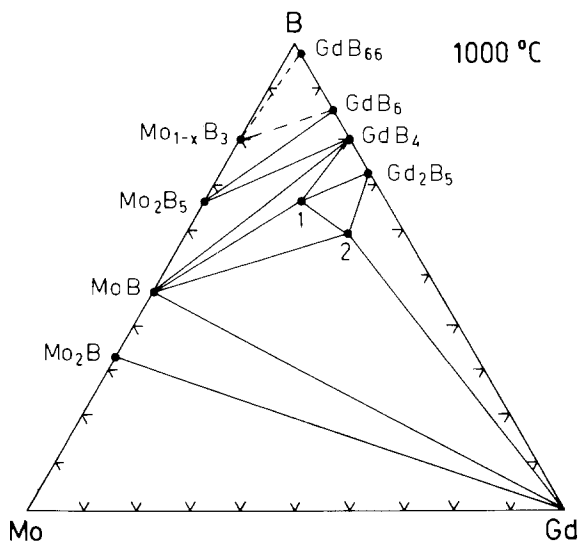


Fig. 78. Gd–Mo–B, isothermal section at 1000°C. 1: GdMoB<sub>4</sub>, 2: Gd<sub>3</sub>MoB<sub>7</sub>.

### Gd–Ni–B

Ternary phase equilibria in the system Gd–Ni–B have been mainly investigated by Kuz'ma and co-workers. Confirming earlier results (see Gd–Ni–B) but without further experimental details Kuz'ma et al. (1983) presented two partial isothermal sections (fig. 79): a) at 800°C for the region 0–40% Gd, and b) at 600°C for the region 40–100% Gd. The ternary boundary systems are in accordance with the literature data; for nickel and gadolinium borides see also Y–Ni–B and Gd–Co–B, respectively. Intermetallics Gd–Ni correspond to a recent compilation by Iandelli and Palenzona (1979): Gd<sub>2</sub>Ni<sub>17</sub> (Th<sub>2</sub>Ni<sub>17</sub>-type), GdNi<sub>5</sub> (CaCu<sub>5</sub>-type), Gd<sub>2</sub>Ni<sub>7</sub> (Ce<sub>2</sub>Ni<sub>7</sub>-type), GdNi<sub>3</sub> (PuNi<sub>3</sub>-type), GdNi<sub>2</sub> (MgCu<sub>2</sub>-type), GdNi (CrB-type) and Gd<sub>3</sub>Ni (Fe<sub>3</sub>C-type). Mutual solid solubilities of the binary compounds were negligible and a rough estimate can be inferred from the detailed investigation of the system Gd–Co–B by Stadelmaier and Lee (1978) (see there). The existence of eleven ternary compounds has been reported, confirming the earlier data on GdNi<sub>12</sub>B<sub>6</sub> (SrNi<sub>12</sub>B<sub>6</sub>-type), Gd<sub>3</sub>Ni<sub>7</sub>B<sub>2</sub> (Dy<sub>3</sub>Ni<sub>7</sub>B<sub>2</sub>-type), Gd<sub>3</sub>Ni<sub>13</sub>B<sub>2</sub> (Nd<sub>3</sub>Ni<sub>13</sub>B<sub>2</sub>-type) and GdNi<sub>4</sub>B (CeCo<sub>4</sub>B-type). Approximate formulas were applied to the remaining compounds such as Gd<sub>2</sub>Ni<sub>2</sub>B, Gd<sub>2</sub>Ni<sub>4</sub>B<sub>3</sub>, GdNi<sub>12</sub>B<sub>7</sub>, GdNi<sub>6</sub>B<sub>3</sub>, GdNi<sub>3</sub>B<sub>2</sub>, GdNi<sub>2</sub>B<sub>4</sub> and Gd<sub>4</sub>NiB<sub>13</sub>. The phase equilibria in the boron-rich region were not investigated and are proposed, including a three-phase equilibrium: GdB<sub>66</sub> + NiB + B (Gd, <2.5 a/o Ni), see fig. 79.

### References

- Iandelli, A. and A. Palenzona, 1979, Crystal chemistry of intermetallic compounds, in: Handbook on the Physics and Chemistry of Rare Earths, Vol. 2, eds. K.A. Gschneidner, Jr. and L. Eyring (North-Holland, Amsterdam) pp. 1–54.  
 Kuz'ma, Yu.B., N.S. Bilonishko, N.F. Chaban and S.V. Chernjak, 1983, J. Less-Common Metals **90**, 217.

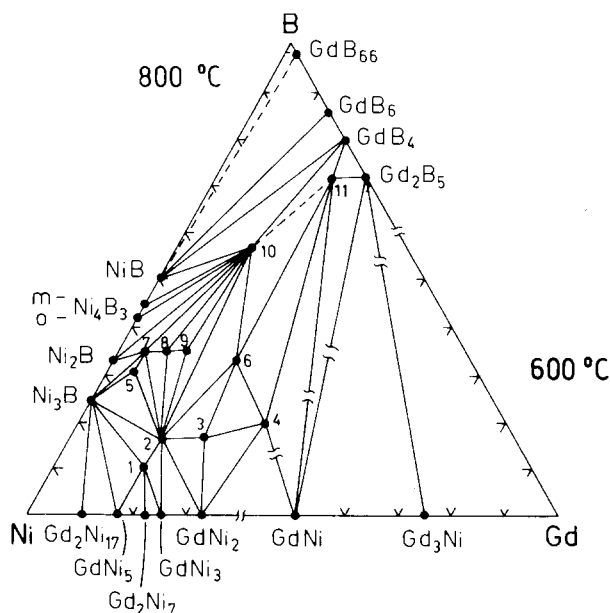


Fig. 79. Gd-Ni-B, partial isothermal sections at 800°C (0–40 a/o Gd) and at 400°C (40–100 a/o Gd). 1:  $\text{Gd}_3\text{Ni}_{13}\text{B}_2$ , 2:  $\text{GdNi}_4\text{B}$ , 3:  $\text{Gd}_3\text{Ni}_7\text{B}_2$ , 4:  $\text{Gd}_2\text{Ni}_2\text{B}$ , 5:  $\text{GdNi}_{12}\text{B}_6$ , 6:  $\text{Gd}_2\text{Ni}_4\text{B}_3$ , 7:  $\text{GdNi}_{12}\text{B}_{7-7}$ , 8:  $\text{GdNi}_6\text{B}_3$ , 9:  $\text{GdNi}_3\text{B}_2$ , 10:  $\text{GdNi}_2\text{B}_4$ , 11:  $\text{Gd}_4\text{NiB}_{13}$ .

### Gd-W-B

Two ternary compounds  $\text{GdWB}_4$  and  $\text{Gd}_3\text{WB}_7$  were found to determine the phase equilibria of the 1000°C isothermal section of the Gd-W-B system. The metal-rich region (0–85 a/o B, fig. 80) has been investigated by Chaban (1982) by means of X-ray analysis of arc melted alloys subsequently annealed at 1000°C for more than 1000 h in evacuated silica tubes. Due to the sluggish solid state transformation of the W-monoboride, alloys near this region had to be subjected to prolonged heat treatments. The binary boundary systems are in agreement with literature data and mutual solid solubilities of W- and Gd-borides were claimed to be negligible.  $\text{GdWB}_4$ , earlier reported by Kuz'ma and Svarichevskaya (1972) with  $\text{YCrB}_4$ -type, was confirmed; the crystal structure of  $\text{Gd}_3\text{WB}_7$  was suspected to be of the  $\text{Y}_3\text{ReB}_7$ -type (no data given).

The phase equilibria at higher boron concentrations (fig. 80) are proposed and are likely to generate the two three-phase equilibria:  $\text{W}_{1-x}\text{B}_3 + \text{GdB}_6 + \text{GdB}_{66}$  and  $\text{GdB}_{66} + \text{W}_{1-x}\text{B}_3 + \text{B}(\text{W}, \text{Gd})$ .

### Reference

Chaban, N.F., 1982, *Poroshk. Metall.* **229**(1), 61.

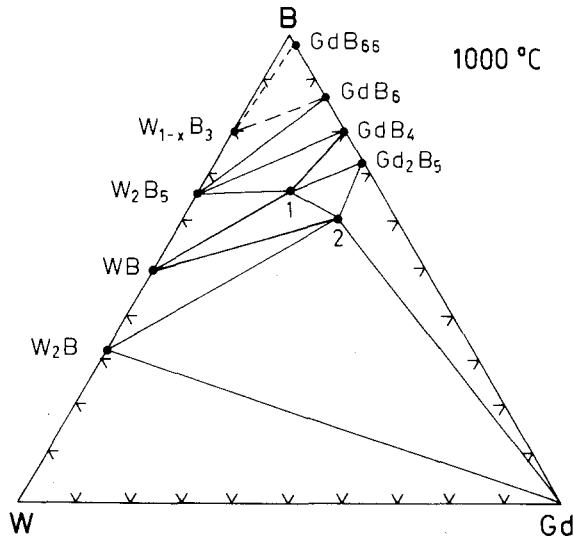


Fig. 80. Gd-W-B, isothermal section at 1000°C, 1: GdWB<sub>4</sub>, 2: Gd<sub>3</sub>WB<sub>7</sub>.

### *Ho-Ni-B*

The existence of the compound Ho<sub>3</sub>Ni<sub>13</sub>B<sub>2</sub> with a Nd<sub>3</sub>Ni<sub>13</sub>B<sub>2</sub>-type of structure [P6/mmm,  $a = 4.943(2)$ ,  $c = 10.90(1)$ ] was recently reported by Kuz'ma et al. (1983); however, no experimental details have been presented.

### *Reference*

Kuz'ma, Yu.B., N.S. Bilonishko, N.F. Chaban and G.V. Chernjak, 1983, *J. Less-Common Metals* **90**, 217.

### *La-Tm-B*

In accordance with the instability of TmB<sub>6</sub>, Kasaya et al. (1983) observed a limited solid solubility range La<sub>1-x</sub>Tm<sub>x</sub>B<sub>6</sub> restricted to values  $x < 0.5$ . Samples were prepared by borothermal reduction of the mixed oxides; however, no temperature was reported. Lattice parameters were found to vary linearly from  $a = 4.156$  (LaB<sub>6</sub>) to  $a = 4.134$  for  $x \approx 0.5$ . From this a value of  $a = 4.11$  is extrapolated for a hypothetical (mixed valent) TmB<sub>6</sub>. Magnetic susceptibility measurements and L<sub>III</sub>-absorption spectroscopy indicate a mixed valency of Tm (in the order of 2.65 for La<sub>0.53</sub>Tm<sub>0.47</sub>B<sub>6</sub>, 2.62 for La<sub>0.78</sub>Tm<sub>0.22</sub>B<sub>6</sub> and 2.66 for La<sub>0.88</sub>Tm<sub>0.12</sub>B<sub>6</sub>).

### *Reference*

Kasaya, M., F. Iga, H. Yashima, T. Satoh, M. Ohashi, S. Nakai and T. Kasuya, 1983, *J. Magn. Magn. Mater.* **31-34**, 389.

*Nd-Co-B*

The existence of ten ternary Nd-Co-B compounds was recently reported by Bilonishko and Kuz'ma (1983) from a röntgenographic and metallographic study of the phase equilibria in two partial isothermal sections at 600°C (for the region 0–33 a/o Nd) and at 400°C for the region 33–100 a/o Nd; see fig. 81. Samples were prepared from Nd ingots (99.07%) and powders of Co (99.9%) and B (99.3%) by arc melting under a protective atmosphere of argon and subsequent heat treatment in evacuated silica tubes for 700 h.

The binary system Nd-Co as presented by Bilonishko and Kuz'ma (1983) is in essential agreement with what is presently known in the literature:  $\text{Nd}_2\text{Co}_{17}$  (Th<sub>2</sub>Zn<sub>17</sub>-type),  $\text{NdCo}_5$  (CaCu<sub>5</sub>-type),  $\text{Nd}_2\text{Co}_7$  (Gd<sub>2</sub>Co<sub>7</sub>-type?),  $\text{NdCo}_3$  (PuNi<sub>3</sub>-type),  $\text{NdCo}_2$  (MgCu<sub>2</sub>-type),  $\text{Nd}_2\text{Co}_{1.7}$  (Pr<sub>2</sub>Co<sub>1.7</sub>-type),  $\text{Nd}_7\text{Co}_3$ ,  $\text{Nd}_3\text{Co}$  (Fe<sub>3</sub>C-type). At variance with a DTA-investigation of the Nd-Co system by Ray et al. (1973), who gave evidence for the existence of  $\text{Nd}_2\text{Co}_3$  (La<sub>2</sub>Co<sub>3</sub>-type) and  $\text{Nd}_5\text{Co}_{19}$  (Ce<sub>5</sub>Co<sub>19</sub>-type), these two phases were not observed by Bilonishko and Kuz'ma (1983), possibly due to retarded kinetics of the peritectic formation at their low temperature annealing conditions.

Severe doubts exist in the characterization of phases such as  $\text{Nd}_{\sim 7}\text{Co}_{\sim 3}$  (eventually described with Ce<sub>7</sub>Ni<sub>3</sub>-type) and  $\text{Nd}_{24}\text{Co}_{11}$  with the Ce<sub>24</sub>Co<sub>11</sub>-type. It is, however, most probable that both the latter phases indeed correspond to  $\text{Nd}_5\text{Co}_2$ , whose crystal structure was recently determined to be of the Mn<sub>5</sub>C<sub>2</sub>-type (Moreau and Paccard,

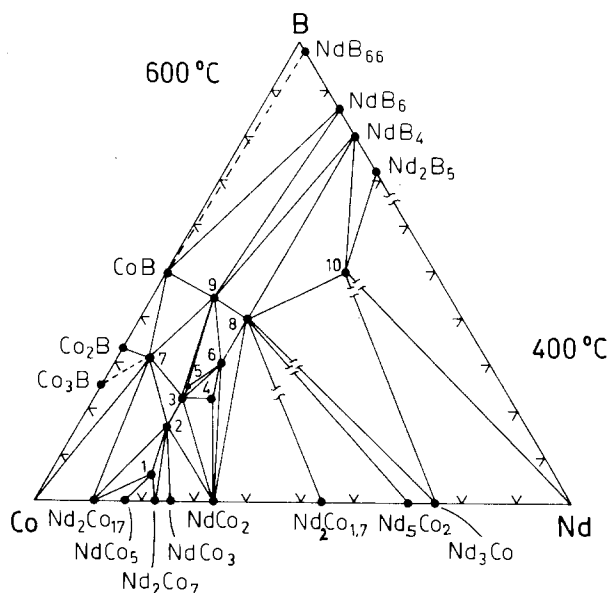


Fig. 81. Nd-Co-B, partial isothermal sections at 600°C (0–33 a/o Nd) and at 400°C (33–100 a/o Nd). 1:  $\text{Nd}_2\text{Co}_9\text{B}$ , 2:  $\text{NdCo}_4\text{B}$ , 3:  $\text{Nd}_3\text{Co}_{11}\text{B}_4$ , 4:  $\text{Nd}_2\text{Co}_5\text{B}_2$ , 5:  $\text{Nd}_2\text{Co}_7\text{B}_3$ , 6:  $\text{Nd}_2\text{Co}_3\text{B}_3$ , 7:  $\text{NdCo}_{11}\text{B}_6$ , 8:  $\text{NdCo}_2\text{B}_2$ , 9:  $\text{NdCo}_4\text{B}_4$ , 10:  $\text{Nd}_2\text{CoB}_3$ .

1976). Some more clarification is also needed regarding the observed polymorphic behaviour of  $\text{Nd}_2\text{Co}_7$ , which according to Singh and Raman (1968) crystallises from the melt with a  $\text{Gd}_2\text{Co}_7$ -type but on annealing was claimed to transform into the  $\text{Ce}_2\text{Ni}_7$ -type.

Singh and Raman (1968) furthermore claim the existence of two polymorphic forms of  $\text{Nd}_3\text{Co}$ , whose Nd-rich  $\beta$ -form has not yet been evaluated ( $\alpha$ - $\text{Nd}_3\text{Co}$  was said to be  $\text{Fe}_3\text{C}$ -type). These data concerning  $\text{Nd}_3\text{Co}$  and  $\text{Nd}_2\text{Co}_7$  are at variance with Ray et al. (1973) who failed to observe indications for a thermal arrest associated with the proposed phase transformations.

For a discussion of the Co–B and Nd–B binary systems, see Gd–Co–B and Nd–Cr–B, respectively.

Mutual solid solubilities of the binary compounds were observed to be negligible and phase equilibria are characterized by the existence of ten ternary compounds, seven of which have been defined earlier (see table 26).

The crystal structures of the remaining three phases with approximate formulas  $\text{Nd}_2\text{Co}_9\text{B}$ ,  $\text{Nd}_2\text{Co}_5\text{B}_3$  and  $\text{Nd}_2\text{CoB}_3$  have not yet been solved. Preliminary X-ray studies, however, suggested an orthorhombic symmetry for  $\text{Nd}_2\text{Co}_5\text{B}_3$  ( $Ccca$ ,  $a = 5.13$ ,  $b = 38.2$ ,  $c = 10.77$ ) representing a new  $\text{CaCu}_5$ -derivative structure according to the geometrical relation  $a \approx a_0$ ,  $b \approx 4\sqrt{3}a$ ,  $c \approx 3c_0$ . Similarly  $\text{Nd}_2\text{CoB}_3$  was found to be of trigonal symmetry [ $a = 5.423(4)$ ,  $c = 24.31(4)$ ] and is supposed to derive from the  $\text{AlB}_2$ -type.

The boron-rich part of the phase diagram is tentative insofar as it is likely to involve three-phase equilibria such as:  $[\text{NdB}_{66} + \text{CoB} + \text{B}(\text{Nd}, < 2 \text{ a/o Co})]$ ,  $[\text{NdB}_{6+x} + \text{CoB} + \text{NdB}_{66}]$  and  $[\text{NdB}_6 + \text{NdB}_{6+x} + \text{CoB}]$ .

### References

- Bilonishko, N.S. and Yu.B. Kuz'ma, 1983, *Izv. Akad. Nauk SSSR, Neorg. Mater.* **19**(3), 485.  
 Moreau, J.M. and D. Paccard, 1976, *Acta Cryst.* **B32**, 1654.  
 Ray, A.E., A.T. Biermann, R.S. Harmer and J.E. Davison, 1973, *Cobalt* **3**, 103.  
 Singh, P.P. and A. Raman, 1968, *Mater. Res. Bull.* **3**(10), 843.

### Nd–Rh–B

Some information about the complicated phase equilibria in the Nd–Rh–B system has recently been reported by Vlasse et al. (1983) concerning the range of  $\text{Nd}_{1-x}\text{Rh}_x\text{Rh}_3\text{B}_2$  for values of  $0 < x < 0.52$ . A “multiphase” region has been observed between  $\text{NdRh}_3\text{B}_2$  with the  $\text{CeCo}_3\text{B}_2$ -type and a new phase  $(\text{Nd}_{1-x}\text{Rh}_x)\text{Rh}_3\text{B}_2$ , revealing a homogeneous region for  $0.29 < x < 0.52$  (data seem to apply for as-cast conditions). The crystal structure of the new compound has been characterized and refined from diffractometer counter data of single crystals obtained from arc melted alloys (purity of starting materials 99.9%).  $\text{Nd}_{0.71}\text{Rh}_{3.29}\text{B}_2$  crystallizes in a new  $\text{CaCu}_5$ -derivative type, exhibiting a statistical distribution of Nd, Rh-atoms on the R-sites:  $a = 5.595(2)$ ,  $c = 2.855(1)$ ;  $P\bar{6}2m$ ; Rh in  $3g$  (0.5052(7), 0, 0.5); (Nd + Rh) in  $1a$  (0, 0, 0), and B in  $2c$  ( $\frac{1}{3}, \frac{2}{3}, 0$ ). The reliability factor was  $R = 0.08$ . X-ray and pycnometric densities were given for  $\text{Nd}_{0.67}\text{Rh}_{3.33}\text{B}_2$  and they compare well:  $\rho_x = 9.92$ ,  $\rho_E = 9.94 \text{ kg/dm}^3$ .

Despite the fact that the phase relationship between the two compounds  $\text{NdRh}_3\text{B}_2$  and  $\text{Nd}_{1-x}\text{Rh}_x\text{Rh}_3\text{B}_2$  ( $0.29 < x < 0.52$ ) and a further compound “ $\text{Nd}_{0.5}\text{Rh}_3\text{B}_2$ ”, reported by Felner and Nowik (1980), remained unsolved,  $\text{Nd}_{0.5}\text{Rh}_3\text{B}_2$  according to its lattice dimensions of  $a \approx 5.65$  and  $c \approx 17.1$  seems to be another  $\text{CaCu}_5$ -derivative type whose structure is still unknown. However, the existence of a compound with a formula  $\text{Nd}_{0.5}\text{Rh}_3\text{B}_2$  was recently confirmed by Majkrzak et al. (1982), who observed this compound as a minor constituent in an alloy “ $\text{NdRh}_6\text{B}_6$ ” and in equilibrium with the bulk phase  $\text{NdRh}_4\text{B}_4$  ( $\text{CeCo}_4\text{B}_4$ -type) and small amounts of  $\text{RhB}$  ( $\text{NiAs}$ -type).

Majkrzak et al. (1982), from a neutron diffraction study of  $\text{NdRh}_4\text{B}_4$  with the  $\text{CeCo}_4\text{B}_4$ -type, were able to observe two antiferromagnetic transitions at  $T_{\text{N1}} = 1.5$  K and  $T_{\text{N2}} = 1.0$  K. In both cases the Nd-moments appeared to be aligned along the  $c$ -axis with a sinusoidal modulation along [100] in the higher temperature modification and along [110] in the lower one.

### References

- Felner, I. and I. Nowik, 1980, *Phys. Rev.* **45**(26), 2128.  
Majkrzak, C.F., D.E. Cox, G. Shirane, H.A. Mook, H.C. Hamaker, H.B. MacKay, Z. Fisk and M.B. Maple, 1982, *Phys. Rev. B* **26**(1), 245.  
Vlasse, M., T. Ohtani, B. Chevalier and J. Etourneau, 1983, *J. Solid State Chem.* **46**, 188.

### Sc-Fe-B

Phase equilibria in two partial isothermal sections of the system Sc-Fe-B were derived by Stepanchikova and Kuz'ma (1981) by means of X-ray diffraction and metallographic analysis of 46 samples which were arc melted and subsequently annealed in evacuated silica tubes for 4300 h at  $700^\circ\text{C}$  (region 0–50 a/o B) and at  $1000^\circ\text{C}$  (region 50–100 a/o B), respectively (fig. 82). Starting materials were Sc ingots of 99.75% purity and powders of Fe (99.99%) and B (99.4%). For a discussion of the Fe-B and Sc-B binary boundary systems, see Y-Fe-B and Sc-Co-B, respectively. In accordance with literature data two intermetallic Sc-Fe compounds were observed:  $\text{Sc}_7\text{Fe}$  and the laves type  $\text{ScFe}_2$ .

The mutual solubility of the binary compounds were observed to be very small (see details given). There is, however, a considerable solubility of both Sc and Fe in  $\beta$ -rh B of the order of 1–2 a/o.

The ternary phase equilibria are dominated by the existence of one ternary compound  $\text{ScFeB}_4$ , whose crystal structure has not yet been evaluated.

### Reference

- Stepanchikova, G.F. and Yu.B. Kuz'ma, 1981, *Vestn., Lvov Univ., Ser. Khim.* **23**, 48.

### Sc-Ni-B

Stepanchikova and Kuz'ma (1981) derived the phase equilibria in an isothermal section of the Sc-Ni-B system by means of X-ray powder diffraction and metallographic analysis of 155 alloys. The specimens were prepared by arc melting

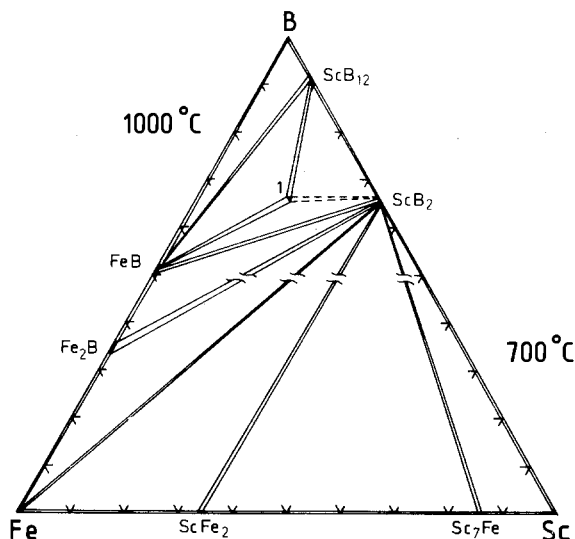


Fig. 82. Sc-Fe-B, partial isothermal sections at 1000°C (50–100 a/o B) and at 700°C (0–50 a/o B). 1: ScFeB<sub>4</sub>.

compacts of Sc ingots (99.75%) and Ni (99.96%) and B (99.4%) powders and subsequent heat treatment at 800°C for 720 h (in evacuated silica tubes).

The ternary Sc-Ni phases observed are in accordance with literature data: ScNi<sub>5</sub> (CaCu<sub>5</sub>-type), Sc<sub>2</sub>Ni<sub>7</sub> (Ce<sub>2</sub>Ni<sub>7</sub>-type), ScNi<sub>2</sub> (MgCu<sub>2</sub>-type), ScNi (CsCl-type) and Sc<sub>2</sub>Ni (Ti<sub>2</sub>Ni-type). For a discussion of nickel and scandium borides, see Y-Ni-B and Sc-Co-B, respectively.

The mutual solid solubility of the binary compounds was found to be very small (no details given). It is noteworthy, however, that  $\beta$ -rh boron shows a remarkable solubility for both Ni and Sc ( $\approx 1$ –2 a/o).

Ternary phase equilibria in fig. 83 reveal the existence of five ternary compounds, confirming the earlier data concerning the Cr<sub>23</sub>C<sub>6</sub>-type compound Sc<sub>3.4</sub>Ni<sub>20-19</sub>B<sub>6</sub> (see also Sc-Ni-B). ScNi<sub>3</sub>B was observed to crystallize with the ordered and filled-up Cu<sub>3</sub>Au-type,  $a = 3.776(5)$ , revealing the Sc atoms in the 1a-site of Pm3m.

The crystal structures of the remaining phases with approximate formulas ScNiB<sub>4</sub>, Sc<sub>4</sub>Ni<sub>15</sub>B<sub>6</sub> and ScNi<sub>4</sub>B<sub>4</sub> have not yet been solved, but X-ray data suggest a tetragonal symmetry for the latter according to  $a = 7.75$  and  $c = 15.57$ . Despite a preliminary space group I4<sub>1</sub>/amd was assigned, a LuRu<sub>4</sub>B<sub>4</sub>-type (however, with actual symmetry I4<sub>1</sub>/acd) is likely to be related considering the unit cell dimensions.

#### Reference

Stepanchikova, G.F. and Yu.B. Kuz'ma, 1981, Vestn. Lvov Univ., Ser. Khim. 23, 48.

#### Sm-M-B (M = Ba, Ca, Dy, Eu, Gd, La, Nd, Pr, Yb)

The valency of Sm in hexaboride solutions Sm<sub>1-x</sub>M<sub>x</sub>B<sub>6</sub> has been studied by Aivazov et al. (1982) for the metals M = Ce, Eu, Gd, La, Nd and Pr and by



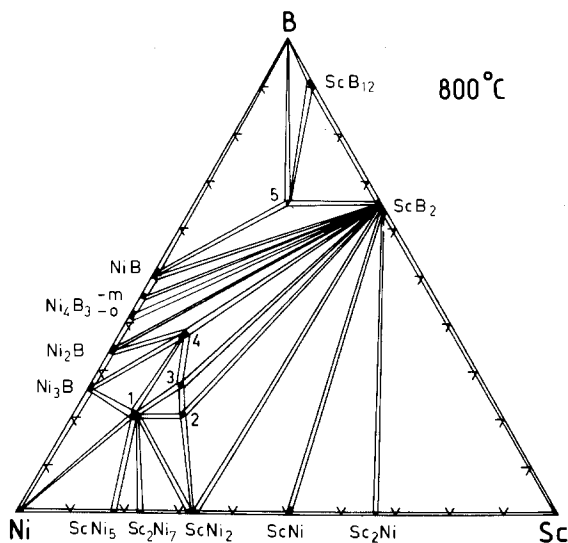


Fig. 83. Sc-Ni-B, isothermal section at 800°C. 1:  $\text{Sc}_3\text{Ni}_{20}\text{B}_6$ , 2:  $\text{ScNi}_3\text{B}$ , 3:  $\text{Sc}_4\text{Ni}_{15}\text{B}_6$ , 4:  $\text{ScNi}_4\text{B}_4$ , 5:  $\text{ScNiB}_4$ .

Konovalova et al. (1982) for  $M = \text{Ba}, \text{Ca}, \text{Dy}, \text{Eu}, \text{Gd}, \text{La}$  and  $\text{Yb}$ , by means of X-ray diffraction analysis and  $L_{\text{III}}$  atomic spectroscopy. Except for the case of  $M = \text{Ba}$  a complete solid solution with the  $\text{CaB}_6$ -type was observed from the vacuum sintered alloys, exhibiting a positive deviation from Vegard's rule for  $M = \text{Gd}, \text{La}, \text{Nd}, \text{Pr}$ , but a negative one for  $M = \text{Ca}, \text{Eu}$  and the limited solid solution (due to vacuum sintering) with  $M = \text{Ba}$ . In accordance with the data reported by Tarascon et al. (1980) for  $M = \text{Yb}, \text{Sr}, \text{La}, \text{Y}, \text{Th}$  substitution of  $\text{Sm}$  by  $\text{Ba}, \text{Eu}, \text{Yb}, \text{Ca}$  is found to raise the effective valence of  $\text{Sm}$ , whereas substitution of  $\text{Sm}$  by one of the trivalent rare earths  $\text{Dy}, \text{Gd}$  and  $\text{La}$  tends to lower it.

With respect to the two basically isostructural forms called  $\alpha$ - and  $\beta$ - $\text{SmB}_6$  by Aivazov et al. (1982) (which probably correspond to  $\text{SmB}_6$  and  $\text{SmB}_{6+x}$  as quoted by Storms) a positive deviation from Vegard's rule was observed on substitution of  $\text{Sm}$  by  $\text{Nd}$  for solid solutions  $(\text{Sm}_{1-x}\text{Nd}_x)_y\text{B}_6$ .

### References

- Aivazov, M.I., S.V. Aleksandrovich, B.A. Evseev, V.S. Mkrtschian, V.N. Sorokin and O.M. Tsarev, 1982, *Fiz. Tverd. Tela* **24**(9), 2667; *Izv. Akad. Nauk SSSR, Neorg. Mater.* **18**(9), 1518.  
 Konovalova, E.S., Yu.B. Paderno, T. Lundström, L.D. Finkelshtein, N.N. Efremova and E.M. Dudnik, 1982, *Poroshk. Metall.* **238**(10), 78.  
 Tarascon, J.M., Y. Ishikawa, B. Chevalier, J. Etourneau and P. Hagenmuller, 1980, *J. Physique (Paris)* **41**, 1135.

### Sm-Re-B

Phase equilibria in an isothermal section of the  $\text{Sm-Re-B}$  system, fig. 84, have been evaluated by Mikhalenko et al. (1982) by means of X-ray diffraction and metal-

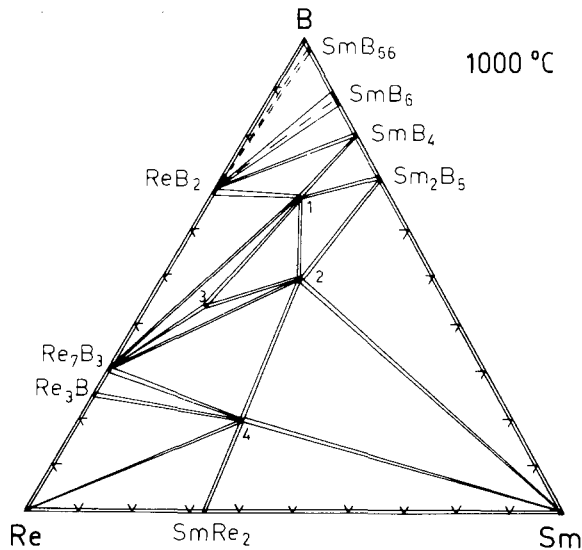


Fig. 84. Sm-Re-B, isothermal section at 1000°C. 1:  $\text{SmReB}_4$ , 2:  $\text{SmReB}_2$ , 3:  $\text{SmRe}_4\text{B}_4$ , 4:  $\text{Sm}_3\text{Re}_5\text{B}_2$ .

lographic analysis of 120 alloys prepared by arc melting and subsequent annealing in evacuated silica tubes at 1000°C for 1200 h. Etching was possible in concentrated nitric acid and microhardness was tested at a load of 100–200 g. Starting materials were Sm ingots of 99.7% purity and Re (99.7%) and B (99.7%) powders.

As far as the binary systems are concerned agreement exists with what is known in the literature;  $\text{SmRe}_2$  is a  $\text{MgZn}_2$ -type compound; for a discussion of the Re-B and Sm-B systems, see Dy-Re-B and Sm-Co-B. Mutual solubilities of the binary compounds were observed to be small.

Four ternary compounds are involved in the phase equilibria; the crystal structures of some of them,  $\text{SmReB}_2$ ,  $\text{Sm}_3\text{Re}_5\text{B}_2$  and  $\text{SmRe}_4\text{B}_4$ , have not yet been solved, but preliminary data suggest  $\text{SmRe}_4\text{B}_4$  to be isostructural with the structure type of  $\text{CeRe}_4\text{B}_4$  [ $a = 7.466(7)$ ,  $c = 10.59(1)$ ].  $\text{SmReB}_4$ , as defined from X-ray powder diffraction data, is  $\text{YCrB}_4$ -type,  $\text{P6mm}$ ,  $a = 6.014(2)$ ,  $b = 11.631(4)$  and  $c = 3.629(1)$ . Using the atomic parameters as derived for  $\text{YMoB}_4$  the agreement was poor ( $R = 0.174$ ) and suggests further refinement.

#### Reference

Mikhaleenko, C.I., Yu.B. Kuz'ma and O.K. Tschyr, 1982, *Poroshk. Metall.* (9), 50.

#### Tb-Ni-B

The crystal structure of  $\text{Tb}_3\text{Ni}_{13}\text{B}_2$  has been determined by Kuz'ma et al. (1983) to be of the  $\text{Nd}_3\text{Ni}_{13}\text{B}_2$ -type ( $\text{P6}/\text{mmm}$ ). The lattice parameters as derived from powder X-ray data were given as  $a = 4.954(2)$ ,  $c = 10.893(5)$ .

*Reference*

Kuz'ma, Yu.B., N.S. Bilonishko, N.F. Chaban and G.V. Chernjak, 1983, *J. Less-Common Metals* **90**, 219.

*Tm-Fe-B*

According to recent X-ray powder diffraction data of arc melted alloys heat treated for 270 h at 800°C in evacuated silica tubes, TmFe<sub>4</sub>B was found to adopt the CeCo<sub>4</sub>B-type of structure with space group P6/mmm and unit cell dimensions as follows:  $a = 4.973(2)$ ,  $c = 6.970(8)$  (Chernjak, 1983).

*Reference*

Chernjak, G.F., 1983, *Izv. Akad. Nauk SSSR, Neorg. Mater.* **19**(3), 485.

*Tm-Ni-B*

Tm<sub>3</sub>Ni<sub>13</sub>B<sub>2</sub> was recently reported to adopt the Nd<sub>3</sub>Ni<sub>13</sub>B<sub>2</sub>-type of structure with space group P6/mmm and unit cell dimensions as follows:  $a = 4.925(1)$ ,  $c = 10.86(1)$  (Kuz'ma et al., 1983).

*Reference*

Kuz'ma, Yu.B., N.S. Bilonishko, N.F. Chaban and G.V. Chernjak, 1983, *J. Less-Common Metals* **90**, 219.

*Tm-Rh-B*

Recent neutron diffraction data of TmRh<sub>4</sub>B<sub>4</sub> obtained by Majkrzak et al. (1983) revealed antiferromagnetic ordering at  $T_N = 0.7$  K (in zero applied magnetic field) with the Tm<sup>3+</sup> moments aligned along [010] and with a sinusoidal modulation along [101]. Furthermore, from preliminary neutron diffraction data in an applied field it was reported that a ferromagnetic component can be introduced at field strengths for which the electrical resistivity is still zero.

*Reference*

Majkrzak, C.F., S.K. Satija, G. Shirane, H.C. Hamaker, Z. Fisk and M.B. Maple, 1983, *Phys. Rev. B* **27**(5), 2889.

*Tm-Yb-B*

Kasaya et al. (1983) investigated the mixed valency behaviour of Tm in the concentrational section Yb<sub>1-x</sub>Tm<sub>x</sub>B<sub>6</sub> by means of susceptibility measurements and L<sub>III</sub> absorption spectroscopy. Due to the thermodynamic instability of TmB<sub>6</sub> a rather limited solid solubility is observed for  $0 < x < 0.5$ . Lattice parameters show a negative deviation from Vegard's rule. Samples were prepared by borothermal reduction of the mixed oxides in vacuum and exact values of  $x$  were derived from X-ray fluorescence analysis.

*Reference*

Kasaya, M., F. Iga, H. Yashima, T. Satoh, M. Ohashi, S. Nakai and T. Kasuya, 1983, *J. Magn. Magn. Mater.* **31–34**, 389.

*Yb–Co–B*

Some information about phase equilibria in the Yb–Co–B system at 800°C were given by Chaban (1981), who when preparing the compound  $\text{YbCo}_4\text{B}_4$  found it in equilibrium with  $\text{Co}_2\text{B}$ ,  $\text{CoB}$  and  $\text{YCo}_3\text{B}_2$ . Samples were prepared by arc melting compacts of Yb ingot (99.2%) and Co (99.9%) and B (99.3%) powders and subsequent heat treatment in evacuated silica tubes for 400 h at 800°C.  $\text{YbCo}_4\text{B}_4$  crystallizes with the  $\text{CeCo}_4\text{B}_4$ -type,  $\text{P4}_2/\text{nmc}$ ,  $a = 4.989(3)$ ,  $c = 6.979(5)$ .

*Reference*

Chaban, N.F., 1981, *Vestn. Lvov Univ., Ser. Khim.* **23**, 44.

**Quaternary systems**

Since the manuscript of this chapter was written quite a number of papers have been published dealing with the physical properties of ternary and quaternary boride systems containing rare earth elements and platinum metals. It was the original intention of this manuscript to only cover the structural properties and the phase equilibria in ternary and higher order boride systems. However, for a detailed discussion of the interesting and unusual, puzzling low temperature behavior of these alloys the reader is referred to the excellent review articles by Maple et al. (1982), Fischer and Maple (1982) and more recently by Maple (1983a, b, c).

For some of the  $\text{RRh}_4\text{B}_4$  compounds the type of magnetic ordering at low temperatures has been established by means of recent neutron diffraction studies ( $\text{NdRh}_4\text{B}_4$ ,  $\text{ErRh}_4\text{B}_4$ ,  $\text{TmRh}_4\text{B}_4$ ) and according to the new features derived a series of the earlier known low temperature phase diagrams of higher order have to be reinvestigated (especially those containing erbium- or thulium-rhodium borides): i.e. a strong interaction of the  $\text{Er}^{3+}$  and  $\text{Tm}^{3+}$  moments is expected for the  $(\text{Tm}_x\text{Er}_{1-x})\text{Rh}_4\text{B}_4$  system (see Lambert et al. 1983).

Similarly the  $(\text{Er}_{1-x}\text{Ho}_x)\text{Rh}_4\text{B}_4$  system has been reexamined. By means of low temperature neutron diffraction measurements Mook et al. (1982) observed a region of mixed magnetic phases separating the phase fields where the  $\text{Er}^{3+}$  and  $\text{Ho}^{3+}$  magnetic moments independently order ferromagnetically (fig. 85). According to the complicated ordering behavior of  $\text{ErRh}_4\text{B}_4$  a region was observed in which the sinusoidally modulated phase coexists with the ferromagnetic domains (shaded area, see also  $\text{ErRh}_4\text{B}_4$ ).

A careful further investigation of the  $\text{Ho}(\text{Rh}_{1-x}\text{Ir}_x)_4\text{B}_4$  system by means of low temperature specific heat, ac magnetic susceptibility and electrical resistance measurements interestingly revealed the existence of two distinct magnetic ordering transitions for those compositions where  $0.2 < x < 0.5$  (Yang et al., 1982). Specific heat and neutron diffraction data confirm antiferromagnetic ordering for  $x > 0.5$ ,

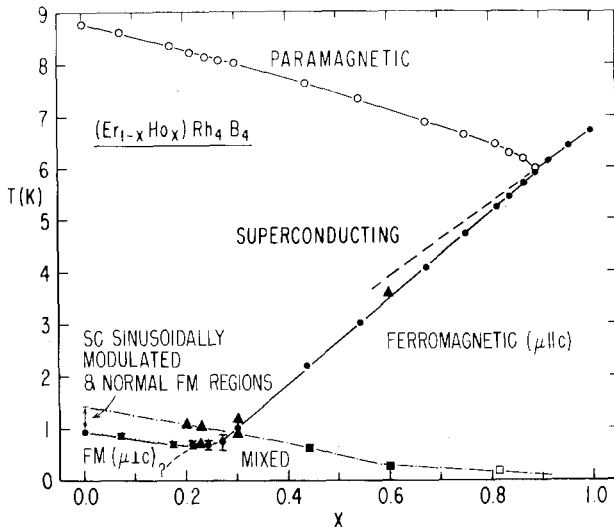


Fig. 85. Low temperature phase diagram for the system  $(Er_{1-x}Ho_x)Rh_4B_4$ , after Mook et al. (1982).

and for the alloy  $Ho(Rh_{0.3}Ir_{0.7})_4B_4$  the magnetic structure (below  $T_N = 2.7$  K) has been derived to be a body-centered tetragonal superstructure of the normal  $CeCo_4B_4$ -type cell according to  $a = \sqrt{2}a_0$  and  $c = 2c_0$ . The structure is described as an alternating stacking of antiferromagnetic planes, and with  $\mu = 9.6\mu_B$  at  $T = 1.5$  K was refined

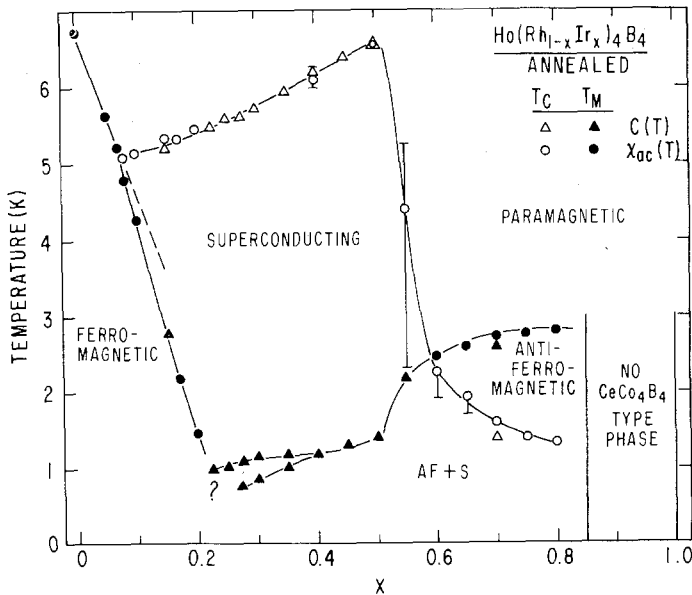


Fig. 86. Low temperature phase diagram for the system  $Ho(Rh_{1-x}Ir_x)_4B_4$ , after Yang et al. (1982).

to  $R = 0.10$ . Furthermore the antiferromagnetic to superconducting transition at  $T_c = 1.35$  K was found to be of second order. Alloys  $0.07 < x < 0.2$  exhibit reentrant superconductivity due to mean field ferromagnetic ordering (fig. 86).

### References

- Fischer, Ø. and M.B. Maple, 1982, Superconducting ternary compounds: prospects and perspectives, in: Superconductivity in Ternary Compounds I, Topics of Current Physics, Vol. 32, eds. Ø. Fischer, and M.B. Maple (Springer, Berlin) pp. 1–24.
- Lambert, S.E., L.D. Woolf and M.B. Maple, 1983, J. Low Temp. Phys., to be published.
- Maple, M.B., 1983a, Coexistence of superconductivity and magnetism, in: Proc. Intern. School of Low Temperature Physics, 3rd Course, Advances in Superconductivity, July 3–14, 1982, Erice, Italy, eds. B. Deaver and J. Ruvald.
- Maple, M.B., 1983b, J. Magn. Magn. Mater. **31–34**, 479.
- Maple, M.B., 1983c, Superconductivity and magnetic order: low-temperature phase diagrams, in: Proc. Mater. Res. Soc. 1982, Annual Meeting 1982.
- Maple, M.B., H.C. Hamaker and L.D. Woolf, 1982, Superconductivity, magnetism and their mutual interaction in ternary rare earth rhodium borides and some ternary rare earth transition metal stannides, in: Superconductivity in Ternary Compounds II, Topics in Current Physics, Vol. 34 (Springer, Berlin) pp. 99–141.
- Mook, H.A., O.A. Pringle, S. Kawarazaki, S.K. Sinha, G.W. Crabtree, D.H. Hinks, M.B. Maple, Z. Fisk, D.C. Johnston, L.D. Woolf and H.C. Hamaker, 1982, Proc. IVth Conf. on Superconductivity in d- and f-Band Metals, Karlsruhe, June 28–30, 1982, p. 201.
- Yang, K.N., S.E. Lambert, H.C. Hamaker, M.B. Maple, H.A. Mook and H.C. Ku, 1982, Proc. IVth Conf. on Superconductivity in d- and f-Band Metals, Karlsruhe, June 28–30, p. 217.

### *Er–Co–Rh–B*

Isino et al. (1983) investigated magnetic and superconductivity properties in the concentrational section  $\text{ErCo}_x\text{Rh}_{4-x}\text{B}_4$ . Samples were arc melted and heat treated for ten days at  $1050^\circ\text{C}$ . Rh-rich compositions  $0 \leq x \leq 1.2$  were found to be of  $\text{LuRu}_4\text{B}_4$ -type; alloys in the range  $1.6 \leq x \leq 2.0$  were claimed to be of a new tetragonal ferromagnetic phase, whereas for compositions  $2.8 \leq x \leq 4$  the  $\text{CeCo}_4\text{B}_4$ -type was obtained.

### Reference

- Isino, M., K. Tsunokuni, H. Iwasaki and Y. Muto, 1983, J. Magn. Magn. Mater. **31–34**, 519.

### Acknowledgements

The generous financial support of the Austrian Bundesministerium für Wissenschaft und Forschung (Dr. H. Schläger) for the computerized literature search is gratefully acknowledged.

The author desires to thank all those who have kindly authorized the reproduction of diagrams and tables, in particular the following: Academic Press, Izv. Akad. Nauk, North-Holland Publ. Comp., Elsevier Sequoia, S.A., Pergamon Press Ltd., Plenum Publ. Corp. and Dr. Riederer Verlag GmbH.

Furthermore the author wants to express his gratitude to Prof. M.B. Maple of the Institute for Pure and Applied Physical Sciences at the University of California, La Jolla, and to Prof. E. Parthé of the Laboratoire de Cristallographie aux Rayons X, Université de Genève, for kindly making available to him a series of forthcoming papers.

Last but not least I wish to express my special gratitude to Mrs. E. Berlakovich and Ch. Fisman for their patience in the tedious business of typing the different versions of the manuscript. I am also most grateful to Mr. M. Gitschthaler of the Drafting Office for his effective activity in doing all the draft work and photography.

## Chapter 50

### PREPARATION OF DIVALENT YTTERBIUM AND SAMARIUM DERIVATIVES AND THEIR USE IN ORGANIC CHEMISTRY

H.B. KAGAN and J.L. NAMY

*Laboratoire de Synthèse Asymétrique, associé au CNRS (LA no. 255),  
Université Paris-Sud, 91405 Orsay, France*

---

Contents	
1. Introduction	526
2. Preparation of divalent ytterbium and samarium compounds	526
2.1. Introduction	526
2.2. A classification of the main preparative methods	527
2.3. Details on preparative methods	528
3. Some physical properties	536
3.1. Thermochemical and redox properties; UV-visible absorption spectroscopy	536
3.2. Magnetism, conductivity	537
3.3. Solvation, solubility and volatility	542
3.4. Structure and bonding	543
4. Chemical properties	548
4.1. Reaction with oxygen, water and halogens	548
4.2. Electron transfer to some inorganic complexes	549
4.3. Use of $\text{SmI}_2$ and $\text{YbI}_2$ in organic chemistry	550
4.4. Reactions of divalent organo-lanthanides with organic or inorganic compounds	560
4.5. Some catalytic reactions induced by divalent Yb and Sm species	563
4.6. Reactions of ytterbium in liquid ammonia	563
5. Conclusion	563
6. Recent developments	564
References	564

---

#### Abbreviations

Ac	Acetyl	$\text{Et}_2\text{O}$	Diethyl ether
bipy	1,1'-bipyridine	HMPA	Hexamethylphosphotriamide
COT	Cyclooctatetraene	Me	Methyl
Cp	Cyclopentadienyl	o-Phen	ortho-phenanthroline
DME	Dimethoxyethane	r.t.	room temperature
dmpe	$(\text{CH}_3)_2\text{PCH}_2\text{CH}_2\text{P}(\text{CH}_3)_2$	THF	Tetrahydrofuran
Et	Ethyl	tmeda	$(\text{CH}_3)_2\text{NCH}_2\text{CH}_2\text{N}(\text{CH}_3)_2$
		tol	Toluene

---



## 1. Introduction

The divopositive oxidation state is unusual among the lanthanides. The more easily available divalent species are europium, ytterbium and samarium, although other divalent lanthanide compounds are known. Several reviews dealing, at least partly, with divalent lanthanides can be found in the literature. The most recent and detailed paper is that of Johnson (1977), which includes preparations and physical properties. Two other reviews are also available (Asprey et al., 1960; Marks, 1978). Thermochemical properties have been reviewed by Morss (1976).

Derivatives of divalent lanthanide compounds are gaining interest amongst scientists for two reasons:

(i) Materials with unusual physical properties such as laser effects, magnetism or electrical conductivity are to be expected.

(ii) The reducing character of divalent lanthanides should be helpful, especially in organic chemistry, for devising new reagents or catalysts.

The availability of pure lanthanides for a moderate price (because of the progress in processing) enhances the interest of chemists for this family of chemicals.

The divalent oxidation state is quite accessible in the case of samarium ( $4f^6$ ) and ytterbium ( $4f^{14}$ ), which are nevertheless characterized by strongly negative redox potentials. In this account we will survey the preparation and chemical properties of molecular divalent samarium and ytterbium compounds. We will consider briefly some of their physical properties. We will restrict this survey to species that have organic surroundings: organometallics, organic salts or inorganic salts in an organic medium. The chemical properties of these compounds will be discussed in detail. The main results are relevant to organic chemistry.

It may be pointed out that divalent europium ( $4f^7$ ) compounds are readily accessible but their derivatives appear to be poor reductants, although in a recent paper the reduction of pyruvic acid with  $\text{Eu}^{2+}$  ions was described (Konstantatos et al., 1982). Other molecular divalent lanthanide compounds are very difficult to obtain. A recent paper was devoted to the reduction of some organic compounds by low-valent cerium compounds (Imamoto et al., 1982), but the nature of the species involved has not yet been established.

We hope that this review will be useful to those who want to study new materials or chemical reagents.

## 2. Preparation of divalent ytterbium and samarium compounds

### 2.1. Introduction

Lanthanides form a unique family of elements. They possess a partially filled 4f electronic subshell and a xenon core. The divalent state is easily attained with europium ( $\text{Eu}^{2+}$ :  $4f^7$ ), samarium ( $\text{Sm}^{2+}$ :  $4f^6$ ) and ytterbium ( $\text{Yb}^{2+}$ :  $4f^{14}$ ), where

half-filled, nearly half-filled or filled 4f subshells are obtained. This fact was recognized long ago and was the basis of one process for the separation of these three elements from the other rare earths, the reducing agent usually being sodium amalgam (Marsh, 1942, 1943, 1946). Divalent europium is quite stable; for example, it can remain in water for quite a long time in contrast to  $\text{Sm}^{2+}$  and  $\text{Yb}^{2+}$  which reduce water.  $\text{Tm}^{2+}$  ( $4f^{13}$ ) and  $\text{Dy}^{2+}$  ( $4f^{10}$ ) are even less stable than divalent samarium and ytterbium. The methods of preparation of  $\text{Sm}^{2+}$  and  $\text{Yb}^{2+}$  compounds have varied widely. The first divalent samarium derivatives,  $\text{SmCl}_2$  and  $\text{SmI}_2$ , were prepared by Matignon et al. (1906a,b) who reduced the trihalides with hydrogen or ammonia at high temperature. The divalent state of ytterbium was obtained for the first time by Klemm et al. (1929); these authors isolated  $\text{YbCl}_2$ .

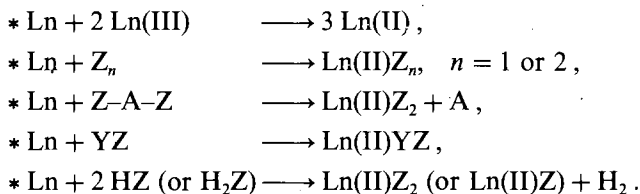
Since these early times many new preparations of  $\text{Yb}^{2+}$  and  $\text{Sm}^{2+}$  derivatives have been devised. The main techniques involve the reduction of a trivalent salt by any of several kinds of reagents including the lanthanide metal. Another class of syntheses involves metathesis which allows the transformation of one divalent compound into another. Some methods require quite vigorous conditions but gentle techniques are also available. The reaction conditions are important to define because some divalent derivatives are stable only for a given set of experimental conditions.

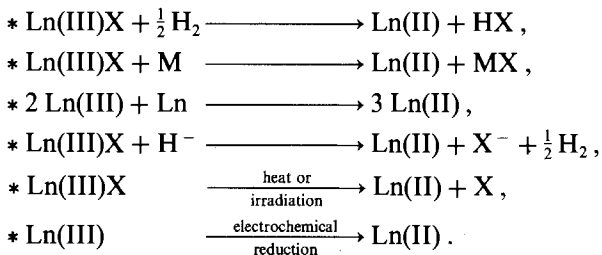
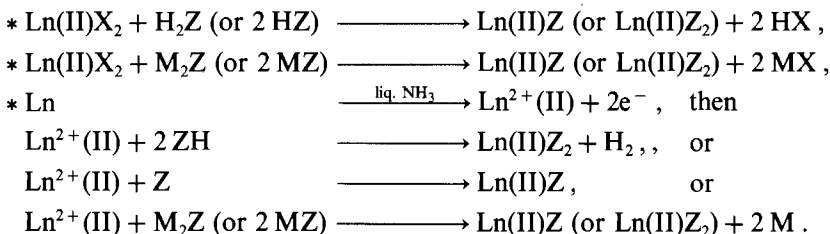
## 2.2. A classification of the main preparative methods

The preparation of inorganic compounds has been reviewed recently by Johnson (1977). Since this review was published, synthesis of  $\text{SmO}$ ,  $\text{YbO}$  (Leger et al., 1981) and of  $\text{LnFX}$  (Beck, 1978) ( $\text{Ln} = \text{Sm}, \text{Yb}$ ;  $\text{X} = \text{Cl}, \text{Br}, \text{I}$ ) has been described.

An examination of the preparation of all the molecular divalent samarium and ytterbium compounds leads to the schematic classification given below, where A, X, Y, Z are atoms or groups of atoms, M is a metal or the cation of a metal, H is hydrogen and Ln stands for Yb or Sm. The preparation of "organic" divalent compounds is detailed in the text and in tables 1–3 of section 2.3. The following classification takes into account the fact that divalent lanthanide compounds can be derived either from the corresponding metal, from the corresponding trivalent lanthanide precursor or from another divalent lanthanide compound. Reaction types marked with an asterisk are described more fully below.

### *Preparations starting from the lanthanide metal*



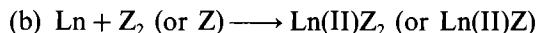
*Preparations starting from trivalent lanthanide compounds**Preparations starting from divalent lanthanide compounds**2.3. Details on preparative methods**2.3.1. Preparations starting from the lanthanide metal*

This method has been used widely to prepare inorganic salts (halides, oxides, sulfides, . . .). Only a few of the compounds falling within the scope of this article were obtained in this way.

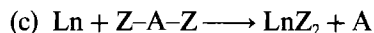
An organometallic compound synthesized utilizing this scheme is dicyclopentadienyl ytterbium ( $\text{YbCp}_2$ ), which is made by the reduction of dicyclopentadienyl ytterbium chloride ( $\text{YbCp}_2\text{Cl}$ ) with ytterbium in tetrahydrofuran (Calderazzo et al., 1966). Unfortunately, experimental details were not reported.

Watson et al. (1981) pointed out the possibility of the reduction of ytterbium triiodide in ytterbium diiodide with ytterbium in tetrahydrofuran at room temperature.

A similar reaction involving samarium ( $\text{Sm} + 2 \text{SmI}_3 \rightarrow 3 \text{SmI}_2$ ) has been observed by Namy et al. (1982).



To our knowledge no "organic" compounds have been prepared in this way.

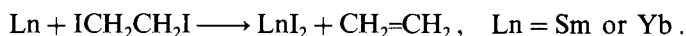


The difference between the redox potentials of the lanthanides and mercury suggests the route  $\text{Ln} + \text{HgZ}_2 \rightarrow \text{LnZ}_2 + \text{Hg}$  as a method of preparing divalent Yb or Sm compounds.

Success was limited in the case of  $\text{Ln(CN)}_2$  (McColm et al., 1972). Divalent polyfluorophenyl ytterbium and samarium compounds were synthesized by the

reaction between the corresponding lanthanide metal and mercury compounds in tetrahydrofuran, but the products were of low thermal stability. Ytterbium metal failed to react with diphenyl mercury (Deacon et al., 1976, 1977, 1979). Reaction of bis(phenylethynyl) mercury with ytterbium metal yields bis(phenylethynyl) ytterbium (Deacon et al., 1978).

Formally analogous to the preceding cases, the preparation of  $\text{YbI}_2$  and  $\text{SmI}_2$  in tetrahydrofuran was performed by reaction between the metal and 1,2-diiodoethane or diiodomethane at room temperature. Reaction conditions are very mild and yields of the diiodides are quantitative (Namy et al., 1977, 1981). The reaction with 1,2-diiodoethane can be written as follows:



$\text{YbBr}_2$  was prepared in a similar way from Yb metal and 1,2-dibromoethane but yields are only 60–80% (Watson, 1980).

(d)  $\text{Ln} + \text{YZ} \longrightarrow \text{Ln(II)YZ}$

Ytterbium readily reacts with alkyl and aryl iodides (RI) in tetrahydrofuran. The solutions contain predominantly  $\text{Yb(II)RI}$  species. Samarium reacts less readily and the percentage of the bivalent state is considerably lower (D.F. Evans et al., 1971). Reaction of ytterbium metal with ether solution of pentamethylcyclopentadienyl iodide ( $\text{C}_5\text{Me}_5\text{I}$ ) and LiI, affords sequentially complexes of stoichiometry  $\text{Li}[\text{Yb}(\text{C}_5\text{Me}_5)_3(\text{OEt}_2)_2]$  and  $\text{Li}[\text{Yb}(\text{C}_5\text{Me}_5)_2\text{I}_2(\text{OEt}_2)_2]$ . Presumably the first step generates a Yb(II) species such as  $\text{Yb(II)(C}_5\text{Me}_5\text{)I}$  (Watson et al., 1980, 1981). These reactions are similar to preparations of Grignard reagents.

(e)  $\text{Ln} + 2 \text{HZ (or H}_2\text{Z)} \longrightarrow \text{Ln(II)Z}_2 \text{ (or Ln(II)Z)} + \text{H}_2$  (see table 1).

A metal vapor technique provides a very interesting route to the preparation of  $\text{Sm(II)}$  or  $\text{Yb(II)}$  organometallic species. Thus W.J. Evans et al. (1980, 1981a, 1982) were able to prepare several substituted dicyclopentadienyl samarium and ytterbium complexes.  $\text{Sm}(\text{C}_5\text{Me}_5)_2$  was the first known soluble divalent organosamarium complex.

The same authors also investigated co-condensation of the Yb metal vapor with 1-hexyne. Organolanthanide products were made in which ytterbium is present predominantly as  $\text{Yb}^{2+}$  (85–92%). These complexes are highly associated in solution. Oligomerisation may occur via alkynide bridge (W.J. Evans et al., 1981b).

### 2.3.2. Preparations starting from trivalent lanthanide compounds

(a)  $\text{Ln(III)X} + \frac{1}{2} \text{H}_2 \longrightarrow \text{Ln(II)} + \text{HX}$

The first divalent lanthanide compounds ( $\text{SmCl}_2$  and  $\text{SmI}_2$ ) were made by the hydrogen reduction of trihalide (Matignon et al., 1906a,b). All the dihalides of Sm and Yb can be prepared by this means although it seems that complete reduction is not achieved in the case of samarium compounds. In the field related to "organic" compounds reduction of  $[\text{Yb}(\text{MeC}_5\text{H}_4)_2\text{Me}]_2$  by hydrogen in  $\text{Yb}(\text{MeC}_5\text{H}_4)_2$  was reported. At 50°C in toluene the reaction is very slow (two weeks) (Zinnen et al., 1980).

TABLE I



References	metal Ln	HZ or H <sub>2</sub> Z	Ln(II)Z <sub>2</sub> or Ln(II)Z	Conditions, remarks
Zinnen et al. (1980)	Yb(C <sub>6</sub> H <sub>10</sub> )	MeC <sub>3</sub> H <sub>5</sub>	Yb(MeC <sub>3</sub> H <sub>4</sub> ) <sub>2</sub>	THF, 25°C, Yb(C <sub>6</sub> H <sub>10</sub> ) obtained from co-condensation of Yb metal vapor with hex-3-yne at -196°C
W.J. Evans et al. (1981)	Sm	Me <sub>3</sub> C <sub>3</sub> H in hexane, then THF	Sm(C <sub>3</sub> Me <sub>3</sub> ) <sub>2</sub> (THF) <sub>2</sub>	-120°C, Sm metal vapor, co-condensation with C <sub>5</sub> (CH <sub>3</sub> ) <sub>3</sub> H, extraction with THF
W.J. Evans (1982)	Sm	Me <sub>4</sub> EtC <sub>3</sub> H in hexane	Sm(C <sub>3</sub> Me <sub>4</sub> Et) <sub>2</sub>	similar conditions as above
W.J. Evans et al. (1981b)	Yb	H-C≡C-C <sub>4</sub> H <sub>9</sub>		-196°C, Yb metal vapor, co-condensation with 1-hexyne

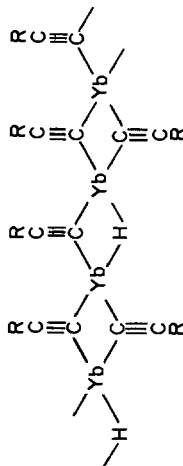


TABLE 2  

$$\text{Ln(III)X} + \text{M} \longrightarrow \text{Ln(II)} + \text{MX}$$

References	Trivalent lanthanide compounds	Metal M	Divalent lanthanide compounds obtained	By-products; conditions and remarks
Rosmanith (1979)	$\text{YbCl}_3$	$\text{Li/naphthalene}$	$\text{YbCl}_2$	$\text{LiCl}$ ; THF, r.t.
Rosmanith (1979)	$\text{SmCl}_3$	$\text{Li/naphthalene}$	$\text{SmCl}_2$	$\text{LiCl}$ ; THF, r.t.
Kamenskaya et al. (1977)	$\text{YbCl}_3$	$\text{Na/HMPA}$	$\text{YbCl}_2$	$\text{NaCl}$ ; half-life for $\text{Yb}^{2+}$ : 31 h, for $\text{Sm}^{2+}$ : 2 h
Kamenskaya et al. (1977)	$\text{SmCl}_3$	$\text{Na/HMPA}$	$\text{SmCl}_2$	as above
Namy et al. (1983)	$\text{SmI}_3$	potassium graphite ( $\text{C}_3\text{K}$ )	$\text{SmI}_2$	$\text{KI}$ ; THF, r.t.
Clifford et al. (1948)	$\text{SmCl}_3$	$\text{Mg/EtOH/HCl}$	$\text{SmCl}_2$	$\text{MgCl}_2$ ; r.t., $\text{SmCl}_2$ not isolated
Calderazzo et al. (1966)	$\text{YbCp}_2\text{Cl}$	$\text{Na}$	$\text{YbCp}_2$	$\text{NaCl}$ ; $\text{Na}$ dispersion, THF, r.t.
Watt et al. (1969)	$\text{SmCp}_3$	potassium naphthalene ( $\text{KC}_{10}\text{H}_8$ )	$\text{SmCp}_2$	$\text{KCp}$ , naphthalene; THF, r.t.
Lappert et al. (1980)	$\text{Yb}[\text{Me}_3\text{SiC}_3\text{H}_4]_2\text{Cl}$	$\text{Na/Hg}$	$\text{Yb}[\text{Me}_3\text{SiC}_3\text{H}_4]_2$	$\text{NaCl}$ ; THF, r.t.
Watson et al. (1981)	$\text{K}[\text{YbCl}_2\text{C}_3\text{Me}_3]_2$	$\text{Na/Hg}$	$\text{Yb}(\text{C}_3\text{Me}_3)_2\text{DME}$ $\text{Yb}(\text{C}_3\text{Me}_3)_2\text{CH}_3\text{CN}$	$\text{NaCl}$ ; $\text{KCl}$ ; $\text{DME}$ or $\text{CH}_3\text{CN}$ , r.t.

(b)  $\text{Ln(III)X} + \text{M} \longrightarrow \text{Ln(II)} + \text{MX}$  (see table 2)

Reduction of Ln(III) salts by Ln metals is considered in section 2.3.1.

Other metals than Sm or Yb are able to reduce Ln(III) species to Ln(II). These are alkali or alkaline earth metals and aluminium. We will also consider, in this paragraph, reduction by alkali arene compounds. This type of reaction is capable of wide range application. Both divalent inorganic and organometallic compounds were prepared by this means. Reduction of  $\text{SmCl}_3$  or  $\text{YbCl}_3$  by Li/naphthalene in tetrahydrofuran provides an interesting route to  $\text{SmCl}_2$  or  $\text{YbCl}_2$  in an organic medium (Rossmann, 1979).  $\text{SmCl}_2$  and  $\text{YbCl}_2$  may be obtained from trivalent salts by Na reduction in hexamethyl phosphotriamide; unfortunately, divalent compounds are reactive towards this solvent (Kamenskaya et al., 1977).  $\text{SmI}_2$  may be synthesized by reduction of  $\text{SmI}_3$  using potassium graphite ( $\text{C}_8\text{K}$ ) in THF at room temperature. The reaction is very fast and yields are quantitative (Namy et al., 1983).

Samarium dichloride has been prepared by reduction of ethanolic solutions of  $\text{SmCl}_3$  with magnesium and hydrochloric acid (aqueous or anhydrous). Nevertheless, isolation of the pure compound from the reaction medium has not been achieved (Clifford et al., 1948).

Some divalent organometallic compounds have been synthesized by reduction of trivalent ones.

Ytterbium dicyclopentadienide was prepared by reducing dicyclopentadienyl ytterbium chloride with finely dispersed sodium metal in tetrahydrofuran (Calderazzo et al., 1966). Samarium(II) dicyclopentadienide was isolated as the 1-tetrahydrofuranate. This compound was prepared by reaction between  $\text{Sm}(\text{C}_5\text{H}_5)_3$  and potassium naphthalene in tetrahydrofuran (Watt et al., 1969). It is insoluble in this solvent and very air-sensitive. Desolvation of the compound at elevated temperature under reduced pressure is accompanied by decomposition.

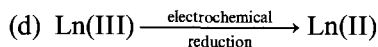
Lappert et al. (1980) have reported preparation of substituted dicyclopentadienide ytterbium. Reduction of  $[\text{Yb}(\text{SiMe}_3\text{C}_5\text{H}_4)_2\text{Cl}]_2$  by Na/Hg in tetrahydrofuran yields the purple toluene soluble  $\text{Yb}(\text{SiMe}_3\text{C}_5\text{H}_4)_2(\text{THF})_2$ , from which  $\text{Yb}(\text{SiMe}_3\text{C}_5\text{H}_4)_2(\text{tmeda})$  and  $\text{Yb}(\text{SiMe}_3\text{C}_5\text{H}_4)_2$  are obtained (Lappert et al., 1980).

The same reducing system (Na/Hg) will transform the potassium salt  $\text{K}[\text{YbCl}_2(\text{C}_5\text{Me}_5)_2]$  into the divalent complexes  $\text{Yb}(\text{C}_5\text{Me}_5)_2\text{DME}$  and  $\text{Yb}(\text{C}_5\text{Me}_5)_2\text{CH}_3\text{CN}_{1,2}$ , using as solvent DME and  $\text{CH}_3\text{CN}$ , respectively (Watson et al., 1981).

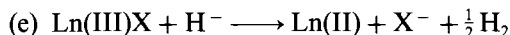
(c)  $\text{Ln(III)X} \xrightarrow[\text{or irradiation}]{\text{thermal dissociation}} \text{Ln(II)} + \text{X}$

The thermal decomposition of trihalides is a good way to prepare divalent ytterbium and samarium halides (especially iodides). For example, Baernighausen (1961) has prepared excellent samples of Sm or Yb dihalide by the thermal decomposition of trihalide hydrates. Only a few preparations involve this type of reaction in the field of divalent organometallic compounds.

Photolysis of  $[\text{Yb}(\text{MeC}_5\text{H}_4)_2\text{Me}]_2$  in toluene yields, after 32 h,  $\text{Yb}(\text{MeC}_5\text{H}_4)_2$  in 25% conversion and methane. It is also possible to perform this conversion thermally using a mixed pentane-ether solvent at  $80^\circ\text{C}$  in a pressure vessel (80% yield after 8 h) (Zinnen et al., 1980).



Electrochemical reduction of some Sm(III) salts in acetonitrile have been reported (Kulyako et al., 1975; Dyke et al., 1972).



This method could be useful to prepare divalent lanthanide compounds but few examples have been reported.

Reduction of  $[\text{Yb}(\text{C}_5\text{Me}_5)_2\text{DME}]\text{PF}_6$  was performed with KH in DME at 20°C. Formation of  $\text{Yb}(\text{C}_5\text{Me}_5)_2\text{DME}$  with rapid hydrogen evolution was observed. A similar reaction occurs when neopentyl lithium was used instead of KH (Watson et al., 1981).

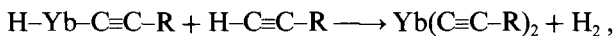
### 2.3.3. Preparations starting from divalent lanthanide compounds



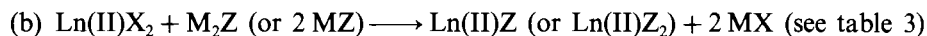
This type of reaction is in wide use in organometallic chemistry. In the specific case of Ln(II) chemistry a possible side reaction is the oxidation in Ln(III) derivatives with an acid compound ( $\text{H}_2\text{Z}$ ,  $\text{HZ}$  or  $\text{HX}$ ).

$\text{Yb}(\text{C}\equiv\text{C}-\text{C}_6\text{H}_5)_2$  was prepared in this manner by reaction between  $\text{Yb}(\text{C}_6\text{F}_5)_2$  and  $2 \text{C}_6\text{H}_5\text{C}\equiv\text{C}-\text{H}$  in THF. This compound has been isolated without supporting ligands and is exceptionally air-sensitive (Deacon, 1978).

In order to explain the experimental results observed in the reaction of 1-hexyne with Yb metal vapor, W.J. Evans (1981b) proposed the following scheme:



in which the  $\text{H}-\text{Yb}-\text{C}\equiv\text{C}-\text{R}$  initially formed reacts with additional acetylenic compound to form a new divalent species.



Metathetical reactions between a divalent lanthanide compound and a metallic derivative (usually  $\text{M}$  = alkaline earth) allow preparation of a great variety of divalent lanthanide compounds.

For the preparation of samarium or europium carbonates, the rare earth(II) sulfate crystals were suspended in water, then concentrated  $(\text{NH}_4)_2\text{CO}_3$  or  $\text{K}_2\text{CO}_3$  solutions were introduced and allowed to contact the sulfate crystal. Some oxidation of the lanthanide occurs simultaneously (Asprey et al., 1964). Clifford et al. (1948) also reported preparation of samarium carbonate by metathesis of the dichloride. The water insoluble and unstable citrate was prepared in the same way (Clifford et al., 1948).

Besides their interesting properties as reducing agents,  $\text{SmI}_2$  and  $\text{YbI}_2$  are useful intermediates to prepare easily a wide variety of other divalent lanthanide derivatives through exchange reactions in THF solution with the appropriate sodium salts. Thus were synthesized  $\text{Sm}(\text{OEt})_2$ ,  $\text{Sm}(\text{OAc})_2$ ,  $\text{SmCp}_2$ ,  $\text{Yb}(\text{OEt})_2$ ,  $\text{Yb}(\text{OAc})_2$ ,  $\text{YbCp}_2$  (Namy et al., 1981).

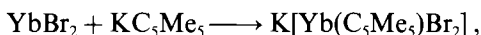
In a similar way Watson (1980) prepared  $\text{Yb}(\text{C}_5\text{Me}_5)_2$ , which was isolated as bis ether adducts from diethyl ether, tetrahydrofuran or dimethoxyethane via the



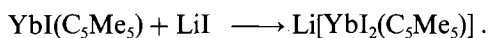
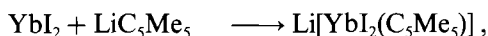
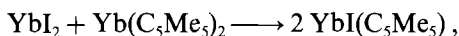
TABLE 3  
 $\text{Ln(II)X}_2 + \text{M}_2\text{Z} \longrightarrow \text{Ln(II)Z} + 2 \text{MX}$   
 $\text{Ln(II)X}_2 + 2 \text{MZ} \longrightarrow \text{Ln(II)Z}_2 + 2 \text{MX}$

References	Divalent lanthanide compounds Ln(II)X <sub>2</sub>	M <sub>2</sub> Z or MZ	Divalent lanthanide compounds obtained	By-products; conditions and remarks
Asprey et al. (1964)	SmSO <sub>4</sub>	K <sub>2</sub> CO <sub>3</sub> or (NH <sub>4</sub> ) <sub>2</sub> CO <sub>3</sub>	SmCO <sub>3</sub>	NaCl; H <sub>2</sub> O, r.t.
Clifford et al. (1948)	SmCl <sub>2</sub>	sodium citrate	samarium (II) citrate	NaCl; H <sub>2</sub> O-EtOH, no further experimental details
Namy et al. (1981)	YbI <sub>2</sub>	NaOC <sub>2</sub> H <sub>5</sub>	Yb(OC <sub>2</sub> H <sub>5</sub> ) <sub>2</sub>	NaI; THF, r.t., NaI separated by heptane precipitations
Namy et al. (1981)	SmI <sub>2</sub>	NaOC <sub>2</sub> H <sub>5</sub>	Sm(OC <sub>2</sub> H <sub>5</sub> ) <sub>2</sub>	as above
Namy et al. (1981)	YbI <sub>2</sub>	NaOAc	Yb(OAc) <sub>2</sub>	NaI; THF, r.t., slow exchange, insoluble product
Namy et al. (1981)	SmI <sub>2</sub>	NaOAc	Sm(OAc) <sub>2</sub>	as above
Namy et al. (1981)	YbI <sub>2</sub>	NaCp	YbCp <sub>2</sub>	NaI; THF, r.t., NaI separated by heptane precipitations
Namy et al. (1981)	SmI <sub>2</sub>	NaCp	SmCp <sub>2</sub>	NaI; THF, r.t., SmCp <sub>2</sub> purple insoluble product very air sensitive
Watson (1980)	YbBr <sub>2</sub>	K(C <sub>3</sub> Me <sub>5</sub> )	Yb(C <sub>3</sub> Me <sub>5</sub> ) <sub>2</sub>	KBr; Et <sub>2</sub> O, DME, r.t.
Tilley et al. (1980)	YbCl <sub>2</sub>	Na(C <sub>3</sub> Me <sub>5</sub> )	Yb(C <sub>3</sub> Me <sub>5</sub> ) <sub>2</sub>	NaCl
Watson et al. (1981)	Yb(C <sub>3</sub> Me <sub>5</sub> ) <sub>2</sub>	LiI	[YbI <sub>2</sub> (C <sub>3</sub> Me <sub>5</sub> ) <sub>2</sub> Li]	Li(C <sub>3</sub> Me <sub>5</sub> )
Watson et al. (1981)	Yb(C <sub>3</sub> Me <sub>5</sub> ) <sub>2</sub>	LiCH <sub>3</sub>	[Yb(CH <sub>3</sub> ) <sub>2</sub> C <sub>3</sub> Me <sub>5</sub> ]Li	Li(C <sub>3</sub> Me <sub>5</sub> )

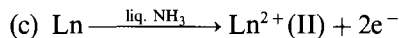
overall reaction sequence depicted by the equations below and driven by precipitation of KBr:



The same organometallic compound was obtained by Tilley et al. (1980). It is readily prepared from sodium pentamethylcyclopentadienide and ytterbium dichloride in refluxing tetrahydrofuran. The diethylether complex  $\text{Yb}(\text{C}_5\text{Me}_5)_2(\text{OEt})_2$  may be isolated by crystallization of the THF complex from diethylether. The hemitoluene complex  $\text{Yb}(\text{C}_5\text{Me}_5)_2(\text{THF})_{\frac{1}{2}} \text{tol}$  can be isolated by recrystallization of the THF complex from toluene. It is possible to generate  $\text{YbIC}_5\text{Me}_5$  and  $\text{Li}[\text{YbI}_2\text{C}_5\text{Me}_5]$  as depicted in the following schemes:



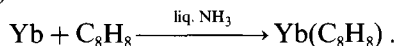
Addition of LiI in ether to a solution of the THF solvate of  $\text{YbIC}_5\text{Me}_5$  in ether resulted in precipitation of  $\text{Li}[\text{YbI}_2\text{C}_5\text{Me}_5]$  (Watson et al., 1981). Watson (1980) has reported that the divalent complex  $\text{Yb}(\text{C}_5\text{Me}_5)_2$  undergoes interesting ring displacement by reactions with LiI or LiMe to produce  $\text{Li}[\text{Yb}(\text{C}_5\text{Me}_5)\text{I}_2]$  and  $\text{Li}[\text{Yb}(\text{C}_5\text{Me}_5)\text{Me}_2]$ , respectively.



Europium and ytterbium metal dissolve in liquid ammonia to give blue solutions containing the ammoniated electron. They are the only lanthanide metals to do so; samarium does not undergo this reaction (Thompson et al., 1966; Warf, 1970).

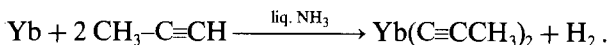
Paramagnetic resonance studies and electronic spectra of solutions of Eu and Yb give evidence that the metals dissolve to give ammoniated divalent cations (Thompson et al., 1966a,b).

On standing, the solutions of Eu and Yb decompose with the formation of a precipitate. The europium precipitate consists of the amide  $\text{Eu}(\text{NH}_2)_2$ , but the ytterbium precipitate is only 20–75% in  $\text{Yb}(\text{NH}_2)_2$  (Hadenfeldt et al., 1970). Solution of ytterbium in liquid ammonia has been used to synthesize organometallic compounds. Addition of cyclooctatetraene to ytterbium dissolved in anhydrous ammonia yields cyclooctatetraenyl ytterbium, which is insoluble in ammonia, hydrocarbons and ethers but dissolves in more basic solvents such as pyridine or DMF (Hayes, 1969):



Ytterbium reacts very rapidly with cyclopentadiene at liquid ammonia temperatures or lower (Calderazzo et al., 1966; Fischer et al., 1965). After evaporation of the ammonia three compounds have been isolated by fractional sublimation of the reaction mixture:  $\text{YbCp}_3$ ,  $n\text{NH}_3$  (deep green);  $\text{YbCp}_2$  (red) perhaps contaminated with  $\text{YbCp}_2\text{H}$ ; and a yellow product which seems to be a mixture of  $\text{Yb}_2\text{Cp}_4\text{N}_2\text{H}_4$

and  $\text{Yb}_2\text{Cp}_3\text{N}_2\text{H}_4$  (Hayes, 1969). A solution of ytterbium in liquid ammonia reacts with propyne to form the methylacetylide (Murphy et al., 1971):



$\text{Yb}(\text{bipy})_4$  and  $\text{Yb}(\text{o-Phen})_4$  can be prepared by the reaction of bipyridine or o-phenanthroline with ytterbium in liquid ammonia. After removal of the ammonia the complex may be dissolved in THF. Magnetic moments correspond to two unpaired electrons, the presence of which suggests that the two 6s electrons of ytterbium metal have been transferred to the ligands (Feistel et al., 1968).  $\text{Yb}(\text{CN})_2$  may also be obtained by reaction of solutions of Yb metal in liquid ammonia with  $\text{NH}_4\text{CN}$ . The initial precipitate formed is a mixture containing a high percentage of dicyanide but also some tricyanide (McColm, 1972).

#### 2.4. Conclusions

Various methods may be considered for the synthesis of divalent ytterbium or samarium compounds. Some of them, such as metathetical reactions, have been widely used but others that until now include only a few examples seem to be very attractive, for example, electrochemical reductions.

### 3. Some physical properties

#### 3.1. Thermochemical and redox properties; UV-visible absorption spectroscopy

3.1.1. *Thermochemical properties of the lanthanide elements and ions* have recently been reviewed by Johnson (1977) and Morss (1976). It is well known that with any particular ligand, the thermodynamic stability of the dipositive oxidation state of the lanthanide varies according to the sequence:  $\text{Eu} > \text{Yb} > \text{Sm}$ . The ease of preparation of divalent compounds is in the same order. For example, co-condensation of Yb metal vapor with 1-hexyne yields a compound in which Yb is present as 85–92%  $\text{Yb}^{2+}$ ; in the case of samarium, trivalent products are obtained (W.J. Evans et al., 1981). Eu and Yb cyclooctatetraenyl have been prepared (Hayes et al., 1969), but the samarium compound is as yet unknown.

In the reaction of Eu and Yb metals with iodobenzene, divalent species are obtained in 99% and 86% yields, respectively. In the case of Sm only 50% of the total samarium is in the bivalent state (D.F. Evans, 1971). It is clear that samarium has the most unstable bivalent state of the three metals. This can be seen from the reduction potentials referred to the standard hydrogen electrode (Morss, 1976; Johnson, 1974):

$$E^0(\text{Eu}^{3+} - \text{Eu}^{2+}) = -0.35 \text{ V},$$

$$E^0(\text{Yb}^{3+} - \text{Yb}^{2+}) = -1.10 \text{ V},$$

$$E^0(\text{Sm}^{3+} - \text{Sm}^{2+}) = -1.50 \text{ V}.$$

Sm(II) is the most reactive of the readily accessible divalent lanthanides and it is interesting that, from comparison of reduction potentials of various salts,  $\text{SmI}_2$  appears as the strongest reducing agent soluble in organic media. Reducing properties of this salt are described in section 4. Two other divalent samarium compounds, soluble in tetrahydrofuran and hence of possible great utility, have recently been prepared by W.J. Evans et al. (1981a, 1982):  $\text{Sm}(\text{C}_5\text{Me}_5)_2$  and  $\text{Sm}(\text{C}_5\text{Me}_4\text{Et})_2$ .

3.1.2. *UV-visible absorption spectroscopy* of  $\text{Ln}^{3+}$  ions has been widely studied. A lot of data are also available in the case of  $\text{Yb}^{2+}$  and  $\text{Sm}^{2+}$  in a host lattice (Dyke et al., 1972; Fong, 1967; Johnson et al., 1969; McClure et al., 1968; Wang et al., 1973). Some studies deal with the absorption spectra of aqueous  $\text{Sm}^{2+}$  and  $\text{Yb}^{2+}$  (Butement, 1948; Farragi et al., 1972; Ganopol'skii et al., 1966; Johnson et al., 1968). Only a few results are available in the case of molecular samarium and ytterbium divalent compounds in an organic medium (see table 4).

The UV-visible absorption spectra of samarium diiodide in THF and of samarium(II) perchlorate in acetonitrile are quite similar. Elaborate discussion of these data may be found in Namy et al. (1981) and Dyke et al. (1972). It appears that for samarium, similar spectra are obtained from the dipositive ions in host lattices.

### 3.2. *Magnetism, conductivity*

Magnetic susceptibility measurements have been used widely for the characterization of oxidation states of the lanthanide elements. Calculation of the molar susceptibilities and effective magnetic moments for the ions  $\text{Sm}^{2+}$  and  $\text{Yb}^{2+}$  lead to the following conclusions:

$\text{Yb}^{2+}$  is either diamagnetic or has only a small temperature independent paramagnetism, suggesting the configuration  $[\text{Xe}] 4f^{14}$ .

The effective moment of  $\text{Sm}^{2+}$  at 35°C is about  $3.64 \mu_B$ . The moments of  $\text{Sm}^{2+}$  and  $\text{Eu}^{3+}$  are nearly the same, indicating that both ions have the electronic configuration  $[\text{Xe}] 4f^6$  (Selwood, 1956).

The effective magnetic moments for  $\text{Yb}^{3+}$  and  $\text{Sm}^{3+}$  at 35°C have been found to be  $4.5 \mu_B$  (W.J. Evans et al., 1981a) and  $1.58 \mu_B$  (D.F. Evans et al., 1971), respectively.

Thus magnetic susceptibility measurements provide an interesting means of evaluating percentages of  $\text{Ln}^{2+}$  and  $\text{Ln}^{3+}$  ions in a mixture of species. Effective magnetic moments of divalent samarium and ytterbium compounds are listed in table 5.

Magnetic susceptibilities were determined with a Gouy balance or using a nmr method originally employed by D.F. Evans (1959). This last method has been used successfully with minor modifications for some organolanthanides (D.F. Evans, 1971). The nmr method, which is very simple to use, is quite applicable in the case of species soluble in an organic medium.

Valence change at high pressure in systems containing lanthanoids is a topic which is of great interest (Jayaraman, 1980). In rare earth systems involving Ce, Sm, Eu, Yb and Tm a change in the valence state of the lanthanide ion can be induced by

TABLE 4  
The UV-visible spectra of some divalent ytterbium and samarium compounds.

References	Compounds	Medium	Band positions (nm)	Remarks
Calderazzo et al. (1966)	YbCp <sub>2</sub>	THF		violet-red solutions; does not show any band around 1000 nm, confirming the ab- sence of trivalent ytterbium species
D.F. Evans et al. (1971)	C <sub>2</sub> H <sub>5</sub> SmI and C <sub>6</sub> H <sub>5</sub> SmI	THF	612-553	possibly charge transfer
Deacon et al. (1979)	Sm/(C <sub>6</sub> F <sub>5</sub> ) <sub>2</sub> Hg	THF	1380, 1220-1260, 1060-1080 615-540 400	Sm <sup>3+</sup> species; charge transfer; f→f transition of Sm(II) and Sm(III)
Deacon et al. (1979)	Yb/(o-HC <sub>6</sub> F <sub>4</sub> ) <sub>2</sub> Hg	THF	978-980 418	Yb <sup>3+</sup> species; 5d←4f transition or metal←ligand charge transfer of polyfluorophenyl ytterbium (II) species
Namy et al. (1981)	SmI <sub>2</sub>	THF	617, 565, 418, 365, 350, 282	see discussion in Namy et al. (1981)
Namy et al. (1981)	YbI <sub>2</sub>	THF	390, 342, 307	see discussion in Namy et al. (1981)
Dyke et al. (1972)	Sm(II)(ClO <sub>4</sub> ) <sub>2</sub>	CH <sub>3</sub> CN	625, 518, 425, 357, 291	see discussion in Dyke et al. (1972)

TABLE 5  
The magnetic properties of some divalent Sm and Yb compounds.

References	Compounds	$\mu_{\text{eff}} (\mu_B)$	Remarks
Tilley et al. (1980)	Yb(C <sub>5</sub> Me <sub>5</sub> ) <sub>2</sub> (THF)	diamagnetic	
W.J. Evans et al. (1981a)	Sm(C <sub>5</sub> Me <sub>5</sub> ) <sub>2</sub> (THF)	3.6 (25°C)	
W.J. Evans et al. (1981a)	SmH(C <sub>5</sub> Me <sub>5</sub> )(THF)	2.86 (25°C)	less than that expected for a pure Sm(II) complex
W. J. Evans (1982)	Sm(C <sub>5</sub> Me <sub>4</sub> Et) <sub>2</sub> (THF) <sub>2</sub>	3.85 (25°C)	
Zinnen et al. (1980)	mixture containing YbH(MeC <sub>5</sub> H <sub>4</sub> ) <sub>2</sub> and Yb(MeC <sub>5</sub> H <sub>4</sub> ) <sub>2</sub>	2-4	obtained from reaction of [YbMe(MeC <sub>5</sub> H <sub>4</sub> ) <sub>2</sub> ] <sub>2</sub> with H <sub>2</sub> in toluene at 50°C
W.J. Evans et al. (1980)	Yb(C <sub>9</sub> H <sub>14</sub> ) <sub>n</sub>	85-92% Yb <sup>2+</sup> <sup>a)</sup>	
Watt et al. (1981)	SmCp <sub>2</sub> (THF)	3.6 ± 0.2 (25°C)	
Hayes et al. (1969)	YbC <sub>8</sub> H <sub>8</sub>	diamagnetic	
Namy et al. (1981)	SmI <sub>2</sub> in THF	3.52 (25°C)	
Namy et al. (1981)	YbI <sub>2</sub> in THF	diamagnetic	
D.F. Evans et al. (1971)	CH <sub>3</sub> YbI	86% Yb <sup>2+</sup> <sup>a)</sup>	
D.F. Evans et al. (1971)	C <sub>2</sub> H <sub>5</sub> YbI	83% Yb <sup>2+</sup> <sup>a)</sup>	
D.F. Evans et al. (1971)	C <sub>6</sub> H <sub>5</sub> YbI	86% Yb <sup>2+</sup> <sup>a)</sup>	
D.F. Evans et al. (1971)	C <sub>6</sub> H <sub>5</sub> SmI	50% Sm <sup>2+</sup> <sup>a)</sup>	

<sup>a)</sup>Percentage of Yb (Sm) as Yb<sup>2+</sup> (Sm<sup>2+</sup>), as indicated by  $\mu_{\text{eff}}$ .

high pressure, temperature or by chemical substitution (Maple et al., 1971). Usually the change is from a lower to a higher valence state. The reason for this electronic transition is in the small energy difference between the 4f<sup>n</sup> and 4f<sup>n-1</sup> electronic configurations. The valence transition leads not to an integral valence but to an intermediate valence state.

The divalent state of Sm, Eu, Tm and Yb should become unstable under high pressure. This can be foreseen from the fact that they have smaller ionic radii in their trivalent state and hence high pressure could favor the higher valence state. Recent high pressure experiments on a series of lanthanoid compounds, in particular the monochalcogenides Sm, Eu, Yb, Tm, have demonstrated the occurrence of such transformations.

When SmS is subjected to pressure it transforms according to



A semiconductor-to-metal transition results, and approximately 10<sup>22</sup> electrons per cm<sup>3</sup> are released from the localized 4f state into the conducting 5d state. This valence change and 4f electron delocalization occurs in SmS near 7000 bar. The electrical conductivity of SmS abruptly increases at the transition pressure as would be

TABLE 6  
The solubility in THF of some divalent samarium and ytterbium derivatives.

References	Compound	Color and solubility in THF	Isolated complexes with THF (or other ligands)
Rossmannith (1979)	SmCl <sub>2</sub>	red; $0.14 \times 10^{-2}$ M (22°C)	
Rossmannith (1979)	YbCl <sub>2</sub>	yellow; 0.19 M (25°C)	YbCl <sub>2</sub> (THF)
Watson (1980)	YbBr <sub>2</sub>	very sparingly soluble; white-yellow	YbBr <sub>2</sub> (THF)
Namy et al. (1981)	SmI <sub>2</sub>	blue-green; 0.1 M (20°C)	
Namy et al. (1981)	YbI <sub>2</sub>	yellow-green; $4 \times 10^{-2}$ M (20°C)	YbI <sub>2</sub> (THF) <sub>3-4</sub> ; YbI <sub>2</sub> (CH <sub>3</sub> CN) <sub>5</sub>
Namy et al. (1981) } Watt et al. (1969) }	SmCp <sub>2</sub>	purple; insoluble	SmCp <sub>2</sub> (THF), SmCp <sub>2</sub> (THF) <sub>2</sub>
Fischer et al. (1966) } Calderazzo et al. (1966) }	YbCp <sub>2</sub>	violet-red; soluble	YbCp <sub>2</sub> (THF) (yellow)
W.J. Evans et al. (1981a)	Sm(MeC <sub>5</sub> H <sub>4</sub> ) <sub>2</sub>	insoluble	
Zinnen et al. (1980)	Yb(MeC <sub>5</sub> H <sub>4</sub> ) <sub>2</sub>	purple; soluble	Yb(MeC <sub>5</sub> H <sub>4</sub> ) <sub>2</sub> (THF) (yellow)
W.J. Evans et al. (1981a)	Sm(C <sub>5</sub> Me <sub>5</sub> ) <sub>2</sub>	purple; soluble	Sm(C <sub>5</sub> Me <sub>5</sub> ) <sub>2</sub> (THF) <sub>2</sub>
Tilley et al. (1980) } Watson (1980) } Watson et al. (1981) }	Yb(C <sub>5</sub> Me <sub>5</sub> ) <sub>2</sub>	deep purple; soluble in THF, Et <sub>2</sub> O and in aliphatic and aromatic hydrocarbons	Yb(C <sub>5</sub> Me <sub>5</sub> ) <sub>2</sub> (THF) <sub>2</sub> (red) Yb(C <sub>5</sub> Me <sub>5</sub> ) <sub>2</sub> (THF) (orange) Yb(C <sub>5</sub> Me <sub>5</sub> ) <sub>2</sub> (Et <sub>2</sub> O) (green) Yb(C <sub>5</sub> Me <sub>5</sub> ) <sub>2</sub> (THF) hemitoluene (brown-red) Yb(C <sub>5</sub> Me <sub>5</sub> ) <sub>2</sub> (DME)

W.J. Evans (1982)	$\text{Sm}(\text{C}_3\text{Me}_4\text{Et})_2$	purple; soluble	$\text{Sm}(\text{C}_3\text{Me}_4\text{Et})_2(\text{THF})_2$
Lappert et al. (1980)	$\text{Yb}(\text{Me}_3\text{SiC}_3\text{H}_4)_2$	purple; soluble in THF, toluene	$\text{Yb}(\text{Me}_3\text{SiC}_3\text{H}_4)_2(\text{THF})_2$ (purple) (mp = 120°C) $\text{Yb}(\text{Me}_3\text{SiC}_3\text{H}_4)_2$ (green) (mp = 308–310°C) $\text{Yb}(\text{Me}_3\text{SiC}_3\text{H}_4)_2(\text{tmeda})$ (blue) (mp = 115°C)
Namy et al. (1981)	$\text{Sm}(\text{OAc})_2$	white; insoluble	$\text{Sm}(\text{OAc})_2(\text{THF})$
Namy et al. (1981)	$\text{Yb}(\text{OAc})_2$	yellow; insoluble	$\text{Yb}(\text{OAc})_2(\text{THF})$
Namy et al. (1981)	$\text{Yb}(\text{OC}_2\text{H}_5)_2$	colorless; soluble	
Namy et al. (1981)	$\text{Sm}(\text{OC}_2\text{H}_5)_2$	colorless; soluble	
Deacon et al. (1979)	$\text{Yb}(\text{C}_6\text{F}_5)_2$	orange; soluble	
Deacon et al. (1979)	$\text{Yb}[(\text{C}_6\text{H}_5)_3\text{C}\equiv\text{C}]_2$	purple black; soluble	
D.F. Evans et al. (1971)	$\text{CH}_3\text{YbI}$	brown; 0.1–0.4 M	
D.F. Evans et al. (1971)	$\text{C}_2\text{H}_5\text{YbI}$	brown; 0.1–0.4 M	
D.F. Evans et al. (1971)	$\text{C}_6\text{H}_5\text{YbI}$	brown; 0.1–0.4 M	
D.F. Evans et al. (1971)	$\text{C}_6\text{H}_5\text{SmI}$	deep blue green; 0.2 M	



expected for a semiconductor-to-metal transition. All the Yb monochalcogenides undergo a valence change which is believed to occur continuously with pressure.

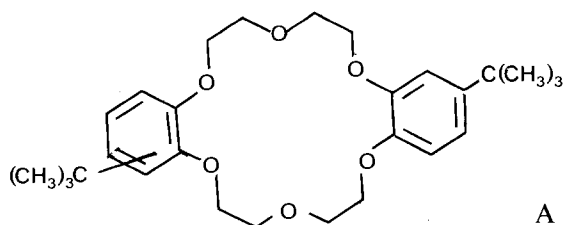
No organic or organometallic compounds have yet been studied under these conditions. They could also be very interesting materials if such valence changes are observed.

### 3.3. Solvation, solubility and volatility

Divalent samarium and ytterbium compounds appear to have strong interactions with solvents, which affect their appearance markedly. In some cases desolvation is accompanied by decomposition. In water, the blood red  $\text{Sm}^{2+}$  and the green  $\text{Yb}^{2+}$  ions are oxidized quite rapidly.  $\text{Yb}^{2+}$  is more stable than  $\text{Sm}^{2+}$  but considerably less than  $\text{Eu}^{2+}$ . The rates of oxidation are in the same sequence as the values of  $-E^0(\text{M}^{3+}/\text{M}^{2+})$  (see section 3.1. above).

It is interesting that appreciable amounts of  $\text{Sm}^{2+}(\text{aq.})$  persist in oxygen-free aqueous solution for at least 1 h (Morss, 1976). Hence reduction of various organic substrates could probably be studied in this medium. Solvents which were used for  $\text{Sm}(\text{II})$  and  $\text{Yb}(\text{II})$  chemistry are acetonitrile, diethylether, tetrahydrofuran, dimethoxyethane, hexamethylphosphotriamide, ethanol and ammonia.

Ammonia has been used for  $\text{Yb}(\text{II})$  compounds because preparations may be performed in some cases in this medium (see section 2.3.3 above). Divalent compounds are soluble in, but reactive towards HMPA and ethanol (Kamenskaya et al., 1977; Clifford et al., 1948) (see section 2.3.1 above). The most widely used solvent is THF. Solubilities in THF are compiled in table 6. It is classical to ascribe a Lewis character to many trivalent lanthanide derivatives. Fewer data are available on divalent species. Hydration enthalpies of  $\text{Ln}^{2+}$  ions have been evaluated (Morss, 1976). Structural investigations establish that very often  $\text{Sm}^{2+}$  and  $\text{Yb}^{2+}$  derivatives are coordinated to the oxygen or nitrogen in various kinds of ligands. If one considers that these compounds are bases, it follows that  $\text{Sm}^{2+}$  or  $\text{Yb}^{2+}$  are Lewis acid centers. Such isolated complexes are listed in table 6. In a very interesting work the influence of 4,4'(5')-diterbutylbenzo-18 crown-6 **A** in propylene carbonate on the electrochemical properties of  $\text{Sm}^{2+}$  and  $\text{Yb}^{2+}$  was investigated (Massaux et al., 1980). These ions form adducts with this crown ether which are 3.6 and 4.6 orders of magnitude more stable than those of the corresponding trivalent ions, respectively. This effect is attributed both to the larger sizes of the divalent ions ( $\text{Sm}^{2+}$ :  $r = 1.11 \text{ \AA}$ ;  $\text{Yb}^{2+}$ :  $r = 0.93 \text{ \AA}$ ), which are better accommodated in the internal cavity of the cycle, and to the smaller charge.



Some anionic organoytterbium complexes have been studied. For example,  $\text{Yb}(\text{C}_5\text{Me}_5)_2$  reacts with  $\text{LiX}$  ( $\text{X} = \text{I}, \text{Me}$ ) to lead to  $\text{Li}[\text{Yb}(\text{C}_5\text{Me}_5)\text{X}_2]$  and  $\text{Li}(\text{C}_5\text{Me}_5)$  (Watson, 1980) (see section 2.3.3 above).

Divalent lanthanide compounds are generally non-volatile; this observation is consistent with a polymeric constitution. However, some organometallic compounds have been sublimed.  $\text{Yb}(\text{Me}_3\text{SiC}_5\text{H}_4)_2$  sublimes at  $300^\circ\text{C}/10^{-3}$  Torr (Lappert et al., 1980) and  $\text{YbCp}_2$  sublimes at  $360^\circ\text{C}/10^{-3}$  Torr with considerable decomposition (Calderazzo et al., 1966).

### 3.4. Structure and bonding

In contrast to trivalent lanthanides only a few divalent organolanthanides were fully characterized.

$\text{Sm}(\text{C}_5\text{Me}_5)_2(\text{THF})_2$  was isolated and its X-ray crystal structure obtained (W.J. Evans et al., 1981a) (fig. 1). The average  $\text{Sm}-\text{C}(\eta^5)$  and  $\text{Sm}-\text{O}$  bond lengths are 2.86(3) and 2.63(1) Å, respectively. Each  $\text{Sm}^{2+}$  atom is eight-coordinated. The  $^1\text{H}$  nmr spectrum of this compound (in  $\text{C}_6\text{D}_6$ ) was the first reported nmr spectrum of a divalent samarium complex. It gives singlets at  $\delta = 2.45$  ppm (30 H) and  $\delta = 4.43$  ppm (7 H) and a broad signal at  $\delta = 17.99$  ppm. The signal at 2.45 ppm was assigned to the methyl groups of  $\text{C}_5\text{Me}_5$  and the  $\delta$  4.32 absorption to the  $\alpha$ - $\text{CH}_2$  group in the THF moiety; the broad signal is attributed to the  $\alpha$ - $\text{CH}_2$  in THF. The  $^{13}\text{C}$  nmr spectrum in  $\text{C}_6\text{D}_6$  was also studied. The signals are at  $-73.7$  ppm (singlet,

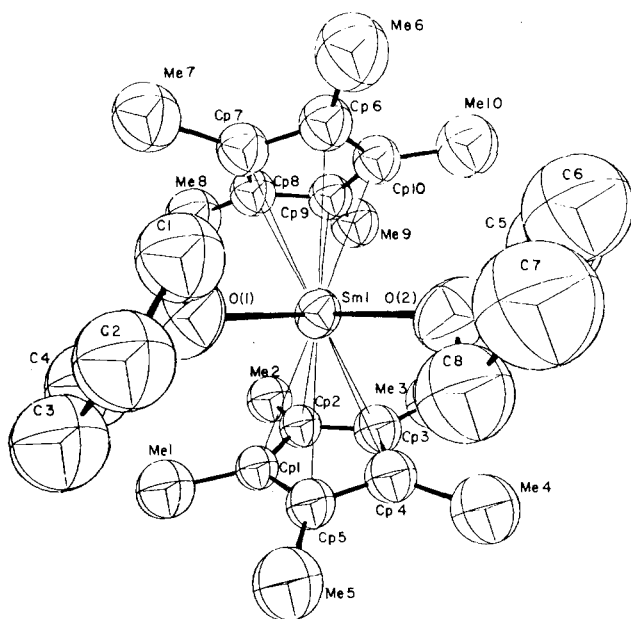


Fig. 1. The molecular structure of  $\text{Sm}(\text{C}_5\text{Me}_5)_2(\text{THF})_2$  according to W.J. Evans et al. (1981a). There are two crystallographically independent molecules in the unit cell, with identical bonding parameters.

$C_5Me_5$ ), 33.4 ppm (triplet,  $J = 125$  Hz, THF), 9.62 ppm (quartet,  $J = 117$  Hz, 5 Me), 149.5 ppm (weak, THF).

X-ray diffraction patterns of  $SmCp_2(THF)$  were obtained but the crystal structure was not solved (Watt et al., 1969). The X-ray structure of  $Yb(MeC_5H_4)_2(THF)$  is one of the first obtained for a divalent organoytterbium complex (Zinnen et al., 1980). Each ytterbium center is formally ten-coordinated, surrounded by three cyclopentadienyl rings and one THF molecule. There is one terminal cyclopentadienyl ring (A) and two bridging cyclopentadienyl rings (B and C, fig. 2). The average Yb–C distance in these three cases is 2.76, 2.91 and 2.87 Å, respectively. In the solid state the complex forms chains oriented along the  $b$ -axis in which the repeating units,  $Yb(\mu-MeC_5H_4)_2(THF)$ , are related by a two-fold screw axis and are connected by one bridging  $MeC_5H_4$  group per ytterbium (fig. 2).  $^1H$  nmr in THF- $d_6$  shows signals at  $\delta = 2.07$  ppm (s) and 5.47 ppm (s).  $^{13}C$  nmr in THF- $d_6$  indicates signals at 15.3, 105.8, 107.5 and 116.8 ppm.

The crystal structure of  $Yb(C_5Me_5)_2(THF)$ ,  $\frac{1}{2}$  tol was also recently described (Tilley

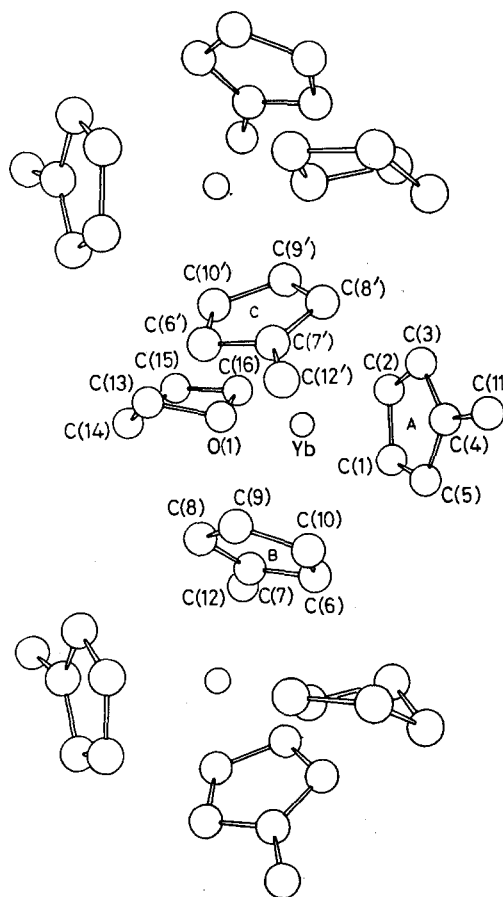


Fig. 2. The structure of  $Yb(MeC_5H_4)_2(THF)$  along the  $b$ -axis vertical, according to Zinnen et al. (1980).

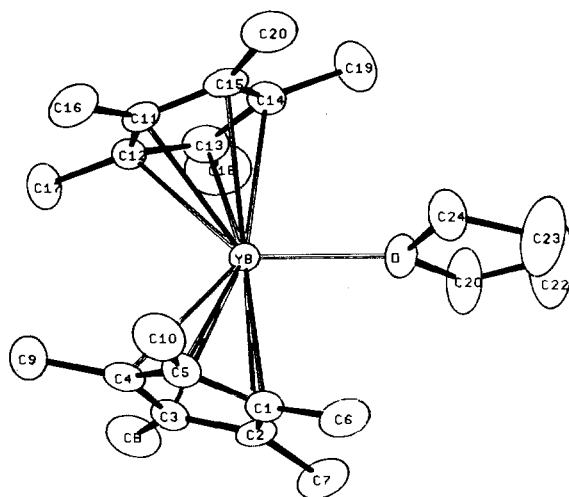


Fig. 3. The molecular structure of  $\text{Yb}(\text{C}_5\text{Me}_5)_2(\text{THF})$  according to Tilley et al. (1980).

et al., 1980). The toluene molecule is not coordinated to the complex and is in a disordered configuration. The structure of the complex can be seen in fig. 3. The pentamethylcyclopentadienyl group is a sterically demanding ligand, which decreases the coordination number around ytterbium atoms and prevents polymerization in the solid state. Each ytterbium atom is coordinated to two  $\text{C}_5\text{Me}_5$  rings and to the oxygen atom of a THF molecule. The three-fold coordination of  $\text{Yb}(\text{II})$  ion is planar. The  $\text{Yb}-\text{O}$  distance is 2.41 Å, the averaged  $\text{Yb}-\text{C}$  distances are 2.66 Å.

$\text{Yb}(\text{C}_5\text{Me}_5)_2(\text{THF})$  has been prepared by the same authors (Tilley et al., 1980) and its nmr spectrum studied at  $-25^\circ\text{C}$  in toluene- $d_8$ . The compound is rigorously diamagnetic ( $f^{14}$  configuration), the  $^1\text{H}$  nmr spectrum shows a singlet at  $\delta = 2.12$  ppm (methyl protons) and multiplets at  $\delta = 3.42$  ppm and 1.41 ppm ( $\alpha$  and  $\beta$  protons of THF).  $^{13}\text{C}$  nmr spectrum shows singlets at 11.5, 25.7, 69.5 and 111 ppm, which account for Me,  $\beta$ -C in THF,  $\alpha$ -C in THF and  $\text{C}_5\text{Me}_5$ , respectively.

The crystal structure of  $\text{Yb}(\text{Me}_3\text{SiC}_5\text{H}_4)_2(\text{THF})_2$  is also available (Lappert et al., 1980). The four ligands are arranged about the ytterbium atom in a distorted tetrahedral fashion. The averaged  $\text{Yb}-\text{C}$  bond lengths are close to 2.75 Å. The  $\text{Yb}-\text{O}$  distances average to 2.405 Å. The molecular structure is shown in fig. 4.

In all the previous structures the cyclopentadienyl rings are pentahapto with Sm or Yb located at a distance which is consistent with an ionic structure involving a  $\text{Ln}^{2+}$  ion. Because of the small number of crystal structures of the divalent organometallics available it is difficult to make a detailed comparison of the bond lengths with those of the analogous trivalent complexes. It was, however, pointed out (W.J. Evans et al., 1981a) that the  $\text{Sm}-\text{C}$  and  $\text{Sm}-\text{O}$  lengths in  $\text{Sm}(\text{C}_5\text{Me}_5)_2(\text{THF})_2$  are in agreement with the larger ionic radius (0.1–0.2 Å) for  $\text{Sm}^{2+}$  compared to  $\text{Sm}^{3+}$ . The ionic structure was also deduced from an interpretation of the IR spectrum of  $\text{SmCp}_2(\text{THF})$  (Watt et al., 1969).

The first tertiary phosphine complex of divalent ytterbium was described by Tilley

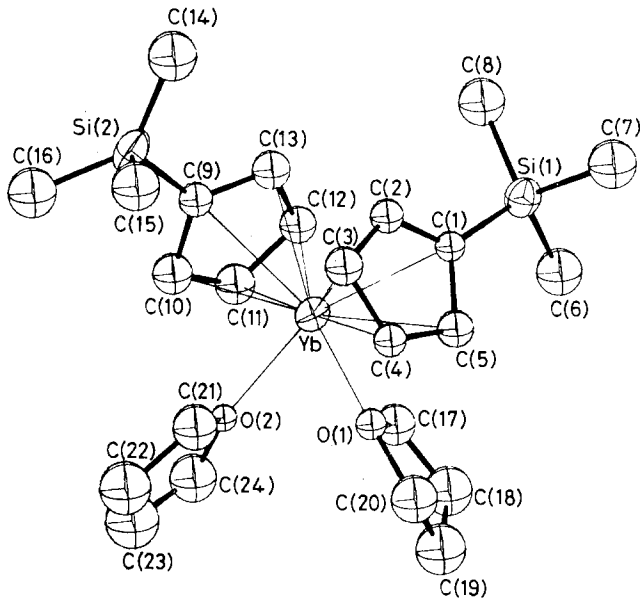


Fig. 4. The molecular structure of  $\text{Yb}(\text{Me}_3\text{SiC}_5\text{H}_4)_2(\text{THF})_2$  according to Lappert et al. (1980).

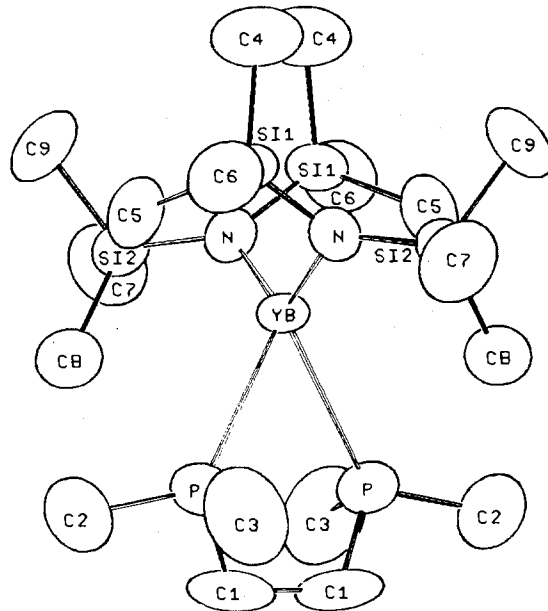


Fig. 5a.

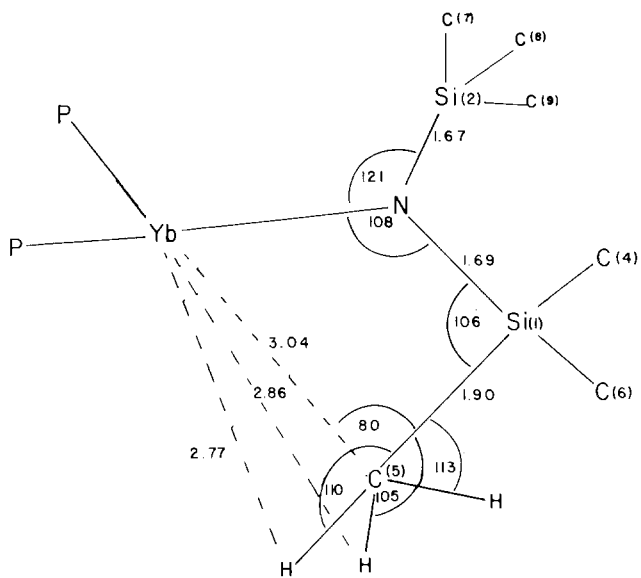


Fig. 5b.

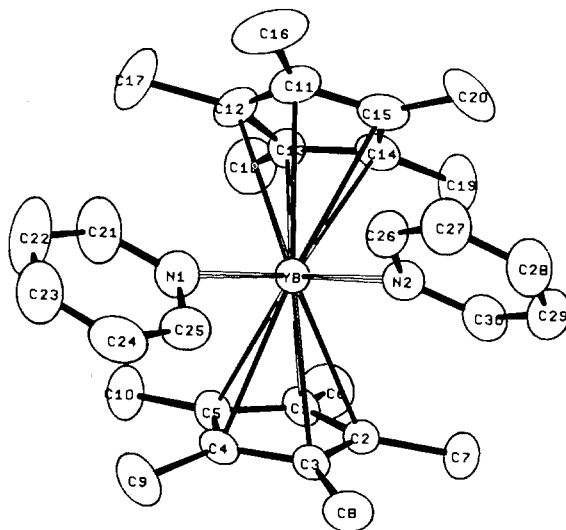
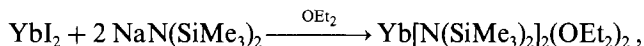


Fig. 5c.

Fig. 5. (a) The structure of  $\text{Yb}[\text{N}(\text{SiMe}_3)_2]_2(\text{dmpe})$ . (b) Details of the  $\text{Yb}-\text{C}(5)$  interactions in  $\text{Yb}[\text{N}(\text{SiMe}_3)_2]_2(\text{dmpe})$ . (c) The structure of  $\text{Yb}(\text{C}_5\text{Me}_5)_2\text{Py}_2$ . (Tilley et al., 1982, 1982a).

et al. (1982). These authors prepared  $\text{Yb}[\text{N}(\text{SiMe}_3)_2]_2$  ( $\text{Me}_2\text{PCH}_2\text{CH}_2\text{PMe}_2$ ) in the following way:



The crystal structure of this lanthanide phosphine complex (purple, diamagnetic) has been solved. The main structure features are indicated in figs. 5a and b. The Yb–P distance is 3.012(4) Å and the Yb–N distance is 2.331(1) Å. The valence angles N–Yb–N, P–Yb–P and N–Yb–P are 123.6(6)°, 68.4(2)° and 101.2(3)°, respectively. A careful inspection of the various bond distances and angles suggests a non-bonded ytterbium–carbon interaction. The carbon atom of a  $\text{CH}_3(\text{Si})$  group is quite close to Yb (3.04 Å), or about the sum of the van der Waals radii of a methyl group (2.0 Å) and of  $\text{Yb}^{2+}$  (1.7 Å). The methyl group (in the  $\gamma$  position with respect to Yb) was described by the authors as semibridging the electropositive Yb atoms. Some geometrical details of the Yb– $\gamma$ C interaction are shown in figs. 5a and b. The complex  $\text{Yb}[\text{N}(\text{SiMe}_3)_2]_2(\text{P-n Bu}_3)_2$  was also prepared from  $\text{Yb}[\text{N}(\text{SiMe}_3)_2]_2(\text{OEt}_2)_2$  by an exchange reaction.

The structure of  $\text{Yb}(\text{C}_5\text{Me}_5)_2\text{Py}_2$  was also recently solved, showing a distorted tetrahedral arrangement at the Yb atom (Tilley et al., 1982a). It is illustrated in fig. 5c.

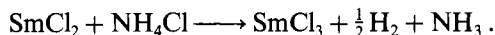
#### 4. Chemical properties

##### 4.1. Reaction with oxygen, water and halogens

Divalent ytterbium and samarium derivatives are generally highly unstable in the presence of oxygen and must be kept under an inert atmosphere. It is the samarium compounds which are the most reactive. Oxidation end-products should be mixtures of various species such as  $\text{LnXO}$ ,  $\text{Ln}_2\text{O}_3$  and  $\text{LnX}_3$ . Organometallics are often extremely sensitive to air, for example,  $\text{Yb}(\text{C}_6\text{F}_5)_2(\text{THF})_4$  (Deacon et al., 1977) and  $\text{SmCp}_2$  (Watt et al., 1969).

It was observed that  $\text{SmI}_2$  and  $\text{SmCl}_2$  can be dissolved into water to give a red bordeaux color which disappears with hydrogen evolution and samarium oxidation (Matignon, 1906a, b).

Oxidation rates of  $\text{Sm}^{2+}$  and  $\text{Yb}^{2+}$  in aqueous solutions have been measured (Faraggi et al., 1972).  $\text{SmCl}_2$  reacts (De Rock et al., 1970) with (aqueous)  $\text{NH}_4\text{Cl}$  according to the equation:

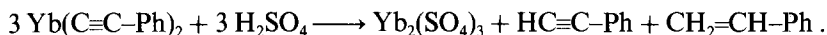


Acidolysis of organometallic divalent lanthanides is classical (D.F. Evans, 1970, 1971). It regenerates the organic moiety as it oxidizes the divalent metal:



In some cases partial hydrogenation of the organic part occurs simultaneously as for

example (Deacon et al., 1979):



Oxidation of  $\text{Sm}^{2+}$  and  $\text{Yb}^{2+}$  by halogens is an easy process (Deacon et al., 1979). It can be of preparative interest in obtaining anhydrous  $\text{Ln}^{3+}$  salts (otherwise prepared after a dehydration step) in some cases. Thus the reaction of iodine in THF solution of  $\text{LnI}_2$  gives rise to anhydrous  $\text{LnI}_3$  which precipitates from the solution in excellent yields (Namy et al., 1981):



Solutions of iodine in THF also oxidize  $\text{Yb}(\text{Me}_3\text{SiC}_5\text{H}_4)_2(\text{THF})_2$  into  $[\text{Yb}(\text{Me}_3\text{SiC}_5\text{H}_4)_2\text{I}]_2$  (Lappert et al., 1980).

#### 4.2. Electron transfer to some inorganic complexes

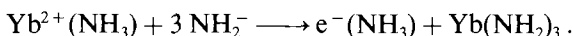
Because of their high negative normal redox potentials,  $\text{Sm}^{2+}$  and  $\text{Yb}^{2+}$  are able to reduce many ions. This property has not yet been used for preparative purposes but it has been exploited in mechanistic studies of electron transfer reactions involving transition metal complexes. Rate constants of reactions between  $\text{Yb}^{2+}$  ions (prepared by electrolytic reduction of  $\text{Yb}^{3+}$ ) and some  $\text{Co}^{2+}$  complexes were measured (Christensen et al., 1970). More accurate kinetic measurements, with the pulse radiolysis technique, have been made (Faraggi et al., 1973) on the reactions of  $\text{Yb}^{2+}$  and  $\text{Sm}^{2+}$  with  $[\text{Co}(\text{NH}_3)_5\text{X}]^{2+}$  ( $\text{X} = \text{F}, \text{Cl}, \text{Br}, \text{I}, \text{N}_3, \text{NCS}, \text{OH}, \text{CN}$ ),  $[\text{Co}(\text{NH}_3)_6]^{3+}$ ,  $[\text{Ru}(\text{NH}_3)_5\text{X}]^{2+}$  ( $\text{X} = \text{Cl}, \text{Br}, \text{I}, \text{OH}$ ) and  $[\text{Ru}(\text{NH}_3)_6]^{3+}$ . The reactions were performed in deaerated aqueous solutions containing tert-butyl alcohol.

It was possible to deduce the second-order rate constants from the decay of  $\text{Yb}^{2+}$  and  $\text{Sm}^{2+}$  monitored spectrophotometrically. Variations of these rate constants with  $\text{Cl}^-$  concentration was also studied.  $\text{Sm}^{2+}$  is always more reactive than  $\text{Yb}^{2+}$  (as expected from the related  $E^0$ ). It was established that the reactions take place mainly by an inner-sphere mechanism in the case of cobalt complexes and by an outer-sphere mechanism with the ruthenium complexes. The reaction with  $[\text{Ru}(\text{NH}_3)_6]^{3+}$  enabled Christensen et al. (1970) to apply the Marcus outer-sphere mechanism theory for calculating the rates of electron exchange  $\text{Ln}^{2+} \rightleftharpoons \text{Ln}^{3+} + \text{e}^-$  ( $\text{Ln} = \text{Sm}$  or  $\text{Yb}$ ). Rates of  $5 \times 10^{-12}$  ( $\text{M}^{-1}\text{s}^{-1}$ ) and  $3 \times 10^{-9}$  ( $\text{M}^{-1}\text{s}^{-1}$ ) were found for  $\text{Sm}$  and  $\text{Yb}$ , respectively. The rate of exchange is very slow and was attributed to the fact that the exchanging electron is in an f orbital.

A new type of linear correlation between electrode potential  $E^0$  and the logarithm of the relative rates of electron transfer (outer-sphere mechanism) towards two oxidants was established by Huck et al. (1980). It involves competition of various divalent ions (mainly lanthanides) towards  $[\text{Co}(\text{NH}_3)_5\text{OH}_2]^{3+}$  and  $[\text{Co}(\text{NH}_3)_6]^{3+}$ . The reaction of  $\text{SmI}_2$  towards various transition metal complexes in THF media could be of preparative interest but the scope of the reaction is still unknown. Preliminary results showed that it is possible to transform some  $\text{Ni}^{2+}$  complexes into  $\text{Ni}^0$  species and  $\text{TiCl}_4$  into low-valence salts (Girard et al., 1982).



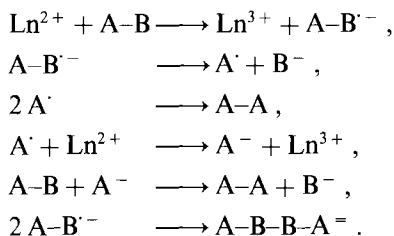
It is appropriate to note in this paragraph the unusual reduction of  $\text{KNH}_2$  by  $\text{YbI}_2$  in liquid ammonia as observed by Salot et al. (1968):



One of the driving forces of the transformation is the insolubility of the resulting ytterbium triamide.

#### 4.3. Use of $\text{SmI}_2$ and $\text{YbI}_2$ in organic chemistry

$\text{SmI}_2$  and  $\text{YbI}_2$ , known as highly reducing agents, are soluble in organic solvents, (e.g. THF). These properties, combined with a new preparation from Sm or Yb metal in THF, made these compounds conveniently available for investigations in organic chemistry (Namy et al., 1977, 1981). The properties of these species towards organic compounds have been actively studied during the last five years (Namy et al., 1977, 1981, 1982; Girard et al., 1980, 1981, 1982; Kagan et al., 1981; Soupe et al., 1982; Danon et al., 1981). The chemistry, which is mediated by  $\text{SmI}_2$  and  $\text{YbI}_2$ , can be interpreted first by electron transfer to an organic substrate (i.e. A-B) that can further decompose or react. The primary products can also react in various ways, for example, a radical  $\text{A}^\cdot$  is able to dimerize or to be transformed into  $\text{A}^-$  by a second electron transfer:



The chemistry following from the use of  $\text{SmI}_2$  and  $\text{YbI}_2$  seems to involve radicals (presence of free radicals or anion radicals) or have carbanion character.

A survey of the main results will be presented here and classified according to the type of reaction.

##### 4.3.1. Reaction with organic halides

Primary or secondary alkyl halides do not react with a 0.1 M THF solution of  $\text{SmI}_2$  at room temperature under nitrogen. However, refluxing in THF for a few hours gives a complete reduction into the alkane when one equivalent of  $\text{SmI}_2$  is used (Girard et al., 1980). Some representative results are indicated in table 7. As predicted from redox potentials the reactivity decreases in RX in the following direction:  $\text{RI} > \text{RBr} > \text{RCl}$ . Alkyl tosylates ROTs could also be reduced, presumably after transformation into RI by metathesis reaction with  $\text{SmI}_2$ , the reaction being faster with a catalytic amount of NaI.

Aromatic or vinylic halides remain unchanged. Only 1-iodonaphtalene could be reduced to naphtalene (Danon et al., 1981), presumably because of the decrease in redox potential introduced by the naphtalene ring. Interestingly

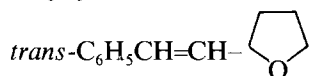
TABLE 7  
The reaction of organic halides or organic sulfonates (Girard et al., 1980).

Compounds	Reaction time	Products	Yield (%)
CH <sub>3</sub> (CH <sub>2</sub> ) <sub>10</sub> CH <sub>2</sub> I	6 h <sup>a)</sup>	CH <sub>3</sub> (CH <sub>2</sub> ) <sub>10</sub> CH <sub>3</sub>	95
CH <sub>3</sub> (CH <sub>2</sub> ) <sub>10</sub> CH <sub>2</sub> OTs	10 h <sup>a)</sup>	CH <sub>3</sub> (CH <sub>2</sub> ) <sub>10</sub> CH <sub>3</sub>	88
PhCH <sub>2</sub> Br	20 min <sup>b)</sup>	PhCH <sub>2</sub> CH <sub>2</sub> Ph	82
PhCH=CH-CH <sub>2</sub> Br	5 min <sup>b)</sup>	(E, E)-(PhCH=CH-CH <sub>2</sub> ) <sub>2</sub>	55
		(E)-(PhCH=CH-CH <sub>2</sub> -CH-CH=CH <sub>2</sub> )	21
		$\begin{array}{c} \text{Ph} \\   \\ \text{Ph}-\text{CH}-\text{CH}-\text{Ph} \\   \quad   \\ \text{CH} \quad \text{CH} \\    \quad    \\ \text{CH}_2 \quad \text{CH}_2 \end{array}$	6

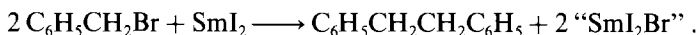
<sup>a)</sup>2 mmol of SmI<sub>2</sub>, 1 mmol of substrate in 55 ml THF; reflux.

<sup>b)</sup>1 mmol of SmI<sub>2</sub>, 1 mmol of substrates; room temperature.

*trans*-C<sub>6</sub>H<sub>5</sub>CH=CHBr leads to

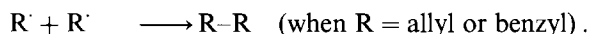
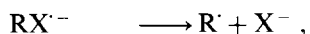
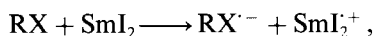


(30% yield) as the sole product. Allylic and benzylic halides are very reactive to SmI<sub>2</sub>. Usually the coupling reaction is finished in a few minutes at room temperature, for example:



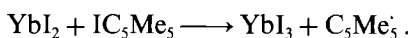
The reaction is very general, unfortunately the regioselectivity in the coupling is not very high (table 7).

The mechanism of these reactions is the following (Kagan et al., 1981):



The reaction  $\text{R}^{\cdot} + \text{SmI}_2 \rightarrow \text{R}^- \text{SmI}_2^+$  was excluded in the case of alkyl halides because it was not possible to isolate the organometallic species RSmI<sub>2</sub>. Related species are known and are quite stable in organic media (see section 4.3.4). Hydrolysis by D<sub>2</sub>O after the disappearance of SmI<sub>2</sub> leads only to RH from RX, which means that the hydrogen is coming from a THF molecule presumably coordinated to a samarium ion (Kagan et al., 1981). When R = allyl or benzyl the radical R<sup>·</sup> is stabilized and can diffuse outside the coordination sphere of Sm<sup>3+</sup> to meet another radical.

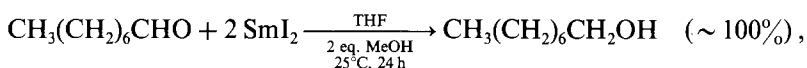
The reaction of  $\text{YbI}_2$  with  $\text{IC}_5\text{Me}_5$  (a tertiary halide) was shown (Watson et al., 1981) to lead to  $\text{YbI}_3$ :



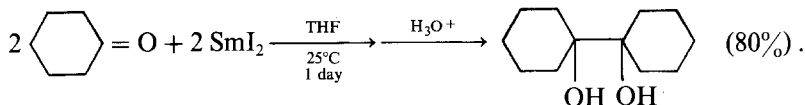
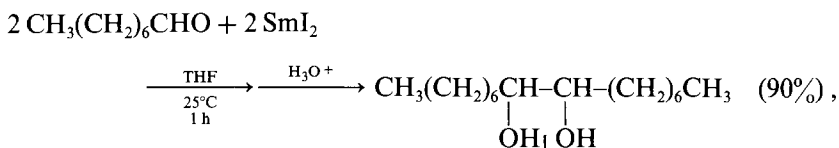
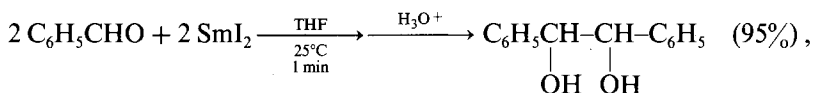
The fate of the organic part was not studied. It was found that trace amounts of  $\text{LiI}$  or  $\text{NBU}_4\text{I}$  catalyze the reaction, presumably via the formation of  $\text{YbI}_3^-$  and a further inner-sphere electron transfer.

#### 4.3.2. Reactions on aldehydes and ketones

THF solutions of  $\text{SmI}_2$  or  $\text{YbI}_2$  are reasonably stable in the presence of 1% methanol. Aldehydes were quantitatively reduced to alcohols by  $\text{SmI}_2$  (2 equivalents) in these solutions, while  $\text{YbI}_2$  was quite inefficient (Namy et al., 1977; Girard et al., 1980). For example:

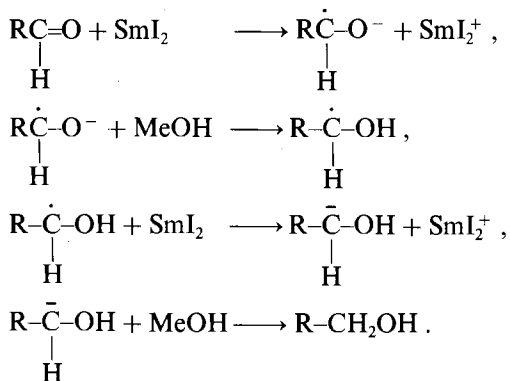


Under the same conditions, 2-octanone, as for many aliphatic ketones, gives a small amount of alcohol (12%). This great difference of reactivity between aliphatic aldehydes and aliphatic ketones was confirmed by competitive reactions, for example, equimolar amounts of octanal and 2-octanone in the presence of 2 equivalents of  $\text{SmI}_2$  gives a 96% reduction of the aldehyde and a 4% reduction of the ketone.  $\text{SmI}_2$  seems to be one of the most selective reagents for the preferred reduction of an aldehyde group in the presence of a ketone. It should be noted that aromatic ketones such as acetophenone are easily reduced by the reagent. It was observed recently (Namy et al., 1983) that aprotic THF solutions of  $\text{SmI}_2$  are excellent reagents for the coupling of aldehydes or ketones into their pinacols. Reactions are very fast at room temperature for aromatic aldehydes, and ketones give the pinacols slowly ( $\sim 1$  day) with a good yield. Some typical examples with  $10^{-1}$  M solutions of  $\text{SmI}_2$  in THF are indicated:



$\text{YbI}_2$  was also found to transform benzophenone into benzopinacol (Deacon et al., 1981). The mechanism of the reductions was discussed by Kagan et al. (1981). The

following pattern was proposed (exemplified in the case of aldehydes):

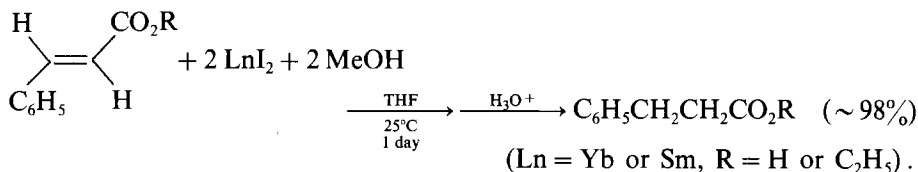


The use of MeOD (instead of MeOH, the proton source) gives 90% RCHDOH and 10% RCH<sub>2</sub>OH. This is in agreement with the protonation by methanol of a transient carbanion. A minor pathway is hydrogen abstraction from THF by the hydroxyalkyl radical. Since pinacol formation is mainly observed in aprotic THF it should be ascribed to the coupling of the initial anion radical.

Carbonyl groups of esters or acids remain unchanged when treated by SmI<sub>2</sub> or YbI<sub>2</sub> solutions.

#### 4.3.3. Reductions of C=C double bonds

Isolated carbon-carbon double bonds do not react with SmI<sub>2</sub> or YbI<sub>2</sub>. On the contrary, conjugated double bonds can be reduced at room temperature. The selectivity is excellent with cinnamic acid or ester (Girard et al., 1980):



For  $\alpha,\beta$ -conjugated ketones or aldehydes there is a competition between C=O and C=C reduction and the selectivity remains to be checked.

#### 4.3.4. Deoxygenation reactions

Sulfoxides



were reduced by two equivalents of SmI<sub>2</sub> into sulfides R-S-R' but phosphine oxides could not be transformed into phosphines. Deoxygenation of epoxides into olefins

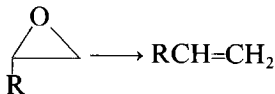
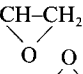
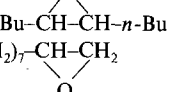



TABLE 8  
The deoxygenation of sulfoxides or epoxides by  $\text{SmI}_2$  (Girard et al., 1980).

Compounds	Reaction conditions <sup>a)</sup>	Products	Yield (%)
Ph-SO-Ph	3 days, 25°C	Ph-S-Ph	88
Ph-SO-Ph	2 h, 65°C	Ph-S-Ph	90
p-Tolyl-SO-Et	4 h, 65°C	p-Tolyl-S-Et	77
PhCH <sub>2</sub> -CH-CH <sub>2</sub> 	1 day, 25°C <sup>b)</sup>	Ph-CH <sub>2</sub> -CH=CH <sub>2</sub>	82
<i>trans</i> - <i>n</i> -Bu-CH-CH- <i>n</i> -Bu 	2 days, 25°C <sup>c)</sup>	<i>trans</i> - <i>n</i> -Bu-CH=CH( <i>n</i> -Bu)	96
CH <sub>3</sub> (CH <sub>2</sub> ) <sub>7</sub> -CH-CH <sub>2</sub> 	2 days, 25°C	CH <sub>3</sub> (CH <sub>2</sub> ) <sub>7</sub> -CH=CH <sub>2</sub>	92

<sup>a)</sup>2 mmol  $\text{SmI}_2$ , 1 mmol of substrate in 50 ml THF.

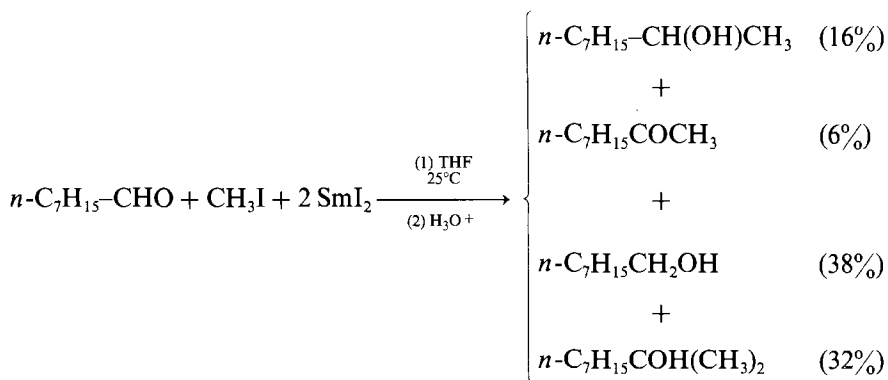
<sup>b)</sup>2 mmol of *t*-BuOH is added.

<sup>c)</sup>4 mmol of  $\text{SmI}_2$ , 4 mmol of *t*-BuOH.

was surprisingly easy even at room temperature. The best results were obtained by use of an excess of  $\text{SmI}_2$  in presence of tert-butyl alcohol. Various examples of deoxygenation are listed in table 8. Mechanisms of these reactions are not well understood, neither has it been established whether the olefin formation could be stereospecific. The nature of the inorganic material formed ( $\text{SmIO} + \text{SmI}_3$ ) is not known.

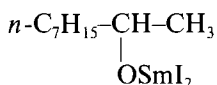
#### 4.3.5. Alkylation of ketones by organic halides

If one considers the reaction mechanisms described in sections 4.3.1. and 4.3.2. it appears that radicals and carbanions could be involved in reactions between aldehydes or alkyl halides and  $\text{SmI}_2$ . It was hypothesized by Namy et al. (1977) that it could be possible to trap one of the intermediates of the aldehyde reduction by replacing methanol by an electrophile such as  $\text{CH}_3\text{I}$ . C-C bond formation was indeed observed but the reaction mixture is quite complicated:

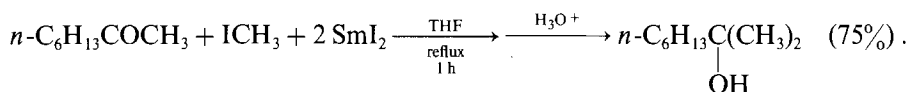


The same types of reactions occur with various aldehydes and alkyl halides. The

pattern of products was interpreted as the result of the initial formation of



which reacts rapidly with aldehyde to give  $n\text{-C}_7\text{H}_{15}\text{COCH}_3$  and  $n\text{-C}_7\text{H}_{15}\text{CH}_2\text{OSmI}_2$  by a Meerwein-Ponndorf reaction. The tertiary alcohol comes from the reaction of the ketone and  $\text{CH}_3\text{I}$  in the presence of  $\text{SmI}_2$ . This interpretation has two consequences: secondary diiodo samarium alkoxides should be efficient reagents for the reduction of aldehydes (this has not yet been checked) and the ketones should react easily with alkyl halides. This latter reaction was indeed proved to be a very general and useful reaction (Girard et al., 1980). A typical example of the reaction is:



The ester groups remain unchanged under the same conditions. The reaction is quite general for ketones and various types of halides. The order of reactivity is  $\text{RI} > \text{RBr} > \text{RCl}$ . Tertiary alcohols are obtained quantitatively by simultaneous increase of the amounts of  $\text{SmI}_2$  and  $\text{RCH}_2\text{X}$ . A promising feature of the  $\text{SmI}_2$ -promoted alkylation method is the ability to replace  $\text{RX}$  by alkyl-sulfonates (ROTs or ROMes). The yields can be increased by the addition of a catalytic amount of sodium iodide. Some representative results of ketone alkylation with 2-octanone as substrate are reported in table 9. The major by-products in reactions performed under standard conditions (2 equivalents of  $\text{SmI}_2$ ) are the alkanes arising from alkyl halide and the alcohol coming from the reduction of the ketone. Surprisingly, allylic or benzylic halides, which are prone to fast self-coupling by  $\text{SmI}_2$ , cleanly react with ketones to give tertiary alcohols (see table 9 in the case of 2-octanone).

$\text{SmI}_2$  allows the use of functionalized halides where there is one site which selectively reacts (Girard et al., 1980):

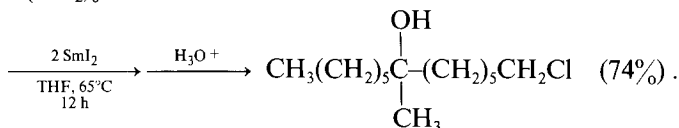
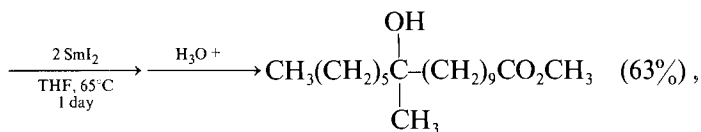
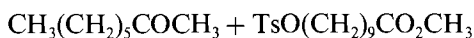
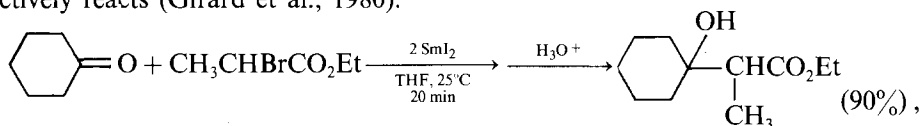


TABLE 9  
The alkylation of 2-octanone by organic halides mediated by  $\text{SmI}_2^a$  (Girard et al., 1980).

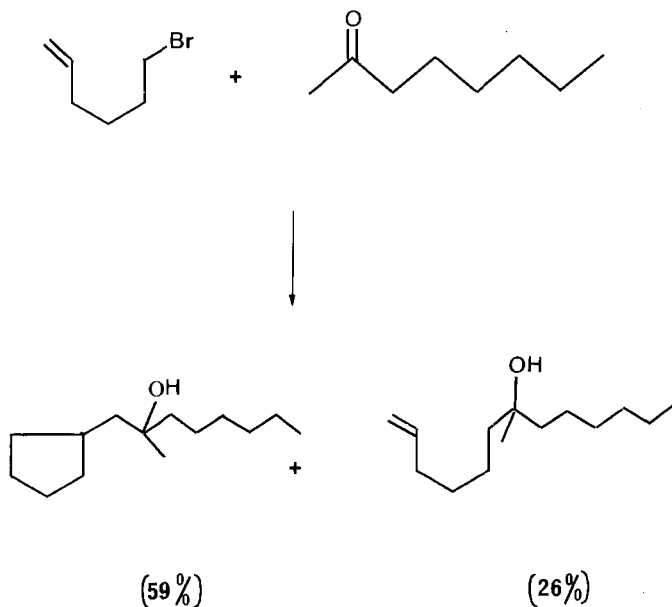
Organic halides	Reaction time	Products	Yield (%)
<i>n</i> -BuI	8 h <sup>b</sup>	$\text{CH}_3(\text{CH}_2)_5-\underset{\text{CH}_3}{\text{C}}(\text{OH})\text{Bu}$	74
<i>n</i> -BuOTs	12 h <sup>b</sup>	$\text{CH}_3(\text{CH}_2)_5-\underset{\text{CH}_3}{\text{C}}(\text{OH})\text{Bu}$	49
$\text{ICH}_2-\text{CH}=\text{CH}_2$	25 min <sup>c</sup>	$\text{CH}_3(\text{CH}_2)_5-\underset{\text{CH}_3}{\text{C}}(\text{OH})\text{CH}_2\text{CH}=\text{CH}_2$	72
$\text{PhCH}_2\text{Br}$	30 min <sup>c</sup>	$\text{CH}_3(\text{CH}_2)_5-\underset{\text{CH}_3}{\text{C}}(\text{OH})-\text{CH}_2-\text{Ph}$	69

<sup>a</sup>) 2 mmol  $\text{SmI}_2$ , 1 mmol of halides, 1 mmol of ketone in 55 ml THF.

<sup>b</sup>) Reflux in THF.

<sup>c</sup>) 25°C.

The mechanism of the ketone alkylations mediated by  $\text{SmI}_2$  was investigated by Kagan et al. (1981). The initial formation of a radical  $\text{R}^\cdot$  arising from  $\text{RX}$  was detected by the use of hexenyl bromide and a ketone:



The cyclopentane ring in the product comes from the classical cyclization of the radical  $\cdot\text{CH}_2-(\text{CH}_2)_3-\text{CH}=\text{CH}_2$ . The fate of the  $\text{R}^\cdot$  radical in the reaction medium is not yet elucidated. (Is it always rapidly reduced by  $\text{SmI}_2$  into  $\text{R}^-$  (as found in the

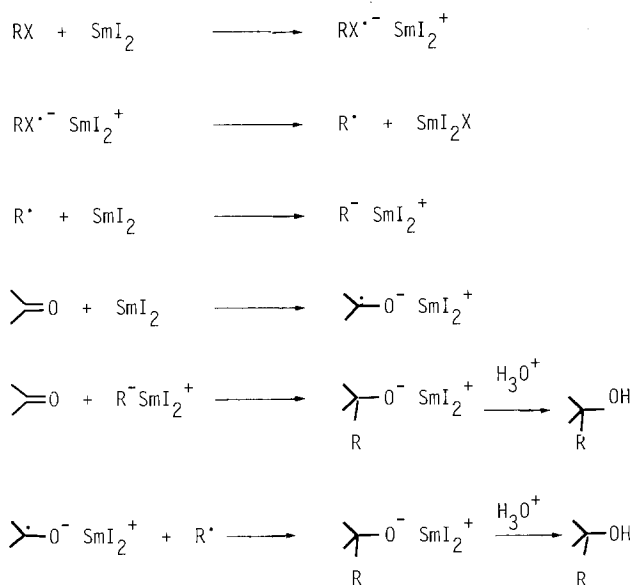


Fig. 6. The mechanism of ketone alkylation by  $\text{SmI}_2$  (Kagan et al., 1981).

case of tetrahydrofurfuryl bromide) or does it couple to the ketyl radical coming from a one-electron transfer between  $\text{SmI}_2$  and the ketone?) The main patterns of the mechanism are indicated in fig. 6. The radical mechanism explains the presence of minor by-products such as



or the pinacol (arising from the ketyl radical) well.

#### 4.3.6. Additions on aldehydes

It was not possible to get clean reactions between aldehydes and alkyl halides in the presence of  $\text{SmI}_2$ . The reason is the very fast Meerwein-Ponndorf reaction quoted in section 4.3.5. It was, however, found that halides such as allyl iodide or benzyl bromide are so reactive towards aldehyde groups that the secondary samarium alkoxide which appears in the solution cannot compete for the remaining aldehyde (Soupe et al., 1982). In this way several homoallylic or homobenzylic alcohols could be obtained. Some examples are listed in table 10. The reaction failed on aromatic aldehydes because the pinacol formation is faster.

#### 4.3.7. Reactions with nitrogen derivatives

Only few details of these reactions are presently known (Danon et al., 1981). Nitroaromatic compounds are rapidly reduced to amines by  $\text{SmI}_2$  in THF, while aromatic or aliphatic nitriles remain unchanged. This allowed some selective



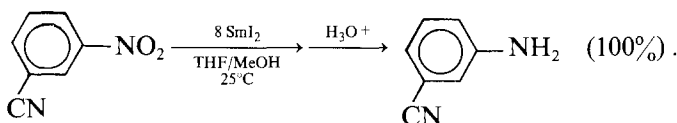
TABLE 10

The reaction of aldehydes with activated organic halides in presence of  $\text{SmI}_2^a$  (Soupe et al., 1982).

Aldehyde	Halide	Products	Yield (%)
$n\text{-C}_7\text{H}_{15}\text{CHO}$	$\text{ICH}_2\text{CH}=\text{CH}_2$	$n\text{-C}_7\text{H}_{15}\text{CH}(\text{OH})\text{CH}_2\text{CH}=\text{CH}_2$	75
$n\text{-C}_7\text{H}_{15}\text{CHO}$	$\text{PhCH}_2\text{Br}$	$n\text{-C}_7\text{H}_{15}\text{CH}(\text{OH})\text{CH}_2\text{Ph}$	86
$n\text{-C}_7\text{H}_{15}\text{CHO}$	$p\text{-NCC}_6\text{H}_4\text{CH}_2\text{Br}$	$n\text{-C}_7\text{H}_{15}\text{CH}(\text{OH})\text{CH}_2(p\text{-NCC}_6\text{H}_4)$	75
$\text{CH}_3\text{CHO}$	$\text{PhCH}_2\text{Br}$	$\text{CH}_3\text{CH}(\text{OH})\text{CH}_2\text{Ph}$	80
$i\text{PrCHO}$	$\text{PhCH}_2\text{Br}$	$i\text{PrCH}(\text{OH})\text{CH}_2\text{Ph}$	88

<sup>a</sup>) Reactions performed in 20 ml THF at room temperature with 2 mmol  $\text{SmI}_2$ , 1 mmol RCHO and 1 mmol organic halide. The reaction time is less than 5 min.

reductions such as the following example:



#### 4.3.8. Coupling of acid chlorides

A very fast reaction occurs between acid chlorides  $\text{RCOCl}$  and two equivalents of diiodosamarium in THF solution at room temperature (Girard et al., 1981). The  $\alpha$ -diketone  $\text{RCOCOR}$  is obtained in good yields (table 11). The mechanism of this unusual coupling should start from an acyl radical,  $\text{RCO}^\cdot$ , which either dimerizes or is further reduced into a samarium acyl anion (fig. 7).

To decide between these two options the case of  $\text{PhCH}_2\text{COCl}$  was investigated (Soupe et al., 1981), because it is known that  $\text{PhCH}_2\text{CO}^\cdot$  is rapidly decarbonylated ( $k = 5.2 \times 10^7 \text{ s}^{-1}$ ) (Griller et al., 1980). The reaction with  $\text{SmI}_2$  gave  $\text{PhCH}_2\text{COCOCH}_2\text{Ph}$  with 75% yield. This is a good argument for a very fast reduction of the acyl radical by  $\text{SmI}_2$  into an acyl anion, which is then acylated by the acid chloride into  $\alpha$ -diketone. The transient  $\text{RCO}^- \text{SmI}_2^+$  species should be a versatile reagent for organic synthesis if it can be isolated or trapped.

TABLE 11

The coupling of acid chlorides by  $\text{SmI}_2^a$  (Girard et al., 1981).

Acid chloride	Reaction time at 25°C in THF	Products	Yield (%)
$\text{PhCOCl}$	2 min	$\text{Ph-CO-CO-Ph}$	78
$p\text{-ClC}_6\text{H}_4\text{COCl}$	4 min	$p\text{-ClC}_6\text{H}_4\text{CO-CO-}(p\text{-ClC}_6\text{H}_4)$	72
$n\text{-C}_8\text{H}_{17}\text{COCl}$	10 min	$n\text{-C}_8\text{H}_{17}\text{CO-CO-}(n\text{-C}_8\text{H}_{17})$	50
$\text{Cl}(\text{CH}_2)_4\text{COCl}$	8 min	$\text{Cl}(\text{CH}_2)_4\text{CO-CO-}(\text{CH}_2)_4\text{Cl}$	54

<sup>a</sup>) 2.5 mmol of the acid chloride are slowly added to 5 mmol of  $\text{SmI}_2$  in 50 ml THF at room temperature.

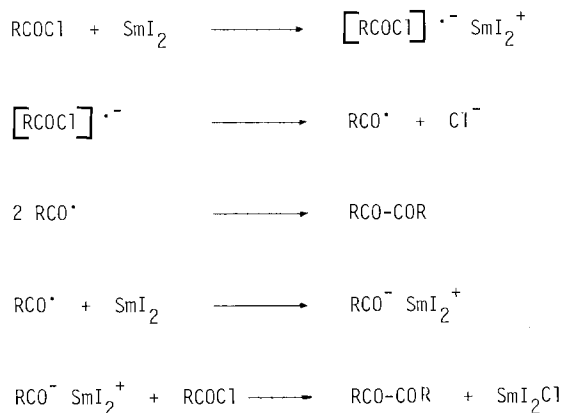


Fig. 7. Possible mechanisms of coupling of acid chlorides promoted by  $\text{SmI}_2$ .

#### 4.3.9. Fragmentation reactions

Ananthanaryan et al. (1982) recently used  $\text{SmI}_2$  as a unique reducing agent for the reactions of fig. 8. These transformations could not be adequately performed by any of the usual reducing reagents. The success of these fragmentations appears to be connected with the ability of  $\text{SmI}_2$  to reduce rapidly an intermediate radical to an anion, which is the starting point of the fragmentation. The tentative mechanisms of the two reactions are indicated in fig. 9.

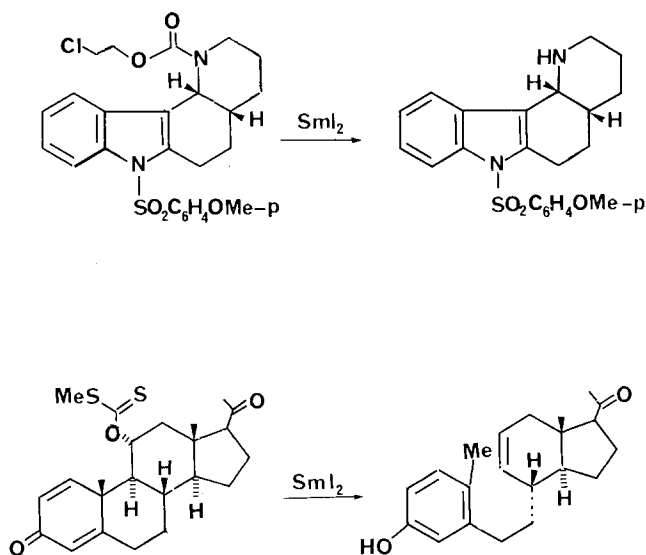


Fig. 8. Fragmentation reactions induced by  $\text{SmI}_2$  (Ananthanaryan et al., 1982).

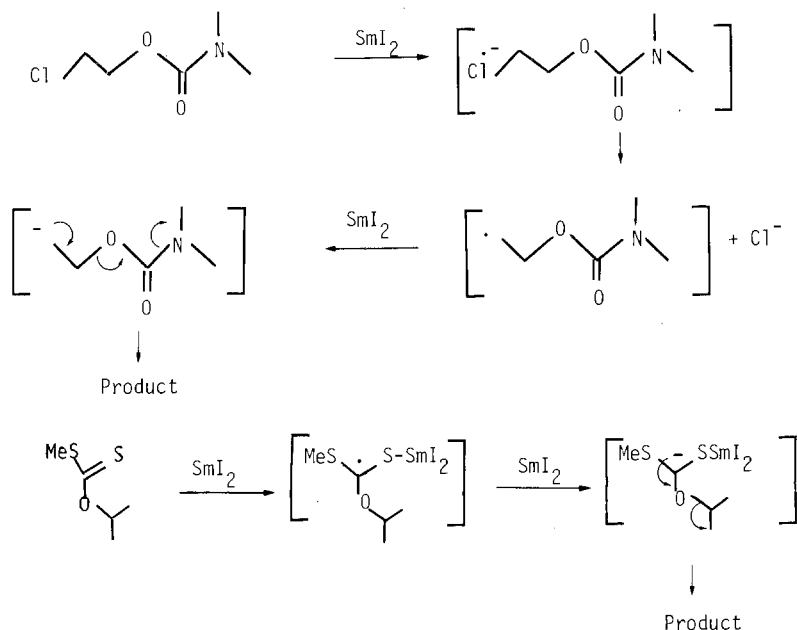


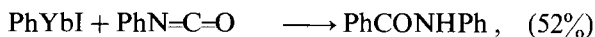
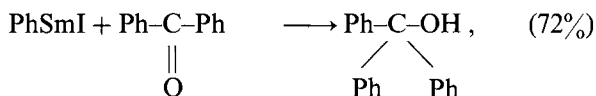
Fig. 9. The mechanism of some fragmentation reactions induced by SmI<sub>2</sub> (Ananthanaryan et al., 1982).

#### 4.4. Reactions of divalent organolanthanides with organic or inorganic compounds

##### 4.4.1. Organic compounds

Until recently the divalent organolanthanides were only briefly studied as Grignard-like reagents. D.F. Evans et al. (1970, 1971) prepared organometallic compounds of divalent ytterbium by the reaction of ytterbium metal on alkyl or aryl iodides in THF at  $-20^{\circ}\text{C}$ . Magnetic susceptibility measurements showed that 75–92% of the ytterbium is present in the divalent state. The solutions react on aldehydes or ketones as typical Grignard reagents.

Some examples are indicated below:



Samarium reacts more slowly with organic iodides such as iodoethane or iodobenzene and needs initiation by iodine and higher temperatures ( $30^{\circ}\text{C}$ ). The various characterizations of the THF solutions indicate that there is a mixture of divalent and trivalent species; this is not unexpected because of the greater instability of the divalent state when Sm is compared to Yb. Thus PhSmI represents only 50%

TABLE 12  
The reactions of diorganoytterbium compounds on aldehydes or ketones (Deacon et al., 1981).

YbR <sub>2</sub> <sup>a)</sup>	Carbonyl compound	Products	Yield (%)
Yb(PhC≡C) <sub>2</sub>	CH <sub>3</sub> CHO	(PhC≡C)MeCH(OH)	63
Yb(PhC≡C) <sub>2</sub>	CH <sub>3</sub> COCH <sub>3</sub>	(PhC≡C)Me <sub>2</sub> C(OH)	34
Yb(PhC≡C) <sub>2</sub>	PhCHO	(PhC≡C)PhCH(OH)	71
Yb(PhC≡C) <sub>2</sub>	Ph <sub>2</sub> CO	(PhC≡C)Ph <sub>2</sub> C(OH)	42
		Ph <sub>2</sub> C(OH)-C(OH)Ph <sub>2</sub>	14
Yb(C <sub>6</sub> F <sub>5</sub> ) <sub>2</sub>	CH <sub>3</sub> CHO	(C <sub>6</sub> F <sub>5</sub> )MeCH(OH)	57
Yb(C <sub>6</sub> F <sub>5</sub> ) <sub>2</sub>	PhCHO	(C <sub>6</sub> F <sub>5</sub> )PhCH(OH)	43
Yb(C <sub>6</sub> F <sub>5</sub> ) <sub>2</sub>	Ph <sub>2</sub> CO	Ph <sub>2</sub> C(OH)-C(OH)Ph <sub>2</sub>	84

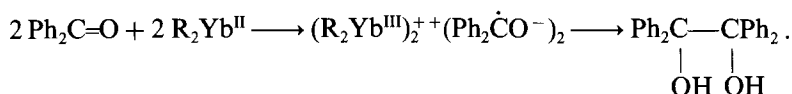
<sup>a)</sup>Formed "in situ" by reaction of Yb with R<sub>2</sub>Hg in THF at room temperature.

of the total samarium which is present. The THF solutions also give Grignard-type reactions, on benzophenone, for example.

Recently the reactions of "PhYbI" reagent prepared according to D.F. Evans (1970, 1971) were reinvestigated by Fugawa et al. (1981, 1982). It was found that there is an unusual selectivity towards ester functions compared to ketones. This reverse trend compared to Grignard reagents could be useful in synthesis. It is also interesting that a large amount of ketone was formed from the esters as well as from benzoyl chloride.

Deacon et al. (1981) prepared diorganoytterbium compounds and found that they react at room temperature in THF to various ketones and aldehydes. Some results are listed in table 12.

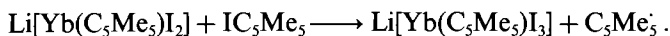
In several cases benzophenone gave benzopinacol, which means that the reagent R<sub>2</sub>Yb can also behave as an electron donor:



The color of the radical anion Ph<sub>2</sub>CO<sup>•-</sup> was detected.

Reduction or pinacol formation was not observed with other carbonyl compounds (benzaldehyde, acetone, ...).

Diorganoytterbium complexes react with some nucleophiles (LiI, LiCH<sub>3</sub>, ...) to give anionic organoytterbium complexes where there is no change in the oxidation state of ytterbium (Watson et al., 1981). These reactions are discussed in section 1. Yb(C<sub>5</sub>Me<sub>5</sub>)<sub>2</sub> was shown (Watson et al., 1981; Tilley et al., 1981) to react with CH<sub>2</sub>Cl<sub>2</sub> to give Yb(C<sub>5</sub>Me<sub>5</sub>)<sub>2</sub>Cl and with FeCp<sub>2</sub><sup>+</sup>PF<sub>6</sub><sup>-</sup> in DME to yield Yb(C<sub>5</sub>Me<sub>5</sub>)<sub>2</sub>DME<sup>+</sup>PF<sub>6</sub><sup>-</sup>. An anionic complex of Yb<sup>2+</sup> could be also easily oxidized:



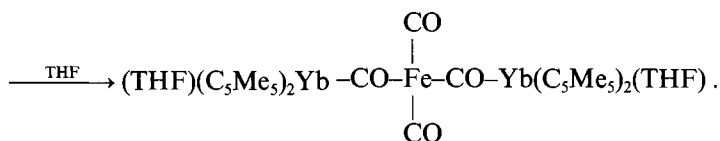
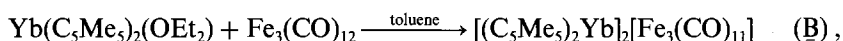
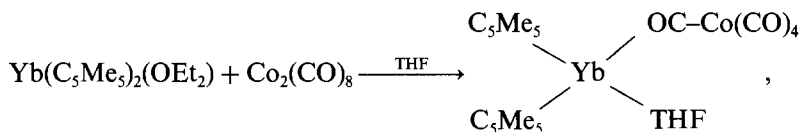
YbI(C<sub>5</sub>Me<sub>5</sub>) was postulated by Watson et al. (1981) as an intermediate in the

transformation

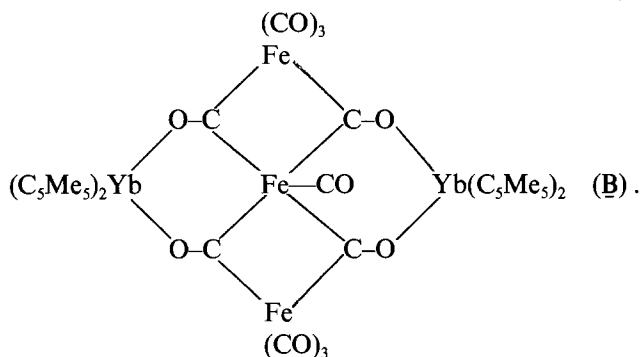


#### 4.4.2. Inorganic compounds

An interesting reaction was observed when  $\text{Yb}(\text{C}_5\text{Me}_5)_2(\text{OEt}_2)$  was opposed to various carbonyl complexes (Tilley et al., 1982). Mixed complexes were obtained with bridged carbon monoxide, the oxygen and carbon being bound to ytterbium and to the transition metal, respectively. The following reactions were studied:



The structure of **B** was elucidated. The trivalent state of Yb was demonstrated by the paramagnetism of the complex. The crystal structure showed that the cluster unit is bound by CO bridges to  $\text{Yb}(\text{C}_5\text{Me}_5)_2$  units:



This entry into families of complexes where CO is O-bonded to a lanthanide ion could be of interest as an activating process of carbon monoxide. Reactions of various divalent organolanthanides with CO and NO were briefly mentioned in the literature without the structure of the reaction products being given. Thus  $\text{Sm}(\text{C}_5\text{Me}_5)_2(\text{THF})_2$  reacts rapidly with CO and NO (W.J. Evans et al., 1981).

#### 4.5. *Some catalytic reactions induced by divalent Yb and Sm species*

In pioneering experiments W.J. Evans et al. (1979, 1981b) prepared, at low temperatures, various divalent organolanthanides by co-condensation of the lanthanide metals with unsaturated hydrocarbons such as cyclopentadiene or alkynes containing acidic hydrogen. Some of the organolanthanides formed showed catalytic activities. Thus  $\text{Sm}(\text{C}_5\text{Me}_5)_2(\text{THF})_2$  polymerizes ethylene (W.J. Evans et al., 1981a). It catalyzes hydrogenation of 3-hexyne into cis-hexene (cis/trans > 99/1). The reaction conditions are quite mild: 25°C and 1 atm of hydrogen, with a turnover number of  $0.85 \times 10^{-3} \text{ min}^{-1}$  (based on  $\text{H}_2$  uptake). The mechanism of the reaction is not established but is believed to involve the addition of a hydride Ln-H on the triple bond followed by hydrogenolysis with  $\text{H}_2$  (W.J. Evans et al., 1981a).

#### 4.6. *Reactions of ytterbium in liquid ammonia*

As was mentioned in section 2.3.3, ytterbium metal dissolves in liquid ammonia to yield ammoniated electrons and  $\text{Yb}^{2+}$  ions. This solution was used by White et al. (1978) to perform reductions of various aromatic systems, similar to the Birch reactions which use lithium or sodium as the metal. The addition of benzoic acid or anisole dissolved in a 10:1 mixture of THF-tert-butyl alcohol, to an ytterbium-ammonia solution gives 1,4-dihydrobenzoic acid (56% yield). Triple bonds are cleanly reduced to trans olefins (i.e.  $\text{PhC}\equiv\text{CPh} \rightarrow \text{trans-PhCH}=\text{CHPh}$  75%). The C=C double bonds of conjugated ketones are also reduced by this system. Since the reaction medium initially contains both solvated electrons and  $\text{Yb}^{2+}$  ions it is likely that the above reactions are not directly connected with the presence of divalent ytterbium species.

### 5. Conclusion

Divalent samarium and ytterbium derivatives can now be prepared by a wide variety of methods. Of the new organometallic compounds recently obtained only a few have been fully characterized and their crystal structures described. Progress toward a better understanding of the bonding properties can be expected in the near future. Mild methods are now also available for synthesis of many simple divalent Sm or Yb derivatives. The study of the reactivity of divalent samarium and ytterbium compounds is at its beginning. Because of the achievements of the last few years one can expect that organic chemistry will benefit increasingly from this class of compounds. Amongst the potential applications are the selective C-C bond formation, unusual electron transfer reactions or homogeneous catalysis. Inorganic chemistry and material science should also profit from the renewed activity in the field of divalent lanthanides.

## 6. Recent developments

Di(alkynyl) mercurials and ytterbium metal in THF or DME give  $(RC\equiv C)_2Yb$ . These compounds were also obtained by ligand exchange between  $(C_6F_5)_2Yb$  or  $(tBuC\equiv C)_2Yb$  and  $PhC\equiv CH$  (Deacon et al., 1982). It was similarly shown (Suleimanov et al., 1982) that  $HgCp_2$  reacts in THF with an excess of ytterbium or samarium amalgam to give  $LnCp_2 \cdot (THF)_n$ , where  $Ln = Yb$  or  $Sm$ . Yields are 30–40%.  $SmI_2$  was found to be an efficient reagent for the reductive cleavage of the O–N bond of isoxazoles (Natale, 1982).

## References

- Ananthanaryan, T.P., T. Gallagher and P. Maganus, 1982, *J. Chem. Soc., Chem. Commun.*, 709.
- Asprey, L.B. and B.B. Cunningham, 1960, *Prog. Inorg. Chem.* **8**, 267.
- Asprey, L.B., F.H. Ellinger and E. Staritzky, 1964, in: *Rare Earth Research*, vol. 2, ed. K.S. Vorres (Gordon and Breach, New York) p. 11.
- Baernighausen, H., 1961, *J. Prakt. Chem.* **14**, 313.
- Beck, H.P., 1978, *J. Solid State Chem.* **23**, 213.
- Butement, F.D.S., 1948, *Trans. Faraday Soc.* **44**, 617.
- Calderazzo, F., R. Pappalardo and S. Losi, 1966, *J. Inorg. Nucl. Chem.* **28**, 987.
- Christensen, R.J., and J.H. Espenson, 1970, *J. Chem. Soc., Chem. Commun.*, 756.
- Clifford, A.F. and H.C. Beachell, 1948, *J. Amer. Chem. Soc.* **70**, 2730.
- Danon, L., J.L. Namy and H.B. Kagan, 1981, unpublished results.
- Deacon, G.B. and A.J. Koplick, 1978, *J. Organometal. Chem.* **146**, C43.
- Deacon, G.B. and T.D. Tuong, 1981, *J. Organometal. Chem.* **205**, C4.
- Deacon, G.B. and P.G. Vince, 1976, *J. Organometal. Chem.* **112**, C1.
- Deacon, G.B., W.D. Raverty and D.G. Vince, 1977, *J. Organometal. Chem.* **135**, 103.
- Deacon, G.B., A.J. Koplick, W.D. Raverty and D.G. Vince, 1979, *J. Organometal. Chem.* **182**, 121.
- Deacon, G.B., A.J. Koplick and T.D. Tuong, 1982, *Aust. J. Chem.* **35**, 941.
- De Rock, C.W. and D.D. Radtke, 1970, *J. Inorg. Nucl. Chem.* **32**, 3687.
- Dyke, J.M. and N.S. Hush, 1972, *J. Electroanal. Chem.* **36**, 337.
- Evans, D.F., 1959, *J. Chem. Soc.*, 2003.
- Evans, D.F., G.V. Fazakerley and R.F. Phillips, 1970, *J. Chem. Soc., Chem. Commun.*, 244.
- Evans, D.F., G.V. Fazakerley and R.F. Phillips, 1971, *J. Chem. Soc.*, 1931.
- Evans, W.J., 1982, personal communication.
- Evans, W.J., S.G. Engerer, P.A. Piliero and A.L. Wayda, 1979, *J. Chem. Soc., Chem. Commun.*, 1007.
- Evans, W.J., I. Bloom, W.E. Hunter and J.L. Atwood, 1981a, *J. Amer. Chem. Soc.* **103**, 6507.
- Evans, W.J., S.G. Engerer and K.M. Colison, 1981b, *J. Amer. Chem. Soc.* **103**, 6672.
- Farragi, M. and A. Feder, 1973, *Inorg. Chem.* **12**, 236.
- Farragi, M. and Y. Tendler, 1972, *J. Chem. Phys.* **56**, 3287.
- Feistel, G.R. and T.P. Mathai, 1968, *J. Amer. Chem. Soc.* **90**, 2988.
- Fisher, E.O. and H. Fisher, 1965, *J. Organometal. Chem.* **3**, 181.
- Fong, F.K., 1967, *Prog. Solid State Chem.* **3**, 135.
- Fugawa, T., Y. Fujiwara, K. Yokoo and H. Taniguchi, 1981, *Chem. Lett.* 1771.
- Fugawa, T., Y. Fujiwara and H. Taniguchi, 1982, *Chem. Lett.*, 601.
- Ganopol'skii, V.T., V.F. Barkovskii and N.P. Ipatova, 1966, *Zh. Prikl. Spektrosk.* **5**, 805.
- Girard, P., J.L. Namy and H.B. Kagan, 1980, *J. Amer. Chem. Soc.* **102**, 2693.
- Girard, P., R. Couffignal and H.B. Kagan, 1981, *Tetrahedron Lett.*, 3959.
- Girard, P., J.L. Namy, J. Collin and H.B. Kagan, 1982, unpublished results.
- Griller, D. and K.U. Ingold, 1980, *Acc. Chem. Res.* **13**, 317.
- Hadenfeldt, C., H. Jacobs and R. Juza, 1970, *Z. Anorg. Allg. Chem.* **379**, 144.
- Hayes, R.G. and J.L. Thomas, 1969a, *Inorg. Chem.* **8**, 2521.
- Hayes, R.G. and J.L. Thomas, 1969b, *J. Amer. Chem. Soc.* **91**, 6876.
- Huck, H.M. and K. Wieghardt, 1980, *Angew. Chem. Int. Engl. Ed.* **19**, 558.
- Imamoto, T., T. Kusumoto, Y. Hatanaka and M. Yokohama, 1982, *Tetrahedron Lett.*, 1353.
- Jayaraman, A., 1980, *Angew. Chem. Int. Engl. Ed.* **19**, 587.
- Johnson, D.A., 1974, *J. Chem. Soc. Dalton Trans.*, 1671.
- Johnson, D.A., 1977, in: *Advances in Inorganic Chemistry and Radiochemistry*, vol. 20, eds. H.J. Emeleus and A.G. Sharpe (Academic Press, New York) p. 1.

- Johnson, K.E. and J.N. Sandoe, 1969, *J. Chem. Soc. A*, 1694.
- Johnson, K.E., J.R. MacKenzie and J.N. Sandoe, 1968, *J. Chem. Soc. A*, 2644.
- Kagan, H.B., J.L. Namy and P. Girard, 1981, *Tetrahedron* **37**, suppl. 1, 175.
- Kamenskaya, A.N., N.B. Mikheev and N.A. Konovalova, 1977, *Zh. Neorg. Khim.* **22**, 2130 [*Chem. Abstr.* **87**, 126525 q].
- Klemm, W. and W. Schuth, 1929, *Z. Anorg. Allg. Chem.* **184**, 352.
- Konstantatos, J. and E. Vrachnou-Astra, 1982, *Inorg. Chem.* **21**, 122.
- Kulyako, Yu.M., B.F. Myasocdov and I.S. Sklyarenko, 1945, *Zh. Neorg. Khim.* **20**, 1799.
- Lappert, M.F., P.I.W. Yanow, J.L. Atwood, R. Shakir and J. Holton, 1980, *J. Chem. Soc., Chem. Commun.*, 987.
- Leger, J.M., N. Yacoubi and J. Lories, 1981, *J. Solid State Chem.* **36**, 261.
- McClure, D.S. and Z. Kiss, 1963, *J. Chem. Phys.* **39**, 3251.
- McColm, I.J. and S. Thompson, 1972, *J. Inorg. Nucl. Chem.* **34**, 3801.
- Maple, M.B. and D.K. Wohlleben, 1971, *Phys. Rev. Lett.* **27**, 511.
- Marks, T.J., 1978, *Progr. Inorg. Chem.* **24**, 51.
- Marsh, J.K., 1942, *J. Chem. Soc.*, 398.
- Marsh, J.K., 1943, *J. Chem. Soc.*, 531.
- Marsh, J.K., 1946, *J. Chem. Soc.*, 20.
- Massaux, J., J.F. Desreux, C. Delchambre and G. Duyckaerts, 1980, *Inorg. Chem.* **19**, 1893.
- Matignon, C.A. and E. Cazes, 1906a, *Ann. Chim. Phys.* **8**, 417.
- Matignon, C.A. and E. Cazes, 1906b, *C.R. Hebd. Seances Acad. Sci. Paris* **142**, 83.
- Morss, L.R., 1976, *Chem. Rev.* **76**, 827.
- Murphy, E. and G.E. Toogood, 1971, *Inorg. Nucl. Chem. Lett.* **7**, 755.
- Namy, J.L., P. Girard and H.B. Kagan, 1977, *Nouv. J. Chim.* **1**, 5.
- Namy, J.L., P. Girard, H.B. Kagan and P. Caro, 1981, *Nouv. J. Chim.* **5**, 479.
- Namy, J.L., J. Soupe and H.B. Kagan, 1983, *Tetrahedron Lett.*, 765.
- Natale, N.R., 1982, *Tetrahedron Lett.*, 5009.
- Rossmannith, K., 1979, *Monatsh. Chem.* **110**, 109.
- Salot, S. and J.C. Warf, 1968, *J. Am. Chem. Soc.* **90**, 1932.
- Selwood, P.W., 1956, *Magnetochemistry*, 2nd Ed. (Interscience, New York/London) p. 157.
- Soupe, J., J.L. Namy and H.B. Kagan, 1981, unpublished results.
- Soupe, J., J.L. Namy and H.B. Kagan, 1982, *Tetrahedron Lett.* **23**, 3497.
- Suleimanov, G.Z., L.F. Rybakova, Ya.A. Nurev, T.Kh. Kurbanov and I.P. Beletskaya, 1982, *J. Organometal. Chem.* **235**, C19.
- Thompson, D.S., D.W. Schaefer and J.S. Waugh, 1966a, *Inorg. Chem.* **5**, 325.
- Thompson, D.S., E.E. Hazen and J.S. Waugh, 1966b, *J. Chem. Phys.* **44**, 2954.
- Tilley, T.D. and R.A. Andersen, 1981, *Inorg. Chem.* **20**, 3267.
- Tilley, T.D. and R.A. Andersen, 1982, *J. Amer. Chem. Soc.* **104**, 1772.
- Tilley, T.D., R.A. Andersen and B. Spencer, 1980, *Inorg. Chem.* **19**, 2999.
- Tilley, T.D., R.A. Andersen and A. Zalkin, 1982, *J. Amer. Chem. Soc.* **104**, 3725.
- Tilley, T.D., R.A. Andersen, B. Spencer and A. Zalkin, 1982a, *Inorg. Chem.* **21**, 2647.
- Wang, P.J. and H. Drickhamer, 1973, *J. Chem. Phys.* **58**, 4444.
- Warf, J.C., 1970, *Angew. Chem. Int. Engl. Ed.* **9**, 383.
- Watson, P.L., 1980, *J. Chem. Soc., Chem. Commun.*, 652.
- Watson, P.L., J.F. Whitney and R.L. Harlow, 1981, *Inorg. Chem.* **20**, 3271.
- Watt, G.W. and E.W. Gillow, 1969, *J. Amer. Chem. Soc.* **91**, 775.
- White, J.D. and G.L. Larson, 1978, *J. Org. Chem.* **43**, 4555.
- Zinnen, H.A., J.J. Pluth and W.J. Evans, 1980, *J. Chem. Soc., Chem. Commun.*, 810.



## SUBJECT INDEX

- activation
  - for H<sub>2</sub> absorption 18
- activation energy
  - for atomic motion of metal atoms 45
  - for decomposition of ternary hydrides 45
  - for diffusion of H atoms 29, 31
- AIB<sub>2</sub>-related ternary structures 207
- AlB<sub>2</sub>-type 166
- amorphous alloys 47
- anionic organoytterbium complexes 543
- antiferromagnetic coupling or interaction 15, 68, 73
- application of hydrides 80
- aqueous Sm<sup>2+</sup>
  - absorption spectra 537
- aqueous Yb<sup>2+</sup>
  - absorption spectra 537
- Arrhenius plots
  - of H<sub>2</sub> absorption 32
  - of H atom diffusion 28
- asymptotic Curie temperature 67
- atomic disordering
  - upon H<sub>2</sub>-absorption 54, 68
- B-B linkage in ternary borides 266
- BaAl<sub>4</sub>-type derivative 211, 220, 223, 225
- BaCd<sub>11</sub>-type derivative 272
- BaCuSn<sub>2</sub>-type 197
- band model
  - for 3d electrons 13, 43, 75
- band structure calculation
  - for intermetallics 14
  - for ternary hydrides 40
- bis(phenylethynyl) ytterbium 529
- boron compounds
  - (see quaternary and higher order systems)
  - (see ternary systems)
- bulk modulus 9
- Ca<sub>3</sub>Ag<sub>8</sub>-type derivative 169
- CaBe<sub>2</sub>Ge<sub>2</sub>-type 220
- CaCu<sub>5</sub>-type derivative 229, 231, 232, 233, 235
- CaIn<sub>2</sub>-type 169
- calorimetric measurements
  - pertaining to H<sub>2</sub> sorption 28, 34, 35, 42, 43
- Carnot efficiency 84
- CaTiO<sub>3</sub>-type 211
- CeAl<sub>2</sub>Ga<sub>2</sub>-type 211
- Ce<sub>2</sub>Co<sub>15</sub>Al<sub>2</sub>-type 257
- CeCo<sub>3</sub>B<sub>2</sub>-type 232, 235
- CeCo<sub>3</sub>B<sub>2</sub>-type derivative 233
- CeCo<sub>4</sub>B-type 231
- CeCo<sub>4</sub>B<sub>4</sub>-type 263
- Ce<sub>2</sub>Co<sub>5</sub>B<sub>2</sub>-type 203
- Ce<sub>2</sub>Co<sub>7</sub>B<sub>3</sub>-type 232
- Ce<sub>3</sub>Co<sub>11</sub>B<sub>4</sub>-type 231
- Ce<sub>3</sub>Co<sub>8</sub>Si-type 184
- CeCr<sub>2</sub>Al<sub>20</sub> 284
- CeCr<sub>2</sub>B<sub>6</sub>-type 269
- CeCu<sub>2</sub>-type 164
- CeCu<sub>2</sub>-type derivative 160
- CeFeSi-type 154
- CeMn<sub>4</sub>Al<sub>8</sub>-related type 271, 277
- CeMn<sub>4</sub>Al<sub>8</sub>-type 277
- Ce<sub>2</sub>Mn<sub>7</sub>Al<sub>10</sub>-type 268
- CeNi<sub>3</sub>-type derivative 184, 191
- Ce<sub>2</sub>Ni<sub>7</sub>-type derivative 203
- Ce<sub>2</sub>NiGa<sub>10</sub>-type 241
- Ce(Ni<sub>1.25</sub>Si<sub>1.75</sub>)<sub>2</sub> (AIB<sub>2</sub>-type) 166
- CeNiSi<sub>2</sub>-type 197
- CeNi<sub>2</sub>Si<sub>2</sub>-type 211
- Ce<sub>2</sub>Ni<sub>15</sub>Si<sub>2</sub>-type 253
- Ce<sub>2</sub>Ni<sub>17</sub>Si<sub>5</sub>-type 272
- Ce<sub>2</sub>Ni<sub>17</sub>Si<sub>9</sub> 281
- Ce<sub>3</sub>Ni<sub>2</sub>Si<sub>8</sub>-type 203
- Ce<sub>3</sub>Ni<sub>6</sub>Si<sub>2</sub>-type 169
- Ce<sub>5</sub>Ni<sub>2</sub>Si<sub>3</sub>-type 139
- Ce<sub>6</sub>Ni<sub>2</sub>Si<sub>3</sub>-type 126
- Ce<sub>7</sub>Ni<sub>2</sub>Si<sub>5</sub>-type 140
- Ce<sub>14</sub>Ni<sub>8</sub>Si<sub>9</sub>-type 141
- Ce<sub>15</sub>Ni<sub>4</sub>Si<sub>13</sub>-type 140
- CeNi<sub>5</sub>Sn-type 242
- CeRe<sub>4</sub>Si<sub>2</sub>-type 243
- charge transfer 13, 43, 55, 61, 75, 77
- chemisorption of H<sub>2</sub> 23
- clusters of 3d atoms 54, 58, 69, 73
- compensation
  - of sublattice magnetization 15, 70
- compensation temperature 16, 70, 97-102
- compounds
  - intermetallic of rare earths 4
- compressibility
  - correlation with H<sub>2</sub> absorption 42
- concentration fluctuations of H atoms 67
- conductivity of ternary hydrides 79
- CrB-type 129, 130
- Cr<sub>23</sub>C<sub>6</sub>-type derivative 280
- critical pressure and temperature
  - for H<sub>2</sub> absorption 18
- crystal field effects 11
- crystal structure
  - of intermetallics 6, 51, 52, 97-103

- of ternary hydrides 48,103  
 crystallization of amorphous alloys 47  
 CsCl-type derivative 194  
 Cu<sub>3</sub>Au filled-up variant 202  
 Cu<sub>3</sub>Au-type 202  
 Curie temperature 12, 16, 17, 58, 97–103  
 Curie–Weiss law 54  
 cyclooctatetraenyl ytterbium 535
- decomposition of ternary hydrides 44, 53, 54  
 density of states 13, 17, 43, 53, 76  
 dicyclopentadienyl samarium complexes 529  
 dicyclopentadienyl ytterbium 528  
 dicyclopentadienyl ytterbium complexes 529
- diffraction  
 neutron 48, 57, 64  
 X-ray 44, 48, 54, 55, 58
- diffusion  
 of H atoms 32  
 of metal atoms 28
- diorgano ytterbium complexes  
 reaction with nucleophiles 561
- diorgano ytterbium compounds  
 reaction with ketones and aldehydes 561
- dipolar relaxation in PMR 28
- dipositive oxidation state of lanthanide  
 thermodynamic stability of 536
- distortion (*see* lattice distortion)
- distribution of H atoms  
 in ternary hydrides 39, 49, 65
- divalent polyfluorophenyl samarium compounds 528
- divalent polyfluorophenyl ytterbium compounds 528
- DyFe<sub>6</sub>Al<sub>6</sub> 277  
 Dy<sub>3</sub>Ni<sub>7</sub>B<sub>2</sub>-type 191
- electric resistivity  
 in ternary hydrides 79
- electrochemical cells 85
- electronegativity 8, 62, 74
- electron paramagnetic resonance 54, 79
- electrons  
 concentration 11, 67  
 conduction 11  
 Coulomb repulsion 13, 54  
 spin polarized 12, 17, 75  
 wavefunction 11
- energy bands 13, 42, 75
- energy carrier 80
- enhancement 54
- enthalpy  
 of formation of intermetallics 9  
 of formation of ternary hydrides 32, 37  
 of formation of vacancies 10
- entropy  
 configurational, of H atoms 35, 49  
 excess in ternary hydrides 35  
 of formation of ternary hydrides 32  
 of H<sub>2</sub> 35  
 vibrational, of H atoms 35
- ErIr<sub>3</sub>B<sub>2</sub>-type 233  
 Er<sub>21</sub>Ni<sub>10</sub>Ga<sub>4</sub>-type 123  
 Er<sub>4</sub>Ni<sub>3</sub>Si or Er(Ni<sub>0.75</sub>Si<sub>0.25</sub>) (CrB-type) 129  
 Er<sub>2</sub>Pd<sub>2</sub>Si-type 144  
 Eu<sup>2+</sup>  
 reduction potential 536  
 compounds 526
- EuNi<sub>12</sub>B<sub>8</sub> 283
- exchange  
 interaction between 3d moments 13, 75  
 interaction between 4f moments 11, 67  
 splitting of 3d band 14, 77
- Fe<sub>2</sub>As-type derivative 154  
 FeB-type 129, 130  
 Fe<sub>3</sub>C-type derivative 192  
 Fe<sub>2</sub>P-type derivative 157  
 Fermi energy 11  
 Fermi wave vector 12, 67
- ferromagnetic coupling or ordering 15, 56, 63, 68, 78
- Gd<sub>3</sub>Cu<sub>4</sub>Ge<sub>4</sub>-type 173  
 Gd<sub>4</sub>Ni<sub>3</sub>Cu or Gd(Ni<sub>0.75</sub>Cu<sub>0.25</sub>) (FeB-type) 129  
 Gd<sub>3</sub>NiSi<sub>2</sub>-type 139
- H atom diffusion in metals 28  
 H–H distance 51, 89  
 H<sub>2</sub>  
 absorption in intermetallics 17, 32, 47, 80, 88  
 pressure above ternary hydrides 17  
 pressure composition isotherms 17  
 purification 82  
 storage 84  
 H<sub>2</sub> getters 82  
 heat capacity measurements 28,43  
 heat of formation (*see* enthalpy)  
 heat pumps 82  
 HfFe<sub>6</sub>Ge<sub>6</sub>-type 273  
 HfFe<sub>2</sub>Si<sub>2</sub>-type 221  
 Hf<sub>3</sub>Ni<sub>2</sub>Si<sub>3</sub>-type 149  
 Hf<sub>3</sub>P<sub>2</sub> filled-up variant 139  
 HoCoGa<sub>5</sub>-type 247  
 Ho<sub>2</sub>CoGa<sub>8</sub>-type 228  
 Ho<sub>4</sub>Co<sub>3</sub> filled-up variant 126  
 Ho<sub>6</sub>Co<sub>7</sub>Ga<sub>21</sub>-type 228  
 HoNiAl-type 157  
 Ho<sub>3</sub>Ni<sub>2</sub>Ga<sub>9</sub> 210  
 Ho<sub>4</sub>Ni<sub>10</sub>Ga<sub>21</sub>-type 268  
 hybridization of 3d electron states 14, 77
- hydrogen  
 bonding in intermetallics 75  
 hyperfine fields 54, 74  
 splitting 59, 74  
 hysteresis  
 sorption hysteresis 26
- indirect exchange interaction 11
- intermetallic compounds of rare earths 4

- isomer shift  
 change upon H absorption  
 59, 63, 74, 76  
 in intermetallics 15
- isotherms  
 pressure composition 17
- isotope separation 87
- kinetics of H<sub>2</sub> sorption 20
- La<sub>3</sub>Al<sub>11</sub>-type derivative 210
- Lacher model 34
- LaCoAl<sub>4</sub>-type 237
- La<sub>3</sub>Co<sub>2</sub>Sn<sub>7</sub>-type 201
- LaIrSi 164
- LaIr<sub>2</sub>Si<sub>2</sub> 220
- La<sub>3</sub>Ni<sub>4</sub>Ga<sub>2</sub> 153
- lanthanide metals  
 cocondensation with un-  
 saturated hydrocarbons  
 563
- lanthanide phosphine complex  
 crystal structure 546
- lanthanoid systems  
 valence change at high pres-  
 sure 537
- LaPd<sub>3</sub>B 211
- LaPtSi-type 162
- La<sub>2</sub>Re<sub>3</sub>B<sub>7</sub>-type 237
- LaRe<sub>2</sub>Si<sub>2</sub>-type 222
- La<sub>3</sub>Rh<sub>4</sub>Ge<sub>4</sub> 175
- lattice expansion  
 upon H<sub>2</sub> absorption 26,  
 48, 51, 60, 67, 68
- lattice disorder  
 upon H<sub>2</sub> absorption 56
- lattice distortion or deforma-  
 tion  
 upon H<sub>2</sub> absorption 26,  
 41, 48
- Laves phases  
 ordering in ternary 151,  
 165, 166
- Ln(CN)<sub>2</sub> 528
- LnFX  
 synthesis of 527
- long-range periodicity  
 loss during H<sub>2</sub> absorption  
 48
- low-valent Ce compounds  
 reduction of organic com-  
 pounds by 526
- LuRh<sub>4</sub>B<sub>4</sub>-type 267
- LuRuB<sub>2</sub>-type 197
- LuRu<sub>4</sub>B<sub>4</sub>-type 267
- magnetic interactions  
 between 3d moments 13,  
 53, 54, 57, 63  
 between 4f moments 11,  
 67  
 between 4f and 3d moments  
 15, 67
- magnetic measurements  
 results of in intermetallics  
 and their hydrides  
 96-103
- magnetic moments  
 of 3d electrons 13  
 of 4f electrons 11
- magnetic properties  
 of intermetallics 10  
 of ternary hydrides 53
- magnetic susceptibilities  
 methods of measuring 537
- magneto-volume effects 58
- mean free path reduction of  
 conduction electrons  
 68
- metastable character  
 of ternary hydrides 44
- Mg<sub>3</sub>Cr<sub>2</sub>Al<sub>18</sub>-related type 284
- MgCuAl<sub>2</sub>-type 199
- Mg<sub>2</sub>Cu<sub>3</sub>Si-related type 151
- Mg<sub>2</sub>Cu<sub>3</sub>Si-type 151, 166
- Mg<sub>6</sub>Cu<sub>16</sub>Si<sub>7</sub>-related type 209
- Mg<sub>6</sub>Cu<sub>16</sub>Si<sub>7</sub>-type 209
- MgZn<sub>2</sub>-type 151, 165, 166
- MgZn<sub>2</sub>-type derivative 166
- Miedema model 8, 37
- miscibility gap 17
- MnCu<sub>2</sub>Al-type 194
- molecular field model 16
- Mo<sub>2</sub>NiB<sub>2</sub>-related type 144
- Mössbauer effect spectroscopy  
 results of in intermetallics  
 15, 43  
 results of in ternary hy-  
 drides 47, 54, 59, 62,  
 70, 73, 74
- NaZn<sub>13</sub>-type derivative 281
- NbCoB<sub>2</sub>-related type 195
- Nb<sub>2</sub>Cr<sub>4</sub>Si<sub>5</sub>-type 226
- NdCo<sub>4</sub>B<sub>4</sub>-type 262
- Nd<sub>3</sub>Ni<sub>13</sub>B<sub>2</sub>-type 229
- NdNiGa<sub>2</sub>-type 198
- NdRe<sub>4</sub>Si<sub>2</sub>-type 245
- neutron diffraction 48, 51, 57,  
 64
- neutron moderators 88
- neutron scattering 29, 35
- NMR  
 results of measurements in  
 ternary hydrides 28
- organometallic divalent lantha-  
 nides  
 acidolysis 548
- paramagnetic Curie tempera-  
 ture 12
- Pauli paramagnetism 15, 54,  
 63
- PbCl<sub>2</sub>-type derivative 160
- PbFCl-type 154
- phase diagrams 6  
 La-Ni diagram 5
- phase separation during de-  
 composition of ternary  
 hydrides 44
- photoemission spectroscopy  
 results in intermetallics 15  
 results in ternary hydrides  
 24
- PhSmI  
 in THF solutions 560
- physical properties of ternary  
 hydrides 47
- "PhYbI"  
 selectivity towards ester  
 functions 561
- plateau pressure 17
- poisoning  
 of surface during H<sub>2</sub> ab-  
 sorption 24
- PrCo<sub>2</sub>Ga-type 191
- preparation  
 of intermetallics 4  
 of ternary hydrides 18
- pressure composition isotherms  
 17, 32
- PrNi<sub>2</sub>Al<sub>3</sub> 235
- PrNi<sub>2</sub>Al<sub>5</sub>-type 252
- Pr<sub>2</sub>Ni<sub>2</sub>Al 144
- PrNiGa<sub>3</sub> 225
- Pr<sub>14</sub>Ni<sub>6</sub>Si<sub>11</sub>-type 141
- proton magnetic resonance (*see*  
 NMR)
- Pr(Pt<sub>0.5</sub>Ge<sub>0.5</sub>)<sub>2</sub> (CeCu<sub>2</sub>-type)  
 164

- $\text{Pr}_3\text{Rh}_4\text{Sn}_{13}$  240  
 quasi-elastic neutron scattering 29  
 quaternary and higher order systems  
   B-Ca-Rh-Sc 503  
   B-Ce-Ir-Os 482  
   B-Co-Er-Rh 522  
   B-Dy-Ir-Rh 482  
   B-Dy-Rh-Ru 484  
   B-Er-Gd-Rh 484  
   B-Er-Ho-Rh 485, 520  
   B-Er-Ir-Rh 486  
   B-Er-Rh-Ru 488  
   B-Er-Rh-Sm 489  
   B-Er-Rh-Tm 490, 520  
   B-Er-Rh-Y 491  
   B-Gd-Rh-Y 491  
   B-Ho-Ir-Rh 492, 520  
   B-Ho-Lu-Rh 493  
   B-Ir-La-Os 494  
   B-Ir-Lu-Y 495  
   B-Ir-Os-Pr 500  
   B-Ir-Os-Sm 500  
   B-Ir-R-Rh 501  
   B-Ir-Rh-Sc-Y 504  
   B-La-Lu-Rh-Ru 494  
   B-La-Rh-Y 495  
   B-La-U-Y 495  
   B-Lu-R-Ru 496  
   B-Lu-Rh-Th 497  
   B-Lu-Rh-Th-Y 499  
   B-Lu-Rh-Tm 498  
   B-Lu-Rh-Y 499  
   B-Lu-Ru-Sc 496  
   B-Lu-U-Y 499  
   B-R-Rh-Ru 502  
   B-R-Rh-Sc 502  
   B-Rh-Ru-Y 505  
   B-Rh-Sc-Th 504  
   B-Rh-Th-Y 504  
   B-Ru-Sc-Y 504  
   B-Ru-Th-Y 505  
 rare earth intermetallics  
   composition and structure 4  
    $\text{H}_2$  absorption characteristics 17, 90-95  
   magnetic properties 10  
   relative stability 8  
 $\text{Re}_3\text{B}$ -type derivative 199  
 Rees model 34  
 resistivity (*see* electrical resistivity)  
 reviews  
   on metal hydrides 3  
   on rare earth intermetallics 6, 11  
 $\text{Rh}_{20}\text{Si}_{13}$  filled-up variant 139  
 rigid band model 42  
 RKKY interaction 12, 68, 72  
 samarium (II) dicyclopentadienide 532  
 saturation magnetization  
    $\text{H}_2$  induced reduction 67  
 $\text{Sc}_2\text{Co}_{21}\text{B}_6$  280  
 $\text{Sc}_2\text{CoSi}_2$ -type 145  
 $\text{Sc}_2\text{Co}_3\text{Si}$ -type 151  
 $\text{Sc}_2\text{Co}_3\text{Si}_5$  223  
 $\text{Sc}_3\text{Co}_2\text{Si}_3$ -type 149  
 $\text{Sc}_4\text{CoSi}$  or  $\text{Sc}_2(\text{Co}, \text{Si})(\text{Ti}_2\text{Ni})$ -type 123  
 $\text{Sc}_4\text{CoSi}_7$ -type 169  
 $\text{Sc}_5\text{Co}_4\text{Si}_{10}$ -type 182  
 $\text{Sc}_2\text{Cr}_4\text{Si}_5$  226  
 $\text{ScFe}_6\text{Ge}_6$  273  
 $\text{ScFeSi}_2$  201  
 $\text{ScFe}_2\text{Si}_2$  221  
 $\text{Sc}_2\text{Fe}_3\text{Si}_5$ -type 222  
 $\text{ScIr}_3\text{B}_4$  251  
 $\text{ScMnSi}_2$  199  
 $\text{Sc}_4\text{Mn}_4\text{Si}_7$  180  
 $\text{Sc}(\text{Ni}_{.5}\text{Al}_{.5})_2$  ( $\text{MgZn}_2$ -type) 165  
 $\text{Sc}_6\text{Ni}_7\text{Al}_{16}$  209  
 $\text{Sc}_3\text{Ni}_4\text{Ge}_4$  173  
 $\text{ScNiSi}_3$ -type 224  
 $\text{ScNi}_2\text{Si}_3$ -type 236  
 $\text{Sc}_6\text{Ni}_{16}\text{Si}_7$  209  
 $\text{ScRe}_2\text{Si}_3$ -type 236  
 $\text{Sc}_2\text{Re}_3\text{Si}_4$ -type 204  
 $\text{Sc}_3\text{Re}_2\text{Si}_3$ -type 149  
 $\text{Sc}_4\text{Rh}_7\text{Ge}_6$  202  
 $\text{ScRhSi}$ -type 160  
 $\text{ScRhSi}_2$  195  
 $\text{ScRh}_3\text{Si}_7$ -type 270  
 $\text{Sc}_2\text{RuAl}_3$  166  
 $\text{Sc}_2\text{Ru}_5\text{B}_4$  226  
 $\text{ScRuGe}$  157  
 secondary diiodo samarium alkoxides  
   as efficient reagents for reduction of aldehydes 555  
 Sm  
   reaction with organic iodides 560  
 $\text{Sm}^{2+}$   
   effective moment 537  
   electrochemical properties 542  
   electron transfer reactions involving transition metal complexes 549  
   oxidation by halogens 549  
   oxidation by halogens to obtain anhydrous  $\text{Ln}^{3+}$  salts 549  
   oxidation rate in aqueous solution 542, 548  
   redox potential 549  
   reduction potential 536  
   size of divalent ion 542  
 $\text{Sm}^{2+}$  and  $\text{Sm}^{3+}$   
   ionic radii compared 545  
 $\text{Sm}^{2+}$  compounds  
   interactions with solvents 542  
   magnetic moments of 537  
   main preparative methods 527  
   solubility in THF 542  
 $\text{Sm}^{2+}$  derivatives 527  
 $\text{Sm}(\text{C}_5\text{Me}_5)_2$   
   preparation of 529, 537  
 $\text{Sm}(\text{C}_5\text{Me}_5)_2(\text{THF})_2$   
   crystal structure 543  
   reaction with CO and NO  
     polymerization of ethylene 562  
   Sm-C and Sm-O lengths in 545  
 $\text{Sm}(\text{C}_5\text{Me}_4\text{Et})_2$   
   preparation of 537  
 $\text{SmCO}_3$   
   preparation of 533  
 $\text{SmCl}_2$  532  
 $\text{Sm}(\text{ClO}_4)_2$   
   UV-visible absorption spectra of 537  
 $\text{Sm}_{26}\text{Co}_{11}\text{Ga}_6$ -type 126  
 $\text{SmCp}_2$   
   synthesis of 533  
 $\text{SmCp}_2(\text{THF})$   
   IR spectrum of 545  
   X-ray diffraction patterns 544

- $\text{Sm}_{17}(\text{Fe}_4\text{B}_4)_{15}$ -type 249  
 Sm halides  
   preparation of 532  
 $\text{SmI}_2$  529, 533  
   as reagent for coupling of aldehydes or ketones into pinacols 552  
   as reducing agent in organic media 537  
   as selective reagent for reduction of an aldehyde group in presence of a ketone 552  
   catalytic coupling of allylic or benzylic halides with ketones 555  
   coupling of allylic and benzylic halides 551  
   electron transfer to an organic substrate 550  
   fragmentation reactions 559  
   mediation of mechanism of ketone alkylations 556  
   promotion of reaction between halides and aldehydes 557  
   reaction towards various transition metal complexes 549  
   reaction with acid chlorides 558  
   reaction with aromatic aldehydes 552  
   reaction with aromatic or vinylic halides 550  
   reduction of aldehydes into alcohols 552  
   reduction of aliphatic ketones 552  
   reduction of alkyl halides into alkane 550  
   reduction of alkyl tosylates 550  
   reduction of aromatic ketones 552  
   reduction of conjugated double bonds 553  
   reduction of nitroaromatic compounds to amines 557  
   reduction of sulfoxides to sulfides 553  
   UV-visible absorption spectra of 537  
 Sm iodides  
   preparation of 532  
 $\text{Sm}(\text{Mn}_{.17}\text{Ga}_{.83})_2$  ( $\text{CaIn}_2$ -type) 169  
 SmO 527  
 $\text{Sm}(\text{OAc})_2$   
   synthesis of 533  
 $\text{Sm}(\text{OEt})_2$   
   synthesis of 533  
 Sm(II) organometallic species  
   preparation by metal vapor technique 529  
 SmS 539  
 sorption hysteresis 26  
 specific heat measurements  
   results of in intermetallics and hydrides 35, 42, 43  
 spin-lattice relaxation in PMR 28  
 $\text{SrNi}_{12}\text{B}_6$ -type 283  
 $\text{SrSi}_2$ -type derivative 164  
 stability  
   relative of intermetallics 8  
   of ternary hydrides 39  
 Stoner criterion 13  
 structure (see crystal structure)  
 substituted dicyclopentadienide ytterbium 532  
 superconduction  
   in ternary hydrides 80  
 superparamagnetism  
   in ternary hydrides 54  
 surface effects  
   during  $\text{H}_2$  absorption 24  
 surface migration of H atoms 23  
 $\text{Ta}_3\text{B}_4$ -type derivative 142  
 technical applications of metal hydrides 80  
 ternary systems  
   Al-B-Ce 340  
   Al-B-La 401  
   Al-B-Lu 417  
   Al-B-Y 460  
   Al-B-Yb 479  
   B-Ca-Er 367  
   B-Ca-Y 461  
   B-Ce-Co 341  
   B-Ce-Cr 344  
   B-Ce-Cu 345  
   B-Ce-Eu 346  
   B-Ce-Fe 346  
   B-Ce-Ge 348  
   B-Ce-Hf 348  
   B-Ce-Ir 348  
   B-Ce-La 349  
   B-Ce-Mn 349  
   B-Ce-Mo 350  
   B-Ce-Nb 351  
   B-Ce-Ni 352  
   B-Ce-Os 354  
   B-Ce-Re 354  
   B-Ce-Rh 354  
   B-Ce-Ru 354  
   B-Ce-Si 355  
   B-Ce-Sm 356  
   B-Ce-Ta 356  
   B-Ce-Th 357  
   B-Ce-U 357  
   B-Ce-V 358  
   B-Ce-W 359  
   B-Co-Dy 360  
   B-Co-Er 368  
   B-Co-Eu 376  
   B-Co-Gd 381  
   B-Co-Ho 395  
   B-Co-La 402  
   B-Co-Lu 418  
   B-Co-Nd 423, 513  
   B-Co-Pr 430  
   B-Co-Sc 433  
   B-Co-Sm 438  
   B-Co-Tb 448  
   B-Co-Tm 455  
   B-Co-Y 461  
   B-Co-Yb 479, 520  
   B-Cr-Dy 361  
   B-Cr-Er 369  
   B-Cr-Gd 384, 508  
   B-Cr-Ho 396  
   B-Cr-La 404  
   B-Cr-Lu 419  
   B-Cr-Nd 424  
   B-Cr-Pr 430  
   B-Cr-Sc 435  
   B-Cr-Sm 442  
   B-Cr-Tb 448  
   B-Cr-Tm 456  
   B-Cr-Y 463  
   B-Cu-Gd 385  
   B-Dy-Fe 361  
   B-Dy-Ge 361  
   B-Dy-Ir 362

ternary systems (*cont'd*)

- B-Dy-La 505  
 B-Dy-Mn 363  
 B-Dy-Mo 363  
 B-Dy-Ni 363, 506  
 B-Dy-Os 363  
 B-Dy-Re 364, 506  
 B-Dy-Rh 365  
 B-Dy-Ru 365  
 B-Dy-Si 366  
 B-Dy-U 366  
 B-Dy-V 367  
 B-Dy-W 367  
 B-Er-Fe 369, 507  
 B-Er-Gd 370  
 B-Er-Ho 370  
 B-Er-Ir 370  
 B-Er-La 371  
 B-Er-Mn 371  
 B-Er-Mo 371  
 B-Er-Ni 371, 507  
 B-Er-Os 372  
 B-Er-Re 373  
 B-Er-Rh 373, 507, 520  
 B-Er-Ru 374  
 B-Er-U 375  
 B-Er-V 376  
 B-Er-W 376  
 B-Er-Yb 376  
 B-Eu-Gd 376  
 B-Eu-Hf 377  
 B-Eu-Ir 377  
 B-Eu-La 377  
 B-Eu-Ni 378  
 B-Eu-Os 378  
 B-Eu-Pd 379  
 B-Eu-Rh 379  
 B-Eu-Ru 379  
 B-Eu-Sm 508  
 B-Eu-Sr 380  
 B-Eu-Ta 380  
 B-Eu-W 380  
 B-Eu-Yb 381  
 B-Fe-Gd 386  
 B-Fe-Ho 396  
 B-Fe-La 405  
 B-Fe-Lu 419  
 B-Fe-Nd 425  
 B-Fe-Pr 431  
 B-Fe-Sc 435, 515  
 B-Fe-Sm 442  
 B-Fe-Tb 448  
 B-Fe-Tm 456, 519  
 B-Fe-Y 465  
 B-Gd-Ge 387  
 B-Gd-Hf 387  
 B-Gd-Ir 388  
 B-Gd-La 389  
 B-Gd-Mn 389  
 B-Gd-Mo 390, 509  
 B-Gd-Ni 390, 510  
 B-Gd-Os 390  
 B-Gd-Re 391  
 B-Gd-Rh 392  
 B-Gd-Ru 392  
 B-Gd-Si 393  
 B-Gd-Ti 393  
 B-Gd-V 394  
 B-Gd-W 394, 511  
 B-Gd-Zr 394  
 B-Ge-La 406  
 B-Ge-Tb 450  
 B-Ge-Y 466  
 B-Hf-La 407  
 B-Ho-Ir 397  
 B-Ho-La 397  
 B-Ho-Mn 398  
 B-Ho-Mo 398  
 B-Ho-Ni 398, 512  
 B-Ho-Os 398  
 B-Ho-Re 399  
 B-Ho-Rh 400  
 B-Ho-Ru 401  
 B-Ho-V 401  
 B-Ho-W 401  
 B-Ho-Y 401  
 B-In-Sc 435  
 B-Ir-La 407  
 B-Ir-Lu 419  
 B-Ir-Nd 426  
 B-Ir-Pr 432  
 B-Ir-Sc 436  
 B-Ir-Sm 444  
 B-Ir-Tb 450  
 B-Ir-Tm 456  
 B-Ir-Y 467  
 B-Ir-Yb 480  
 B-La-Mo 407  
 B-La-Nd 408  
 B-La-Ni 408  
 B-La-Os 410  
 B-La-Re 411  
 B-La-Rh 412  
 B-La-Ru 412  
 B-La-Si 412  
 B-La-Sm 413  
 B-La-Ta 415  
 B-La-Tm 512  
 B-La-U 415  
 B-La-W 416  
 B-La-Y 416  
 B-La-Yb 417  
 B-Lu-Ni 419  
 B-Lu-Os 420  
 B-Lu-Re 421  
 B-Lu-Rh 421  
 B-Lu-Ru 423  
 B-Lu-U 423  
 B-M-Sm 516  
 B-Mn-Tb 451  
 B-Mn-Y 467  
 B-Mo-Tb 451  
 B-Mo-Y 468  
 B-Nd-Ni 426  
 B-Nd-Os 428  
 B-Nd-Rh 428, 514, 520  
 B-Nd-Ru 429  
 B-Nd-Si 429  
 B-Ni-Pr 432  
 B-Ni-Sc 436, 515  
 B-Ni-Sm 444  
 B-Ni-Tb 451, 518  
 B-Ni-Tm 456, 519  
 B-Ni-Y 469  
 B-Ni-Yb 480  
 B-Os-Pr 432  
 B-Os-Sc 436  
 B-Os-Sm 445  
 B-Os-Tb 451  
 B-Os-Tm 457  
 B-Os-Y 471  
 B-Os-Yb 480  
 B-Pb-Sc 437  
 B-Pd-R 338  
 B-Pr-Rh 432  
 B-Pr-Ru 433  
 B-R-Rh 339  
 B-Re-Sm 517  
 B-Re-Tb 452  
 B-Re-Tm 458  
 B-Re-Y 472  
 B-Rh-Sc 437  
 B-Rh-Sm 445  
 B-Rh-Tb 453  
 B-Rh-Tm 458, 519, 520  
 B-Rh-Y 473  
 B-Rh-Yb 481  
 B-Ru-Sc 437  
 B-Ru-Sm 446

- ternary systems (*cont'd*)
- B-Ru-Tb 453
  - B-Ru-Tm 459
  - B-Ru-Y 473
  - B-Ru-Yb 481
  - B-Sc-Sn 438
  - B-Sc-Tl 438
  - B-Si-Tb 454
  - B-Si-Y 474
  - B-Sm-Sr 447
  - B-Sm-Th 447
  - B-Sm-Y 447
  - B-Sm-Yb 448
  - B-Tb-V 454
  - B-Tb-W 454
  - B-Tb-Y 455
  - B-Th-Y 475
  - B-Tm-Yb 519
  - B-U-Y 476
  - B-V-Y 477
  - B-W-Y 477
  - B-Y-Yb 478
- ThCr<sub>2</sub>Si<sub>2</sub>-type 211
- thermal compressor 86
- thermal conductivity 79
- thermodynamic description of
- H<sub>2</sub> sorption 32
- ThMn<sub>12</sub>-type derivative 277
- Th<sub>6</sub>Mn<sub>23</sub>-type derivative 209
- Th<sub>2</sub>Ni<sub>17</sub>-type derivative 253
- ThSi<sub>2</sub>-type derivative 162
- Th<sub>2</sub>Zn<sub>17</sub>-type derivative 257, 268
- TiFeSi-type with disorder 165
- TiFeSi<sub>2</sub>-type 199
- TiMnSi<sub>2</sub>-type 199
- Ti<sub>2</sub>Ni-type 123
- TiNiSi-type 160
- transition metal compounds
- composition and structure 4
  - H<sub>2</sub> absorption characteristics 17, 90-96
  - magnetic properties 10
  - relative stability 8
- trivalent lanthanide derivatives
- Lewis character 542
- U<sub>2</sub>Co<sub>3</sub>Si<sub>5</sub>-type 223
- U<sub>2</sub>Ni<sub>2</sub>Si<sub>7</sub>-type 228
- U<sub>3</sub>Ni<sub>4</sub>Si<sub>4</sub>-type 175
- U<sub>4</sub>Re<sub>7</sub>Si<sub>6</sub>-type 202
- vacancy formation 10, 45
- valence changes
- H<sub>2</sub> induced 54, 58, 78
- Van 't Hoff equation for H<sub>2</sub>
- absorption 32
- vibrational spectrum of H atoms 35
- volume expansion 27, 41, 48, 59, 66, 70
- V-phase type 180
- V<sub>12</sub>P<sub>7</sub> filled-up variant 126
- V<sub>6</sub>Si<sub>5</sub>-type derivative 226
- W<sub>2</sub>CoB<sub>2</sub>-related type 144
- W<sub>3</sub>CoB<sub>3</sub>-related type 141
- W<sub>2</sub>Cr<sub>21</sub>C<sub>6</sub>-type derivative 280
- Y<sub>3</sub>Co<sub>3</sub>Ga 141
- Y<sub>10</sub>Co<sub>7</sub>Ga<sub>3</sub>-type 139
- YCrB<sub>4</sub>-type 239
- Y<sub>2</sub>Fe<sub>4</sub>Si<sub>9</sub>-type 247
- YMnGa or Y(Mn, Ga)<sub>2</sub> 165
- Y<sub>2</sub>MnGa<sub>5</sub> or Y(Mn, Ga)<sub>17</sub>(Ga, Si)<sub>3</sub> (Cu<sub>3</sub>Au-type) 202
- YNiAl<sub>2</sub> 199
- YNiAl<sub>4</sub>-type 239
- YNi<sub>5</sub>Si<sub>3</sub>-type 258
- YNi<sub>10</sub>Si<sub>2</sub> 281
- Y<sub>3</sub>NiSi<sub>3</sub> 142
- YPd<sub>2</sub>Si-type 192
- YPd<sub>2</sub>Sn 194
- Y<sub>2</sub>ReB<sub>6</sub>-type 206
- Y<sub>3</sub>ReB<sub>7</sub>-type 181
- YRe<sub>4</sub>Si<sub>2</sub>-type 243
- Y<sub>3</sub>Rh<sub>2</sub>-type derivative 123
- YZn<sub>3</sub>-type derivative 195
- Yb<sup>2+</sup>
- electrochemical properties 542
  - electron transfer reactions involving transition metal complexes 549
  - oxidation by halogens 549
  - oxidation by halogens to obtain anhydrous Ln<sup>3+</sup> salts 549
  - oxidation rate in aqueous solution 542, 548
  - redox potential 549
  - reduction potential 536
  - size of divalent ion 542
  - tertiary phosphine complex of 545
- Yb<sup>2+</sup> ion and Co<sup>2+</sup> complexes
- reactions between 549
- Yb<sup>2+</sup> compounds
- interactions with solvents 542
  - magnetic moments of 537
  - main preparative methods 527
  - solubility in THF 542
- Yb<sup>3+</sup>
- effective magnetic moment 537
- Yb(bipy)<sub>4</sub>
- preparation of 536
- YbBr<sub>2</sub> 529
- Yb(C≡CCH<sub>3</sub>)<sub>2</sub> 536
- Yb(C≡C-C<sub>6</sub>H<sub>5</sub>)<sub>2</sub> 533
- Yb(C<sub>6</sub>F<sub>5</sub>)<sub>2</sub> 533
- Yb(C<sub>5</sub>Me<sub>5</sub>)<sub>2</sub> 533, 535
- Yb(C<sub>5</sub>Me<sub>5</sub>)<sub>2</sub>DME 532, 533
- Yb(C<sub>5</sub>Me<sub>5</sub>)<sub>2</sub>(OEt)<sub>2</sub> 535
- reaction with carbonyl complexes 562
- Yb(C<sub>5</sub>Me<sub>5</sub>)<sub>2</sub>(THF)
- nmr spectrum 545
- Yb(C<sub>5</sub>Me<sub>5</sub>)<sub>2</sub>(THF),  $\frac{1}{2}$  tol 535
- crystal structure 544
- Yb(II)(C<sub>5</sub>Me<sub>5</sub>)<sub>2</sub> 529
- Yb(CN)<sub>2</sub> 536
- YbCl<sub>2</sub> 532
- YbCp<sub>2</sub> 533, 535
- YbI<sub>2</sub> 528, 529, 533, 535
- electron transfer to an organic substrate 550
  - reaction with tertiary halide 552
  - reduction of benzophenone to benzopinacol 552
  - reduction of conjugated double bonds 553
  - reduction of KNH<sub>2</sub> 550
- YbI<sub>3</sub>
- reduction of 528
- Yb(MeC<sub>5</sub>H<sub>4</sub>)<sub>2</sub> 529, 532
- Yb(MeC<sub>5</sub>H<sub>4</sub>)<sub>2</sub>(THF)
- X-ray structure 544
- Yb(Me<sub>3</sub>SiC<sub>3</sub>H<sub>4</sub>)<sub>2</sub>(THF)<sub>2</sub>
- crystal structure 545
- Yb metal
- dissolution in liquid ammonia 535
  - in preparation of organometallic compounds 560

- Yb metal vapor  
  reaction with 1-hexyne  
    533
- YbMo<sub>2</sub>Al<sub>4</sub>-type 245
- Yb monochalcogenides 539
- Yb(NH<sub>2</sub>)<sub>2</sub> 535
- YbO 527
- Yb(OAc)<sub>2</sub> 533
- Yb(OEt)<sub>2</sub> 533
- Yb(o-Phen)<sub>4</sub> 536
- Yb(II) organometallic species  
  preparation by metal vapor  
    technique 529
- Yb<sub>3</sub>Rh<sub>4</sub>Sn<sub>13</sub>-type 240
- ytterbium dicyclopentadienide  
  532
- Zr<sub>4</sub>Co<sub>4</sub>Ge<sub>7</sub>-type 180
- ZrFeSi<sub>2</sub>-type 201
- ZrFe<sub>4</sub>Si<sub>2</sub>-type 243
- ZrIr<sub>3</sub>B<sub>4</sub>-type 251
- ZrNiAl-type 157
- ZrOS-type 164
- ZrSi<sub>2</sub>-type derivative 169
- Zr<sub>5</sub>Si<sub>4</sub>-type derivative 204
- ZrZn<sub>22</sub>-type derivative 284